

Jacob Fraden

# Handbook of Modern Sensors

Physics, Designs, and Applications

*Fifth Edition*

 Springer

---

# Handbook of Modern Sensors



---

Jacob Fraden

# Handbook of Modern Sensors

Physics, Designs, and Applications

Fifth Edition

 Springer

Jacob Fraden  
Fraden Corp.  
San Diego, CA, USA

ISBN 978-3-319-19302-1                      ISBN 978-3-319-19303-8 (eBook)  
DOI 10.1007/978-3-319-19303-8

Library of Congress Control Number: 2015947779

Springer Cham Heidelberg New York Dordrecht London  
© Springer International Publishing Switzerland 2004, 2010, 2016  
© American Institute of Physics 1993, 1997

This work is subject to copyright. All rights are reserved by the Publisher, whether the whole or part of the material is concerned, specifically the rights of translation, reprinting, reuse of illustrations, recitation, broadcasting, reproduction on microfilms or in any other physical way, and transmission or information storage and retrieval, electronic adaptation, computer software, or by similar or dissimilar methodology now known or hereafter developed.

The use of general descriptive names, registered names, trademarks, service marks, etc. in this publication does not imply, even in the absence of a specific statement, that such names are exempt from the relevant protective laws and regulations and therefore free for general use.

The publisher, the authors and the editors are safe to assume that the advice and information in this book are believed to be true and accurate at the date of publication. Neither the publisher nor the authors or the editors give a warranty, express or implied, with respect to the material contained herein or for any errors or omissions that may have been made.

Printed on acid-free paper

Springer International Publishing AG Switzerland is part of Springer Science+Business Media  
(www.springer.com)

---

## Preface

Numerous computerized appliances wash clothes, prepare coffee, play music, guard homes, and perform endless useful functions. However, no electronic device operates without receiving external information. Even if such information comes from another electronic device, somewhere in the chain, there is at least one component that perceives external input signals. This component is a sensor. Modern signal processors are the devices that manipulate binary codes generally represented by electric impulses. As we live in an analog world that mostly is not digital or electrical (apart from the atomic level), sensors are the interface devices between various physical values and the electronic circuits that “understand” only the language of moving electrical charges. In other words, sensors are eyes, ears, and noses of the silicon chips. This book is about the man-made sensors that are very much different from the sensing organs of living organisms.

Since the publication of the previous edition of this book, sensing technologies have made remarkable leaps. Sensitivities of sensors have become higher, their dimensions smaller, selectivity better, and prices lower. A new, major field of application for sensors—mobile communication devices—has been rapidly evolving. Even though such devices employ sensors that operate on the same fundamental principles as other sensors, their use in mobile devices demands specific requirements. Among these are miniature dimensions and complete integration with the signal processing and communication components. Hence, in this new edition, we address in greater detail the mobile trend in sensing technologies.

A sensor converts input signals of a physical nature into electrical output. Thus, we will examine in detail the principles of such conversions and other relevant laws of physics. Arguably one of the greatest geniuses who ever lived, Leonardo da Vinci, had his own peculiar way of praying (according to a book I read many years ago, by Akim Volinsky, published in Russian in 1900). Loosely, it may be translated into modern English as something like, “*Oh Lord, thank you for following Thy own laws.*” It is comforting indeed that the laws of Nature do not change—it is our appreciation of the laws that is continually refined. The sections of the book that cover these laws have not changed much since the previous editions. Yet, the sections that describe the practical designs have been revised substantially. Recent ideas and developments have been added, while obsolete and less interesting designs were dropped.

In the course of my engineering work, I often wished for a book which combined practical information on the many subjects relating to the most important physical principles, design, and use of various sensors. Of course, I could browse the Internet or library bookshelves in search of texts on physics, chemistry, electronics, technical, and scientific magazines, but the information is scattered over many publications and websites, and almost every question I was pondering required substantial research. Little by little, I gathered practical information on everything which is in any way related to various sensors and their applications to scientific and engineering measurements. I also spent endless hours at a lab bench, inventing and developing numerous devices with various sensors. Soon, I realized that the information I had collected would be quite useful to more than one person. This idea prompted me to write this book, and this fifth updated edition is the proof that I was not mistaken.

The topics included in the book reflect the author's own preferences and interpretations. Some may find a description of a particular sensor either too detailed or broad or perhaps too brief. In setting my criteria for selecting various sensors for this new edition, I attempted to keep the scope of this book as broad as possible, opting for many different designs described briefly (without being trivial, I hope), rather than fewer treated in greater depth. This volume attempts (immodestly perhaps) to cover a very broad range of sensors and detectors. Many of them are well known, but describing them is still useful for students and for those seeking a convenient reference.

By no means this book is a replacement for specialized texts. It gives a bird's-eye view at a multitude of designs and possibilities, but does not dive in depth into any particular topic. In most cases, I have tried to strike a balance between details and simplicity of coverage; however simplicity and clarity were the most important requirements I set for myself. My true goal was not to pile up a collection of information but rather to entice the reader into a creative mindset. As Plutarch said nearly two millennia ago, "*The mind is not a vessel to be filled but a fire to be kindled. . .*"

Even though this book is for scientists and engineers, as a rule, the technical descriptions and mathematic treatments generally do not require a background beyond a high school curriculum. This is a reference text which could be used by students, researchers interested in modern instrumentation (applied physicists and engineers), sensor designers, application engineers, and technicians whose job is to understand, select, or design sensors for practical systems.

The previous editions of this book have been used quite extensively as desktop references and textbooks for the related college courses. Comments and suggestions from sensor designers, application engineers, professors, and students have prompted me to implement several changes and to correct errors. I am deeply grateful to those who helped me to make further improvements in this new edition. I owe a debt of gratitude and many thanks to Drs. Ephraim Suhir and David Pintsov for assisting me in mathematical treatment of transfer functions and to Dr. Sanjay V. Patel for his further contributions to the chapter on chemical sensors.

---

# Contents

<b>1</b>	<b>Data Acquisition</b> . . . . .	1
1.1	Sensors, Signals, and Systems . . . . .	1
1.2	Sensor Classification . . . . .	7
1.3	Units of Measurements . . . . .	10
	References . . . . .	11
<b>2</b>	<b>Transfer Functions</b> . . . . .	13
2.1	Mathematical Models . . . . .	13
2.1.1	Concept . . . . .	15
2.1.2	Functional Approximations . . . . .	15
2.1.3	Linear Regression . . . . .	19
2.1.4	Polynomial Approximations . . . . .	19
2.1.5	Sensitivity . . . . .	21
2.1.6	Linear Piecewise Approximation . . . . .	21
2.1.7	Spline Interpolation . . . . .	22
2.1.8	Multidimensional Transfer Functions . . . . .	23
2.2	Calibration . . . . .	24
2.3	Computation of Parameters . . . . .	26
2.4	Computation of a Stimulus . . . . .	28
2.4.1	Use of Analytical Equation . . . . .	29
2.4.2	Use of Linear Piecewise Approximation . . . . .	29
2.4.3	Iterative Computation of Stimulus (Newton Method) . . . . .	32
	References . . . . .	34
<b>3</b>	<b>Sensor Characteristics</b> . . . . .	35
3.1	Sensors for Mobile Communication Devices . . . . .	35
3.1.1	Requirements to MCD Sensors . . . . .	36
3.1.2	Integration . . . . .	37
3.2	Span (Full-Scale Input) . . . . .	38
3.3	Full-Scale Output . . . . .	39
3.4	Accuracy . . . . .	39
3.5	Calibration Error . . . . .	42
3.6	Hysteresis . . . . .	43
3.7	Nonlinearity . . . . .	44
		vii



3.8	Saturation . . . . .	45
3.9	Repeatability . . . . .	46
3.10	Dead Band . . . . .	47
3.11	Resolution . . . . .	48
3.12	Special Properties . . . . .	48
3.13	Output Impedance . . . . .	48
3.14	Output Format . . . . .	48
3.15	Excitation . . . . .	49
3.16	Dynamic Characteristics . . . . .	49
3.17	Dynamic Models of Sensor Elements . . . . .	54
	3.17.1 Mechanical Elements . . . . .	54
	3.17.2 Thermal Elements . . . . .	55
	3.17.3 Electrical Elements . . . . .	57
	3.17.4 Analogies . . . . .	58
3.18	Environmental Factors . . . . .	58
3.19	Reliability . . . . .	61
	3.19.1 MTTF . . . . .	61
	3.19.2 Extreme Testing . . . . .	62
	3.19.3 Accelerated Life Testing . . . . .	63
3.20	Application Characteristics . . . . .	65
3.21	Uncertainty . . . . .	65
	References . . . . .	67
<b>4</b>	<b>Physical Principles of Sensing . . . . .</b>	<b>69</b>
4.1	Electric Charges, Fields, and Potentials . . . . .	70
4.2	Capacitance . . . . .	76
	4.2.1 Capacitor . . . . .	78
	4.2.2 Dielectric Constant . . . . .	79
4.3	Magnetism . . . . .	83
	4.3.1 Faraday Law . . . . .	86
	4.3.2 Permanent Magnets . . . . .	88
	4.3.3 Coil and Solenoid . . . . .	89
4.4	Induction . . . . .	90
	4.4.1 Lenz Law . . . . .	94
	4.4.2 Eddy Currents . . . . .	95
4.5	Resistance . . . . .	96
	4.5.1 Specific Resistivity . . . . .	98
	4.5.2 Temperature Sensitivity of a Resistor . . . . .	99
	4.5.3 Strain Sensitivity of a Resistor . . . . .	102
	4.5.4 Moisture Sensitivity of a Resistor . . . . .	104
4.6	Piezoelectric Effect . . . . .	104
	4.6.1 Ceramic Piezoelectric Materials . . . . .	108
	4.6.2 Polymer Piezoelectric Films . . . . .	112
4.7	Pyroelectric Effect . . . . .	113
4.8	Hall Effect . . . . .	119

4.9	Thermoelectric Effects . . . . .	123
4.9.1	Seebeck Effect . . . . .	123
4.9.2	Peltier Effect . . . . .	128
4.10	Sound Waves . . . . .	129
4.11	Temperature and Thermal Properties of Materials . . . . .	132
4.11.1	Temperature Scales . . . . .	133
4.11.2	Thermal Expansion . . . . .	135
4.11.3	Heat Capacity . . . . .	137
4.12	Heat Transfer . . . . .	138
4.12.1	Thermal Conduction . . . . .	139
4.12.2	Thermal Convection . . . . .	141
4.12.3	Thermal Radiation . . . . .	142
	References . . . . .	153
<b>5</b>	<b>Optical Components of Sensors . . . . .</b>	<b>155</b>
5.1	Light . . . . .	155
5.1.1	Energy of Light Quanta . . . . .	155
5.1.2	Light Polarization . . . . .	157
5.2	Light Scattering . . . . .	157
5.3	Geometrical Optics . . . . .	159
5.4	Radiometry . . . . .	160
5.5	Photometry . . . . .	166
5.6	Windows . . . . .	169
5.7	Mirrors . . . . .	171
5.7.1	Coated Mirrors . . . . .	172
5.7.2	Prismatic Mirrors . . . . .	173
5.8	Lenses . . . . .	174
5.8.1	Curved Surface Lenses . . . . .	174
5.8.2	Fresnel Lenses . . . . .	176
5.8.3	Flat Nanolenses . . . . .	179
5.9	Fiber Optics and Waveguides . . . . .	179
5.10	Optical Efficiency . . . . .	183
5.10.1	Lensing Effect . . . . .	183
5.10.2	Concentrators . . . . .	185
5.10.3	Coatings for Thermal Absorption . . . . .	186
5.10.4	Antireflective Coating (ARC) . . . . .	187
	References . . . . .	188
<b>6</b>	<b>Interface Electronic Circuits . . . . .</b>	<b>191</b>
6.1	Signal Conditioners . . . . .	193
6.1.1	Input Characteristics . . . . .	194
6.1.2	Amplifiers . . . . .	198
6.1.3	Operational Amplifiers . . . . .	199
6.1.4	Voltage Follower . . . . .	201

---

6.1.5	Charge- and Current-to-Voltage Converters . . . . .	201
6.1.6	Light-to-Voltage Converters . . . . .	203
6.1.7	Capacitance-to-Voltage Converters . . . . .	205
6.1.8	Closed-Loop Capacitance-to-Voltage Converters . . . . .	207
6.2	Sensor Connections . . . . .	209
6.2.1	Ratiometric Circuits . . . . .	209
6.2.2	Differential Circuits . . . . .	212
6.2.3	Wheatstone Bridge . . . . .	212
6.2.4	Null-Balanced Bridge . . . . .	215
6.2.5	Bridge Amplifiers . . . . .	216
6.3	Excitation Circuits . . . . .	218
6.3.1	Current Generators . . . . .	220
6.3.2	Voltage Generators . . . . .	222
6.3.3	Voltage References . . . . .	223
6.3.4	Oscillators . . . . .	224
6.4	Analog-to-Digital Converters . . . . .	225
6.4.1	Basic Concepts . . . . .	226
6.4.2	V/F Converters . . . . .	227
6.4.3	PWM Converters . . . . .	231
6.4.4	R/F Converters . . . . .	232
6.4.5	Successive-Approximation Converter . . . . .	234
6.4.6	Resolution Extension . . . . .	235
6.4.7	ADC Interface . . . . .	237
6.5	Integrated Interfaces . . . . .	239
6.5.1	Voltage Processor . . . . .	239
6.5.2	Inductance Processor . . . . .	240
6.6	Data Transmission . . . . .	241
6.6.1	Two-Wire Transmission . . . . .	242
6.6.2	Four-Wire Transmission . . . . .	243
6.7	Noise in Sensors and Circuits . . . . .	243
6.7.1	Inherent Noise . . . . .	244
6.7.2	Transmitted Noise . . . . .	247
6.7.3	Electric Shielding . . . . .	252
6.7.4	Bypass Capacitors . . . . .	255
6.7.5	Magnetic Shielding . . . . .	256
6.7.6	Mechanical Noise . . . . .	258
6.7.7	Ground Planes . . . . .	258
6.7.8	Ground Loops and Ground Isolation . . . . .	259
6.7.9	Seebeck Noise . . . . .	261
6.8	Batteries for Low-Power Sensors . . . . .	263
6.8.1	Primary Cells . . . . .	264
6.8.2	Secondary Cells . . . . .	265
6.8.3	Supercapacitors . . . . .	265

6.9	Energy Harvesting . . . . .	266
6.9.1	Light Energy Harvesting . . . . .	267
6.9.2	Far-Field Energy Harvesting . . . . .	268
6.9.3	Near-Field Energy Harvesting . . . . .	269
	References . . . . .	269
<b>7</b>	<b>Detectors of Humans . . . . .</b>	<b>271</b>
7.1	Ultrasonic Detectors . . . . .	273
7.2	Microwave Motion Detectors . . . . .	276
7.3	Micropower Impulse Radars . . . . .	281
7.4	Ground Penetrating Radars . . . . .	284
7.5	Linear Optical Sensors (PSD) . . . . .	285
7.6	Capacitive Occupancy Detectors . . . . .	289
7.7	Triboelectric Detectors . . . . .	292
7.8	Optoelectronic Motion Detectors . . . . .	294
7.8.1	Sensor Structures . . . . .	295
7.8.2	Multiple Detecting Elements . . . . .	297
7.8.3	Complex Sensor Shape . . . . .	297
7.8.4	Image Distortion . . . . .	297
7.8.5	Facet Focusing Elements . . . . .	298
7.8.6	Visible and Near-IR Light Motion Detectors . . . . .	299
7.8.7	Mid- and Far-IR Detectors . . . . .	301
7.8.8	Passive Infrared (PIR) Motion Detectors . . . . .	302
7.8.9	PIR Detector Efficiency Analysis . . . . .	305
7.9	Optical Presence Sensors . . . . .	309
7.9.1	Photoelectric Beam . . . . .	309
7.9.2	Light Reflection Detectors . . . . .	310
7.10	Pressure-Gradient Sensors . . . . .	311
7.11	2-D Pointing Devices . . . . .	313
7.12	Gesture Sensing (3-D Pointing) . . . . .	314
7.12.1	Inertial and Gyroscopic Mice . . . . .	315
7.12.2	Optical Gesture Sensors . . . . .	315
7.12.3	Near-Field Gesture Sensors . . . . .	316
7.13	Tactile Sensors . . . . .	318
7.13.1	Switch Sensors . . . . .	319
7.13.2	Piezoelectric Tactile Sensors . . . . .	320
7.13.3	Piezoresistive Tactile Sensors . . . . .	323
7.13.4	Tactile MEMS Sensors . . . . .	326
7.13.5	Capacitive Touch Sensors . . . . .	326
7.13.6	Optical Touch Sensors . . . . .	330
7.13.7	Optical Fingerprint Sensors . . . . .	331
	References . . . . .	332

<b>8</b>	<b>Presence, Displacement, and Level</b> . . . . .	335
8.1	Potentiometric Sensors . . . . .	336
8.2	Piezoresistive Sensors . . . . .	340
8.3	Capacitive Sensors . . . . .	342
8.4	Inductive and Magnetic Sensors . . . . .	345
8.4.1	LVDT and RVDT . . . . .	346
8.4.2	Transverse Inductive Sensor . . . . .	348
8.4.3	Eddy Current Probes . . . . .	349
8.4.4	Pavement Loops . . . . .	351
8.4.5	Metal Detectors . . . . .	352
8.4.6	Hall-Effect Sensors . . . . .	353
8.4.7	Magneto-resistive Sensors . . . . .	358
8.4.8	Magnetostrictive Detector . . . . .	361
8.5	Optical Sensors . . . . .	362
8.5.1	Optical Bridge . . . . .	363
8.5.2	Proximity Detector with Polarized Light . . . . .	363
8.5.3	Prismatic and Reflective Sensors . . . . .	364
8.5.4	Fabry-Perot Sensors . . . . .	366
8.5.5	Fiber Bragg Grating Sensors . . . . .	368
8.5.6	Grating Photomodulators . . . . .	370
8.6	Thickness and Level Sensors . . . . .	371
8.6.1	Ablation Sensors . . . . .	372
8.6.2	Film Sensors . . . . .	373
8.6.3	Cryogenic Liquid Level Sensors . . . . .	375
	References . . . . .	376
<b>9</b>	<b>Velocity and Acceleration</b> . . . . .	379
9.1	Stationary Velocity Sensors . . . . .	382
9.1.1	Linear Velocity . . . . .	382
9.1.2	Rotary Velocity Sensors (Tachometers) . . . . .	384
9.2	Inertial Rotary Sensors . . . . .	385
9.2.1	Rotor Gyroscope . . . . .	386
9.2.2	Vibrating Gyroscopes . . . . .	387
9.2.3	Optical (Laser) Gyroscopes . . . . .	390
9.3	Inertial Linear Sensors (Accelerometers) . . . . .	392
9.3.1	Transfer Function and Characteristics . . . . .	393
9.3.2	Inclinometers . . . . .	397
9.3.3	Seismic Sensors . . . . .	400
9.3.4	Capacitive Accelerometers . . . . .	401
9.3.5	Piezoresistive Accelerometers . . . . .	404
9.3.6	Piezoelectric Accelerometers . . . . .	405
9.3.7	Thermal Accelerometers . . . . .	406
9.3.8	Closed-Loop Accelerometers . . . . .	410
	References . . . . .	411

---

<b>10</b>	<b>Force and Strain</b> . . . . .	413
10.1	Basic Considerations . . . . .	413
10.2	Strain Gauges . . . . .	416
10.3	Pressure-Sensitive Films . . . . .	418
10.4	Piezoelectric Force Sensors . . . . .	420
10.5	Piezoelectric Cables . . . . .	424
10.6	Optical Force Sensors . . . . .	426
	References . . . . .	428
<b>11</b>	<b>Pressure Sensors</b> . . . . .	429
11.1	Concept of Pressure . . . . .	429
11.2	Units of Pressure . . . . .	431
11.3	Mercury Pressure Sensor . . . . .	432
11.4	Bellows, Membranes, and Thin Plates . . . . .	433
11.5	Piezoresistive Sensors . . . . .	435
11.6	Capacitive Sensors . . . . .	440
11.7	VRP Sensors . . . . .	442
11.8	Optoelectronic Pressure Sensors . . . . .	443
11.9	Indirect Pressure Sensor . . . . .	445
11.10	Vacuum Sensors . . . . .	447
	11.10.1 Pirani Gauge . . . . .	447
	11.10.2 Ionization Gauges . . . . .	449
	11.10.3 Gas Drag Gauge . . . . .	450
	References . . . . .	451
<b>12</b>	<b>Flow Sensors</b> . . . . .	453
12.1	Basics of Flow Dynamics . . . . .	453
12.2	Pressure Gradient Technique . . . . .	456
12.3	Thermal Transport Sensors . . . . .	458
	12.3.1 Hot-Wire Anemometers . . . . .	459
	12.3.2 Three-Part Thermoanemometer . . . . .	463
	12.3.3 Two-Part Thermoanemometer . . . . .	465
	12.3.4 Microflow Thermal Transport Sensors . . . . .	468
12.4	Ultrasonic Sensors . . . . .	470
12.5	Electromagnetic Sensors . . . . .	472
12.6	Breeze Sensor . . . . .	474
12.7	Coriolis Mass Flow Sensors . . . . .	475
12.8	Drag Force Flowmeter . . . . .	477
12.9	Cantilever MEMS Sensors . . . . .	478
12.10	Dust and Smoke Detectors . . . . .	479
	12.10.1 Ionization Detector . . . . .	479
	12.10.2 Optical Detector . . . . .	481
	References . . . . .	483

<b>13</b>	<b>Microphones</b> . . . . .	485
13.1	Microphone Characteristics . . . . .	487
13.1.1	Output Impedance . . . . .	487
13.1.2	Balanced Output . . . . .	487
13.1.3	Sensitivity . . . . .	487
13.1.4	Frequency Response . . . . .	488
13.1.5	Intrinsic Noise . . . . .	488
13.1.6	Directionality . . . . .	489
13.1.7	Proximity Effect . . . . .	492
13.2	Resistive Microphones . . . . .	493
13.3	Condenser Microphones . . . . .	493
13.4	Electret Microphones . . . . .	495
13.5	Optical Microphones . . . . .	497
13.6	Piezoelectric Microphones . . . . .	500
13.6.1	Low-Frequency Range . . . . .	500
13.6.2	Ultrasonic Range . . . . .	501
13.7	Dynamic Microphones . . . . .	504
	References . . . . .	505
<b>14</b>	<b>Humidity and Moisture Sensors</b> . . . . .	507
14.1	Concept of Humidity . . . . .	507
14.2	Sensor Concepts . . . . .	511
14.3	Capacitive Humidity Sensors . . . . .	512
14.4	Resistive Humidity Sensors . . . . .	515
14.5	Thermal Conductivity Sensor . . . . .	516
14.6	Optical Hygrometers . . . . .	517
14.6.1	Chilled Mirror . . . . .	517
14.6.2	Light RH Sensors . . . . .	518
14.7	Oscillating Hygrometer . . . . .	519
14.8	Soil Moisture . . . . .	520
	References . . . . .	523
<b>15</b>	<b>Light Detectors</b> . . . . .	525
15.1	Introduction . . . . .	525
15.1.1	Principle of Quantum Detectors . . . . .	526
15.2	Photodiode . . . . .	530
15.3	Phototransistor . . . . .	536
15.4	Photoresistor . . . . .	538
15.5	Cooled Detectors . . . . .	540
15.6	Imaging Sensors for Visible Range . . . . .	543
15.6.1	CCD Sensor . . . . .	544
15.6.2	CMOS Imaging Sensors . . . . .	545
15.7	UV Detectors . . . . .	546
15.7.1	Materials and Designs . . . . .	546
15.7.2	Avalanche UV Detectors . . . . .	547

15.8	Thermal Radiation Detectors . . . . .	549
15.8.1	General Considerations . . . . .	549
15.8.2	Golay Cells . . . . .	551
15.8.3	Thermopiles . . . . .	552
15.8.4	Pyroelectric Sensors . . . . .	558
15.8.5	Microbolometers . . . . .	564
	References . . . . .	567
<b>16</b>	<b>Detectors of Ionizing Radiation . . . . .</b>	<b>569</b>
16.1	Scintillating Detectors . . . . .	570
16.2	Ionization Detectors . . . . .	574
16.2.1	Ionization Chambers . . . . .	574
16.2.2	Proportional Chambers . . . . .	575
16.2.3	Geiger–Müller (GM) Counters . . . . .	576
16.2.4	Semiconductor Detectors . . . . .	578
16.3	Cloud and Bubble Chambers . . . . .	582
	References . . . . .	583
<b>17</b>	<b>Temperature Sensors . . . . .</b>	<b>585</b>
17.1	Coupling with Object . . . . .	585
17.1.1	Static Heat Exchange . . . . .	585
17.1.2	Dynamic Heat Exchange . . . . .	589
17.1.3	Sensor Structure . . . . .	592
17.1.4	Signal Processing of Sensor Response . . . . .	594
17.2	Temperature References . . . . .	596
17.3	Resistance Temperature Detectors (RTD) . . . . .	597
17.4	Ceramic Thermistors . . . . .	599
17.4.1	Simple Model . . . . .	601
17.4.2	Fraden Model . . . . .	602
17.4.3	Steinhart and Hart Model . . . . .	604
17.4.4	Self-Heating Effect in NTC Thermistors . . . . .	607
17.4.5	Ceramic PTC Thermistors . . . . .	611
17.4.6	Fabrication . . . . .	615
17.5	Silicon and Germanium Thermistors . . . . .	617
17.6	Semiconductor <i>pn</i> -Junction Sensors . . . . .	620
17.7	Silicon PTC Temperature Sensors . . . . .	624
17.8	Thermoelectric Sensors . . . . .	626
17.8.1	Thermoelectric Laws . . . . .	628
17.8.2	Thermocouple Circuits . . . . .	630
17.8.3	Thermocouple Assemblies . . . . .	633
17.9	Optical Temperature Sensors . . . . .	635
17.9.1	Fluoroptic Sensors . . . . .	635
17.9.2	Interferometric Sensors . . . . .	637
17.9.3	Super-High Resolution Sensing . . . . .	637
17.9.4	Thermochromic Sensors . . . . .	638
17.9.5	Fiber-Optic Temperature Sensors (FBG) . . . . .	639



---

17.10	Acoustic Temperature Sensors . . . . .	640
17.11	Piezoelectric Temperature Sensors . . . . .	641
	References . . . . .	642
<b>18</b>	<b>Chemical and Biological Sensors . . . . .</b>	<b>645</b>
18.1	Overview . . . . .	646
	18.1.1 Chemical Sensors . . . . .	646
	18.1.2 Biochemical Sensors . . . . .	647
18.2	History . . . . .	647
18.3	Chemical Sensor Characteristics . . . . .	648
	18.3.1 Selectivity . . . . .	648
	18.3.2 Sensitivity . . . . .	650
18.4	Electrical and Electrochemical Sensors . . . . .	651
	18.4.1 Electrode Systems . . . . .	651
	18.4.2 Potentiometric Sensors . . . . .	655
	18.4.3 Conductometric Sensors . . . . .	656
	18.4.4 Metal Oxide Semiconductor (MOS) Chemical Sensors . . . . .	661
	18.4.5 Elastomer Chemiresistors . . . . .	663
	18.4.6 Chemicapacitive Sensors . . . . .	666
	18.4.7 ChemFET . . . . .	668
18.5	Photoionization Detectors . . . . .	669
18.6	Physical Transducers . . . . .	671
	18.6.1 Acoustic Wave Devices . . . . .	671
	18.6.2 Microcantilevers . . . . .	674
18.7	Spectrometers . . . . .	676
	18.7.1 Ion Mobility Spectrometry . . . . .	677
	18.7.2 Quadrupole Mass Spectrometer . . . . .	678
18.8	Thermal Sensors . . . . .	679
	18.8.1 Concept . . . . .	679
	18.8.2 Pellister Catalytic Sensors . . . . .	680
18.9	Optical Transducers . . . . .	681
	18.9.1 Infrared Detection . . . . .	681
	18.9.2 Fiber-Optic Transducers . . . . .	682
	18.9.3 Ratiometric Selectivity (Pulse Oximeter) . . . . .	683
	18.9.4 Color Change Sensors . . . . .	686
18.10	Multi-sensor Arrays . . . . .	688
	18.10.1 General Considerations . . . . .	688
	18.10.2 Electronic Noses and Tongues . . . . .	688
18.11	Specific Difficulties . . . . .	692
	References . . . . .	693
<b>19</b>	<b>Materials and Technologies . . . . .</b>	<b>699</b>
19.1	Materials . . . . .	699
	19.1.1 Silicon as Sensing Material . . . . .	699
	19.1.2 Plastics . . . . .	703

---

19.1.3	Metals . . . . .	708
19.1.4	Ceramics . . . . .	710
19.1.5	Structural Glasses . . . . .	710
19.1.6	Optical Glasses . . . . .	711
19.2	Nano-materials . . . . .	714
19.3	Surface Processing . . . . .	715
19.3.1	Spin Casting . . . . .	715
19.3.2	Vacuum Deposition . . . . .	716
19.3.3	Sputtering . . . . .	717
19.3.4	Chemical Vapor Deposition (CVD) . . . . .	718
19.3.5	Electroplating . . . . .	719
19.4	MEMS Technologies . . . . .	721
19.4.1	Photolithography . . . . .	722
19.4.2	Silicon Micromachining . . . . .	723
19.4.3	Micromachining of Bridges and Cantilevers . . . . .	727
19.4.4	Lift-Off . . . . .	728
19.4.5	Wafer Bonding . . . . .	729
19.4.6	LIGA . . . . .	730
	References . . . . .	731
<b>Appendix . . . . .</b>		<b>733</b>
<b>Index . . . . .</b>		<b>753</b>



---

## About the Author

**Jacob Fraden** holds a Ph.D. in medical electronics and is President of Fraden Corp., a technology company that develops sensors for consumer, medical, and industrial applications. He has authored nearly 60 patents in the areas of sensing, medical instrumentation, security, energy management, and others.

*“It’s as large as life, and twice as natural”*

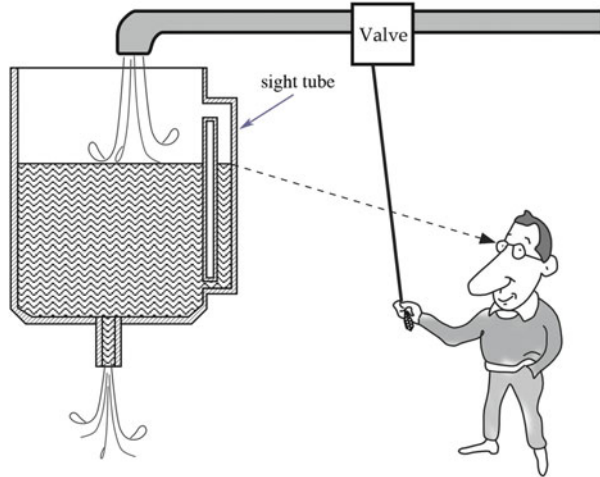
—Lewis Carroll, “Through the Looking Glass”

---

## 1.1 Sensors, Signals, and Systems

A sensor is often defined as a “*device that receives and responds to a signal or stimulus*”. This definition is broad. In fact, it is so broad that it covers almost everything from a human eye to a trigger in a pistol. Consider the level-control system shown in Fig. 1.1 [1]. The operator adjusts the level of fluid in the tank by manipulating its valve. Variations in the inlet flow rate, temperature changes (these would alter the fluid’s viscosity and consequently the flow rate through the valve), and similar disturbances must be compensated for by the operator. Without control the tank is likely to flood, or run dry. To act appropriately, the operator must on a timely basis obtain information about the level of fluid in the tank. In this example, the information is generated by the sensor, which consists of two main parts: the sight tube on the tank and the operator’s eye, which produces an electric response in the optic nerve. The sight tube by itself is not a sensor, and in this particular control system, the eye is not a sensor either. Only the combination of these two components makes a narrow-purpose sensor (detector) that is *selectively* sensitive to the fluid level. If a sight tube is designed properly, it will very quickly reflect variations in the level, and it is said that the sensor has a fast speed response. If the internal diameter of the tube is too small for a given fluid viscosity, the level in the tube may lag behind the level in the tank. Then, we have to consider a phase characteristic of such a sensor. In some cases, the lag may be quite acceptable, while in other situations, a better sight tube design would be required. Hence, the sensor’s performance must be assessed only as part of a data acquisition system.

**Fig. 1.1** Level-Control System. Sight tube and operator's eye form a sensor—device that converts information into electrical signal



This world is divided into natural and man-made objects. The natural sensors, like those found in living organisms, usually respond with signals having electrochemical character; that is, their physical nature is based on ion transport, like in the nerve fibers (such as an optic nerve in the fluid tank operator). In man-made devices, information is also transmitted and processed in electrical form, however, through the transport of electrons. Sensors intended for the artificial systems must speak the same language as the systems “speak”. This language is electrical in its nature and the sensor shall be capable of responding with the output signals where information is carried by displacement of electrons, rather than ions.<sup>1</sup> Thus, it should be possible to connect a sensor to an electronic system through electrical wires, rather than through an electrochemical solution or a nerve fiber. Hence, in this book, we use a somewhat narrower definition of a sensor, which may be phrased as

A sensor is a device that receives a stimulus and responds with an electrical signal.

The term *stimulus* is used throughout this book and needs to be clearly understood. The stimulus is the quantity, property, or condition that is received and converted into electrical signal. Examples of stimuli are light intensity and wavelength, sound, force, acceleration, distance, rate of motion, and chemical composition. When we say “electrical,” we mean a signal which can be channeled, amplified, and modified by electronic devices. Some texts (for instance, [2]) use a different term, *measurand*, which has the same meaning as stimulus, however with the stress on quantitative characteristic of sensing.

We may say that a sensor is a translator of a generally nonelectrical value into an electrical value. The sensor's output signal may be in form of voltage, current, or charge. These may be further described in terms of amplitude, polarity, frequency,

<sup>1</sup> There is a very exciting field of the optical computing and communications where information is processed by a transport of photons. That field is beyond the scope of this book.

phase, or digital code. The set of output characteristics is called the *output signal format*. Therefore, a sensor has input properties (of any kind) and electrical output properties.

Any sensor is an energy converter. No matter what you try to measure, you always deal with energy transfer between the object of measurement to the sensor. The process of sensing is a particular case of information transfer, and any transmission of information requires transmission of energy. One should not be confused by the obvious fact that transmission of energy can flow both ways—it may be with a positive sign as well as with a negative sign; that is, energy can flow either from the object to the sensor or backward—from the sensor to the object. A special case is when the net energy flow is zero, and that also carries information about existence of that particular situation. For example, a thermopile infrared radiation sensor will produce a positive voltage when the object is warmer than the sensor (infrared flux is flowing to the sensor). The voltage becomes negative when the object is cooler than the sensor (infrared flux flows from the sensor to the object). When both the sensor and the object are at exactly the same temperature, the flux is zero and the output voltage is zero. This carries a message that the temperatures are equal to one another.

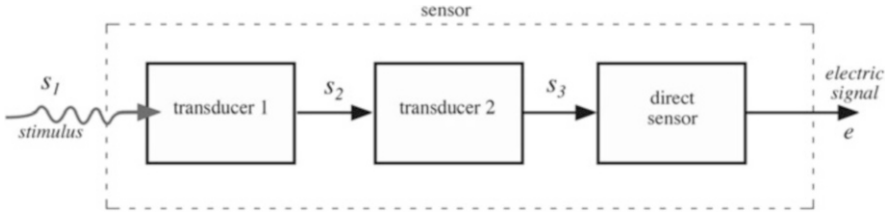
The terms *sensor* and term *detector* are synonyms, used interchangeably and have the same meaning. However, detector is more often used to stress qualitative rather than quantitative nature of measurement. For example, a PIR (passive infrared) detector is employed to indicate just the existence of human movement but generally cannot measure direction, speed, or acceleration.

The term *sensor* should be distinguished from *transducer*. The latter is a converter of any one type of energy or property into another type of energy or property, whereas the former converts it into *electrical signal*. An example of a transducer is a loudspeaker which converts an electrical signal into a variable magnetic field and, subsequently, into acoustic waves.<sup>2</sup> This is nothing to do with perception or sensing. Transducers may be used as *actuators* in various systems. An actuator may be described as opposite to a sensor—it converts electrical signal into generally nonelectrical energy. For example, an electric motor is an actuator—it converts electric energy into mechanical action. Another example is a pneumatic actuator that is enabled by an electric signal and converts air pressure into force.

Transducers may be parts of a *hybrid* or *complex* sensor (Fig. 1.2). For example, a chemical sensor may comprise two parts: the first part converts energy of an exothermal chemical reaction into heat (transducer) and another part, a thermopile, converts heat into an electrical output signal. The combination of the two makes a hybrid chemical sensor, a device which produces *electrical* signal in response to a chemical reagent. Note that in the above example a chemical sensor is a complex sensor—it is comprised of a nonelectrical transducer and a simple (direct) sensor converting heat to electricity. This suggests that many sensors incorporate at least

---

<sup>2</sup>It is interesting to note that a loudspeaker, when connected to an input of an amplifier, may function as a microphone. In that case, it becomes an acoustical sensor.



**Fig. 1.2** Sensor may incorporate several transducers. Value  $s_1$ ,  $s_2$ , etc. represent various types of energy. Direct sensor produces electrical output  $e$

one *direct*-type sensor and possibly a number of transducers. The direct sensors are those that employ certain physical effects to make a *direct* energy conversion into a generation or modulation of an electrical signal. Examples of such physical effects are the photoeffect and Seebeck effect. These will be described in Chap. 4.

In summary, there are two types of sensors, *direct* and *hybrid*. A direct sensor converts a stimulus into an electrical signal or modifies an externally supplied electrical signal, whereas a hybrid sensor (or simply—a sensor) in addition needs one or more transducers before a direct sensor can be employed to generate an electrical output.

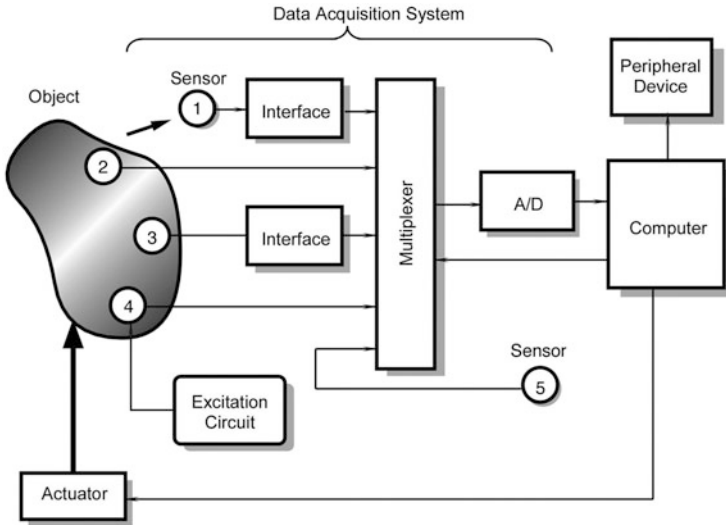
A sensor does not function by itself; it is always part of a larger system that may incorporate many other detectors, signal conditioners, processors, memory devices, data recorders, and actuators. The sensor's place in a device is either intrinsic or extrinsic. It may be positioned at the input of a device to perceive the outside effects and to inform the system about variations in the outside stimuli. Also, it may be an internal part of a device that monitors the devices' own state to cause the appropriate performance. A sensor is always part of some kind of a data acquisition system. In turn, such a system may be part of a larger control system that includes various feedback mechanisms.

To illustrate the place of sensors in a larger system, Fig. 1.3 shows a block diagram of a data acquisition and control device. An object can be anything: a car, space ship, animal or human, liquid, or gas. Any material object may become a subject of some kind of a measurement or control. Data are collected from an object by a number of sensors. Some of them (2, 3, and 4) are positioned directly on or inside the object. Sensor 1 perceives the object without a physical contact and, therefore, is called a *noncontact* sensor. Examples of such a sensor is a radiation detector and a TV camera. Even if we say “noncontact”, we remember that energy transfer always occurs between a sensor and object.

Sensor 5 serves a different purpose. It monitors the internal conditions of the data acquisition system itself. Some sensors (1 and 3) cannot be directly connected to standard electronic circuits because of the inappropriate output signal formats. They require the use of interface devices (signal conditioners) to produce a specific output format.

Sensors 1, 2, 3, and 5 are *passive*. They generate electric signals without energy consumption from the electronic circuits. Sensor 4 is *active*. It requires an operating





**Fig. 1.3** Positions of sensors in data acquisition system. Sensor 1 is noncontact, sensors 2 and 3 are passive, sensor 4 is active, and sensor 5 is internal to data acquisition system

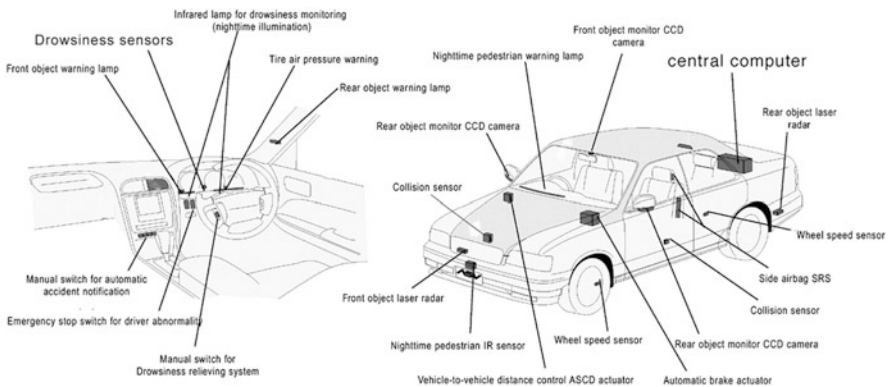
signal that is provided by an excitation circuit. This signal is modified by the sensor or modulated by the object's stimulus. An example of an active sensor is a thermistor that is a temperature-sensitive resistor. It needs a current source, which is an excitation circuit. Depending on the complexity of the system, the total number of sensors may vary from as little as one (a home thermostat) to many thousands (a space station).

Electrical signals from the sensors are fed into a multiplexer (MUX), which is a switch or a gate. Its function is to connect the sensors, one at a time, to an analog-to-digital converter (A/D or ADC) if a sensor produces an analog signal, or directly to a computer if a sensor produces signals in a digital format. The computer controls a multiplexer and ADC for the appropriate timing. Also, it may send control signals to an actuator that acts on the object. Examples of the actuators are an electric motor, a solenoid, a relay, and a pneumatic valve. The system contains some peripheral devices (for instance, a data recorder, display, alarm, etc.) and a number of components that are not shown in the block diagram. These may be filters, sample-and-hold circuits, amplifiers, and so forth.

To illustrate how such a system works, let us consider a simple car door monitoring arrangement. Every door in a car is supplied with a sensor that detects the door position (open or closed). In most cars, the sensor is a simple electric switch. Signals from all door switches go to the car's internal processor (no need for an ADC as all door signals are in a digital format: ones or zeros). The processor identifies which door is open (signal is zero) and sends an indicating message to the peripheral devices (a dashboard display and an audible alarm). A car driver (the actuator) gets the message and acts on the object (closes the door) and the sensor outputs the signal "one".

An example of a more complex device is an anesthetic vapor delivery system. It is intended for controlling the level of anesthetic drugs delivered to a patient through inhalation during surgical procedures. The system employs several active and passive sensors. The vapor concentration of anesthetic agents (such as halothane, isoflurane, or enflurane) is selectively monitored by an active piezoelectric sensor being installed into a ventilation tube. Molecules of anesthetic vapors add mass to the oscillating crystal in the sensor and change its natural frequency, which is a measure of the vapor concentration. Several other sensors monitor the concentration of  $\text{CO}_2$ , to distinguish exhale from inhale, and temperature and pressure, to compensate for additional variables. All these data are multiplexed, digitized, and fed into the digital signal processor (DSP) which calculates the actual vapor concentration. An anesthesiologist presets a desired delivery level and the processor adjusts the actuators (valves) to maintain anesthetics at the correct concentration.

Another example of a complex combination of various sensors, actuators, and indicating signals is shown in Fig. 1.4. It is an Advanced Safety Vehicle (ASV) that was developed by Nissan. The system is aimed at increasing safety of a car. Among many others, it includes a drowsiness warning system and drowsiness relieving system. This may include the eyeball movement sensor and the driver head inclination detector. The microwave, ultrasonic, and infrared range measuring sensors are incorporated into the emergency braking advanced advisory system to illuminate the break lamps even before the driver brakes hard in an emergency, thus advising the driver of a following vehicle to take evasive action. The obstacle warning system includes both the radar and infrared (IR) detectors. The adaptive cruise-control system works if the driver approaches too closely to a preceding vehicle; the speed is automatically reduced to maintain a suitable safety distance. The pedestrian monitoring system detects and alerts the driver to the presence of pedestrians at night as well as in vehicle blind spots. The lane-control system helps in the event the system detects and determines that incipient lane deviation is not the driver's intention. It issues a warning and automatically steers the vehicle, if necessary, to prevent it from leaving its lane.



**Fig. 1.4** Multiple sensors, actuators, and warning signals are parts of the Advanced Safety Vehicle (Courtesy of Nissan Motor Company)

In the following chapters we focus on sensing methods, physical principles of sensor operations, practical designs, and interface electronic circuits. Other essential parts of the control and monitoring systems, such as actuators, displays, data recorders, data transmitters, and others are beyond the scope of this book and mentioned only briefly.

The sensor's packaging design may be of a general purpose. A special packaging and housing should be built to adapt it for a particular application. For instance, a micromachined piezoresistive pressure sensor may be housed into a watertight enclosure for the invasive measurement of the aortic blood pressure through a catheter. The same sensor will be given an entirely different packaging when intended for measuring blood pressure by a noninvasive oscillometric method with an inflatable cuff. Some sensors are specifically designed to be very selective in a particular range of input stimulus and be quite immune to signals outside the desirable limits. For instance, a motion detector for a security system should be sensitive to movement of humans and not responsive to movement of smaller animals, like dogs and cats.

---

## 1.2 Sensor Classification

Sensor classification schemes range from very simple to the complex. Depending on the classification purpose, different classification criteria may be selected. Here are several practical ways to look at sensors.

1. All sensors may be of two kinds: *passive* and *active*. A passive sensor does not need any additional energy source. It generates an electric signal in response to an external stimulus. That is, the input stimulus energy is converted by the sensor into the output signal. The examples are a thermocouple, a photodiode, and a piezoelectric sensor. Many passive sensors are *direct* sensors as we defined them earlier.

The *active* sensors require external power for their operation, which is called an *excitation signal*. That signal is modified (modulated) by the sensor to produce the output signal. The active sensors sometimes are called *parametric* because their own properties change in response to an external stimulus and these properties can be subsequently converted into electric signals. It can be stated that a sensor's parameter modulates the excitation signal and that modulation carries information of the measured value. For example, a thermistor is a temperature-sensitive resistor. It does not generate any electric signal, but by passing electric current (excitation signal) through it its resistance can be measured by detecting variations in current and/or voltage across the thermistor. These variations (presented in ohms) directly relate to temperature through a known transfer function. Another example of an active sensor is a resistive strain gauge in which electrical resistance relates to strain in the material. To measure the resistance of a sensor, electric current must be applied to it from an external power source.

2. Depending on the selected reference, sensors can be classified into *absolute* and *relative*. An absolute sensor detects a stimulus in reference to an absolute physical scale that is independent on the measurement conditions, whereas a relative sensor produces a signal that relates to some special case. An example of an absolute sensor is a thermistor—a temperature-sensitive resistor. Its electrical resistance directly relates to the absolute temperature scale of Kelvin. Another very popular temperature sensor—a thermocouple—is a relative sensor. It produces an electric voltage that is function of a temperature gradient across the thermocouple wires. Thus, a thermocouple output signal cannot be related to any particular temperature without referencing to a selected baseline. Another example of the absolute and relative sensors is a pressure sensor. An absolute pressure sensor produces signal in reference to vacuum—an absolute zero on a pressure scale. A relative pressure sensor produces signal with respect to a selected baseline that is not zero pressure—for example, to the atmospheric pressure.
3. Another way to look at a sensor is to consider some of its properties that may be of a specific interest [3]. Below are the lists of various sensor characteristics and properties (Tables 1.1, 1.2, 1.3, 1.4, and 1.5).

**Table 1.1** Sensor specifications

Sensitivity	Stimulus range (span)
Stability (short and long term)	Resolution
Accuracy	Selectivity
Speed of response	Environmental conditions
Overload characteristics	Linearity
Hysteresis	Dead band
Operating life	Output format
Cost, size, weight	Other

**Table 1.2** Sensing element material

Inorganic	Organic
Conductor	Insulator
Semiconductor	Liquid gas or plasma
Biological substance	Other

**Table 1.3** Conversion phenomena

Physical	Thermoelectric Photoelectric Photomagnetic Magnetoelectric Electromagnetic Thermoelastic Electroelastic Thermomagnetic Thermo-optic Photoelastic Other	Chemical	Chemical transformation Physical transformation Electrochemical process Spectroscopy Other
		Biological	Biochemical transformation Physical transformation Effect on test organism Spectroscopy Other

**Table 1.4** Field of applications

Agriculture	Automotive
Civil engineering, construction	Domestic, appliances
Distribution, commerce, finance	Environment, meteorology, security
Energy, power	Information, telecommunication
Health, medicine	Marine
Manufacturing	Recreation, toys
Military	Space
Scientific measurement	Other
Transportation (excluding automotive)	

**Table 1.5** Stimuli

Stimulus	Stimulus		
<i>Acoustic</i>	<i>Mechanical</i>	Position (linear, angular)	
Wave amplitude, phase		Acceleration	
Spectrum polarization		Force	
Wave velocity		Stress, pressure	
Other		Strain	
<i>Biological</i>		Mass, density	
Biomass (types, concentration states)		Moment, torque	
Other		Speed of flow, rate of mass transport	
<i>Chemical</i>		Shape, roughness, orientation	
Components (identities, concentration, states)		Stiffness, compliance	
Other	<i>Radiation</i>	Viscosity	
<i>Electric</i>		Crystallinity, structural integrity	
Charge, current		Other	
Potential, voltage		Type	
Electric field (amplitude, phase, polarization, spectrum)		Energy	
Conductivity		Intensity	
Permittivity		Other	
Other		<i>Thermal</i>	Temperature
<i>Magnetic</i>			Flux
Magnetic field (amplitude, phase, polarization, spectrum)			Specific heat
Magnetic flux	Thermal conductivity		
Permeability	Other		
Other			
<i>Optical</i>			
Wave amplitude, phase, polarization, spectrum			
Wave velocity			
Refractive index			
Emissivity, reflectivity, absorption			
Other			

### 1.3 Units of Measurements

In this book, we use base units which have been established in The 14th General Conference on Weights and Measures (1971). The base measurement system is known as SI which stands for French “*Le Système International d’Unités*” (Table 1.6) [4]. All other physical quantities are derivatives of these base units.<sup>3</sup> Some of them are listed in Table A.3.

Often it is not convenient to use base or derivative units directly—in practice quantities may be either too large or too small. For convenience in the engineering work, multiples and submultiples of the units are generally employed. They can be obtained by multiplying a unit by a factor from the Appendix Table A.2. When pronounced, in all cases the first syllable is accented. For example, 1 ampere (A) may be multiplied by factor of  $10^{-3}$  to obtain a smaller unit; 1 milliampere (1 mA) which is one thousandth of an ampere or 1 kilohm (1 k $\Omega$ ) is one thousands of Ohms, where 1  $\Omega$  is multiplied by  $10^3$ .

Sometimes, two other systems of units are used. They are the Gaussian System and the British System, and in the U.S.A. its modification is called the

**Table 1.6** SI basic units

Quantity	Name	Symbol	Defined by... (year established)
Length	meter	m	...the length of the path traveled by light in vacuum in 1/299,792,458 of a second... (1983)
Mass	kilogram	kg	...after a platinum-iridium prototype (1889)
Time	second	s	...the duration of 9,192,631,770 periods of the radiation corresponding to the transition between the two hyperfine levels of the ground state of the cesium-133 atom (1967)
Electric current	ampere	A	force equal to $2 \times 10^{-7}$ N/m of length exerted on two parallel conductors in vacuum when they carry the current (1946)
Thermodynamic temperature	kelvin	K	The fraction 1/273.16 of the thermodynamic temperature of the triple point of water (1967)
Amount of substance	mole	mol	...the amount of substance which contains as many elementary entities as there are atoms in 0.012 kg of carbon 12 (1971)
Luminous intensity	candela	cd	...intensity in the perpendicular direction of a surface of 1/600,000 m <sup>2</sup> of a blackbody at temperature of freezing Pt under pressure of 101,325 N/m <sup>2</sup> (1967)
Plane angle	radian	rad	(supplemental unit)
Solid angle	steradian	sr	(supplemental unit)

<sup>3</sup>The SI is often called the *modernized metric system*.

*US Customary System.* The United States is the only developed country where SI still is not in common use. However, with the increase of globalization, it appears unavoidable that America will convert to SI in the future, though perhaps not in our lifetime. Still, in this book, we will generally use SI; however, for the convenience of the reader, the US customary system units will be used in places where US manufacturers employ them for the sensor specifications.

For conversion to SI from other systems<sup>4</sup> use Table A.4 of the Appendix. To make a conversion, a non-SI value should be multiplied by a number given in the table. For instance, to convert acceleration of 55 ft/s<sup>2</sup> to SI, it must to be multiplied by 0.3048:

$$55 \text{ ft/s}^2 \times 0.3048 = 16.764 \text{ m/s}^2$$

Similarly, to convert electric charge of 1.7 faraday, it must be multiplied by  $9.65 \times 10^{19}$ :

$$1.7 \text{ faraday} \times 9.65 \times 10^{19} = 1.64 \times 10^{20} \text{ C}$$

The reader should consider a correct terminology of the physical and technical terms. For example, in the U.S.A. and several other countries, electric potential difference is called “*voltage*”, while in other countries “*electric tension*” or simply “*tension*” is in common use, such as *spannung* in German, *напряжение* in Russian, *tensione* in Italian, and 电压 in Chinese. In this book, we use terminology that is traditional in the United States of America.

---

## References

1. Thompson, S. (1989). *Control systems: Engineering & design*. Essex, England: Longman Scientific & Technical.
2. Norton, H. N. (1989). *Handbook of transducers*. Englewood Cliffs, NJ: Prentice Hall.
3. White, R. W. (1991). A sensor classification scheme. In *Microsensors* (pp. 3–5). New York: IEEE Press.
4. Thompson, A., & Taylor, B. N. (2008). *Guide for the use of the international system of units (SI)*. NIST Special Publication 811, National Institute of Standards and Technology, Gaithersburg, MD 20899, March 2008.

---

<sup>4</sup> Nomenclature, abbreviations, and spelling in the conversion tables are in accordance with ASTM SI10-02 IEEE/ASTM SI10 *American National Standard for Use of the International System of Units (SI): The Modern Metric System*. A copy is available from ASTM, 100 Barr Harbor Dr., West Conshohocken, PA 19428-2959, USA. [www.astm.org/Standards/SI10.htm](http://www.astm.org/Standards/SI10.htm)

*Everything is controlled by probabilities.  
I would like to know—who controls probabilities?*

Stanisław Jerzy Lec

Since most of stimuli are not electrical, from its input to the output a sensor may perform several signal conversion steps before it produces and outputs an electrical signal. For example, pressure inflicted on a fiber optic pressure sensor, first, results in strain in the fiber, which, in turn, causes deflection in its refractive index, which, in turn, changes the optical transmission and modulates the photon density, and finally, the photon flux is detected by a photodiode and converted into electric current. Yet, in this chapter we will discuss the overall sensor characteristics, regardless of a physical nature or steps that are required to make signal conversions inside the sensor. Here, we will consider a sensor as a “black box” where we are concerned only with the relationship between its output electrical signal and input stimulus, regardless of what is going on inside. Also, we will discuss in detail the key goal of sensing: determination of the unknown input stimulus from the sensor’s electric output. To make that computation we shall find out how the input relates to the output and vice versa?

---

## 2.1 Mathematical Models

An ideal or theoretical input–output (stimulus–response) relationship exists for every sensor. If a sensor is ideally designed and fabricated with ideal materials by ideal workers working in an ideal environment using ideal tools, the output of such a sensor would always represent the *true value* of the stimulus. This ideal input–output relationship may be expressed in the form of a table of values, graph, mathematical formula, or as a solution of a mathematical equation. If the input–output function is

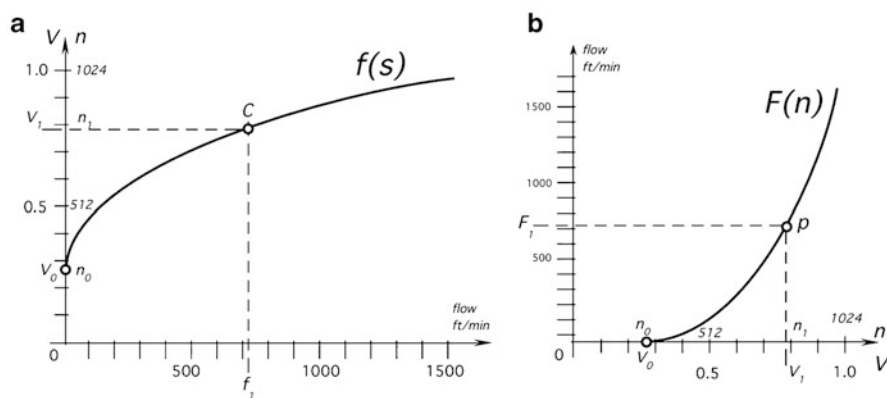


time invariant (does not change with time) it is commonly called a *static transfer function* or simply *transfer function*. This term is used throughout this book.

A static transfer function represents a relation between the input stimulus  $s$  and the electrical signal  $E$  produced by the sensor at its output. This relation can be written as  $E = f(s)$ . Normally, stimulus  $s$  is unknown while the output signal  $E$  is measured and thus becomes known. The value of  $E$  that becomes known during measurement is a number (voltage, current, digital count, etc.) that represents stimulus  $s$ . A job of the designer is to make that representation as close as possible to the true value of stimulus  $s$ .

In reality, any sensor is attached to a measuring system. One of the functions of the system is to “break the code  $E$ ” and infer the unknown value of  $s$  from the measured value of  $E$ . Thus, the measurement system shall employ an inverse transfer function  $s = f^{-1}(E) = F(E)$ , to obtain (compute) value of the stimulus  $s$ . It is usually desirable to determine a transfer function not just of a sensor alone, but rather of a system comprising the sensor and its interface circuit.

Figure 2.1a illustrates the transfer function of a thermo-anemometer—the sensor that measures mass flow of fluid. In general, it can be modeled by a square root function  $f(s)$  of the input airflow rate. The output of the sensor can be in volts or in digital count received from the analog-to-digital converter (ADC), as shown on the y-axis of Fig. 2.1a for a 10-bit ADC converter. After the output count  $n = f(s)$  is measured, it has to be translated back to the flow rate by use of the inverse transfer function. The monotonic square root function  $f(s)$  has parabola  $F(n)$  as its inverse. This parabola is shown in Fig. 2.1b, illustrating the relation between the output counts (or volts) and the input flow rate. Graphically, the inverse function can be obtained by a *mirror reflection* with respect to the bisector of the right angle formed by  $x$  and  $y$ -axes.



**Fig. 2.1** Transfer function (a) and inverse transfer function (b) of thermo-anemometer

### 2.1.1 Concept

Preferably, a physical or chemical law that forms a basis for the sensor's operation should be known. If such a law can be expressed in form of a mathematical formula, often it can be used for calculating the sensor's inverse transfer function by inverting the formula and computing the unknown value of  $s$  from the measured output  $E$ . Consider for example a linear resistive potentiometer that is used for sensing displacement  $d$  (stimulus  $s$  is this example). The Ohm's law can be applied for computing the transfer function as illustrated in Fig. 8.1. In this case, the electric output  $E$  is the measured voltage  $v$  while the inverse transfer function is given as

$$d = F(E) = \frac{D}{v_0}v \quad (2.1)$$

where  $v_0$  is the reference voltage and  $D$  is the maximum displacement (full scale); both being the constants. By using this function we can compute displacement  $d$  from the measured voltage  $v$ .

In practice, readily solvable formulas for many transfer functions, especially for complex sensors, does not exist and one has to resort to various approximations of the direct and inverse transfer functions, which are subjects of the following section.

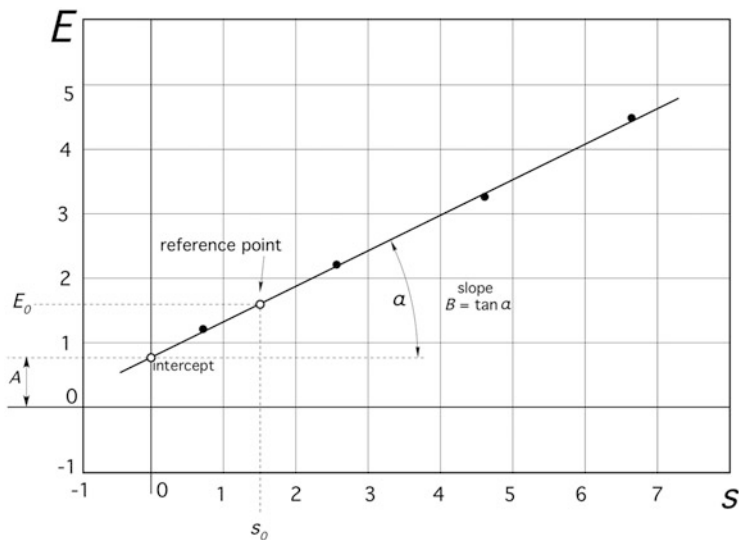
### 2.1.2 Functional Approximations

Approximation is a selection of a suitable mathematical expression that can fit the experimental data as close as possible. The act of approximation can be seen as a *curve fitting* of the experimentally observed values into the approximating function. The approximating function should be simple enough for ease of computation and inversion and other mathematical treatments, for example, for computing a derivative to find the sensor's sensitivity. The selection of such a function requires some mathematical experience. There is no clean-cut method for selecting the most appropriate function to fit experimental data—eyeballing and past experience perhaps is the only practical way to find the best fit. Initially, one should check if one of the basic functions can fit the data and if not, then resort to a more general curve-fitting technique, such as a polynomial approximation, e.g., as described below. Here are some most popular functions used for approximations of transfer functions.

The simplest model of a transfer function is *linear*. It is described by the following equation:

$$E = A + Bs. \quad (2.2)$$

As shown in Fig. 2.2, it is represented by a straight line with the intercept  $A$ , which is the output signal  $E$  at zero input signal  $s = 0$ . The slope of the line is  $B$ .



**Fig. 2.2** Linear transfer function. *Black dots* indicate experimental data

Sometimes it is called *sensitivity* since the larger this coefficient the greater the stimulus influence. The slope  $B$  is a tangent of the angle  $\alpha$ . The output  $E$  may be the amplitude of voltage or current, phase, frequency, pulse-width modulation (PWM), or a digital code, depending on the sensor properties, signal conditioning, and interface circuit.

Note that Eq. (2.2) assumes that the transfer function passes, at least theoretically, through zero value of the input stimulus  $s$ . In many practical cases it is just difficult or impossible to test a sensor at a zero input. For example, a temperature sensor used on a Kelvin scale cannot be tested at the absolute zero ( $-273.15\text{ }^{\circ}\text{C}$ ). Thus, in many linear or quasilinear sensors it may be desirable to reference the sensor not to the zero input but rather to some more practical input reference value  $s_0$ . If the sensor response is  $E_0$  for some known input stimulus  $s_0$ , Eq. (2.2) can be rewritten in a more practical form:

$$E = E_0 + B(s - s_0) \quad (2.3)$$

The reference point has coordinates  $s_0$  and  $E_0$ . For a particular case where  $s_0 = 0$ , Eq. (2.3) becomes Eq. (2.2) and  $E_0 = A$ . The inverse linear transfer function for computing the input stimulus from the output  $E$  is

$$s = \frac{E - E_0}{B} + s_0 \quad (2.4)$$

Note that three constants shall be known for computing the stimulus  $s$ : sensitivity  $B$  and coordinates  $s_0$  and  $E_0$  of the reference point.

Very few sensors are truly linear. In the real world, at least a small nonlinearity is almost always present, especially for a broad input range of the stimuli. Thus, Eqs. (2.2) and (2.3) represent just a linear approximation of a nonlinear sensor's response, where a nonlinearity can be ignored for the practical purposes. In many cases, when nonlinearity cannot be ignored, the transfer function still may be approximated by a group of linear functions as we shall discuss below in greater detail (Sect. 2.1.6).

A nonlinear transfer function can be approximated by a nonlinear mathematical function. Here are few useful functions.

The *logarithmic* approximation function (Fig. 2.3) and the corresponding inverse function (which is exponential) are respectively:

$$E = A + B \ln s, \tag{2.5}$$

$$s = e^{\frac{E-A}{B}}, \tag{2.6}$$

where  $A$  and  $B$  are the fixed parameters.

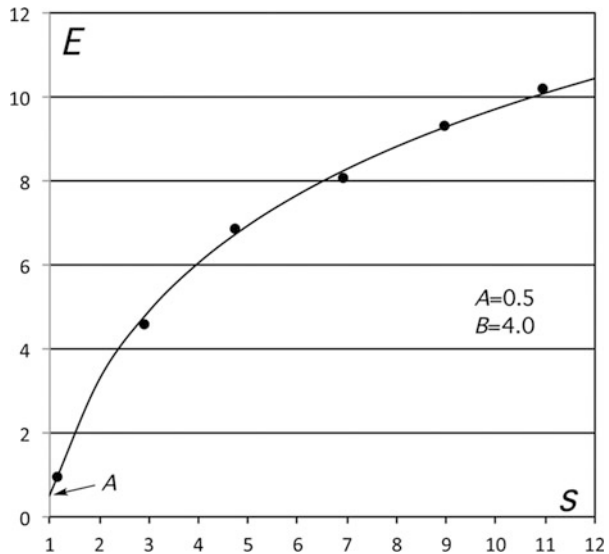
The *exponential* function (Fig. 2.4) and its inverse (which is logarithmic) are given by:

$$E = Ae^{ks}, \tag{2.7}$$

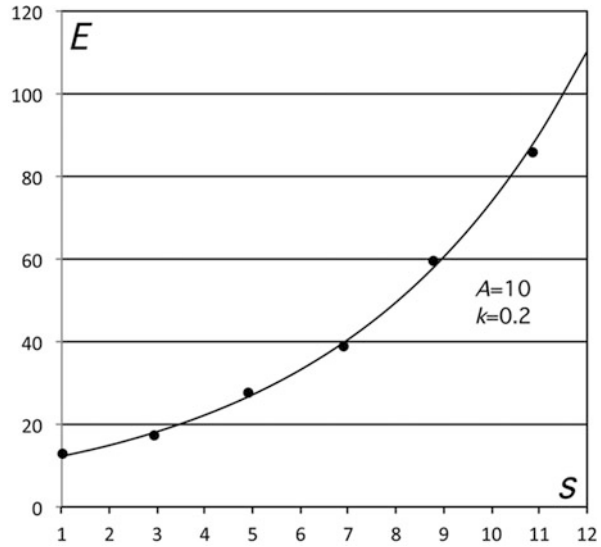
$$s = \frac{1}{k} \ln \frac{E}{A}, \tag{2.8}$$

where  $A$  and  $k$  are the fixed parameters.

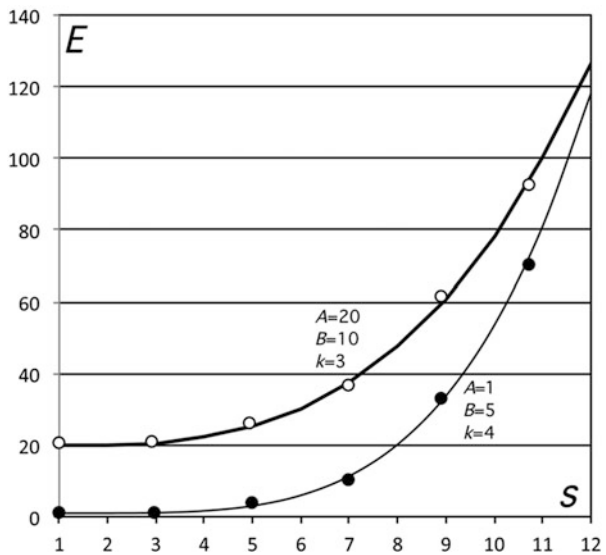
**Fig. 2.3** Approximation by logarithmic function. Dots indicate experimental data



**Fig. 2.4** Approximation by an exponential function. Dots indicate experimental data



**Fig. 2.5** Power functions



The *power* function (Fig. 2.5) and its inverse can be expressed as

$$E = A + Bs^k, \tag{2.9}$$

$$s = \sqrt[k]{\frac{E - A}{B}}, \tag{2.10}$$

where  $A$  and  $B$  are fixed parameters and  $k$  is the power factor.

All the above three nonlinear approximations possess a small number of parameters that shall be determined during calibration. A small number of parameters makes them rather convenient, provided that they can fit response of a particular sensor. It is always useful to have as small a number of parameters as possible, not the least for the sake of lowering cost of the sensor calibration. The fewer parameters, the smaller the number of the measurements to be made during calibration.

### 2.1.3 Linear Regression

If measurements of the input stimuli during calibration cannot be made consistently with high accuracy and large random errors are expected, the minimal number of measurements will not yield a sufficient accuracy. To cope with random errors in the calibration process, a method of *least squares* could be employed to find the slope and intercept. Since this method is described in many textbooks and manuals, only the final expressions for the unknown parameters of a linear regression are given here for reminder. The reader is referred to any textbook on statistical error analysis. The procedure is as follows:

1. Measure multiple ( $k$ ) output values  $E$  at the input values  $s$  over a substantially broad range, preferably over the entire sensor span.
2. Use the following formulas for a linear regression to determine intercept  $A$  and slope  $B$  of the best-fitting straight line of Eq. (2.2):

$$A = \frac{\Sigma E \Sigma s^2 - \Sigma s \Sigma s E}{k \Sigma s^2 - (\Sigma s)^2}, \quad B = \frac{k \Sigma s E - \Sigma s \Sigma E}{k \Sigma s^2 - (\Sigma s)^2}, \quad (2.11)$$

where  $\Sigma$  is the summation over all  $k$  measurements. When the constants  $A$  and  $B$  are found, Eq. (2.2) can be used as a linear approximation of the experimental transfer function.

### 2.1.4 Polynomial Approximations

A sensor may have such a transfer function that none of the above basic functional approximations would fit sufficiently well. A sensor designer with a reasonably good mathematical background and physical intuition may utilize some other suitable functional approximations, but if none is found, several old and reliable techniques may come in handy. One is a polynomial approximation, that is, a power series.

Any continuous function, regardless of its shape, can be approximated by a power series. For example, the exponential function of Eq. (2.7) can be

approximately calculated from a third-order polynomial by dropping all the higher terms of its series expansion<sup>1</sup>:

$$E = Ae^{ks} \approx A \left( 1 + ks + \frac{k^2}{2!} s^2 + \frac{k^3}{3!} s^3 \right) \quad (2.12)$$

In many cases it is sufficient to see if the sensor's response can be approximated by the second or third degree polynomials to fits well enough into the experimental data. These approximation functions can be expressed respectively as

$$E = a_2 s^2 + a_1 s + a_0 \quad (2.13)$$

$$E = b_3 s^3 + b_2 s^2 + b_1 s + b_0 \quad (2.14)$$

The factors  $a$  and  $b$  are the constants that allow shaping the curves (2.13) and (2.14) into a great variety of the practical transfer functions. It should be appreciated that the quadratic (second order) polynomial of Eq. (2.13) is a special case of the third degree polynomial when  $b_3 = 0$  in Eq. (2.14). Similarly, the first-order (linear) polynomial of Eq. (2.2) is a special case of the quadratic polynomial of Eq. (2.13) with  $a_2 = 0$ .

Obviously, the same technique can be applied to the inverse transfer function as well. Thus, the inverse transfer function can be approximated by a second or third degree polynomial:

$$s = A_2 E^2 + A_1 E + A_0 \quad (2.15)$$

$$s = B_3 E^3 + B_2 E^2 + B_1 E + B_0 \quad (2.16)$$

The coefficients  $A$  and  $B$  can be converted into coefficients  $a$  and  $b$ , but the analytical conversion is rather cumbersome and rarely used. Instead, depending in the need, usually either a direct or inversed transfer function is approximated from the experimental data points, but not both.

In some cases, especially when more accuracy is required, the higher order polynomials should be considered because the higher the order of a polynomial the better the fit. Still, even a second-order polynomial often may yield a fit of sufficient accuracy when applied to a relatively narrow range of the input stimuli and the transfer function is monotonic (no ups and downs).

---

<sup>1</sup>This third-order polynomial approximation yields good approximation only for  $ks \ll 1$ . In general, the error of a power series approximation is subject of a rather nontrivial mathematical analysis. Luckily, in most practical situations that analysis is rarely needed.

### 2.1.5 Sensitivity

Recall that the coefficient  $B$  in Eqs. (2.2) and (2.3) is called *sensitivity*. For a nonlinear transfer function, sensitivity is not a fixed number, as would be the case in a linear transfer function. A nonlinear transfer function exhibits different sensitivities at different points in intervals of stimuli. In the case of nonlinear transfer functions, sensitivity is defined as a first derivative of the transfer function at the particular stimulus  $s_i$ :

$$b_i(s_i) = \frac{dE(s_i)}{ds} = \frac{\Delta E_i}{\Delta s_i}, \quad (2.17)$$

where,  $\Delta s_i$  is a small increment of the input stimulus and  $\Delta E_i$  is the corresponding change in the sensor output  $E$ .

### 2.1.6 Linear Piecewise Approximation

A linear piecewise approximation is a powerful method to employ in a computerized data acquisition system. The idea behind it is to break up a nonlinear transfer function of any shape into sections and consider each such section being linear as described by Eq. (2.2) or (2.3). Curved segments between the sample points (knots) demarcating the sections are replaced with straight-line segments, thus greatly simplifying behavior of the function between the knots. In other words, the knots are graphically connected by straight lines. This can also be seen as a polygonal approximation of the original nonlinear function. Figure 2.6 illustrates

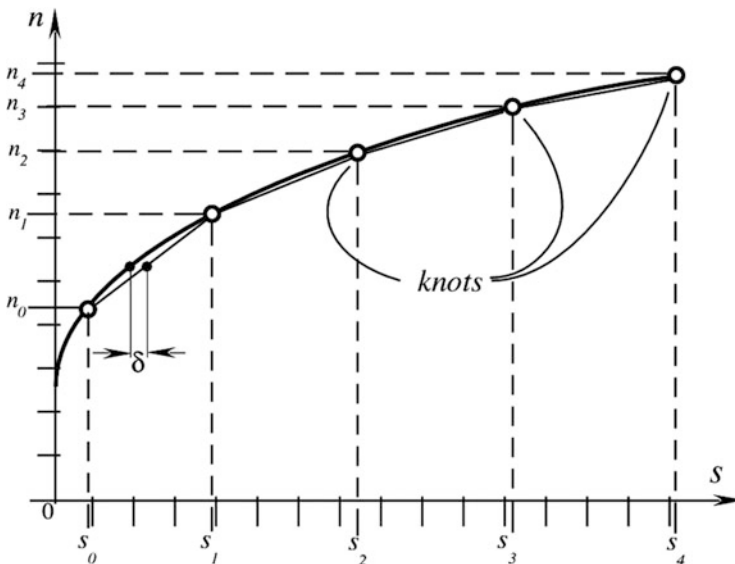


Fig. 2.6 Linear piecewise approximation



the linear piecewise approximation of a nonlinear function with the knots at input values  $s_0, s_1, s_2, s_3, s_4$ , and the corresponding output values  $n_0, n_1, n_2, n_3, n_4$  (in this example, the digital counts from an ADC).

It makes sense to select knots only for the input range of interest (a span—see definition in the next chapter); thus in Fig. 2.6 a section of the curve from 0 to  $s_0$  is omitted as being outside of the practically required span limits.

An error of a piecewise approximation can be characterized by a maximum deviation  $\delta$  of the approximation line from the real curve. Different definitions exist for this maximum deviation (mean square, absolute max, average, etc.); but whatever is the adopted metric, the larger  $\delta$  calls for a greater number of samples, that is a larger number of sections with the idea of making this maximum deviation acceptably small. In other words, the larger the number of the knots the smaller the error. The knots do not need to be equally spaced. They should be closer to each other where nonlinearity is high and farther apart where nonlinearity is small.

While using this method, the signal processor should store the knot coordinates in a memory. For computing the input stimulus  $s$  a linear interpolation should be performed (see Sect. 2.4.2).

### 2.1.7 Spline Interpolation

Approximations by higher order polynomials (third order and higher) have some disadvantages; the selected points at one side of the curve make strong influence on the remote parts of the curve. This deficiency is resolved by the *spline* method of approximation. In a similar way to a linear piecewise interpolation, the spline method is using different third-order polynomial interpolations between the selected experimental points called knots [1]. It is a curve between two neighboring knots and then all curves are “stitched” or “glued” together to obtain a smooth combined curve fitting. Not necessarily it should be a third-order curve—it can be as simple as the first-order (linear) interpolation. A linear spline interpolation (first order) is the simplest form and is equivalent to a linear piecewise approximation as described above.

The spline interpolation can utilize polynomials of different degrees, yet the most popular being cubic (third order) polynomials. Curvature of a line at each point is defined by the second derivative. This derivative should be computed at each knot. If the second derivatives are zero, the cubic spline is called “relaxed” and it is the choice for many practical approximations. Spline interpolation is the efficient technique when it comes to an interpolation that preserves smoothness of the transfer function. However, simplicity of the implementation and the computational costs of a spline interpolation should be taken into account particularly in a tightly controlled microprocessor environment.

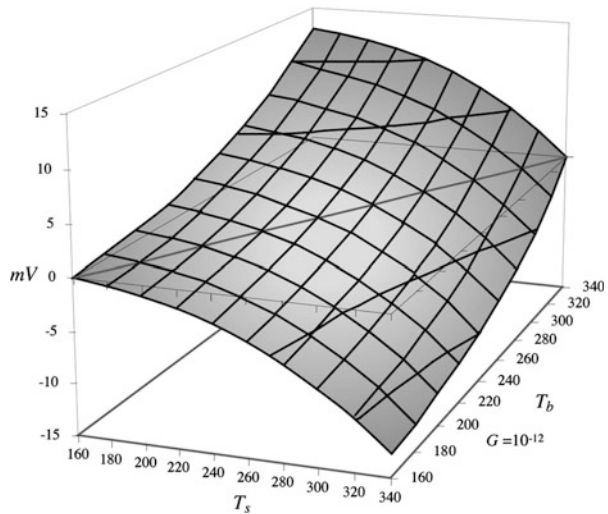
### 2.1.8 Multidimensional Transfer Functions

A sensor transfer function may depend on more than one input variable. That is, the sensor's output may be a function of several stimuli. One example is a humidity sensor whose output depends on two input variables—relative humidity and temperature. Another example is the transfer function of a thermal radiation (infrared) sensor. This function<sup>2</sup> has two arguments—two temperatures:  $T_b$ , the absolute temperature of an object of measurement and  $T_s$ , the absolute temperature of the sensing element. Thus, the sensor's output voltage  $V$  is proportional to a difference of the fourth-order parabolas:

$$V = G(T_b^4 - T_s^4), \quad (2.18)$$

where  $G$  is a constant. Clearly, the relationship between the object's temperature  $T_b$  and the output voltage  $V$  is not only nonlinear but also in a nonlinear way depends on the sensing element surface temperature  $T_s$ , which should be measured by a separate contact temperature sensor. The graphical representation of a two-dimensional transfer function of Eq. (2.18) is shown in Fig. 2.7.

**Fig. 2.7** Two-dimensional transfer function of thermal radiation sensor. Temperatures are in K



<sup>2</sup>This function is known as the Stefan-Boltzmann law (Sect. 4.12.3).

## 2.2 Calibration

If tolerances of a sensor and interface circuit (signal conditioning) are broader than the required overall accuracy, a calibration of the sensor or, preferably, a combination of a sensor and its interface circuit is required for minimizing errors. In other words, a calibration is required whenever a higher accuracy is required from a less accurate sensor. For example, if one needs to measure temperature with accuracy, say  $0.1\text{ }^{\circ}\text{C}$ , while the available sensor is rated as having accuracy of  $1\text{ }^{\circ}\text{C}$ , it does not mean that the sensor cannot be used. Rather this particular sensor needs calibration. That is, its unique transfer function should be determined. This process is called *calibration*.

A calibration requires application of several precisely known stimuli and reading the corresponding sensor responses. These are called the *calibration points* whose input–output values are the point coordinates. In some lucky instances only one pair is required, while typically 2–5 calibration points are needed to characterize a transfer function with a higher accuracy. After the unique transfer function is established, any point in between the calibration points can be determined.

To produce the calibration points, a standard reference source of the input stimuli is required. The reference source should be well maintained and periodically checked against other established references, preferably traceable to a national standard, for example a reference maintained by NIST<sup>3</sup> in the U.S.A. It should be clearly understood that the calibration accuracy is directly linked to accuracy of a reference sensor that is part of the calibration equipment. A value of uncertainty of the reference sensor should be included in the statement of the overall uncertainty, as explained in Sect. 3.21.

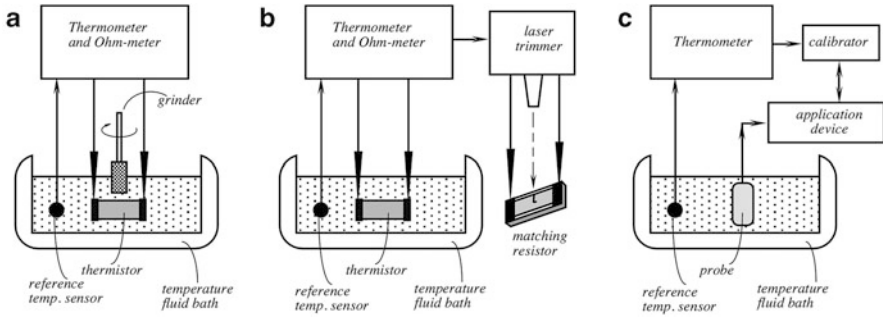
Before calibration, either a mathematical model of the transfer function has to be known or a good approximation of the sensor’s response over the entire span shall be found. In a great majority of cases, such functions are smooth and monotonic. Very rarely they contain singularities and if they do, such singularities are the useful phenomena that are employed for sensing (an ionizing particle detector is an example).

Calibration of a sensor can be done in several possible ways, some of which are the following:

1. Modifying the transfer function or its approximation to fit the experimental data. This involves computation of the coefficients (parameters) for the selected transfer function equation. After the parameters are found, the transfer function becomes unique for that particular sensor. The function can be used for computing the input stimuli from any sensor response within the range. Every calibrated sensor will have its own set of the unique parameters. The sensor is not modified.
2. Adjustment of the data acquisition system to trim (modify) its output by making the outputs signal to fit into a normalized or “ideal” transfer function.

---

<sup>3</sup> NIST—National Institute of Standards and Technology: [www.nist.gov](http://www.nist.gov)



**Fig. 2.8** Calibration of thermistor: grinding (a), trimming reference resistor (b), and determining calibrating points for characterizing transfer function (c)

An example is a scaling and shifting the acquired data (modifying the system gain and offset). The sensor is not modified.

3. Modification (trimming) the sensor's properties to fit the predetermined transfer function, thus the sensor itself is modified.
4. Creating the sensor-specific reference device with the matching properties at particular calibrating points. This unique reference is used by the data acquisition system to compensate for the sensor's inaccuracy. The sensor is not modified.

As an example, Fig. 2.8 illustrates three methods of calibrating a thermistor (temperature sensitive resistor). Figure 2.8a shows a thermistor that is immersed into a stirred liquid bath with a precisely controlled and monitored temperature. The liquid temperature is continuously measured by a precision reference thermometer. To prevent shorting the thermistor terminals, the liquid should be electrically nonconductive, such as mineral oil or Fluorinert™. The resistance of the thermistor is measured by a precision Ohmmeter. A miniature grinder mechanically removes some material from the thermistor body to modify its dimensions. Reduction in dimensions leads to increase in the thermistor electrical resistance at the selected bath temperature. When the thermistor's resistance matches a predetermined value of the “ideal” resistance, the grinding stops and the calibration is finished. Now the thermistor response is close to the “ideal” transfer function, at least at that temperature. Naturally, a single-point calibration assumes that the transfer function can be fully characterized by that point.

Another way of calibrating a thermistor is shown in Fig. 2.8b where the thermistor is not modified but just measured at a selected reference temperature. The measurement provides a number that is used for selecting a conventional (temperature stable) matching resistor as a unique reference. That resistor is for use in the interface scaling circuit. The precise value of such a reference resistor is achieved either by a laser trimming or selection from a stock. That individually matched pair thermistor–resistor is used in the measurement circuit, for example, in

a Wheatstone bridge. Since it is a matching pair, the response of the bridge will scale to correspond to an “ideal” transfer function of a thermistor.

In the above examples, methods (a) and (b) are useful for calibration at one temperature point only, assuming that other parameters of the transfer function do not need calibration. If such is not the case, several calibrating points at different temperatures and resistances should be generated as shown in Fig. 2.8c. Here, the liquid bath is sequentially set at two, three, or four different temperatures and the thermistor under calibration produces the corresponding responses, that are used by the calibrating device to generate the appropriate parameters for the inverse transfer function that will be stored in the application device (e.g., a thermometer).

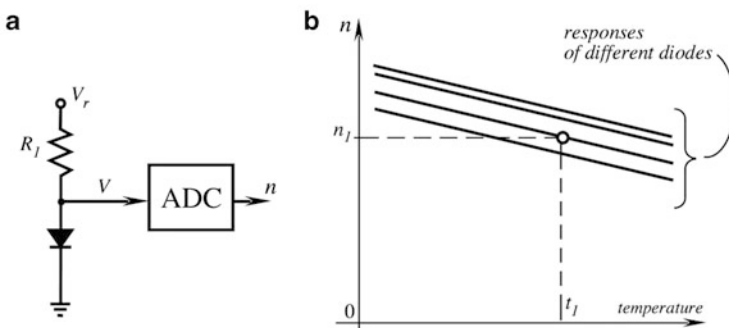
### 2.3 Computation of Parameters

If a transfer function is linear, as in Eq. (2.2), then calibration should determine constants  $A$  and  $B$ . If it is exponential as in Eq. (2.7), the constants  $A$  and  $k$  should be determined, and so on.

To calculate parameters (constants) of a linear transfer function one needs two data points defined by two calibrating input–output pairs. Consider a simple linear transfer function of Eq. (2.3). Since two points are required to define a straight line, a two-point calibration shall be performed. For example, if one uses a forward-biased semiconductor p–n junction (Fig. 2.9a) as a temperature sensor (see Sect. 17.6), its transfer function is linear (Fig. 2.9b) with temperature  $t$  being the input stimulus and the ADC count  $n$  from the interface circuit is the output:

$$n = n_1 + B(t - t_1). \quad (2.19)$$

Note that  $t_1$  and  $n_1$  are the coordinates of the first reference calibrating point. To fully define the line, the sensor shall be subjected to two calibrating temperatures ( $t_1$  and  $t_2$ ) for which two corresponding output counts ( $n_1$  and  $n_2$ ) will be registered. At the first calibrating temperature  $t_1$ , the output count is  $n_1$ .



**Fig. 2.9** A p–n junction temperature sensor (a) and transfer functions for several sensors (b). Each diode will produce different  $n_1$  at the same temperature  $t_1$

After subjecting the sensor to the second calibrating temperature  $t_2$ , we receive the digital counts for the second calibrating point. The count is

$$n_2 = n_1 + B(t_2 - t_1) \quad (2.20)$$

from which the sensitivity (slope) is computed as

$$B = \frac{n_2 - n_1}{t_2 - t_1} \quad (2.21)$$

and Eq. (2.19) becomes a linear transfer function with now three known parameters:  $B$ ,  $n_1$ , and  $t_1$ . The sensitivity (slope)  $B$  is in count/degree. In example of Fig. 2.9, the slope  $B$  is negative since a p–n junction has a negative temperature coefficient (NTC). Note that the parameters found from calibration are unique for the particular sensor and must be stored in the measurement system to which that particular sensor is connected. For another similar sensor, these parameters will be different (perhaps except  $t_1$ , if all sensors are calibrated at exactly the same temperature). After calibration is done, any temperature within the operating range can be computed from the ADC output count  $n$  by use of the inverse transfer function

$$t = t_1 + \frac{n - n_1}{B} \quad (2.22)$$

In some fortunate cases, parameter  $B$  may be already known with a sufficient accuracy so that no computation of  $B$  is needed. In a p–n junction of Fig. 2.9a, the slope  $B$  is usually very consistent for a given lot and type of the semiconductor wafer and thus can be considered as a known parameter for all diodes in the production lot. However, all diodes may have different offsets, so a single-point calibration is still needed to find out  $n_1$  for each individual sensor at the calibrating temperature  $t_1$ .

For nonlinear transfer functions, calibration at one data point may be sufficient only in some rare cases when other parameters are already known, but often two and more input–output calibrating pairs would be required. When a second or a third degree polynomial transfer functions are employed, respectively three and four calibrating pairs are required. For a third-order polynomial

$$E = b_3s^3 + b_2s^2 + b_1s + b_0 \quad (2.23)$$

to find four parameters  $b_0$  to  $b_3$ , four experimental calibrating input–output pairs (calibrating points) are required:  $s_1$  and  $E_1$ ,  $s_2$  and  $E_2$ ,  $s_3$  and  $E_3$ , and  $s_4$  and  $E_4$ .

Plugging these experimental pairs into Eq. (2.23) we get a system of four equations

$$\begin{aligned} E_1 &= b_3s_1^3 + b_2s_1^2 + b_1s_1 + b_0 \\ E_2 &= b_3s_2^3 + b_2s_2^2 + b_1s_2 + b_0 \\ E_3 &= b_3s_3^3 + b_2s_3^2 + b_1s_3 + b_0 \\ E_4 &= b_3s_4^3 + b_2s_4^2 + b_1s_4 + b_0 \end{aligned} \quad (2.24)$$

To solve this system for the parameters, first we compute the determinants of the system:

$$\begin{aligned}\Delta &= \left( \frac{s_1^2 - s_2^2}{s_1 - s_2} - \frac{s_1^2 - s_4^2}{s_1 - s_4} \right) \left( \frac{s_1^3 - s_2^3}{s_1 - s_2} - \frac{s_1^3 - s_3^3}{s_1 - s_3} \right) - \left( \frac{s_1^2 - s_2^2}{s_1 - s_2} - \frac{s_1^2 - s_3^2}{s_1 - s_3} \right) \left( \frac{s_1^3 - s_2^3}{s_1 - s_2} - \frac{s_1^3 - s_4^3}{s_1 - s_4} \right) \\ \Delta_a &= \left( \frac{s_1^2 - s_2^2}{s_1 - s_2} - \frac{s_1^2 - s_4^2}{s_1 - s_4} \right) \left( \frac{E_1 - E_2}{s_1 - s_2} - \frac{E_1 - E_3}{s_1 - s_3} \right) - \left( \frac{s_1^2 - s_2^2}{s_1 - s_2} - \frac{s_1^2 - s_3^2}{s_1 - s_3} \right) \left( \frac{E_1 - E_2}{s_1 - s_2} - \frac{E_1 - E_4}{s_1 - s_4} \right) \\ \Delta_b &= \left( \frac{s_1^3 - s_2^3}{s_1 - s_2} - \frac{s_1^3 - s_3^3}{s_1 - s_3} \right) \left( \frac{E_1 - E_2}{s_1 - s_2} - \frac{E_1 - E_4}{s_1 - s_4} \right) - \left( \frac{s_1^3 - s_2^3}{s_1 - s_2} - \frac{s_1^3 - s_4^3}{s_1 - s_4} \right) \left( \frac{E_1 - E_2}{s_1 - s_2} - \frac{E_1 - E_3}{s_1 - s_3} \right),\end{aligned}\tag{2.25}$$

from which the polynomial coefficients are calculated in the following fashion:

$$\begin{aligned}b_3 &= \frac{\Delta_a}{\Delta}; \\ b_2 &= \frac{\Delta_b}{\Delta}; \\ b_1 &= \frac{1}{s_1 - s_4} [E_1 - E_4 - b_3(s_1^3 - s_4^3) - b_2(s_1^2 - s_4^2)]; \\ b_0 &= E_1 - b_3s_1^3 - b_2s_1^2 - b_1s_1\end{aligned}\tag{2.26}$$

If the determinant  $\Delta$  is small, some considerable inaccuracy will result. Thus, the calibrating points should be spaced within the operating range as far as possible from one another.

When dealing with a large inertia or temperatures, calibration may be a slow process. To reduce the manufacturing cost, it is important to save time and thus to minimize the number of calibration points. Therefore, the most economical transfer function or the approximation should be selected. Economical means having the smallest number of the unknown parameters. For example, if an acceptable accuracy can be achieved by a second-order polynomial, a third order should not be used.

---

## 2.4 Computation of a Stimulus

A general goal of sensing is to determine the value of the input stimulus  $s$  from the measured output signal  $E$ . This can be done by two methods.

1. From an *inverted* transfer function  $s = F(E)$ , that may be either an analytical or approximation function, or
2. From a *direct* transfer function  $E = f(s)$  by use of an iterative computation.

### 2.4.1 Use of Analytical Equation

This is a straight approach when an analytical equation for the transfer equation is known. Simply measure the output signal  $E$ , plug it into the formula, and compute the sought input stimulus  $s$ . For example, to compute a displacement from resistance of a potentiometric sensor, use Eq. (2.4). For other functional models, use respective Eqs. (2.4), (2.6), (2.8), and (2.10).

### 2.4.2 Use of Linear Piecewise Approximation

Refer to Sect. 2.1.6 for description of the approximation. For computing stimulus  $s$ , the very first step is to find out where it is located, in other words, between which knots lays the output signal  $E$ ? The next step is to use the method of *linear interpolation* for computing the input stimulus  $s$ .

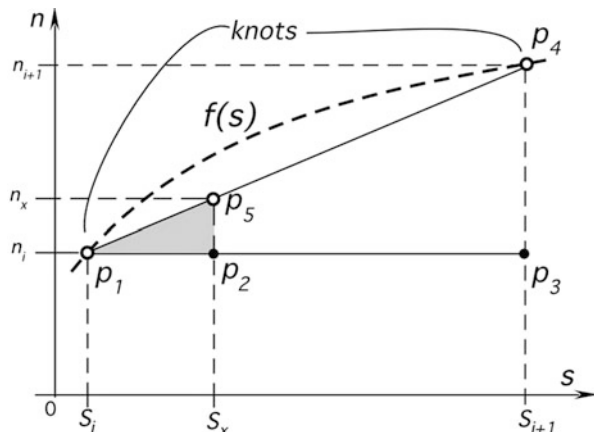
Here how it works.

First, determine where the output is located, that is, in between which knots? For example, we found that the output is somewhere in between the knots  $p_1$  and  $p_4$  as illustrated in Fig. 2.10. The sensor's output  $E = n$  is in counts from the ADC. A large triangle is formed with the corners at the points  $p_1, p_3$ , and  $p_4$ . The unknown stimulus  $s_x$  corresponds to the measured ADC output counts  $n_x$ . This is indicated by the point  $p_5$  on the approximation straight line, thus forming a smaller triangle between the points  $p_1, p_2$ , and  $p_5$ . Both triangles are similar, which allows us to derive a linear equation for computing the unknown stimulus  $s_x$  from the value of  $n_x$ :

$$s_x = s_i + \frac{n_x - n_i}{n_{i+1} - n_i} (s_{i+1} - s_i) \quad (2.27)$$

This equation is easy to program and compute by an inexpensive microprocessor, which keeps in its memory a look-up table containing the knot coordinates (Table 2.1).

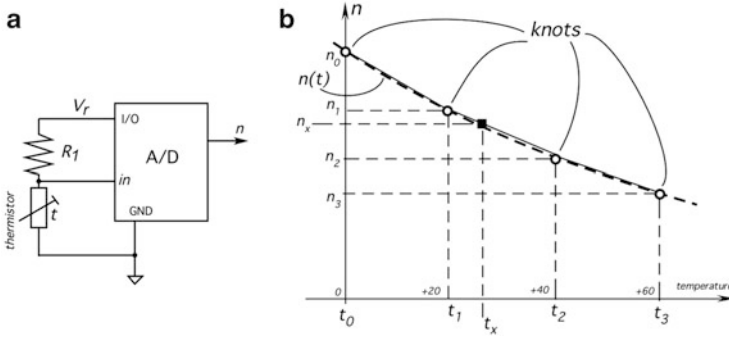
**Fig. 2.10** Computation of stimulus from linear piecewise approximation





**Table 2.1** Look-up table of knots for computing the input from the measured output

Knot	0	1	2	...	$i$	...	$k$
Output	$n_0$	$n_1$	$n_2$	...	$n_i$	...	$n_k$
Input	$s_0$	$s_1$	$s_2$	...	$s_i$	...	$s_k$



**Fig. 2.11** Thermistor circuit (a) and its linear piecewise approximation (b) with four knots

For illustration, let us compare uses of a full functional model of the transfer function and a linear piecewise approximation. Obviously, the full functional model gives the most accurate computation. Figure 2.11a shows a thermistor temperature sensor with a pull-up resistor  $R_1$  connected to a 12-bit analog-to-digital (ADC) converter (a full scale  $N_0 = 4095$  counts corresponding to the reference voltage  $V_r$ ). The thermistor is used to measure temperature in the total input span from 0 to  $+60^\circ\text{C}$ .

The output count of the thermistor measurements circuit can be modeled by a nonlinear function of temperature:

$$n_x = N_0 \frac{R_r e^{\beta(T_x^{-1} - T_r^{-1})}}{R_1 + R_r e^{\beta(T_x^{-1} - T_r^{-1})}}, \tag{2.28}$$

where  $T_x$  is the measured temperature,  $T_r$  is the reference temperature,  $R_r$  is resistance of the thermistor at reference temperature  $T_r$ , and  $\beta$  is the characteristic temperature. All temperatures and  $\beta$  are in degrees kelvin.

After manipulating Eq. (2.28), we arrive at the inverse transfer function that enables us to compute the input temperature in kelvin:

$$T_x = \left[ \frac{1}{T_r} + \frac{1}{\beta} \ln \left( \frac{n_x}{N_0 - n_x} \frac{R_1}{R_r} \right) \right]^{-1} \tag{2.29}$$

The above Eqs. (2.28) and (2.29) contain two unknown parameters:  $R_r$  and  $\beta$ . Thus, before we proceed further, the entire circuit, including the ADC, shall be

calibrated at temperature  $T_r$  and also at some other temperature  $T_c$ . In the circuit, we use a pull-up resistor  $R_1 = 10.0 \text{ k}\Omega$ . For calibration, we select two calibrating temperatures in the operating range as  $T_r = 293.15 \text{ K}$  and  $T_c = 313.15 \text{ K}$ , which correspond to  $20 \text{ }^\circ\text{C}$  and  $40 \text{ }^\circ\text{C}$ , respectively.

During calibration, the thermistor sequentially is immersed into a fluid bath at these two temperatures and the ADC output counts are registered respectively as

$$\begin{aligned} n_r &= 1863 \text{ at } T_r = 293.15 \text{ K} \\ n_c &= 1078 \text{ at } T_c = 313.15 \text{ K} \end{aligned}$$

By substituting these pairs into Eq. (2.28) and solving the system of two equations, we arrive at parameter values  $R_r = 8.350 \text{ k}\Omega$  and  $\beta = 3895 \text{ K}$ . This completes the calibration.

Now, since all parameters in Eqs. (2.28) and (2.29) are fully characterized, Eq. (2.29) can be used for computing temperature from any ADC count in the operating range. We assume this is the most accurate way of computing true temperature. Now, let us see what involves using the linear piecewise approximation.

Let us break up the transfer function of Eq. (2.28) just into three sections (Fig. 2.11b) with two end knots at  $0$  and  $60 \text{ }^\circ\text{C}$  (the span limits) and two equally spaced central knots at  $20$  and  $40 \text{ }^\circ\text{C}$ . We will use linear approximations between the neighboring knot temperatures<sup>4</sup>  $t_0 = 0 \text{ }^\circ\text{C}$  and  $t_1 = t_r = 20 \text{ }^\circ\text{C}$ ,  $t_2 = 40 \text{ }^\circ\text{C}$ , and  $t_3 = 60 \text{ }^\circ\text{C}$ .

From calibration, we find the ADC outputs at these knot temperatures:

$$\begin{aligned} n_0 &= 2819 \text{ for } t_0 = 0 \text{ }^\circ\text{C} \\ n_1 &= n_r = 1863 \text{ for } t_1 = t_r = 20 \text{ }^\circ\text{C} \\ n_2 &= 1078 \text{ for } t_2 = 40 \text{ }^\circ\text{C} \\ n_3 &= 593 \text{ for } t_3 = 60 \text{ }^\circ\text{C} \end{aligned}$$

The count–temperature coordinate pairs are plugged into a look-up Table 2.2.

As an example, to compare temperatures computed from the functional model of Eq. (2.29) and Table 2.2, consider that at some unknown temperature the ADC outputs count  $n_x = 1505$ . We need to find that temperature. From Table 2.2 we determine that this measured count  $n_x$  is situated somewhere between the knots 1 and 2. To find temperature  $t_s$ , the measured counts and the knot values are plugged into Eq. (2.27) to arrive at

**Table 2.2** Look-up table for computation of temperature

Knot	0	1	2	3
Counts	2819	1863	1078	593
Temp ( $^\circ\text{C}$ )	0	20	40	60

<sup>4</sup>Note that the reference temperature in Celsius  $t_r = t_1 = T_r - 273.15$ , where  $T_r$  is in kelvin.

$$t_x = t_1 + \frac{n_x - n_1}{n_2 - n_1} (t_2 - t_1) = 20 + \frac{1505 - 1863}{1078 - 1863} (40 - 20) = 29.12^\circ\text{C} \quad (2.30)$$

Now, to compare two methods of calculation, use a real transfer function Eq. (2.29) by plugging into it the same  $n_x = 1505$ . After calculation, we get the stimulus temperature  $t_x = 28.22^\circ\text{C}$ . This number is lower than the one computed from Eq. (2.30). Hence, the linear piecewise approximation with only two central knots overestimates temperature by  $0.90^\circ\text{C}$  which may be a too much of an error. For a more demanding application, to reduce errors use more than two central knots.

### 2.4.3 Iterative Computation of Stimulus (Newton Method)

If the *inverse* transfer function is not known, the iterative method allows using a *direct* transfer function to compute the input stimulus. A very powerful method of iterations is the Newton or secant method<sup>5</sup> [1–3]. It is based on first *guessing* the initial reasonable value of stimulus  $s = s_0$  and then applying the Newton algorithm to compute a series of new values of  $s$  converging to the sought stimulus value. Thus, the algorithm involves several steps of computation, where each new step brings us closer and closer to the sought stimulus value. When a difference between two consecutively computed values of  $s$  becomes sufficiently small (less than an acceptable error), the algorithm stops and the last computed value of  $s$  is considered a solution of the original equation and thus the value of the unknown stimulus is found. Newton's method converges remarkably quickly, especially if the initial guess is reasonably close to the actual value of  $s$ .

The output signal is represented through the sensor's transfer function is  $f(s)$  as  $E = f(s)$ . It can be rewritten as  $E - f(s) = 0$ . The Newton method prescribes computing the following *sequence* of the stimuli values for the measured output value  $E$ :

$$s_{i+1} = s_i - \frac{f(s_i) - E}{f'(s_i)} \quad (2.31)$$

This sequence after just several steps converges to the sought input  $s$ . Here,  $s_{i+1}$  is the computed stimulus value at the iteration  $i + 1$ , wherein  $s_i$  is the computed value at a prior iteration  $i$  and  $f'(s_i)$  is the first derivative of the transfer function at input  $s_i$ . The iteration number is  $i = 0, 1, 2, 3, \dots$ . Note that the same measured value  $E$  is used in all iterations.

Start by guessing stimulus  $s_0$ , then use Eq. (2.31) to calculate the next approximation to the true stimulus  $s$ . Then, do it again by using the result from the prior approximation of  $s$ . In other words, computation of the subsequent  $s_i$  is performed

<sup>5</sup> This method is also known as the Newton–Raphson method, named after Isaac Newton and Joseph Raphson.

several times (iterations) until the incremental change in  $s_i$  becomes sufficiently small, preferably in the range of the sensor resolution.

To illustrate use of the Newton method let us assume that our direct transfer function is a third degree polynomial:

$$f(s) = as^3 + bs^2 + cs + d, \quad (2.32)$$

having coefficients  $a = 1.5$ ,  $b = 5$ ,  $c = 25$ ,  $d = 1$ . The next step is plugging Eqs. (2.32) into (2.31) to arrive at the iteration of  $s_{i+1}$ :

$$s_{i+1} = s_i - \frac{as_i^3 + bs_i^2 + cs_i + d - E}{3as_i^2 + 2bs_i + c} = \frac{2as_i^3 + bs_i^2 - d + E}{3as_i^2 + 2bs_i + c} \quad (2.33)$$

This formula is used for all subsequent iterations. Let us assume, for example, that we measured the sensor's response  $E = 22.000$  and our guess for the true stimulus is  $s_0 = 2$ . Then Eq. (2.33) will result in the following iterative sequence of the computed stimuli  $s_{i+1}$ :

$$\begin{aligned} s_1 &= \frac{2 \cdot 1.5 \cdot 2^3 + 5 \cdot 2^2 - 1 + 22}{3 \cdot 1.5 \cdot 2^2 + 2 \cdot 5 \cdot 2 + 25} = 1.032 \\ s_2 &= \frac{2 \cdot 1.5 \cdot 1.032^3 + 5 \cdot 1.032^2 - 1 + 22}{3 \cdot 1.5 \cdot 1.032^2 + 2 \cdot 5 \cdot 1.032 + 25} = 0.738 \\ s_3 &= \frac{2 \cdot 1.5 \cdot 0.738^3 + 5 \cdot 0.738^2 - 1 + 22}{3 \cdot 1.5 \cdot 0.738^2 + 2 \cdot 5 \cdot 0.738 + 25} = 0.716 \\ s_4 &= \frac{2 \cdot 1.5 \cdot 0.716^3 + 5 \cdot 0.716^2 - 1 + 22}{3 \cdot 1.5 \cdot 0.716^2 + 2 \cdot 5 \cdot 0.716 + 25} = 0.716 \end{aligned} \quad (2.34)$$

We see that after just the third iteration, the sequence of  $s_i$  converges to 0.716.

Hence, at step 4, the Newton algorithm stops and the stimulus value is deemed to be  $s = 0.716$ . To check accuracy of this solution, plug the  $s$  number into Eq. (2.32) and obtain  $f(s) = E = 22.014$ , which is within 0.06 % of the actually measured response  $E = 22.000$ .

It should be noted that the Newton method results in large errors when the sensor's sensitivity becomes low. In other words, the method will fail where the transfer function flattens (1st derivative approaches zero). In such cases, the so-called Modified Newton Method may be employed. In some cases when the first derivative cannot be easily computed analytically, one uses instead a sensitivity value devised from  $\Delta s$  and  $\Delta E$  as in (2.17).

## References

1. Stoer, J., & Bulirsch, R. (1991). *Introduction to numerical analysis* (2nd ed., pp. 93–106). New York, NY: Springer.
2. Kelley, C. T. (2003). *Solving nonlinear equations with Newton's method. Number 1 in Fundamental algorithms for numerical calculations*. Philadelphia, PA: SIAM.
3. Süli, E., & Mayers, D. (2003). *An introduction to numerical analysis*. Cambridge, UK: Cambridge University Press.

*O, what men dare do! What men may do!  
What men daily do, not knowing what they do.*

—Shakespeare, *Much Ado About Nothing*

When selecting a sensor—the first thing to do is to outline requirements for the particular application. When knowing what is needed, one is ready to evaluate what is available. The evaluation starts by studying the sensor’s data sheet that specifies all its essential characteristics. The task then is to match the requirements to availability. It is tempting to get the best available sensor, yet selecting a too good sensor means that you will be paying for an overkill—not a good engineering practice. In this chapter we review the most typical sensor characteristics and requirements that are usually specified in data sheets, or at least should be specified.

---

## 3.1 Sensors for Mobile Communication Devices

In the past decade, a major market for sensors has emerged—the *Mobile Communication Devices* (MCD), such as smartphones, smartwatches, and tablets. Nowadays, MCD becomes a bionic extension of ourselves. No longer a telephone is just for the far (*tele*) transmission of sound (*phone*)—it has been evolving into our personal cyber-valet that can perform a multitude of services. For doing any useful job, an MCD needs information from the outside of its own shell by using a number of either external or built-in sensors and detectors. Some sensors are used for the human-to-MCD interface: for receiving the operator’s commands (keypad, microphone, accelerometer), while other sensors are required for perceiving the environment (light, pressure, chemistry, etc.). Today a generic MCD contains a rather limited number of sensors, yet they support thousands of the apps for many

industrial, scientific, consumer, and medical purposes. These currently built-in sensors are:

Imaging camera—takes still photo and video.

Microphone—detects sound mostly in the audible frequency range.

Accelerometer—detects motion of the MCD and direction of the gravity force.

Gyroscope—measures spatial orientation of the MCD.

Magnetometer (compass)—detects strength and direction of magnetic fields.

GPS—an RF receiver and processor for identifying global coordinates.

Proximity detector—detects closeness of the MCD to the user's body.

Yet, the above sensors perceive a rather limited number of stimuli and cannot support many emerging MCD applications. These emerging application areas include:

*Industrial* for detecting noncontact temperature, thermal imaging, humidity, air flow, ionizing radiation, smell, dielectric constant of objects, material composition, range (distance), air pressure, produce freshness, etc.

*Medical* for the inner (core) and skin body temperatures, thermal imaging, arterial blood pressure, EKG, blood factors (glucose, cholesterol, hemoglobin oxygen saturation), deep body imaging, smell (e-nose), behavior modification, etc.

*Military* for night vision, detecting poisonous gases, proximity, ionizing radiation, explosives, chemical and biological agents, etc.

*Consumer* for the body core temperature, heart rate, radon gas, pregnancy detection, breathalyzer for alcohol and hydrogen sulfide, food composition, behavior modification, proximity, UV level, electromagnetic pollution, surface temperature, etc.

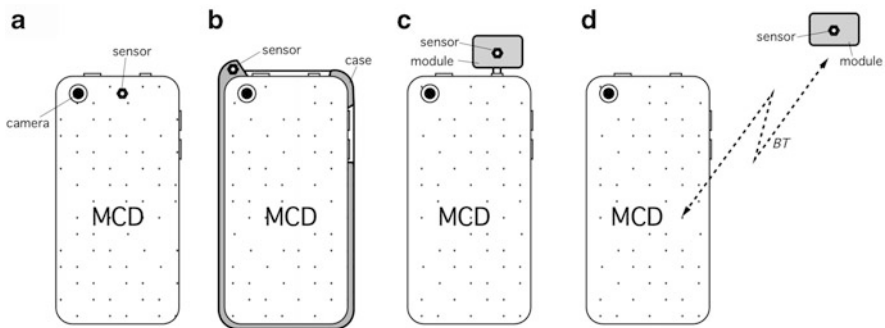
### 3.1.1 Requirements to MCD Sensors

Since an MCD sensor is intended for embedding into a small hand-held device, it should be designed in a specific way. Perhaps the most important feature that an MCD sensor shall have is a full integration with the supporting components, including among others, signal conditioning, data processing, and communication circuits. The general idea is that an MCD sensor shall be more than just a sensor, it has to be an integrated self-containing *sensing module*—a miniature instrument that detects, conditions, digitizes, processes, outputs, and communicates information. Other important requirements to MCD sensing modules include low power consumption, small size/weight, high accuracy, stability, short response time, and several others. Table 3.1 summarizes ten essential requirements to an MCD sensor [1]. To emphasize their importance, we call them “*10 Commandments*” of the Mobile Sensor Design. All and every requirement is critical and shall not be ignored. Even if any one of the “commandments” is not met, such a sensor may not be fully suitable for mobile applications.

There are four possible ways of coupling a sensing module to an MCD. Figure 3.1 illustrates that a sensing module can be embedded directly into the MCD housing (a), incorporated into a removable protective case (jacket) that

**Table 3.1** “10 Commandments” of mobile sensor design

1	Intelligent sensor: built-in signal conditioner and DSP
2	Built-in communication circuit ( $I^2C$ , NFC, Bluetooth, etc.)
3	Integrated supporting components (optics, thermostat, blower, etc.)
4	High selectivity of the sensed signal (reject interferences)
5	Fast response
6	Miniature size to fit a mobile device
7	Low power consumption
8	High stability in changing environment
9	Lifetime stability: no periodic recalibration or replacement
10	Low cost at sufficiently high volumes



**Fig. 3.1** Four possible ways of coupling sensing module to mobile communication device

envelops an MCD (b), it can be configured as an external device for plugging into one of the communication ports of an MCD (c), and finally the module can be totally external to an MCD (d) and communicate with it wirelessly.

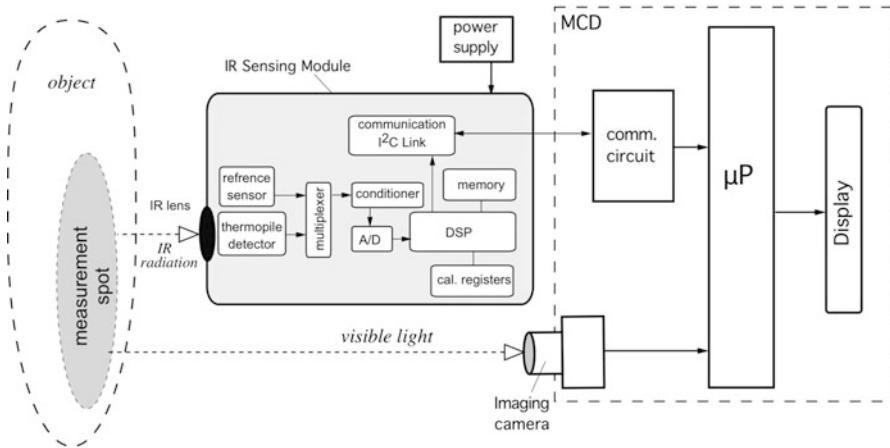
All these possible options are workable from the engineering standpoint, yet from a convenience and practicality perspective, it appears that option b is the most attractive for coupling with a *generic* MCD that is used by a consumer. Positioning sensors inside a protective case allows hiding them ergonomically and inconspicuously and making the sensors instantly available whenever needed without additional actions by an operator. The sensing “smart case” communicates with an MCD either by wires or preferably wirelessly, for example through NFC<sup>1</sup> or Bluetooth.

### 3.1.2 Integration

Integration of various functions into a sensing module is based on the reality that a sensing element rarely operates by itself—it needs numerous supporting components, such as voltage or current references, signal conditioners, heaters,

<sup>1</sup> NFC stands for *near-field communication*.





**Fig. 3.2** Block-diagram of thermal radiation (IR) sensing module for MCD

multiplexers, gas blowers, lenses, digital signal processors (DSP), and many others. To illustrate the point, refer to Fig. 3.2 that shows a sensing module with an integrated noncontact infrared (IR) thermometer [2]. This module can be directly incorporated into an MCD housing (option a) or be part of a “smart” case (option b).

The IR sensing module operates in concert with the MCD’s internal digital imaging camera that functions as a viewfinder for the IR lens. Both the imaging and IR lenses are aimed at the object’s preferred measurement location (the measurement spot). Thermal IR radiation that is naturally emanated from the spot surface is focused by a narrow-angle IR lens on the thermal radiation detector, such as a thermopile or microbolometer. The detecting element converts the radiation into minute electrical voltage that together with the reference temperature sensor’s output are multiplexed and fed into the signal conditioner. The conditioner filters out some interfering voltages and brings the measured signals to the levels suitable for conversion to a digital format by a high-resolution analog-to-digital converter (ADC). The digitalized signals are processed by a digital signal processor (DSP) to compute temperature of the object and then send it through a serial digital communication link ( $I^2C$ ) to the MCD for display and interpretation. As it can be appreciated, this sensing module is the entire noncontact IR thermometer that requires no or very few external components for interfacing with an MCD. Any sensor intended for an MCD should follow the similar approach—a complete integration of all essential functions into a single small housing.

### 3.2 Span (Full-Scale Input)

A dynamic range of stimuli that may be converted by a sensor is called a *span* or an *input full scale* (FS). It represents the highest possible input value, which can be applied to the sensor without causing unacceptably large error. For sensors with

**Table 3.2** Relationship between power, force (voltage, current), and decibels

Power ratio	1.023	1.26	10.0	100	10 <sup>3</sup>	10 <sup>4</sup>	10 <sup>5</sup>	10 <sup>6</sup>	10 <sup>7</sup>	10 <sup>8</sup>	10 <sup>9</sup>	10 <sup>10</sup>
Force ratio	1.012	1.12	3.16	10.0	31.6	100	316	10 <sup>3</sup>	3162	10 <sup>4</sup>	3 × 10 <sup>4</sup>	10 <sup>5</sup>
Decibels	0.1	1.0	10.0	20.0	30.0	40.0	50.0	60.0	70.0	80.0	90.0	100.0

very broad and nonlinear response characteristics, the dynamic ranges of the input stimuli are often expressed in decibels, which is a logarithmic measure of ratios of either power or force (voltage). It should be emphasized that decibels do not measure absolute values, but a *ratio* of the values only. A decibel scale represents signal magnitudes by much smaller numbers that in many cases is by far more convenient. Being a nonlinear scale, it may represent low-level signals with high resolution, while compressing the high-level numbers. In other words, the logarithmic scale for small objects works as a microscope and for the large objects as a telescope. By definition, decibels are equal to ten times the log of the ratio of powers (Table 3.2):

$$1 \text{ dB} = 10 \log \frac{P_2}{P_1}. \quad (3.1)$$

In a similar manner, decibels are equal to 20 times the log of the force, or current, or voltage:

$$1 \text{ dB} = 20 \log \frac{E_2}{E_1} \quad (3.2)$$

---

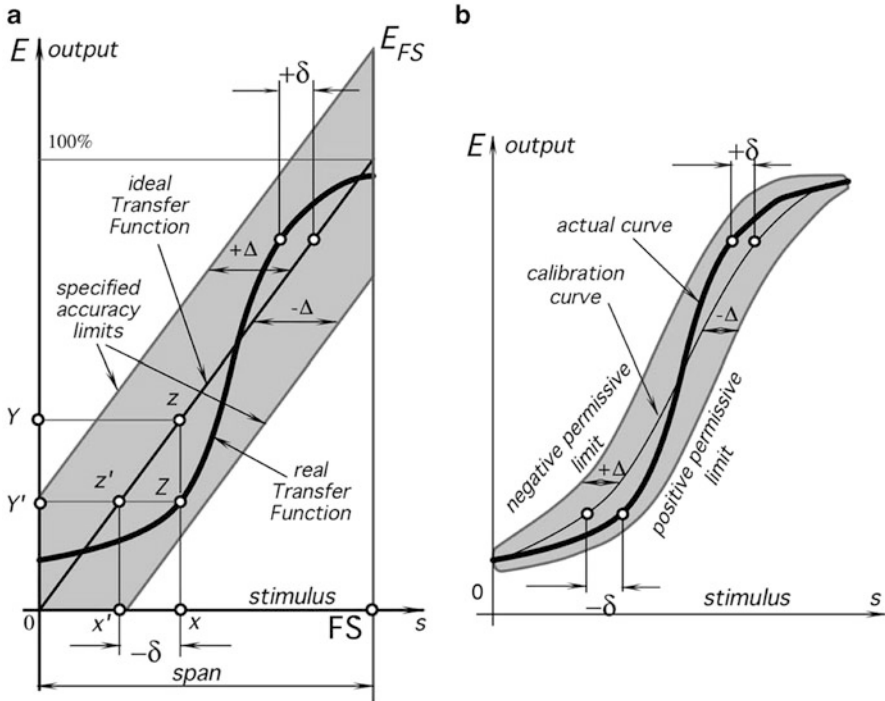
### 3.3 Full-Scale Output

Full-scale output (FSO) for an analog output is the algebraic difference between the electrical output signals measured with maximum input stimulus and the lowest input stimulus applied. For a digital output it is the maximum digital count the A/D convertor can resolve for the absolute maximum FS input. This must include all deviations from the ideal transfer function. For instance, the FSO output in Fig. 3.3a is represented by  $E_{\text{FS}}$ .

---

### 3.4 Accuracy

A very important characteristic of a sensor is accuracy, which really means inaccuracy. Inaccuracy is measured as a highest deviation of a value represented by the sensor from the ideal or true value of a stimulus at its input. The true value is



**Fig. 3.3** Transfer function (a) and calibrated accuracy limits (b). Errors are specified in terms of input values

attributed to the input stimulus and accepted as having a specified uncertainty (see below) because one never can be absolutely sure what the true value is.

The deviation from an ideal (true) transfer function can be described as a difference between the value that is computed back from the output, and the actual input stimulus value. For example, a linear displacement sensor ideally should generate 1 mV per 1 mm displacement. That is, its transfer function is a line with a slope (sensitivity)  $B = 1$  mV/mm. However, in the experiment, a reference displacement of  $s = 10$  mm produced an output of  $E = 10.5$  mV. Since we assume that the slope is 1 mV/mm, converting this number back into the displacement value by using the inverted transfer function ( $1/B = 1$  mm/mV), we calculate the displacement as  $s_x = E/B = 10.5$  mm. The result overestimates the displacement by  $s_x - s = 0.5$  mm. This extra 0.5 mm is an erroneous deviation in the measurement, or error. Therefore, in a 10 mm range the sensor's absolute inaccuracy is 0.5 mm, or in relative terms, the inaccuracy is  $0.5 \text{ mm}/10 \text{ mm}$  times  $100\% = 5\%$ . For a larger displacement, the error may be larger. If we repeat this experiment over and over again without any random error and every time we observe an error of 0.5 mm we may say that the sensor has a *systematic* inaccuracy of 0.5 mm over a 10 mm span. Naturally, a random component is always present, so the systematic error may be represented as an average or mean value of multiple errors.

Figure 3.3a shows an ideal or theoretical linear transfer function (thin line). In the real world, any sensor performs with some kind of imperfection. A possible real transfer function is represented by a thick line, which generally may be neither linear nor monotonic. A real function rarely coincides with the ideal. Because of the material variations, workmanship, design errors, manufacturing tolerances, and other limitations, it is possible to have a large family of the real transfer functions, even when the sensors are tested under presumably identical conditions. However, all runs of the real transfer functions must fall within the limits of a specified accuracy. These permissive limits differ from the ideal transfer function line by  $\pm\Delta$ . The real functions deviate from the ideal by  $\pm\delta$  where  $\delta \leq \Delta$ .

For example, let us consider a stimulus having value,  $x$ . Ideally, we would expect this value to correspond to point  $z$  on the transfer function, resulting in the output value  $Y$ . Instead, the real function will respond at point  $Z$  producing output value  $Y'$ . When we compute the value of a stimulus from the output  $Y'$ , we have no idea how the real transfer function differs from the expected “ideal” so we use the ideal inverted transfer function for calculation. The measured output value  $Y'$  corresponds to point  $z'$  on the ideal transfer function, which, in turn, relates to a “would-be” input stimulus  $x'$  whose value is smaller than  $x$ . Thus, in this example an imperfection in the sensor’s performance leads to the measurement error  $-\delta$ .

The accuracy rating includes combined effects of part-to-part variations, hysteresis, dead band, calibration, and repeatability errors (see below). The specified accuracy limits generally are used in the worst-case analysis to determine the worst possible performance of the entire system.

To improve accuracy, a number of the error-contributing factors should be reduced. This can be achieved by not fully trusting the manufacturer’s specified tolerances, but rather calibrating each sensor individually under selected conditions. Figure 3.3b shows that  $\pm\Delta$  may more closely follow the real transfer function, meaning a better sensor’s accuracy. This can be accomplished by a multiple-point calibration of each individual sensor and a curve fitting as described above. Thus, the specified accuracy limits are established not around the theoretical (ideal) transfer function, but around the actual calibration curve, which is adjusted during the calibration procedure. Then, the permissive limits become narrower as they do not embrace part-to-part variations between the purchased sensors as they are geared specifically to the particular device. Clearly, this method allows for a more accurate sensing, albeit in some applications it may be prohibitive because of a higher cost.

Often, inaccuracy (accuracy) is defined as a *maximum*, or *typical*, or *average* error.

Inaccuracy rating may be represented in several forms, some of which are:

1. Directly in terms of measured value of a stimulus ( $\Delta$ ).

This form is used when error is independent on the input signal magnitude. Often, it relates to additive noise or systematic bias, but also combines with all other conceivable error sources, like calibration, manufacturer’s tolerances, etc. For example, it can be stated as 0.15 °C for a temperature sensor or 10 fpm (foot-

per-minute) for a flow sensor. Usually, a specific range of the stimulus accompanies this statement, then the accuracy specification may read:

10 fpm in the range from below 100 ft/min, and

20 fpm in the range over 100 ft/min

2. In percentage of the input span (full scale).

This form #2 is useful for a sensor with a linear transfer function and closely relates to the above form #1. It is just another way of stating the same thing because the input range must be specified for nearly any sensor. This form is not useful for a sensor with a nonlinear transfer function, unless a small quasilinear range is specified. For example, a thermo-anemometer (see Sect. 12.3) has a response that can be modeled by a square root function—that is—it is more sensitive at low-flow rates and less sensitive at high flows. Let us assume that the sensor has a span of 3000 fpm and its accuracy is stated as 3 % of the full scale, which is the other way to say 90 fpm. However, for measuring low-flow rates, say from 30 to 100 fpm, this full-scale error of 90 fpm looks huge and in fact is misleading due to a nonlinearity.

3. In percentage of the measured signal.

This is a multiplicative way of expressing error because the error magnitude is shown as fraction of the signal magnitude. It is useful for a sensor with a highly nonlinear transfer function. Considering the same example from the form #2 above, the 3 % of the measured signal is more practical for low-flow rates because it will be just few fpm, while for the high-flow rate range it will be in tens of fpm and is also reasonable and realistic. Still, using this form is not generally recommended because typically the error varies with a stimulus. It makes more sense to break up the total nonlinear span into smaller quasilinear sections. Then, form #2 should be used instead for each individual section.

4. In terms of the output signal. This is useful for sensors with a digital output format so the error can be expressed, for example, in units of LSB.

Which particular method to use? The answer often depends on the application.

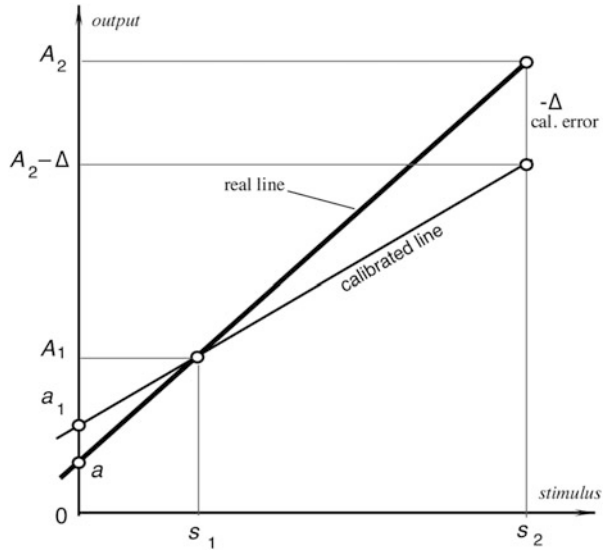
In modern sensors, specification of accuracy often is replaced by a more comprehensive value of uncertainty (Sect. 3.21) because uncertainty is comprised of all distorting effects both systematic and random and is not limited to inaccuracy of a sensor alone.

---

## 3.5 Calibration Error

Calibration error is the inaccuracy permitted when a sensor is calibrated in the factory. This error is of a systematic nature, meaning that it is added to all possible real transfer functions. It shifts accuracy for each stimulus point by a constant. This error is not necessarily uniform over the range and may change depending on the type of error. For example, let us consider a two-point calibration of a real linear transfer function (thick line in Fig. 3.4). To determine the slope and the intercept of

**Fig. 3.4** Calibration error



the function, two stimuli,  $s_1$  and  $s_2$ , are applied to the sensor. The sensor responds with two corresponding output signals  $A_1$  and  $A_2$ . Let us say the first response was measured absolutely accurately, while the other response was measured with error  $-\Delta$ . This causes errors in the slope and intercept calculation. A new erroneous intercept  $a_1$  will differ from the true intercept,  $a$ , by

$$\delta_a = a_1 - a = \frac{\Delta}{s_2 - s_1}, \tag{3.3}$$

and the slope will be calculated with error:

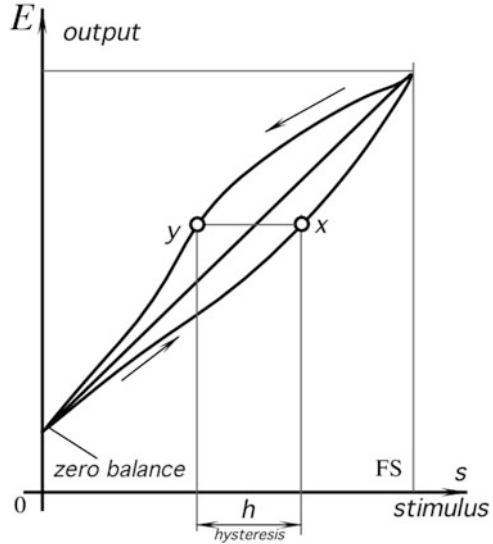
$$\delta_b = -\frac{\Delta}{s_2 - s_1} \tag{3.4}$$

Another source of errors in calibration is a reference sensor. No accurate calibration is possible if one uses a not-so-accurate reference. Thus, it is essential to use and maintain the high precision reference signal sources and/or sensors (meters) that are traceable to the National standards.

### 3.6 Hysteresis

A hysteresis error is a deviation of the sensor’s output at a specified point of the input signal when it is approached from the opposite directions (Fig. 3.5). For example, a displacement sensor when the object moves from left to right at a certain

**Fig. 3.5** Transfer function with hysteresis

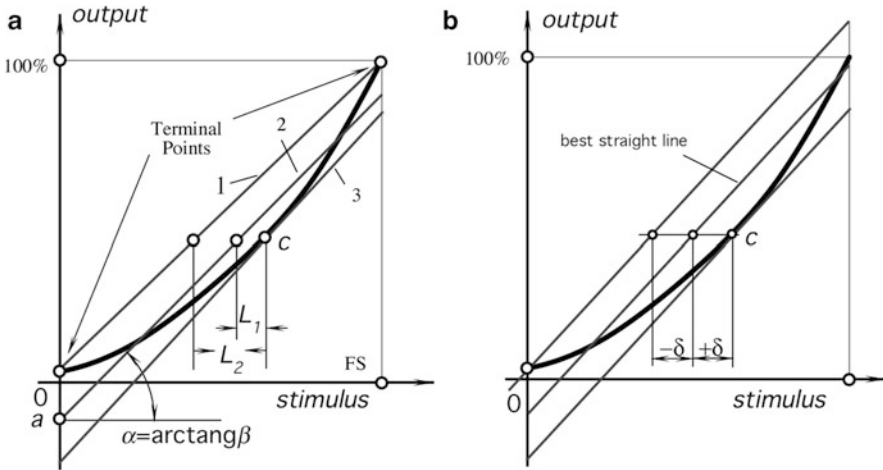


point produces voltage, which differs by 20 mV from that when the object moves from right to left. If the sensitivity of the sensor is 10 mV/mm, the hysteresis error in terms of displacement units is 2 mm. The typical causes for hysteresis are a geometry of design, friction, and structural changes in the materials, especially in plastics and epoxy.

### 3.7 Nonlinearity

Nonlinearity error is specified for sensors whose transfer functions may be approximated by straight lines, Eq. (2.2 or 2.3). A nonlinearity is a maximum deviation ( $L$ ) of a real transfer function from the approximation straight line. The term “linearity” actually means “nonlinearity”. When more than one calibration run is made, the worst linearity seen during any one calibration cycle should be stated. Usually, it is specified either in percentage of a span or in terms of the measured value, for instance, in kPa or °C. “Linearity”, when not accompanied by a statement explaining what sort of straight line it is referring to, is meaningless. There are several ways of specifying nonlinearity, depending on how the line is superimposed on the transfer function. One way is to use the terminal points (Fig. 3.6a), that is, to determine the output values at the smallest and highest stimuli and to draw a straight line through these two points (line 1). Here, near the terminal points, the nonlinearity error is the smallest and it is higher somewhere in between.

In some applications, higher accuracy may be desirable in particular narrower section of the input range. For instance, a medical thermometer should have the best accuracy in a fever borderline region which is between 36 and 38 °C. It may have a



**Fig. 3.6** Linear approximations of nonlinear transfer function (a) and independent linearity (b)

somewhat lower accuracy beyond these limits. Thus, a sensor preferably is calibrated in the region where the highest accuracy is desirable. Then, the approximation line may be drawn through the calibration point  $c$ , line 3 in Fig. 3.6a. As a result, nonlinearity has the smallest value near the calibration point and increases toward the ends of the span. In this method, the line is often determined as tangent to the transfer function in point  $c$ . If the actual transfer function is known, the slope of the line can be found from Eq. (2.17).

*Independent linearity* is referred to the so-called best straight line, Fig. 3.6b, which is a line midway between two parallel straight lines closest together and enveloping all output values on a real transfer function. It often is used when all stimuli in the range are equally important.

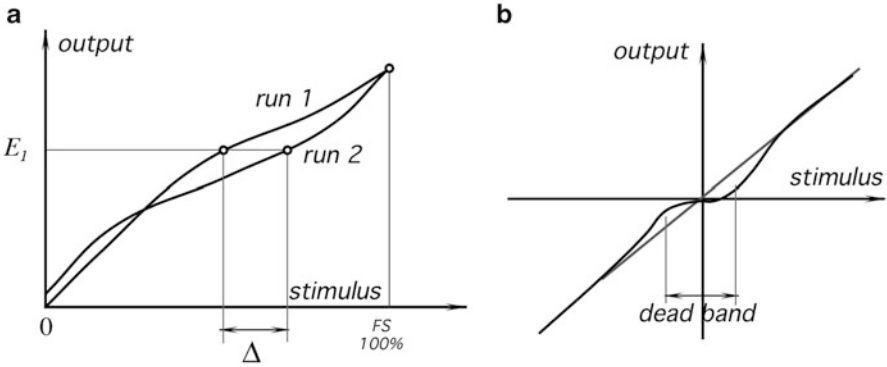
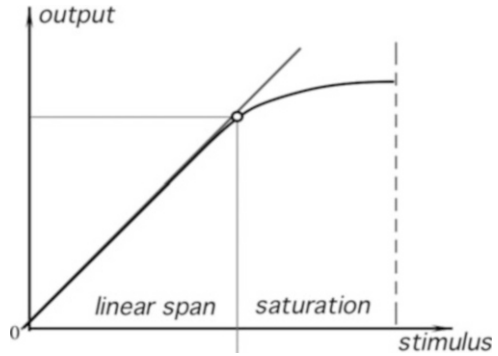
Depending on the specification method, approximation lines may have different intercepts and slopes. Therefore, the nonlinearity measures may differ quite substantially from one another. A user should be aware that manufacturers sometimes publish the smallest possible number to specify nonlinearity without defining what method was used.

### 3.8 Saturation

Every sensor has its operating limits. Even if it is considered linear, at some levels of the input stimuli, its output signal no longer will be responsive. Further increase in stimulus does not produce a desirable output. It is said that the sensor exhibits a span-end nonlinearity or saturation, Fig. 3.7.



**Fig. 3.7** Transfer function with saturation



**Fig. 3.8** Repeatability error (a). The same output signal  $E_1$  corresponds to two different input signals. Dead-band zone in transfer function (b)

### 3.9 Repeatability

Repeatability (reproducibility) error is caused by the inability of a sensor to represent the same value under presumably identical conditions. The repeatability is expressed as a maximum difference between the output readings as determined by two run cycles (Fig. 3.8a), unless otherwise specified. It is usually represented as percentage of FS:

$$\delta_r = \frac{\Delta}{FS} 100\% \tag{3.5}$$

The possible sources of a repeatability error may be thermal noise, build up charge, material plasticity, etc.

---

### 3.10 Dead Band

Dead band is the insensitivity of a sensor in a specific range of the input signals (Fig. 3.8b). In that range, the output may remain near a certain value (often zero) over an entire dead-band zone.

---

### 3.11 Resolution

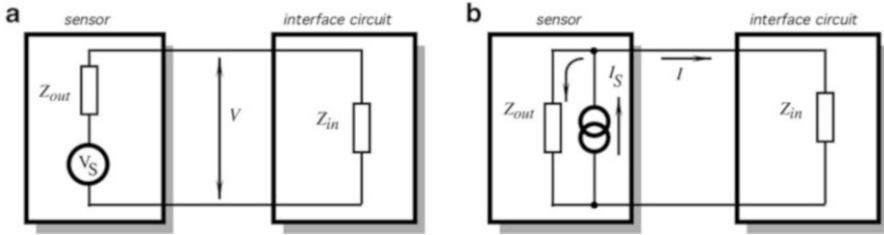
Resolution describes the smallest increment of a stimulus that can be sensed. When a stimulus continuously varies over the range, the output signals of some sensors will not be perfectly smooth, even under the no-noise conditions. The output may change in small steps. This is typical for potentiometric transducers, occupancy infrared detectors with grid masks, and other sensors where the output signal change is enabled only upon a certain degree of stimulus variation. Besides, any signal that is converted into a digital format is broken into small steps where a number is assigned to each step. The magnitude of the input variation, which results in the output smallest step, is specified as a *resolution* under specified conditions (if any). For instance, for the motion detector the resolution may be specified as follows: “*resolution—the minimum equidistant displacement of an object for 20 cm at a 5 m distance*”. For a wire-wound potentiometric angular sensor, resolution may be specified as “*a minimum angle of 0.5°*”. Sometimes, it may be specified as percent of a full scale (FS). For instance, for the angular sensor having 270° FS, the 0.5° resolution may be specified as 0.18 % of FS. It should be noted that the step size may vary over the range, hence, the resolution may be specified as typical, average, or worst.

The resolution of a sensor with a digital output format is given by the number of bits. For instance, resolution may be specified as “*8-bit resolution*”. This statement to make sense must be accomplished with either of FS value or the value of LSB (least significant bit). When there are no measurable steps in the output signal, it is said that the sensor has continuous or infinitesimal resolution (sometimes erroneously referred to as “infinite resolution”).

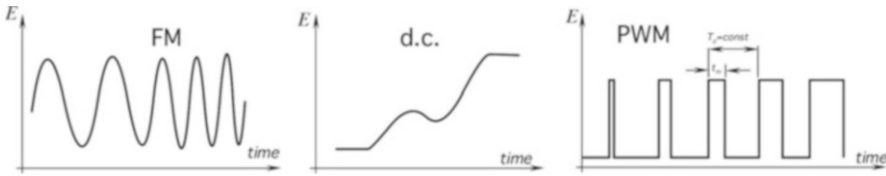
---

### 3.12 Special Properties

Special input properties may be needed to specify for some sensors. For instance, light detectors are sensitive within a limited optical bandwidth. Therefore, it is appropriate to specify for them a spectral response.



**Fig. 3.9** Sensor connection to interface circuit: sensor has voltage output (a), sensor has current output (b)



**Fig. 3.10** Examples of output signals: sine wave constant amplitude with frequency modulation (FM), analog signal (d.c.) changing within the output range, and pulse-width modulation (PWM) of rectangular pulses of a constant period but variable width

### 3.13 Output Impedance

Output impedance  $Z_{out}$  is important to know for better interfacing a sensor with an electronic circuit. Electrically, the output impedance is connected to the input impedance  $Z_{in}$  of the interface circuit either in parallel (voltage connection) or in series (current connection). Figure 3.9 shows these two connections. The output and input impedances generally should be represented in a complex form, as they may include the reactive components (capacitors and inductors). To minimize signal distortions, a current generating sensor (Fig. 3.9b) should have an output impedance  $Z_{out}$  as high as possible, while the interface circuit's input impedance should be low. Contrary, for the voltage connection (Fig. 3.9a), a sensor shall have a lower  $Z_{out}$ , while the interface circuit should have  $Z_{in}$  as high as practical.

### 3.14 Output Format

*Output Format* is a set of the output electrical characteristics that are produced by the sensor alone or by its integrated excitation circuit and signal conditioner. The characteristics may include voltage, current, charge, frequency, amplitude, phase, polarity, shape of a signal, time delay, and digital code. Figure 3.10 shows examples of the output electrical signals in form of current or voltage. A sensor manufacturer

should provide sufficient information on the output format to allow for efficient applications.

The most popular digital communication between an integrated sensor and peripheral device is a serial link. As the name implies, a serial link sends and receives bytes of information in a serial fashion—one bit at a time. These bytes are transmitted using either a binary format or a text (ASCII) format. For communicating an integrated sensor with a digital output format, the most popular formats are PWM (pulse-width modulation) and  $I^2C$  and its variations.

The  $I^2C$  (pronounced I-squared-C) protocol was developed by Philips Semiconductors for sending data between the  $I^2C$  devices over two wires. It sends information from a sensor to a peripheral device serially using two lines: one line for data (SDA) and one for clock (SCL). The protocol is based on a concept of the master and slave devices. A master device is a controller (often a microprocessor) that is in charge of the bus at the present time and controls the clock. It also generates START and STOP signals. Slaves simply listen to the bus and act on controls or data that they sent. The master can send data to a slave or receive data from a slave—slaves do not transfer data among themselves. The basic communication speed is selected between 0 and 100 kHz. Some sensors are relatively slow (contact temperature sensors, for example), thus a slow slave module may need to stop the bus while it collects and processes data. It can do this while holding the clock line (SCL) low forcing the master into the wait state. The master must then wait until SCL is released before proceeding.

---

### 3.15 Excitation

Excitation is the signal needed to enable operation of an active sensor. Excitation is specified as a range of voltage and/or current, or in some cases it may be light, magnetic field and any other type of a signal. For some sensors, the frequency and shape of the excitation signal, and its stability, must also be specified. Spurious variations in the excitation may alter the sensor transfer function, produce noise, and cause output errors. An example of an excitation signal is electric current passing through a thermistor to measure its temperature-dependent resistance.

An example of the excitation signal specification is:

Maximum current through a thermistor	in still air	50 $\mu$ A
	in water	1 mA

---

### 3.16 Dynamic Characteristics

Under the static conditions (a very slow-changing input stimulus) a sensor is described by a time-invariant transfer function, accuracy, span, calibration, etc. However, when an input stimulus varies with an appreciable rate, a sensor response

generally does not follow it with a perfect fidelity. The reason is that both the sensor and its coupling with the stimulus source cannot always respond instantly. In other words, a sensor may be described by a time-dependent characteristic that is called *dynamic*. If a sensor does not respond instantly, it may represent the stimulus as somewhat different from the real, that is, the sensor responds with a dynamic error. A difference between a static and dynamic error is that the latter is always time-dependent. If a sensor is part of a control system, which has its own dynamic characteristics, the combination may cause at best a delay in representing a true value of a stimulus or, at worst, cause spurious oscillations.

The *warm-up time* characteristic is a time delay between applying power to the sensor or the excitation signal and the moment when the sensor can operate within its specified accuracy. Many sensors have a negligibly short warm-up time. However, some sensors, especially those that operate in a thermally controlled environment (a thermostat, e.g.) and many chemical sensors employing heaters, may require seconds and even minutes of a warm-up time before they are fully operational within the specified accuracy limits.

In the control theory, it is common to describe the input-output relationship through a constant-coefficient linear differential equation. Then, the sensor's dynamic (time-dependent) characteristics can be studied by evaluating such an equation. Depending on the sensor design, differential equations can be of several orders.

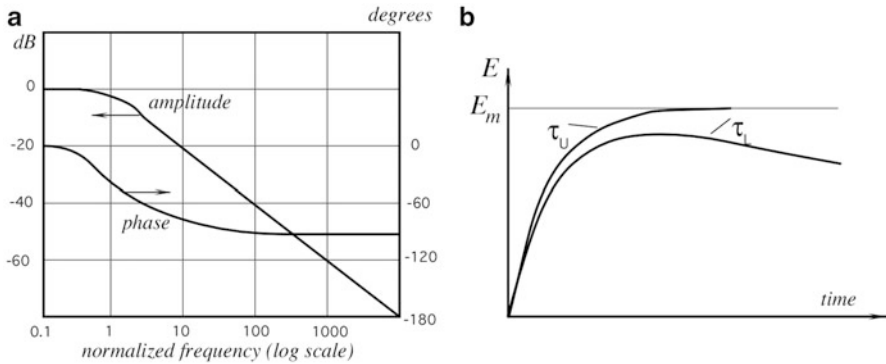
A *Zero-Order* sensor is characterized by a transfer function that is time-independent. Such a sensor does not incorporate any energy storage devices, like a capacitor. A zero-order sensor responds instantaneously. In other words, such a sensor does not need any dynamic characteristics to be specified. Naturally, nearly any sensor still has a finite time to respond, but such time is negligibly short and thus can be ignored.

A *First-Order* differential equation describes a sensor that incorporates one energy storage component. The relationship between the input  $s(t)$  and output  $E(t)$  is a first-order differential equation

$$b_1 \frac{dE(t)}{dt} + b_0 E(t) = s(t) \quad (3.6)$$

An example of a first-order sensor is a temperature sensor where the energy storage is a thermal capacity of the sensor within an encapsulation.

A dynamic characteristic of a first-order sensor may be specified by a manufacturer in various ways. A typical is a frequency response, which specifies how fast the sensor can react to a change in the input stimulus. The frequency response is expressed in Hz or rad/s to specify the relative reduction in the output signal at a certain frequency of the stimulus (Fig. 3.11a). A commonly used reduction number (frequency limit) is  $-3$  dB. It shows at what frequency the output voltage (or current) drops by about 30 %. The frequency response limit  $f_u$  is often called the *upper cutoff frequency*, as it is considered the highest frequency that a sensor can process.



**Fig. 3.11** Frequency characteristic (a) and response of first-order sensor (b) with limited upper and lower cutoff frequencies.  $\tau_u$  and  $\tau_L$  are the corresponding time constants

The frequency response directly relates to a *speed response*, which is defined in the units of input stimulus per unit of time. How to specify, frequency or speed, in any particular case, depends on the sensor type, application, and preference of a designer.

Another way of specifying speed response is by the time that is required by the output to reach an arbitrary, say 63 or 90 %, level of a steady state or maximum response upon exposure to the input step stimulus. For the first-order response, it is very convenient to use the so-called *time constant*. Time constant  $\tau$  is a measure of the sensor’s inertia. In electrical terms, it is a product of the electrical capacitance and resistance:  $\tau = CR$ . In thermal terms, a thermal capacity and thermal conductivity or thermal resistance should be used instead. Practically, a time constant can be easily measured.

A solution of Eq. (3.6) gives the first-order system time response:

$$E = E_m \left( 1 - e^{-t/\tau} \right), \tag{3.7}$$

where  $E_m$  is steady-state settled output,  $t$  is time, and  $e$  is the base of natural logarithm.

Substituting  $t = \tau$ , we arrive at:

$$\frac{E}{E_m} = 1 - \frac{1}{e} = 0.6321 \tag{3.8}$$

This means that after the elapsed time is equal to one time constant, the sensor’s response reaches about 63 % of its steady-state level  $E_m$ . Similarly, it can be shown that after two time constants, the transition will be at a 86.5 % level and after three time constants it will climb to 95 % of the value that would be reached after waiting infinitely long.

A cutoff frequency shows what is the lowest or highest frequency of stimuli the sensor can process? The upper cutoff frequency shows how fast the sensor reacts, while the lower cutoff frequency shows how the sensor can process a slow-changing stimulus. Figure 3.11b depicts the sensor's response when both upper and lower cutoff frequencies are limited. As a rule of thumb, a simple formula can be used to establish a connection between the cutoff frequency  $f_c$  (either upper and lower) and a time constant in a first-order sensor:

$$f_c \approx \frac{0.159}{\tau} \quad (3.9)$$

A phase shift at a specific frequency defines how the output signal lags behind the stimulus, Fig. 3.11a. The shift is measured in angular degrees or rads and is usually specified for sensors that process periodic signals. If a sensor is part of a feedback control system, it is very important to know the phase characteristic. The phase lag reduces the phase margin of the system and may result in the overall instability.

A *Second-Order* differential equation describes a sensor that incorporates two energy storage components. The relationship between the input  $s(t)$  and output  $E(t)$  is a differential equation

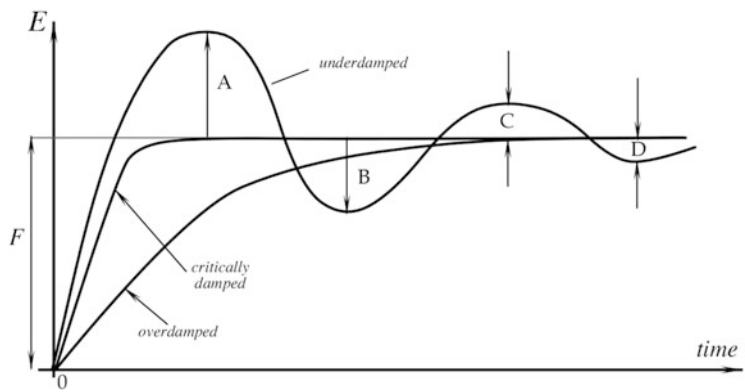
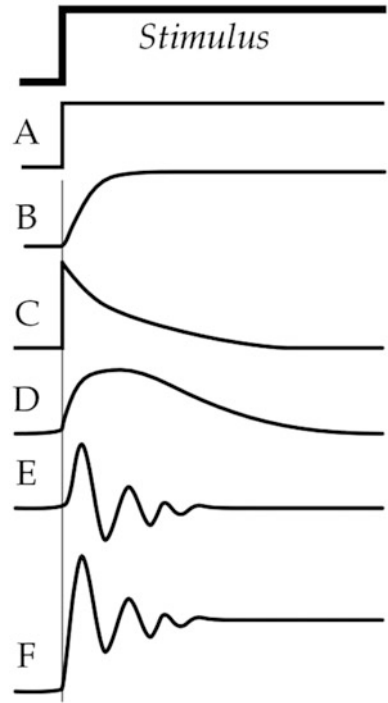
$$b_2 \frac{d^2 E(t)}{dt^2} + b_1 \frac{dE(t)}{dt} + b_0 E(t) = s(t) \quad (3.10)$$

An example of a second-order sensor is an accelerometer that incorporates an inertial mass and a spring.

A second-order response is specific for a sensor whose response includes a periodic signal. Such a periodic response may be very brief and we say that the sensor is damped, or it may be of a prolonged time and even may oscillate continuously. For many sensors such a continuous oscillation is a malfunction and must be avoided.

Any second-order sensor may be characterized by a resonant (natural) frequency, which is a number expressed in Hz or rad/s. The natural frequency shows where the sensor's output signal increases considerably while the stimulus does not. When the sensor behaves as if the output conforms to the standard curve of a second-order response, the manufacturer will state the natural frequency and the damping ratio of the sensor. The resonant frequency may be related to mechanical, thermal, or electrical properties of the detector. Generally, the operating frequency range for a sensor should be selected well below (at least by 60 %) or above the resonant frequency. However, in some sensors, a resonant frequency is the operating point. For instance, in glass breakage detectors (used in the security systems) a resonant makes the sensor selectively sensitive to a narrow bandwidth of stimuli, which is specific for the acoustic spectrum, produced by shattered glass. Figure 3.12 illustrates responses of the sensors having different cutoff frequencies.

**Fig. 3.12** Types of dynamic responses unlimited upper and lower frequencies (A); first-order limited upper cutoff frequency (B); first-order limited lower cutoff frequency (C); first-order limited both upper and lower cutoff frequencies (D); narrow bandwidth response (resonant) (E); wide bandwidth with resonant (F)



**Fig. 3.13** Responses of sensors with different damping characteristics

Damping is the progressive reduction or suppression of oscillations in a sensor having higher than the first-order response. When sensor's response is fast but without an overshoot, the response is said to be *critically damped* (Fig. 3.13). *Underdamped* response is when the overshoot occurs and the *overdamped* response is slower than the critical. The damping ratio is a number expressing the quotient of



the actual damping of a second-order linear sensor by its critical damping. Damping in a sensor may be performed by a special component (damper) that has viscous properties, for example—fluid (air, oil, water).

For an oscillating response, as shown in Fig. 3.13, a damping factor is a measure of damping, expressed (without sign) as the quotient of the greater by the littlest of pair of consecutive swings in opposite directions of the output signal, about an ultimately steady-state value. Hence, the damping factor can be measured as:

$$\text{Damping factor} = \frac{F}{A} = \frac{A}{B} = \frac{B}{C} = \dots \quad (3.11)$$

---

## 3.17 Dynamic Models of Sensor Elements




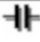






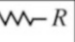
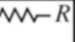
To determine a sensor's dynamic response a variable stimulus should be applied to its input while observing the output values. Generally, a test stimulus may have any shape or form, which should be selected according to the practical need. For instance, while determining a natural frequency of an accelerometer, sinusoidal vibrations of different frequencies are the best. On the other hand, for a temperature probe, a step-function of temperature would be preferable. In many other cases, a step or square-pulse input stimulus is often employed. The reason is that the steps or pulses have a theoretically infinite frequency spectrum. That is, the sensor simultaneously is tested at all frequencies.

A mathematical modeling of a sensor is a powerful tool in assessing its performance. A modeling may address both responses: static and dynamic. The models usually deal with the sensor's transfer function. Here we briefly outline how some sensors can be evaluated dynamically. The dynamic models may have several independent variables, however, one of them must be time. The resulting model is referred to as a lumped parameter model. In this section, the mathematical models are formed by applying physical laws to some simple lumped parameter sensor elements. In other words, for the analysis, a sensor is divided into simple elements and each element is considered separately. However, once the equations describing the elements have been formulated, individual elements can be recombined to yield the mathematical model of the original sensor. The treatment is intended not to be exhaustive, but rather to introduce the topic.

### 3.17.1 Mechanical Elements

Dynamic mechanical elements are made of masses, or inertias, which have attached springs and dampers. Often the damping is viscous, and for the rectilinear motion the retaining force is proportional to velocity. Similarly, for the rotational motion, the retaining force is proportional to angular velocity. Also, the force, or torque,

**Table 3.3** Mechanical, thermal, and electrical analogies

MECHANICAL	THERMAL	ELECTRICAL	
MASS  $F = M \frac{d(v)}{dt}$	CAPACITANCE  C $Q = C \frac{dT}{dt}$	INDUCTOR  L $V = L \frac{di}{dt}$	CAPACITOR  $i = C \frac{dV}{dt}$
SPRING  k $F = k \int v dt$	CAPACITANCE  C $T = \frac{1}{C} \int Q dt$	CAPACITOR  C $V = \frac{1}{C} \int i dt$	INDUCTOR  L $i = \frac{1}{L} \int V dt$
DAMPER  b $F = bv$	RESISTANCE  R $Q = \frac{1}{R} (T_2 - T_1)$	RESISTOR  R $V = Ri$	RESISTOR  R $i = \frac{1}{R} V$

exerted by a spring, or shaft, is usually proportional to displacement. The various elements and their governing equations are summarized in Table 3.3.

One of the simplest methods of producing the equations of motion is to isolate each mass or inertia and to consider it as a free body. It is then assumed that each of the free bodies is displaced from the equilibrium position, and the forces or torques acting on the body then drive it back to its equilibrium position. Newton’s second law of motion can then be applied to each body to yield the required equation of motion.

For a rectilinear system Newton’s second law indicates that for a consistent system of units *the sum of forces equals to the mass multiplied the acceleration*. In the SI system of units, force is measured in newtons (N), mass in kilograms (kg), and acceleration in meters per second squared (m/s<sup>2</sup>).

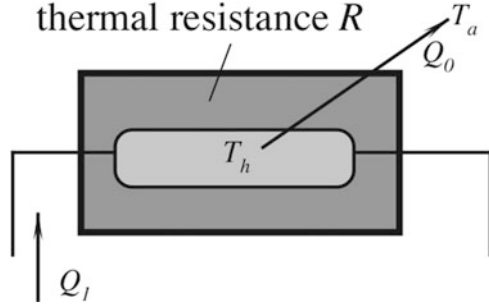
For a rotational system, Newton’s law becomes: *the sum of the moments equals the moment of inertia multiplied by the angular acceleration*. The moment, or torque, has units of newton-meters (Nm), the inertia units of kilogram per meter squared (kg/m<sup>2</sup>), and the angular acceleration units of radians per second squared (rad/s<sup>2</sup>).

Detailed mathematical model of a linear accelerometer in given in Sect. 9.3.1.

### 3.17.2 Thermal Elements

Thermal elements include such components as heat sinks, heating and refrigeration elements, insulators, heat reflectors, and absorbers. If heat is of a concern, a sensor should be regarded as a component of a larger device. In other words, heat conduction through the housing and the mounting elements, air convection, and radiative heat exchange with other objects should not be discounted (see discussion is Sect. 17.1).

**Fig. 3.14** Thermal model of a heating element



Heat may be transferred by three mechanisms: conduction, natural and forced convection, and thermal radiation (Sect. 4.12). For simple lumped parameter models, the first law of thermodynamics may be used to determine the temperature changes in a body. The rate of change of a body's internal energy is equal to the flow of heat into the body less the flow of heat out of the body, very much like fluid moves through pipes into and out of a tank. This balance may be expressed as

$$C \frac{dT}{dt} = \Delta Q, \quad (3.12)$$

where  $C = Mc$  is the thermal capacity of a body (J/K),  $T$  is the temperature (K),  $\Delta Q$  is the heat flow rate (W),  $M$  is the mass of the body (kg), and  $c$  is the specific heat of the material (J/kg K). The heat flow rate through a body is a function of the thermal resistance of the body. This is normally assumed to be linear, and therefore

$$\Delta Q = \frac{T_1 - T_2}{r}, \quad (3.13)$$

where  $r$  is the thermal resistance (K/W) and  $T_1 - T_2$  is a temperature gradient across the element, where heat conduction is considered.

For illustration, we analyze a heating element (Fig. 3.14) having temperature  $T_h$ . The element is coated with insulation. The temperature of the surrounding air is  $T_a$ . The value  $Q_1$  is the rate of heat supply to the element, and  $Q_0$  is the rate of heat loss. From Eq. (3.12) we get:

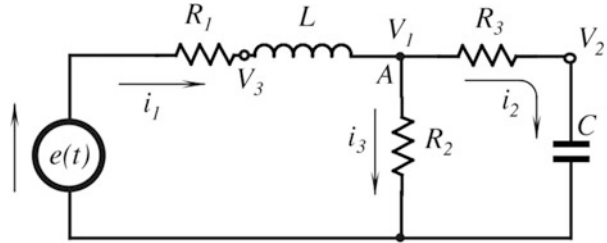
$$C \frac{dT_h}{dt} = Q_1 - Q_0, \quad (3.14)$$

but, from Eq. (3.13):

$$Q_0 = \frac{T_h - T_a}{r}, \quad (3.15)$$

and as a result, we obtain a differential equation:

**Fig. 3.15** Electrical circuit diagram with resistive, capacitive, and inductive components



$$\frac{dT_h}{dt} + \frac{T_h}{rC} = \frac{Q_1}{C} + \frac{T_a}{rC}, \quad (3.16)$$

This is a first-order differential equation which is typical for thermal systems. A thermal element, if not part of a control system with a feedback loop, is inherently stable. A response of a simple thermal element may be characterized by a thermal time constant which is a product of thermal capacity and thermal resistance:  $\tau_T = Cr$ . The time constant is measured in units of time (s) and, for a passively cooling element, is equal to time which takes to reach about 63 % of the initial temperature gradient.

### 3.17.3 Electrical Elements

There are three basic electrical elements: the capacitor, the inductor, and the resistor. Again, the governing equation describing the idealized elements are given in Table 3.3. For idealized elements, the equations describing the sensor's behavior may be obtained from the Kirchhoff's laws which directly follow from the law of conservation of energy:

*Kirchhoff's first law:* The total current flowing toward a junction is equal to the total current outflowing from that junction, i.e., the algebraic sum of the currents flowing through a junction is zero.

*Kirchhoff's second law:* In a closed circuit, the algebraic sum of the voltages across each part of the circuit is equal to the applied e.m.f.

Let us assume that we have a sensor whose elements may be represented by a circuit shown in Fig. 3.15. To find the circuit equation, we will use the first Kirchhoff's law, which sometimes is called Kirchhoff's current law. For the node, A

$$i_1 - i_2 - i_3 = 0, \quad (3.17)$$

and for each current

$$\begin{aligned}
 i_1 &= \frac{e - V_3}{R_1} = \frac{1}{L} \int (V_3 - V_1) dt \\
 i_2 &= \frac{V_1 - V_2}{R_3} = C \frac{dV_2}{dt} \\
 i_3 &= \frac{V_1}{R_2}.
 \end{aligned} \tag{3.18}$$

When these expressions are substituted into Eq. (3.17), the resulted equation becomes

$$\frac{V_3}{R_1} + \frac{V_1 - V_2}{R_3} + 2\frac{V_1}{R_2} + C \frac{dV_2}{dt} - \frac{1}{L} \int (V_3 - V_1) dt = \frac{e}{R_1}. \tag{3.19}$$

In the above equation,  $e/R_1$  is the forcing input, and the measurable outputs are  $V_1$ ,  $V_2$ , and  $V_3$ . To produce the above equation, three variables  $i_1$ ,  $i_2$ , and  $i_3$  have to be specified and three equations of motion derived. By applying Eq. (3.17) of constrain  $i_1 - i_2 - i_3 = 0$  it has been possible to condense all three equations of motion into a single expression. Note that each element in this expression has a unit of current (ampere).

### 3.17.4 Analogies

Above, we considered mechanical, thermal, and electrical elements separately. However, the dynamic behavior of these systems are analogous. It is possible, for example, to take mechanical elements or thermal components, convert them into an equivalent electric circuit, and analyze the circuit by using Kirchhoff's laws. Table 3.3 gives the various lumped parameters for the mechanical, thermal, and electrical circuits, together with their governing equations. For the mechanical components, Newton's second law was used and for thermal we apply Newton's law of cooling.

In the first column there are the linear mechanical elements and their equations in terms of force ( $F$ ). In the second column there are the linear thermal elements and their equations in terms of heat ( $Q$ ). In the third and fourth columns are the electrical analogies (capacitor, inductor, and resistor) in terms of voltage and current ( $V$  and  $i$ ). These analogies may be quite useful in a practical assessment of a sensor and for the analysis of its mechanical or thermal interface with the object and environment.

---

## 3.18 Environmental Factors

Every sensor is subject to various environmental influences during both a nonoperational storage and operational functionality. All possible environmental factors that may affect the sensor performance are generally specified by manufacturers.

*Storage conditions* are the nonoperating environmental limits to which a sensor may be subjected during a specified period without permanently altering its performance when operating under normal conditions. Usually, storage conditions include the highest and lowest storage temperatures and maximum relative humidities at these temperatures. Word “*noncondensing*” may be added to the relative humidity number. Depending on the sensor’s nature, some specific limitation for storage need to be considered. For instance, maximum pressure, presence of some gases, or contaminating fumes.

Short- and long-term stabilities (drifts) are parts of the accuracy specification. A *short-term stability* is manifested as changes in the sensor’s performance within minutes, hours, or even days. Eventually, it is another way to express repeatability (see above) as drift may be bidirectional. That is, the sensor’s output signal may increase or decrease, which in other terms may be described as ultralow frequency noise.

A *long-term stability* (aging) may be related to degrading of the sensor materials, which is an irreversible change in the material’s electrical, mechanical, chemical, or thermal properties. A long-term drift is usually unidirectional. It happens over a relatively long time span, such as months and years. A long-term stability is very important for sensors that are used for precision measurements. Aging greatly depends on the environmental storage and operating conditions, how well the sensor components are isolated from the environment, and what materials are used for their fabrication. Aging phenomenon is typical for sensors having organic components and, in general, is not an issue for a sensor made with only nonorganic materials. For instance, a glass-coated metal-oxide thermistor exhibits much greater long-term stability as compared with an epoxy-coated thermistor.

A powerful way of improving a long-term stability is to pre-age the sensor at extreme conditions. The extreme conditions may be cycled from the lowest to the highest. For instance, a sensor may be periodically swung from freezing to hot temperatures. Such an *accelerated aging* not only enhances stability of the sensor’s characteristics, but also improves reliability, as the pre-aging process reveals many hidden defects. For instance, stability of thermistors may be greatly improved if they are pre-aged at +150 °C for a month before they are calibrated and installed into a product.

Environmental conditions to which a sensor is subjected *during normal operation* do not include variables that the sensor measures. For instance, an air pressure sensor usually is subjected not only to air pressure, but to other influences as well, such as temperature of air, humidity, vibration, ionizing radiation, electromagnetic fields, gravitational forces, etc. All these factors may and usually do affect the sensor’s performance. Both static and dynamic variations of these conditions should be considered. Some environmental conditions usually are of a multiplicative nature, that is, they alter a transfer function of the sensor, for instance changing a sensitivity. One example is a resistive strain gauge whose sensitivity increases with temperature.

Environmental stability is a very important requirement. Both the sensor designer and application engineer should consider all possible external factors that may affect the sensor's performance. Take for example a piezoelectric accelerometer that may generate spurious signals if affected by a sudden change in ambient temperature, electrostatic discharge, triboelectric effect, vibration of a connecting cable, electromagnetic interferences (EMI), etc. Even if a manufacturer does not specify such effects, an application engineer should simulate them while prototyping the product. If, indeed, the environmental factors degrade the sensor's performance, additional corrective measures may be required (see Sect. 6.7). Examples are placing the sensor in a protective enclosure, electrical shielding, using a thermal insulation or thermostat, and employing a differential design.

Temperature effects must be known and accounted for. The operating temperature range is a span of the ambient temperatures given by their upper and lower extremes (" $-20$  to  $+150$  °C", e.g.) wherein the sensor maintains its specified accuracy. Many sensor characteristics change with temperature and their transfer functions may shift significantly. Special compensating elements are often incorporated either directly into the sensor or signal conditioning circuits, to compensate for temperature errors. The simplest way of specifying tolerances of thermal effects is provided by the error-band concept, which is simply the error band that is applicable over the operating temperature band. A temperature band may be divided into sections while the error band is separately specified for each section. For example, a sensor may be specified to have an accuracy of  $\pm 1\%$  in the range from  $0$  to  $50$  °C,  $\pm 2\%$  from  $-20$  to  $0$  °C, and from  $+50$  to  $100$  °C, and  $\pm 3\%$  beyond these ranges within the operating limits which are from  $-20$  to  $+150$  °C.

Temperatures will also affect the dynamic characteristics, particularly when they employ viscous damping. A relatively fast temperature change may cause the sensor to generate a spurious output signal. For instance, a dual pyroelectric sensor in an infrared motion detector is nearly insensitive to slow varying ambient temperature. However, when temperature changes fast, the sensor will generate electric current, that may be recognized by its processing circuit as a valid response, thus causing a false positive detection.

A *self-heating error* may be specified when an excitation signal is absorbed by a sensor and changes its temperature by such a degree that it may affect accuracy. For instance, a thermistor temperature sensor requires passage of electric current, causing a heat dissipation within the sensor's body. If a coupling with the environment is poor, the sensor's temperature may increase significantly due to a self-heating effect. This will result in errors since the sensor temperature will go up. A coupling with environment depends on the media where the sensor operates—a dry contact, liquid, air, etc. The worst thermal coupling may be through still air. For thermistors, the manufacturers often specify the self-heating errors in air, stirred liquid, or other media.

A resistive sensor's temperature increase above its surroundings may be found from formula:

$$\Delta t^\circ = \frac{V}{R(\xi v c + \alpha)} \quad (3.20)$$

where  $\xi$  is the sensor's mass density,  $c$  is specific heat,  $v$  is the volume of the sensor,  $\alpha$  is the coefficient of thermal coupling between the sensor and the outside (thermal conductivity),  $R$  is electrical resistance of the sensor, and  $V$  is the effective constant voltage across the resistance. If a self-heating results in errors, Eq. (3.20) may be used as a design guidance. For instance, to increase  $\alpha$ , a thermistor should be well coupled to the object by increasing the contact area, applying thermally conductive grease, or using thermally conductive adhesives. Also, the higher resistance sensors and lower measurement voltages are preferable.

## 3.19 Reliability

Reliability is ability of a product (sensor, e.g.) to perform a required function under stated conditions for a stated period of time. Reliability can be expressed in statistical terms as the probability that the device will function without failure over a specified time or a number of uses. Reliability specifies a *failure*—that is—a temporary or permanent malfunction of a sensor. While reliability is an important requirement, it is seldom specified however by the sensor manufacturers. The reason for that is, perhaps, the absence of a commonly accepted measure(s) for sensor reliability.

### 3.19.1 MTTF

For many repairable electronic devices, the procedure for predicting the in-service reliability is the MTBF (mean-time-between-failures) whose calculation is described in the MIL-HDBK-217 standard [3]. Since sensors are, as a rule, nonrepairable devices and so after a failure they should be replaced, not repaired. Thus sensors are more conveniently characterized by the MTTF—*mean-time to-failure*, an average time of operation before the device fails. The MTTF determines the dependability of the device and is computed as:

$$\text{MTTF} = \frac{1}{n} \sum_i (t_{fi} - t_{0i}) \quad (3.21)$$

where  $t_0$ —time of the test start,  $t_f$ —time of failure,  $n$ —total devices tested, and  $i$  is the number of a device. This means that each tested device shall run to its failure (recoverable or catastrophic) and the average work time till failure is computed.



The MTTF tests should be performed under the extreme (off normal or typical) operating conditions.

### 3.19.2 Extreme Testing

A device reliability can be inferred after tests at extreme conditions. One approach (suggested by MIL-STD-883 [4]) is 1000 h, loaded at maximum temperature. This test does not qualify, however, for such important impacts as rapid temperature changes and many other factors, like humidity, ionizing radiation, shock and vibrations, etc.

Extreme tests are especially helpful in the sensor design phase to uncover hidden problems. During the extreme tests, a sensor may be subjected to some strong environmental factors, which potentially can alter its performance or uncover hidden defects. Among additional tests that may reveal such issues are:

- High temperature/high humidity, while being fully electrically powered. For instance, a sensor may be subjected to its maximum allowable temperature at 85–90 % relative humidity (RH) and kept under these conditions during 500 h. This test is very useful for detecting contaminations and evaluation of packaging integrity. Failures are more likely to occur at 85 °C and 85 % RH. This test sometimes is called an “85–85 test (temperature-humidity bias)”.
- Mechanical shocks and vibrations may be used to simulate adverse environmental conditions, especially in evaluating wire bonds, adhesion of epoxy, etc. A sensor may be dropped to generate high-level accelerations (up to 3000 g’s of force). The drops should be made on different axes. Harmonic vibrations should be applied to the sensor over the range, which includes its natural frequency.
- Extreme storage conditions may be simulated, for instance at +100 and –40 °C while maintaining a sensor for at least 1000 h under these conditions. This test simulates storage and shipping conditions and usually is performed on nonoperating devices. The upper and lower temperature limits must be consistent with the sensor’s physical nature. For example, TGS pyroelectric sensors manufactured in the past by Philips were characterized by a Curie temperature of +60 °C. Approaching and surpassing this temperature resulted in a permanent destruction of the sensor sensitivity. Hence, temperature of such sensors should never exceed +50 °C which shall be clearly specified and marked on its packaging material.
- Thermal shock or temperature cycling (TC) is subjecting a sensor to alternate extreme conditions. For example, it may be dwelled for 30 min at –40 °C, then rapidly moved to +100 °C for 30 min, and then back to cold. The method must specify total number of cycling, like 100 or 1000. This test helps to uncover die bond, wire bond, epoxy connections, and packaging integrity.
- To simulate sea conditions, sensors may be subjected to a salt spray atmosphere for a specified time, for example 24 h. This helps to uncover its resistance to corrosion and structural defects.

### 3.19.3 Accelerated Life Testing

Another important method reliability of testing would be an accelerated life (AL) qualification. It is a procedure that emulates the sensor's operation, providing the real-world stresses, but compressing years into weeks. Three goals are behind such a test: to establish MTTF; identify first failure points that can then be remedied by the design changes; and identify the overall system practical lifetime.

#### 3.19.3.1 Environmental Acceleration

One possible way of compressing time is to use the same profile as the actual operating cycle, including maximum loading and power-on, power-off cycles, but expanded *environmental* highest and lowest ranges (temperature, humidity, and pressure). The highest and lowest limits should be substantially broader than normal operating conditions. Performance characteristics may be outside specifications, but must return to those when the device is brought back to the specified operating range. For example, if a sensor is specified to operate up to 50 °C at the highest relative humidity (RH) of 85 % at maximum supply voltage of +15 V, it may be cycled up to 100 °C a 99 % RH and at +18 V power supply (still lower than the maximum permissible voltages). To estimate number of the test cycles ( $n$ ), the following empirical formula developed by Sundstrand Corporation, Rockford, IL and Interpoint Corp., Redmond, WA [1] may be useful:

$$n = N \left( \frac{\Delta T_{\max}}{\Delta T_{\text{test}}} \right)^{2.5} \quad (3.22)$$

where  $N$  is the estimated number of cycles per lifetime,  $\Delta T_{\max}$  is the maximum specified temperature fluctuation, and  $\Delta T_{\text{test}}$  maximum cycled temperature fluctuation during the test. For instance, if the normal temperature is 25 °C, the maximum specified temperature is 50 °C, cycling was up to 100 °C, and over the lifetime (say, 10 years) the sensor was estimated being subjected to 20,000 cycles, then the number of test cycles is calculated as:

$$n = 20,000 \cdot \left( \frac{50 - 25}{100 - 25} \right)^{2.5} = 1283. \quad (3.23)$$

As a result, the accelerated life test requires about 1300 cycles instead of 20,000. It should be noted, however, that the 2.5 power factor was derived from a solder fatigue multiple, since that element is heavily influenced by cycling. Some sensors have no solder connections at all, while some might have components that are even more sensitive to cycling substances than solder, for instance, electrically conductive epoxy. Then, the factor should be selected somewhat smaller. As a result of the AL test, the reliability may be expressed as a probability of failure. For instance, if 2 out of 100 sensors (with an estimated lifetime of 10 years) failed the AL test, the

reliability is specified as 98 % over 10 years. For a better understanding of accelerated life tests and accelerated aging, refer to the excellent text [5]. Getting maximum reliability information in short time and at minimum cost is the major goal of a manufacturer. At the same time, it is impractical to wait for failures, when the lifetime of typical today's sensors is hundreds of thousands of hours. Accelerated testing is therefore both a must and a powerful means in production.

### 3.19.3.2 HALT Testing

To uncover potential problems during the R&D process, *Highly Accelerated Life Testing* (HALT) [6] is currently widely employed in different modifications. In this testing the sensor is considered as a “black box” with no regard to its internal structure or functionality. HALT is for determining the product's reliability weaknesses, assess its reliability limits, ruggedize the product by applying elevated stresses (not necessarily mechanical and not necessarily limited to the anticipated field stresses) that could cause field failures. HALT often involves transitional stressing, rapid thermal changes, and other means that enable one to carry out testing in a time and cost effective fashion. HALT is sometimes referred to as a “discovery” test. It is not a qualification test (QT) that is a “pass/fail” test essential in the product fabrication and reliability assurance. Over the years, HALT has demonstrated its ability to improve robustness through a “test-fail-fix” process, in which the applied stresses and stimuli are somewhat above the specified operating limits. This “somewhat above” is based, however, on the intuition, rather than on calculations. There is a general perception that HALT might be able to quickly precipitate and identify failures of different origins.

### 3.19.3.3 FOAT Testing

A highly focused and highly cost effective *failure-oriented accelerated testing* (FOAT) may be conducted in addition to and in some cases instead of HALT [7]. Unlike HALT, FOAT concerns with the actual physical or chemical effects inside the sensor. The testing is based on a theoretical model of the transfer function and other properties of the device that can be analytically or numerically modeled. The FOAT's objective is to use a particular predictive model (e.g., Arrhenius model) to confirm (after HALT is conducted) the actual mechanism of failure, and establish the numerical characteristics (activation energy, time constant, sensitivity factors, etc.) and to improve the design. The FOAT models allow to predict failures. Obviously, the major assumption is that the model is valid for the sensor at the actual operation conditions. Therefore, HALT can be used for “rough tuning” the device's reliability, while FOAT should be employed whenever a “fine tuning” is needed. FOAT and HALT could be carried out separately, or might be partially combined in a particular accelerated test effort.

Some useful failure predictions could be based on the recently suggested multiparametric Boltzmann-Arrhenius-Zhurkov (BAZ) model [8]. This model assumes that reliability of the device is based on FOAT and aimed at prediction of the probability of failure of the product.

## 3.20 Application Characteristics

Design, weight, and overall dimensions are geared to specific areas of applications. As indicated above in Sect. 3.1, mobile devices have a specific set of requirements to sensors. The overall dimensions and power consumption are just two of the critical requirements. Dimensions for such sensors shall be very small—on the order of several millimeters, while the supplied power typically should not exceed 10 mW.

Price may be a secondary issue when the sensor's reliability and accuracy are of a paramount importance. If a sensor is intended for a life support equipment, weapon or spacecraft, a high price tag may be well justified to assure high accuracy and reliability. On the other hand, for a very broad range of the high-volume consumer applications, including nearly all uses in mobile communication devices, the price of a sensor or sensing module may be a major decision factor of a design.

---

## 3.21 Uncertainty

Nothing is perfect in this World, at least in a sense that we perceive it. All materials are not exactly as we think they are. Our knowledge even of the purest of the materials is always approximate; machines are not perfect and never produce perfectly identical parts according to drawings. All components experience drifts related to the environment and their aging; external interferences may enter the system, alter its performance, and modify the output signal. Workers are not consistent and the human factor is nearly always present. Manufacturers fight an everlasting battle for the uniformity and consistency of the processes, yet the reality is that every part produced is never ideal and carries an uncertainty of its properties. Any measurement system consists of many components, including sensors. Thus, no matter how accurate the measurement is, it is only an approximation or estimate of the true value of the specific quantity subject to measurement, that is the stimulus or measurand. The result of measurement should be considered complete only when accompanied by a quantitative statement of its uncertainty. We simply never can be 100 % sure of the measured value.

When taking individual measurements (samples) under real conditions we expect that stimulus  $s$  is represented by the sensor as having a somewhat different value  $s'$ , so that error of measurement is expressed as

$$\delta = s' - s, \quad (3.24)$$

The difference between *error*, as defined by Eq. (3.24), and *uncertainty*, should always be clearly understood. An error can be compensated to a certain degree by correcting its systematic component. The result of such a correction can unknowably be very close to the unknown true value of the stimulus and thus it will have a very small error. Yet, in spite of a small error, the uncertainty of measurement may be very large since we cannot really trust that the error is indeed

that small. In other words, an error is what we unknowably get when we measure, while uncertainty is what we think how large that error might be [9].

The International Committee for Weight and Measures (CIPM) considers that uncertainty consists of many factors that can be grouped into two classes or types [10, 11]:

- A: those, which are evaluated by statistical methods;  
 B: those, which are evaluated by other means.

This division is not clear-cut and the borderline between A and B is somewhat illusive. Generally, A components of uncertainty arise from random effects, while the B components arise from systematic effects.

Type A uncertainty is generally specified by a standard deviation  $\sigma_i$ , equal to the positive square root of the statistically estimated variance  $\sigma_i^2$ , and the associated number of degrees of freedom  $\nu_i$ . For such a component the *standard uncertainty* is  $u_i = \sigma_i$ . Standard uncertainty represents each component of uncertainty that contributes to the total uncertainty of the measurement result.

Evaluation of a Type A standard uncertainty may be based on any valid statistical method for treating data. Examples are calculating standard deviation of the mean of a series of independent observations, using the method of least squares. If the measurement situation is especially complicated, one should consider obtaining the guidance of a statistician.

Evaluation of a Type B of standard uncertainty is usually based on scientific judgment using all the relevant information available, such may include

- Previous measurement data.
- Experience with or general knowledge of the behavior and property of relevant sensors, materials, and instruments.
- Manufacturer's specifications.
- Data obtained during calibration and other reports.
- Uncertainties assigned to reference data taken from handbooks and manuals.

For detailed guidance of assessing and specifying standard uncertainties one should consult specialized texts, for instance [12].

When both A and B uncertainties are evaluated, they should be combined to represent the *combined standard uncertainty*. This can be done by using a conventional method for combining standard deviations. This method is often called the law of propagation of uncertainty and in common parlance is known as "root-sum-of-squares" or "RSS" method of combining uncertainty components estimated as standard deviations:

$$u_c = \sqrt{u_1^2 + u_2^2 + \cdots + u_i^2 + \cdots + u_n^2}, \quad (3.25)$$

where  $n$  is a number of standard uncertainties in the uncertainty budget.

**Table 3.4** Uncertainty budget for a thermistor thermometer

Source of uncertainty	Standard uncertainty (°C)	Type
<i>Calibration of sensor</i>		
Reference temperature source	0.03	A
Coupling between reference and sensor	0.02	A
<i>Measured errors</i>		
Repeated observations	0.02	A
Sensor inherent noise	0.01	A
Amplifier noise	0.005	A
DVM error	0.005	A
Sensor aging	0.025	B
Thermal loss through connecting wires	0.015	A
Dynamic error due to sensor's inertia	0.005	B
Transmitted noise	0.02	A
Misfit of transfer function	0.02	B
<i>Ambient drifts</i>		
Voltage reference	0.01	A
Bridge resistors	0.01	A
Dielectric absorption in A/D capacitor	0.005	B
Digital resolution	0.01	A
<i>Combined standard uncertainty</i>	<b>0.062</b>	

To illustrate the concept, Table 3.4 shows an example of the uncertainty budget for an electronic thermometer with a thermistor sensor, which measures temperature of a water bath. While compiling such a table one shall be very careful not to oversee any standard uncertainty not only in a sensor, but also in the interface instrument, experimental setup, and the object of measurement. This shall be done for various environmental conditions, which may include temperature, humidity, atmospheric pressure, power supply variations, transmitted noise, aging, and many other factors.

No matter how accurately any individual measurement is made, that is, how close the measured temperature is to true temperature of an object, one never can be sure that it is indeed accurate. The combined standard uncertainty of 0.062 °C does not mean that error of measurement is no greater than 0.062 °C. That value is just a standard deviation and if an observer has enough patience she may find that individual errors may be much larger. The word “uncertainty” by its very nature implies that the uncertainty of the measurement is an estimate and generally does not have well-defined limits.

---

## References

1. Fraden, J. (2015). Medical sensors for mobile communication devices, Chapt. D-11. In H. Eren & J. G. Webster (Eds.), *The E-medicine, E-health, M-health, telemedicine and telehealth handbook*. Boca Raton, FL: CRC Press.

2. Fraden, J., et al. (2012, September 25). Wireless communication device with integrated electromagnetic sensors. *U.S. Patent No. 8,275,413*.
3. U.S. Dept. of Defense. (1991, December 2). *Military handbook. Reliability prediction of electronic equipment* (Mil-HDBK-217F).
4. Department of Defense. (1996, December 31). *Test method standard. Microcircuits* (MIL-STD-883E).
5. Suhir, E. (2007). How to make a device into a product. Accelerated life testing (ALT), its role attributes, challenges, pitfalls and interaction with qualification tests, Chapt. 8. In E. Suhir, Y. C. Lee, & C. P. Wong (Eds.), *Micro- and opto-electronic materials and structures: physics, mechanics, design, reliability, packaging* (Vol. 2, pp. 203–230). New York: Springer.
6. Suhir, E., et al. (2014, March). *Highly accelerated life testing (HALT), failure oriented accelerated Testing (FOAT), and their role in making a viable device into a reliable product*. 2014 I.E. Aerospace Conference, Big Sky, Montana.
7. Suhir, E. (2014, March 9–13). *Failure-oriented-accelerated-testing (FOAT) and its role in making a viable IC package into a reliable product*. SEMI-THERM 2014, San Jose, CA.
8. Suhir, E., et al. (2014, March). *Application of multi-parametric BAZ Model in aerospace optoelectronics*. IEEE Aerospace Conference, Big Sky, Montana.
9. Taylor, B. N., et al. (1994). *Guidelines for evaluation and expressing the uncertainty of NIST Measurement Results* (NIST Technical Note 1297).
10. CIPM. (1981). *BIPM Proc.-Verb. Com. Int. Poids et Mesures* (in French) 49, 8–9, No. 26.
11. International Organization for Standardization. (1993). *ISO Guide to the expression of uncertainty in measurements*. Geneva, Switzerland: Author.
12. Better reliability via system tests. (1991, August 19). *Electronic Engineering Times*, CMP Publication, 40–41.

*“The way we have to describe Nature is generally incomprehensible to us.”*

—Richard P. Feynman,  
“QED. The Strange Theory of Light and Matter”

*“It should be possible to explain the laws of physics to a barmaid.”*

—Albert Einstein

Since a sensor is a converter of generally nonelectrical effects into electrical signals, one and often several transformation steps are required before the electric output signal can be generated. These steps involve changes of types of energy or physical properties of materials, wherein the final step shall produce electrical signal of a desirable format. As it was mentioned in Chap. 1, generally there are two types of sensors: *direct* and *complex*. A direct sensor is the one that can directly convert a nonelectrical stimulus into electric output signal. Many stimuli cannot be directly converted into electricity, thus multiple conversion steps would be required. If, for instance, one wants to detect displacement of an opaque object, a fiber optic sensor can be employed. A pilot light beam (excitation signal) is generated by the light emitting diode (LED). Then the light flux enters the optical fiber and propagates through it, then exits toward the object and is reflected from its surface. The reflected photon flux enters the receiving optical fiber and propagates toward a photodiode, where it is detected to produce electric current representing a distance from the fiber optic end to the object. We see that such a sensor involves transformation of electrical current into photons, propagation of photons through some refractive media (the fiber), reflection from the object, propagation again through the fiber, and conversion back into electric current. Therefore, such a sensing process includes two energy conversion steps and also manipulation of light.



There are several physical effects that result in a direct generation of electrical signals in response to nonelectrical influences and thus can be used in direct sensors. Examples are thermoelectric (Seebeck) effect, piezoelectricity, and photoeffect. Other conversions of energy that do not produce electric output are performed by devices known as *transducers*. The physical effects that can be used to convert one type of energy or property into another nonelectrical energy or property are outside of the scope of this book. However, since the optical transducers are often used in many sensors, in the next chapter we will examine them in greater detail.

In this chapter we describe various physical effects that can be used for a *direct* conversion of stimuli into electric signals. Since all such effects are based on fundamental principles of physics, first we briefly review these principles.

---

## 4.1 Electric Charges, Fields, and Potentials

There is a well-known phenomenon to those who live in dry climates—the possibility of the generation of sparks by friction involved in walking across the carpet. This is a result of the so-called *triboelectric effect* that is a process of an electric charge separation<sup>1</sup> due to object movements, friction of clothing fibers, air turbulence, atmosphere electricity, etc. There are two kinds of charges. Like charges repel and the unlike charges attract each other. Benjamin Franklin (1706–1790), among his other remarkable achievements, was the first American physicist. He named one charge *negative* and the other *positive*. These names have remained to this day. He made an elegant experiment with a kite flying in a thunderstorm to prove that the atmospheric electricity is of the same kind as produced by friction. In doing the experiment, Franklin was extremely lucky, as several Europeans who were trying to repeat his test were severely injured by the lightning and one was killed.<sup>2</sup>

A triboelectric effect is a result of a mechanical charge redistribution. For instance, rubbing a glass rod with silk strips off electrons from the surface of the rod, thus leaving an abundance of positive charges, i.e., giving the rod a positive charge. It should be noted that the electric charge is conserved—it is neither created nor destroyed. Electric charges can be only moved from one place to another. Giving negative charge means taking electrons from one object and placing them onto another (charging it negatively). The object, which loses some amount of electrons, is said gets a positive charge.

A triboelectric effect influences an extremely small number of electrons as compared with the total electronic charge in an object. Actual amount of charges in any object is very large. To illustrate this let us consider a total number of

---

<sup>1</sup> Prefix *tribo-* means “friction”.

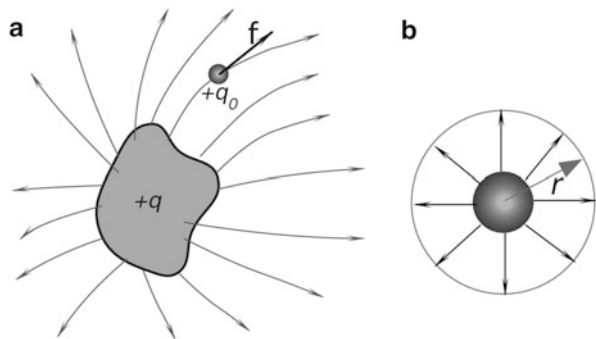
<sup>2</sup> A Russian physicist of German extraction Georg Wilhelm Richmann (1711–1753) was killed in St. Petersburg during a thunderstorm experiment when a ball lightning having a size of a fist jumped from the electrometer and struck him in a forehead.

electrons in an old US copper penny<sup>3</sup> [1]. The coin weighs 3.1 g, therefore, it can be shown that the total number of atoms in it is about  $2.9 \times 10^{22}$ . A copper atom has a positive nuclear charge of  $4.6 \times 10^{-18}$  C and, respectively, the same electronic charge of the opposite polarity. A combined charge of all electrons in a penny is  $q = (4.6 \times 10^{-18} \text{ C/atom}) (2.9 \times 10^{22} \text{ atoms}) = 1.3 \times 10^5 \text{ C}$ , a very large charge indeed. This electronic charge from a single copper penny may generate sufficient current of 0.91 A to operate a 100 W light bulb for 40 h.

With respect to electric charges, there are three kinds of materials: *conductors*, *isolators*, and *semiconductors*. In conductors, electric charges (electrons) are free to move through the material, whereas in isolators they are not. Although there is no perfect isolator, the isolating ability of fused quartz is about  $10^{25}$  times as great as that of copper, so that for practical purposes many materials are considered perfect isolators. The semiconductors are intermediate between conductors and isolators in their ability to conduct electricity. Among the elements, silicon and germanium are well-known examples. In semiconductors, the electrical conductivity may be greatly increased by adding small amounts of other elements, traces of arsenic or boron are often added to silicon for this purpose. For the sensing technologies, semiconductors are very interesting materials because their ability to conduct electricity can be manipulated by applying external inputs, like electric and magnetic fields and light.

Figure 4.1a shows an object which carries a positive electric charge  $q$ . If a small *positive* electric test charge  $q_0$  is positioned in the vicinity of a charged object, it will be subjected to a repelling electric force. If we place a negative charge on the object, it will attract the test charge. In a vector form,<sup>4</sup> the repelling (or attracting) force is shown as  $\mathbf{f}$ . A fact that the test charge is subjected to force without a physical contact between charges means that the volume of space which is occupied by the test charge may be characterized by a so-called *electric field*.

**Fig. 4.1** Positive test charge in vicinity of charged object (a) and electric field of spherical object (b)



<sup>3</sup> Now, the U.S. pennies are just copper-plated (2.5 % of copper), but till 1982 they did contain 95 % of copper.

<sup>4</sup> The bold face indicates a vector notation.

The electric field in each point is defined through the force as

$$\mathbf{E} = \frac{\mathbf{f}}{q_0}. \quad (4.1)$$

Here  $\mathbf{E}$  is vector of the same direction as  $\mathbf{f}$  because  $q_0$  is scalar. Formula (4.1) expresses an electric field as a force divided by a property of a test charge. The test charge must be very small not to disturb the electric field. Ideally, it should be infinitely small, however, since the charge is quantized, we cannot contemplate a free test charge whose magnitude is smaller than the electronic charge:  $e = 1.602 \times 10^{-19}$  C.

The field is indicated in Fig. 4.1a by the *field lines*, which in every point of space are tangent to the vector of force. By definition, the field lines start on the positive object and end on the negative. The density of field lines indicates the magnitude of electric field  $\mathbf{E}$  in any particular volume of space.

For a physicist, any field is a physical quantity that can be specified simultaneously for all points within a given region of interest. Examples are pressure field, temperature field, electric field, and magnetic field. A field variable may be a scalar (for instance, temperature field) or a vector (for instance, a gravitational field around the earth). The field variable may or may not change with time. A vector field may be characterized by a distribution of vectors, which form the so-called flux (symbol  $\Phi$ ). Flux is a convenient description of many fields, such as electric, magnetic, thermal, etc. The word flux is derived from the Latin word *fluere* (to flow). A familiar analogy of flux is a stationary, uniform field of fluid flow (water) characterized by a constant flow vector  $\mathbf{v}$ , the constant velocity of the fluid at any given point. In case of electric field, nothing flows in a formal sense. If we use  $\mathbf{E}$  – vector representing electric field – the field lines form flux. If we imagine a hypothetical closed surface (Gaussian surface)  $S$ , a connection between the charge  $q$  and flux can be established as

$$\varepsilon_0 \Phi_E = q, \quad (4.2)$$

where  $\varepsilon_0 = 8.8541878 \times 10^{-12}$  C<sup>2</sup>/Nm<sup>2</sup> is the vacuum permittivity constant. By integrating flux over the surface we arrive at:

$$\varepsilon_0 \oint \mathbf{E} ds = q, \quad (4.3)$$

where the integral is equal to  $\Phi_E$ . In the above equations, known as Gauss' law, charge  $q$  is the net charge surrounded by the Gaussian surface. If a surface encloses equal and opposite charges, the net flux  $\Phi_E$  is zero. The charge outside the surface makes no contribution to the value of  $q$ , nor does the exact location of the inside charges affect this value. Gauss' law can be used to make an important prediction, namely: *An exact charge on an insulated conductor is in equilibrium, entirely on its outer surface.* This hypothesis was shown to be true even before either Gauss' law or Coulomb law was advanced. The Coulomb law itself can be derived from the

Gauss' law. It states that the force acting on a test charge is inversely proportional to a squared distance from the charge

$$f = \frac{1}{4\pi\epsilon_0} \frac{qq_0}{r^2}. \quad (4.4)$$

Another result of Gauss' law is that the electric field outside any spherically symmetrical distribution of charge, Fig. 4.1b, is directed radially and has magnitude (note that magnitude is not a vector)

$$E = \frac{1}{4\pi\epsilon_0} \frac{q}{r^2}, \quad (4.5)$$

where  $r$  is the distance from the sphere's center.

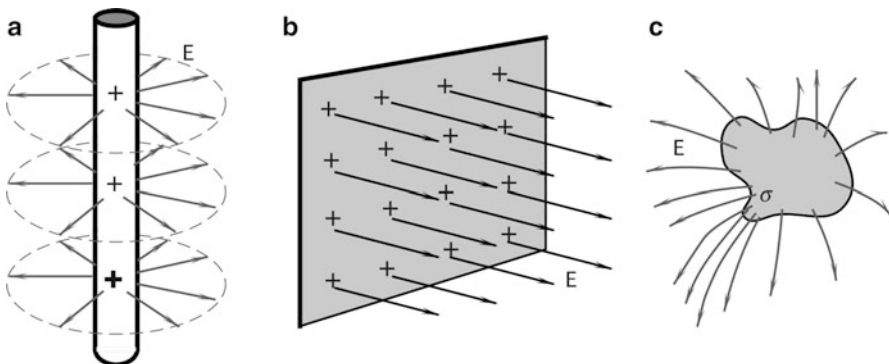
Similarly, the electric field inside a uniform sphere of charge  $q$  is directed radially and has magnitude

$$E = \frac{1}{4\pi\epsilon_0} \frac{qr}{R^3}, \quad (4.6)$$

where  $R$  is the sphere's radius and  $r$  is the distance from the sphere's center. It should be noted that electric field in the center of the sphere ( $r = 0$ ) is equal to zero.

If electric charge is distributed along an infinite (or, for the practical purposes, long) line (Fig. 4.2a), the electric field is directed perpendicularly to the line and has the magnitude

$$E = \frac{\lambda}{2\pi\epsilon_0 r}, \quad (4.7)$$



**Fig. 4.2** Electric field around infinite line (a) and near-infinite sheet (b). Pointed conductor concentrates electric field (c)

where  $r$  is the distance from the line and  $\lambda$  is the linear charge density (charge per unit length).

The electric field resulted from an infinite sheet of charge, Fig. 4.2b, is perpendicular to the plane of the sheet and has magnitude

$$E = \frac{\sigma}{2\epsilon_0}, \quad (4.8)$$

where  $\sigma$  is the surface charge density (charge per unit area). However, for an isolated conductive object, the electric field is two times stronger

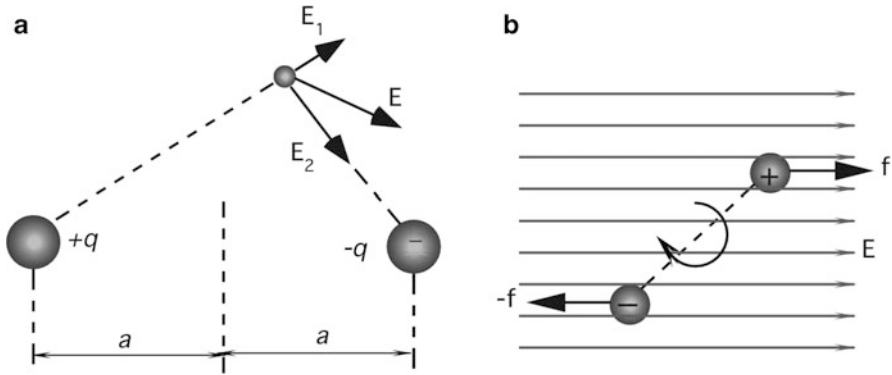
$$E = \frac{\sigma}{\epsilon_0}. \quad (4.9)$$

The apparent difference between electric fields is a result of different geometries—the former is an infinite sheet and the latter is an object of an arbitrary shape. A very important consequence of Gauss' law is that electric charges are distributed only on the outside surface. This is a result of repelling forces between charges of the same sign—all charges try to move as far as possible from one another. The only way to do this is to move to the foremost distant place in the material, which is the outer surface. Of all places on the outer surface the most preferable places are the areas with the highest curvatures. This is why pointed conductors are the best concentrators of the electric field as in Fig. 4.2c. A very useful scientific and engineering tool that is based on this effect is a Faraday cage—a room entirely covered by either grounded conductive sheets or a metal net. No matter how strong the external electric field, it will be essentially zero inside the cage. This makes metal airplanes, cars, and ships the best protectors during thunderstorms, because they act as virtual Faraday cages. It should be remembered, however, that the Faraday cage, while being a perfect shield against electric fields, is of little use to protect against magnetic fields, unless it is made of a thick ferromagnetic material.

An *electric dipole* is a combination of two opposite charges, which are placed at a distance  $2a$  apart, Fig. 4.3a. Each charge will act on a test charge with force that defines electric fields  $\mathbf{E}_1$  and  $\mathbf{E}_2$  produced by the individual charges. A combined electric field of a dipole,  $\mathbf{E}$ , is a vector sum of two fields. The magnitude of the field is

$$E = \frac{1}{4\pi\epsilon_0} \frac{2aq}{r^3}, \quad (4.10)$$

where  $r$  is the distance from the center of the dipole. The essential properties of the charge distribution are magnitude of the charge  $q$  and the separation  $2a$ . In formula (4.10) charge and distance are entered only as a product. This means that, if we measure  $E$  at various distances from the electric dipole (assuming that distance is much longer than  $a$ ), we can never deduce  $q$  and  $2a$  separately, but only the product  $2aq$ . For instance, if  $q$  is doubled and  $a$  is cut in half, the electric field will not



**Fig. 4.3** Electric dipole (a); electric dipole in electric field is subjected to rotating force (b)

change. The product  $2aq$  is called the electric dipole moment  $p$ . Thus, Eq. (4.10) can be rewritten as

$$E = \frac{1}{4\epsilon_0 r^3} p \quad (4.11)$$

The spatial position of a dipole may be specified by its moment in a vector form:  $\mathbf{p}$ . Not all materials have a dipole moment; gases such as methane, acetylene, ethylene, carbon dioxide, and many others have no dipole moment. On the other hand, carbon monoxide has a weak dipole moment ( $0.37 \times 10^{-30}$  C m) and water has a strong dipole moment ( $6.17 \times 10^{-30}$  C m).

Dipoles are found in crystalline materials and form a foundation for such sensors as piezo- and pyroelectric detectors. Usually, a dipole is part of a crystal, which defines its initial orientation. When a dipole is placed in an electric field, it becomes subjected to a rotation force: Fig. 4.3b. An electric field, if strong enough, will align the dipole along its lines. Torque which acts on a dipole in a vector form is

$$\boldsymbol{\tau} = \mathbf{p} \times \mathbf{E}. \quad (4.12)$$

Work must be done by an external agent to change the orientation of an electric dipole in an external electric field. This work is stored as potential energy  $U$  in the system consisting of the dipole and the arrangement used to set up the external field. In a vector form this potential energy is

$$U = -\mathbf{p} \cdot \mathbf{E}. \quad (4.13)$$

A process of dipole orientation is called *poling*. The aligning electric field must be strong enough to overcome a retaining force in the crystalline structure of the material. To ease this process, the material during the poling is heated to increase mobility of its molecular structure. The poling of a ceramic or crystalline polymer is used in fabrication of piezo- and pyroelectric materials.

The electric field around the charged object can be described not only by the vector  $\mathbf{E}$ , but by a scalar quantity, the *electric potential*  $V$  as well. Both quantities are intimately related and usually it is a matter of convenience which one to use in practice. A potential is rarely used as a description of an electric field in a specific point of space, however, a potential difference (*voltage*) between two points is the most common quantity in electrical engineering practice. To find the voltage between two arbitrary points, we may use the same technique as above—a small positive test charge  $q_0$ . If the electric charge is positioned in point A, it stays in equilibrium being under influence of force  $q_0\mathbf{E}$ . It may remain there theoretically infinitely long. Now, if we try to move it to another point B, we have to work against the electric field. Work,  $-W_{AB}$ , which is done against the field (that is why it has a negative sign) to move the charge from A to B defines voltage between these two points

$$V_B - V_A = -\frac{W_{AB}}{q_0}. \quad (4.14)$$

Correspondingly, the electrical potential at point B is smaller than at point A. The SI unit for voltage is  $1 \text{ V} = 1 \text{ J/C}$ . For convenience, point A is chosen to be very far away from all charges (theoretically at an infinite distance) and the electric potential at that point is considered to be zero. This allows us to define electric potential at any other point as

$$V = -\frac{W}{q_0}. \quad (4.15)$$

This equation tells us that the potential near the positive charge is positive, because moving the positive test charge from infinity to the point in a field, must be made against a repelling force. This will cancel the negative sign in Eq. (4.15). It should be noted that the potential difference between two points is independent on a path at which the test charge is moving. It is strictly a description of the electric field difference between the two points. If we travel through the electric field along a straight line and measure  $V$  as we go, the rate of change of  $V$  with distance  $l$  that we observe is the components of  $\mathbf{E}$  in that direction

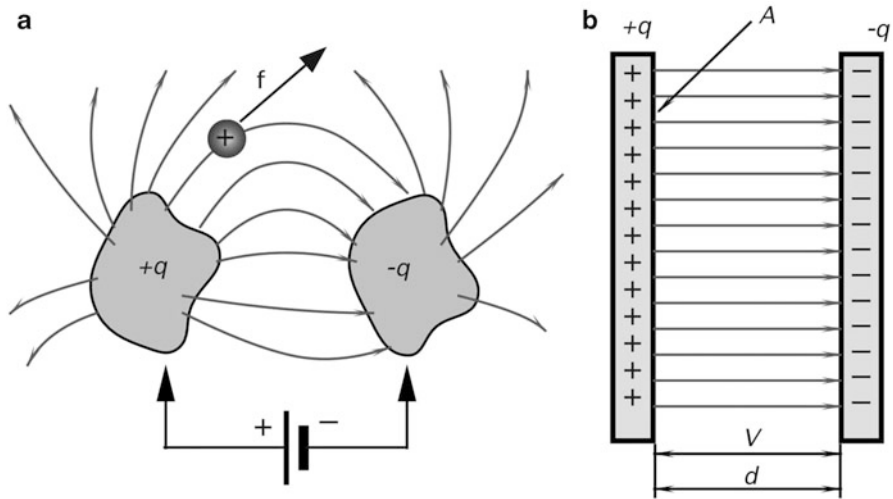
$$E_l = -\frac{dV}{dl}. \quad (4.16)$$

The minus sign tells us that  $\mathbf{E}$  points in the direction of decreasing  $V$ . As it follows from Eq. (4.16), the appropriate unit for electric field is volts/meter (V/m).

---

## 4.2 Capacitance

Let us take two isolated conductive objects of arbitrary shape (plates) and connect them to the opposite poles of a battery, Fig. 4.4a. The plates will receive equal amounts of opposite charges. That is, a negatively charged plate will receive



**Fig. 4.4** Electric charge and voltage define capacitance between two objects (a); parallel-plate capacitor (b)

additional electrons while there will be a deficiency of electrons in the positively charged plate. Now, let us disconnect the battery. If the plates are totally isolated and exist in a vacuum, they will remain charged theoretically infinitely long. A combination of the plates, which can hold an electric charge, is called a *capacitor*. If a small *positive* electric test charge,  $q_0$ , is positioned between the charged objects, it will be subjected to an electric force from the positive plate to the negative. The positive plate will repel the positive test charge and the negative will attract it, thus resulting in a combined push-pull force. Depending on the position of the test charge between the oppositely charged objects, the force will have a specific magnitude and direction that is characterized by vector  $\mathbf{f}$ .

The capacitor may be characterized by  $q$ , the magnitude of charge on either conductor, shown in Fig. 4.4a, and by  $V$ , the positive potential difference between the conductors. It should be noted that  $q$  is not a net charge on the capacitor, which is zero. Further,  $V$  is not the potential of either plate, but the potential *difference* between them. The ratio of charge to voltage is constant for each capacitor:

$$\frac{q}{V} = C. \quad (4.17)$$

This fixed ratio,  $C$  is called the *capacitance* of the capacitor. Its value depends on the shapes and relative position of the plates. The ratio,  $C$ , also depends on the medium in which the plates are immersed. Note, that  $C$  is always positive since we use the same sign for both  $q$  and  $V$ . The SI unit for capacitance is  $1 \text{ F} = 1 \text{ C/V}$  which is represented by the abbreviation F. A farad is a very large capacitance, hence, in practice submultiples of the farad are generally used:



1 picofarad (pF)	$10^{-12}$ F
1 nanofarad (nF)	$10^{-9}$ F
1 microfarad ( $\mu$ F)	$10^{-6}$ F

When connected into an electronic circuit, capacitance may be represented as a *complex resistance*  $Z$ .

$$Z_c = \frac{V}{i} = -\frac{1}{j\omega C}, \quad (4.18)$$

where  $j = \sqrt{-1}$  and  $i$  is the sinusoidal current having a frequency of  $\omega$ , meaning that the complex resistance of a capacitor drops at higher frequencies. This is called Ohm's law for the capacitor. The minus sign and complex argument indicate that the voltage across the capacitor lags by  $90^\circ$  behind the current.

Capacitance is a very useful physical phenomenon in the sensor designer's toolbox. Manipulating capacitance, according to Eq. (4.18), allows a direct conversion of an input stimulus into electric voltage or current. A capacitive sensor can be successfully employed for measuring distance, area, volume, pressure, force, chemical composition, etc. The following background establishes fundamental properties of a capacitor and gives few useful formulas.

### 4.2.1 Capacitor

Figure 4.4b shows a parallel-plate capacitor in which the conductors take the form of two plane parallel plates of area  $A$  separated by a distance  $d$ . If  $d$  is much smaller than the plate dimensions, the electric field between the plates will be uniform, which means that the field lines (lines of force  $\mathbf{f}$ ) will be parallel and evenly spaced. The laws of electromagnetism require that there be some "fringing" of the lines at the edges of the plates, but for a small enough  $d$  we can neglect it for our present purpose.

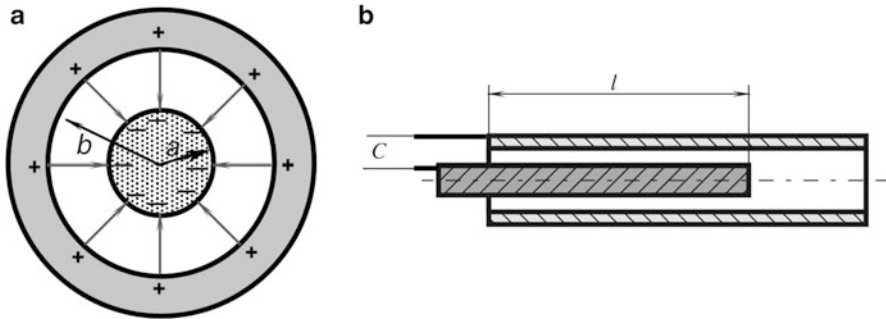
To calculate the capacitance we must relate  $V$  (the potential difference between the plates) to  $q$ , which is charge on the capacitor as in Eq. (4.17):

$$C = \frac{q}{V}. \quad (4.19)$$

Alternatively, the capacitance of a flat capacitor in vacuum can be found from

$$C = \frac{\epsilon_0 A}{d}. \quad (4.20)$$

It could be jokingly said that to make a capacitive sensor one needs a bad capacitor; traditionally all electronic components are fabricated as insensitive as possible to any environmental influences. Yet, to make a sensor—one of the capacitor parameters should be "spoiled"—so the capacitance will change under an external influence. In a capacitive sensor, capacitance is modulated (modified) by an



**Fig. 4.5** Cylindrical capacitor (a); capacitive displacement sensor (b)

external stimulus or by a signal from an intermediate transducer. Thus, to vary capacitance, the stimulus needs to change one of the parameters that define the capacitance. These parameters for a flat-plate capacitor are established by the key formula (4.20). It shows a relationship between the plate area and distance between the plates. Varying one of them will change the capacitance that according to Eq. (4.19) affects voltage  $V$  that in turn can be measured quite accurately by an appropriate circuit. It should be noted that Eq. (4.20) holds only for capacitors of the parallel-plate type with nothing in-between the plates. A change in geometry will require different formulas. A ratio,  $A/d$ , may be called a geometry factor for a parallel-plate capacitor.

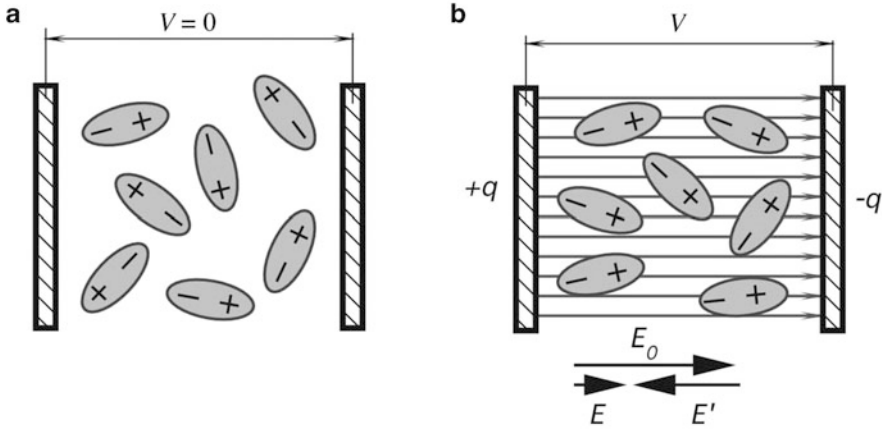
A cylindrical capacitor which is shown in Fig. 4.5a consists of two coaxial cylinders of radii  $a$  and  $b$ , and length  $l$ . For the case when  $l \gg b$  we can ignore fringing effects and calculate capacitance from the following formula:

$$C = \frac{2\pi\epsilon_0 l}{\ln \frac{b}{a}}. \quad (4.21)$$

In this formula  $l$  has a meaning of length of the overlapping conductors (Fig. 4.5b) and  $2\pi l(\ln b/a)^{-1}$  may be called a geometry factor for a coaxial capacitor. A useful displacement sensor can be built with such a capacitor if the inner conductor can be made movable in and out of the outer conductor. According to Eq. (4.21), capacitance of such a sensor is in a linear relationship with the displacement,  $l$ . It should be noted however that the cylindrical capacitive displacement sensor is not a very practical device, because it is technologically challenging to fabricate a coaxial structure by using MEMS technologies (Chap. 19).

## 4.2.2 Dielectric Constant

Equation (4.20) holds for a parallel-plate capacitor with its plates in vacuum (or air, for most practical purposes). In 1837, Michael Faraday first investigated the effect of completely filling the space between the plates with a dielectric. He had found



**Fig. 4.6** Polarization of dielectric. Dipoles are randomly oriented without external electric field (a); dipoles align with electric field (b)

that the effect of the filling is to increase the capacitance of the device by a factor of  $\kappa$ , which is known as the dielectric constant of the material.

The increase in capacitance due to the dielectric presence is a result of molecular polarization. In some dielectrics (for instance, in water), molecules have a permanent dipole moment, while in other dielectrics, molecules become polarized only when an external electric field is applied. Such polarization is called *induced*. In both cases, either permanent electric dipoles or those acquired by induction tend to align molecules with an external electric field. This process is called *dielectric polarization*. It is illustrated in Fig. 4.6a that shows the permanent dipoles before and in Fig. 4.6b after an external electric field is applied to the capacitor. In the former case, there is no electric field between the capacitor plates and all dipoles are randomly oriented. After the capacitor is charged, the dipoles will align with the electric field lines, however, thermal agitation will prevent a complete alignment. Each dipole forms its own electric field which is predominantly oppositely directed with the external electric field,  $\mathbf{E}_0$ . Due to a combined effect of a large number of dipoles ( $\mathbf{E}'$ ), the electric field in the capacitor becomes weaker ( $\mathbf{E} = \mathbf{E}_0 + \mathbf{E}'$ ), where the field,  $\mathbf{E}_0$ , would be in the capacitor without the dielectric.

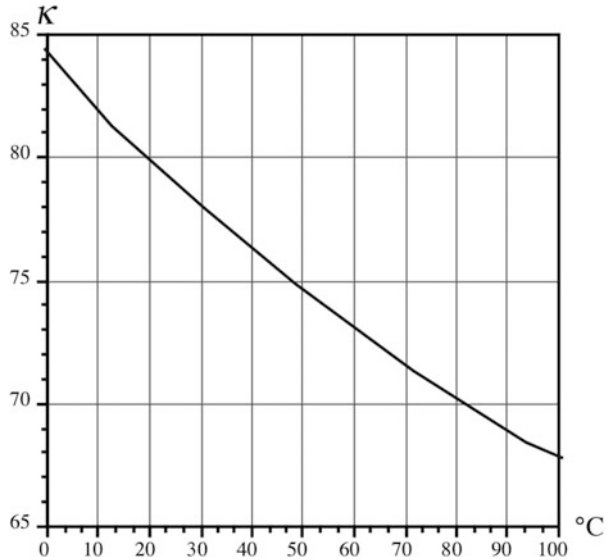
Reduced electric field leads to a smaller voltage across the capacitor:  $V = V_0/\kappa$ . Substituting it into Eq. (4.19) we arrive at the expression for a capacitor with dielectric

$$C = \kappa \frac{q}{V_0} = \kappa C_0. \quad (4.22)$$

For the parallel-plate capacitor we thus have

$$C = \kappa \epsilon_0 \frac{A}{d}. \quad (4.23)$$

**Fig. 4.7** Dielectric constant of water as a function of temperature



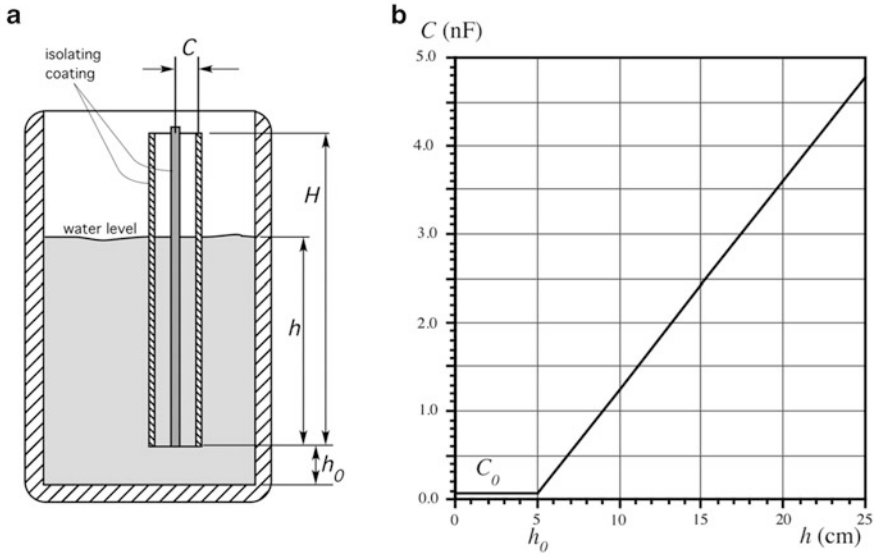
In a more general form, the capacitance between two objects of any shape may be expressed through a geometry factor,  $G$

$$C = \epsilon_0 \kappa G, \quad (4.24)$$

where  $G$  depends on the shape of the objects and their separation. Thus, Eq. (4.24) establishes that a capacitance can also be modulated by varying the geometry and the dielectric constant,  $\kappa$ . Table A.5 gives dielectric constants,  $\kappa$ , for different materials. Since the dielectric constant depends on material, temperature, and humidity/moisture content—all these variables can be used in the capacitive sensors as inputs to modulate capacitance.

Dielectric constants must be specified for a test frequency and temperature. Some dielectrics have a very uniform dielectric constant over a broad frequency range (for instance, polyethylene), while others display strong negative frequency dependence, that is, a dielectric constant decreases with frequency. Temperature dependence is also negative. Figure 4.7 illustrates  $\kappa$  for water as function of temperature.

To illustrate how capacitance can be employed in sensing, consider a capacitive water level sensor, Fig. 4.8a. The sensor is fabricated in form of a coaxial capacitor where the surface of each conductor (electrode) is coated with a thin isolating layer to prevent electric short circuit through water. The isolator is a dielectric, which we disregard in the following analysis because it does not change in the process of measurement. The coaxial sensor is immersed in a water tank so that water can fill in-between the capacitive electrodes. When water level increases, water fills more and more space between the sensor's conductors, thus changing the average dielectric constant between the conductors and according to Eq. (4.24)



**Fig. 4.8** Capacitive water level sensor (a); capacitance as function of water level (b) (sensor’s dimensions are  $a = 10$  mm,  $b = 12$  mm,  $H = 200$  mm, liquid—water)

subsequently changing the sensor’s capacitance). Total capacitance of the coaxial sensor is

$$C_h = C_1 + C_2 = \epsilon_0 G_1 + \epsilon_0 \kappa G_2, \tag{4.25}$$

where  $C_1$  is capacitance of the water-free portion of the sensor and  $C_2$  is capacitance of the water-filled portion. The corresponding geometry factors are designated  $G_1$  and  $G_2$ .

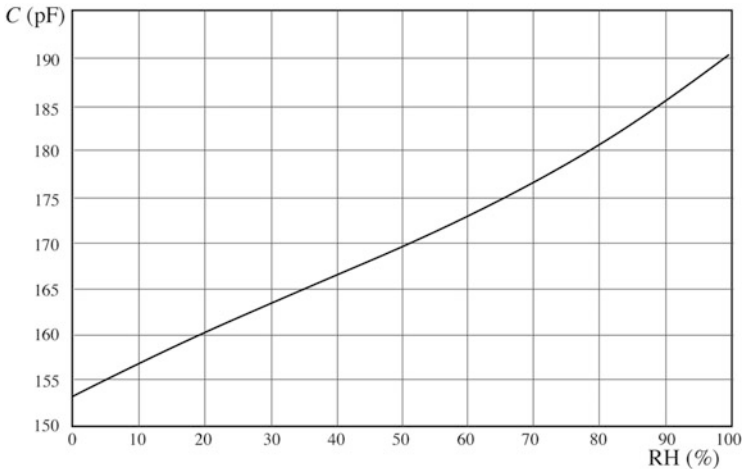
From formulas (4.21) and (4.25), total sensor capacitance can be found as:

$$C_h = \frac{2\pi\epsilon_0}{\ln\frac{b}{a}} [H + h(\kappa_w - 1)], \tag{4.26}$$

where  $h$  is the height of the water-filled portion of the sensor and  $\kappa_w$  is the water dielectric constant at a calibrating temperature. If the water is at or below the level  $h_0$ , the capacitance remains constant because  $h = 0$  and no water is present in-between the sensor electrodes.

$$C_{\min} = \frac{2\pi\epsilon_0}{\ln\frac{b}{a}} H \tag{4.27}$$

Figure 4.8b shows the water level-capacitance dependence. It is a straight line from level  $h_0$ . Since the dielectric constant of water is temperature-dependent (Fig. 4.7) this water level sensor shall be combined with a temperature sensor, for



**Fig. 4.9** Transfer function of capacitive relative humidity sensor

instance, a thermistor or RTD that would monitor water temperature for compensating the transfer function by the electronic signal conditioner.

The slope of the transfer function Eq. (4.26) depends on type of the liquid. For instance, if instead of water the sensor measures a level of transformer oil, it is expected to be about 22 times less sensitive (see Table A.5) because  $\kappa$  for oil is much smaller than for water.

Another example of a capacitive sensor is a humidity sensor. In such a sensor, a dielectric filling between the capacitor plates is fabricated of a material that is hygroscopic, that is, it can absorb water molecules. The material dielectric constant varies with the amount of absorbed moisture. According to Eq. (4.24), this changes the capacitance that can be measured and converted to the value of relative humidity. Figure 4.9 illustrates the dependence between a capacitance and a relative humidity of such a sensor. The dependence is not perfectly linear but this usually can be taken care of during the signal processing.

---

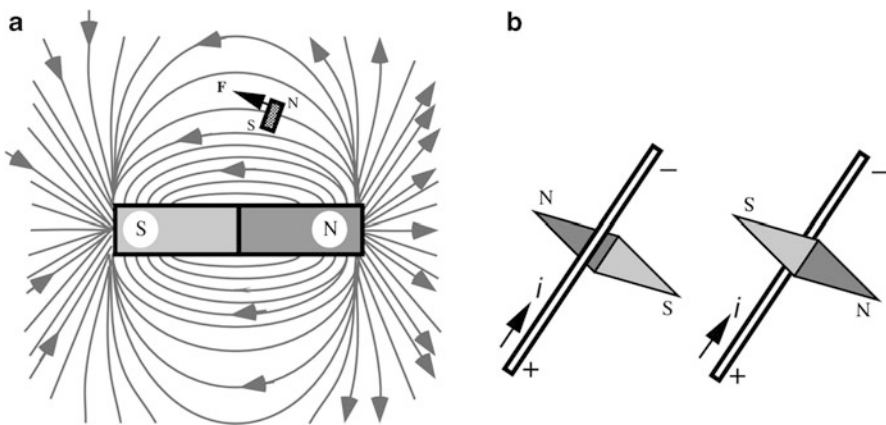
### 4.3 Magnetism

Magnetic properties were discovered in prehistoric times in certain specimens of an iron ore mineral known as magnetite ( $Fe_3O_4$ ). It was also discovered that pieces of soft iron that rubbed against a magnetic material acquired the same property of acting as a magnet, i.e., attracting other magnets and pieces of iron. The first comprehensive study of magnetism was made by William Gilbert. His greatest contribution was his conclusion that the earth acts as a huge magnet. The word magnetism comes from the district of Magnesia in Asia Minor, which is one of the places at which the magnetic stones were found.

There is a strong similarity between electricity and magnetism. One manifestation of this is that two electrically charged rods have like and unlike ends, very much in the same way as two magnets have opposite ends. In magnets, these ends are called S (south) and N (north) poles in analogy with the planet Earth. The like poles repel and the unlike attract. Contrary to electric charges, the magnetic poles always come in pairs. This is proven by breaking magnets into any number of parts. Each part, no matter how small, will have a north pole and a south pole. This suggests that the cause of magnetism is associated with atoms or their arrangements or, more probably, with both.

If we place a magnetic pole in a certain space, that space about the pole appears to have been altered from what it was before. To demonstrate this, bring into that space a piece of iron. Now, it will experience a force that it will not experience if the magnet is removed. This altered space is called a *magnetic field*. The field is considered to exert a force on any magnetic body brought into the field. If that magnetic body is a small bar magnet or a magnetic needle, the magnetic field will be found to have direction. By definition, the direction of this field at any point is given by the direction of the force exerted on a small unit north pole. Directions of the field lines are by definition from north to south pole. Figure 4.10a shows the direction of the field by arrows. A tiny test magnet is attracted in the direction of the force vector  $\mathbf{F}$ . Naturally, about the same force but of the opposite direction is exerted on the south pole of the test magnet.

The above description of the magnetic field was made for a permanent magnet. However, the magnetic field does not change its nature if it is produced by a different device—electric current passing through a conductor. It was Hans Christian Oersted (Ørsted), a Danish professor of physics, who in 1820 discovered that a magnetic field could exist where there were no magnets at all. In a series of experiments in which he was using an unusually large Voltaic pile (battery) so as to produce a large current, he happened to note that a compass in the near vicinity

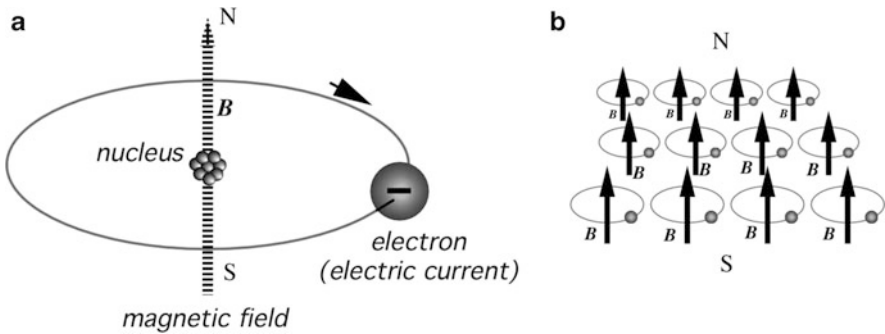
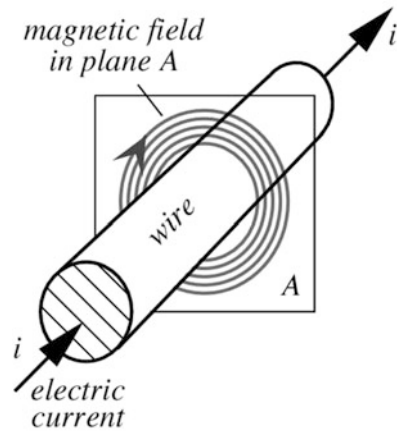


**Fig. 4.10** Test magnet in magnetic field (a); compass needle rotates in accordance with direction of electric current (b)

was behaving oddly. Further investigation showed that the compass needle always oriented itself at right angles to the current carrying wire, and that it reversed its direction if either current was reversed, or the compass was changed from a position below the wire to the one above (Fig. 4.10b). Stationary electric charges make no effect on a magnetic compass (in this experiment, a compass needle is used as a tiny test magnet). It was clear that the moving electric charges were the cause of the magnetic field. It can be shown that magnetic field lines around a wire are circular and their direction depends on the direction of electric current, i.e., moving electrons (Fig. 4.11). Above and below the wire, magnetic field lines are pointed in the opposite direction. That is why the compass needle turns around when it is placed below the wire.

A fundamental property of magnetism is that moving electric charges (electric current) essentially produce a magnetic field. Knowing this, Albert Einstein came up with explanation of the nature of a permanent magnet. A simplified model of a magnetic field origination process is shown in Fig. 4.12a. An electron continuously

**Fig. 4.11** Electric current sets circular magnetic field around conductor



**Fig. 4.12** Moving electron sets magnetic field (a); superposition of field vectors results in combined magnetic field of magnet (b)



spins in an eddy motion around the atom. The electron movement constitutes a circular electric current around the atomic nucleus. That current is a cause for a small magnetic field. In other words, a spinning electron forms a permanent magnet of atomic dimensions. Now, let us imagine that many of such atomic magnets are aligned in an organized fashion (Fig. 4.12b), so that their magnetic fields add up. The process of magnetization then becomes quite obvious—nothing is added or removed from the material—only orientation of atoms is made. The atomic magnets may be kept in the aligned position in some materials that have an appropriate chemical composition and a crystalline structure. Such materials are called *ferromagnetics*.

### 4.3.1 Faraday Law

Michael Faraday pondered the question, “*If an electric current is capable of producing magnetism, is it possible that magnetism can be used to produce electricity?*” It took him 9 or 10 years to discover how. If an electric charge is moved across a magnetic field, a deflecting force is acting on that charge. It must be emphasized that it is not important what actually moves—either the charge or the source of the magnetic field. What matters is a *relative displacement* of those. A discovery that a moving electric charge can be deflected as a result of its interaction with the magnetic field is a fundamental in electromagnetic theory. Deflected electric charges result in an electric field generation, which, in turn, leads to a voltage difference in a conducting material, thus producing an electric current.

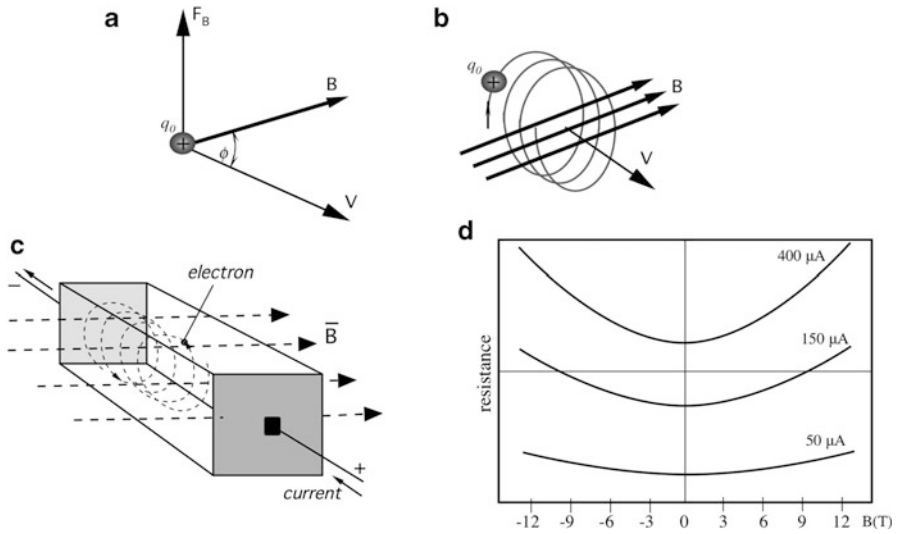
The intensity of a magnetic field at any particular point is defined by vector  $\mathbf{B}$  that is tangent to a magnetic field line at that point. For a better visual representation, the number of the field lines per unit cross-sectional area (perpendicular to the lines) is proportional to the magnitude of  $\mathbf{B}$ . Where the lines are close together,  $\mathbf{B}$  is large and where they are far apart,  $\mathbf{B}$  is small.

The flux of magnetic field can be defined as

$$\Phi_B = \oint \mathbf{B}ds, \quad (4.28)$$

where the integral is taken over the surface for which  $\mathbf{F}_B$  is defined.

To define the magnetic field vector  $\mathbf{B}$  we use a laboratory procedure where a positive electric charge  $q_0$  is used as a test object. The charge is projected through the magnetic field with velocity  $\mathbf{v}$ . A sideways deflecting force  $\mathbf{F}_B$  acts on the charge (Fig. 4.13a). By “sideways” we mean that  $\mathbf{F}_B$  is at a right angle to  $\mathbf{v}$ . It is interesting to note that vector  $\mathbf{v}$  changes its direction while moving through the magnetic field. This results in a spiral rather than parabolic motion of the charge (Fig. 4.13b). The spiral movement is a cause for a *magnetoresistive effect*, which forms a foundation for the magnetoresistive sensors. A magnetoresistor shown in Fig. 4.13c is placed in magnetic field  $\mathbf{B}$  and supplied with constant electric current. The swirling electronic path reflects in change of the resistance (Fig. 4.13c), thus for



**Fig. 4.13** Positive charge projected through magnetic field is subjected to sideways force (a); spiral movement of electric charge in magnetic field (b); magnetoresistor (c), and dependence of resistance on magnetic field and current (d)

a known current, voltage across the resistor represents strength of the magnetic field. The reason why the resistance goes up is a longer path for electrons to travel inside the material, thus experience a higher resistance to their travel.

Deflecting force  $F_B$  is proportional to charge, velocity, and magnetic field

$$F_B = q_0 v B. \tag{4.29}$$

Vector  $F_B$  is always at right angles to the plane formed by  $v$  and  $B$  and thus is always at right angles to  $v$  and to  $B$ ; that is why it is called a sideways force. The magnitude of magnetic deflecting force, according to the rules for vector products, is

$$F_B = q_0 v B \sin \phi, \tag{4.30}$$

where  $\phi$  is the angle between vectors  $v$  and  $B$ . The magnetic force vanishes if  $v$  is parallel to  $B$ . The above Eq. (4.30) is used for definition of the magnetic field in terms of deflected charge, its velocity, and deflecting force. Therefore, the units of  $B$  is  $(N/C)/(m/s)^{-1}$ . In the System SI its given name is *tesla* (abbreviated T). Since coulomb/second is an ampere, we have  $1 T = 1 N/(A \cdot m)$ . An older unit for  $B$  still is sometimes in use. It is the gauss:

$$1 T = 10^4 G$$

### 4.3.2 Permanent Magnets

Permanent magnets are useful components for fabricating magnetic sensors for detection of motion, displacement, position, proximity, etc. To select the magnet for any particular application, the following characteristics should be considered:

- Residual inductance ( $B$ ) in gauss or milli-tesla (mT)—how strong the magnet is?
- Coercive force ( $H$ ) in oersteds (Oe) or kA/m—how well will the magnet resist external demagnetization forces? For a comparison, 1 Oe = 0.08 kA/m.
- Maximum energy product, MEP, ( $BH_{\max}$ ) is gauss-oersteds times  $10^6$  or kJ/m<sup>3</sup>. A million of gauss-oersted is often indicated as MGOe (mega-gauss-oersted). For a comparison, 1MGOe = 7.96 kJ/m<sup>3</sup>. A strong magnet that is also very resistant to demagnetization forces has a high MEP. Magnets with higher MEP are better, stronger, and more expensive.
- Temperature coefficient in %/°C shows how much  $B$  changes with temperature?

Magnets are produced from special alloys (see Table A.6). Examples are *rare earth* (e.g., samarium)-cobalt alloys. These are the best magnets, however, they are too hard for machining, and must be ground if shaping is required. Their maximum MEP is about  $16 \times 10^6$  or 16MGOe. Another popular alloy is *Alnico*, which contains aluminum, nickel, cobalt, iron, and some additives. These magnets can be cast, or sintered by pressing metal powders in a die and heating them. Sintered Alnico is well suited to mass production. *Ceramic magnets* contain barium or strontium ferrite (or another element from that group) in a matrix of a ceramic material that is compacted and sintered. They are poor conductors of heat and electricity, chemically inert, and have high value of  $H$ .

Another alloy for the magnet fabrication is *Cunife*, which contains copper, nickel, and iron. It can be stamped, swaged, drawn, or rolled into final shape. Its MEP is about  $1.4 \times 10^6$ . *Iron-chromium* magnets are soft enough to undergo machining before the final aging treatment hardens them. Their maximum MEP is  $5.25 \times 10^6$ . *Plastic and rubber* magnets consist of barium or strontium ferrite in a plastic matrix material. They are very inexpensive and can be fabricated in many shapes. Their maximum MEP is about  $1.2 \times 10^6$ .

A neodymium magnet (also known as NdFeB, NIB, or *Neo* magnet), a type of rare-earth magnet, is a permanent magnet made from an alloy of neodymium, iron, and boron to form the Nd<sub>2</sub>Fe<sub>14</sub>B tetragonal crystalline structure. This material is currently the strongest type of permanent magnet. In practice, the magnetic properties of Neodymium magnets depend on the alloy composition, microstructure, and manufacturing technique employed. Neodymium magnets have very much higher coercivity and energy product, but lower Curie temperature than other types of magnets.

In the 1990s it was discovered that certain molecules containing paramagnetic metal ions are capable of storing a magnetic moment at very low temperatures. In fact, these magnets are large molecules with strong magnetic properties. Such magnets are called *single molecule magnets* (SMM). Most SMM's contain manganese, but can also be found with vanadium, iron, nickel, and cobalt clusters.

Advantages of SMMs include strong residual inductance, solubility in organic solvents, and subnanoscale dimensions. More recently it has been found that some chain systems can also display a magnetization which persists for long times at relatively higher temperatures. These systems have been called single-chain magnets (SCM).

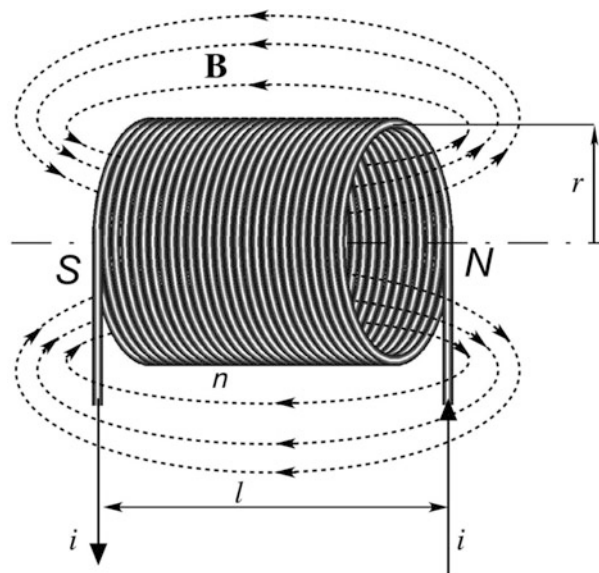
For selecting a permanent magnet for a practical application, one can use a helpful magnet calculator on the Internet ([www.kjmagnetics.com/calculator.asp](http://www.kjmagnetics.com/calculator.asp)).

### 4.3.3 Coil and Solenoid

A *solenoid* and *coil* are made in form of a long wire wound in helix and carrying current  $i$ . Solenoids and coils are practical devices for producing magnetic fields. Solenoids are often used as actuators for converting electric currents to mechanical forces. But they also are the basis for many useful sensors, especially for detecting movement and proximity. Word solenoid is derived from Greek: σωλήνας (pipe) and εἶδος (form). The difference between a coil and solenoid is that the former may have any loopy shape, while the latter is a tightly packed coil in form of a cylinder. In the following discussion we assume that a solenoid is very long as compared with its diameter. The solenoid magnetic field is the *vector sum* of the fields' setup by all the turns that make up the solenoid.

If a coil has widely spaced turns, the magnetic fields tends to cancel between the wires. At points inside the solenoid and reasonably far from the wires, magnetic vector  $\mathbf{B}$  is parallel to the solenoid axis. In the limiting case of adjacent very tightly packed wires as shown in Fig. 4.14, the solenoid becomes essentially a cylindrical

**Fig. 4.14** Solenoid or coil



current sheet. If we apply Ampere's law to that current sheet, the magnitude of magnetic field inside the solenoid becomes

$$B = \mu_0 i_o n, \quad (4.31)$$

where  $n$  is the number of turns per unit length and  $i_o$  is the current through the solenoid wire. Although, this formula was derived for an infinitely long solenoid, it holds quite well for actual solenoids for internal points near the center of the solenoid. It should be noted that  $B$  does not depend on the diameter or the length of the solenoid and that  $B$  is constant over the solenoid cross-section. Since the solenoid's diameter is not part of the equation, multiple layers of winding can be used to produce a magnetic field of higher strength. Magnetic field outside of a solenoid is weaker than that of the inside.

---

## 4.4 Induction

In 1831, Michael Faraday in England and Joseph Henry in the U.S.A. discovered one of the most fundamental effects of electromagnetism: an ability of a varying magnetic field to induce electric current in a wire. Magnetic field is nonspecific in its origin, so it is not important how the field is produced—either by a permanent magnet or by a solenoid—the effect is the same. Electric current is generated as long as the magnetic field *changes*. A stationary magnetic field produces no current.

Faraday's law of induction says that the induced voltage, or *electromotive force* (e.m.f.), is equal to the rate at which the magnetic flux through the circuit changes. If the rate of change is in Wb/s, the e.m.f. ( $e$ ) will be in volts:

$$e = -\frac{d\Phi_B}{dt}. \quad (4.32)$$

The minus sign is an indication of the direction of the induced e.m.f. If varying magnetic flux is applied to a solenoid, e.m.f. appears in every turn and all these e.m.f.'s must be added up. If a coil is wound in such a manner as each turn has the same cross-sectional area, the flux through each turn will be the same, then the induced voltage is

$$V = -N \frac{d\Phi_B}{dt}, \quad (4.33)$$

where  $N$  is the number of turns. This equation may be rewritten in form that is of interest to a sensor designer or an application engineer

$$V = -N \frac{d(BA)}{dt}. \quad (4.34)$$

The equation means that voltage in a pick-up circuit can be produced by either changing amplitude of magnetic field ( $B$ ) or changing area of the circuit ( $A$ ). Thus, induced voltage depends on:

- Moving the source of magnetic field (magnet, coil, wire, etc.) with respect to a receiving coil.
- Varying current in the coil or wire, which produces the magnetic field.
- Changing orientation of the magnetic source with respect to the pick-up circuit.
- Changing geometry of a pick-up circuit, for instance, by stretching it or squeezing, or changing the number of turns in a coil.

If electric current passes through a coil, which is situated in close proximity with another coil, according to Faraday's law, e.m.f. in the second coil will appear. However, the magnetic field penetrates not only the second coil, but the first coil as well. Thus, the magnetic field sets e.m.f. in the same coil where it is originated. This is called *self-induction* and the resulting voltage is called a *self-induced e.m.f.* The Faraday's law for a central portion of a solenoid is

$$\nu = -\frac{d(n\Phi_B)}{dt}. \quad (4.35)$$

The number in parenthesis is called the flux linkage and is an important characteristic of the device. For a simple coil with no magnetic material in the vicinity, this value is proportional to current through coil

$$n\Phi_B = Li, \quad (4.36)$$

where  $L$  is the proportionality constant, which is called the *inductance* of the coil. Then, Eq. (4.35) can be rewritten as

$$\nu = -\frac{d(n\Phi_B)}{dt} = -L\frac{di}{dt}. \quad (4.37)$$

From this equation we can define inductance as

$$L = -\frac{\nu}{\frac{di}{dt}}. \quad (4.38)$$

If no magnetic material is introduced in the vicinity of an *inductor* (a device possessing inductance), the value defined by Eq. (4.38) depends only on the geometry of the device. The SI unit for inductance is the volt-second/ampere, which was named after American physicist Joseph Henry (1797–1878):  $1\text{ H} = 1\text{ V} \cdot \text{s}/\text{A}$ . Abbreviation for henry is H.

Several conclusions can be drawn from Eq. (4.37):

- Induced voltage is proportional to the rate of change in current through the inductor.

- Voltage is essentially zero for dc.
- Voltage increases linearly with the current rate of change.
- Voltage polarity is different for increased and decreased currents flowing in the same direction.
- Induced voltage is always in the direction that opposes the change in current.

Like capacitance, inductance can be calculated from geometrical factors. For a closely packed coil, just like the one shown in Fig. 4.14, the inductance is

$$L = \frac{n\Phi_B}{i}. \quad (4.39)$$

If  $n$  is the number of turns per unit length, the number of flux linkages in the coil length,  $l$ , is

$$N\Phi_B = (nl) \cdot (BA), \quad (4.40)$$

where  $A$  is the cross-sectional area of the coil. For the solenoid without a magnetic core,  $B = \mu_0 ni$ , then the coil inductance is:

$$L = \frac{N\Phi_B}{i} = \mu_0 n^2 l A. \quad (4.41)$$

It should be noted that  $lA$  is the volume of a solenoid that often is called  $G$ —a *geometry factor*.

If a magnetic core is inserted into the inner space of the solenoid, inductance will depend on two additional factors: the relative magnetic permeability,  $\mu_r$ , of the core material, and  $g$ , the core geometry factor,  $g$ :

$$L = \mu_0 \mu_r n^2 g G \quad (4.42)$$

Note that factor  $g$  depends on size and shape of the magnetic core, its depth of insertion, and closeness to the ends of the solenoid. Another point that should be considered is that relative permeability  $\mu_r$  of a ferromagnetic material changes with current  $i$ , thus, Eq. (4.42) needs a correction coefficient  $\eta_i$  that is function of the current passing through the solenoid coil having a magnetic core (with no core  $\mu_r = \eta_i = 1$ ):

$$L = \mu_0 \mu_r n^2 \eta_i g G \quad (4.43)$$

This equation suggest that inductance  $L$  can be modulated by every factor at its right side (except  $\mu_0$  that is a universal constant): the number of the coil turns can vary, all dimensions of the coil can be changed, the core shape and depth of insertion can be changed, and even the core material can be modified. This makes the inductive sensors very useful in many applications, for example to measure displacement for detecting force, pressure, position, and other variables.

When connected into an electronic circuit, inductance may be represented as a “complex resistance”

$$\frac{V}{i} = j\omega L, \quad (4.44)$$

where  $j = \sqrt{-1}$  and  $i$  is a sinusoidal current having frequency of  $\omega = 2\pi f$ , meaning that the complex resistance of an inductor increases at higher frequencies. This is called Ohm’s law for an inductor. Complex notation indicates that current lags behind voltage by  $90^\circ$  and thus a coil is called a *reactive* component.

If two coils are brought in the vicinity of one another and one coil conducts electric current, the magnetic field produced by that coil interacts with electrons in the second coil and induces in it e.m.f.:

$$v_2 = -M_{21} \frac{di_1}{dt} \quad (4.45)$$

where  $M_{21}$  is the coefficient of *mutual inductance* between two coils. The calculation of a mutual inductance is not a simple exercise and in many practical cases can be easier performed experimentally. Nevertheless, for some relatively simple combinations mutual inductances have been calculated. For example, a coil having  $N$  turns which is placed around a long solenoid, with  $n$  turns per unit length, the mutual inductance is

$$M = \mu_0 \pi R^2 n N, \quad (4.46)$$

where  $R$  is the solenoid diameter.

If two coils are brought in the vicinity of one another, their mutual inductance can be expressed as:

$$M_{12} = N_1 N_2 P_{21}, \quad (4.47)$$

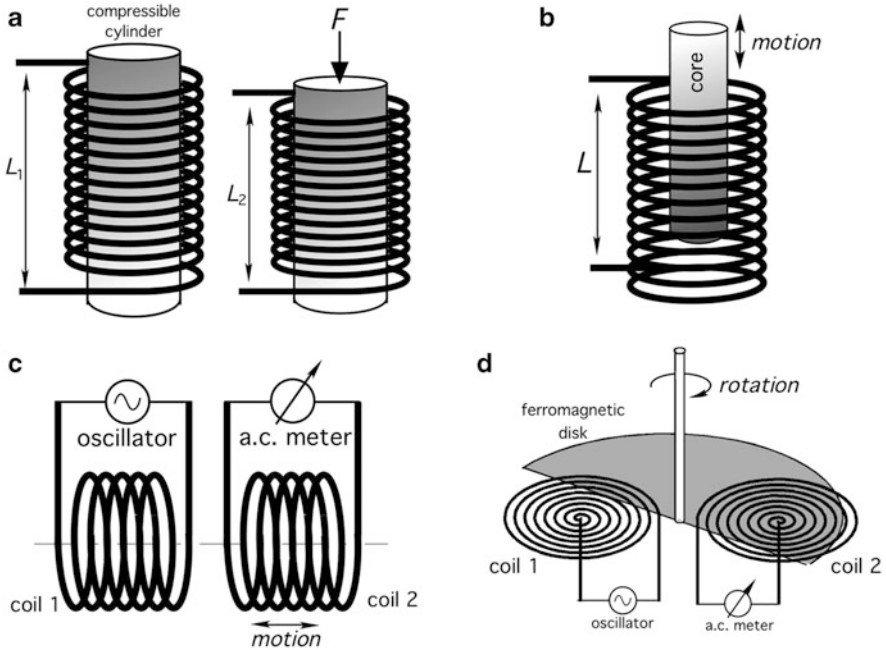
where  $N_1$  and  $N_2$  are numbers of turns in the first and second coils respectively, while  $P_{21}$  is permanence of space where the magnetic flux propagates. The meaning of permanence is similar to an electric resistance but used for the magnetic flux. It is proportional to the magnetic permeability of the coil-coupling material and its geometry, thus forming the basis for designing many useful sensors.

Another useful way of expressing mutual inductance is through inductivities of the coils and the coupling coefficient  $0 \leq k \leq 1$ :

$$M = k\sqrt{L_1 L_2} \quad (4.48)$$

To illustrate how a coil inductance and mutual inductance can be employed in sensors, Fig. 4.15 shows four conceptual designs. If a coil is wound around a pliant cylinder having a spring action, according to Eq. (4.43), the coil geometry  $G$  can be varied by application to the core an external force,  $F$ , Fig. 4.15a. This causes a





**Fig. 4.15** Examples of sensors with coils. A changing geometry coil (a), solenoid with a moving core (b), two moving coils (c), and variable mutual inductance coils (d)

change in the coil inductance,  $L$ . If the coil is part of an electronic  $LC$  oscillator, the applied force,  $F$ , will modulate the output frequency.

A solenoid may have inside a movable ferromagnetic core, Fig. 4.15b, that while moving, according to the Eq. (4.43), will vary the factor  $g$ , because only a portion of the core that is inside the solenoid modulates the solenoid inductance. Thus, the deeper inside the core is inserted, the higher the inductance value. Figure 4.15c shows the mutually movable coils. The left coil is fed by excitation signal from an oscillator. The output coil will output a.c. voltage in proportion to the coil coupling, because change in  $P_{21}$  in Eq. (4.47) modulates the mutual inductance. Another way of modulating the coil coupling is illustrated in Fig. 4.15d, where two coils are coupled via a movable (rotating) ferromagnetic semidisk—the coupling media. The coupling is at its maximum when the overlapping areas of the semidisk with both coils are the largest, while the coupling is the lowest when no ferromagnetic material is positioned over any coil.

#### 4.4.1 Lenz Law

In many sensor applications involving inductive coupling, one should always consider that current induced in the secondary coil produces its own magnetic field that works backward toward the primary coil. This phenomenon is known as

Lenz Law<sup>5</sup> that states: *The induced current will appear in such a direction that it opposes the current that produced it.* The minus sign in Eq. (4.35) suggests this opposition. Thus, the induced current tends to reduce the originating current in the primary coil. It can be said that Lenz Law is similar to Newton's third law of motion (i.e., to every action there is always an equal and opposite reaction). Lenz's law refers to induced currents, which means that it applies only in closed conduction circuits. Note that the opposing magnetic flux in a coil reduces its inductance. Lenz law has a very broad range of applications, including electromagnetic braking, induction cooktops, metal detectors, and many others.

### 4.4.2 Eddy Currents

Eddy current is an electrical phenomenon discovered in 1851 by French physicist Léon Foucault. Thus, this current sometimes is called *Foucault current*. It appears in two cases: (1) when a conductor is exposed to a changing magnetic field due to relative motion of the field source and conductor, and (2) due to changing intensity of the magnetic field. These effects cause a circulating flow of electrons, or a circular current, within the body of the conductor. The conductor may be magnetic or not. The eddy currents circulate in the planes that are perpendicular to the magnetic flux. If they are induced by a coil, they normally travel parallel to the coil's winding and the flow is limited to the area of the inducing magnetic field. Eddy currents concentrate near the surface adjacent to an excitation coil and their strength decreases with distance from the coil. Eddy current density decreases exponentially with depth. This phenomenon is known as the skin effect.

These circulating eddies of current create induced magnetic fields that oppose the change of the original magnetic field due to Lenz's law, thus causing repulsive or drag forces between the conductor and the magnet or the inducing coil. The stronger the applied magnetic field, or the greater the electrical conductivity of the conductor, or the faster the field that the conductor is exposed to changes, then the greater the currents that are developed and the greater the opposing field.<sup>6</sup> The skin effect arises when the eddy currents flowing in the test object at any depth produce magnetic fields which oppose the primary field, thus reducing the net magnetic flux and causing a decrease in current flow as the depth increases. Alternatively, eddy currents near the surface can be viewed as shielding the coil's magnetic field, thereby weakening the magnetic field at greater depths and reducing induced currents.

---

<sup>5</sup> Lenz Law is named after the German scientist H.F.E. Lenz in 1834.

<sup>6</sup> Eddy currents are employed for inductive cooking. A coil positioned under a pot induces strong circular currents in the pot base. For converting eddy currents into thermal energy, the base shall have not too high and not too low electrical resistance. That is why neither glass or ceramic, nor copper or aluminum cookware can be used for inductive cooking.

## 4.5 Resistance

In any material, electrons move randomly like gas in a closed container. There is no preferred direction and an average concentration of electrons in any part of material is uniform (assuming that the material is homogeneous). Let us take a bar of an arbitrary material. The length of the bar is  $l$ . When the ends of the bar are connected to the battery having voltage  $V$  (Fig. 4.16), electric field  $\mathbf{E}$  will be setup within the material. It is easy to determine strength of the electric field

$$E = \frac{V}{l} \quad (4.49)$$

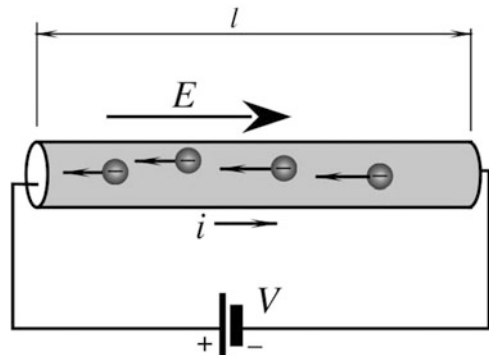
For instance, if the bar has a length of  $l = 1$  m and the battery delivers 1.5 V, the electric field has the strength of 1.5 V/m. The field acts on free electrons and sets them in motion against the direction of the field. Thus, the electric current starts flowing through the material. We can imagine a cross-section of the material through which passes electric charge  $q$ . The rate of the electric charge flowing (unit of charge per unit of time) is called electric current

$$i = \frac{dq}{dt} \quad (4.50)$$

The SI unit of current is ampere (A):  $1 \text{ A} = 1 \text{ C/s}$ . In SI, ampere is defined as electric current which is maintained in two infinitely long parallel wires separated by 1 m in free space, which produce a force between the two wires (due to their magnetic field) of  $2 \times 10^{-7}$  N for each meter of length. An ampere is quite strong electric current. In sensor technologies, generally much smaller currents are used, therefore, submultiples of A are often employed:

1 milliampere (mA)	$10^{-3}$ A
1 microampere ( $\mu\text{A}$ )	$10^{-6}$ A
1 nanoampere (nA)	$10^{-9}$ A
1 picoampere (pA)	$10^{-12}$ A
1 femtoampere (fA)	$10^{-15}$ A

**Fig. 4.16** Voltage across a material sets electric current



No matter what the cross-section of the material is, whether it is homogeneous or not, the electric current through any cross-section is always the same for a given electric field. It is similar to a water flow through a combination of serially connected pipes of different diameters—the rate of flow is the same throughout of the pipe combination. The water flows faster in the narrow sections and slower in the wide section, but amount of water passing through any cross-section per unit of time is constant. The reason for that is very simple—water in the pipes is neither drained out, nor created. The same reason applies to electric current. One of the fundamental laws of physics is the law of conservation of charge. Under steady-state conditions, charge in a material is neither created nor destroyed. *Whatever comes in must go out.* In this section, we do not consider any charge storages (capacitors), and all materials we discuss are said have pure *resistive* properties.

The mechanism of electrical conduction in a simplified form may be described as follows. A conducting material, say a copper wire, can be modeled as a semirigid spring-like periodic lattice of positive copper ions. They are coupled together by strong electromagnetic forces. Each copper atom has one conduction electron, which is free to move about the lattice. When electric field  $\mathbf{E}$  is established within the conductor, force  $-e\mathbf{E}$  acts on each electron ( $e$  is the electron charge). The electron accelerates under the force and moves. However, the movement is very short as the electron collides with the neighboring copper atoms, which constantly vibrate with intensity that is determined by the material temperature. The electron transfers its kinetic energy to the lattice and is often captured by the positive ion. When captured, it frees another electron, which keeps moving in the electric field until, in turn, it collides with the next portion of the lattice. The average time between collisions is designated as  $\tau$ . It depends on the material type, structure, and impurities. For instance, at room temperature, a conduction electron in pure copper moves between collisions for an average distance of  $0.04 \mu\text{m}$  with  $\tau = 2.5 \times 10^{-14} \text{ s}$ . In effect, electrons that flow into the material near the negative side of the battery are not the same that outflow to the positive terminal. However, the constant drift or flow of electrons is maintained throughout the material. Collisions of electrons with the material atoms further add to the atomic agitation and, subsequently, raise the material temperature. This is why passing of electric current through a resistive material results in the so-called Joule heat liberation.

It was arbitrarily decided to define the direction of current flow along with the direction of the electric field, i.e., in the *opposite direction* of the electronic flow. Hence, the electric current flows from the positive to negative terminal of the battery while electrons actually move in the opposite direction. It is interesting to note that unlike water flowing through a pipe, electrons do not need to initially “fill up” the conductor before they start flowing out at a positive side. Electrons are always present in a conductor, so it is already filled-up. Since electric field in a conductor propagates with the speed of light in the conductor’s material, electric current appears at all parts of the conductor nearly instantaneously.

### 4.5.1 Specific Resistivity

If we fabricate two geometrically identical rods from different materials, say from copper and glass, and apply to them the same voltage, the electric fields in the rods will be the same, but the resulting currents will be quite different. A material may be characterized by its ability to pass electric current. It is called *resistivity* and material is said to have electrical *resistance* that is defined by Ohm's law, meaning that a ratio of voltage to current is a constant

$$R = \frac{V}{i}. \quad (4.51)$$

For the pure resistance (no inductance or capacitance) voltage and current are in-phase with each other, meaning that they are changing simultaneously.

Any material has electric resistivity<sup>7</sup> and therefore is called a *resistor*. The SI unit of resistance is 1 ohm ( $\Omega$ ) = 1 V/1 A. Other multiples and submultiples of  $\Omega$  are:

1 milliohm (m $\Omega$ )	$10^{-3} \Omega$
1 kilohm (k $\Omega$ )	$10^3 \Omega$
1 Megohm (M $\Omega$ )	$10^6 \Omega$
1 Gigohm (G $\Omega$ )	$10^9 \Omega$
1 Terohm (T $\Omega$ )	$10^{12} \Omega$

If we again compare electric current with water flow, pressure across the pipe line (say, in pascal) is analogous of voltage (V) across the resistor, electric current (C/s) is analogous of water flow (l/s), and electric resistance ( $\Omega$ ) corresponds to water flow resistance in the pipe (no special unit). It is clear that resistance to water flow is smaller when the pipe is short, wide, and has no obstructions. When the pipe has, for instance, a filter installed in it, resistance to water flow will be higher. Consider a human body where arterial blood flow may be restricted by cholesterol deposits on the inner lining of arteries. These deposits increase the flow resistance (called vascular resistance). The arterial blood pressure increases to compensate for rise in the vascular resistance, so the heart pumps stronger. If arterial pressure cannot keep-up with increase in the vascular resistance, the heart pumping force is no longer sufficient for providing a necessary blood flow to vital organs, including the heart itself. This may result in a heart attack or other complications.

The basic laws that govern the electric circuit designs are called Kirchhoff's Laws, after the German physicist Gustav Robert Kirchhoff (1824–1887). These laws were originally conceived by considering a similarity to the plumbing networks, which as we have seen, are analogous to the electric networks.

Resistance is a characteristic of a device. It depends on both: the material type and geometry of the resistor. Material itself can be characterized by a *specific resistivity*,  $\rho$ , which is defined as

<sup>7</sup> Excluding superconductors which are beyond the scope of this book.

$$\rho = \frac{E}{j}, \quad (4.52)$$

where current density  $j = i/a$  ( $a$  is the area of the material cross-section). The SI unit of resistivity is  $\Omega \cdot \text{m}$ . Resistivities of some materials are given in Appendix (Table A.7). Quite often, a reciprocal quantity is used, which is called *conductivity*,  $\sigma = 1/\rho$ . The SI unit of conductivity is *siemens* having dimension  $[1/\Omega]$ . Sometimes, siemens is called *mho*—that is “ohm” spelled backwards.

Specific resistivity of a material can be expressed through the mean time between collisions,  $\tau$ , the electronic charge,  $e$ , the mass of electron,  $m$ , and a number of conduction electrons per unit volume of the material,  $n$ :

$$\rho = \frac{m}{ne^2\tau}. \quad (4.53)$$

To find the resistance of a conductor the following formula is frequently used:

$$R = \rho \frac{l}{a}, \quad (4.54)$$

where  $a$  is the cross-sectional area and  $l$  is the length of the conductor. The ratio  $l/a$  is called a *geometry factor* of a resistor.

Formula (4.54) establishes the fundamental relationship between resistance and its parameters. Thus, if one wants to design a resistive sensor, she should find ways of modulating either the specific resistivity or geometry factor,  $l/a$ . Below we review several resistive sensors that use modulation of the variables in Eq. (4.54).

## 4.5.2 Temperature Sensitivity of a Resistor

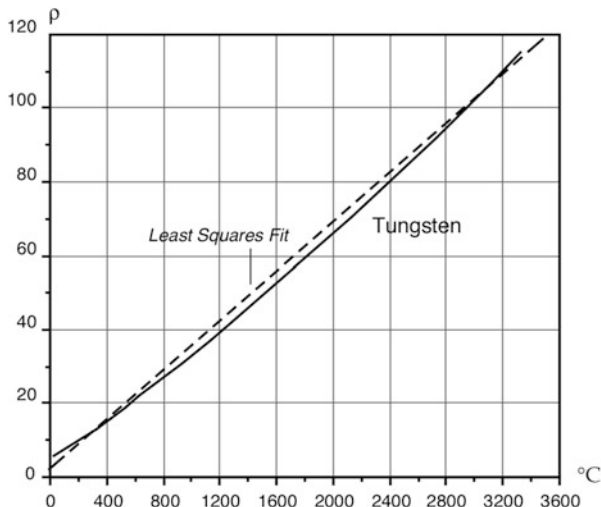
In reality, the specific resistivity of a material is not constant. It changes somewhat with temperature,  $t$ , and in a relatively narrow temperature range may be linearly approximated through the thermal sensitivity (slope)  $\alpha$ , which is the *temperature coefficient of resistivity* (TCR).

$$\rho = \rho_0 \left( 1 + \alpha \frac{t - t_0}{t_0} \right) \quad (4.55)$$

where  $\rho_0$  is the specific resistivity at reference temperature  $t_0$  (commonly  $t_0 = 0$  or  $25^\circ\text{C}$ ). In a broader range, resistivity is a nonlinear function of temperature.

For nonprecision applications over a broad temperature range, resistivity of tungsten, as shown in Fig. 4.17, may be modeled by a best-fit straight line. When a better accuracy is required, the linear Eq. (4.55) should not be employed. Instead, a higher order polynomial may be employed. For instance, over a broader temperature range, tungsten resistivity may be found from the second-order approximation:

**Fig. 4.17** Specific resistivity of tungsten as function of temperature



$$\rho = 4.45 + 0.0269t + 1.914 \times 10^{-6}t^2, \quad (4.56)$$

where  $t$  is temperature in  $^{\circ}\text{C}$  and  $\rho$  is in  $\Omega \cdot \text{m}$ .

Metals have positive temperature coefficients<sup>8</sup> (PTC)  $\alpha$ , while many semiconductors and oxides have negative temperature coefficients of resistance (NTC). As a rule, the NTC resistors have high temperature nonlinearity.

When a conventional resistor is used in an electronic circuit, its resistance shall be as temperature independent as possible. A “good” resistor may have  $\alpha = 10^{-5}$  or even lower. However, in sensing technologies, it is often desirable to have a “bad” resistor whose temperature coefficient of resistivity  $\alpha$  is high and predictable. A strong  $\alpha$  allows fabricating two types of temperature sensors: one is known as a *thermistor* (a contraction of words *thermal* and *resistor*) and the other is a *resistance temperature detector* (RTD).<sup>9</sup> The most popular RTD is a platinum (Pt) sensor that operates over a broad temperature range up to  $600^{\circ}\text{C}$ . Resistance of a Pt RTD is shown in Fig. 4.18. The best-fit straight line is given by equation:

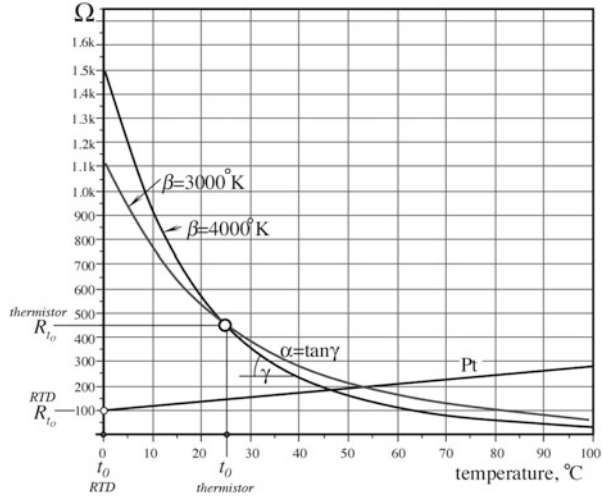
$$R = R_0(1 + 36.79 \times 10^{-4}t), \quad (4.57)$$

where the calibrating resistance  $R_0$  is measured at  $0^{\circ}\text{C}$ ,  $t$  is in  $^{\circ}\text{C}$  and  $R$  is in  $\Omega$ . A slight nonlinearity of the Pt resistance curve, if not corrected, may lead to an appreciable error over a broad temperature range. A more precise approximation

<sup>8</sup> Since resistance of a metal increases with temperature, a tungsten filament in a light bulb acts as a self-regulator of temperature, so the filament does not burn out. When temperature increases, the resistance goes up, and the current drops, causing the temperature to come down. If coefficients  $\alpha$  for metals were negative, the filaments would instantly burn out and we would not have incandescent electric lights.

<sup>9</sup> See Sect. 17.1.

**Fig. 4.18** Resistance-temperature characteristics for two thermistors and Pt RTD ( $R_0 = 1\text{ k}$ ); note different reference temperatures for thermistors ( $t_0 = 25\text{ }^\circ\text{C}$ ) and RTD ( $t_0 = 0\text{ }^\circ\text{C}$ )



of the Pt resistance is a second-order polynomial which gives accuracy better than  $0.01\text{ }^\circ\text{C}$ :

$$R = R_0(1 + 39.08 \times 10^{-4}t - 5.8 \times 10^{-7}t^2)\Omega \tag{4.58}$$

It should be noted, however, that the coefficients in Eqs. (4.57 and 4.58) somewhat depend on the material purity and manufacturing technologies. To compare accuracies of the linear and second-order models of the platinum thermometer, we use the following example. If a Pt RTD sensor at a reference temperature  $0\text{ }^\circ\text{C}$  has resistivity  $R_0 = 100\text{ }\Omega$ , for  $+150\text{ }^\circ\text{C}$  the linear approximation gives

$$R = 100(1 + 36.79 \times 10^{-4} \times 150) = 155.18\Omega,$$

while from the second-order approximation (Eq. 4.58)

$$R = 100(1 + 39.08 \times 10^{-4} \times 150 - 5.8 \times 10^{-7} \times 150^2) = 157.32\Omega.$$

The difference between the two is  $2.13\text{ }\Omega$ . This is equivalent to an error at  $+150\text{ }^\circ\text{C}$  of approximately  $-5.8\text{ }^\circ\text{C}$ , meaning that a linear approximation gives a lower reading with the error of nearly  $-4\text{ }\%$ .

Another type of the resistive temperature sensors includes thermistors that are resistors with large, either negative (NTC), or positive (PTC) temperature coefficients. For temperature measurements usually the NTC are employed, while the PTCs thermistors due to their very high nonlinearity are used for applications where a lesser accuracy is traded for a very high sensitivity in a selected region. The thermistors are ceramic semiconductors commonly made of oxides of one or more



of the following metals: nickel, manganese, cobalt, titanium, iron. Oxides of other metals are occasionally used.

Resistances of thermistors vary from a fraction of an ohm to many Megohms. Thermistors can be produced in form of disks, droplets, tubes, flakes, or thin films deposited on ceramic substrates. Also, a thick-film paste can be printed on ceramic substrate to form a thick-film thermistor. Also resistance of a semiconductors (Ge and Si) may be controlled to create either NTC or PTC to form semiconductive RTDs and thermistors.

Thermistors possess nonlinear temperature-resistance characteristics (Fig. 4.18), which are generally approximated by one of several different equations that are covered in detail in Chap. 17. The most popular of the thermistor's transfer function approximations is the exponential form

$$R_t = R_0 e^{\beta \left( \frac{1}{T} - \frac{1}{T_0} \right)} \quad (4.59)$$

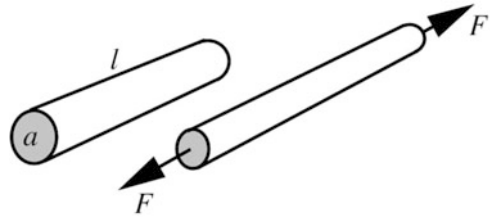
where  $T$  is the thermistor temperature,  $T_0$  is the calibrating temperature,  $R_0$  is its resistance at the calibrating temperature  $T_0$ , and  $\beta$  is the thermistor material's characteristic temperature. All temperatures and  $\beta$  are in kelvin. Commonly,  $\beta$  ranges between 2600 and 4200 K (the value can reach even 6000 K for a semiconductive thermistor made of Germanium) and for a relatively narrow temperature range  $\beta$  can be considered temperature-independent, which makes Eq. (4.59) a reasonably good approximation. When higher accuracy is required, other approximations are employed. Figure 4.18 shows resistance/temperature dependencies for two thermistors having  $\beta = 3000$  and  $4000$  K and also for the platinum RTD. The platinum temperature sensor is substantially less sensitive and more linear with a positive slope, while NYC thermistors are nonlinear with a higher sensitivity and variable negative slope.

Traditionally, in data sheets, thermistors are specified at a reference temperature of  $t_0 = 25$  °C ( $T_0 = 298.15$  K), while RTDs are specified at  $t_0 = 0$  °C ( $T_0 = 273.15$  K).

### 4.5.3 Strain Sensitivity of a Resistor

Electrical resistance of a material changes when the material is mechanically deformed. *Strain* is a measure of the deformation. A mechanical deformation modulates either the specific resistivity or the geometry factor as shown by Eq. (4.54). The resistor's strain sensitivity is called the *piezoresistivity* from the Greek word  $\pi\acute{\iota}\epsilon\sigma\eta$  (pressure). As we have seen before, a "good" resistor better be stable, while having a "bad" resistor gives us an opportunity to make a sensor. In this case, we are talking about a strain sensor that may be used to measure strain. Also it may serve as part in many other complex sensors, such as displacement, force, pressure sensors, etc.

**Fig. 4.19** Strain changes geometry of conductor and its resistance



To deform a resistor and cause strain, it should be stressed. The *stress*,  $\sigma$ , relates to force as

$$\sigma = \frac{F}{a} = E \frac{dl}{l} = Ee \quad (4.60)$$

where  $E$  is Young's modulus of the material,  $F$  is the applied force, and  $a$  is the cross-sectional area. In this equation, the ratio  $dl/l = e$  is strain which is a normalized *deformation* of the material.

Figure 4.19 shows a cylindrical conductor (wire) that is stretched by the applied force  $F$ . Volume  $v$  of the material stays constant (no material is added or removed), while the length increases, and the cross-sectional area becomes smaller. As a result, Eq. (4.54) can be rewritten as

$$R = \frac{\rho l^2}{v} \quad (4.61)$$

Note that the ratio is a constant for a given material and design. After differentiating, we can define a sensitivity of the wire resistor with respect to the elongation:

$$\frac{dR}{dl} = 2 \frac{\rho}{v} l \quad (4.62)$$

It follows from this equation that the strain sensitivity of a wire becomes higher for the longer and thinner wires with a high specific resistivity. The normalized incremental resistance of the strained wire is a linear function of strain,  $e$ , and it can be expressed as:

$$\frac{dR}{R} = S_e e, \quad (4.63)$$

where  $S_e$  is known as the *gauge factor* or *sensitivity* of the strain gauge element. For metallic wires it ranges from 2 to 6. It is much higher for the semiconductor gauge, where it is between 40 and 200, because in semiconductors the geometry factor plays a much smaller role than change in the specific resistivity due to deformation of the crystalline structure of the material. When a semiconductor material is stressed, its resistivity changes depending on the type of material and the doping

dose (see Sect. 10.2). However, the strain sensitivity in a semiconductor is temperature-dependent that requires a proper compensation when used over a broad temperature range.

#### 4.5.4 Moisture Sensitivity of a Resistor

By selecting material for a resistor, one can control its specific resistivity and its susceptibility to environmental factors. One of the factors that may greatly affect  $\rho$  is the amount of moisture that can be absorbed by the resistor. A moisture-dependent resistor can be fabricated of a hygroscopic material whose specific resistivity is strongly influenced by concentration of the absorbed water molecules. This is a basis for the resistive humidity sensors that are called *hygristors*.

A typical resistive hygristor is comprised of a ceramic substrate that has two silk-screen printed conductive interdigitized<sup>10</sup> electrodes (Fig. 4.20a). The electrodes are conductors where the space between them is covered by hygroscopic semiconductive gel that forms a matrix to suspend conductive particles (see Sect. 14.4). This structure forms a resistor between two electrodes. The gel [2] is typically fabricated of hydroxyethylcellulose, nonyl phenyl polyethylene glycol ether (a tongue twister for a nonchemist!), and other organic materials with addition of carbon powder. The gel is thoroughly milled to produce a smooth mixture. Another type of a hygristor is fabricated of lithium chloride (LiCl) film and a binder. The coated substrates are cured under controlled temperature and humidity.

Resistance of the coating changes with humidity in a nonlinear way as shown in Fig. 4.20b, which should be taken into account during calibration and data processing. The response time for many hygristors ranges from 10 to 30 s. It can be shortened in moving air. The resistance range varies from 1 k $\Omega$  to 100 M $\Omega$ .

Hygristors are the active sensors, that is, they require an excitation signal to produce an electrical output. It is important to use only symmetrical AC excitation current with no DC bias to prevent polarization of the coating, otherwise the sensor will be destroyed.

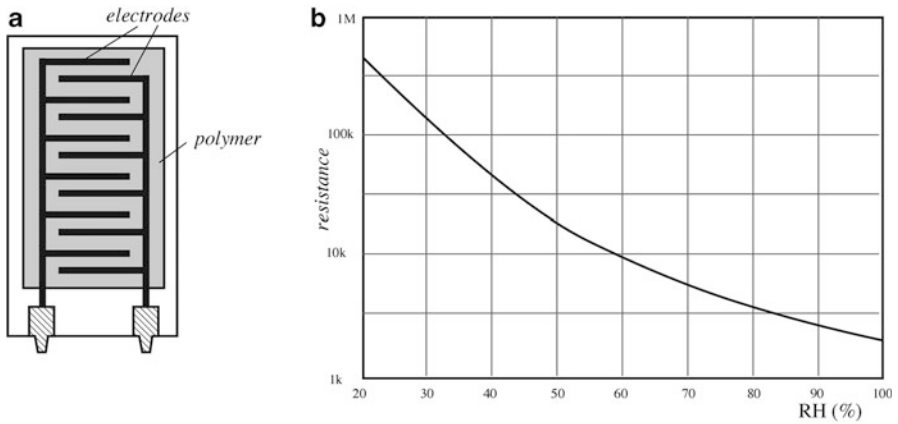
---

## 4.6 Piezoelectric Effect

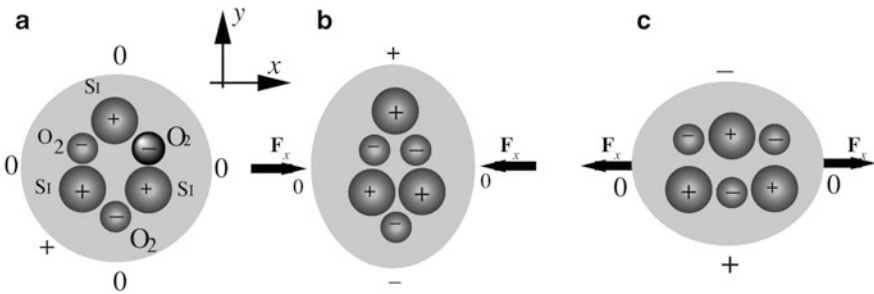
The piezoelectric effect is generation of electric charge by a crystalline material upon subjecting it to stress, or more accurately—a redistribution of the electric charge. The effect exists in natural crystals, such as quartz (chemical formula SiO<sub>2</sub>), and poled (artificially polarized) man-made ceramics and some polymers, such as PVDF. It is said that piezoelectric material possess ferroelectric properties. The name was given by an analogy with ferromagnetic properties, though there is no iron in most piezoelectrics. Unlike piezoresistivity that is manifested by change

---

<sup>10</sup>The term is based on a similarity between the electrode shape and shapes of human fingers (digits).



**Fig. 4.20** Hygristor design (a) and its transfer function (b)



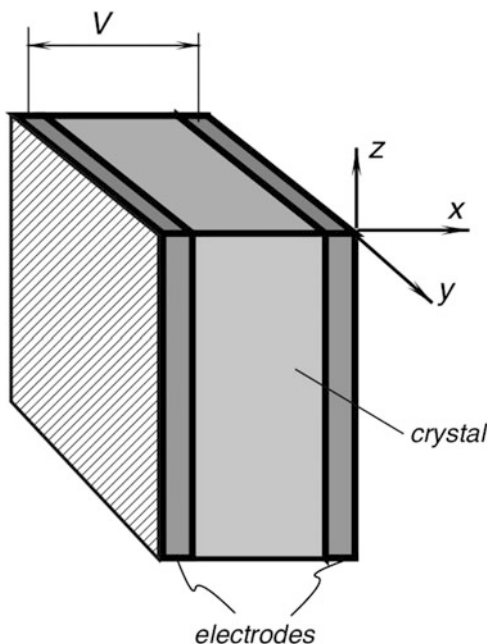
**Fig. 4.21** Piezoelectric effect in quartz crystal

of a resistance when pressed, piezoelectricity is manifested in appearance of electric charge on the surface in response to pressure.

The Curie brothers discovered the piezoelectric effect in quartz in 1880, but very little practical use was made until 1917 when another Frenchman, professor P. Langevin used x-cut plates of quartz to generate and detect sound waves in water. His work led to the development of sonar.

A simplified, yet quite explanatory model of the piezoelectric effect was proposed in 1927 by A. Meissner [3]. A quartz crystal is modeled as a helix, Fig. 4.21a, with one silicon, Si, and two oxygen, O<sub>2</sub>, atoms alternating around the helix. A quartz crystal is cut along its axes  $x$ ,  $y$ , and  $z$ , thus Fig. 4.21a is a view along the  $z$ -axis. In a single crystal-cell, there are three atoms of silicon and six oxygen atoms. Oxygen is being lumped in pairs. Each silicon atom carries four positive charges and a pair of oxygen atoms carries four negative charges (two per atom). Therefore a quartz cell is electrically neutral under the no-stress conditions. When external force,  $F_x$ , is applied along the  $x$ -axis, the hexagonal lattice becomes deformed. Figure 4.21b shows a compressing force, which shifts atoms in a crystal

**Fig. 4.22** Piezoelectric sensor is formed by applying electrodes to a poled crystalline material



in such a manner as a positive charge is built up at the silicon atom side and the negative at the oxygen pair side. Thus, the crystal develops an electric charge disbalance along the  $y$ -axis. If the crystal is stretched along the  $x$ -axis (Fig. 4.21c), a charge of opposite polarity is built along the  $y$ -axis, which is the result of a different deformation. This simple model illustrates that crystalline material can develop electric charge on its surface in response to a mechanical deformation. A similar explanation may be applied to the pyroelectric effect that is covered in the next section of this chapter.

To pickup an electric charge, at least two conductive electrodes must be applied to the crystal at the opposite sides of the cut (Fig. 4.22). As a result, a piezoelectric sensor becomes a capacitor with a dielectric material in-between the metal plates, where the dielectric is a piezoelectric crystalline material. The dielectric acts as a generator of electric charge, resulting in voltage  $V$  across the capacitor. Although charge in a crystalline dielectric is formed at the location of an acting force, metal electrodes equalize charges along the surface making the capacitor not selectively sensitive. However, if electrodes are formed with a complex pattern (e.g., multiple electrodes), it is possible to determine the exact location of the applied force by measuring the response from a selected electrode.

It can be said that strain in the material charges the capacitor. A piezoelectric sensor is a direct converter of a mechanical stress into electricity. The piezoelectric effect is a reversible physical phenomenon. This means that stress produces electricity, while voltage applied across the crystal produces mechanical strain—the material deformation. So the piezoelectric material can convert strain to electricity

and convert electricity to strain. It is possible by placing several electrodes on the crystal to use one pair of the electrodes to deliver voltage to the crystal and cause strain, and the other pair of the electrodes to pick up charge resulting from developed strain. This method is used quite extensively in various piezoelectric transducers and devices. For example in the crystal oscillators.

The magnitude of the piezoelectric effect in a simplified form can be represented by the vector of polarization [4]:

$$\mathbf{P} = \mathbf{P}_{xx} + \mathbf{P}_{yy} + \mathbf{P}_{zz}, \quad (4.64)$$

where  $x, y, z$  refer to a conventional orthogonal system related to the crystal axes. In terms of axial stress,  $\boldsymbol{\sigma}$ , we can write<sup>11</sup>

$$\begin{aligned} \mathbf{P}_{xx} &= d_{11}\boldsymbol{\sigma}_{xx} + d_{12}\boldsymbol{\sigma}_{yy} + d_{13}\boldsymbol{\sigma}_{zz}, \\ \mathbf{P}_{yy} &= d_{21}\boldsymbol{\sigma}_{xx} + d_{22}\boldsymbol{\sigma}_{yy} + d_{23}\boldsymbol{\sigma}_{zz}, \\ \mathbf{P}_{zz} &= d_{31}\boldsymbol{\sigma}_{xx} + d_{32}\boldsymbol{\sigma}_{yy} + d_{33}\boldsymbol{\sigma}_{zz}, \end{aligned} \quad (4.65)$$

where constants  $d_{mn}$  are the piezoelectric coefficients along the orthogonal axes of the crystal cut. Dimensions of these coefficients are C/N (coulomb/newton), i.e., charge unit per unit force. Depending on the material, all coefficients  $d$  may be quite different and for practical purposes the material should be used with the predominant direction where the coefficient is the largest.

Charge generated by the piezoelectric crystal is proportional to the applied force. For instance, in the  $x$ -direction the charge is

$$Q_x = d_{11}F_x. \quad (4.66)$$

Since a crystal with the deposited electrodes forms a capacitor having capacitance,  $C$ , voltage,  $V$ , which develops across the electrodes is:

$$V = \frac{Q_x}{C} = \frac{d_{11}}{C}F_x, \quad (4.67)$$

In turn, the capacitance can be represented by Eq. (4.23) through the electrode surface area,<sup>12</sup>  $a$ , crystal thickness,  $l$ , and  $\kappa$ —a dielectric constant:

$$C = \kappa\epsilon_0\frac{a}{l}. \quad (4.68)$$

Then, the sensor output voltage is

<sup>11</sup> The complete set of coefficients also includes shear stress and the corresponding  $d$ -coefficients.

<sup>12</sup> The electrode area, not the crystal area! Piezoinduced charge can be collected only over the area covered by the electrode.

$$V = \frac{d_{11}}{C} F_x = \frac{d_{11}l}{\kappa\epsilon_0a} F_x. \quad (4.69)$$

The formula suggests that to get a higher output voltage, the piezoelectric material shall have a smaller electrode area but a larger thickness. It also indicates that the transfer function of force to voltage is linear. But it should be remembered that voltage represented by Eq. (4.69) is the peak voltage of a decaying transient, since a piezoelectric sensor is an a.c. sensor that responds only to *changing forces* but not to a constant force, as it will be explained below.

### 4.6.1 Ceramic Piezoelectric Materials

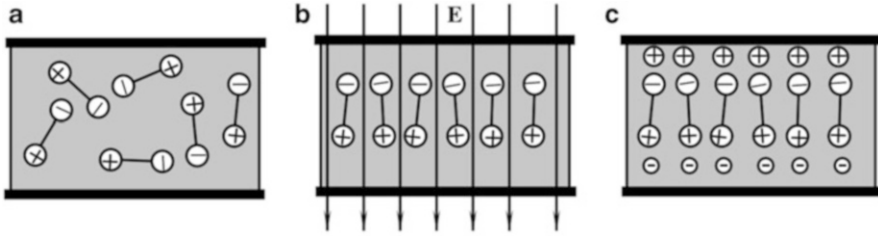
A popular ceramic material for piezoelectric sensors is *lead zirconium titanate* (PZT) having formula  $\text{Pb}(\text{Zr},\text{Ti})\text{O}_3$ . The sensor manufacturing begins with high purity metal oxides (lead oxide, zirconium oxide, titanium oxide, etc.) in form of fine powders having various colors. The powders are milled to a specific fineness, and mixed thoroughly in chemically correct proportions. In a process called “calcining”, the mixtures are then exposed to an elevated temperature, allowing the ingredients to react to form a powder, each grain of which has a chemical composition close to the desired final composition. At this stage, however, the grain does not have yet the desired crystalline structure.

The next step is to mix the calcined powder with solid and/or liquid organic binders (intended to burn out during firing) and mechanically form the mixture into a “cake” which closely approximates a shape of the final sensing element. To form the “cakes” of desired shapes, several methods can be used. Among them are pressing (under force of a hydraulic powered piston), casting (pouring viscous liquid into molds and allowing to dry), extrusion (pressing the mixture through a die, or a pair of rolls to form thin sheets), tape casting (pulling viscous liquid onto a smooth moving belt).

After the “cakes” have been formed, they are placed into a kiln and exposed to a very carefully controlled temperature profile. After burning out of organic binders, the material shrinks by about 15 %. The “cakes” are heated to a red glow and maintained at that state for some time, which is called the “soak time”, during which the final chemical reaction occurs. The crystalline structure is formed when the material is cooled down. Depending on the material, the entire firing may take 24 h.

When the material is cold, the contact electrodes are applied to its surface. This can be done by several methods. The most common of them are: a fired-on silver (a silk-screening of silver-glass mixture and refiring), an electroless plating (a chemical deposition in a special bath), and a sputtering (an exposure to metal vapor in a partial vacuum).

Crystallinities (crystal cells) in the material can be considered electric dipoles. In some materials, like quartz, these cells are naturally oriented along the crystal axes,



**Fig. 4.23** Thermal poling of piezo- and pyroelectric material

thus giving the material sensitivity to stress. In other materials, the dipoles are randomly oriented and the materials need to be “poled” to possess piezoelectric properties. To give a crystalline material the piezoelectric properties, several poling techniques can be used. The most popular poling process is a thermal poling, which includes the following steps:

1. A crystalline material (ceramic or polymer film—see next section), which has randomly oriented dipoles, Fig. 4.23a, is warmed up slightly below its Curie temperature. In some cases (e.g., for a PVDF film) the material is stretched (strained) to give the crystals a predominant orientation. High temperature results in a stronger agitation of dipoles and permits to orient them more easily in a desirable direction.
2. Material is placed in strong electric field,  $E$ , as illustrated in Fig. 4.23b, where dipoles align along the field lines. The alignment is not total. Many dipoles deviate from the field direction quite strongly, however, a statistically predominant orientation of the dipoles is maintained.
3. The material is cooled down while the electric field across its thickness is maintained.
4. The electric field is removed and the poling process is complete. As long as the poled material is maintained below the Curie temperature, its polarization remains permanent. The dipoles stay “frozen” in the direction, which was given to them by the electric field at high temperature, as shown in Fig. 4.23c.

Another method called a corona discharge poling. It is used to produce polymer piezo/pyroelectric films (see Sect. 4.6.2). The film is subjected to a corona discharge from an electrode at several million volts per cm of film thickness for 40–50 s [5, 6]. Corona polarization is uncomplicated to perform and can be easily applied before electric breakdown occurs, making this process useful at room temperature.

The final operation includes cutting, machining, and grinding. After the piezo (pyro) element is prepared, it is installed into a sensor’s housing, where its electrodes are bonded to the electrical terminals and/or other electronic components.

After poling, the crystal remains permanently polarized, with an electric charge formed at the electrodes for a relatively short time. There is a sufficient amount of

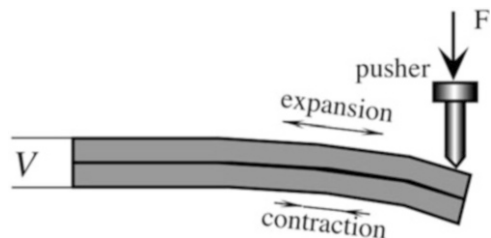


free charge carriers, which move in the electric field setup inside the bulk material and there are plenty charged ions in the surrounding air. The charge carriers move toward the poled dipoles and neutralize their charges as in Fig. 4.23c. Hence, after a while, the poled piezoelectric material becomes electrically discharged as long as it remains under steady-state conditions. When stress is applied, or air blows near its surface (Sect. 12.6) the balanced state is degraded and the piezoelectric material develops electric charges on its opposite surfaces. If the stress is maintained, the charges again will be neutralized by the internal leakage. Thus, a piezoelectric sensor is responsive only to a *changing stress* rather than to a steady level of it. In other words, a piezoelectric sensor is an a.c. device, rather than a d.c. device.

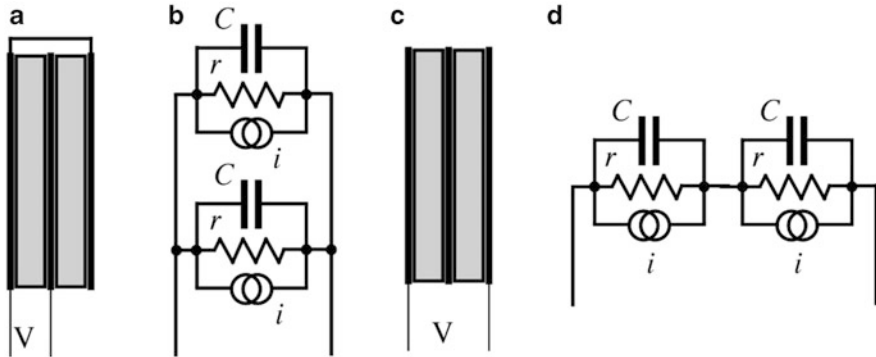
Piezoelectric directional sensitivities ( $d$  coefficients) are temperature-dependent. For some materials (quartz), sensitivity drops with a slope of about  $-0.016\ \%/^{\circ}\text{C}$ . For others (the PVDF films and ceramics) at temperatures below  $40\ ^{\circ}\text{C}$  it may go down, while at higher temperatures it increases with a raise in temperature. Nowadays, the most popular materials for fabrication piezoelectric sensors are ceramics [7–9]. The earliest of the ferroelectric ceramics was barium titanate, a polycrystalline substance having the chemical formula  $\text{BaTiO}_3$ . The stability of permanent polarization relies on the coercive force of the dipoles. In some materials, polarization may decrease with time. To improve stability of a poled material, impurities have been introduced into the basic material with the idea that the polarization may be “locked” into a position [4]. While the piezoelectric constant changes with operating temperature, a dielectric constant,  $\kappa$ , exhibits a similar dependence. Thus, according to Eq. (4.69), variations in these values tend to cancel each other as they are entered into numerator and denominator. This results in a better stability of the output voltage,  $V$ , over a broad temperature range.

The piezoelectric elements may be used as a single crystal, or in a multilayer form where several plates of the material are laminated together. This must be done with the electrodes placed in-between. Figure 4.24 shows a two-layer force sensor.<sup>13</sup> When an external force  $F$  is applied, the upper part of the sensor expands while the bottom compresses. If the layers are laminated correctly, this produces a double output signal. Double sensors can have either a parallel connection as shown in Fig. 4.25a, or a serial connection as in Fig. 4.25c. The electrical equivalent circuit

**Fig. 4.24** Laminated two-layer piezoelectric sensor



<sup>13</sup> Remember, a piezoelectric sensor is an AC device, so it will not respond to a constant or slowly changing force.



**Fig. 4.25** Parallel (a) and serial (c) laminated piezoelectric sensors and their corresponding equivalent circuits (b and d)

of the piezoelectric sensor is a parallel connection of a stress-induced current source ( $i$ ), leakage resistance ( $r$ ), and capacitance ( $C$ ). Depending on the layer connection equivalent circuits for the laminated sensors are as shown in Fig. 4.25b, d. The leakage resistors  $r$  are very large—on the orders of  $10^{12}$ – $10^{14}$   $\Omega$ , meaning that the sensor has an extremely high output impedance. This requires special interface circuits, such as charge- to-voltage or current-to-voltage converters, or the voltage amplifiers with very high input resistances and very low input capacitances.

Since silicon does not possess piezoelectric properties, such properties can be added on by depositing crystalline layers of piezoelectric materials. The three most popular materials are zinc oxide (ZnO), aluminum nitride (AlN), and PZT ceramic, basically the same material used for fabrication of discrete piezoelectric sensors as described above.

Zinc oxide in addition to the piezoelectric properties also is pyroelectric. It was the first and most popular material for development of the ultrasonic acoustic sensors, surface acoustic wave (SAW) devices, microbalances, etc. One of its advantages is the ease of chemical etching in production of MEMS devices. The zinc oxide thin films are usually deposited on silicon by employing the sputtering technology.

Aluminum nitride, AlN, is an excellent piezoelectric material because of its high acoustic velocity and its endurance in humidity and high temperature. Its piezoelectric coefficient is somewhat lower than of ZnO but higher than of other thin-film piezoelectric materials, excluding ceramics. The high acoustic velocity makes it an attractive choice in the GHz frequency range. Usually, the AlN thin films are fabricated by using the chemical vapor deposition (CVD) or reactive molecular beam epitaxy (MBE) technologies. However, the drawback of using these deposition methods is the need for high heating temperature (up to 1300 °C) of the substrate.

The PZT thin films possesses a larger piezoelectric coefficient than ZnO or AlN, and also a high pyroelectric coefficient, which makes it a good candidate for

fabrication of thermal radiation detectors. A great variety of deposition techniques is available for the PZT, among which are the electron-beam evaporation [10], RF sputtering [11], ion-beam deposition [12], epitaxial growth by RF sputtering [13], magnetron sputtering [14], laser ablation [15], and sol-gel [16].

#### 4.6.2 Polymer Piezoelectric Films

In 1969, H. Kawai discovered a strong piezoelectricity in PVDF (polyvinylidene fluoride) and in 1975 the Japanese company Pioneer, Ltd. developed the first commercial product with the PVDF as piezoelectric loudspeakers and earphones [17]. PVDF is a semicrystalline polymer with an approximate degree of crystallinity of 50 % [18]. Like other semicrystalline polymers, PVDF consists of a lamellar structure mixed with amorphous regions. The chemical structure of it contains the repeat unit of doubly fluorinated ethene  $\text{CF}_2\text{-CH}_2$ :



PVDF molecular weight is about  $10^5$ , which corresponds to about 2000 repeat units. The film is quite transparent in the visible and near-IR region, and is absorptive in the mid- and far-infrared portions of the electromagnetic spectrum. The polymer melts near  $170^\circ\text{C}$ . Its density is about  $1780\text{ kg/m}^3$ . It is a mechanically durable and flexible material.

PVDF does not have a higher, or even as high piezoelectric coefficient as other commonly used materials, like  $\text{BaTiO}_3$  or PZT. However, it has a unique quality not to depolarize while being subjected to very high alternating electric fields. This means that even though the value of  $d_{31}$  of PVDF is about 10 % of PZT, the maximum strain observable in PVDF will be ten times larger than in PZT since the maximum permissible field is a hundred times greater for PVDF. The film exhibits good stability: when stored at  $60^\circ\text{C}$  it loses its sensitivity by about 1–2 % over 6 months. Comparative characteristics for various piezoelectric materials are given in Table A.8. Another advantage of piezofilm over piezoceramic is its low acoustic impedance, which is closer to that of water, human tissue, and other organic materials. For example, the acoustic impedance of piezofilm is only 2.6 times that of water, whereas piezoceramics are typically 11 times greater. A close impedance match permits more efficient transduction of acoustic signals in water and tissue.

Like some other ferroelectric materials, PVDF is also pyroelectric (Sect. 4.7 below), producing electrical charge in response to a change in temperature. PVDF strongly absorbs infrared energy in the 7–20  $\mu\text{m}$  wavelengths, covering the same wavelength spectrum as heat from the human body. However, in spite that the film can absorb thermal radiation, a pyroelectric sensor has the film sandwiched between two thin metal electrodes that can be quite reflective, so no infrared radiation can

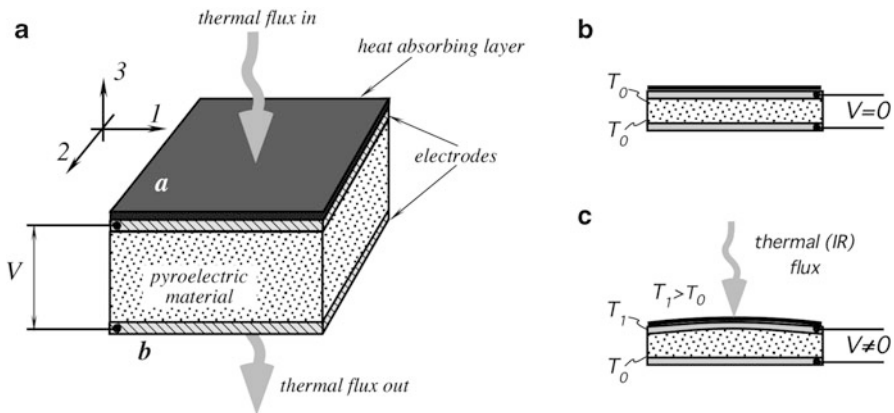
penetrate the electrodes and be absorbed by the film. To resolve this difficulty, the electrode that is exposed to thermal radiation either is coated with a heat-absorbing layer or is made of Nichrome—a metal alloy having high infrared absorptivity. When the thermal radiation is absorbed, it is converted into heat that quickly propagates through the PVDF film by means of thermal conduction.

The PVDF film makes a useful human motion sensor as well as pyroelectric sensor for more sophisticated applications like vidicon cameras for night vision and laser beam profiling sensors. Also, it has a broad range of applications in robotics, medicine, prosthetics [19], and even in Space exploration for detecting micrometeorites. The copolymers of PVDF permit use at higher temperatures (135 °C) and offer desirable new sensor shapes, like cylinders and hemispheres. Piezoelectric cable is also produced using the copolymer (Sect. 10.5).

### 4.7 Pyroelectric Effect

The pyroelectric materials are crystalline substances capable of generating an electrical charge in response to heat flow. The pyroelectric effect very closely relates to the piezoelectric effect. Before going further, we recommend that the reader should familiarize herself with Sect. 4.6.

Like piezoelectrics, the pyroelectric materials are used in form of thin ceramic slices or films with the charge pick-up electrodes deposited on the opposite sides, Fig. 4.26a. A pyroelectric sensor is essentially a capacitor that can be electrically charged by thermal flux. Even though there is no difference of the origin of heat—either from contacting a warm/cold surface, or by absorbing thermal radiation, the result is the same—electric charge is generated.



**Fig. 4.26** Pyroelectric sensor has two electrodes at opposite sides of crystal (a). Thermal radiation is applied along axis 3 from top and absorbed by heat-absorbing layer. Heat conductively travels through pyroelectric material and is partially emanated downward from side *a*. Pyroelectric sensor in neutral state (b); heat expands upper layer, resulting in piezoelectric charge (c)

The detector does not require any external electrical bias (excitation signal), thus it is a direct converter of a heat flow into electricity. It needs only an appropriate electronic interface circuit to measure the charge. Contrary to thermoelectrics (thermocouples) that produce a steady voltage when two dissimilar metal junctions are held at steady but different temperatures (Sect. 4.9), pyroelectrics generate charge only in response to a *change* in temperature. Since a change in temperature essentially causes propagation of heat, a pyroelectric device is a heat *flow* detector rather than heat detector. When a pyroelectric crystal is exposed to a heat flow (for instance, from an infrared radiation source or from touching a warm or cold object), temperature of the exposed side is elevated and the side becomes a source or sink of heat which propagates through the pyroelectric material towards or from its opposite side. Hence, there is an outflow of heat from the crystal to the environment, as it is shown in Fig. 4.26a.

A crystal is considered to be pyroelectric if it exhibits a spontaneous temperature-dependent polarization. Of the 32 crystal classes, 21 are noncentrosymmetric and 10 of these exhibit pyroelectric properties. Beside the pyroelectric properties, all these materials exhibit piezoelectric properties as well—they generate electrical charge in response to mechanical stress. Thus, when a pyroelectric sensor is designed, it is very important to minimize all potential mechanical disturbances.

Pyroelectricity was observed for the first time in tourmaline crystals in the eighteenth century (some claim that the Greeks noticed it 23 centuries ago). Later, in the nineteenth century, Rochelle salt was used to make pyroelectric sensors. A large variety of materials became available after 1915: KDP ( $\text{KH}_2\text{PO}_4$ ), ADP ( $\text{NH}_4\text{H}_2\text{PO}_4$ ),  $\text{BaTiO}_3$ , and a composite of  $\text{PbTiO}_3$  and  $\text{PbZrO}_3$  known as PZT. Presently, more than 1000 materials with a reversible polarization are known. They are called ferroelectric crystals.<sup>14</sup> The most important among them are triglycine sulfate (TGS) and lithium tantalate oxide ( $\text{LiTaO}_3$ ). In 1969 H. Kawai discovered strong piezoelectricity in the plastic materials, polyvinyl fluoride (PVF) and polyvinylidene fluoride (PVDF) [20]. These materials also possess substantial pyroelectric properties.

A pyroelectric material can be considered as a composition of a large number of minute crystallinities, where each behaves as a small electric dipole. All these dipoles are randomly oriented, see Fig. 4.23a. Above a certain temperature, known as the *Curie point*, the crystallinities have no dipole moment. Manufacturing (poling) of pyroelectric materials is similar to that of the piezoelectrics (see Sect. 4.6.1).

There are several mechanisms by which changes in temperature will result in pyroelectricity. Temperature changes may cause shortening or elongation of individual dipoles. It may also affect the randomness of the dipole orientations due to thermal agitation. These phenomena are called *primary* pyroelectricity. There is also *secondary* pyroelectricity that, in a simplified way, may be described as a result

---

<sup>14</sup>This is a misnomer as the prefix *ferro*, meaning *iron*, is used despite the fact that most ferroelectric materials do not have iron in their lattice. It is used by analogy with ferromagnetics.

of the piezoelectric effect, that is, development of strain in the material due to thermal expansion. Figure 4.26b shows a pyroelectric sensor whose temperature  $T_0$  is homogeneous over its volume. That is, the sensor generates zero voltage across the electrodes. Now, let us assume that heat is applied to the top side of the sensor, Fig. 3.26c, in form of thermal (infrared) radiation. The radiation is absorbed by the heat-absorbing layer (e.g., goldblack or organic paint) and warms up the upper side of the pyroelectric material. As a result of the heat absorption, the upper side becomes warmer (the new warmer temperature is  $T_1$ ) which causes the top side of the sensor to expand. The expansion leads to flexing (straining) of the crystalline material, which, in turn, produces stress and a change in a dipole orientation. Being a piezoelectric, the stressed material generates electric charges of the opposite polarities on the electrodes and thus a voltage is observed across the electrodes. Hence, we may regard a secondary pyroelectricity as a sequence of the events: thermal radiation—heat absorption—thermally induced stress—electric charge.

Let us analyze properties of a pyroelectric material. The dipole moment,  $M$ , of the bulk pyroelectric sensor is

$$M = \mu Ah, \tag{4.71}$$

where  $\mu$ —the dipole moment per unit volume,  $A$  is the sensor’s area and  $h$  is the thickness. The charge,  $Q_a$ , which can be picked up by the electrodes, develops the dipole moment across the material

$$M_o = Q_a \cdot h. \tag{4.72}$$

$M$  must be equal to  $M_o$ , so that

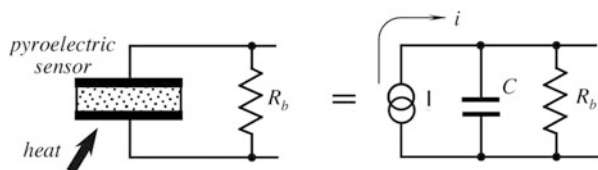
$$Q_a = \mu \cdot A \tag{4.73}$$

As the temperature varies, the dipole moment also changes, resulting in an induced charge. Thermal absorption may be related to a dipole change, so that  $\mu$  must be considered as function of both temperature,  $T_a$ , and an incremental thermal energy,  $\Delta W$ , absorbed by the material

$$\Delta Q_a = A \cdot \mu(T_a, \Delta W). \tag{4.74}$$

Figure 4.27 depicts a pyroelectric detector (pyroelectric element) connected to resistor  $R_b$  that represents either the internal leakage resistance or a combined input resistance of the interface circuit, which is connected to the element. The equivalent electrical circuit of the sensor is shown at right. It consists of three components: a

**Fig. 4.27** Pyroelectric sensor and its equivalent circuit



current source that generates the heat-induced current,  $i$ , (remember that current is a movement of electric charges), sensor's capacitance,  $C$ , and leakage resistance,  $R_b$ .

The output signal from the pyroelectric sensor can be taken in form of either charge (current) or voltage, depending on the application. Being a capacitor, the pyroelectric device is discharged when connected to a resistor,  $R_b$ . Electric current through the resistor and voltage across the resistor represent the heat flow-induced charge. It can be characterized by two pyroelectric coefficients [21]

$$P_Q = \frac{dP_s}{dT} \quad \text{Pyroelectric charge coefficient,} \quad (4.75)$$

$$P_V = \frac{dE}{dT} \quad \text{Pyroelectric voltage coefficient,} \quad (4.76)$$

where  $P_s$  is the spontaneous polarization (which is the other way to say: “*electric charge*”),  $E$  is the electric field strength, and  $T$  is temperature in K. Both coefficients are related by way of the electric permittivity,<sup>15</sup>  $\kappa$  and electric permittivity of free space,  $\epsilon_0$

$$\frac{P_Q}{P_V} = \frac{dP_s}{dE} = \kappa\epsilon_0. \quad (4.77)$$

The polarization is temperature dependent and, as a result, both pyroelectric coefficients of Eqs. (4.75 and 4.76) are also functions of temperature.

If a pyroelectric material is exposed to a heat source, its temperature rises by  $\Delta T$  and the corresponding charge and voltage changes can be described by the following equations

$$\Delta Q = P_Q A \Delta T \quad (4.78)$$

$$\Delta V = P_V h \Delta T \quad (4.79)$$

Remembering that the sensor's capacitance can be defined as

$$C_e = \frac{\Delta Q}{\Delta V} = \kappa\epsilon_0 \frac{A}{h}, \quad (4.80)$$

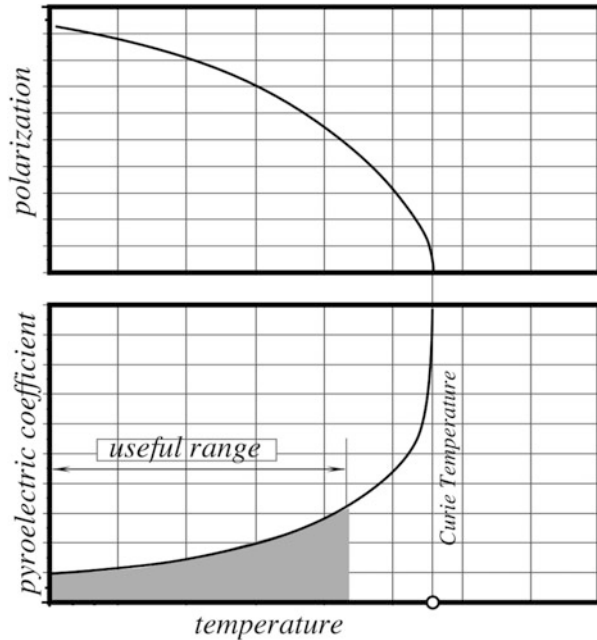
then, from Eqs. (4.78–4.80) it follows that:

$$\Delta V = P_Q \frac{A}{C_e} \Delta T = P_Q \frac{\kappa\epsilon_0}{h} \Delta T \quad (4.81)$$

Thus, the peak output voltage is proportional to the sensor's temperature rise and

<sup>15</sup> Electric permittivity is the same thing as dielectric constant.

**Fig. 4.28** Polarization of a pyroelectric crystal. The sensor must be stored and operated below Curie temperature



pyroelectric charge coefficient and inversely proportional to the sensing element thickness.

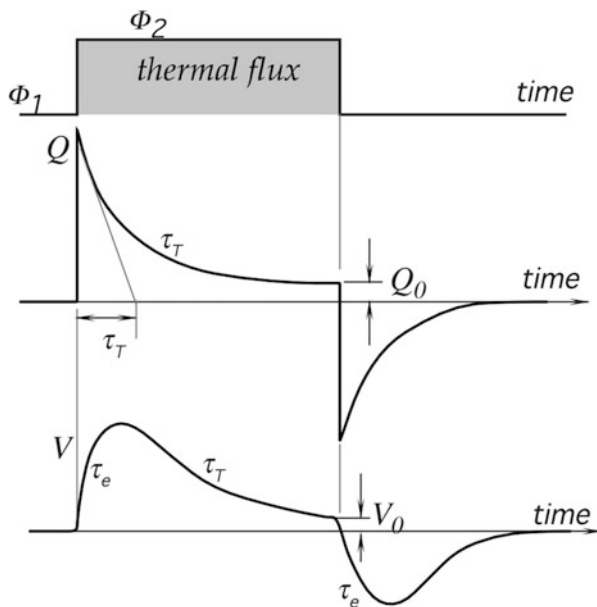
When the pyroelectric element is subjected to a thermal gradient, its polarization (electric charge developed across the crystal) varies with temperature of the crystal. A typical polarization-temperature curve is shown in Fig. 4.28. The voltage pyroelectric coefficient,  $P_v$ , is a slope of the polarization curve. It increases dramatically near the Curie temperature at what the polarization disappears and the material permanently loses its pyroelectric properties. The curves imply that the sensor's sensitivity increases with temperature at the expense of nonlinearity.

Piezo- and pyroelectric materials such as lithium-tantalite and the polarized ceramics are typical materials to produce the pyroelectric sensors. During recent years, a deposition of pyroelectric thin films has been intensively employed in the MEMS technologies. Especially effective is use of lead-titanate-oxide ( $\text{PbTiO}_3$ ) that is a ferroelectric ceramic having both a high pyroelectric coefficient and a high Curie temperature of about  $490^\circ\text{C}$ . This material can be easily deposited on the silicon substrates by the so called sol-gel spin casting deposition method [22] as described in Sect. 19.3.1.

Figure 4.29 shows the timing diagrams for a pyroelectric sensor when it is exposed to a step function of thermal flux. It is seen that the electric charge reaches its peak value almost instantaneously, and then decays with a *thermal time constant*,  $\tau_T$ . The physical meaning is this: a thermally induced polarization occurs initially in the most outer layer of the crystalline material (just few atomic layers), whose



**Fig. 4.29** Response of a pyroelectric sensor to a thermal step function. Magnitudes of charge  $Q_0$  and voltage  $V_0$  are exaggerated for clarity



temperature nearly instantaneously raises to its maximum level. This creates the highest thermal gradient across the material thickness, leading to the maximum polarization. Then, heat propagates through the material, being absorbed by its mass in proportion to thermal capacity,  $C_T$ , while some of the heat is lost to the surroundings through a thermal resistance,  $R_T$ . This diminishes the initial gradient that generates the electric charge. The thermal time constant is a product of the sensors' thermal capacity and thermal resistance:

$$\tau_T = C_T R_T = c A h R_T, \quad (4.82)$$

where  $c$  is the specific heat of the pyroelectric element. The thermal resistance  $R_T$  is function of all thermal losses to the surroundings through convection, conduction, and thermal radiation. For the low frequency applications, it is desirable to use sensors with  $\tau_T$  as large as practical, while for the high speed applications (for instance, to measure laser pulses), a thermal time constant should be dramatically reduced. For that purpose, the pyroelectric material may be laminated with a heat sink: a piece of aluminum or copper.

When a pyroelectric sensor is exposed to a heat source, we consider a thermal capacity of the source being very large (an infinite heat source), and thermal capacity of the sensor small. Therefore, the surface temperature  $T_b$  of a target can be considered constant during the measurement, while temperature of the sensor  $T_s$  is a function of time. That time function is dependent on properties of the sensing element: its density, specific heat, and thickness as per Eq. (4.82). If the input thermal flux has shape of a step function of time and the sensor is freely mounted in air, the output current can be approximated by an exponential function, so that

$$i = i_0 e^{-t/\tau_T}, \quad (4.83)$$

where  $i_0$  is peak current.

In Fig. 4.29, as long as a heat source is present, the charge  $Q$  and voltage  $V$  do not completely return to zero, no matter how much time has elapsed. Thermal energy enters the pyroelectric material from side a (Fig. 4.26), resulting in the material temperature increase. Subsequently, the sensor's response decays with a thermal time constant  $\tau_T$ . However, since the other side b of the sensor faces a cooler environment, part of the thermal energy leaves the sensor and is lost to its surroundings. Because the sides a and b face objects of different temperatures (one is a heat source and the other is the environment), a continuous heat flow exists through the pyroelectric material and it maintains a continuous, albeit small, level of polarization. Thus, electric current generated by the pyroelectric sensor has the same shape as the thermal flow through the sensing material. An accurate measurement can demonstrate that as long as heat continues to flow, the pyroelectric sensor generates a constant voltage  $v_0$ , whose magnitude is proportional to the heat flow, thus making the device a heat flow sensor. The output voltage greatly depends on the sensing element capacitance and input resistance of the interface circuit that define the voltage rise time. It is characterized by the electric time constant  $\tau_e$  being a product of the sensor capacitance and input resistance.

---

## 4.8 Hall Effect

This physical effect was discovered in 1879 in Johns Hopkins University by E. H. Hall. Initially, the effect had a limited, however, a very valuable application as a tool for studying electrical conduction in metals, semiconductors, and other conductive materials. Nowadays, the Hall sensors are widely used for detecting magnetic fields, position, and displacement of objects [23, 24].

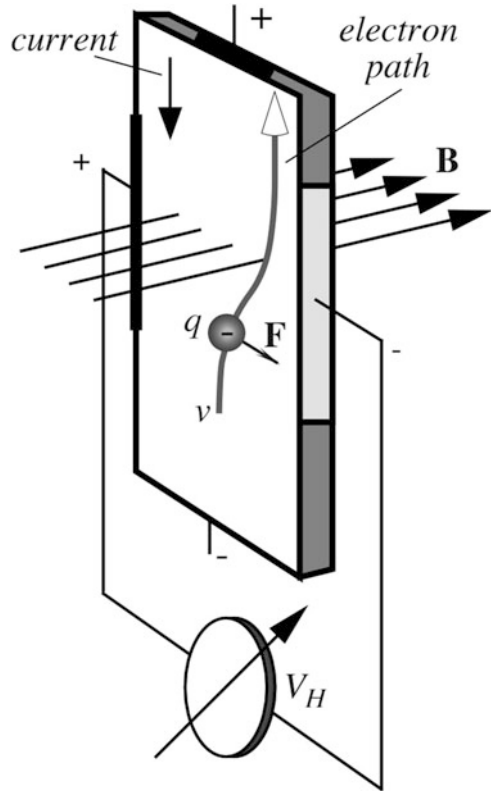
The effect is based on interaction between moving electric carriers and external magnetic field, known as Faraday's law: development of electromotive force as electric charge moves in magnetic field. In metals, these electric carriers (charges) are electrons. When an electron moves through a magnetic field, upon it acts the sideways force:

$$\mathbf{F} = q\mathbf{v}\mathbf{B}, \quad (4.84)$$

where  $q = 1.6 \times 10^{-19}$  C is an electronic charge,  $\mathbf{v}$  is the speed of an electron, and  $\mathbf{B}$  is the magnetic field. Vector notation (bold face) is indication that the force direction and its magnitude depend on the spatial relationship between the magnetic field and the direction of the electron movement. The unit of  $\mathbf{B}$  is  $1 \text{ T} = 1 \text{ N}/(\text{A} \cdot \text{m}) = 10^4 \text{ G}$ .

Let us assume that electrons move inside a flat conductive strip that is placed in magnetic field  $\mathbf{B}$  (Fig. 4.30). The strip has two additional contacts at its left and right sides that are connected to a voltmeter. Two other contacts are placed at the

**Fig. 4.30** Concept of Hall effect sensor. Magnetic field deflects movement of electric charges

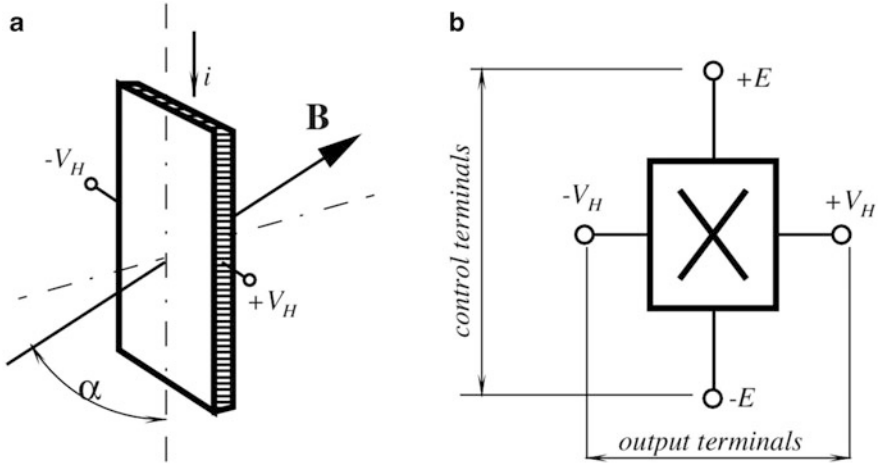


upper and lower ends of the strip. These are connected to a source of electric current. Due to the magnetic field, the deflecting force shifts the moving electrons toward the right side of the strip, which becomes more negative than the left side. The stronger the electric current and the stronger the magnetic field, the larger the number of the shifted electrons. That is, the magnetic field and electric current produce the so-called *transverse Hall potential difference*  $V_H$ . The sign and amplitude of this potential depend on both magnitude and directions of magnetic field and electric current. At a fixed temperature it is given by

$$V_H = hiB \sin \alpha, \quad (4.85)$$

where  $\alpha$  is the angle between the magnetic field vector and the Hall plate (Fig. 4.31), and  $h$  is the coefficient of overall sensitivity whose value depends on the plate material, its geometry (active area), and temperature.

The overall sensitivity depends on the *Hall coefficient*, which can be defined as the transverse electric potential gradient per unit magnetic field intensity per unit current density. According to the free electron theory of metals, the Hall coefficient is given by



**Fig. 4.31** Output signal of a Hall sensor depends on angle between magnetic field vector and plate (a); four terminals of Hall sensor (b)

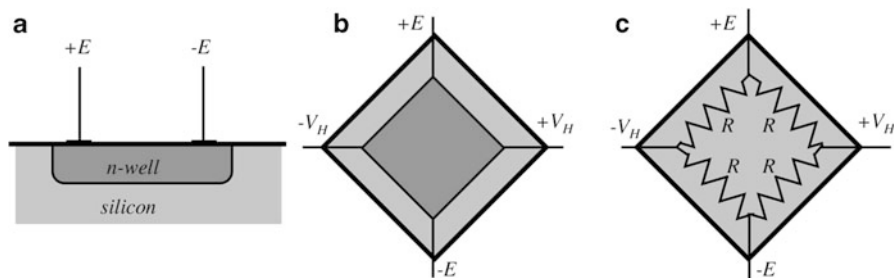
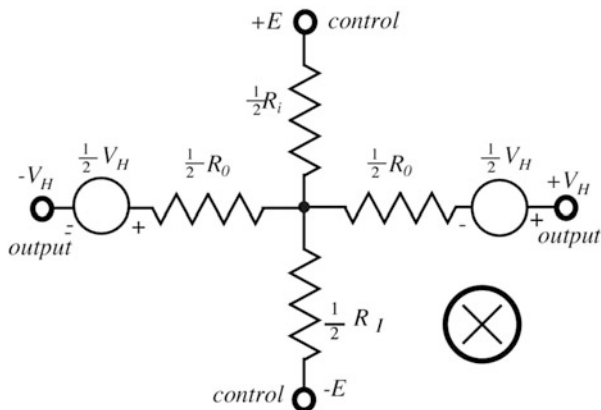
$$H = \frac{1}{Ncq}, \tag{4.86}$$

where  $N$  is the number of free electrons per unit volume and  $c$  is the speed of light. Depending on the material crystalline structure, charges may be either electrons (negative) or holes (positive). As a result, the Hall effect may be either negative or positive.

A linear Hall effect sensor is usually packaged in a four-terminal housing. Terminals for applying the control current are called the *control* terminals and a resistance between them is called the *control resistance*  $R_i$ . The terminals where the output voltage is observed are called the *differential output terminals* and a resistance between them is called the *differential output resistance*,  $R_o$ . The sensor's equivalent circuit (Fig. 4.32) may be represented by the cross-connected resistors and two voltage sources connected in series with the output terminals. The cross  $\otimes$  in Figs. 4.31b and 4.32 indicates the direction of the magnetic field from the viewer to the symbol plane.

The sensor is specified by its resistances,  $R_i$  and  $R_o$ , across both pairs of terminals, the offset voltage at no magnetic field applied, the sensitivity, and the temperature coefficient of sensitivity. Many Hall effect sensors are fabricated from silicon and fall into two general categories—the basic sensors and integrated sensors. Other materials used for the element fabrication include InSb, InAs, Ge, and GaAs. In the silicon element, an interface electronic circuit are frequently incorporated into the same wafer. This integration is especially important since the Hall effect voltage is quite small. An example of an integration is the three-axis compass AK8975 for smartphones manufactured by AsahiKasei.

**Fig. 4.32** Equivalent circuit of Hall sensor



**Fig. 4.33** Silicon Hall effect sensor with n-well (a and b) and equivalent resistive bridge circuit (c)

In a discrete Hall Effect sensor, a built-in interface circuit may contain a threshold device thus making an integrated sensor a two-state device. That is, it generates “zero” when magnetic field strength is below the threshold, and produces “one” when magnetic field is strong enough to cross the threshold.

Because of a natural piezoresistivity of silicon, all Hall effect sensors are susceptible to mechanical stress effects. Caution should be exercised to minimize application of stress to the leads or the housing. The sensor is also sensitive to temperature variations because temperature influences resistance of the element. If the element is fed by a voltage source, temperature will change the control resistance, and subsequently the control current. Hence, it is preferable to connect the control terminals to a current source rather than to a voltage source.

One way to fabricate the Hall sensor is to use a silicon *p*-substrate with ion-implanted *n*-wells, Fig. 4.33a. Electrical contacts provide connections to the power supply terminals and form the sensor outputs. A Hall element is a simple square where a well with four electrodes attached to the diagonals, Fig. 4.33b. A helpful way of looking at the Hall sensor is to picture it as a resistive bridge

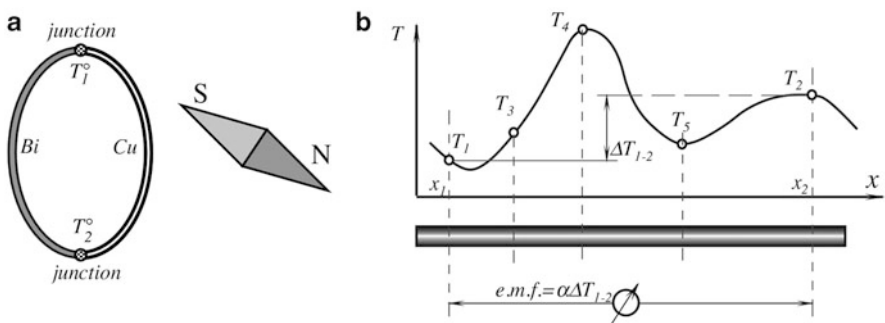
depicted in Fig. 4.33c. This representation makes its practical applications more conventional because the bridge circuits are the most popular circuits with well-established methods of design (Sect. 6.2.3). For examples of practical designs with the Hall Effect sensors see Sect. 8.4.6.

## 4.9 Thermoelectric Effects

### 4.9.1 Seebeck Effect

In 1821, Thomas Johann Seebeck (1770–1831), an Estonian born and Berlin and Göttingen educated physician, accidentally joined semicircular pieces of bismuth and copper while studying thermal effects on galvanic arrangements [25]. A nearby compass indicated a magnetic disturbance, Fig. 4.34a. Seebeck experimented repeatedly with different metal combinations at various temperatures, noting related magnetic field strengths. Curiously, he did not believe that an electric current was flowing, and preferred to describe that effect as “thermomagnetism” [26].

If we take a conductor and place one end of it into a cold place and the other end into a warm place, energy will flow from the warm to cold part. The energy takes the form of heat. Intensity of the heat flow is proportional to the thermal conductivity of the conductor. Besides, the thermal gradient also sets an *electric field* inside the conductor (this directly relates to Thompson effect<sup>16</sup>). The thermally induced electric field results in incremental voltage:



**Fig. 4.34** Seebeck experiment (a), varying temperature along a conductor is a source of a thermoelectric e.m.f. (b)

$$dV_a = \alpha_a \frac{dT}{dx} dx, \quad (4.87)$$

where  $dT$  is the temperature gradient across small length  $dx$  and  $\alpha_a$  is the *absolute* Seebeck coefficient of the material [27]. If the material is homogeneous,  $\alpha_a$  is not function of length and Eq. (4.87) becomes:

$$dV_a = \alpha_a dT. \quad (4.88)$$

Equation (4.88) is the principle mathematical expression of a thermoelectric effect. Figure 4.34b shows a conductor having nonuniform temperature  $T$  along its length  $x$ . A temperature gradient between any arbitrary points defines an electromotive force (e.m.f.) between these points. Other possible temperatures between the selected points (temperatures  $T_3$ ,  $T_4$ , and  $T_5$ , for example) make no effect whatsoever on the value of e.m.f. between points 1 and 2—only temperatures of these two points matter.

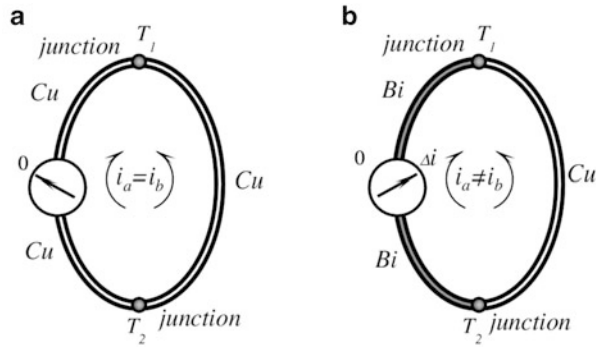
To measure e.m.f., we would like to connect a voltmeter to the conductor as shown in Fig. 4.34b and this is not as simple as may first look. To measure thermally induced e.m.f. we would need to attach the voltmeter probes. However, the probes are also made of conductors that may be different from the conductor we study. As a result, the probe contacts will introduce their own e.m.f. and disturb our experiment. Let us consider a simple measurement electric circuit where a current loop is formed. We cut the left side of the conductor (Cu) and insert the current meter into the cut in series with the wire, Fig. 4.35a. If the entire loop is made of a uniform material, say copper, then no current will be observed, even if the temperature along the conductor is not uniform. Electric fields in the left and right arms of the loop produce equal currents  $i_a = i_b$  which cancel one another, resulting in zero net current. A thermally induced e.m.f. exists in every thermally nonhomogeneous conductor, but it cannot be directly measured.

In order to observe *thermoelectricity*, it is in fact necessary to have a circuit composed of two *different* materials,<sup>17</sup> and we can then measure the *net* difference between their thermoelectric properties. Figure 4.35b shows a loop of two dissimilar metals which produces net current  $\Delta i = i_a - i_b$ . The actual current depends on many factors, including the shape and size of the conductors. If, on the other hand, instead of current we measure the net voltage across the broken conductor, the potential will depend *only* on the materials and the temperature difference. It does not depend on any other factors. A thermally induced potential difference is called

<sup>16</sup> A Thomson effect was discovered by William Thomson around 1850. It consists of absorption or liberation of heat by passing current through a homogeneous conductor which has a temperature gradient across its length. Unlike the Joule effect (liberated heat is proportional to square of current), the heat is linearly proportional to current. Heat is absorbed when the current and heat flow in opposite directions, and heat is produced when they flow in the same direction.

<sup>17</sup> Or perhaps the same material in two different states, for example, one under strain, the other is not.

**Fig. 4.35** Thermoelectric loop Joints of identical metals produce zero net current at any temperature difference (a); joints of dissimilar metals produce net current  $\Delta i$  (b)



the *Seebeck potential*. Note that the only way to eliminate influence of the voltmeter terminals is to connect it into a cut as shown in Fig. 4.35b, that is, both terminals of the voltmeter must be connected to the same type of a conductor.

What happens when two conductors are joined together? Free electrons in metal may behave as an ideal gas. Kinetic energy of electrons is function of the material temperature. However, in different materials, energies and densities of free electrons are not the same. When two dissimilar materials at the same temperature are brought into a contact, free electrons diffuse through the junction [27]. The electric potential of the material accepting electrons becomes more negative at the interface, while the material emitting electrons becomes more positive. Different electronic concentrations across the junction set up an electric field, which balances the diffusion process and the equilibrium is established. If the loop is formed and both junctions are at the same temperature, the electric fields at both junctions cancel each other, which is not the case when the junctions are at different temperatures.

A subsequent investigation has shown the Seebeck effect to be fundamentally electrical in nature. It can be stated that the thermoelectric properties of a conductor are in general just as much bulk properties as are the electrical and thermal conductivities. Coefficient  $\alpha_a$  is a unique property of a material.

When a combination of two dissimilar materials (A and B) is used, the Seebeck potential is determined from a *differential* Seebeck coefficient

$$\alpha_{AB} = \alpha_A - \alpha_B, \tag{4.89}$$

and the net voltage of the junction is

$$dV_{AB} = \alpha_{AB}dT. \tag{4.90}$$

The above equation can be used to determine a differential coefficient:



$$\alpha_{AB} = \frac{dV_{AB}}{dT} \quad (4.91)$$

Note that the Seebeck coefficient is not strictly a constant. It is somewhat temperature dependent and thus the Seebeck potential will be different at different temperatures. Voltage as function of a temperature gradient for a thermocouple with a high degree of accuracy can be approximated by a second-order equation

$$V_{AB} = a_0 + a_1T + a_2T^2 \quad (4.92)$$

Then a differential Seebeck coefficient for a thermocouple can be found by differentiating Eq. (4.92) by temperature:

$$\alpha_{AB} = \frac{dV_{AB}}{dT} = \alpha_1 + 2\alpha_2T \quad (4.93)$$

It is seen that the coefficient is a linear function of temperature. Sometimes this coefficient  $\alpha_{AB}$  is called the *sensitivity* of a thermocouple junction. A junction that is kept at a cooler temperature traditionally is called a *cold junction* and the warmer is a *hot junction*.

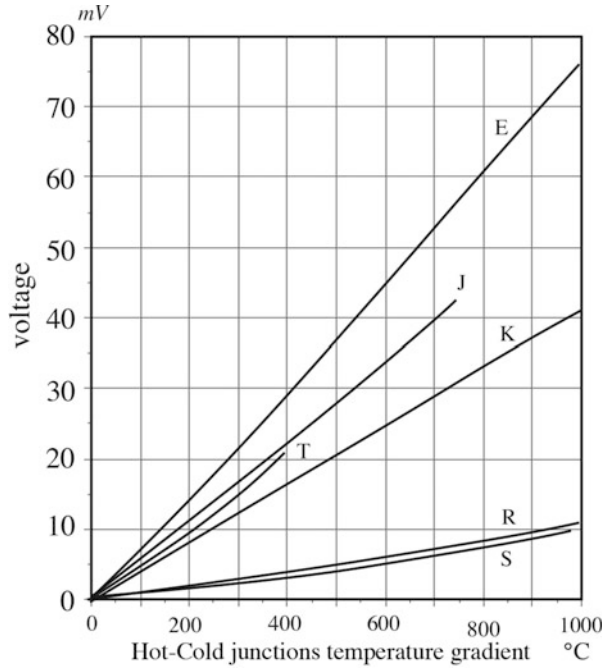
There is a very useful property of a joint: the Seebeck coefficient does not depend on the nature of the junction, metals may be pressed together, welded, fused, soldered, twisted, etc. What counts is temperature of the junction and the actual metals. The Seebeck effect is a direct conversion of thermal energy into electric energy.

Table A.11 gives values of the thermoelectric coefficients and volume resistivities for some thermoelectric materials. It is seen that to achieve the best sensitivity, the junction materials shall be selected with the opposite signs for  $\alpha$  and those coefficients should be as large as practical.

In 1826, A. C. Becquerel suggested to use the Seebeck's discovery for temperature measurements. Nevertheless, the first practical thermocouple was constructed by Henry LeChatelier almost 60 years later [28]. He had found that the junction of platinum and platinum-rhodium alloy wires produces "the most useful voltage". Thermoelectric properties of many combinations have been well documented and for many years used for measuring temperature. Table A.10 gives sensitivities of some practical thermocouples (at 25 °C) and Fig. 4.36 shows the Seebeck voltages for the standard types of thermocouples over a broad temperature range.

It should be emphasized once again that a thermoelectric sensitivity is not constant over the temperature range and it is customary to reference thermocouples at 0 °C. Besides the thermocouples, the Seebeck effect also is employed in *thermopiles* that are, in essence, multiple serially connected thermocouples. Nowadays, thermopiles are most extensively used for detecting thermal radiation (Sect. 15.8.3). The original thermopile was made of wires and intended for increasing the output voltage. It was invented by James Joule (1818–1889) [29].

**Fig. 4.36** Output voltage from standard thermocouples as functions of cold-hot temperature gradient



Nowadays, the Seebeck effect is used in fabrication of the integral MEMS sensors where pairs of materials are deposited on surfaces of the semiconductor wafers. Quite sensitive thermoelectric sensors can be fabricated of silicon, since silicon possess a strong Seebeck coefficient. The Seebeck effect results from the temperature dependence of the Fermi energy  $E_F$ , and the total Seebeck coefficient for  $n$ -type silicon may be approximated as a function of its electrical resistivity:

$$\alpha_a = \frac{mk}{q} \ln \frac{\rho}{\rho_0}, \tag{4.94}$$

where  $\rho_0 \approx 5 \times 10^{-6} \Omega \cdot \text{m}$  and  $m \approx 2.5$  are constants,  $k$  is the Boltzmann constant, and  $q$  is the electronic charge. The doping concentrations used in practice may achieve very large Seebeck coefficients up to 0.6 mV/K. Examining Table A.11, it can be seen that Seebeck coefficients for metals are much smaller than for silicon and that influence of the aluminum terminals on chips is negligible compared to the Seebeck coefficient for silicon. We conclude this discussion of the thermoelectric effect by a remark that the effect allows fabrication a *relative* temperature sensor but not an absolute sensor. In other words, a thermocouple or thermopile sensor will measure only a temperature *gradient*. To measure an absolute temperature, a cold or hot junction temperature must be either known or independently measured by another sensor—the reference absolute sensor, such as a thermistor.

### 4.9.2 Peltier Effect

In the early nineteenth century, a French watchmaker turned physicist, Jean Charles Athanase Peltier (1785–1845) discovered that if electric current passes from one substance to another (Fig. 4.37), then heat may be given or absorbed at the junction [30]. Heat absorption or production is a function of the current direction

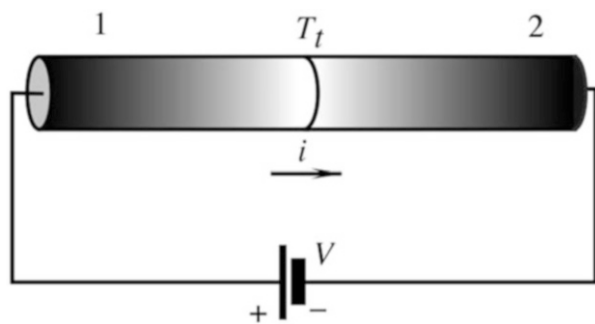
$$dQ_p = \pm p i dt, \quad (4.95)$$

where  $i$  is the current and  $t$  is time. The coefficient  $p$  has a dimension of voltage and represents thermoelectric properties of the material. It should be noted that produced and absorbed heat does not depend on temperature at the other sides of the material.

The Peltier effect concerns the reversible absorption of heat, which usually takes place when an electric current crosses a junction between two dissimilar metals. The effect takes place whether the current is introduced externally, or is induced by the thermocouple junction itself (due to Seebeck effect).

The Peltier effect is used for two purposes: it can produce heat or “produce” cold (remove heat), depending on the direction of electric current through the junction. This makes it quite useful for the devices where precision thermal control is required. Apparently, the Peltier effect is of the same nature as the Seebeck effect. It should be well understood that the Peltier heat is different from that of the Joule. The Peltier heat depends *linearly* on magnitude of the current flow as contrasted to Joule heat.<sup>18</sup> The magnitude and direction of Peltier heat does not depend in any way on the actual nature of the contact. It is purely a function of two different bulk materials that have been brought together to form the junction and each material makes its own contribution depending on its thermoelectric properties. The Peltier effect is a basis for operation of thermoelectric coolers, which are used for cooling

**Fig. 4.37** Peltier effect



<sup>18</sup> Joule heat is produced when electric current passes in any direction through a conductor having finite resistance. Released thermal power of Joule heat is proportional to squared current:  $P = i^2/R$ , where  $R$  is resistance of a conductor.

of the photon detectors operating in the far-infrared spectral range (Sect. 15.5) and the chilled mirror hygrometers (Sect. 14.6.1).

To summarize the Seebeck and Peltier effects we should remember that thermoelectric currents may exist whenever the junctions of a circuit formed of at least two dissimilar metals are exposed to different temperatures. This temperature difference is always accompanied by irreversible Fourier heat conduction, while the passage of electric currents is always accompanied by irreversible Joule heating effect. At the same time, the passage of electric current always is accompanied by reversible Peltier heating or cooling effects at the junctions of the dissimilar metals, while the combined temperature difference and passage of electric current always is accompanied by reversible Thomson heating or cooling effects along the conductors. The two reversible heating-cooling effects are manifestations of four distinct e.m.f.'s, which make up the net Seebeck e.m.f.

$$E_s = p_{AB_{T_2}} - p_{AB_{T_1}} + \int_{T_1}^{T_2} \sigma_A dT - \int_{T_1}^{T_2} \sigma_B dT = \int_{T_1}^{T_2} \alpha_{AB} dT, \quad (4.96)$$

where  $\sigma$  is a quantity called the Thomson coefficient, which Thomson referred to as the *specific heat of electricity* because of an apparent analogy between  $\sigma$  and the usual specific heat,  $c$ , of thermodynamics. The quantity of  $\sigma$  represents the rate at which heat is absorbed, or liberated, per unit temperature difference per unit mass [31, 32].

---

## 4.10 Sound Waves

Alternate physical compression and expansion of medium (solids, liquids, and gases) with certain frequencies are called sound waves. The medium contents oscillate in the direction of wave propagation, hence these waves are called *longitudinal* mechanical waves. The name *sound* is associated with the hearing range of a human ear which is approximately from 20 to 20,000 Hz. Longitudinal mechanical waves below 20 Hz are called *infrasound* and above 20,000 Hz (20 kHz) *ultrasound*. If the classification was made by other animals, like dogs, the range of sound waves surely would be wider since dogs can hear up to 45 kHz.

Detection of infrasound is of interest with respect to analysis of building structures, earthquake prediction, and other geometrically large sources. When infrasound is of a relatively strong magnitude it can be if not heard, at least felt by humans, producing quite irritating psychological effects (panic, fear, etc.).<sup>19</sup>

---

<sup>19</sup> There is an anecdote about the American physicist R. W. Wood (1868–1955). His friend, a theatrical director from New York, asked Wood to invent a mysterious sound effect for a play about time travel. Wood built a huge organ pipe (sort of a whistle) for the infrasonic frequency of about 8 Hz. When during a dress rehearsal, Wood activated the pipe, the entire building and everything in it started vibrating. The terrified audience ran out to the street, feeling uncontrollable fear and panic. Needless to say, the pipe was never used during performances.

Audible waves are produced by vibrating strings (string music instruments), vibrating air columns (wind music instruments), and vibrating plates (some percussion instruments, vocal cords, loudspeakers). Whenever sound is produced, air is alternately compressed and rarefied. These disturbances propagate outwardly. A spectrum of waves may be quite different—from simple monochromatic sounds from a metronome or an organ pipe, to a rich multiharmonic violin sound. Acoustic noise may have a very broad spectrum. It may be of a uniform distribution of density or it may be “colored” with predominant harmonics at some of its portions.

When a medium is compressed, its volume changes from  $V$  to  $V - \Delta V$ . The ratio of change in pressure,  $\Delta p$ , to relative change in volume is called the bulk modulus of elasticity of medium:

$$B = -\frac{\Delta p}{\Delta V/V} = \rho_0 v^2, \quad (4.97)$$

where  $\rho_0$  is the density outside the compression zone and  $v$  is the speed of sound in the medium. Then speed of sound can be defined as

$$v = \sqrt{\frac{B}{\rho_0}}, \quad (4.98)$$

Hence, the speed of sound depends on the elastic ( $B$ ) and inertia ( $\rho_0$ ) properties of the medium. Since both variables are functions of temperature, the speed of sound also depends on temperature. This feature forms a basis for the acoustic thermometers (Sect. 17.10). For solids, longitudinal velocity can be defined through its Young modulus  $E$  and Poisson ratio  $\nu$ :

$$v = \sqrt{\frac{E(1-\nu)}{\rho_0(1+\nu)(1-2\nu)}} \quad (4.99)$$

Table A.15 provides speeds of longitudinal waves in some media.

If we consider propagation of a sound wave in an organ tube, each small volume element of air oscillates about its equilibrium position. For a pure harmonic tone, the displacement of a particle from the equilibrium position may be represented by:

$$y = y_m \cos \frac{2\pi}{\lambda}(x - vt), \quad (4.100)$$

where  $x$  is the equilibrium position of a particle and  $y$  is a displacement from the equilibrium position  $y_m$  that is the amplitude, and  $\lambda$  is the wavelength. In practice, it is more convenient to deal with pressure variations in sound waves rather than with displacements of the particles. It can be shown that the pressure exerted by the sound wave is:

$$p = k\rho_0 v^2 y_m \sin(kx - \omega t), \quad (4.101)$$

where  $k = \frac{2\pi}{\lambda}$  is a wave number,  $\omega$  is angular frequency, and the front terms before  $\sin$  represent an amplitude,  $p_m$ , of the sound pressure. Therefore, a sound wave may be considered as a pressure wave. It should be noted that  $\sin$  and  $\cos$  in Eqs. (4.100 and 4.101) indicate that the displacement wave is  $90^\circ$  out of phase with the pressure wave.

Pressure at any given point in media is not constant and changes continuously, and the difference between the instantaneous and the average pressure is called an *acoustic pressure*  $P$ . During the wave propagation, vibrating particles oscillate near a stationary position with the instantaneous velocity  $\xi$ . The ratio of the acoustic pressure and the instantaneous velocity (do not confuse it with a wave velocity!) is called an *acoustic impedance*:

$$\mathbf{Z} = \frac{\mathbf{P}}{\xi}, \quad (4.102)$$

which is a complex quantity that is characterized by an amplitude and a phase. For an idealized media (no loss) the  $\mathbf{Z}$  is real and is related to the wave velocity as:

$$Z = \rho_0 v. \quad (4.103)$$

We can define *intensity*  $I$  of a sound wave as the power transferred per unit area. Also, it can be expressed through the acoustic impedance:

$$I = P\xi = \frac{P^2}{Z}. \quad (4.104)$$

It is common, however, to specify sound not by intensity but rather by a related parameter  $\beta$ , called the *sound level* and defined with respect to a reference intensity  $I_0 = 10^{-12} \text{ W/m}^2$

$$\beta = 10 \log_{10} \left( \frac{I}{I_0} \right) \quad (4.105)$$

The magnitude of  $I_0$  was chosen because it is the lowest ability of a human ear. The unit of  $\beta$  is a decibel (dB), named after Alexander Graham Bell. If  $I = I_0$ ,  $\beta = 0$ .

Pressure levels also may be expressed in decibels as:

$$\Pi = 20 \log_{10} \left( \frac{P}{p_0} \right), \quad (4.106)$$

where  $p_0 = 2 \cdot 10^{-5} \text{ N/m}^2$ .

Examples of some sound levels are given in Table 4.1. Since the response of a human ear is not the same at all frequencies, sound levels are usually referenced to  $I_0$  at 1 kHz where the ear is most sensitive.

**Table 4.1** Sound levels ( $\beta$ ) referenced to  $I_0$  at 1000 Hz

Sound source	dB
Theoretical limit at 1 atm. pressure	194
Supersonic boom	160
Hydraulic press at 1 m	130
Threshold of pain	130
10 W Hi-Fi speaker at 3 m	110
Unmuffled motorcycle	110
Jet ski	100
Subway train at 5 m	100
Pneumatic drill at 3 m	90
Niagara Falls	85
Heavy traffic	80
Automobiles at 5 m	75
Vacuum cleaner	70
Conversation at 1 m	60
Accounting office	50
City street (no traffic)	30
Whisper at 1 m	20
Rustle of leaves	10
Threshold of hearing	0

Since sound is a propagating pressure wave, theoretically it can be measured by pressure sensors adapted for the media where the wave propagates. Sound pressure in several respects differs from other types of pressure (mostly by frequency and intensity ranges), thus a sound (acoustic) sensor should have a special set of characteristics for the efficient conversion of the oscillating pressure into useful electrical signals. Some of these characteristics are the sensitivity, frequency range, and directionality. These are discussed in greater detail in Chap. 13.

## 4.11 Temperature and Thermal Properties of Materials

Our bodies have a sense of temperature, which by no means is an accurate method to measure outside heat. Human senses are not only nonlinear, but also relative with respect to our previous experience. Nevertheless, we can easily tell the difference between warmer and cooler objects. Then, what is going on with these objects that they produce different thermal perceptions?

Every single particle in this Universe exists in perpetual motion. Temperature of a volume of a material, in the simplest way, can be described as a measure of an average kinetic energy of vibrating particles. The stronger the particle movement the higher temperature. Of course, molecules and atoms in a given volume of material do not move with equal intensities. That is, microscopically, they all are at different temperatures. The average kinetic energy of a very large number of moving particles determines *macroscopic* temperature of an object.

These processes are studied by thermodynamics and statistical mechanics. Here, however, we are concerned with the methods and devices that are capable of measuring macroscopic average kinetic energy of vibrating particles, which is the other way to say temperature of the object. Since temperature is related to movement of molecules, it is closely associated with pressure, which is defined as the force applied by moving molecules per unit area.

When atoms and molecules in a material move, they interact with each other, that happen to be brought in contact with them. A jiggling atom agitates a neighboring atom and transfers to it portion of its kinetic energy, so the neighbor starts vibrating more intensely and kicks and pulls its next neighbors with the increased forces. This agitation propagates through the material, elevating its temperature. Since an atom contains moving electrons swirling around its nucleus like a cloud of the electric current, thermal agitation causes that current to move and thus producing *electromagnetic* waves. Hence, every vibrating atom acts as a microscopic radio transmitter that emanates electromagnetic radiation to the surrounding space in relation to its own jiggling. These two types of activities form a basis for heat transfer from warmer to cooler objects—conduction and radiation. The stronger the atomic jiggling the hotter the temperature and the stronger the electromagnetic radiation. Special devices (we call them *thermometers*), which either contact the object or receive its electromagnetic radiation, produce physical responses, or signals. These signals becomes a measure of the object's temperature.

The word *thermometer* first appeared in literature in 1624 in a book by J. Leurechon, entitled *La Récréation Mathématique* [27]. The author described a glass water-filled thermometer whose scale was divided by  $8^\circ$ . The first pressure-independent thermometer was built in 1654 by Ferdinand II, Grand Duke of Tuscany<sup>20</sup> in form of an alcohol-filled hermetically sealed tube.

Thermal energy is what we call heat. Heat is measured in *calories*.<sup>21</sup> One calorie (cal) is equal to amount of heat which is required to warm up by  $1^\circ\text{C}$  1 g of water at normal atmospheric pressure. In the U.S.A., a British unit of heat is generally used, which is 1 Btu (British thermal unit):  $1 \text{ Btu} = 252.02 \text{ cal}$ .

### 4.11.1 Temperature Scales

There are several scales to measure temperature. To make a linear scale (for convenience, all thermometers have linear scales), at least two reference points are required. Usually one of these points is called a zero point. A first zero for a scale was established in 1664 by Robert Hooke at a point of freezing distilled water.

---

<sup>20</sup> More precisely, not “*by him*” but rather “*for him*”. The Duke was obsessed with new technologies, and had several hygrometers, barometers, thermometers, and telescopes installed in his Pitti palace in Florence.

<sup>21</sup> A *calorie* that measures energy in food is actually equal to 1000 physical calories that is called a *kilocalorie*.



In 1694 Carlo Renaldi of Padua suggested to take a melting point of ice (zero point) and a boiling point of water (second point) to define a linear span of his thermometer. He divided the span by 12 equal parts. Unfortunately, his suggestion had been forgotten for almost 50 years. In 1701, Newton also suggested for the zero point to use the temperature of melting ice and for the second point he chose the armpit temperature of a “*healthy Englishman*”, he labeled that point “12”. At Newton’s scale, water was boiling at point No. 34. Daniel Gabriel Fahrenheit, a Dutch instrument maker, in 1706 selected zero for his thermometer at the coldest temperature he could produce by mixing water, ice, and sal-ammoniac or household salt. For the sake of convenience, he established the other point at  $96^\circ$ , which was “*found in the blood of a healthy man*”.<sup>22</sup> On his scale, the melting point of pure water was at  $32^\circ$  and boiling at  $212^\circ$ . In 1742, Andreas Celsius, professor of astronomy at the University of Uppsala (Sweden), proposed a scale with zero as the melting point of ice and 100 at boiling point of water. He divided the span by 100 equal parts—degrees.

Nowadays, in science and engineering, Celsius and Kelvin scales are generally employed. The Kelvin scale is arbitrarily based on the so-called *triple point of water*. There is a fixed temperature at a unique pressure of 4.58 mmHg where water vapor, liquid, and ice can coexist. This unique temperature is 273.16 K (degrees kelvin) which approximately coincides with  $0^\circ\text{C}$ . The Kelvin scale is linear with zero intercept (0 K) at a lowest temperature where kinetic energy of all moving particles is equal to zero. This point cannot be exactly attained in practice and is a strictly theoretical limit. It is called the *absolute zero*. Kelvin and Celsius scales have the same slopes,<sup>23</sup> i.e.,  $1^\circ\text{C} = 1\text{ K}$  and  $0\text{ K} = -273.15^\circ\text{C}$ . So the Kelvin scale is a shifted Celsius scale:

$$^\circ\text{C} = ^\circ\text{K} - 273.15^\circ \quad (4.107)$$

The boiling point of water is at  $100^\circ\text{C} = 373.15^\circ\text{K}$ . In the past, the Celsius scale sometimes was called “centigrade scale”. Now, this term is no longer in use.

A slope of the Fahrenheit scale is steeper, because  $1^\circ\text{C} = 1.8^\circ\text{F}$ . The Celsius and Fahrenheit scales cross at  $-40^\circ\text{C}$  and F. The conversion between the two scales is

$$^\circ\text{F} = 32 + 1.8^\circ\text{C} , \quad (4.108)$$

which means that at  $0^\circ\text{C}$ , temperature on the Fahrenheit scale is  $+32^\circ\text{F}$ .

<sup>22</sup> After all, Fahrenheit was a toolmaker and for him 96, but not 100, was a convenient number because to engrave the graduation marks, he could easily do so by dividing a distance between the marks by two: 96, 48, 24, etc. With respect to nationality of the blood, he did not care if it was blood of an Englishman or not. Now, it is known that blood temperature of a healthy person is not really constant. It varies between approximately 97 and 99.5 °F (36 and 37.5 °C) but during his times, Fahrenheit could not find a better thermostat than a human body.

<sup>23</sup> There is a difference of  $0.01^\circ$  between the Kelvin and Celsius scales, as Celsius’ zero point is defined not at a triple point of water as for the Kelvin, but at temperature where ice and air-saturated water are at equilibrium at atmospheric pressure.

### 4.11.2 Thermal Expansion

Essentially, all solids expand in volume with an increase in temperature. This is a result of vibrating atoms and molecules. When the temperature goes up, an average distance between the atoms increases, which leads to an expansion of a whole body.<sup>24</sup> The change in any linear dimension: length, width, or height is called a *linear expansion*. A length,  $l_2$ , at temperature,  $T_2$ , depends on length,  $l_1$ , at initial temperature  $T_1$  and can be approximated by a linear equation:

$$l_2 = l_1[1 + \alpha(T_2 - T_1)] , \quad (4.109)$$

where  $\alpha$ , called the *coefficient of linear expansion*, has different values for different materials:

$$\alpha = \frac{\Delta l}{l} \frac{1}{\Delta T} \quad (4.110)$$

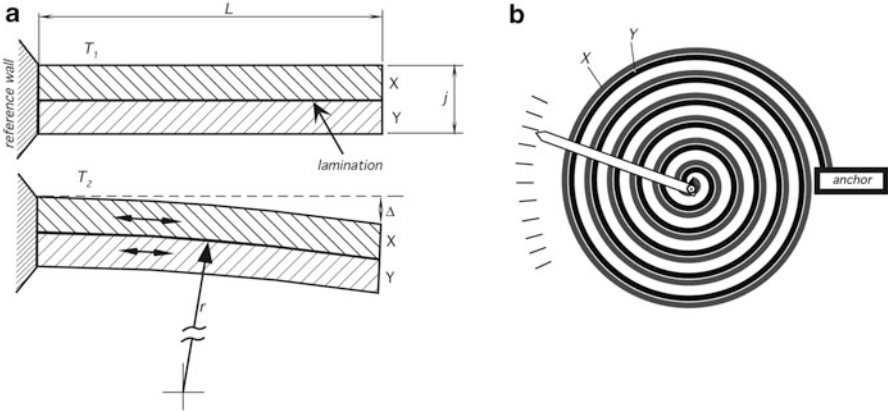
where  $\Delta T = T_2 - T_1$ . Table A.16 gives values of  $\alpha$  for different materials. Strictly speaking,  $\alpha$  depends on the actual temperature and thus is not strictly linear. However, for most engineering purposes, small variations in  $\alpha$  may be neglected. For the so-called *isotropic* materials,  $\alpha$  is the same for any direction. The fractional change in area,  $A$ , of an object and its volume,  $V$ , with a high degree of accuracy can be respectively represented by:

$$\Delta A = 2\alpha A \Delta T , \quad (4.111)$$

$$\Delta V = 3\alpha V \Delta T . \quad (4.112)$$

Thermal expansion is a useful phenomenon that can be employed in many sensors where thermal energy is either measured or used as an excitation signal. Consider two laminated plates, X and Y, that are fused together at temperature  $T_1$  (Fig. 4.38a). The plates have the same thickness, surface areas, and identical moduli of elasticity. Their coefficients of thermal expansion,  $\alpha_1$  and  $\alpha_2$ , however, are different. The fused plates are anchored at the left-hand side to a reference wall. Now, if we apply heat to the structure, that is, if we increase its temperature from  $T_1$  to  $T_2$ , plate X will expand more than plate Y (for  $\alpha_1 > \alpha_2$ ). The joint between the plates will restrain plate X from a uniform expansion, while forcing plate Y to expand more, than its coefficient of expansion would require. This results in formation of the internal stress and the structure will warp downwardly. Contrary, if we cool the structure, it will warp upwardly. The radius of warping can be estimated from equation [33]:

<sup>24</sup>This assumes that there is no phase change during warming up, like from solid to liquid.



**Fig. 4.38** Warping of laminated plate where two materials have different coefficients of thermal expansion (a); bimetal coil used as temperature transducer (b)

$$r \approx \frac{2j}{3(\alpha_X - \alpha_Y)(T_2 - T_1)} \quad (4.113)$$

The warping results in deflection of the nonanchored portion of the laminated plates. The deflection is strongest at the end of the structure. This deflection can be measured as a representative of the temperature change with respect to the reference temperature (we may call it calibration temperature). At the calibration temperature the plate is flat, however, any convenient shape at a calibration temperature may be selected. A bimetal plate is a transducer of temperature into a displacement but not a sensor in formal sense as we define it, since it does not produce electric output signals.

Most of such bimetal plate transducers are made of iron-nickel-chrome alloys. They are useful in a temperature range from  $-75^\circ\text{C}$  and up to  $+600^\circ\text{C}$ . For relatively small temperature changes, radius of curvature is quite large (several meters) and thus the tip deflection is rather small. A bimaterial plate tip deflection can be computed from

$$\Delta = r \left( 1 - \cos \frac{180L}{\pi r} \right), \quad (4.114)$$

where  $r$  is found from Eq. (4.113) and  $L$  is the length the plate. For example, for a bimetal plate made of brass ( $\alpha = 20 \times 10^{-6}$ ) and chromium ( $\alpha = 6 \times 10^{-6}$ ) having  $L = 50$  mm and  $j = 1$  mm, for a  $10^\circ\text{C}$  gradient the deflection is only  $\Delta \approx 0.26$  mm. This deflection is not easy to observe with a naked eye, thus, in a practical thermometer a bimetal plate is usually preshaped in form of a coil, Fig. 4.38b. This allows for a dramatic increase in  $L$  and achieving a much larger  $\Delta$ . In the same example, for  $L = 200$  mm, the deflection becomes 4.2 mm—a significant

improvement. In modern sensors, the bimaterial structure is fabricated by employing a micromachining technology (MEMS).

### 4.11.3 Heat Capacity

When an object is warmed up, its temperature increases. By warming we mean transfer of a certain amount of heat (thermal energy) into the object. Heat is stored in the object in form of a kinetic energy of vibration atoms. Since different materials are composed of atoms having different atomic weights, which even may be locked into crystalline structures, the kinetic energy of the atomic vibration also will be different. The amount of heat that an object can store is analogous to the amount of water that a water tank can store. Naturally, it cannot store more than its volume, which is a measure of a tank's capacity. Similarly, every object may be characterized by a heat capacity which depends on both: the material properties of the object and its mass,  $m$ :

$$C = cm, \quad (4.115)$$

where  $c$  is a constant, which characterizes thermal properties of material. It is called the *specific heat* and is defined as:

$$c = \frac{Q}{m\Delta T} \quad (4.116)$$

The specific heat describes the material while a thermal capacity describes the object, which is made of that material. Strictly speaking, specific heat is not constant over an entire temperature range of a phase of the material. It often changes dramatically when a phase of the material changes, say from solid to liquid. Microscopically, specific heat reflects structural changes in the material. For instance, the specific heat of water is almost constant between 0 and 100 °C (liquid phase). Almost, but not exactly: it is higher near freezing, and decreases slightly when the temperature goes to about 35 °C and then slowly rises again from 38 to 100 °C. Remarkably, the specific heat of water is the lowest near 37 °C—a biologically optimal temperature of warm-blooded animals.<sup>25</sup>

Table A.17 gives the specific heat for various materials. Some other published tables provide specific heat in cal/(g °C). The relationship between cal/(g °C) and j/(g °C) is as follows

---

<sup>25</sup> Likely, this is because of a better compatibility between the animal protein molecules and structures of the water crystals at that temperature that is manifested by the water specific heat.

$$1 \frac{j}{g^{\circ}C} = 0.2388 \frac{\text{cal}}{g^{\circ}C}. \quad (4.117)$$

It may be noted, that generally, the heavier the material the lower its specific heat. A concept of thermal capacity is very important for development of temperature sensors. It follows from Eq. (4.116) that for the same temperature increase, a smaller thermal energy needs to be transferred from the object to a lighter sensor with smaller specific heat. Hence, a temperature sensor having smaller heat capacity will disturb the measured object to a lesser degree and respond faster.

---

## 4.12 Heat Transfer

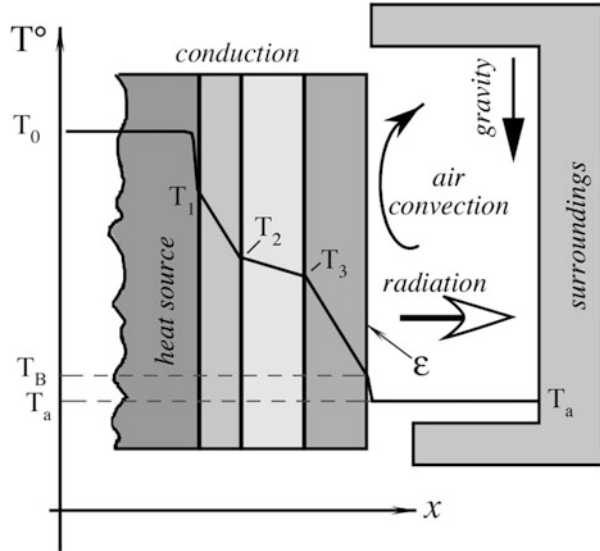
There are two fundamental properties of heat, which should be well recognized:

1. Heat is totally *not specific*, that is, once it is produced, it is impossible to say what origin it has.
2. Heat *can not be contained*, which means that it flows spontaneously from warmer to the cooler part of the system and there is no method known to modern science to stop the heat flow entirely.

Thermal energy may be transferred from one object to another by three ways: conduction, convection, and radiation. While conduction and radiation relate to solids, liquids, and gases, convection can transfer heat by an intermediate fluid (liquid or gas). A measurement of any physical quantity always requires transfer of energy. One of the objects being involved in thermal exchange may be a thermal sensor. Its purpose would be to measure the amount of heat that represents certain information about the object producing that heat. Such information may be the temperature, chemical reaction, position of the object, heat flow, etc.

For illustrating the ways heat propagates, let us consider a sandwich-like multi-layer object, where each layer is made of a different material. When heat moves through the layers, a temperature profile within each material depends on its thickness and thermal conductivity. Figure 4.39 shows three laminated layers where the first layer is attached to a heat source—a device having an “infinite” heat capacity and a high thermal conductivity. One of the best solid materials to act as an infinite heat source is a thermostatically controlled bulk copper. In liquids, an “infinite” heat capacity can be attributed to a stirred liquid, like water in a temperature controlled bath. Temperature within the source is higher and constant, except of a thin boundary region at the joint of the laminated materials. Heat propagates from one material to another by conduction, gradually dropping towards ambient temperature. The temperature within each material drops with different rates depending on the thermal properties of the material. The last layer loses heat to air through the natural (gravitational) convection and to the surrounding objects through the infrared (thermal) radiation. Thus, Fig. 4.39 illustrates all three possible ways to transfer heat from one object to another: conduction, convection, and

**Fig. 4.39** Temperature profile in laminated materials



radiation. Naturally, the same consideration is applicable if instead of a heat source we will use a heat sink whose temperature is lower than that of surroundings.

### 4.12.1 Thermal Conduction

Heat conduction requires a physical contact between two bodies. Thermally agitated particles in a warmer body jiggle and transfer kinetic energy to a cooler body by agitating its particles. As a result, the warmer body loses heat while the cooler body gains heat. Heat transfer by conduction is analogous to water flow or to electric current. For instance, heat passage through a rod is governed by a law that is similar to Ohm’s law. A heat flow rate (thermal “current”) is proportional to a temperature gradient (thermal “voltage”) across the material ( $dT/dx$ ) and a cross-sectional area  $A$ :

$$H = \frac{dQ}{dt} = -kA \frac{\Delta T}{dx}, \tag{4.118}$$

where  $k$  is called *thermal conductivity*. The minus sign indicates that heat flows in the direction of temperature decrease (a negative derivative is required to cancel the minus sign). A good thermal conductor has a high  $k$  (most of metals) while thermal insulators (most of dielectrics) have a low  $k$ . Thermal conductivity is considered constant, however it somewhat increases with temperature. To calculate heat conduction through, say, an electric wire, temperatures at both ends ( $T_1$  and  $T_2$ ) must be used in equation:

$$H = kA \frac{T_1 - T_2}{L}, \quad (4.119)$$

where  $L$  is the length of the wire. Quite often, a thermal resistance  $r$  is used instead of a thermal conductivity:

$$r = \frac{L}{k}, \quad (4.120)$$

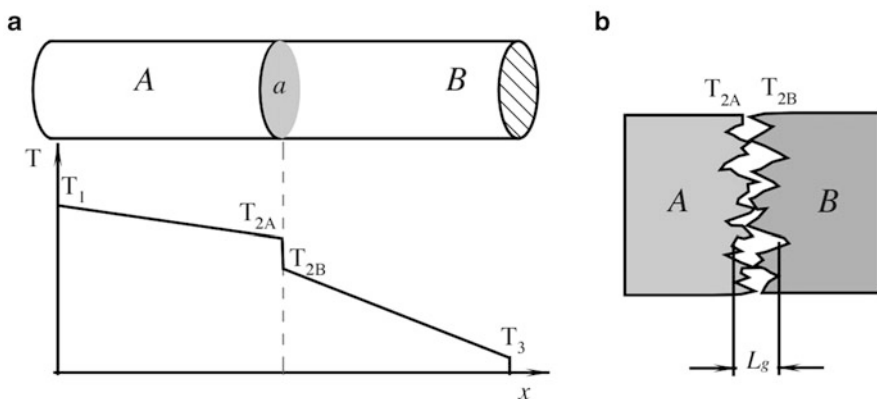
then, Eq. (4.119) can be rewritten as:

$$H = A \frac{T_1 - T_2}{r}. \quad (4.121)$$

Values of thermal conductivities for some materials are shown in Table A.17.

Figure 4.39 shows an idealized temperature profile within the layers of laminated materials having different thermal conductivities. This may be the case when the materials are fused together. In the real world, heat transfer through an interface of two adjacent materials may be different from that idealized case. If we press together two materials and observe the heat propagation through the assembly, a temperature profile may look like the one shown in Fig. 4.40a. If the sides of the materials are well insulated, the heat flux (“thermal current”) must be the same through both materials. The sudden temperature drop at the boundary region, having surface area,  $a$ , is the result of a thermal *contact resistance*. Heat transfer through the assembly can be described as:

$$H = \frac{T_1 - T_3}{R_A + R_c + R_B}, \quad (4.122)$$



**Fig. 4.40** Temperature profile in joint (a) and a microscopic view of surface contact (b)

where  $R_A$  and  $R_B$  are thermal resistances of two materials and  $R_c$  is the contact resistance:

$$R_c = \frac{1}{h_c a}. \quad (4.123)$$

The quantity  $h_c$  is called the contact coefficient. This factor can be very important in a number of sensor applications because many heat-transfer situations involve mechanical joining of two materials. Microscopically, the joint may look like the one shown in Fig. 4.40b. No real surface is perfectly smooth, and the actual surface roughness is believed to play a central role in determining the contact resistance. There are two principal contributions to the heat transfer at the joint:

1. The material-to-material conduction through the actual physical contact.
2. The conduction through trapped gases (air) in the void spaces created by the rough surfaces.

Since thermal conductivity of gases is much smaller as compared with many solids, the trapped gas creates the most resistance to heat transfer. Then, the contact coefficient can be defined as

$$h_c = \frac{1}{L_g} \left( \frac{a_c}{a} \frac{2k_A k_B}{k_A + k_B} + \frac{a_v}{a} k_f \right), \quad (4.124)$$

where  $L_g$  is the thickness of the void space,  $k_f$  is the thermal conductivity of the fluid (for instance, air) filling the void space,  $a_c$  and  $a_v$  are areas of the contact and void, respectively, and  $k_A$  and  $k_B$  are the respective thermal conductivities of the materials. The main problem with this theory is that it is very difficult to determine experimentally areas  $a_c$  and  $a_v$ , and distance  $L_g$ . This analysis, however, allows us to conclude that the contact resistance should increase with a decrease in the ambient gas pressure. On the other hand, contact resistance decreases with an increase in the joint pressure. This is a result of a deformation of the high spots of the contact surface which leads to enlarging  $a_c$  and creating a greater contact area between the materials. The joint surfaces should be as smooth as practical. To decrease the thermal resistance, a dry contact between materials should be avoided. Before joining, surfaces may be coated with fluid having low thermal resistance. For instance, thermal grease is often used for the purpose.

### 4.12.2 Thermal Convection

Another way to transfer heat is convection. Convection requires an intermediate agent (fluid: gas or liquid) which takes heat from a warmer body, carries it to a cooler body, releases heat, and then may or may not return back to a warmer body to pick up another portion of heat. Heat transfer from a solid body to a moving agent or



within the moving agent is also called convection. Convection may be natural (gravitational) or forced (produced by a mechanism). With the natural convection of air, buoyant forces produced by gravitation act upon air molecules. Warmed up air rises carrying heat away from a warm surface. Cooler air descends toward the warmer object. Forced convection of air is produced by a fan or blower. Forced convection is used in liquid thermostats to maintain the temperature of a device at a predetermined level. Efficiency of a convective heat transfer depends on the rate of media movement, temperature gradient, surface area of an object, and thermal properties of moving medium. An object whose temperature is different from the surroundings will lose (or receive) heat, which can be determined from the Newton's Law of cooling which is governed by equation similar to that of a thermal conduction:

$$H = \alpha A(T_1 - T_2), \quad (4.125)$$

where the convective coefficient  $\alpha$  depends on the fluid's specific heat, viscosity, and a rate of movement. The coefficient is not only gravity-dependent, its value changes somewhat with the temperature gradient. For a horizontal plate in air, the value of  $\alpha$  for the gravitational convection may be estimated from

$$\alpha = 2.49\sqrt[4]{T_1 - T_2} \text{ W/m}^2\text{K}, \quad (4.126)$$

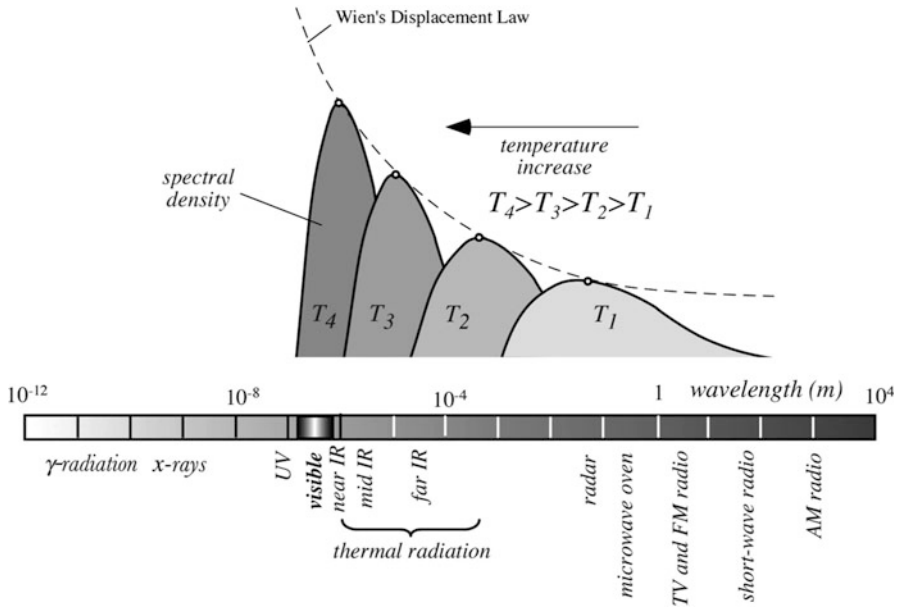
while for a vertical plate it is:

$$\alpha = 1.77\sqrt[4]{T_1 - T_2} \text{ W/m}^2\text{K}. \quad (4.127)$$

It should be noted, however, that these values are applicable for one side of a plate only, assuming that the plate is a surface of an infinite heat source (that is, its temperature does not depend on heat loss) and the surroundings have constant temperature. If volume of air is small, like in the air gap between two surfaces of different temperatures, movement of gaseous molecules becomes very restricted due to viscosity, hence the convective heat transfer becomes insignificant. In these cases, thermal conductivity of air and radiative heat transfer should be considered instead.

### 4.12.3 Thermal Radiation

It was mentioned above that in any object every atom and every molecule vibrate. The average kinetic energy of vibrating particles is represented by temperature. Each vibrating atom contains a nucleus and an electronic cloud, which is an orbiting electric charge. According to laws of electrodynamics, a moving electric charge is associated with a variable electric field that produces an alternating magnetic field. In turn, when the magnetic field changes, it results in a coupled with it changing electric field, and so on. Thus, a vibrating particle is a source of electromagnetic



**Fig. 4.41** Spectrum of electromagnetic radiation

field (EMF) which propagates outwardly with the speed of light and is governed by the laws of optics, that is, the electromagnetic waves can be reflected, filtered, focused, etc. The electromagnetic radiation associated with heat is called *thermal radiation*. Figure 4.41 shows the total electromagnetic radiation spectrum spreading from  $\gamma$  rays to radio waves. Thermal radiation is predominantly situated in the mid- and far-infrared (IR) spectral ranges.

The wavelength of the radiation directly relates to frequency,  $\nu$ , by means of speed of light  $c$  in a particular media

$$\lambda = \frac{c}{\nu} \tag{4.128}$$

A relationship between  $\lambda$  and temperature is more complex and governed by Planck's Law, which was discovered<sup>26</sup> in 1901. It establishes radiant flux density  $W_\lambda$  as function of a wavelength  $\lambda$  and absolute temperature  $T$ . Radiant flux density is power of electromagnetic radiation per unit of wavelength:

<sup>26</sup>In 1918, Max K. E. L. Planck (Germany, Berlin University) was awarded Nobel Prize in recognition of his services he rendered to the advancement of Physics by his discovery of energy quanta.

$$W_\lambda = \frac{\varepsilon(\lambda)C_1}{\pi\lambda^5(e^{C_2/\lambda T} - 1)}, \quad (4.129)$$

where  $\varepsilon(\lambda)$  is the emissivity of a surface from which the EMF is emanated,  $C_1 = 3.74 \times 10^{-12} \text{ W cm}^2$  and  $C_2 = 1.44 \text{ cm K}$  are constants, and  $e$  is the base of natural logarithms. Note that this fundamental equation defines the radiant power at a specific wavelength as function of the surface temperature  $T$ .

Temperature is a result of averaged kinetic energies of an extremely large number of vibrating particles. However, all particles do not vibrate with the same frequency or magnitude. Different permissive frequencies (also wavelengths and energies) are spaced very close to one another, which makes the material capable of radiating of a virtually infinite number of frequencies, spreading from very long to very short wavelengths. Since temperature is a statistical representation of average kinetic energy, it determines the highest probability for the particles to vibrate with a specific frequency and to have a specific wavelength. This most probable wavelength is established by the Wien's law,<sup>27</sup> which can be found by equating to zero a first derivative of Eq. (4.129). The result of the calculation is a wavelength near which most of the radiant power is concentrated:

$$\lambda_m = \frac{2898}{T}, \quad (4.130)$$

where  $\lambda_m$  is in  $\mu\text{m}$  and  $T$  in K. Wien's law states that the higher the temperature the shorter the wavelength (Fig. 4.41). In view of Eq. (4.128), the Wien's law also states that the most probable frequency in the entire spectrum is proportional to the absolute temperature:

$$\nu_m = 10^{11}T [\text{Hz}]. \quad (4.131)$$

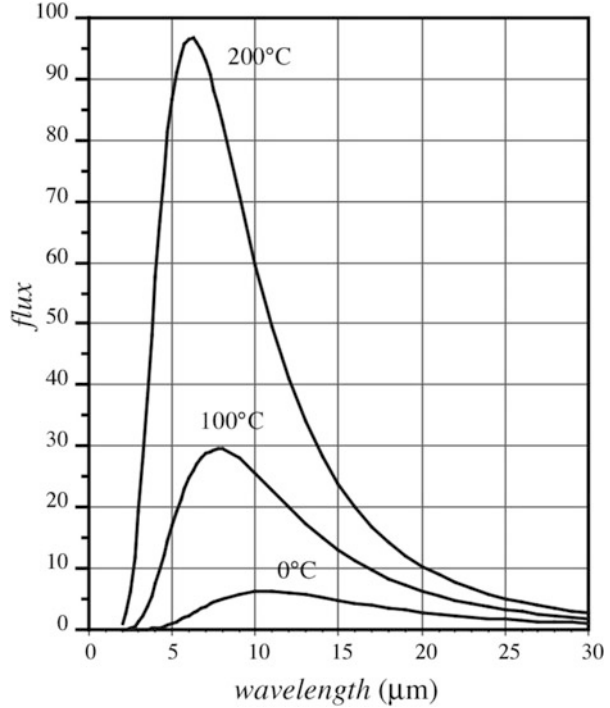
For instance, at normal room temperature, most of the mid- and far-infrared energy is radiated from an object near 30 THz ( $30 \times 10^{12} \text{ Hz}$ ). According to the Planck's equation, radiated frequencies and wavelengths depend only on temperature, while the magnitude of radiation also depends on the emissivity  $\varepsilon(\lambda)$  of the surface, which we discuss below in detail as it is an important characteristic of a thermal radiation sensor.

Figure 4.42 shows the radiant flux density for three different temperatures for an infinitely wide bandwidth ( $\lambda_1 = 0$  and  $\lambda_2 = \infty$ ). It is seen, that the radiant energy is distributed over the spectral range highly nonuniformly, with a clearly pronounced maximum defined by the Wien's law. A hot object radiates a significant portion of its energy in the visible range, while power radiated by cooler objects is concentrated in the near-, mid-, and far-infrared (IR) portions of the spectrum.

---

<sup>27</sup> In 1911, Wilhelm Wien (Germany, Würzburg University) was awarded Nobel Prize for his discoveries regarding the laws governing the radiation of heat.

**Fig. 4.42** Spectral flux density for three temperatures for ideal radiator emanating toward infinitely cold space



Theoretically, a thermal radiation bandwidth is infinitely wide. However, when detecting that radiation, properties of the real world sensors must be accounted for. Any sensor is capable of measuring only a limited spectral range (bandwidth) of radiation. In order to determine the total radiated power within a particular bandwidth, Eq. (4.129) is integrated within the range limits from  $\lambda_1$  to  $\lambda_2$ :

$$\Phi_{bo} = \frac{1}{\pi} \int_{\lambda_1}^{\lambda_2} \frac{\varepsilon(\lambda) C_1 \lambda^{-5}}{e^{C_2/\lambda T} - 1} d\lambda, \tag{4.132}$$

Equation (4.132) is quite complex and cannot be solved analytically for any particular bandwidth. A solution can be found either numerically or by an approximation. A useful approximation for a broad bandwidth (when  $\lambda_1$  and  $\lambda_2$  embrace over 50 % of the total radiated power) is a fourth-order parabola, which is known as the *Stefan-Boltzmann law*

$$\Phi_{bo} = A \varepsilon \cdot \sigma \cdot T^4. \tag{4.133}$$

Here  $\sigma = 5.67 \times 10^{-8} \text{ W/m}^2 \text{ K}^4$  (Stefan-Boltzmann constant),  $A$  is the geometry factor, and emissivity  $\varepsilon$  is assumed to be wavelength independent [34]. This equation defines total thermal radiation flux emanated in all directions from a

surface having temperature  $T$  and emissivity  $\varepsilon$  toward infinitely cold space (at absolute zero). In reality, any surface faces other surfaces that have their own temperatures and thus absorbs from them their thermal flux. This concept is fundamental for development of thermal radiation sensors and thus is discussed below in greater detail.

#### 4.12.3.1 Emissivity

While wavelengths of the radiated IR light are temperature dependent, the magnitude of radiation is also function of the surface property, which is called *emissivity*,  $\varepsilon$ . Emissivity is measured on a scale from 0 to 1. It is a ratio of the actual radiant flux that is emanated from a surface to that would be emanated from an ideal emitter ( $\varepsilon = 1$ ) having the same temperature. There is a principal equation that connects emissivity  $\varepsilon$ , transparency  $\gamma$ , and reflectivity  $\rho$  of an object:

$$\varepsilon + \gamma + \rho = 1 \quad (4.134)$$

In 1860, Kirchhoff had found that emissivity and absorptivity,  $\alpha$ , are the same thing. As a result, for an opaque object ( $\gamma = 0$ ), reflectivity,  $\rho$ , and emissivity,  $\varepsilon$ , are connected by a simple relationship:  $\rho = 1 - \varepsilon$ .

The Stefan-Boltzmann law, Eq (4.133), specifies the radiant power (flux) that would be emanated from a surface of temperature,  $T$ , toward an infinitely cold space. When thermal radiation flux emanated from the object's surface is detected by a thermal sensor<sup>28</sup> having its own temperature, the opposite flowing radiation from the sensor toward the object must also be accounted for. A thermal sensor is capable of responding only to a *net* thermal flux, i.e., flux  $\Phi_{bo}$  from the object to the sensor minus flux  $\Phi_s$  from the sensor toward the object. The sensor's surface that faces the object has emissivity,  $\varepsilon_s$  (and, subsequently reflectivity  $\rho_s = 1 - \varepsilon_s$ ). Since the sensor is only partly absorptive, not the entire flux,  $\Phi_{bo}$ , is absorbed and utilized. Thus, one part of it,  $\Phi_{ba}$ , is absorbed by the sensor while another part,  $\Phi_{br}$ , is reflected back toward object<sup>29</sup> and lost (Fig. 4.43). The reflected flux is proportional to the sensor's coefficient of reflectivity

$$\Phi_{br} = -\rho_s \Phi_{bo} = -A\varepsilon(1 - \varepsilon_s)\sigma T^4 \quad (4.135)$$

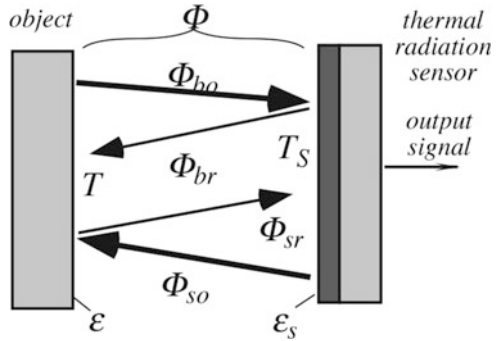
A negative sign indicates an opposite direction with respect to flux  $\Phi_{bo}$ . As a result, the net flux originated by the object and utilized by the sensor depends on both the object and sensor's emissivities:

$$\Phi_b = \Phi_{bo} + \Phi_{br} = A\varepsilon\varepsilon_s\sigma T^4. \quad (4.136)$$

<sup>28</sup> Here we discuss the so-called *thermal* sensors as opposed to quantum sensors that are described in Chap. 14.

<sup>29</sup> This simplified analysis assumes that there are no other objects in the sensor's field of view.

**Fig. 4.43** Thermal radiation exchange between object and thermal radiation sensor



Depending on its temperature  $T_s$ , the sensor’s surface radiates its own thermal flux that in a similar way results in the net thermal flux emanated by the sensor’s surface:

$$\Phi_s = -A\epsilon\epsilon_s\sigma T_s^4. \tag{4.137}$$

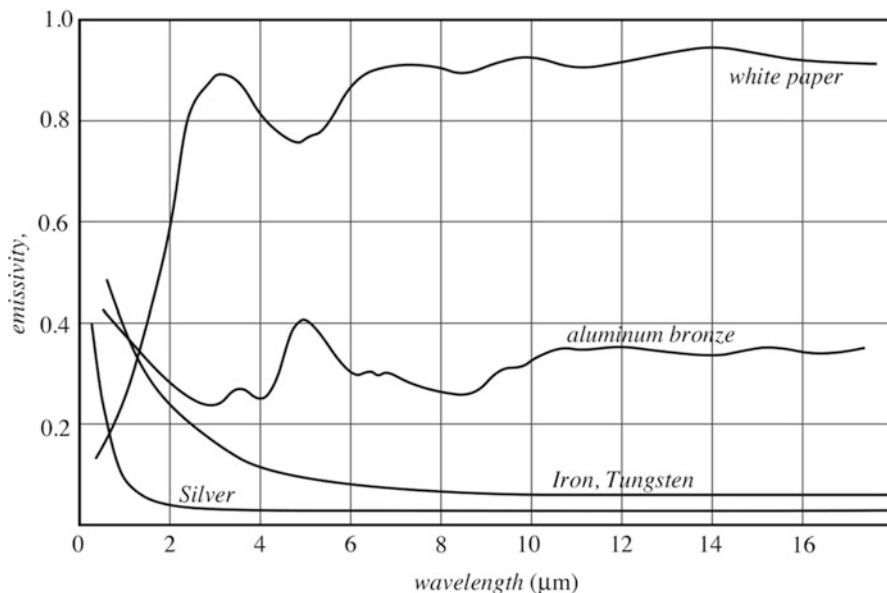
Two fluxes that originate by the object and sensor are combined into the final net flux existing between these two surfaces (object and sensor):

$$\Phi = \Phi_b + \Phi_s = A\epsilon\epsilon_s\sigma(T^4 - T_s^4). \tag{4.138}$$

This is a mathematical model of a net thermal flux that is converted by a thermal sensor into the output signal. It establishes a connection between thermal power absorbed by the sensor, and absolute temperatures of both the object and sensor. The important implication of this model is that the thermal radiation sensor will respond according to two temperatures: the object and the sensor itself.

The surface emissivity of a media is function of its dielectric constant and, subsequently, refractive index  $n$ . The highest possible emissivity is 1. It is attributed to the so-called *blackbody*—an ideal emitter of electromagnetic radiation. The name implies its appearance at normal room temperatures because emissivity of an ideal blackbody is wavelength independent—it is a unity all over the spectrum. If the object is opaque ( $\gamma = 0$ ) and nonreflective ( $\rho = 0$ ) according to Eq. (4.134), it becomes an ideal emitter and absorber of electromagnetic radiation (since  $\epsilon = \alpha$ ). Thus, a blackbody is an ideal emitter and absorber of light. It reflects nothing—that is why it looks black. In practice, a true blackbody does not exist. However it can be approached quite closely in a specially designed instrument, as we discuss below. A well-designed blackbody should have emissivity near  $\epsilon = 0.999$ . A lower emissivity approximately from 0.97 to 0.99 is attributed to the so-called *graybody*.

It should be noted that emissivity of a real surface is generally wavelength dependent (Fig. 4.44). For example, a white sheet of paper is very much reflective in the visible spectral range and emits no visible light. However, in the mid- and far-infrared spectral ranges its reflectivity is low and emissivity is high (about 0.92), thus making paper a good emitter of thermal radiation. Some materials, like



**Fig. 4.44** Wavelength dependence of surface emissivities

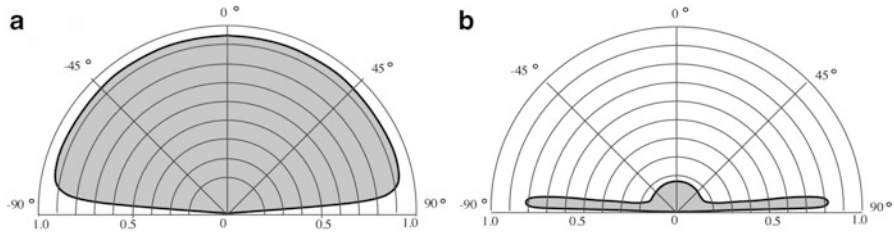
polymers and gases, have highly nonuniform emissivities (absorptivities) at different wavelengths, but within even a very narrow spectral range they still must obey Eq. (4.134). For example, polyethylene, which is widely used for fabrication of the far-infrared lenses, heavily absorbs (emits) in narrow bands around 3.5, 6.8, and 13.5  $\mu\text{m}$ , while being quite transparent (nonemissive) in other bands.

For many practical purposes, emissivity of an opaque material in a relatively narrow spectral range of thermal radiation may be considered constant. For precision noncontact IR measurements, when thermal radiation must be detected with accuracy better than 1 %, surface emissivity either must be known, or special methods to reduce effects of emissivity on accuracy should be employed. One such method is the so-called dual-band IR detectors.<sup>30</sup> The other method takes the benefit of a thermally balanced infrared sensor.<sup>31</sup>

For a nonpolarized mid- and far-infrared light in normal direction, emissivity may be expressed through refractive index by the equation

<sup>30</sup> Dual-band detectors use two narrow spectral ranges to detect the IR flux. Then, by using a radiometric technique of a signal processing, temperature of an object is calculated. During the calculation, emissivity and other multiplicative constants are cancelled out.

<sup>31</sup> In a thermally balanced IR sensor, the sensor's temperature is constantly controlled (warmed up or cooled down) to bring the net thermal flux close to zero. Then, according to Eq. (4.138), the emissivities are multiplied by zero and thus their values no longer make any difference.



**Fig. 4.45** Spatial emissivities for nonmetal (a) and polished metal (b)

$$\epsilon = \frac{4n}{(n + 1)^2}. \tag{4.139}$$

All nonmetals are very good diffusive emitters of thermal radiation with a remarkably constant emissivity defined by Eq. (4.139) within a solid angle of about  $\pm 70^\circ$  from normal.<sup>32</sup> Beyond that angle, emissivity begins to decrease rapidly to zero with the angle approaching  $90^\circ$  from normal. Near  $90^\circ$  emissivity is very low. A typical calculated graph of the directional emissivity of nonmetals into air is shown in Fig. 4.45a. It should be emphasized that the above considerations are applicable only to wavelengths in the mid- and far-infrared spectral range and are not true for the visible light, since emissivity of thermal radiation is a result of electromagnetic effects which occur at an appreciable depth below the surface of a dielectric.

Metals behave quite differently. Their emissivities greatly depend on surface finish. Generally, polished metals are poor emitters (good reflectors) within the solid angle of  $\pm 70^\circ$  while their emissivity increases at larger angles (Fig. 4.45b). This implies that even a very good metal-coated mirror reflects poorly at angles approaching  $90^\circ$  from normal. Table A.18 gives typical emissivities of some materials in a temperature range between 0 and  $100^\circ\text{C}$  in a normal direction.

Unlike most solid bodies, gases in many cases are transparent to thermal radiation. When they absorb and emit radiation, they usually do so only in certain narrow spectral bands. Some gases, such as  $\text{N}_2$ ,  $\text{O}_2$ , and others of nonpolar symmetrical molecular structure, are essentially transparent at low temperatures, while  $\text{CO}_2$ ,  $\text{H}_2\text{O}$ , and various hydrocarbon gases radiate and absorb to an appreciable extent. When infrared light enters a layer of gas, its absorption has an exponential decay profile, governed by *Beer's law*

$$\frac{\Phi_x}{\Phi_o} = e^{-\alpha_\lambda x}, \tag{4.140}$$

where  $\Phi_o$  is the incident thermal flux,  $\Phi_x$  is the flux at thickness  $x$ , and  $\alpha_\lambda$  is the spectral coefficient of absorption (emissivity). The above ratio is called a

<sup>32</sup>Normal means perpendicular to surface.



*monochromatic transmissivity*  $\gamma_\lambda$  at a specific wavelength  $\lambda$ . If gas is nonreflecting, then its emissivity at a specific wavelength  $\lambda$  is defined as

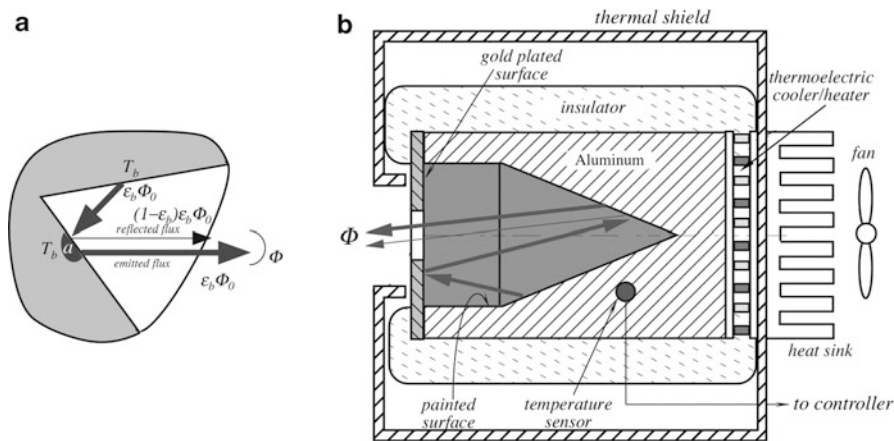
$$\varepsilon_\lambda = 1 - \gamma_\lambda = 1 - e^{-\alpha\lambda}. \quad (4.141)$$

It should be emphasized that since gasses absorb only in narrow bands, emissivity and transmissivity must be specified separately for any particular wavelength. For instance, water vapor is highly absorptive at wavelengths of 1.4, 1.8, and 2.7  $\mu\text{m}$  and is very transparent at 1.6, 2.2, and 4  $\mu\text{m}$ .

It is known that emissivity is essential when an infrared sensor is used for a noncontact temperature measurement—see Eq. (4.138). For calibrating such a noncontact thermometer or verifying its accuracy, a laboratory standard source of radiative heat must be constructed. The source shall exhibit precisely known emissivity and that emissivity preferably should approach unity as close as practical. In other words, this source is a blackbody. A nonunity emissivity would result in reflection (Eq. 3.134) of thermal radiation from the surrounding objects that may introduce a significant error in the measured infrared flux. There is no known material that has emissivity of one. Thus, a practical way to artificially simulate such a surface is employing the *cavity effect*, which is the basis for constructing a blackbody.

#### 4.12.3.2 Cavity Effect

An interesting effect develops when thermal radiation is measured from a cavity. For this purpose, a *cavity* means a void of a generally irregular shape inside a body whose inner wall temperature is uniform over its entire surface, Fig. 4.46a. Emissivity of the cavity opening or aperture (not of the cavity inner surface!) dramatically increases approaching unity at any wavelength, as compared with a



**Fig. 4.46** Cavity effect enhances emissivity (a); construction of a practical blackbody with a dual-cavity surface (b)

flat surface. The cavity effect is especially pronounced when the inner walls of a void have relatively high emissivity ( $>0.95$ ). Let us consider a nonmetal surface of a cavity. All nonmetals are diffuse emitters. Also, they are diffuse reflectors as shown in Fig. 4.45a. We assume that temperature and emissivity of the cavity walls are homogeneous over the entire area. According to Stefan-Boltzmann Law, Eq. (4.133), an ideal surface would emanate from some elementary area  $a$ , the ideal infrared photon flux  $\Phi_o = a\sigma T_b^4$ . However, the real surface has a lower emissivity  $\epsilon_b$ , and, as a result, the flux radiated from that area is smaller:  $\Phi_r = \epsilon_b\Phi_o$ . Since the cavity is thermally homogeneous, the flux which is emitted by any other part of the cavity in the direction toward area  $a$  is also equal to  $\Phi_r$ . A substantial portion of that incident flux  $\Phi_r$  is absorbed by the surface of area  $a$ , while a smaller part is diffusely reflected:

$$\Phi_p = \rho\Phi_r = (1 - \epsilon_b)\epsilon_b\Phi_o, \quad (4.142)$$

and the combined radiated and reflected flux from area  $a$  toward the cavity aperture is

$$\Phi = \Phi_r + \Phi_p = \epsilon_b\Phi_o + (1 - \epsilon_b)\epsilon_b\Phi_o = (2 - \epsilon_b)\epsilon_b\Phi_o. \quad (4.143)$$

If the aperture were a flat plate having emissivity,  $\epsilon_b$ , it would radiate flux  $\Phi_r = \epsilon_b\Phi_o$ . However, since in reality it is an opening (hole) in a cavity, by definition, the effective emissivity of the aperture from Eq. (4.143) is expressed as

$$\epsilon_e = \frac{\Phi}{\Phi_o} = (2 - \epsilon_b)\epsilon_b \quad (4.144)$$

Equation (4.144) suggests that due to just a single internal reflection (in reality there are many more), a perceived (effective) emissivity of a cavity aperture is equal to the inner wall surface emissivity magnified by a factor of  $(2 - \epsilon_b)$ . For example, assuming that the cavity wall is painted by an acrylic paint (typical emissivity 0.95), the aperture effective emissivity becomes  $\epsilon_e = (2 - 0.95)0.95 = 0.9975$ .

For a cavity effect to work, the effective emissivity must be attributed only to the cavity opening from which radiation escapes. If during measuring of thermal radiation, an IR sensor is inserted into the cavity too deeply facing its wall directly and occluding the internally reflected rays, the cavity effect will disappear and the emissivity becomes closer to that of the wall surface, which is always lower than unity.

When measuring infrared emission from a cavernous surface, cavity effect changes a perceived emissivity of a surface and, if not accounted for, may cause error in evaluation of the radiated power and subsequently, the measured temperature. To illustrate this, Fig. 4.47 shows two photographs of a human face—one is taken in visible light and the other in mid-infrared. Note that in the IR image, the areas at the nostrils appear a little bit brighter (that is—warmer). Yet the skin temperature in these spots is the same as nearby. Two wrinkles above the mustache cause the cavity effect that increases the wrinkle emissivity from a typical human



**Fig. 4.47** Photographs in visible light and IR thermal radiation that is naturally emanated from the object. Note the brighter (appearing warmer) areas at wrinkles and skin folds near nose—a result of cavity effect. Eyeglasses appear black (cold) because glass is opaque in mid- and far-infrared spectral ranges and does not pass thermal radiation from eyes. (Photo: courtesy of *Infrared Training Center*, [www.infraredtraining.com](http://www.infraredtraining.com))

skin emissivity of 0.96 to some higher value. This enhances intensity of the emanated thermal crease, creating an illusion of a warmer skin inside the wrinkle.

Design and fabrication of a blackbody is not a trivial task. For a cavity effect to work, a blackbody must satisfy the following conditions:

1. The cavity shall have the inner surface area much larger than the IR light exit—the aperture.
2. Shape of the cavity must allow for multiple inner reflections before light may escape from the aperture or any light entering the aperture from the outside should be totally lost inside. Thus, the cavity shall be a light trap.
3. The cavity wall temperature must be highly uniform all over its entire surface.

Figure 4.46b shows an efficient way of fabricating a blackbody [35] whose aperture emissivity approaches 0.999. The cavity body is fabricated of a solid copper or aluminum having a shape of an inverted cone, allowing multiple inner reflections. An imbedded temperature sensor and a thermoelectric heater/cooler with a control circuit (not shown) form a thermostat that maintains temperature of the cavity on a preset level with accuracy and stability better than  $\pm 0.02$  °C. The set temperature may be above or below the ambient temperature. The entire metal body is covered with a thermally insulating layer. To minimize thermal loss from the cavity to surroundings, an additional thermal shield envelops the entire assembly. Temperature of the shield is close to the cavity temperature and thus a heat flow through the insulation is drastically reduced. This helps in making temperature of the cavity walls highly stable and uniform.

The inner portion of the cavity should be painted with organic paint. Visible color of paint is not important as there is no correlation between the paint

reflectivity in a visible range (that determines color) and its emissivity in the infrared spectral ranges. The most troublesome portion of the cavity is located near the aperture, since it is very difficult to assure temperature of the aperture surrounding wall be totally independent of the ambient temperature and equal to the rest of the cavity walls. To minimize effects of the ambient temperature and increase a virtual cavity size, the inner surface of the front wall around the aperture is highly polished and gold-plated. Thus, the front side of the cavity has a very low emissivity and thus its temperature is not that critical. Besides, the gold surface reflects rays emitted by the right-side parts of the cavity walls that have high emissivity and thus enhances the cavity effect. This is called a dual-cavity surface. It should be stressed again that the blackbody near-unity emissivity is attributed only to the virtual surface of an aperture, which reality is a hole.

---

## References

1. Halliday, D., et al. (1986). *Fundamentals of physics* (2nd ed.). New York: John Wiley & Sons.
2. Crotzer, D., et al. (1993) Method for manufacturing hygriators. *U.S. Patent No. 5,273,777*.
3. Meissner, A. (1927). Über piezoeletrische Krystalle bei Hochfrequenz. *Zeitschrift für Technische Physik*, 8(74).
4. Neubert, H. K. P. (1975). *Instrument transducers. An introduction to their performance and design* (2nd ed.). Oxford: Clarendon.
5. Radice, P. F. (1982). Corona discharge poling process. *U.S. Patent No. 4,365,283*.
6. Southgate, P. D. (1976). Room-temperature poling and morphology changes in pyroelectric polyvinylidene fluoride. *Applied Physics Letters*, 28, 250.
7. Jaffe, B., et al. (1971). *Piezoelectric ceramics*. London: Academic.
8. Mason, W. P. (1950). *Piezoelectric crystals and their application to ultrasonics*. New York: Van Nostrand.
9. Megaw, H. D. (1957). *Ferroelectricity in crystals*. London: Methuen.
10. Oikawa, A., et al. (1976). Preparation of Pb(Zr, Ti)O<sub>3</sub> thin films by an electron beam evaporation technique. *Applied Physics Letters*, 29, 491.
11. Okada, A. (1977). Some electrical and optical properties of ferroelectric lead-zirconite-lead-titanate thin films. *Journal of Applied Physics*, 48, 2905.
12. Castelano, R. N., et al. (1979). Ion-beam deposition of thin films of ferroelectric lead-zirconite-titanate (PZT). *Journal of Applied Physics*, 50, 4406.
13. Adachi, H., et al. (1986). Ferroelectric (Pb, La)(Zr, Ti)O<sub>3</sub> epitaxial thin films on sapphire grown by RF-planar magnetron sputtering. *Journal of Applied Physics*, 60, 736.
14. Ogawa, T., et al. (1989). Preparation of ferroelectric thin films by RF sputtering. *Journal of Applied Physics*, 28, 11–14.
15. Roy, D., et al. (1991). Excimer laser ablated lead zirconite titanate thin films. *Journal of Applied Physics*, 69, 1.
16. Yi, G., et al. (1989). Preparation of PZT thin film by sol-gel processing: Electrical, optical, and electro-optic properties. *Journal of Applied Physics*, 64, 2717.
17. Tamura, M., et al. (1975). Electroacoustical transducers with piezoelectric high polymer. *Journal of the Audio Engineering Society*, 23(31), 21–26.
18. Eliason, S. (1984). Electronic properties of piezoelectric polymers. *Report TRITA-FYS 6665 from Dept. of Applied Physics*, The Royal Inst. of Techn., Stockholm, Sweden.
19. Dargahi, J. (2000). A piezoelectric tactile sensor with three sensing elements for robotic, endoscopic and prosthetic applications. *Sensors and Actuators A: Physical*, 80(1), 1–90.

20. Kawai, H. (1969). The piezoelectricity of poly (vinylidene fluoride). *Japanese Journal of Applied Physics*, 8, 975–976.
21. Meixner, H., et al. (1986). Infrared sensors based on the pyroelectric polymer polyvinylidene fluoride (PVDF). *Siemens Forsch-u Entwicl Ber Bd*, 15(3), 105–114.
22. Ye, C., et al. (1991). Pyroelectric PbTiO<sub>3</sub> thin films for microsensor applications. In: *Transducers'91 International Conference on Solid-State Sensors and Actuators. Digest of Technical Papers* (pp. 904–907). ©IEEE
23. Beer, A. C. (1963). Galvanomagnetic effect in semiconductors. In F. Seitz & D. Turnbull (Eds.), *Suppl. to solid state physics*. New York: Academic.
24. Putlye, E. H. (1960). The Hall effect and related phenomena. In C. A. Hogarth (Ed.), *Semiconductor monographs*. London: Butterwort.
25. Williams, J. (1990). Thermocouple measurement, AN28. In: *Linear applications handbook*. © Linear Technology Corp.
26. Seebeck, T. (1822–1823). Magnetische Polarisation der Metalle und Erze durch Temperatur-Differenz. *Abhaandulgen der Preussischen Akademic der Wissenschaften* (pp. 265–373).
27. Benedict, R. P. (1984). *Fundamentals of temperature, pressure, and flow measurements* (3rd ed.). New York: John Wiley & Sons.
28. LeChatelier, H. (1962). Copt. Tend., 102, 188629. In: D. K. C. MacDonald (Eds.), *Thermoelectricity: An introduction to the principles*. New York: John Wiley & Sons.
29. Carter, E. F. (1966). Dictionary of inventions and discoveries. In F. Muller (Ed.), *Crane*. New York: Russak.
30. Peltier, J. C. A. (1834). Investigation of the heat developed by electric currents in homogeneous materials and at the junction of two different conductors. *Annals of Physical Chemistry*, 56(2nd ser.), 371–386.
31. Thomson, W. (1854, May). On the thermal effects of electric currents in unequal heated conductors. *Proceedings of the Royal Soc.* (Vol. VII).
32. Manual on the use of thermocouples in temperature measurement. (1981). *ASTM Publication code number 04-470020-40*. Philadelphia: ASTM.
33. Doebelin, E. O. (1990). *Measurement systems: Application and design* (4th ed.). New York: McGraw-Hill.
34. Holman, J. P. (1972). *Heat transfer* (3rd ed.). New York: McGraw-Hill Book.
35. Fraden, J. (2002). Blackbody cavity for calibration of infrared thermometers. *U.S. Patent No. 6447160*.

*“Where the telescope ends, the microscope begins.  
Which of the two has the grander view?”*

—Victor Hugo

---

## 5.1 Light

### 5.1.1 Energy of Light Quanta

Light is a very efficient form of energy for sensing a great variety of stimuli. Among many others, these include distance, motion, temperature, chemical composition, pressure, etc. Light has an electromagnetic nature. It may be considered as propagation of either quanta of energy or electromagnetic waves. This confusing duality nowadays is well explained by quantum electrodynamics [1] and both the quantum and wave properties are used for sensing.

Different portions of the wave frequency spectrum are given special names, for example: ultraviolet (UV), visible, near-, mid- and far-infrared (IR), microwaves, radio waves, etc. The name “light” was arbitrarily given to electromagnetic radiation which occupies wavelengths from approximately 0.1 to 100  $\mu\text{m}$ . Light below the shortest wavelength that we can see—violet—is called *ultraviolet* (UV) and above the longest that we can see—red—is called *infrared* (IR). The UV upper wavelength limit is near 0.38  $\mu\text{m}$ . The IR range is arbitrarily subdivided into three regions: near-infrared (from about 0.75 to 1.5  $\mu\text{m}$ ), mid-infrared (1.5 to 5  $\mu\text{m}$ ), and far-infrared (5 to 100  $\mu\text{m}$ ).

Different portions of the radiation spectrum are studied by separate branches of physics and employed by different branches of engineering. The entire electromagnetic spectrum is represented in Fig. 4.41. It spreads from  $\gamma$  rays (the shortest wavelength is around 1 pm) to radio waves (the longest with the wavelength of hundreds of meters). In this section, we will briefly review those properties of light and the optical components which are mostly concerned with the visible and

near-IR portions of the electromagnetic spectrum. Thermal radiation (mid- and far-IR regions) is covered in Sect. 4.12.3.

The velocity of light  $c_0$  in vacuum is independent of wavelengths and can be expressed through  $\mu_0 = 4\pi \times 10^{-7}$  H/m and  $\epsilon_0 = 8.854 \times 10^{-12}$  F/m, which are the magnetic and electric permittivities of free space:

$$c_0 = \frac{1}{\sqrt{\mu_0 \epsilon_0}} = 299,792,458.7 \pm 1.1 \text{ m/s}. \quad (5.1)$$

However, when light propagates in some media, not in vacuum, its speed is lower. The frequency of light waves in vacuum or any particular medium relates to its wavelength  $\lambda$  by the Eq. (4.128) which we rewrite here as

$$\nu = \frac{c}{\lambda}, \quad (5.2)$$

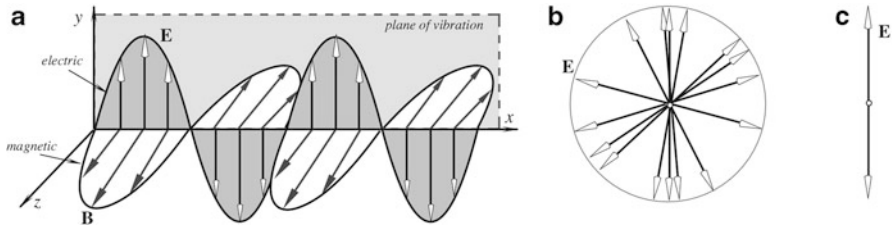
where  $c$  is the speed of light in a medium.

The energy of a quanta of light or photon relates to its frequency as

$$E = h\nu, \quad (5.3)$$

where  $h = 6.63 \times 10^{-34}$  J·s ( $4.13 \times 10^{-15}$  eV·s) is the Planck's constant. The photon energy  $E$  is measured in  $1.602 \times 10^{-19}$  J = 1 eV (electron-volt). It is worth recalling here the Wien's Law—see Eq. (4.130), stating that the higher the object's temperature, the shorter wave of light it radiates. Considering Eqs. (5.2) and (5.3) it is easy to arrive at a conclusion that photon energy is proportional to the object's absolute temperature. Thus, the hotter the object the more powerful photons it emanates.

The UV and visible photons carry relatively large energy and are not difficult to detect by the sensors based on the photoeffect. However, when temperature of an object drops and the emanated wavelength increases, moving to the infrared portion of the spectrum, the detection becomes more and more difficult. For example, a near-infrared photon having a wavelength of 1  $\mu\text{m}$  has the energy of 1.24 eV. Hence, an optical quantum detector operating in the range of 1  $\mu\text{m}$  must be capable of responding to that level of energy. If we keep moving even further toward the mid- and far-infrared spectral ranges, we deal with smaller and smaller energies. Human skin (at 34 °C) radiates the near- and far-infrared photons with energies near 0.13 eV which is an order of magnitude lower than the red light, making them much more difficult to detect. This is the reason, why low-energy radiation is often detected by *thermal detectors* rather than *quantum detectors*. Unlike quantum (photon) detectors that respond to individual quanta of light, thermal detectors are much less sensitive since they respond to temperature increase of the sensing element upon absorption light quanta and that requires a lot of photons.



**Fig. 5.1** Traveling electromagnetic wave has electric and magnetic field vectors (a); unpolarized electric field viewed along  $x$ -axis (magnetic vectors are not shown but they are always there) (b); vertically polarized electric field (c)

### 5.1.2 Light Polarization

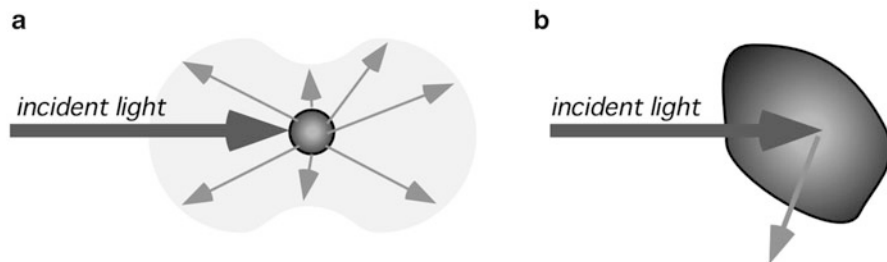
The electromagnetic wave (now we ignore the quantum properties of light) has the additional characteristic that is *polarization*—more specifically, *plane polarization*. This means that the alternating electric field vectors in space are parallel to each other for all points in the wave. The magnetic field vectors are also parallel to each other, but in dealing with the polarization issues related to sensor technologies, we focus our attention on the electric field, to which most detectors of the electromagnetic radiation are sensitive. Figure 5.1a shows the polarization feature. The wave in the picture is traveling in the  $x$ -direction. It is said the wave to be polarized in the  $y$ -direction because the electric field vectors are all parallel to this axis. The plane defined by the direction of propagation (the  $x$ -axis) and the direction of polarization (the  $y$ -axis) is called the *plane of vibration*. In a polarized light, there are no other directions for the field vectors.

Figure 5.1b shows a randomly polarized light which is the type of light that is produced by the Sun and various incandescent light sources, however, the emerging beam in most laser configurations is polarized. If unpolarized light passes through a polarization filter (Polaroid), only specific planes can pass through and the output electric field will be as shown in Fig. 5.1c. The polarization filter transmits only those wavetrain components whose electric vectors vibrate parallel to the filter direction and absorbs those that vibrate at right angles to this direction. The emerging light will be polarized according to the filter orientation. This polarizing direction in the filter is established during the manufacturing process by embedding certain long-chain molecules in a flexible plastic sheet and then stretching the sheet so that the molecules are aligned in parallel to each other. The polarizing filters are most widely used in the liquid crystal displays (LCD) and in some optical sensors that are described in the corresponding sections of this book.

## 5.2 Light Scattering

In empty space and away from the astronomically massive objects, light travels along straight lines. But if space is not entirely empty, this rule may be broken. Scattering is an electromagnetic phenomenon where light is forced to deviate from





**Fig. 5.2** Scattering of light from small (a) and large (b) particle

a straight path by one or more localized nonuniformities in the medium [2]. Examples of nonuniformities are smoke particles, dust, bacteria, water droplets, and gaseous molecules. When a particle is larger than the wavelength of incident light and happens to be in the light path, it serves as a reflector (Fig. 5.2b). The reflection is governed by general laws of reflection as described below.

Smaller particles cause a different type of scattering. It is typical for particles that are at least ten times smaller than the wavelength of light. In a simplified way, the scattering mechanism by a small particle can be explained as absorption of the light energy and re-emitting it in all directions (Fig. 5.2a). A scattering theory studies electromagnetic radiation (light) scattered by a small spherical volume of variant refractive indices, such as a bubble, droplet, or even a density fluctuation. This effect was first modeled by Lord Rayleigh, from whom it gets its name. For a very small particle, the exact shape of the scattering particle is usually not very significant and can often be treated as a sphere of the equivalent volume. The inherent scattering that light undergoes passing through a pure gas is due to microscopic density fluctuations as the gas molecules move around, which are normally small enough in scale for Rayleigh's model to apply.

Scattering depends on size of the particle or irregularity, the wavelength of light, and angle between the scattered and incident lights. This scattering mechanism is the primary cause for blue color of the Earth's sky on a clear day, as the shorter blue wavelengths of sunlight passing overhead are more strongly scattered than the longer red wavelengths at angles significantly deviating from the direction of the light beam coming from the Sun. However, at a sunset, at angles closer to the direction to the Sun, the sky appears orange and red because of a stronger scattering of longer (red) wavelengths. At night, the sky appears black because the sun light rays pass above the atmosphere and thus are not scattered toward the earth observer. Therefore, a sensor that employs scattering by small particles can operate either on a principle of measuring the light intensity or a shift in the scattered light spectrum.

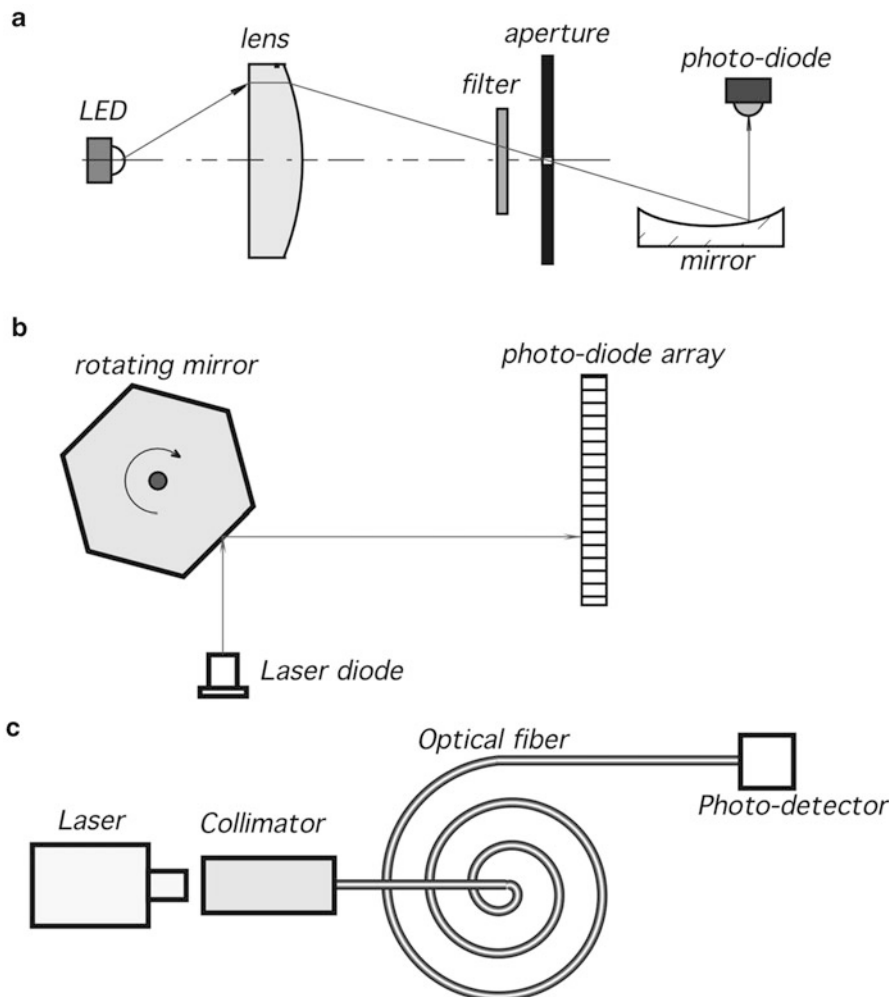
Light scattering is a phenomenon that can be used for detecting small impurities in gases and liquids and for sensing concentration of particles in a fluid. Examples of the applications are a smoke detector and air cleanliness monitor that senses presence and density of dust.

## 5.3 Geometrical Optics

Light modifications, such as reflection, refraction, absorption, interference, polarization, and speed are the powerful utensils in the sensor designer’s toolbox. Optical components help to manipulate light in many ways. Below we discuss these components from the standpoint of geometrical optics or ray optics. We will describe light propagation in terms of “rays”. The “ray” in geometrical optics is an abstraction that can be used to approximately model how light will propagate. Light rays are defined to propagate in a rectilinear path as they travel in a homogeneous medium. We consider light as a moving front or a ray which is perpendicular (normal) to that front. To do so, we will not discuss optical elements whose dimensions are too small as compared with the wavelength. In cases of very small objects, the methods of quantum electrodynamics (QED) need to be employed [1]. When using geometrical optics, we omit properties of light that are better described by quantum mechanics and quantum electrodynamics. Here, we will generally ignore not only the quantum properties of light but the wave properties as well. Just briefly we will address the emerging field of nano-optics. For more detailed discussions of the geometrical optics we refer the reader to special texts, for example [3–5].

Before light can be manipulated, first we need to have the light generated. There are several ways to produce light. Some sources of light are natural and exist without our will or effort, while some must be incorporated into a measurement device. The natural sources of light include celestial objects, such as sun, moon, stars, fire, etc. Also, natural sources of light in the mid- and far-infrared spectral ranges include all material objects that radiate electromagnetic waves depending on their temperatures, as it was described in Chap. 4. These include fire, exothermic chemical reactions, living organisms, and other natural sources whose thermal radiation can be selectively detected by the special optical devices. The man-made sources of light include filaments in the electric bulbs, light emitting diodes (LED), gas discharge lamps, lasers, laser diodes, heaters, etc.

After light is generated, it can be manipulated in many ways. Figure 5.3 shows several examples of manipulation of light in sensors. Most of these methods involve changing direction of light, while some use a selective blocking of certain wavelengths. The latter is called filtering. The light direction can be changed by use of *reflection* with the help of mirrors, prisms, optical waveguides, optical fibers, and many reflective objects. Also, the light direction can be changed by *refraction* with the help of lenses, prisms, windows, chemical solutions, crystals, organic materials, and biological objects. While passing through these objects, properties of light may be modified (modulated) by a measured stimulus. Then, the task of a sensor designer is to arrange a conversion of such a modulation into electrical signals that can be related to the stimulus. Which characteristics of light can be modulated? The intensity, direction of propagation, polarization, spectral contents—all these can be modified—and even the speed of light and phase of its wave can be changed.



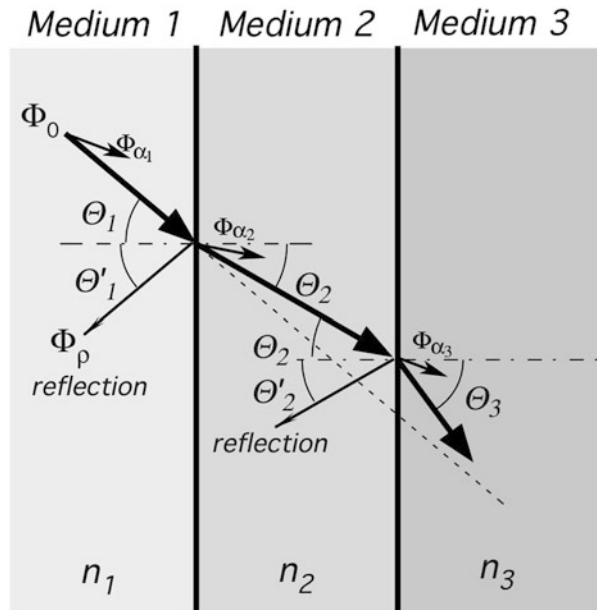
**Fig. 5.3** Examples of optical systems that use refraction (a) and reflection (a–c)

When developing sensors, one may be concerned either with radiometry or photometry. The former deals with the light power and its manipulation, while the latter is about illumination (brightness) and its control.

## 5.4 Radiometry

Let us consider light traveling through a three-layer material. All layers are made of different substances (materials) that we call media. Figure 5.4 shows what happens to a ray of light which travels from the first medium into a flat plate of a second

**Fig. 5.4** Light passing through materials with different refractive indices. Fluxes  $\Phi_\alpha$  are absorbed by respective media layers



medium, and then to a third medium. Examples of the media are air, glass, and water. Part of the incident light is reflected from a planar boundary between the first and second media according to the *law of reflection* which historically is attributed to Heron of Alexandria (first century AD) who noticed that angle of incidence equals angle of reflection

$$\Theta_1 = \Theta'_1 \tag{5.4}$$

This could be restated by saying that reflected light takes the shortest path or the shortest time to travel between two points. The latter definition can be derived from the Fermat's principle. A mirror-like reflection is called a *specular* reflection. Reflection not necessarily should be specular as defined by Eq. (5.4). When light strikes a rough or granular boundary between two media, it bounces off in all directions due to the microscopic irregularities of the interface. This is called *diffuse* reflection. The exact form of reflection depends on structure of the surface and the light wavelength.

While passing through a boundary between Medium 1 and Medium 2, a part of the original light flux enters Medium 2 at a different angle. The new angle  $\Theta_2$  is governed by the *refraction law* which was discovered in 1621 by Willebrord Snell (1580–1626) and is known as *Snell's law*

$$n_1 \sin \Theta_1 = n_2 \sin \Theta_2, \tag{5.5}$$

where  $n_1$  and  $n_2$  are the *indices of refraction* of two media.

In any medium light moves slower than in vacuum. An *index of refraction* is a ratio of velocity of light in vacuum,  $c_0$ , to that in a medium,  $c$

$$n = \frac{c_0}{c}, \quad (5.6)$$

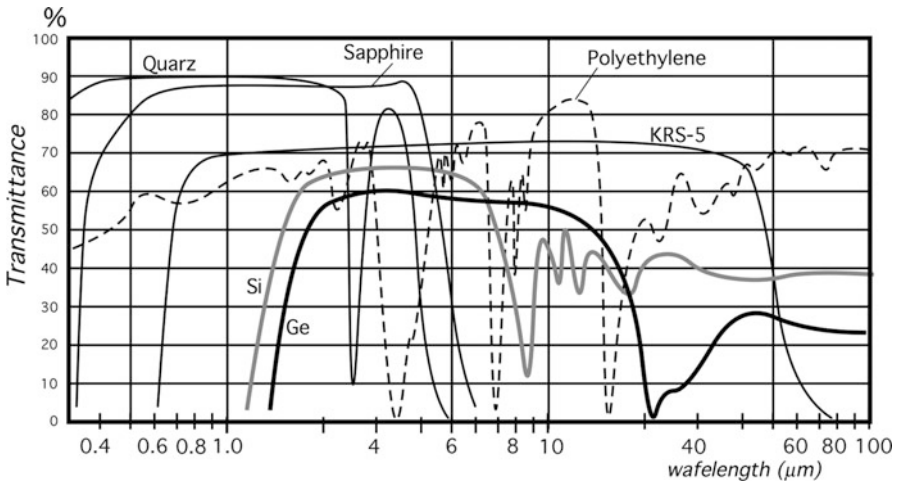
Since  $c < c_0$ , the refractive index of a medium is always more than unity. The velocity of light in a medium directly relates to a dielectric constant  $\epsilon_r$  of a medium, which subsequently determines the refractive index

$$n = \sqrt{\epsilon_r} \quad (5.7)$$

Generally,  $n$  is function of a wavelength. A wavelength dependence of index of refraction is manifested in a prism which was used by Sir Isaac Newton in his experiments with the light spectrum. In the visible range, the index of refraction  $n$  is often specified at a wavelength of  $0.58756 \mu\text{m}$ , the yellow-orange helium line. Indices of refraction for some materials are presented in Table A.19.

A refractive index dependence of wavelengths is called *dispersion*. The change in  $n$  with the wavelength is usually very gradual, and often negligible, unless the wavelength approaches a region where the material is not transparent.

While propagating through the medium, portions of light flux  $\Phi_\alpha$  in each medium, as shown in Fig. 5.4, is absorbed by the material and in most cases is converted into heat. Coefficient of absorption  $\alpha$  is also wavelength dependent and thus the medium transparency changes over the light spectrum. Figure 5.5 illustrates transparency curves of some optical materials employed in various optical sensors.



**Fig. 5.5** Transparency characteristics for various optical materials

It is important to remember that whenever electromagnetic radiation, including light, comes to a boundary between media having different indices of refraction, a reflection always takes place. However, whenever the indices of refraction are the same—there is no reflection and the light propagates right through both media without changing its direction. This suggests that reflection and refraction are intimately connected.

A portion of light flux that is not absorbed by the first medium is reflected from a boundary at angle  $\Theta'_1$ , and depends on the light velocities in two adjacent media. Amount of reflected flux  $\Phi_\rho$  relates to incident flux  $\Phi_0$  through the *coefficient of reflection*  $\rho$  which can be expressed by means of refractive indices

$$\rho = \frac{\Phi_\rho}{\Phi_0} = \left( \frac{n_1 - n_2}{n_1 + n_2} \right)^2. \quad (5.8)$$

Equations (4.139) and (5.8) indicate that both the reflection and absorption (the same as emissivity  $\varepsilon$ ) depend solely on refractive indices of the material at a particular wavelength.

If the light flux enters from air into an object having refractive index  $n$ , Eq. (5.8) is simplified as

$$\rho = \left( \frac{n - 1}{n + 1} \right)^2, \quad (5.9)$$

Before light exits Medium 2 (Fig. 5.4) and enters the Medium 3, having refractive index  $n_3$ , other parts of it are absorbed and reflected internally from the second boundary between the  $n_2$  and  $n_3$  media at angle  $\Theta'_2$ . The remaining portion of light exits at angle  $\Theta_3$  which is also governed by the Snell's law. If Media 1 and 3 are the same (for instance, air), then  $n_1 = n_3$  and  $\Theta_1 = \Theta_3$ . This case is illustrated in Fig. 5.6. It follows from Eq. (5.8) that coefficients of reflection are the same for light striking a boundary from either direction—approaching from the higher or lower index of refraction.

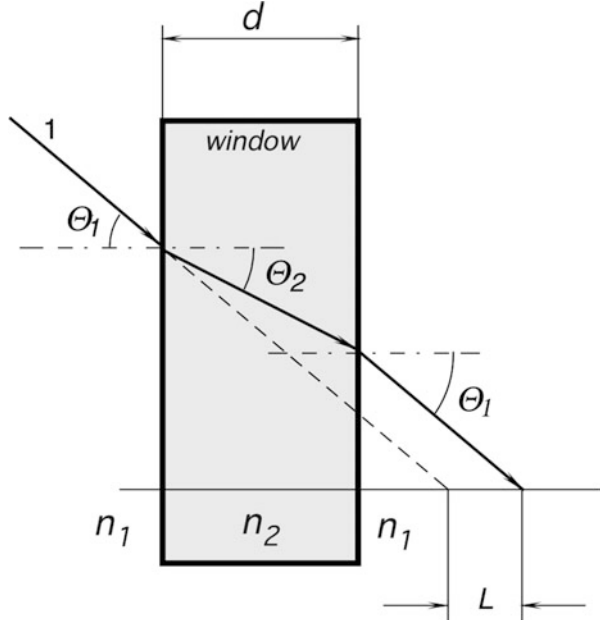
A combined coefficient of two reflections from both surfaces of a plate can be found from a simplified formula

$$\rho_2 \approx \rho_1(2 - \rho_1), \quad (5.10)$$

where  $\rho_1$  is the reflective coefficient from one surface. In reality, the light reflected from the second boundary is reflected again from the first boundary back to the second boundary, and so on. Thus, assuming that absorption in the material is negligibly small, the total reflective loss within the plate can be calculated through the refractive index of the material

$$\rho_2 \approx 1 - \frac{2n}{n^2 + 1} \quad (5.11)$$

**Fig. 5.6** Light passing through optical plate



Reflection increases for higher differences in refractive indices. For instance, if visible light travels without absorption from air through a heavy flint glass plate, two reflectances result in a loss of about 11 % of the flux power, while for the air-germanium-air interfaces (in the mid- and far-infrared spectral ranges) the reflective loss is about 59 %. To reduce losses, optical materials are often given antireflective coatings (ARC) which have refractive indices and thickness geared to specific wavelengths and serve as optical buffers.

The radiant energy balance Eq. (4.134) should be modified to account for two reflections in an optical material:

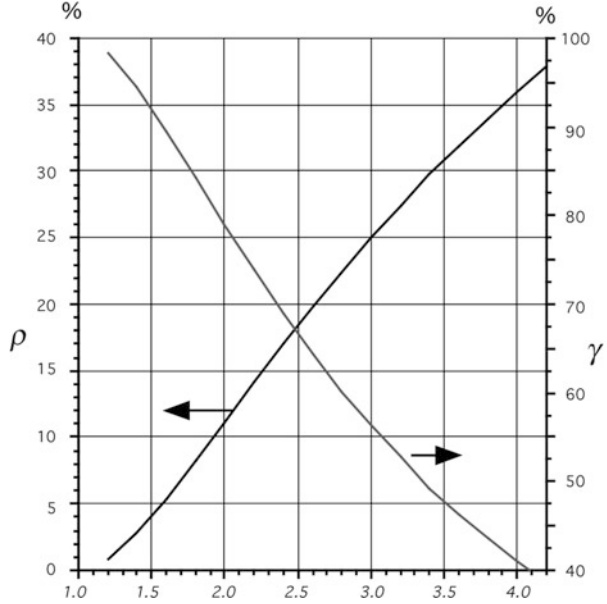
$$\rho_2 + \alpha + \gamma = 1, \quad (5.12)$$

where  $\alpha$  is a coefficient of absorption and  $\gamma$  is a coefficient of transmittance. In a transparency region,  $\alpha \approx 0$ , therefore, the overall transmittance can be approximately estimated as:

$$\gamma = 1 - \rho_2 \approx \frac{2n}{n^2 + 1}. \quad (5.13)$$

In the above example, transmittance of a glass plate is 88.6 % (visible) while transmittance of a germanium plate is 41 % (far IR). However, in the visible range, germanium transmittance is zero, which means that 100 % of visible light is reflected and absorbed. Figure 5.7 shows reflectance and transmittance of a thin

**Fig. 5.7** Reflectance and transmittance of a thin plate as functions of a refractive index



**Fig. 5.8** Radiant energy distribution at optical plate

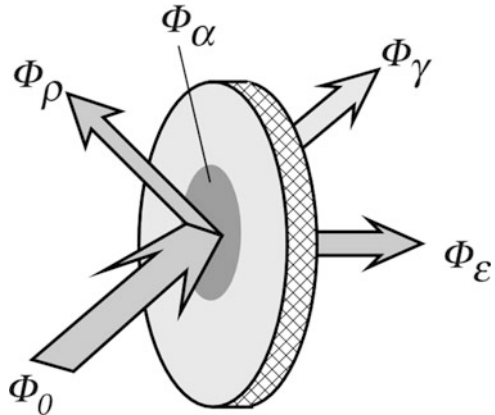


plate as functions of the refractive indices. Here a plate means any optical device (like a thin window or a lens) operating within its useful spectral range, that is, where its absorptive loss is very small ( $\alpha \approx 0$ ).

Figure 5.8 shows a light energy distribution within an optical plate when incident light flux  $\Phi_0$  strikes its surface. A part of incident flux  $\Phi_\rho$  is reflected, another part  $\Phi_\alpha$  is absorbed by the material, and the third part  $\Phi_\gamma$  is transmitted through. The absorbed portion of light is converted into heat, a portion of which  $\Delta P$  is lost to a supporting structure and surroundings through thermal conduction and convection. The rest of the absorbed light, raises temperature of the material. The temperature increase may be of



concern when the material is used as a window in a powerful laser. Another application where temperature increase may cause problems is in far-infrared detectors. The problem is associated with the flux  $\Phi_\epsilon = \Phi_\alpha - \Delta P$  which is radiated by the material due to its temperature change. This is called a *secondary radiation*. Naturally, the radiated spectrum relates to a temperature of the material, its chemical composition and is situated in the mid- and far-infrared regions of the optical spectrum. The spectral distribution of the secondary radiation corresponds to the absorption distribution of the material because absorptivity and emissivity is the same thing.

For materials with a relatively low absorption, the absorption coefficient can be determined through a temperature rise in the material

$$\alpha = \frac{mc}{\Phi_\gamma} \frac{2n}{n^2 + 1} \left( \frac{dT_g}{dt} + \frac{dT_L}{dt} \right) T_0, \quad (5.14)$$

where  $m$  and  $c$  are the mass and the specific heat of the optical material,  $T_g$  and  $T_L$  are the slopes of the rising and lowering parts of the temperature curve of the material, respectively, at test temperature  $T_0$ . Strictly speaking, light in the material is lost not only due to absorption but to scattering as well. A combined loss within material depends on its thickness and can be expressed through the so-called *attenuation coefficient*,  $g$ , and thickness of the sample  $h$ . The transmission coefficient can be determined from Eq. (5.13) which is modified to account for the attenuation:

$$\gamma \approx (1 - \rho_2)e^{-gh}. \quad (5.15)$$

The attenuation (or *extinction*) coefficient  $g$  is usually specified by manufacturers of optical materials.

---

## 5.5 Photometry

When using the light sensitive devices (photodetectors), it is critical to take into consideration both the sensor and light source. In some applications, light is received from independent sources, while in others the light source is part of the measurements system. In any event, the so-called photometric characteristics of the optical system should be accounted for. Such characteristics include light, emittance, luminance, brightness, etc.

To measure radiant intensity and brightness, special units have been devised. Radiant flux (energy emitted per unit time) which is situated in a visible portion of the spectrum is referred to as *luminous flux*. This distinction is due to the inability of the human eye to respond equally to like power levels of different visible wavelengths. For instance, one red and one blue light of the same intensity will produce very different sensations—the red will be perceived as much brighter.<sup>1</sup>

---

<sup>1</sup>This is the reason why “stop” in a traffic light is red—much easier to notice at longer distances.

**Table 5.1** Radiometric and photometric terminology

Description	Radiometric	Photometric
Total flux	Radiant flux ( $\Phi$ ) in watts	Luminous flux ( $\Phi$ ) in lumens
Emitted flux density at a source surface	Radiant emittance ( $W$ ) in watts/cm <sup>2</sup>	Luminous emittance ( $L$ ) in lumens/cm <sup>2</sup> (lamberts) or lumens/ft <sup>2</sup> (foot-lamberts)
Source intensity (point source)	Radiant intensity ( $I_r$ ) in watts/steradian	Luminous intensity ( $I_L$ ) in lumens/steradian (candela)
Source intensity (area source)	Radiance ( $B_r$ ) in watts/steradian/cm <sup>2</sup>	Luminance ( $B_L$ ) in lumens/steradian/cm <sup>2</sup> (lambert)
Flux density incident on a receiver surface	Irradiance ( $H$ ) in watts/cm <sup>2</sup>	Illuminance ( $E$ ) in lumens/cm <sup>2</sup> (candle) or lumens/ft <sup>2</sup> (foot-candela)

Hence, comparing lights of different colors, the watt becomes a poor measure of brightness and a special unit called a *lumen* was introduced. It is based on a standard radiation source with molten platinum formed in a shape of a blackbody and visible through a specified aperture within a solid angle of one steradian. A solid angle is defined in a spherical geometry as

$$\omega = \frac{A}{r^2}, \quad (5.16)$$

where  $r$  is the spherical radius and  $A$  is the spherical surface of interest. When  $A = r$ , then the unit is called a spherical radian or *steradian* (see Table 5.1).

Illuminance is given as

$$E = \frac{d\Phi}{dA}, \quad (5.17)$$

that is, a differential amount of luminous flux ( $\Phi$ ) over a differential area ( $A$ ). It is most often expressed in lumens per square meter (square foot), or foot-meter (foot-candle). The luminous intensity specifies flux over solid angle:

$$I_L = \frac{d\Phi}{d\omega}, \quad (5.18)$$

most often it is expressed in lumens per steradian or candela. If the luminous intensity is constant with respect to the angle of emission, the above equation becomes

$$I_L = \frac{\Phi}{\omega}. \quad (5.19)$$

If the wavelength of the radiation varies, but the illumination is held constant, the radiative power in watts is found to vary. A relationship between illumination and radiative power must be specified at a particular frequency. For specifications, a

very exact wavelength has been selected,  $0.555 \mu\text{m}$ , which is the peak of the spectral response of a human eye. At this wavelength,  $1 \text{ W}$  of radiative power is equivalent to  $680 \text{ lm}$ . For convenience of the reader, some useful terminology is given in Table 5.1.

In selection of electro-optical sensors, the design considerations of light sources are of prime concern. A light source will effectively appear as either a *point source*, or as an *area source*, depending upon the relationship between the size of the source and the distance between the source and the detector. Point sources are arbitrarily defined as those whose diameter is less than  $10 \%$  of the distance between the source and the detector. While it is usually desirable that a photodetector is aligned such that its surface area is tangent to the sphere with the point source at its center, it is possible that the plane of the detector can be inclined from the tangent plane. Under this condition, the incident flux density (irradiance) is proportional to the cosine of the inclination angle  $\varphi$ :

$$H = \frac{I_r}{\cos \varphi}, \quad (5.20)$$

and the illuminance

$$E = \frac{I_L}{r^2} \cos \varphi. \quad (5.21)$$

The area sources are arbitrarily defined as those whose diameter is greater than  $10 \%$  of the separation distance. A special case that deserves some consideration occurs when radius  $R$  of the light source is much larger than the distance  $r$  to the sensor. Under this condition

$$H = \frac{B_r A_s}{r^2 + R^2} \approx \frac{B_r A_s}{R^2}, \quad (5.22)$$

where  $A_s$  is the area of the light source and  $B_r$  is the radiance. Since the area of the source  $A_s = \pi R^2$ , irradiance is:

$$H \approx B_r \pi = W, \quad (5.23)$$

that is, the emitted and incident flux densities are equal. If the area of the detector is the same as area of the source, and  $R \gg r$ , the total incident energy is approximately the same as the total radiated energy, that is, a unity coupling exists between the source and the detector. When the optical system is comprised of channeling, collimating, or focusing components, its efficiency and, subsequently, coupling coefficient, must be considered. Important relationships for point and area light sources are given in Tables 5.2 and 5.3.

**Table 5.2** Point source relationships

Description	Radiometric	Photometric
Point source intensity	$I_r$ , W/sr	$I_L$ , lm/sr
Incident flux density	Irradiance, $H = \frac{I_r}{r^2}$ , W/m <sup>2</sup>	Illuminance, $E = \frac{I_L}{r^2}$ , lm/m <sup>2</sup>
Total flux output of a point source	$P = 4\pi I_r$ , W	$F = 4\pi I_L$ , lm

**Table 5.3** Area source relationships

Description	Radiometric	Photometric
Point source intensity	$B_r$ , W/(cm <sup>2</sup> sr)	$B_L$ , lumens/(cm <sup>2</sup> sr)
Emitted flux density	$W = \pi B_r$ , W/cm <sup>2</sup>	$L = \pi B_L$ , lumens/cm <sup>2</sup>

## 5.6 Windows

The main purpose of windows is to protect interiors of optical sensors and detectors from environment. A good window should transmit light rays in a specific wavelength range with minimal distortions. Therefore, windows should possess appropriate characteristics adapted for a particular application. For instance, if an optical detector operates under water, perhaps its window should possess the following properties: a mechanical strength to withstand water pressure, a low water absorption, a transmission band corresponding to the wavelength of interest, and an appropriate refractive index preferably should be close to that of water. A useful window shape that can better withstand high pressures is spherical as shown in Fig. 5.9. To minimize optical distortions, three limitations should be applied to a spherical window: an aperture  $D$  (its largest dimension) should be smaller than the window's spherical radius  $R_1$ , a thickness  $d$  of the window should be uniform, and much smaller than radius  $R_1$ . If these conditions are not met, the window becomes a concentric spherical lens.

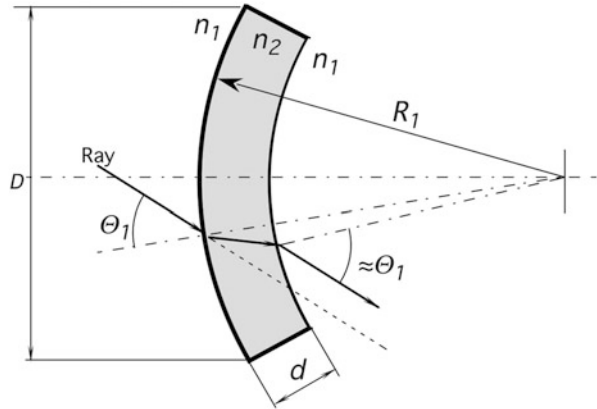
A surface reflectivity of a window should be considered for its overall performance. To minimize a reflective loss, windows may be given antireflective coatings (ARC) which are applied on either one or both sides of the window (Sect. 5.10.4). These are the coatings that give blue and amber appearances to photographic lenses and filters. Due to refraction in the window (see Fig. 5.6), a passing ray is shifted by a distance  $L$  which for small angles  $\Theta_1$  may be found from formula:

$$L = d \frac{n-1}{n}, \quad (5.24)$$

where  $n$  is the refractive index of the material.

Sensors operating in the mid- and far-infrared ranges require special windows which are opaque in the visible and ultraviolet (UV) spectral regions and quite transparent in the wavelength of interest. Several materials are available for fabrication of such windows. Spectral transmittances of some materials are shown in

**Fig. 5.9** Spherical window



**Fig. 5.10** Spectral transmittance of a silicon window. Note that majority of loss is due to a reflection from two surfaces

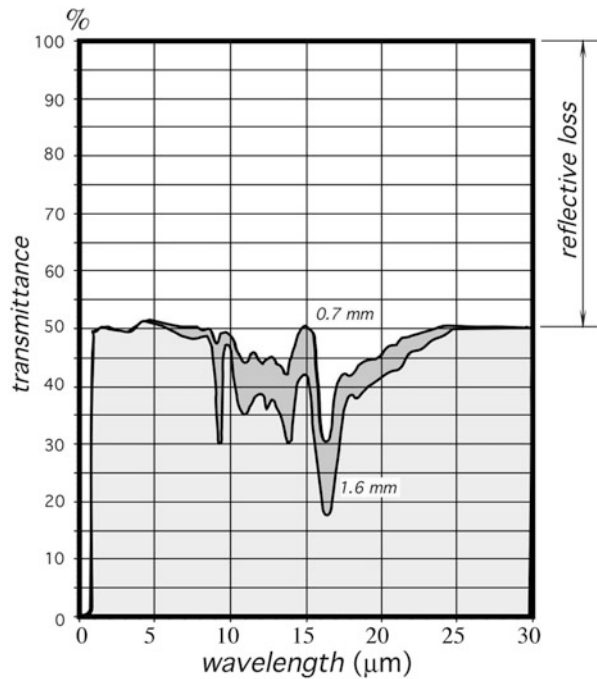


Fig. 5.5 When selecting material for a mid- and far-infrared window, the refractive index shall be seriously considered because it determines coefficients of reflectivity, absorptivity, and eventually transmittance. Figure 5.10 shows spectral transmittances of two silicon windows having different thicknesses. Total radiation (100 %) at the window is divided into three portions: reflected (average of about 50 % over the entire spectral range), absorptive (varies at different wavelengths), and transmitted, which is whatever is left after reflection and absorption. Since all windows are characterized by specific spectral transmissions, often they are called *filters*.

## 5.7 Mirrors

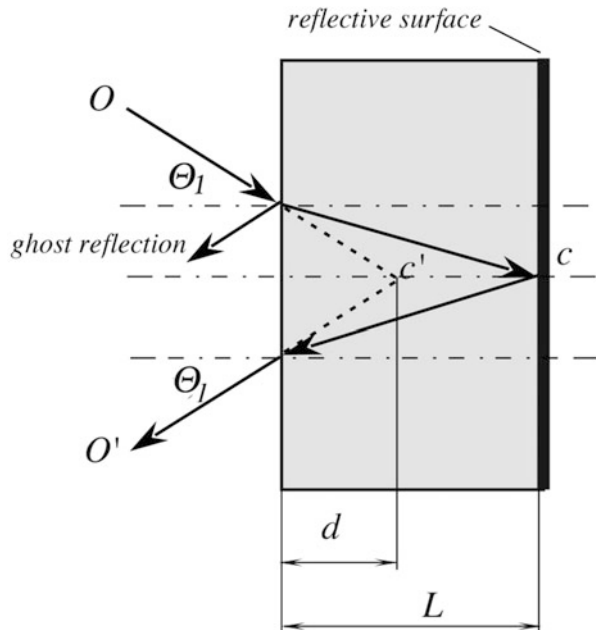
A mirror is the oldest optical instrument ever used or designed. Whenever light passes from one medium to another, there is some reflection. To enhance a reflectivity, a single or multilayer reflecting coating is applied either on the front (first surface) or the rear (second surface) of a plane-parallel plate or other substrate of any desirable shape. The first surface mirrors are the most accurate. In the second surface mirror, light first must enter a plate having generally a different index of refraction than the outside medium. A second surface mirror in effect is a combination of a mirror and window.

Several effects in the second surface mirror shall be taken into consideration. First, due to refractive index  $n$  of a plate, a reflective surface appears closer (Fig. 5.11). A virtual thickness  $d$  of the carrier for smaller angles  $\Theta_1$  may be found from a simple formula:

$$d \approx \frac{L}{n} \quad (5.25)$$

A front side of the second surface mirror may also reflect a substantial amount of light creating the so-called *ghost reflection*. A glass surface typically reflects in air about 4 % of visible light.

**Fig. 5.11** Second surface mirror



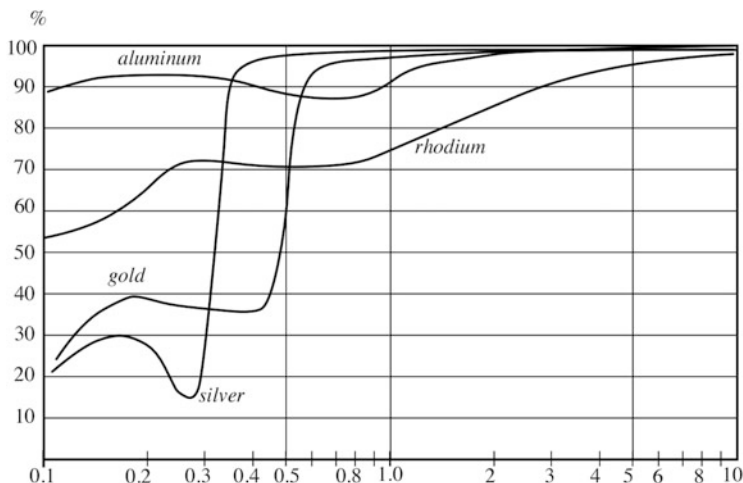


Fig. 5.12 Spectral reflectances of some mirror coatings

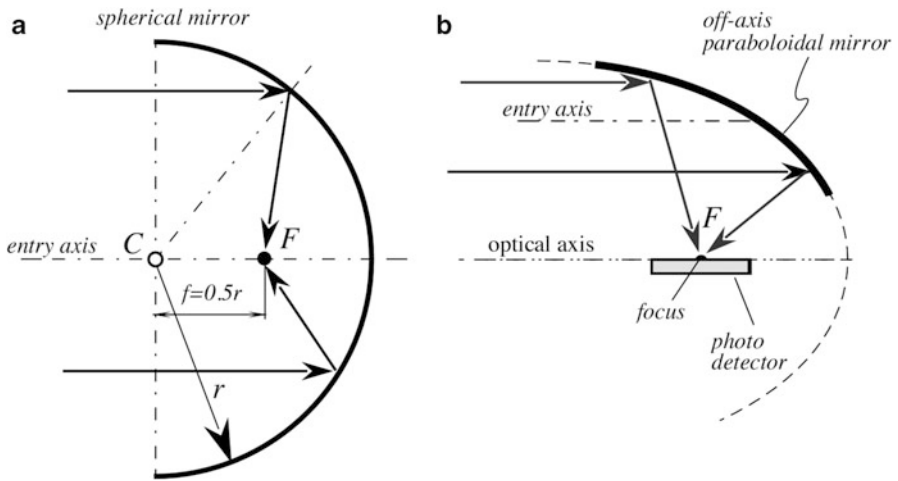
### 5.7.1 Coated Mirrors

Reflecting coatings applied to a surface for operation in the visible and near-infrared range can be silver, aluminum, chromium, and rhodium. Gold is preferable for the mid- and far-infrared spectral range devices. By selecting an appropriate coating, the reflectance may be achieved of any desired value from nearly 0 to almost 1 (Fig. 5.12).

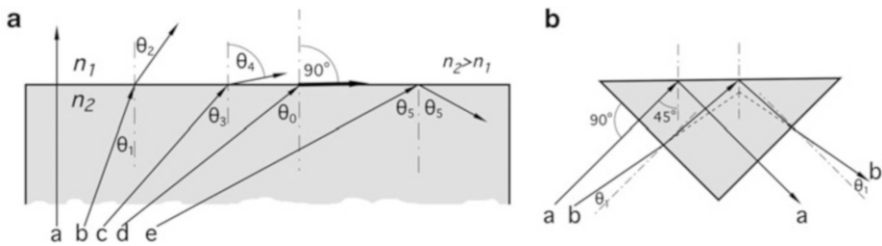
The best mirrors for a broadband use have pure metallic layers, vacuum, or electrolytically deposited on glass, fused silica, or metal substrates. Before the reflective layer deposition, to achieve a leveling effect a mirror may be given an undercoat of copper, zirconium-copper, or molybdenum.

A reflective surface may be sculptured practically in any shape to divert the direction of the light travel. In optical systems, curved mirrors produce effects equivalent to that of lenses. The advantages they offer include (1) higher transmission, especially in the longer wavelength spectral range where lenses become less efficient due to higher absorption and reflectance loss, (2) absence of distortions incurred by refracting surfaces due to dispersion (chromatic aberrations), (3) lower size and weight as compared with many types of lenses. Spherical mirrors are used whenever light must be collected and focused.<sup>2</sup> However, spherical mirrors are good only for the parallel or near parallel beams of light that strike a mirror close to normal. These mirrors suffer from imaging defects called aberrations. Figure 5.13a shows a spherical mirror with the center of curvature in point C. A focal point is located at a distance of 1/2 of the radius from the mirror surface. A spherical mirror is astigmatic, meaning that the off-axis rays are focused away from its focal point.

<sup>2</sup> *Focus* is from the Latin meaning *fireplace*—a gathering place in a house.



**Fig. 5.13** Spherical (a) and parabolic (b) first surface mirrors



**Fig. 5.14** Internal reflections (a) and prismatic mirror (b)

Nevertheless, such mirrors prove very useful in detectors where no quality imaging is required, for instance in infrared motion detectors which are covered in detail in Sect. 7.8.8.

A parabolic mirror is quite useful for focusing light off-axis. When it is used in this way, there is complete access to the focal region without shadowing, as shown in Fig. 5.13b.

### 5.7.2 Prismatic Mirrors

Figure 5.14a illustrates passing light rays from a media having refractive index  $n_2$  to another media of a lower refractive index  $n_1$ . Ray “a” is normal to the boundary and passes through without change in its direction (though portion of its energy is still reflected back). Ray “b” approaches the boundary at angle  $\theta_1$  and according to Eq. (5.5) exits at a larger angle  $\theta_2$ . Similarly behaves the ray “c” having a larger



entrance angle  $\Theta_3$ . If the entry angle still increases, at a certain angle  $\Theta_0$  the ray “d” bends so much that after exiting it propagates along the boundary at the angle of  $90^\circ$ . This special entry angle is called the angle of *total internal reflection* (TIR). It is a function of both refractive indices:

$$\Theta_0 = \arcsin\left(\frac{n_1}{n_2}\right). \quad (5.26)$$

Ray “e” enters even at a larger angle  $\Theta_5$  and thus instead of crossing the boundary, it is reflected, like from a mirror, at the same angle  $\Theta_5$ . Note that the TIR effect appears only when the rays try to exit from the media of a higher refractive index into the media of a lower refractive index. TIR forms a reflector that may serve as a second-surface mirror without the need for reflective coatings. Usually it is employed in a prism as shown in Fig. 5.13b. The prismatic shape allows the rays to enter the prism body at small angles ( $\Theta_1$ ), while approaching from inside the upper surface at the angles exceeding TIR. As a result, the rays are reflected from the upper surface and exit the prism from the right-side slope. The total internal reflectors are the most efficient in the visible and near-infrared spectral ranges as the reflectivity coefficient is close to unity. The TIR principle is fundamental for operation of optical fibers and fiber-optic sensors.

---

## 5.8 Lenses

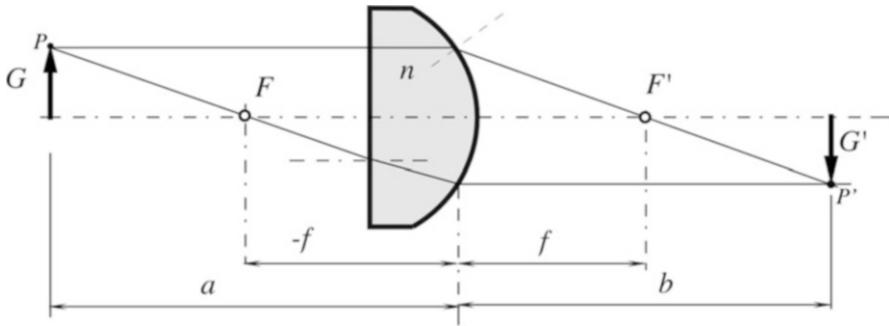
Like the mirrors, lenses<sup>3</sup> are employed in sensors and detectors to divert the direction of light rays and arrange them in a desirable fashion. But unlike the mirrors that use reflection, lenses use refraction—the effect based on Snell Law (Sect. 5.4) and Eq. (5.5). The main idea behind the lens is a bending of light ray while crossing the lens surface and entering and exiting to another medium, such as air. By sculpturing the lens surface, rays can be predictably diverted to a desired location, for example—a focal point or *focus*.

### 5.8.1 Curved Surface Lenses

Figure 5.15 shows a *plano-convex* lens which has one surface spherical and the other is flat. The lens has two focuses—one at each side:  $F$  and  $F'$ , which are positioned at equal distances  $-f$  and  $f$  from the lens. When light rays from object  $G$  enters the lens, their directions change according to Snell’s law. Light changes direction only at a boundary between the lens and outside. Inside the lens light propagates along straight lines.

---

<sup>3</sup>The word *lens* is from the Latin name for lentils. A lentil seed is flat and round with its sides bulging outward—just like a convex lens.



**Fig. 5.15** Geometry of a plano-convex lens

A useful property of a lens (and a curved mirror as well) is that it forms an image of object  $G$ . To better understand how that comes about, consider that the object is illuminated (unless it glows) and each point  $P$  on its surface reflects light rays toward every point on the lens surface that faces the object. In other words, each point of the object projects endless number of rays toward the lens surface. To determine where the image of point  $P$  will be formed, there is no need to trace all possible rays that strike the lens. It is sufficient to evaluate just two rays—we know from the plane geometry that coordinates of a point is fully defined by crossing of two straight lines, so we need just two rays. These two rays that we evaluate are: 1—parallel to the optical axis, and 2—passing through the lens focus.

After exiting the lens, ray 1 (parallel to the axis) goes through focus  $F'$ . The other ray 2 first passes through focus  $F$  and upon exiting the lens, propagates in parallel with the optical axis. Then, both rays cross at point  $P'$  that is the image of point  $P$ . The entire multitude of the rays passing through the lens from point  $P$  converges at the same image point  $P'$  (if we ignore several optical aberrations, such as spherical, *e.g.*).

The formed image  $G'$  is inverted and positioned at a distance  $b$  from the lens. That distance may be found from a thin lens equation:

$$\frac{1}{f} = \frac{1}{a} + \frac{1}{b}. \quad (5.27)$$

Lenses may have different shapes, for example:

- Biconvex (positive), when both sides are curved to bulge out.
- Plano-convex (positive) when one side is curved to bulge out and one is flat.
- Biconcave (negative) when both sides are curved to cave in.
- Plano-concave (negative) when one side caves in and the other is flat. Other combinations are possible, such as meniscuses.

A thin biconvex lens whose radii of curvatures are much larger than thickness of the lens has a focal distance  $f$  that may be found from the equation

$$\frac{1}{f} = (n - 1) \left( \frac{1}{r_1} + \frac{1}{r_2} \right), \quad (5.28)$$

where  $r_1$  and  $r_2$  are radii of the lens curvatures.

For the thick lenses where thickness  $t$  is comparable with the radii of curvature a focal distance may be found from formula

$$\frac{1}{f} = (n - 1) \left[ \frac{1}{r_1} - \frac{1}{r_2} + \frac{(n - 1)t}{nr_1r_2} \right]. \quad (5.29)$$

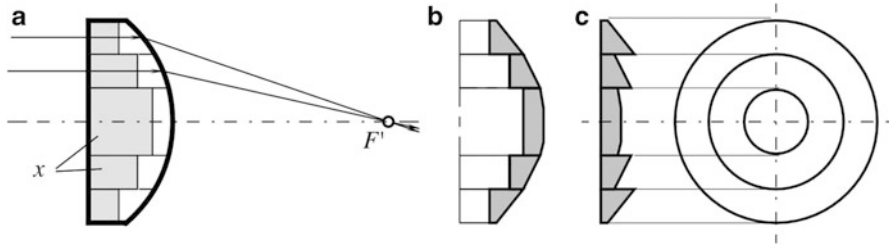
Several lenses may be combined into a more complex system. For two lenses separated by a distance  $d$ , a combination focal length may be found from equation

$$f = \frac{f_1 f_2}{f_1 + f_2 - d}. \quad (5.30)$$

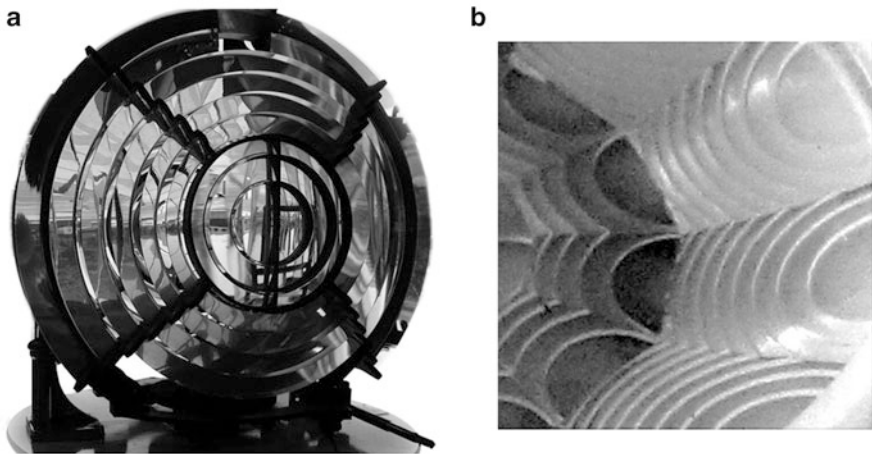
## 5.8.2 Fresnel Lenses

Fresnel lenses are optical elements with the step-profiled surfaces. They prove to be very useful in sensors and detectors where a high quality of imaging is not required, while minimizing the lens weight and cost are the key requirements. Major applications include light condensers, magnifiers, and focusing element in the infrared thermometers and occupancy detectors. Fresnel lenses may be fabricated of glass, acrylic (visible and near-infrared range), silicon or polyethylene (mid- and far-infrared ranges). The history of Fresnel lenses began in 1748, when Count Buffon proposed grinding out a solid piece of glass lens in steps of the concentric zones in order to reduce thickness of the lens to a minimum and to lower energy loss. He realized that only the surface of a lens is needed to refract light, because once the light is inside the lens, it travels in a straight line. His idea was modified in 1822 by Augustin Fresnel (1788–1827), who constructed a lens in which the centers of curvature of the different rings receded from the axis according to their distances from the center, so as to practically eliminate spherical aberration.

The concept of that lens is illustrated in Fig. 5.16, where a regular plano-convex lens is depicted (a). The lens is sliced into several concentric rings. After slicing, all rings still remain lenses that refract parallel incident rays into a common focus defined by Eq. (5.27). A change in an angle occurs when a ray exits a curved surface, not inside the lens, hence the section of a ring marked by the letter  $x$  does not contribute to the focusing properties, while having negative effects of contributing to the lens weight and light absorption. If all such useless sections are removed, the lens will look like it is shown in Fig. 5.16b and will fully retain its ability to focus light rays. Now, all of the rings may be shifted with respect to one



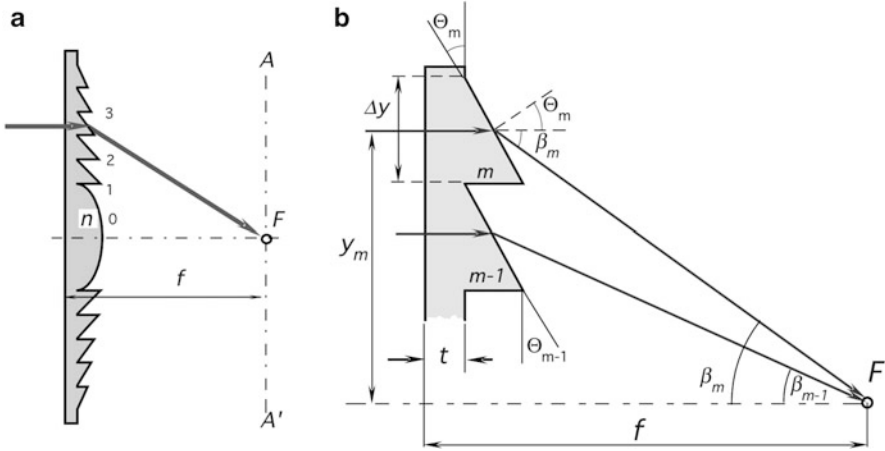
**Fig. 5.16** Concept of a Fresnel lens



**Fig. 5.17** Fresnel lens for lighthouse (a) and section of plastic multifaceted Fresnel lens (b)

another to align their flat surfaces, Fig. 5.16c. The resulting near-flat but grooved lens has nearly the same focusing properties as the original plano-convex lens.

A Fresnel lens basically consists of a series of concentric prismatic grooves, designed to cooperatively direct incident light rays into a common focus. It has several advantages over a conventional lens, such as low weight, thin size, ability to be curved (for a plastic lens) to any desirable shape, and, most importantly, a lower absorption loss of the light flux. This is the prime reason why this type of a lens is almost exclusively has been used in lighthouses to form parallel beams of light, Fig. 5.17a. A lower absorption loss is very important for fabrication of the mid- and far-infrared lenses where absorption in the material may be significant. This is the reason why low-cost polymer Fresnel lenses are used almost exclusively in the passive-infrared (PIR) motion detectors. In such detectors, however, the entire lens is used quire rarely. Typically, small portions of many lenses are “stitched” together to form a single multifaceted lens, Fig. 5.17b, that has an ability to focus different portions of the outside space into a single focal point. This is covered in Sect. 7.8.5.



**Fig. 5.18** Grooves of Fresnel lens (a); computation of groove angle (b)

When fabricating a Fresnel lens, it is difficult to produce and maintain a curved surface of each small groove; hence, the profile of a groove is approximated by a flat surface, Fig. 5.18a, and essentially becomes a refracting prism. This demands that the steps be positioned close to each other. In fact, the closer the steps the more accurate the lens. The limiting factor is the ability to tool and fabricate such closely positioned curved grooves. There are several ways of designing grooves of the lens. The most common is the so-called constant step where all grooves have the same pitch—the distance between the neighboring grooves.

A computation of the lens is essentially the computation of a groove angle, depending on its number [6]. We assume that a monochromatic parallel beam is incident normally from the left onto a flat surface of the lens. The refraction takes place only at the grooved side. Applying Snell's law of refraction of a ray passing through the center of the groove, we arrive at:

$$\sin \Theta_m = n \sin (\Theta_m + \beta_m) , \quad (5.31)$$

where  $n$  is the refractive index of the material at the desired wavelength and the angles are defined in Fig. 5.18b. Let  $y_m$  be a distance from the optical axis to the  $m$ th groove, then for that particular groove:

$$\Theta_m = \tan^{-1} \left[ \frac{y_m}{n \sqrt{y_m^2 + (f-t)^2} - (f-t)} \right] , \quad (5.32)$$

where  $f$  is the focal length and  $t$  is the mean lens thickness. This equation can be rewritten in a dimensionless form, considering:

$$y'_m = \frac{y_m}{f} \text{ and } t' = \frac{t}{f} \quad (5.33)$$

and finally we arrive at the basic formula for computing a Fresnel lens:

$$\Theta_m = \tan^{-1} \left[ \frac{y'_m}{n\sqrt{y'^2_m + (1-t')^2} - (1-t')} \right]. \quad (5.34)$$

The angles  $\Theta'_m$  of the refracting prisms are selected such that all the central rays of a particular wavelength have a common focus. A refractive index  $n$  for a visible spectrum may be found from Table A.19. For the mid- and far-infrared spectral ranges, low-density polyethylene (LDPE) has a refractive index 1.510 while the high-density polyethylene (HDPE) has  $n = 1.540$ . For the integrated IR sensors, nowadays Fresnel lenses are fabricated of Si or Ge—these materials have much larger refractive indices and thus focal points are positioned much closer to the lens' grooved surfaces.

A plastic Fresnel lens may be slightly bent if it is required for a sensor design. However, a bend changes positions of the focal points. If a lens is bent with its grooves inside the curvature, all angles  $\Theta'_m$  change depending on the radius of curvature. A new focal distance can be found from inverting Eq. (5.32) and solving it for  $f$ .

### 5.8.3 Flat Nanolenses

Recent developments in MEMS fabrications on a nanoscale lead to a design of the ultrathin flat lenses that are not only incredibly thin, but also do not suffer from aberrations (spherical, chromatic, etc.) that are typical for lenses with spherical surfaces [7]. The operating principle of the nanolens is based on a controlled phase shift of light having different wavelengths that impinge on the lens surface. The surface carries microscopic V-shaped gold structures that are smaller than the light wavelength and thus scatter light with a predefined phase delay. By rotating and modifying shapes of the V-reflectors, the lens regenerates beams of light that converge in a common focus, similar to conventional lenses.

It should be noted that the nanostructure that requires use of gold complicates the manufacturing technology as gold is known as contaminant for a microelectronic circuitry (see Sect. 19.3.2) and thus the nanolenses should be processed on a dedicated equipment.

---

## 5.9 Fiber Optics and Waveguides

Although light does not go around the corner, it can be channeled along complex paths by the use of waveguides. To operate in the visible and near-infrared spectral ranges, the guides may be fabricated of glass or polymer fibers. For the mid- and

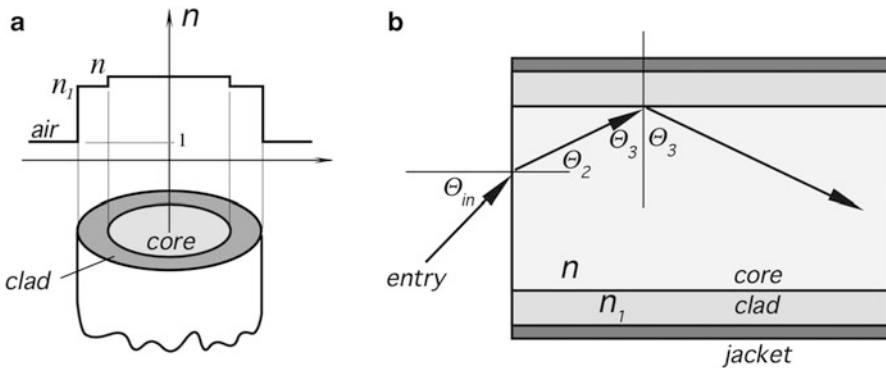
far-infrared spectral ranges, the waveguides are made of special materials having low absorption in these parts of the spectrum, or the guides are hollow tubes with highly reflective inner surfaces. A tubular waveguide operates on the principle of a first-surface reflection where light beams travel inside the tube in a zigzag pattern. A fiber operates on the principle of TIR (see Sect. 5.7.2) and can be used to transmit light energy in the otherwise inaccessible areas. Besides, since glass and most of plastics are not transparent in the optical range of thermal radiation, they can channel light without any transport of heat from the light source.

The surface and ends of a fiber are polished. An outside cladding may be added along its length. When glass is hot, the fibers can be bent to curvature radii of 20–50 times their section diameter and after cooling, to 200–300 diameters. Plastic fibers fabricated of polymethyl methacrylate may be bent at much smaller radii than glass fibers.

A typical attenuation due to light absorptive and reflective losses for a 0.25-mm polymer fiber is in the range of 0.5 dB/m of length. Light propagates through a fiber by means of a total internal reflection (TIR), as shown in Fig. 5.19b. It follows from Eq. (5.26) that light passing to air from a medium having a refractive index  $n$  is subject to the limitation of an angle of total internal reflection (TIR). For a cladding having refractive index  $n_1$ , Eq. (5.26) is rewritten here as

$$\Theta_0 = \arcsin\left(\frac{n_1}{n}\right) \quad (5.35)$$

Figure 5.19a shows a profile of the index of refraction for a single fiber with the cladding that must have a lower index of refraction to assure a total internal reflection at the boundary. For example, a silica-clad fiber may have compositions set so that the core (fiber) material has an index of refraction of 1.5 and the clad has an index of refraction of 1.485. To protect the clad fiber, it is typically enclosed in some kind of protective rubber or plastic jacket.



**Fig. 5.19** Optical fibers. Step-index multiple fiber (a); determination of maximum angle of entry (b)

When light enters the fiber, it is important to determine the maximum angle of entry, which will result in total internal reflections, Fig. 5.19b. If we take that minimum angle of an internal reflection  $\Theta_0 = \Theta_3$ , then the maximum angle  $\Theta_2$  can be found from Snell's law:

$$\Theta_{2(\max)} = \arcsin\left(\frac{\sqrt{n^2 - n_1^2}}{n}\right), \quad (5.36)$$

Applying Snell's law again and remembering that for air  $n \approx 1$ , we arrive at:

$$\sin\Theta_{\text{in}(\max)} = n_1 \sin\Theta_{2(\max)} \quad (5.37)$$

Combining Eqs. (5.36) and (5.37), we obtain the largest angle with the normal to the fiber end for which the total internal reflection will occur in the core:

$$\Theta_{\text{in}(\max)} = \arcsin\left(\sqrt{n^2 - n_1^2}\right). \quad (5.38)$$

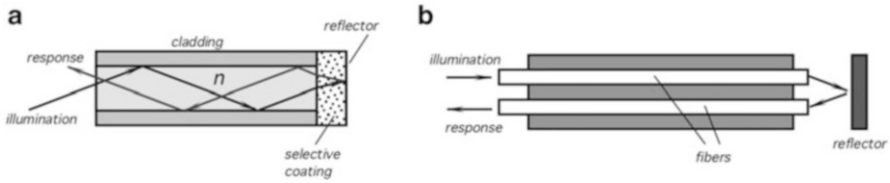
Light rays entering the fiber at angles greater than  $\Theta_{\text{in}(\max)}$  will pass through to the cladding and jacket and will be lost. For data transmission, this is an undesirable event. However, in a specially designed fiber-optic sensor, the maximum entry angle can be a useful phenomenon for modulating light intensity. Sometimes, the value of  $\Theta_{\text{in}(\max)}$  is called the *numerical aperture* of the fiber. Due to variations in the fiber properties, bends, and skewed paths, the light intensity does not drop to zero abruptly but rather gradually diminishes to zero while approaching  $\Theta_{\text{in}(\max)}$ . In practice, the numerical aperture is defined as the angle at which light intensity drops by some arbitrary number (e.g.,  $-10$  dB of the maximum value).

One of the useful properties of fiber-optic sensors is that they can be formed into a variety of geometrical shapes depending on the desired application. The fibers are very useful for design of miniature optical sensors which are responsive to such stimuli as pressure, temperature, chemical concentration, and so forth. The basic idea for use of the fiber optics in sensing is to modulate one or several characteristics of light in a fiber.

A stimulus may act on a fiber either directly or it can be applied to a component attached to the fiber's outer surface or the polished end to produce an optically detectable signal. To make a fiber chemical sensor, a special solid phase of a reagent may be formed in the optical path coupled to the fiber. The reagent interacts with the analyte to produce an optically detectable effect (e.g., to modulate the index of refraction or coefficient of absorption). A cladding on a fiber may be created from a chemical substance whose refractive index may be changed in the presence of some fluids [8]. When the angle of total internal reflection changes, the light intensity varies.

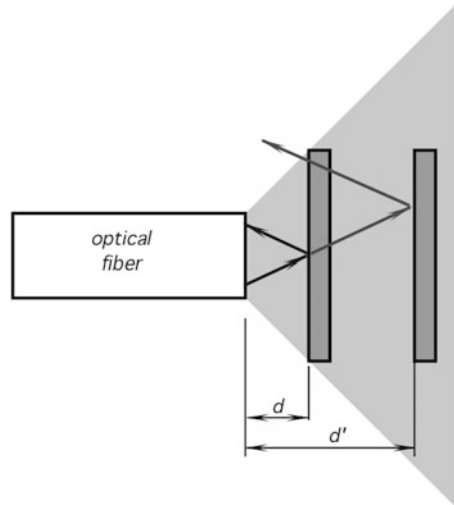
Optical fibers may be used in two modes. In the first mode, Fig. 5.20a, the same fiber is used to transmit the excitation signal and to collect and conduct an optical





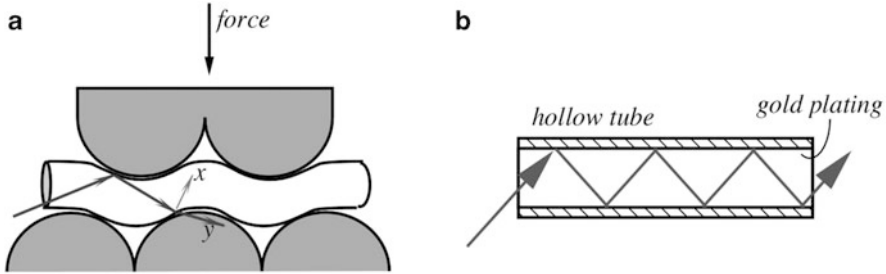
**Fig. 5.20** Single (a) and dual (b) fiber-optic sensors

**Fig. 5.21** Fiber-optic displacement sensor utilizes modulation of reflected light intensity



response back to the processing device. In the second mode, two or more fibers are employed where the excitation (illumination) function and collection function are carried out by separate fibers, Fig. 5.20b. The most commonly used type of fiber-optic sensor is an intensity sensor, where light intensity is modulated by an external stimulus [9]. Figure 5.21 shows a displacement sensor where a single-fiber waveguide emits light toward the reflective surface. Its operation is based on variations in the optical coupling between the fiber end and the tested object. Light travels along the optical fiber and exits in a conical profile toward the object. If the object is close to the fiber end (distance  $d$ ), the optical coupling is the highest and most of light is reflected into the fiber and propagates back to the light detector at the other end of the fiber. If the object moves away, some of the rays are reflected outside of the fiber end, and fewer photons are returned back. Due to a conical profile of the emitted light, a quasilinear relationship between the distance  $d$  and the intensity of the returned light can be achieved over a limited range.

The so-called microbend strain gauge can be designed with an optical fiber being squeezed between two deformers, as shown in Fig. 5.22a. The external force that is applied to the upper deformer bends the fiber, thus altering angles of the internal reflective surface. As a result, a light beam, which normally would be reflected in



**Fig. 5.22** Fiber-optic microbend strain gauge (a) and waveguide for far-infrared radiation (b)

direction  $x$ , approaches the lower part of the fiber at an angle which is less than  $\Theta_0$ —the TIR angle, Eq. (5.35). Instead of being reflected, light is refracted, moves in the direction  $y$  through the fiber wall and is lost. The closer the deformers come to each other, the more bending of the fiber, the more light goes astray and less light is transmitted along the fiber.

When operating in the spectral range where loss inside a fiber is too great (mid- and far-infrared spectral ranges), hollow tubes are generally used for channeling light beams, Fig. 5.22b. The tubes are highly polished inside and coated with reflective metals. For instance, to channel thermal radiation, a tube is coated inside by two layers: nickel as a leveling underlayer and the optical-quality gold having thickness in the range 500–1000 Å. Hollow waveguides may be bent to radii of 20 or more of their diameters.

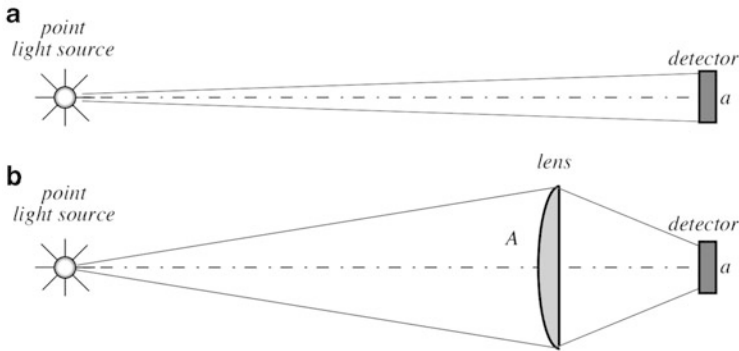
While fiber optics use the effect of total internal reflection, tubular waveguides use a first surface mirror reflection, which is always less than 100 %. As a result, loss in a hollow waveguide is function of the number of reflections; that is, loss is higher for a smaller diameter and longer length of a tube. At length/diameter ratios more than 20, hollow waveguides become quite inefficient and fiber-optic devices should be considered; for example, AMTIR (Table A.19).

## 5.10 Optical Efficiency

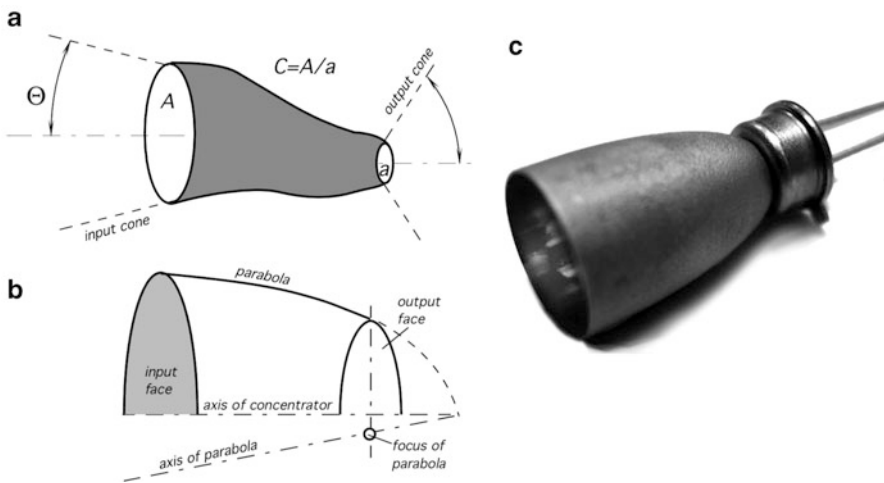
### 5.10.1 Lensing Effect

A light detector (Chap. 15) usually operates in conjunction with some kind of an optical system that may be as simple as a window or spectral filter. Often, an optical system includes lenses, mirrors, fiber optics, and other elements that alter direction of light. In many applications, a sensor works together with a light source whose properties shall match those of the sensor, both spectrum-wise and space-wise.

Several factors are critical in designing the optical components. Let us, for instance, take a point light source whose light should be sensed by a photodetector (Fig. 5.23a). In most cases, the detector's output signal is proportional to the received photonic power, which, in turn, proportional to the detector's surface



**Fig. 5.23** Efficiency of optical system depends on (a) its surface area  $a$  and (b) input aperture  $A$  of system



**Fig. 5.24** Nonimaging concentrator. General schematic (a); concentrator having a parabolic profile (b) and sensor attached to concentrator (c)

area (input aperture). Yet, the sensing area of a detector is usually small. For example, a thermopile pixel of the sensor shown in Fig. 15.25a has a sensing area about  $0.08 \text{ mm}^2$  and thus it will receive a very small portion of the entire photon flux that is emanated from the object. Fig. 5.24b shows how use of a focusing lens having an aperture larger than the sensing element can dramatically increase the received light flux. This is why high quality photo cameras have sizable lenses. The lens receives incident light flux just like a funnel, bringing it to a small sensing area. Efficiency of a single lens depends on its refractive index  $n$  (see Sect. 5.4). The overall improvement in the sensitivity can be estimated by use of Eqs. (5.8) and (5.11) to account for the reflective loss:

$$k \approx \frac{A}{a} \left[ 1 - 2 \left( \frac{n-1}{n+1} \right)^2 \right], \quad (5.39)$$

where  $A$  and  $a$  are the respective effective areas (apertures) of the lens and sensing area of a photodetector.

For glasses and most plastics operating in the visible and near-infrared spectral ranges, Eq. (15.39) can be simplified to

$$k \approx 0.92 \frac{A}{a}. \quad (5.40)$$

Thus, the amount of light received by the sensing element is proportional to the lens area. It should be pointed out that arbitrary placement of a lens may be more harmful than helpful. That is, a lens system must be carefully planed to be effective. For instance, many photodetectors have built-in lenses which are effective for parallel rays. If an additional lens is introduced in front of such a detector, it will create nonparallel rays at the input, resulting in misalignment of the optical system and poor performance. Thus, whenever additional optical devices need to be employed, detector's own optical properties must be considered.

### 5.10.2 Concentrators

There is an important issue of increasing density of the photon flux impinging on the sensor's surface. In many cases, when only the energy factors are of importance, while focusing or imaging is not required, special optical devices can be used quite effectively. These are the so-called nonimaging collectors, or concentrators [10–12]. They have some properties of the waveguides and some properties of the imaging optics (like lenses and curved mirrors). The most important characteristic of a concentrator is a ratio of the input aperture area and area of the output aperture. The ratio is called the *concentration ratio*  $C$ . Its value is always more than unity. That is, the concentrator collects light from a larger area and directs it to a smaller area, Fig. 5.24a, where the sensing element is positioned. A theoretical maximum for  $C$  is:

$$C_{\max} = \frac{1}{\sin^2 \Theta_i}, \quad (5.41)$$

where  $\Theta_i$  is the maximum input semiangle. Under these conditions, the light rays emerge at all angles up to  $\pi/2$  from the normal to the exit face. This means that the exit aperture diameter is smaller by  $\sin \Theta_i$  times the input aperture. This gives an advantage in the sensor design as its linear dimensions can be reduced by that number while maintaining a near equal efficiency. The input rays entering

at angle  $\Theta$  will emerge within the output cone with the angles dependent of point of entry.

The concentrators can be fabricated with reflective surfaces (mirrors) or refractive bodies (Fresnel lenses, e.g.), or as combinations of both. A practical shape of the reflective parabolic concentrator is shown in Fig. 5.24b. It is interesting to note that the “cone” light receptors in a retina of a human eye have a shape similar to that shown in Fig. 5.24b [11].

The tilted parabolic concentrators may have very high efficiency—they can collect and concentrate well over 90 % of the incoming radiation. If a lesser efficiency is acceptable, a conical rather than paraboloid concentrator can be employed. Some of the incoming rays will be turned back after several reflections inside the cone, however, its overall efficiency is still near 80 %. Clearly, the cones are easier to fabricate than the paraboloids of revolution.

### 5.10.3 Coatings for Thermal Absorption

All thermal radiation sensors (Sect. 15.8) rely on absorption or emission of electromagnetic waves in the mid- and far-infrared spectral ranges. According to Kirchhoff’s discovery, absorptivity  $\alpha$  and emissivity  $\varepsilon$  is the same thing (see Sect. 4.12.3). Their value for the efficient sensor’s operation must be maximized, i.e., it should be made as close to unity as possible. This can be achieved by either a special surface processing of a sensing element to make it highly emissive, or by covering it with a coating having high emissivity. Any such coating should have a good thermal conductivity and a very small thermal capacity, which means it shall be thin, but not too thin—a preferred thickness is at least 1 maximum wavelength it should absorb.

Several methods are known to give a surface the emissive (absorptive) properties. Among them a deposition of thin metal films (like Nichrome) having reasonably good emissivity, a galvanic deposition of porous platinum black [13], and evaporation of metal in atmosphere of low-pressure nitrogen [14]. The most effective way to create a highly absorptive (emissive) material is to form it with a porous surface [15]. Particles with sizes much smaller than the wavelength generally absorb and diffract light. High emissivity of a porous surface covers a broad spectral range, however, it decreases with the increased wavelength. A film of goldblack with a thickness corresponding to  $500 \mu\text{g}/\text{cm}^2$  has an emissivity over 0.99 in the near-, mid-, and far-infrared spectral ranges.

To form porous platinum black, the following electroplating recipe can be used [14]:

Platinum chloride	$\text{H}_2\text{PTCl}_6$ aq	2 g
Lead Acetate	$\text{Pb}(\text{OOCCH}_3)_2 \cdot 3\text{H}_2\text{O}$	16 mg
Water		58 g

Out of this galvanic bath the films were grown at room temperature on silicon wafers with a gold underlayer film. A current density  $30 \text{ mA/cm}^2$  was used. To achieve absorption better than 0.95, a film of  $1.5 \text{ g/cm}^2$  is needed.

To form a goldblack by evaporation, the process is conducted in a thermal evaporation reactor in a nitrogen atmosphere of 100 Pa pressure. The gas is injected via a microvalve, and the gold source is evaporated from the electrically heated tungsten wire from a distance of about 6 cm. Due to collisions of evaporated gold with nitrogen, the gold atoms lose their kinetic energy and are slowed down to thermal speed. When they reach the surface, their energy is too low to allow a surface mobility and they stick to the surface on the first touch event. Gold atoms form a surface structure in form of needles with linear dimensions of about 25 nm. The structure resembles a surgical cotton wool. For the best results, goldblack should have a thickness in the range from 250 to  $500 \text{ }\mu\text{g/cm}^2$ .

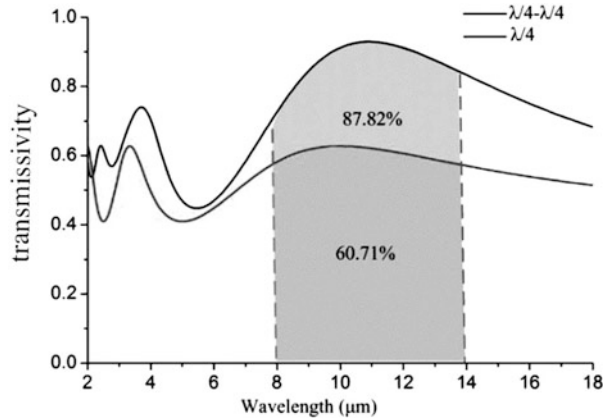
Another popular method of enhancing emissivity is to oxidize a surface metal film to form metal oxide, which generally is highly emissive. This can be done by a metal deposition in a partial vacuum.

Another method of improving the surface emissivity is to coat a surface with organic paint (visible color of the paint is not important). These paints have the far-infrared emissivity from 0.92 to 0.97, however, the organic materials have low thermal conductivity and cannot be effectively deposited with thicknesses less than  $10 \text{ }\mu\text{m}$ . This may significantly slow the sensor's speed response. In the micromachined sensors, the top surface may be given a passivation glass layer, which not only provides an environmental protection, but also has emissivity of about 0.95 in the far-infrared spectral range.

#### 5.10.4 Antireflective Coating (ARC)

Windows and lenses for use in the mid- and far-infrared spectral ranges are fabricated of materials having high refractive indices that cause a strong reflection at the boundary with air. For example, a Ge plate, in the wavelength from 4 to  $16 \text{ }\mu\text{m}$  due to a reflective loss, has transmission of only about 40 %. To reduce reflective loss, both sides of the window or lens may be coated (vacuum evaporation) with the antireflective coating (ARC) to form a gradual transition from air to the lens (window) refractive index. For example, an ARC layer having thickness of a quarter wavelength ( $\lambda/4$ ) of  $\text{YbFe}_3$  (Ytterbium Fluoride) is applied on the front and back surface of a lens.  $\text{YbFe}_3$  has a relatively low-refractive index (1.52), yet is transparent in a broad wavelength range from UV to over  $12 \text{ }\mu\text{m}$ . Thus, its thin layer serves as a “buffer”—reducing reflection and passing more light through the window boundary. For even a further improvement in

**Fig. 5.25** Optical transmissivity of single- and double-ARC layers on Ge (adapted from [16])



transmission, a multilayer ARC may be applied. As a result, the transmission of light, especially in the mid- and far-infrared ranges, is substantially increased, as shown in Fig. 5.25.

## References

1. Feynman, R. P. (2006). *QED: The strange theory of light and matter*. Princeton, NJ: Princeton University Press.
2. Stover, J. C. (1995). *Optical scattering: Measurement and analysis*. Bellingham, WA: SPIE Optical Engineering Press.
3. Begunov, B. N., et al. (1988). *Optical instrumentation. Theory and design*. Moscow: Mir Publishers.
4. Katz, M. (1994). *Introduction to geometrical optics*. New York: Penumbra Publishing.
5. Kingslake, R. (1978). *Lens design fundamentals*. New York: Academic Press.
6. Sirohi, R. S. (1979). Design and performance of plano-cylindrical fresnel lens. *Applied Optics*, 45(4), 1509–1512.
7. Aieta, F., et al. (2012). Aberration-free ultrathin flat lenses and axicons at telecom wavelengths based on plasmonic metasurfaces. *Nano Letters*. dx.doi.org/10.1021/nl302516v
8. Giuliani, J. F. (1989). Optical waveguide chemical sensors. In *Chemical sensors and microinstrumentation. Chapt. 24*. Washington, DC: American Chemical Society.
9. Johnson, L. M. (1991). Optical modulators for fiber optic sensors. In E. Udd (Ed.), *Fiber optic sensors: Introduction for engineers and scientists*. Hoboken, NJ: John Wiley & Sons.
10. Welford, W. T., et al. (1989). *High collection nonimaging optics*. San Diego: Academic.
11. Winston, R., et al. (1971). Retinal cone receptor as an ideal light collector. *Journal of the Optical Society of America*, 61, 1120–1121.
12. Leutz, R., et al. (2001). *Nonimaging fresnel lenses: Design and performance of solar concentrators*. Berlin: Springer Verlag.
13. Persky, M. J. (1999). Review of black surfaces for space-borne infrared systems. *Review of Scientific Instruments*, 70(5), 2193–2217.

14. Lang, W., et al. (1991). Absorption layers for thermal infrared detectors. In: *Transducers'91. International Conference on Solid-State Sensors and Actuators. Digest of technical papers* (pp. 635–638). IEEE.
15. Harris, L., et al. (1948). The Preparation and Optical Properties of Gold Blacks. *J. of the Opt. Soc. of Am.*, 38, 582–588.
16. Jiang, B. et al. (2013). Design and analysis of hermetic single chip packaging for large format thermistor. *Applied Mechanics and Materials*. 3, 1-x manuscripts.

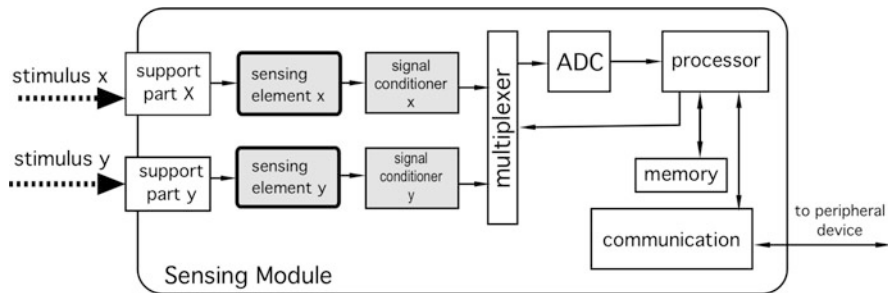


*“Engineers like to solve problems.  
If there are no problems handily available,  
they will create their own problems.”*

—Scott Adams

A system designer is rarely able to connect a sensor directly to processing, monitoring, or recording instruments, unless a sensor has a built-in electronic circuit with an appropriate output format. When a sensor generates an electric signal, that signal often is either too weak, or too noisy, or it contains undesirable components. Besides, the sensor output may be not compatible with the input parameters of a data acquisition system, that is, it may have a wrong output format. To mate a sensor and a processing device, they either must share a “common value” or use in-between some kind of a “mating” device. In other words, signals from a sensor usually have to be conditioned and modified before they are fed into a processing device (a load). Such a load usually requires voltage or current as its analog input signal, or a digital code. Nowadays, it is preferable if the sensor’s output is preprocessed and presented at the output in a ready-to-use form. An example is an accelerometer that outputs a digital signal with an encoded number of measured  $g$ . Thus, a great majority of sensors that produce analog signals require the interface circuits.

Trend in modern sensor designs focuses on integration of sensing components with signal conditioning, converting, and communication circuits. Such a combination is called a *sensing module*. As an illustration, consider Fig. 6.1 that shows an integrated sensing module having two sensing elements that selectively respond to two input stimuli. For operation, a sensing element may require some supporting parts. For example, an RH (relative humidity) sensor may need a protective grid or



**Fig. 6.1** Block diagram of sensing module

even blower for delivering sampled air to the sensing element. Another example is an imaging sensor that requires a focusing lens. Another type of a supporting part is required for an *active sensor*—a pilot signal generator (called excitation generator). For example, a hygistor (moisture sensitive resistor) for its operation requires a.c. current, thus the sensing element shall be appended with an a.c. current generator.

Since a typical sensing element produces low-level analog signals, its output signals need amplification, filtering, impedance matching, and perhaps a level shifting, before it can be digitized. All these functions are performed by signal conditioners. Since a module may comprise more than one channel, outputs of all signal conditioners should be converted into a common digital format. One option is to have one analog-to-digital converter (ADC) per channel, but in most cases it is more convenient and economical to have a single high-quality ADC common for all channels. Thus, the outputs of all signal conditioners shall be connected one at a time to the common ADC. This function is performed by a switching analog gate or *multiplexer* (MUX).

ADC generates a digital code that is fed into a processor for an on-board computation of the input stimuli. For example, if the stimulus is temperature, the processor should compute its value in a selected scale with acceptable resolution—for example, in degree Celsius with a resolution of 0.02 °C. Due to various imperfections, often accuracy cannot be achieved unless the entire system from the input to the processor is individually calibrated. A calibration process requires determination of certain unique parameters that are stored in the sensing module's memory. And finally, the processed information must be communicated in a selected format to the outside peripheral device. This is the function of a communication circuit. An example is an  $I^2C$  serial communication link that requires only two wires for transmitting multichannel digital information.

In this chapter we will discuss some electronic interface components. These may be parts of the sensing module, or used separately for supporting the nonintegrated sensors. For details of digital signal processors, memory, and communication devices, the reader is referred to specialized texts.




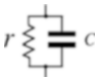


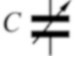
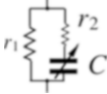

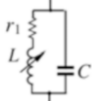
## 6.1 Signal Conditioners

A signal conditioning circuit has a specific purpose—to bring a signal from the sensing element up to the format that is compatible with the load device—typically an ADC. To do its job effectively, a signal conditioner must be a faithful slave of two masters: the sensing element (sensor) and the load device. The signal-conditioner input characteristics shall be compatible to the output characteristics of the sensor while its output should generate voltage for ease of interfacing with an ADC or other load. This book, however, is about sensors; therefore, below we discuss only typical front stages of the signal conditioning circuits that are coupled to various sensors.

The front end of a signal conditioner depends on type of the sensor’s output electrical characteristics. Table 6.1 lists five basic types of the sensor output properties: voltage, current, resistive, capacitive, and inductive. Selecting the appropriate input stage of a signal conditioner is essential for the optimal data collection.

A difference between a voltage-generating and current-generating sensors should be clearly understood. The former has a relatively low-output impedance. Its output voltage is little dependent on the load but the current is function of the load. This sensor resembles a battery whose voltage is driven by a stimulus.

**Table 6.1** Sensor types and corresponding inputs of signal conditioners

Sensor type	Sensor impedance	Signal conditioner front stage
Voltage out 	Very low resistive 	High input resistance amplifier (“voltmeter”)
Current out 	Very high complex 	High input impedance amplifier or low input resistance circuit (“amperemeter”)
Resistive 	Resistive 	Resistance-to-voltage converter (“Ohm-meter”)
Capacitive 	Complex 	Capacitance-to-voltage converter (“capacitance meter”)
Inductive 	Complex 	Inductance meter

The latter sensor has a large output impedance, typically much larger than the load, and thus produces current that is mainly independent of the load.

### 6.1.1 Input Characteristics

The input part of a signal conditioner may be specified through several standard parameters. These are useful for calculating how accurately the circuit can process the sensor's output signals and what would be the circuit's contribution to the total error budget?

The *input impedance* shows by how much the circuit loads the sensor at different frequencies. The impedance may be expressed in a complex form as:

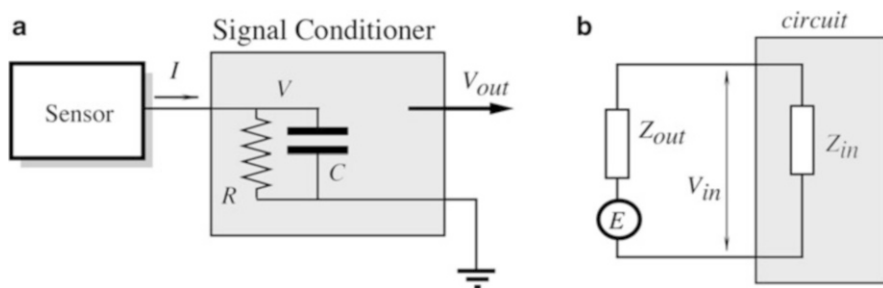
$$\mathbf{Z} = \frac{\mathbf{V}}{\mathbf{I}}, \quad (6.1)$$

where  $\mathbf{V}$  and  $\mathbf{I}$  are the complex notations for the voltage and current across the input impedance. For example, if input of a signal conditioner is modeled as a parallel connection of the input resistance,  $R$  and input capacitance,  $C$ , (Fig. 6.2a), the complex input impedance may be represented as

$$\mathbf{Z} = \frac{R}{1 + j\omega RC}, \quad (6.2)$$

where  $\omega$  is the circular frequency and  $j = \sqrt{-1}$  is the imaginary unity.

Formula (6.2) suggests that the input impedance is function of the signal frequency. With increase in the signal rate of change, the input impedance becomes lower. On the other hand, at very low frequencies, a circuit, having a relatively low-input capacitance  $C$  and resistance  $R$ , has an input impedance that is almost equal to the input resistance:  $\mathbf{Z} \approx R$ . Relatively low, here means that the reactive part of the above equation becomes negligibly small, i.e., the following holds



**Fig. 6.2** Complex input impedance of interface circuit (a), and equivalent circuit of voltage-generating sensor (b)

$$RC \frac{1}{\omega}. \quad (6.3)$$

The product  $RC$  is called a time constant  $\tau$  that is measured in seconds. Whenever the input impedance of a circuit is considered, the output impedance of the sensor must be taken into account for a very obvious reason—when the sensor is attached, the impedances are connected in parallel. For example, if the sensor is of a capacitive nature (Table 6.1), to define a frequency response of the input stage, sensor's capacitance with its resistive components  $r_1$  and  $r_2$  must be connected in parallel with the circuit's input capacitance.

Figure 6.2b shows an equivalent circuit for a voltage-generating sensor. The signal-conditioner's front end comprises the sensor output,  $Z_{\text{out}}$ , and the circuit input,  $Z_{\text{in}}$ , impedances (we use here scalar notations). Output signal from the sensor is represented by a voltage source,  $E$ , which is connected in series with the output impedance  $Z_{\text{out}}$ . Note that an ideal voltage source  $E$  by definition has a zero internal impedance. Its real impedance is modeled by  $Z_{\text{out}}$ . If the impedance is low, especially its resistive part over the entire frequency range, the sensor and signal-conditioner's reactive components (capacitive and/or inductive) can be safely ignored.

However, if the sensor's output impedance has a sizable value, it cannot be ignored. Let us analyze a voltage-generating sensor (see Table 6.1). By accounting for both impedances (the sensor's output and signal-conditioner's input), the signal-conditioner input voltage,  $V_{\text{in}}$  is represented by

$$V_{\text{in}} = E \frac{Z_{\text{in}}}{Z_{\text{in}} + Z_{\text{out}}}. \quad (6.4)$$

In any particular case, the output impedance of a sensor should be defined. This helps to analyze a frequency response and phase lag of the sensor-conditioner combination. For instance, a piezoelectric sensor that can be represented by a very high-output resistance (on the order of  $10^{11} \Omega$ ) shunted by a capacitance (in the order of 10 pF) is modeled as a current-generating sensor.

To illustrate importance of the input impedance characteristics, let us consider a purely resistive sensor  $Z_{\text{out}} = R_{\text{out}}$  connected to the input impedance as shown in Fig. 6.2a, b. A combined resistance at the circuit's input becomes:

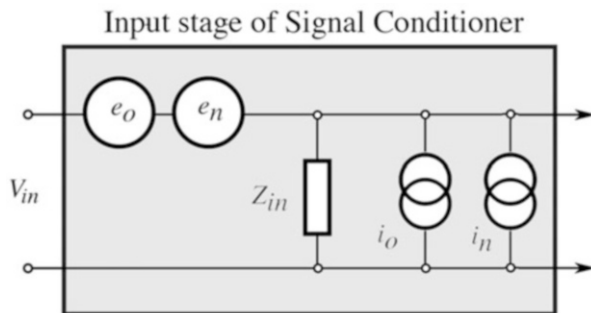
$$R_{\text{in}} = \frac{R_{\text{out}}R}{R_{\text{out}} + R} \quad (6.5)$$

The circuit's input voltage as function of frequency,  $f$ , can be expressed by a formula:

$$V_{\text{in}} = \frac{E}{\sqrt{1 + \left(\frac{f}{f_c}\right)^2}} \quad (6.6)$$

where  $f_c = (2\pi R_{\text{in}}C)^{-1}$  is the corner frequency (i.e., the frequency where the voltage amplitude drops by 3 dB). If we assume a required accuracy in detection of the

**Fig. 6.3** Equivalent circuit of electrical noise sources at input stage



amplitude as 1 %, we can calculate the maximum stimulus frequency, which can be processed by the circuit:

$$f_{\max} \approx 0.14f_c, \quad (6.7)$$

or  $f_c \approx 7f_{\max}$ ; that is, the impedance must be selected in such a way as to assure a sufficiently high-corner frequency. For example, if the stimulus' expected highest frequency is 1 kHz, the corner frequency of the signal conditioner must be selected at least at 7 kHz. In practice,  $f_c$  is selected even higher, because of additional frequency limitations in the subsequent circuits.

For a voltage-generating sensor  $R_{\text{out}} \ll R$ , then according to Eq. (6.5),  $R_{\text{in}} \approx R_{\text{out}}$ , thus  $f_c$  becomes very large. This lead to  $V_{\text{in}} \approx E$ , and as a result, the input stage of a signal conditioner does not distort the sensor's signal. Therefore, for the voltage-generating sensors, an input resistance of a signal conditioner should be as high as practical. The input capacitance makes no difference because it is shunted by a low-output resistance of the sensor.

Figure 6.3 is a more detailed equivalent circuit of the input properties of a signal conditioner, for instance, an amplifier. The circuit is modeled by the input impedance  $Z_{\text{in}}$  and several generators producing interfering signals. They represent voltages and currents that are spuriously generated by the circuit itself or picked up from various external sources, even if the sensor generates no signal. These undesirable voltages and currents may pose substantial problems if not handled properly. Besides, many such noise generators are temperature dependent.

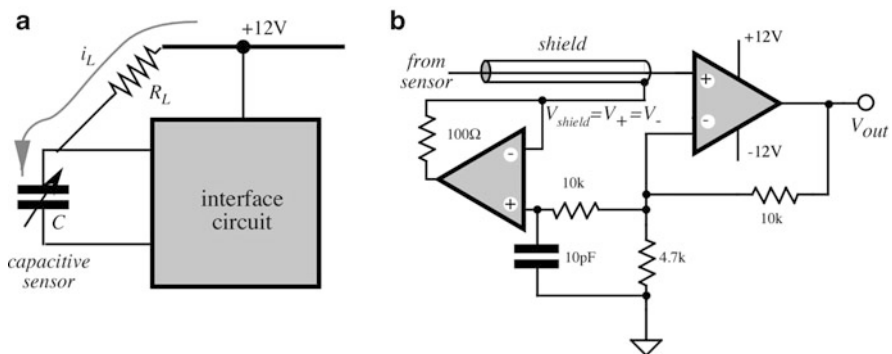
Voltage  $e_o$  is nearly constant and called the input *offset voltage*. If the input terminals of the signal conditioner are shorted together (zero input signal), that voltage would simulate a presence of a virtual d.c. voltage input signal having value  $e_o$ . It should be noted that the offset voltage source is connected in series with the input and its resulting error is independent of the output impedance of the sensor or its signal, that is, the offset voltage has an *additive nature*.

The input *bias current*  $i_o$  is also generated internally by the front stage or introduced from some external interfering sources, such as circuit board leakage currents. Its value is quite high for many input bipolar transistors, much smaller for JFETs, and further much lower for the CMOS circuits. This current may present a

serious problem when a sensor has a high-output impedance (a current-generating sensor). The bias current passes through the output resistance of the sensor, resulting in a spurious voltage drop. This voltage drop may be of a significant magnitude. For instance, if a piezoelectric sensor is connected to a circuit having a combined (Eq. 6.5) input resistance of  $1\text{ G}\Omega$  ( $10^9\ \Omega$ ) and the input bias current is  $100\text{ pA}$  ( $10^{-10}\text{ A}$ ), the voltage drop at the input becomes equal to  $1\text{ G}\Omega \times 100\text{ pA} = 0.1\text{ V}$ —a very high erroneous value, indeed. Error resulting from a bias current is proportional to the combined resistance of the sensor and interface circuit. This error is negligibly small for sensors having low-output resistances (voltage generating) and thus can be ignored. For instance, an inductive detector is not sensitive to bias currents.

A circuit board *leakage current* may be a source of errors while working with the current-generating sensors. This spurious current may be resulted from a reduced surface resistance in a printed circuit board (PCB). Possible causes for that are a poor quality PCB material, surface contaminations by a solder flux residue (a poorly washed PCB), moisture condensation, and degraded conformal coating. Figure 6.4a shows that a power supply bus and board resistance,  $R_L$ , may cause leakage current,  $i_L$ , through the front stage combined impedance. If the sensor is capacitive, its output capacitance will be very quickly charged by the PCB leakage current. This will not only cause error, but may even lead to a sensor's destruction if the sensor uses chemical compounds (e.g., a humidity sensor).

There are several techniques known to minimize the board leakage current effect. One is a careful board layout to keep higher voltage conductors away from the high-impedance components. A leakage through the board thickness in the multilayer boards should not be overlooked. Another method is electrical guarding, which is an old trick. The so-called driven shield is also highly effective. Here, the input circuit is surrounded by a conductive trace that is connected to a low-impedance point at the same potential as the input. The guard absorbs leakage from other points on the board, drastically reducing spurious currents that may reach the input terminal. To be completely effective, there should be guard rings on



**Fig. 6.4** Circuit board leakage affects input stage (a); driven shield of input stage (b)

both sides of the PCB. As an example, an amplifier is shown with a guard ring, driven by a relatively low impedance of the amplifier's inverting input.

It is highly advisable to position high-input impedance signal conditioners as close as possible to the sensors. However, sometimes the connecting lines cannot be avoided. The coaxial shielded cables with good isolation are recommended [1]. Polyethylene or virgin (not reconstructed) Teflon is best for critical applications. However, even short cable runs can reduce bandwidth unacceptably with high sensor resistances. These problems can be largely avoided by bootstrapping the cable's shield. Figure 6.4b shows a voltage follower connected to the inverting input of an amplifier. The follower drives the shield of the cable, thus reducing the cable capacitance, the leakage, and spurious voltages resulting from cable flexing. A small capacitance at the follower's noninverting input improves its stability.

Another problem that must be avoided is connecting to input of a signal conditioner any components, besides a sensor, that potentially may cause problems. An example of such a "troublemaker" is a ceramic capacitor. In a hope to filter out high frequency transmitted noise at the input, a designer quite frequently uses filter capacitors either at the input, or in the feedback circuit of an input stage. If for a cost saving or the space saving reason a ceramic capacitor is selected—she may get what she is not expecting. Many capacitors possess the so-called dielectric absorption which is manifested as a memory effect. If such a capacitor is subjected to a charge spike either from a sensor, or from a power supply, or just from any external noise source, the charge will alter the capacitor's dielectric properties in such a way that the capacitor starts behaving like a small battery. That spurious "battery" may take a long time to lose its charge—from few seconds to many hours. Voltage generated by that "battery" is added to the sensor's output signal and may cause significant errors. If a capacitor must be employed at the input stage, a film capacitor should be used instead of ceramic.

### 6.1.2 Amplifiers

Many sensing elements produce weak output signals. Magnitudes of these signals may be on the order of microvolts ( $\mu\text{V}$ ) for the voltage-generating sensors or picoamperes (pA) for the current-generating sensors. On the other hand, standard electronic data processors, such as analog-to-digital converters (ADC), frequency modulators, data recorders, etc. require input signals of sizable magnitudes—in the order of volts (V). Therefore, amplification of the sensor output signals has to be made with a voltage gain up to 10,000 and a current gain up to one million. Amplification is part of a signal conditioning. There are several standard configurations of the amplifiers that might be useful for amplifying low-level signals. These amplifiers may be built of discrete components, such as semiconductors, resistors, capacitors, and inductors. Nowadays, amplifiers are frequently composed of standard building blocks, such as operational amplifiers (OP-AMPS) that are augmented with various discrete components.



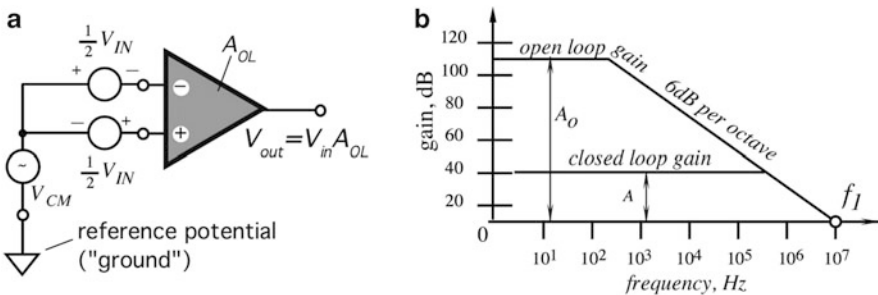
The purpose of an amplifier is much broader than just increasing the signal magnitude. An amplifier also is an impedance matching device, an enhancer of a signal-to-noise ratio, a frequency filter, and an isolator between the sensor and rest of the circuit.

### 6.1.3 Operational Amplifiers

One of the principle building blocks for amplifiers is the so-called *operational amplifier* or OP-AMP, which is either an integrated (monolithic) or hybrid (a combination of monolithic and discrete parts) circuit. An integrated OP-AMP may contain hundreds of transistors, diodes, as well as resistors and capacitors. An analog circuit designer, by arranging around the OP-AMP discrete components (resistors, capacitors, inductors, etc.), may create endless number of useful circuits—not only amplifiers, but also many other circuits as well. OP-AMPs are also used as cells in custom-made integrated circuits—*analog or mixed technology*. A custom circuit is called *application-specific integrated circuit* or ASIC, for short. Below, we will describe some typical circuits with OP-AMP, which are often used as front ends of various signal-conditioning circuits.

As a building block, a good operational amplifier has the following properties (a symbol representation of OP-AMP is shown in Fig. 6.5a):

- Two inputs: one is inverting (–) and the other is noninverting (+).
- High-input resistance (on the order of  $G\Omega$ ).
- Low-output resistance (a fraction of  $\Omega$ ), mostly independent of a load.
- Ability to drive capacitive loads without becoming unstable.
- low input offset voltage  $e_0$  (few mV or even few  $\mu\text{V}$ ).
- low input bias current  $i_0$  (few pA or even less).
- Very high *open-loop gain*  $A_{OL}$  (at least  $10^4$  and preferably over  $10^6$ ). That is, the OP-AMP must be able to magnify (amplify) a voltage difference  $V_{in}$ , between its two inputs by a factor of  $A_{OL}$ .



**Fig. 6.5** General symbol of operational amplifier (a), and gain-frequency characteristic of OP-AMP (b)

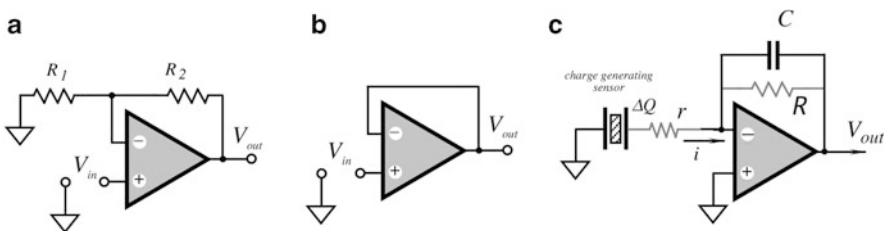
- High common mode rejection ratio (CMRR). That is, the amplifier suppresses the in-phase equal magnitude input signals (common-mode signals)  $V_{CM}$  applied to its both inputs.
- Low intrinsic noise.
- Broad operating frequency range.
- Low sensitivity to variations in the power supply voltage.
- High environmental stability of its own characteristics.

For detailed information and application guidance the reader should refer to data sheets and catalogues published by the respective manufacturers and available online. Such catalogues usually contain selection guides for every important feature of an OP-AMP. For instance, OP-AMPs are grouped by such criteria as low offset voltages, low-bias currents, low noise, bandwidth, etc.

Figure 6.5a depicts an operational amplifier without feedback components. Therefore, it operates under the so-called *open-loop* conditions. An open-loop gain,  $A_{OL}$ , of an OP-AMP is always specified but is not a very stable parameter. Its frequency dependence may be approximated by a graph of Fig. 6.5b. The  $A_{OL}$  changes with the load resistance, temperature, and power supply fluctuations. Many amplifiers have an open-loop gain temperature coefficient in the order of 0.2–1 %/°C and the power supply gain sensitivity in the order of 1 %/%. An OP-AMP as a linear circuit is very rarely used with an open loop (without the feedback components) because the high open-loop gain may result in circuit instability, a strong temperature drift, noise, etc. For instance, if the open-loop gain is  $10^5$ , the input voltage drift of 10  $\mu$ V (ten microvolts) would cause the output drifts by about 1 V.

Ability of an OP-AMP to amplify small magnitude high-frequency signals is specified by the *gain-bandwidth product* (GBW) which is equal to the frequency  $f_1$  where the amplifier's open-loop gain becomes equal to unity. In other words, above the  $f_1$  frequency, the amplifier cannot amplify.

An example of a feedback with a resistive divider  $R_1$  and  $R_2$  is shown in Fig. 6.6a. The input voltage is applied to a noninverting (+) input of the OP-AMP. This input has a very high-input impedance. The feedback resistors convert the Op-AMP to a noninverting amplifier, where the resulting closed-loop gain:



**Fig. 6.6** Noninverting amplifier (a); voltage follower (b); charge-to-voltage converter (c)

$$A = 1 + \frac{R_2}{R_1} \quad (6.8)$$

Considering the  $A_{OL}$  being very large, the closed-loop gain  $A$  depends only on the feedback components and is nearly constant over a broad frequency range (see Fig. 6.5b). However,  $f_1$  is still the frequency limiting factor, regardless of the feedback. Linearity, gain stability, and output impedance—all are improved by the amount of a feedback. The feedback may have various linear components, including resistors, capacitors, inductors, as well as nonlinear components, such as diodes. As a general rule for a moderate accuracy, the open-loop gain of an OP-AMP should be at least 100 times greater than the closed-loop gain at the highest frequency of interest. For even higher accuracy, the ratio of the open- and closed-loop gains should be 1000 or more.

### 6.1.4 Voltage Follower

A voltage follower shown in Fig. 6.6b is an electronic circuit that provides impedance conversion from a high to low level. It is a particular case of the amplifier shown in Fig. 6.6a where  $R_1$  is removed (“infinite” value) and  $R_2 = 0$ . Then, according to Eq. (6.8) the closed-loop gain is unity. A typical follower has high-input impedance (very high-input resistance and low-input capacitance) and very low-output resistance (the output capacitance makes no difference). A good follower has a voltage gain being very close to unity (typically, 0.999 over a broad frequency range). The buffering properties—high-input and low-output impedances make it indispensable for interfacing between many sensors and signal processing devices.

When designing a follower, these tips might be useful:

- For the current-generating sensors, the input bias current of the follower must be at least 100 times smaller than the sensor’s current.
- The input offset voltage must be either trimmable or smaller than the required LSB.
- A temperature coefficient of the bias current and the offset voltage should not result in errors of more than 1 LSB over an entire temperature range.

### 6.1.5 Charge- and Current-to-Voltage Converters

Charge-to-voltage converters (CVC) are employed to convert signals from the charge-generating sensors. Like a voltage follower, a CVC is a buffer between the charge sensor and ADC that requires voltage from a low-impedance source. A basic circuit of a CVC is shown in Fig. 6.6c. Capacitor,  $C$ , is connected into a negative feedback network of an OP-AMP. Its leakage resistance  $R$  must be substantially larger than impedance of the capacitor at the lowest operating

frequency. A good film capacitor is usually recommended along with a good quality printed circuit board where the components are coated with conformal coating.

A transfer function of the converter is:

$$V_{\text{out}} = -\frac{\Delta Q}{C}. \quad (6.9)$$

If the sensor is of a capacitive nature (many charge-generating sensors are), connecting it to an inverting input of OP-AMP may cause instability at high frequencies. In other words, the amplifier may oscillate—a highly undesirable behavior. To prevent oscillations, a small resistor  $r$  should be added in series with the capacitive sensor.

Note, that when the OP-AMP operates, the feedback keeps voltage at its inverting input ( $-$ ) very close to the noninverting voltage that in this circuit is zero (ground). That is why the noninverting input is called a *virtual ground* as compared to the real ground of the noninverting input. In many practical circuits, a provision should be made to periodically discharge the feedback capacitor, for example by use of a parallel analog switch.

Many sensors can be modeled as current generators. An example is a photodiode. A current-generating sensor is represented by a very large leakage resistance,  $r$ , connected in parallel with a current generator (a double-circle symbol) that by definition has an infinitely high internal resistance, Fig. 6.7a. To convert current to voltage, it shall be pushed through a load resistor  $R$ . The sensor current,  $i_0$ , has two ways to outflow: through the sensor's internal leakage resistance,  $r$ , as current  $i_r$ , and also through the load resistor as  $i_{\text{out}}$ . Current  $i_r$  is useless, thus to minimize error, leakage resistance  $r$  of the sensor must be much larger than the load resistor  $R$ .

According to Ohm's law, output voltage  $V$  is proportional to magnitude of the current and resistor  $R$ . Note that this voltage also appears across the sensor. This could be undesirable, since it may cause some errors, including nonlinearity and frequency limitations. To alleviate that problem, a special electronic circuit called current-to-voltage converter is employed. One of its functions is to keep voltage

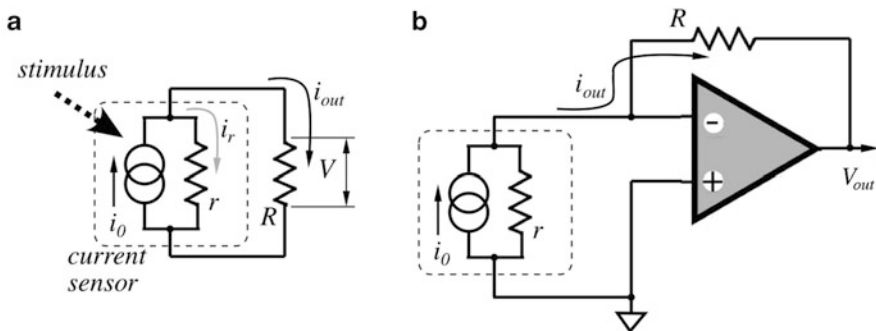


Fig. 6.7 Current-to-voltage converters

across the sensor on a constant level, often zero. Figure 6.7b shows a converter where the sensor is connected to a virtual ground (inverting input of the OP-AMP) and thus always is at a zero potential (the same as the grounded noninverting input). This is because of a very large  $A_{OL}$  that via the feedback keeps both inputs of the OP-AMP very close to one another. Another advantage of the virtual ground input is that the output voltage does not depend on the sensor's capacitance, no matter how large, and, as a result, has a much wider frequency response comparing with the basic circuit of Fig. 6.7a. The output voltage of the circuit:

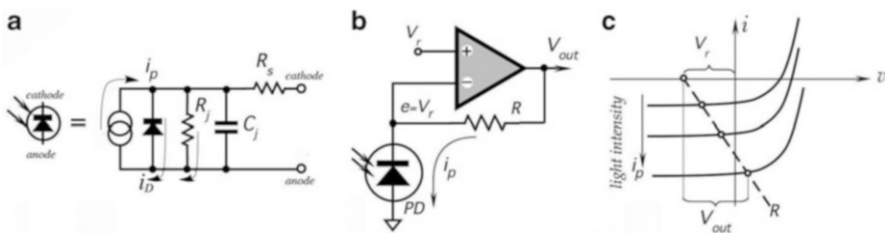
$$V_{out} = -iR \tag{6.10}$$

Minus sign indicates that the output voltage is negative (below ground) for the positive (flowing in) currents.

### 6.1.6 Light-to-Voltage Converters

Light-to-voltage converters are required for converting output signals from photosensors to voltage. For detecting extremely low-intensity light—typically few photons—a photomultiplier is generally employed (Sect. 16.1); however, for less demanding applications, three types of photosensors are available: a photodiode, phototransistor, and photoresistor (Chap. 15). They all employ a photoeffect that was discovered by A. Einstein and won him the Nobel Prize. These photo sensors are called *quantum* detectors. The difference between a photodiode and a phototransistor is in construction of a semiconductor chip. A photodiode has one p-n junction, while a phototransistor has two junctions where the base of the transistor may be floating or may have a separate terminal. The base current is a photoinduced current that is multiplied by the transistor's  $\beta$  (current gain) to produce the collector current, that in turn can be converted to voltage as described above. Thus, a phototransistor is equivalent to a photodiode with a built-in current amplifier. The quantum detectors are the *current-generating* sensors having very large internal resistances.

From the electrical point of view, a photodiode can be represented by an equivalent circuit shown in Fig. 6.8a. It consists of a current generator (internal



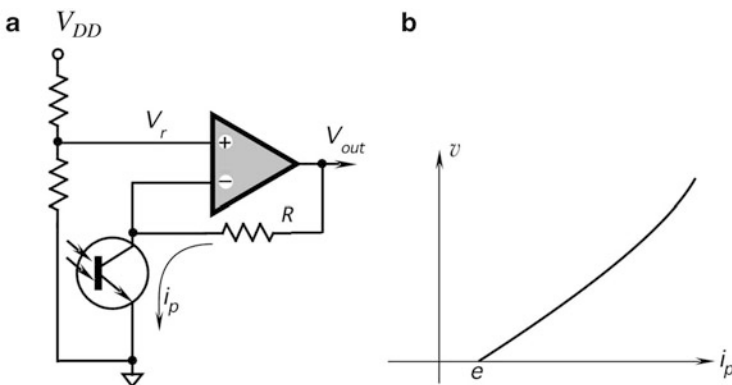
**Fig. 6.8** Equivalent circuit of photodiode (a). Reverse-biased photodiode with current-to-voltage converter (b). Load diagram of circuit (c)

input impedance is infinitely large), a parallel regular diode (like a rectifier diode), resistance of the diode junction  $R_j$ , capacitance of the junction  $C_j$ , and a serial resistance  $R_s$ . The current generator produces current proportional to the absorbed photon flux. This current flows in the direction from the cathode to the anode of the photodiode, that is in the opposite direction to that where the diode would normally conduct. Note that for very strong illuminations, the portion  $i_D$  of the photocurrent  $i_p$  will start flowing through a nonlinear rectifier diode which will degrade the sensor's linearity.

A photodiode can be used in a voltaic or current modes. In the voltaic mode, a photodiode is connected to a very high resistor ( $10^7$ – $10^9 \Omega$ ) and a good voltage amplifier. The diode will work like a battery where voltage is nearly proportional to the light intensity. This voltage is the result of a photocurrent  $i_p$  passing through the internal junction resistance  $R_j$ . In a current mode, the photodiode is either kept with a constant voltage across its terminals or virtually shorted (a voltage across the diode is held at zero) and current  $i_p$  is drawn to the current-to-voltage converter as described below. This mode is far more popular, especially for applications where a high-speed response is required.

A circuit with an operational amplifier is shown in Fig. 6.8b. Note that the reference voltage  $V_r$  creates a constant reverse bias across the photodiode. Figure 6.8c shows the operating points for a load feedback resistor  $R$ . Advantages of the circuits used with a reverse-biased photodiode are high-speed response and wide linear range of output. Therefore, this circuit is generally used. Frequently when illumination flux is rather small, the bias voltage is not applied, but rather the noninverting input of the OP-AMP is grounded.

The interface circuits for a phototransistor are similar, except that they have to provide a voltage across the collector-emitter terminals as shown in Fig. 6.9a. The transfer function of this circuit is shown in Fig. 6.9b. A phototransistor circuit is more sensitive to light but for the price of higher nonlinearity at stronger irradiances.



**Fig. 6.9** Light-to-Voltage converted with phototransistor (a); transfer function (b)

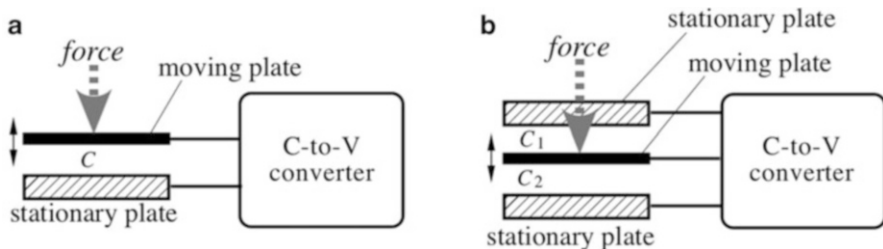
### 6.1.7 Capacitance-to-Voltage Converters

Capacitive sensors are very popular. Nowadays, micromachining technologies allow fabrication of small monolithic capacitive sensors. Examples include a pressure transducer with a thin silicon diaphragm as a movable plate of the variable-gap capacitor. In a mechanical capacitive sensor, for example, an accelerometer or pressure sensor, a moving plate of a capacitor (diaphragm or proof mass), moves with respect to a stationary plate, thus modulating the capacitance that exists between the plates. This sensor is called a capacitive displacement sensor and presently is one of the widely produced sensors by employing MEMS technologies.

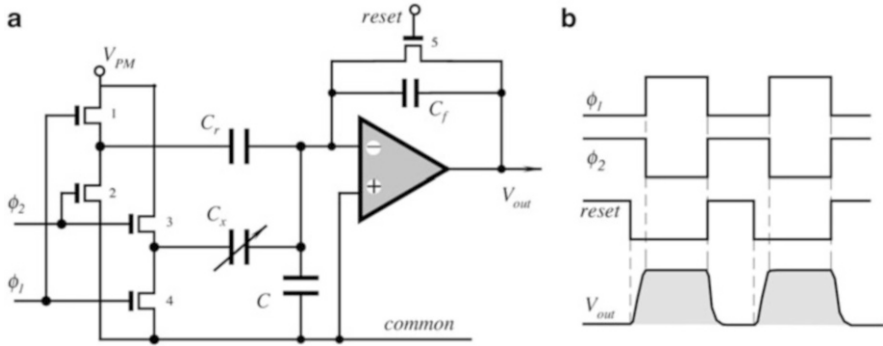
All capacitive sensors can be divided into asymmetrical and symmetrical structures. In a mechanical asymmetrical structure, Fig. 6.10a, the capacitance  $C$  change is measured only between the force-sensitive moving plate and a single stationary conductive plate (electrode). In a symmetrical structure, Fig. 6.10b, the capacitance measurement is performed between the moving plate and two conductive electrodes placed on both sides of the plate, rendering the differential capacitance ( $C_1 - C_2$ ) measurement possible.

The principle problem with these tiny capacitors is a relatively low capacitance value per unit area of the plate (about  $2 \text{ pF/mm}^2$ ) which may result in large die sizes. A typical capacitive pressure sensor offers a zero pressure capacitance on the order of few picofarads, so that a 10-bit resolution requires the detection of capacitive shifts on the order of  $15 \text{ fF}$  or less ( $1 \text{ femtofarad} = 10^{-15} \text{ F}$ ). This difficulty may be reduced by further narrowing a gap between the plates (down to a couple of micrometers) or even maintaining the gap on a nearly constant level by providing a force feedback, as described in Sect. 6.1.8. It is obvious that any external measurement circuit will be totally impractical, as a parasitic capacitance of connecting conductors at best can be on the order of  $1 \text{ pF}$ —too much with respect to the sensor capacitance. Therefore, the only way to make such a sensor practical is to build a signal conditioning and other interface circuits as an integral part of the sensor itself.

One quite effective way of designing such a capacitance-to-voltage ( $C/V$ ) is to use a switched capacitor technique. The technique is based on a charge transfer from one capacitor to another by the solid-state analog switches.



**Fig. 6.10** Asymmetrical (a) and symmetrical (b) capacitive displacement sensor



**Fig. 6.11** Simplified schematic (a) and timing diagrams (b) of capacitance-to-voltage converter using switched-capacitors technique

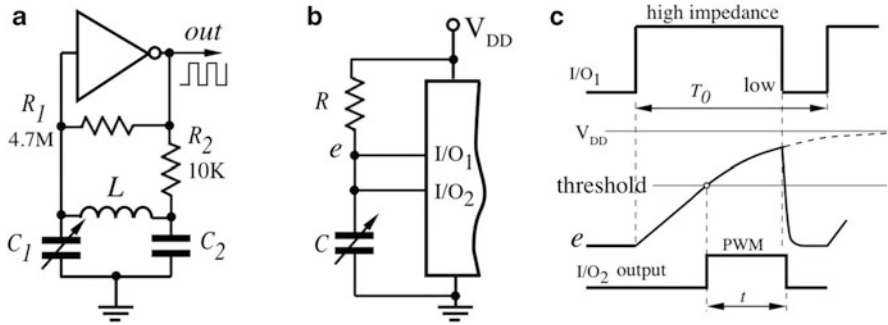
Figure 6.11a shows a simplified circuit diagram of a differential switched-capacitor converter [2], where variable capacitance  $C_x$  and reference capacitance  $C_r$  are parts of a symmetrical silicon pressure sensor. The same circuit can be used for an asymmetrical sensor with  $C_r$  being a trimmed reference capacitor.

Monolithic MOS switches (1–4) are driven by the opposite phase clock pulses,  $\phi_1$  and  $\phi_2$ . When the clocks switch, a charge appears at the common capacitance node—inverting input of OP-AMP. The charge is supplied by the constant voltage source,  $V_{PM}$ , and is proportional to  $(C_x - C_r)$  and, therefore to the applied pressure in the sensor. This charge is fed to a charge-to-voltage converter which includes an operational amplifier, integrating capacitor  $C_f$ , and MOS discharge (reset) switch 5. The output signal is the variable-amplitude pulses shown in Fig. 6.11b. These pulses can be demodulated to produce a linear signal or can be directly converted into digital data. So long as the open-loop gain of the integrating OP-AMP is high, the output voltage is insensitive to the input capacitance  $C$ , offset voltage, and temperature drift. The minimum detectable signal (noise floor) is determined by the component noise and temperature drifts of the components.

When the MOS switch goes from the on-state to the off-state, the switching signal at the gate injects some charge from the gate to the inverting input of the OP-AMP. An injection charge results in the offset voltage at the amplifier output. This error can be compensated for by a charge-cancelling device [3], which can improve the signal-to-noise ratio by two orders of magnitude of the uncompensated charge.

For the capacitive sensors having much larger capacitances (10–1000 pF), simpler techniques can be employed. One is use of an  $RC$  or  $LC$  oscillator that converts value of a variable  $C$  into a variable frequency or duty cycle of an a.c. signal. Figure 6.12a illustrates an  $LC$  oscillator whose frequency depends on both the variable capacitor and fixed inductor:





**Fig. 6.12** LC oscillator (a); microcontroller converter of capacitance to PWM signal (b); timing diagram of PWM converter (c)

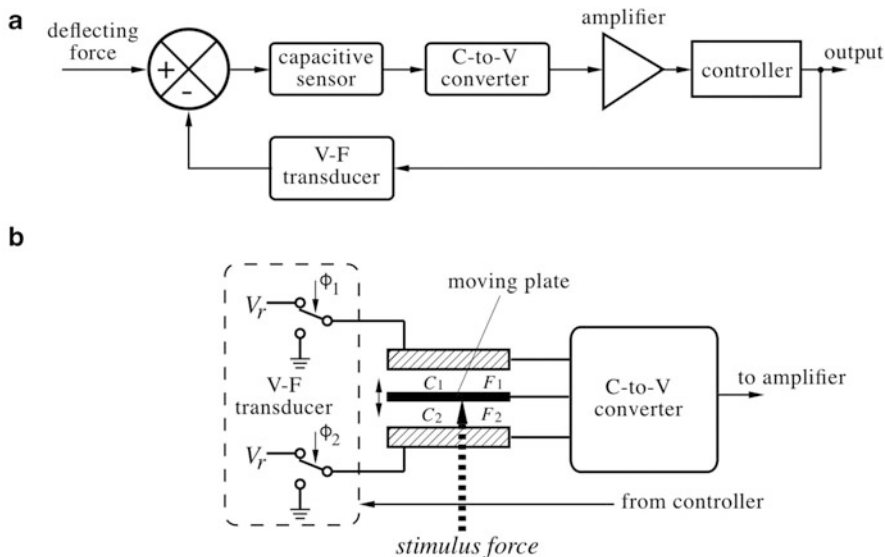
$$f = \frac{1}{2\pi\sqrt{L\frac{C_1+C_2}{C_1C_2}}} \tag{6.11}$$

Another circuit has a relaxation network of a fixed resistor  $R$  and variable sensor’s capacitance  $C$ , Fig. 6.11b. The network is connected to a microcontroller having two I/O ports, where  $I/O_1$  generates the tristate square pulses with a period  $T_0$ , alternating between a high impedance and ground low. The other  $I/O_2$  is a digital input with a triggering threshold of about  $0.5V_{DD}$ . Preferably, it should have a Schmitt-trigger input. During the  $I/O_1$  low state, capacitor  $C$  is discharged, see Fig. 6.11c. When the  $I/O_1$  goes high impedance, the sensor’s capacitor  $C$  charges through resistor  $R$  to  $V_{DD}$  voltage. At the moment of crossing the threshold, the  $I/O_2$  registers the crossover and the microcontroller computes duty cycle  $M$  that is proportional to the sensor capacitance  $C$ :

$$M = \frac{0.693R}{T_0} C \tag{6.12}$$

### 6.1.8 Closed-Loop Capacitance-to-Voltage Converters

Closed feedback loop in a capacitance-to-voltage converter has the ability to extend a dynamic range, increase linearity, flatten frequency response, and improve cross-axis rejection in accelerometers. The idea behind the method is to generate a compensating force that would prevent the moving plate of a capacitive sensor from shifting from its balance position [4]. It is a practical implementation of the null-balanced bridge concept as described in Sect. 6.2.4. Figure 6.13a illustrates the closed-loop block diagram where the capacitive sensor is subjected to a difference force: the deflecting force caused by a mechanical stimulus (pressure, acceleration, sound, etc.) minus the feedback force from the voltage-to-force transducer (V-F). The difference force is sensed by a capacitive displacement sensor, converted into electric signal, amplified, and applied to the controller that modulates the V-F transducer. The mechanical feedback maintains the difference force applied to



**Fig. 6.13** Block diagram of closed-loop capacitive signal conditioner (a) and use of voltage-to-force transducer to generate electrostatic forces for balancing symmetrical capacitive sensor (b)

the moving plate of the sensor close to zero, thus the stimulus and compensating forces are nearly equal in magnitude. As a result, instead of measuring the deflecting force produced by the stimulus, the voltage that controls the V-F transducer is used as the output signal.

Design of a V-F transducer is not a trivial task. The most practical method for use with MEMS is to employ an electrostatic force that appears between the plates of a symmetrical capacitive sensor in response to a voltage gradient across the plates. This force  $F_e$  can be expressed through  $U$ —the potential difference between the capacitor plates (voltage), the distance between the plates  $d$ ,  $\epsilon_0\kappa$ —dielectric constant of the space between the plates, and the plate area  $A$ :

$$F_e = \frac{\epsilon_0\kappa}{2} \int_A \frac{U^2}{d^2} dA, \quad (6.13)$$

The electrostatic feedback force can be generated by a pulsed voltage. If the pulse rate of the applied voltage is essentially above the transducer dynamic response cutoff frequency (that is, the lowest natural frequency of the sensor), the moving plate is subjected to an average electrostatic force. Note that the C-to-V converter uses a.c. signal to measure capacitances  $C_1$  and  $C_2$  between the plates, however, frequency of this a.c. signal must be much higher than the electrostatic modulation rate. Thanks to the frequency difference, it is easy to separate them by employing the appropriate filters.

Figure 6.13b illustrates the V-F transducer where two switches alternate voltage  $V_r$  and ground for applying to the upper and lower electrodes, where the moving plate is at virtual ground (zero) potential. The stimulus force is applied to the moving plate whose movement is suppressed by the electrostatic forces  $F_1$  and  $F_2$  produced by the applied voltage  $V_r$  with the phase and pulse-width modulation (PWM) of the switching pulses. Phases of these pulses  $\phi_1$  and  $\phi_2$  are arranged to oppose the stimulus force. A differential capacitive sensor based on controlled force equilibrium excels by its linearity and low temperature dependence, since the central plate can be kept stationary by virtue of the applied feedback.

---

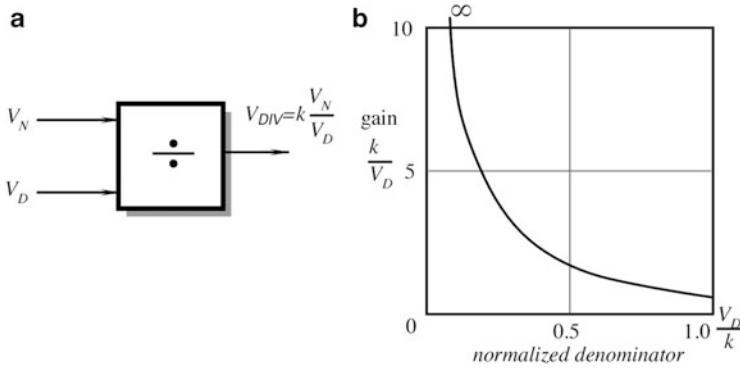
## 6.2 Sensor Connections

A sensor may be directly connected to a signal conditioner, but often it is desirable to reduce errors and noise caused by various interfering sources even before the signal is conditioned. Some errors can be reduced or even entirely eliminated by use of special sensor connections in front of the signal conditioner. Below are descriptions of the most popular techniques.

### 6.2.1 Ratiometric Circuits

A powerful method of improving accuracy of a sensor is a *ratiometric* technique. It should be emphasized, however, that the method is useful only if a source of error has a *multiplicative* nature but not additive. That is, the technique is useless for reduction, for instance, thermal noise. On the other hand, it is quite potent to solve problems as dependence of sensor's sensitivity to such factors as power supply instability, ambient temperature, humidity, pressure, effects of aging, etc. The technique essentially requires the use of two sensors where one is the acting sensor that responds to an external stimulus and the other is a compensating sensor, which is either shielded from that stimulus or is insensitive to it. Both sensors must be exposed to all other external effects, which may multiplicatively change their performance. The second sensor, which is often called *reference*, must be subjected to a reference stimulus, which is ultimately stable during the lifetime of the product. In many practical systems, the reference sensor is not necessarily exactly similar to the acting sensor, however its physical properties, which are subject to instabilities, should be the same.

A ratiometric technique essentially requires the use of a division. It can be performed by two standard methods: digital and analog. In a digital form, output signals from both the acting and the reference sensors are multiplexed and converted into binary codes in an analog-to-digital converter (ADC). Subsequently, a computer or a microprocessor performs the operation of a division. In an analog form, a divider may be part of a signal conditioner. A "divider", Fig. 6.14a, produces an output voltage or current proportional to a ratio of two input voltages or currents or numbers:

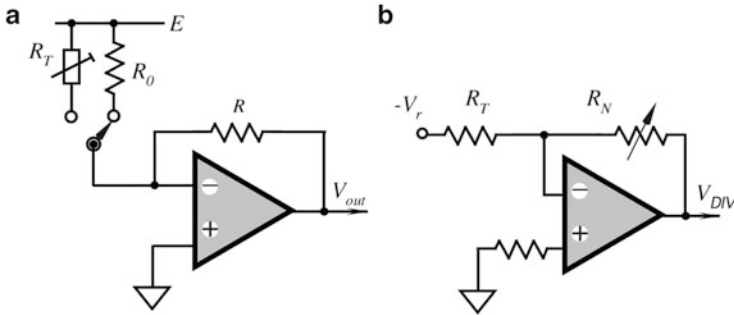


**Fig. 6.14** Symbol of divider (a) and gain of divider as function of denominator (b)

$$V_{DIV} = k \frac{V_N}{V_D}, \quad (6.14)$$

where the numerator is denoted as  $V_N$ , the denominator  $V_D$ , and  $k$  is equal to the output voltage, when  $V_N = V_D$ . The operating ranges of the variables (quadrants of operation) are defined by the polarity and magnitude ranges of the numerator and denominator inputs, and the output. For instance, if  $V_N$  and  $V_D$  are both either positive or negative, the divider is of a 1-quadrant type. If the numerator is bipolar, the divider is 2-quadrant. Generally, the denominator is restricted to a single polarity, since the transition from one polarity to another would require the denominator to pass through zero, which would call for an infinite output (unless the numerator is also zero). In practice,  $V_D$  is a signal from a reference sensor, which usually has a relatively constant value.

Division has long been the most difficult of the four arithmetic functions to implement. This difficulty stems primarily from the nature of division: the magnitude of a ratio becomes quite large, approaching infinity, for a denominator that is approaching zero (and a nonzero numerator). Thus, an ideal divider must have a potentially infinite gain and infinite dynamic range. For a real divider, both of these factors are limited by the magnification of drift and noise at low values of  $V_D$ . That is, the gain of a divider for a numerator is inversely dependent on the value of the denominator, Fig. 6.14b. Thus, the overall error is the net effect of several factors, such as gain dependence of denominator, numerator, and denominator input errors, like offsets, noise, and drift (which must be much smaller than the smallest values of input signals). Besides, the output of the divider must be constant for constant ratios of numerator and denominator, independent of their magnitudes. For example,  $10/10 = 0.01/0.01 = 1$  and  $1/10 = 0.001/0.01 = 0.1$ . In practice, some simple division circuits are used quite extensively. An example is an amplifier of Fig. 6.15b whose output signal is function of the resistor ratio (note that the reference voltage  $V_r$  is negative):



**Fig. 6.15** Ratiometric temperature detector (a) and analog divider of resistive values (b)

$$V_{DIV} = V_r \frac{R_N}{R_T}, \quad (6.15)$$

The most popular and efficient ratiometric circuits are based on the Wheatstone bridge designs which are covered below.

To illustrate effects of a ratiometric technique, consider Fig. 6.14a that shows a simple temperature detector where the acting sensor is a negative temperature coefficient (NTC) thermistor  $R_T$ . A reference resistor  $R_0$  has a value equal to resistance of the thermistor at some reference temperature, for instance at 25 °C. Both are connected via an analog multiplexer to the amplifier with a feedback resistor  $R$ . Let us assume that there is a some drift in the sensor value that can be described by a function of time  $a(t)$  so that the sensor's resistance becomes  $R_T(t) = a(t)R_T$ . Property of the resistor  $R_0$  is such that it also changes with the same function, so  $R_0(t) = a(t)R_0$ . The output signals of the amplifier produced by the sensor and the reference resistor respectively are:

$$V_D = -\frac{ER}{a(t)R_T} = -\frac{ER}{a(t)R_T}, \quad (6.16)$$

$$V_N = -\frac{ER}{a(t)R_0} = -\frac{ER}{a(t)R_0}. \quad (6.17)$$

It is seen that both voltages are functions of a power supply voltage  $E$  and the circuit gain, which is defined by resistor  $R$ . They also are functions of the drift  $a(t)$ . The multiplexing switch causes two voltages  $V_N$  and  $V_D$  to appear sequentially at the amplifier's output. If these voltages are fed into a divider circuit, the resulting signal is expressed as

$$N_{DIV} = k \frac{V_N}{V_D} = k \frac{R_T}{R_0}, \quad (6.18)$$

where  $k$  is the divider's factor (gain). Therefore, the divider's output signal does not depend on neither power supply voltage nor the amplifier gain. It also not a subject

of the multiplicative drift  $a(t)$ . Thus, all these negative factors are rendered irrelevant. The divider's output depends only on the sensor and its reference resistor. This is true only if spurious variables, such as function  $a(t)$ , the power supply, or amplifier's gain, do not change rapidly. That is, they should not change appreciably during the multiplexing period. This requirement determines the rate of multiplexing.

### 6.2.2 Differential Circuits

Beside multiplicative interferences, the additive interferences are very common and pose serious problems for low-level output signals. Consider for example a pyroelectric sensor, Fig. 15.26a, where a heat flow sensitive ceramic plate is supported inside a metal can. Since a pyroelectric is also a piezoelectric, besides heat flow the sensor is susceptible to mechanical stress interferences. Even a slight vibration will generate a spurious piezoelectric signal that may be several orders of magnitude higher than a pyroelectric current. The solution is to fabricate the sensor with dual electrodes deposited on the same ceramic substrate as shown in Fig. 15.26b. This essentially creates two identical sensors on the same ceramic plate. Both sensors respond to all stimuli nearly identically. Since they are oppositely connected and assuming that  $V_{\text{pyro}}$  and  $V_{\text{piezo}}$  from one sensor are respectively equal to those of the other sensor, the resulting output voltage is essentially zero:

$$V_{\text{out}} = (V_{\text{pyro1}} + V_{\text{piezo1}}) - (V_{\text{pyro2}} + V_{\text{piezo2}}) = 0 \quad (6.19)$$

If one of the sensors is blocked from receiving thermal radiation ( $V_{\text{pyro2}} = 0$ ), then  $V_{\text{out}} = V_{\text{pyro1}}$ . In other words, thanks to subtraction ( $V_{\text{piezo1}} = V_{\text{piezo2}}$  are subtracted), the combined sensor becomes insensitive to piezoelectric spurious signals.

A differential method where a sensor is fabricated in a symmetrical form and connected to a symmetrical signal conditioning circuit (e.g., differential amplifier) so that one signal is subtracted from another, is a very powerful way of noise and drift reductions. Yet, this method is effective only if a dual sensor is fully symmetrical. An asymmetry will produce a proportional loss of noise cancellation. For example, if asymmetry is 5 %, interference will be cancelled by no more than 95 %.

### 6.2.3 Wheatstone Bridge

The Wheatstone bridge circuits are popular and very effective implementations of both the ratiometric technique (division) and differential techniques (subtraction) before a sensor is coupled to a signal conditioner. A general circuit of the bridge is shown in Fig. 6.16a. Impedances  $\mathbf{Z}$  may be either active or reactive, that is they may be either simple resistances, like in the piezoresistive strain gauges, or capacitors, or inductors, or combinations of the above. For a pure resistor, the impedance is  $R$ , for an ideal capacitor, the magnitude of its impedance is equal to  $1/(2\pi fC)$  and for an

inductor, it is  $2\pi fL$ , where  $f$  is frequency of the current passing through the bridge arms, while at least one arm is the sensor. The bridge output voltage is represented by:

$$V_{\text{out}} = \left( \frac{\mathbf{Z}_1}{\mathbf{Z}_1 + \mathbf{Z}_2} - \frac{\mathbf{Z}_3}{\mathbf{Z}_3 + \mathbf{Z}_4} \right) V_{\text{ref}} = V_{\text{ref}} \left[ \left( 1 + \frac{\mathbf{Z}_2}{\mathbf{Z}_1} \right)^{-1} - \left( 1 + \frac{\mathbf{Z}_4}{\mathbf{Z}_3} \right)^{-1} \right], \quad (6.20)$$

The bridge is considered to be in a balanced state when the following condition is met:

$$\frac{\mathbf{Z}_1}{\mathbf{Z}_2} = \frac{\mathbf{Z}_3}{\mathbf{Z}_4}. \quad (6.21)$$

Under the balanced condition, the output voltage is zero. When at least one impedance in the bridge changes, the bridge becomes imbalanced and the output voltage goes either in a positive or negative direction, depending on direction of the impedance change. To determine the bridge sensitivity with respect to each impedance, partial derivatives may be obtained from Eq. (6.20):

$$\begin{aligned} \frac{\partial V_{\text{out}}}{\partial \mathbf{Z}_1} &= \frac{\mathbf{Z}_2}{(\mathbf{Z}_1 + \mathbf{Z}_2)^2} V_{\text{ref}} \\ \frac{\partial V_{\text{out}}}{\partial \mathbf{Z}_2} &= -\frac{\mathbf{Z}_1}{(\mathbf{Z}_1 + \mathbf{Z}_2)^2} V_{\text{ref}} \\ \frac{\partial V_{\text{out}}}{\partial \mathbf{Z}_3} &= -\frac{\mathbf{Z}_4}{(\mathbf{Z}_3 + \mathbf{Z}_4)^2} V_{\text{ref}} \\ \frac{\partial V_{\text{out}}}{\partial \mathbf{Z}_4} &= \frac{\mathbf{Z}_3}{(\mathbf{Z}_3 + \mathbf{Z}_4)^2} V_{\text{ref}} \end{aligned} \quad (6.22)$$

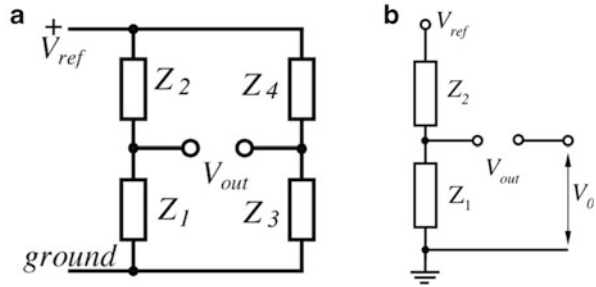
By summing these equations, we obtain the bridge sensitivity:

$$\frac{\delta V_{\text{out}}}{V_{\text{ref}}} = \frac{\mathbf{Z}_2 \delta \mathbf{Z}_1 - \mathbf{Z}_1 \delta \mathbf{Z}_2}{(\mathbf{Z}_1 + \mathbf{Z}_2)^2} - \frac{\mathbf{Z}_4 \delta \mathbf{Z}_3 - \mathbf{Z}_3 \delta \mathbf{Z}_4}{(\mathbf{Z}_3 + \mathbf{Z}_4)^2}, \quad (6.23)$$

It should be noted that according to Eq. (6.20), the Wheatstone bridge possesses both properties: ratiometric and differential. The ratios  $\mathbf{Z}_2/\mathbf{Z}_1$  and  $\mathbf{Z}_4/\mathbf{Z}_3$  are ratiometric, while the difference in the parenthesis represents a differential property, thus making the Wheatstone bridge a very useful circuit.

A closer examination of Eq. (6.23) shows that only the adjacent pairs of the impedances (i.e.,  $\mathbf{Z}_1$  and  $\mathbf{Z}_2$ ,  $\mathbf{Z}_3$  and  $\mathbf{Z}_4$ ) have to be identical in order to achieve the ratiometric compensation (such as the temperature stability, drift, etc.). For the differential properties, impedances in the balanced bridge do not have to be equal, as long as the balance ratio of Eq. (6.21) is satisfied.

**Fig. 6.16** General circuit of Wheatstone bridge (a) and half-bridge (b)



In many practical circuits, only one impedance is used as a sensor, thus for  $Z_1$  as a sensor, the bridge sensitivity becomes:

$$\frac{\delta V_{out}}{V_{ref}} = \frac{\delta Z_1}{4Z_1}. \quad (6.24)$$

A simplified version of the bridge is shown in Fig. 6.16b, where only two serial impedances are used as a voltage divider. The second divider is replaced by a fixed reference voltage  $V_0$ . As a result, the circuit that is called a *half-bridge* has no differential properties, but still possess the ratiometric properties because its output voltage is represented by:

$$V_{out} = V_{ref} \left( 1 + \frac{Z_2}{Z_1} \right)^{-1} - V_0. \quad (6.25)$$

The resistive bridges are commonly used with strain gauges, piezoresistive pressure transducers, thermistor thermometers, hygriators, and many other sensors when immunity against environmental factors is required. Similar arrangements are used with the capacitive and magnetic sensors for measuring force, displacement, moisture, etc.

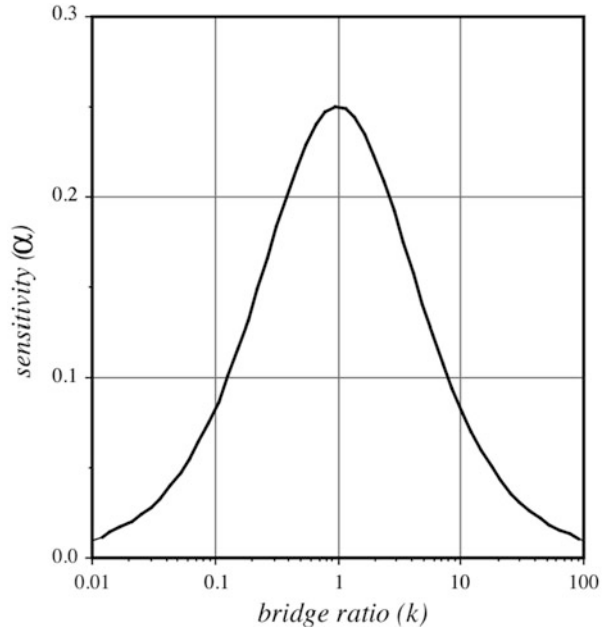
The basic Wheatstone bridge circuit (Fig. 6.16a) generally operates when the bridge is disbalanced. This is called the *deflection* method of measurement. It is based on detecting voltage  $V_{out}$  across the bridge diagonal. Let us consider a bridge with a sensor in place of impedance  $Z_1$ . When the sensor's impedance changes by the value  $\Delta$ , the new impedance becomes  $Z_v = Z_1(1 + \Delta)$ . The bridge output voltage is a nonlinear function of a disbalance  $\Delta$ . However, for a small change ( $\Delta < 0.05Z_1$ ), which often is the case, the bridge output may be considered quasilinear. The bridge maximum sensitivity is obtained when  $Z_1 = Z_2$ . When  $Z_1 \gg Z_2$  or  $Z_2 \gg Z_1$ , the bridge output voltage decreases. Assuming that  $k = Z_1/Z_2$ , the bridge sensitivity may be expressed as:

$$\alpha = \frac{k}{(k + 1)^2} \quad (6.26)$$

A normalized graph calculated from this equation is shown in Fig. 6.17. It indicates that the maximum sensitivity is achieved at  $k = 1$ , however, sensitivity



**Fig. 6.17** Sensitivity of disbalanced bridge as function of impedance ratio



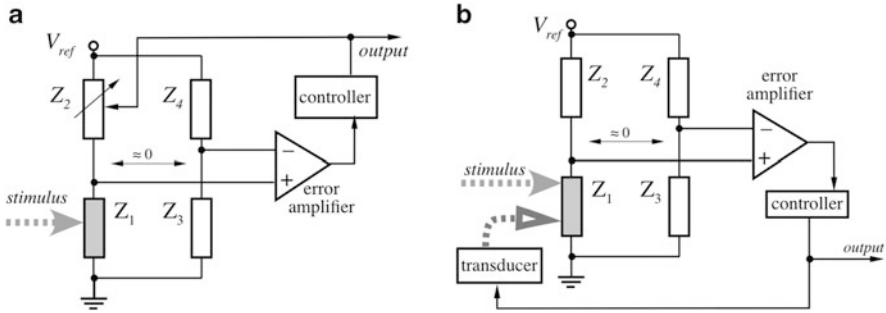
drops relatively little for the range where  $0.5 < k < 2$ . If the bridge is fed by a current source  $i_{\text{ref}}$ , rather by a voltage source  $V_{\text{ref}}$ , its output voltage for small  $\Delta$  and a single variable component (sensor) is represented by:

$$V_{\text{out}} = i_{\text{ref}} \frac{k\Delta}{2(k+1)}, \quad (6.27)$$

### 6.2.4 Null-Balanced Bridge

Another method of using a bridge circuit is called *null-balanced*. The method overcomes the limitation of small changes ( $\Delta$ ) in the bridge arm to achieve a good linearity over a broad span of the input stimuli. The null-balance essentially requires that the bridge is *always* maintained near the balanced state. To satisfy the requirement for a bridge balance of Eq. (6.21), there are two methods to balance the bridge:

1. One of the impedances of the bridge, other than the sensor, is changing together with the sensor to keep the bridge balanced. Figure 6.18a illustrates this concept. The error amplifier magnifies the small bridge disbalances. The controller modifies value of  $Z_2$  on command from the error amplifier. In effect, this is a closed-loop control circuit of the PID type (proportional-integral-differential). The output voltage is obtained from the control signal that balances the bridge



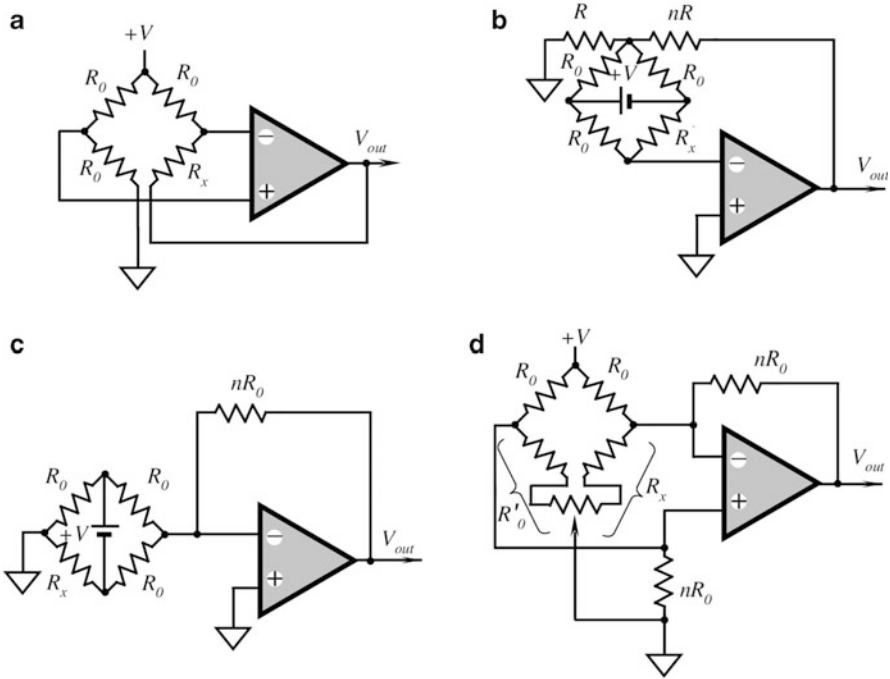
**Fig. 6.18** Balancing of Wheatstone bridge by feedback to nonsensing impedance (a) and to sensor (b)

via  $Z_2$ . Consider the example: both  $Z_1$  and  $Z_2$  may be photoresistors—the light sensitive resistors where  $Z_1$  is used for sensing an external light intensity. The  $Z_2$  photoresistor could be optically coupled with a light emitting diode (LED) that is part of the controller. The controller modulates LED to modify  $Z_2$  for balancing the bridge. When the bridge is balanced, the LED light is nearly equal to light sensed by  $Z_1$ . Therefore, electric current through the LED becomes a measure of the resistance  $Z_1$ , and, subsequently, of the light intensity detected by the sensor. Note that using impedance  $Z_2$  for the feedback, rather than  $Z_3$  or  $Z_4$ , is preferable as the bridge not only will stay balanced, but also the voltage across the sensor remains constant and the value of  $k$  will be close to unity, assuring the best linearity and sensitivity of the circuit.

- The bridge balancing feedback is provided directly to the same sensor as measures the stimulus. Thus, the feedback shall be of the same nature and magnitude but of the opposite sign as the stimulus, Fig. 6.18b. When both the stimulus and “counter-stimulus” are equal to one another in magnitudes and opposite in phase, the bridge is balanced and the output of the controller becomes a measure of the stimulus. This approach was exemplified for mechanical forces in Sect. 6.1.8. It can be used when an appropriate transducer is available for converting voltage to the counter-stimulus. For example, a bidirectional force can be generated by an electrostatic effect and thus this method is useful for differential pressure sensors, accelerometers, and microphones, but there is no known way of generating, for example, “negative light” if one would like to use this option with photodetectors.

### 6.2.5 Bridge Amplifiers

The *bridge amplifiers* for resistive sensors are probably the most frequently used front stages of signal conditioners. They may be of various configurations, depending on the required bridge grounding and availability of either grounded or floating reference voltages. Below we review some basic circuits with operational



**Fig. 6.19** Connection of operational amplifiers to resistive bridge circuits (deflection method)

amplifiers. Figure 6.19a shows the so-called active bridge, where a variable resistor (the sensor) is floating, i.e., isolated from ground, and is connected into a feedback of the OP-AMP. If a resistive sensor’s transfer function can be approximated by a linear function:

$$R_x \approx R_0(1 + \alpha), \tag{6.28}$$

where  $\alpha$  is a small normalized input stimulus, then the output voltage of this circuit is:

$$V_{out} = \frac{V}{2}(1 - \alpha). \tag{6.29}$$

A circuit with a floating bridge and floating reference voltage source  $V$  is shown in Fig. 6.19b. This circuit may provide gain that is determined by the feedback resistor whose value is  $nR_0$ , so the output voltage is:

$$V_{out} = V \left( \frac{1 + \alpha}{2 + \alpha} - \frac{1}{2} \right) (n + 1). \tag{6.30}$$

Note that when floating, the sensor and reference voltage source shall have no connection whatsoever to ground neither directly nor through any other circuit.

All connecting wires to the amplifier must be very short, so the amplifier should be located close the sensor.

A bridge with the grounded sensor  $R_x$  but a floating reference voltage  $V$  is shown in Fig. 6.19c. The output voltage is:

$$V_{\text{out}} = V \left( \frac{1 + \alpha}{2 + \alpha} - \frac{1}{2} \right) n \quad (6.31)$$

Perhaps the most popular resistive bridge amplifier circuit is shown in Fig. 6.19d. It is for the grounded resistive sensor  $R_x$  with the amplifier having gain  $n$ . Its output voltage is:

$$V_{\text{out}} = Vn \left[ \frac{1}{2n + 1} \left( 1 + n \frac{2 + \alpha}{1 + \alpha} \right) - 1 \right]. \quad (6.32)$$

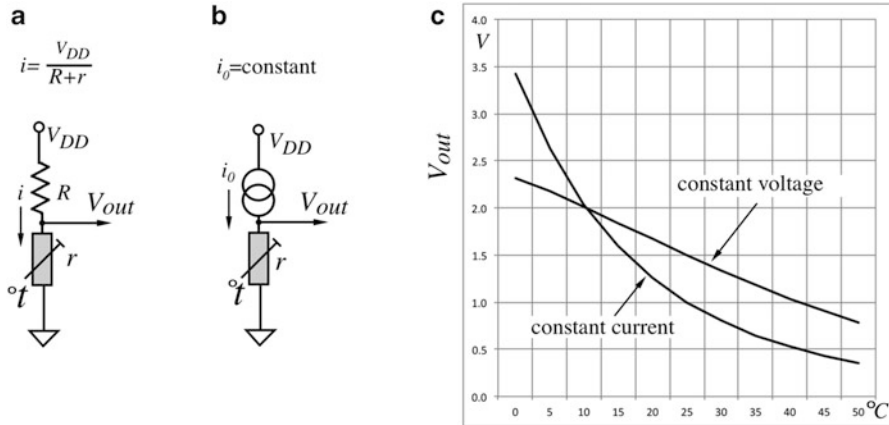
Note that the circuit may contain a balancing potentiometer whose resistance sectors should be included into the corresponding arms of the bridge. The potentiometer is used to adjust the bridge component tolerances or offset the bridge balance by some fixed bias. When the bridge is perfectly balanced, its output voltage  $V_{\text{out}}$  is equal to zero. To better utilize the operational amplifier open-loop gain, the value of  $n$  should not exceed 100.

Note that circuits Fig. 6.19b–d are nonlinear with respect to  $\alpha$ , even if the sensor is linear, while circuit Fig. 6.19a is linear. The reason for this is that in circuit of Fig. 6.19a, the sensor is supplied with a constant current being independent of the sensor's resistance, as it will be explained in the next section. In other circuits, the sensor's current varies when the sensor resistance changes, thus producing a nonlinear output, albeit for small  $\alpha$ , this nonlinearity is usually very small.

### 6.3 Excitation Circuits

External signals are required for operation of the so-called *active* sensors. Examples are the absolute temperature sensors (thermistors and RTDs), pressure sensors (piezoresistive and capacitive), and displacement sensors (electromagnetic, capacitive and resistive). Different active sensors need different types of external signals for their operation. Depending on the sensor, these may be constant voltage, constant current, sinusoidal, or pulsing currents. It may even be light, magnetic field, or ionizing radiation. The names for that external signal is the *excitation signal* or *pilot signal*. In many cases, stability and precision of excitation signals directly relate to the sensor's accuracy and stability. Hence, it is imperative to generate the signal with such accuracy that the overall performance of the sensing system is not degraded. Below, we review several basic circuits, which feed sensors with the appropriate electric excitation signals.

When selecting the excitation circuit, one should think not only about the sensor but also what kind of signal processing is expected. Excitation signal is generally



**Fig. 6.20** Generating of excitation currents by a constant voltage source  $V_{DD}$  (a) and by constant current source  $i_0$  (b); voltages across thermistor  $r$  at two different excitation currents as functions of temperature (c)

multiplicative to the sensor’s transfer function and thus directly defines the shape and behavior of the output. To illustrate this, consider two possible circuits shown in Fig. 6.20a, b. These circuits are intended to pump electric current through a thermistor (temperature-dependent resistor) having resistance  $r$ . Each resistance  $r$  corresponds to a unique temperature. Thus, to measure temperature, one needs to measure resistance. However, to measure resistance it is necessary to force electric current  $i$  through that resistance. Then according to Ohm’s law, the voltage  $V_{out}$  across the thermistor is function of current  $i$ , resistance  $r$ , and subsequently—temperature:

$$V_{out} = ir \tag{6.33}$$

Figure 6.20a shows that current through  $r$  is also function of a pull-up fixed resistor  $R$  connected to a constant voltage source  $V_{DD}$ . Since  $r$  has a highly nonlinear transfer function with a negative temperature coefficient (NTC), resistance  $r$  and the current vary dramatically over a temperature range. Luckily, a combination of a variable resistor  $r$  and variable current  $i$  cause a linearization of the output voltage  $V_{out}$  in a narrow temperature range—see Fig. 6.20c, line “constant voltage”. The linearization works only in a narrow temperature range, yet for many nondemanding applications it may be what is needed. On the other hand, circuit in Fig. 6.20b shows that instead of resistor  $R$ , a constant current generator is used. It produces fixed current  $i_0$  that is independent of the thermistor resistance and power supply voltage  $V_{DD}$  and, as a result, according to Eq. (6.33),  $V_{out}$  is directly proportional to  $r$ . Figure 6.20c shows the line “constant current” that is highly nonlinear with temperature. Both circuits are useful, but which one to employ—depends on how  $V_{out}$  is going to be processed.

### 6.3.1 Current Generators

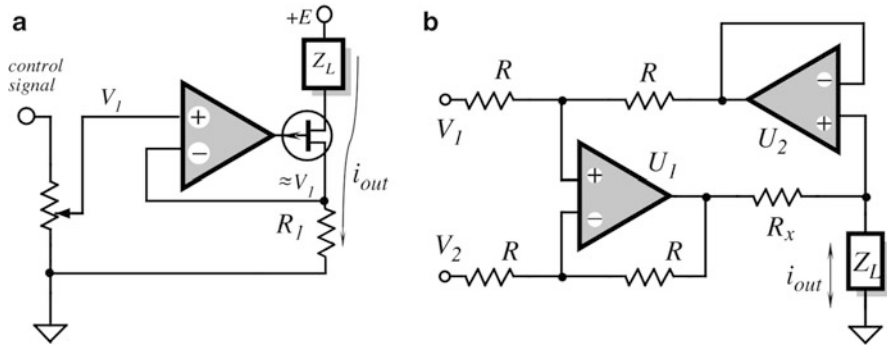
Current generators are often used as excitation circuits to feed sensors with predetermined currents that, within limits, are independent of the sensor properties, stimulus value, or environmental factors. In general terms, a current generator (current pump or current source or current sink) is a device that produces electric current independent of the load impedance. That is, within the capabilities of the generator, the amplitude of its output current remains substantially independent of any changes in the load and power supply voltage. It is said that an ideal current generator has infinitely high output resistance, so any series load will not change the output current. When generating a fixed current for a variable load, according to Ohm's Law, the corresponding voltage across the load changes in synch with the load.

Usefulness of the current generators for the sensor interfaces is in their ability to produce excitation currents of precisely controlled magnitude and shape. Hence, a current generator should not only produce current which is load-independent, but it also must be controllable from an external signal source (e.g., a wave-form generator), which in most cases has a voltage output.

There are two main characteristics of a current generator: the output resistance and voltage compliance. The output resistance should be as high as practical. A voltage compliance is the highest voltage which can be developed across the load without affecting the output current. For a high-resistive load, according to Ohm's law, Eq. (6.33), a higher voltage is required for a given current. For instance, if the required excitation current is  $i = 10$  mA and the highest load impedance at any given frequency is  $Z_L = 10$  k $\Omega$ , a voltage compliance of at least  $iZ_L = 100$  V would be needed. Below, we show some useful circuits with the increased voltage compliance where the output currents can be controlled by external signals.

A *unipolar* current generator is called either a current *source* (generates the out-flowing current), or a current *sink* (generates the in-flowing currents). Here, unipolar means that it can produce currents of any shape flowing in one direction only, usually toward the ground. Many of such generators utilize current-to-voltage characteristics of transistors. A voltage controlled current source or sink may include an operational amplifier, Fig. 6.21a. In such a circuit, a precision and stable resistor  $R_1$  defines the output current,  $i_L$ , that flows through the load impedance  $Z_L$ . The circuit contains a feedback loop through the OP-AMP that keeps voltage across resistor  $R_1$  constant and thus assuring a constant current. To maximize the voltage compliance, a voltage drop across the sensing resistor  $R_1$  should be as small as possible. For a better performance, current through the base of the output transistor should be as small as possible, hence, a field effect rather than bipolar transistor is used as an output current delivering device. Note that in that circuit the load is not grounded.

For many sensors, *bipolar* current generators may be required. Such a generator feeds a sensor with the excitation current that may flow in both directions (in- and out-flowing). In cases where the sensor must be grounded, a useful current pump is the circuit invented by Brad Howland at MIT [5]. One of its implementations is shown in Fig. 6.21b. The pump operation is based on utilizing both the negative and



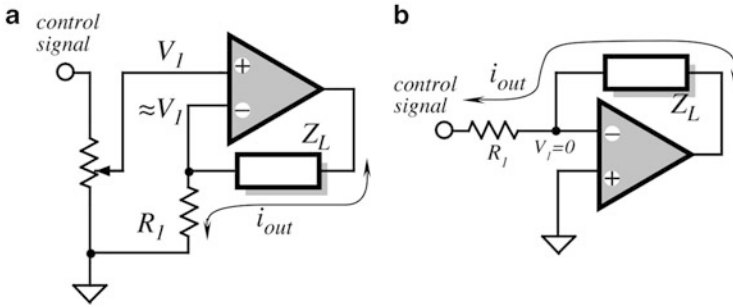
**Fig. 6.21** Current sink with JFET transistor (a) and Howland current pump (b)

positive feedbacks around the operational amplifier. The load is connected to the positive loop. In that circuit all resistors should be nearly equal with high tolerances. Resistor  $R_x$  should be of a relatively low value for a sufficient output current magnitude. The circuit is stable for most of the resistive loads, however, to insure stability, a few picofarad capacitor may be added in a negative feedback or/and from the positive input of the operational amplifier  $U_1$  to ground. When the load is inductive, an infinitely large compliance voltage would be required to deliver the set current when a fast transient control signal is applied. Therefore, the real current pump will produce a limited rising slope of the output current. The flowing current will generate an inductive spike across the output terminal, which may be fatal to the operational amplifier. It is advisable, for large inductive loads, to clamp the load with diodes to the power supply buses. The output current of the Howland pump is defined by the equation

$$i_L = \frac{(V_1 - V_2)}{R_s}. \quad (6.34)$$

The advantage of this circuit is that resistors  $R$  may be selected with a relatively high value and housed in the same thermally homogeneous packaging for better thermal tracking.

When the sensor is floating (not connected to ground), a simpler current source can be used. Figure 6.22 shows a noninverting (b) and inverting (a) circuits with operational amplifiers where the load (sensor) is connected as a feedback. Current through the load  $Z_L$  is equal to  $V_I/R_1$  and is load independent. The load current follows variations in  $V_I$  within the operating limits of the amplifier. An obvious limitation of the circuit is that the load is “floating”, i.e., it is not connected to the ground bus or any other reference potential. For some applications, this is quite all right, however, many sensors need to be grounded or otherwise referenced. A circuit shown in Fig. 6.22b keeps one side of the load impedance near the ground potential, because a noninverting input of the OP-AMP is a virtual ground. Nevertheless, even in this circuit, the load is still fully isolated from the ground.



**Fig. 6.22** Bidirectional current sources with floating loads (sensors)

### 6.3.2 Voltage Generators

As opposed to current generators, voltage generators (voltage sources or voltage drivers) must produce output voltages which over broad ranges of the loads and operating frequencies are independent of the load impedances and thus of the output currents. Sometimes, the voltage generators are called *hard voltage sources*. Usually, when a sensor that has to be driven by hard voltage is purely resistive, a driver can be a simple output stage which can deliver a sufficient current magnitude. However, when the load contains capacitances or inductances, that is, the load is reactive, the output stage of a voltage generator becomes a more complex device.

In many instances, even when the load is purely resistive, there still can be some capacitance associated with it. This may happen when the load is connected through lengthy wires or coaxial cables. A coaxial cable behaves as a capacitor connected from its central conductor to its shield if the length of the cable is less than  $1/4$  of the wavelength in the cable at the frequency of interest  $f$ . For a coaxial cable, this maximum length is given by

$$l_{\max} \leq 0.0165 \frac{c}{f}, \quad (6.35)$$

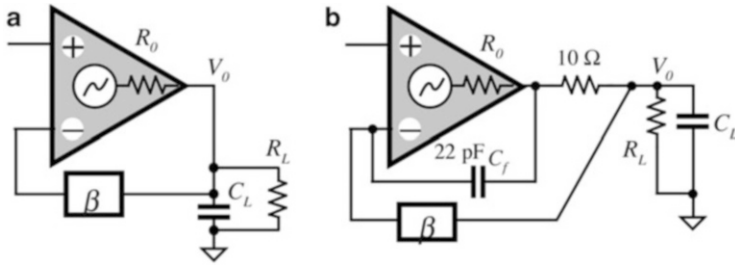
where  $c$  is the velocity of light in a coaxial cable dielectric.

For instance, if  $f = 100$  kHz,  $l_{\max} \leq 0.0165 \frac{3 \times 10^8}{10^5} = 49.5$ , that is, a cable less than 49.5 m (162.4 ft) long will behave as a capacitor connected in parallel with the load, Fig. 6.23a. For example, cable R6-58A/U has the capacitance of 95 pF/m. This capacitance must be considered for two reasons: for the speed and stability of the circuits having a feedback coefficient  $\beta$ . The instability results from the phase shift produced by the output resistance of the voltage driver  $R_o$  and the loading capacitance  $C_L$ :

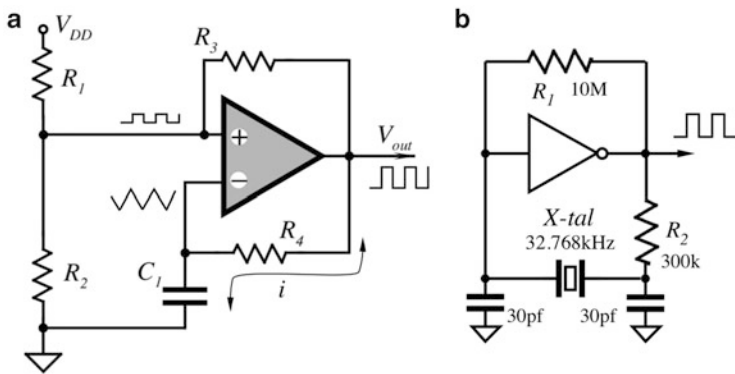
$$\varphi = \arctan(2\pi f R_o C_L). \quad (6.36)$$

For example, if  $R_o = 100 \Omega$  and  $C_L = 1000$  pF, at  $f = 1$  MHz, the phase shift  $\varphi \approx 32^\circ$ . This shift significantly reduces the phase margin in a feedback network that may cause a substantial degradation of the response and a reduced ability to





**Fig. 6.23** Driving capacitive load. The load capacitor is coupled to driver’s input through feedback (a); decoupling of capacitive load (b)



**Fig. 6.24** Square-wave oscillator with OP-AMP (a) and crystal oscillator using a digital inverter (b)

drive the capacitive loads. The instability may be either overall, when an entire system oscillates, or localized when the driver alone becomes unstable. The local instabilities often can be cured by large by-pass capacitors (on the order of 10  $\mu$ F) across the power supply or the so-called Q-spoilers consisting of a serial connection of 3–10  $\Omega$  resistor and a disc ceramic capacitor connected from the power supply pins of the driver chip to ground.

To make a driver stage more tolerant to capacitive loads, it can be isolated by a small serial resistor as it is shown in Fig. 6.24b. A small capacitive feedback ( $C_f$ ) to the inverting input of the amplifier, and a 10  $\Omega$  resistor may allow to drive loads as large as 0.5  $\mu$ F. However, in any particular case it is recommended to find the best values for the resistor and capacitor experimentally.

### 6.3.3 Voltage References

A voltage reference is an electronic device for generating precisely known constant voltage that is affected very little by variations in power supply, temperature, load, aging, and other factors. Many voltage references are available in a monolithic form

for a large variety of the output voltages. Most of them operate with the so-called internal band-gap circuits. A good voltage reference should be a good voltage source, that is, it shall possess two critical features: have a very high stability of the output voltage and low-output resistance.

### 6.3.4 Oscillators

Oscillators are generators of variable electrical signals. Some of them are for generating a single signal wave (called “one-shot”), while others are free running. In many applications, free-standing oscillators may be replaced with digital outputs of a microprocessor or microcontroller, where the square-wave single or free-running pulses may be generated at one of the I/O ports.

Any oscillator essentially is comprised of a circuit with a gain stage, nonlinearity, and a certain amount of a positive feedback. By definition, an oscillator is an unstable circuit (as opposed to an amplifier that better be stable!) whose timing characteristics are either steady or changeable according to a predetermined functional dependence. The latter is called a *modulation*. Generally, there are three types of the electronic oscillators classified according to their time-keeping components: the *RC*, *LC*, and crystal oscillators (mechanical).

An *RC*-oscillators is called a *relaxation oscillator* because its functionality is based on a capacitor discharge (relaxation of a charge). The operating frequency is defined by a capacitor (*C*) and resistor (*R*)

An *LC* oscillator contains capacitive (*C*) and inductive (*L*) components that define the operating frequency.

In crystal oscillators, operating frequency is defined by a mechanical resonant in the specific cuts of piezoelectric crystals, usually quartz or ceramic. There is a great variety of the oscillation circuits, coverage of which is beyond the scope of this book. Just as an introduction, below we briefly describe a couple of practical circuits.

Many free-running oscillators (multivibrators) can be built with logic circuits, for instance—with NOR, NAND gates, or binary inverters. These circuits possess input nonlinearities, such as thresholds, that upon crossing, produce sharp transients at the outputs. Also, many multivibrators can be designed with comparators or operational amplifiers having a high open-loop gain. In all these oscillators, a combination of a capacitor and a resistor, or a crystal is a time-keeping combination.

In an *RC*-multivibrator, a voltage across a charging or discharging capacitor is compared with either constant or changing thresholds. When the capacitor charges, the moment of a threshold crossing is detected and causing generation of the output pulse transient. The transient is fed back to the *RC*-network (positive feedback) to cause the capacitor discharging that goes on until the next moment of comparison and generation of another pulse transient. Then, the cycle repeats.

This basic principle essentially requires the following minimum components: a capacitor, a charging circuit, and a threshold device (a comparator which is a nonlinear circuit). Several monolithic relaxation oscillators are available from many manufacturers, for instance a very popular timer, type 555, that can operate in either monostable (one-shot), or astable (free-running) modes. A great variety of oscillating circuits the reader can find in many books on operational amplifiers and digital systems, for instance [6].

A very popular free-running square-wave oscillator, Fig. 6.24a, can be built with one OP-AMP or a voltage comparator.<sup>1</sup> The amplifier is surrounded by two feedback loops—one is negative (to the inverting input) and the other is positive (to the noninverting input). A positive feedback (via  $R_3$ ) controls the threshold level, while the negative loop charges and discharges timing capacitor  $C_1$ , through resistor  $R_4$ . Frequency of this oscillator can be determined from

$$f = \frac{1}{R_4 C_1} \left[ \ln \left( 1 + \frac{R_1 || R_2}{R_3} \right) \right]^{-1}, \quad (6.37)$$

where  $R_1 || R_2$  is an equivalent resistance of parallel-connected  $R_1$  and  $R_2$ .

A crystal oscillator is shown in Fig. 6.24b. It utilizes a digital voltage inverter that can be described as an inverting amplifier having very high gain in a very narrow linear range, that is near its threshold value (about 50 % of the power supply voltage). To bias the input close to that linear range, a feedback resistor  $R_1$  is used as a negative feedback. The inverter amplifies the input signal so much that the output voltage is saturated either to ground or the positive power supply rail. It also flips its phase by 180°. The crystal inverts the output by another 180°, thus providing a positive feedback to the input, causing continuous oscillations.

---

## 6.4 Analog-to-Digital Converters

The conversion of an analog signal to a digital format involves quantization of the input, so it necessarily introduces a small amount of error. The converter periodically samples the analog signal and, at specific moments, performs conversions. The result is a sequence of digital values that have been converted from a continuous-time and continuously variable analog signal to a discrete-time and discrete-value digital signal.

---

<sup>1</sup> A voltage comparator differs from an operational amplifier by its faster transient response and special output circuit, which is easier interfaceable with digital circuits. A comparator may have a built-in hysteresis input circuit and it's called Schmitt trigger. Schmitt trigger is a digital comparator having two thresholds: upper and lower. When the input voltage transient goes upward and crosses the upper threshold, the trigger output switches high. When voltage moves downward and crosses the lower threshold, the output switches low. It was invented in 1934 by Otto H. Schmitt.

### 6.4.1 Basic Concepts

The analog-to-digital converters (abbreviated as A/D, or ADC, or A2D, or A-to-D) range from discrete circuits, to monolithic ICs (integrated circuits), to high-performance hybrid circuits, modules, and even boxes. Also, the converters are available as standard cells for custom and semicustom application-specific integrated circuits (ASIC). The ADCs transform continuous analog data—usually voltage—into an equivalent discrete digital format, compatible with digital data processing devices. Key characteristics of ADC include absolute and relative accuracy, linearity, no-missing codes, resolution, conversion speed, stability, and price. When price is of a major concern, a monolithic ADC as an embedded part of a microcontroller is the most efficient.

The most popular ADC converters are based on a successive-approximation technique because of an inherently good compromise between speed and accuracy. However, other popular techniques are used in a large variety of applications, especially when no high-conversion speed is required and only a small number of channels is needed. These include dual-ramp, quad-slope, pulse-width modulators (PWM), voltage-to-frequency (V/F) converters, and resistance-to-frequency (R/F) converters. The art of ADC is well developed. Here, we briefly review some popular architectures of ADCs, however, for detailed descriptions the reader should refer to specialized texts, such as [7].

The best-known digital code is *binary* (base 2). Binary codes are most familiar in representing integers, i.e., in a natural binary integer code having  $n$  bits, the LSB (least significant bit) has a weight of  $2^0$  (i.e., 1), the next bit has a weight of  $2^1$  (i.e., 2), and so on up to MSB (most significant bit), which has a weight of  $2^{n-1}$  (i.e.,  $2^n/2$ ). The value of a binary number is obtained by adding up the weights of all nonzero bits. When the weighted bits are added up, they form a unique number having any value from 0 to  $2^n - 1$ . Each additional trailing zero-bit, if present, essentially doubles the size of the number.

When converting signals from analog sensors, because full scale is independent of the number of bits of resolution, a more useful coding is *fractional* binary which is always normalized to a full scale. Integer binary can be interpreted as fractional binary if all integer values are divided by  $2^n$ . For example, the MSB has a weight of  $1/2$  (i.e.,  $2^{n-1}/2^n = 2^{-1}$ ), the next bit has a weight of  $1/4$  (i.e.,  $2^{-2}$ ), and so forth down to the LSB, which has a weight of  $1/2^n$  (i.e.,  $2^{-n}$ ). When the weighted bits are added up, they form a number with any of  $2^n$  values, from 0 to  $(1 - 2^{-n})$  of full scale. Additional bits simply provide more fine structure without affecting the full-scale range. To illustrate these relationships, Table 6.2 lists 16 permutations of 5-bit's worth of 1's and 0's, with their binary weights, and the equivalent numbers expressed as both decimal and binary integers and fractions.

When all bits are "1" in natural binary, the fractional number value is  $1 - 2^{-n}$ , or normalized full-scale less 1 LSB ( $1 - 1/16 = 15/16$  in the example). Strictly speaking, the number that is represented, written with an "integer point", is 0.1111 (=  $1 - 0.0001$ ). However, it is almost a universal practice to write the

**Table 6.2** Integer and fractional binary codes

Decimal fraction	Binary fraction	MSB $\times 1/2$	Bit2 $\times 1/4$	Bit3 $\times 1/6$	Bit4 $\times 1/16$	Binary integer	Decimal integer
0	0.0000	0	0	0	0	0000	0
1/16 (LSB)	0.0001	0	0	0	1	0001	1
2/16 = 1/8	0.0010	0	0	1	0	0010	2
3/16 = 1/8 + 1/16	0.0011	0	0	1	1	0011	3
4/16 = 1/4	0.0100	0	1	0	0	0100	4
5/16 = 1/4 + 1/16	0.0101	0	1	0	1	0101	5
6/16 = 1/4 + 1/8	0.0110	0	1	1	0	0110	6
7/16 = 1/4 + 1/8 + 1/16	0.0111	0	1	1	1	0111	7
8/16 = 1/2 (MSB)	0.1000	1	0	0	0	1000	8
9/16 = 1/2 + 1/16	0.1001	1	0	0	1	1001	9
10/16 = 1/2 + 1/8	0.1010	1	0	1	0	1010	10
11/16 = 1/2 + 1/8 + 1/16	0.1011	1	0	1	1	1011	11
12/16 = 1/2 + 1/4	0.1100	1	1	0	0	1100	12
13/16 = 1/2 + 1/4 + 1/16	0.1101	1	1	0	1	1101	13
14/16 = 1/2 + 1/4 + 1/8	0.1110	1	1	1	0	1110	14
15/16 = 1/2 + 1/4 + 1/8 + 1/16	0.1111	1	1	1	1	1111	15

code simply as the integer 1111 (i.e., “15”) with the fractional nature of the corresponding number understood: “1111”  $\rightarrow$  1111/(1111 + 1), or 15/16.

For convenience, Table 6.3 lists bit weights in binary for numbers having up to 20 bits. However, the practical range for the vast majority of sensors rarely exceeds 16 bits.

The weight assigned to the LSB is the resolution of numbers having  $n$  bits. The dB column represents the logarithm (base 10) of the ratio of the LSB value to unity (full scale), multiplied by 20. Each successive power of 2 represents a change of 6.02 dB [i.e.,  $20 \log_{10}(2)$ ] or “6 dB/octave”.

## 6.4.2 V/F Converters

A voltage-to-frequency (V/F), as the name implies, converts voltage to a variable frequency of pulses, in other words—input voltage modulates frequency. This is called *frequency modulation* or FM. V/F can provide a high-resolution conversion, that is also useful for some additional sensor features, such as a voltage isolation, communication, and storage of data. The converter accepts analog output from a sensor, which can be either voltage or current (in latter case, of course, it should be called a current-to-voltage converter). Here we will discuss a conversion of voltage to frequency, or, in other words, to a *number of square pulses per unit of time*. A frequency is a digital format because pulses can be gated (selected for a given interval of time) and then counted, resulting in a binary

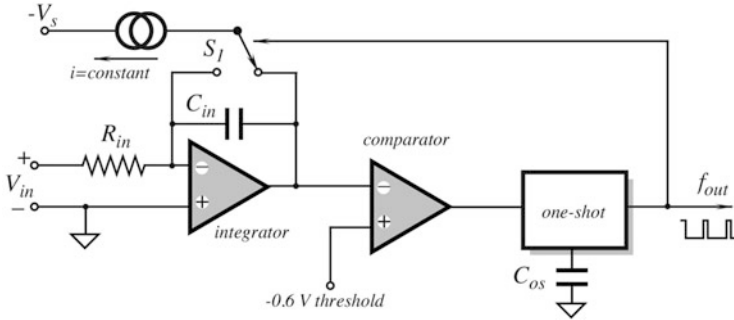
**Table 6.3** Binary bit weights and resolutions

BIT	$2^{-n}$	$1/2^n$ fraction	dB	$1/2^n$ decimal	%	ppm
FS	$2^0$	1	0	1.0	100	1,000,000
MSB	$2^{-1}$	1/2	-6	0.5	50	500,000
2	$2^{-2}$	1/4	-12	0.25	25	250,000
3	$2^{-3}$	1/8	-18.1	0.125	12.5	125,000
4	$2^{-4}$	1/16	-24.1	0.0625	6.2	62,500
5	$2^{-5}$	1/32	-30.1	0.03125	3.1	31,250
6	$2^{-6}$	1/64	-36.1	0.015625	1.6	15,625
7	$2^{-7}$	1/128	-42.1	0.007812	0.8	7812
8	$2^{-8}$	1/256	-48.2	0.003906	0.4	3906
9	$2^{-9}$	1/512	-54.2	0.001953	0.2	1953
10	$2^{-10}$	1/1024	-60.2	0.0009766	0.1	977
11	$2^{-11}$	1/2048	-66.2	0.00048828	0.05	488
12	$2^{-12}$	1/4096	-72.2	0.00024414	0.024	244
13	$2^{-13}$	1/8192	-78.3	0.00012207	0.012	122
14	$2^{-14}$	1/16,384	-84.3	0.000061035	0.006	61
15	$2^{-15}$	1/32,768	-90.3	0.0000305176	0.003	31
16	$2^{-16}$	1/65,536	-96.3	0.0000152588	0.0015	15
17	$2^{-17}$	1/131,072	-102.3	0.00000762939	0.0008	7.6
18	$2^{-18}$	1/262,144	-108.4	0.000003814697	0.0004	3.8
19	$2^{-19}$	1/524,288	-114.4	0.000001907349	0.0002	1.9
20	$2^{-20}$	1/1,048,576	-120.4	0.0000009536743	0.0001	0.95

number. All V/F converters are of the *integrating* type because the number of pulses per second, or *frequency*, is proportional to the *average* value of the input voltage.

By using a V/F converter, a conversion to a digital format can be performed in the most simple and economical manner. The time required to convert an analog voltage into a digital number relates to a full-scale frequency of the V/F converter and the required resolution. Generally, the V/F converters are relatively slow, as compared with successive-approximation devices, however, they are quite appropriate for many sensor applications. When acting as an ADC, the V/F converter is coupled to a counter which is clocked with the required sampling rate. For instance, if a full-scale frequency of the converter is 32 kHz, and the counter is clocked eight times per second, the highest number of pulses which can be accumulated every counting cycle is 4000 which approximately corresponds to a resolution of 12 bit (see Table 6.3). By using the V/F converter and counter, an integrator can be build for the applications, where the stimulus needs to be integrated over a certain time. The counter accumulates pulses over the gated interval rather than as an average number of pulses per counting cycle.

Another useful feature of a V/F converter is that output pulses can be easily transmitted through communication lines. The pulsed signal is much less susceptible to noisy environment than a high-resolution analog signal. In the ideal



**Fig. 6.25** Charge-balance V/F converter

case, the output frequency  $f_{\text{out}}$  of the converter is proportional to the input voltage  $V_{\text{in}}$ :

$$\frac{f_{\text{out}}}{f_{\text{FS}}} = \frac{V_{\text{in}}}{V_{\text{FS}}}, \quad (6.38)$$

where  $f_{\text{FS}}$  and  $V_{\text{FS}}$  are the full-scale frequency and input voltage, respectively. For a given linear converter, ratio  $f_{\text{FS}}/V_{\text{FS}} = G$  is constant and is called a conversion factor:

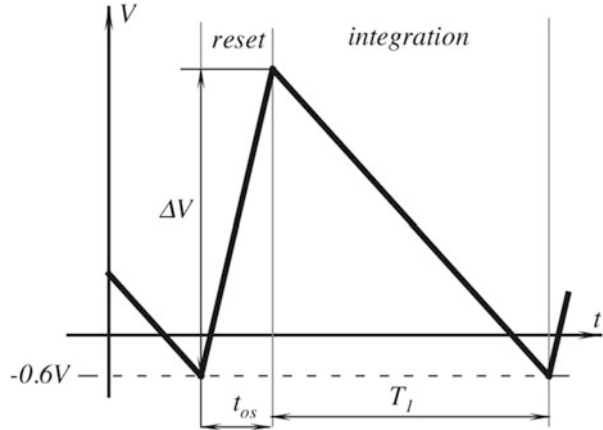
$$f_{\text{out}} = GV_{\text{in}}. \quad (6.39)$$

There are several known types of V/F converters. The most popular of them are the multivibrator and the charge-balance circuit.

A *multivibrator* V/F converter employs a free-running square-wave oscillator where charge-discharge currents of a timing capacitor are controlled by the input signal. However, a more accurate type is the *charge-balance* type of converter that employs an analog integrator and a voltage comparator as shown in Fig. 6.25. This circuit has such advantages as high speed, high linearity, and good noise rejection. The circuit is available in an integral form from several manufacturers, for instance, AD652 from Analog Devices and LM331 from Texas Instruments.

The converter operates as follows. Input voltage  $V_{\text{in}}$  is applied to an integrator through the input resistor  $R_{\text{in}}$ . The integrating capacitor is connected as a negative feedback loop to the operational amplifier whose output voltage is compared with a small negative threshold of  $-0.6$  V. The integrator generates a saw-tooth voltage (Fig. 6.26) that at the moment of comparison with the threshold results in a transient at the comparator's output. That transient enables a one-shot generator to produce a square pulse of a fixed duration  $t_{\text{os}}$ . A precision current source generates constant current  $i$  which is alternatively applied either to the summing node of the integrator, or to its output. The switch  $S_1$  is controlled by the one-shot pulses. When the current source is connected to the summing node, it delivers a precisely defined packet of charge  $\Delta Q = it_{\text{os}}$  to the integrating capacitor. The same summing node also receives

**Fig. 6.26** Integrator output in charge-balanced V/F converter



an input charge through the resistor  $R_{in}$ , thus the net charge is accumulated on the integrating capacitor  $C_{in}$ .

When the threshold is reached, the one-shot generator is triggered and the switch  $S_1$  changes its state to high, thus initiating a reset period. During the reset period, the current source delivers its current to the summing node of the integrator. The input current charges the integrating capacitor upward. The total voltage between the threshold value and the end of the deintegration is determined by the duration of a one-shot pulse:

$$\Delta V = t_{os} \frac{dV}{dt} = t_{os} \frac{i - I_{in}}{C_{in}}. \quad (6.40)$$

When the output signal of the one-shot circuit goes low, switch  $S_1$  diverts current  $i$  to the output terminal of an integrator, which makes no effect on the state of the integrating capacitor  $C_{in}$ . That is, the current source sinks a portion of the output current from the operational amplifier. This time is called the integration period. During the integration, the positive input voltage delivers current  $I_{in} = V_{in}/R_{in}$  to the capacitor  $C_{in}$ . This causes the integrator to ramp down from its positive voltage with the rate proportional to  $V_{in}$ . The amount of time required to reach the comparator's threshold is:

$$T_1 = \frac{\Delta V}{dV/dt} = t_{os} \frac{i - I_{in}}{C_{in}} \frac{1}{I_{in}/C_{in}} = t_{os} \frac{i - I_{in}}{I_{in}}. \quad (6.41)$$

It is seen that the capacitor value does not affect duration of the integration period.

The output frequency is determined by:

$$f_{out} = \frac{1}{t_{os} + T_1} = \frac{I_{in}}{t_{os}i} = \frac{V_{in}}{R_{in}} \frac{1}{t_{os}i}. \quad (6.42)$$

Therefore, the frequency of one-shot pulses is proportional to the input voltage. It depends also on quality of the integrating resistor, stability of the current generator,



and a one-shot circuit. With a careful design, this type of a V/F converter may reach nonlinearity error below 100 ppm and can generate frequencies from 1 Hz to 1 MHz.

A major advantage of the integrating-type converters, such as a charge-balanced V/F converter, is the ability to reject large amounts of additive noise. By integrating of the measurement, noise is reduced or even totally eliminated. Pulses from the converter are accumulated for a gated period  $T$  in a counter. Then, the counter behaves like a filter having a transfer function in the form

$$H(f) = \frac{\sin \pi f T}{\pi f T}, \quad (6.43)$$

where  $f$  is the frequency of pulses. For low frequencies, value of this transfer function  $H(f)$  is close to unity, meaning that the converter and the counter make correct measurements. However, for a frequency  $1/T$  the transfer function  $H(1/T)$  is zero, meaning that these frequencies are completely rejected. For example, if gating time  $T = 16.67$  ms which corresponds to a frequency of 60 Hz (the power line frequency which is a source of substantial noise in many sensors) the 60 Hz noise will be rejected. Moreover, the multiple frequencies (120 Hz, 180 Hz, 240 Hz, and so on) will also be rejected.

### 6.4.3 PWM Converters

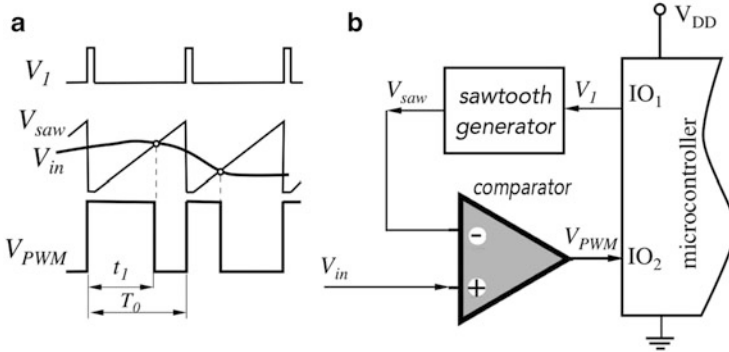
The *pulse-width modulation* (PWM) in many respects is similar to FM. The main difference is that in PWM, period  $T_0$  of the square pulses remains constant (therefore frequency of pulses is also constant), while the pulse duration  $t_{\text{PWM}}$  is proportional to the input voltage. In other words, a duty cycle  $D$  is proportional to voltage:

$$D = \frac{t_{\text{PWM}}}{T_0} = kV_{\text{in}}, \quad (6.44)$$

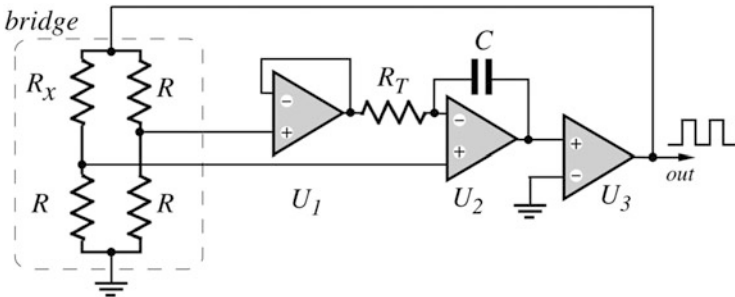
where  $k$  is the conversion constant. Theoretically, duty cycle varies from 0 to 1, however, practically, it has a bit narrower range, typically from 0.05 to 0.95, thus utilizing the period  $T_0$  with about 0.9 or 90 % efficiency.

To make conversion from PWM signal to a binary code, a PWM pulse can be used as a gating function for a high-frequency pulse train and the subsequent counting of the gated pulses. For example, if period  $T_0$  is 10 ms (the PWM conversion is with frequency  $F_0 = 1/T_0 = 100$  Hz) and the pulse train is of 1 MHz ( $10^6$  Hz), then with a PWM efficiency 0.9, each PWM pulse can gate maximum  $10^6/10^2 \times 0.9 = 9000$  high-frequency pulses. This is approximately equivalent to a 13-bit resolution (see Table 6.3).

A PWM modulator can be implemented with a saw-tooth generator as shown in Fig. 6.27. The reset pulses (voltage  $V_1$ ) of a fixed period  $T_0$  are generated by the microcontroller at its  $\text{IO}_1$ . Each  $V_1$  pulse starts generation by the saw-tooth generator of a positive ramp  $V_{\text{saw}}$ . Input voltage  $V_{\text{in}}$  and  $V_{\text{saw}}$  are fed to the



**Fig. 6.27** Voltages (a) and block diagram of PWM converter with a microcontroller (b)



**Fig. 6.28** Schematic of R/F converter for Wheatstone bridge

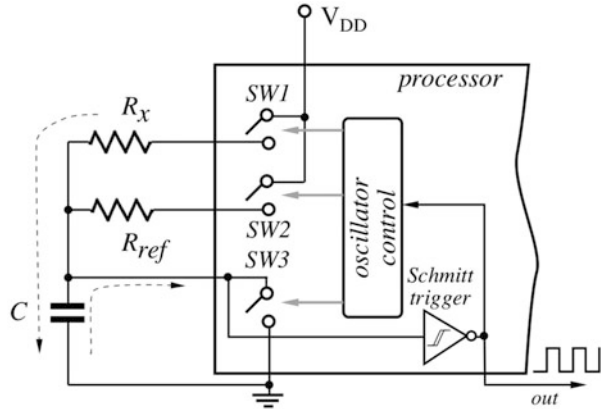
respective noninverting and inverting inputs of the analog comparator, whose output is a PWM pulse  $V_{PWM}$ . The next reset pulse clears and restarts the saw-tooth generator and a new cycle starts. The PWM pulses may be provided to the IO<sub>2</sub> of the microcontroller whose firmware may control a further conversion of PWM to a binary code.

### 6.4.4 R/F Converters

For a resistive sensor, a conversion to a digital format can be performed without an intermediate conversion of resistance to voltage. In a direct conversion, the sensor is used as a component in a pulse modulator, usually as a frequency modulator of an oscillator.

As a first example of this approach we discuss an R/F converter for a resistive Whetstone bridge, where resistance of the sensor  $R_x = R + \Delta R$ . Figure 6.28 illustrates a simplified schematic [8] of a bridge being part of a free-running relaxation-type oscillator. The oscillator comprises a timing capacitor  $C$  and timing resistor  $R_T$  that define the base frequency  $f_0$  when the bridge is perfectly balanced.

**Fig. 6.29** Ratiometric resistance-to-frequency converter



The circuit also contains a voltage follower  $U_1$ , integrator  $U_2$ , and comparator  $U_3$ . A positive feedback from  $U_3$  to the resistive bridge results in a continuous generation of square pulses whose frequency deviation  $\Delta f$  is a linear function of the bridge disbalance  $\Delta R$ :

$$\Delta f = \frac{\Delta R}{2R} f_0 \quad (6.45)$$

Another R/F approach utilizes a microprocessor as illustrated in Fig. 6.29. A resistive sensor  $R_x$ , for example—a thermistor or resistive humidity sensor, and a reference resistor  $R_{ref}$  are connected to a capacitor  $C$ . Under command of the oscillator control circuit, the capacitor can be charged from the power supply voltage  $V_{DD}$  via one of these resistors and discharged to ground through the solid-state switch SW3. Initially, the switch SW2 stays open, while the sensing resistor  $R_x$  is connected to the capacitor via the charging SW1 that is alternatively turned on and off out of phase with the discharging SW3. The capacitor  $C$  develops a saw-tooth voltage that is fed to a Schmitt trigger producing pulses whose frequency  $f_x$  is function of the sensor resistor  $R_x$  and capacitor  $C$ . The processor for some fixed time accumulates and counts these pulses to measure their frequency related to the stimulus.

The next phase is generating the reference pulses by the same circuit, except that the switch SW1 stays open and SW2 alternates with SW3 to use  $R_{ref}$  for charging  $C$ . The new frequency is  $f_{ref}$  and again for the same fixed time the processor accumulates and counts these reference pulses. After both frequencies are measured, the output digital number representing the stimulus that modulates  $R_x$  is computed as a ratio:

$$x = \frac{f_{ref}}{f_x} = \frac{R_x}{R_{ref}} \quad (6.46)$$

Thanks to the ratiometric technique, output (Eq. 6.46) depends only on resistors  $R_{ref}$  and  $R_x$ , while all other factors, such as capacitance  $C$ , power supply

voltage, thermal effects, circuit characteristics, and other interfering factors are cancelled out. This method was utilized in the integrated circuit S1C6F666 from Epson.

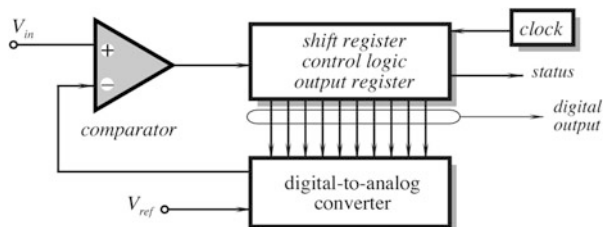
### 6.4.5 Successive-Approximation Converter

These converters are widely used in a monolithic form thanks to their high speed (up to 1 MHz sampling rates) and high resolution (16 bit and higher). Conversion time is fixed and independent of the input signal. Each conversion is unique, as the internal logic and registers are cleared after each conversion, thus making these ADC converters suitable for a multichannel multiplexing. The converter (Fig. 6.30) consists of a precision voltage comparator, a module comprising shift registers and a control logic, and a digital-to-analog converter (DAC) that serves as a feedback from the digital outputs to the input analog comparator.

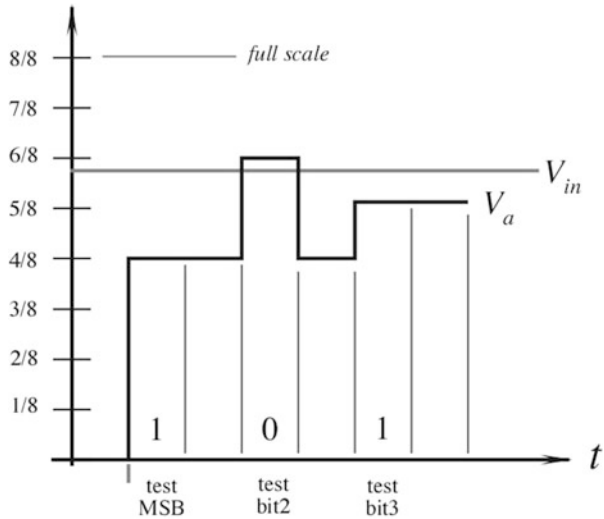
The conversion technique consists of comparing the unknown input,  $V_{in}$ , against a precise voltage,  $V_a$ , or current generated by the DAC. The conversion technique is similar to a weighing process using a balance, with a set of  $n$  binary weights (for instance, 1/2 kg, 1/4 kg, 1/8 kg, 1/16 kg, etc. up to total of 1 kg). Before the conversion cycles, all the registers must be cleared and the comparator's output is HIGH. The DAC has MSB (1/2 scale) at its inputs and generates an appropriate analog voltage,  $V_a$ , equal to 1/2 of a full-scale input signal. If the input is still greater than the DAC voltage (Fig. 6.31), the comparator remains HIGH, causing "1" at the register's output. Then, the next bit (2/8 = 1/4 of FS) is tried. If the second bit does not add enough weight to exceed the input, the comparator remains HIGH ("1" at the output), and the third bit is tried. However, if the second bit tips the scale too far, the comparator goes LOW resulting in "0" in the register, and the third bit is tried. The process continues in order of descending bit weight until the last bit has been tried. After the completion, the status line indicates the end of conversion and data can be read from the register as a valid number corresponding to the input signal.

To make the conversion valid, the input signal  $V_{in}$  must not change until all the bits are tried, otherwise, the digital reading may be erroneous. To avoid any problems with the changing input, a successive-approximation converter usually is supplied with a sample-and-hold (S&H) circuit. This circuit is a short-time analog memory that samples the input signal and stores it as a dc voltage during an entire conversion cycle.

**Fig. 6.30** Block Diagram of successive-approximation DAC



**Fig. 6.31** 3-Bit weighing in successive-approximation ADC



### 6.4.6 Resolution Extension

In a typical data acquisition system, many low-cost monolithic microcontrollers contain analog-to-digital converters, whose maximum resolutions are limited to 10 or 12 bits. When the resolution of a built-in converter is higher, or an external converter of a high resolution is used, the cost may become prohibitively high. In many applications, 12 bits may be not sufficient for a correct representation of a minimum increment of a stimulus (the required input resolution  $R_0$ ). There are several ways of resolving this problem. One is to use an analog amplifier in front of the ADC. For example, an amplifier of gain 4 will effectively increase the input resolution  $R_0$  by two bits, say from 12 to 14. Of course, the price to pay is an uncertainty in the amplifier's characteristics. Another method of achieving higher resolution is to use a dual-slope ADC converter whose resolution limited only by the available counter rate and the speed response of a comparator.<sup>2</sup> And another method is to use a 12-bit ADC converter (for instance, of a successive-approximation type) with a resolution extension circuit. Such a circuit can boost the resolution by several bits, for instance from 12 to 15. A block diagram of the resolution extension circuit is shown in Fig. 6.32a. In addition to a conventional 12-bit ADC converter, it includes a digital-to-analog converter (DAC), a subtraction circuit, and an amplifier having gain  $A$ . In the ASIC or discrete circuits, a DAC may be shared with the ADC part (see Fig. 6.30).

<sup>2</sup> A resolution should not be confused with accuracy.

The input signal  $V_m$  has a full-scale value  $E$ , thus for instance, if we have a 12-bit ADC, the initial resolution will be:

$$R_0 = E/(2^{12} - 1) = E/4095, \quad (6.47)$$

which is expressed in volts per bit. For instance, for  $E = 5$  V, the 12-bit resolution is 1.22 mV/bit. Initially, the multiplexer (MUX) connects the input signal to the ADC which produces the output digital value,  $M$ , which is expressed in bits. Then, the microprocessor outputs that value to the DAC that produces the output analog voltage  $V_c$ , which is an approximation of the input signal. This voltage is subtracted from the input signal and the difference is amplified by the amplifier to value

$$V_D = (V_m - V_c) \cdot A \quad (6.48)$$

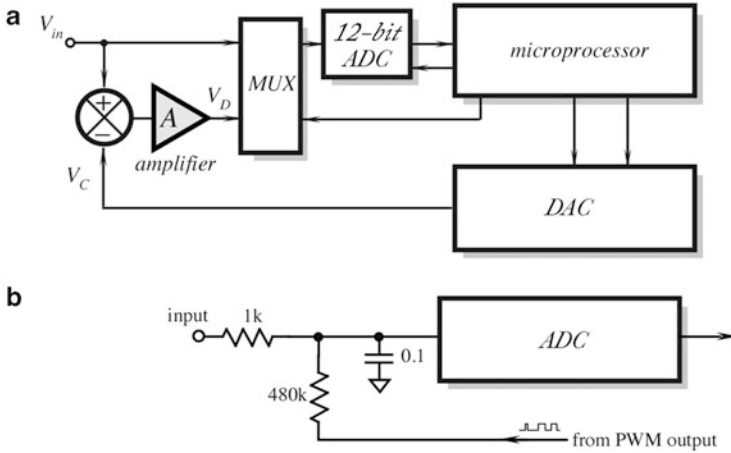
The voltage  $V_D$  is an amplified error between the actual and digitally represented input signals. For a full-scale input signal, the maximum error ( $V_m - V_c$ ) is equal to a resolution of an ADC converter, therefore, for an 12-bit conversion  $V_D = 1.22 \cdot A$  mV. The multiplexer connects that voltage to the ADC converter which converts  $V_D$  to a digital value  $C$ :

$$C = \frac{V_D}{R_0} = (V_m - V_c) \frac{A}{R_0}. \quad (6.49)$$

As a result, the microprocessor combines two digital values:  $M$  and  $C$ , where  $C$  represents the high-resolution bits. If  $A = 255$ , then for the 5-V full-scale,  $\text{LSB} \approx 4.8 \mu\text{V}$  which corresponds to a total resolution of 20 bit. In practice, it is hard to achieve such a high resolution because of the errors originated in the DAC, reference voltage, amplifier's drift, noise, etc. Nevertheless, the method is quite efficient when a modest resolution of 14 or 15 bit is deemed to be sufficient.

Another powerful method of a resolution extension is based on the so-called *oversampling* [9]. The idea works only if the input analog signal is changing between the sampling points. For example, if the ADC conversion steps are at 50 mV, 70 mV, 90 mV, etc., while the input signal is steady 62 mV, the digital number will indicate 70 mV, thus producing a digitization error of 8 mV and no oversampling would make any difference. However, if the input signal changes with the maximum spectral frequency  $f_m$ , according to the Nyquist-Shannon-Kotelnikov theorem,<sup>3</sup> the sampling frequency  $f_s > 2f_m$ . The oversampling requires a much higher sampling frequency than defined by the Nyquist. Specifically, it is based on the formula

<sup>3</sup> A fundamental theorem of the information theory. It states that the minimum sampling must be twice as fast as the highest frequency of the signal.



**Fig. 6.32** Resolution enhancement circuit with DAC (a); adding artificial noise to input signal for oversampling (b)

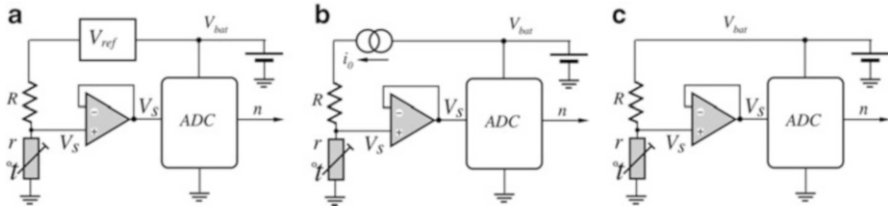
$$f_{os} > 2^{2+n} f_m, \tag{6.50}$$

where  $n$  is a number of the extension bits. For example, if we have a 10-bit ADC and would like to generate with it a number of 12-bits ( $n = 2$ ), the sampling rate must be at least 16 times higher than  $f_m$ . The oversampling allows trading a resolution of an ADC conversion for the maximum converted frequency. Thus, this method is useful for converting relatively slow changing signals as compared with the maximum sampling rate of an ADC.

As it was said above, the method requires the signal to change between samplings. If the analog signal does not include natural variations or inherent noise, an artificial noise can be added to the input signal or the ADC reference voltage to jitter signal between the samples. A practical method of adding artificial noise is shown in Fig. 6.32b. The microcontroller generates PWM (Pulse-Width Modulated) random-width pulses that are smoothed by a capacitor and added to the analog input signal. The magnitude of jittering must correspond to at least 0.5 LSB of the original resolution but preferably should be about 2 LSB. After sampling, to get an increased resolution,  $2^{2+n}$  samples from the ADC are added and the result is right-shifted  $n$  times. For the above example, 16 sequential 10-bit numbers are added and then right-shifted two times, resulting in a 12-bit output number.

### 6.4.7 ADC Interface

When a sensor or sensing circuit, such as the Wheatstone bridge, is connected to an ADC, it is important to assure that the coupling between the two does not introduce an unexpected error. As we indicated above, a sensor can be powered either by a voltage source (Sect. 6.3.2) or by a current source (Sect. 6.3.1). Further, a voltage



**Fig. 6.33** Powering the sensor circuit with constant voltage (a), constant current (b), and ratiometric voltage (c)

source can be connected by two options: constant voltage and ratiometric. On the other hand, ADC also requires a voltage reference, that may be either internal or external. Thus, to avoid a mismatch between the sensor and ADC, a coupling between the sensor and ADC should consider how the sensor and ADC are referenced? Figure 6.33 illustrates three possibilities for powering (referencing) a resistive sensor—in this example a thermistor  $r$  with a pull-up resistor  $R$ .

A power supply that feeds the sensor may be not very stable, have some ripples, noise, and even may drift substantially during operation. An example is a battery producing voltage  $V_{\text{bat}}$  that drops during discharge. The sensor that requires an excitation power may be fed by a constant voltage as shown in Fig. 6.33a. A constant voltage is produced by a precision voltage reference  $V_{\text{ref}}$  whose value is independent of the battery voltage  $V_{\text{bat}}$  (see Sect. 6.3.3). Thus, the sensor's voltage divider outputs  $V_r$  that depends only on the sensor, pull-up resistor, and reference voltage. This method is used when ADC has its own precision voltage reference, thus conversion to a digital format is not affected by the battery.

Some sensor applications require a constant current  $i_0$  excitation (Fig. 6.33b). In that case, the divider output  $V_r$  depends on two factors: the constant current and sensor resistance  $r$ . As in the previous case, to be independent of the battery, the ADC must have its own voltage reference.

An efficient way of powering a sensor is to use a ratiometric technique, where both the sensor and ADC are powered from the same voltage source (battery) that does not have to be regulated (Fig. 6.33c). It is important that ADC uses  $V_{\text{bat}}$  as its reference. Thus, the output ADC counts are proportional to the battery voltage. Here is how it works.

Voltage from the sensor at the ADC input depends on the battery:

$$V_r = \frac{r}{r+R}V_{\text{bat}}, \quad (6.51)$$

while ADC transfer function is also battery dependent. Its output digital count  $n$  is:

$$n = \frac{V_r}{V_{\text{bat}}}N_{\text{FS}}, \quad (6.52)$$



where  $N_{FS}$  is the maximum ADC count or MSB (most significant bit) corresponding to the maximum (full-scale) input voltage. Substituting Eq. (6.51) into Eq. (6.52) we arrive at the output count as function of the sensor resistance:

$$n = \frac{r}{r + R} N_{FS} \quad (6.53)$$

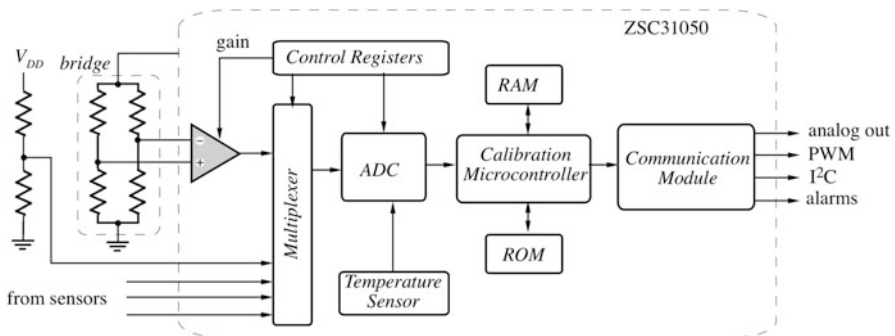
We see that the digital output is independent of the power supply voltage and relates only to the sensor's and pull-up resistances.

## 6.5 Integrated Interfaces

In the past, an application engineer had to design her own interface circuit and often that was a challenge. The modern trend in signal conditioning is to integrate in a single chip the amplifiers, multiplexers, ADC, memory, and other circuits (see Sect. 3.1.2). This frees the application engineers from designing the interface and signal-conditioning circuits—few engineers might have an experience in designing such systems. Thus, standardized interfaces are the reliable and efficient solutions. Below are two examples of many highly useful commercially available integrations.

### 6.5.1 Voltage Processor

Figure 6.34 illustrates an integrated signal conditioning circuit on a single chip ZSC31050 from the German company ZMDI ([www.zmdi.com](http://www.zmdi.com)). It is optimized for several low-voltage and low-power multiple sensors, including a resistive bridge. The differential voltage from the bridge sensor is preamplified by the programmable gain amplifier and, along with several other sensor signals, fed to the multiplexer. The multiplexer transmits the signals, including one from the internal temperature sensor, to the ADC in a specific sequence. Next, the ADC converts



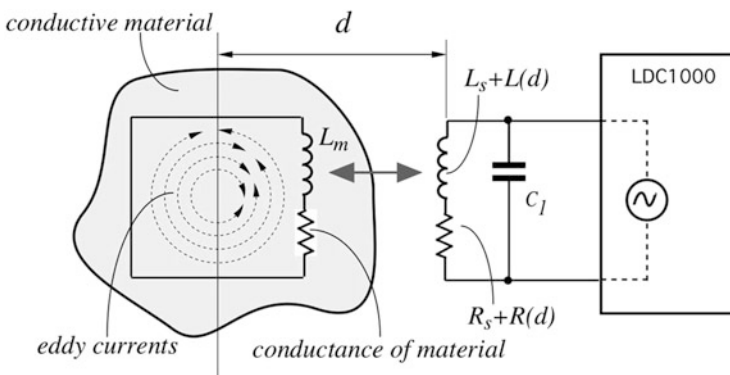
**Fig. 6.34** Integrated ZMDI Signal Conditioner

these signals into 15-bit digital values. The digital signal correction takes place in the calibration microcontroller. The correction is based on sensor-specific formulas residing in the ROM and the sensor-specific calibrating coefficients (stored in the EEPROM during calibration). Depending on the programmed output configuration, the corrected sensor signal goes to the output through the communication module as analog voltage, PWM signal, or in various communication formats, includes a serial link  $I^2C$ . The configuration data and the correction parameters can be programmed into the EEPROM via the digital interfaces. The modular circuit concept used in the design of the ZSC31050 allows fast customization of the IC for high-volume applications.

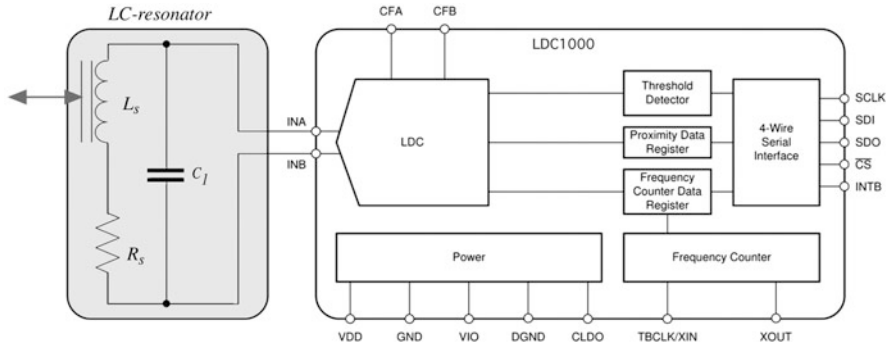
### 6.5.2 Inductance Processor

Magnetic sensors operating on the inductive principle are highly popular for detecting proximity, presence of magnetic and conductive objects, measuring electrical impedance, etc. Many of these sensors are described throughout this book. The chip LDC1000 from TI is an integrated inductance-to-digital converter (LDC) that monitors a combined impedance of an external resonant tank consisting of an inductive coil ( $L$ ) and capacitor ( $C$ ). Loss of power in the tank is function of its inductive coupling with the outside. By monitoring the loss through measuring the LC-resonator's parallel loss resistivity it is possible to monitor the external conductive objects with high degree of accuracy.

Consider Fig. 6.35 where inductance  $L$  of the sensing coil causes the circular eddy currents in a conductive material positioned at some distance  $d$  from the coil. An a.c. current flowing through a coil generates an a.c. magnetic field. If a conductive material, such as a target made of metal, is brought into the vicinity of the coil, the alternate magnetic field will induce circulating eddy currents inside the target. These eddy currents are a function of the distance, size, and



**Fig. 6.35** Generation of eddy currents in conductive material



**Fig. 6.36** Block diagram of integrated inductance-to-digital converter (adapted from TI data sheet of LDC1000)

composition of the target. The eddy currents then generate their own magnetic field, that according to Lenz law, opposes the original field generated by the coil. This mechanism is best compared to a transformer, where the coil is the primary core and the eddy current is the secondary core. The inductive coupling between both cores depends on distance and shape. Hence the resistance and inductance of the secondary core shows up as a distant-dependent loss resistive  $R(d)$  and inductive  $L(d)$  components on the primary side (coil). The conductive material shifts the resonant frequency of the LC-resonator and increases the loss resistance.

When the resonant shifts, a value of the power loss is the measure of the external object properties (distance, composition, size, etc.). The integrated circuit (Fig. 6.36) LDC1000 does not measure the series loss resistance directly; instead it measures the equivalent parallel resonance impedance of the LC circuit that operates in the range from 5 kHz to 5 MHz. The measured impedance is digitized with a 16-bit resolution and processed by the integrated circuit.

## 6.6 Data Transmission

Signal from a sensor may be transmitted to a receiving end of the system either in a digital format or analog. In most cases, a digital format essentially requires use of an analog-to-digital converter at the sensor's site. Transmission in a digital format has several advantages, the most important of which is a noise immunity. Since transmission of digital information is beyond the scope of this book we will not discuss it further. In many cases, however, digital transmission cannot be done for some reasons. Then, the sensor's output signal is transmitted to the receiving site in an analog form. Depending on connection, transmission methods can be divided into a two, four, and six-wire methods.

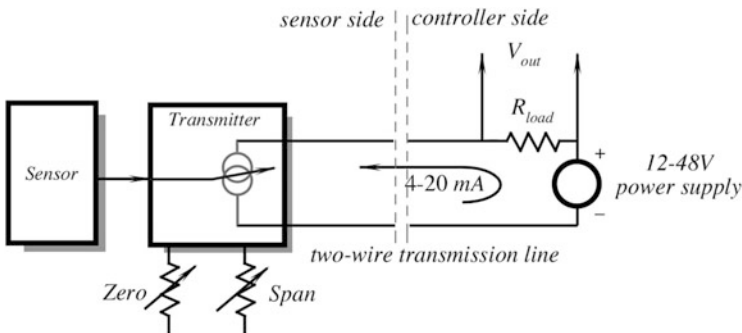
### 6.6.1 Two-Wire Transmission

The two-wire analog transmitters are used to couple sensors to control and monitoring devices in the process industry [10]. For example, when a temperature measurement is taken within a process, a two-wire transmitter relays that measurement to the control room or interfaces the analog signal directly to a process controller. Two wires can be used to transmit either voltage or current, however, current was accepted as an industry standard. The current carried by a two-wire loop varies in the range from 4 to 20 mA which represents the entire span of input stimuli. The minimum stimulus corresponds to 4 mA while the maximum to 20 mA.

Two wires form a loop (Fig. 6.37) of serially connected *two-wire transmitter*, conductors, power supply, and the load resistor  $R_{load}$ . The transmitter may be a voltage-to-current converter. That is, it converts the sensor signal into a variable current in a 4–20 mA range. The load resistor  $R_{load}$  develops output voltage representing the stimulus. When the sensor signal varies, the transmitter's output current varies accordingly and so the voltage across  $R_{load}$ . For example, if  $R_{load} = 250 \Omega$ , the output voltage varies from 1 to 5 V.

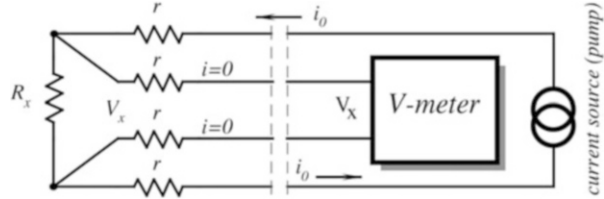
The same current that carries information about the stimulus may also be used by the transmitter side to harvest its operating power. The lowest sensor signal produces a 4 mA current that often is sufficient for powering the transmitting side of the loop. Thus, the same two-wire loop is used for both the information transmission and delivering power to the sensor and transmitter.

The advantage of a two-wire current loop is that the loop current is independent of  $R_{load}$  and the connecting wires resistance, obviously within the limits. Since the current is produced by a current generator having very large output impedance (see Sect. 6.3.1), it remains independent on many disturbing factors, including voltages induced to the loop by external noise sources.



**Fig. 6.37** Two-wire 4–20 mA analog data transmission

**Fig. 6.38** Remote measurements of resistive sensor by 4-wire transmission



## 6.6.2 Four-Wire Transmission

Sometimes, it is desirable to connect a resistive sensor to a remotely located interface circuit. When such a sensor has a relatively low resistance (for instance, it is normal for piezoresistors or RTDs to have resistances on the order of  $100\ \Omega$ ), the connecting wire resistances pose a serious problem since they alter the excitation voltage across the sensor and add up to the sensor's resistance. The problem can be solved by using the so-called *four-wire* method shown in Fig. 6.38. The method allows measuring resistance of a remote sensor without accounting for the connecting conductors. A sensor is connected to the interface circuit through four wires. Two pairs of wires form two loops: a current loop (excitation) and voltage loop. The excitation loop includes two wires that are connected to a current source-generating excitation current  $i_0$ . The voltage loop wires are attached to a voltmeter or amplifier. A constant current source (current pump) has a very high-output resistance (see Sect. 6.3.1), therefore current  $i_0$  in the current loop is independent of the sensor  $R_x$  and any resistance  $r$  of the wire loop. Thus, effect of wires is eliminated.

The input impedance of a voltmeter or amplifier is very high in comparison with any resistances in the voltage loop, hence no current is diverted from the current loop to the voltmeter, therefore wire resistances  $r$  that are in the voltage loop also can be ignored. A voltage drop across the sensor resistor  $R_x$  is

$$V_x = R_x i_0, \quad (6.54)$$

which is independent of any resistances  $r$  of the connecting wires. The four-wire method is a very powerful means of measuring resistances of remote detectors and is used in industry and science quite extensively.

## 6.7 Noise in Sensors and Circuits

*Noise* in sensors and circuits may present a substantial source of errors and should be seriously considered. Like diseases, noise is never eliminated, just prevented, cured, or endured, depending on its nature, seriousness, and the cost/difficulty of treating. There are two basic types of noise for a given circuit: they are *inherent* noise, which is noise arising within the circuit, and *interference (transmitted)* noise, which is noise picked up from outside the circuit.

Any sensor, no matter how well it was designed, never produces electric signal, which is an ideal representation of the input stimulus. Often, it is a matter of judgment to define the goodness of the signal. The criteria for this are based on the specific requirements to accuracy and reliability. Distortions of the output signal can be either *systematic* or *stochastic*. The former are related to the sensor's transfer function, its linearity, dynamic characteristics, etc. They all are the results of the sensor's design, manufacturing tolerances, material quality, and calibration. During a reasonably short time, these factors either do not change or may drift relatively slowly. They can be well defined, characterized, and specified (see Chap. 3). In many applications, such a determination may be used as a factor in the error budget and can be accounted for. Stochastic disturbances, on the other hand, often are irregular, unpredictable to some degree and may change rapidly. Generally, they are termed *noise*, regardless of their nature and statistical properties. It should be noted that word *noise*, in association with audio equipment noise, is often mistaken for an irregular, somewhat fast changing signal. We use this word in a much broader sense for all disturbances, either in stimuli, environment, or in components of the sensors and circuits from dc to the upper operating frequencies.

### 6.7.1 Inherent Noise

Signal which is amplified and converted from a sensor into a digital format should be regarded not just by its magnitude and spectral characteristics, but also in terms of a digital resolution. When a conversion system employs an increased digital resolution, the value of the least-significant bit (LSB) decreases. For example, the LSB of a 10-bit system with a 5 V full scale is about 5 mV, the LSB of 16 bits is 77  $\mu\text{V}$ . This by itself poses a significant problem. It makes no sense to employ, say a 16-bit resolution system, if a combined noise is, for example, 300  $\mu\text{V}$ . In a real world, the situation is usually much worse. There are just few sensors that are capable of producing a 5 V full-scale output signals. Most of them require amplification. For instance, if a sensor produces a full-scale output of 5 mV, at a 16-bit conversion it would correspond to a LSB of 77 nV—an extremely small signal which makes amplification an enormous task by itself. Whenever a high resolution of a conversion is required, all sources of noise must be seriously considered. In electrical circuits, noise can arise within the monolithic amplifiers and other components which are required for the feedback, biasing, filtering, etc.

Input offset voltages and bias currents may drift. In d.c. circuits, they are indistinguishable from the low magnitude signals produced by a sensor. These drifts are usually slow (within a bandwidth of tenths and hundredths of a Hz), therefore they are often called ultralow frequency noise. They are equivalent to random or predictable (e.g., temperature dependent) changing voltage and current offsets and biases. To distinguish them from the higher frequency noise, the equivalent circuit (Fig. 6.3) contains two additional generators. One is a *voltage offset* generator  $e_0$  and the other is a *current bias* generator  $i_0$ . The noise signals (voltage and current) result from physical mechanisms within the resistors and

semiconductors that are used to fabricate the circuits. There are several sources of noise whose combined effect is represented by the noise voltage and current generators.

One cause for noise is a discrete nature of electric current because current flow is made up of moving charges, and each charge carrier transports a definite value of charge (charge of an electron is  $1.6 \times 10^{-19}$  C). At the atomic level, current flow is very erratic. The motion of the current carriers resembles popcorn popping. This term was chosen as a good analogy for current flow and has nothing to do with the “popcorn noise” which we will discuss below. Just as popcorn, the electron movement may be described in statistical terms. Therefore, one never can be sure about very minute details of current flow. The movement of carriers are temperature related and noise power, in turn, is also temperature related. In a resistor, these thermal motions cause *Johnson noise* [11]. The mean-square value of noise voltage (which is representative of noise power) can be calculated from

$$\overline{e_n^2} = 4kTR\Delta f \text{ [V}^2/\text{Hz}] , \quad (6.55)$$

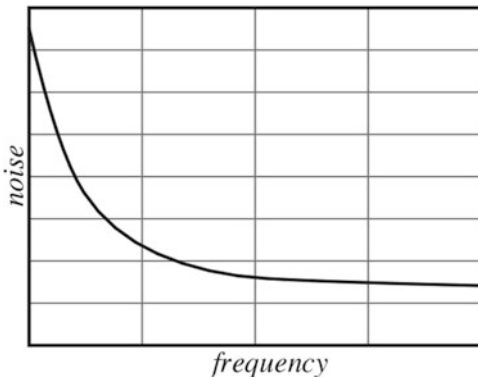
where  $k = 1.38 \times 10^{-23}$  J/K (Boltzmann constant),  $T$  is temperature in K,  $R$  is the resistance in  $\Omega$ , and  $\Delta f$  is the bandwidth over which the measurement is made, in Hz.

For practical purposes, noise generated by a resistor at room temperature may be estimated from a simplified formula  $\overline{e_n} \approx 0.13\sqrt{R \cdot \Delta f}$  in nV. For example, if noise bandwidth is 100 Hz and the resistance of concern is 10 M $\Omega$  ( $10^7 \Omega$ ), the average Johnson noise voltage at room temperature is estimated as  $\overline{e_n} \approx 0.13\sqrt{10^7}\sqrt{100} \approx 4 \mu\text{V}$ .

Even a simple resistor is a source of noise, behaving as a perpetual generator of random electric signal. Naturally, relatively small resistors generate extremely small noise, however, in some sensors Johnson noise must be taken into account. For instance, a typical pyroelectric detector uses a bias resistor on the order of 50 G $\Omega$ . If a sensor is used at room temperature within a bandwidth of 10 Hz, one may expect the average noise voltage across the resistor to be on the order of 0.1 mV—a pretty high value. To keep noise at bay, bandwidths of the interface circuits must be maintained small, just wide enough to pass the minimum required signal. It should be noted that noise voltage is proportional to square root of the bandwidth. It implies that if we reduce the bandwidth 100 times, average noise voltage will be reduced by a factor of 10. Johnson noise magnitude is constant over a broad range of frequencies. Hence, it is often called *white noise* because of the similarity to white light, which is composed of all the frequencies in the visible spectrum.

Another type of noise results from dc current flows in semiconductors. It is called *shot noise*—the name which was suggested by Schottky not in association with his own name but rather because this noise sounded like “a hail of shot striking the target” (nevertheless, shot noise is often called *Schottky noise*). Shot noise is also white noise. Its value becomes higher with increase in the bias current. This is the reason why in FET and CMOS semiconductors the current noise is quite small.

**Fig. 6.39** Spectral distribution of  $1/f$  “pink” noise



For a bias current of 50 pA, it is equal to about  $4 \text{ fA}/\sqrt{\text{Hz}}$ —an extremely small current that is equivalent to movement of about 6000 electrons per second. A convenient equation for shot noise is

$$i_{\text{sn}} = 5.7 \times 10^{-4} \sqrt{I \Delta f}, \quad (6.56)$$

where  $I$  is a semiconductor junction current in pA and  $\Delta f$  is a bandwidth of interest in Hz.

Another a.c. noise mechanism exists at low frequencies (Fig. 6.39). Both the noise voltage and noise current sources have a spectral density roughly proportional to  $1/f$ , which is called the *pink noise*, because of the higher noise contents at lower frequencies (lower frequencies are also at red side of the visible spectrum and red mixing with white makes pink). This  $1/f$  noise occurs in all conductive materials, therefore it is also associated with resistors. At extremely low frequencies, it is impossible to separate the  $1/f$  noise from dc drift effects. The  $1/f$  noise is sometimes called a *flicker* noise. Mostly it is pronounced at frequencies below 100 Hz, where many sensors operate. It may dominate Johnson and Schottky noise and becomes a chief source of errors at these frequencies. The magnitude of pink noise depends on current passing through the resistive or semiconductive material. Nowadays progress in semiconductor technology resulted in significant reduction of  $1/f$  noise in semiconductors, however, when designing a circuit, it is a good engineering practice to use metal film or wirewound resistors in sensors and the front stages of interface circuits wherever significant currents flow through the resistor and low noise at low frequencies is a definite requirement.

Combined noise from all voltage and current sources is given by the sum of squares of individual noise voltages:

$$e_E = \sqrt{e_{n1}^2 + e_{n2}^2 + \dots + (R_1 i_{n1})^2 + (R_1 i_{n2})^2 + \dots}. \quad (6.57)$$

A combined random noise may be presented by its *root mean square* (r.m.s.) value, that is



**Table 6.4** Peak-to-peak value vs. r.m.s. (for Gaussian distribution)

Nominal p-p voltage	% of time that noise will exceed nominal p-p value
$2 \times \text{r.m.s.}$	32.0
$3 \times \text{r.m.s.}$	13.0
$4 \times \text{r.m.s.}$	4.6
$5 \times \text{r.m.s.}$	1.2
$6 \times \text{r.m.s.}$	0.27
$7 \times \text{r.m.s.}$	0.046
$8 \times \text{r.m.s.}$	0.006

$$E_{\text{rms}} = \sqrt{\frac{1}{T} \int_0^T e^2 dt}, \quad (6.58)$$

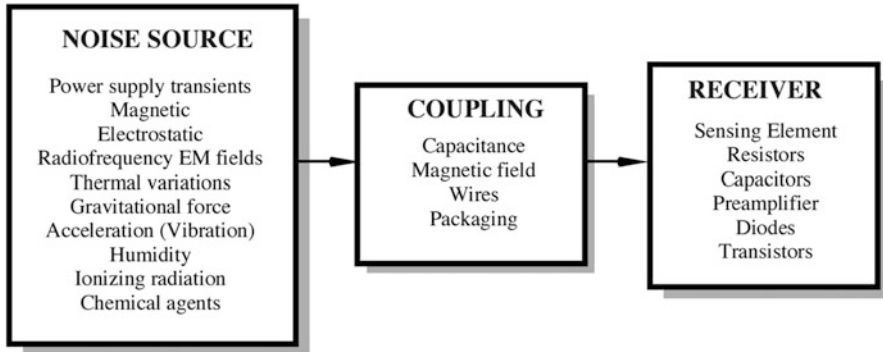
where  $T$  is total time of observation,  $e$  is noise voltage, and  $t$  is time.

Also, noise may be characterized in terms of the peak values which are the differences between the largest positive and negative peak excursions observed during an arbitrary interval. For some applications, in which peak-to-peak (p-p) noise may limit the overall performance (in a threshold-type devices), p-p measurement may be essential. Yet, due to a generally Gaussian distribution of noise signal, p-p magnitude is very difficult to measure in practice. Because r.m.s. values are so much easier to measure repeatedly, and they are the most usual form for presenting noise data noncontroversially, the Table 6.4 should be useful for estimating the probabilities of exceeding various peak values given by the r.m.s. values. The casually-observed p-p noise varies between  $3 \times \text{r.m.s.}$  and  $8 \times \text{r.m.s.}$ , depending on patience of the observer and amount of data available.

### 6.7.2 Transmitted Noise

A large portion of the environmental stability is attributed to immunity of the sensor and interface circuit to noise which is originated in external sources. Figure 6.40 shows a diagram of the transmitted noise propagation. Noise comes from a source which often cannot be identified. Examples of the transmitted noise sources are voltage surges in power lines, lightnings, changes in ambient temperature, sun activity, etc. These interferences propagate toward the sensors and interface circuits, and to present a problem eventually must appear at the outputs. However, before that, they somehow affect the sensing element inside the sensor, its output terminals, or the electronic components in the circuit. Both the sensor and circuit act as receivers of the interferences.

There can be several classifications of transmitted noise, depending on how it affects the output signal, how it enters the sensor or circuit, etc.



**Fig. 6.40** Sources and coupling of transmitted noise

With respect to its relation to the output signals, noise can be either *additive* or *multiplicative*.

### 6.7.2.1 Additive Noise

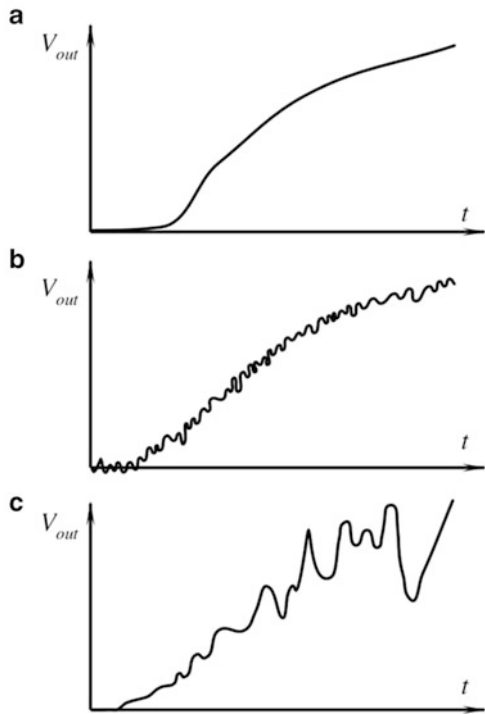
Additive noise  $e_n$  is added to the useful signal  $V_s$  and mixed with it as a fully independent voltage (or current)

$$V_{\text{out}} = V_s + e_n. \quad (6.59)$$

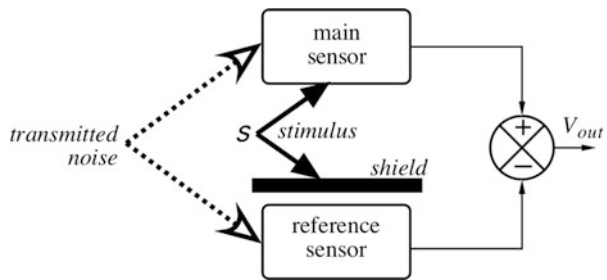
An example of such a disturbance is depicted in Fig. 6.41b. It can be seen, that the noise magnitude does not change when the actual (useful) signal changes. As long as the sensor and interface electronics can be considered linear, the additive noise magnitude is totally independent of the signal magnitude and, if the signal is equal to zero, the output noise still will be present.

To improve noise stability against transmitted additive noise, quite often sensors are combined in pairs, that is, they are fabricated in a dual form whose output signals are subtracted from one another (Fig. 6.42). This method is called a *differential* technique (see Sect. 6.2.2). One sensor of the pair (it is called the main sensor) is subjected to the stimulus of interest  $s_1$ , while the other (reference) is shielded from the stimulus perception. Since additive noise is specific for the linear or quasilinear sensors and circuits, the reference sensor does not have to be subjected to any particular stimulus. Often, it may be equal to zero. It is anticipated that both sensors are subjected to identical transmitted noise (noise generated inside the sensor cannot be cancelled by a differential technique), which is a *common-mode* noise. This means that the noisy effects at both sensors are in-phase and have the same magnitude. If both sensors are identically influenced by the common-mode spurious stimuli, the subtraction removes the noise component. Such a sensor is often called either a dual or a *differential* sensor. Quality of the noise rejection is measured by a number which is called the *common-mode rejection ratio* (CMRR):

**Fig. 6.41** Types of noise: noise-free signal (a); additive noise (b); multiplicative noise (c)



**Fig. 6.42** Differential technique. Shield prevents stimulus  $s$  from reaching reference sensor



$$CMMR = 0.5 \frac{S_1 + S_0}{S_1 - S_0}, \tag{6.60}$$

where  $S_1$  and  $S_0$  are output signals from the main and reference sensors, respectively. CMRR may depend on magnitude of stimuli and usually becomes smaller at greater input signals. The ratio shows how many times stronger the actual stimulus will be represented at the output, with respect to a common mode noise having the same magnitude. The value of the CMRR is a measure of the sensor's symmetry. To be an effective means of noise reduction, both sensors must be positioned as close as possible to each other, they must be very identical and subjected to the same

environmental conditions. Also, it is very important that the reference sensor is reliably shielded from the actual stimulus, otherwise the combined differential response will be diminished.

### 6.7.2.2 Multiplicative Noise

Multiplicative noise affects the sensor's transfer function or the circuit's nonlinear components in such a manner as  $V_s$  signal's value becomes altered or *modulated* by the noise:

$$V_{\text{out}} = [1 + N(t)]V_s, \quad (6.61)$$

where  $N(t)$  is a dimensionless function of noise. An example of such noise is shown in Fig. 6.41c. Multiplicative noise at the output disappears or becomes small (it also may become additive) when the signal magnitude nears zero. Multiplicative noise grows together with the signal's  $V_s$  magnitude. As its name implies, multiplicative noise is a result of multiplication (which essentially is a nonlinear operation) of two values where one is a useful signal and the other is a noise-dependent spurious signal.

To reduce transmitted multiplicative noise, a ratiometric technique should be used instead of a differential (see Sect. 6.2.1). Its principle is quite simple. Like for a differential technique, the sensor is fabricated in a dual form where one part is subjected to the stimulus of interest and both parts are subjected to the same environmental conditions that may cause transmitted multiplicative noise. The first, main sensor is responsive to a stimulus  $s_1$  and is affected by a transmitted noise. The second sensor is called *reference* because a constant fixed reference stimulus  $s_0$  is applied to its input. For example, let us consider a transmitted noise being an ambient temperature that affects both the main and reference sensor identically. The output voltage of a main sensor may be approximated by

$$V_1 \approx F(T)f(s_1), \quad (6.62)$$

where  $F(T)$  is a temperature-dependent function affecting the sensor's transfer function and  $T$  is temperature. Note that  $f(s_1)$  is a noise-free sensor's transfer function. The reference sensor whose fixed reference input is  $s_0$  generates voltage

$$V_0 \approx F(T)f(s_0). \quad (6.63)$$

Taking ratio of the above equations we arrive at

$$\frac{V_1}{V_0} = \frac{1}{f(s_0)}f(s_1). \quad (6.64)$$

Since  $f(s_0)$  is constant, the ratio is not temperature dependent, and thus effect of temperature as a transmitted noise is eliminated. It should be emphasized however, that the ratiometric technique is useful only when the anticipated noise has a

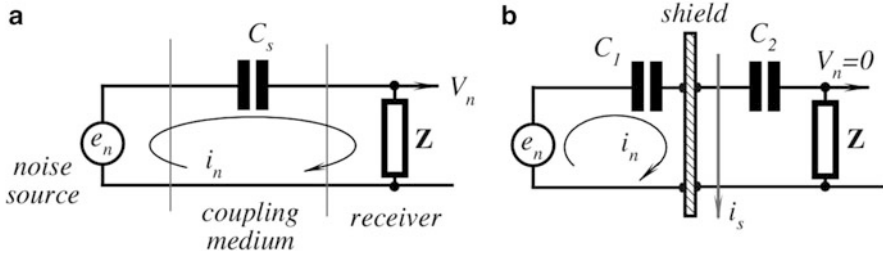
multiplicative nature, while a differential technique works only for additive transmitted noise. Neither technique is useful for inherent noise that is generated internally in sensors and circuits. Also, the reference sensor output may not be zero, nor too small, otherwise Eq. (6.4) will increase enormously. Value of the reference stimulus should be selected near the center of the input stimulus span, as long as the output  $f(s_0)$  is far away from zero.

While inherent noise is mostly Gaussian, the transmitted noise is usually less suitable for conventional statistical description. Transmitted noise may be monotonic and systematic (like temperature effects), periodic, irregularly recurring, or essentially random, and it ordinarily may be reduced substantially by a careful sensor design and taking precautions to minimize electrostatic and electromagnetic pickup from power sources at line frequencies and their harmonics, radio broadcast stations, arcing of mechanical switches, and current and voltage spikes resulting from switching in reactive (having inductance and capacitance) circuits. Temperature effects can be reduced by placing a sensor in a thermostat. The electrical precautions may include filtering, decoupling, shielding of leads and components, use of guarding potentials, elimination of ground loops, physical reorientation of leads, components and wires, use of damping diodes across relay coils and electric motors, choice of low impedances where possible, and choice of power supply and references having low noise. Transmitted noise from vibration may be reduced by proper mechanical design. A list outlining some of the sources of transmitted noise, their typical magnitudes, and some ways of dealing with them is given in Table 6.5.

The most frequent channel for coupling electrical noise is a “parasitic” capacitance. Such a coupling exists everywhere. Any object is capacitively coupled to another object. For instance, a human standing on isolated earth develops a

**Table 6.5** Typical sources of transmitted electric noise (adapted from [12])

External source	Typical magnitude	Typical cure
60/50 Hz power	100 pA	Shielding; attention to ground loops; isolated power supply
120/100 Hz supply ripple	3 $\mu$ V	Supply filtering
180/150 Hz magnetic pickup from saturated 60/50 Hz transformers	0.5 $\mu$ V	Reorientation of components
Radio broadcast stations	1 mV	Shielding
Switch-arcing	1 mV	Filtering of 5–100 MHz components; attention to ground loops and shielding
Vibration	10 pA (10–100 Hz)	Proper attention to mechanical coupling; elimination of leads with large voltages near input terminals and sensors
Cable vibration	100 pA	Use a low noise (carbon coated dielectric) cable
Circuit boards	0.01–10 pA/ $\sqrt{\text{Hz}}$ below 10 Hz	Clean board thoroughly; use Teflon insulation where needed and guard well



**Fig. 6.43** Capacitive coupling (a) and electric shield (b)

capacitance to ground on the order of 700 pF, electrical connectors have a pin-to-pin capacitance of about 2 pF, and an optoisolator has an emitter-detector capacitance of about 2 pF. Figure 6.43a shows that an electrical noise source is connected to the sensor's internal impedance  $Z$  through a coupling capacitance  $C_s$ . That impedance may be a simple resistance or a combination of resistors, capacitors, inductors, and nonlinear elements, like diodes and transistors. Voltage across the impedance is a direct result of the noise signal, the value of coupling capacitance  $C_s$  and impedance  $Z$ . For instance, a pyroelectric detector may have an internal impedance which is equivalent to a parallel connection of a 30 pF capacitor and a 50 G $\Omega$  resistor. Let us assume that the impedance is coupled to a moving person through just 1 pF, while the person on her body carries a surface electrostatic charge of 1000 V. If we limit the main frequency of human movement to 1 Hz, the sensor would pickup the electrostatic interference of about 30 V! This is over five orders of magnitude higher than the sensor would normally produce in response to thermal radiation received from the human body.

Since many sensors and virtually all electronic circuits have some nonlinearities, the high-frequency interference signals may be rectified and appear at the output as a d.c. or slow changing noise voltage.

### 6.7.3 Electric Shielding

Interferences attributed to electric fields can be significantly reduced by appropriate shielding of the sensor and circuit, especially high impedance and nonlinear components. Each shielding problem must be analyzed separately and carefully. It is very important to identify the noise source and how it is coupled to the circuit. Improper shielding and guarding may only make matters worse or create a new problem.

A shielding serves two purposes [13]. First, it confines noise to a small region. This will prevent noise from getting into nearby circuits. However, the problem with such shields is that the noise captured by the shield can still cause problems if a return path that the noise is not carefully planned and implemented by an understanding of the ground system and making the connections correctly.

Second, if noise source is present in the circuit, shields can be placed around critical parts to prevent noise from getting into sensitive portions of the detectors and circuits. These shields may consist of metal boxes around circuit regions or cables with shields around the center conductors.

As it was shown in Sect. 4.1, noise that resulted from electric fields can be well controlled by metal enclosures because electric charge cannot exist on the interior of a closed conductive surface. Coupling by a mutual, or stray, capacitance can be modeled by a circuit shown in Fig. 6.43a. The parasitic capacitance  $C_s$  is the stray capacitance (having impedance  $Z_s$  at a particular frequency) between the noise source and the circuit impedance  $Z$ , which acts as a receiver of the noise. Voltage  $V_n$  is a result of the capacitive coupling. A noise current is defined as

$$i_n = \frac{e_n}{Z + Z_s}, \quad (6.65)$$

and actually produces noise voltage

$$V_n = \frac{e_n}{\left(1 + \frac{Z_s}{Z}\right)}. \quad (6.66)$$

For example, if  $C_s = 2.5$  pF,  $Z = 10$  k $\Omega$  (resistor) and  $e_n = 100$  mV, at 1.3 MHz, the output noise will be 67 mV.

One might think that 1.3 MHz noise is relatively easy to filter out from low-frequency signals produced by a sensor. In reality, it cannot be done, because many sensors and, especially the front stages of the amplifiers, contain nonlinear components (semiconductor junctions) which act as rectifiers. As a result, after passing a nonlinear component, the spectrum of high-frequency noise shifts into a low-frequency region making the noise signal similar to voltages produced by a sensor.

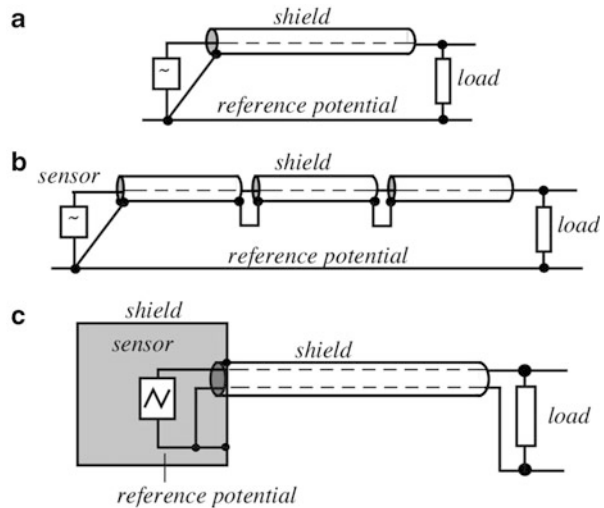
When a shield is added, the coupling changes as shown in Fig. 6.43b. With the assumption that the shield has zero impedance, the noise current at the left side will be  $i_n = e_n/Z_c$ . On the other side of the shield, noise current will be essentially zero since there is no driving source at the right side of the circuit. Subsequently, the noise voltage over the receiving impedance will also be zero and the sensitive circuit becomes effectively shielded from the noise source.

There are several practical rules that should be observed when applying electrostatic shields:

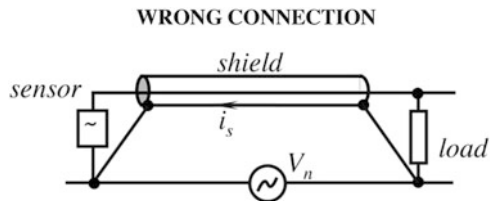
- An electrostatic shield, to be effective, should be connected to the reference potential of any circuitry contained within the shield. If the reference is connected to ground (chassis of the frame or to earth), the shield must be connected to that ground. Grounding of shield is *useless* if current from the reference is not returned to the ground.
- If a shielding cable is used, its internal shield must be connected to the signal referenced node at the signal source side, Fig. 6.44a.

- If the shield is split into sections, as might occur if connectors are used, the shield for each segment must be tied to those for the adjoining segments, and ultimately connected only to the signal referenced node, Fig. 6.44b.
- The number of separate shields required in a data acquisition system is equal to the number of independent signals that are being measured. Each signal should have its own shield, with no connection to other shields in the system, unless they share a common reference potential (signal “ground”). In that case, all connections must be made by separate jumping wires connected to each shield at a *single point*.
- A shield must be grounded only at one point—preferably next to the sensor. A shielded cable must never be grounded at both ends (Fig. 6.45). The potential difference ( $V_n$ ) between two “grounds” will cause shield current  $i_s$  to flow which may induce a noise voltage into the center conductor via magnetic coupling.
- If a sensor is enclosed into a shield box and data are transmitted via a shielded cable, Fig. 6.44c, the cable shield must be connected to the box. It’s a good practice to use a separate conductor for the reference potential (“ground”) inside the shield, and not to use the shield for any other purposes except shielding: *do not allow shield current to exist*.

**Fig. 6.44** Connections of an input cable to reference potential



**Fig. 6.45** Cable shield is erroneously grounded at both ends





- Never allow the shield to be at any potential with respect to the reference potential (except in case of driven shields as shown in Fig. 6.4b). The shield voltage couples to the center conductor (or conductors) via a cable capacitance.
- Connect shields to a ground via short wires to minimize inductance.

### 6.7.4 Bypass Capacitors

The bypass capacitors are used to maintain a low power supply impedance at the point of a load. Parasitic resistance and inductance in supply lines mean that the power supply impedance can be quite high. As the frequency goes up, the parasitic inductive becomes troublesome and may result in circuit oscillation or ringing effects. Even if the circuit operates at lower frequencies, the bypass capacitors are still important as high-frequency noise may be transmitted to the circuit and power supply conductors from external sources, for instance radio stations. At high frequencies, no power supply or regulator has zero output impedance. What type of capacitor to use is determined by the application, frequency range of the circuit, cost, board space, and some other considerations. To select a bypass capacitor one must remember that a practical capacitor at high frequencies may be far away from the idealized capacitor which is described in textbooks.

A generalized equivalent circuit of a capacitor is shown in Fig. 6.46. It is comprised of a nominal capacitance  $C$ , leakage resistance  $r_l$ , lead inductances  $L$ , and resistances  $R$ . Further, it includes dielectric absorption terms  $r$  and  $c_a$ , which are manifested in capacitor’s “memory”. In many interface circuits, especially amplifiers, analog integrators and current (charge)-to-voltage converters, dielectric absorption is a major cause for errors. In such circuits, film capacitors should be used whenever possible.

In bypass applications,  $r_l$  and dielectric absorption are second order terms but series  $R$  and  $L$  are of importance. They limit the capacitor’s ability to damp transients and maintain a low power supply output impedance. Often, bypass capacitors must be of large values (10  $\mu\text{F}$  or more) so they can absorb longer transients, thus electrolytic capacitors are often employed. Unfortunately, these capacitors have large series  $R$  and  $L$ . Usually, tantalum capacitors offer better results, however, a combination of aluminum electrolytic with nonpolarized (ceramic or film) capacitors may offer even further improvement. Nowadays, high-volume ceramic capacitors are available for low price.

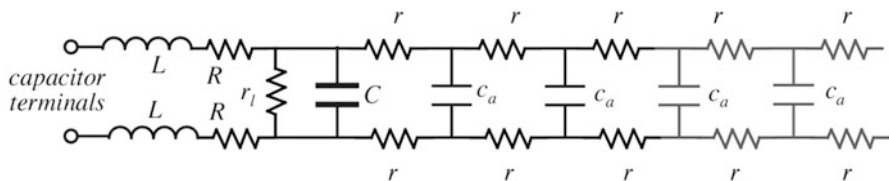


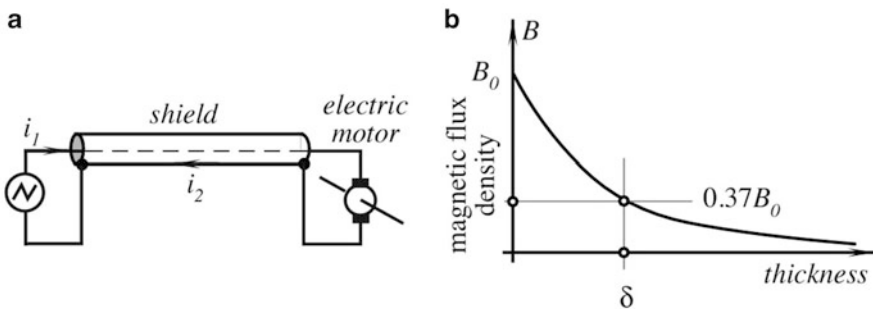
Fig. 6.46 Equivalent circuit of a capacitor

A combination of wrong types of bypass capacitors may lead to ringing, oscillation, and crosstalk between data communication channels. The best way to specify a correct combination of bypass capacitors is to first try them on a breadboard.

### 6.7.5 Magnetic Shielding

Proper shielding may dramatically reduce noise resulting from electrostatic and electrical fields. Unfortunately, it is much more difficult to shield against magnetic fields because they penetrate conducting materials. A typical shield placed around a conductor and grounded at one end has little if any effect on the magnetically induced voltage in that conductor. When magnetic field  $B_0$  penetrates the shield, its amplitude drops exponentially as shown in Fig. 6.47b. The skin depth  $\delta$  of the shield is the depth required for the field attenuation to 37% of that in the air. Table 6.6 lists typical values of  $\delta$  for several materials at different frequencies. At high frequencies, any material from the list may be used for effective magnetic shielding, however at a lower range, steel yields a much better performance. The high-frequency magnetic shielding by an electrically conductive material arises thanks to the induced eddy currents. These circular currents according to Lenz law (Sect. 4.4.1) generate their own magnetic fields that oppose the originating field and thus provide shielding. At lower frequencies however, eddy currents have much lower efficiencies.

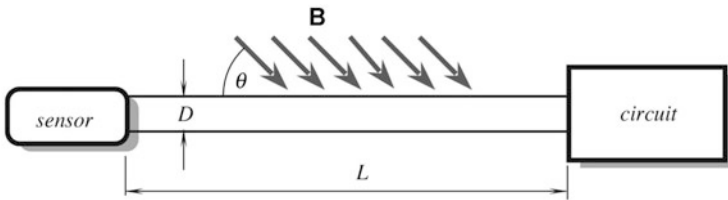
For improving low-frequency magnetic field shielding, a shield consisting of a high-permeability magnetic material (e.g., mumetal) should be considered. However, the mumetal effectiveness drops at higher frequencies and strong magnetic fields. An effective magnetic shielding can be accomplished with thick steel shields at higher frequencies. Since magnetic shielding is very difficult, the most effective approach at low frequencies is to minimize the strength of magnetic fields, minimize the magnetic loop area at the receiving end, and select the optimal geometry of conductors. Some useful practical guidelines are as follows:



**Fig. 6.47** Reduction of transmitted magnetic noise. Powering load device through coaxial cable (a); magnetic shielding improves with thickness of shield (b)

**Table 6.6** Skin depth  $\delta$  (mm) versus frequency

Frequency	Copper	Aluminum	Steel
60 Hz	8.5	10.9	0.86
100 Hz	6.6	8.5	0.66
1 kHz	2.1	2.7	0.20
10 kHz	0.66	0.84	0.08
100 kHz	0.2	0.3	0.02
1 MHz	0.08	0.08	0.008



**Fig. 6.48** Receiver’s loop formed by long conductors

- Locate the receiving circuit as far as possible from the source of the magnetic field.
- Avoid running wires parallel to the magnetic field; instead, cross the magnetic field at right angles.
- Shield the magnetic field with an appropriate material for the frequency and strength.
- Use a twisted pair of wires for conductors carrying the high-level current that is the source of the magnetic field. If the currents in the two wires are equal and opposite, the net field in any direction over each cycle of twist will be zero. For this arrangement to work, none of the current can be shared with another conductor, for example, a ground plane, which may result in ground loops.
- Use a shielded cable with the high-level source circuit’s return current carried by the shield, Fig. 6.47a. If the shield current  $i_2$  is equal and opposite to that of the center conductor  $i_1$ , the center conductor field and the shield field will cancel, producing a zero net field. This case seems a violation of a rule “no shield currents” for the receiver’s circuit, however, the shielded cable here is not used to electrostatically shield the center conductor. Instead, the geometry produces a cancellation of the magnetic field which is generated by current supplied to a “current-hungry” device (an electric motor in this example).
- Since magnetically induced noise depends on area of the receiver loop, the induced voltage due to magnetic coupling can be reduced by making the loop’s area smaller.

What is the receiver’s loop? Figure 6.48 shows a sensor which is connected to the load circuit via two conductors having length  $L$  and separated by distance  $D$ . The rectangular circuit forms a loop area  $a = L \times D$ . The voltage induced in series with the loop is proportional to magnetic field  $B$ , the area and cosine of its angle to

the field. Thus, to minimize noise, the loop should be oriented at right angles to the field, and its area should be minimized.

The area can be decreased by reducing the length of the conductors and/or decreasing the distance between the conductors. This is easily accomplished with a twisted pair, or at least with a tightly cabled pair of conductors. It is a good practice to pair the conductors so that the circuit wire and its return path will always be together. This requirement shall not be overlooked. For instance, if wires are correctly positioned by a designer, a service technician may reposition them during the repair work. A new wire location may create a disastrous noise level. Hence, a general rule is—know the area and orientation of the wires and permanently secure the wiring.

### 6.7.6 Mechanical Noise

*Vibration and acceleration effects* are also sources of transmitted noise in sensors which otherwise should be immune to them. These effects may alter transfer characteristics (multiplicative noise), or the sensor may generate spurious signals (additive noise). If a sensor incorporates certain mechanical elements, vibration along some axes with a given frequency and amplitude may cause resonant effects. For some sensors, acceleration is a source of noise. For instance, pyroelectric detectors possess piezoelectric properties. The main function of a pyroelectric detector is to respond to thermal radiation. However, such environmental mechanical factors as fast changing air pressure, strong wind, or structural vibrations cause the sensor to respond with output signals which often are indistinguishable from responses to normal stimuli. If this is the case, a differential noise cancellation may be quite efficient (see Sect. 6.7.2).

### 6.7.7 Ground Planes

For many years ground planes have been known to electronic engineers and printed circuit designers as a “mystical and ill-defined” cure for spurious circuit operation. Ground planes are primarily useful for minimizing circuit inductance. They do this by utilizing the basic magnetic theory. Current flowing in a wire produces an associated magnetic field (Sect. 4.3). The field’s strength is proportional to the current  $i$  and inversely related to the distance  $r$  from the conductor:

$$B = \frac{\mu_0 i}{2\pi r}. \quad (6.67)$$

Thus, we can imagine a current carrying wire surrounded by a magnetic field. Wire inductance is defined as energy stored in the field setup by the wire’s current. To compute the wire’s inductance requires integrating the field over the wire’s length and the total area of the field. This implies integrating on the radius from the wire

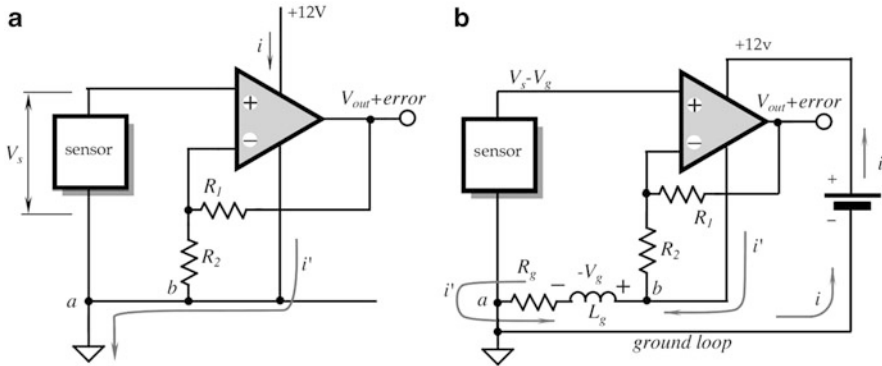
surface to infinity. However, if two wires carrying the same current in opposite directions are in close proximity, their magnetic fields are cancelled. In this case, the virtual wire inductance is much smaller. An opposite flowing current is called *return current*. This is the underlying reason for ground planes. A ground plane provides a return path directly under the signal carrying conductor through which return current can flow. Return current has a direct path to ground, regardless of the number of branches associated with the conductor. Currents will always flow through the return path of the lowest impedance. In a properly designed ground plane this path is directly under the signal conductor. In practical circuits, a ground plane is one side of the board and the signal conductors are on the other. In the multilayer boards, a ground plane is usually sandwiched between two or more conductor planes. Aside from minimizing parasitic inductance, ground planes have additional benefits. Their flat surface minimizes resistive losses due to “skin effect” (a.c. current travel along a conductor’s surface). Additionally, they aid the circuit’s high-frequency stability by referring stray capacitance to the ground. Even though ground planes are very beneficial for digital circuits, using them for current return of analog sensor signals are dangerous—likely digital currents in a ground will create strong interferences in the analog part of the circuit.

Some practical suggestions:

- Make ground planes of as much area as possible on the components side (or inside for the multilayer boards). Maximize the area especially under traces that operate with high frequency or digital signals.
- Mount components that conduct fast transient currents (terminal resistors, ICs, transistors, decoupling capacitors, etc.) as close to the board as possible.
- Wherever a common ground reference potential is required, use separate conductors for the reference potential and connect them all to the ground plane at a common point to avoid voltage drops due to ground currents.
- Use separate nonoverlapping ground planes for digital and analog sections of the circuit board and connect them at one point only at the power supply terminals.
- Keep the trace length short. Inductance varies directly with length and no ground plane will achieve perfect cancellation.

### 6.7.8 Ground Loops and Ground Isolation

When a circuit is used for low-level input signals, a circuit itself may generate enough noise and interferences to present a substantial problem for accuracy. Sometimes, when a circuit is correctly designed on paper and a bench breadboard shows quite a satisfactory performance, when a production prototype with the printed circuit board is tested, the accuracy requirement is not met. A difference between a breadboard and PC-board prototypes may be in the physical layout of conductors. Usually, conductors between electronic components are quite

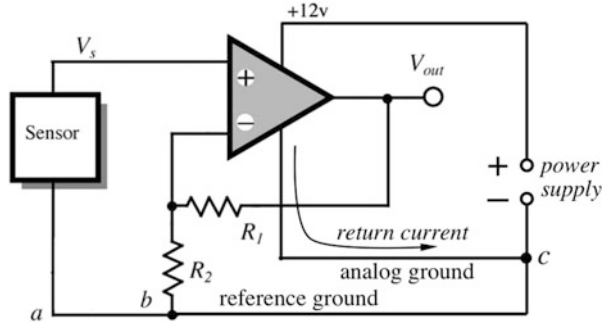


**Fig. 6.49** Wrong connection of ground terminal to circuit (a); path of supply current through ground conductors (b)

specific—they may connect a capacitor to a resistor, a gate of a JFET transistor to the output of an operational amplifier, etc. However, there are at least two conductors, which, in most cases are common for the majority of the electronic circuit. These are the power supply bus and the ground bus. Both of them may carry undesirable signals from one part of the circuit to another, specifically, they may couple strong output signals to the sensors and input stages.

A power supply bus carries supply currents to all stages. A ground bus also carries supply currents, but, in addition, it is often used to establish a reference base for an electrical signal. For any measurement circuit electrical cleanliness of a reference is essential. Interaction of the two functions (power supply and reference) may lead to a problem which is known as *ground loop*. We illustrate it in Fig. 6.49a where a sensor is connected to a noninverting input of an amplifier which may have a substantial gain. The amplifier is connected to the power supply and draws current  $i$  which is returned to the ground bus as  $i'$ . The sensor generates voltage  $V_s$  which is fed to the input of the amplifier. A ground wire is connected to the circuit at point  $a$ —right next to the sensor's terminal. A circuit has no visible error sources, nevertheless, the output voltage contains substantial error. A noise source is developed in a wrong connection of ground wires. Figure 6.49b shows that the ground conductor is not ideal. It may have some finite resistance  $R_g$  and inductance  $L_g$ . In this example, supply current, while returning to the battery from the amplifier, passes through the ground bus between points  $b$  and  $a$  resulting in voltage drop  $V_g$ . This drop, however small, may be comparable with signals produced by the sensor. It should be noted that voltage  $V_g$  is serially connected with the sensor and directly applied to the amplifier's input. In other words, the sensor is not referenced to a clean ground. Ground currents may also contain high-frequency components, than the bus inductance will produce quite strong spurious high-frequency signals which not only add noise to the sensor, but may cause circuit instability as well.

**Fig. 6.50** Correct grounding of a sensor and interface circuit



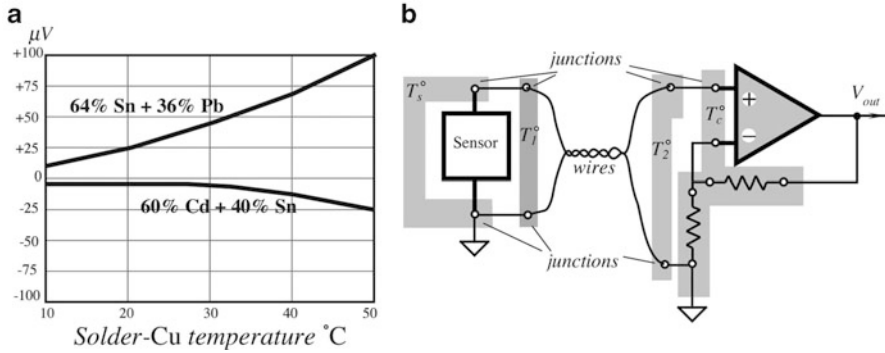
As an example, consider a thermocouple temperature sensor which generates voltage corresponding to  $50 \mu\text{V}/^\circ\text{C}$  of the object's temperature. A low noise amplifier has quiescent current,  $i = 1 \text{ mA}$ , which passes through the ground loop having resistance  $R_g = 0.2 \Omega$ . The ground-loop voltage  $V_g = iR_g = 0.2 \text{ mV}$  corresponding to an error of  $-4^\circ\text{C}$ ! The cure is usually quite simple—ground loops must be broken. The most critical rule of the circuit board design: *never use the same conductor for the reference potential and power supply currents*. A circuit designer should always separate a reference ground from the current carrying grounds, especially serving digital devices. Thus, it is advisable to have at least three grounds: reference, analog, and digital.

The *reference ground* shall be used only for connecting the sensor components that produce low-level input signals, all front stage amplifier input components that need be referenced to a ground potential, and the reference input of an ADC. The *analog ground* shall be used exclusively for returning stronger currents from the analog interface circuits. And the *digital ground* shall be used only for binary signals, like microprocessors, digital gates, etc. There may be a need for additional “grounds”, for example those that carry relatively strong currents, especially containing high-frequency signals (LEDs, relays, motors, heaters, etc.). Figure 6.50 shows that moving the ground connection from the sensor's point *a* to the power terminal point *c* prevents formation of spurious voltages across the ground conductor connected to the sensor and a feedback resistor  $R_2$ .

A rule of thumb is to *join all “grounds” on a circuit board only at one point*, preferably at the power source. Grounding at two or more spots may form ground loops which often is very difficult to diagnose.

### 6.7.9 Seebeck Noise

This noise is a result of the Seebeck effect (Sect. 4.9.1) which is manifested as generation of an *electromotive force (e.m.f.)* when two dissimilar metals are joined together. The Seebeck *e.m.f.* is small and for many sensors may be simply ignored. However, when absolute accuracy on the order of  $10\text{--}100 \mu\text{V}$  is required, that noise



**Fig. 6.51** Seebeck *e.m.f.* developed by solder-copper joints (a) (adapted from [14]); maintaining joints at the same temperature reduces Seebeck noise (b)

should be taken into account. A connection of two dissimilar metals produces a temperature sensor. However, when temperature sensing is not a desired function, a thermally induced *e.m.f.* is a spurious signal. In electronic circuits, connection of dissimilar metals can be found everywhere: connectors, switches, relay contacts, sockets, wires, etc. For instance, the copper PC board cladding connected to kovar<sup>TM4</sup> input pins of an integrated circuit creates an offset voltage of  $40 \mu\text{V} \times \Delta T$  where  $\Delta T$  is the temperature gradient in  $^\circ\text{C}$  between two dissimilar metal contacts on the board. The common lead-tin solder, when used with the copper cladding, creates a thermoelectric voltage between 1 and  $3 \mu\text{V}/^\circ\text{C}$ . There are special cadmium-tin solders available to reduce these spurious signals down to  $0.3 \mu\text{V}/^\circ\text{C}$ . Figure 6.51a shows Seebeck *e.m.f.* for two types of solder. Connection of two identical wires fabricated by different manufacturers may result in voltage having slope on the order of  $200 \text{ nV}/^\circ\text{C}$ .

In many cases, Seebeck *e.m.f.* may be eliminated by a proper circuit layout and thermal balancing. It is a good practice to limit the number of junctions between the sensor and front stage of the interface circuit. Avoid connectors, sockets, switches, and other potential sources of *e.m.f.* to the extent possible. In some cases this will not be possible. In these instances, attempt to balance the number and type of junctions in the circuit's front stage so that differential cancellations occur. Doing this may involve deliberately creating and introducing junctions to offset necessary junctions. Junctions which intent to produce cancellations must be maintained at the same temperature. Figure 6.51b shows a remote sensor connection to an amplifier where the sensor junctions, input terminal junctions, and amplifier components junctions are all maintained while at different but properly arranged

<sup>4</sup>Trademark of Westinghouse Electric Corp.



temperatures. Such thermally balanced junctions must be maintained at a close physical proximity and preferably on common heat sinks. Air drafts and temperature gradients in the circuit boards and sensor enclosures must be avoided.

## 6.8 Batteries for Low-Power Sensors

Modern development of integrated sensors and need for long-term remote monitoring and data acquisition demand use of reliable and high-energy density power sources. History of battery development goes back to Volta and shows a remarkable progress during last decades. Well-known old electrochemical power sources improve dramatically. Examples are C-Zn, alkaline, Zn-air, NiCd, and lead-acid batteries. Nowadays, Zn-air, Ni-metal-hydride, and especially lithium batteries (such as Li-MnO<sub>2</sub>) are the most popular energy sources.

All batteries can be divided into two groups: *primary*—single use devices, and *secondary* (rechargeable)—multiple use devices.

Often, batteries are characterized by energy per unit weight, however, for miniature sensor applications energy per unit volume often becomes more critical (see Table A.20)

In general, energy delivered by a battery depends upon the rate at which power is withdrawn. Typically, as the current increases the amount of energy delivered decreases. Battery energy and power are also affected by construction of battery, the size, and the duty cycle of current delivery. Manufacturers usually specify batteries as ampere-hours or watt-hours when discharged at a specific rate to a specific voltage cutoff.

If the battery capacitance is  $C$  (in mA h) and the average current drain is  $I$  (mA), the time of a battery discharge (lifetime for a primary cell when in use) is defined as

$$t = \frac{C}{In}, \quad (6.68)$$

where  $n$  is a duty cycle. For instance, if the battery is rated as having capacity of 100 mA h, the load current consumption is 5 mA and the circuit works only 3 min every hour (duty cycle is 3/60), the battery will last approximately for

$$t = \frac{C}{In} = \frac{100}{5 \frac{3}{60}} = 400 \text{ h}$$

Yet, the manufacturer's specification shall be used with a grain of salt and *only as a guideline*, because the specified discharge rate rarely coincides with the actual power consumption. Also, a capacity is rated for a specific cutoff voltage because when a battery discharges its output voltage drops. For example, a fresh battery capacity is specified as 220 mA h for a cutoff voltage 2.6 V, while the load needs minimum 2.8 V for its operation. Thus, the actual battery capacity will be less than specified by the manufacturer.

It is highly recommended to determine battery life experimentally, rather than rely on calculation. When designing electronic circuit, its power consumption shall be determined during various operating modes and over the operating temperature range. Then, these values of power consumption should be used in simulation of the battery load to determine the useful life with a circuit-specific cutoff voltage in mind. The accelerated life tests of a battery shall be used with caution, since the useful capacity of a battery greatly depends on the load, operational current profile, and a real duty cycle.

Sometimes, a circuit draws high currents during short times (pulse mode) and the battery ability to deliver such pulse current should be evaluated since the battery internal resistance may be a limiting factor, so the battery would not be able to deliver as much current as needed. A solution is to augment the battery with a large parallel capacitor, for example 10–100  $\mu\text{F}$ , that can be used as a charge storage tank for quick delivering the current bursts. Another advantage of the parallel capacitor is that it prolongs the battery life in pulsing applications [15].

## 6.8.1 Primary Cells

The construction of a battery cell determines its performance and cost. Most primary cells (disposable batteries) employ single thick electrodes arranged in parallel or concentric configuration and aqueous electrolytes. Most small secondary cells (rechargeable batteries) are designed differently—they use “wound” or “jelly roll” construction, in which long thin electrodes are wound into a cylinder and placed into a metal container. This results in a higher power density, but with decreased energy density and higher cost. Due to low conductivity of electrolytes, many lithium primary cells also use “wound” construction [16].

### 6.8.1.1 Alkaline Manganese Batteries

Demand for these batteries grew significantly, especially after a major improvement—elimination of mercury from the zinc anode. The alkaline batteries are capable of delivering high currents, have improved power/density ratio and at least 5 years of shelf life (Table A.20)

### 6.8.1.2 Primary Lithium Batteries

Most of these batteries are being produced in Japan and China. Popularity of lithium-manganese dioxide cells grows rapidly since they were first introduced by Sony in 1991. They have higher operating voltage, wide range of sizes and capacities, and excellent shelf life (Table A.21). Lithium iodine cells have very high-energy density and allow up to 10 years of operation in a pacemaker (implantable heart rate controller). However, these batteries are designed with a low conductivity solid-state electrolyte and allow operation with very low current drain (in the order of microamperes), which is quite sufficient for many passive sensors.

Amount of lithium in batteries is quite small, because just 1 g is sufficient for producing capacity of 3.86 A h. Lithium cells are exempt from environmental regulations, but still are considered hazardous because of their flammability and thus restricted for transporting by aircrafts. Lithium-ion cells with cobalt cathodes should never rise above 130 °C (265 °F) because at 150 °C (302 °F) the cell becomes thermally unstable.

For portable equipment, thin batteries are highly desirable due to their small thickness. There is a tradeoff between thickness and surface area—the area becomes larger for thinner batteries. For example, lithium/manganese dioxide battery CP223045 has thickness 2.2 mm with the surface area 13.5 cm<sup>2</sup>. It has an impressive capacity of 450 mA h with only 2 % self-discharge per year.

### 6.8.2 Secondary Cells

Secondary cells (Tables A.22 and A.23) are *rechargeable batteries*.

*Sealed lead acid* batteries offer small size at large capacities and allow about 200 cycles of life at discharge times as short as 1 h. The main advantages of these cells are low initial cost, low self-discharge, and an ability to support heavy loads and to withstand harsh environments. Besides, these batteries have long life. The disadvantages include relatively large size and weight as well as potential environmental hazard due to presence of lead and sulfuric acid.

Sealed *Nickel-Cadmium* (NiCd) and *Nickel-Metal Hydrate* (Ni-MH) are the most widely used secondary cells, being produced at volumes over one billion cells per year. Typical capacity for an “AA” cell is about 2000 mA h and even higher from some manufacturers. The NiCd cells are quite tolerant of overcharge and overdischarge. An interesting property of NiCd is that charging is the endothermic process that is the battery absorbs heat, while other batteries warm up when charging. Cadmium, however, presents potential environmental problem. Bi-MH and modern NiCd do not exhibit “memory” effect, that is, a partial discharge does not influence their ability to fully recharge. The Nickel-Metal Hydrate cells are nearly direct replacement for NiCd, yet they yield better capacity, but have somewhat poorer self-discharge.

A *Lithium Ion Polymer battery* (LiPo or LIP) contain a nonliquid electrolyte, which makes it a solid-state battery. This allows fabricating it in any size and shape, however, these batteries are most expensive.

Rechargeable *alkaline batteries* have low cost and good power density. However, their life cycles are quite low.

### 6.8.3 Supercapacitors

Supercapacitors (SC) or ultracapacitors fill the gap between secondary batteries and regular capacitors. They are characterized by very large capacitances ranging from 1 to 200 F and a low internal resistance ranging from 0.07 to

0.7  $\Omega$  ([www.maxwell.com](http://www.maxwell.com)). While supercapacitors have energy densities that are approximately 10 % of the conventional batteries, their power density is generally 10–100 times greater. This results in much shorter charge/discharge times than for batteries. While working in tandem with a regular primary or secondary battery for applications that require both a constant low-power discharge for continual function and a pulse power for peak loads they relieve batteries of peak power functions resulting in an extension of battery life and reduction of the overall battery size and cost. The SC main advantage is a long life—about 0.5 million cycles, much exceeding that of a secondary cell that has a typical charge-discharge cycles ranging from 500 to 10,000 (for lithium-ion cells). On a negative side, a SC has a relatively large leakage current and its typical operating voltage is not exceeding 2.8 V. This precludes the SC from replacing batteries for a prolonged storage of electric charge. Thus, these capacitors are the most beneficial when their charge can be constantly replenished either from a battery or energy harvester.

---

## 6.9 Energy Harvesting

Providing electric power for a sensing module does not always have a simple solution. When electric power line is available or a battery can be periodically replaced—there is no issue. However, replacing a battery is not always easy or even possible. In such special cases, energy should be obtained or harvested from ambient sources [21]. This requires receiving one type of energy and converting it to d.c. electric power. Examples of the potential sources for energy harvesting are:

*Thermal*, where energy can be obtained from thermal gradients. For example, a temperature difference between a human body and environment can be converted into electricity by thermoelectric elements.

*Mechanical*, when energy is obtained by stressing a special transducer or moving a coil or magnet. For example, a piezoelectric element may be built into a shoe sole and stressed at every step to generate voltage spikes that can charge a capacitor or battery. Another example is a floating sensing module with a built-in electromagnetic transducer for converting mechanical energy of water waves to electric power.

*Light* of different wavelengths can be converted to electricity by use of a photoeffect or thermoelectric effect.

*Acoustic*, when sound (pressure waves) can be converted to electricity by use of special microphones or hydrophones.

*Electromagnetic* (RF) sources (far-field), such as radio stations emitting electromagnetic fields that can be detected and converted to a d.c. power.

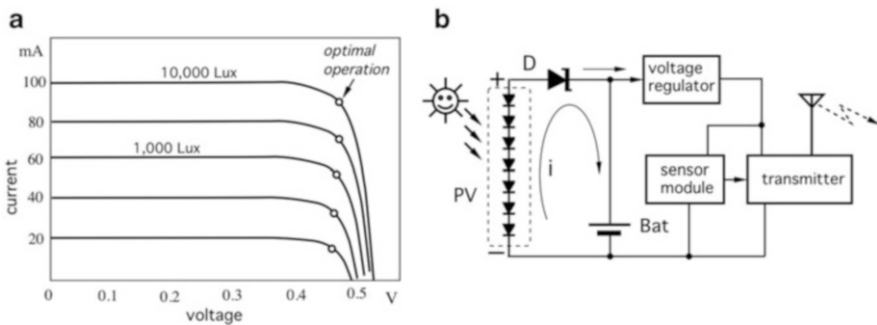
*Magnetic* (RF) sources (near field), such as power transformers and variable magnetic filed transmitters in close proximities.

### 6.9.1 Light Energy Harvesting

Quanta of light carries a substantial energy depending on its wavelength, Eq. (5.3). Portion of that energy can be captured and used for powering electronic circuits. From low-energy light known as thermal radiation, electric power can be harvested by using pyroelectric cells [17]. In these cells, light first is converted into heat and subsequently heat is converted to electricity. For visible light, the most common type of a conversion device is a photovoltaic (PV) or solar cell. These cells are similar in many ways to a battery because they supply direct current. A PV cell has a positive and a negative side, just like a battery.

Photovoltaic cells are made from single crystal silicon  $pn$  junctions, the same as photodiodes with a very large light sensitive region. But unlike photodiodes, they are used without the reverse bias. When illuminated, the light energy causes electrons to flow through the  $pn$  junction and generates an open circuit voltage of about 0.58 V (for an individual solar cell). To boost output voltage (and power), individual solar cells can be connected together in series to form a solar panel. The amount of available current from a PV cell depends upon the light intensity, size of the cell, and its efficiency which is generally rather low: 15–20 %. To increase the overall efficiency of the cell, commercially available solar cells use polycrystalline silicon or amorphous silicon, which have no crystalline structure, and can generate maximum currents between 20 and 40 mA/cm<sup>2</sup>.

For a given illumination, a cell has a flat ampere-voltage characteristic shown in Fig. 6.52a. The optimal operating point is where the cell can deliver maximum power, that is where the product of current and voltage is the highest. These points are indicated by the dots. The higher illumination the stronger the PV current,  $i$ . For illustration of the PV energy harvesting, consider a panel of seven solar cells connected in series as shown in Fig. 6.52b. They deliver about 4 V that charge a secondary battery whose purpose is to provide power in darkness, when the PV cells output no current. To prevent a current reverse flow in darkness, a diode  $D$  is used in the current path. Whenever ambient light comes on, the battery is trickle-charged. The battery output may be regulated to provide a fixed voltage to the sensing



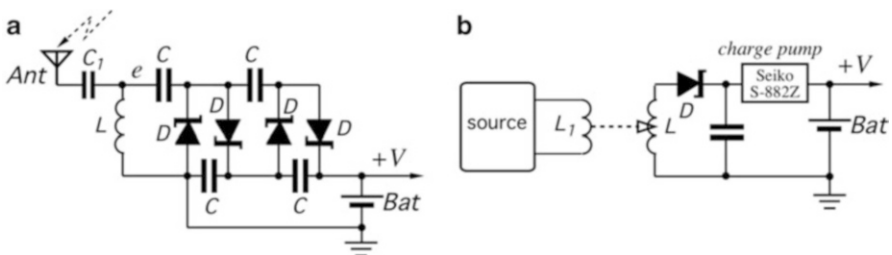
**Fig. 6.52** Volt-ampere characteristic of photovoltaic cell (a) and use of photovoltaic battery to power sensing module (b)

module and data transmitter, for example Bluetooth. Obvious disadvantages of light harvesting include a need for the solar panels being exposed to bright ambient light and a potential soiling of the panels by airborne dirt.

## 6.9.2 Far-Field Energy Harvesting

Ambient space around us is “packed” with electromagnetic fields (EMF) of endless frequencies having substantial combined energy. Harvesting that entire energy is not possible with modern technologies, yet tapping of small incident EMF at selected frequencies is quite practical [18, 19]. The key point is—what frequency? The answer depends on proximity of EMF sources, such as radio stations, wireless routers, etc. Since the EMF strength drops dramatically when moving away from the source, typical distances between the EMF source and harvester preferably are no more than 3 m (10 ft). The harvesting range must be at least 70 % of the wavelength of EMF or longer. Therefore, this type of the electromagnetic reception is called a *far-field* harvesting. In some occasions, when the transmitter emits significant EMF power (e.g., broadcasting or communication station), the harvesting range may be as long as 40 m. The RF to d.c. power conversion system operates more efficiently in UHF frequencies in the industrial, scientific, and medical bands (ISM band) of 902–928 MHz. In this frequency range, RF power is transmitted more efficiently for longer distances and experiences lower propagational losses than higher frequency bands (i.e., 2.4 GHz).

Harvested EMF energy is used for charging battery as shown in Fig. 6.53a. The circuit includes the antenna with an  $LC_1$  resonant tank that is tuned to a selected frequency. The tuning may be fixed or automatically adjustable to maximize the output power. The antenna preferably should be placed on the outside surface of the converter. The RF voltage from the resonant tank is rather small for rectification and charging the battery, thus first it passes through a voltage multiplier called the Villard cascade, consisting of several diodes ( $D$ ) and capacitors ( $C$ ) that rectify and multiply the d.c. output to the level that is sufficient for charging the battery.



**Fig. 6.53** Far-field energy harvesting circuit (a) and near-field magnetic coupling (b) with charge pump

### 6.9.3 Near-Field Energy Harvesting

In the near-field harvester, only the magnetic component of the EMF vector is employed, thus this method of energy harvesting resembles a transformer with two magnetically coupled coils [20] as illustrated in Fig. 6.53b. Note that voltage after the rectifier is rather small (about 0.5 V), thus a charge pump is employed to increase that voltage to about 2 V. This type of a coupling dramatically limits the range of energy transfer—typically it does not exceed 5 cm and must be less than 70 % of the wavelength. Due to its magnetic nature, a near-field energy transfer sometimes is called a coupling to H-field. These fields are abundant in close vicinity of many appliances that use high electric currents. In some cases, H-field in the RF range is specially generated by a radio antenna for providing power to a wireless circuit, for example for RFID tags. Thus, one coil that emanates EMF (for example in the NFC frequency of 13.56 MHz) has to be inductively coupled with a receiving coil and battery charger. The RF signal may be modulated to enable transfer of data along with supplying energy.

---

### References

1. Widlar, R. J. (1980). Working with high impedance Op Amps, AN24. *Linear application handbook*. National Semiconductor.
2. Park, Y. E., et al. (1983). An MOS switched-capacitor readout amplifier for capacitive pressure sensors. *IEEE Custom IC Conf.* (pp. 380–384).
3. Cho, S. T., et al. (1991). A self-testing ultrasensitive silicon microflow sensor. *Sensor Expo Proceedings* (p. 208B-1).
4. Ryhänen, T. (1996). Capacitive transducer feedback-controlled by means of electrostatic force and method for controlling the profile of the transducing element in the transducer. *U.S. Patent 5531128*.
5. Pease, R. A. (1983, January 20). Improve circuit performance with a 1-op-amp current pump. *EDN* (pp. 85–90).
6. Bell, D. A. (1981). *Solid state pulse circuits* (2nd ed.). Reston, VA: Reston Publishing Company.
7. Sheingold, D. H. (Ed.). (1986). *Analog-digital conversion handbook* (3rd ed.). Englewood Cliffs, NJ: Prentice-Hall.
8. Johnson, C., et al. (1986). Highly accurate resistance deviation to frequency converter with programmable sensitivity and resolution. *IEEE Transactions on Instrumentation and Measurement, IM-35*, 178–181.
9. AVR121: Enhancing ADC resolution by oversampling. (2005). *Atmel Application Note 8003A-AVR-09/05*.
10. Coats, M. R. (1991). New technology two-wire transmitters. *Sensors*, 8(1).
11. Johnson, J. B. (1928). Thermal agitation of electricity in conductors. *Physical Review*, 32, 97–109.
12. Rich, A. (1991). Shielding and guarding. In: *Best of analog dialogue*. ©Analog Devices.
13. Ott, H. W. (1976). *Noise reduction techniques in electronic systems*. New York: John Wiley & Sons.
14. Pascoe, G. (1977, February 6). The choice of solders for high-gain devices. *New Electronics* (U.K.).
15. Jensen, M. (2010). White Paper SWRA349. *Texas Instruments*.

16. Powers, R. A. (1995). Batteries for low power electronics. *Proceedings of the IEEE*, 83(4), 687–693.
17. Batra, A., et al. (2011). Simulation of energy harvesting from roads via pyroelectricity. *Journal of Photonics for Energy*, 1(1), 014001.
18. Le, T. T., et al. (2009). RF energy harvesting circuit. *U.S. Patent publ. No. 2009/0152954*.
19. Mickle, M. H., et al. (2006). Energy harvesting circuit. *U.S. Patent No. 7084605*.
20. Butler, P. (2012). Harvesting power in near field communication (NFC) device. *U.S. Patent No. 8326224*.
21. Safak, M. (2014). Wireless sensor and communication nodes with energy harvesting. *Journal of Communication, Navigation, Sensing and Services*, 1, 47–66.



*“Never confuse motion with action”*

—Ernest Hemingway

Detection of humans embraces a very broad spectrum of applications, including security, surveillance, energy management (electric lights control), personal safety, man-machine interface, friendly home appliances, point-of-sale advertisements, robotics, automotive, interactive toys, novelty products, etc. Detectors of human bodies loosely can be subdivided into the following categories.

*Occupancy* sensors detect presence of people (and sometimes animals) in a monitored area.

*Motion* detectors respond only to moving objects. Unlike occupancy sensors that produce signals whenever a subject is stationary or not, motion detectors are selectively sensitive to moving subjects.

*Position* detectors are the quantitative sensors that measure at least one coordinate of the object location, for instance—a distance of a hand from the sensor.

*Tactile sensors* respond to small forces or a mere physical coupling between the detector and part of the subject’s body, be it a human or a human equivalent (robot).

One of the most important applications is security. Sept. 11 has changed the way people think about the airport, aviation, and security in general. The threat is expanding interest in more reliable systems to detect and possibly identify people within the protected perimeters.

Depending on the application, presence of humans may be detected through any means that is associated with some kind of a human body’s property or body’s actions [1]. For instance, a detector may be sensitive to the body image, optical contrast, weight, heat, sounds, dielectric constant, smell, etc. The following types of detectors are presently used for the occupancy and motion sensing of people:

1. *Air pressure sensors*—detect minute variations in air pressure resulted from opening doors and windows.
2. *Capacitive*—detectors of human body capacitance.
3. *Acoustic*—detectors of sound produced by people.
4. *Photoelectric*—interruption of light beams by moving objects.
5. *Optoelectric*—detection of variations in illumination or optical contrast in the protected area.
6. *Pressure mat switches*—pressure-sensitive long strips used on floors beneath the carpets to detect weight of an intruder.
7. *Stress detectors*—strain gauges imbedded into floor beams, staircases, and other structural components.
8. *Switch sensors*—electrical contacts connected to doors and windows.
9. *Magnetic switches*—noncontact versions of switch sensors.
10. *Vibration detectors*—react to the vibration of walls or other building structures. Also, may be attached to doors or windows to detect movements.
11. *Glass breakage detectors*—sensors reacting to specific vibrations produced by shattered glass.
12. *Infrared motion detectors*—devices sensitive to heat waves naturally emanated from warm or cold moving objects.
13. *Microwave detectors*—active sensors responsive to microwave electromagnetic signals reflected from objects.
14. *Ultrasonic detectors*—devices similar to microwave detectors except that instead of electromagnetic radiation, ultrasonic air waves are used.
15. *Video presence detectors*—a video equipment that compares a reference image stored in memory with the current image from a protected area.
16. *Image recognition*—image analyzers that compare facial features with database.
17. *Laser system detectors*—similar to photoelectric detectors, except that they use narrow light beams and combinations of reflectors.
18. *Triboelectric detectors*—sensors capable of detecting static electric charges carried by moving objects.

One of the major aggravations in detecting occupancy or intrusion is a *false-positive* detection. The term “false positive” means that the system indicates an intrusion when there is none. In some noncritical applications where false positive detections occur once in a while, for instance, in an interactive toy or motion controlled lights switch, this may be not a serious problem: the lights will be erroneously turned on for a short time, which unlikely do any harm.<sup>1</sup> In other systems, especially used for security and military purposes, false positive detections, while generally not as dangerous as false negative ones (missing an intrusion), may become a serious problem.<sup>2</sup> While selecting a sensor for critical

---

<sup>1</sup> Perhaps just steering up some suspicion about living in a haunted house.

<sup>2</sup> A very nice movie “*How to Steal a Million*” (1966) was based on a plot where multiple false-positive alarms were so irritating that the guards disabled the electronic protection system in the museum—exactly what the perpetrator planned.

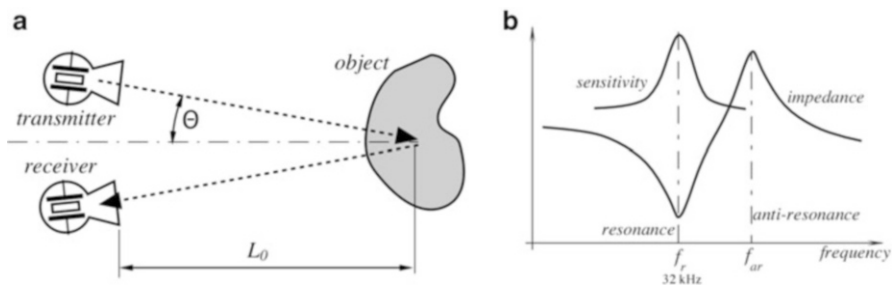
applications, considerations should be given to its reliability, selectivity, and noise immunity. It is often a good practice to form a multiple sensor arrangement with differential interface circuits. It may dramatically improve a reliability of a system, especially in presence of external transmitted noise. Another efficient way of reducing erroneous detections is using sensors operating on different physical principles, for instance, combining capacitive and infrared detectors is an efficient method, as they are receptive to different kinds of transmitted noise.

## 7.1 Ultrasonic Detectors

Transmission and reception of ultrasonic waves (USW) energy is a basis for very popular ultrasonic range meters, proximity detectors, and velocity meters. USW are mechanical acoustic waves covering frequency range well beyond the capabilities of human ears, i.e., over 20 kHz. However, these frequencies may be quite perceptible by smaller animals, like dogs, cats, rodents, and insects. Indeed, the ultrasonic detectors are the biological ranging devices in bats and dolphins.

When USW are incident on an object, part of their energy is absorbed and part is reflected. In many practical cases, USW energy is reflected in a diffuse manner. That is, regardless of the direction where the waves come from, they are reflected almost uniformly within a wide solid angle, which may approach  $180^\circ$ . If the object moves, frequency of the reflected wavelength will differ from the transmitted waves. This is called the Doppler effect.<sup>3</sup>

A distance  $L_0$  to the object can be calculated through the speed  $v$  of the USW in the media (see Table A.15), and the angle,  $\Theta$ , Fig. 7.1a:



**Fig. 7.1** Ultrasonic proximity measurement: basic arrangement (a); impedance characteristic of piezoelectric transducer (b)

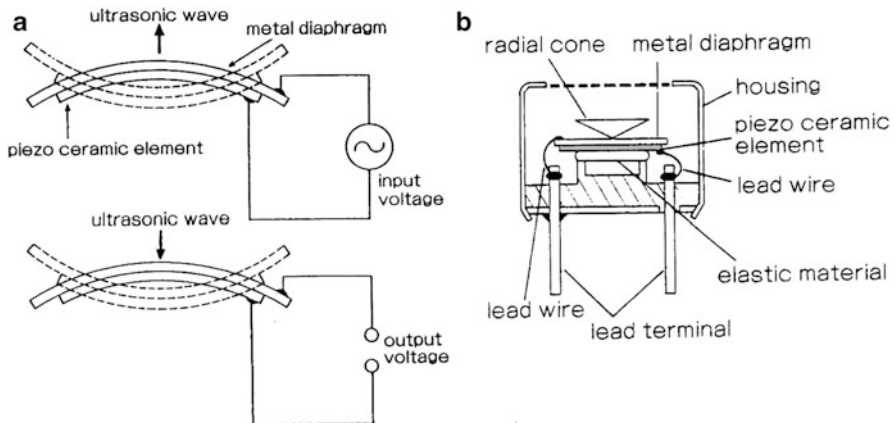
<sup>3</sup> See Sect. 7.2 for description of the Doppler effect for microwaves. The effect is fully applicable to propagation of any energy having wave nature, including ultrasonic.

$$L_0 = \frac{vt \cos\Theta}{2}, \quad (7.1)$$

where  $t$  is the time for the ultrasonic waves to travel to the object and back to the receiver (thus the denominator 2). If a transmitter and a receiver are positioned close to each other as compared with the distance to the object, then  $\cos\Theta \approx 1$ . USW have an obvious advantage over the microwaves: they propagate with the speed of sound, which is much slower than the speed of light at what the microwaves propagate. Thus, time  $t$  is much longer and its measurement can be accomplished easier and cheaper.

For generating any mechanical waves, including ultrasonic, movement of a surface is required. This movement creates compression and rarefaction of medium that can be gas (air), liquids, or solids. There are two main types of the ultrasonic transducers for operation in air: piezoelectric and electrostatic [2]. Electrostatic transducers have high sensitivity and bandwidth but require higher voltage for polarization and operation. The most common type of the excitation device that can generate surface movement in the ultrasonic range is a *piezoelectric* transducer operating in the so-called *motor* mode. A piezoelectric device directly converts electrical energy into mechanical energy. Piezoelectric transducers require lower-voltage excitation signals (10–20  $V_{\text{rms}}$ ), so the excitation stages are simpler and lower cost.

Figure 7.2a shows that the input voltage applied to the piezoelectric plate causes it to flex and transmit ultrasonic waves. Because piezoelectricity is a reversible phenomenon, the ceramic plate generates voltage when incoming ultrasonic waves make it to flex. In other words, the element may work as both the sonic generator (transmitter) and microphone (receiver). A typical operating frequency of the transmitting piezoelectric element is near 32 kHz. For better efficiency, frequency



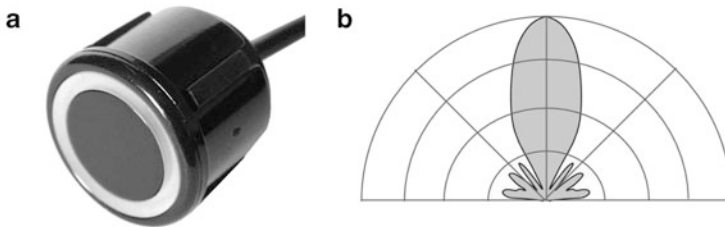
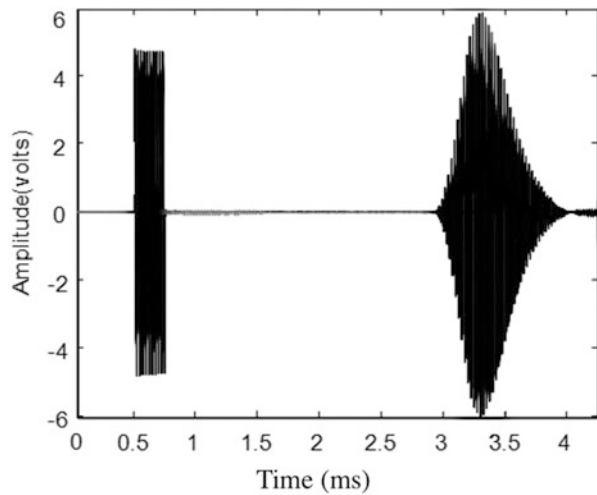
**Fig. 7.2** Piezoelectric USW transducer. Input voltage flexes the element and transmits ultrasonic waves, while incoming waves produce output voltage (a). Open aperture type of USW transducer for operation in air (b) (Courtesy of Nippon Ceramic, Japan)

of the driving oscillator should be adjusted to the resonant frequency  $f_r$  of the piezoelectric ceramic (Fig. 7.1b) where sensitivity and efficiency of the element is the best. A typical design of an air-operating sensor is shown in Figs. 7.2b and 7.4a. A directional sensitivity diagram (Fig. 7.4b) is important for a particular application. The narrower the diagram, the more sensitive the transducer.

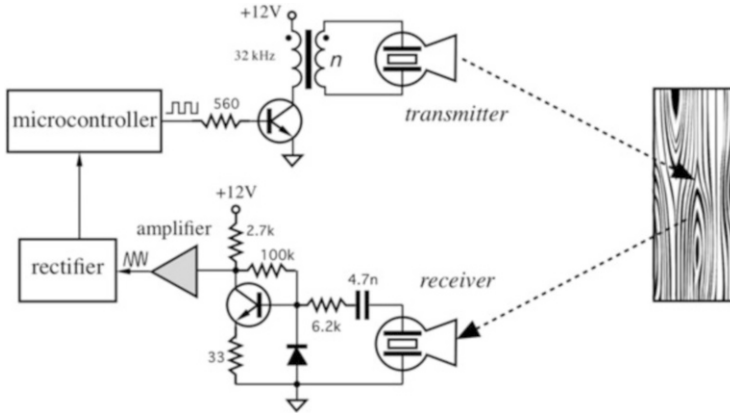
There are two possible operating modes for a USW transducer: a pulsed mode and continuous mode. When the measurement circuit operates in a pulsed mode and since piezoelectric crystal has a reversible nature, in most designs the same transducer is used for both—transmission and reception of the US signals [3]. The USW transducer transmits short bursts of sonic energy, detects reflected signal, and measures time of arrival of the received burst for computing a range to the object. Figure 7.3 illustrates shapes of the transmitted and received sonic bursts. Since time delay can be measured quite accurately, pulsed USW detectors can measure range with a high resolution. One popular application of this method is in the parking assistance detectors for a car.

In a system with continuous transmission of the USW, separate piezoelectric elements are employed for the transmitter and receiver. Figure 7.5 illustrates a

**Fig. 7.3** Transmitted and received USW signals in pulsed mode (adapted from [2])



**Fig. 7.4** USW transducer for air (a); directional diagram (b)



**Fig. 7.5** Simplified schematic of USW proximity detector operating in continuous mode

simplified circuit of a continuous USW detector. The transmitting transducer emanates a continuous stream of USW toward the object. The transmitting square pulses of 32 kHz are generated by the microcontroller and turn on and off the output transistor. To increase the detection range, the transformer amplifies the pulse amplitude, typically over 20 V. The reflected USW energy is received, amplified, filtered, and rectified. The rectified signal representing magnitude of the received energy is digitized by the microcontroller's ADC and compared with a software threshold. The stronger the amplitude the closer the object to the detector. Exceeding the threshold is the indication of a critical proximity. Unlike the pulsed USW device that measures a propagational time delay, the continuous device monitors only a magnitude of the received sonic waves and thus accurate distance measurement is not possible, yet for a great majority of applications such a qualitative detection is sufficient. Example of the applications include robotics and door openers.

## 7.2 Microwave Motion Detectors

The microwave detectors offer an attractive alternative to other devices when it is required to cover large areas and operate over an extended temperature range under the influence of strong ambient interferences, such as wind, acoustic noise, fog, dust, moisture, and so forth. These detectors emit pulses of electromagnetic energy toward the monitored area. The operating principle of a microwave detector is based on radiation of electromagnetic radio-frequency (RF) waves toward a protected area. The electromagnetic waves backscattered (reflected) from objects whose sizes are comparable with or larger than the wavelength of the transmitted signal. The reflected waves are received, amplified, and analyzed. A time delay between the sent (pilot) signal and reflected received signal is used for measuring

distance to the object, while the frequency shift is used for calculating speed of the object motion.

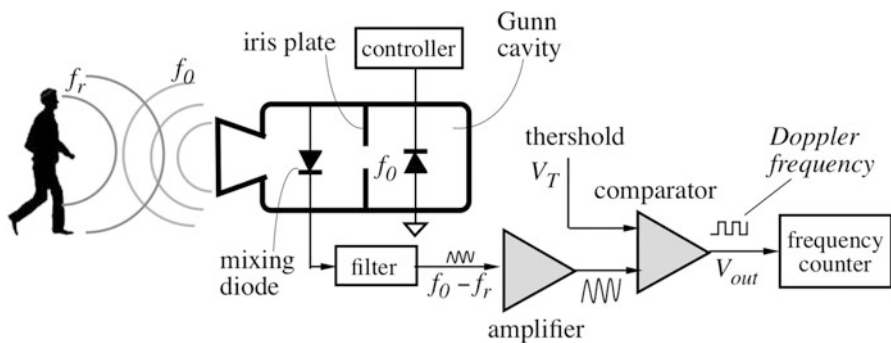
The microwave detectors belong to the class of devices known as *radars*. Radar is an acronym for *RA*dio *D*etection *A*nd *R*anging.

The standard radar frequencies are

Band	Frequency range (GHz), $f$	Wavelength range (cm), $\lambda$
K <sub>a</sub>	26.0–40.0	0.8–1.1
K	18.0–26.5	1.1–1.67
X	8.0–12.5	2.4–3.75
C	4.0–8.0	3.75–7.50
S	2.0–4.0	7.5–15
L	1.0–2.0	15–30
P	0.3–1.0	30–100

The name *microwave* is arbitrarily assigned to the wavelengths shorter than 4 cm (K<sub>a</sub>, K, and X bands). They are long enough ( $\lambda = 3$  cm at X-band) to pass freely through most contaminants, such as fog and airborne dust, and short enough for being reflected by larger objects. Other frequencies and types of energy (e.g., ultrasonic, and light,) are also used in a similar manner to the microwaves. For example, traffic police use laser guns to identify speeders. In the laser detectors, series of short (nanosecond) pulses of infrared laser light is emitted and the laser gun measures the time it takes for the bursts of light to be reflected and detected, just as in the microwave radars.

The microwave part of the detector (Fig. 7.6) consists of a Gunn oscillator, antenna, and mixer diode. The Gunn oscillator is a diode mounted in a small precision cavity that, upon application of power, oscillates at microwave frequencies. The oscillator produces electromagnetic waves (frequency  $f_0$ ), part of which is directed through an iris and mixing cavity into a waveguide and focusing antenna that directs the radiation toward the object. The iris controls the amount of microwave energy that reaches the mixing diode. Focusing characteristics of the



**Fig. 7.6** Microwave motion detector with Gunn oscillator and mixing diode

antenna are determined by the application. As a general rule, the narrower the directional diagram of the antenna, the more sensitive it is (the antenna has a higher gain). Another general rule is that a narrow-beam antenna is much larger, whereas a wide-angle antenna can be quite small. Typical radiated power of the transmitter is 10–20 mW. The Gunn oscillator is quite sensitive to stability of the applied dc voltage from the controller and, therefore, must be powered by a good quality voltage regulator. The oscillator may run continuously, or it can be pulsed, depending on the design.

A smaller part of the microwave oscillations is coupled to the Schottky mixing diode and serves as a reference signal. In many cases, the transmitter and receiver are contained in one module called a *transceiver*. The target reflects some waves back toward the antenna, which directs the received radiation toward the mixing diode. This induces electric current in the diode, containing a multitude of harmonic related to the object presence and movement. For the microwave and ultrasonic occupancy and motion detectors, Doppler effect is the basis for operation. It should be noted that a Doppler effect device is a true motion detector because it is responsive only to moving targets. Here is how it works.

The antenna transmits a pilot signal having frequency  $f_0$  which is defined through the wavelength  $\lambda_0$  as

$$f_0 = \frac{c_0}{\lambda_0}, \quad (7.2)$$

where  $c_0$  is the speed of light in air. When the target moves toward or away from the transmitting antenna, frequency of the reflected radiation changes. Thus, if the target is moving away with velocity  $v$ , the reflected frequency will decrease and it will increase for the approaching targets. This is called the Doppler effect, after the Austrian scientist Christian Johann Doppler (1803–1853).<sup>4</sup> Although the effect first was discovered for sound, it is applicable to electromagnetic radiation as well. However, in contrast to sound waves that propagate with the velocities related movement of both the source of sound and target, electromagnetic waves propagate with the speed of light, which is an absolute constant, independent of the light source speed. The frequency of reflected electromagnetic waves can be predicted by the Einstein's Special Theory of Relativity as

$$f_r = f_0 \frac{\sqrt{1 - \left(\frac{v}{c_0}\right)^2}}{1 + \frac{v}{c_0}}, \quad (7.3)$$

---

<sup>4</sup> During Doppler times, the acoustical instruments for precision measurements did not exist. To prove his theory, Doppler placed trumpeters on a railroad flatcar and musicians with a sense of absolute pitch near the tracks. A locomotive engine pulled the flatcar back and forth at different speeds for 2 days. The musicians on the ground "recorded" the trumpet notes as the train approached and receded. The equations held up.



where  $v$  is speed of the target movement toward or away from the detector. Note that the target speed  $v$  may be positive for the approaching target or negative for the going away target.

For practical purposes when detecting relatively slow moving objects, the quantity  $(v/c_0)^2$  is very small as compared with unity; hence, it can be ignored. Then, equation for the frequency of the reflected waves becomes:

$$f_r = f_0 \frac{1}{1 + \frac{v}{c_0}} \quad (7.4)$$

As follows from Eq. (7.4), due to a Doppler effect, the reflected waves have a different frequency  $f_r$ . The mixing diode combines the radiated (reference) and reflected frequencies and, being a nonlinear device, produces the induced signal which contains multiple harmonics of both frequencies. The induced electric current through the diode may be represented by a polynomial:

$$i = i_0 + \sum_{k=1}^n a_k (U_1 \cos 2\pi f_0 t + U_2 \cos 2\pi f_r t)^k, \quad (7.5)$$

where  $i_0$  is a d.c. component,  $a_k$  are the harmonic coefficients which depend on a diode operating point,  $U_1$  and  $U_2$  are amplitudes of the reference and received signals, respectively, and  $t$  is time. The induced current through the diode contains an infinite number of harmonics, among which there is a harmonic of a differential frequency:  $\Delta f = a_2 U_1 U_2 \cos 2\pi (f_0 - f_r) t$ , which is called a Doppler frequency.

The Doppler frequency in the mixing diode can be found from Eq. (7.4):

$$\Delta f = f_0 - f_r = f_0 \frac{1}{1 + \frac{v}{c_0}} = f_0 \frac{v}{v + c_0}, \quad (7.6)$$

and since  $c_0 \gg v$ , the following holds after substituting Eq. (7.2):

$$\Delta f \approx \frac{v}{\lambda_0} \quad (7.7)$$

Therefore, the signal frequency at the output of the mixer is proportional to the velocity of a moving target. For instance, if a person walks toward the detectors with a velocity of 0.6 m/s, a Doppler frequency for the X-band detector is  $\Delta f = 0.6 / 0.03 = 20$  Hz.

Equation (7.7) holds true only for movements in the normal direction (to or away from the detector). When the target moves at angles  $\Theta$  with respect to the detector, the Doppler frequency is

$$\Delta f \approx \frac{v}{\lambda_0} \cos \Theta \quad (7.8)$$

This implies that Doppler detectors theoretically become insensitive when a target moves at angles approaching  $90^\circ$ .

For the supermarket door openers and security alarms, instead of measuring frequency, a threshold comparator is used to indicate presence of a moving target at a predetermined range. It should be noted that even if Eq. (7.8) predicts that the Doppler frequency is near zero for targets moving at angles  $\Theta = 90^\circ$ , entering of a target into a protected area at any angle results in an abrupt change in the received signal amplitude, and the output voltage from the mixer changes accordingly. Usually, this is sufficient to trigger response of a threshold detector.

A signal from the mixer is in the range from microvolts to millivolts, so amplification is needed for the signal processing. Because the Doppler frequency is in the audio range, the amplifier is relatively simple. However, it generally must be accompanied by the so-called notch filters, which reject a power line frequency and the main harmonic from full-wave rectifiers and fluorescent light fixtures: 60 and 120 Hz (or 50 and 100 Hz).

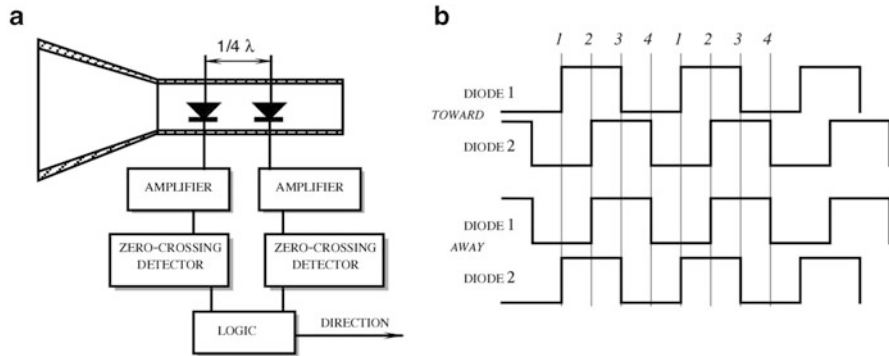
For reliable operation, the received microwave power must be sufficiently high. It depends on several factors, including the antenna aperture area  $A$ , target area  $a$ , and distance to the target  $r$ :

$$P_r = \rho \frac{P_0 A^2 a}{4\pi \lambda^2 r^4}, \quad (7.9)$$

where  $P_0$  is the transmitted power. For effective detection, the target's cross-sectional area  $a$  must be relatively large, because for  $\lambda^2 \leq a$ , the received signal is drastically reduced. Further, the coefficient of reflectivity  $\rho$  of a target in the operating wavelength is also very important for magnitude of the received signal. Generally, conductive materials and objects with high dielectric constants are good reflectors of electromagnetic radiation, whereas many dielectrics absorb energy and reflect very little. Plastics and ceramics are quite transmissive and can be used as windows in the microwave detectors.

The best target for a microwave detector is a smooth, flat conductive plate positioned normally toward the detector. A flat conductive surface makes a very good specular reflector; however, it may render the detector inoperable at angles other than  $0^\circ$ . Thus, the angle  $\Theta = 45^\circ$  can completely divert a reflective signal from the receiving antenna. This method of diversion, along with coating the target by materials having high absorptivity of electromagnetic radiation, has been used quite effectively in designs of the Stealth bombers, which are invisible on the radar screens.

To detect whether a target moves toward or away from the antenna, the Doppler concept can be extended by adding another mixing diode to the transceiver module. The second diode is located in the waveguide in such a manner that the Doppler signals from both diodes differ in phase by one-quarter of the wavelength or by  $90^\circ$  (Fig. 7.7a). These outputs are amplified separately and converted into square pulses that can be analyzed by a logic circuit. The circuit is a digital phase discriminator that determines the direction of motion (Fig. 7.7b). Door openers and traffic controls are two major applications for this type of module. Both applications



**Fig. 7.7** Block diagram (a) and timing diagrams (b) of microwave Doppler motion detector with directional sensitivity

need the ability to acquire a great deal of information about the target for discrimination before enabling a response. In door openers, limiting the field of view and transmitted power may substantially reduce the number of false-positive detections. While for the door openers a direction discrimination is optional, for traffic control it is a necessity to reject signals from the vehicles moving away.

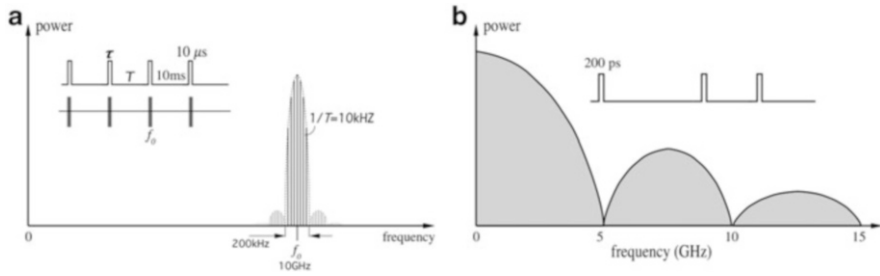
If the module is used for intrusion detection, vibrations of the building structures may cause false-positive detections. A direction discriminator will respond to vibration with an alternate signal, while a response to an intruder is a steady logic signal. Hence, the direction discriminator is an efficient way of improving reliability of detection, the reader should familiarize herself with Sect. 4.4.

Generally, a transmission and reception are alternated in time. That is, the receiver is disabled during a transmission, otherwise, a strong transmitted power not only will saturate the receiving circuitry but also may damage its sensitive components. In nature, bats use ultrasonic ranging to catch their small prey. The bats become deaf for the short time when the ultrasonic burst of energy is transmitted. This temporary blinding of the receiver is the main reason why radars and pulsed acoustic rangars are not effective at short distances—it is just not enough time to disable and enable the receiver.

Whenever a microwave detector is used in the United States, it must comply with the strict requirements (e.g., MSM20100) imposed by the Federal Communication Commission. Similar regulations are enforced in many other countries. Also, emission of the transmitter must be below 10 mW/cm<sup>2</sup> as averaged over any 0.1-h period, as specified by OSHA 1910.97 for the frequency range from 100 MHz to 100 GHz.

### 7.3 Micropower Impulse Radars

In 1993, U.S. Lawrence Livermore National Laboratory developed the first *micropower impulse radar* (MIR) which is a low-cost noncontact ranging sensor [4–6]. The operating principle of the MIR fundamentally is the same as of a



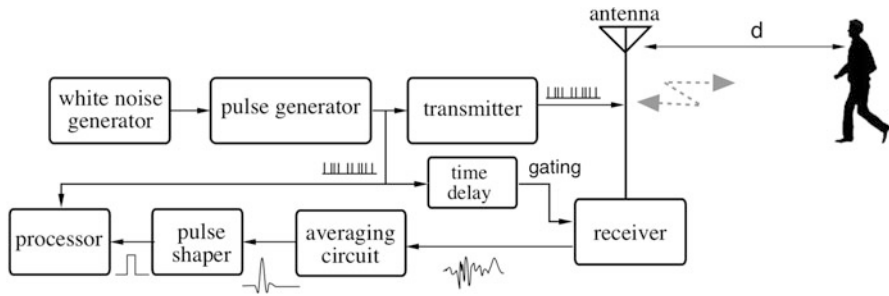
**Fig. 7.8** Radio spectrum of conventional radar transmitted signal with carrier frequency  $f_0 = 10\text{ GHz}$  (a) and of UWB radar (b)

conventional pulse radar system as described above, however with several significant differences. The MIR (Fig. 7.8) consists of a white noise generator whose output signal triggers a pulse generator. The pulse generator produces pulses with the average rate of 1 MHz and about 20 % variability. Each pulse has extremely short duration ( $\tau = 200\text{ ps}$ ), while the repetition of these pulses is random, according to a triggering by the noise generator. The pulses are spaced with respect to one another in a Gaussian noise-like pattern. It can be said that the pulses have a pulse-position modulation (PPM) by white noise with the maximum index of 20 %. These pulses are called the *pilot pulses*. Since they are triggered by noise, it is impossible to predict when the next pulse will appear. Because of the unpredictable modulation pattern, ultra-wide bandwidth, and extremely low spectral density of the transmitted signal, the MIR system is practically stealthy. Moreover, due to a random period of the transmitted pulses, the spectrum is continuous and to any nonsynchronous receiver it would appear as white noise.

Unlike a conventional pulse radar where a sine-wave carrier of high frequency is modulated by the pilot pulses (similar to Fig. 7.3) and then the carrier frequency bursts are radiated by the antenna, in the MIR the pilot pulses are transmitted themselves, without any carrier signal. Since in MIR a pilot pulse is very short, it has extremely wide frequency spectrum. Thus, this radar is often called the *ultra-wide band* (UWB) radar. To illustrate this point, refer to Fig. 7.8a that illustrates a radio spectrum of transmitted frequencies from a conventional radar. A controller in this radar modulates carrier frequency  $f_0$  (for example, 10 GHz in the X-band) by the square pulses of fixed duration  $\tau$  (for example,  $10\ \mu\text{s}$ ), repeating with fixed intervals  $T$  (for example, 10 ms). The transmitted spectrum is relatively narrow (after a tuned antenna it is only 200 kHz wide) and discrete with the harmonic intervals equal to  $1/T$ , centering around the carrier frequency  $f_0$ .

For the MIR (UWB) radar with the pulses of 200 ps, the spectrum is continuous and has no carrier frequency (Fig. 7.8b) and thus it spreads from d.c. to tens of GHz.

The UWB radio transmitter produces the infinite number of very low-power harmonics that propagate from the antenna to surrounding space. Electromagnetic waves reflect from the objects and return back to the antenna (Fig. 7.9). The same random pulse generator that forms the transmitted pulses, also gates the ultrawide



**Fig. 7.9** Block-diagram of UWB micropower impulse radar

band receiver with a predetermined delay from each transmitted pulse. This enables a synchronous reception by the MIR only of those reflected pulses that arrive during a specific time window, in other words – within a specific range of distances,  $d$ . At all other times, the receiver is turned off. Another reason for gating the receiver is to reduce its power consumption.

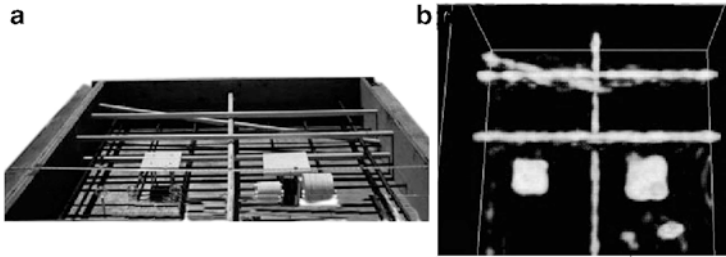
Each received pulse is very weak and buried in noise, that is it has a very small signal-to-noise ratio—well below unity. Thus, a large number of these pulses are averaged before further processing. For example, for the mean period  $T = 1$  MHz, 1000 received pulses are averaged to arrive at the 1 kHz combined pulses. Averaging improves a signal-to-noise ratio by about 30 times. The averaged pulses are shaped (a square-wave form is restored), and a time delay with respect to the respective transmitted pulses is measured by the processor, just like in a conventional radar. A time delay is proportional to distance  $d$  from the antenna to the object from which the radio waves are reflected:  $t_d = 2d/c_0$ , where  $c_0$  is the speed of light.

A spatial distribution of the transmitted energy is determined by type of the antenna. For a dipole antenna it covers nearly  $360^\circ$ , but it may be shaped to a desired pattern by employing a horn, reflector, or lens.

The average duty cycle of the transmitted pulses is very small (about 0.02 %) and since they are spaced randomly, practically any number of identical MIR systems may operate in the same space in spite of the overlapping spectra. There is a negligible chance that pulses from different transmitters would coincide, and even if they do, interferences will be nearly eliminated by the averaging circuit.

Other advantages of the MIR are a low cost and extremely small power consumption of the radio receiver—about  $12 \mu\text{W}$ . The total power consumption of the entire MIR system is near  $50 \mu\text{W}$ , thus two AA alkaline batteries may power it continuously for several years. The MIR has a short operating range, usually no longer than several meters.

Applications for the MIR include range meters, intrusion alarms, level detectors, vehicle ranging devices, automation systems, detection of objects hidden behind walls, penetrating imaging, robotics, medical instruments [7], weapons, novelty products, and even toys where relatively short range of detection is required. As an example, Fig. 7.10 illustrates detection of steel bars through a layer of concrete.

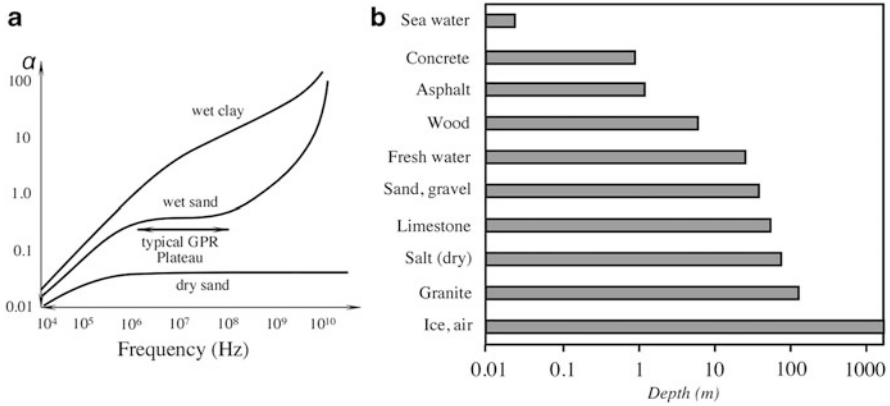


**Fig. 7.10** MIR imaging of steel bars in concrete. Internal elements of a concrete slab before pouring (a). Reconstructed 3-D MIR image of the steel bars embedded in finished 30-cm-thick concrete slab (b)

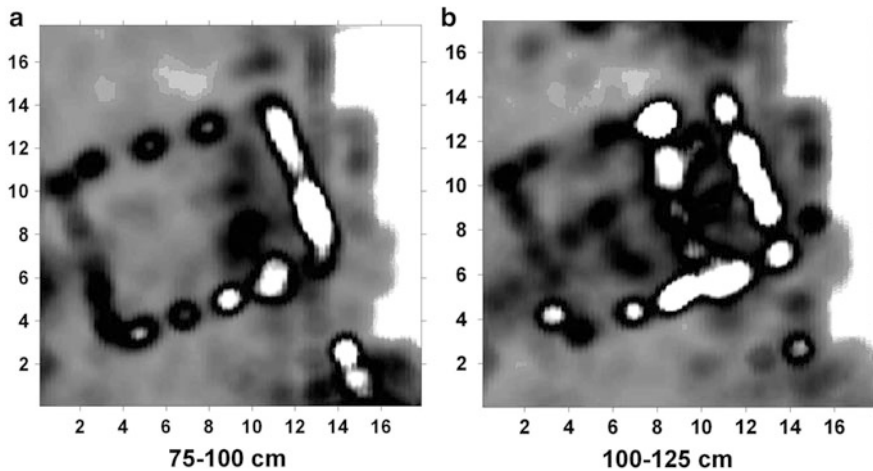
## 7.4 Ground Penetrating Radars

Civil engineering, archeology, forensic science, security (to detect illegal tunnels, explosive devices, etc.)—these are just few examples of many applications of the high frequency ground penetrating radars (GPR). The radar operation is rather classical—it transmits radio waves and receives the reflected signal. The time delay between the transmitted and received signal is the measure of a distance to the reflecting surface. While the radars that operate in air and Space have ranges that may reach thousands of kilometers, the GPR range at best is just several hundred meters. A practical GPR operates at frequencies from 500 MHz to 1.5 GHz ([www.sensoft.ca](http://www.sensoft.ca)). Radio waves do not penetrate far through soils, rocks, and most man-made materials such as concrete. The exponential attenuation coefficient,  $\alpha$ , is primarily determined by electrical conductivity of the material. In simple uniform materials this is usually the dominant factor. In most materials, energy is also lost to scattering from material variability and to water contents. Water has two effects: first, it contains ions, which contribute to bulk conductivity. Second, a water molecule absorbs electromagnetic energy at high frequencies typically above 1 GHz. Figure 7.11a shows that attenuation varies with excitation frequency and material. At low frequencies ( $<1$  MHz), the attenuation is primarily controlled by a d.c. conductivity. At high frequencies ( $>1$  GHz), water is a strong energy absorber, thus, the practical maximum distance increases for dry materials, Fig. 7.11b. An example of data presented on the radar monitor is shown in Fig. 7.12.

Lowering frequency improves depth of exploration because attenuation primarily increases with frequency. As frequency decreases, however, two other fundamental aspects of the GPR measurement come into play. First, reducing frequency results in loss of a resolution. Second, if frequency is too low, electromagnetic fields no longer travel as waves but diffuse which is the realm of inductive EM or eddy current measurements.



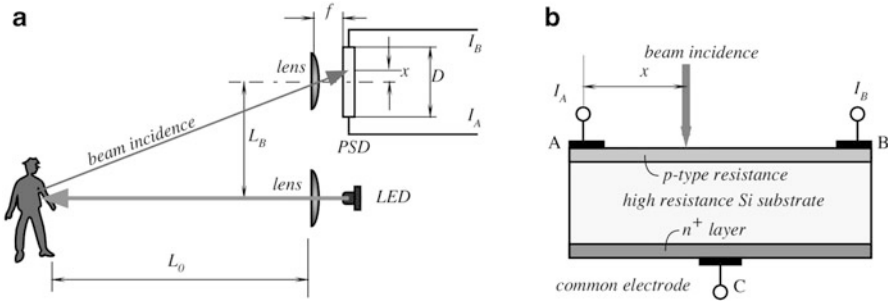
**Fig. 7.11** Attenuation of radio waves in different materials (a). Maximum depth for various materials (b)



**Fig. 7.12** Images of depth slices in Roman Temple at Petra (Jordan), showing different levels of temple at different depths (courtesy of Prof. L. Conyers, *University of Denver*)

## 7.5 Linear Optical Sensors (PSD)

For precision position measurements over short and long ranges, optical systems operating in the near infrared can be quite effective. An example is a *position-sensitive detector* (PSD) that originally was produced for precision position sensing and autofocus in photographic and video cameras. The position measuring module is of an active type: it incorporates a light-emitting diode (LED) and a photosensitive PSD. The LED serves as an illuminator of the objects.



**Fig. 7.13** The PSD sensor measures distance by applying triangular principle (a) and design of one-dimensional PSD (b)

Position of an object is determined by applying the principle of a triangular measurement. Figure 7.13 shows that the near-infrared LED through a collimator lens produces a narrow-angle beam ( $<2^\circ$ ) of a 0.7 ms wide pulse. On striking the object, the beam is reflected back to the detector. The received low intensity light is focused on a photosensitive surface of the PSD. The PSD is not a digital device, it is a linear sensor that allows infinitesimal resolution of detection. It generates the output currents  $I_B$  and  $I_A$  which are proportional to distance  $x$  of the light spot on its surface, from the central position.

Intensity of a received beam greatly depends on the reflective properties of an object. Diffusive reflectivity in the near-infrared spectral range is close to that in the visible range, hence, intensity of the light incident on PSD has a great deal of variations. Nevertheless, accuracy of the measurement depends very little on intensity of the received light.

A PSD operates on the principle of photoeffect. It makes use of a surface resistance of a silicon photodiode. Unlike MOS and CCD sensors incorporating multielement photodiode arrays, the PSD has a nondiscrete sensitive area. It provides one-dimensional, or two-dimensional [8] position signals from a light spot traveling over its sensitive surface. A sensor is fabricated of a piece of high resistance silicon with two layers ( $p$  and  $n^+$  types), Fig. 7.13b. A one-dimensional sensor has two electrodes (A and B) formed on the upper layer to provide electrical contacts to the  $p$ -type resistance. There is a common electrode (C) at the center of the bottom layer. Photoelectric effect occurs in the  $pn$ -junction. The distance between two upper electrodes is  $D$ , and the corresponding resistance between these two electrodes is  $R_D$ . Let us assume that the beam incidence strikes the surface at distance  $x$  from the A electrode. Then, the corresponding resistance between that electrode and the point of incidence is, respectively,  $R_x$ . The photoelectric current  $I_0$  produced by the beam is proportional to its intensity. That current will flow to both outputs (A and B) of the sensors in the corresponding proportions to the resistances and, therefore, to the distances between the point of incidence and the electrodes



$$I_A = I_0 \frac{R_D - R_x}{R_D} \text{ and } I_B = I_0 \frac{R_x}{R_D}. \quad (7.10)$$

If the resistances-versus-distances are linear, they can be replaced with the respective distances on the surface

$$I_A = I_0 \frac{D - x}{D} \text{ and } I_B = I_0 \frac{x}{D}. \quad (7.11)$$

To eliminate dependence of the photoelectric current (and of the light intensity), we can use a ratiometric technique of the signal processing, that is we take a ratio of the currents

$$P = \frac{I_A}{I_B} = \frac{D}{x} - 1, \quad (7.12)$$

which we can rewrite for the value of  $x$ :

$$x = \frac{D}{P + 1}. \quad (7.13)$$

To compute distance  $L_0$  refer to Fig. 7.13a where the lens with the focal distance  $f$  focuses the beam incidence on the PSD surface at the shift  $x$  from the center. Solving two triangles for  $L_0$  yields

$$L_0 = f \frac{L_B}{x}, \quad (7.14)$$

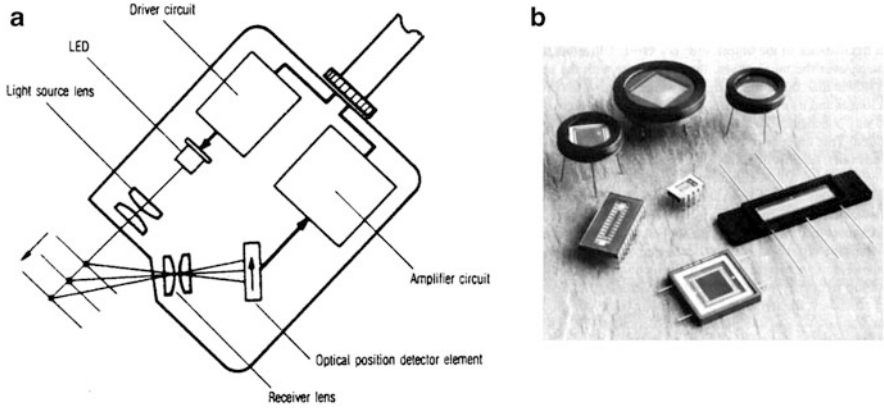
Substituting Eq. (7.13) to Eq. (7.14) we arrive at the distance in terms of the currents ratio

$$L_0 = f \frac{L_B}{D} (P + 1) = k(P + 1), \quad (7.15)$$

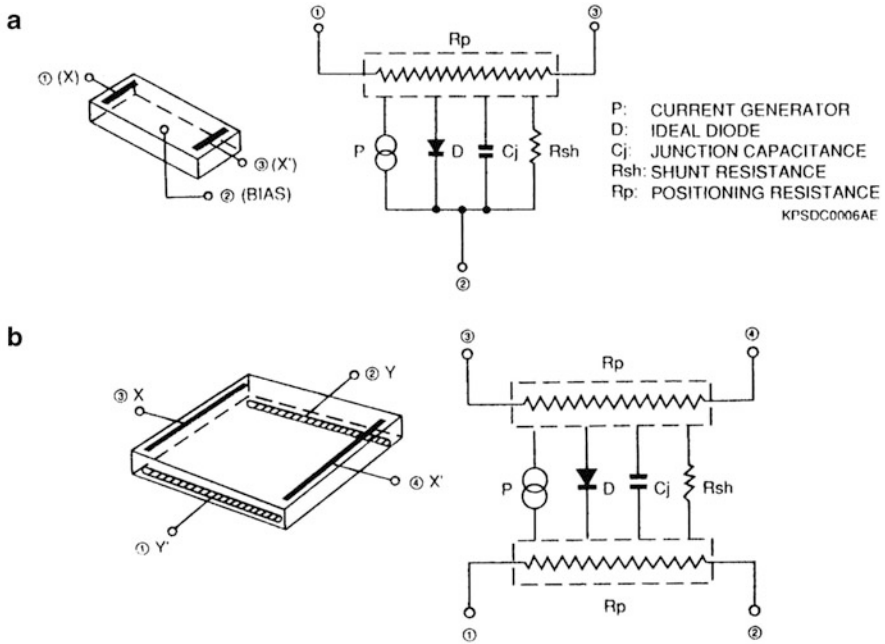
where  $k$  is called the module's geometrical constant. Therefore, the distance from the detector to the object linearly affects ratio of the PSD output currents.

A PSD with a triangulation principle is implemented in an industrial optical displacement sensor, Fig. 7.14a, where PSD is used for measuring a small displacements at the operating distances of several centimeters. Such optical sensors are highly efficient for the production line measurements of height of a device (the PC-board inspection, liquid and solids level control, laser torch height control, etc.), for measuring eccentricity of a rotating object, thickness and precision displacement measurements, detection of presence or absence of an object (e.g., medicine bottle caps), etc. [8].

The PSD elements are produced of two basic types: one- and two-dimensional. The equivalent circuits of both are shown in Fig. 7.15. Since the equivalent circuit has a distributed capacitance and resistance, the PSD time constant varies depending on the position of the light spot. In response to an input step function,



**Fig. 7.14** Optical-position sensor (a) (From Keyence Corp. of America, Fair Lawn, N.J.) and samples of different PSD (b)



**Fig. 7.15** Equivalent circuits for one- (a) and two-dimensional (b) position-sensitive detectors (Courtesy of Hamamatsu Photonics K.K., Japan)

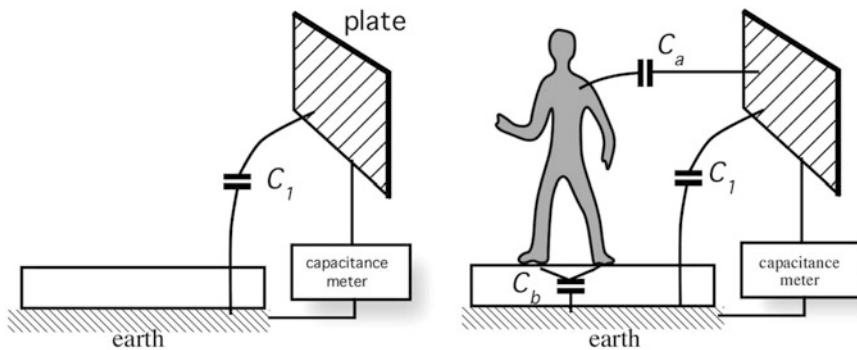
a small area PSD has rise time in the range of 1–2  $\mu$ s. Its spectral response is approximately from 320 to 1100 nm, that is, the PSD covers the UV, visible, and near-infrared spectral ranges. Small area one-dimensional PSDs have the sensitive surfaces ranging from 1  $\times$  2 to 1  $\times$  12 mm, while the large area two-dimensional sensors have square areas with the side ranging from 4 to 27 mm.

## 7.6 Capacitive Occupancy Detectors

Being a conductive medium with a high dielectric constant, a human body develops a strong coupling capacitance to its surroundings.<sup>5</sup> This capacitance greatly depends on such factors as body size, clothing, type of the surrounding objects, weather, and so forth. However wide the coupling range is, the capacitance may vary from few picofarads to several nanofarads. When a person moves, the coupling capacitance varies, thus making it possible to discriminate static objects from moving objects.

Any object forms some degree of a capacitive coupling with respect to another object. If a human (or for that purpose—anything) moves into vicinity of the stationary objects whose coupling capacitance with each other has been previously established, a new capacitive value arises between the surrounding objects as a result of presence of an intruding body. Figure 7.16 shows that capacitance between a test plate and earth<sup>6</sup> is equal to  $C_1$ . When a person moves into vicinity of the plate, it forms two additional capacitors: one between the plate and its own body,  $C_a$ , and the other between the body and the earth,  $C_b$ . The resulting capacitance  $C$  between the plate and the earth becomes larger by the incremental capacitance  $\Delta C$

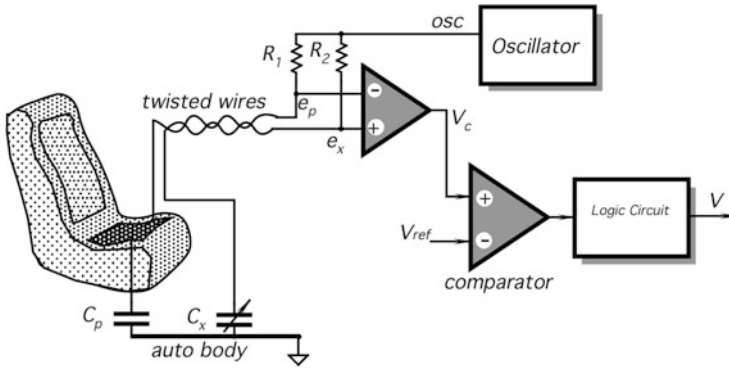
$$C = C_1 + \Delta C = C_1 + \frac{C_a C_b}{C_a + C_b}. \quad (7.16)$$



**Fig. 7.16** Intruder brings in an additional capacitance to a detection circuit

<sup>5</sup> At 40 MHz, the dielectric constants of muscle, skin, and blood are quite large—about 97. For fat and bones, it is near 15.

<sup>6</sup> Here, by “earth” we mean any large object, such as the earth, lake, metal fence, car, ship, airplane, and so forth.

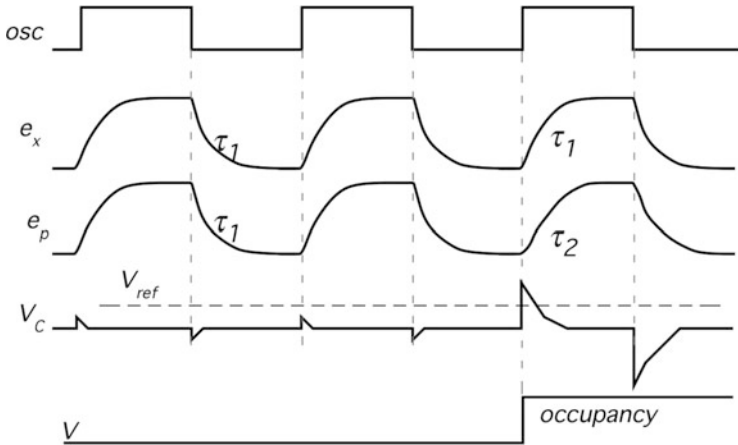


**Fig. 7.17** Capacitive intrusion detector for automotive applications

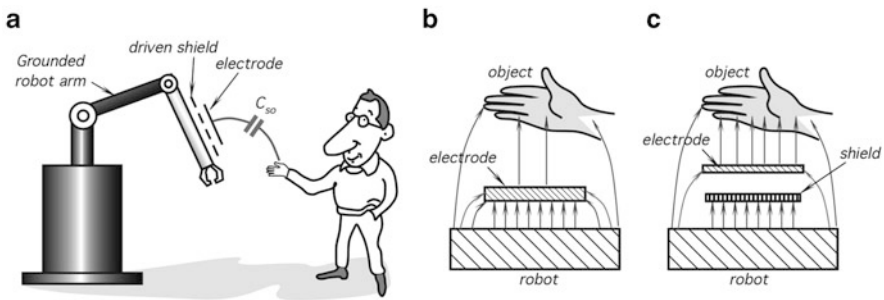
With the appropriate apparatus, this phenomenon can be used for occupancy detection. We just need to measure capacitance between a test plate (the probe) and a reference plate (the earth).

Figure 7.17 illustrates the capacitive security system for an automobile [9]. The sensing probe is imbedded into a car seat. It can be fabricated as a metal plate, metal net, conductive fabric, etc. The probe forms one plate of a capacitor  $C_p$ . The other plate of the capacitor is formed either by a body of an automobile, or by a separate plate positioned under a floor mat. A reference capacitor  $C_x$  is composed of a simple fixed or trimming capacitor which should be placed close to the seat probe. The probe plate and the reference capacitor are, respectively, connected to two inputs of a charge detector (resistors  $R_1$  and  $R_2$ ). The conductors preferably should be twisted to reduce introduction of spurious signals as much as possible. For instance, strips of a twinflex cabling were found quite adequate. A differential charge detector is controlled by an oscillator which produces square pulses, Fig. 7.18. Under a no-seat-occupied condition, the reference capacitor is adjusted to be approximately equal to  $C_p$ . Resistors and the corresponding capacitors define time constants of the networks. Both  $RC$  circuits have nearly equal time constants  $\tau_1$ . Voltages across the resistors are fed into the inputs of a differential amplifier, whose output voltage  $V_c$  is near zero because it rejects the in-phase (common mode) signals. Small spikes at the output are the result of some unavoidable imbalance. When a person is positioned on the seat, her body forms an additional capacitance in parallel with  $C_p$ , thus increasing a time constant of the  $R_1C_p$  network from  $\tau_1$  to  $\tau_2$ . This causes the increased spike amplitudes at the output of a differential amplifier. The comparator compares  $V_c$  with a predetermined threshold voltage  $V_{ref}$ . When the spikes exceed the threshold, the comparator sends an indicating signal to the logic circuit that generates signal  $V$  manifesting the car occupancy. It should be noted that a capacitive detector is an active sensor, because it essentially required an oscillating pilot signal for measuring the capacitance value.

When a capacitive occupancy (proximity) sensor is used near or on a metal device, its sensitivity may be severely reduced due to a stray capacitive coupling

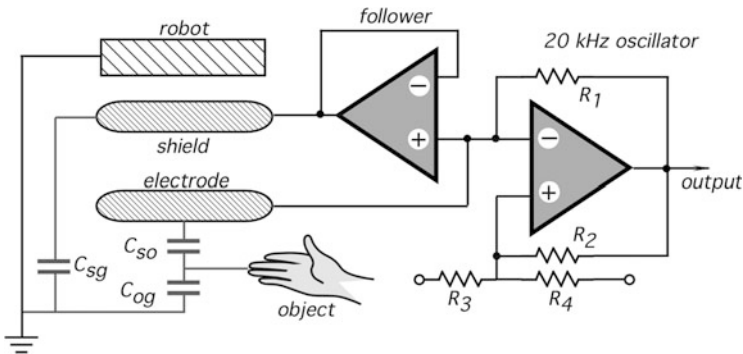


**Fig. 7.18** Timing diagrams for a capacitive intrusion detector



**Fig. 7.19** Capacitive proximity sensor. A driven shield is positioned on metal arm of grounded robot (a). Without shield, the electric field is distributed between electrode and robot (b), while driven shield directs electric field from electrode toward object (c)

between the electrode and device’s metallic parts [10]. An effective way of reducing that stray capacitance is to use driven shields. Figure 7.19a shows a robot with a metal arm. The arm moves near people and other potentially conductive objects with which it potentially could collide if the robot’s control computer is not provided with the advance warning on proximity to the obstacles. An obstacle (object), while approaching the arm, forms a capacitive coupling with it, which is equal to  $C_{s0}$ . To form a capacitive sensor, the arm is covered with an electrically isolated conductive sheath—the *electrode*. The nearby massive metal arm (Fig. 7.19b) forms a much stronger capacitive coupling with the electrode which drags the electric field away from the obstacle. An elegant solution is to decouple the electrode from the robot arm by a driven shield as shown in Fig. 7.19c. The sensor’s assembly is a multilayer cover for the robotic arm, where the bottom layer is an insulator, then there is a large electrically conductive shield, then another



**Fig. 7.20** Simplified circuit diagram of frequency modulator controlled by input capacitance formed by obstacle (object)

layer of insulation, and on the top is a narrower sheet of the electrode. To reduce a capacitive coupling between the electrode and arm, the shield must be maintained at the same potential as the electrode, that is, its voltage needs to be driven by the electrode voltage (hence the name *driven shield*). As a result, no electric field is formed between them. The electric field is squeezed out from beneath the electrode and distributed toward the obstacle for a reliable detection.

Figure 7.20 shows a simplified circuit diagram of a square-wave oscillator whose frequency depends on the net input capacitance, comprised of  $C_{sg}$  (sensor-to-ground),  $C_{so}$  (sensor-to-object), and  $C_{og}$  (object-to-ground). The electrode is connected to the driven shield through a voltage follower. A frequency-modulated signal is fed into the robot's computer for controlling the arm movement. This arrangement allows detection of proximity to conductive objects over the range up to 30 cm.

## 7.7 Triboelectric Detectors

Any object can accumulate on its surface static electricity. These naturally occurring charges arise from the *triboelectric effect*, that is a process of charge separation due to object movements, friction of clothing fibers, air turbulence, atmosphere electricity, etc. (see Sect. 4.1). Usually, air contains either positive or negative ions that can be attracted to human body, thus modifying its charge. Under the idealized static conditions, an object is not charged—its bulk charge is equal to zero. In reality, any object that at least temporarily is isolated from ground can exhibit some degree of its bulk charge imbalance. In other words, it becomes a carrier of electric charges.

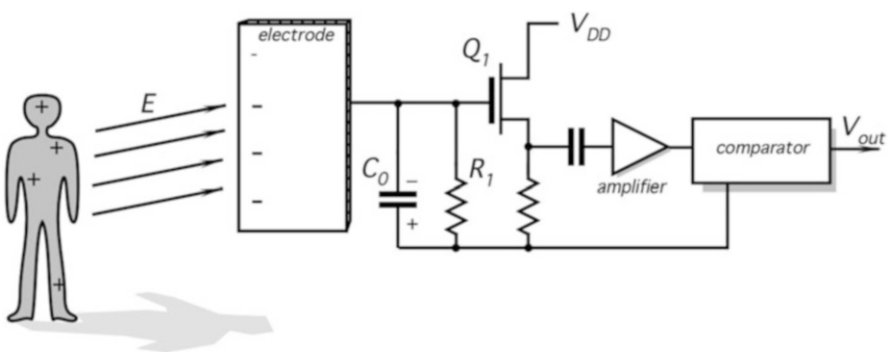
Any electronic circuit is made of conductors and dielectrics. If a circuit is not electrically shielded, all its components exhibit a certain capacitive coupling to the surrounding objects. To sense external electric fields, a pick-up electrode can be

added to the circuit's input to increase its coupling to the environment, very much like in the capacitive detectors that were covered in the previous Sect. 6.6. The electrode can be fabricated in form of a conductive surface that is well isolated from ground. The difference between the triboelectric and capacitive sensors is that in the former no pilot signal is generated to measure capacitance, but rather an electric charge that is accumulated on the object is detected, so the triboelectric detector is passive, while capacitive is active.

Electric field is established between the surrounding objects and the electrode whenever at least one of them carries electric charges. In other words, all distributed capacitors formed between the electrode and environmental objects are charged by the static or slow changing electric fields that resulted from a triboelectric effect. Under a no-occupancy condition, electric field in the electrode vicinity is either constant or changes relatively slow.

If a charge carrier (a human or animal) changes its position: moves away or a new charge-carrying object enters into vicinity of the electrode, a static electric field is disturbed. This results in a redistribution of charges between the coupling capacitors. The charge magnitude depends on the atmospheric conditions and nature of the objects. For instance, a person in dry man-made clothes<sup>7</sup> walking along a carpet carries much stronger charge than a wet intruder who has come in from the rain. An electronic circuit can be adapted for sensing these variable charges at its input. In other words, it can be made capable of converting the induced variable charges into electric signals that may be amplified and further processed.

Figure 7.21 shows a monopolar triboelectric motion detector. It is comprised of a conductive electrode connected to an analog impedance converter made with a MOS transistor  $Q_1$ , a bias resistor  $R_1$ , input capacitance  $C_0$ , gain stage, and a window comparator [11]. While the rest of the electronic circuit may be shielded, the sensing electrode is exposed to the environment and forms a coupling capacitor



**Fig. 7.21** Monopolar triboelectric motion detector

<sup>7</sup> Many “man-made” objects are made by women, so do not look for any sexism here.

$C_p$  with the surrounding objects. In Fig. 7.21, static electricity is exemplified by positive charges distributed along the person's body. Being a charge carrier, the person becomes a source of an electric field, having intensity  $E$ . The field induces a charge of the opposite sign in the electrode. Under the static conditions, when the person does not move, the field intensity is constant and the input capacitance  $C_0$  is discharged through a bias resistor  $R_1$ . To make the circuit sensitive to relatively slow motions, resistor  $R_1$  should be selected of a very high value: on the order of  $10^{10} \Omega$  or higher. When the person moves, intensity  $E$  of the electric field changes. This induces a corresponding variable electric charge in the input capacitor  $C_0$  and results in appearance of a variable electric voltage across the bias resistor. That voltage is fed to the gain stage whose output signal is applied to a window comparator. The comparator compares the signal with two thresholds, as it is illustrated in a timing diagram of Fig. 7.22b. A positive threshold is normally higher than the baseline static signal, while the negative threshold is lower. During human movement, a signal at the comparator's input deflects either upward or downward, crossing one of the thresholds. The output signals from the window comparator are square pulses that can be utilized and further processed by the conventional data processing devices. Since a triboelectric detector is passive and relies on detection of electric fields that penetrate many nonconductive objects, it may be hidden in or behind nonconductive objects such as wood, bricks, etc.

There are several possible sources of interferences that may cause spurious detections. A triboelectric detector may be subjected to a transmitted noise. Among the noise sources are 60 or 50 Hz power line signals, electromagnetic fields generated by radio stations, power electric equipment, lightnings, etc. Most of these interferences generate electric strong fields which are distributed around the detector quite uniformly and thus can be compensated for by employing a differential input circuit with a large common-mode rejection ratio.

---

## 7.8 Optoelectronic Motion Detectors

By far the most popular intrusion sensors are the optoelectronic motion detectors. They rely on electromagnetic radiation in the optical spectral range, specifically having wavelengths from 0.4 to 20  $\mu\text{m}$ . This covers visible, near-, and part of far-infrared (IR) ranges. The detectors are primarily used for indication of movement of people and animals. They operate over distances ranging up to several hundred meters and, depending on the need, may have either a narrow or wide angle of view.

The operating principle of the optical motion detectors is based on detection of light reflected or emanated from surface of a moving object into the surrounding space. The light may be originated either by an external light source and then reflected by the object or it may be produced by the object itself in form of a natural IR (thermal) emission. The former case is classified as an active detector and the latter—a passive. Hence, an active detector requires an additional light source, for instance, daylight, electric lamp, infrared LED projector, laser, etc. Passive infrared



(PIR) detectors perceive mid- and far-infrared natural emission from objects having temperatures that are different from the surroundings. Both types of detectors use a variable *optical contrast* as means of the object recognition.

The optoelectronic detectors are used almost exclusively for detecting movement qualitatively rather than quantitatively. In other words, optoelectronic detectors are very useful for indicating whether an object moves or not, while they cannot reliably distinguish one moving object from another and cannot be utilized for accurate measurement of a distance to a moving object or its velocity. Major application areas for the optoelectronic motion detectors are in security systems (to detect intruders), in energy management (to turn lights on and off), and in the so-called “smart” homes where they can control various appliances, such as air conditioners, cooling fans, audio players, etc. They also may be used in robots, toys, point-of-sale advertisements, and novelty products. The most important advantage of an optoelectronic motion detector is simplicity, reliability, and low cost.

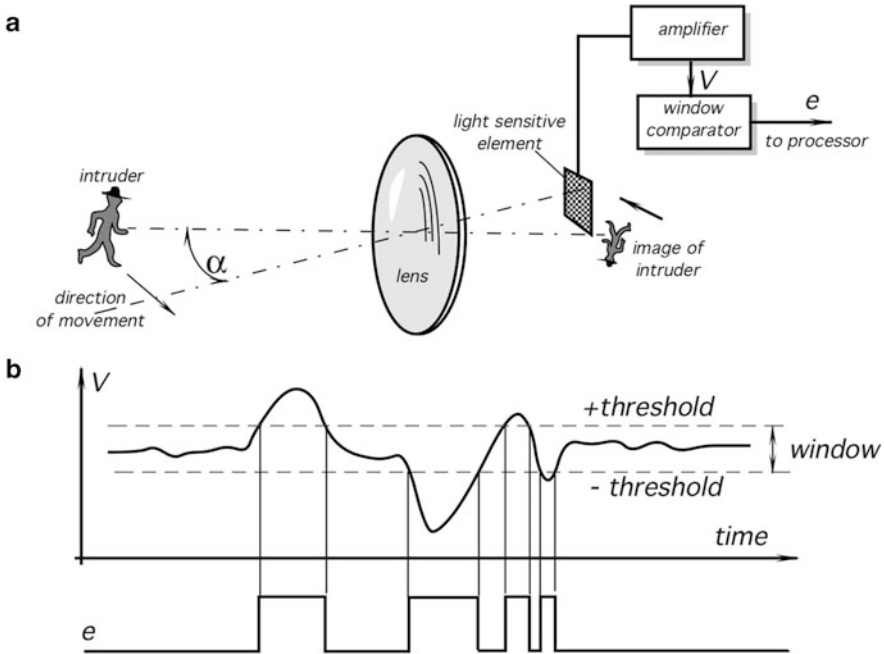
### 7.8.1 Sensor Structures

A general structure of an optoelectronic motion detector is shown in Fig. 7.22a. Regardless what kind of a sensing element is employed, the following components are essential: a focusing device (a lens or curved mirror), a light detecting element, and a threshold comparator. An optoelectronic motion detector resembles a photographic camera. Its focusing component creates on a focal plane an image of the field of view. While there is no shutter like in a film camera, in place of an imaging sensor or film, a light sensitive element is used. The element converts the optical energy received from the image into electric signal. Since the image is not being processed as it would be in a multipixel sensor in a video camera, the motion-sensing element can be considered as a single-pixel optoelectronic detector.<sup>8</sup>

Let us assume that the motion detector is mounted in a room. A focusing lens creates an image of the room on a focal plane where the light sensitive element is positioned. If the room is unoccupied, the image is static and the output signal from the element is steady-stable, depending on the optical power received from the room. When an “intruder” enters the room and keeps moving, her image on the focal plane also moves. At a certain moment, the intruder’s body is displaced from an arbitrary reference position by the angle  $\alpha$  and her image overlaps with the sensing element. This is an important point to understand—a detection is produced only at the moment when the object’s image either coincides with the element surface or clears it. That is, no crossing—no detection. Assuming that the intruder’s body creates an image whose photon flux is different from that being detected from

---

<sup>8</sup> In a differential sensor, as described below, two “pixels” are employed.



**Fig. 7.22** General arrangement of optoelectronic motion detector. Lens forms image of moving object (intruder). When image crosses sensor's optical axis it coincides with light-sensing element (a). Sensor responds with electric signal that is amplified and compared with window thresholds in comparator (b)

the static surroundings, the light sensitive element responds with a deflecting voltage  $V$ . In other words, to cause detection, a moving image shall have a certain degree of an optical contrast with its surroundings.

Figure 7.22b shows that the output signal  $V$  is compared with two thresholds in a window comparator. The purpose of the comparator is to convert the signal into two logic levels: 0—no motion detected and 1—motion is detected. In most cases, signal  $V$  from the sensing element first must be amplified and conditioned before it becomes suitable for the threshold comparison. Operation of this circuit is identical to the threshold circuits described earlier for other types of motion detectors.

It may be noted in Fig. 7.22 that the detector has quite a narrow field of view: if the intruder moves, her image will overlap with the sensor only once. After that—no detection. This is the result of a small area of the sensing element. Sometimes, when only a narrow field of view is required it is quite all right, however, in the majority of practical cases, a wider field of view is desirable, so the intruder image should cross the sensing element multiple times—across the field of view. This can be achieved by several methods described below.

### 7.8.2 Multiple Detecting Elements

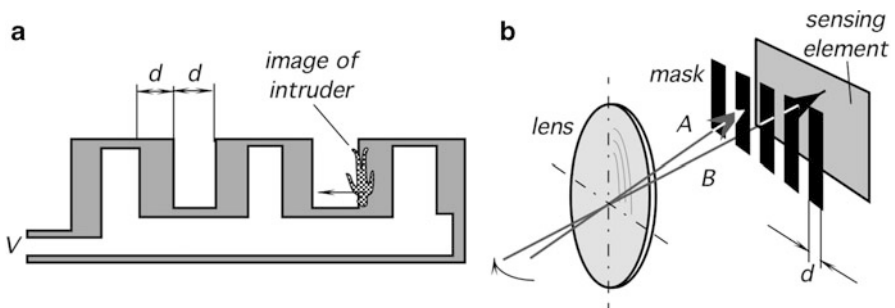
An array of detecting elements (multiple pixels) may be placed in the focal plane of a focusing mirror or lens. Each individual element covers a narrow field of view, while in combination they protect larger area. All detectors in the array either shall be multiplexed or otherwise interconnected to produce a combined detection signal.

### 7.8.3 Complex Sensor Shape

If the detecting element's surface area is sufficiently large to cover the entire angle of view, the area may be optically broken into smaller elements, thus creating an equivalent of a multiple detector array. To break up the surface area into several parts, one way is to shape the sensing (detecting) element in an odd pattern like that shown in Fig. 7.23a. Each part of the element acts as a separate light detector. All such detectors are electrically connected either in parallel or in series, being arranged in a serpentine pattern. The parallel or serially connected detectors generate a combined output signal, for instance, voltage  $v$ , when image of the object moves along the element surface crossing alternatively sensitive and non-sensitive areas. This results in an alternate signal  $v$  at the detector terminals. For a better sensitivity, such sensitive and nonsensitive areas should be sufficiently large to cover the entire angle of view.

### 7.8.4 Image Distortion

Instead of making the detector in a complex shape, the image of an entire field of view may be broken into several parts. This can be done by placing a distortion mask [12] in front of the detector having a sufficiently large area as is depicted in Fig. 7.23b. The mask is opaque and allows formation of an image on the detector's surface only within its clearings. The mask operation is analogous to the complex sensor's shape as described above. A limitation of this method is the need of a sensing element having large surface area.



**Fig. 7.23** Complex shape of a sensing element (a); and image distortion mask (b)

### 7.8.5 Facet Focusing Elements

A common way of broadening the field of view while employing a small area detector is to use multiple focusing devices. A focusing mirror or a lens may be divided into arrays of smaller mirrors or lenses (see Fig. 5.17b) called *facets*, resembling an eye of an insect. Each facet works as an individual lens (mirror) creating its own image on a common focal plane, while receiving images from different sections of the field of view. All facets form multiple images as shown in Fig. 7.24a. When the object moves, the image made by each individual facet also moves across the focal plane. Since numerous lenses produce numerous images, at least one image will cross the sensing element causing it to generate an alternating signal. By combining multiple facets it is possible to shape any desirable detecting pattern in the field of view, in both horizontal and vertical planes. To develop the lens and design the detector, first a field of view and ranges shall be defined. Then the facet focal distances, their number, and the pitch of the facets (a distance between the optical axes of two adjacent facets) may be calculated by applying the rules of geometrical optics. The following practical formulas may be applied to find the focal length of a single-facet lens:

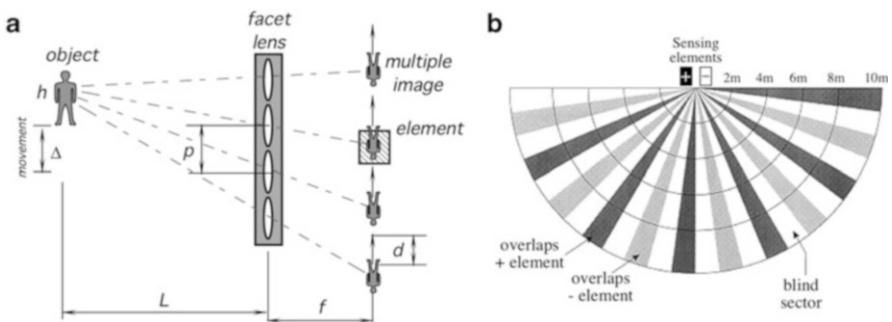
$$f = \frac{Ld}{\Delta}, \quad (7.17)$$

and the facet pitch is

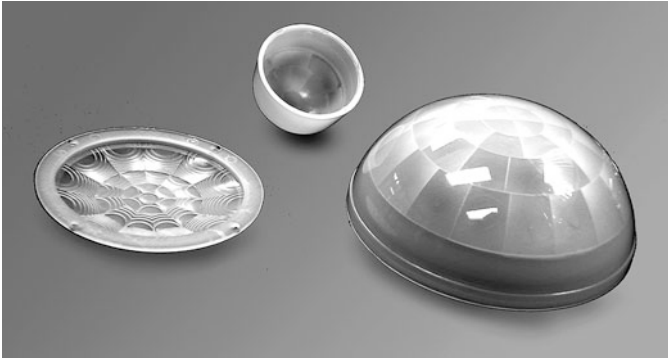
$$p = 2nd, \quad (7.18)$$

where  $L$  is distance to the object,  $d$  is width of the sensing element,  $n$  is number of the sensing elements (evenly spaced), and  $\Delta$  is the object's minimum displacement which must result in detection.

For example, if the sensor has two sensing elements of  $d = 1$  mm each, that are positioned at 1 mm apart, and the object's minimum displacement  $\Delta = 25$  cm at a distance  $L = 10$  m, the facet focal length is calculated from Eq. (7.17) as



**Fig. 7.24** Facet lens creates multiple images near-sensing element (a); sensitive zones created by complex facet lens on a double-element sensor (b)



**Fig. 7.25** Various infrared faceted Fresnel lenses molded of HDP

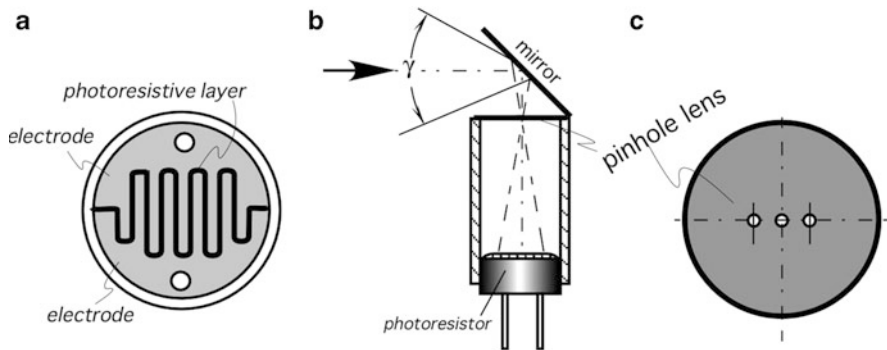
$f = 1000 \text{ cm} \times 0.1 \text{ cm} / 25 \text{ cm} = 4 \text{ cm}$ , and per Eq. (7.18) the lens facets should be positioned with a pitch of  $p = 8 \text{ mm}$  from one another.

Figure 7.24b shows a field coverage diagram for a motion detector with two sensing elements (plus and minus). Each element for each facet forms its own segment (zone) for generating an output when the image overlaps the element. When the object moves, it crosses the zone boundaries, thus modulating the sensor's output. Even though each zone is narrow, a combination of many covers up to a  $180^\circ$  field of detection. Currently, the facet lenses are primarily used in the mid- and far-infrared spectral ranges. These lenses are molded of high-density polyethylene, HDP (Fig. 7.25) and are quite inexpensive.

### 7.8.6 Visible and Near-IR Light Motion Detectors

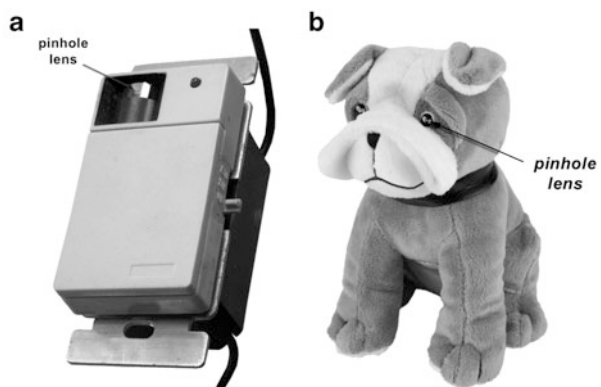
Visible and near-infrared light motion detectors rely on sources of light that illuminate objects. Illuminating light is reflected by the object's surface toward the focusing device of the motion detector. The light sources may be sun, incandescent lamps, or invisible near-infrared (IR) light-emitting diodes (LEDs). The use of visible light for detecting moving objects goes back to 1932 when during the pradar era, inventors were looking for ways of detecting moving cars and flying airplanes. In one invention [13], an airplane detector was built in form of a photographic camera where the focusing glass lens was aimed at the sky. The image of a moving plane was focused on a selenium photodetector which reacted to a changing contrast in the sky image. Such a detector could operate only at daytime to detect planes flying below clouds. Obviously, those detectors were not too practical. Another version of a visible light motion detector was patented and produced for less demanding applications: controlling lights in a room [12] and making interactive toys [14].

To turn lights off in a nonoccupied room, the visible light motion detector<sup>9</sup> was combined with a timer and a solid-state relay. The detector was activated only in the illuminated room. Visible light photons carry a relatively high energy and may be detected by quantum photovoltaic or photoconductive cells whose detectivity is quite high (see Chap. 15). Thus, the optical system may be simplified. In “Motion Switch” that operates in the visible spectrum of light, the focusing device was built in the form of a pinhole lens (Figs. 7.26b and 7.27a). Such a lens is just a tiny hole in an opaque foil. To avoid a light diffraction, a hole diameter must be substantially larger than the longest detectable wavelength (red). The “Motion Switch” had a three-facet pinhole lens with apertures of 0.2 mm in diameter (Fig. 7.26c). A pinhole lens has a theoretically infinite depth of the focusing range, hence, a



**Fig. 7.26** Simple optical motion detector for light switch and toys. Sensitive surface of photoresistor forms complex-sensing element (a); Flat mirror and pinhole lens form image on surface of photoresistor (b); pinhole lens (c)

**Fig. 7.27** “Motion Switch” [12] with a photoresistor and pinhole lens for turning lights off in unoccupied room (a); interactive toy (b) that reacts to child movement—dog barks when child motion is detected [14]



<sup>9</sup>“Motion Switch” of Fig. 7.27a for some time was manufactured by *Intermatic, Inc.*

photodetector can be positioned at any distance from the lens. For practical reasons, that distance was calculated for the projected object displacements, view angle, and the photoresistor sensing area. The photoresistor was selected with a serpentine pattern of the sensing element (Fig. 7.26a) and connected to a resistive bridge and high-pass filter with a cut-off frequency 0.25 Hz. When a room was illuminated, the motion sensor acted as a miniature photographic camera: an image from the lens' field of view was created on the surface of a photoresistor. Moving people in the room caused the image to move across the serpentine pattern of the photoresistor (Fig. 7.23a), resulting in modulation of the electric current passing through the photoresistor. If no motion was detected within 10 min from the last event, the built-in timer disabled the solid-state relay to turn lights off. Thanks to its low cost, this type of a motion sensor was also used in interactive toys that react to movement of children [14]. An example of such a toy is shown in Fig. 7.27b where a pinhole lens was built into the "eye" of a mechanized barking dog. Normally, the dog was sitting quietly but when motion in its vicinity was detected, the dog started moving and barking. If you pet it on the back, the barking stopped and the dog wagged the tail (a tactile sensor was installed on the back under the coat).

### 7.8.7 Mid- and Far-IR Detectors

The most popular version of an optical motion detector operates in the spectral range of thermal radiation, the other name for which is mid- and far-infrared (IR). Such detectors are responsive to radiative heat exchange between a sensing element and moving object [15–17]. Here we will discuss detection of moving people, however the technique is applicable to any warm or cold object having thermal contrast with the environment.

The principle of thermal motion detection is based on the physical theory of natural emission of electromagnetic radiation from a surface whose temperature is above absolute zero. The fundamentals of this theory are described in Sect. 4.12.3. We recommend that the reader first familiarize herself with that section before going further.

For motion detection, it is essential that surface temperature of a moving object be different from that of the surrounding objects, so a thermal contrast would exist, just as a visible contrast in the optical sensors described above. All objects emanate thermal radiation from their surfaces. Intensity of that radiation is governed by the Stefan-Boltzmann law Eq. (4.133). If the object is warmer than the surroundings, its thermal radiation is shifted toward shorter wavelengths and intensity becomes stronger. Most objects whose movement is to be detected have nonmetal surfaces, hence they radiate thermal energy quite uniformly within a hemisphere, Fig. 4.45a. Moreover, dielectric objects generally have high emissivity of thermal radiation. Human skin is a quite good emitter of thermal radiation. Its emissivity is well over 90 % (see Table A.18). Most of the natural and synthetic fabrics also have high emissivities between 0.74 and 0.95.

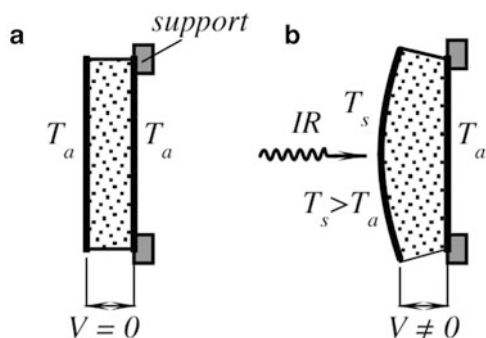
### 7.8.8 Passive Infrared (PIR) Motion Detectors

The passive infrared (PIR) motion detectors became very popular for use in the security and energy management systems. The PIR-sensing element is responsive to mid- and far-infrared radiation within a spectral range from approximately 4 to 20  $\mu\text{m}$  where most of the thermal power emanated by humans is concentrated (surface temperatures ranging from about 26 to 37  $^{\circ}\text{C}$ ). There are three types of the sensing elements that are potentially useful for that detector: bolometers, thermopiles, and pyroelectrics; however the pyroelectric elements are used almost exclusively for motion detection thanks to their simplicity, low cost, high responsivity, and a broad dynamic range. A pyroelectric effect is described in Sect. 4.7 and some detectors are covered in Sect. 15.8.4. Here, we are going to see how that effect may be employed in a practical PIR motion sensor design.

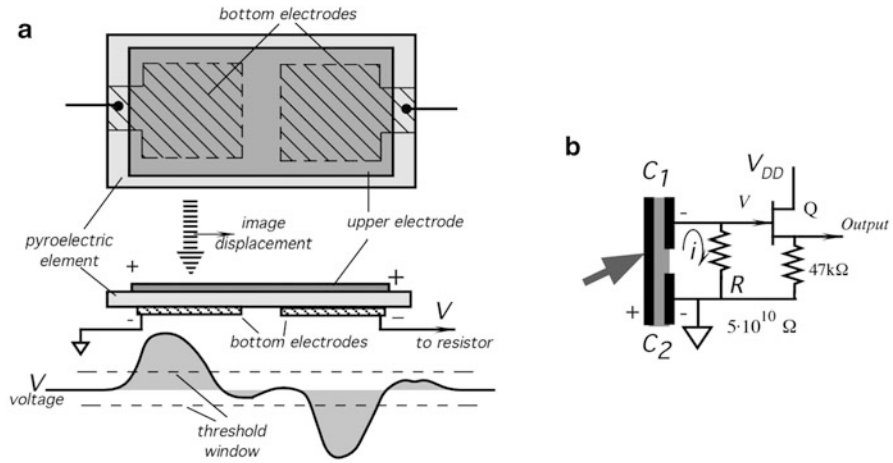
A pyroelectric ceramic plate (sensing element) generates electric charge in response to a thermal energy flowing through its body. The plate has two deposited electrodes: one—on its upper side, while the other—on the bottom side. In a very simplified way, a pyroelectric response may be described as a secondary effect of a thermal expansion (Fig. 7.28). Since all pyroelectrics are also piezoelectrics, IR heat absorbed by the front electrode causes the upper side temperature  $T_s$  to increase over the base temperature  $T_a$ . As a result, the upper side size expands, causing a mechanical stress in the piezoelectric crystals. In turn, the stress leads to development of a piezoelectric charge. This IR-induced charge is manifested as voltage across the electrodes. Unfortunately, piezoelectric properties of the element have also a negative effect. If the sensor is subjected to a minute mechanical stress due to any external force, like sounds or structural vibrations, it generates a spurious charge which often is indistinguishable from that caused by the infrared heat.

To separate thermally induced charges from the mechanically induced charges, a pyroelectric sensor is usually fabricated in a symmetrical form, Fig. 7.29a. Two identical sensing elements are positioned inside the sensor's housing. The elements are connected to the interface circuit in such a manner as to produce the out-of-phase signals when subjected to the same in-phase inputs. The idea is based on the fact that the piezoelectric or spurious thermal interferences are applied to both sensing elements simultaneously (in phase) and thus will be canceled at the input of

**Fig. 7.28** Simplified model of pyroelectric effect as secondary effect of piezoelectricity. Initially, the element has uniform temperature (a); upon exposure to thermal radiation, its front side warms up and expands, causing stress-induced voltage across electrodes (b)







**Fig. 7.29** Dual-pyroelectric sensor. Pyroelectric plate has front (*upper*) electrode and two bottom electrodes (a). Moving thermal image travels from left side of sensor to right, generating alternate voltage across bias resistor,  $R$  (b)

the electronic circuit. On the other hand, since the IR flux that is focused by the lens is absorbed by only one element at a time, cancellation is avoided. This arrangement is called a differential PIR detector.

One way of fabricating a differential PIR detector is to deposit two pairs of the electrodes on both sides of a single-pyroelectric plate. Each pair forms a capacitor that may be charged either by heat or by a mechanical stress. The electrodes on the upper side of the sensor are connected together, forming one continuous electrode, while two bottom electrodes are separated, thus creating two opposite-serially connected capacitors. Depending on the side where the electrodes are positioned, the output signal will have either a positive or negative polarity for a thermally induced response. In some applications, a more complex pattern of the sensing electrodes may be required (for instance, to form predetermined detection zones), so that more than one pair of the electrodes are needed. In such a case, for better rejection of the in-phase signals (common-mode rejection), the sensor still should have an even number of pairs where positions of the pairs alternate for a better geometrical symmetry.

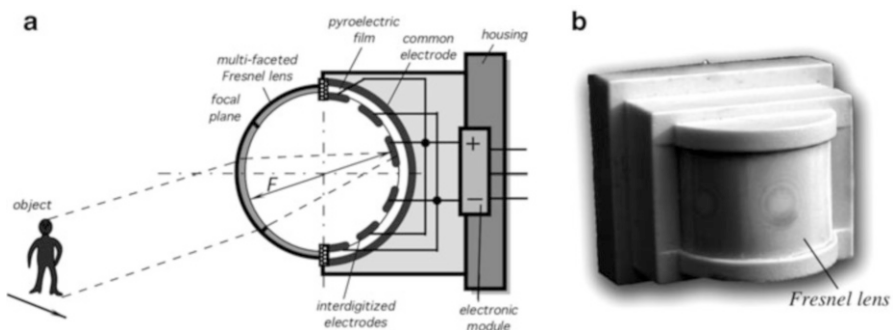
A symmetrical sensing element should be mounted in a way to assure that both parts of the element generate the equal (but out-of-phase) signals if subjected to the same external factor. At any moment, the optical component (e.g., a Fresnel lens,) must focus thermal image of an object on a surface of one part of the sensor only, otherwise signals will be cancelled. The element generates a charge only across the electrode pair that is subjected to a heat flux. When a thermal image moves from one electrode to another, the current  $i$  flowing from the sensing element to the bias resistor  $R$ , Fig. 7.29b, changes from zero, to positive, then back to zero, then to negative, and again back to zero, Fig. 7.29a—lower portion. A JFET transistor  $Q$  is used as an impedance converter and a voltage follower (the gain is close to unity).

The resistor  $R$  value must be very high. For example, a typical alternate current generated by the element in response to a moving person is on the order of  $1 \text{ pA}$  ( $10^{-12} \text{ A}$ ). For example, if a desirable output voltage for a maximum distance is  $v = 10 \text{ mV}$ , according to Ohm's law, the resistor value should be  $R = v/i = 10 \text{ G}\Omega$  ( $10^{10} \Omega$ ).

Table A.9 lists several crystalline materials that possess pyroelectric properties and can be used for fabrication of PIR-sensing elements. Most often used are the ceramic elements, thanks to their low cost and ease of fabrication. The pyroelectric coefficients of ceramics to some degree may be controlled by varying the ceramic porosity (creating voids inside the sensing plate body). An interesting pyroelectric material is a polymer film PVDF which while being not as sensitive as most of the ceramic crystals, has advantages of being flexible and inexpensive. Besides, it can be produced in any size, and may be bent or folded in any desirable fashion (see Sect. 4.6.2).

Besides the sensing element, the IR motion detector needs a focusing device. Some detectors employ parabolic mirrors while the Fresnel plastic lenses (Sect. 5.8.2) become more and more popular because of low cost, ability to be molded in any desirable shape (Fig. 7.25) and, in addition, they act as windows—protecting interior of the sensor from elements.

To illustrate how a plastic Fresnel lens and a PVDF film can work together, let us look at the motion detector depicted in Fig. 7.30a. It uses a high-density polyethylene multifaceted curved lens and curved PVDF film sensor [15]. The sensor design combines two methods described above: a facet lens and a complex electrode shape. The lens and the film are curved with the same radii of curvature equal to one-half of the focal distance  $f$ , thus assuring that the film is always positioned in the focal plane of the corresponding facet of the lens. The film has a pair of large interdigitized electrodes that are connected to the positive and negative inputs of a differential amplifier located in the electronic module. The amplifier rejects common-mode interference and amplifies a thermally induced voltage. The front side of the film facing the lens is coated with an organic coating to improve its



**Fig. 7.30** PIR motion detector uses curved Fresnel lens and curved pyroelectric PVDF film. Internal structure of sensor (a); external appearance of the sensor (b)

absorptivity in the mid- and far-infrared spectral ranges. This design results in a fine resolution (detecting small displacements at longer distances), and small size of the sensor, Fig. 7.30b. Small sensors are especially useful for installation into products where minimizing the overall dimensions is critical. For instance, one such application is a light switch where the PIR detector is incorporated into a wall plate of the switch.

### 7.8.9 PIR Detector Efficiency Analysis

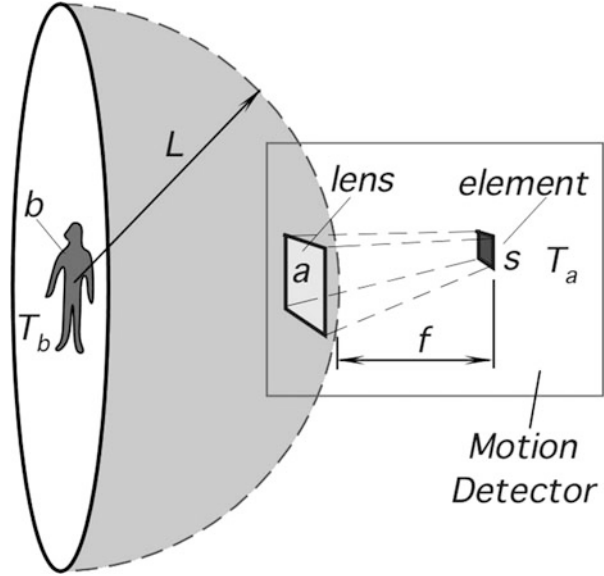
Regardless of the type of the optical device employed, majority of modern PIR detectors operate on the same physical effect—pyroelectricity. To analyze performance of such a sensor, first we shall calculate the infrared power (flux) which is converted into an electric charge by the sensing element. The optical device focuses thermal radiation forming a miniature thermal image on a surface of the sensor. The photon energy of an image is absorbed by the sensing element and converted into heat. That heat while propagating through the pyroelectric element, in turn, is converted into a minute electric charge. And finally, the charge causes a very small electric current passing through the input of an interface circuit. The maximum operating distance for given conditions can be determined by a noise level in the detector. For reliable detection, the worst-case noise power must be at least ten times smaller than that of the signal detected by a moving person.

A pyroelectric sensor is a converter of thermal energy flow into electric charge. Energy flow essentially demands a presence of a thermal gradient across the sensing element. In the detector, the element of thickness  $h$  has the front side exposed to the lens, while the opposite side faces the detector's interior housing, which normally is at ambient temperature  $T_a$ . The front side of the sensor element is covered with a heat absorbing coating to increase its emissivity  $\epsilon_s$  to the highest possible level, preferably close to unity. When thermal flux  $\Phi_s$  is absorbed by the element's front side, the front side temperature goes up and heat starts propagating through the sensor toward its rear side. Thanks to the pyroelectric effect, electric charge develops on the element surfaces in response to the heat flow.

To estimate a IR power level at the sensor's heat absorbing surface, let us make some assumptions. For the simplicity sake, let us consider an idealized person whose effective surface area is  $b$  (Fig. 7.31), temperature along this surface ( $T_b$ ) is distributed uniformly and expressed in degree K. The person is moving along an equidistant path located at distance  $L$  from the PIR detector's lens and, being a diffuse emitter, radiates IR energy uniformly within a hemisphere having a surface area of  $A = 2\pi L^2$ . Also, we assume that the focusing device makes a sharp image of the object. For this calculation we select a lens which has a surface area  $a$ . The sensor's temperature in K is  $T_a$ —the same as that of ambient.

Total infrared power (flux) lost to surroundings from the object can be determined from the Stefan-Boltzmann law

**Fig. 7.31** Formation of thermal image on sensing element of PIR motion detector



$$\Phi = b\epsilon_a\epsilon_b\sigma(T_b^4 - T_a^4), \tag{7.19}$$

where  $\sigma$  is the Stefan-Boltzmann constant,  $\epsilon_b$  and  $\epsilon_a$  are the object and the surrounding emissivities, respectively [see Eq. (4.138)]. If the object is warmer than the surroundings (which is usually the case), the net infrared power is distributed toward an open space having ambient temperature  $T_a$ . Since the object is a diffusive emitter, we may consider that the same flux density may be detected at any point along the equidistant surface. In other words, intensity of the infrared power is distributed uniformly along the spherical surface having radius  $L$ . The above assumptions are rather stretched, yet they should allow us to get an estimate of the sensor's response.

Assuming that the surroundings and the object's surface are ideal emitters and absorbers ( $\epsilon_b = \epsilon_a = 1$ ) and the sensing element's emissivity is  $\epsilon_s$ , the net radiative flux density at distance  $L$  can be derived as

$$\phi = \frac{b}{2\pi L^2} \epsilon_s \sigma (T_b^4 - T_a^4) \tag{7.20}$$

The lens efficiency (transmission coefficient) is  $\gamma$ , which theoretically may as large as 0.92 depending on properties of the lens material and the lens design. For high-density polyethylene (HDPE) the transmission value of a Fresnel lens is in the range from 0.5 to 0.75. After ignoring a minor nonlinearity related to the fourth power of temperatures in Eq. (7.20), thermal power absorbed by the element is expressed as

$$\Phi_s \approx a\gamma\phi \approx \frac{2\sigma\epsilon_s}{\pi L^2} abyT_a^3(T_b - T_a) \tag{7.21}$$

Note that infrared flux which is focused by the lens on the surface of the sensing element is inversely proportional to the squared distance ( $L$ ) from the object and directly proportional to the areas of the lens and the object. For a multifaceted lens, the lens area  $a$  relates only to a single facet and not to the total lens area.

If the object is warmer than the sensor, the flux  $\Phi_s$  is positive. If the object is cooler, the flux becomes negative, meaning it changes its direction: the heat goes from the sensor to the object. This may happen when a person walks into a warm room from the cold outside. Surface of her clothing will be cooler than the sensor and thus the flux becomes negative. In the following discussion we will consider that the object is warmer than the sensor and the flux is positive.

Upon influx of the infrared radiation, temperature of the sensor element increases with a rate that can be derived from the absorbed thermal power  $\Phi_s$  and thermal capacity  $C$  of the element

$$\frac{dT}{dt} \approx \frac{\Phi_s}{C}, \quad (7.22)$$

where  $t$  is time. This equation is valid during a relatively short interval, immediately after the sensor is exposed to the thermal flux, and can be used for evaluating the peak signal.

The peak electric current generated by the sensor in response to a thermal influx can be found from the fundamental formula:

$$i = \frac{dQ}{dt}, \quad (7.23)$$

where  $Q$  is the electric charge developed by the pyroelectric sensor. This charge depends on the sensor's pyroelectric coefficient  $P$ , sensor's area  $s$ , and temperature change  $dT$ :

$$dQ = PsdT \quad (7.24)$$

Thermal capacity  $C$  can be derived through a specific heat  $c$  of the material, area  $s$ , and thickness of the element  $h$

$$C = csh. \quad (7.25)$$

By substituting Eqs. (7.22), (7.24), and (7.25) into Eq. (7.23), we arrive at the peak current which is generated by the sensor in response to the incident thermal flux:

$$i = \frac{PsdT}{dt} = \frac{Ps\Phi_s}{csh} = \frac{P}{hc}\Phi_s. \quad (7.26)$$

To establish relationship between the current and moving objects, the flux from Eq. (7.21) has to be substituted into Eq. (7.26)

$$i \approx \frac{2Pa\sigma\gamma}{\pi hc} bT_a^3 \frac{\Delta T}{L^2}, \quad (7.27)$$

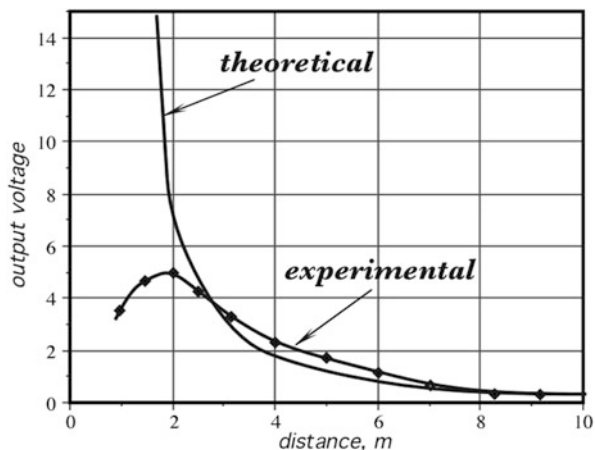
where  $\Delta T = (T_b - T_a)$ .

Several conclusions can be drawn from Eq. (7.27). The first part of the equation (the first ratio) characterizes a detector while the rest relates to an object. The pyroelectric current  $i$  is directly proportional to the temperature difference (thermal contrast) between the object and its surroundings. It is also proportional to the surface area  $b$  of the object which faces the detector. A contribution of the ambient temperature  $T_a$  is not that strong as it might appear from its third power. The ambient temperature must be entered in kelvin, hence, its variations become relatively small with respect to the scale. The thinner the sensing element the more sensitive the detector. The lens area also directly affects the signal magnitude. On the other hand, pyroelectric current does not depend on the sensor's area as long as the lens focuses the entire image on the sensing element.

To evaluate Eq. (7.27) further, let us calculate voltage across the bias resistor. That voltage can be used as the output signal of the motion detector. We select a pyroelectric PVDF film sensor with typical properties:  $P = 25 \mu\text{C}/\text{K m}^2$ ,  $c = 2.4 \times 10^6 \text{ J}/\text{m}^3 \text{ K}$ ,  $h = 25 \mu\text{m}$ , lens area  $a = 1 \text{ cm}^2$ ,  $\gamma = 0.6$ , and the bias resistor  $R = 10^9 \Omega$  (1 G $\Omega$ ). We assume that the object's surface temperature is  $27^\circ\text{C}$  and surface area  $b = 0.1 \text{ m}^2$ . The ambient temperature is  $t_a = 20^\circ\text{C}$ . The output current is calculated from Eq. (7.27) as function of distance  $L$  from the detector to the object, then converted to voltage, and shown in Fig. 7.32.

The theoretical graph of Fig. 7.32 was calculated under the assumption that the optical system makes a sharp image at all distances and that image is no larger than the sensing element area. In practice, this is not always true, especially at shorter ranges where the image is not only out of focus but also may overlap the out-of-phase elements of a differential sensor. A reduction in the signal amplitude at shorter distances becomes apparent, thus the experimental voltage does not go as high as calculated from the theoretical equation.

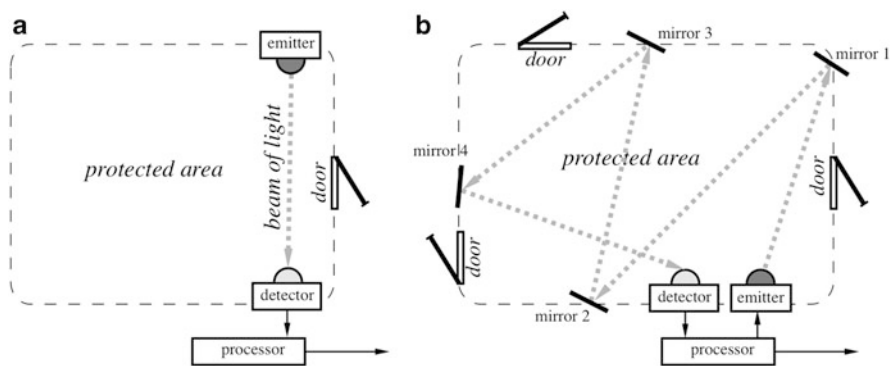
**Fig. 7.32** Calculated and experimental amplitudes of output signals in a PIR detector



## 7.9 Optical Presence Sensors

### 7.9.1 Photoelectric Beam

The old but efficient light-beam interrupters are still widely used in security systems, thanks to their high reliability and long detection range (up to 500 m). The idea behind these detectors is similar to a trip wire: an intruder occludes a beam of light. Figure 7.33a illustrates this principle. A photoelectric-beam interrupter comprises an optical coupler (emitter-detector) that is installed near the entrance to a protected area. The emitter sends a narrow-beam infrared light (typical wavelength 940 nm) toward a detector. Under normal conditions, the detector registers a steady light intensity. To eliminate possible influence of ambient light, the emitter modulates the light beam by an a.c. signal, such as short square pulses (turning the beam on and off). At the detector side, only the a.c. component is registered, so any potential offset from steady light sources is rejected. An intruder interrupts the beam and the detector registers an abrupt reduction in the light intensity. If reduction is below a preset threshold, the alarm is actuated. In cases when the protected area has multiple points of entry (e.g., several doors and windows) one optocoupler still can be used to cover several zones at once as shown in Fig. 7.33b. Here, a beam from the emitter is directed toward the detector through multiple reflections inside the protected area. Several reflectors (mirrors) are positioned near the perimeter and adjusted to divert the beam sequentially from one mirror to another and finally—to the detector. To avoid false positive detections, the optocoupler and all mirrors must be securely fixed at their locations to prevent vibrations and movements that may cause spurious diversions of the light beam. Obvious disadvantages of the photoelectric-beam interrupters are their susceptibility to airborne contaminants that may soil optical components, reduced reliability at fog and relatively high-power consumption.

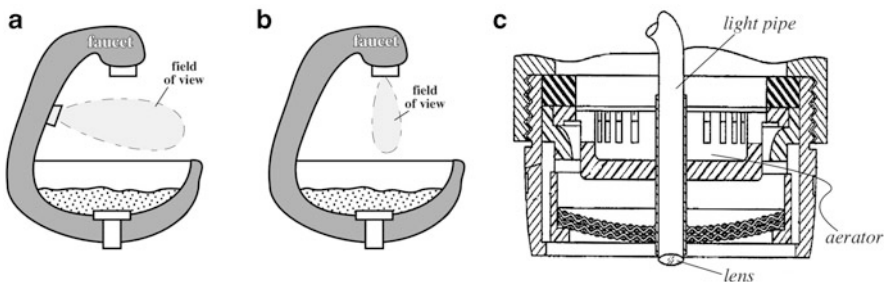


**Fig. 7.33** Photoelectric-beam interrupters as intrusion detectors. Direct (a) and reflective coupling (b)

## 7.9.2 Light Reflection Detectors

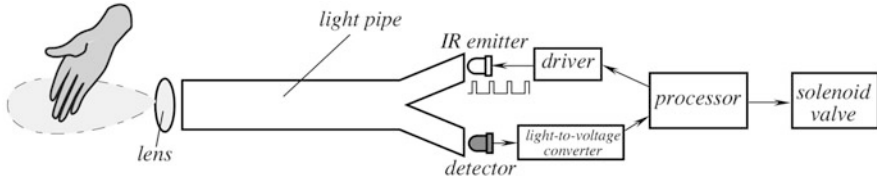
A reflection of light is the optical phenomenon that is used quite extensively in detecting not only motion but also a mere presence of an object in a monitored area. The operating principle is very simple. Just like the optointerrupters, the sensor contains two key components: a source of light (usually a near-infrared LED—the emitter) and a photodetector. The LED emits a pilot light that illuminates objects within the field of view of the photodetector. The detector measures intensity of light reflected by the objects. Before monitoring, a background reflection from the objects (reference) is established. As new object appears in the field of view, it either absorbs more light or reflects more. In most cases it alters the established reference level by the increment that can be detected by a threshold detector in the electronic processor. This sensor will not measure distance to the object because the registered light intensity depends on many unknown factors, such as size of the object, its shape, material, surface finish, and distance to the sensor. This sensor is merely a presence detector, yet in many practical applications it is just what's needed. Nowadays, the emitters and detectors are controlled by intelligent integrated circuits that improve reliability of detection and reject spurious signals [18]. An example is a presence detector for a bathroom faucet that is used to control flow of water when hands are placed under the faucet [19, 20] to actuate water flow. A similar detector is frequently employed in hand dryers, toilet tanks, light switches, gesture controllers for home appliances (stereo player, air conditioner, etc.), robotic vacuum cleaners, and many other products.

Figure 7.34a, b show two possible locations of the sensor in a water fixture. One location is on the spout while in the other the sensor is built-in directly into the faucet. It is important to make sure that the detection area is situated where the hands are normally being placed. Figure 7.34c illustrated the faucet having a light pipe and other parts that are normally needed for dispensing water. The light pipe is similar to a fiber-optic that is used for transmitting and receiving reflected light—see Fig. 5.20b.



**Fig. 7.34** Installation of optical presence detector into spout (a) and faucet (b). Cross-sectional view (c) of faucet with light pipe (adapted from [20])





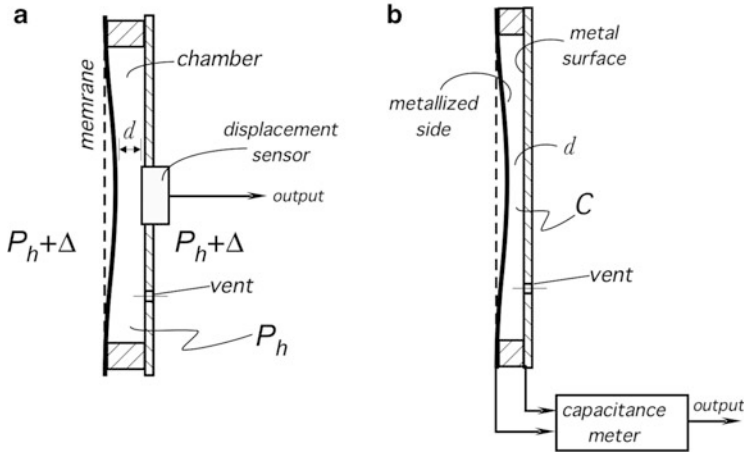
**Fig. 7.35** Block-diagram of the water-flow controller with optical presence detector

Figure 7.35 shows a block diagram of the water-flow control system. The light pipe can be a bundle of the optical fibers or a solid translucent rod molded of polycarbonate resin. The emitted light produced by the LED emitter is modulated by the short pulses with relatively high frequency of 1 kHz. This helps in separating the reflected pulsed light from a background (ambient) illumination. The ambient light may contain three types of components: steady level, slow changing, and ripple or flickering from fluorescent lights with the mains frequency of 50 or 60 Hz. These spurious components are reduced by use of high-pass filters or synchronous detectors for rectifying the detected signal.

## 7.10 Pressure-Gradient Sensors

An efficient sensor can be designed to detect intrusion into a closed room by monitoring small variations in the atmospheric air pressure resulted from opening doors, windows, or movement of people. In principle, variations in air pressure can be monitored by a conventional air pressure sensor. However, it is not a practical solution. A conventional air pressure sensor is characterized by a relatively large span of the input pressures. Yet, pressure variations that are associated with intrusion are very small—over three orders of magnitude smaller than the conventional pressure sensor's span. In fact, these variations approach the noise floor of a sensor. Besides, such a sensor is just not sensitive enough for them. Appending it with a high-gain amplifier is not a solution because noise will be amplified as well. A practical solution would be designing a sensor with a narrow pressure span but high sensitivity. It is also desirable to make the sensor responsive only to pressure changes rather than to an absolute value of pressure. Preferably, such a sensor should output a signal similar to a first derivative of the air pressure. Since the only purpose of the sensor is detecting intrusion and not measuring the actual air pressure, accuracy requirements can be significantly relaxed.

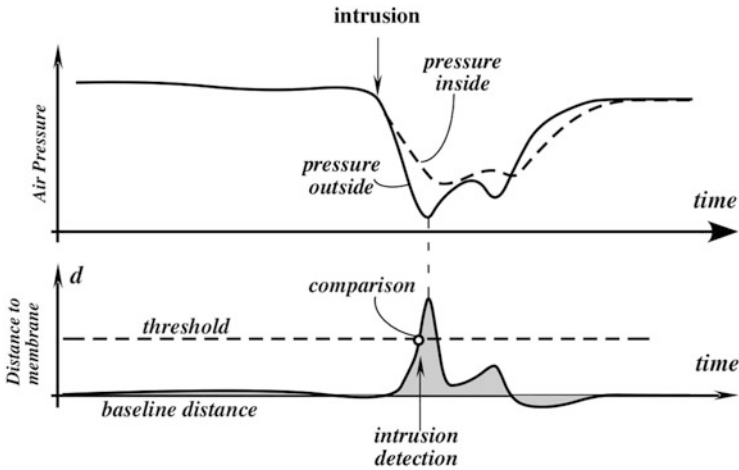
A high sensitivity can be achieved by making the sensing membrane very thin with a relatively large area. An example of the intrusion air pressure sensor design [21] is shown in Fig. 7.36. The main part of the sensor is an enclosed chamber. The left wall of the chamber is covered with a thin stretched membrane made of a plastic or metal foil having thickness on the order of 20  $\mu\text{m}$ . The membrane area should be relatively large, about 200  $\text{mm}^2$  or larger. The right side of the chamber is a rigid backplate with a small venting hole whose purpose is to equalize air pressures



**Fig. 7.36** Air pressure gradient sensor (a) and pressure gradient sensor with capacitive displacement detector (b)

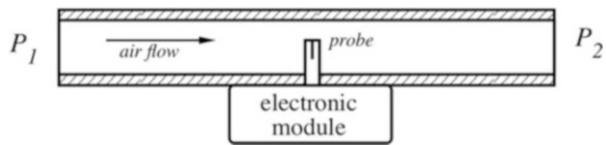
inside and outside of the chamber. A distance  $d$  from the membrane to backplate is monitored by a built-in displacement sensor. All exterior surfaces of the sensor are exposed to ambient air. When all doors and window in the monitored room are closed and the room is unoccupied, the ambient air pressure is either static or changes slowly. Thanks to a vent hole in the backplate, pressures  $P_h$  inside and outside of the sensor's chamber are equal and the membrane is flat. When a door or window opens, the ambient air pressure changes slightly but rapidly by the increment  $\Delta$ . Because the vent is very narrow and air has a finite viscosity, air pressure  $P_h$  inside the chamber cannot change instantly, thus any changes inside the chamber will lag behind the outside changes. The phase lag creates a temporary air pressure differential across the membrane which deflects to or from the backplate in relation to the differential pressure amplitude and sign. The distance  $d$  from the membrane to the backplate is monitored by a displacement sensor and is used as an indication of the intrusion. When the differential pressure is small, the membrane remains substantially flat and the distance  $d$  is at its base level. Figure 7.37 illustrates the timing diagrams of air pressures inside and outside of the sensing chamber and the differential pressure across the membrane. The signal representative of displacement  $d$  is compared with a threshold to detect an intrusion.

There are numerous ways of designing a displacement sensor for monitoring the membrane deflection, many of which are discussed in Chap. 8. As an example, Fig. 7.36b illustrates a capacitive displacement sensor, where the sensing chamber was built in the form of a flat capacitor with two plates. The first plate of a capacitor is a metal foil (or metallized plastic membrane) and the other plate is a metal layer on the backplate. The baseline gap  $d$  between the membrane and backplate should be rather small—0.5 mm or less. For example, if the membrane and base have an overlapping area of 400 mm<sup>2</sup> and the gap is 0.5 mm, the baseline capacitance is 17 pF.



**Fig. 7.37** Timing diagrams for pressure gradient detector

**Fig. 7.38** Concept of thermoanemometer as detector of minute pressure gradients



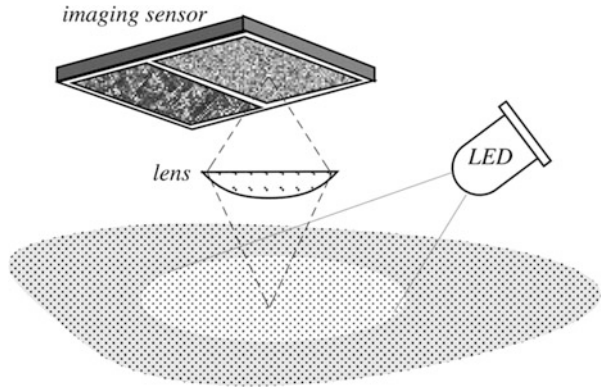
The value of capacitance  $C$  will change when distance  $d$  varies according to the air pressure differential (see Eq. 4.20). The capacitance variations are measured and converted into a useful signal.

An alternative design includes a pressure gradient detector with a thermoanemometer as a flow sensor [22] whose functionality is described in detail in Sect. 11.9. This sensor responds to miniscule pressure differences by monitoring very small air currents in a protected area. A conceptual design is shown in Fig. 7.38. It contains a test tube with a small air-flow sensor positioned in the center. If there is a pressure gradient across the left-right tube outlets ( $P_1 > P_2$ ), air will flow inside the tube and be measured by a thermal anemometer. Since thermal anemometer’s output is nonlinear, Fig. 12.9b, with a higher sensitivity at small flows, the sensor is responsive to minute variations in room pressures caused by opening/closing of doors and windows and even people walking.

## 7.11 2-D Pointing Devices

Personal computers presented a need for another displacement sensor that is called a pointing device. Such a device for sensing movement of a human hand is a mouse (or a tracking ball). It is intended for moving a pointer to a desired  $x$ - $y$  coordinate on a computer monitor. The first mice used mechanical rollers coupled to optical encoder disks (similar to that shown in Fig. 8.44) or electromagnetic pickups.

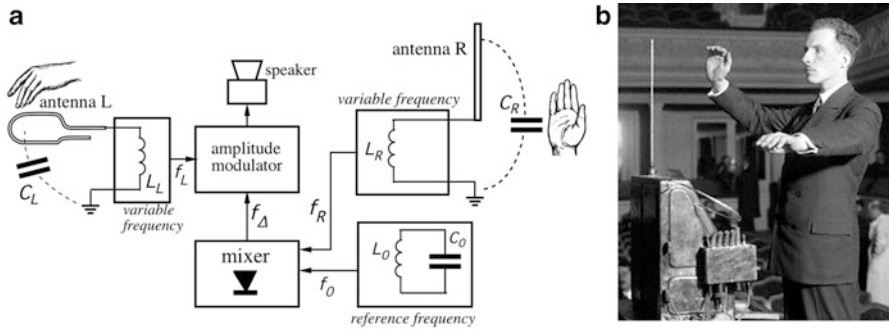
**Fig. 7.39** Concept of optical pointing device (mouse)



Later, Steve Kirsch invented an optical mouse that required a special reflective pad with a coordinate grid [23]. The newest mice and trackballs employ an optical pickup with illumination by a red (or infrared) LED or laser diode. A typical optical pointing device contains three essential components: an illuminator, CMOS optoelectronic image sensor, and digital signal processing (DSP) chip (Fig. 7.39). The optoelectronic image sensor takes successive pictures of the surface on which the mouse operates, or of a surface pattern on the tracking ball. The DSP chip compares the successive images. Changes between one frame and the next are processed by the image processing part of the chip and translated into movement along the two axes using an optical-flow estimation algorithm. For example, the Avago Technologies ADNS-2610 optical mouse sensor processes 1512 frames per second: each frame consisting of a rectangular array of  $18 \times 18$  pixels, and each pixel can sense 64 different levels of gray. This advance enabled the mouse to detect relative motion on a wide variety of surfaces, translating the movement of the mouse into the movement of the cursor and eliminating the need for a special mouse-pad.

## 7.12 Gesture Sensing (3-D Pointing)

To control human-machine interface devices, modern computing moves from an  $x$ - $y$  human detection to a three-dimensional sensing of the operator's body. This allows commanding a computer by gestures—motions of hands, head, and torso. Some gesture sensors require the small sensing devices being attached directly to the operator limbs, while others are totally contactless. The earliest noncontact gesture sensor was part of the world first electronic music instrument that was invented [24] in 1919 by the Russian engineer Лев Сергеевич Термен, known in the West as Léon Theremin. Figure 7.40a illustrates a block diagram of his musical instrument called “*Theremin*” or “*Thereminvox*”. The operating principle is based on movement of hands that modulate capacitances between the right hand and ground ( $C_R$ ) and the left hand and ground ( $C_L$ ). The Theremin player moves her hands near two antennas.



**Fig. 7.40** Block diagram of Thereminvox (a) and Léon Theremin in 1927 playing his instrument (b)

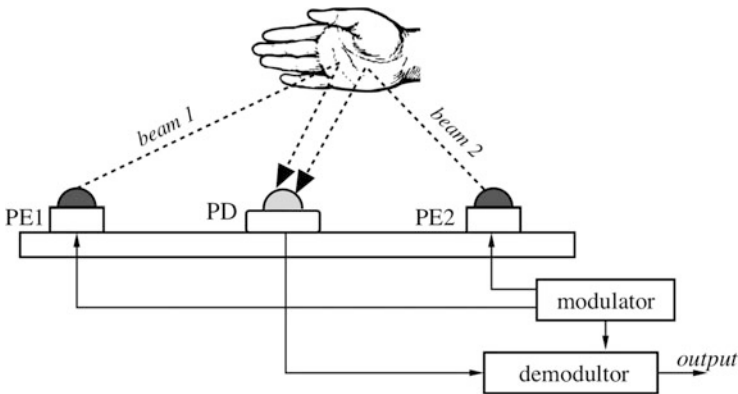
Proximity of the right hand to the vertical antenna changes the capacitance  $C_R$  and thus modulates high frequency  $f_R$  of the LC-oscillator. A reference high-frequency oscillator produces a fixed frequency  $f_0$  that along with  $f_R$  is sent to the mixer. The mixer, being a non-linear circuit, extracts a differential beat-frequency  $f_\Delta$  in the audible range. The hand movement changes the pitch of generated sound over a six-octave range. The beat-frequency method is known in electronics as a heterodyne. The left hand controls the frequency  $f_L$  that modulates the oscillations amplitude, that is—controls the volume. Theremin’s sound resembles sometime the cello or violin, sometime the flute, and often the human voice.

### 7.12.1 Inertial and Gyroscopic Mice

A sensing device attached to the operator’s wrist is often called the “air mouse” since it does not require a contact with any surface or even proximity to a stationary-sensing surface. It is the inertial mouse that uses a miniature accelerometer and gyroscope for detecting movement for every axis supported. The sensing module wirelessly communicates with the computer. The user requires only small wrist rotations to move the monitor cursor or perform other controls.

### 7.12.2 Optical Gesture Sensors

A detector based on reflectance of light can be employed for detecting presence, position, and movement of the operator hand (Fig. 7.41). The detection system consists of several strategically placed point light emitters (PE) and at least one photodetector (PD). The emitters are fed by the alternate current pulses generated by the modulator, so only one PE illuminates at a time. This allows not only cancelling the ambient background illumination, but also, by use of a synchronous demodulator, to determine from which particular PE the reflected light beam is

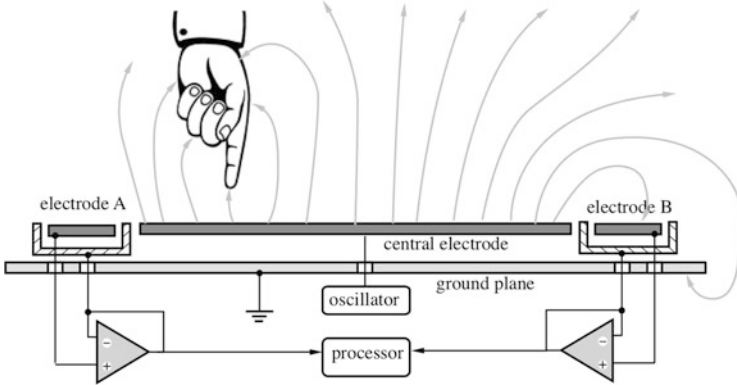


**Fig. 7.41** Optical gesture sensor

detected. The operating principle of the device is based on measuring change in the detected light intensity [25]—the closer the operator’s hand to the detecting device the stronger the PD response. Thus, by combining responses from several PE, it is possible to determine both a distance to the base and position of the hand with respect to all PE, that is, a 3-D coordinates of the hand. A signal processing from the device is based on computation of both—the static coordinate and a phase lags in the PD responses for monitoring a rate and direction of motion.

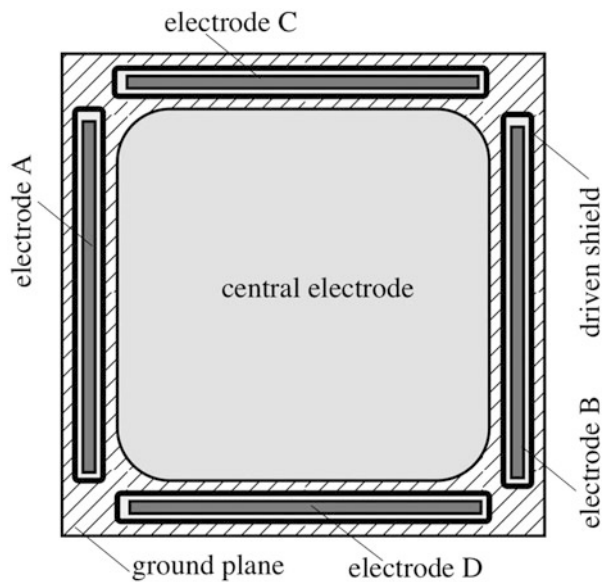
### 7.12.3 Near-Field Gesture Sensors

A detector of Fig. 7.19 for proximity detection uses the subject’s capacitive coupling to a conductive object. In a somewhat similar manner, a 3-D gesture sensor may be designed for detecting variations in electric fields near the sensing electrodes. Figure 7.42 shows an electric field produced by the central electrode that is attached to the output of an oscillator. The oscillator generates a sine-wave voltage having frequency of about 100 kHz. This frequency corresponds to very long electromagnetic waves (about 3 km), that are much longer than dimensions of the sensor and subject. Thus, in vicinity of the central electrode, mostly the electric field vectors exist, but not magnetic. The electric field lines propagate from the central electrode outwardly to the surrounding objects having near the ground electric potentials. Since human subjects have very large dielectric constants—in the range of 90, we are strongly capacitively coupled to ground. As a result, bringing part of the human body, such as hand or finger, into the near field will attract the electric field lines, as shown at the left side of Fig. 7.42. If the hand is not there, the electric field lines pass mostly through the detecting electrodes A and B and appear as a.c. voltages at the inputs of the voltage followers made of operational amplifiers (see Fig. 6.6b). A human hand being positioned near the electrode A diverts the electric field lines away from the electrode A, causing a drop in the



**Fig. 7.42** Near-field gesture sensor

**Fig. 7.43** Top view of electrode arrangement for near-field gesture sensing



voltage amplitude. The closer to the electrode the stronger the voltage drop at the corresponding voltage follower.

To minimize a stray coupling and increase sensitivity, the sensing electrodes A and B are surrounded by the driven electric shields that are connected to the outputs of the respective voltage followers. Functionality of a driven shield is similar to arrangements of Figs. 7.19 and 6.4b.

For a spatial detection of a human hand, the electrodes are arranged in a rectangular manner (Fig. 7.43) that allows detection of the coordinates [26]. Commercial integrated circuits for the near-field gesture sensing are available from several manufacturers, for example, from Microchip Technology, Inc.

### 7.13 Tactile Sensors

In general, the tactile sensors belong to the special class of force or pressure transducers that are characterized by small thicknesses, or to the class of proximity sensors that respond to a very close presence ( $< 1$  mm) or contact by a “digit”—human or mechanical. Examples of applications of the tactile sensors include robotics where the sensor can be positioned on the “fingertip” of a mechanical actuator to provide a feedback upon developing a contact with an object—very much like the live tactile sensors work in human skin. They are used for fabricating the “touchscreen” displays, keyboards, and other devices where a physical contact has to be sensed. A very broad area of applications is the biomedical field where tactile sensors can be used in dentistry for the crown or bridge occlusion investigation, in studies of forces developed by a human foot during locomotion. They can be installed in artificial knees for balancing of the prosthesis operation, etc. Another interesting area is identification of humans by their fingerprints.

The tactile sensors loosely can be subdivided into several subgroups:

*Touch Sensors.* These sensors detect and/or measure contact forces at defined points. A touch sensor may be analog, being capable of measuring the touch force, and binary (threshold), namely—touch or no touch.

*Contact Sensors.* These sensors detect physical coupling between two objects, regardless of forces. A touch by a finger may be detected by monitoring a contact area between the finger and the panel. An example is a capacitive touchscreen on a touch-sensitive monitor (e.g., smartphone).

*Spatial Sensors.* These sensors detect and measure the spatial distribution of forces perpendicular to a predetermined sensory area or physical contacts, and the subsequent interpretation of the spatial information. A spatial-sensing array can be considered to be a coordinated group of touch sensors.

*Slip Sensors.* These sensors detect and measure the movement of an object relative to the sensor. This can be achieved either by a specially designed slip sensor or by the interpretation of the data from a touch sensor, contact sensor, or a spatial array.

Requirements to tactile sensors are based on investigation of human sensing and analysis of grasping and manipulation. An example of the desirable characteristics of a touch or tactile sensor suitable for the majority of industrial applications are as follows:

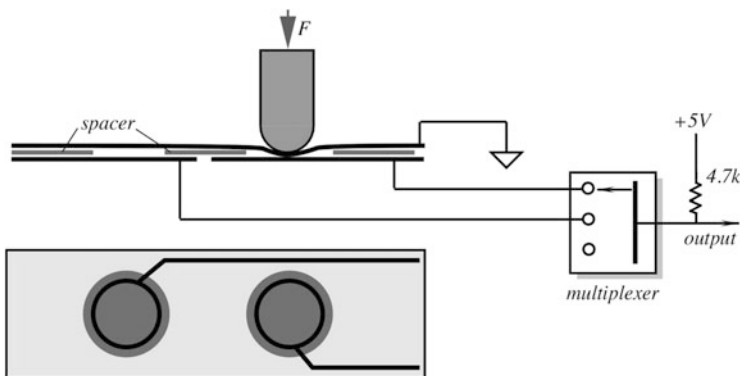
1. A touch sensor should ideally be a single-point contact, through the sensory area can be of any size. In practice, an area of  $1\text{--}2$  mm<sup>2</sup> is considered satisfactory.
2. The sensitivity depends on the application, in particular any physical barrier between the sensor and the object is a factor. For a force-type tactile sensor, sensitivity within the range  $0.4\text{--}10$  N, together with an allowance for accidental mechanical overload, is considered satisfactory for most applications.
3. A minimum sensor bandwidth of 100 Hz.
4. The sensor characteristics must be stable and repeatable with low hysteresis. A linear response in an analog sensor is not absolutely necessary as information processing techniques can be used to compensate for any moderate nonlinearities.



If a tactile array is being considered, the majority of applications can be undertaken by an array 10–20 sensors square, with a spatial resolution of 1–2 mm. In robotics and in design of prosthesis, a grasping force at a “finger” tip should be measured. Thus, these tactile sensors can be integrated into the “skin” to respond in real time, the magnitude, location, and direction of the forces at the contact point.

### 7.13.1 Switch Sensors

A simple tactile sensor producing an “on-off” output can be formed with two leaves of foil and a spacer (Fig. 7.44). The spacer has round (or any other suitable shape) holes. One leaf is grounded and the other is connected to a pull-up resistor. The grounded leaf may be a conductive cladding on a circuit board. A multiplexer can be used if more than one sensing area is required. When an external force is applied to the upper conductor over the hole in the spacer, the top leaf flexes and upon reaching the lower conductor, makes an electric contact, grounding the pull-up resistor. The output signal becomes zero indicating the applied force. The upper and lower conducting leaves can be fabricated by a silk-screen printing of conductive ink on the backing material, like Mylar<sup>®</sup> or polypropylene. Multiple-sensing spots can be formed by printing rows and columns by a conductive ink. Touching of a particular area on a sensor will cause the corresponding row and column to join thus indicating force at a particular location. These sensors are widely used in low cost consumer products, such as TV remote controls and toys.

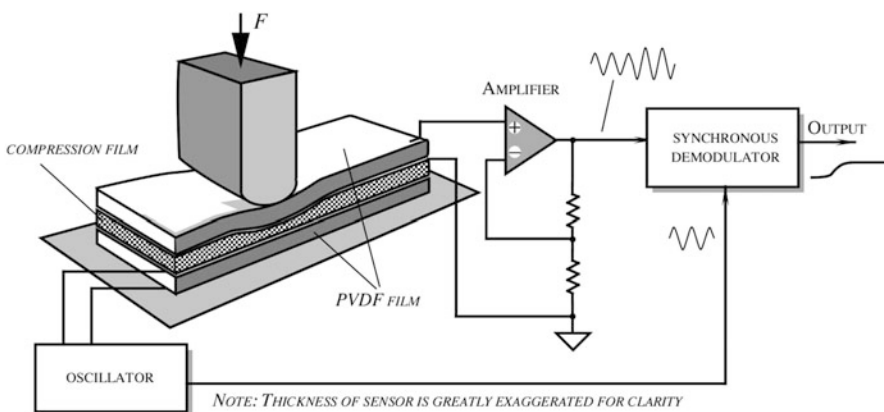


**Fig. 7.44** Membrane switch as tactile sensor

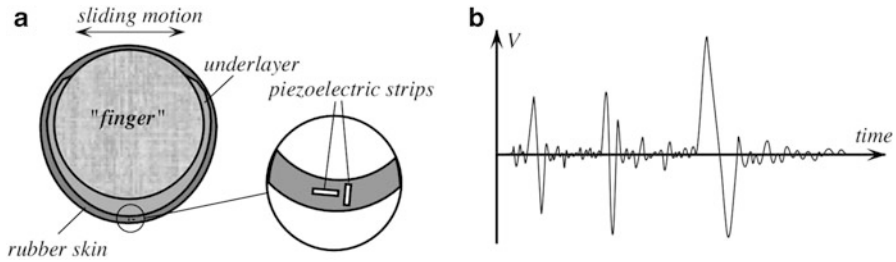
### 7.13.2 Piezoelectric Tactile Sensors

Efficient tactile sensors can be designed with piezoelectric films, such as polyvinylidene fluoride (PVDF) used in the active or passive modes (see Sect. 4.6.2). An active ultrasonic coupling touch sensor with the piezoelectric films is illustrated in Fig. 7.45 where three films are laminated together (there are also the additional protective layers that are not shown in the figure). The upper and bottom films are PVDF, while the center film is for the acoustic coupling between the two. Softness of the center film determines sensitivity and operating range of the sensor. A practical material for the center film is silicone rubber. The bottom piezoelectric film acts as a vibration transmitter and is driven by an ac voltage from an oscillator. This excitation signal results in mechanical contractions of the film that are coupled to the compression film and, in turn, to the upper piezoelectric film, which acts as a receiver. Since piezoelectricity is a reversible phenomenon, the upper film produces alternating voltage upon being subjected to mechanical vibrations from the compression film. These oscillations are amplified and fed into a synchronous demodulator. The demodulator is sensitive to both the amplitude and the phase of the received signal. When compressing force  $F$  is applied to the upper film, a mechanical coupling between the three-layer assembly changes. This modulates the amplitude and phase of the received signal. These changes are recognized by the demodulator and appear at its output in form of a variable voltage.

Within certain limits, the output signal linearly depends on the force. If the 25  $\mu\text{m}$  PVDF films are laminated with a 40  $\mu\text{m}$  silicone rubber compression film, the thickness of an entire assembly (including protective layers) does not exceed 200  $\mu\text{m}$ . The PVDF film electrodes may be fabricated with a cell-like pattern on either the transmitting or receiving side. This would allow to use an electronic multiplexing of the cells to achieve spatial recognition of the applied stimuli. The sensor also can be used for measuring small displacements. Its accuracy is



**Fig. 7.45** Active piezoelectric tactile sensor



**Fig. 7.46** Tactile sensor with piezoelectric film for detecting sliding forces. Cross-sectional view (a) and typical response (b) (adapted from [27])

better than  $\pm 2 \mu\text{m}$  over a few millimeter range. Advantages of this sensor is in its simplicity and a d.c. response, that is, in the ability to recognize static forces.

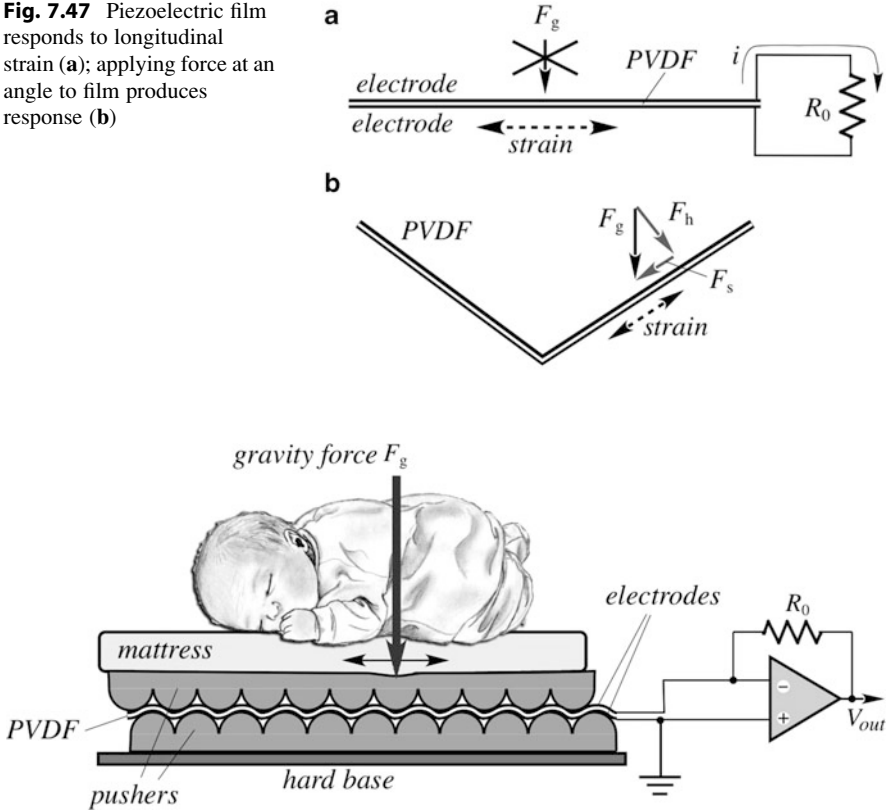
A piezoelectric tactile sensor for detecting touch and sliding motions can be fabricated with the PVDF film strips imbedded into a rubber skin, Fig. 7.46a. This sensor is passive, so the output signal is generated by the piezoelectric film without the need for any excitation signal. As a result, it produces a response proportional to the rate of stress, rather than to the stress magnitude. The design of this sensor is tailored to the robotic applications where it is desirable to sense sliding motions causing fast vibrations. The piezoelectric sensor is directly interfaced with a rubber skin, thus the electric signal produced by the strips reflect movements of the elastic rubber that are caused by the uneven friction forces.

The sensor is built on a rigid structure (a robot's "finger") which has a foamy compliant underlayer (1 mm thick), around which a silicon rubber "skin" is wrapped. It is also possible to use a fluid underlayer for a better smooth surface tracking. Because the sensing strips are located at some depth beneath the skin surface, and because the piezoelectric film responds differently in different directions, a signal magnitude is not the same for movements in any direction. The sensor responds with a bipolar signal, Fig. 7.46b, to surface discontinuity or bumps as small as  $50 \mu\text{m}$  high.

Electronics for musical instruments present a special problem in drums and pianos. The very high dynamic range and frequency response requirements for the drum triggers and piano keyboards are met by piezoelectric film impact elements. Laminates of piezo film are incorporated in the foot pedal switches for bass drums, and triggers for snares and tom-toms. The piezoelectric film impact switches are force sensitive, faithfully duplicating the effort of the drummer or pianist. In electronic pianos, the piezoelectric film switches respond with a dynamic range and time constant that is remarkably similar to a piano keystrokes.

It should be noted that piezoelectric films mostly respond when stretched, while compression generates much weaker signals. Thus, the designs should apply forces along the film surface. This is illustrated in Fig. 7.47a where the longitudinal strain in the film produces current  $i$  through the load resistor  $R_0$ . The transverse force  $F_g$  makes almost no signal. To resolve this difficulty, the film may be positioned or

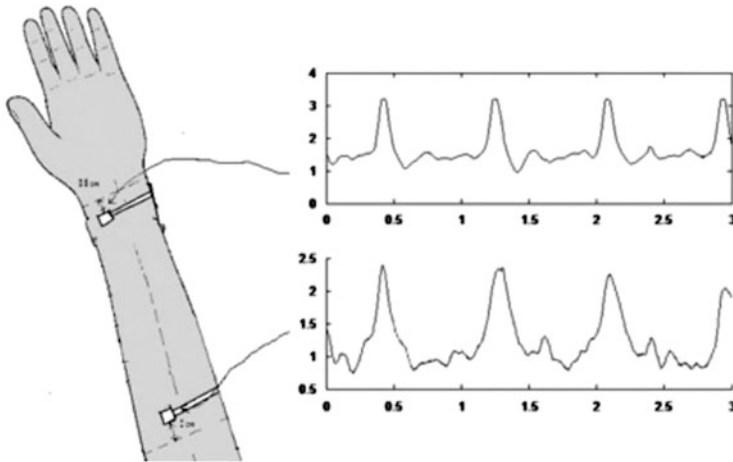
**Fig. 7.47** Piezoelectric film responds to longitudinal strain (a); applying force at an angle to film produces response (b)



**Fig. 7.48** Piezoelectric film respiration rate sensor

folded at an angle to the applied force as shown in Fig. 7.47b. The force vector  $F_g$  can be replaced by a sum of two vectors:  $F_s$  and  $F_h$ , where vector  $F_s$  is parallel with the film surface and thus causes a strain. This approach is illustrated in Fig. 7.48 that shows the PVDF film sensor for detecting breathing rate of a sleeping child. The minute movements of the child's body resulted from respirations were monitored in order to detect apnea—a cessation of breathing [28]. The sensor was placed under the mattress in a crib. The body of a normally breathing baby slightly shifts horizontally with each inhale and exhale due to a moving diaphragm in the chest. The diaphragm movement causes displacement of the body's center of gravity and thus shifting horizontally the gravitational force  $F_g$  applied normally to the plane of the mattress. This force movement is detected by the PVDF film sensor. The film sheet has two electrodes deposited on its front and backsides. The sensor assembly consists of three layers where the PVDF film is sandwiched between two preformed pushers that are made, for instance, from silicone rubber.

The pushers have the corrugated or bump-shaped surfaces that squeeze the PVDF film in-between the alternating bumps. The bumps fold the film and thus apply a force to the film at an angle. Under a shifting force, the PVDF film is



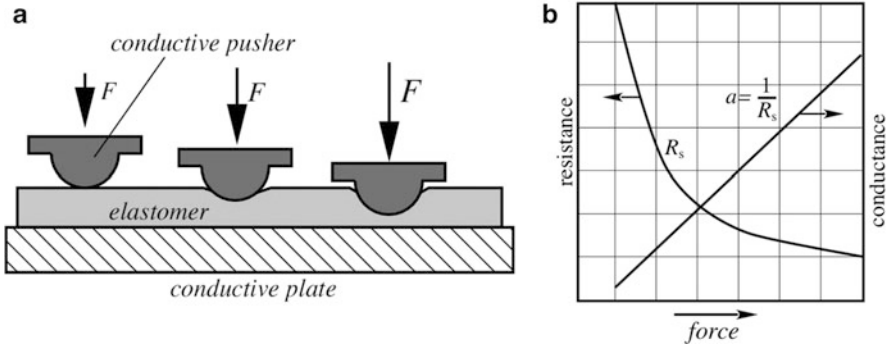
**Fig. 7.49** Recording of arterial oscillations from two piezoelectric film sensors

variably stressed by the bumps and subsequently generates a variable electric charge. The charge causes electric current flowing through the current-to-voltage converter that produces the output voltage  $V_{out}$ . The amplitude of that variable voltage within certain limits is proportional to the variations in gravitational force. Operation of this sensor is similar to a piezoelectric cable placed under the mattress, as illustrated in Fig. 10.11. Note that this design resembles the one shown in Fig. 5.22 for the fiber-optic force sensor.

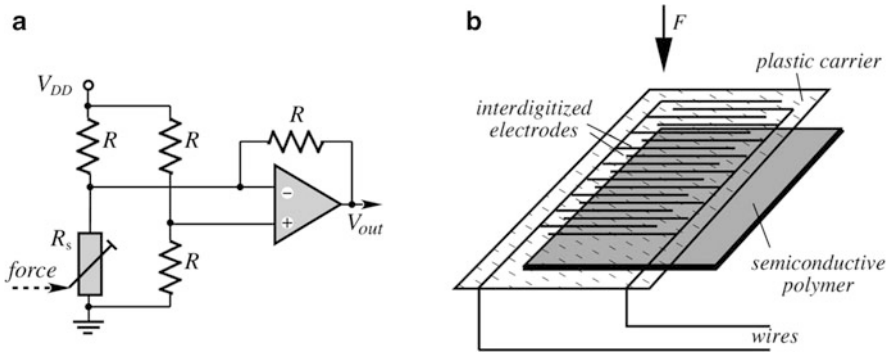
Small thickness, high sensitivity, and no energy consumption of the piezoelectric film permits designing a great variety of medical sensors for monitoring minute motions of human tissues. As an example, Fig. 7.49 shows recordings of the arterial oscillations from two piezoelectric film sensors adhered to the patient's skin over the radial artery at two locations: wrist and middle arm.

### 7.13.3 Piezoresistive Tactile Sensors

Another type of a tactile sensor contains a piezoresistive element. It can be fabricated by using materials having electrical resistance dependent on strain. The sensor incorporates a force-sensitive resistor (FSR) whose resistance varies when subjected to pressure [29]. The FSRs are conductive elastomers or pressure-sensitive inks. A conductive elastomer is fabricated of silicone rubber, polyurethane, and other compounds that are impregnated with conductive particles or fibers. For instance, conductive rubber can be fabricated by using carbon powder as an impregnating material. Operating principles of the elastomeric tactile sensors are based either on varying the contact area when the elastomer is squeezed between two conductive parts, Fig. 7.50a, or on changing the elastomer thickness.



**Fig. 7.50** FSR tactile sensor. Through thickness application with elastomer (a); transfer function for resistance  $R_0$  and conductance  $a$  (b)



**Fig. 7.51** Interface circuit for elastomer tactile sensor (a) and tactile sensor with polymer FSR (b)

When the external force varies, a contact area at the interface between the pusher and elastomer changes and the elastomer volume between the pusher and plate becomes smaller, resulting in reduction of the electrical resistance.

At a certain pressure, the contact area reaches its maximum and the transfer function, Fig. 7.50b, goes to saturation. The elastomer resistance  $R_s$  changes with the force highly nonlinearly, however its reciprocal function, the conductivity  $a$ , is nearly linear with respect to the force:

$$a \approx kF, \tag{7.28}$$

where  $k$  is the force coefficient that depends on the elastomer conductive properties and geometry. This linear feature may be utilized in the interface circuit shown in Fig. 7.51a, where the force-sensitive resistor  $R_s$  is part of the resistive bridge connected to an operational amplifier. The output voltage of the amplifier is a nearly linear function of the applied force  $F$ :

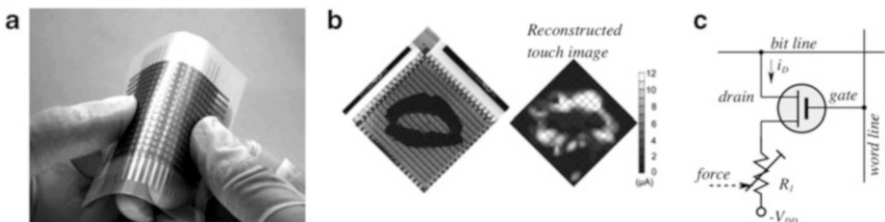
$$V_{\text{out}} = \frac{V_{\text{DD}}}{2} \left( \frac{R}{R_s} - 1 \right) \approx \frac{V_{\text{DD}}}{2} (Ra - 1) = \frac{V_{\text{DD}}}{2} (RkF - 1) \quad (7.29)$$

It should be noted, however, that the elastomer conductivity may noticeably drift when the polymer is subjected to prolonged pressure or temperature changes.

A thin FSR tactile sensor can be fabricated with a semiconductive polymer whose resistance varies with pressure. A design of the sensor resembles a membrane switch, Fig. 7.51b, [13]. Unlike a strain gauge, the FSR has a significantly wider dynamic range: typically three decades of resistance change over a 0–3 kg force range and a much lower accuracy (typically  $\pm 10\%$ ). However, in many applications, where an accurate force measurement is not required, a low cost of the sensor makes it an attractive alternative. A typical thickness of a FSR polymer sensor is on the range of 0.25 mm (0.010") but even thinner sheets are also available.

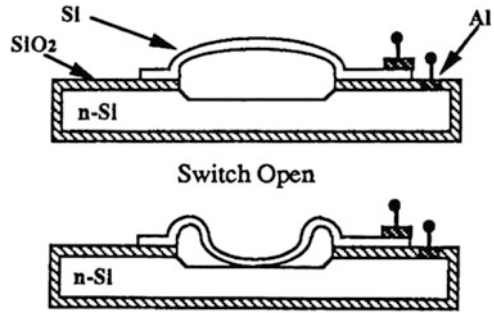
A combination of a conductive rubber as FSR and the organic field effect transistors (FET) as multiplexers allows fabrication of an electronic pressure-sensitive skin suitable for robotic applications. The skin has of a multitude of the miniature pressure sensors that is appended with a flexible switching matrix. The organic FET is selected for the “skin” because organic circuits are inherently flexible and potentially low in cost, even for a large skin area [30]. An important step in production of a good artificial “electronic skin” is to fabricate large-area tactile sensors with mechanical flexibility. The organic FET transistors are integrated within a graphite-containing rubber to form a wide area as illustrated in Fig. 7.52a. The skin is electrically functional even when it is wrapped around a cylindrical bar with only a 2-mm radius. A pitch of the embedded FETs is 10 dpi that is sufficient for generating a recognizable image as shown in Fig. 7.52b. The basic idea behind the sensor is to modulate electric currents through the FETs by the variable rubber resistances attached to the FET drains and multiplex the FETs by applying control voltages to the gates. Figure 7.52c illustrates connection of the FET into a matrix.

The overall configuration is similar to a memory cell or a pixel of a charge-coupled device (CCD): gate electrodes of each line are connected to a word line, whereas drain electrodes are connected to a bit line. As pressure is applied on the skin in the vicinity of a particular cell and varies from 0 to 30 kPa ( $\approx 300$  g force/cm), the resistance of the rubbery sheet varies from 10 M $\Omega$  to 1 k $\Omega$  and the transconductance of the FET, as well as the measured current  $i_D$ , increases.



**Fig. 7.52** Electronic skin with embedded organic FETs (a), 16  $\times$  16 FET matrix responds to a “kiss” by a lip-shaped rubber stamp (b), and connection of FET (c). (Adapted from [30])

**Fig. 7.53** Micromachined silicon threshold switch with trapped gas (from [16])



### 7.13.4 Tactile MEMS Sensors

Subminiature tactile sensors are especially in high demand in robotics, where a good spatial resolution, high sensitivity, and wide dynamic range are required. A plastic deformation in silicon can be used for fabrication of a threshold tactile sensor with a mechanical hysteresis [31]. In one design [32], the expansion of trapped gas in a sealed cavity formed by wafer bonding is used to plastically deform a thin silicon membrane bonded over the cavity, creating a spherically shaped cap. The structure shown in Fig. 7.53 is fabricated by MEMS processing a silicon wafer. At normal room temperature and above the critical force, the upper electrode will buckle downward, making contact with the lower electrode. Experiments have shown that the switch has hysteresis of about 2 psi of pressure with a closing action near 13 psi. The closing resistance of the switch is on the order of 10 k $\Omega$ , which for the micropower circuits is usually low enough.

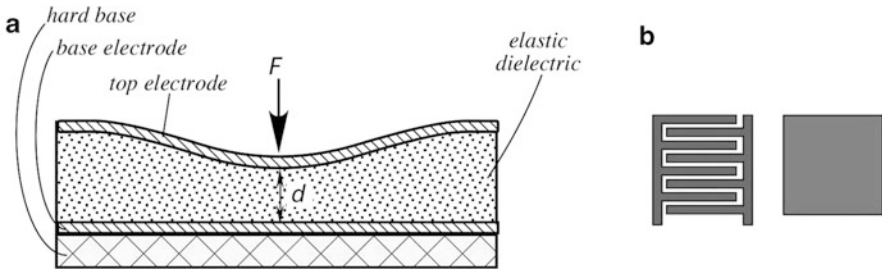
### 7.13.5 Capacitive Touch Sensors

A capacitive touch sensor is based on fundamental equations for the parallel-plate and coaxial capacitors (Sect. 4.2). A capacitive touch sensor relies on the applied force that either changes the distance between the plates or varies surface area of the capacitor electrodes (plates). In the sensor two conductive plates are separated by a dielectric medium, which may also be used as an elastomer to give the sensor its force-to-capacitance characteristics, Fig. 7.54a.

To maximize change in the capacitance when force is applied, it is preferable to use a high-permittivity dielectric polymer such as polyvinylidene fluoride (PVDF).

To measure change in a capacitance, a number of techniques can be employed. If the capacitor is not too small (on the order of 1 nF or larger), the most popular technique is using a current source with a resistor and measure a time delay caused by a variable capacitance. Another approach is using a capacitive sensor as part of an oscillator with an LC or RC circuit, and measuring the frequency response. Significant problem with capacitive sensors may arise if they are in close proximity





**Fig. 7.54** Capacitive parallel-plate touch sensor (a); interdigitized and single electrodes for touchscreen (b)

with metal structures. The effect can be minimized by a good circuit layout and a differential capacitor design.

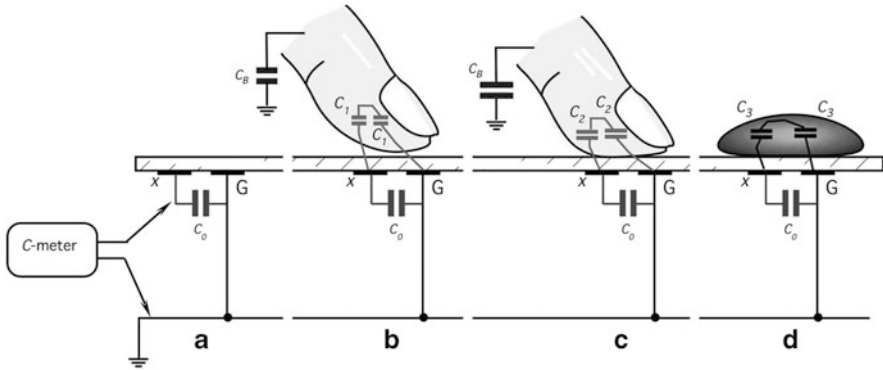
Capacitive sensors are popular in touchscreen panels that typically are made of glass or a clear polymer coated with a transparent conductor such as indium tin oxide (ITO) that combines electrical conductivity and optical clarity. This type of a sensor is basically a capacitor in which the plates are the overlapping areas between the horizontal and vertical axes in a grid pattern. Each plate may be a dual-interdigitized or single-plate electrode (Fig. 7.54b). Since a human body has a high dielectric constant, touching the sensor electrode will affect distribution of the electric field around the contact and create a measurable change in the capacitance. These sensors work on proximity of the conductive medium (finger), thus they do not have to be directly touched for triggering. It is a durable technology that has been used in a wide range of applications including point-of-sale systems, industrial controls, and public information kiosks. However, it only responds to a finger contact and will not work with a gloved hand or pen stylus unless the stylus is conductive.

Many popular touchscreens for computer monitors employ capacitive sensors. The screen is formed of glass where each sensing element has two electrodes deposited on the glass inner surface as shown in Fig. 7.55a. One of the electrodes (G) is grounded and the other is connected to the capacitance meter (C-meter). Some small baseline capacitance  $C_0$  exists between the two electrodes and that capacitance is monitored by the C-meter.

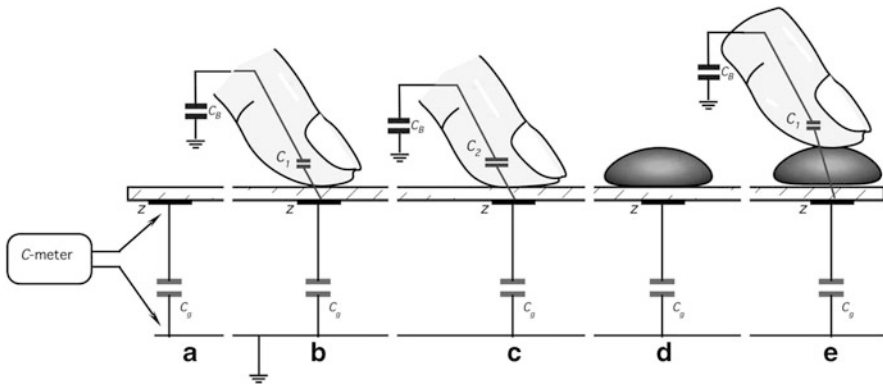
When a finger comes in proximity of the electrodes (Fig. 7.55b), it develops with each electrode a capacitive coupling  $C_1$ . In response, the capacitance monitor will register a new combined capacitance

$$C_{m1} = C_0 + 0.5C_1, \quad (7.30)$$

which is much larger than  $C_0$ . If the finger is pressed harder, due to the fingertip elasticity the contact area with the touchscreen increases and that causes a larger capacitive coupling  $C_2 > C_1$  as shown in Fig. 7.55c. This will further increase the combined monitored capacitance and thus can be used as an indication of a harder pressing.



**Fig. 7.55** Dual-electrode touchscreen. No touch (a), light touch (b), strong touch (c) and water droplet (d)



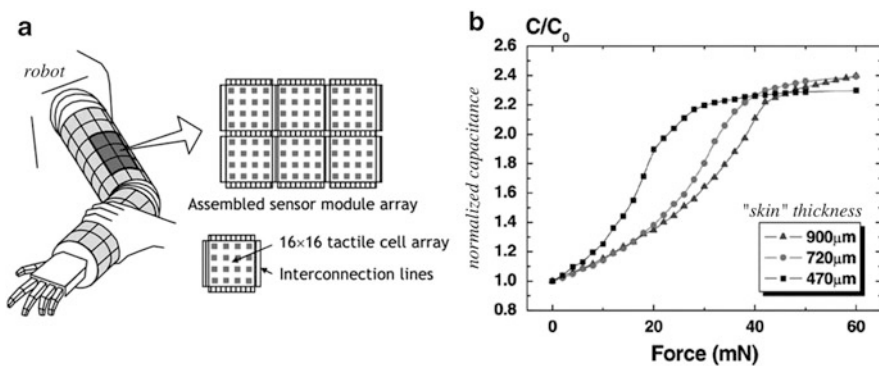
**Fig. 7.56** Single electrode touchscreen. No touch (a), light touch (b), strong touch (c), water droplet (d), and touching through water droplet (e)

Now, let us assume that a droplet of water is deposited on the touchscreen above the electrodes as shown in Fig. 7.55d. Being electrically conductive with a dielectric constant between 76 and 80, water forms with the electrodes a strong coupling  $C_3$  which is comparable with that of a finger and, as a result, the touchscreen will indicate a false touch. Sensitivity to water droplets is a disadvantage of a dual-electrode touchscreen where one electrode is grounded.

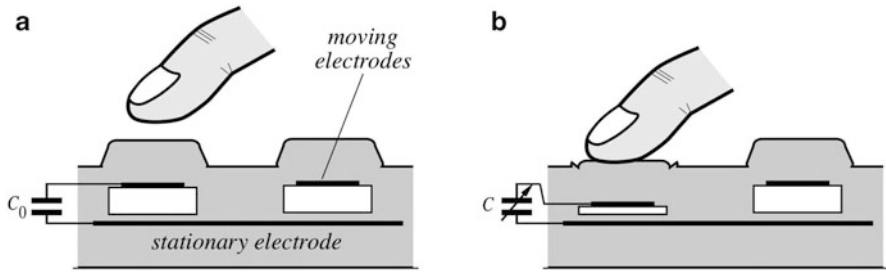
To resolve sensitivity to water droplets, an improvement of a capacitive touchscreen that contains a single-electrode pattern was proposed [33]. No electrode in that screen is grounded. Under the no-touch condition, only a small capacitance  $C_0$  exists between the electrode and ground (earth) as indicated in Fig. 7.56a and it is monitored by a C-meter. A human body naturally forms a strong capacitive coupling  $C_B$  to the surrounding objects. This capacitance is several orders of magnitude larger than  $C_0$ . Hence, a human body may be considered

having a low impedance to “ground”. When a finger comes into vicinity of the electrode (Fig. 7.56b), a capacitance  $C_1$  is formed between the fingertip and electrode. This capacitance is electrically connected in parallel with the baseline capacitance  $C_0$ , causing the C-meter to respond. Like in a two-electrode screen, a stronger pressing will create a larger capacitance as shown in Fig. 7.56c. However, when a water droplet is deposited on the screen (Fig. 7.56d), it will cause no false detection as the water droplet is not coupled to ground. It is interesting to note that as shown in Fig. 7.56e touching the water droplet will form a capacitive coupling to ground and the touch will be correctly detected. Therefore, this electrode arrangement is more robust under the adverse environmental conditions. Arranging the electrode pattern in rows and columns and processing signals by the appropriate circuit can make a reliable spatial touch recognition by an special electronic circuit such as, for example, the Fujitsu controller FMA1127. A similar approach can be used to form proximity detectors on surfaces of many shapes. For example, a proximity sensor can be formed on a doorknob for the security purposes. It will respond not only to touching but even to approaching the door knob surface by as far as 5 cm.

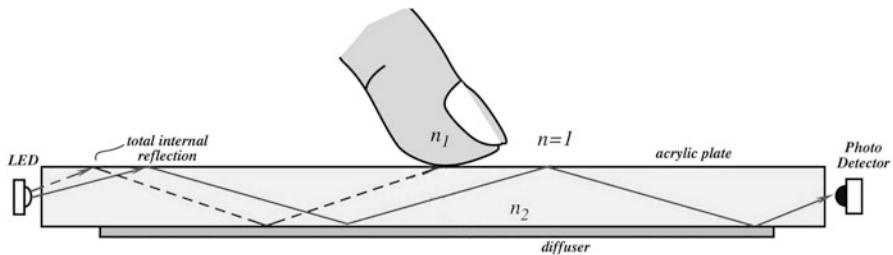
A multielement capacitive “skin” can be developed for covering larger areas of complex shapes, such as the robot’s arms shown in Fig. 7.57a. The skin is a combination of modules that are the sensing arrays having  $16 \times 16$  matrix of miniature-sensing elements [34]. Each element is comprised of a flexible molded elastomer having a small pusher on the top and a cavity inside as shown in Fig. 7.58. The cavity is sandwiched between two electrodes: the stationary and movable that form the baseline capacitance  $C_0$ . When an external force is applied to the pusher, the cavity collapses bringing the electrodes closer to one another. This results in change in capacitance that for a full compression more than doubles as shown in the response curves of Fig. 7.57b.



**Fig. 7.57** Modules of sensing arrays form robotic skin (a). Normalized change of capacitance for different skin thicknesses (b)



**Fig. 7.58** Cross-sectional view of the sensing element (a). Sensing cavity collapses under external force (b)



**Fig. 7.59** Concept of optical touchscreen

### 7.13.6 Optical Touch Sensors

A conventional optical-touch systems uses an array of infrared (IR) light-emitting diodes (LEDs) on two adjacent bezel edges of a display, with the photodetectors placed on two opposite bezel edges to analyze the system and determine a touch event (Fig. 7.59). The LED and photodetectors pairs create a grid of light beams across the display. An object (such as a finger or pen) that touches the screen changes reflection due to a difference between refractive properties of air and a finger. Since the acrylic or glass refractive index  $n_2$  is larger than the human skin refractive index  $n_1$ , at the point of touch, the angle of total internal reflection (TIR) increases. This results in a light beam passing through the boundary to the skin and not being transmitted toward the detector (see detailed explanation in the next Sect. 7.13.7). This results in a measured decrease in the detected light intensity. The photodetector output signals can be used to locate the touch-point coordinate.

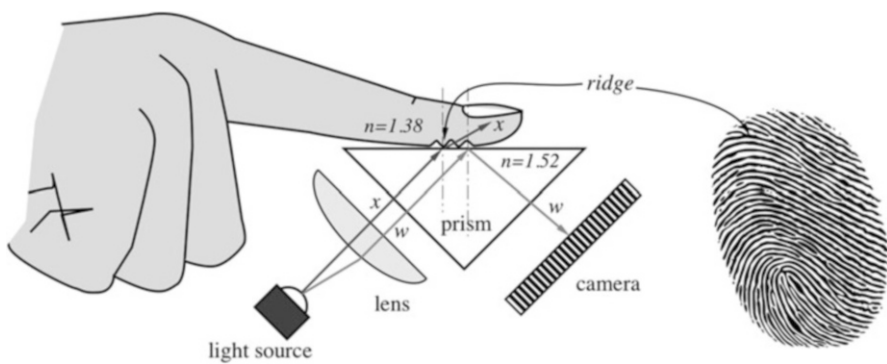
Widespread adoption of infrared touchscreens has been hampered by two factors: a relatively high cost of the technology compared to competing capacitive technologies and somewhat reduced performance in bright ambient light.

The latter problem is the result of background light increasing the noise floor at the photodetectors, sometimes to such a degree that the touchscreen's LED light cannot be detected at all, causing a temporary failure of the touchscreen. This is most pronounced in direct sunlight conditions since the sun emanates very high energy in the infrared region.

However, certain features of the infrared touch remain desirable and represent attributes of the ideal touchscreen, including the option to eliminate the glass or plastic overlay that most other touch technologies require in front of the display. In many cases, this overlay is coated with an electrically conducting transparent material such as ITO, which reduces the optical quality of the display. This advantage of the optical touchscreens is important for applications that require higher clarity.

### 7.13.7 Optical Fingerprint Sensors

Fingerprints are one of many forms of biometrics used for identifying and verifying individuals. A fingertip recognition is employed by various security systems, personal banking, medical records, and device protection. The analysis of fingerprints for the matching with a database generally requires a comparison of several features of the print pattern. These include the aggregate characteristics of ridges and minutia points, which are unique features. To identify a touch by a particular human finer tip, the pattern of the skin surface shall be reliably recognized. Before performing the recognition, first a quality image shall be obtained by a special fingertip sensor. Sensors for such detections include ultrasonic, capacitive, and optical. Below we discuss the optical sensor whose operating principle is based on differences between refractive indices of glass, air, and human skin. Figure 7.60 illustrates a conceptual design of the sensor. Its key element is a glass prism with the base surface facing up. A light source (for example, LED) with a collimator lens produces parallel beams of light that enter the prism and, in



**Fig. 7.60** Optical fingerprint sensor uses a difference between refractive indices of glass ( $n_2$ ) and skin ( $n_1$ )

absence of a finger, are being reflected towards the imaging camera. Light is reflected from the base surface because the rays enter at angles that exceed the angle of total internal reflection or TIR (see Sect. 5.7.2). The TIR can be computed from Eq. (5.26). A prism made of crown glass has a refractive index  $n_2 = 1.52$ , thus the TIR for a boundary with air (refractive angle  $n = 1$ ) is  $41^\circ$ . Since the light rays enter at larger angles of about  $45^\circ$ , they are fully diverted toward the imaging camera that registers a uniform light surface.

When a fingertip touches the prism surface, the contacts occur only at the skin ridges while the skin valleys have air trapped inside. As a result, two types of the boundaries form on the prism surface: glass-skin and glass-air. Since a typical skin refractive index in the visible and near-infrared spectral ranges is about  $n_1 = 1.38$  [35], the glass-skin boundary forms the TIR angle:

$$\Theta_{2-1} = \arcsin\left(\frac{n_1}{n_2}\right) = \arcsin\left(\frac{1.38}{1.52}\right) \approx 65^\circ \quad (7.31)$$

This wide TIR angle does not reflect the light rays  $x$  arriving at  $45^\circ$  and passes them outside of the prism where they are lost and do not reach the camera. From these spots, the camera registers black. On the other hand, the skin valleys have trapped air, thus their TIR remains  $41^\circ$  and the light rays  $w$  are reflected toward the camera, forming the white areas. A disadvantage of this method is that the sensor may fail if the fingertip is wet or soiled with dirt that fills in the fingertip valleys.

---

## References

1. Blumenkrantz, S. (1989). *Personal and organizational security handbook*. Washington, DC: Government data publications.
2. Sarabia, E. G., et al. (2013). Accurate estimation of airborne ultrasonic time-of-flight for overlapping echoes. *Sensors*, 13(11), 15465–15488.
3. Kyrynyuk, V. et al. (2014). Automotive ultrasonic distance measurement for park-assist systems. AN76530. cypress.com
4. McEwan, T. E. (1994, November 1). Ultra-wideband radar motion sensor. *U.S. Patent No. 5,361,070*.
5. Azevedo, S. G., et al. (1995). Landmine detection and imaging using micropower impulse radar (MIR). *Proceedings of the Workshop on Anti-personnel Mine Detection and Removal*, July 1, 1995, Lausanne, Switzerland (pp. 48–51).
6. Boles, S. et al. (1995). Signal processing for ultra-wide band impulse radar. *U.S. Patent No. 5381151*.
7. Staderini, E. M. (2002). UWB radars in medicine. *IEEE Aerospace and Electronic Systems Magazine*, 17(1), 13–18.
8. van Drecht, J., et al. (1991). Concepts for the design of smart sensors and smart signal processors and their applications to PSD displacement transducers. In: *Transducers'91. International Conference on Solid-State Sensors and Actuators. Digest of technical papers* (pp. 475–478). ©IEEE.
9. Long, D. J. (1975, August 5). Occupancy detector apparatus for automotive safety system. *U.S. Patent No. 3,898,472*.

10. Gao, X. (2013). *Microchip capacitive proximity design guide*. AN1492, DS01492A, Microchip Technology Inc.
11. Fraden, J. (1991, May 28). Apparatus and method for detecting movement of an object. *U.S. Patent No. 5,019,804*.
12. Fraden, J. (1984, May 22). Motion discontinuance detection system and method. *U.S. Patent No. 4,450,351*.
13. Fitz Gerald, A. S. (1932, February 4). Photo-electric system. *U.S. Patent No. 2,016,036*.
14. Fraden, J. (1984, October 30). Toy including motion-detecting means for activating same. *U.S. Patent No. 4,479,329*.
15. Fraden, J. (1988, September 6). Motion detector. *U.S. Patent No. 4,769,545*.
16. Fraden, J. (1990, January 23). Active infrared motion detector and method for detecting movement. *U.S. Patent No. 4,896,039*.
17. Fraden, J. (1992). Active far infrared detectors. In: *Temperature. Its measurement and control in science and industry* (Vol. 6, Part 2, pp. 831–836). New York: ©AIP.
18. APDS-9700. (2010). *Signal conditioning IC for optical proximity sensors*. Avago Technologies. [www.avagotech.com](http://www.avagotech.com)
19. Parsons, N. E., et al. (2003, September 16). Automatic flow controller employing energy-conservation mode. *U.S. Patent No. 6,619,614*.
20. Parsons, N. E., et al. (2008, July 8). Passive sensors for automatic faucets and bathroom flushers. *U.S. Patent No. 7,396,000*.
21. Fraden, J. (2007, August 31). Alarm system with air pressure detector. *U.S. Patent Publication No. US 2008/0055079*.
22. Fraden, J. (2009, February 17). Detector of low levels of gas pressure and flow. *U.S. Patent No. 7,490,512*.
23. Kirsch, S. T. (1985, October 8). Detector for electro-optical mouse. *U.S. Patent No. 4546347*.
24. Theremin, L. (1928, February 28). Method of and apparatus for the generation of sounds. *U.S. Patent No. 1661058*.
25. Silicon Laboratories Inc. (2011). *Infrared gesture sensing*. AN580. [www.silabs.com](http://www.silabs.com)
26. Microchip Technology. (2013). *Gest IC design guide: Electrodes and system design*. MGC3130. Microchip Technology.
27. Measurement Specialties. (1999, April). Piezo film sensors technical manual. Norristown, PA: Measurement Specialties. [www.msiusa.com](http://www.msiusa.com)
28. Fraden, J. (1985). Cardio-respiration transducer. *U.S. Patent No. 4509527*.
29. Del Prete, Z., et al. (2001). A novel pressure array sensor based on contact resistance variation: Metrological properties. *Review of Scientific Instruments*, 72(3), 1548–1553.
30. Someya, T., et al. (2004). A large-area, flexible pressure sensor matrix with organic field-effect transistors for artificial skin applications. *Proceedings of the National Academy of Sciences of the United States of America*, 101(27), 9966–9970.
31. Mei, T., et al. (2000). An integrated MEMS three-dimensional tactile sensor with large force range. *Sensors and Actuators*, 80, 155–162.
32. Huff, M. A., et al. (1991). A threshold pressure switch utilizing plastic deformation of silicon. In: *Transducers'91. International Conference on Solid-State Sensors and Actuators. Digest of technical papers* (pp. 177–180). ©IEEE.
33. Fujitsu Microelectronics America. (2009). *Touch screen controller technology and application trends*. Fujitsu Technology Backgrounder.
34. Lee, H.-K., et al. (2006). A flexible polymer tactile sensor: Fabrication and modular expandability for large area deployment. *Journal of Microelectromechanical Systems*, 15(6), 1681–1686.
35. Ding, H., et al. (2006). Refractive indices of human skin tissues at eight wavelengths and estimated dispersion relations between 300 and 1600 nm. *Physics in Medicine and Biology*, 51, 1479–1489.
36. Parsons, N. E., et al. (1999, November 16). Object-sensor-based flow-control system employing fiber-optic signal transmission. *U.S. Patent No. 5,984,262*.

*There are two ways of making progress.  
One is to do something better,  
the other is to do something for the first time.*

Detectors of *presence* indicate position of an object at a selected position or within a predefined system of coordinates. By definition, the presence detector is a static, time invariant device.

*Displacement* is a shift of an object from one position to another for a specific distance or angle. Displacement is measured when the object is referenced to its own prior position rather than to an external reference or coordinates. Yet, regardless of the reference, measurements of displacement and position are closely related and thus many sensors designed for a position can be used for measuring shifting (displacement).

*Proximity* detectors indicate when a critical distance is reached. These detectors may be responsive to either live or inanimate objects. Detection of live subjects was described in Chap. 7. In effect, a proximity sensor is a threshold version of a position detector. A *position* sensor measures distance to the object from a certain reference point, while a proximity sensor generates output signals when a certain distance to the object has reached. For instance, many moving mechanisms in process control and robotics use a simple proximity sensor—the end switch. It is a mechanical electrical switch having normally open or normally closed contacts. When a moving object activates the switch by a physical contact, the switch sends a signal to the control circuit. The signal is an indication that the object has reached the end position. Obviously, such contact switches have several drawbacks, among which are a mechanical load on a moving object and hysteresis. Displacement and proximity often are measured by the same sensors.

Displacement sensors are the essential parts of many complex sensors where detection and gauging of shifting of a sensing component is one of several steps in a signal conversion. For example, Fig. 7.36 illustrates a special kind of an air pressure



sensor where a variable air pressure is translated into displacement of a membrane. Subsequently, the displacement is converted into the electrical output signal representing the pressure variations. It is fair to say that displacement sensors are the most widely employed sensors.

When describing displacement sensors in this chapter we consider them as the zero-order devices (see Sect. 3.16) that instantly respond to stimuli. Thus, we do not discuss responses that are functions of time, which by definition, relate to dynamic sensors. Those sensors are covered elsewhere in this book. Here we will concern only with the mechanisms of converting a displacement into electrical output.

When designing or selecting displacement sensors, first, the following questions should be answered:

1. How big is the displacement and of what type (linear, circular)?
2. What resolution and accuracy are required?
3. What is the measured (moving) object made from (metal, plastic, fluid, ferro-magnetic, etc.)?
4. How much space is available for mounting the detector?
5. What are the environmental conditions (humidity, temperature, sources of interference, vibration, corrosive materials, etc.)?
6. How much power is available for the sensor?
7. How much mechanical wear can be expected over the lifetime of the device?
8. What is the production quantity of the sensing assembly (limited number, medium volume, mass production)?
9. What is the target cost of the detecting assembly?

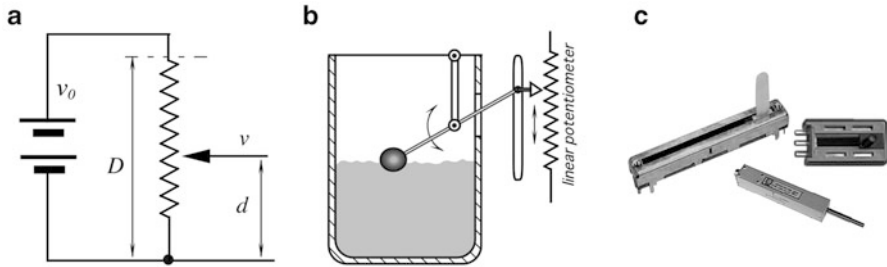
A careful analysis will pay big dividends in the long term.

---

## 8.1 Potentiometric Sensors

A presence or displacement transducer may be built with a linear or rotary *potentiometer*, or a *pot* for short. The operating principle of this sensor is based on Eq. (4.54) for a wire resistance. From the formula, it follows that a resistance linearly relates to the wire length. Thus, by making an object to control the length of the wire, as is done in a pot, a displacement measurement can be performed. Since a resistance measurement requires passage of electric current through the pot wire, the potentiometric transducer is an active type. That is, it requires an excitation signal, for instance, d.c. current. A moving object is mechanically coupled to the pot wiper, whose movement causes the resistance change (Fig. 8.1a). In many practical circuits, a resistance measurement is replaced by a measurement of voltage drop. Voltage across the wiper of a linear pot is proportional to the displacement  $d$

$$v = v_0 \frac{d}{D}, \quad (8.1)$$



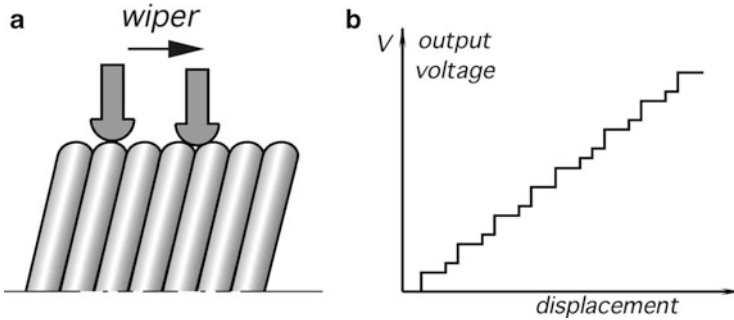
**Fig. 8.1** Potentiometer as position sensor (a); fluid level sensor with float (b); linear potentiometers (c)

where  $D$  is the full-scale displacement, and  $v_0$  is excitation voltage across the pot. This assumes that there is no electrical loading effect from the interface circuit. If there is an appreciable load, the linear relationship between the wiper position and output voltage will not hold. The output signal is proportional to the excitation voltage applied across the sensor. This voltage, if not maintained constant, may be a source of error. This issue may be resolved by using a ratiometric analog-to-digital converter (ADC) in a microcontroller (see Sect. 6.4.7), so the voltage influence will be cancelled. A potentiometric sensor with respect to the pot resistance is a ratiometric device, hence resistance of the pot is not part of the equation, as long as the resistive element is uniform over its entire length. In other words, only a ratio of the resistances is important, not the resistance value. This means that the pot stability (for instance, over a temperature range) makes no effect on accuracy. For low-power applications, high impedance pots are desirable, however, the loading effect must be always considered, thus a voltage follower may be required. The wiper of the pot is usually electrically isolated from the sensing shaft. To illustrate an application of a potentiometric sensor, Fig. 8.1b shows a liquid level sensor with a float being connected to the potentiometer wiper. Different applications require different potentiometer designs, some of which are illustrated in Fig. 8.1c.

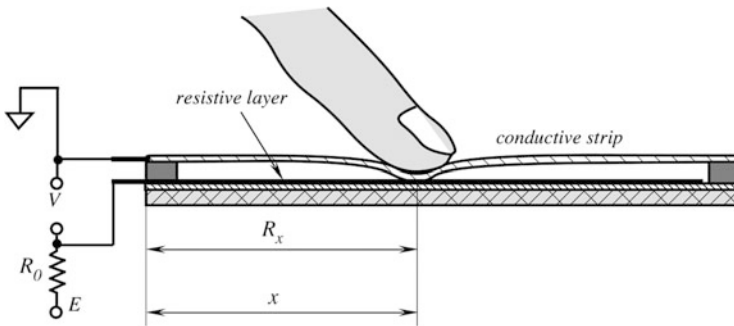
Figure 8.2a shows one problem associated with a wire-wound potentiometer. The wiper may, while moving across the winding, make contact with either one or two wires, thus resulting in uneven voltage steps, Fig. 8.2b, or a variable resolution. Therefore, when a coil potentiometer with  $N$  turns is used, only the average resolution  $n$  should be considered

$$n = 100/N\%. \quad (8.2)$$

The force which is required to move the wiper comes from the measured object and the resulting energy is dissipated in form of heat. Wire-wound potentiometers are fabricated with thin wires having a diameter in the order of 0.01 mm. A good coil potentiometer can provide an average resolution of about 0.1 % of FS (full scale), while the high-quality resistive film potentiometers may yield an infinitesimal (continuous) resolution which is limited only by uniformity of the resistive



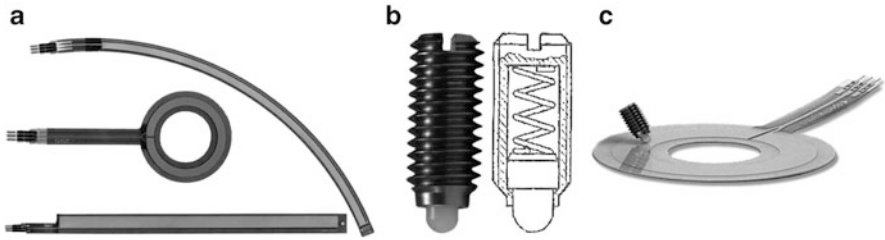
**Fig. 8.2** Uncertainty caused by wire-wound potentiometer. Wiper may contact one or two wires at a time (a); uneven voltage steps (b)



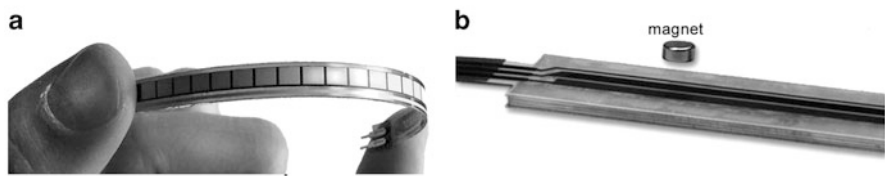
**Fig. 8.3** Principle of a pressure-sensitive potentiometric position sensor

material and noise floor of the interface circuit. The continuous resolution pots are fabricated with conductive plastic, carbon film, metal film, or a ceramic-metal mix, known as *cermet*. The wipers of precision potentiometers are made from precious metal alloys. Angular displacements sensed by the angular potentiometers may range from approximately  $10^\circ$  to over  $3000^\circ$  for the multiturn pots (with gear mechanisms).

A concept of another implementation of a potentiometric position sensor with a continuous resolution is shown in Fig. 8.3. The sensor consists of two strips—the upper strip is made of flexible plastic sheet having a metalized surface. This is a contact or wiper strip. The bottom strip is rigid and coated with a resistive material of a total resistance ranging from several kilohms to Megaohms. The upper conductive strip (wiper) and the bottom resistive strip are connected into an electric circuit. When a pusher (e.g., a fingertip) is pressed against the upper strip at a specific distance  $x$  from the end, the contact strip flexes, touching the bottom strip and making an electric contact at the pressure point. That is, the contact strip works as a wiper in a pot. The contact between two strips changes the output voltage from  $E$  to  $ER_x/R_0$  which is proportional to distance  $x$  from the left side of the sensor.



**Fig. 8.4** Various shapes of pressure-sensitive potentiometers (a), wiper with spring-loaded tip (b) and circular SoftPot with wiper (c) (Courtesy of spectrasymbol.com)



**Fig. 8.5** Flex Sensor (a) and MagnetoPot (b) (Courtesy of spectrasymbol.com)

Practical examples of various shapes of the pressure-sensitive potentiometers are shown in Fig. 8.4a where a resistive layer is deposited on a polyester substrate. The pusher (wiper) slides along the sensor causing a variable output voltage, Fig. 8.4a, b. The overall resistance varies from 1 to 100 k $\Omega$  with a wiper force being in the range from 1 to 3 N. Note that the wipers should be fabricated of a slippery material, such as *derlin* or *nylon*. Alternatively, a roller can be used as a wiper.

Another interesting potentiometric sensor uses the piezoresistive properties of carbon-impregnated plastics. The operating principle of such a sensor is based on change in resistance in response to a mechanical deformation. Carbon-impregnated layer is deposited on a substrate that is fabricated of polyester, fiberglass, or polyimide. When deformed, the carbon particles density varies and subsequently varies the overall resistance. It is the same principle that is used in strain gauges and is the basis of a Flex Sensor, Fig. 8.5a. Such sensors may be used for motion control, medical devices, musical instruments, robotics, and other devices where bends or mutual rotation of joined parts have to be monitored. It should be noted that the bend sensors change resistance to any deformation of the substrate, including local multiple bends and linear stresses. Also, they possess a very noticeable hysteresis and may be the source of noise.

While being quite useful in many applications, potentiometers with contact wipers have several drawbacks:

1. Noticeable mechanical load (friction)
2. Need for a physical coupling with the object
3. Low speed

4. Friction and excitation voltage cause heating of the potentiometer
5. Low environmental stability (wear, susceptibility to dust, etc.).
6. Large size

A potentiometric sensor where the physical contact between the wiper and a resistive layer and thus friction are eliminated uses a wiper layer impregnated with ferromagnetic particles. When an external magnetic field is present at a specific location above the potentiometer, the contact layer is pulled up to the conductive layer making an electrical contact, just like the wiper in Fig. 8.3. This magnetic potentiometer is sealed so it can be used as an immersed sensor for measuring, for example, level of a liquid. It is important to select the appropriate magnet that is sufficiently strong for the sensor operation (see Sect. 4.3.2). Even though such a contactless potentiometer has no friction, a magnetic drag is still a force that opposes the magnet motion. That force should be considered and accounted for in the sensitive applications.

## 8.2 Piezoresistive Sensors

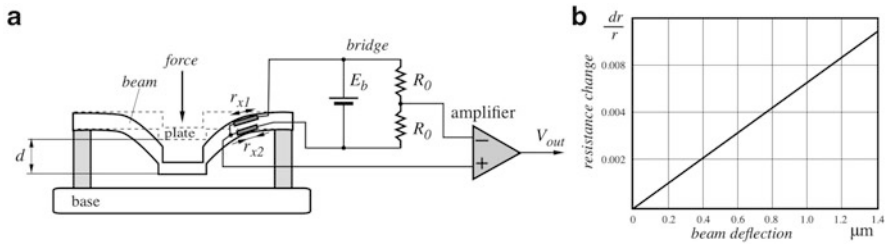
The piezoresistive effect (see Sect. 4.5.3) is the change of material electrical resistance in response to stress or material deformation. A stress/strain-sensitive resistor can be incorporated into a mechanical structure that is deformed and the resistance change and amount of strain is calculated to relate them to a deformation. Sensitivity of a piezoresistive element is quantified as *gauge factor*, which is defined as the relative change in resistance per unit strain  $\varepsilon$ :

$$G = \frac{\Delta r/r}{\varepsilon} \quad (8.3)$$

By considering Eq. (4.54), a normalized change in the piezoresistance can be expressed as:

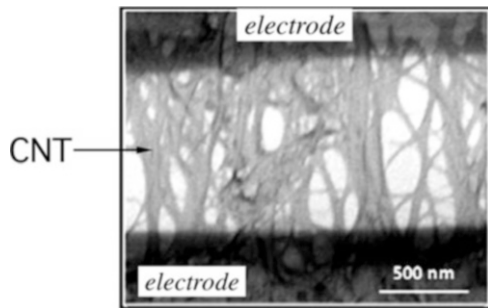
$$\frac{\Delta r}{r} = \frac{\Delta \rho}{\rho} + \frac{\Delta(l/a)}{l/a} = \frac{\Delta \rho}{\rho} + \left( \frac{\Delta l}{l} - \frac{\Delta a}{a} \right), \quad (8.4)$$

where  $\rho$  is the specific resistivity,  $l$  is the length and  $a$  is a cross-section area of the sensing resistor. Thus, the sensor's response depends on the material resistive properties and geometry. To illustrate how sensor converts displacement to electrical output, Fig. 8.6a shows a plate that is supported by several silicon beams. One of the beams has two strain-sensitive resistors,  $r_{x1}$  and  $r_{x2}$ , embedded into its upper and lower sides respectively. An external force pushes the plate downward by distance  $d$ . The plate shifts to a new position, bending and straining the supporting beams, which subsequently deform the embedded piezoresistors. Note that when the plate goes down, the upper resistor  $r_{x1}$  is stretched, so its resistance increases, while the lower resistor  $r_{x2}$  is compressed, causing the resistance decrease.



**Fig. 8.6** Displacement sensor with two piezoresistors embedded into supporting beam. Relative dimensions and displacement are exaggerated for clarity (a); normalized resistance change as function of the beam tip displacement for Si piezoresistor (b)

**Fig. 8.7** Parallel carbon nanotube mesh between electrodes forms subminiature strain gauge sensor. (Adapted from [2])



Both resistors are connected to a Wheatstone bridge circuit that converts the resistance changes to a voltage change, representing the plate displacement. This type of displacement sensors is widely used with the Micro-Electro-Mechanical Systems (MEMS) technologies for fabricating force and pressure sensors, accelerometers, and many other sensors that require displacement transducers for their operations.

A piezoresistor embedded in a thin MEMS beam must be localized as close to the cantilever surface as possible for maximizing sensitivity. A choice must also be made as to the dopant type and resistor orientation to achieve good sensitivity. The sensitivity of a piezoresistor varies proportionately to the doping thickness. The gauge factor of Eq. (8.3) can be calculated directly by straining the cantilevers and measuring the resistance change. An example response of a Si piezoresistor to a beam deflection is shown in Fig. 8.6b.

Progress in nanotechnologies allows development of sensitive displacement sensors on a nanoscale with use of carbon nanotubes (CNT) [1, 2]. A CNT strain gauge contains a large number of nanotubes attached in parallel between two electrodes (Fig. 8.7). When due to strain, the electrodes move apart, the CNT mesh stretches and its resistance increases accordingly. To allow bidirectional measurements, at a zero-strain the CNT network is prestressed (biased), so the electrodes can move closer or farther apart to modulate the resistance toward decrease or increase.

### 8.3 Capacitive Sensors

The capacitive displacement sensors have very broad applications—they are employed directly and also as building blocks in other sensors where displacements are the result of force, pressure, temperature, acceleration, etc. The ability of capacitive detectors to sense virtually all materials makes them an attractive choice for many uses. Equation (4.20) defines that capacitance of a flat capacitor is inversely proportional to distance between the plates and directly proportional to the overlapping area of the plates. The operating principle of a capacitive gauge is based on either changing the geometry (i.e., a distance between the capacitor plates or the overlapping area), or variations in the dielectric materials positioned between the plates. When the capacitance changes, it can be converted into a variable electrical output signal by one of several well known circuits.

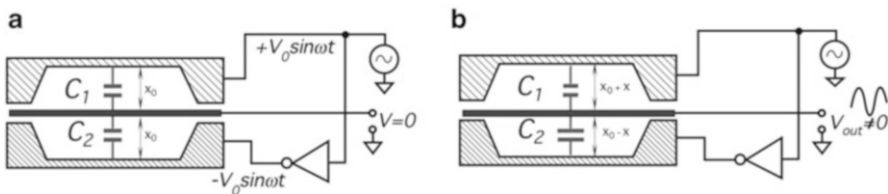
As it is with many sensors, a capacitive sensor can be either *monopolar* (using just one capacitor), *differential* (using two capacitors), or a capacitive bridge can be employed (using four capacitors). When two or four capacitors are used, one or two capacitors may be either fixed or variable, changing with the opposite phases.

As an introductory example, consider three equally spaced plates (Fig. 8.8a). The plates form two capacitors  $C_1$  and  $C_2$ . The upper and lower plates are fed with the out-of-phase sinewave signals, that is, their signal phases are shifted by  $180^\circ$ . Both capacitors are nearly equal one another and thus the central plate has almost no voltage with respect to ground—the charges on  $C_1$  and  $C_2$  cancel each other. Now, let us assume that the central plate moves downward by distance  $x$ , Fig. 8.8b. This causes changes in the respective capacitance values:

$$C_1 = \frac{\epsilon A}{x_0 + x} \quad \text{and} \quad C_2 = \frac{\epsilon A}{x_0 - x}, \quad (8.5)$$

and the central plate signal  $V$  increases in proportion to the displacement while the phase of that signal is indication of the central plate direction—up or down. The amplitude of the output signals is

$$V_{\text{out}} = V_0 \left( -\frac{x}{x_0 + x} + \frac{\Delta C_0}{C_0} \right). \quad (8.6)$$



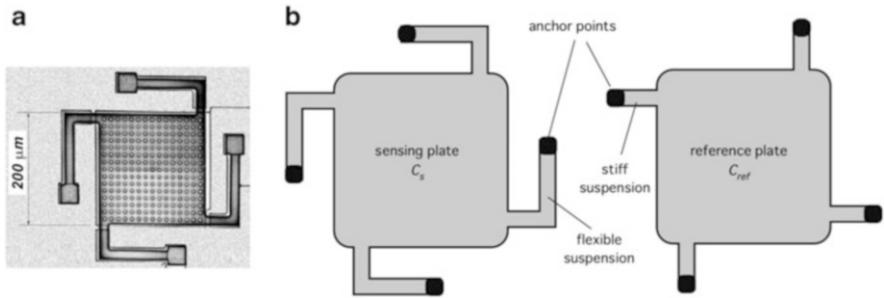
**Fig. 8.8** Operating principle of differential flat-plate capacitive sensor. Balanced (a) and disbalanced (b) positions

As long as  $x \ll x_0$ , the output voltage may be considered a linear function of displacement. The second summand represents an initial capacitance mismatch and is the prime cause for the output offset. The offset is also caused by fringing effects at the peripheral portions of the plates and by the so-called electrostatic force that is a result of the charge attraction and repulsion which is applied to the plates of the sensor, causing the plates to behave like springs. The instantaneous value of the electrostatic force resulted from voltage difference on the plates  $\Delta V$  is

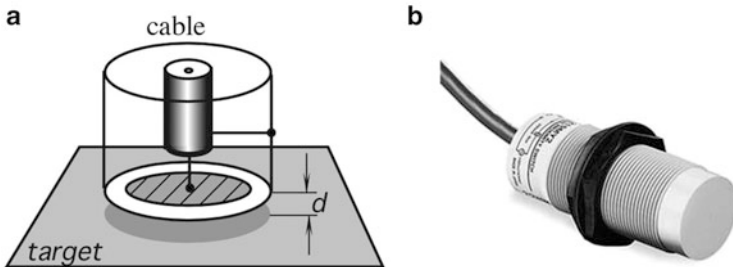
$$F = -\frac{1}{2} \frac{C \Delta V^2}{x_0 + x} \tag{8.7}$$

In another design, two separate silicon plates are fabricated by using a MEMS technology (Fig. 8.9). One plate serves for a displacement measurement, while the other is for reference. Both plates have nearly the same surface areas, however the measurement plate is supported by four flexible suspensions, while the reference plate is held by the stiff suspensions. This particular design is especially useful for accelerometers.

In many practical applications, especially when measuring a distance to an electrically conductive object, the object’s surface itself may serve as a capacitor’s plate. A design of a monopolar capacitive sensor is shown in Fig. 8.10, where one



**Fig. 8.9** Dual-plate capacitive displacement sensor (adapted from [3]). Micromachined sensing plate (a) and different suspensions for sensing and reference plates (b)



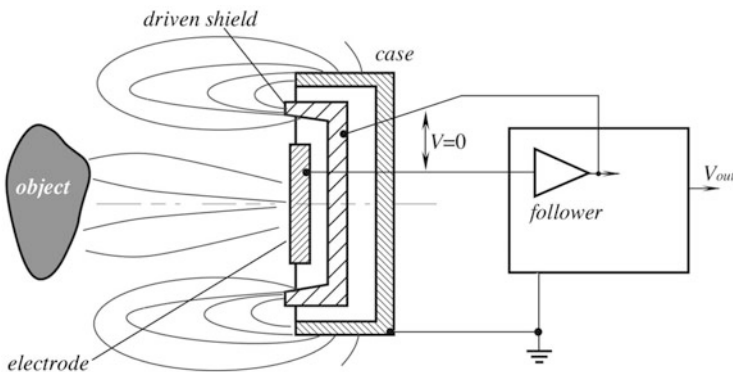
**Fig. 8.10** Capacitive probe with guard ring. Internal view (a); outside view (b)



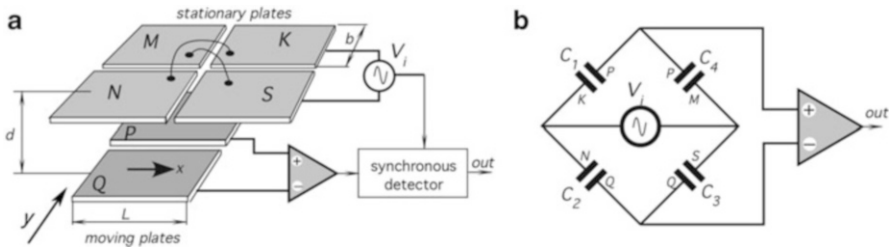
plate of a capacitor is connected to the central conductor of a coaxial cable, while the other plate is formed by a target (object). Note that the probe plate is surrounded by a grounded guard to minimize a fringing effect for improving linearity. A typical capacitive probe operates at frequencies in the 3 MHz range and can detect very fast moving targets, since a frequency response of a probe with a built-in electronic interface is in the range of 40 kHz. A capacitive proximity sensor can be highly efficient when used with electrically conductive objects. The sensor measures a capacitance between the electrode and the object. Nevertheless, even for the nonconductive objects, these sensors can be employed quite efficiently though with lesser accuracy. Any object, conductive or nonconductive, that is brought in the vicinity of the electrode, has its own dielectric properties that will alter the capacitance between the electrode and the sensor housing and, in turn, will produce a measurable response.

To improve sensitivity and reduce fringing effects, the monopolar capacitive sensor may be supplied with a driven shield. The idea behind a driven shield is to eliminate electric field between the sensing electrode and undesirable parts of the object, thus making the parasitic capacitance being virtually nonexistent (see Fig. 7.19). A driven shield is positioned around the nonoperating sides of the electrode and fed with voltage equal to that at the central electrode. Since the shield and the electrode voltages are in-phase and have the same magnitude, no electric field exists between the two and all components positioned behind the shield make no effect on the operation. The driven shield technique for a capacitive proximity sensor is illustrated in Fig. 8.11.

Nowadays, capacitive bridges become increasingly popular in designs of the displacement sensors [4]. A linear bridge capacitive position sensor is shown in Fig. 8.12a. The sensor comprises two planar electrode sets that are parallel and adjacent to each other with a constant separation distance,  $d$ . For increasing capacitance, spacing between the plate sets is made relatively small. The stationary electrode set contains four rectangular elements while the moving electrode set contains two rectangular elements. All six elements are of about the same size



**Fig. 8.11** Driven shield around the electrode in capacitive proximity sensor



**Fig. 8.12** Parallel-plate capacitive bridge sensor. Plate arrangement (a) and equivalent circuit diagram (b). (Adapted from [5])

(side dimension is  $b$ ). The size of each plate can be as large as mechanically practical, whenever a broad range of linearity is desired. The four electrodes of the stationary set are cross-connected electrically, thus forming a bridge-type capacitive network.

The bridge excitation source provides a sinusoidal voltage (5–50 kHz) and the voltage difference between the pair of moving plates is sensed by a differential amplifier whose output feeds the input of a synchronous detector. The capacitance of two parallel plates at fixed separation distance is proportional to the overlapping areas of either plate that directly faces the corresponding area of the other plate. Figure 8.12b shows the equivalent circuit of the sensor that has a configuration of a capacitive bridge. A value of capacitor  $C_1$  is

$$C_1 = \frac{\epsilon_0 b}{d} \left( \frac{L}{2} + x \right) \tag{8.8}$$

The other capacitances are derived from the identical equations. Note that the opposite capacitors are nearly equal:  $C_1 = C_3$  and  $C_2 = C_4$ . A mutual shift of the plates with respect to a fully symmetrical position results in the bridge disbalance and the phase-sensitive output of the differential amplifier. An advantage of the capacitive bridge circuit is the same as of any bridge circuit—linearity and external noise immunity. The same method can be applied to any symmetrical arrangement of a sensor, for instant to detect a rotary motion.

## 8.4 Inductive and Magnetic Sensors

One of many advantages of using magnetic field for sensing position and distance is that any nonmagnetic material can be penetrated by the filed with no loss of position accuracy. Stainless steel, aluminum, brass, copper, plastics, masonry, and woods can be penetrated, meaning that accurate position with respect to the probe at the opposite side of a wall can be determined nearly instantly. Another advantage is that the magnetic sensors can work in severe environments and corrosive situations

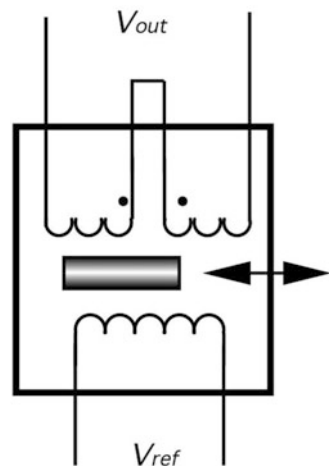
because the probes and targets can be coated with inert materials that will not adversely affect the magnetic fields. Before going further, it is recommended that the readers should familiarize themselves with Sect. 4.4.

### 8.4.1 LVDT and RVDT

Position and displacement may be sensed by methods of electromagnetic induction. A magnetic flux coupling between two coils is altered by movement of an object and subsequently converted into voltage. Variable inductance sensors that use a nonmagnetized ferromagnetic medium to alter the reluctance (magnetic resistance) of the flux path are known as variable-reluctance transducers [6]. The basic arrangement of a multi-induction transducer contains at least two coils—primary and secondary. The primary one carries the ac excitation ( $V_{ref}$ ) that induces a steady a.c. voltage in the secondary coil (Fig. 8.13). The induced amplitude depends on the flux coupling between the coils. There are two techniques to change the coupling. One is the movement of an object made of a ferromagnetic material within the flux path. This changes the reluctance of the path, which, in turn, alters the coupling between the coils. This is the basis for operation of LVDT (linear variable differential transformer), RVDT (rotary variable differential transformer), and the mutual inductance proximity sensors. The other method is to physically move one coil with respect to another.

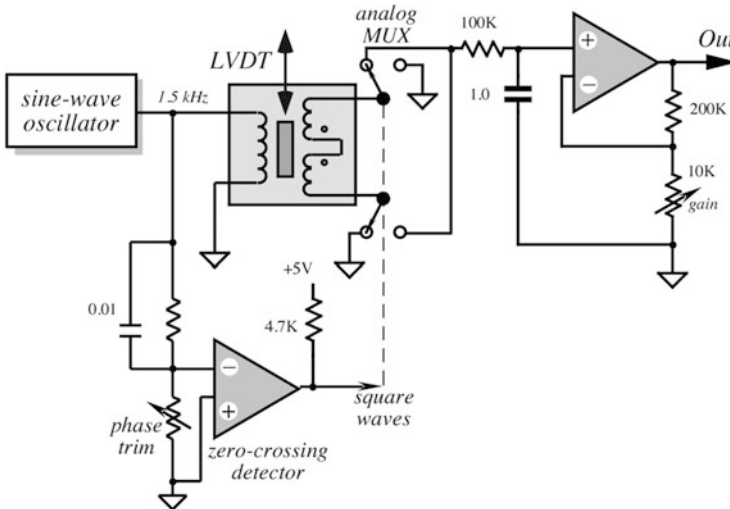
Consider LVDT as a transformer with a mechanically actuated core. The primary coil is driven by a sine wave (excitation signal) having a stabilized amplitude. Sine wave eliminates error related harmonics in the transformer. An a.c. signal is induced in the secondary coils. A core made of a ferromagnetic material is inserted coaxially into the cylindrical opening without physically touching the coils. The two secondaries are connected in the opposed phase. When the

**Fig. 8.13** Circuit diagram of LVDT sensor



core is positioned in the magnetic center of the transformer, the secondary output signals cancel, and there is no output voltage. Moving the core away from the central position unbalances the induced magnetic flux ratio between the secondaries, developing an output. As the core moves, the reluctance of the flux path changes. Hence, the degree of flux coupling depends on the axial position of the core. At a steady state, the amplitude of the induced voltage is proportional, in the linear operating region, to the core displacement. Consequently, voltage may be used as measure of a displacement. The LVDT provides the direction as well as magnitude of the displacement. The direction is determined by the phase angle between the primary (reference) voltage and the secondary voltage. Excitation voltage is generated by a stable oscillator. To exemplify how the sensor works, Fig. 8.14 shows the LVDT connected to a synchronous detector that rectifies the sine wave and presents it at the output as a d.c. signal. The synchronous detector is comprised of an analog multiplexer (MUX) and a zero-crossing detector which converts the sine wave into the square pulses compatible with the control input of the multiplexer. A phase of the zero-crossing detector should be trimmed for the zero output at the central position of the core. The output amplifier can be trimmed to a desirable gain to make the signal compatible with the next stage, such as ADC. The synchronized clock to the multiplexer means that the information presented to the RC-filter at the input of the amplifier is the amplitude and phase sensitive. The output voltage represents how far the core is from the center and on which side.

For LVDT to measure transient motions accurately, frequency of the oscillator must be at least ten times higher than the highest significant frequency of the movement. For a slow changing process, stable oscillator may be replaced by coupling to a power line frequency of 60 or 50 Hz.



**Fig. 8.14** Simplified circuit diagram of interface for LVDT sensor

Advantages of the LVDT and RVDT are the following: (1) the sensor is a noncontact device with no or very little friction resistance with small resistive forces; (2) hysteresis (magnetic and mechanical) are negligible; (3) output impedance is very low; (4) low susceptibility to noise and interferences; (5) construction is solid and robust, (6) infinitesimal resolution is possible.

One useful application for the LVDT sensor is in the so-called *gauge heads* which are used in tool inspection and gauging equipment. In that case, the inner core of the LVDT is spring loaded to return the measuring head to a preset reference position.

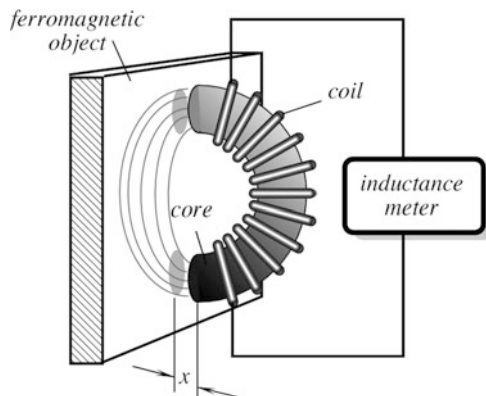
The RVDT operates on the same principle as LVDT, except that a rotary ferromagnetic core is used. The prime use for the RVDT is measurement of the angular displacements. A typical linear range of measurement is about  $\pm 40^\circ$  with a nonlinearity error of about 1 %.

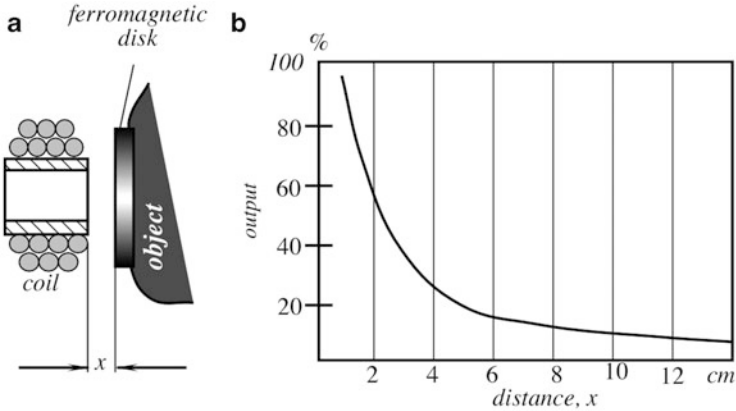
### 8.4.2 Transverse Inductive Sensor

Another electromagnetic position sensing device is called a *transverse inductive proximity sensor*. It is useful for sensing relatively small displacements of ferromagnetic materials. As the name implies, the sensor measures the distance to an object which alters the magnetic field in the coil. The coil inductance is measured by an external electronic circuit (Fig. 8.15). A self-induction principle is the foundation for the operation of this sensor. When it moves into the vicinity of a ferromagnetic object, its magnetic field changes, thus altering inductance of the coil. The advantage of the sensor is that it is a noncontact device whose interaction with the object is only through magnetic field. An obvious limitation is that it is useful only for the ferromagnetic objects at relatively short distances.

A modified version of the transverse transducer is shown in Fig. 8.16a. To overcome the limitation for measuring only ferrous materials, a ferromagnetic disk is attached to a displacing object while the coil has a stationary position. Alternatively, the coil may be attached to the object and the core is stationary.

**Fig. 8.15** Transverse inductive proximity sensor





**Fig. 8.16** Transverse sensor with auxiliary ferromagnetic disc (a) and output signal as function of distance (b)

This proximity sensor is useful for measuring small displacements only, as its linearity is poor in comparison with LVDT. However, it is quite useful as a proximity detector for indication of close proximity to an object which is made of any solid material. Magnitude of the output signal as function of distance to the disk is shown in Fig. 8.16b.

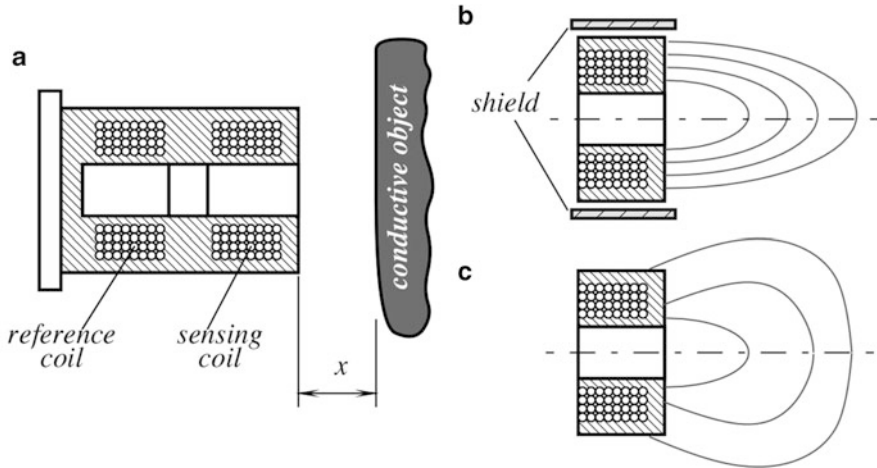
### 8.4.3 Eddy Current Probes

To sense proximity of nonmagnetic but conductive materials the effect of eddy currents is employed in a dual-coil sensor (Fig. 8.17a).<sup>1</sup> One coil is used as a reference or receiving, while the other is for sensing the magnetic currents induced in the conductive object. Eddy currents produce the magnetic field which opposes that of the sensing coil, thus resulting in a disbalance with respect to the reference coil. The closer the object to the coil the larger the change in the magnetic impedance. The depth of the object where eddy currents are produced is defined by

$$\delta = \frac{1}{\sqrt{\pi f \mu \sigma}}, \quad (8.9)$$

where  $f$  is the frequency and  $\sigma$  is the target conductivity. Naturally, for effective operation, the object thickness should be larger than that depth. Hence, eddy detectors should not be used for detecting film metallized or foil objects. Generally, relationship between the coil impedance and distance to the object  $x$  is nonlinear and temperature dependent. The operating frequency of the eddy current sensors

<sup>1</sup> See Sect. 4.4.2 for description of eddy currents.



**Fig. 8.17** Electromagnetic proximity sensor with eddy currents (a). Sensor with shielded front end (b); unshielded sensor (c)

depends on physical dimensions. The small size probes (1–4 cm in diameter) operate in the range from 50 kHz to 10 MHz.

Figure 8.17b, c shows two configurations of the eddy current probes: with the shield and without one. The shielded sensor has a metal guard around the ferrite core and the coil assembly. It focuses and directs the electromagnetic field to the front of the sensor. This allows the sensor to be installed and even imbedded into a metal structure with little influence on the detection range. The unshielded sensor can sense at its sides as well as from the front. As a result, the detecting range of an unshielded sensor is usually somewhat greater than that of the shielded sensor of the same diameter; however, to operate properly, the unshielded sensors require non-metallic surrounding objects.

In addition to position and motion detections, eddy sensors can be used to determine material thickness, nonconductive coating thickness, conductivity and plating measurements, and hidden cracks in the material. A crack detection and surface flaws become the most popular applications for the sensors. Cracks interrupt flow of eddy currents and result in abrupt change in the sensor's output signal.

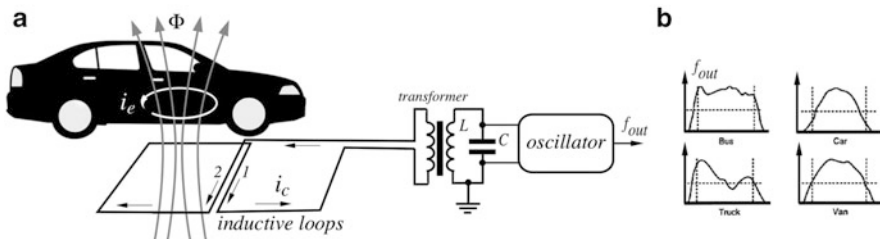
Depending on the applications, eddy probes may be of many coil configurations: very small in diameter (2–3 mm), or quite large (25 mm). Some companies even make custom designed probes to meet unique requirements of the customers ([www.olympus-ims.com](http://www.olympus-ims.com)). One important advantage of the eddy current sensors is that they do not need magnetic material for the operation, thus they can be quite effective at high temperatures (well exceeding the Curie temperature of a magnetic material), and for measuring distance to or level of conductive liquids, including molten metals. Another advantage of the detectors is that they are not mechanically coupled to the object and thus the loading effect is very low.

The eddy current proximity sensor shown in Fig. 8.17 is intended for detecting relatively small distances to conductive objects. However, if the coil dimensions are made substantially larger and its magnetic field is allowed to spread out further, the same operating principle can be employed for detecting if not distance to, but at least presence of a conductive object. Examples of other eddy currents detectors include hand-held metal detectors, security gates for detecting presence of metal objects on human subjects (e.g., for airports), and pavement loops for detecting presence and passage of vehicles.

### 8.4.4 Pavement Loops

To monitor presence of a vehicle at a specific location—for controlling traffic lights, opening gates, and generating warning signals, various sensors are currently in use. They include digital cameras with the image processing software and the in-ground magnetic sensors. The latter comprise large interconnected loops [7] that are buried into a pavement and connected to an electronic control circuit shown in Fig. 8.18a. Typically, several loops are serially connected for covering larger areas. The control circuit contains an oscillator that generates sine-wave current  $i_c$  (frequency is in the order of 10 kHz), that travels through the loops and produces alternate magnetic fields below and above the ground surface. The fields that are directed in-ground are of no interest for this device, while the above-ground fields are used for detection.

The loops may have different shapes: circular, oval, or rectangular that are shown in Fig. 8.18a. Note a mutual position of the wires 1 and 2 belonging to the adjacent rectangular loops. The wires are specifically laid out for conducting the excitation current  $i_c$  in the same direction to prevent cancellation of a magnetic field [8]. However, a cancellation would pose no problem if circular loops are separated from one another by at appreciable distances of at least one radius.



**Fig. 8.18** Magnetic loops detect induced eddy currents (a); frequency signatures from various vehicles (b)



All loops in the network have a combined inductance  $L_C$  that via a transformer is brought in the LC resonant tank that controls the oscillator frequency  $f_{\text{out}}$ :

$$f_{\text{out}} = \frac{1}{2\pi\sqrt{LC}}, \quad (8.10)$$

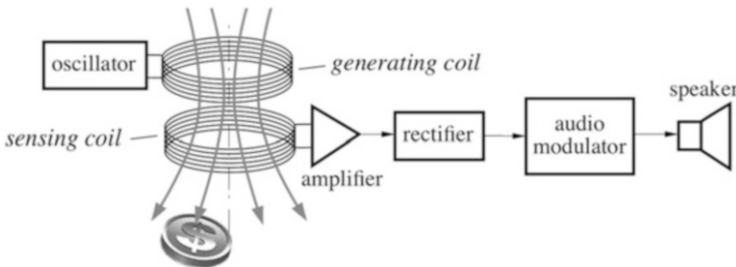
where  $L$  is the combined tank inductance which defines the oscillator resonance. In accordance with Eq. (4.42), the loop inductance is defined through its magnetic flux  $\Phi$ , number of wire turns  $n$ , and excitation current  $i_c$ :

$$L_C = n \frac{\Phi}{i_c} \quad (8.11)$$

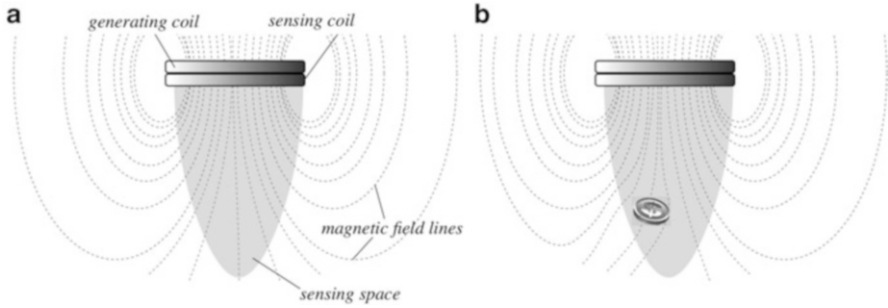
When no metal objects are present in vicinity of the loops, the combined loop inductance  $L_C$  remains constant and the oscillator produces a baseline frequency. As soon as a vehicle enters the space above the loop, the magnetic flux induces eddy currents  $i_e$  in metal components of the vehicle. According to Lenz Law (see Sect. 4.4.1), these circular currents produce their own magnetic flux that opposes the originating flux  $\Phi$ . As a result, the net magnetic flux through the loop drops. From Eq. (8.11) it follows that drop in a magnetic flux results in reduction in the loop inductance  $L_C$ . Subsequently, according to Eq. (8.10) the oscillator's frequency goes up and after demodulation it is used as indicator of the vehicle presence. This frequency modulation represents several variables: the vehicle size and shape (Fig. 8.18b), its speed of motion, position over the loops, weather conditions, etc.

### 8.4.5 Metal Detectors

Eddy currents are employed in various metal detectors. There are several design options for the detectors, such as the number of loops (coils), their dimensions, shapes, single- or multifrequency. Figure 8.19 illustrates a block diagram of a double-loop single-frequency hand-held metal detector. It contains two closely positioned coils working as a transformer. The generating coil is connected to the output of a high frequency oscillator and used for producing a magnetic flux.



**Fig. 8.19** Block diagram of double-loop metal detector



**Fig. 8.20** Magnetic field produced by generating coil (a); eddy currents in metal object distort magnetic field (b)

The second coil is for receiving the flux and converting it back into an alternate electric voltage that is amplified and demodulated. The design of the coils allows magnetic flux to spread out at a significant range and form a sensing space (Fig. 8.20). Any variations in flux measured by the receiving coil, if strong enough, are the indications of conductive objects present in the sensing space. When a conductive object (a mine, coin, metal jewelry, etc.) enters the sensing space, eddy currents develop inside the object, close to its surface. The currents produce their own magnetic fields that oppose and distort the magnetic field produced by the generating coil. This distortion modulates voltage that is detected by the receiving coil and after processing by the circuit, changes a pitch of sound in the speaker.

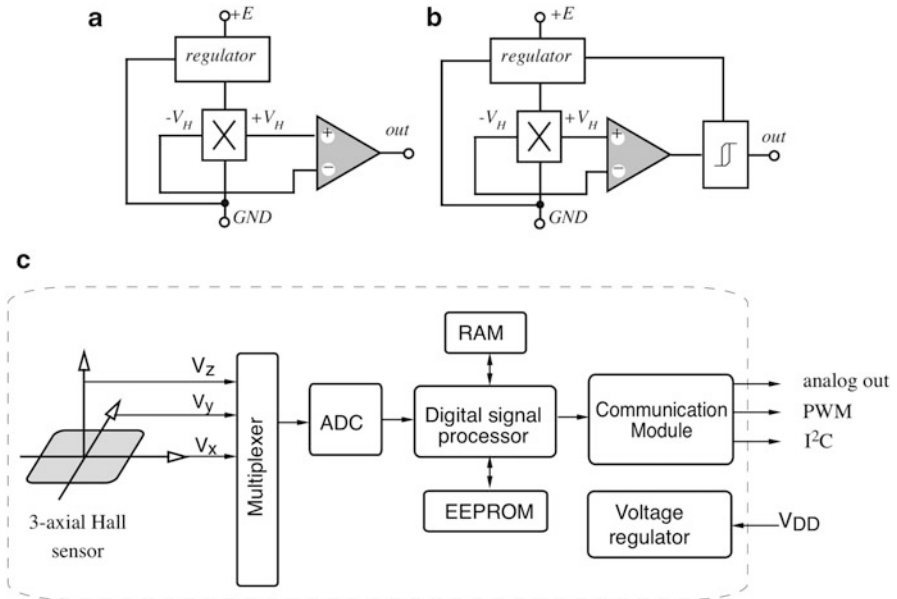
### 8.4.6 Hall-Effect Sensors

Probably the most widely used magnetic detectors are the Hall-effect sensors.<sup>2</sup> Many smartphones and tablets employ these sensors for detecting the Earth magnetic field for controlling the electronic compasses.

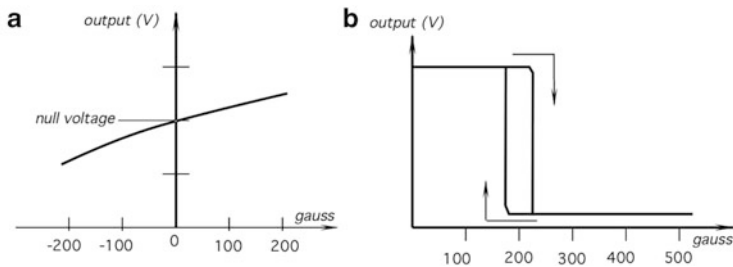
The Hall sensors are produced in three configurations: analog (linear), bilevel (digital), and integrated (multiaxial), as shown in Fig. 8.21. The analog sensors usually incorporate amplifiers for easier interface with the peripheral circuits, they operate over a broader voltage range, and are stable for a noisy environment. These sensors are not quite linear (Fig. 8.22a) with respect to the magnetic field density and, therefore, for precision measurements require a calibration. The end-of-span nonlinearity may be up to  $-1.5\%$ . Besides, the linear sensor sensitivity is temperature dependent [9].

A bilevel sensor, in addition to an amplifier, contains a Schmitt trigger with a built-in hysteresis of the threshold levels. The output signal as function of a magnetic field density is shown in Fig. 8.22b. The signal is bilevel and has a clearly pronounced hysteresis with respect to the magnetic field. When the applied

<sup>2</sup> See Sect. 4.8 for operating principle of the Hall sensor.



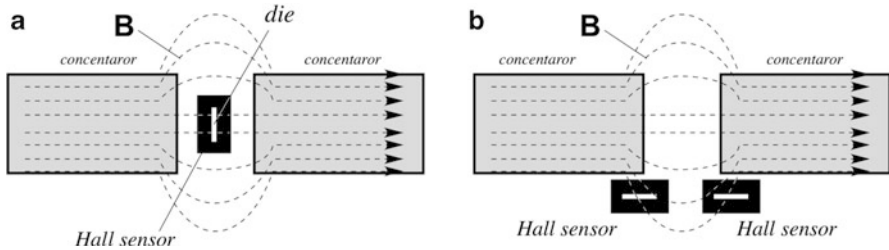
**Fig. 8.21** Circuit diagrams of linear (a), digital (b), and integrated (c) Hall-effect sensors



**Fig. 8.22** Transfer functions of linear (a) and a threshold (b) Hall-effect sensors

magnetic flux density exceeds the upper threshold, the trigger provides a clean positive transient from the OFF to ON position. When the flux drops and its signal crosses the lower threshold, the transition is negative. The hysteresis eliminates spurious oscillations by introducing a dead-band zone in which the action is disabled after the threshold value has passed. The Hall sensors are usually fabricated as monolithic silicon chips and encapsulated into small epoxy or ceramic packages.

A much more complex sensor is a combination of several Hall-effect sensors as shown in the block diagram of Fig. 8.21c. It is a system of three or more sensors that detect magnetic field in all three spatial directions. Outputs from the orthogonal Hall sensors are fed into the ADC, typically having a 15-bit resolution. A digital



**Fig. 8.23** Concepts of conventional magnetic concentrator (a) and integrated magnetic concentrator (b)

signal processor is programmable and the serial interface provides information on both the intensity and spatial orientation of the magnetic field.

A Hall sensor responds only to the magnetic flux that is perpendicular to the sensing-plate surface (see Fig. 4.30). Thus, the flux that is parallel to the die surface ( $x$ - and  $y$ -directions) would not be sensed. To make the Hall sensors responsive to the planar fluxes, either the magnetic field lines should be rotated or the sensing plate should be rotated. Rotation of the sensing plate is not practical, as that would increase thickness of the sensor packaging and size of the die. Rotation of the magnetic field is accomplished by the so-called integrated magnetic concentrator or IMC, for short [10]. The concept works as follows. Figure 8.23a illustrates a conventional magnetic concentrator fabricated of a magnetic material, for example of FeNi alloy. The concentrator has a gap where the Hall sensor is positioned. The outside magnetic field is attracted to the concentrator as it presents a path of least resistance. Then, magnetic flux  $\mathbf{B}$  inside the concentrator jumps across the gap. In doing so, it fringes to the outside along the curved paths. The flux inside the gap passes through the sensor in a normal (perpendicular) direction to the die plane. This is a popular way of directing magnetic flux through a Hall sensor in many practical applications. Yet, if the Hall sensor is rotated by  $90^\circ$  as shown in Fig. 8.23b and positioned outside of the gap at its edges where the curved fringing flux lines exist, some portion of the magnetic flux will be passing through the rotated die at angles approaching normal and the Hall sensor will respond. In other words, the IMC rotates the magnetic flux to direct it at the  $90^\circ$  angle to the sensing Hall plate.

Note that in this arrangement, the die plane is parallel to the concentrator plane. This allows an integration of a silicon die and a thin layer of the IMC in a small flat chip. The ferromagnetic IMC film with a gap is deposited on the Hall plate. Therefore, several Hall sensors may be positioned in a single flat die, yet they will be responsive to three-dimensional magnetic fluxes. In practice, the IMC layer may have various shapes: bars, discs, hexagons, etc., while its thickness is selected in the order of  $1 \mu\text{m}$  [11]. In the integrated sensor, the IMC layer is deposited on a die surface by a sputtering technique (see Sect. 19.3.3).

For a position and displacement measurements of nonmagnetic materials, the Hall-effect sensors should be provided with the magnetic field sources and interface

electronic circuits. Magnetic field has two important characteristics for this application—a flux density and polarity (or orientation). For a better responsivity, magnetic field lines must be normal (perpendicular) to the flat face of the sensor and be at a correct polarity. A magnetic flux concentrator is recommended to direct flux to the correct section of the sensor.

Before designing a position or proximity detector with a Hall sensor, an overall analysis should be performed in approximately the following manner.

The field strength of the magnet should be investigated.

The strength will be the greatest at the pole face, and will decrease with increasing distance from the magnet.

The field may be measured by a gaussmeter or by a calibrated analog Hall sensor. For a bilevel-type Hall sensor, the longest distance at which the sensor's output goes from ON (high) to OFF (low) is called a *release point*. It can be used to determine a critical distance where the sensor is useful.

A magnetic field strength is not linear with distance and depends greatly upon the magnet shape, the magnetic circuit, and the path traveled by the magnet. The Hall conductive strip (plate) is situated at some depth within the sensor's housing. This determines the minimum operating distance. A magnet must operate reliably with the total effective air gap in the working environment. It must fit the available space, be mountable, affordable, and available.<sup>3</sup>

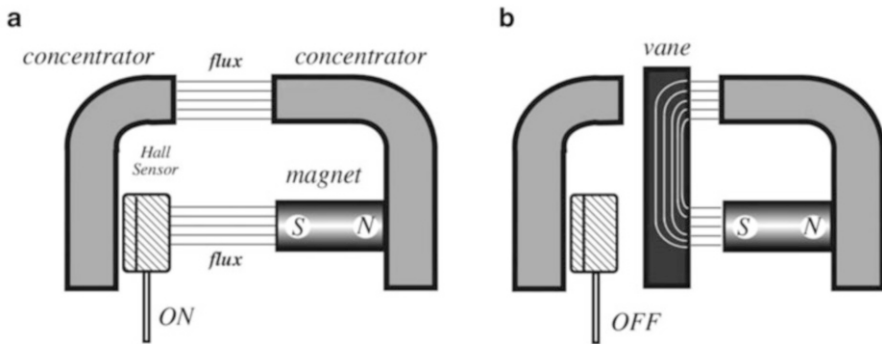
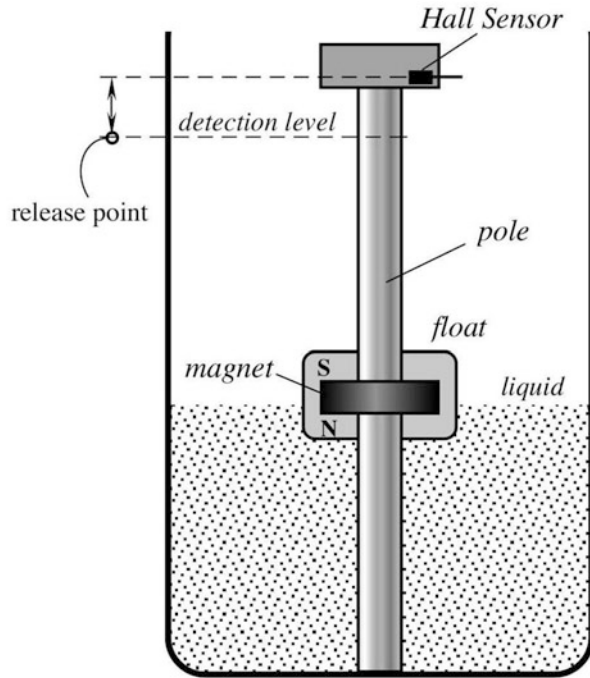
As a first example of the Hall sensor application, consider a liquid level detector with a float (Fig. 8.24). A permanent magnet is imbedded inside a float having a hole in the center. The float can freely slide up and down over the pole that is positioned inside the tank containing liquid. The float position corresponds to the liquid level. A bilevel Hall sensor is mounted at the top of the pole which should be fabricated on a nonmagnetic material. When the liquid level rises and reaches the detection level (release point), the Hall switch triggers and sends signal to the monitoring device. When the liquid level drops below the release point plus the threshold hysteresis, the output voltage changes indicating that the liquid level dropped. The detection point depends on the key factors—the magnet strength and shape, the Hall sensor's sensitivity, the hysteresis, and presence of ferromagnetic components in the vicinity of the Hall sensor.

The Hall sensors can be used with a flux interrupter attached to a moving object. In this mode, the activating magnet and the Hall sensor are mounted on a single rugged assembly of a flux concentrator, with a small air gap between them (Fig. 8.25). Thus, the sensor is held in the ON position by the activating magnet. If a ferromagnetic plate, or vane, is placed between the magnet and the Hall sensor, the vane forms a magnetic shunt that diverts the magnetic flux away from the sensor. This causes the sensor to flip to the OFF position. The Hall sensor and the magnet could be molded into a common housing, thus eliminating the alignment problem. The ferrous vanes which interrupt the magnetic flux could have linear or rotating motion. An example of such a device is an automobile distributor.

---

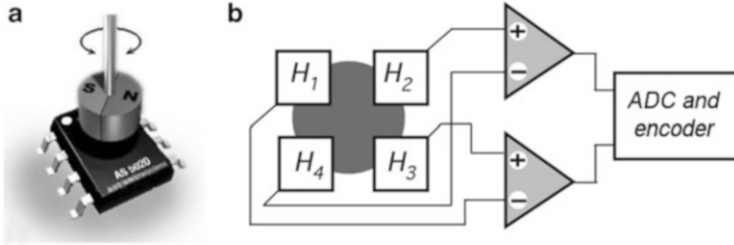
<sup>3</sup>For more information on permanent magnets see Sect. 4.3.2.

**Fig. 8.24** Liquid level detector with a Hall sensor

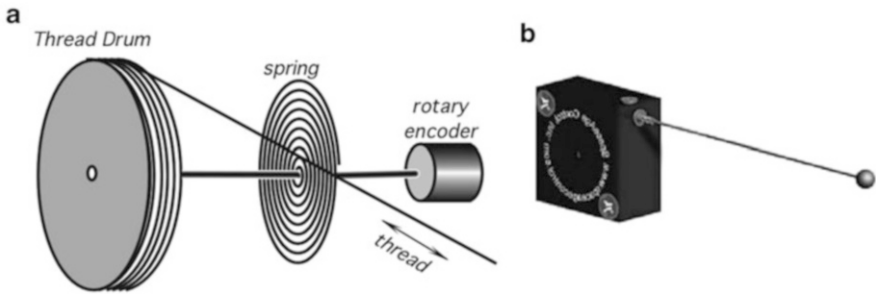


**Fig. 8.25** Bilevel Hall-effect sensor in interrupter switching mode. Magnetic flux turns sensor on (a); magnetic flux is shunted by vane (b)

Like many other sensors, four Hall sensors can be connected into a bridge circuit to detect linear or circular motion. Figure 8.26a, b illustrates this concept where the sensor is fabricated using MEMS technology on a single chip and packaged in a SOIC-8 plastic housing. A circular magnet is positioned above the chip and its angle of rotation and direction is sensed and converted into a digital code. The properties of an ADC determine the maximum speed response, while the Hall sensors allow the magnet to rotate with a rate of up to 30,000 rpm. Such an



**Fig. 8.26** Angular Hall-sensor bridge integrated circuit (a) and internal-sensor interface (b) (Courtesy of Austria Micro Systems: [www.ams.com](http://www.ams.com))



**Fig. 8.27** Conversion of linear displacement (length of a thread or cable) into rotary motion (a) and cable position sensor (b) (Courtesy of SpaceAge Control, Inc.)

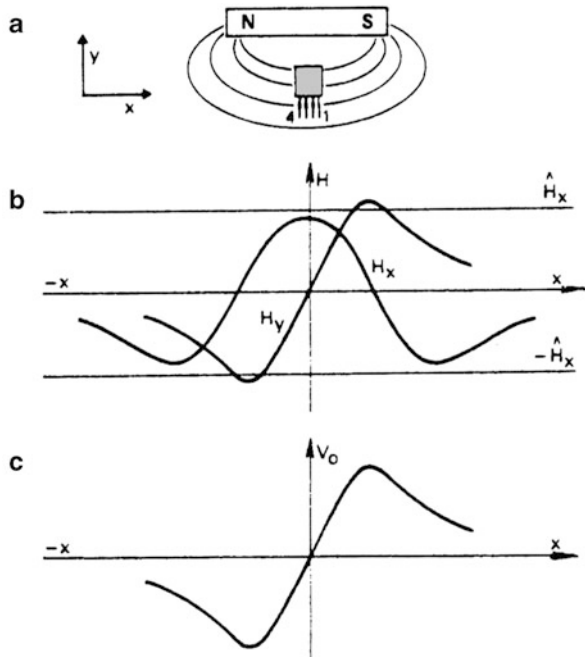
integrated sensor permits a friction-free precision linear and angular sensing of position, precision angular encoding, and even to make a programmable rotary switch. Thanks to a bridge connection of the individual sensors, the circuit is highly tolerant to the magnet misalignment and external interferences, including the magnetic fields.

A rotary motion can be digitally encoded with high precision. To take advantage of this feature, a linear distance sensor can be built with a converter of a linear into a rotary motion as shown in Fig. 8.27. Such sensors are produced, for example, by *SpaceAge Control, Inc.* ([www.spaceagecontrol.com](http://www.spaceagecontrol.com)). A cable or thread is wound up on a drum that is coaxially connected to a magnetic rotary encoder.

### 8.4.7 Magneto-resistive Sensors

These sensors are similar in application to the Hall-effect sensors, however, their operating principle is quite different (see Sect. 4.3 and Fig. 4.13). Like the Hall sensors, for functioning they require an external magnetic field. Hence, whenever the magneto-resistive sensor is used as a proximity, position, or rotation detector it must be combined with a source of a magnetic field. Usually, the field is originated

**Fig. 8.28** Magnetoresistive sensor in field of a permanent magnet (a) as a function of its displacement  $x$  parallel to the magnetic axis (b); output voltage (c)



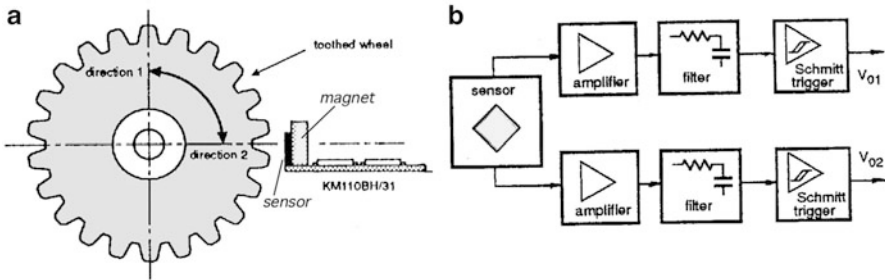
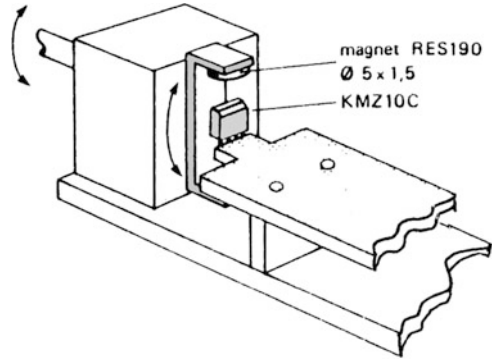
in a permanent magnet that is attached to the sensor. Figure 8.28 shows a simple arrangement for using a sensor-permanent-magnet combination to measure linear displacement. It reveals some of the problems likely to be encountered if proper account is not taken of the following effect. When the sensor is placed in the magnetic field, it is exposed to the fields in both the  $x$ - and  $y$ -directions. As shown in Fig. 8.28b, both vectors  $H_x$  and  $H_y$  vary with displacement  $x$ . If the magnet is oriented with its axis parallel to the sensor strips (i.e., in the  $x$ -direction) as shown in Fig. 8.28a, magnetic vector  $H_x$  then provides the auxiliary field, and the variation in  $H_y$  can be used as a measure of  $x$  displacement. Therefore, the output signal (Fig. 8.28c) has the same shape as the  $H_y$  vector.

Figure 8.29 shows how a magnetoresistive sensor can be useful for measuring angular displacement. The sensor itself is located in the magnetic field produced by two permanent magnets fixed to a rotatable frame. The output of the sensor will then be a measure of the rotation of the frame. Figure 8.30a depicts the use of a single KM110B sensor for detecting rotation and direction of a toothed wheel. Note that this sensor has a permanently attached magnet producing magnetic field in the  $x$ -direction. The method of directional detection is based on a separate signal processing for the sensor's two half-bridge outputs.

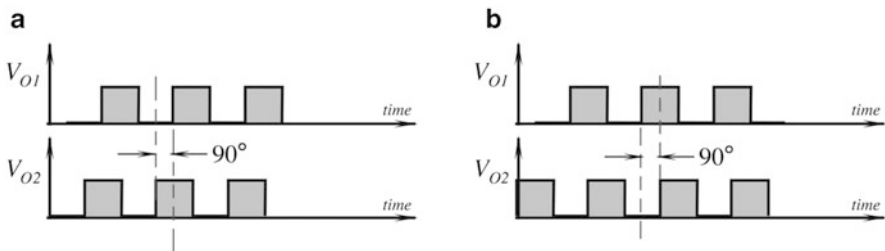
The sensor operates like a magnetic Wheatstone bridge measuring nonsymmetrical magnetic conditions such as when the teeth or pins move in front of the sensor. The mounting of the sensor and the magnet is critical, so the angle between the sensor's symmetry axis and that of the toothed wheel must be kept near zero.



**Fig. 8.29** Angular measurement with the KMZ10 sensor



**Fig. 8.30** Optimum operating position of magnetoresistive module with permanent magnet is positioned behind on sensor (a). Block diagram of module (b)



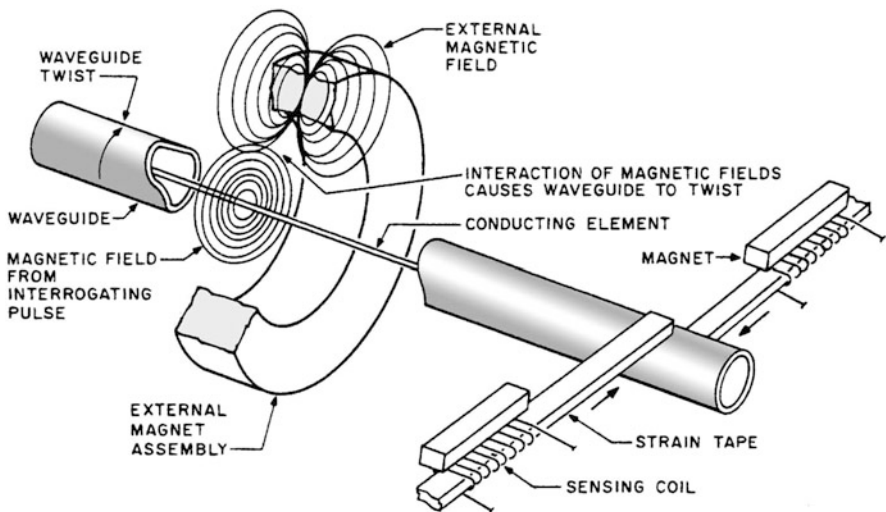
**Fig. 8.31** Output signal from the amplifiers for direction 1 (a) and 2 (b)

Further, both axes (sensor's and wheel's) must coincide. The circuit of Fig. 8.30b connects both bridge outputs to the corresponding amplifiers, and, subsequently, to the low-pass filters and Schmitt triggers to form the rectangular output signals. A phase difference between both outputs (Fig. 8.31a, b) is an indication of a rotation direction.

### 8.4.8 Magnetostrictive Detector

A transducer which can measure displacement of an object with high resolution across long distances can be built by using magnetostrictive and ultrasonic technologies. The transducer is comprised of two major parts: a long waveguide (up to 7 m long) and a permanent ring magnet (Fig. 8.32). The magnet can move freely along the waveguide without touching it. A position of that magnet with respect to the waveguide is the stimulus that is converted by the sensor into an electrical output signal. A waveguide contains a conductor (conducting element), which upon applying an electrical pulse, sets up a magnetic field over its entire length. Another magnetic field produced by the permanent magnet exists only in its vicinity. Thus two magnetic fields may be setup at the point where the permanent magnet is located. A superposition of two fields results in the net magnetic field which can be found from the vector summation. This net field, while being helically formed around the waveguide, causes it to experience a minute torsional strain, or twist at the location of the magnet. This twist is known as Wiedemann effect.<sup>4</sup>

Therefore, electric pulses injected into the waveguide's coaxial conductor produce mechanical twist pulses which propagate along the waveguide with the speed of sound specific for its material. When the pulse arrives to the excitation head of



**Fig. 8.32** Magnetostrictive detector uses ultrasonic waves to detect position of permanent magnet

<sup>4</sup> Internally, ferromagnetic materials have a structure that is represented by domains, each of which is a region of uniform magnetic polarization. When a magnetic field is applied, the boundaries between the domains shift and the domains rotate, both these effects causing a change in the material's dimensions.

**Fig. 8.33** Commercial sensors based on Wiedemann effect (TWK-Elektronik, Germany)

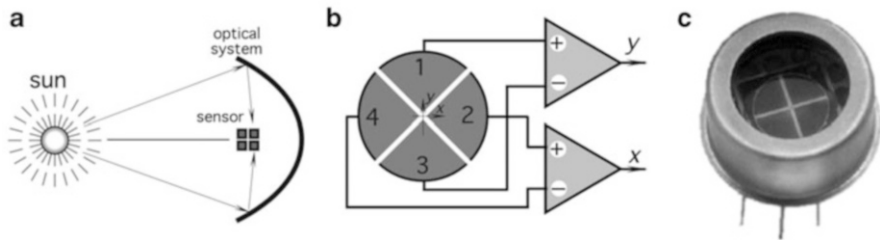


the sensor, the moment of its arrival is precisely measured. One way to detect that pulse is to use a detector that can convert an ultrasonic twitch into electric output. This can be accomplished by piezoelectric sensors, or as it is shown in Fig. 8.32, by the magnetic reluctance sensor. The sensor consists of two tiny coils positioned near two permanent magnets. The coils are physically coupled to the waveguide and can jerk whenever the waveguide experiences the twitch. This sets up short electric pulses across the coils. Time delay of these pulses from the corresponding excitation pulses in the coaxial conductor is the exact measure of the ring magnet position. An appropriate electronic circuit converts time delay into a digital code representative of position of the permanent magnet on the waveguide. The advantage of this sensor is in its high linearity (in the order of 0.05 % of the full scale), good repeatability (in the order of 3  $\mu\text{m}$ ), and a long-term stability. The sensor can withstand aggressive environments, such as high pressure, high temperature, and strong radiation. Another advantage of this sensor is its low temperature sensitivity which by a careful design can be achieved in the order of 20 ppm/ $^{\circ}\text{C}$ .

Applications of this sensor include hydraulic cylinders, injection molding machines (to measure linear displacement for mold clamp position, injection of molding material, and ejection of the molded part), mining (for detection of rocks movements as small as 25  $\mu\text{m}$ ), rolling mills, presses, forges, elevators, and other devices where fine resolution along large dimensions is a requirement. These sensors are produced in a great variety of configurations and lengths (Fig. 8.33).

## 8.5 Optical Sensors

After the mechanical contact and potentiometric sensors, optical sensors are probably the most popular for measuring position and displacement. Their main advantages are simplicity, the absence of a loading effect, and relatively long operating distances. They are insensitive to stray magnetic fields and electrostatic interferences, which makes them quite suitable for many sensitive applications. An optical position sensor usually requires at least three essential components: a light source, a photodetector, and light guidance devices, which may include lenses, mirrors, optical fibers, etc. Examples of the single- and dual-mode fiber-optic proximity sensors are shown in Figs. 5.20b and 5.21. The similar arrangements are often implemented without the optical fibers, when light is guided toward a target by focusing lenses, and is diverted back to the detectors by reflectors.



**Fig. 8.34** Four-quadrant photodetector. Object is focused on sensor (a). Connection of sensing elements to difference amplifiers (b). Packaging of the sensor (c) (from Advanced Photonix, Inc.)

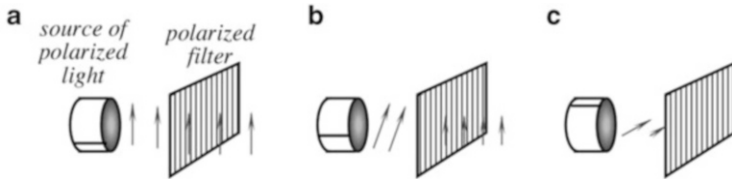
### 8.5.1 Optical Bridge

A concept of a bridge circuit, like a classical Wheatstone bridge, is employed in many optical sensors. An example is a four-quadrant photodetector consisting of four light detectors connected in a bridge-like circuit. The object that is detected must have an optical contrast against the background. Consider a positioning system of a space vehicle, Fig. 8.34a. An image of the sun or any other sufficiently bright celestial object is focused by an optical system (e.g., a telescope) on a four-quadrant photodetector. The opposite parts of the detector are connected to the corresponding inputs of two difference amplifiers, Fig. 8.34b. Each amplifier produces the output signal proportional to a displacement of the image from the optical center of the sensor along the corresponding axis. When the image is perfectly centered, both amplifiers produce zero outputs. This may happen only when the optical axis of the telescope passes through the object.

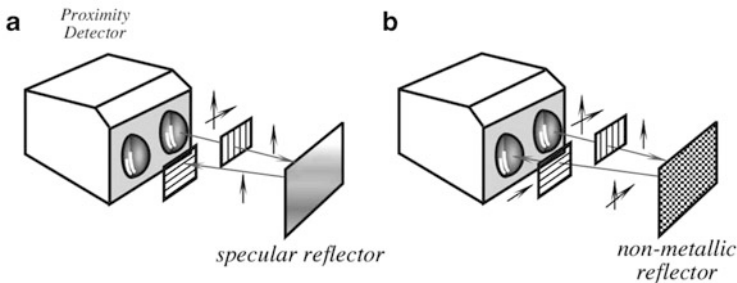
### 8.5.2 Proximity Detector with Polarized Light

One method of building a better optoelectronic proximity sensor is to use polarized light. Each light photon has specific magnetic and electric field directions perpendicular to each other and to the direction of propagation. Direction of the electric field is the direction of the light *polarization* (see Sect. 5.1.2). Most of the light sources produce light with randomly polarized photons. To make light polarized, it can be directed through a polarizing filter, that is, a special material which transmits light polarized only in one direction and absorbs and reflects photons with wrong polarizations. However, any direction of polarization can be represented as a geometrical sum of two orthogonal polarizations: one is the same as the filter, and the other is nonpassing. Thus, by rotating the polarization of light before the polarizing filter we may *gradually* change the light intensity at the filter's output (Fig. 8.35).

When polarized light strikes an object, the reflected light may retain its polarization (specular reflection) or the polarization angle may change. The latter is typical for many nonmetallic objects. Thus, to make a sensor nonresponsive to



**Fig. 8.35** Passing polarized light through polarizing filter. Direction of polarization is the same as of filter (a). Direction of polarization is rotated with respect to filter (b). Direction of polarization is perpendicular with respect to filter (c)



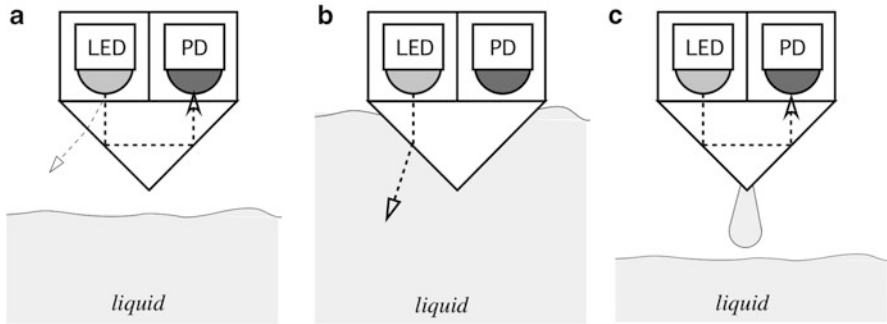
**Fig. 8.36** Proximity detector with two polarizing filters positioned at a  $90^\circ$  angle with respect to one another. Polarized light returns from the metallic object within the same plane of polarization (a); nonmetallic object depolarizes light, thus allowing it to pass through the polarizing filter (b)

reflective objects (like metal cans, foil wrappers, and the like), it may include two perpendicularly positioned polarizing filters: one at the light source and the other at the detector, Fig. 8.36a, b.

The first filter is positioned at the emitting lens (light source) to polarize the outgoing light. The second filter is at the receiving lens (detector) to allow passage of only those components of light, which have a  $90^\circ$  rotation with respect to the outgoing polarization. Whenever light is reflected from a specular reflector (metal), its polarization direction does not change and the receiving filter will not allow the light to pass to a photodetector. However, when light is reflected in a nonspecular manner, its components will contain a sufficient amount of polarization to go through the receiving filter and activate the detector. Therefore, the use of polarizers reduces false-positive detections of nonmetallic objects. This detector not only identifies proximity of a nonmetal object, but it also makes a distinction between metals and nonmetals.

### 8.5.3 Prismatic and Reflective Sensors

Fiber-optic sensors can be used quite effectively as proximity and level detectors. One example of the displacement sensor is shown in Fig. 5.21, where intensity

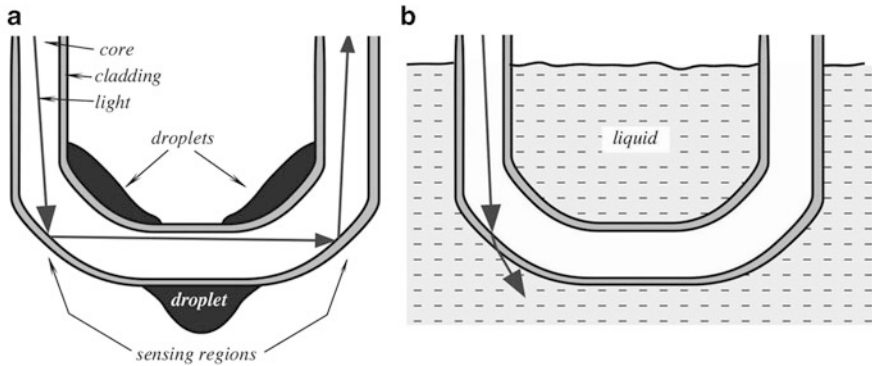


**Fig. 8.37** Prismatic liquid level detector utilizing change in refractive index. Position away from liquid (a); touching liquid (b); droplets do not create false detection (c)

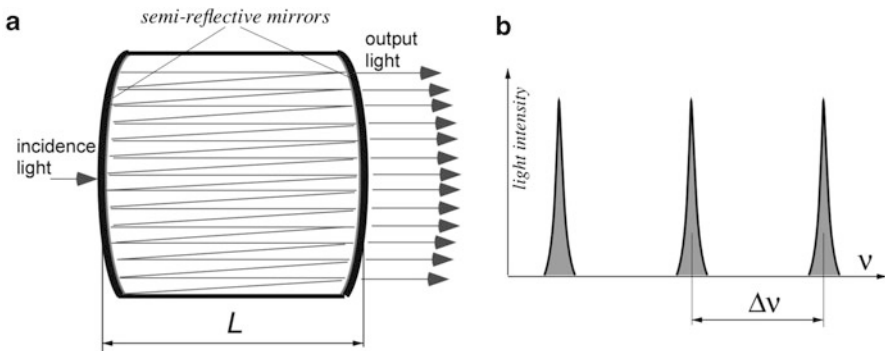
of the reflected light is modulated by distance  $d$  to the reflective surface. This principle has been implemented in numerous commercial products, including APDS-9130 from Avago Technologies ([www.avagotech.com](http://www.avagotech.com)), which is a fully integrated sensor meeting all 10 *commandments* described in Sect. 3.1.1. One of its prime applications is a smartphone proximity detector—to indicate when the telephone is brought close to an ear. The detector incorporates lenses for the LED emitter and photodetector, ADC, signal processor, and  $I^2C$  communication link.

To detect level of liquid, an optical detector with a prism is shown in Fig. 8.37. It utilizes the difference between refractive indices of air (or gaseous phase of a material) and the measured liquid. The sensor contains a light-emitting diode (LED) and photodetector (PD), operating in the near-infrared spectral range. When the sensor is above the liquid level, the LED sends most of its light to the receiving PD due to a total internal reflection in the prism (see Sect. 5.7.2). Some light rays approaching the prism's reflective surface at angles less than the angle of total internal reflection are lost to the surrounding. When the prism reaches the liquid level and is at least partially immersed, the angle of a total internal reflection changes because the refractive index of a liquid is higher than that of air. Under these conditions, a greater number of light rays is not reflected but pass to the liquid. This reduces the light intensity that is detected by the PD. The light is converted into an electrical signal that may activate, for example, a switch. Note that gravity draws the liquid droplets to the tip of the prism, so they do not cover most of the prism surface and thus make no effect on detection, Fig. 8.37c. The prismatic liquid level detectors operating on this principle are produced by Gems Sensors & Controls ([www.gemssensors.com](http://www.gemssensors.com)).

Another version of the sensor is shown in Fig. 8.38. The optical fiber is U-shaped and upon being immersed into liquid, modulates the intensity of passing light. The detector has two sensitive regions near the bends where the radii of curvatures are the smallest. The entire assembly is packaged into a 5-mm diameter probe and has a repeatability error of about 0.5 mm. That shape of the sensing element draws liquid droplets away from the sensing regions when the probe is elevated above the liquid level.



**Fig. 8.38** U-shaped fiber-optic liquid level sensor. When sensor is above liquid, passing light is strongest (a); when sensitive regions touch liquid, light is diverted to liquid and intensity drops (b)



**Fig. 8.39** Multiple-ray interference inside Fabry-Perot cavity (a). Transmitted frequencies of light (b)

### 8.5.4 Fabry-Perot Sensors

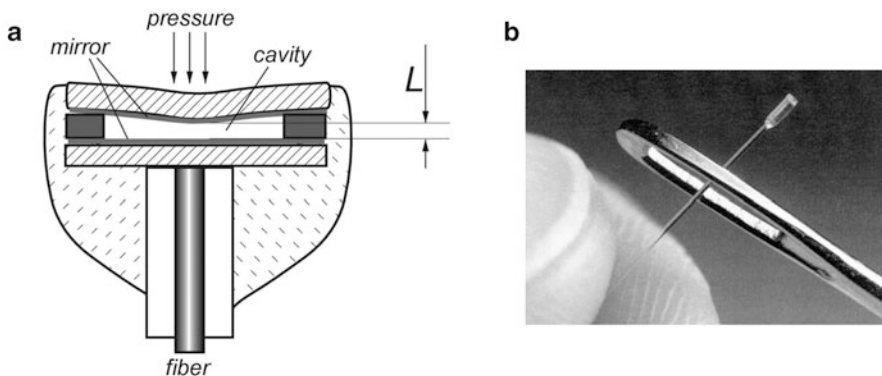
For measuring displacements on the nanoscale with high precision in harsh environment, the so-called Fabry-Perot (FP) optical cavity can be employed [12]. The cavity contains two semi-reflective mirrors facing each other and separated by distance  $L$ , Fig. 8.39a. The cavity is injected with light from a controlled source (a laser, for example). The photons inside the cavity bounce back and forth between the two mirrors, interfering with each other in the process. In fact, the cavity is a storage tank for light. At some frequencies of the photons, light can pass out of the cavity. A Fabry-Perot interferometer is basically a frequency filter whose transmission frequency is intimately related to the length  $L$  of the cavity, Fig. 8.39b. As the cavity length changes, the frequencies at which it transmits light change accordingly. If you make one of the mirrors movable, by monitoring the optical transmission frequency, very small changes in the cavity length can be

resolved. The narrow bands of transmitted light are separated by frequencies that are inversely proportional to the cavity length:

$$\Delta\nu = \frac{c}{2L} \quad (8.12)$$

where  $c$  is the speed of light. For practical cavities with the mirror separation in the order of  $1\ \mu\text{m}$ , typical values of  $\Delta\nu$  are between 500 MHz and 1 GHz. Thus, by detecting the frequency shift of the transmitted light with respect to a reference light source, changes in the cavity dimensions can be measured with accuracy comparable with the wavelength of light. Whatever may cause changes in the cavity dimensions (mirror displacement), may be the subject of measurements. These include strain, force, pressure, and temperature [13, 14]. The FP sensor detects changes in the optical path length induced by either a change in the refractive index of the cavity (affects the speed of light) or change in a physical length of the cavity. Micromachining techniques make Fabry-Perot sensors more attractive by reducing size and cost of the sensing element. Another advantage of the miniature Fabry-Perot sensor is that low coherence light sources, such as light-emitting diodes (LEDs) or even light bulbs, can be used to generate the interferometric signal.

A pressure sensor with a FP cavity is shown in Fig. 8.40a. Pressure is applied to the upper membrane. Under pressure, the diaphragm deflects inwardly thus reducing the cavity dimension  $L$ . The cavity is monolithically built by the MEMS technology. The mirrors can be either the dielectric layers or metal layers deposited or evaporated during the manufacturing process. The thickness of each layer must be tightly controlled to achieve the target performance of a sensor. A commercial ultraminiature pressure sensor produced by FISO Technologies ([www.fiso.com](http://www.fiso.com)) is shown in Fig. 7.40b. The FOP-260 sensor released in 2014 has very small temperature coefficient of sensitivity ( $<0.03\%$ ) with an outside diameter of only 0.25 mm which makes it ideal for such critical applications as implanted medical devices and other invasive instruments.



**Fig. 8.40** Construction of Fabry-Perot pressure sensor (a) and view of FISO FOP-M pressure sensor (b)



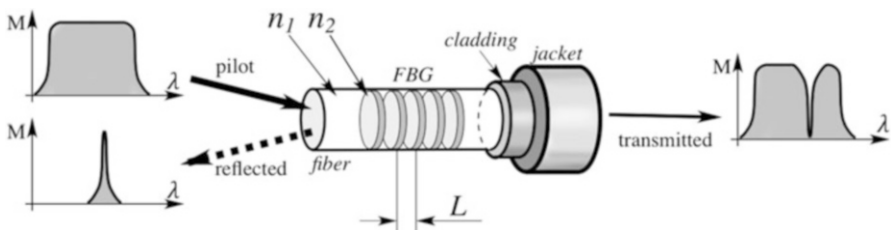
### 8.5.5 Fiber Bragg Grating Sensors

A typical fiber-optic cable generally may transmit a broad spectral range of light from UV to near IR. The cable is characterized by several fundamental parameters, all of which: length and refractive index of the core, can be modulated, at least in theory, by external stimuli. A modulation of the length and refractive index is a foundation of the so-called Fiber Bragg Grating (FBG) sensors [15]. A conventional optical fiber is a thin strand of glass or plastic that transmits light by means of total internal reflections (see Sect. 5.9). An optical cable is composed of three main components: the core, cladding, and jacket (Fig. 5.19). The cladding has a lower refractive index than the core and thus reflects stray light back into the core, ensuring the transmission of light through the core with minimal loss. The outer jacket protects the fiber from external conditions and physical damage.

Unlike a regular optical fiber having the core of a fixed refractive index, the FBG index is not uniform throughout the fiber length. Thus, the FBG not only transmits light but also reflects some back, in other words, it is a distributed reflector inside the optical fiber. It reflects back only the specific wavelengths and transmits the rest, working as a filter. The FBG fiber has periodic changes in the refractive index (Fig. 8.41) called the *gratings*. They can be presented as sections of the fiber having shapes of disks. The basic core refractive index is  $n_1$ , while the grating discs have index  $n_2$ .

The grating is fabricated by using an intense UV source such as a UV laser. A germanium-doped silica fiber is photosensitive, which means that the refractive index of the core changes when exposed to UV light. The amount of the change depends on the intensity and duration of the exposure as well as the photosensitivity of the fiber. Exposure to UV light permanently modifies the refractive index of the core at specific locations, so the FBG discs inside the fiber are positioned at distances  $L$  from one another.

When operating, the fiber is illuminated from a broad spectrum pilot light source, such as an LED. The pilot light enters the fiber end and propagates toward the FBG. The waves of the specific wavelength  $\lambda$  are reflected back, while the rest of the wavelengths propagate along the fibers toward the other end and are not used in the sensor. Small graphs in Fig. 8.41 illustrate spectral intensities  $M$  at both sides



**Fig. 8.41** Concept of FBG sensor

of the fiber. The wavelength that is reflected back and detected depends on the grating period  $L$  and the fiber average refractive index  $n$ :

$$\lambda = 2nL \quad (8.13)$$

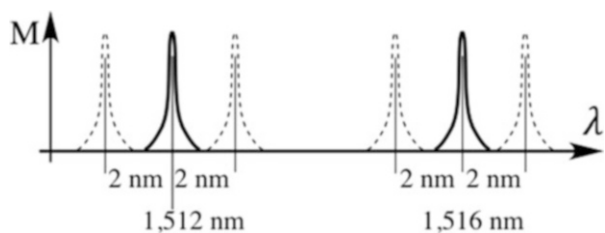
It follows from this equation that if we measure the reflected wavelength  $\lambda$ , the refractive index and grating period can be used as the sensor inputs. In other words, they can be modulated by a stimulus, causing variations in  $\lambda$ . To modulate  $n$  and  $L$ , the FBG can be subjected to strain  $\varepsilon$  and temperature  $T$ , then the FBG normalized wavelength variation is:

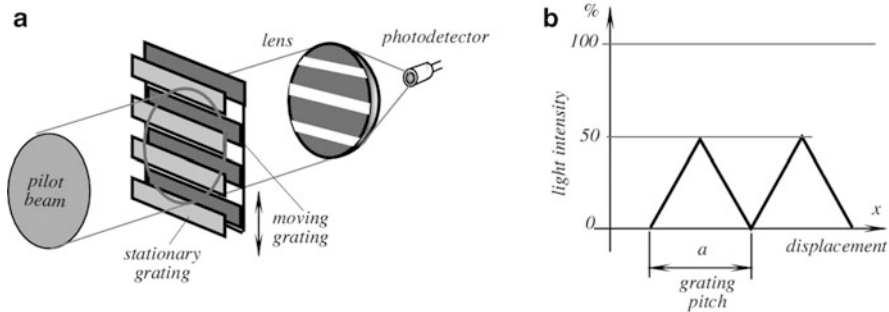
$$\frac{\Delta\lambda}{\lambda} = (1 - p_\varepsilon)\varepsilon + (\alpha_L + \alpha_n)T \quad (8.14)$$

The first summand in the equation depends on the strain factor  $p_\varepsilon$ . When the fiber is strained, the distance between the FBG discs changes, resulting in modulation of  $\lambda$ . The second summand describes sensitivity of  $\lambda$  to temperature  $T$ . Change in temperature causes thermal expansion or contraction of the fiber with the coefficient  $\alpha_L$ , and the subsequent variations of distances  $L$  between the disks. Temperature also causes change in the refractive index with coefficient  $\alpha_n$ . Thus, the FBG can function as both a strain gauge (displacement sensor) and temperature sensor. The wavelength shifts due to strain are typically more pronounced than temperature, and often cover a 5 nm output span. The temperature sensing span is up to 1 nm.

Advantages of the FBG sensors include ruggedness, immunity to electromagnetic interferences (EMI), high stability, and ability for a chain connection. The last feature allows using a single fiber for monitoring a multitude of locations. For that, the fiber is manufactured with different periods  $L$  at separate portions. Each period results in its own wavelength of the reflected light. This is called a wavelength division multiplexing (WDM). As a result of the WDM, the detector will register different reflected wavelengths corresponding to different positions of the fiber (Fig. 8.42). The number of sensors that can be incorporated within a single fiber depends on the wavelength range of operation of each sensor and the total available wavelength range. Because typical FBG system provides a measurement range of 60–80 nm, each fiber array of sensors can usually incorporate anywhere from one to more than 80 sensors—as long as the reflected wavelengths do not overlap in the optical spectrum.

**Fig. 8.42** Spectral response of WDM fiber





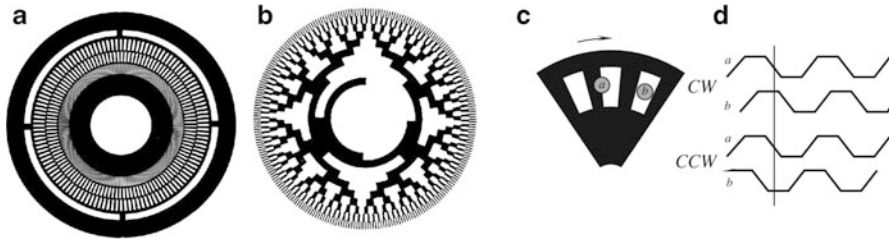
**Fig. 8.43** Optical displacement sensor with grating light modulator. Conceptual schematic (a) and transfer function (b)

### 8.5.6 Grating Photomodulators

A linear optical displacement transducer can be fabricated with two overlapping gratings which serve as a light intensity modulator (Fig. 8.43a). The incoming pilot beam strikes the first, stationary grating mask which allows only about 50 % of light to pass toward the second, moving grating mask. The moving mask is mechanically coupled to the measured object. When the opaque sectors of the moving mask are precisely aligned with the transmitting sectors of the stationary mask, the light will be completely occluded. Shifting the moving mask opens the light passages more and more, and thus the transmitted light beam can be modulated from 0 to 50 % of the pilot beam (Fig. 8.43b). The transmitted beam is focused on a sensitive surface of a photodetector which converts light into electric current. This displacement sensor is a linear transducer as the light intensity is proportional to displacement.

This type of a linear modulator was used in a sensitive hydrophone [16] to measure displacements of a diaphragm. The grating pitch was  $10\ \mu\text{m}$  which means that the full-scale displacement was  $5\ \mu\text{m}$ . The light source was a 2-mW He-Ne laser whose light was coupled to the grating through an optical fiber. The tests of the hydrophone demonstrated that the device was sensitive with a dynamic range of 125 dB of pressure as referenced to  $1\ \mu\text{Pa}$ , with a frequency response up to 1 kHz.

A grating principle of a digital light modulation has been employed in very popular rotating or linear encoders, where a moving mask, that is usually fabricated in form of a disk, has transparent and opaque sections (Fig. 8.44). The photodetector gives a binary output—on and off—thus, the encoding disk functions as an interrupter of light beams within an optocoupler. When the opaque section of the disk breaks the light beam, the detector is turned off (indicating digital ZERO), and when the light passes through a transparent section, the detector is on (indicating digital ONE). The optical encoders typically employ infrared emitters and detectors operating in the spectral range from 820 to 940 nm. The disks are made from laminated plastic and the opaque lines are produced by a photographic process. Alternatively, the discs are fabricated of metal plates using a photoetching



**Fig. 8.44** Incremental (a) and absolute (b) optical encoding disks. When wheel rotates clockwise (CW), signal in channel a leads b by  $90^\circ$  (c). When wheel rotates counter-clockwise (CCW), signal in channel b leads a by  $90^\circ$  (d)

technology.<sup>5</sup> Plastic disks are light, have low inertia, low cost, and excellent resistance to shock and vibration. However, they have a limited operating temperature range.

There are two types of encoding disks: the incremental, which produces a transient whenever it is rotated for a pitch angle, and the absolute, whose angular position is encoded in a combination of opaque and transparent areas along the radius. The encoding can be based on any convenient digital code. The most common are the gray code, binary, and BCD (binary coded decimals).

The incremental encoding systems are more commonly used than the absolute systems, because of their lower cost and complexity, especially in applications, where a displacement (incremental count) is desirable instead of a position. When employing the incremental encoding disks, the basic sensing of movement can be made with a single optical channel (an emitter-detector pair), while the speed and incremental position, and direction sensing, must use two. The most commonly used approach is a quadrature sensing, where the relative position of the output signals from two optical channels are compared. The comparison provides the direction information, while either of the individual channels gives the transition signal which is used to derive either count or speed information (Fig. 8.44c, d).

## 8.6 Thickness and Level Sensors

In many industrial applications, measurement of material thickness is essential for manufacturing, process and quality control, safety, airspace, etc. Manual methods of using, say a caliper or micrometer, are rarely useful in the automatic high-speed manufacturing processes or at difficult-to-reach places. The methods of thickness gauging are ranging from optical to ultrasonic to X-ray. Here we briefly review some interesting methods.

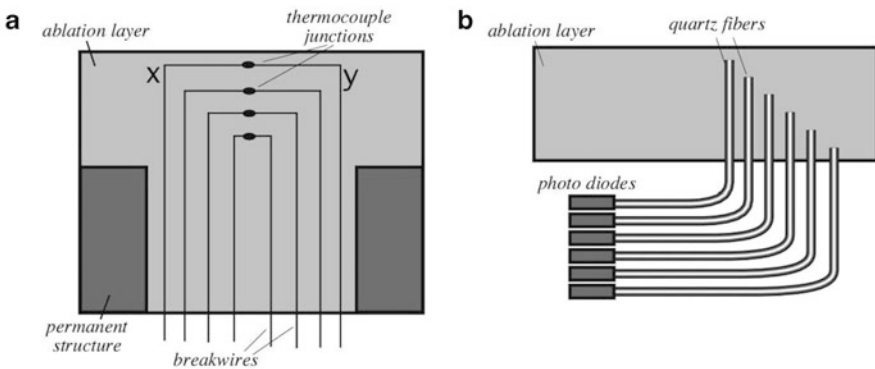
<sup>5</sup> Photoetching or photochemical milling parts may be fabricated of a variety materials, including Elgiloy, Nitinol, Titanium, and Kapton<sup>®</sup> (polyimide film). However, the encoding discs having thickness of 0.005" typically are etched from stainless steel or Beryllium-Copper alloy.

### 8.6.1 Ablation Sensors

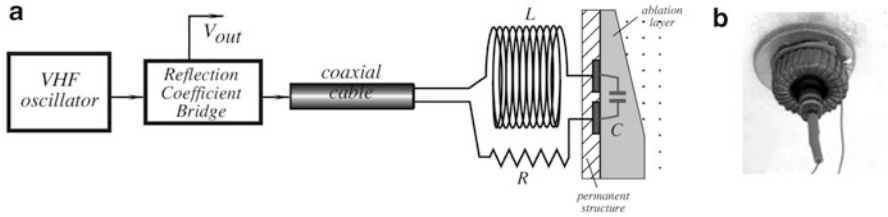
Ablation is a removal of material from the surface by some erosive processes. Specifically it relates to dissipation of heat by melting and removal of the sacrificial protective layer such as in a spacecraft during the atmospheric re-entry. Aerospace vehicles subjected to significant aerodynamic heating often rely on ablating thermal protection systems (TPSs) to keep the internal structure and equipment below critical operating temperatures. An ablating TPS undergoes chemical decomposition or phase change (or both) below the internal structure's critical temperature. Incident thermal energy is then channeled into melting, subliming, or decomposing the ablator. Ablator recession rate is directly proportional to the thermal heat flux at the surface. A measure of the ablator thickness is required to estimate surface heat flux and estimate the level of thermal protection. Thus an ablation sensor is kind of a position sensor that detects position of the ablation layer's outer surface and provides a measure of the remaining thickness. The ablation sensors can be embedded into the ablation layer (intrusive sensors) or be noninvasive.

The intrusive sensors include the breakwire ablation gage, radiation transducer (RAT) sensor, and light pipe. The breakwire ablation gage consists of several thin wires implanted at various known levels in an ablator. As the material progressively erodes, each successive wire is broken and results in an open circuit. Figure 8.45a illustrates this concept. In some cases [17] a breakwire doubles as a thermocouple (TC) and each is situated so that no breakwire TC is directly above another. This arrangement allows an unobstructed conduction path through the ablator to each breakwire TC, including those at lower levels. Although the breakwire method provides temperature time histories until the last TC is exposed and destroyed, this method only provides recession data at a few distinct points.

The light-pipe sensor consists of the quartz fibers implanted in an ablator and terminated at known depths (Fig. 8.45b). When the TPS recedes to where a fiber terminates, light transmits down to a photodiode. This method provides recession



**Fig. 8.45** Breakwire concept with thermocouples consisting of metals x and y (a), and light-pipe concept (b)



**Fig. 8.46** Block diagram of resonant ablation gauge (a) and sensor prototype (b)

data at distinct points only and does not provide temperature data, as the breakwire method does.

Entirely noninvasive sensor for measuring the ablation layer can be built by using a capacitive method. The sensor is made in form of two electrodes that may have a variety of shapes [18]. The sensor is placed in series with an inductor and a resistor forming a resistive, inductive, and capacitive (RLC) termination to a waveguide (i.e., a coaxial cable). The arrangement shown in Fig. 8.46 is similar to a transmitter-antenna configuration. The RLC termination has a resonant frequency approximated by

$$f_0 = \frac{1}{2\pi\sqrt{LC}} \quad (8.15)$$

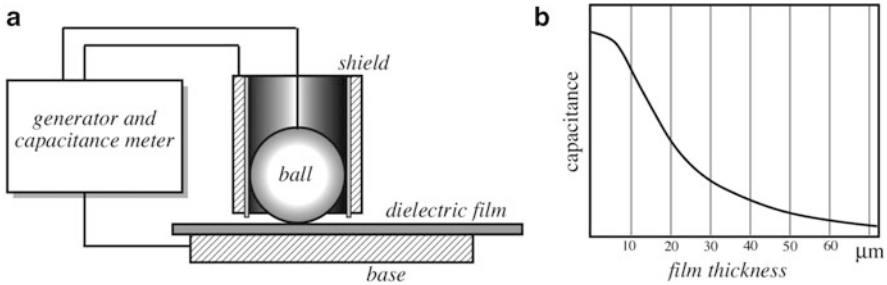
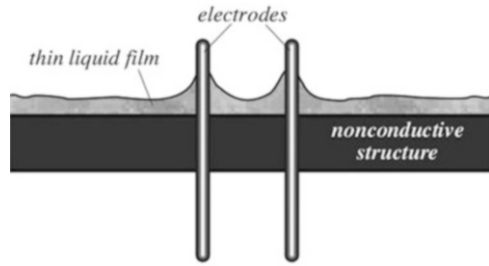
When electromagnetic energy at the resonant frequency is sent down the waveguide, all the energy dissipates in the resistor. If, however, the resonant frequency of the termination changes (say, because of a change in capacitance), a fraction of the energy is reflected back toward the source. As the capacitance continues to change, the energy reflected increases. Antennas that work like this are said to be out of tune. In this situation, one could use a commercially available reflection coefficient bridge (RCB) between the radio frequency (RF) source and the waveguide termination. The RCB generates a DC voltage proportional to the energy reflected. Then the antenna can be adjusted until the bridge output voltage is a minimum and the energy transmitted is a maximum.

### 8.6.2 Film Sensors

Sensors for measuring thickness of films range from mechanical gauges to ultrasonic probes to optical to electromagnetic and capacitive types. The method of measurement greatly depends on the film composition (conductive, isolating, ferromagnetic, etc.), thickness range, motion, temperature stability, and other factors.

Coating thickness gauges (also referred to as paint meters) are used to measure dry film thickness. Dry nonconductive film thickness can be measured by ultrasonic gauges on any substrate or by electromagnetic sensors on either magnetic surfaces

**Fig. 8.47** Measurement of thin film liquid by capacitive method



**Fig. 8.48** Dry dielectric film capacitive sensor (a) and shape of transfer function (b). (Adapted from [20])

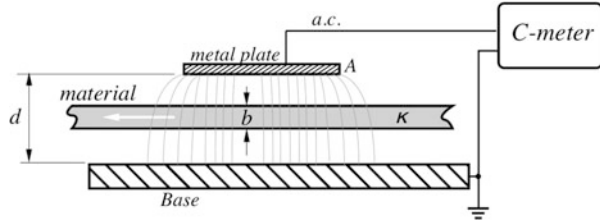
or nonmagnetic metal surfaces such as stainless steel or aluminum. The latter method is based on effects of eddy currents induced in the substrate. The operating principle is shown in Fig. 8.17.

Here is an example of a simple capacitive sensor that can measure thickness of nonconductive liquid film [19]. The liquid film thickness was measured via capacitance between two small wire probes protruding into the liquid (Fig. 8.47). The liquid acted as a dielectric between two plates of a capacitor with the plates being two small wire probes. Since the liquid has a different dielectric constant than air, a change in liquid level results in a change in the probe's capacitance. The capacitance changes were measured by incorporating the probe into a frequency modulation circuit. This type of a liquid sensor is more efficient for measuring liquids having high dielectric constants, such as water or methanol.

For measuring dry dielectric films a spherical electrode was found to be more efficient [20]. The capacitance is measured between the metal sphere (a stainless steel ball having a diameter between 3 and 4 mm) and a conductive base (Fig. 8.48). To minimize a fringing effect, the ball was surrounded by a driven shield that helps in directing the electric field only toward the base electrode through the film. A practical measurement range as follows from the calibration curve shown in Fig. 8.48b is between 10 and 30  $\mu\text{m}$ .

Another capacitive method employs a parallel-plate capacitor with the planar electrode area  $A$ , as shown in Fig. 8.49. The electrode is a metal plate positioned at a distance  $d$  from a conductive base. A nonconductive film having a dielectric

**Fig. 8.49** Planar electrode capacitive sensor for measuring thickness of dielectric film



constant  $\kappa$  moves in the gap between the plates. The capacitance measurement circuit (C-meter) generates a high frequency signal to measure capacitance between the plate and base. Presence in the gap of a dielectric material of thickness  $b$  modifies capacitance according to formula (4.23) and thus, for a combination of the film and empty space in a gap, the measured capacitance is:

$$C = A\epsilon_0 \left[ d - b \left( 1 - \frac{1}{\kappa} \right) \right]^{-1}, \quad (8.16)$$

from where the film thickness can be derived as function of the measured capacitance  $C$ :

$$b = \left( d - \frac{A\epsilon_0}{C} \right) \left( 1 - \frac{1}{\kappa} \right)^{-1} \quad (8.17)$$

For small thickness variations, this equation may be considered linear. When using capacitive methods, temperature effects should not be overlooked, since the film dielectric constant  $\kappa$  is likely temperature dependent. Thus, an appropriate temperature compensation circuit should be considered whenever an absolute accuracy is required. However, when only the thickness variations from a reference thickness  $b_0$  are needed (relative accuracy), a ratiometric formula should be employed. It contains no dielectric constant:

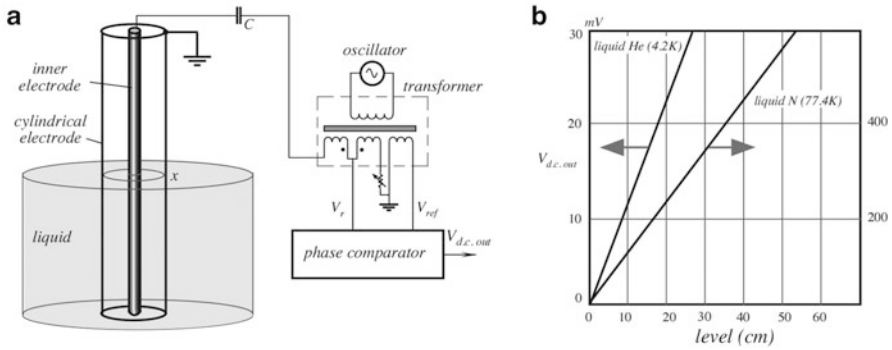
$$\delta = \frac{b}{b_0} = \frac{\left( d - \frac{A\epsilon_0}{C} \right)}{\left( d - \frac{A\epsilon_0}{C_0} \right)}, \quad (8.18)$$

where  $C_0$  is the capacitance measured from a reference film having “ideal” thickness  $b_0$ . Naturally, both the reference and monitored films should be measured under the same conditions (temperature, humidity, etc.). Use of this method is limited to measuring thickness of only dielectric films.

### 8.6.3 Cryogenic Liquid Level Sensors

There are many ways of detecting levels of liquids. They include use of the resistive (Fig. 8.1a), optical (Figs. 8.37 and 8.38), magnetic (Fig. 8.24), and capacitive (Fig. 4.8) sensors. The choice of a particular sensor depends on many factors, but





**Fig. 8.50** Transmission line probe (a) and transfer functions (b). (Adapted from [21])

probably the defining parameter is type of a liquid. One of the most challenging types are liquid gases, especially liquid helium which has low density and low dielectric constant, not mentioning its storage in the enclosed Dewar bottles at a cryogenic temperature. In such difficult cases, a transmission line sensor may be quite efficient. Such sensor may be constructed as shown in Fig. 8.50.

The probe resembles a capacitive level sensor shown in Fig. 4.8; however, its operation does not rely on the liquid dielectric constant as is the case of Fig. 4.8. The probe looks like a long tube with an inner electrode surrounded by the outer cylindrical electrode. The probe is immersed into liquid which may freely fill the space between the electrodes. The electrodes are fed with a high frequency signal (about 10 MHz). A length of the probe can be of any practical length, but for a linear response it is advisable to keep it less than  $1/4\lambda$  [21]. The high frequency signal propagates along the transmission line that is formed by the two electrodes. The liquid fills the space between the electrodes up to a particular level  $x$ . Since the dielectric constant of liquid is different from its vapor, the properties of the transmission line depend on position of the borderline between liquid and vapor, in other words, on the liquid level. The high frequency signal is partially reflected from the liquid-vapor borderline and propagates back toward the upper portion of the sensor. To some degree, it resembles a radar that sends a pilot signal and received the reflection. By measuring a phase shift between the transmitted and reflected signals, a position of the borderline can be computed. The phase shift measurement is resolved by a phase comparator that produces a d.c. voltage at its output. A higher dielectric constant produces a better reflection and thus sensitivity of the sensor improves accordingly (Fig. 8.50b).

## References

1. Wilkinson, P., et al. (2008). Nanomechanical properties of piezoresistive cantilevers: Theory and experiment. *Journal of Applied Physics*, 104, 103527.
2. Cullinan, M., et al. (2010). Carbon nanotubes as piezoresistive microelectromechanical sensors: Theory and experiment. *Physical Review*, B82, 115428.

3. Young, D., et al. (1996, June). A micromachined variable capacitor for monolithic low-noise VCOs. *Solid-State Sensor and Actuator Workshop*. Hilton Head, SC.
4. Barker, M. J., et al. (1997). A two-dimensional capacitive position transducer with rotation output. *Review of Scientific Instruments*, 68(8), 3238–3240.
5. Peters, R. D. (1994, November 3). Symmetric differential capacitance transducer employing cross coupled conductive plates to form equipotential pairs. *U.S. Patent No. 5461319*.
6. De Silva, C. W. (1989). *Control sensors and actuators*. Englewood Cliffs, NJ: Prentice Hall.
7. Bruce, R. (1984, February 7). Loop detector for traffic signal control. *U.S. Patent No. 4430636*.
8. Lees, R. H. (2002, January 8). Inductive loop sensor for traffic detection. *U.S. Patent No. 6337640*.
9. Hall effect sensing and application. Honeywell, Inc. [www.honeywell.com/sensing](http://www.honeywell.com/sensing)
10. Popovic, R. S., et al. (2002). Hall ASICs with integrated magnetic concentrators. *Proceedings of the Sensors Expo & Conference*, Boston, USA.
11. Palumbo, V., et al. (2013). Hall current sensor IC with integrated Co-based alloy thin film magnetic concentrator. *EPJ Web of Conferences* 40, 16002.
12. Born, M., et al. (1984). *Principles of optics* (6th ed.). London: Pergamon.
13. Lee, C. E., et al. (1991). Fiber-optic Fabry-Perot temperature sensor using a low-coherence light source. *Journal of Lightwave Technology*, 9, 129–134.
14. Wolthuis, R. A., et al. (1991). Development of medical pressure and temperature sensors employing optical spectrum modulation. *IEEE Transactions on Biomedical Engineering*, 38, 974–980.
15. Hill, K. O., et al. (1978). Photosensitivity in optical fiber waveguides: Application to reflection fiber fabrication. *Applied Physics Letters*, 32(10), 647.
16. Spillman, W. B., Jr. (1981). Multimode fiber-optic hydrophone based on a schlieren technique. *Applied Optics*, 20, 465.
17. In-Depth Ablative Plug Transducers (1992). Series #S-2835, Hycal Engineering, 9650 Telstar Avenue, P. O. Box 5488, El Monte, California.
18. Noffz, G. K., et al. (1996). *Design and laboratory validation of a capacitive sensor for measuring the recession of a thin-layered ablator*. NASA Technical Memorandum 4777.
19. Brown, R. C., et al. (1978). The use of wire probes for the measurement of liquid film thickness in annular gas-liquid flows. *The Canadian Journal of Chemical Engineering*, 56, 754–757.
20. Graham, J., et al. (2000). Capacitance based scanner for thickness mapping of thin dielectric films. *Review of Scientific Instruments*, 71(5), 2219–2223.
21. Bruschi, L., et al. (1999). Level meter for dielectric liquids. *Review of Scientific Instruments*, 70(2), 1514.

*“Eppur si muove!”* (“*And yet it does move*” (Lat.)—the remark by Galilei after his trial by the Inquisition in 1633.)

An object can be in either of two states—stationary or in motion. When we think of motion, we should consider a frame of reference, since an object may be moving with respect to one system of coordinates, yet be stationary with respect to the another system of coordinates, if that systems moves together with the object. A stationary object is described by its position within the selected coordinates—just like a chess figure position on a specific square has a coordinate notation, for example e2 (Fig. 9.1).

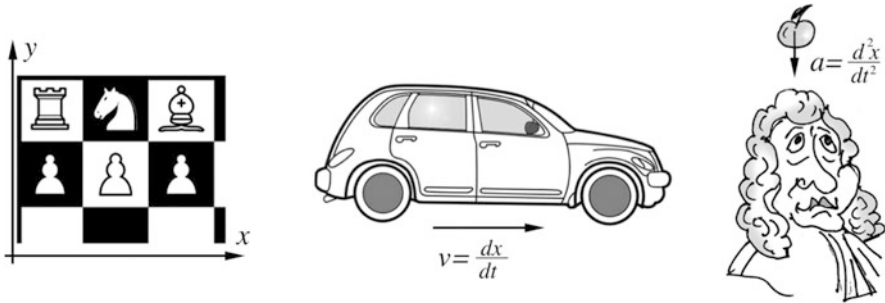
### *Linear Motion*

When position changes, we say that the object moves with a specific speed (rate of motion) and acceleration, if any. Newton’s first law states that in absence of any acting forces, an object will retain its position if it was stationary, or if it was moving—will keep moving with a constant speed along a straight line. Einstein’s Special Theory of Relativity took this law on a new level for cases when the rate of motion is extremely high, approaching that of the speed of light, which, as it was postulated and later shown experimentally, is a universal constant.

In this book we concern mostly with objects whose speed of motion is much slower than the speed of light, thus we will generally use the Newton’s Laws.<sup>1</sup> If the object moves along a straight line  $x$ , at any moment we define its average *velocity* as a ratio of distance versus time:

---

<sup>1</sup> In some cases, like for a Doppler effect, e.g., we must consider the Einstein equations of Special Theory of Relativity, as in Eq. (7.3).



**Fig. 9.1** Stationary objects have fixed coordinates. Linear steady motion is rate of coordinate change, while force (gravity in the picture) acting on apple causes acceleration

$$\bar{v} = \frac{\Delta x}{\Delta t}, \quad (9.1)$$

where  $\Delta x$  is the distance between two checkpoints and  $\Delta t$  is time of travel.

At any particular moment the instantaneous velocity is defined as

$$v = \frac{dx}{dt} \quad (9.2)$$

If motion is not steady (for example, a car driver presses either the brake or accelerator pedals), the speed varies in time. Moving from one speed to another causes either an acceleration or deceleration. According to the Newton's second Law, this essentially requires application of force—like the brakes or additional torque from the engine. An instantaneous acceleration is a speed of the speed, or a second derivative of coordinate  $x$ :

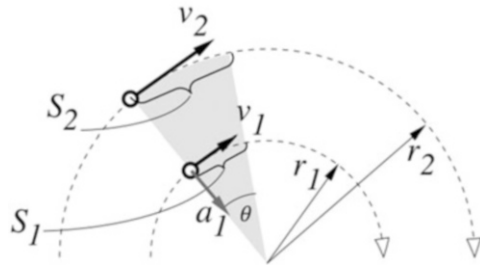
$$a = \frac{dv}{dt} = \frac{d^2x}{dt^2} \quad (9.3)$$

Pondering about acceleration led Einstein to development of the General Theory of Relativity. It is substantially based on the Equivalency Principle, which states that a force arisen from an acceleration and force resulted from an attraction by a massive body (gravity) are indistinguishable and thus acceleration and gravity are just different ways of describing the same phenomenon. For our purpose, it means that for measuring acceleration and gravity we should use the same sensors—accelerometers.

### Rotary Motion

When an object moves along a curved trajectory, several properties of such movement should be considered. Any curvature, at least over a short distance, can be described by a radius  $r$  of the trajectory indicated by dotted lines in Fig. 9.2. A rotation is described by an average *angular velocity* that is the rate of rotation by angle  $\Theta$  over a time interval.

**Fig. 9.2** Vectors of rotary motion



$$\bar{\omega} = \frac{\Delta\Theta}{\Delta t} \tag{9.4}$$

The instantaneous angular velocity then is defined as

$$\omega = \frac{d\Theta}{dt} \tag{9.5}$$

The angular velocity is a vector quantity where direction of the vector is *along the axis* of rotation.

At any moment, the moving object is characterized by a linear instantaneous velocity (speed)  $v$  that is tangential to the radius of rotation and relates to the angular velocity as

$$v = \omega r \tag{9.6}$$

Note that for all rotating together objects, no matter how far away from the center, the angular velocity is the same, while the linear velocity depends on distance (radius)  $r$  from the center. This is because at different radii,  $r_1$  and  $r_2$ , the object moves for different distances  $S_1$  and  $S_2$ , while rotating for the same angle  $\Theta$ .

If the angular velocity changes, we speak of the angular acceleration:

$$\alpha = \frac{d\omega}{dt} = \frac{d^2\Theta}{dt^2} \tag{9.7}$$

Now, consider the tangential velocity  $v_1$ . When the object rotates with a constant angular velocity, the tangential velocity continuously changes direction but its magnitude remains the same. Yet, whenever the velocity changes, either in direction or magnitude, it gives rise to acceleration, which during a uniform rotary motion is directed toward the center of rotation and has value

$$a = \frac{v^2}{r} \tag{9.8}$$

The acceleration also changes its direction but not magnitude, as long as the angular velocity is constant.

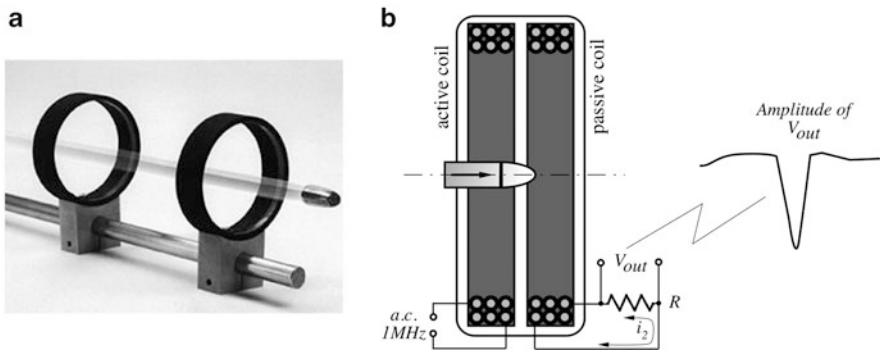
To measure velocity or acceleration, both linear and rotary, we should select physical effects where electric signals can be generated as functions of these variables. Below we describe several popular solutions.

## 9.1 Stationary Velocity Sensors

### 9.1.1 Linear Velocity

Velocity is a distance that is traveled by an object per unit of time [Eq. (9.1)]. Therefore, the most obvious way of determining velocity is first measuring two items: the distance and time, and then taking a ratio of such. For that, two checkpoints separated by a known distance  $\Delta x$  should be established. Each checkpoint needs a fast-acting presence detector to indicate the moment when the moving object passes by it. Which detector to use? A selection depends on several factors, including the expected speed of movement, required accuracy, material of the moving target, its size, etc. Many such detectors are described in the previous chapters of this book. As an illustration, consider a measurement of speed of a projectile, such as a bullet. We know that a bullet moves very fast, having the muzzle speed something in the order of 1 km/s, it is made of metal (meaning—it is conductive), its size varies but the length may be on the order of 20 mm at a diameter in the order of 10 mm.

Instantaneous location of such a fast object may be detected by a photo-interrupter, high-speed video camera, piezoelectric film detector (Sect. 4.6.2), one of various magnetic sensors, etc. As an example, we describe a direct measurement of a bullet velocity by employing eddy currents. The work was performed at Impact Physics Laboratory of U.S. Air Force (model KD-2300 from Kaman Instrumentation Corp.) The test setup contains two double rings that serve as checkpoints separated by a fixed and known distance, Fig. 9.3a.



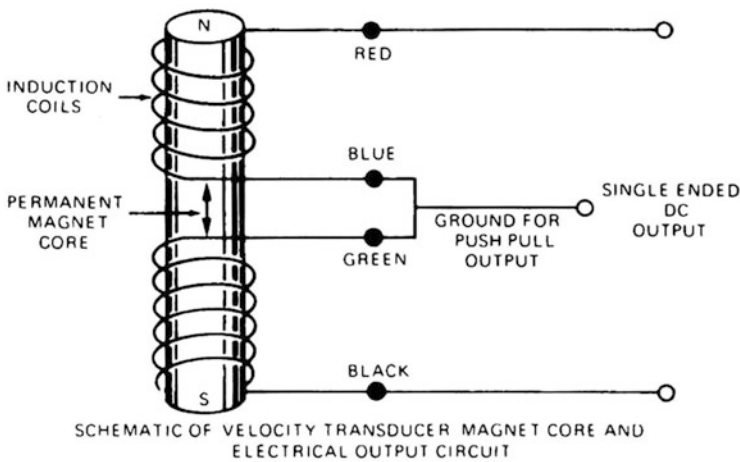
**Fig. 9.3** Setup for directly measuring bullet velocity (a); double coil that induces and detects eddy currents in bullet (b)

Each double ring comprises two coils where one coil is active for generating alternate magnetic field. For that purpose, it is supplied by a.c. current having frequency 1 MHz—sufficiently high for accurately detecting a fast moving bullet. The second one is a passive coil being magnetically coupled with the active coil and thus it produces an induced a.c. current  $i_2$ . Two joined coils form a transformer. When the bullet enters a void in the center of the first ring, magnetic field from the active coil induces in the bullet eddy currents (see Sect. 8.4.3). These circulating eddies of electrons create their own magnetic fields that, due to the Lenz’s law, oppose changes in the originating magnetic field. As a result, a magnitude of the output a.c. current in the passive coil starts dropping. When the bullet passes the ring center the amplitude is the lowest. This is the precise indication of the bullet’s position at the first checkpoint. After certain time, the bullet passes the second double ring where it induces another current spike, which indicates presence of a bullet at the second checkpoint. The time difference  $\Delta t$  between the spikes is what it takes for the bullet to travel between the rings separated by a known distance  $\Delta x$  and thus is the measure of its velocity according to Eq. (9.1).

Another example of a velocity sensor is the LVT—linear velocity transducer (Fig. 9.4) that employs the Faraday law of electromagnetism. The coil is stationary, while the core magnet is attached to the object of interest and moves inside the coil with velocity  $v$ . Voltage across the coil is generated when the moving magnet interacts with a wire:

$$V = Blv, \tag{9.9}$$

where  $B$  is strength of the magnetic field and  $l$  is the wire length. Thus, the voltage is proportional to the speed of the magnet movement. In the LVT, both ends of the



**Fig. 9.4** Operating principle of electromagnetic velocity sensor (Courtesy of Trans-Tek, Inc., Ellington, CT)

magnet are inside the coil. With a single coil, this would give a zero output because the voltage generated by one end of the magnet would cancel the voltage generated by the other end. To overcome this limitation, the coil is divided into two sections.

The north pole of the magnet induces a current in one coil, while the south pole induces a current in the other coil. The two coils are connected in a series-opposite direction to obtain an output proportional to the magnet's velocity. Maximum detectable velocity depends primarily on the input stages of the interface electronic circuit. Minimum detectable velocity depends on the noise floor, and especially of transmitted noise from a nearby high a.c. current-carrying equipment. This design is very similar to an LVDT position sensor (Sect. 8.4.1), except that LVDT is an active sensor with a moving ferromagnetic core, while the LVT is a passive device with a moving permanent magnet. In other words, the LVT is a passive voltage generating sensor which does not need an excitation signal. An angular version of the LVT (called RVT—rotary velocity transducer) may measure rotation rate continuously for any number of turns. Stationary velocity sensors detect velocity along a distance that is limited by the size of the sensor, so in most cases these sensors measure vibration velocity.

### 9.1.2 Rotary Velocity Sensors (Tachometers)

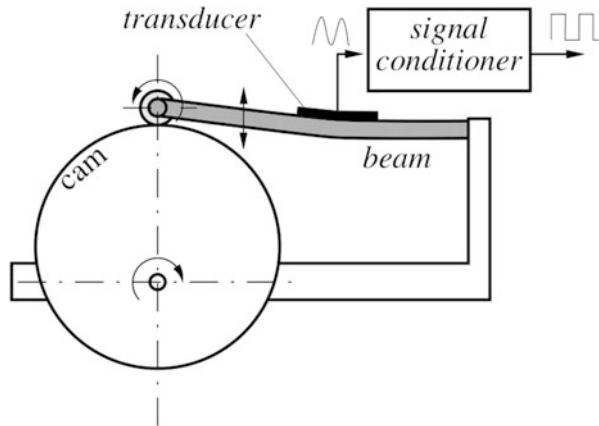
For measuring angular velocity, rotating sprocket wheels with the position sensors are often employed. This concept is illustrated in Fig. 8.26. Naturally, output signals from this sensor have a discrete format—the higher the pitch of the sprockets the finer the resolution.

For detecting the wheel rotation, many types of position sensors can be employed, like the magnetic (Hall-sensors, magnetoresistors as in Fig. 8.25, and the reed switches) and optical (photo-interrupters). One of the most popular is a magnetic rotary sensor (Fig. 8.22a, b). The key feature of all these devices is that the sensor is stationary and physically attached to the frame of reference (a car body, for example), while the wheels rotate. In many applications, especially in mobile devices, this arrangement is not possible and therefore an inertial sensor—a gyroscope—is the choice for measuring angular velocity.

Another type of a tachometer uses an eccentric wheel (cam) illustrated in Fig. 9.5. When rotating, the cam bends the resilient beam whose right side is anchored to a support structure. A strain transducer is applied to the beam surface. The transducer may be of any suitable design, for example, a strain gauge (Fig. 10.2) or piezoelectric element (Fig. 10.8). When the beam flexes up and down, the transducer converts mechanical strains to a variable electrical signal that, in turn, is converted by the signal conditioner to rectangular pulses—one per the wheel turn.



**Fig. 9.5** Cam tachometer with flexing beam

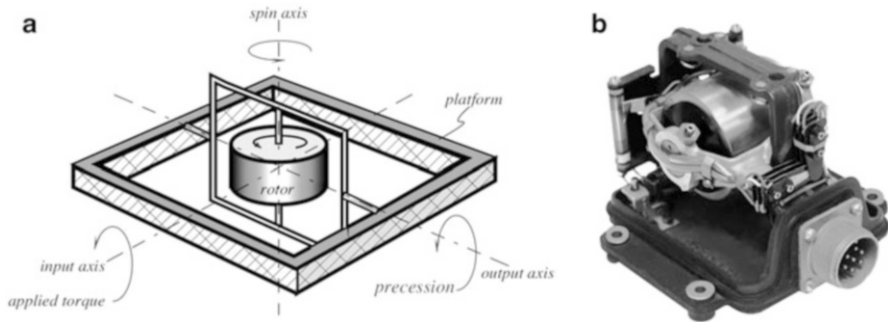


## 9.2 Inertial Rotary Sensors

Inertial rotary sensor is a self-contained device in which measurements are provided by one or more gyroscopes. This sensor is used to track the position and orientation of an object relative to the prior sensor orientation and velocity, rather than to a stationary coordinate system. A complete inertial sensor typically contains three orthogonal rate-gyroscopes, measuring *angular velocities*.

Before advancement of a GPS (*global positioning system*), besides a magnetic compass, a rotating wheel gyroscope probably was the most common mobile navigation sensor for detecting deviation from a selected direction of motion. In other words, a gyroscope was measuring an angular rotation of the direction of motion. Word mobile means being attached to a moving object. In many cases where a geomagnetic field was either absent (in Space), or is altered by presence of some disturbances, a gyroscope was an indispensable sensor for monitoring angular velocity of a vehicle, such as an aircraft or missile, Fig. 9.6b. Nowadays, applications of gyroscopes are much broader than just for navigation. They are used in the stabilization devices, weapons, robotics, tunnel mining, and—in very large quantities—in mobile communications devices, such as smartphones.

The earliest known gyroscope containing a rotating massive sphere was made in 1817 by German Johann Bohnenberger. In 1832, American Walter R. Johnson developed a gyroscope that was based on a rotating disk. In 1852 Léon Foucault used a rotating disc in an experiment involving the rotation of the Earth. Foucault coined the name *gyroscope* from the Greek *gyros*—circle or rotation—and *skopeein*—to see.



**Fig. 9.6** Conceptual design of mechanical gyroscope (a) and early autopilot gyroscope (b)

### 9.2.1 Rotor Gyroscope

A gyroscope, or a *gyro* for short, is a “keeper of direction”, like a pendulum in a clock is a “keeper of time”. A keeper of direction means that it produces an output signal whenever angular velocity deviates from zero, which happens when the platform starts rotating. A gyro operation is based on the fundamental principle of the conservation of angular momentum: *in any system of particles, the total angular momentum of the system relative to any point fixed in space remains constant, provided no external forces act on the system.*

A mechanical gyro is comprised of a massive disk free to rotate about a spin axis (Fig. 9.6a) which itself is confined within a framework that is free to rotate about one or two axes. Hence, depending on the number of rotating axes, a gyro can be either of a single-, or two-degree-of-freedom types. Two qualities of a gyro account for its usefulness: (1) the spin axis of a free gyroscope will remain fixed with respect to space, provided there are no external forces to act upon it, and (2) a gyro can be made to deliver a torque (or output signal) which is proportional to the angular velocity about an axis perpendicular to the spin axis.

When the wheel (rotor) freely rotates, it tends to preserve its axial position. If the gyro platform rotates around the input axis, the gyro will develop a torque around a perpendicular (output) axis, thus turning its spin axis around the output axis. This phenomenon is called *precession* of a gyro. It can be explained by the Newton’s law of motion for rotation: *the time rate of change of angular momentum about any given axis is equal to the torque applied about the given axis.* That is, when a torque  $T$  is applied about the input axis, and the speed  $\omega$  of the wheel is held constant, the angular momentum of the rotor may be changed only by rotating the projection of the spin axis with respect to the input axis. In other words, the rate of rotation of the spin axis about the output axis is proportional to the applied torque:

$$T = I\omega\Omega, \quad (9.10)$$

where  $\Omega$  is the angular velocity about the output axis and  $I$  is the inertia of a gyro wheel about the spin axis. To determine the direction of precession, the following

rule can be used: *precession is always in such a direction as to align the direction of rotation of the wheel with the direction of rotation of the applied torque.*

Accuracy of a mechanical gyro greatly depends on the effects which may cause additional unwanted torques and cause drifts. The sources of these are friction, imbalanced rotor, magnetic effects, etc. One method which has been widely used to minimize rotor friction is to eliminate the suspension entirely by floating the rotor and the driving motor in a viscous, high-density liquid, such as one of the fluorocarbons. This method requires close temperature control of the liquid and also may suffer from aging effects. The other method of friction reduction is to use the so-called gas bearings, where the shaft of the rotor is supported by high-pressure helium, hydrogen, or air. And even a better solution is to support the rotor in vacuum by an electric field (electrostatic gyros). In another version—a magnetic gyro consists of a rotor supported by a magnetic field. In that case, the system is cryogenically cooled to temperatures where the rotor becomes superconductive. Then, an external magnetic field produces enough counter-field inside the rotor that the rotor floats in a vacuum. These magnetic gyroscopes sometimes are called cryogenic gyros.

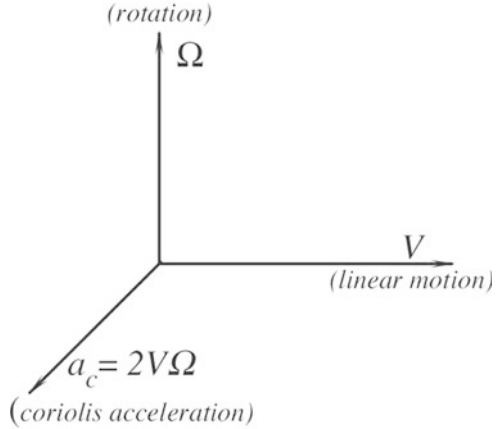
While a spinning-rotor gyroscope for many years was the only practical choice, its operating principle really does not lend itself to design of a small monolithic sensor that is required by many mobile applications. Conventional spinning-rotor gyroscopes contain parts such as gimbals, support bearings, motors, and rotors which need accurate machining and assembly; these aspects of construction prohibit conventional mechanical gyroscopes from ever becoming a low-cost portable device. Wear on the motors and bearings during operation means that the gyroscope will only meet the performance specifications for a set number of running hours. Thus, other methods for sensing a direction and angular velocity have been developed. Often, a GPS would be the ideal choice. Yet, it just cannot be employed in Space, under water, in tunnels, inside buildings, or whenever the size and cost are of a paramount importance. Besides, spatial resolution of the GPS is just nearly not sufficient for many hand-held devices.

## 9.2.2 Vibrating Gyroscopes

If, as illustrated in Fig. 9.2, the object initially rotates with radius  $r_1$ , it is characterized by a tangential velocity  $v_1$ . When a rotating object moves farther away from the center to the new radius  $r_2$ , it will have a faster tangential velocity  $v_2$ . Thus, when the object moves away from the center the tangential velocity increases, meaning that the object accelerates. This phenomenon was discovered in 1835 by Gaspard G. de Coriolis (1792–1843), a French mathematician—and the effect is known as *Coriolis acceleration*. This acceleration  $\mathbf{a}_c$  in a vector notation is described as:

$$\mathbf{a}_c = -2\boldsymbol{\Omega}\mathbf{V}, \quad (9.11)$$

**Fig. 9.7** Vector of Coriolis acceleration



where  $\mathbf{V}$  is the velocity of the object moving within the rotating system, and  $\mathbf{\Omega}$  is the angular vector which has magnitude equal to the rotation velocity  $\omega$  and is directed along the axis of rotation. If the object has mass  $m$ , the Coriolis acceleration produces force that in a vector notation is

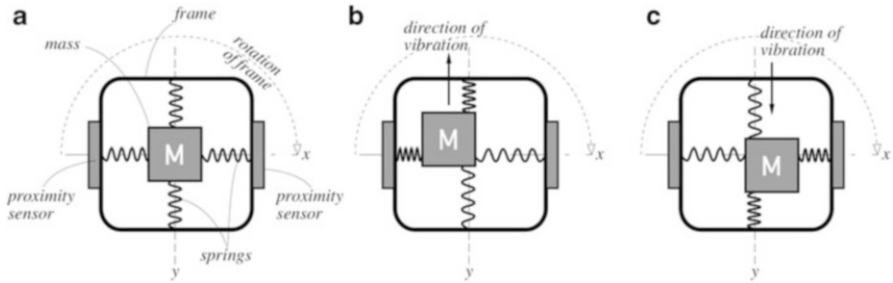
$$\mathbf{F}_c = -2\mathbf{\Omega}\mathbf{V}m \quad (9.12)$$

This force is called a *fictitious force* as it arises not from an interaction between different objects but rather from a rotation of a single object. The Coriolis acceleration, which is directly proportional to the rate of turn, occurs in the third axis that is perpendicular to the plane containing the other two axes. Figure 9.7 shows that the Coriolis acceleration vector is perpendicular to the plane where the vectors of angular velocity and object's velocity are positioned.

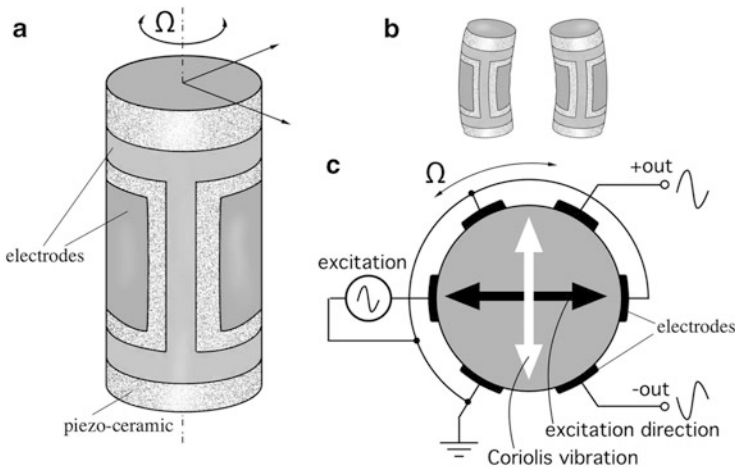
Since the force magnitude is function of the angular velocity, this suggests that the angular velocity sensor can be designed by incorporation a force sensor that converts the Coriolis force into an electrical signal. The object having mass does not need to move in one direction only, it can go back and forth within the reference frame whose angular velocity we measure. In other words, the object may oscillate in one direction, while the frame rotation will produce the Coriolis force in another direction. We can measure that force for generating an output electrical signal.

Figure 9.8 is a conceptual illustration of how the oscillating gyro works. The massive object  $M$  is forced by an external drive to oscillate along the  $y$ -axis with frequency of several kHz [1]. So the mass goes up and down with high velocity that has a sinusoidal form. When the frame rotates, a Coriolis force arises and pushes the mass either to the left or to the right. The shift is measured by the proximity or displacement sensors positioned along the  $x$ -axis. The shift also follows the sinusoidal function having a magnitude proportional to the angular velocity.

The vibrating gyros are fabricated in very large quantities. Use of the MEMS micromachined technology takes advantage of the techniques developed in the electronic industry and is highly suited to a high-volume manufacture. There are



**Fig. 9.8** Conceptual diagram of vibrating gyroscope. Massive object M is supported within frame by four springs and forced to oscillate along y-direction (a). When frame rotates and object oscillates upward (b), Coriolis force shifts it to left. When object oscillates downward (c), force shifts it to the right



**Fig. 9.9** Piezoelectric ceramic vibrating gyro has a cylindrical shape (a). Alternate voltage applied to electrodes flexes cylinder along one axis (b); axial view of gyro cylinder, where Coriolis force flexes it along perpendicular axis (c). [Adapted from [www.nec-tokin.com](http://www.nec-tokin.com)]

several practical ways of building a vibrating gyro, however, all of them can be divided into three principle groups [2]:

1. Simple oscillators (mass on a string, beams)
2. Balanced oscillators (tuning forks)
3. Shell resonators (“wine glass”, cylinder, ring)

All three categories have been implemented in the actual designs.

As an example, a modern vibrating gyro is shown in Fig. 9.9. It uses a piezoelectric ceramic (see Sect. 4.6.1) that is formed in shape of a small cylinder (0.8 mm in diameter and 9 mm in length) with six electrodes deposited on it sides.

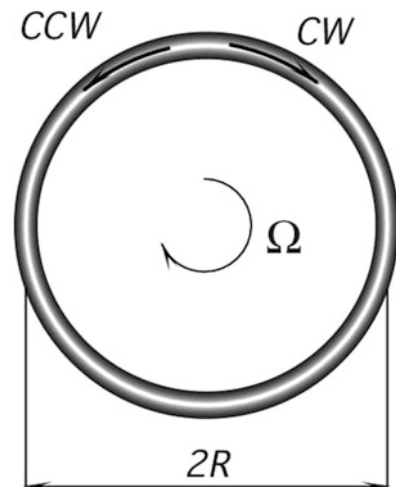
The design takes advantage of a reversible phenomenon of a piezoelectric effect: application of electric charge strains the piezoelectric material, thus converting electric signal into deformation. On the other hand, a strain produces an electric charge, thus converting mechanical force into electrical signal. The driving pair of the electrodes is supplied with a.c. voltage from an external oscillator. It flexes the cylinder in a direction indicated by the black arrow in Fig. 9.9c. When the cylinder rotates around its vertical axis with an angular velocity  $\Omega$ , the arising Coriolis force flexes it in the direction of the white arrow—the higher the angular velocity the stronger the flexing. This rotation-related flexing induces piezoelectric charges in a pick-up pair of the electrodes: +out and –out that generate the out-of-phase sinusoidal voltages. These voltages are amplified and processed by a signal conditioner for serving as the gyro output signals. Advantages of this design are a small size and ease of production, meaning a lower cost. A sensitivity of this sensor to angular velocity is fairly good—about 0.6 mV/deg/s. This miniature gyro is widely used in the camera stabilization devices, game controllers, and supplementary sensors for GPS (to continue navigating during times when the satellite RF signals are lost), robots, and virtual reality systems.

### 9.2.3 Optical (Laser) Gyroscopes

A ring laser gyroscope (RLG) is another inertial navigation sensor. It is characterized by very high reliability (no moving parts) and very high accuracy with the angular uncertainty on the order  $0.01^\circ/h$ . A major advantage of the optical gyros is their ability to operate under hostile environments that would be difficult, if not impossible, for the mechanical gyros.

Operation of the RLG is based on employing the so-called Sagnac effect, which is illustrated in Fig. 9.10 [3]. Two beams of light generated by a laser propagate in

**Fig. 9.10** Sagnac effect



opposite directions within an optical ring having refractive index  $n$  and radius  $R$ . One beam goes in clockwise (CW) direction, while the other in a counterclockwise (CCW) direction. The amount of time which takes light to travel within the ring takes  $\Delta t = 2\pi R/nc$ , where  $c$  is the speed of light. Now, let us assume that the ring rotates with angular rate  $\Omega$  in the clockwise direction. In that case, light will travel different paths at two directions. The CW beam will travel  $l_{\text{cw}} = 2\pi R + \Omega R \Delta t$ , while the CCW beam will travel  $l_{\text{ccw}} = 2\pi R - \Omega R \Delta t$ . Hence, the difference between the paths is

$$\Delta l = \frac{4\pi\Omega R^2}{nc}. \quad (9.13)$$

Therefore, to accurately measure  $\Omega$ , a technique must be developed to determine  $\Delta l$ . There are three basic methods known for the path detection: (1) optical resonators, (2) open-loop interferometers, and (3) closed-loop interferometers.

For the RLG, the measurements of  $\Delta l$  are made by taking advantages of the lasing characteristics of an optical cavity (that is, of its ability to produce coherent light). For lasing to occur in a closed optical cavity, there must be an integer number of wavelengths about the complete ring. The light beams, which does not satisfy this condition, interfere with themselves as they make subsequent travel about the optical path. In order to compensate for a change in the perimeter due to rotation, the wavelength  $\lambda$  and frequency  $\nu$  of the light must change

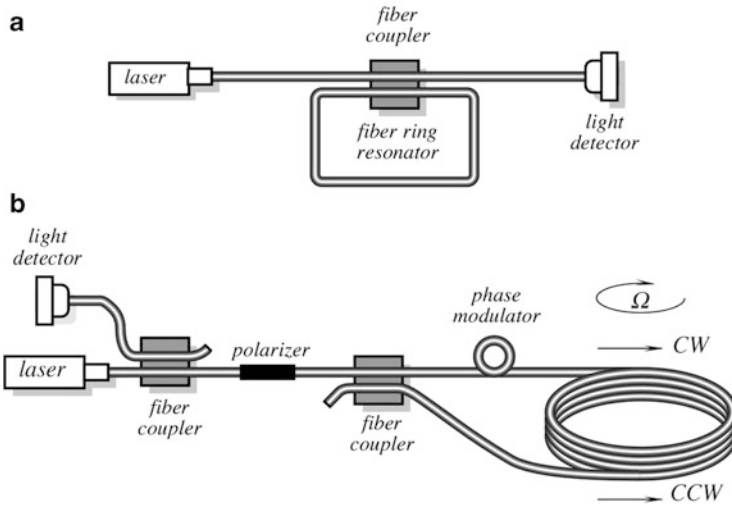
$$-\frac{d\nu}{\nu} = \frac{d\lambda}{\lambda} = \frac{dl}{l}. \quad (9.14)$$

The above is a fundamental equation relating frequency, wavelength, and perimeter change in the ring laser. If the ring laser rotates at a rate  $\Omega$ , then Eq. (9.14) indicates that light waves stretch in one direction and compress in the other direction to meet the criteria for the lasing of an integral number of wavelengths about the ring (somewhat similar to the Doppler effect). This, in turn, results in a net frequency difference between the light beams. If the two beams are bit together (mixed), the resulting signal has frequency

$$F = \frac{4A\Omega}{\lambda nl}, \quad (9.15)$$

where  $A$  is the area enclosed by the ring.

In practice, optic gyros are designed with either a fiber ring resonator, or the fiber coil where the ring has many turns of the optical fiber [4]. The optic ring resonator is shown in Fig. 9.11a. It consists of a fiber loop formed by a fiber beam splitter that has a very low cross-coupling ratio. When the incoming beam is at the resonant frequency of the fiber ring, the light couples into the fiber cavity and the intensity in the exiting light drops. The coil fiber gyro (Fig. 9.11b) contains a light source and the detector coupled to the fiber. The light polarizer is positioned between the detector and the second coupler to insure that both counter-propagating beams



**Fig. 9.11** Fiber optic ring resonator (a); fiber optic analog coil gyro (b) (adapted from [3])

traverse the same path in the fiber optic coil [5]. The two beams mix and impinge onto the detector, which monitors the cosinusoidal intensity changes caused by the rotationally induced phase changes between the beams. This type of optical gyro provides a relatively low cost, small size rotation sensitive sensor with a dynamic range up to 10,000. Applications include yaw and pitch measurements, attitude stabilization, and gyro compassing.

### 9.3 Inertial Linear Sensors (Accelerometers)

Linear accelerometers belong to the class of inertial sensors that do not require referencing to a stationary coordinate system. They are attached to moving platforms. The name “inertial” refers to an essential component that has a substantial inertia to motion. In navigational devices, accelerometers work together with gyroscopes, typically containing three orthogonal rate-gyroscopes and three orthogonal accelerometers, measuring angular velocity and linear acceleration, respectively. By processing signals from these devices it is possible to track the position and orientation of a moving object.

Accelerometers are used for measuring acceleration resulted from subjecting an object to external forces, including gravity. While gravity is usually a constant force directed toward the center of gravity of a massive object, other forces may vary in magnitude and direction in the broad magnitude and frequency ranges. Thus, a typical accelerometer should be responsive to various forms of accelerations—from constant to slow moving to strong impacts and vibrations.



As it follows from the Newton’s second law, acceleration in a vector notation is defined as

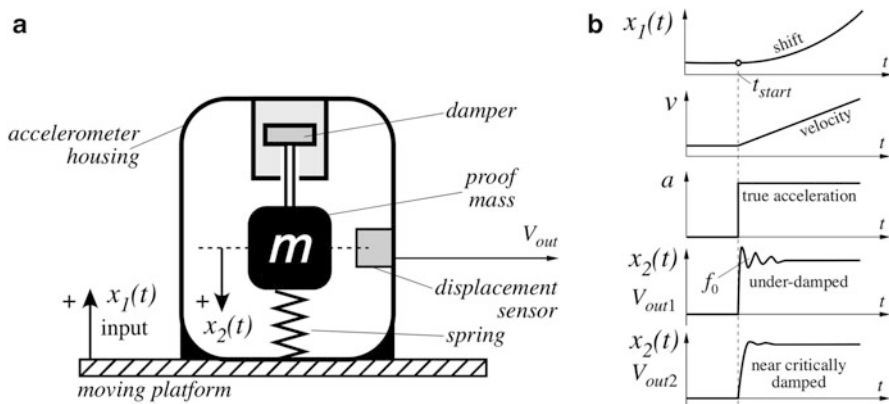
$$\mathbf{a} = \frac{\mathbf{F}}{m}, \tag{9.16}$$

where  $\mathbf{F}$  is the force vector and  $m$  is mass of the object (scalar value) that is subjected to the force causing an acceleration. Thus, mass, acceleration, and force are all interconnected. The direction of acceleration is the same as that of the force. Equation (9.16) suggests that for measuring acceleration we need to provide a known mass  $m$  and measure the force magnitude  $F$  that is exerted by that mass on a force sensor. The force sensor is an essential part of an accelerometer. The force sensor comprises two components: a spring that deforms under influence of the force and a deformation sensor to determine the deformation magnitude. For a compression spring, deformation is measured as change in the spring length by a displacement sensor. For details on force sensors, refer to Chap. 10.

### 9.3.1 Transfer Function and Characteristics

A one-axis accelerometer can be specified as a single-degree-of-freedom device, which has a massive object (sometimes called *proof mass* or *seismic mass*), a spring-like supporting system, a frame structure with damping properties (Fig. 3.15a), and also a displacement sensor. To make a functional accelerometer, its housing is attached to a moving platform (Fig. 9.12a).

The proof mass,  $m$ , is supported by a compressible spring that allows the mass to shift up and down. In turn, the mass is attached to two additional components: a damper and a displacement sensor. A damper slows down the mass motions while the displacement sensor determines the mass position with respect to the neutral (at no acceleration).



**Fig. 9.12** Concept of linear mechanical accelerometer (a) and timing diagrams (b)

The platform with the attached accelerometer housing may be stationary or it may travel along coordinate  $x$ . Consider the distance change as having the shape of a parabolic function [Fig. 9.12b:  $x$ -curve]. The entire assembly accelerates upward with the speed,  $v$ , changing linearly while the acceleration,  $a$ , that is a step-function we are attempting to measure. When the motion starts, due to its inertia, the proof mass tends to remain in place and thus exerts force  $F$  on the spring, squeezing it for a distance  $\Delta x = x_2 - x_1$ . The spring is characterized by stiffness  $k$ . The spring counteracts the force  $F$  so that the following equation holds:

$$F = ma = k\Delta x = k(x_2 - x_1), \quad (9.17)$$

from which we can determine the proof mass displacement as

$$x_2 - x_1 = \frac{m}{k}a. \quad (9.18)$$

where the ratio

$$S = \frac{m}{k} = \frac{1}{\omega_0^2} = \frac{1}{(2\pi f_0)^2} \quad (9.19)$$

is called the “static sensitivity” of an accelerometer. Note that sensitivity  $S$  is inversely proportional to the squared  $f_0$ —a natural (resonant) frequency in Hz of the proof mass assembly (including all attached components). Notation  $\omega_0$  is a circular frequency in rad/s.

As follows from Eq. (9.19), to increase the natural frequency, the proof mass must be reduced and the spring stiffness shall increase. Another conclusion from this equation is that the higher the natural frequency the less sensitive the accelerometer.

So far we discussed the static properties of an accelerometer. Now we need to consider time dependent characteristics of the moving mass. When acceleration onsets, the proof mass compresses the spring with force  $F$ . At some moment, the spring will push the mass upward until the spring expands beyond its original size. Then the motion reverses again, the spring compresses, and the process repeats. In other words, the mass oscillates. To minimize undesirable oscillations of the proof mass, it is connected to a damper (“shock absorber”) that slows down the mass movement by absorbing its kinetic energy in relationship with the speed of the mass motion. The damper exerts on the mass a damping force proportional to the speed of the mass displacement:

$$F_b = b \frac{d(x_2 - x_1)}{dt} = b \left( \frac{dx_2}{dt} - \frac{dx_1}{dt} \right) \quad (9.20)$$

where  $b$  is the dumping coefficient which is defined through a parameter called a damping ratio  $\zeta$  as:

$$b = 2\zeta\sqrt{km}, \quad (9.21)$$

To account for all forces acting on the proof mass (inertial force, spring force, and damping force) we shall write a second order linear differential equation:

$$m \frac{d^2 x_2}{dt^2} + b \left( \frac{dx_2}{dt} - \frac{dx_1}{dt} \right) + k(x_2 - x_1) = 0, \quad (9.22)$$

Let's call  $x_2 - x_1 = z$  which is a relative shift of the proof mass being translated by the displacement sensor into output voltage  $V_{\text{out}}$ . Then, considering Eq. (9.16) which is the Newton second Law, Eq. (9.22) can be rewritten as

$$m \frac{d^2 z}{dt^2} + b \frac{dz}{dt} + kz = -ma = -F. \quad (9.23)$$

Its solution for a relative displacement  $z(t)$  is:

$$z(t) = B e^{-\zeta \sqrt{\frac{k}{m}} t} \text{Sin}(2\pi f_d t + \varphi) - Sa, \quad (9.24)$$

where the factor  $B$  and phase shift  $\varphi$  depend on position of the proof mass at the moment of onset of acceleration.

The damped frequency  $f_d$  is different from the natural frequency  $f_0$  and defined as:

$$f_d = f_0 \sqrt{1 - \zeta^2} \text{ only for } \zeta < 1 \quad (9.25)$$

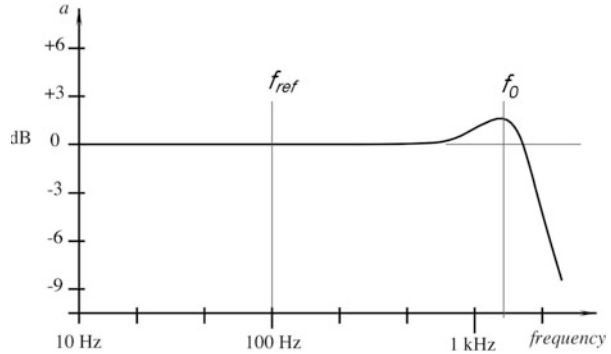
Several conclusions can be drawn from the solution (9.24). The output has a decaying oscillatory nature characterized by the first summand. The decay rate is exponential with a time constant:

$$\tau = \frac{1}{\zeta} \sqrt{\frac{m}{k}}. \quad (9.26)$$

Thus, the higher the damping ratio  $\zeta$ , the quicker the spurious oscillations disappear. If  $\zeta \ll 1$ , then Eq. (9.24) has a noticeable oscillatory "underdamped" response shown in Fig. 9.12b as output voltage  $V_{\text{out}1}$ . For  $\zeta \gg 1$ , the response is overdamped with no oscillations, slow, and lagging behind the true acceleration  $a$ . A critical or near critically damped response ( $\zeta \approx 1$ ) has a shape that is closer to the true acceleration and is the optimal parameter. Another conclusion is that after the oscillations disappear, the output characterized by the second summand is proportional to acceleration  $a$  multiplied by the sensitivity factor defined by Eq. (9.19). Depending on particular applications, the mass, spring, and damper should be carefully selected.

A correctly designed, installed, and calibrated accelerometer should have one clearly identifiable resonant (natural) frequency, and a flat frequency response where the most accurate measurement can be made (Fig. 9.13). Within this flat region, the output of the accelerometer will correctly reflect the change without

**Fig. 9.13** A frequency response of an accelerometer where  $f_n$  is natural frequency;  $f_{ref}$  is reference frequency



multiplying the signal by any variations in the frequency characteristic of the accelerometer. Viscous damping is used in many accelerometers to improve the useful frequency range by limiting effects of the resonant. As a damping medium, silicone oil is used quite often. A damper is important in sensors where the operating frequency is close to the natural frequency. However, when the natural frequency is much higher than the operating bandwidth limit, a mechanical damper may be replaced by a hardware or software low-pass filter in the signal conditioner.

When calibrated, several characteristics of an accelerometer should be determined:

1. *Sensitivity* is the ratio of an electrical output to the mechanical input. It is usually expressed in terms of volts per unit of acceleration under the specified conditions. For instance, the sensitivity may be specified as 1 V/g (unit of acceleration:  $g = 9.80665 \text{ m/s}^2$  at sea level,  $45^\circ$  lat.) The sensitivity is typically measured at a single reference frequency of a sine-wave shape.<sup>2</sup> In the U.S.A. it is 100 Hz, while in most European countries it is 160 Hz (outside of the power line frequency and its harmonics).
2. *Frequency response* is the output signal over a range of frequencies where the sensor should be operating. It is specified with respect to a reference frequency which is where the sensitivity is specified.
3. *Resonant (natural) frequency* in an undamped sensor shows as a clearly defined peak that can be 3–4 dB higher than the response at the reference frequency. In a near critically damped device, the resonant may not be clearly visible, therefore, the phase shift is measured. At the resonant frequency, it is  $180^\circ$  of that at the reference frequency. For a 1 % accuracy the highest operating frequency should be at least 2.5 times lower than the resonant frequency of the accelerometer. When designing an accelerometer, the proof mass should be selected as small as practical (without compromising sensitivity) while the support springs should be

<sup>2</sup> These frequencies are chosen because they are removed from the power line frequencies and their harmonics.

stiff and sort—this helps to make the natural frequency much higher than the operating range.

4. *Zero stimulus output* is specified for the position of the sensor where its sensitive (active) axis is either perpendicular to Earth's gravity or during a free-fall (weightlessness). That is, in accelerometers that include a d.c. component in the output signals, the gravitational effect should be eliminated before the output at a no-mechanical input is determined.
5. *Linearity* of the accelerometer is specified over the dynamic range of the input signals.

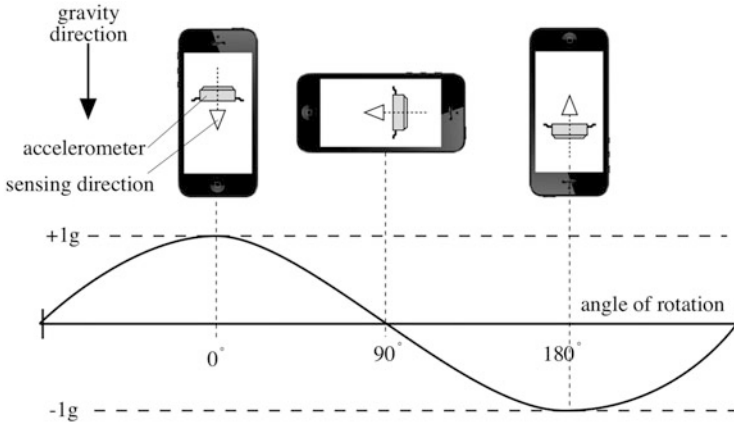
When specifying an accelerometer for a particular application, one should answer a number of questions, such as:

1. What is the anticipated magnitude of vibration or linear acceleration?
2. What is the operating temperature and how fast the ambient temperature may change?
3. What is the anticipated frequency range?
4. What linearity and accuracy are required?
5. What is the maximum tolerable size?
6. What kind of power supply is available?
7. Are any corrosive chemicals or high moisture present?
8. What is an anticipated overshock?
9. Are intense acoustic, electromagnetic, or electrostatic fields present?
10. Is the machinery grounded?

### 9.3.2 Inclinometers

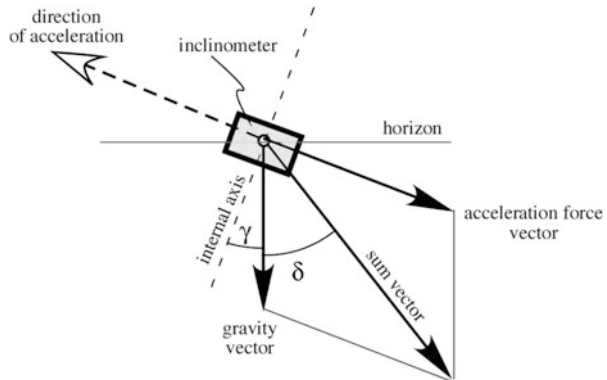
Inclination detectors are employed in ground and air-based vehicles, road construction, machine tools, inertial navigation systems, video monitors of mobile hand-held devices (to control orientation of an image), robots, electronic games, and other applications requiring a gravity reference.

Earth gravity is characterized by a constant force directed toward the Earth center and causing acceleration of  $1g \approx 9.8 \text{ m/s}^2$ . This value changes somewhat at different locations on the planet. One popular application of an accelerometer is sensing a gravity direction rather than measuring its magnitude. These special accelerometers are often called *inclinometers* or *tilt detectors*. According to the Einstein's theory of General Relativity, if we want to detect direction and magnitude of a gravitational force, an accelerometer is our sensor. Due to a relatively small value of the earth gravity, a tilt accelerometer does not need a broad span of the input signals, however, a practical device should be sensitive in all three axes and also have some additional features, like being able to respond to tapping and detect impacts resulted from dropping of the device. Thus, for a tilt accelerometer a minimum input span of  $2g$  should be sufficient. However, there is always a trade-off between the angular resolution and span.



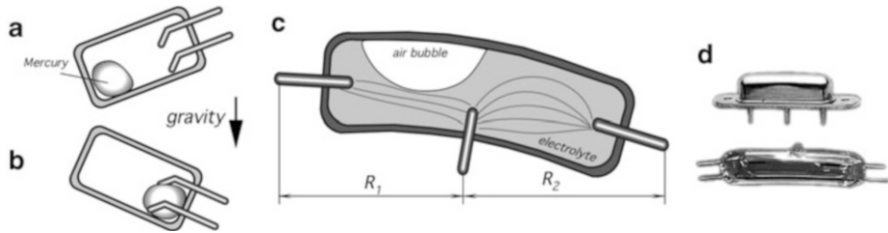
**Fig. 9.14** Sensing of smartphone orientation

**Fig. 9.15** Error of tilt accelerometer in accelerating vehicle



An example of a commercial tilt accelerometer is BMA220 from Bosch. It is very small ( $2 \times 2 \times 1$  mm), senses accelerations along all three axes, has a free-fall detection (zero gravity), and offers a high resolution [6]. An example of its application is shown in Fig. 9.14 where a smartphone is rotated around one axis resulting in the sinusoidal output of the accelerometer. A three-axial accelerometer responds with similar signals along each axis allowing a correct spatial detection.

When an inclinometer is positioned on an accelerating vehicle, it produces an erroneous signal because the response is a sum of two vectors—earth gravity and acceleration force as shown in Fig. 9.15. The inclinometer cannot tell them apart. In a stationary or steady moving vehicle, an inclinometer will measure angle  $\alpha$  between its own internal axis and the gravity vector. If the vehicle carrying the inclinometer accelerates, an acceleration force acting on the proof mass will appear in the opposite direction from the direction of motion. The two vectors, gravity and acceleration, will sum and the inclinometer will respond with an erroneous angle  $\delta$ .



**Fig. 9.16** Conductive gravitational sensors. Mercury switch in the open position (a) and closed (b) positions; electrolytic tilt sensor (c) and electrolytic sensor housings (d)

If only a low-resolution direction of the gravitational force is of interest, a simpler and cheaper tilt or inclination detector may be considered. A response of such a detector is not function of the gravity vector magnitude but only of its direction. The detector has its own internal axis with respect to which the gravity direction is measured. A response is an electric signal representative of an angle between the internal axis and the gravity vector. An old and still quite popular detector is a mercury switch, Fig. 9.16a, b. The switch is made of a non-conductive (often glass) tube having two electrical contacts and a drop of mercury. When the sensor is positioned with respect to the gravity force in such a way as the mercury slides away from the contacts, the switch is open. Tilting the switch causes the mercury drop to move to the contacts and touch both of them, thus closing the switch. One popular application of this design is in a household thermostat, where the mercury switch is mounted on a bimetal coil (see Fig. 4.38) that serves as an air temperature sensor. Winding or unwinding the coil in response to the room temperature affects the switch inclination. Opening and closing the switch controls a heating/cooling system. Since this tilt sensor is a threshold device, the obvious limitation is an on-off operation: a “bang-bang” controller in the engineering jargon.

To measure inclination with an infinitesimal resolution, a more complex sensor is required. One elegant design is shown in Fig. 9.16c. It is called the *electrolytic tilt sensor*. A small slightly curved glass tube is filled with partly conductive electrolyte. Three electrodes are built into the tube: two at the ends and the third electrode is at the center of the tube. An air bubble resides in the tube and may move along its length as the tube tilts. Electrical resistances between the center electrode and each of the end electrodes depend on position of the bubble. As the tube shifts away from the balance position, the resistances increase or decrease proportionally. The electrodes are connected into a bridge circuit which is excited by an a.c. current to avoid damage to the electrolyte and electrodes. The electrolytic tilt sensors are available<sup>3</sup> in different designs (Fig. 9.16d) for a wide spectrum of angular ranges from  $\pm 0.5^\circ$  to  $\pm 80^\circ$ . Correspondingly, the shapes of the glass tubes vary from slightly curved to doughnut-like.

<sup>3</sup>The Fredericks Company. P.O. Box 67, Huntingdon Valley, PA 19006.

### 9.3.3 Seismic Sensors

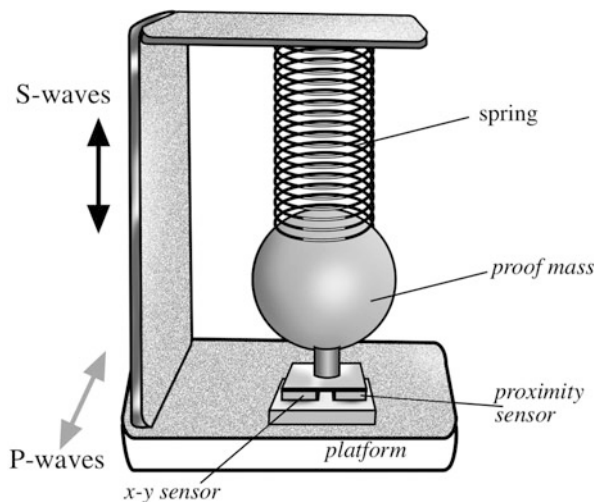
Earth masses (e.g., tectonic plates), due to their huge masses, are characterized by motions of very low frequencies in the infrasound range. Therefore, movements of ground are better represented by velocity rather than acceleration. Since *seismometers* or *seismographs* contain the same basic components as accelerometers (proof mass, springs, force sensors, dampers), we briefly review them here.

For measuring very slow earth movements, a seismic sensor shall be slow but very sensitive, thus it employs a large proof mass and a soft spring—see Eq. (9.19) for sensitivity. During measurements, position of the proof mass is considered fixed (due to a large inertia) while the platform, attached to the ground, moves. This kind of a sensor is used for detecting earthquakes and ground vibrations caused by human activities.

Earth movement is characterized by two kinds of soil displacements. The first are elastic longitudinal P-waves—horizontal shifts manifested by compression and rarefaction of soil when the soil density varies (similarly to sound waves). “P” stands for *primary* because due to its higher speed the wave arrives first from a remote earthquake. In the P-waves, the soil vibrates along the wave propagation direction. Other motions are the S-waves (“S” stands for *secondary*)—transverse displacements without change in soil density. They vibrate at a right angle to the direction of propagation. P-waves can travel through solids and liquid, whereas S-waves can travel only through solids.

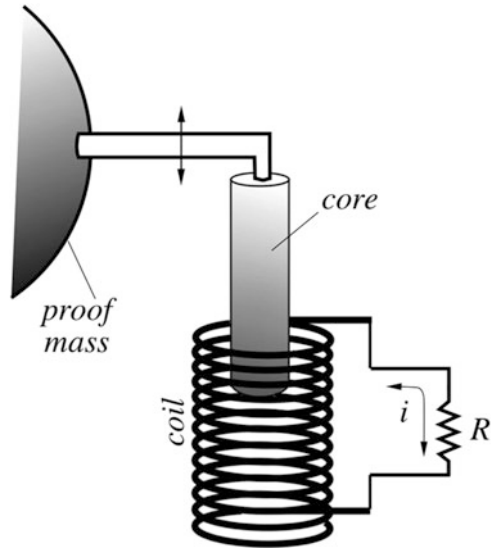
Therefore, depending on the wave type the sensing elements should be oriented at different directions. This is illustrated in Fig. 9.17 that is a concept of a pendulum-type seismometer. A large proof mass is supported by a soft spring and can move both vertically and horizontally, that is in the  $x$ - $y$ - $z$  directions, depending on motion of the platform that is solidly attached to ground. Two separate types of

**Fig. 9.17** Concept of a three-axial “pendulum” seismograph





**Fig. 9.18** Electromagnetic damper



transducers respond to different motions—an  $x$ - $y$  sensor responds to the P-waves, while a proximity sensor responds to the S-waves in a vertical direction. A great variety of displacement sensors may be employed for the purpose. We indicated above that seismometers measure ground velocity rather than acceleration, thus electromagnetic velocity transducers are often employed, such as shown in Fig. 9.2. Another type of a displacement transducer that is useful for seismometers is capacitive. For example,  $x$ - $y$  sensing can be successfully performed by a capacitive sensor similar to that shown in Fig. 8.12, while proximity may be detected also by a capacitive sensor that is conceptually shown in Fig. 8.8.

Like in an accelerometer, the seismograph has a very pronounced mechanical resonance that, if not damped, will register long spurious oscillations. A damping mechanism may be a viscous liquid (e.g., mineral oil), but the most efficient is an electromagnetic damper [7]. Its operating principle is based on moving a ferromagnetic core into a coil connected to a loss resistor (Fig. 9.18). The induced current flowing through a load resistor creates its own magnetic field that, according to Lenz law, counteracts the original magnetic field thus resisting motions of the core. This slows down the seismic mass and damps oscillations with the oscillation energy dissipating in the resistor in form of heat. Such a damper should be used for all sensed axes.

### 9.3.4 Capacitive Accelerometers

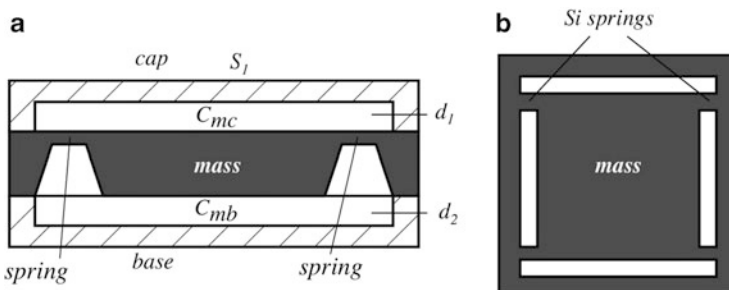
The conceptual design of a mechanical linear accelerometer (Fig. 9.12) can be implemented in a great variety of ways. Design options primarily are driven by selection of the type of a displacement sensor or transducer for monitoring shifts of the proof mass with respect to the housing.

A capacitive transducer is one of the proven and reliable elements that lends itself to microminiaturization, high accuracy, and low cost. The transducer essentially contains at least two conductors where the first one is anchored to the accelerometer housing, while the other is connected to the proof mass that moves inside the housing in response to acceleration. These conductors form a capacitor whose value is function of their overlapping area  $A$  and a mutual distance  $d$ —see Eq. (4.23). Depending on design, either the overlapping area or the distance may be made variable. A maximum proof mass displacement which typically is measured by the capacitive accelerometer rarely exceeds  $20\ \mu\text{m}$ . Hence, such a small displacement requires a reliable compensation of drifts and various interferences. This is usually accomplished by use of a differential technique, where an additional capacitor is formed in the same MEMS structure. A value of the second capacitor must be close to that of the first one, and it should be subjected an acceleration with a  $180^\circ$  phase shift. Then, acceleration can be represented by a difference in values between these two capacitors. See the concept in Fig. 8.8.

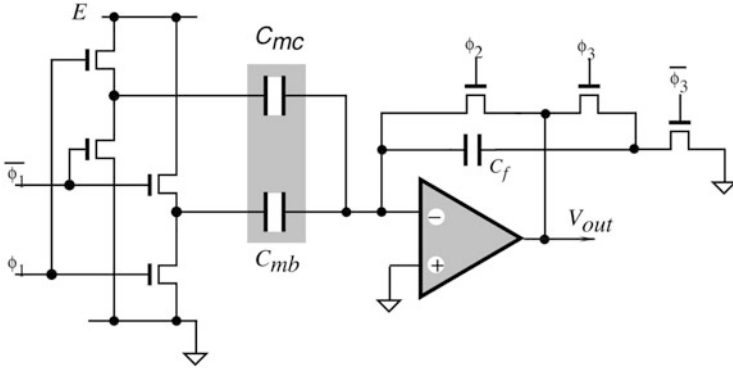
Figure 9.19a shows a cross-sectional diagram of a MEMS capacitive accelerometer where an internal mass is sandwiched between the upper cap and the base [8]. The mass is supported by four silicon springs (Fig. 9.19b). The upper plate and the base are separated from it by respective distances  $d_1$  and  $d_2$ . All three parts are micromachined from a silicon wafer. Note that there is no damper. Figure 9.20 is a simplified circuit diagram for a capacitance-to-voltage converter that in many respects is similar to the circuit of Fig. 6.11.

A parallel plate capacitor  $C_{mc}$  between the mass and the cap electrodes has a plate area  $S_1$ . The plate spacing  $d_1$  can be reduced by an amount  $\Delta$  when the mass moves toward the upper plate. A second capacitor  $C_{mb}$  having a different plate area  $S_2$  appears between the mass and the base. When mass moves toward the upper plate and away from the base, the spacing  $d_2$  increases by  $\Delta$ . The value of  $\Delta$  is equal to the mechanical force  $F_m$  acting on the mass divided by the spring constant  $k$  of the silicon springs:

$$\Delta = \frac{F_m}{k}. \quad (9.27)$$



**Fig. 9.19** Capacitive accelerometer with a differential capacitor side cross-sectional view (a); top view of a seismic mass supported by four silicon springs (b)



**Fig. 9.20** Circuit diagram of capacitance-to-voltage conversion suitable for integration on silicon

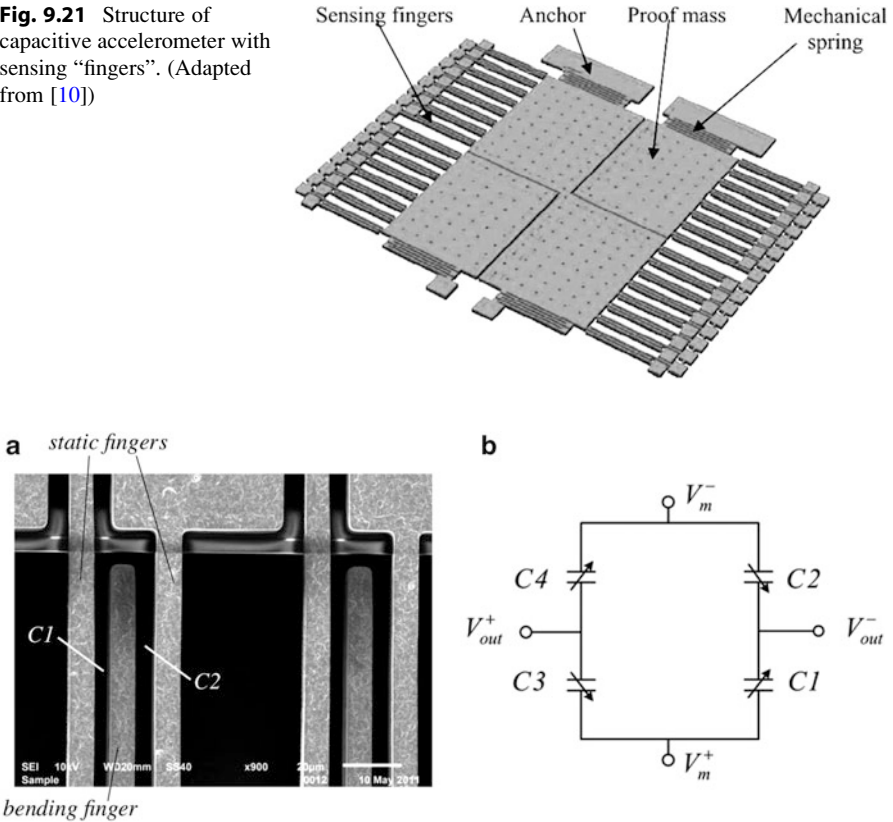
Strictly speaking, the accelerometer equivalent circuit is valid only when electrostatic forces do not affect the mass position, that is, when the capacitors depend linearly on  $F_m$  [9]. When accelerometer capacitors are applied to a switched-capacitor summing amplifier, the output voltage depends on value of the capacitors, and subsequently on the force:

$$V_{out} = 2E \frac{C_{mc} - C_{mb}}{C_f}. \tag{9.28}$$

The above equation is true for small changes in the sensor’s capacitances. The accelerometer output is also a function of temperature and a capacitive mismatch. It is advisable that it be calibrated over the entire temperature range and appropriate corrections are made during the signal processing. Another effective method of assuring high stability is to design self-calibrating systems which make use of the electrostatic forces appearing in the accelerometer assembly when voltage is applied to either a cap or a base electrode.

Figure 9.21 illustrates design of an advanced accelerometer where the proof mass displacement is measured by capacitive “fingers” [10] that slide with respect to one another and thus modulate the overlapping area. The overall capacitance is proportional to the number of the narrow fingers. The proof mass is separated into four sections where each is supported by the individual serpentine spring and connected to its own set of the capacitive fingers. When the proof mass moves, the bending fingers shift as shown in Fig. 9.22a. The overlapping area changes, thus modulating the respective capacitances. The structure forms four sets of the sensing capacitors that are connected into the bridge circuit as shown in Fig. 9.22b. Each set of the capacitors has sensitivity of about 1.6 fF/g.

**Fig. 9.21** Structure of capacitive accelerometer with sensing “fingers”. (Adapted from [10])



**Fig. 9.22** Downward bending of fingers modulates capacitances C1 and C2 (a); capacitive bridge (b)

### 9.3.5 Piezoresistive Accelerometers

As a sensing element a piezoresistive accelerometer incorporates strain gauges that measure strain in the mass-supporting springs. The strain can be directly correlated with the magnitude and rate of the mass displacement and, subsequently, with an acceleration. These devices can sense accelerations within a broad frequency range: from near d.c. up to 13 kHz. With a proper design, they can withstand overshock up to 10,000  $g$ . Naturally, a dynamic range (span) is somewhat narrower (1000  $g$  with error less than 1 %). The overshock is a critical specification for many applications. Piezoresistive accelerometers with discrete, epoxy-bonded strain gauges tend to have undesirable output temperature coefficients. Since they are manufactured separately, the gauges require individual thermal testing and parameter matching. This difficulty is virtually eliminated in modern sensors that use MEMS technology of the silicon wafers. The concept of a piezoresistive Si strain gauge that monitors deflection of a proof mass is given in Fig. 8.6.

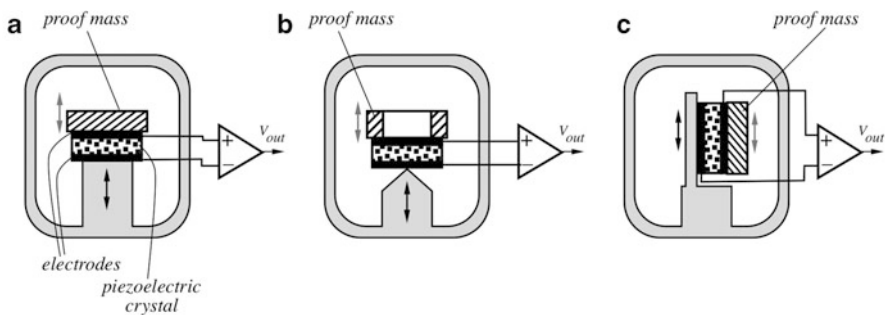
### 9.3.6 Piezoelectric Accelerometers

The piezoelectric effect (do not confuse it with a piezoresistive effect!) has a natural application in sensing vibration and acceleration. The effect allows a direct conversion of mechanical energy into electrical (see Sect. 4.6). These sensors operate from frequency as low as 2 Hz and up to about 5 kHz, they possess good off-axis noise rejection, high linearity, and a wide operating temperature range (up to 120 °C). While quartz crystals are occasionally used as sensing elements, the most popular are the ceramic piezoelectric materials, such as barium titanate, lead zirconite titanate (PZT), and lead metaniobite. A piezoelectric crystal is sandwiched between the supporting structure and proof mass which exerts on it a force proportional to acceleration. In these sensors, a proof mass is directly coupled to the piezoelectric crystal with no intermediate springs. The crystal itself acts as a spring, thus due to its rather high stiffness, a natural frequency of the sensor is high—typically over 2 kHz [11].

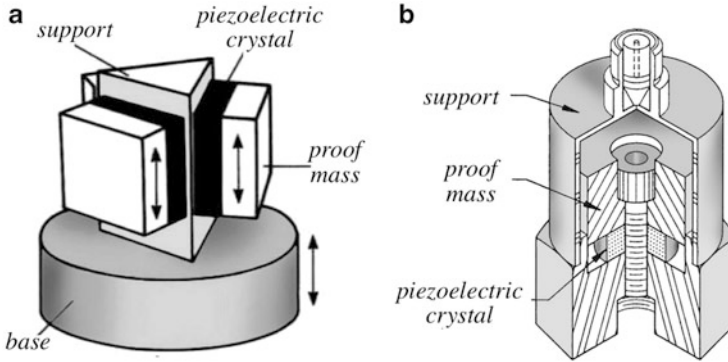
There are several possible variations for mounting the crystal and proof mass on the accelerometer housing, some of which are shown in Fig. 9.23. In the compression coupling, the crystal is sandwiched between a vibrating base and proof mass (a). The flexural coupling causes the crystal to bend around a central support pin (b), while the shear coupling causes the piezoelectric dipoles in the crystal to tilt under influence of a shearing force (c). All these mechanical strains develop electric charges across the piezoelectric crystal.

As in any piezoelectric sensor, the crystal is given two thin electrodes for picking up electric charges (see Fig. 4.22). Since a piezoelectric sensor essentially is a charge generator with extremely high output impedance, for assuring a broad frequency response, the interface electronic circuit shall use a front stage in form of a charge-to-voltage converter that conceptually is shown in Fig. 6.6c.

Two practical accelerometer designs are shown in Fig. 9.24. The first uses a shearing mounting of the proof mass [11], while the second employs compression of the crystal.



**Fig. 9.23** Piezoelectric accelerometer options. Compression coupling (a), flexural coupling (b), and shear coupling (c)



**Fig. 9.24** Brüel and Kjær Delta Shear piezoelectric accelerometer (a) and compression-type piezoelectric accelerometer with PZT ceramic crystal (b)

In miniature piezoelectric accelerometers, a silicon support structure is usually employed. Since silicon does not possess piezoelectric properties, a thin film of lead titanate can be deposited on a micromachined silicon cantilever to fabricate an integral miniature sensor.

### 9.3.7 Thermal Accelerometers

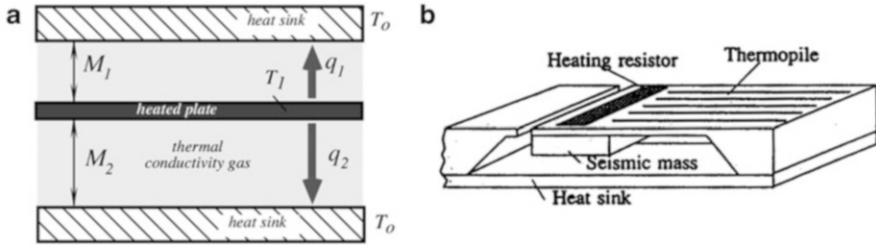
#### 9.3.7.1 Heated Plate Accelerometer

A heated plate accelerometer, as any accelerometer, contains a proof mass that is suspended by a thin cantilever and positioned in close proximity with a heat sink, or between two heat sinks, Fig. 9.25a [12]. The seismic mass and the cantilever structure are fabricated by using a MEMS technology. The space between these components is filled with a thermally conductive gas. The seismic mass is heated by a surface-deposited or imbedded heater to a defined temperature  $T_1$ . Since the basic idea behind any accelerometer is measurement of a displacement of a seismic (proof) mass, a fundamental formula for a conductive heat transfer can be used for computing motions of the heated seismic mass (see Eq. 4.121).

Under the no-acceleration conditions, a thermal equilibrium is established between the mass and heat sinks: the amounts of heat  $q_1$  and  $q_2$  conducted to the heat sinks through gas from the seismic mass is function of distances  $M_1$  and  $M_2$ .

The temperature at any point  $x$  in the cantilever beam supporting the seismic mass<sup>4</sup> depends on its distance from the support  $x$  and the gaps at the heat sinks. It can be found from

<sup>4</sup> Here we assume steady-state conditions and neglect radiative and convective heat transfers.



**Fig. 9.25** Thermal accelerometer. Cross-section of heated part (a); accelerometer design shown without roof (b) (adapted from [12])

$$\frac{d^2T}{dx^2} - \lambda^2 T = 0, \tag{9.29}$$

where constant  $\lambda = \sqrt{\frac{K_g(M_1+M_2)}{K_{si}DM_1M_2}}$ ,  $K_g$  and  $K_{si}$  being thermal conductivities of gas and silicon respectively, and  $D$  is the thickness of a cantilever beam. For boundary conditions, where the heat sink temperature is 0, a solution of the above equation for temperature of the beam is

$$T(x) = \frac{P \sinh(\lambda x)}{W D K_{si} \lambda \cosh(\lambda L)}, \tag{9.30}$$

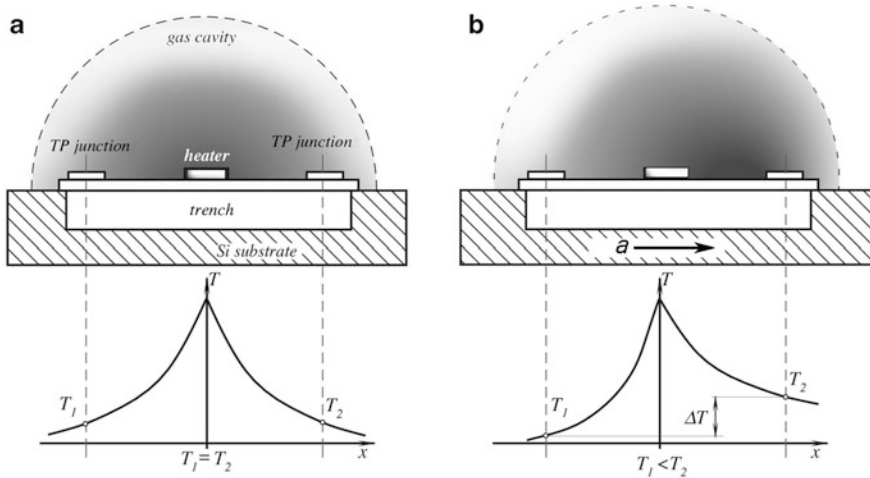
where  $W$  and  $L$  is the width and length of the beam respectively, and  $P$  is the thermal power. To measure that temperature, a temperature sensor can be deposited on the beam. It can be done by integrating silicone diodes into the beam,<sup>5</sup> or by forming serially connected thermocouples (a thermopile) on the beam surface. Eventually, the measured beam temperature in form of an electrical signal is the measure of acceleration. Sensitivity of a heated plate accelerometer (about 1 % of change in the output signal per  $g$ ) is somewhat smaller than that of a capacitive or piezoelectric type, however, it is much less susceptible to such interferences as ambient temperature or electromagnetic and electrostatic noise.

**9.3.7.2 Heated Gas Accelerometer**

Unlike the heated plate accelerometer that uses a *conductive* heat transfer through gas, the heated gas accelerometer (HGA) employs a *convective* heat transfer of heated gas molecules within a sealed cavity.

Heat can be transferred by conduction, convection, and radiation (see Chap. 4). Convection of fluids (liquids or gases) can be either natural, that is, caused by gravity, or forced, arising from an external force, like that produced by e.g., a blower. The HGA accelerometer is fabricated on a micromachined CMOS chip and is a complete biaxial measurement system. The proof mass in this sensor is gas,

<sup>5</sup> See Sect. 17.6 for a description of a Si diode as a temperature sensor.



**Fig. 9.26** Cross-sectional view of HGA sensor along  $x$ -axis (a). Heated gas is symmetrical around the heater (b). Acceleration causes heated gas to shift to right, resulting in temperature gradient

being thermally nonhomogeneous within the sealed cavity. The force that causes the gas convection within the cavity is produced by acceleration. The embedded temperature sensors measure the internal changes in the trapped gas and thermal gradients within the gas make the accelerometer to function.

The sensor contains a micromachined plate adjacent to a sealed cavity filled with gas (Fig. 9.26). The plate is positioned above the etched cavity (trench). A single heat source, centered in the silicon chip, is suspended across the trench. Equally spaced are four temperature sensors (two along the  $x$ -axis and two along the  $y$ -axis) that are the aluminum/polysilicon thermopile (TP) junctions. A thermopile is a set of the serially connected thermocouples. These temperature sensors are located equidistantly on all four sides of the heat source (dual axis). Note that a TP measures only a temperature difference so that the left and right thermopile junctions in fact are a single TP where the left side holds the “cold” junctions while the right side is for the “hot” junctions (see Sect. 17.8 for the operating principle of a thermocouple). A reason for using a thermopile instead of a thermocouple is for a sole purpose—to increase a magnitude of the electrical output signal. Another pair of the TP junctions is for measuring a thermal gradient along the  $y$ -axis.

Under a zero acceleration, a temperature distribution across the gas cavity is symmetrical about the heat source, so that the temperature is the same at all four TP junctions, causing each pair to output a zero voltage. The heater is warmed to a temperature that is well above ambient and typically is near  $200^\circ\text{C}$ . Figure 9.26a shows two TP junctions (TP) sensing a temperature gradient along a single axis. Gas is heated so that it is hottest near the heater and rapidly cools down toward the left and right temperature sensors (the junctions).



When no force acts on gas, temperature has a symmetrical cone-like distribution around the heater, where temperature  $T_1$  at the left junction is equal to temperature  $T_2$  of the right junction. Since cooler gas is denser and more massive, acceleration of the housing in any direction will move gas inside the cavity. A motion disturbs the temperature profile due to a convection heat transfer, causing it to be asymmetrical. Figure 9.26b shows acceleration  $a$  in a direction of the arrow. Under the acceleration force, cooler gaseous molecules lag behind while the warm molecules shift toward the right TP junction and transfer to it a portion of their thermal energy. The temperature, and hence voltage output of the opposite TP junctions will then be different so that  $T_1 < T_2$ . The differential temperature  $\Delta T$  and voltage at the thermopile outputs becomes nearly proportional to the acceleration. There are two identical acceleration signal paths on the device, one to measure acceleration in the  $x$ -axis and one to measure acceleration in the  $y$ -axis. A typical noise floor from the TP sensors is below 1 mg/Hz, allowing the submilli-g signals<sup>6</sup> to be measured at very low frequencies.

This technology has a number of interesting properties:

1. There are no moving parts—the “proof mass” in this accelerometer consists of molecules of gas.
2. The accelerometer exhibits no detectable natural frequency, which makes it virtually immune to out-of-band vibration and shock.
3. An HGA is robust and reliable, providing shock tolerance of 50,000  $g$  (nearly an order of magnitude greater than many capacitive or piezoresistive devices).
4. The HGAs have good zero- $g$  offset stability with time and temperature, and have virtually undetectable thermal hysteresis (an effect that is commonly experienced with many other accelerometer types, limiting their ability to measure small accelerations or tilt angles).
5. The HGA can measure both the dynamic acceleration (e.g., vibration) and static acceleration (e.g., gravity).
6. Another advantage of HGA accelerometers is a low cost and small size. For example, the device MXC6226XC produced by Memscic, Inc. has dimensions  $1.7 \times 1.2 \times 1.0$  mm and incorporates a signal conditioner with the I<sup>2</sup>C serial digital output with the interrupt pin [13, 14].
7. A noticeable limitation of the HGA is a relatively narrow frequency response. A typical  $-3$  dB roll-off occurs at above 30 Hz. However, a great majority of consumer applications (smartphones, toys, video cameras, etc.) does not require a faster response beyond this limit. Note that the maximum operating frequency is limited not by a resonance, as in the mechanical accelerometers, but by the inertia of gas molecules.

---

<sup>6</sup> In terms of an angular rotation, 1 mg (milli-g) corresponds to approximately  $0.06^\circ$  of inclination.

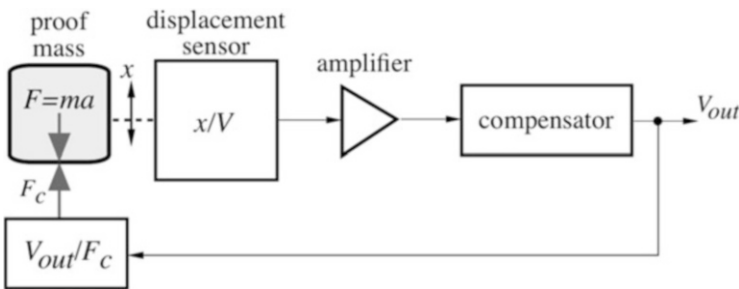
### 9.3.8 Closed-Loop Accelerometers

All accelerometers that we discussed above belong to the class of open-loop devices. For increasing a dynamic range, improving linearity and temperature stability, and reducing other interfering factors, it is desirable to minimize deflection of the proof mass from its neutral position (no acceleration) [15]. This can be achieved by providing a mechanical feedback to the proof mass. The similar idea was discussed in Sect. 6.1.8 for a closed-loop capacitance-to-voltage converter.

The idea behind a feedback (closed-loop) accelerometer is in applying a compensating force to a proof mass to keep it from shifting from the neutral position. Figure 9.27 illustrates the concept.

Position of the proof mass is sensed and converted into a voltage that is amplified for controlling the compensating circuit that produces the output signal that serves as a feedback. The important component of the accelerometer is a voltage-to-force transducer that applies a feedback force to the proof mass for opposing the accelerating input force. Consequently, the proof mass is only being deflected by the difference between these two forces that can be considered as the error signal. That error controls the PID<sup>7</sup> feedback loop. Some sort of a stabilizer may be required in the compensator to ensure stability of the loop.

In a closed-loop accelerometer, the sensitivity  $S$  is not inversely proportional to the square of the natural frequency  $f_0$  of the sensing element, see Eq. (9.19), but depends on the loop gain and the form of a compensation. Another advantage is that possible nonlinearities of the spring and damping are reduced considerably since the proof mass stays close to its neutral position. Furthermore, the bandwidth of the accelerometer can be increased past the natural frequency of the assembly. In many closed-loop accelerometers, feedback forces are commonly generated by electromagnetic transducers. However, in the MEMS devices, the dimensions are so small that electromagnetic transducer is not practical, thus the electrostatic forces can be used instead to provide the feedback. This has the advantage of lower power



**Fig. 9.27** Block diagram of closed-loop accelerometer

<sup>7</sup>Term PID means “*proportional-integral-differential*” to indicate type of a feedback control.

consumption and overcomes the problems of manufacturing micromachined inductors. The drawback of the electrostatic feedback is that the forces are proportional to the square of the potential difference between the plates [see Eq. (6.13)], hence they are always positive. As a result, negative feedback is difficult to generate. For this reason the electrostatically generated feedback relationship is nonlinear.

---

## References

1. Park, S., et al. (2009). Oscillation control algorithms for resonant sensors with applications to vibratory gyroscopes. *Sensors*, 9, 5952–5967.
2. Fox, C. H. J., et al. (1984). *Vibratory gyrosopic sensors*. Symposium Gyro Technology (DGON).
3. Udd, E. (1991). Fiber optic sensors based on the Sagnac interferometer and passive ring resonator. In E. Udd (Ed.), *Fiber optic sensors* (pp. 233–269). New York: John Wiley & Sons.
4. Ezekiel, S., & Arditty, H. J. (Eds.). (1982). *Fiber-optic rotation sensors* (Springer series in optical sciences, Vol. 32). New York: Springer.
5. Fredericks, R. J., et al. (1984). Phase error bounds of fiber gyro with imperfect polarizer/depolarizer. *Electronics Letters*, 29, 330.
6. BMA220 Data sheet (2011). *Bosch Sensortec GmbH*.
7. Havskov, J., et al. (2004). *Instrumentation in earthquake seismology*. New York: Springer.
8. Sensor signal conditioning: An IC designer's perspective. (1991, November). *Sensors*, 23–30.
9. Allen, H., et al. (1989). Accelerometer system with self-testable features. *Sensors and Actuators*, 20, 153–161.
10. Qu, P., et al. (2013). Design and characterization of a fully differential MEMS accelerometer fabricated using MetalMUMPs technology. *Sensors*, 13, 5720–5736.
11. Senldge, M., et al. (1987). *Piezoelectric accelerometers and vibration preamplifiers*. Copenhagen, Denmark: Brüel & Kjær.
12. Haritsuka, R., et al. (1991). A novel accelerometer based on a silicon thermopile. In: *Transducers'91. International conference on solid-state sensors and actuators. Digest of technical papers* (pp. 420–423). ©IEEE.
13. Fennelly, J., et al. (2012, March). Thermal MEMS accelerometers fit many applications. *Sensor Magazine*. [www.sensormagazin.de](http://www.sensormagazin.de)
14. Ultra Low Cost Accelerometer MXC6226XC Data Sheet. (2010). Memsic, Inc. [www.memsic.com](http://www.memsic.com)
15. Dong, Y., et al. (2006). Force feedback linearization for higher-order electromechanical sigma-delta modulators. *Journal of Micromechanics and Microengineering*, 16, S54–S60.

*Engineering is art of converting science into useful things*

## 10.1 Basic Considerations

While the kinematics study positions of objects and their motions, the dynamics answers the question—what causes motion? Classical mechanics deal with moving objects whose velocities are substantially smaller than the speed of light. Moving particles, such as photons, atoms, and electrons, or, on the other side of the scale—planets and stars—are subjects of other branches of physics—quantum mechanics and the theory of relativity. A typical problem of classical mechanics is the question: “*What is motion of an object that initially had a given mass, charge, dipole moment, position, etc. and was subjected to external objects having known mass, charge, velocity, etc.?*” That is, classical mechanics deals with interactions of macro-objects. In a general form, this problem was solved by Sir Isaac Newton (1642–1727) who was born in the year when Galileo died. He brilliantly developed ideas of Galileo and other great mechanics. Newton stated his *First Law* as: “*Every body persists in its state of rest or of uniform motion in a straight line unless it is compelled to change that state by forces impressed on it.*” Sometimes, this is called a law of inertia. Another way to state the first law is to say that: “*If no net force acts on a body, its acceleration is zero.*”

When force is applied to a free body (not anchored to another body), it gives the body an acceleration in direction of the force. Thus, we can define force as a vector value. Newton had found that vector of acceleration  $\mathbf{a}$  is proportional to the acting force  $\mathbf{F}$  and inversely proportional to the property of a body called the mass  $m$  which is a scalar value:

$$\mathbf{a} = \frac{\mathbf{F}}{m}. \quad (10.1)$$

**Table 10.1** Mechanical units (bold face indicates the base units)

System of units	Force	Mass	Acceleration
SI	newton (N)	<b>kilogram</b> (kg)	m/s <sup>2</sup>
British	<b>pound</b> (lb)	slug	ft/s <sup>2</sup>

This equation is known as Newton's *Second Law*—the name given by the great Swiss mathematician and physicist Leonhard Euler in 1752, 65 years after the publication of Newton's *Principia* [1]. The First Law is contained in the second law as a special case: when the net acting force  $\mathbf{F} = 0$ , acceleration  $\mathbf{a} = 0$ .

Newton's second law allows us to establish the mechanical units. In SI terms, mass (kg), length (m), and time (s) are the *base* units (see Table 1.6). Force and acceleration are *derivative* units. The force unit is the force, which will accelerate 1 kg mass to acceleration 1 m/s<sup>2</sup>. This unit is called a *newton*.

In the British and US Customary systems of units, however, force (lb), length (ft), and time (s) were selected as the base units. The mass unit is defined as the mass which is accelerated at 1 ft/s<sup>2</sup> when it is subjected to force of 1 lb. The British unit of mass is *slug*. Hence, the mechanical units are as shown in Table 10.1.

Newton's *Third Law* establishes a principle of a mutual interaction between two bodies:

*“To every action there is always opposed an equal reaction; or, the mutual actions of two bodies upon each other are always equal, and directed to contrary parts.”*

The SI unit of force is one of the fundamental quantities of physics. The measurement of force is required in mechanical and civil engineering, for weighing objects, designing prosthesis, etc. Whenever pressure is measured, it requires the measurement of force. It could be said that force is measured when dealing with solids, while pressure—when dealing with fluids (i.e., liquids or gases). That is, *force is considered when action is applied to a spot, and pressure is measured when force is distributed over a relatively large area.*

Force sensors can be divided into two classes: quantitative and qualitative. A quantitative sensor actually measures the force and represents its value in terms of an electrical signal. Examples of these sensors are strain gauges and load cells being used together with the appropriate interface circuits. The qualitative sensors are the *threshold* devices that are not concerned with a good fidelity of representation of the force value. Their function is merely to indicate whether a sufficiently strong force is applied or not. That is, the output signal indicates when the force magnitude exceeds a predetermined threshold level. An example of these detectors is a computer keyboard where a key makes a contact only when it is pressed sufficiently hard. The qualitative force sensors are frequently used for detection of motion and position. A pressure-sensitive floor mat of a security system and a piezoelectric cable in a pavement are examples of the qualitative force sensors.

The various methods of sensing force can be categorized as follows [2]:

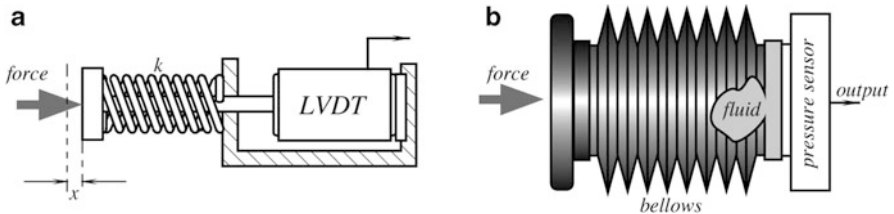
1. By balancing the unknown force against the gravitational force of a standard mass.
2. By measuring the acceleration of a known mass to which the force is applied.
3. By balancing the force against an electromagnetically developed force.
4. By converting the force to a fluid pressure and measuring that pressure.
5. By measuring the strain produced in an elastic member by the unknown force.

Method 1 is a classical balancing beam scale for weighing goods. It consisted of a fulcrum or pivot and a lever with the unknown weight placed on one end of the lever, and a counterweight applied to the other end. However, this scale is not a sensor as it does not output electrical signal. In modern sensors, the most commonly used method is 5, while 3 and 4 are used occasionally.

In many sensors, force is developed in response to some stimulus (an accelerometer is an example). That force is not directly converted into an electric signal, thus some additional steps are usually required. A typical force sensor is a combination of a force-to-displacement transducer and displacement sensor that converts displacement to electrical output. The former may be a simple coil spring, whose compression displacement  $x$  can be defined through the spring coefficient  $k$  and compressing force  $F$  as

$$x = kF \quad (10.2)$$

Spring scales were introduced in the 1760s as a more compact alternative to the popular steelyard balance. In a sensor, the spring is augmented with a displacement-to-electricity transducer. The sensor shown in Fig. 10.1a is comprised of a spring and LVDT displacement sensor (Sect. 8.4.1). Within a linear range of the spring, the LVDT sensor produces voltage that is proportional to the applied force. A similar sensor can be constructed with other types of springs and pressure sensors, such as the one shown in Fig. 10.1b where a pressure sensor is combined with a fluid-filled bellows which is subjected to force. The bellows functions as a force-to-pressure converter (transducer) by distributing a localized force at its input over the sensing membrane of a pressure sensor, that, in turn, comprises another displacement transducer for converting the membrane motion to an electrical output.



**Fig. 10.1** Spring-based force sensor with LVDT (a); force sensor incorporating bellows and pressure sensor (b)

In summary, a typical force sensor combines a resilient element (spring, polymer lattice, silicon cantilever, etc.) and a gauge for measuring the degree of the element compression or strain for the purpose of converting it to electrical output signal. The force sensors are integral parts of the pressure, tactile, and acceleration sensors that are covered in the relevant chapters of this book.

Depending on the applications, configurations, and force ranges, various force sensors are known under different names, such as microforce sensor, compression sensor, load cell, and so on. Yet, regardless what the name is—they all are variations of the basic force sensor.

## 10.2 Strain Gauges

When force is applied to a compressible resilient component, the component is deformed or strained. The degree of strain (deformation) can be used as measure of displacement under influence of force. Thus, a strain gauge serves as a transducer that measures a displacement of one section of a deformable component with respect to its other part. A strain gauge shall be either embedded directly into a resilient component (spring, beam, cantilever, conductive elastomer, etc.) or intimately adhered to one or more of its outside surfaces, so the strain gauge will deform together with the component when force acts upon it.

Strain is deformation of a physical body under action of the applied forces. Several physical effects can be used for measuring strain. Among them are the optical [3], piezoelectric [4], and capacitive [5], but by far the most popular are piezoresistive.

A typical piezoresistive strain gauge is an elastic sensor whose resistance is function of the applied strain (unit deformation). Since all materials resist to deformation, some force must be applied to cause deformation. Hence, electrical resistance can be related to the applied force. That relationship is generally called the piezoresistive effect (see Sect. 4.5.3) and is expressed through the gauge factor  $S_e$  of the conductor, Eq. (4.63):

$$\frac{dR}{R} = S_e e, \quad (10.3)$$

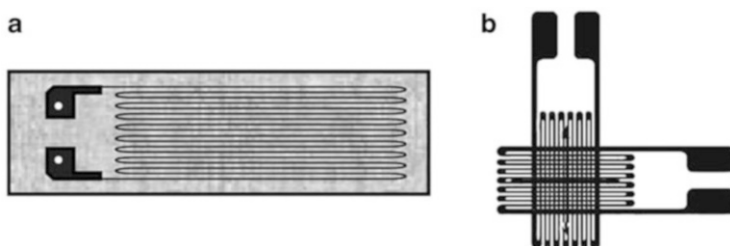
For many materials  $S_e \approx 2$  with the exception of platinum for which  $S_e \approx 6$  [6]. For small variations in resistance not exceeding 2 % (which is usually the case), the resistance of a metallic wire can be approximated by a linear equation:

$$R = R_o(1 + x) = R_o(1 + S_e e), \quad (10.4)$$

where  $R_o$  is the resistance with no stress applied. For semiconductive materials, the relationship depends on the doping concentration, Fig. 19.2a. Resistance decreases with compression and increases with tension. Characteristics of some resistive strain gauges are given in Table 10.2.

**Table 10.2** Characteristics of some resistance strain gauges (after [8])

Material	Gauge factor ( $S_e$ )	Resistance ( $\Omega$ )	TCR ( $^{\circ}\text{C}^{-1}\cdot 10^{-6}$ )	Notes
57 % Cu–43 % Ni	2.0	100	10.8	$S_e$ is constant over wide range of strain. For use under $260^{\circ}\text{C}$
Platinum alloys	4.0–6.0	50	2160	For high temperature use
Silicon	–100 to +150	200	90,000	High sensitivity, good for large strain measurements

**Fig. 10.2** Wire strain gauge bonded to elastic backing (a) and biaxial strain gauge (b)

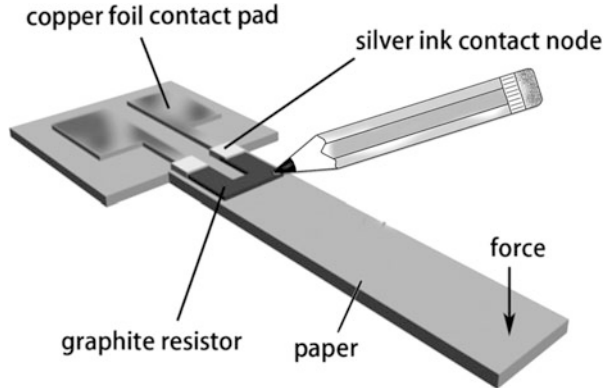
A wire strain gauge is composed of a thin wire bonded with an elastic carrier (backing). The backing, in turn, is applied (glued) to the object where strain is to be measured. Obviously, that strain from the object must be reliably coupled to the gauge wire, while the wire must be electrically isolated from the object. The coefficient of thermal expansion of the backing should be matched to that of the wire. Many metals can be used for making wire strain gauges. The most common materials are alloys *constantan*, *nichrome*, *advance*, and *karma*. Typical nominal resistances vary from 100 to several thousand ohms [7]. To possess good sensitivity, the sensor should have long longitudinal and short transverse segments, Fig. 10.2a, so that transverse sensitivity is no more than a couple of percent of the longitudinal. The gauges may be arranged in many ways to measure strains in different axes. As an example, Fig. 10.2b illustrates a biaxial strain gauge. Typically, the resistive strain gauges are connected into Wheatstone bridge circuits (Sect. 6.2.3).

For the semiconductive strain gauges see Sect. 8.2. It should be noted that semiconductive strain gauges are quite sensitive to temperature variations. Therefore, interface circuits or the gauges must contain temperature compensating networks.

Some soft materials of relatively low conductivity can be used to fabricate thin-film piezoresistive strain gauges for measuring the applied forces. One such material is graphite. A simple test project to fabricate super-low cost strain gauges can demonstrate the concept [9]. A quick-and-easy strain-sensitive resistor can be drawn by a pencil on paper (Fig. 10.3). A pencil of any shade of blackness is



**Fig. 10.3** Graphite strain strain-sensitive resistor can be drawn on paper by pencil

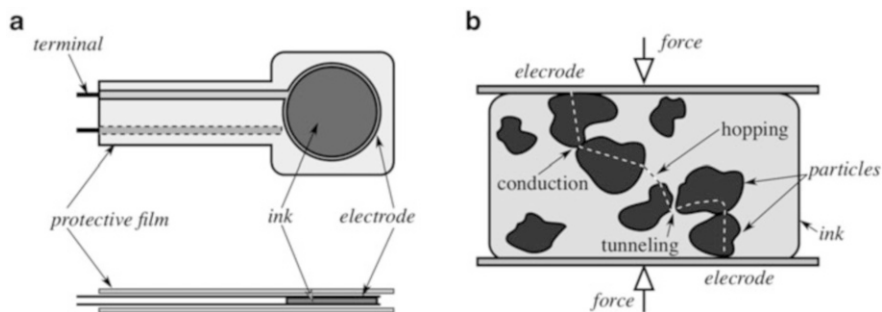


composed of mixture of clay and amorphous graphite in form of very fine flakes. A graphite resistor of any shape can be drawn on a sheet of paper that is cut into a desirable form. Soft pencils (B2 type, for example) with higher concentration of graphite should be used to draw the piezoresistive gauge line. Silver ink or conductive epoxy electrically connect the ends of the gauge line to two copper foil pads for soldering to wires and connecting to the bridge circuit. When paper is flexed by the applied force, the graphite flakes slide with respect to one another, changing the mutual contact areas and subsequently modulating the gauge resistance. A practical resistance of the gauge is about  $500\ \Omega$  with the maximum change in resistance, when flexed, as large as 15 %. The paper backing can be glued to an external beam or cantilever for measuring its strain. Since a manual drawing of the gauge is hardly accurate or consistent, before use such primitive strain gauge together with the interface circuit shall be calibrated.

### 10.3 Pressure-Sensitive Films

Thin- and thick-film sensors, thanks to their very small thickness, flexibility, variable sizes, and low cost are useful for measuring forces in very tight spaces. Due to their unique properties, they often are used as tactile sensors. Their designs and use are similar to the FSR sensors described in Sect. 7.13.3. A typical thick-film sensor consists of five layers: the top and bottom protective films, printed pressure-sensitive film and two electrodes terminals, as shown in Fig. 10.4.

The key component of the thick-film force sensor is a pressure-sensitive layer produced by screen printing the piezoresistive ink with a predefined pattern. The ink is printed as thick films having thickness from 10 to 40  $\mu\text{m}$ . The printed ink is dried at 150  $^{\circ}\text{C}$  and then sintered at temperatures ranging from 700 to 900  $^{\circ}\text{C}$ . The ink is a solution of small submicron particles of various metal oxides, such as  $\text{PbO}$ ,  $\text{B}_2\text{O}_2$ ,  $\text{RuO}_2$  and others, in concentrations varying from 5 to 60 %. Sintering makes grains of conductive and insulating oxides to bind together and give them cohesion



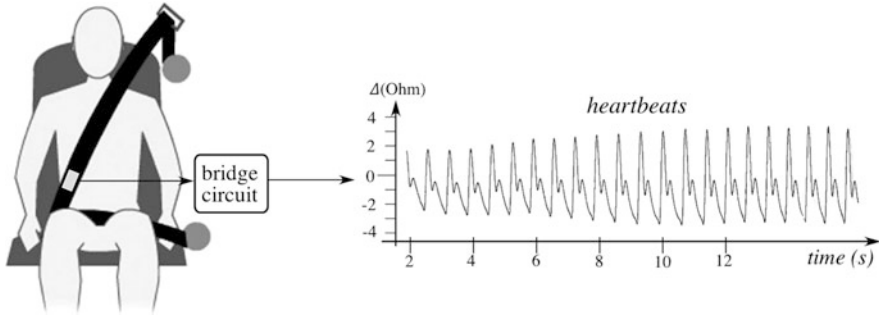
**Fig. 10.4** Composition of thin-film pressure sensor (a) and operating concept of pressure-sensitive ink (b)

and strength. The sintered ink has a large gauge factor, up to ten times more than of metals and is more temperature stable than the semiconductive gauges [10].

The mechanism of converting force to resistance is illustrated in Fig. 10.4b. There are three possible mechanisms to explain while increase in pressure causes increase in the film conductivity. They are the conductivity, electron hopping, and tunneling effect. There are two different types of oxides in the ink—conductive and insulating. The applied pressure causes more conductive particles to touch and form conductive paths. A temperature related tunneling effect appears when the grains (particles) come very close to each other (on the order of 1 nm), while the electron hopping appears when distances between the particles are about 10 nm.

The sensor is essentially a resistor whose conductivity varies linearly vs. applied force. With no force is applied, the resistance is on the order of Megohms (conductivity is very low). As applied force rises, the sensor resistance drops, eventually reaching about 10 k $\Omega$  or lower (conductivity goes up), depending on the ink and geometry. The output, expressed in conductance vs. force, is quite linear (the linearity error typically is less than  $\pm 3\%$ ) as shown in Fig. 7.50b. External circuitry for converting the film conductivity into a linear analog voltage can be relatively simple – one possible design is shown in Fig. 7.51a. These sensors can be fabricated in custom form factors for a great variety of applications. Since sensitivity of the printed ink sensors is quite high, they can register a light touch of only 5 g; however, to enter a relatively linear region, the pressure-sensitive film should be compressed along of at least 80 % of the sensing area with 40 g or more of a bias force.

To illustrate one of the many applications of the thick-film sensors, Fig. 10.5 shows a car safety belt where the film force sensor is positioned on the belt across the belly of a driver. Respiratory and heart failure are conditions that can occur with little warning while driving. To generate an alarm and perhaps even force the vehicle to stop, should the driver experiences an adverse health event, the belt, at least under the laboratory condition, continuously provides signals of a heart rate and respiration [11]. Each heartbeat and each inhale-exhale cause small but measurable tension variation of the safety belt. These tensions result in compressions of the film force sensor whose resistance changes by several ohms—small but



**Fig. 10.5** Thick-film force sensor positioned on safety belt generates patterns corresponding to driver's heartbeats

measurable deviations. With use of a pattern recognition software, it is possible to discriminate the cardiac and respiratory events, filter out motion artefacts,<sup>1</sup> and process the information for extracting vital signs that can be analyzed on-site for producing warning signals.

## 10.4 Piezoelectric Force Sensors

While the tactile sensors that use piezoelectric effect as described in Sect. 7.13.2 are not intended for accurate measurements of force, the same effect can be used quite efficiently for precision measurements. It should be remembered however that a piezoelectric effect is, so to speak, an a.c. phenomenon. In other words, it can convert a changing force into a variable electrical signal, while a steady state force produces no electrical response. However, the applied force can change some properties of the piezoelectric material that would affect an a.c. response when the sensor is supplied with an excitation signal, that is—it is an active sensor. One example of an active approach is shown in Fig. 7.45. Yet, for accurate quantitative measurements this still would not be a right design. A better approach is based on modulating a mechanical resonant frequency of the piezoelectric crystal by the applied force. A basic idea behind such sensor's operation is as follows. Certain cuts of a quartz crystal, when used as resonators in the electronic oscillators, shift the resonant frequency upon being mechanically loaded. The equation describing the natural mechanical frequency spectrum of a piezoelectric oscillator is given by [14]

<sup>1</sup> Word *artefact* in medicine means “spurious or artificial signal” that distorts a legitimate signal.

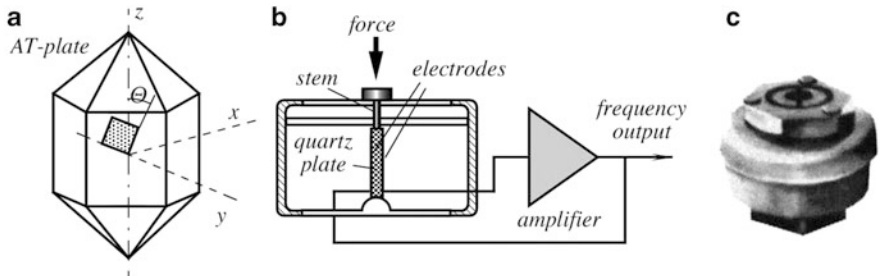
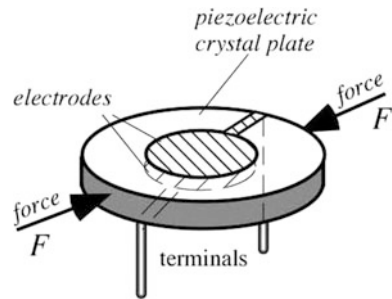
$$f_n = \frac{n}{2l} \sqrt{\frac{c}{\rho}}, \tag{10.5}$$

where  $n$  is the harmonic number,  $l$  is the resonance-determining dimension (e.g., the thickness of a relatively large thin plate or the length of a thin long rod),  $c$  is the effective elastic stiffness constant (e.g., the shear stiffness constant in the thickness direction of a plate or Young’s modulus in the case of a thin rod), and  $\rho$  is density of the crystal material.

The frequency shift induced by external force is due to nonlinear effects in the crystal. In the above equation, the stiffness constant  $c$  changes slightly with the stress. The effect of the stress on the dimension (strain) or the density is negligible. The minimal sensitivity to external force can occur when the squeezed dimension is aligned in certain directions for a given cut. These directions are usually chosen when crystal oscillators are designed, because their mechanical stability is important. However, in the sensor applications, the goal is just the opposite—a sensitivity to force along certain axes should be maximized. For example, the diametric force has been used for a high-performance pressure transducer [12] (Fig. 10.6).

Another design of a sensor that operates over a relatively narrow range from 0 to 1.5 kg is shown in Fig. 10.7. It has a good linearity and over 11-bit resolution. To fabricate the sensor, a rectangular plate is cut of the crystal where only one edge is parallel to the  $x$ -axis, and the face of the plate is cut at the angle of approximately  $\Theta = 35^\circ$  with respect to the  $z$ -axis. This cut is commonly known as *AT-cut* plate, Fig. 10.7a.

**Fig. 10.6** Piezoelectric disk resonator as diametric force sensor



**Fig. 10.7** Quartz force sensor. AT-cut of quartz crystal (a); structure of sensor (b); outside appearance of sensor (c). (Courtesy of Quartzcell, Santa Barbara, California)

The plate is given in the surface electrodes for utilizing a piezoelectric effect (see Fig. 4.22), which are connected in a positive feedback of an oscillator, Fig. 10.7b. A quartz crystal oscillates at a fundamental frequency  $f_o$  (unloaded) which shifts at loading by:

$$\Delta f = F \frac{K f_o^2 n}{l}, \quad (10.6)$$

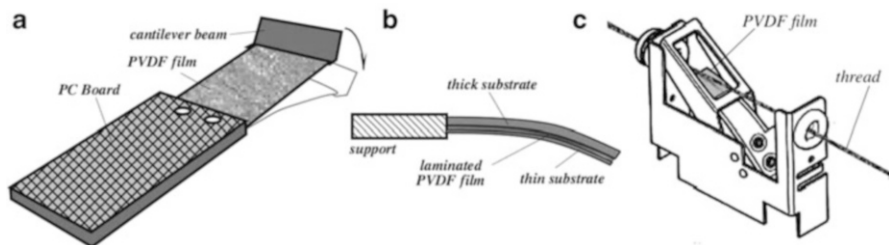
where  $F$  is the applied force,  $K$  is a constant,  $n$  is the number of the overtone mode, and  $l$  is the size of the crystal [13]. To compensate for the frequency variations due to temperature effects, a differential technique can be employed with a double crystal. One-half is used for temperature compensation while the other for measuring force. Each resonator is connected into its own oscillating circuit and the resulting frequencies are subtracted, thus negating temperature effects. A commercial force sensor (load cell) is shown in Fig. 10.7c.

A fundamental problem in all force sensors that use crystal resonators is based on two contradictory demands. On one hand, the resonator shall have the highest possible quality factor which means the sensor has to be decoupled from the environment and possibly should operate in vacuum. On the other hand, application of force or pressure requires relatively rigid structure and substantial loading effect on the oscillation crystal, thus reducing its quality factor. This difficulty may be partially solved by using a more complex sensor structure. For instance, in a photolithographically produced double- and triple-beams structures [14, 15], the so-called string concept is employed. The idea is to match dimensions of the oscillating element to the acoustic quarter-wavelength ( $1/4 \lambda$ ). The total wave reflection occurs at the supporting points through which the external force is coupled and the loading effect on quality factor is significantly reduced.

For measuring extremely small forces, a piezoelectric force sensor can be developed on a nanoscale dimension. Molybdenum disulfate ( $\text{MoS}_2$ ) when formed as a molecular monolayer exhibits strong piezoelectric properties, while in bulk form, it is not piezoelectric. If a two-dimensional  $\text{MoS}_2$  flake having odd number of monolayers is stretched and released, it produces piezoelectric voltage and current outputs. No output is observed for flakes with an even number of layers. A single monolayer flake strained by 0.53 % generates a peak output of 15 mV and current of 20 pA. The output increases with decreasing thickness and reverses sign when the strain direction is rotated by  $90^\circ$  [16].

Below are few examples of force sensors that use the PVDF and copolymer films [17].

Reliability of many conventional contact switches is reduced due to contaminates like moisture and dust which foul the contact points. Piezoelectric film offers exceptional reliability because it is a fully sealed monolithic structure, not susceptible to elements and other conventional switch failure modes. One of the most challenging of all switch applications is found in pinball machines. A pinball machine manufacturer uses a piezoelectric film switch as a replacement for the momentary rollover-type switch. The switch is constructed from a laminated



**Fig. 10.8** PVDF film switch for pinball machine (a), beam switch (b), thread-break sensor (c) (adapted from [17])

piezoelectric film on a spring steel beam, mounted as a cantilever to the end of a circuit board, Fig. 10.8a. The “digital” piezoelectric film switch is connected to a simple MOSFET circuit that consumes no power during the normally open state. In response to a direct contact force, the film beam flexes, generates electric charge, and momentarily triggers the MOSFET. This provides a momentary “high” state of the switch. The sensor does not exhibit corrosion, pitting, or bounce that are normally associated with contact switches. It can survive in excess of ten million cycles without failure. Simplicity of the design makes it effective in applications which include: counter switches for assembly lines and shaft rotation, switches for automated processes, impact detection for machine dispensed products, etc.

The cantilever beam that carries a PVDF film can be modified to adjust switch sensitivity from high to low impact forces. Figure 10.8b shows construction of a beam-type switch. The PVDF film element is laminated to a thicker substrate on one side, and has a much thinner laminated substrate on the other. This moves the neutral axis of the structure out of the piezoelectric film element, resulting in a fully tensile strain in the film when deflected downward, and a fully compressive strain when deflected in the opposite direction. Beam switches are used in shaft rotation counters in natural gas meters and as gear tooth counters in electric utility metering. The beam switch does not require an external power source, so the gas meter is safe from spark hazard. Other examples of applications for the beam switch include a baseball target that detects ball impact, a basketball game where a hoop mounted piezoelectric film sensor counts good baskets, switches inside of an interactive soft doll to detect a kiss to the “cheek” or a “tickle” (the sensor is sewn into the fabric of the doll), coin sensors for vending and slot machines, and as digital potentiometer for high reliability.

Textile plants require the continuous monitoring of often thousands of lines of thread for breakage. An undetected break event can require a large volume of material be discarded, as the labor costs to recover the material exceed the manufacturing cost. Drop switches, where switch contact closure occurs when the thread breaks, are very unreliable. Lint fouls the contact points, resulting in a no-output signal. A piezoelectric film vibration sensor, mounted to a thin steel

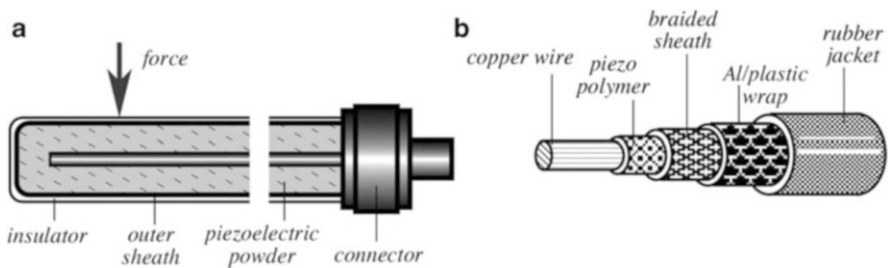
beam, monitors the acoustic signal caused by the abrasion of the thread running across the beam, analogous to a violin string (Fig. 10.8c). The absence of the vibrations instantly triggers the machinery to stop.

## 10.5 Piezoelectric Cables

A piezoelectric effect can be employed for detecting motions of objects exerting gravitational force on a base (floor, ground, pavement, etc.). To sense forces distributed over a relatively large area, the sensor has shape of a long coaxial cable that is placed on a hard base and is compressed when external force acts upon it. The cable length may range from few centimeters to many meters. It can be positioned straight or in any desirable pattern. As any piezoelectric sensor, the cable contains a crystalline material possessing the piezoelectric property and two electrodes placed at the opposite sides of the material. One electrode is the outer cable conductive cladding and the other electrode is the inner conductor, while the crystalline material is positioned in between along the cable length. The cable generates electric signal across the electrodes when subjected to variable compressions.

One type of a piezoelectric cable consists of a solid insulated copper sheath having 3 mm outer diameter, piezoelectric ceramic powder, and an inner copper core, Fig. 10.9a. The powder is tightly compressed between the outer sheath and the core. Usually, the cable is welded at one end and connected to a 50  $\Omega$  extension cable at the other end.

Another method of fabricating piezoelectric cables is to use a PVDF piezopolymer film as a component in the cable insulation, Fig. 10.9b. The PVDF can be made piezoelectric (see Sect. 4.6.2), thus giving the cable sensing properties. When a mechanical force is applied to the cable, the piezoelectric film is stressed, which results in development of electric charges of the opposite polarities on its surfaces. The inner copper wire and the braided sheath serve as the charge pick-up electrodes.



**Fig. 10.9** Piezoelectric cable with crystalline powder (a); polymer film as voltage generating component (b) (adapted from [18])

For a cable to possess piezoelectric properties, its sensing component (the ceramic powder or polymer film) must be poled during the manufacturing process [19]. During poling, the cable is warmed up to near the Curie temperature, and subjected to high voltage to orient dipoles in the crystals, then cooled down while the high voltage is maintained.

As it follows from Eq. (4.66), a piezoelectric material generates electric charge when stressed. The charge is proportional to the compressing force  $F_x$ :

$$Q_x = d_x F_x \quad (10.7)$$

where  $d_x$  is the piezoelectric coefficient along compression coordinate  $x$ .

When connected to a charge-to-voltage converter, Fig. 6.6c, the piezoinduced charge first produces current:

$$i = \frac{dQ_x}{dt} = d_x \frac{dF_x}{dt} = d_x v_F, \quad (10.8)$$

that is converted to the output voltage:

$$V_{\text{out}} = -iR = R d_x v_F, \quad (10.9)$$

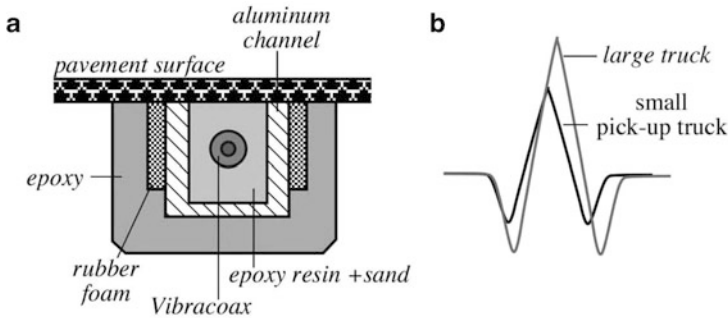
where  $v_F$  is the rate (velocity) of the force change. Therefore, the piezoelectric cable may be considered as the force velocity sensor.

Piezoelectric cables have been used in various experiments for monitoring vibrations in the compressor blades in turboshaft aircraft engines, security sensors for embedding into floors, detection of insects in silos, and automobile traffic analysis.<sup>2</sup> In the traffic applications, the cable is buried in a highway pavement, positioned perpendicular to the traffic flow. In the road traffic applications, the cables are sensitive primarily to the vertical forces. When properly installed, they last for at least 5 years [18]. The long, thin piezoelectric insulating layer provides a relatively low output impedance (600 pF/m), unusual for a piezoelectric device. The dynamic range of the cable is substantial (>200 dB) allowing sensing even such minute signals as distant small amplitude vibrations caused by rain or hail, yet responding linearly to the impacts of heavy trucks. The cables, when installed, have withstood pressures of 100 MPa. The typical operating temperature range is  $-40$  to  $+125$  °C. When the cable sensor is installed into the pavement (Fig. 10.10), its response should be calibrated, because shape of the signal and its amplitude depend not only on the properties of the cable, but also on type of the pavement and subgrade.

In medical research a piezoelectric cable was used for monitoring respiration and patient body motion resulted from the heart contraction—ballistocardiogram (BCD). Figure 10.11 illustrates a recording of the cable response to a 70 kg male patient when the cable was positioned underneath the mattress.

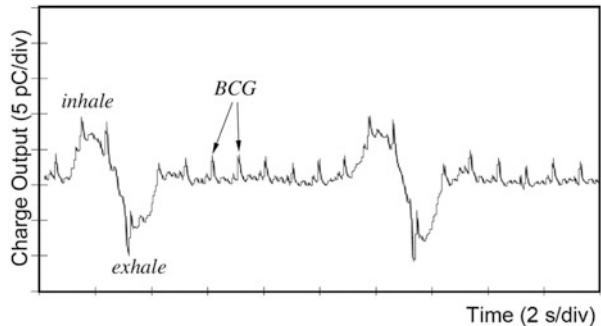
<sup>2</sup> [www.irdinc.com](http://www.irdinc.com)





**Fig. 10.10** Application of piezoelectric cables in highway monitoring installation into pavement (a); shape of electrical response (b)

**Fig. 10.11** Recording of patient respiration and BCD (ballistocardiogram) from a 1-m long piezoelectric cable positioned between the mattress and carpeted floor (Adapted from [19])

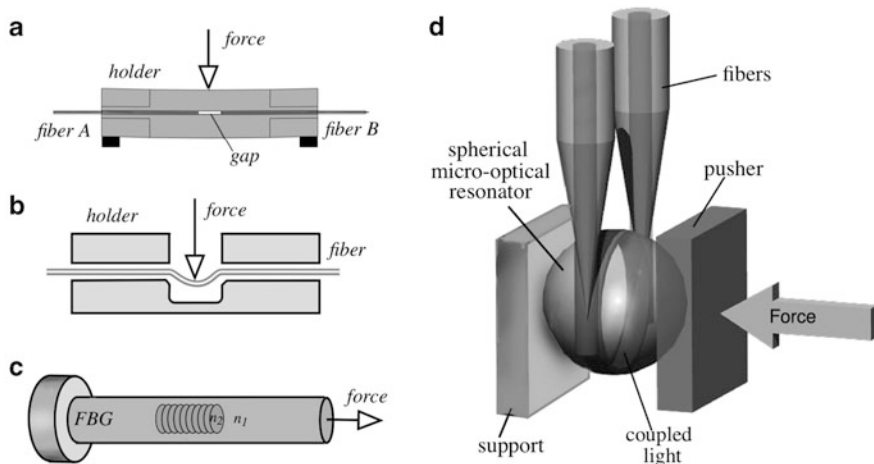


## 10.6 Optical Force Sensors

A great variety of the optical sensors can be employed for measuring force. Just to introduce the topic, we briefly present some methods that are covered in greater detail in other sections of this book for detecting and measuring other types of stimuli, yet the same sensors with slight modifications can be used for detecting force.

Figure 10.12a illustrates a coupling type of the optical sensor. An optical fiber is embedded into a holder that acts as a resilient component (spring). The fiber is positioned inside a narrow channel and split into two sections, A and B, with a small gap in between. Light passes from A to B section through the gap. When force is applied to the holder, it flexes, causing a misalignment between the fiber ends. A degree of the misalignment is proportional to the applied force, thus intensity of light traveling through the fiber is modulated by external force. A photodetector positioned at the other end of section B converts light into electrical output.

Another fiber-optic force sensor is shown in Fig. 10.12b. Here the fiber itself serves as a resilient material that flexes under the influence of external force. Flexing causes the fiber to curve, resulting in loss of intensity of the transmitted light. This concept is the same as of a microbend strain gauge illustrated in Fig. 5.22a.



**Fig. 10.12** Fiber-optic coupling-type sensor (a); fiber-optic bend-type sensor (b); fiber Bragg grating force sensor (c) and whispering gallery optical force sensor (d)

For measuring small forces, the optical fiber may be stretched or compressed as shown in Fig. 10.12c. It employs the so-called Fiber Bragg Grating (FBG) where the optical fiber has sections with different refractive indices:  $n_1$  and  $n_2$ . The fiber works as an optical filter. Its operation is described in Sect. 8.5.5. As an example of many applications, the FBG sensor was employed for a noncontact measuring forces between a small magnet attached to the fiber end and any ferromagnetic material placed within a few millimeters of the magnet. Maintaining the sensor at a constant standoff distance, material loss due to corrosion increased the distance between the magnet and the corroded surface, which was decreasing the magnetic pull force. This caused decrease of the fiber strain and, as a result, shifting the reflected Bragg wavelength of the FBG [20].

Another type of the optical fiber sensor uses a micro-optical resonator coupled to two fibers as shown in Fig. 10.12d. Its advantages include insensitivity to electromagnetic interferences (EMI) and no signal degradation even over very long (hundreds of meters) cable lengths [21]. It can be used at higher temperatures than many conventional electrical sensors, and safe for use with combustible materials and in HERO (Hazards of Electromagnetic Radiation to Ordnance) applications. Operation of the sensor is based on Whispering Gallery Mode (WGM) resonator that is comprised of a micro-optical element (e.g., a ball,) in contact with the optical fibers.<sup>3</sup> Optical resonances within the ball resonator occur when the optical path to complete a round trip inside a resonator in an integer multiple of the light wavelengths, and manifest as peaks in the spectrum. By scanning the wavelength of light used to illuminate the microresonator, the WGM

<sup>3</sup> See description of the WGM sensor in Sect. 17.9.3.

spectrum can be obtained by measuring intensity of the light that is decoupled out of the resonator and returned to the interrogator. WGM resonances are highly sensitive to changes of the microsphere (such as the size, shape, or refractive index) caused by temperature changes or applied forces. Monitoring the shifting ( $\Delta\lambda$ ) of the resonant spectral peaks allows measurement of the applied force with very high accuracy.

---

## References

1. Newton, I. (1687). *Philosophiæ Naturalis Principia Mathematica*. London: Joseph Streater for the Royal Society.
2. Doebelin, E. O. (1966). *Measurement systems: Applications and design*. New York: McGraw-Hill.
3. Ioppolo, T., et al. (2009). High-resolution force sensor based on morphology dependent optical resonances of polymeric spheres. *Journal of Applied Physics*, 105, 013535.
4. Tilmans, H. A. C., et al. (1992). Micro resonant force gauges. *Sensors and Actuators A*, 30, 35–53.
5. Suster, M., et al. (2006). A high-performance MEMS capacitive strain sensing system. *Journal of Microelectromechanical Systems*, 15(5), 1069–1077.
6. Pallás-Areny, R., et al. (2001). *Sensors and signal conditioning* (2nd ed.). New York: John Wiley & Sons.
7. Ștefănescu, D. M. (2011). *Handbook of force transducers. Principles and components*. New York: Springer.
8. Holman, J. P. (1978). *Experimental methods for engineers*. New York: McGraw-Hill Book Co.
9. Ren, T.-L., et al. (2012). Flexible graphite-on-paper piezoresistive sensors. *Sensors*, 12, 6685–6694.
10. Lefort, M.-H., et al. (2000). Thick film piezoresistive ink: Application to pressure sensors. *International Journal of Microcircuits and Electronic Packaging*, 23(2), 191–202.
11. Hadmani, S. T. A., et al. (2014). *The application of a piezo-resistive cardiorespiratory sensor system in an automobile safety belt*. *Proced. Intern. Electronic Conf. on Sensors and Applications*. [www.mdpi.com/journal/sensors](http://www.mdpi.com/journal/sensors)
12. Karrer, E., et al. (1977). A low range quartz pressure transducer. *ISA Transactions*, 16, 90–98.
13. Corbett, J. P. (1991). Quartz steady-state force and pressure sensor. In: *Sensors Expo West Proceedings*, paper 304A-1. Peterborough, NH: Helmers Publishing, Inc.
14. Benes, E., et al. (1995). Sensors based on piezoelectric resonators. *Sensors and Actuators A*, 48, 1–21.
15. Kirman, R. G., et al. (1986). Force sensors. *U.S. Patent No. 4594898*.
16. Wu, W., et al. (2014). Piezoelectricity of single-atomic-layer MoS<sub>2</sub> for energy conversion and piezotronics. *Nature*. doi:10.1038/nature13792.
17. Piezo Film Sensors Technical Manual. (1999, April). Norristown, PA: Measurement Specialties, Inc. [www.msusa.com](http://www.msusa.com)
18. Radice, F. P. (1991). Piezoelectric sensors and smart highways. *Sensors Expo Proceed.*
19. Ebisawa, M., et al. (2007, April 3). Coaxial piezoelectric cable polarizer, polarizing method, defect detector, and defect detecting method. *US Patent No. 7199508*.
20. Pacheco, C. J., et al. (2013). A noncontact force sensor based on a Fiber Bragg Grating and its application for corrosion measurement. *Sensors*, 13(9), 11476–11489.
21. Ioppolo, T., et al. (2008). Micro-optical force sensor concept based on whispering gallery mode resonators. *Applied Optics*, 47(16), 3009–3014.

*“To learn something new,  
first, you must know something old.”*

- My physics teacher

---

## 11.1 Concept of Pressure

The pressure concept was primarily based on the pioneering work of Evangelista Torricelli who for a short time was a student of Galileo. During his experiments with mercury-filled dishes, in 1643, he realized that the atmosphere exerts pressure on earth [1]. A great French experimenter Blaise Pascal, in 1647, conducted an experiment with the help of his brother-in-law, Perier, on the top of the mountain *Puy-de-Dôme* and at its base. He observed that pressure exerted on the column of mercury depends on elevation. He named a mercury-in-vacuum instrument they used in the experiment the *barometer*. In 1660, Robert Boyle stated his famous relationship:

The product of the measures of pressure and volume is constant for a given mass of air at fixed temperature.

In 1738 Daniel Bernoulli developed an impact theory of gas pressure to the point where Boyle's law could be deduced analytically. Bernoulli also anticipated the Charles-Gay-Lussac law by stating that *pressure is increased by heating gas at a constant volume*. For a detailed description of gas and fluid dynamics a reader should be referred to one of the many books on the fundamentals of physics. Below, we briefly summarize the basics that are essential for understanding designs and uses of pressure sensors.

In general terms, matter can be classified into *solids* and *fluids*. The word fluid describes something which can flow. That includes liquids and gases. The distinction between liquids and gases are not quite definite. By varying pressure it is possible to change liquid into gas and vice versa.

It is impossible to apply pressure to fluid in any direction except normal to its surface. At any angle, except  $90^\circ$ , fluid will just slide over, or flow. Therefore, any force applied to fluid is tangential and the pressure exerted on boundaries is normal to the surface. For a fluid at rest, pressure can be defined as the force  $F$  exerted perpendicularly on a unit area  $A$  of a boundary surface:

$$p = \frac{dF}{dA}. \quad (11.1)$$

As it follows from the equation, *pressure is force distributed over area*. Thus, pressure sensors not only very closely relate to force sensors, but very frequently force sensors are employed for pressure measurements and pressure sensors are used to measure force.

Pressure is basically a mechanical concept that can be fully described in terms of the primary dimensions of mass, length, and time. It is a familiar fact that pressure is strongly influenced by the position within the boundaries, however at a given position it is quite independent of direction.

We note the expected variations in pressure with elevation

$$dp = -w dh, \quad (11.2)$$

where  $w$  is the specific weight of the medium on Earth, and  $h$  represents the vertical height.

Pressure is unaffected by the shape of the confining boundaries. Thus, a great variety of pressure sensors can be designed without a concern of shape and dimensions. If pressure is applied to one of the sides of the surface confining liquid or gas, pressure is transferred to the entire surface without diminishing in value.

Kinetic theory of gases states that pressure can be viewed as a measure of the total kinetic energy of the molecules "attacking" the surface

$$p = \frac{2}{3} \frac{KE}{V} = \frac{1}{3} \rho C^2 = NRT, \quad (11.3)$$

where KE is the kinetic energy,  $V$  is the volume,  $C^2$  is an average value of the square of the molecular velocities,  $\rho$  is the density,  $N$  is the number of molecules per unit volume,  $R$  is a specific gas constant, and  $T$  is the absolute temperature.

Equation (11.3) suggests that pressure and density of compressible fluids (gases) are linearly related. Increase in pressure results in the proportional increase in density. For example, at  $0^\circ\text{C}$  and 1 atm pressure, air has a density of  $1.3 \text{ kg/m}^3$ , while at the same temperature and 50 atm of pressure its density is  $65 \text{ kg/m}^3$  which is 50 times higher. Contrary, for liquids the density varies very little over ranges of pressure and temperature. For instance, water at  $0^\circ\text{C}$  and 1 atm has a density of  $1000 \text{ kg/m}^3$ , while at  $0^\circ\text{C}$  and 50 atm its density is  $1002 \text{ kg/m}^3$ , and at  $100^\circ\text{C}$  and 1 atm its density is  $958 \text{ kg/m}^3$ .

Whether the gas pressure is above or below pressure of ambient air, we speak about overpressure or vacuum. Pressure is called *relative* when it is measured with

respect to ambient pressure. It is called *absolute* when it is measured with respect to a vacuum at zero pressure. The pressure of a medium may be static when it is referred to fluid at rest, or dynamic when it is referred to kinetic energy of a moving fluid.

---

## 11.2 Units of Pressure

The SI unit of pressure is the *pascal*:  $1 \text{ Pa} = 1 \text{ N/m}^2$ . That is, one pascal is equal to one newton force uniformly distributed over 1 square meter of surface. Sometimes, in technical systems, the *atmosphere* is used which is denoted 1 atm. One atmosphere is the pressure exerted on 1 square cm by a column of water having height of 1 m at a temperature of +4 °C and normal gravitational acceleration. 1 Pa may be converted into other units by use of the following relationships (see also Table A.4)

$$1 \text{ Pa} = 1.45 \times 10^{-4} \text{ lb/in.}^2 = 9.869 \times 10^{-6} \text{ atm} = 7.5 \times 10^{-4} \text{ cmHg.}$$

One Pa is quite a low pressure. For a practical estimation, it is useful to remember that 0.1 mm H<sub>2</sub>O is roughly equal to 1 Pa. A much larger pressure unit 1 barr = 10<sup>5</sup> Pa.

In industry, another unit of pressure is often used. It is defined as pressure exerted by 1 mm column of mercury at 0 °C at normal atmospheric pressure and normal gravity. This unit is named after Torricelli and is called the *torr*:

$$1 \text{ torr} = 1 \text{ mmHg.}$$

The ideal pressure of the Earth atmosphere is 760 Torr (mmHg) and is called the *physical atmosphere*

$$1 \text{ atm} = 760 \text{ torr} = 101,325 \text{ Pa.}$$

In medicine, the arterial blood pressure (ABP) traditionally is measured in mmHg. For a healthy person a typical ABP is about 120/70 mmHg, where the first number is the systolic pressure (at heart ejecting blood), while the second number is a diastolic pressure (at heart relaxation). These pressures can be expressed as 0.158/0.092 atm, meaning that in the arteries, blood pressure fluctuates, being always higher than the ambient atmospheric pressure by these numbers.

The US Customary System of units defines pressure as a pound per square inch (lbs/sq) or psi. Conversion into SI systems is the following

$$1 \text{ psi} = 6.89 \times 10^3 \text{ Pa} = 0.0703 \text{ atm.}$$

A pressure sensor is a complex sensor. That is, more than one step of the energy conversion is required before pressure can be finally presented as an electrical signal. The operating principle of many pressure sensors is based on the conversion

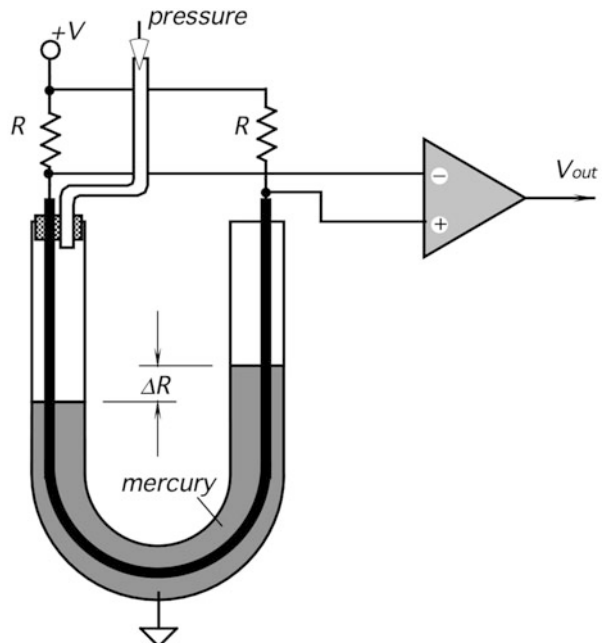
of a result of the pressure exertion on a sensitive element having a defined surface area. In turn, the element is displaced or deformed. As a result, a pressure measurement may be reduced to a measurement of a displacement or strain, which results from application of force. We recommend that the reader first familiarize herself with the displacement sensors covered in Chap. 8 and force sensors of Chap. 10.

### 11.3 Mercury Pressure Sensor

A simple yet efficient sensor is based on the communicating vessels principle (Fig. 11.1). Its prime use is for the measurement of gas pressure. A U-shaped wire is immersed into mercury which shorts the wire resistance in proportion with the height of mercury in each column. The resistors are connected into a Wheatstone bridge circuit that remains in balance as long as the differential pressure in the tube is zero. Pressure is applied to one of the arms of the tube and disbalances the bridge which results in the output signal. The higher the pressure in the left tube the higher the resistance of the corresponding arm and the lower the resistance of the opposite arm. The output voltage is proportional to a difference in resistances  $\Delta R$  of the wire arms that are not shunted by mercury:

$$V_{\text{out}} = V \frac{\Delta R}{R} = V\beta\Delta p. \quad (11.4)$$

**Fig. 11.1** Mercury-filled U-shaped sensor for measuring gas pressure

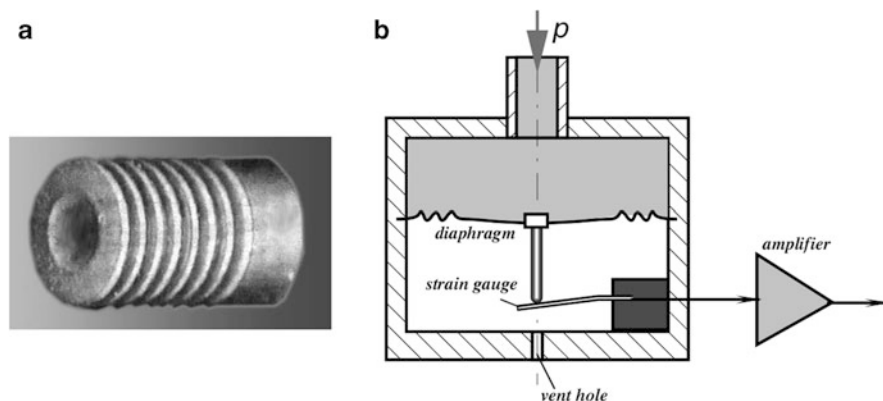


The sensor can be directly calibrated in units of torr. Being simple, this sensor suffers from several drawbacks, such as necessity of precision leveling, susceptibility to shocks and vibration, large size, and contamination of measured gas by mercury vapors.<sup>1</sup>

## 11.4 Bellows, Membranes, and Thin Plates

As it was mentioned above, a typical pressure sensor contains a deformable element whose deformation or movement is measured and converted by the displacement sensor into an electrical signal representative of the pressure value. In pressure sensors, this deformable or sensing element is a mechanical device that undergoes structural changes under strain caused by pressure. Historically, such devices were bourdon tubes (C-shaped, twisted, and helical), corrugated and catenary diaphragms, capsules, bellows, barrel tubes, and other components whose shape was changing under pressure.

A bellows, Fig. 11.2a, is intended for conversion of pressure into a linear displacement which can be measured by an appropriate sensor. Thus, bellows performs the first step in the complex conversion of pressure into electrical signal. The bellows is characterized by a relatively large surface area and, therefore, by a large displacement at low pressures. The stiffness of seamless metallic bellows is proportional to the Young's modulus of the material and inversely proportional to the outside diameter and to the number of convolutions of the bellows. Stiffness also increases with roughly the third power of the wall thickness.

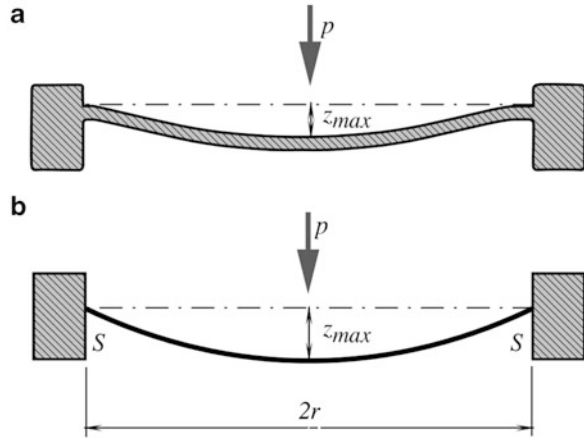


**Fig. 11.2** Steel bellows for pressure transducer (a) and metal corrugated diaphragm for conversion of pressure into linear deflection (b)

<sup>1</sup> Note that this sensor can be used as an inclination sensor when pressures at both sides of the tube are equal.



**Fig. 11.3** Thin plate (a) and membrane (b) under pressure  $p$



A popular example of pressure conversion into a linear deflection is a diaphragm in an aneroid barometer (Fig. 11.2b). A deflecting device always forms at least one wall of a pressure chamber and is coupled to a strain sensor (for instance, a strain gauge like the one shown in Fig. 10.2), which converts deflection into electrical signals by means of piezoresistivity. Nowadays, a great majority of pressure sensors are fabricated with silicon membranes by using the MEMS technologies.

A membrane is a thin diaphragm under radial tension  $S$ , which is measured in N/m (Fig. 11.3b). The stiffness to bending forces can be neglected as the thickness of the membrane is much smaller as compared with its radius (at least 200 times smaller). When pressure is applied to one side of the membrane, it shapes spherically, like a soap bubble. At low pressure,  $p$ , differences across the membrane, the center deflection  $z_{max}$ , and the stress  $\sigma_m^2$  are quasilinear functions of pressure

$$z_{max} = \frac{r^2 p}{4S}, \quad (11.5)$$

$$\sigma_{max} \approx \frac{S}{g}, \quad (11.6)$$

where  $r$  is the membrane radius and  $g$  is the thickness. Stress is generally uniform over the membrane area.

For the membrane, the lowest natural frequency can be calculated from [2]

$$f_0 = \frac{1.2}{\pi r} \sqrt{\frac{S}{\rho g}} \quad (11.7)$$

where  $\rho$  is the membrane material density.

<sup>2</sup> Stress is measured in  $\frac{N}{m^2}$ .

If thickness of the membrane is not negligibly small ( $r/g$  ratio is 100 or less), the membrane is no longer a “membrane” and it is called a *thin plate* (Fig. 11.3a). If the plate is compressed between some kind of clamping rings, it exhibits a noticeable hysteresis due to friction between the thin plate and the clamping rings. A much better arrangement is a one-piece structure where the plate and the supporting components are fabricated of a single bulk of material.

For a plate, the maximum deflection is also linearly related to pressure

$$z_{\max} = \frac{3(1 - \nu^2)r^4 p}{16Eg^3}, \quad (11.8)$$

where  $E$  is Young’s modulus ( $\text{N/m}^2$ ) and  $\nu$  is Poisson’s ratio. The maximum stress at the circumference is also a linear function of pressure:

$$\sigma_{\max} \approx \frac{3r^2 p}{4g^2}. \quad (11.9)$$

The above equations suggest that a pressure sensor can be designed by exploiting the membrane and thin-plate deflections. The next question is: what physical effect to use for the conversion of deflection into an electrical signal? There are several options that we discuss below.

## 11.5 Piezoresistive Sensors

To make a pressure sensor, two essential components are required: a deflection detector and a resilient component having an area  $A$  over which the force  $F$  is distributed. Both these components can be fabricated of silicon. A silicon-diaphragm pressure sensor consists of a thin silicon diaphragm (membrane) having area  $A$ , as an elastic material and the piezoresistive gauge resistors made by diffusive impurities into the diaphragm. Thanks to single crystal silicon superior elastic characteristics, virtually no creep<sup>3</sup> and no hysteresis occur, even under strong static pressure. The gauge factor of silicon is many times stronger than that of thin metal conductors [3]. It is customary to fabricate the strain gauge resistors for connecting as the Wheatstone bridge. The full-scale output of such a circuit is on the order of several hundred millivolts, thus a signal conditioner is required for bringing the output to an acceptable output format. Further, silicon resistors exhibit strong temperature sensitivity, therefore, either the piezoresistors should be temperature compensated or a signal conditioning circuit should include temperature compensation.

<sup>3</sup> Creep (sometimes called *cold flow*) is the tendency of a solid material to move slowly or deform permanently under the influence of stress.

When stress is applied to a semiconductor resistor, having initial resistance  $R$ , the piezoresistive effect results in change in the resistance  $\Delta R$  [4]

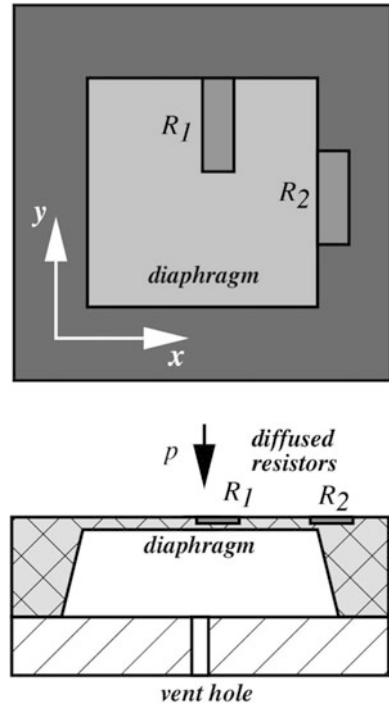
$$\frac{\Delta R}{R} = \pi_1 \sigma_1 + \pi_t \sigma_t \quad (11.10)$$

where  $\pi_1$  and  $\pi_t$  are the piezoresistive coefficients in a longitudinal and transverse directions, respectively. Stresses in longitudinal and transverse directions are designated  $\sigma_1$  and  $\sigma_t$ . The  $\pi$ -coefficients depend on the orientation of resistors on the silicon crystal. Thus, for  $p$ -type diffused resistor arranged in the  $\langle 110 \rangle$  direction or an  $n$ -type silicon square diaphragm with (100) surface orientation as shown in Fig. 11.4, the coefficients are approximately denoted as [4]:

$$\pi_1 = -\pi_t = \frac{1}{2}\pi_{44} \quad (11.11)$$

A change in resistivity is proportional to applied stress and, subsequently, to applied pressure. The resistors are positioned on the diaphragm in such a manner as to have the longitudinal and transverse coefficients of the opposite polarities, therefore resistors change in the opposite directions:

**Fig. 11.4** Position of piezoresistors on a silicon diaphragm



$$\frac{\Delta R_1}{R_1} = -\frac{\Delta R_2}{R_2} = \frac{1}{2}\pi_{44}(\sigma_{1y} - \sigma_{1x}). \quad (11.12)$$

When connecting  $R_1$  and  $R_2$  in a half-bridge circuit, and exciting the bridge with voltage  $E$ , the output voltage is

$$V_{\text{out}} = \frac{1}{4}E\pi_{44}(\sigma_{1y} - \sigma_{1x}). \quad (11.13)$$

The pressure sensitivity  $a_p$  and temperature sensitivity of the circuit  $b_T$  can be found by taking partial derivatives:

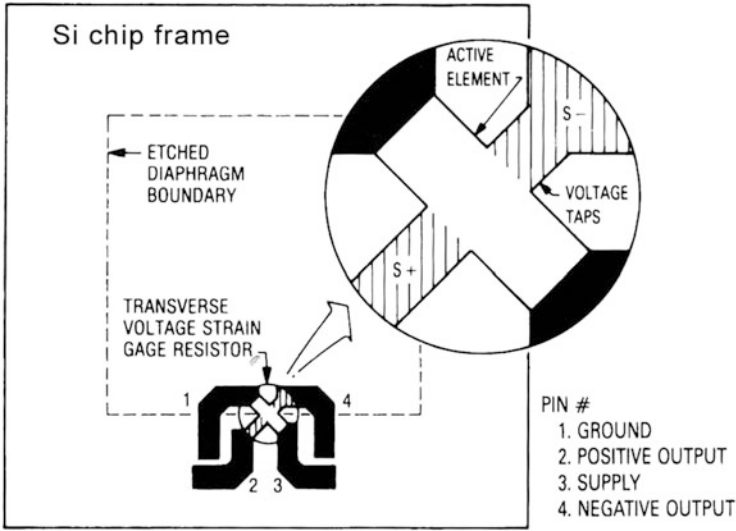
$$a_p = \frac{1}{E} \frac{\partial V_{\text{out}}}{\partial p} = \frac{\pi_{44}}{4} \frac{\partial (\sigma_{1y} - \sigma_{1x})}{\partial p}, \quad (11.14)$$

$$b_T = \frac{1}{a_p} \frac{\partial a_p}{\partial T} = \frac{1}{\pi_{44}} \frac{\partial \pi_{44}}{\partial T}. \quad (11.15)$$

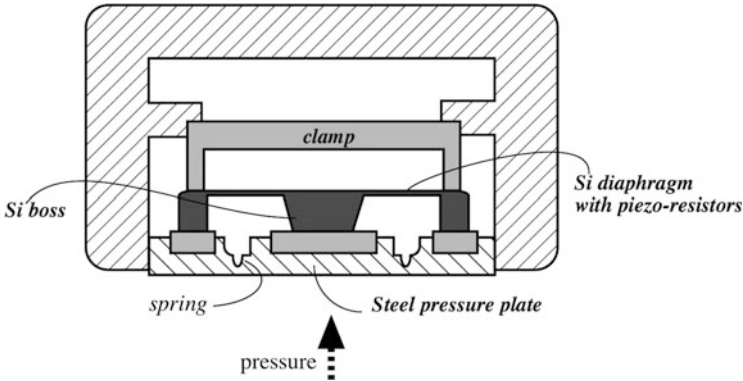
Since  $\partial\pi_{44}/\partial T$  has a negative value, the temperature coefficient of sensitivity is negative, that is, sensitivity decreases at higher temperatures.

There are several methods of fabricating the embedded piezoresistors that can be used for the silicon pressure sensor processing. In one method [5], the starting material is  $n$ -type silicon substrate with (100) surface orientation. Piezoresistors with  $3 \times 10^{18} \text{ cm}^{-3}$  surface-impurity concentration are fabricated using a boron ion implantation. One of them ( $R_1$ ) is parallel and the other is perpendicular to the  $\langle 110 \rangle$  diaphragm orientation. Other peripheral components, like resistors and  $pn$ -junctions used for temperature compensation, are also fabricated during the same implantation process as that for the piezoresistors. They are positioned in a thick-rim area surrounding the diaphragm and, as a result, are insensitive to pressure applied to the diaphragm.

Another approach of stress sensing was used in Motorola MPX pressure sensor chip shown in Fig. 11.5. The piezoresistive element, which constitutes a strain gauge, is ion implanted on a thin silicon diaphragm. Excitation current passes longitudinally through the resistor's taps 1 and 3, while the pressure that stresses the diaphragm is applied at a right angle to the current flow. The stress establishes a transverse electric field in the resistor that is sensed as voltage at taps 2 and 4. The single-element transverse voltage strain gauge can be viewed as the mechanical analog of a Hall effect device (see Sect. 4.8). The use of a single element eliminates the need to closely match the four stresses and temperature sensitive resistors that form a Wheatstone bridge circuit. At the same time, it greatly simplifies the additional circuitry necessary to accomplish a calibration and temperature compensation. Nevertheless, the single-element strain gauge electrically is analogous to the bridge circuit. Its balance (offset) does not depend on the matched resistors, as it would be in a conventional bridge, but instead on how well the transverse voltage taps are aligned.

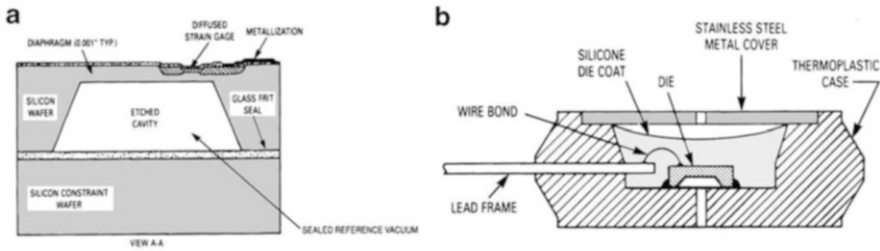


**Fig. 11.5** Basic uncompensated piezoresistive element of Motorola MPX pressure sensor (© of Motorola, Inc. Used with permission)



**Fig. 11.6** Piezoresistive chip inside steel enclosure for measuring high pressures

A diaphragm (membrane) of a piezoresistive sensor in many sensors usually is very thin—in the order of 1  $\mu\text{m}$ , thus its mechanical properties is a limiting factor for the maximum applied pressures. In applications where pressures are very high, the silicon diaphragm is just too weak to be directly subjected to such pressures. Thus, forces applied to the silicon diaphragm should be scaled down by the use of an intermediate pressure plate having a significantly larger stiffness. For example, in automotive industry for measuring pressure in combustion engines where temperature reaches 2000  $^{\circ}\text{C}$  and pressures may exceed 200 bar, a special sensor housing with a scaling pressure plate may be employed. Such a housing should scale down pressure and protect the chip from a harsh environment. Figure 11.6



**Fig. 11.7** Absolute (a) and differential (b) pressure sensor packaging

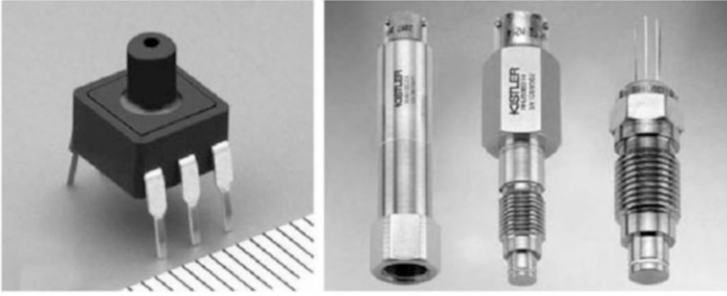
illustrates a housing where pressure sensitive chip with a micromachined Si diaphragm is positioned above the steel plate. High pressures flex the steel plate with a relatively small displacement in the center section that is coupled to the boss. The Si boss is a mechanical extension of the Si diaphragm and flexes it upwards, causing disbalance of the piezoresistive bridge. The scaling factor is controlled by the springs formed around the steel plate.

Pressure sensors are usually available in three basic configurations that permit measurement of *absolute*, *differential*, and *gauge* pressures. Absolute pressure, such a barometric pressure, is measured with respect to a reference vacuum chamber. The chamber may be either external, or it can be built directly into the sensor, Fig. 11.7a. A differential pressure, such as the pressure drop in a pressure-differential flowmeter, is measured by applying pressure to the opposite sides of the diaphragm simultaneously. Gauge pressure is measured with respect to some kind of reference pressure. An example is arterial blood pressure measurement, which is done with respect to the atmospheric pressure. Thus, gauge pressure is a special case of a differential pressure.

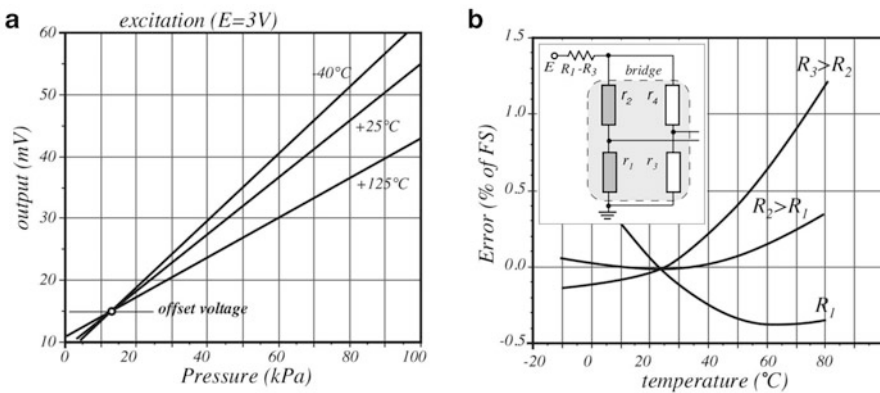
The diaphragm and strain gauge designs are the same for all three configurations, while the packaging makes them different. For example, to make a differential or gauge sensor, a silicon die is positioned inside the chamber (Fig. 11.7b) that has two openings at both sides of the die. To protect them from harsh environment, the interior of the housing may be filled with a silicone gel which isolates the die surface and wire bonds, while allowing the pressure signal to be coupled to the silicon diaphragm. Differential sensors may be incorporated into various porting holders (Fig. 11.8), depending on applications. Certain applications, such as a hot water hammer, corrosive fluids, and load cells, require physical isolation and hydraulic coupling to the chip-carrier package. It can be done with additional diaphragms, plates, and bellows. Silicon oil, such as Dow Corning DS200, can be used to fill the air cavity so that system frequency response is not degraded.

All silicon-based sensors are characterized by temperature dependence. Temperature coefficient of sensitivity  $b_T$  as defined by Eq. (11.15) is usually negative and for the accurate pressure sensing it must be compensated for. Without compensation, the sensor's output voltage may look like the one shown in Fig. 11.9a for three different temperatures.

In many applications, a simple yet efficient temperature compensation can be accomplished by adding to the resistive bridge either a series or parallel



**Fig. 11.8** Examples of pressure sensor housings



**Fig. 11.9** Temperature characteristics of a piezoresistive pressure sensor. Transfer function at three different temperatures (a); full-scale errors for three values of serial compensating resistor connected to bridge circuit (b)

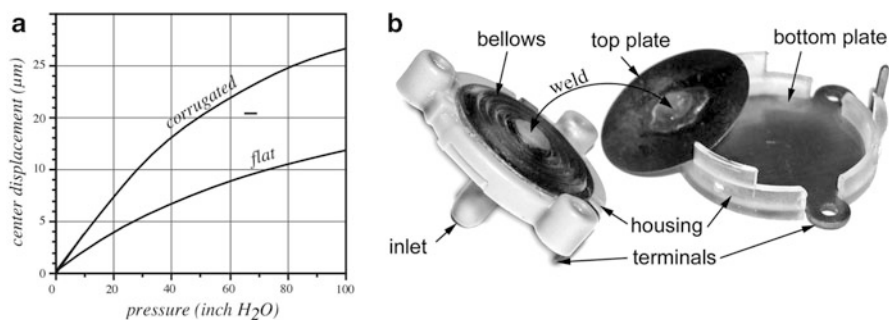
temperature stable resistor [6]. By selecting an appropriate value of the resistor, the sensor's output can be tailored to the desirable operating range, Fig. 11.9b. Whenever a better temperature correction over a broad range is required, more complex compensation circuits with temperature detectors can be employed. A viable alternative is a software compensation where temperature of the pressure transducer is measured by an imbedded temperature sensor. Both data from the pressure and temperature sensors relayed to the processing circuit where numerical compensation is digitally performed. But the best solution is still designing a temperature compensated Si bridge inside the sensor.

## 11.6 Capacitive Sensors

A silicon diaphragm can be used with another pressure-to-electricity conversion device—a capacitive sensor. In a capacitive pressure sensor, the diaphragm displacement modulates capacitance with respect to the reference plate (backplate).

The concept of the capacitive pressure sensor is similar to any capacitive displacement sensors, for examples as illustrated in Fig. 8.8. Capacitive pressure sensors are especially effective for measuring low pressures. The entire sensor can be fabricated from a solid piece of silicon, thus maximizing its operational stability. The diaphragm can be designed to produce up to 25 % capacitance change over a full range. While a piezoresistive diaphragm should be designed to maximize stress at its edges, the capacitive diaphragm utilizes a displacement of its central portion. These diaphragms can be protected against overpressure by including mechanical stops close to either side of the diaphragm (for a differential pressure sensor). Unfortunately, in the piezoresistive diaphragms, the same protection is not quite effective because of small operational displacements. As a result, while the piezoresistive sensors typically have burst pressures of no more than ten times the full-scale rating, the capacitive sensors with overpressure stops can handle a thousand times the rated full-scale pressure. This is especially important for the low-pressure applications, where relatively high-pressure pulses can occasionally occur.

When designing a capacitive pressure sensor, for good linearity it is important to maintain flatness of the diaphragm. Traditionally, these sensors are linear only over the displacements which are much less than their thickness. One way to improve the linear range is to make a diaphragm with groves and corrugations by applying a micromachining technology. Planar diaphragms are generally considered more sensitive than the corrugated diaphragms with the same size and thickness. However, in the presence of the in-plane tensile stresses, the corrugations serve to relieve some of the stresses, thus resulting in better sensitivity and linearity as shown in Fig. 11.10a. As an example, a low-cost pressure sensor for a consumer arterial blood pressure monitor is shown in Fig. 11.10b. The air hose from the arm cuff it attached to the sensor's inlet that is pneumatically coupled to the bellows whose center is welded to a large moving top plate. A capacitance is measured between the top and bottom plates. The sensor housing is fabricated of a molded resin. The sensor exhibits a good linearity and low hysteresis in the pressure range from 20 to 300 mmHg. However, its low temperature stability limits its use to room temperatures.



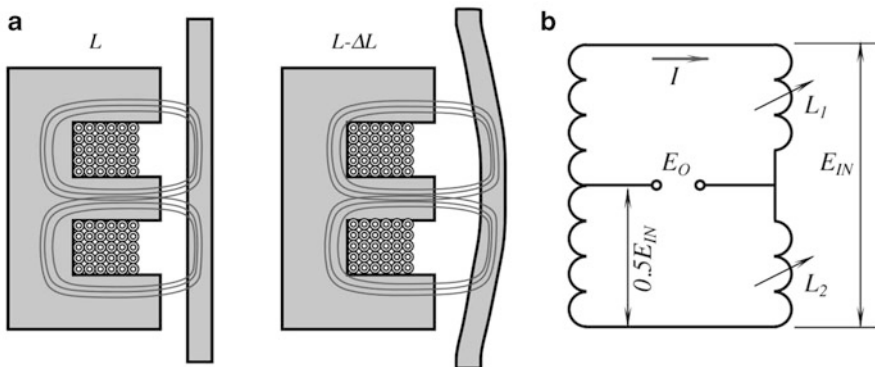
**Fig. 11.10** Central deflection of flat and corrugated diaphragms of the same sizes under in-plane tensile stresses (a). Disassembled pressure sensor for blood pressure monitor. It has bellows welded to moving top plate (b)



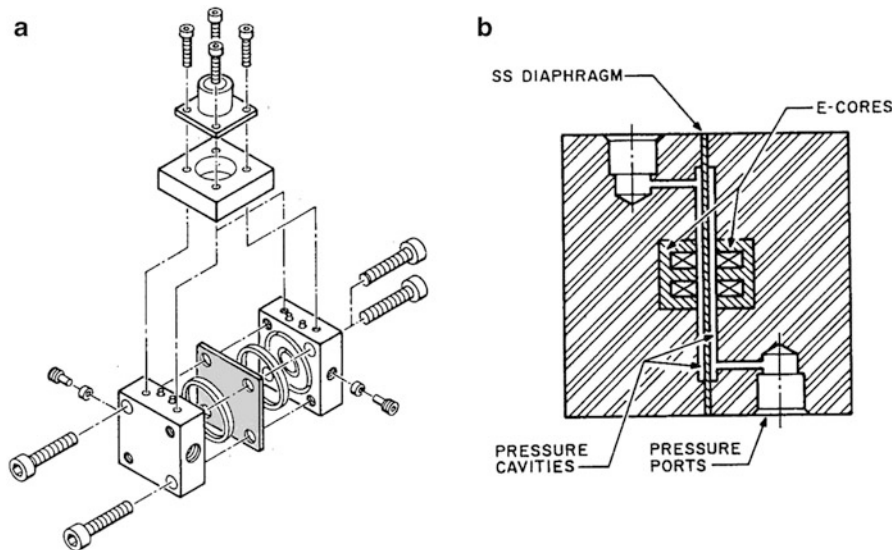
## 11.7 VRP Sensors

When measuring small pressures, deflection of a thin plate or diaphragm can be very small. In fact, it can be so small that use of strain gauges attached to or imbedded into the diaphragm becomes impractical due to the low-output signal. One possible answer to the problem may be a capacitive sensor where a diaphragm deflection is measured by its relative position to a reference base rather than by the internal strain in the material. Such sensors were described above. Another solution which is especially useful for very low pressures is a *variable-reluctance pressure* (VRP) sensor. It uses a magnetically conductive diaphragm to modulate the magnetic resistance of a differential transformer. Figure 11.11a illustrates the basic idea behind magnetic flux modulation. The assembly of an E-shaped core and a coil produces a magnetic flux whose field lines travel through the core, the air gap, and the diaphragm. The permeability of the E-core magnetic material is at least 1000 times higher than that of the air gap [7], and, subsequently, its magnetic resistance is much lower than the resistance of air. Since the magnetic resistance of the air gap is much higher than the resistance of the core, it is the gap that determines inductance of the core-coil assembly. When the diaphragm deflects, the air gap increases or decreases depending on direction of the deflection, thus causing modulation of the inductance.

To fabricate a pressure sensor, a magnetically permeable diaphragm is sandwiched between two halves of the shell (Fig. 11.12). Each half incorporates a E-core/coil assembly. The coils are encapsulated in a hard compound to maintain maximum stability under even very high pressure. Thin pressure cavities are formed at both sides of the diaphragm. The thickness of the diaphragm defines a full-scale operating range, however, under most of the circumstances, total deflection does not exceed 25–30  $\mu\text{m}$  which makes this device very sensitive to low pressures. Further, due to thin pressure cavities, the membrane is physically prevented from excessive deflection under the over-pressure conditions.



**Fig. 11.11** Variable-reluctance pressure sensor. Basic principle of operation (a); equivalent circuit of inductive bridge (b)

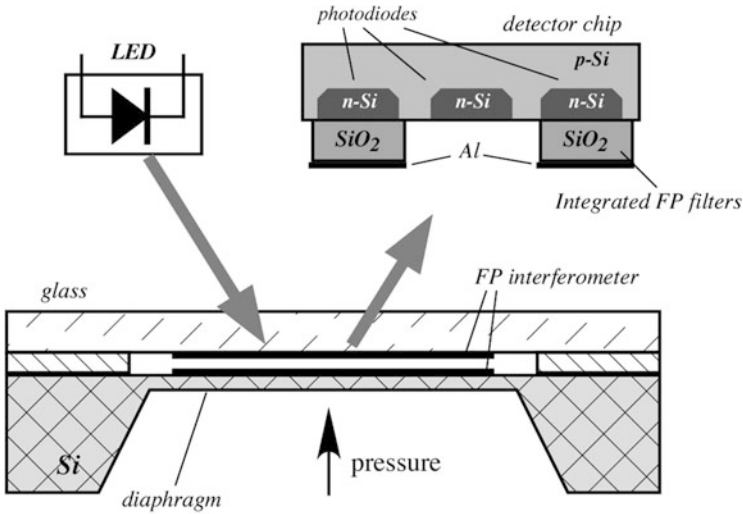


**Fig. 11.12** Construction of VRP sensor for low-pressure measurements. Assembly of sensor (a); double E-core at both sides of cavity (b)

This makes VRP sensors inherently safe devices. When excited by an ac current, a magnetic flux is produced in each core and air gaps at the diaphragm. Thus, the sensors contain two inductances and can therefore be thought of as half of a variable-reluctance bridge where each inductance forms one arm of the bridge (Fig. 11.11b). As a differential pressure across the diaphragm is applied, the diaphragm deflects, one side decreasing and the other increasing, and the air gap reluctances in the electromagnetic circuit change proportionally to the differential pressure applied. . When the bridge is excited by a carrier current, the output signal across the bridge becomes amplitude-modulated by the applied pressure. The amplitude is proportional to the bridge imbalance, while phase of the output signal changes with direction of the imbalance. The a.c. signal can be demodulated to produce a d.c. response. A full-scale pressure on the diaphragm, while being very small, will produce a large output signal that is easily discriminated from noise.

## 11.8 Optoelectronic Pressure Sensors

When measuring low-level pressures or, contrary, when thick membranes are required to enable a broad dynamic range, a diaphragm displacement may be too small to assure a sufficient resolution and accuracy. Besides, most of piezoresistive sensors, and some capacitive, are quite temperature sensitive requiring an additional thermal compensation. An optical readout has several advantages over other technologies, namely, a simple encapsulation, small temperature effects, high



**Fig. 11.13** Schematic of an optoelectronic pressure sensor operating on the interference phenomenon (adapted from [9])

resolution, and accuracy. The optical pressure sensors can be designed with fiber optics, which makes them especially useful for remote sensing where radio frequency interferences present serious problem. Especially promising are the sensors operating with the light interference phenomena [8]. Such sensors use a Fabry-Perot (FP) principle of measuring small displacements as covered in more detail in Section 8.5.4. A simplified circuit of another FP pressure sensor is shown in Fig. 11.13.

The sensor consists of the following essential components: a passive optical pressure chip with a diaphragm (membrane) etched in silicon, a light emitting diode (LED), and a detector chip [9]. A pressure chip is similar to a capacitive pressure sensor, except that a capacitor is replaced by an optical cavity forming a Fabry-Perot interferometer [10] measuring a deflection of the diaphragm. A back-etched single-crystal diaphragm on a silicon chip is covered with a thin metallic layer, and a glass plate with a metallic layer on its backside. The glass is separated from the silicon chip by the gap of a distance  $w$ . Two metallic layers form a variable-gap FP interferometer with a pressure sensitive movable mirror (on the diaphragm) and a plain-parallel stationary fixed half-transparent mirror (on the glass). A detector chip contains three  $pn$ -junction photodiodes. Two of them are covered with integrated optical FP filters of slightly different thicknesses. The filters are formed as first surface silicon mirrors, coated with a layer of  $\text{SiO}_2$  and thin metal (Al) mirrors on their surfaces. An operating principle of the sensor is based on measurement of a wavelength modulation of the reflected and transmitted light depending on the width  $w$  of the FP cavity. The reflection and transmission from the cavity is almost a periodic function of the inverse wavelength,  $1/\lambda$ , of the light with a period equal to

$1/2w$ . Since  $w$  is a linear function of the applied pressure, the reflected light is wavelength modulated.

The detector chip works as a demodulator by generating electrical signals representing the applied pressure. It performs an optical comparison of the sensing cavity with a virtual cavity formed by the height difference between two FP filters. If both cavities are the same, the detector generates the maximum photocurrent, and, when the pressure changes, the photocurrent is cosine-modulated with a period defined by a half the mean wavelength of the light source. The photodiode without the FP filter serves as a reference diode, which monitors the total light intensity arriving at the detector. Its output signal is used for a ratiometric processing of the information. Since the output of the sensor is inherently nonlinear, a linearization by a microprocessor is generally required.

---

## 11.9 Indirect Pressure Sensor

For measuring very small pressure variations on the order of few pascals, the diaphragm-based pressure sensors are not really efficient because it is difficult to make a very thin membrane (diaphragm) that would respond to miniscule pressures.<sup>4</sup> And when such a membrane is constructed, it is fragile and could be easily damaged by an accidental overpressure. Thus, other methods of measuring small pressures were devised. These methods often do not measure pressure directly, that is by measuring force distributed over a specific area, but rather rely on measurement of some other variable that is pressure dependent. Then, pressure can be inferred or computed from value of the variable.

As an illustration, let us assume that we have a large enclosed tank filled with air under low, relatively static pressure  $p_1$  that we would like to measure. This means that pressure  $p_1$  is slightly above the atmosphere pressure  $p$ . To measure the pressure gradient, we will use not a pressure sensor but the airflow sensor. To do that, we attach a small bleed tube to the interior of the tank and open the other end of the tube to the atmosphere. Thanks to a pressure gradient, air will be flowing out of the tank to the atmosphere through the bleed tube. If  $p_1$  is lower than atmosphere  $p$ , the air will flow backwards—from atmosphere into the tank. Since the tank is large and the tube is small, the airflow rate inside the bleed tube is considered constant  $v_2$ . The pressure differential (the tank minus atmosphere) can be derived from the Bernoulli equation (see Sect. 12.2) as

$$\Delta p = p_1 - p_2 = b\rho v_2^2, \quad (11.16)$$

where  $\rho$  is the air density,  $v$  is the mass flow rate, and  $b$  is the scaling coefficient that among other factors depends on size of the bleed tube. This equation is the modified

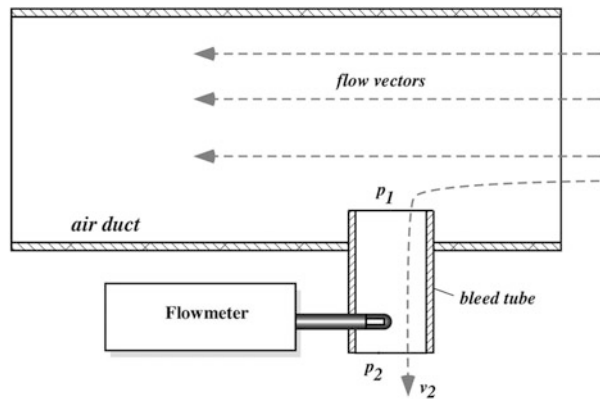
---

<sup>4</sup>Difficult, but not impossible. Thin diaphragms were developed for the vacuum sensors [18], albeit they are expensive and very delicate.

Eq. (12.9) where the flow resistance  $R$  is zero. Note that the air density is proportional to the average pressure which makes the pressure differential nearly independent on the absolute level of pressure. Equation (11.16) shows that the pressure differential can be expressed in terms of flow rate. Thus, we can monitor the differential pressure indirectly, without a conventional pressure sensor. This can be done by measuring the velocity  $v$  (flow rate) of the outflowing or inflowing gas. It is the basis of a low-differential pressure sensor that employs a flowmeter [11]. Since the flow rate is squared, the flow rate can be related to a pressure differential but not to its sign: plus or minus will be lost in the second power of flow rate. This method is primarily useful for monitoring pressure gradients in dynamic gas systems, such as HVAC where gas is moved by a blower. In these cases, depending on orientation of the bleed tube opening, the monitored pressure will be either the static pressure or stagnation (total) pressure that includes the dynamic pressure of the flowing gas, just like in the Pitot tube.<sup>5</sup>

Figure 11.14 shows a practical implementation of the differential pressure sensor with a bleed tube and a flowmeter. An air duct of a HVAC system has air flowing inside of it. The bleed tube is inserted into the air duct perpendicular to the vector of the airflow, thus the open end is exposed only to static pressure  $p_1$ . The other side of the tube is open to the atmosphere having pressure  $p_2$ . According to Eq. (11.15), the pressure differential across the tube will cause airflow through the tube. The bleed tube has a built-in mass flowmeter probe that measures the flow rate  $v$ . The pressure gradient can be calculated from Eq. (11.15). Note that value  $b$  needs a calibration. The simplest and most efficient flowmeter for use in this device is a gas thermoanemometer that is described in Sect. 12.3.3.

**Fig. 11.14** Flow meter as differential pressure sensor (adapted from [11])



<sup>5</sup> Refer to description of Pitot tubes elsewhere.

## 11.10 Vacuum Sensors

Measurement of extremely low pressures is important for processing of the micro-electronic wafers, optical components, chemistry, and other industrial applications. It is also vital for scientific studies, for instance, in the Space exploration. In general, *vacuum* means pressure below atmospheric, but usually the term is used with respect to a near absence of gas pressure. True vacuum is never attained. Even the intrastellar space is not entirely free of matter.

Vacuum can be measured as negative pressure comparing to the atmospheric pressure by conventional pressure sensors, yet this is not quite efficient. Conventional pressure sensors do not resolve extremely low concentrations of gas due to poor signal-to-noise ratio. While a pressure sensor in most cases employs some kind of membrane and a displacement (deflection) transducer, special vacuum sensors operate on different principles. They rely on certain physical properties of gaseous molecules that are related to the number of such molecules per volume of space. These properties may be a thermal conductivity, viscosity, ionization, and others. Here we briefly describe some popular sensor designs.

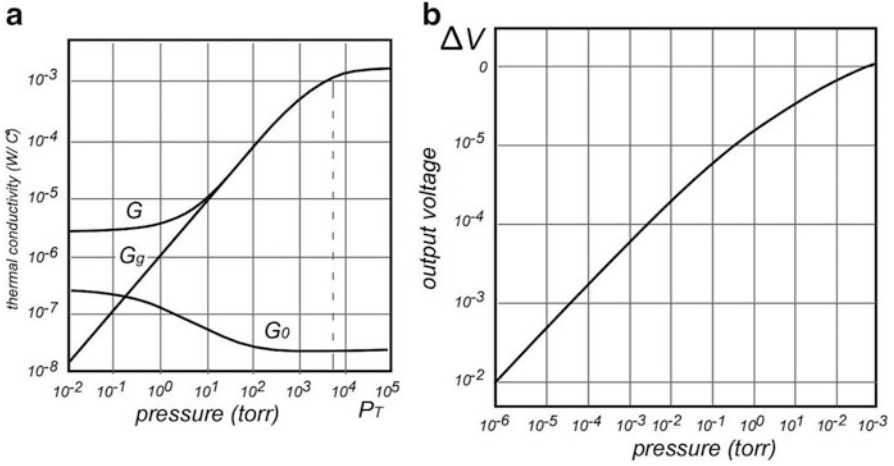
### 11.10.1 Pirani Gauge

Pirani vacuum gauge [12] is the sensor that infers the level of vacuum through thermal conductivity of gas. It is one of the oldest vacuum sensors. The simplest version of the gauge contains a heated plate. A measurement is done by detecting the amount of heat loss from the plate. It assumes that the heat loss is function of the gas pressure. Operation of the Pirani gauge is based on the pioneering works by Von Smoluchowski [13]. He established that when an object is heated, thermal conductivity to the surrounding objects is governed by

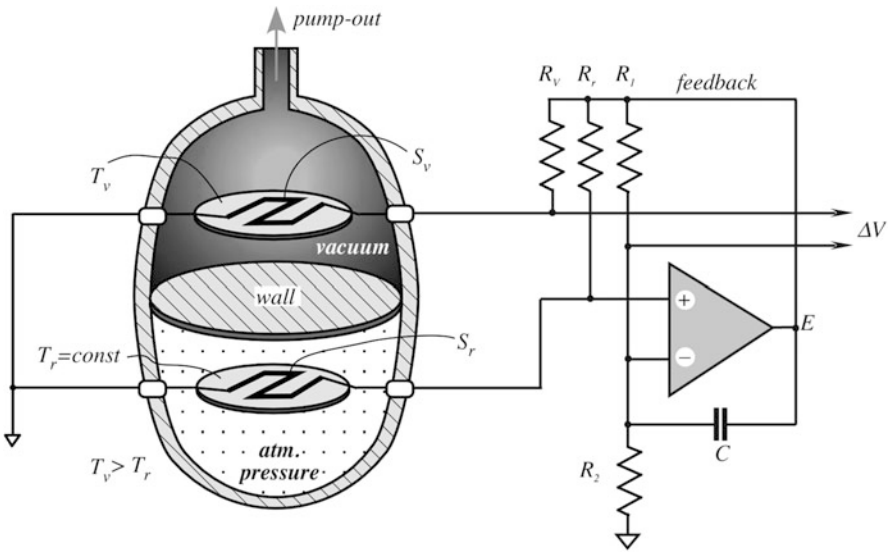
$$G = G_0 + G_g = G_s + G_r + ak \frac{PP_T}{P + P_T} \quad (11.17)$$

where,  $G_s$  is thermal conductivity via the solid supporting elements,  $G_r$  is the radiative heat transfer conductivity,  $G_0 = G_s + G_r$  is the baseline thermal conductivity,  $a$  is the area of a heated plate,  $k$  is a coefficient related to gas properties, and  $P_T$  is a transitional pressure which is the maximum pressure that can be measured. Figure 11.15a illustrates different factors that contribute to a thermal loss from a heated plate. If the conductive (through solid components) and radiative heat loss is accounted for, the gas conductivity  $G_g$  goes linearly down to absolute vacuum. The trick is to minimize the interfering factors that contribute to  $G_0$ . This can be achieved by use of both the heated plate that is suspended with a minimal thermal contact with the sensor housing and by a differential technique that to a large degree cancels the influence of  $G_0$ .

Several designs of the Pirani gauge are known in vacuum technologies. Some employ two plates with different temperatures and the amount of power spent for



**Fig. 11.15** Thermal conductivities from heated plate (a). Transfer function of Pirani vacuum gauge (b)



**Fig. 11.16** Pirani vacuum gauge with NTC thermistors operating in self-heating mode

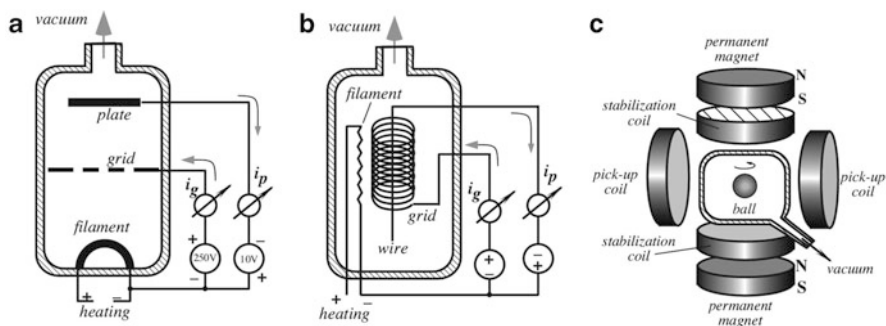
heating them is a measure of the gas pressure. The other use a single plate that measures thermal conductivity of gas by heat loss to the surrounding walls. Temperature measurement is usually done with either a thermocouple or platinum RTD.

Figure 11.16 illustrates one version of the Pirani gauge that employs a thermal balance (differential) technique. The sensing chamber is divided into two identical

sections where one is filled with gas at a reference pressure, say  $1 \text{ atm} = 760 \text{ Torr}$  and the other is connected to vacuum that is to be measured. Each chamber contains a heated plate that is supported by the tiny links to minimize a conductive heat transfer through solids. Both chambers are preferably of the same shape, size, and construction so that the conductive and radiative heat loss would be nearly identical. The better the symmetry the better the cancellation of the spurious thermal conductivity  $G_0$ . The heaters on the plates are warmed up by electric current. In this particular design, each heater is a self-heating thermistor having NTC—a negative temperature coefficient (see Sect. 17.4.4). Resistances of the thermistors are equal and relatively low to allow for a Joule self-heating. The reference thermistor  $S_r$  is connected into a self-balancing bridge that also includes fixed resistors  $R_r$ ,  $R_1$ ,  $R_2$  and an operational amplifier. The bridge automatically sets temperature of  $S_r$  on a constant level  $T_r$  that is higher than and independent of the ambient temperature. This set temperature is defined by the  $S_r$  thermistor and fixed bridge resistors  $R_1$  and  $R_2$ . Note that the bridge is balanced by both the negative and positive feedbacks to both arms of the bridge. Capacitor  $C$  keeps the circuit from oscillating. The same voltage  $E$  that feeds the reference plate is applied to the thermistor  $S_v$  on the sensing plate via  $R_v = R_r$ . The output voltage  $\Delta V$  is taken differentially from the sensing thermistor and the bridge. The shape of the transfer function is shown in Fig. 11.15b. A vacuum sensor often operates with gases that may contaminate the sensing plates so the appropriate coatings and filters should be employed.

### 11.10.2 Ionization Gauges

This ionization sensor resembles a vacuum tube that was used as an amplifier in the old-fashioned radio. The ion current between the plate and filament, Fig. 11.17a, is a nearly linear function of the molecular density (pressure) [14]. The vacuum gauge tube has a reversed connection of voltages: the positive high voltage is applied to a grid while a negative lower voltage is connected to the plate. The output is the ion current  $i_p$  collected by the plate that is proportional to pressure and the electron



**Fig. 11.17** Ionization vacuum gauge (a), Bayard-Alpert gauge (b), and gas drag gauge (c)



current  $i_g$  of the grid. Presently, a further improvement of this gauge is the so-called Bayard-Alpert vacuum sensor [15]. It is more sensitive and stable at much lower pressures. Its operating principle is the same as a vacuum tube gauge, except that the geometry is different—the plate is substituted by the wire surrounded by a grid while the cathode filament is outside, Fig. 11.17b.

### 11.10.3 Gas Drag Gauge

The gas molecules mechanically interact with a moving body. This is the basic idea behind the spinning rotor gauge [16] that is abbreviated SRG. Advantages of SRG are as follows: it does not perturb the vacuum environment with a hot cathode (filament) or high-voltage discharge and it is compatible with a wide variety of gases, including corrosive gases. These characteristics have led to the widespread use of the SRG as a reference standard for calibration of other vacuum gages between  $10^{-4}$  and  $10^{-1}$  Pa ( $10^{-6}$  and  $10^{-3}$  Torr), and offer potential for monitoring chemically active process gases.

The SRG monitor has three main components [17]:

1. The sensor or rotor—a magnetic steel ball located in a thimble that is a thin-walled extension of the vacuum system.
2. The suspension head that is located outside the thimble. It contains permanent and electromagnets for suspending the ball, the suspension coils to sense and stabilize the position of the suspended ball, the inductive drive coils to spin the ball to its operating frequency range, and pickup coils to sense the rotation of the ball.
3. The electronic control unit (controller) which controls all operating functions, amplifies the pickup signal from the rotating ball, and processes the data from the signal to obtain the pressure.

In the current implementation of the device, a small steel ball having diameter of 4.5 mm is magnetically levitated, Fig. 11.17c, inside the thimble coupled to a vacuum chamber and spinning with a rate of 400 Hz. The ball magnetic moment induces a signal in a pick-up coil. The gas molecules exert drag on the ball and slow its rate of rotation. From kinetic theory it can be shown that collisions with gas molecules cause the ball's rotation frequency to exponentially decrease, or the rotation period  $r$  to exponentially increase with time  $t$ :

$$r = \tau_0 e^{KPt}, \quad (11.18)$$

where  $P$  is the pressure, and  $K$  is the calibration constant. This constant is defined as:

$$K = \frac{\pi\rho\alpha c}{10\sigma_{\text{eff}}}, \quad (11.19)$$

where  $\rho$  is the density of the ball,  $\alpha$  is its radius,  $c$  is the mean gas molecular speed (which depends on the gas temperature and molecular weight), and  $\sigma_{\text{eff}}$  is the effective tangential-momentum accommodation coefficient that accounts for the surface roughness of the ball and molecular scattering characteristics. For “smooth” balls  $\sigma_{\text{eff}}$  is typically between 0.95 and 1.07 (more accurate determination requires calibration against a vacuum standard). Thus, pressure can be computed from the inverted Eq. (11.18) by accounting for the slowing of the rotation rate. This requires integration over a specified time interval.

---

## References

1. Benedict, R. P. (1984). *Fundamentals of temperature, pressure, and flow measurements* (3rd ed.). New York, NY: John Wiley & Sons.
2. Clark, S. K., et al. (1979). Pressure sensitivity in anisotropically etched thin-diaphragm pressure sensor. *IEEE Transactions on Electron Devices*, ED-26, 1887–1896.
3. Kurtz, A. D., et al. (1967). Semiconductor transducers using transverse and shear piezoresistance. *Proceedings of the 22nd ISA Conference*, No. P4-1 PHYMMID-67, September 1967.
4. Tanigawa, H., et al. (1985). MOS integrated silicon pressure sensor. *IEEE Transactions on Electron Devices*, ED-32(7), 1191–1195.
5. Petersen, K., et al. (1998). Silicon fusion bonding for pressure sensors. *Rec. of the IEEE Solid-state sensor and actuator workshop* (pp. 144–147).
6. Peng, K. H., et al. (2004). The temperature compensation of the silicon piezo-resistive pressure sensor using the half-bridge technique. In Tanner DM, Ramesham R (Eds.) *Reliability, testing, and characterization of MEMS/MOEMS III, Proc. SPIE*. Vol. 5343.
7. Wolhuis, R., et al. (1991). Development of medical pressure and temperature sensors employing optical spectral modulation. *IEEE Transactions on Bio-medical Engineering*, 38 (10), 974–981.
8. Hälgl, B. (1991). A silicon pressure sensor with an interferometric optical readout. In: *Transducers'91. International conference on solid-state sensors and actuators. Digest of technical papers* (pp. 682–684). IEEE.
9. Vaughan, J. M. (1989). *The Fabry-Perot interferometers*. Bristol: Adam Hilger.
10. Saaski, E.W., et al. (1989). A fiber optic sensing system based on spectral modulation. Paper #86-2803, ©ISA.
11. Fraden, J. (2009). Detector of low levels of gas pressure and flow. U.S. Patent No. 7,490,512. February 17, 2009.
12. von Pirani, M. (1906). Selbszeigendes vakuum-mefsinstrument. *Verhandlungen der Deutschen Physikalischen Gesellschaft, 1906*, 686–694.
13. Von Smoluchovski, M. (1911). Zur theorie der warnteilung in verdunnten gasen und der dabei auftretenden druckkrafte. *Annalen der Physik*, 35, 983–1004.
14. Leck, J. H. (1964). *Pressure measurement in vacuum systems* (2nd ed.). London: Chapman & Hall.
15. Bayard, R. T., et al. (1950). Extension of the low pressure range of the ionization gauge. *Review of Scientific Instruments*, 21, 571. American Institute of Physics.
16. Fremery, J. K. (1946). *Vacuum*, 32, 685.
17. Looney, J. P., et al. (1994). PC-based spinning rotor gage controller. *Review of Scientific Instruments*, 65(9), 3012.
18. Zhang Y., et al. (2001). An ultra-sensitive high-vacuum absolute capacitive pressure sensor. In: *14th IEEE international conference on micro electro mechanical systems*. (Cat. No. 01CH37090). Technical Digest, pp: 166–169.

*A distinguished scientist was asked which two questions he would ask God?*

- Oh, I would ask to explain the theory which links quantum mechanics and general relativity.
- And the second question? Would you ask God to explain turbulence?
- No, I don't wish to embarrass God. . .

---

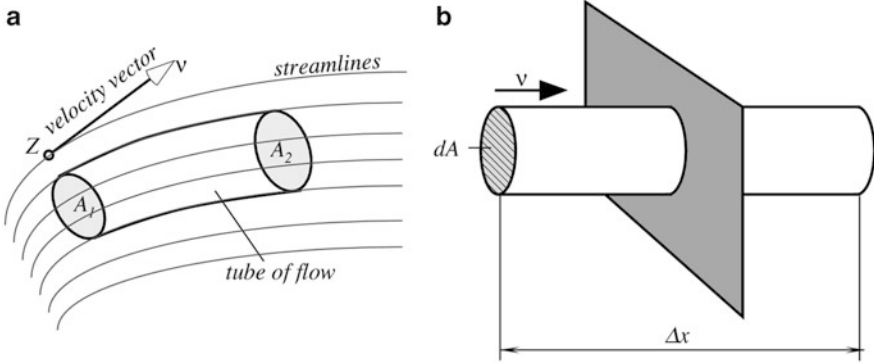
## 12.1 Basics of Flow Dynamics

One of the fundamentals of physics is that mass is a conserved quantity. It cannot be created or destroyed. In the absence of sources or sinks of mass, its quantity remains constant regardless of boundaries. However, if there is influx or outflow of mass through the boundaries, the sum of influx and efflux must be zero. Whatever mass comes in and not stored, it must go out. When both are measured over the same interval of time, mass entering the system ( $M_{in}$ ) is equal to mass leaving the system ( $M_{out}$ ) [1]. Therefore,

$$\frac{dM_{in}}{dt} = \frac{dM_{out}}{dt}. \quad (12.1)$$

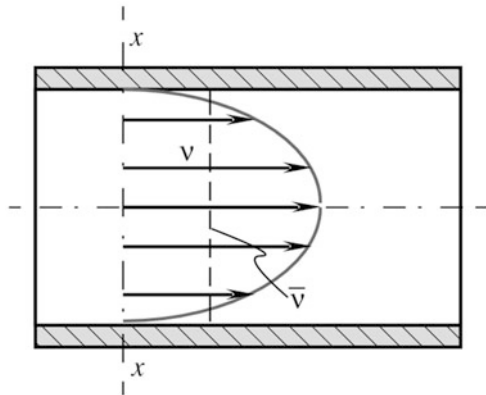
In mechanical engineering, moving media whose flow is measured are liquids (water, oil, solvents, gasoline, etc.), air, and gases (oxygen, nitrogen, CO, CO<sub>2</sub>, methane CH<sub>4</sub>, water vapor, etc.). When we say “flow rate”, “flow velocity”, or “velocity rate” we mean a speed of motion of a miniscule *volume* within the moving fluid.

In a steady flow, the flow velocity at a given point is constant in time. We can draw a streamline through every point in a moving medium (Fig. 12.1a). In a steady flow, the line distribution is time independent. A velocity vector is tangent to a



**Fig. 12.1** Tube of flow (a) and flow of a medium through a plane (b)

**Fig. 12.2** Profile of velocity of flow in a pipe



streamline in every point  $z$ . Any boundaries of flow which envelop a bundle of streamlines is called a *tube of flow*. Since the boundary of such a tube consists of streamlines, no fluid can cross the boundary of a tube of flow and the tube behaves something like a pipe of some shape. The flowing medium can enter such a pipe at one end, having cross-section  $A_1$  and exit at the other end through cross-section  $A_2$ . The velocity of a moving material inside a tube of flow will in general have different magnitudes at different points along the tube.

The volume of moving medium passing a given plane (Fig. 12.1b) in a specified time interval  $\Delta t$  is

$$\Lambda = \frac{V}{\Delta t} = \int \frac{\Delta x}{\Delta t} dA = \int v dA \tag{12.2}$$

where  $v$  is the velocity of moving medium which must be integrated over area  $A$ , while  $\Delta x$  is the displacement of volume  $V$ . Figure 12.2 shows that the velocity of liquid or gas in a pipe may vary over the cross-section. It is often convenient to define an average velocity

$$v_a = \frac{\int v dA}{A} \quad (12.3)$$

When measuring the velocity by a sensor whose dimensions are substantially smaller than the pipe size, one should be aware of a possibility of erroneous detection of either too low or too high velocity, while the average velocity,  $v_a$ , is somewhere in-between. A product of the average velocity and a cross-sectional area is called *flux* or *flow rate*. Its SI unit is  $\text{m}^3/\text{s}$ . The US customary system unit is  $\text{ft}^3/\text{s}$ . The flux can be found by rearranging Eq. (12.3)

$$Av_a = \int v dA \quad (12.4)$$

What a flow sensor usually measures is  $v_a$ . Thus, to determine a flow rate, a cross-section area of tube of flow  $A$  must be known, otherwise the measurement is meaningless.

The measurement of flow is rarely conducted for the determination of a displacement of volume. Usually, what is needed is to determine the *flow of mass* rather than volume. Of course, when dealing with virtually incompressible fluids (water, oil, etc.), either volume or mass can be used. A relationship between mass and volume for an incompressible material is through density  $\rho$

$$M = \rho V. \quad (12.5)$$

The densities of some materials are given in Table A.12. The rate of *mass flow* is defined as

$$\frac{dM}{dt} = \rho A \bar{v} \quad (12.6)$$

The SI unit for mass flow is  $\text{kg}/\text{s}$  while the US customary system unit is  $\text{lb}/\text{s}$ . For a compressible medium (gas) either mass flow or volume flow at a given pressure should be specified.

There is a great variety of sensors which can measure flow velocity by determining the rate of displacement either mass, or volume. Whatever sensor is used, inherent difficulties of the measurement make the process a complicated procedure. It is necessary to take into consideration many of the natural characteristics of the medium, its surroundings, barrel and pipe shapes and materials, medium temperature and pressure, etc.

When selecting any particular sensor for the flow measurement it is advisable to consult with the manufacturer's specifications and very carefully considering the application recommendations for a particular sensor. In this book we do not cover such traditional flow measurement systems as a moving vane or turbine type meters. It is of interest to us to describe sensors without moving components which introduce either no or little restriction into the flow.

## 12.2 Pressure Gradient Technique

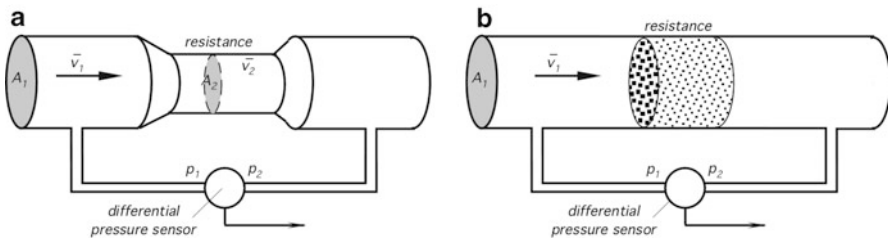
A fundamental equation in fluid mechanics is *Bernoulli equation*<sup>1</sup> which is strictly applicable only to steady flow of nonviscous, incompressible medium

$$p + \rho \left( \frac{1}{2} v_a^2 + gy \right) = \text{const}, \quad (12.7)$$

where  $p$  is the pressure in a tube of flow,  $g = 9.80665 \text{ m/s}^2 = 32.174 \text{ ft/s}^2$  is the Earth gravity constant, and  $y$  is the height of medium displacement. Note that in the Space exploration, the gravity constant should be selected depending on the space body (planet, satellite, comet, etc.). In weightlessness the constant is zero. Bernoulli's equation allows us to find fluid velocity indirectly—by measuring pressures at different points along the flow.

The pressure gradient technique of flow measurement essentially requires an introduction a *flow resistance*. Measuring the pressure gradient across a known resistor allows calculating a flow rate. The concept is analogous to Ohm's law: voltage (pressure) across a fixed resistor is proportional to current (flow). In practice, the restricting elements that cause flow resistances are orifices, porous plugs, and Venturi tubes (tapered profile pipes). Figure 12.3 shows two types of flow resistors. In the first case it is a narrow in the channel, while in the other case there is a porous plug which somewhat restricts the medium flow. A differential pressure sensor (the analog of a voltmeter) is positioned across the resistor. When moving mass enters the higher resistance area, its velocity increases in proportion to the resistance increase

$$v_{1a} = v_{2a}R. \quad (12.8)$$



**Fig. 12.3** Two types of flow resistors: narrow channel (a) and porous plug (b)

<sup>1</sup>The Bernoulli's principle is named after the Dutch-Swiss mathematician Daniel Bernoulli who published his principle in his book *Hydrodynamica* in 1738.

Note that here resistance  $R$  is a dimensionless value. The Bernoulli equation defines differential pressure as<sup>2</sup>

$$\Delta p = p_1 - p_2 = \frac{\rho}{2}(v_{2a}^2 - v_{1a}^2) = k \frac{\rho}{2} v_{2a}^2 (1 - R^2), \quad (12.9)$$

where  $k$  is the correction coefficient which is required because the actual pressure  $p_2$  is slightly lower than the theoretically calculated. From Eq. (12.9) the average flow velocity can be calculated as

$$v_{2a} = \frac{1}{\sqrt{k(1 - R^2)}} \sqrt{\frac{2}{\rho} \Delta p}. \quad (12.10)$$

To determine the mass flow rate per unit time, for incompressible medium, the Eq. (12.10) is simplified to

$$q = \xi A_2 \sqrt{\Delta p}, \quad (12.11)$$

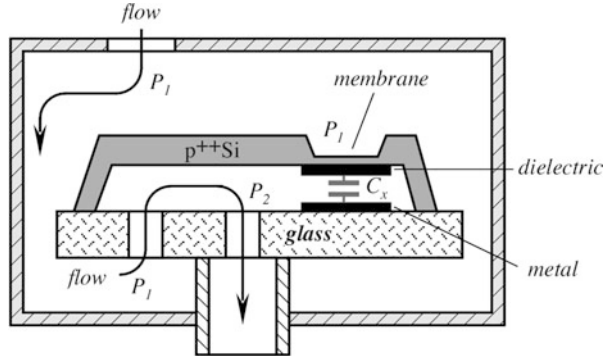
where  $\xi$  is a scaling coefficient which is determined through calibration. The calibration must be done with a specified liquid or gas over an entire operating temperature range since the value of  $\xi$  may be different at different temperatures.

It follows from the above that the pressure gradient technique essentially requires the use of either one differential pressure sensor or two absolute sensors. If a linear representation of the output signal is required, a square root-extraction must be used. The root-extraction can be performed in a microprocessor by using one of the conventional computation techniques. Advantage of the pressure gradient method is in the absence of moving components and use of standard pressure sensors that are readily available. A disadvantage is in the restriction of flow by a resistive device.

As a practical example, consider a microflow sensor that can be constructed by utilizing a capacitive pressure sensor [2] shown in Fig. 12.4. The sensor was fabricated using silicon micromachining and defused boron etch-stops to define the structure. The gas enters the sensor's housing at pressure  $P_1$  through the inlet, and the same pressure is established all around the silicon plate, including the outer side of the etched membrane. The gas flows into the microsensor's cavity through a narrow channel having a relatively high resistance to flow. As a result, pressure  $P_2$  inside the cavity is lower than  $P_1$ , thus creating a pressure differential across the membrane. Therefore, the flow rate can be calculated from Eq. (12.11). The pressure differential causes the membrane deflection that is measured by a capacitive pressure sensor. The capacitance  $C_x$  is formed of a thin, stress compensated,  $p^{++}$  boron-doped silicon membrane suspended above a metal plate. Pressure differential

<sup>2</sup>It is assumed that both pressure measurements are made at the same height ( $y=0$ ) which is usually the case.

**Fig. 12.4** Structure of a gas microflow sensor utilizing capacitive pressure sensor (adapted from [2])



changes capacitance  $C_x$  between the metal plate and the silicon structure with a resolution of 1 mTorr/fF with a full pressure of about 4 Torr. An overall resolution of the sensor is near 14–15 bits and accuracy of the pressure measurement about 9–10 bits. At approximately twice the full scale pressure differential, the membrane touches the metal plate, hence a dielectric layer is required to prevent an electric short, while the substrate glass plate protects the membrane from rupturing. A capacitance measurement circuit (see for example Fig. 9.20) is integrated with the silicon plate using a standard CMOS technology.

## 12.3 Thermal Transport Sensors

A good method of measuring a flow would be by somehow marking the flowing medium and detecting movement of the mark. For example, a mark can be a floating object that can move with the medium while being stationary with respect to the medium (like a raft on a river). The time which it would take the object to move with the flow from one position to another could be used for calculating the flow rate. Such an object may be a float, radioactive element, or dye, such as colored fluid (color smoke or liquid paint). Also, the mark can be a different gas or liquid whose concentration and rate of dilution can be detectable by appropriate sensors.

In medicine, a dye-dilution method of flow measurement is used for studies in hemodynamics. In most instances, however, placing any foreign material into the flowing medium is either impractical or forbidden for some reasons. An alternative would be to change certain physical properties of the moving medium and detect the rate of displacement of the changed portion or rate of its dilution. Usually, the physical property that can be easily modified without causing undesirable effects is temperature.

The sensors that detect the rate of heat dissipation in flowing media are called thermal transport flowmeters or *thermoanemometers*. Thermal transport flowmeters are far more sensitive than other types and have a broad dynamic range. They can be employed for measuring very minute gas or liquid displacements as well as fast and strong currents. Major advantages of these sensors are the absence of moving



components and an ability to measure very low-flow rates. “Paddle wheel”, hinged vane, and pressure differential sensors have low and inaccurate outputs at low-flow rates. If a small diameter of a tubing is required, as in automotive, aeronautic, medical, and biological applications, sensors with moving components become mechanically impractical or difficult to use. In these applications, thermal transport sensors are indispensable. Another advantage of these sensors is their usefulness for detecting the material change in composition because they are sensitive to heat transport in a media that is typically altered by a changing composition or chemical reaction.

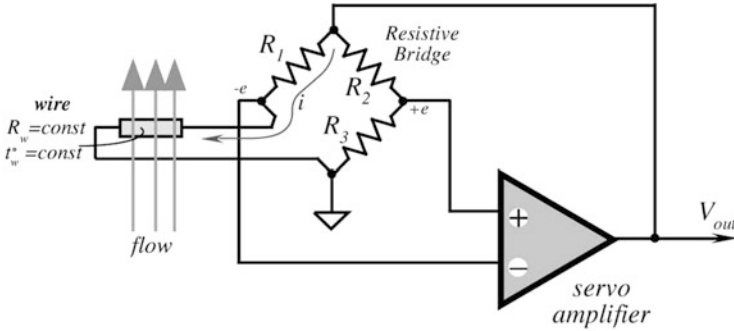
A thermoanemometer design determines its operating limits. At a certain velocity, the molecules of a moving medium while passing near a heater do not have sufficient time to absorb enough thermal energy for developing a temperature change in a temperature sensor. The upper operating limits for the thermal transport sensors usually are determined experimentally. For instance, under normal atmospheric pressure and room temperature (about 20 °C), the maximum air velocity that can be detected by a thermal transport sensor is in the range of 60 m/s (200 ft/s).

The pressure and temperature of a moving medium, especially of gases, make a strong contribution to the accuracy of a volume rate calculation. It is interesting to note that for the mass flow meters, pressure makes very little effect on the measurement as increase in pressure results in a proportional increase in mass.

A typical data processing system for a thermal transport sensing must receive at least three variable input signals: a flowing medium temperature, a temperature differential, and a heating power signal. These signals are multiplexed, converted into digital form, and processed by a computer to calculate characteristics of flow. Data are usually displayed in velocities (m/s or ft/s), volume rates (m<sup>3</sup>/s or ft<sup>3</sup>/s), or mass rate (kg/s or lb/s).

### 12.3.1 Hot-Wire Anemometers

The oldest and best known thermal transport flow sensors are the hot-wire and later developed hot-film anemometers [3]. They have been used quite extensively for measurements of turbulence levels in wind tunnels, flow patterns around models, and blade wakes in radial compressors. A hot-wire thermoanemometer is a single-part sensor as opposed to two- and three-part sensors as described below. The key element of this sensor is a heated wire having typical dimensions 0.00015–0.0002 in. (0.0038–0.005 mm) in diameter and 0.040–0.080 in. (1.0–2.0 mm) in length. The wire resistance typically is between 2 and 3 Ω. The operating principle is based on warming up the wire by electric current to 200–300 °C—well above the flowing media temperature and then measuring temperature of the wire. A high temperature, that typically is well over temperatures of the flowing media, makes the sensor little sensitive to the media temperature and thus no media temperature compensation is required. Under the no-flow condition, temperature of the wire will be constant, but when the media flows, the wire will be cooled. The stronger the



**Fig. 12.5** Null-balanced bridge for a constant temperature hot-wire anemometer

flow the stronger the cooling. Advantage of the hot-wire and hot-film probes is in their fast speed responses—they can resolve frequencies up to 500 Hz.

There are two methods of controlling temperature and measuring a cooling effect—a constant voltage and a constant temperature. In the former method, reduction in the wire temperature is measured, while in the latter case, the temperature is maintained constant at any reasonable flow rate by the increase in supplied electric power. That power is the measure of the flow rate. In a hot-wire anemometer, the wire has a positive temperature coefficient (PTC) and thus is used for a dual purpose: to elevate temperature above the media temperature (to create a cooling effect) and also to measure that temperature because the wire resistance goes down when the wire cools. Figure 12.5 shows a simplified bridge circuit for the constant temperature method. This is a null-balanced bridge that is based on the principle described in Sect. 6.2.4.

The feedback from a servo amplifier keeps the bridge in a balanced state. Resistors  $R_1$ – $R_3$  are constant, while  $R_w$  represents resistance of the hot wire and is temperature dependent. Drop in the wire temperature  $t_w$  causes temporary drop in  $R_w$  and a subsequent reduction in the bridge voltage  $-e$  that is applied to the negative input of a servo amplifier. This leads to increase in  $V_{out}$  which is applied to the bridge as a feedback. When  $V_{out}$  goes up, current  $i$  through the wire increases, leading to increase in temperature. This restores the wire temperature when the flowing media attempt to cool it, so  $t_w$  remains constant over the entire flow rate range. The feedback voltage  $V_{out}$  is the output signal of the circuit and the measure of a mass flow rate. The faster the flow, the higher the voltage.

Under a steady flow rate, the electric power  $Q_e$  supplied to the wire is balanced by the out-flowing thermal power  $Q_T$  carried by the flowing media due to a convective heat transfer. That is,

$$Q_e = Q_T. \quad (12.12)$$

Considering the heating current  $i$ , the wire temperature  $t_w$ , temperature of the fluid  $t_f$ , the wire surface area  $A_w$ , and the heat transfer coefficient  $h$ , we can write the power balance equation

$$i^2 R_w = h A_w (t_w - t_f) \quad (12.13)$$

In 1914 L.V. King [4] developed a solution of a heat loss from an infinite cylindrical body in an incompressible fluid with low Reynolds number. The heat loss coefficient is:

$$h = a + b v_f^c, \quad (12.14)$$

where  $a$  and  $b$  are constant and  $c \approx 0.5$ . This equation is known as King's law.

Combining the above three equations allows us to eliminate the heat transfer coefficient  $h$ :

$$a + b v_f^c = \frac{i^2 R_w}{A_w (t_w - t_f)} \quad (12.15)$$

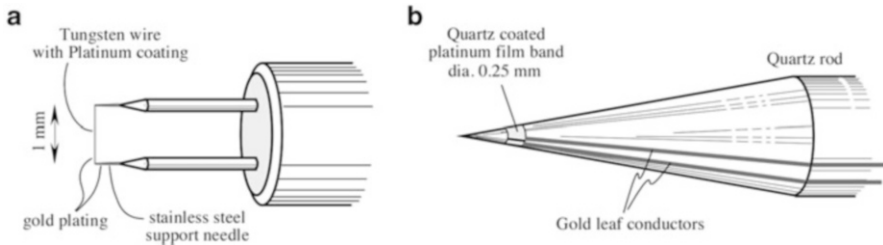
Considering that  $V_{\text{out}} = i(R_w + R_l)$  and  $c = 0.5$ , we can solve this equation for the output voltage as function of the fluid velocity  $\nu$ :

$$V_{\text{out}} = (R_w + R_l) \sqrt{\frac{A_w (a + b \sqrt{\nu}) (t_w - t_f)}{R_w}}. \quad (12.16)$$

Thanks to high temperature gradient ( $t_w - t_f$ ), the output signal depends little of the media temperature  $t_f$ . For efficient operation, the temperature gradient ( $t_w - t_f$ ) and the sensor surface area should be as large as practical.

Since the King's law was derived for an infinite cylinder, its applicability to a practical sensor should be taken with a grain of salt. The hot wire is relatively short (no more than 2 mm) and must be somehow supported by the probe and held steady while inside the flow. Also, electrical resistance of the wire should be relatively low to allow for heating by electric current. At the same time, the wire should have as large thermal coefficient as possible. A very careful design is required to meet these requirements. Heat can be lost from the wire not only by means of convection (the useful effect) but also via thermal radiation and thermal conduction (interfering effects). While thermal radiation is usually negligibly small and can be ignored, conductive heat loss via the support structure may be comparable or even greater than the convective loss. Thus, the heated wire must have as large thermal resistance to the support structure as physically possible. This poses series challenges to the sensor designer.

A typical design of the hot-wire sensor is shown in Fig. 12.6a. The most common wire materials are tungsten, platinum, and a platinum-iridium alloy. Tungsten wires are strong and have a high temperature coefficient of electrical resistance ( $0.004 \text{ }^\circ\text{C}^{-1}$ ). However, they cannot be used at high temperatures in many gases because of poor oxidation resistance. Platinum has good oxidation resistance, has a relatively large temperature coefficient ( $0.003 \text{ }^\circ\text{C}^{-1}$ ), but is very weak, particularly at high temperatures. The platinum-iridium wire is a compromise between tungsten and platinum with good oxidation resistance, and more strength than platinum, but



**Fig. 12.6** Hot-wire probe (a) and a conical hot-film probe (b)

it has a low temperature coefficient of electrical resistance ( $0.00085\text{ }^{\circ}\text{C}^{-1}$ ). Presently, tungsten is the most popular hot-wire material. A thin platinum coating is usually applied to improve bond with the plated ends and the support needles. The needles should be thin but strong and have high thermal resistance (low thermal conductivity) to the probe body. Stainless steel is the most often used material. Hot-wires probes are expensive, extremely fragile, and can be damaged easily mechanically or by an excessive electric pulse.

A hot-film sensor is essentially a conductive film deposited on an insulator, such as a ceramic substrate. The sensor shown in Fig. 12.6b is a quartz cone with a platinum film on the surface. Gold plating on the sides of the cone provides electrical connection. When compared with hot wires, the hot-film sensor has the following advantages:

- Better frequency response (when electronically controlled) than a hot wire of the same diameter because the sensitive part of the film sensor has a larger surface area.
- Lower heat conduction to the supports for a given length to diameter ratio due to the low thermal conductivity of the substrate material. A shorter sensing length can thus be used.
- More flexibility in sensor configuration. Wedge, conical, parabolic, and flat surface shapes are available.
- Less susceptible to fouling and easier to clean. A thin quartz coating on the surface resists accumulation of foreign material.

The metal film thickness on a typical film sensor is less than  $1000\text{ \AA}$ , thus the physical strength and the effective thermal conductivity is determined almost entirely by the substrate material. Most films are made of platinum due to its good oxidation resistance and the resulting long-term stability. A better ruggedness and stability of film sensors have led to their use for many measurements that have previously been very difficult with the more fragile and less stable hot wires. The hot-film probes have been made on cones, cylinders, wedges, parabolas, hemispheres, and flat surfaces. Cylindrical film sensors that are cantilever mounted are also made. This is done by making the cylindrical film sensor from a quartz tube and running one of the electrical leads through the inside of the tube.

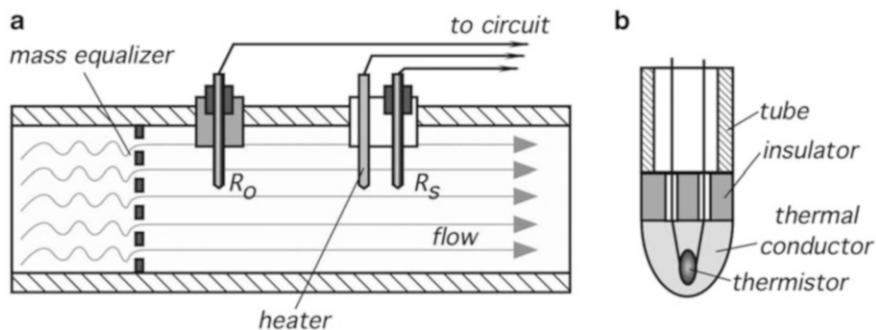
The cone-shaped sensor of Fig. 12.6b is used primarily in water applications where its shape is particularly valuable in preventing lint and other fibrous impurities from getting entangled with sensor. The cone can be used in relatively contaminated water, while cylindrical sensors are more applicable when the water has been filtered.

### 12.3.2 Three-Part Thermoanemometer

The thermal anemometer shown in Fig. 12.7 is used primarily for liquids but also may be useful for gases. It is a very rugged and contamination-resistant device. This sensor is comprised of three small tubes immersed into a moving medium. Two tubes contain temperature detectors  $R_o$  and  $R_s$ . The detectors are thermally coupled to the medium and thermally isolated from the structural elements and the pipe where the flow is measured. In between two detectors, a heating element is positioned. Both detectors are connected to electrical wires through tiny conductors to minimize thermal loss through conduction, Fig. 12.7b.

The sensor operates as follows. The first temperature detector  $R_o$  measures the temperature of the flowing medium. Downstream from the first sensor, the heater warms up the medium and the elevated temperature is measured by the second temperature detector  $R_s$ . In a still medium, heat would be dissipated from the heater through media to both detectors. In a medium with a zero flow, heat moves out from the heater mainly by thermal conduction and gravitational convection. Since the heater is positioned closer to the  $R_s$  detector, that detector will register higher temperature. When the medium flows, heat dissipation increases due to forced convection. The higher the rate of flow the higher the heat dissipation and the lower temperature will be registered by the  $R_s$  detector. Heat loss is measured and converted into the flow rate of medium.

A fundamental relationship of the thermoanemometry is based on King's law as described above for the hot-wire anemometer. An incremental heat change is



**Fig. 12.7** Three-part thermoanemometer. Basic two-sensor design (a); cross-sectional view of a temperature sensor (b)

$$\Delta Q = kl \left( 1 + \sqrt{\frac{2\pi\rho cd\nu}{k}} \right) (t_s - t_f), \quad (12.17)$$

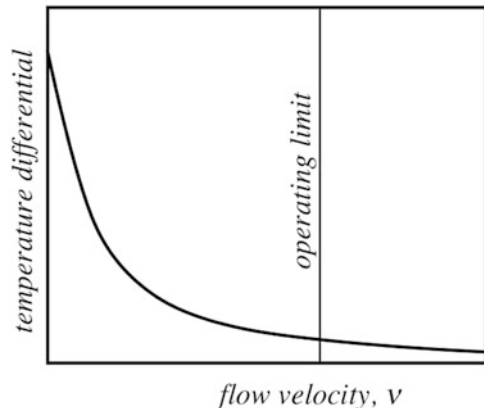
where  $k$  and  $c$  are the thermal conductivity and specific heat of a medium at a given pressure,  $\rho$  is the density of the medium,  $l$  and  $d$  are the length and diameter of the second temperature sensor,  $t_s$  is the surface temperature of the second sensor,  $t_f$  is the temperature of the first sensor (media temperature), and  $\nu$  is the velocity of the medium. Collis and Williams experimentally proved [5] that King's theoretical law needs some correction. For a cylindrical sensor with  $l/d \gg 1$ , a modified King's equation yields the velocity of the medium:

$$v = \frac{K}{\rho} \left( \frac{dQ}{dt} \frac{1}{t_s - t_f} \right)^{1.87}, \quad (12.18)$$

where  $K$  is the calibration constant. It follows from the above that to measure a flow, a temperature gradient between the second sensor and the moving medium, and dissipated heat, must be measured. Then velocity of the fluid or gas becomes although nonlinear, but a quite definitive function of a thermal loss (Fig. 12.8).

For accurate temperature measurements in a flowmeter, any type of temperature detector can be used—resistive, semiconductor, optical, etc. (Chap. 17). Nowadays, however, the majority of manufacturers use resistive sensors. In industry and scientific measurements, RTDs is the prime choice as they assure higher linearity, predictable response, and long-term stability over a broader temperature range. In medicine, thermistors are often preferred thanks to their higher sensitivity. Whenever a resistive temperature sensor is employed, especially for a remote sensing, a four-wire measurement technique should be seriously considered. The technique is a solution for a problem arising from a finite resistance of connecting wires which may be a substantial source of error, especially with low-resistance temperature sensors like RTDs. See Sect. 6.6.2 for description of the four-wire method.

**Fig. 12.8** Transfer function of a thermoanemometer

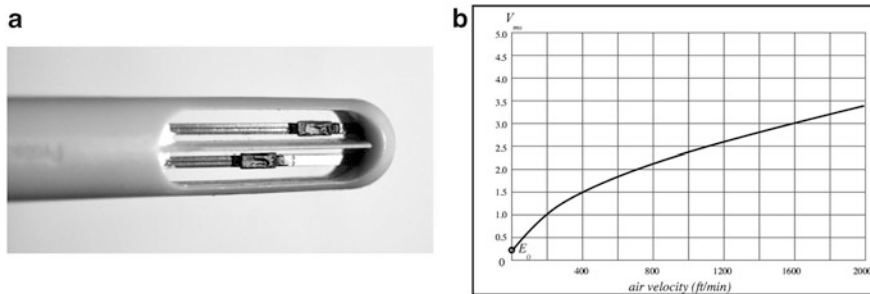


While designing thermal flow sensors, it is important to assure that the medium moves through the detectors without turbulence in a laminar well mixed flow. Thus, the sensor is often supplied with the mixing grids or turbulence breakers which sometimes are called *mass equalizers*, Fig. 12.7a.

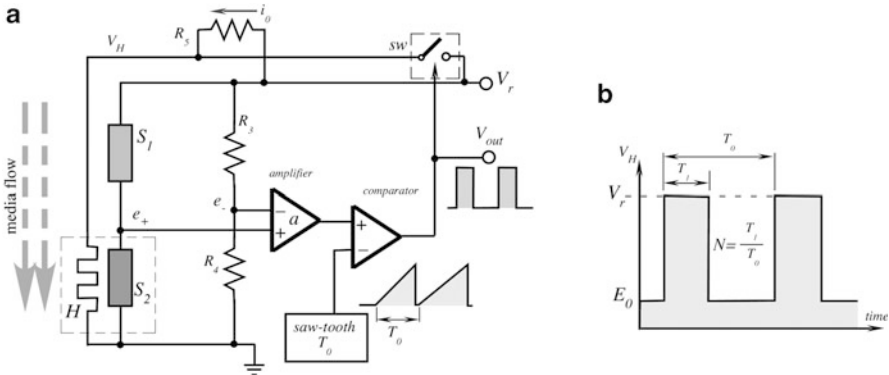
### 12.3.3 Two-Part Thermoanemometer

The hot-wire and hot-film anemometers that were described above are the fast-response sensors. However, they are extremely delicate and expensive devices that is sensitive to many airborne contaminants, like dust and smoke. In many applications, a gas flow should be monitored continuously, for a long time without the need for a fast response. Such sensors should be more resistant to gas impurities and mechanically rugged. Since the speed of response can be sacrificed for the sake of robustness, different design approaches are taken. Three functions should be accomplished by a thermal transport sensor: measuring temperature of the flowing media, heating the media, and monitoring the cooling effect caused by the flow. Figure 12.9a shows a two-part thermoanemometer [6, 7] where one part is the media temperature reference sensor  $S_1$ , while the other part is a combination of the heating  $H$  and temperature sensing  $S_2$  elements that are kept in an intimate thermal coupling with each other. In other words, the second temperature sensor measures temperature of the heater.

Both temperature sensors are the thick-film NTC thermistors (see Sect. 17.4.6) printed on the ceramic substrates. These substrates form two sensing “strips” show in Fig. 12.9a. The second substrate in addition comprises a heating resistor  $H = 150 \Omega$  printed over the thermistor layer  $S_2$  with an electrical isolating barrier in-between. Both strips are coated with thin layers of protective glass or thermally conductive epoxy. The thermistors are connected into a Wheatstone bridge (Fig. 12.10a) where two fixed resistors  $R_3$  and  $R_4$  comprise the other two arms of the bridge [8]. To generate heat, the following condition must be met:  $R_4 < R_3$ . The warm strip is thermally decoupled from the reference strip and both strips are exposed to gas flow. This sensor is not very fast. It can be characterized by a relatively long time constant of about 0.5 s, yet for many applications this is sufficiently small.



**Fig. 12.9** Two-part thermoanemometer probe (a) and transfer function (b) (Courtesy of CleanAlert, LLC)



**Fig. 12.10** Control circuit of a thermoanemometer with PWM modulator (a); heating PWM signal (b)

The thermistor  $S_2$  is warmed up above the media (air) temperature by a constant increment  $\Delta t = 5\text{--}10\text{ }^\circ\text{C}$ . During operation, air moves across both thermistors  $S_1$  and  $S_2$  and removes thermal energy from the warmer thermistor  $S_2$  in relation to the airflow velocity. The convective cooling is compensated for by the electric power provided to the heater  $H$  from a feedback circuit that is similar to Fig. 12.5. However there is a difference—the heating voltage  $V_H$  is a pulse-width modulated (PWM) feedback to the heater whose *r.m.s.* value provides a Joule heat. The PWM signal is formed with the help of a saw-tooth generator having a fixed period  $T_0$  of about 4 ms. The pulses from the comparator control the switch  $sw$  that connects the heater to the reference voltage  $V_r$ . The wider the PWM pulses, the more heat is generated. This PWM signal also serves as the output of the sensor where the duty cycle  $N$  represent the airflow rate.

The sensor is quite rugged and both sensing strips are securely supported by the interior of the probe. The price for the ruggedness is a not too high thermal resistance  $r$  between the strip and probe body. As a result, a significant thermal power  $P_L$  is lost to the supporting structure via thermal conduction. To compensate for this undesirable effect, resistor  $R_5$  provides to  $H$  a compensating current  $i_0$  when the switch  $sw$  is open. This is visible in Fig. 12.10b as a voltage pedestal  $E_0$  across  $H$ .

Initially, at the moment when the reference voltage  $V_r$  is just being turned on, the thermistors are at the same air temperature and thus have nearly equal resistances. The bridge is disbalanced because  $R_4 < R_3$ . The bridge differential voltage ( $e_+ - e_-$ ) is amplified with gain  $a$ , compared with the saw-tooth signal to form a PWM signal. The rectangular PWM pulses from the comparator control the gating switch  $sw$ , resulting in the output voltage pulses  $V_H$  which are applied to the heater  $H$ . The pulses develop a Joule heat in the heater  $H$  and warm up the thermistor  $S_2$ . Temperature of  $S_2$  goes up by  $\Delta t$  above the air temperature and resistance of  $S_2$  drops until the moment when the bridge enters a balanced state:

$$\frac{S_1}{S_2} = \frac{R_3}{R_4} \quad (12.19)$$



The balance is kept by the feedback circuit as long as there is no change in the air movement near the sensing thermistors, so the ratio of Eq. (12.19) is satisfied. Change in the airflow rate (change in cooling) disbalances the bridge and subsequently modulates the duty cycle  $N$  of the PWM signal to restore the ratio of Eq. (12.19). Thus, value of  $N$  reflects the airflow rate.

To obtain the sensor's transfer function, remember that heater  $H$  and thermistor  $S_2$  lose thermal energy to the probe body by means of thermal conduction at a rate

$$P_L = \frac{\Delta t}{r}, \quad (12.20)$$

where  $r$  is a thermal resistance [ $^{\circ}\text{C}/\text{W}$ ] to the support structure. A typical value of  $r$  is on the order of  $50\text{ }^{\circ}\text{C}/\text{W}$  and the design goal is to make that number as large as possible. The compensating power to balance out the loss is provided to  $H$  via  $R_5$  when  $sw$  is open. Its value is

$$P_0 = \frac{E_0^2}{H}(1 - N)^2 \quad (12.21)$$

The flowing air results in a convective heat loss from  $S_2$  that is defined as

$$P_a = k\nu\Delta t, \quad (12.22)$$

where  $\nu$  is the air velocity and  $k$  is the scaling factor. To compensate for the convective cooling, Joule heat power is delivered to  $H$  from the PWM feedback circuit:

$$P_f = \frac{N^2 V_r^2}{H} \quad (12.23)$$

The law of conservation of energy demands that under a steady-state condition

$$P_L + P_a = P_0 + P_f \quad (12.24)$$

Substituting Eqs. (12.20)–(12.23) into Eq. (12.24) we arrive at:

$$\frac{\Delta t}{r} + k\nu\Delta t = i_0^2 H(1 - N)^2 + \frac{N^2 V_r^2}{H} = \frac{E_0^2}{H}(1 - N)^2 + \frac{N^2 V_r^2}{H}, \quad (12.25)$$

from which we derive the output value of the PWM duty cycle  $N$ :

$$N = \sqrt{\frac{(\frac{\Delta t}{r} + k\nu\Delta t)H - i_0^2 H^2}{V_r^2 - i_0^2 H^2}} \approx \sqrt{\frac{((\frac{1}{r} + k\nu)\Delta t - i_0^2 H)H}{V_r}}. \quad (12.26)$$

Since the value in parenthesis is always positive, to prevent a dead-bad zone where the sensor is not responsive, the following condition must be met:

$$\frac{\Delta t}{r} \geq i_0^2 H = \frac{V_r^2 H}{(H + R_5)^2} \quad (12.27)$$

The sensor's response is shown in Fig. 12.9b. In a practical design, thermistors  $S_1$  and  $S_2$  may have manufacturer's tolerances that should be compensated for by trimming one of the resistors  $R_3, R_4$ . If the conductive heat loss is fully compensated by current  $i_0$ , the compensating condition is met:

$$\frac{\Delta t}{r} = i_0^2 H, \quad (12.28)$$

then from the inverted Eq. (12.26) the mass flow rate can be computed from a PWM duty cycle  $N$ :

$$\nu = \frac{V_r^2}{k \Delta t H} N^2 \quad (12.29)$$

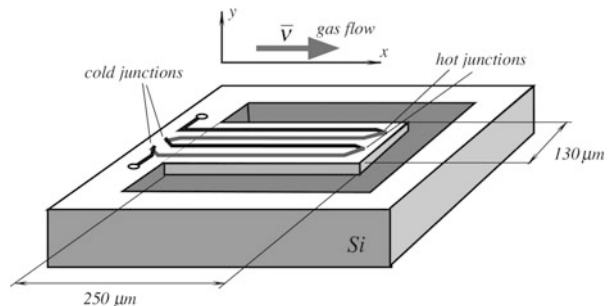
### 12.3.4 Microflow Thermal Transport Sensors

In some applications, such as process control in precise semiconductor manufacturing, chemical and pharmaceutical industries, and biomedical engineering, miniaturized gas flow sensors are in a strong demand. Most of them are thermoanemometers. Miniature flow sensors are fabricated from a silicon crystal by using micromachining technology (MEMS). Many of the microflow sensors use thermopiles as temperature sensors [9, 10].

A cantilever design of a microflow sensor is shown in Fig. 12.11. Thickness of the cantilever may be as low as 2  $\mu\text{m}$ . It is fabricated in the form of a sandwich consisting of layers of field oxide, CVD oxide, and nitrate [11]. The cantilever sensor is heated by an imbedded resistor with a rate of 26 K/mW of the applied electric power, and a typical transfer function of the flow sensor has a negative slope of about 4 mV/(m/s).

Heat is removed from the sensor by three means: conductance  $L_b$  through the cantilever beam, gas flow  $h(\nu)$ , and thermal radiation, which is governed by the

**Fig. 12.11** Micromachined gas flow sensor



Stefan-Boltzmann law. Thus, the thermal power equation has three respective components:

$$P = L_b(T_s - T_b) + h(v)(T_s - T_b) + a\sigma\varepsilon(T_s^4 - T_b^4), \tag{12.30}$$

where  $\sigma$  is the Stefan-Boltzmann constant,  $a$  is the area along which the beam-to-gas heat transfer occurs,  $\varepsilon$  is surface emissivity, and  $v$  is the gas velocity. From the principles of energy and particle conservation we deduce a generalized heat transport equation governing the temperature distribution  $T(x,y)$  in the gas flowing near the sensor's surface

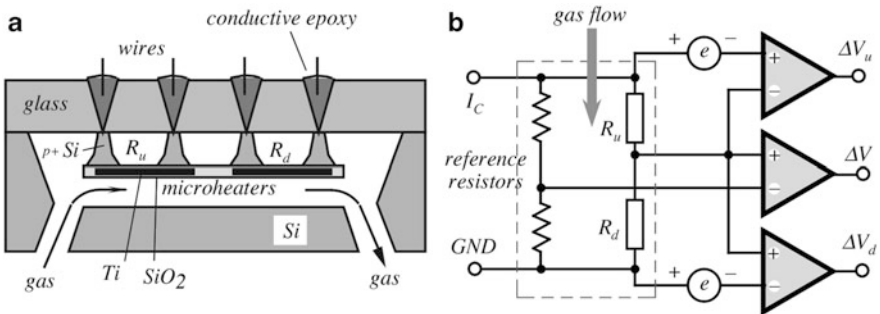
$$\frac{\partial^2 T}{\partial x^2} + \frac{\partial^2 T}{\partial y^2} = \frac{vnc_p}{k_g} \frac{\partial T}{\partial x} \quad \text{for } y > 0, \tag{12.31}$$

where  $n$  is the gas density,  $c_p$  is the molecular gas capacity, and  $k_g$  is the thermal conductivity of gas. It can be shown that solution of this equation for the boundary condition of a vanishing thermal gradient far off the surface is [11]:

$$\Delta V = B \left( \frac{1}{\sqrt{\mu^2 + 1}} - 1 \right), \tag{12.32}$$

where  $V$  is the input voltage,  $B$  is a constant, and  $\mu = Lvnc_p/2\pi k_g$ , and  $L$  is the gas-sensor contact length. This solution coincides very well with the experimental data.

Another design of a thermal transport microsensor is shown in Fig. 12.12a [12] where the titanium films having thickness of 0.1  $\mu\text{m}$  serve as both the temperature sensors and heaters. The films are sandwiched between two layers of  $\text{SiO}_2$ . Titanium was used because of its high TCR (temperature coefficient of resistance) and excellent adhesion to  $\text{SiO}_2$ . Two microheaters are suspended with four silicon girders at a distance of 20  $\mu\text{m}$  from one another. The Ti film resistance is about



**Fig. 12.12** Gas microflow sensor with self-heating titanium resistors sensor design (a); interface circuit (b).  $R_u$  and  $R_d$  are resistances of the up- and downstream heaters respectively (adapted from [12])

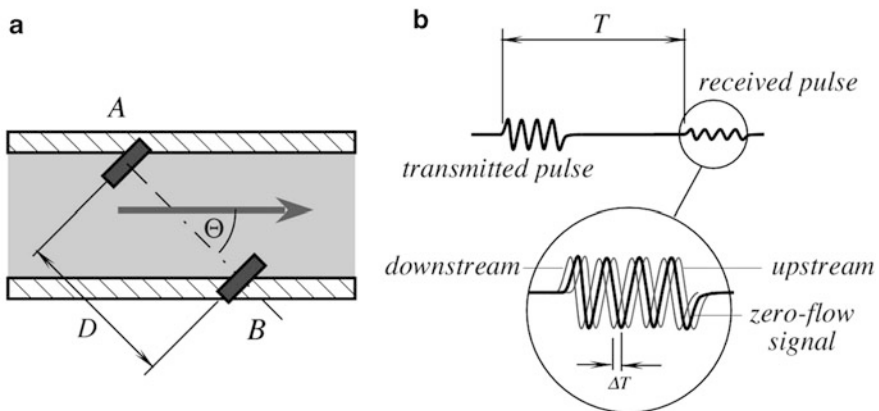
2 k $\Omega$ . Figure 12.12b shows a simplified interface circuit diagram for the sensor, which exhibits an almost linear relationship between the flow and output voltage change  $\Delta V$ .

## 12.4 Ultrasonic Sensors

Flow rate can be measured by employing ultrasonic waves. The main idea behind the principle is the detection of frequency or phase shift caused by flowing medium. One possible implementation is based on the Doppler effect (see Sects. 7.1 and 7.2 for the description of the Doppler effect), while the other relies on the detection of the increase or decrease in effective ultrasound velocity in the medium. Effective velocity of sound in a moving medium is equal to the velocity of sound relative to the medium plus the velocity of the medium with respect to the source of the sound. Thus, a sound wave propagating upstream will have a smaller effective velocity, while the sound propagating downstream will have a higher effective velocity. Since the difference between the two velocities is exactly twice the velocity of the medium, measuring the upstream-downstream velocity difference allows us to determine the velocity of the flow.

Figure 12.13a shows two ultrasonic generators positioned at opposite sides of a tube of flow. Piezoelectric crystals are usually employed for that purpose. Each crystal can be used for either the generation of the ultrasonic waves (motor mode), or for receiving the ultrasonic waves (generator mode). In other words, the same crystal, when needed, acts either as a “speaker” or “microphone”.

Two crystals are separated by distance  $D$  and positioned at angle  $\Theta$  with respect to flow. Also, it is possible to place the small crystals right inside the tube along the flow. That case corresponds to  $\Theta = 0$ . The transit time of sound between two transducers  $A$  and  $B$  can be found through the average fluid velocity  $v_c$



**Fig. 12.13** Ultrasonic flowmeter. Position of transmitter-receiver crystals in flow (a); waveforms in circuit (b)

$$T = \frac{D}{c \pm \nu_c \cos \Theta}, \tag{12.33}$$

where  $c$  is the velocity of sound in the fluid. The plus/minus signs refer to the downstream/upstream directions, respectively. The velocity  $\nu_c$  is the flow velocity averaged along the path of the ultrasound. Gessner [13] has shown that for laminar flow  $\nu_c = 4\nu_a/3$ , and for turbulent flow,  $\nu_c = 1.07\nu_a$ , where  $\nu_a$  is the flow averaged over the cross-sectional area. By taking the difference between the downstream and upstream velocities we arrive at [5]

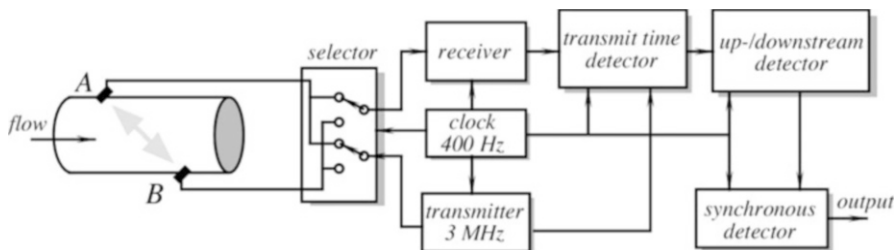
$$\Delta T = \frac{2D\nu_c \cos \Theta}{c^2 + \nu_c \cos^2 \Theta} \approx \frac{2D\nu_c \cos \Theta}{c^2}, \tag{12.34}$$

which is true for the most practical cases when  $c \gg \nu_c \cos \Theta$ . To improve the signal-to-noise ratio, the transit time is often measured for both up- and downstream directions. That is, each piezoelectric crystal at one time works as a transmitter and at the other time as a receiver. This can be accomplished by a selector (Fig. 12.14) which is clocked by a relatively slow sampling rate (400 Hz in this example). The sinusoidal ultrasonic waves (about 3 MHz) are transmitted as bursts with the same slow clock rate (400 Hz). A received sinusoidal burst is delayed from the transmitted one by time  $T$  which is modulated by the flow, Fig. 12.13b. This time is detected by a transit time detector, then the time difference in both directions is recovered by a synchronous detector.

An alternative way of measuring flow with the ultrasonic sensors is to detect a phase difference in transmitted and received pulses in the up- and downstream directions. The phase differential can be derived from Eq. (12.34)

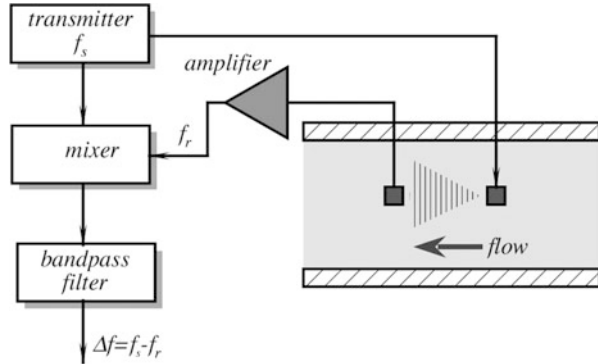
$$\Delta\varphi = \frac{4fD\nu_c \cos \Theta}{c^2}, \tag{12.35}$$

where  $f$  is the ultrasonic frequency. It is clear that the sensitivity is better with the increase in the frequency, however, at higher frequencies one should expect stronger sound attenuation in the system, which may cause reduction in the signal-to-noise ratio.



**Fig. 12.14** Block diagram of ultrasonic flowmeter with alternating transmitter and receiver

**Fig. 12.15** Ultrasonic Doppler flowmeter with continuous transmission



For the Doppler flow measurements, continuous ultrasonic waves can be used. Figure 12.15 shows a flowmeter with a transmitter-receiver assembly positioned inside the flowing stream. Like in a Doppler radio receiver, transmitted and received frequencies are mixed in a nonlinear circuit (a mixer). The output low-frequency differential harmonic is selected by a bandpass filter. That differential is defined as

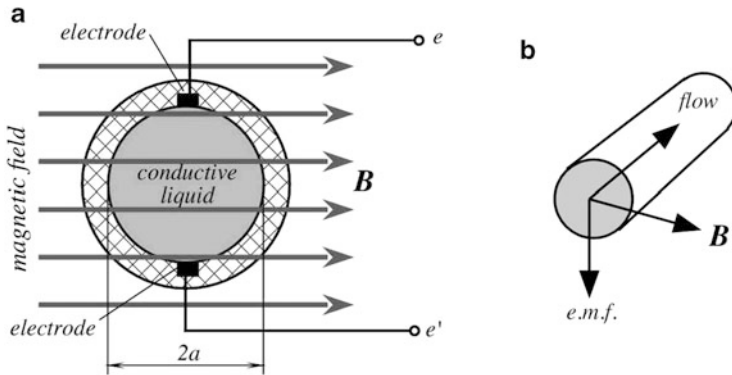
$$\Delta f = f_s - f_r \approx \pm \frac{2f_s v}{c}, \quad (12.36)$$

where  $f_s$  and  $f_r$  are the frequencies in the transmitting and receiving crystals respectively, and the plus/minus signs indicate different directions of flow. An important conclusion from the above equation is that the differential frequency is directly proportional to the flow velocity. Obviously, the piezoelectric crystals must have much smaller sizes than the clearance of the tube of flow. Hence, the measured velocity is not the average but rather a localized velocity of flow. In practical systems, it is desirable to calibrate the ultrasonic sensors with actual fluids over the useful temperature range, so that contribution of a fluid viscosity is accounted for.

An ultrasonic piezoelectric sensors/transducers can be fabricated of small ceramic discs encapsulated into a flowmeter body. The surface of the crystal can be protected by a suitable material, for instance, silicone rubber. An obvious advantage of an ultrasonic sensor is in its ability to measure flow without a direct contact with the fluid.

## 12.5 Electromagnetic Sensors

The electromagnetic flow sensors are useful for measuring the movement of *conductive* liquids. The operating principle is based on the discovery of Faraday and Henry of the electromagnetic induction (see Sects. 4.3 and 4.4). When a



**Fig. 12.16** Principle of electromagnetic flowmeter. Position of electrodes is perpendicular to the magnetic field (a); relationships between flow and electrical and magnetic vectors (b)

conductive media—a wire, for instance, or for this particular purpose—flowing conductive liquid crosses the magnetic flux lines, e.m.f. is generated in the moving conductor (liquid). As follows from Eq. (4.35), the value of e.m.f. is proportional to velocity of moving conductor. Figure 12.16 illustrates a tube of flow positioned into the magnetic field  $\mathbf{B}$ . There are two electrodes incorporated into a tube to pick up the e.m.f. induced in the liquid. The magnitude of the e.m.f. is defined by

$$V = e - e' = 2a\mathbf{B}\nu, \quad (12.37)$$

where  $a$  is the radius of the tube of flow, and  $\nu$  is the velocity of flow.

By solving the Maxwell's equations, it can be shown that for a typical case when the fluid velocity is nonuniform within the cross-sectional area but remains symmetrical about the tube axis (axisymmetrical), the e.m.f generated is the same as that given above, except that  $\nu$  is replaced by the average velocity,  $\nu_a$ , Eq. (12.3):

$$\nu_a = \frac{1}{\pi a^2} \int_0^a 2\pi r \nu r \, dr \quad (12.38)$$

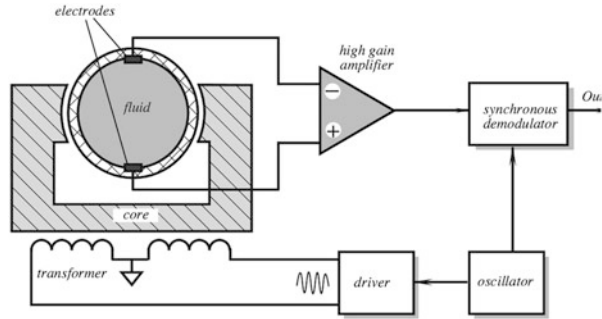
where  $r$  is the distance from the center of the tube. Equation (12.38) can be expressed in terms of the volumetric flow rate

$$\nu_a = \frac{2\Delta\mathbf{B}}{\pi a}. \quad (12.39)$$

It follows from the above equation that the voltage registered across the pick-up electrodes is independent of the flow profile or fluid conductivity. For a given tube geometry and the magnetic flux, it depends only on the instantaneous volumetric flow rate.

There are two general methods of inducing voltage in the pick-up electrodes. The first is a dc method where the magnetic flux density is constant and induced

**Fig. 12.17** Electromagnetic flowmeter with synchronous (phase sensitive) demodulator. Magnetic field is applied to tube by magnetic concentrator (core). Pick-up electrodes contact fluid



voltage is a d.c. or slow changing signal. One problem associated with this method is a polarization of the electrodes due to small but unidirectional current passing through their surface. The other problem is a low-frequency noise which makes it difficult to detect small flow rates.

Another and far better method of excitation is with an alternating magnetic field, which causes appearance of an a.c. voltage across the electrodes (Fig. 12.17). Naturally, the frequency of the magnetic field should meet a condition of the Nyquist rate. That is, it must be at least two times higher than the highest frequency of flow rate variations. In practice, the excitation frequency is selected in the range between 100 and 1000 Hz.

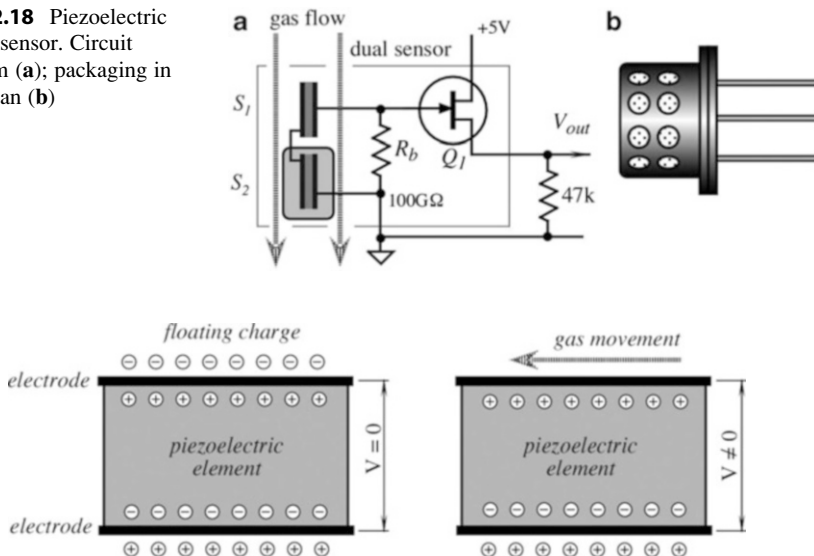
## 12.6 Breeze Sensor

In some applications, it is desirable just to merely detect a change in the air (or any other gas for that matter) movement, rather than to measure its flow rate quantitatively. This task can be accomplished by a breeze sensor, which produces an output transient whenever velocity of the gas flow changes. One example of such a device is a piezoelectric breeze sensor produced by Nippon Ceramic, Japan. A sensor contains a pair of the piezoelectric (or pyroelectric) elements,<sup>3</sup> where one is exposed to ambient air and the other is protected by the encapsulating resin coating. Two sensors are required for a differential compensation of variations in ambient temperature. The elements are connected in a series-opposed circuit, that is, whenever both of them generate the same electric charge in response to a spurious influence, the resulting voltage across the bias resistor  $R_b$  (Fig. 12.18a) is essentially zero. Both elements, the bias resistor, and the JFET voltage follower are

<sup>3</sup> In this sensor, the crystalline element, which is poled during the manufacturing process is the same as used in piezo- or pyroelectric sensors. However, the operating principle of the breeze sensor relates to neither mechanical stress nor heat flow. Nevertheless, for the sake of simplicity, we use the term *piezoelectric*.



**Fig. 12.18** Piezoelectric breeze sensor. Circuit diagram (a); packaging in TO-5 can (b)



**Fig. 12.19** In-breeze sensor, gas movement strips off electric charges from surface of piezoelectric element

encapsulated into a TO-5 metal housing with vents for exposing the  $S_1$  element to gas movement, Fig. 12.18b.

An operating principle of the sensor is illustrated in Fig. 12.19. When airflow is either absent or is very steady, the charge across the piezoelectric element is balanced. The internal electric dipoles, which were oriented during the poling process (Sect. 4.6.1), are balanced by both the free carriers inside the material and by the charged floating air molecules at the element’s surface. In the result, voltage across the piezoelectric elements  $S_1$  and  $S_2$  is zero, which defines the baseline output voltage  $V_{out}$ .

When the gas flow across the  $S_1$  surface changes ( $S_2$  surfaces are protected by resin), the moving gas molecules strip off the floating charges from the element, causing a charge disbalance. This results in appearance of voltage across the element’s electrodes because the internally poled dipoles are no longer balanced by the outside floating charges. The voltage is applied to the JFET follower, that serves as an impedance converter, and appears as a transient in the output terminal.

## 12.7 Coriolis Mass Flow Sensors

Coriolis flowmeters measure flow of mass directly, as opposed to those that measure velocity or volume [14]. Coriolis flowmeters are virtually unaffected by the fluid pressure, temperature, viscosity, and density. As a result, Coriolis meters can be used without recalibration and without compensating for parameters specific

to a particular type of fluid. While these meters were used mainly for liquids when they were first introduced, now they have become adaptable for the gas applications as well.

Coriolis flowmeters are named after Gaspard G. Coriolis (1792-1843), a French civil engineer and physicist. A Coriolis sensor generally consists of one or two vibrating tubes with an inlet and an outlet. A typical material for the tube is stainless steel. It is critical for the meter accuracy to prevent any mechanical or chemical attack of the tube or its lining by the flowing fluid. Many tubes are U-shaped but a wide variety of other shapes have been also employed. The thinner tubes are used for gas while thicker tubes are more appropriate for liquids. The Coriolis tube is set to vibration by an auxiliary electromechanical drive system.

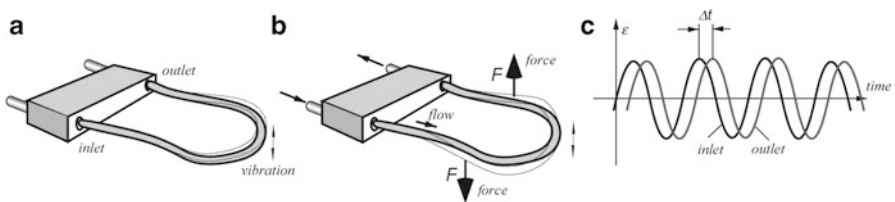
Fluid enters the meter in the inlet. A mass flow is determined based on the action of the fluid on the vibrating tubes. As fluid moves from the inlet to outlet, it develops different forces depending on its acceleration that is the result of the tube vibration.

The Coriolis force induced by the flow is described by the following equation:

$$F = 2m\omega\nu \quad (12.40)$$

where  $m$  is the mass,  $\omega$  is the rotating circular frequency and  $\nu$  is the vector of the average fluid velocity. As a result of these forces, the tube takes on a twisting motion as it passes through the vibrating cycle. The amount of twist is directly proportional to the mass flow through the tube. Figure 12.20a shows the Coriolis flow tube in a no-flow situation, and Fig. 12.20b shows Coriolis tube with the flow.

At a no-flow state, the tube vibrates identically at its inlet and outlet sides with the sine-wave motions with the zero phase shift between them. During flow, the tube twists in response to the flow, and the inlet and outlet sides vibrate differently with a phase shift between them (Fig. 12.20c). The main disadvantage of the Coriolis sensor is its relatively high initial cost. However, the versatility of the Coriolis sensors in handling multiple fluids (water, crude oil, acids, etc.) makes them very useful for the plants where flow of multiple fluid types must be measured. There are also an increasing number of the gas applications for the Coriolis meters. Figure 12.21 illustrates the Coriolis U-shaped sensor that is part of a pipeline for loading crude oil to a tanker. Such sensors are capable of measuring mass flows up to 3200 tons/h.



**Fig. 12.20** Coriolis tube with no flow (a), twist of the tube with flow (b), vibrating phase shift resulted from Coriolis forces (c)

**Fig. 12.21** Coriolis mass flow sensor for use in pipeline (Emerson Electric Co.)



## 12.8 Drag Force Flowmeter

When fluid motion is sporadic, multidirectional, and turbulent, a drag force flow sensor may be quite efficient. Application of such flowmeters include environmental monitoring, meteorology, hydrology, and maritime studies to measure speeds of air or water flow and turbulence close to surface [15]. In the flowmeter, a solid object known as a *drag element* or *target* is exposed to the flow of fluid. The force exerted by the fluid on the drag element is measured and converted to an electrical signal indicative of a value for flow speed. An important advantage of the drag sensor is that it can be made to generate a measurement of flow in two dimensions, or even in three dimensions of flow speed. To implement this feature, the drag element must be symmetrical in the appropriate number of dimensions. For over half a century, these flowmeters have been used by industry, utilities, aerospace, and research laboratories to measure the flow of liquids (including cryogenic), gases, and steam (both saturated and superheated).

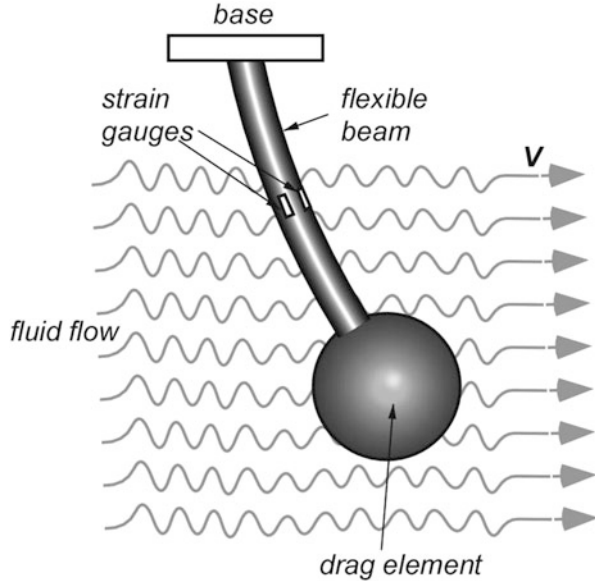
The operation of the sensor is based on strain measurement of deformation of an elastic cantilever, to which a force is applied by a spherical symmetrical drag element (Fig. 12.22). An ideal drag element however is a flat disk [16], because this configuration gives a drag coefficient independent of the flow rate. Using a spherical drag element, which departs from the ideal of a flat disk, the drag coefficient may vary with flow rate, and therefore the gauge must be calibrated and optimized for the conditions of intended use. The strain measurement can be performed with strain gages that should be physically protected from interaction with the moving fluids.

The drag force  $F$ , exerted by incompressible fluid on a solid object exposed to it is given by the drag *equation*:

$$F_D = C_D \rho A v^2 \quad (12.41)$$

where  $\rho$  is fluid density,  $v$  is fluid velocity at the point of measurement,  $A$  is projected area of the body normal to the flow, and  $C_D$  is the overall drag coefficient.  $C_D$  is a dimensionless factor, whose magnitude depends primarily on the physical

**Fig. 12.22** Concept of rag force sensor



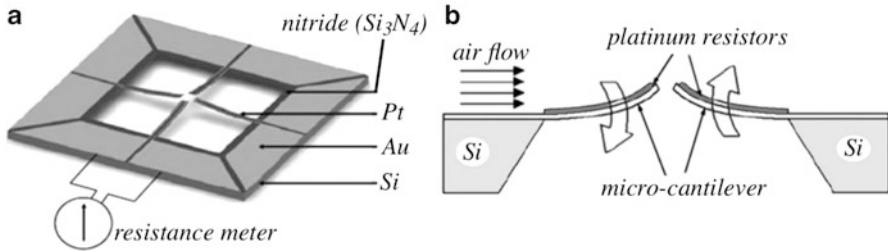
shape of the object and its orientation relative to the fluid stream. If mass of the supporting beam is ignored, the developed strain is

$$\epsilon = \frac{3C_D \rho A v^2 (L - x)}{E a^2 b}, \quad (12.42)$$

where  $L$  is the beam length,  $x$  is the point coordinate on the beam where the strain gauges are located,  $E$  is the Young's modulus of elasticity, and  $a$  and  $b$  are the geometry target factors. It is seen that the strain in a beam is a square law function of the fluid flow rate.

## 12.9 Cantilever MEMS Sensors

Similar to the drag force flow sensors, the cantilever sensors rely on measurement of strain in a beam, where the strain is caused by a flowing media. A cantilever flow sensor based on the MEMS material processing that allowed velocity measurement up to  $45 \text{ m}\cdot\text{s}^{-1}$ , with a response time of about  $0.5 \text{ s}$  and a power consumption of  $0.02 \text{ mW}$ , was realized for bio-medical applications by Wang et al. [17]. Figure 12.23a shows the MEMS sensor for measuring multidirectional flows. The structure contains four prebended beams with platinum piezoresistors deposited on each beam. The beam curvature is modulated by the flow in such a manner as the left beam shown in Fig. 12.23b deflects downward, while the right beam curves upwardly. This results in increase of the left, and decrease of the right resistors in proportion to the force exerted by the flow. The resistors are connected in a Wheatstone bridge circuit whose output voltage represents a flow rate.



**Fig. 12.23** MEMS cantilever sensor (a). Airflow causes bending of the beams and modulation of piezoresistors (b). Adapted from [18]

## 12.10 Dust and Smoke Detectors

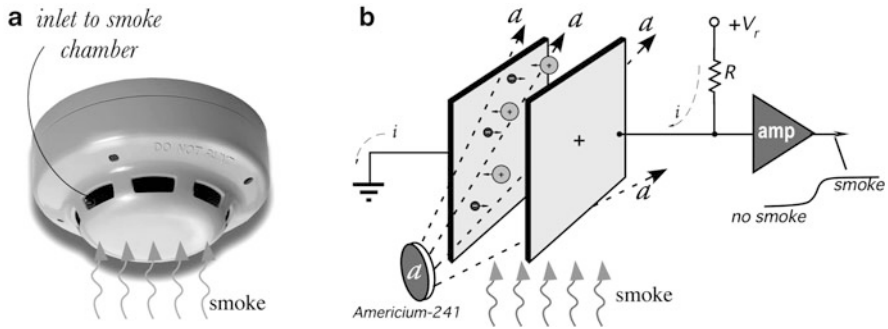
Smoke and air (gas) impurity sensors are intended for detecting presence of the small airborne particles and have wide range of applications. Even though these detectors do not monitor airflow, their operation essentially requires movement of gas through the detection chamber of the sensor. By far the most popular are the smoke detectors that are positioned on or near a ceiling, Fig. 12.24a. The detector has an inlet for air that can flow through passively or can be drawn by a forced convection with help from a fan or blower.

Airborne particles greatly vary in size depending on their origin. Table 12.1 exemplifies some contaminants that either may present health hazard or are the manifestations of certain troubling events (a fire, e.g.). To detect presence of small particles suspended in air, nowadays two types of sensors are widely employed: ionization and optical detectors.

### 12.10.1 Ionization Detector

This detector is especially useful for detecting smoke composed of very small submicron particles, like those generated by large hot fires. The key part of this type of sensor is an *ionization chamber* containing less than a milligram of radioactive element Americium-241 ( $\text{Am}^{241}$ ). This element is a natural source of Alpha particles that resulted from the so-called *alpha decay*. The ionization chamber resembles a capacitor with two opposite electrodes (Fig. 12.24b) having shapes either of parallel plates or a coaxial cylinder, where one plate is electrically connected to ground (or the negative side of the power source) and the other, through resistor  $R$ , is connected to a positive voltage  $+V_r$  (few volts) [19]. The voltage creates an electric field between the plates. Space between the plates is filled with air drawn from air inlets at the sides of the plates.

If alpha particles are absent, no current can pass from the positive plate to grounded plate, because air normally is not electrically conductive. Alpha particles emanated by the radioactive element have kinetic energy about 5 MeV—enough to



**Fig. 12.24** Smoke detector (a) and concept of ionization smoke sensor (b)

**Table 12.1** Sizes of some airborne contaminants

Particle	Particle size (μm)	Particle	Particle size (μm)
Glass wool	1000	Coal dust	1–100
Spanish moss pollen	150–750	Smoke from synthetic materials	1–50
Beach sand	100–10,000	Face powder	0.1–30
Mist	70–350	Asbestos	0.7–90
Pollens	10–1000	Calcium zinc dust	0.7–20
Textile fibers	10–1000	Paint pigments	0.1–5
Fiberglass Insulation	1–1000	Car emission	1–150
Grain dusts	5–1000	Clay	0.1–50
Human hair	40–300	Humidifier	0.9–3
Dust mites	100–300	Copier toner	0.5–15
Saw dust	30–600	Liquid droplets	0.5–5
Cement dust	3–100	Insecticide dusts	0.5–10
Mold spores	10–30	Anthrax	1–5
Textile dust	6–20	Yeast cells	1–50
Spider web	2–3	Carbon black dust	0.2–10
Spores	3–40	Atmospheric dust	0.001–40
Combustion-related carbon monoxide from motor vehicles, wood burning, open burning, industrial processes	up to 2.5	Smoldering or flaming cooking oil	0.03–0.9
Sea salt	0.035–0.5	Combustion	0.01–0.1
Bacteria	0.3–60	Smoke from natural materials	0.01–0.1
Burning wood	0.2–3	Tobacco smoke	0.01–4
Coal flue gas	0.08–0.2	Viruses	0.005–0.3
Oil smoke	0.03–1	Pesticides and herbicides	0.001

ionize air molecules by breaking them into positively charged ions and negatively charged electrons. The charged ions and electrons are being pulled by the electric field in the opposite directions—electrons to the positive plate and ions to the grounded plate. This results in small constant electric current  $i$  flowing from the voltage source  $V_r$ , through resistor  $R$ , the ionized air-filled space between the plates, and to the “ground”. As a result, the input voltage at the amplifier “amp” drops, indicating that no smoke is present in the ionization chamber.

When smoke is drawn into the ionization chamber between the plates, the smoke particles absorb alpha radiation thus reducing the air ionization and subsequently current  $i$  is reduced. This increases voltage at input of the amplifier, manifesting a presence of smoke inside the ionization chamber. Since Americium-241 has a half-life of 432.2 years, lifetime of the ionization source is long enough for all practical purposes.

The reasons why alpha radiation is used instead of beta or gamma is twofold: a higher ability of *alpha* radiation to ionize air and low-penetrating power of the alpha particles,<sup>4</sup> so the radiation will be absorbed by the smoke detector housing, reducing a potential harm to humans.

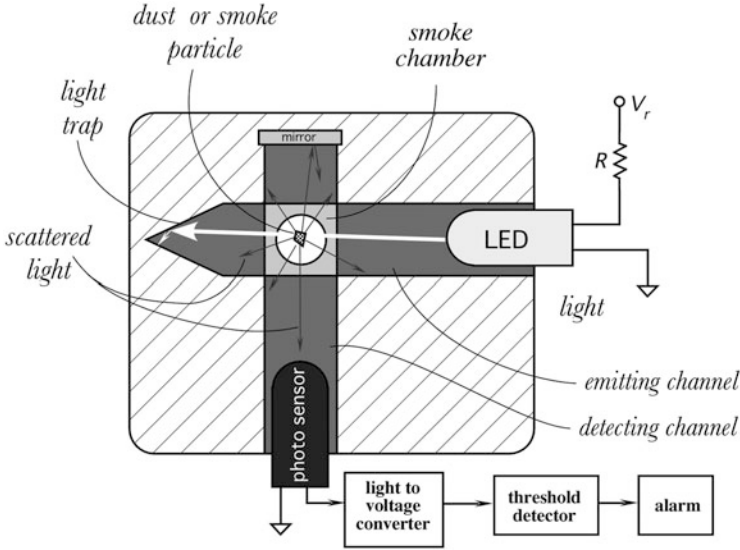
### 12.10.2 Optical Detector

Another type of a smoke or dust detector is based on measuring scattering of light (see Sect. 5.1.3). The optical detector includes a light emitter (incandescent bulb, infrared LED, or a laser diode) and a photosensor, usually a photodiode or photo-transistor (Fig. 12.25). The light emitter and detector are positioned inside a light-tight enclosure in such a way as to prevent any photons reaching the detector from the emitter either directly or by reflections from the enclosure inner walls. The enclosure should also protect the photosensor from ambient light. To achieve these difficult requirements, the light emitter and photosensor are positioned inside the individual emitting and detecting channels that cross each other preferably at a 90° angle. This is not an optimal angle since light scattering is not the strongest at 90° (Fig. 12.26) but this is the best angle for minimizing a chance for stray light passing from the photoemitter to photosensor. Many practical optical smoke detectors [20] use smaller angles on the expense of a larger size and mechanical complexity—to trap the unwanted light before it reaches a photosensor.

The interior walls of the channels have low-light reflectivity surfaces. In addition, the emitting channel has the far end that is conically shaped to prevent a spurious light reflection toward the photosensor. This shape is called a light trap. The emitter and photosensor may have built-in lenses to shape the narrow-angle beams, thus assuring that very little light strikes the chamber walls. The space

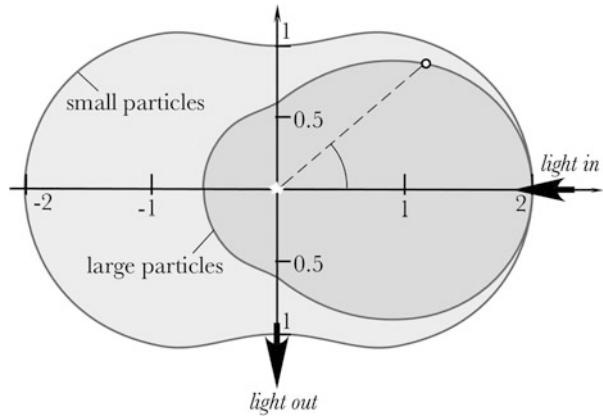
---

<sup>4</sup> Alpha radiation consists of Helium-4 positively charged nucleus and due to high mass travels with the speed of only about 15,000 km/s. Thus, it easily can be stopped by just a thin tissue paper and, due to collisions with air molecules, travels in air at distances no farther than few centimeters.



**Fig. 12.25** Concept of optical smoke detector

**Fig. 12.26** Scattering directional diagram



where two channels cross is called a “scattering chamber” or “smoke chamber” which is open to ambient air or connected to the source of tested air. The smoke chamber has the inlets and outlets for air passing through, but is shielded from ambient light.

In presence of clean air inside the scattering chamber, light beam from the emitter cannot reach the photosensor (in empty space, light cannot go around the corner) and thus the photosensor produces a very low-output current, called the dark current (see Sect. 15.2). When dust or smoke enters the scattering chamber, it appears in the light beam path and some light is scattered by the particles in all



directions (Fig. 12.26), including the direction toward the photosensor. Smaller airborne particles cause the Rayleigh scattering while the larger particles cause specular reflections in many directions (Fig. 5.2), including the direction along the detecting channel toward the photosensor. The detecting channel may have a mirror at the opposite end to bounce some scattered light toward the photosensor, thus increasing the sensor's sensitivity. Whatever is the physical nature of scattering, thanks to air impurities, the photosensor now sees some light "in the tunnel". Small particles being much more numerous create a relatively constant shift in the photocurrent, while the larger particles will glitter and result in a pulsing photocurrent. The effect of appearance of light in the detecting channel resembles appearance of light rays when the Sun is partially covered by clouds—the sunlight rays passing through openings in the cloud become visible due to light scattering by water droplets and airborne dust particles.

A photodiode (light sensor) along with the interface circuit serves as light-to-voltage converter (see Fig. 6.8) whose output is fed to a threshold detector connected to an alarm. For responding to the light pulses resulted from larger particles, the electronic interface circuit should have a sufficiently wide frequency bandwidth. The optical smoke detectors are less prone to false alarms resulted from steam or cooking fumes in kitchen or steam from a bathroom than the ionization smoke alarms. They are especially efficient for detecting smoke from smoldering fires.

---

## References

1. Benedict, R. P. (1984). *Fundamentals of temperature, pressure, and flow measurements* (3rd ed.). New York, NY: John Wiley & Sons.
2. Cho, S. T., et al. (1991). A high performance microflowmeter with built-in self test. In: *Transducers'91. International conference on solid-state sensors and actuators. Digest of technical papers* (pp 400–403), IEEE.
3. Bruun, H. H. (1995). *Hot-wire anemometry. Principles and signal analysis*. Oxford: Oxford Science.
4. King, L. V. (1914). On the convection of heat from small cylinders in a stream of fluid. *Philosophical Transactions of the Royal Society A*, A214, 373.
5. Collis, D. C., et al. (1959). Two-dimensional convection from heated wires at low Reynolds' numbers. *Journal of Fluid Mechanics*, 6, 357.
6. Fraden, J., et al. (2007). Clogging detector for air filter. U.S. Patent No. 7178410, February 20, 2007.
7. Fraden, J. (2009). Detector of low levels of gas pressure and flow. U.S. patent No. 7490512, February 17, 2009.
8. Fraden, J. (2012). Measuring small air pressure gradients by a flow sensor. *IEEE Instrumentation and Measurement Magazine*, 15(5), 35–40.
9. Van Herwaarden, A. W., et al. (1986). Thermal sensors based on the Seebeck effect. *Sensors and Actuators*, 10, 321–346.
10. Nan-Fu, C., et al. (2005). Low power consumption design of micro-machined thermal sensor for portable spirometer. *Tamkang Journal of Science and Engineering*, 8(3), 225–230.
11. Wachutka, G., et al. (1991). Analytical 2D-model of CMOS micromachined gas flow sensors. In: *Transducers'91. International conference on solid-state sensors and actuators. Digest of technical papers*. ©IEEE.

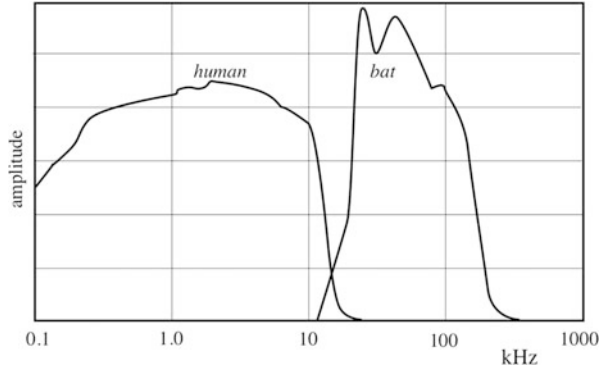
12. Esashi, M. (1991). Micro flow sensor and integrated magnetic oxygen sensor using it. In: *Transducers'91. International conference on solid-state sensors and actuators. Digest of technical papers*. IEEE.
13. Gessner, U. (1969). The performance of the ultrasonic flowmeter in complex velocity profiles. *IEEE Transactions on Bio-medical Engineering, MBE-16*, 139–142.
14. Yoder, J. (2000). Coriolis effect mass flowmeters. In J. Webster (Ed.), *Mechanical variables measurement*. Boca Raton, FL: CRC Press LLC.
15. Philip-Chandy, R., et al. (2000). Drag force flowmeters. In J. Webster (Ed.), *Mechanical variables measurement*. Boca, Raton, FL: CRC Press LLC.
16. Clarke, T. (1986). *Design and operation of target flowmeters. Encyclopedia of fluid mechanics* (Vol. 1). Houston, TX: Gulf Publishing Company.
17. Wang, Y. H., et al. (2007). A MEMS-based air flow sensor with a free-standing micro-cantilever structure. *Sensors*, 7, 2389–2401.
18. Ma, R. H., et al. (2009). A MEMS-based flow rate and flow direction sensing platform with integrated temperature compensation scheme. *Sensors*, 9, 5460–5476.
19. Dobrzanski, J., et al. (1977). Ionization smoke detector and alarm system. U.S. Patent No. 4037206, July 19, 1977.
20. Steele, D. F., et al. (1975). Optical smoke detector. U.S. Patent No. 3863076, January 28, 1975.

“Sound is the vocabulary of nature”

—Pierre Schaeffer, French composer

The fundamentals of acoustics are given in Sect. 4.10 and the reader is encouraged to familiarize herself with materials of that section. Here we will discuss the acoustic sensors for various frequency ranges. The audible range sensors are generally called the *microphones*, however, the name is often used even for the ultrasonic and infrasonic waves. In essence, a microphone is a pressure transducer adapted for transduction of sound waves over a broad spectral range that generally excludes very low frequencies below few Hz. The microphones differ by their sensitivity, directional characteristics, frequency bandwidth, dynamic range, sizes, etc. Also, their designs are quite different depending on the media from which sound waves are sensed. For example, for perception airwaves or vibrations in solids, the sensor is called a *microphone*, while for operation in liquids, it is called a *hydrophone* (even if liquid is not water) from the Greek name of the mythological water serpent *Hydra*. The main difference between a pressure sensor and acoustic sensor is that the latter does not need to measure constant or very slow changing pressures. Its operating frequency range usually starts at several hertz (or as low as tens of millihertz for some special applications), while the upper operating frequency limit is quite high—up to several megahertz for the ultrasonic applications and even gigahertz in a surface acoustic wave device. The operating frequency range of a microphone or hydrophone depends on the particular application. Figure 13.1 illustrates the spectral ranges of a human and bat ears—they differ quite dramatically and practically do not overlap. Thus, a microphone for the human use and for detecting sounds of bats shall have different frequency characteristics.

**Fig. 13.1** Frequency characteristics of human and bat ears



Since acoustic waves are mechanical pressure waves, any microphone or hydrophone has the same basic structure as a pressure sensor; it is comprised of a moving diaphragm and a displacement transducer that converts the diaphragm's deflections into electrical signal. All microphones and hydrophones differ by the designs of these two essential components. Also, they may include some additional parts such as mufflers, focusing reflectors, etc., however, in this chapter we will describe only the sensing parts of some interesting acoustic sensors.

The wavelength depends on the speed of sound  $\nu$  in a media and its frequency,  $f$ :

$$\lambda = \frac{\nu}{f} \quad (13.1)$$

For sound waves in air, the speed of sound  $\nu = 343.59$  m/s (at room temperature and atmospheric pressure). For most of other media, the speed of sound is higher—see Table A.15. In general, the speed of sound in any media depends on temperature and is given by the Newton-Laplace formula:

$$\nu = \sqrt{\frac{K}{\rho}}, \quad (13.2)$$

where  $K$  is the temperature dependent stiffness coefficient that for gases is called the modulus of bulk elasticity and  $\rho$  is the media density.

The sensor's diaphragm is typically much smaller than the wavelength of sound, however when operating at high frequencies of the ultrasonic spectral range, the diaphragm dimensions may be comparable with the wavelength. For example, for the ultrasonic frequency of 100 kHz in air, according to Eq. (13.1), the wavelength is only 3.4 mm, while for an audible frequency of 300 Hz, the wavelength is about 1.1 m.

## 13.1 Microphone Characteristics

### 13.1.1 Output Impedance

One important characteristic of a microphone is its output impedance that is connected to an amplifier through some conductive media, such as a cable. Generally, microphones can be divided into low (50–1000  $\Omega$ ), medium (5000–15,000  $\Omega$ ), and high (20,000+  $\Omega$ ) output impedance devices. The impedance is important for selecting the appropriate cable that would introduce low distortions. There is a limit to how much cable should be used between a high-impedance microphone and the amplifier input. For medium- and high-impedance microphones, any more than about 20 ft will result in a loss of high-frequency components of a signal, and loss of the output level. By using low-impedance microphones and low-impedance cables, the cables can be almost of any practical length, with no serious losses of any kind. Thus, for a serious sound recording, low-output impedance microphones are preferable.

### 13.1.2 Balanced Output

Some high-quality microphones with long connecting lines offer balanced outputs that produce the out-of-phase signals of equal amplitudes. The balanced lines are much less susceptible to RFI (radio frequency interference) and the pick-up of other electrical noise and hum. In a balanced line, the shield of the cable is connected to ground, and the audio signal appears across the two inner conductors that are not connected to ground. Because signal currents are flowing in the opposite directions at any given moment in the pair of signal wires, transmitted noise, which is common to both, is effectively cancelled out.

### 13.1.3 Sensitivity

Sensitivity characteristic shows the ability of a microphone to convert low-level sounds into voltages of acceptable levels. Typically, the microphone output is stated in dB (decibels) compared to a reference level. Most reference levels are well above the output level of the microphone, so the resulting number (in dB) will be negative. Thus, a microphone with a sensitivity rating of  $-55$  dB will provide more signal to the input terminals of an amplifier than one rated at  $-60$  dB.

Some manufacturers rate a microphone sensitivity in terms of its open circuit output voltage per the input sound level. Stated in dB-relative-to-1-V, or in actual millivolts (mV), the output voltage the microphone will deliver for a stated *sound pressure level* (SPL) input. A popular reference sound pressure is 1 Pa (Pascal), which equals 94 dB SPL, thus sensitivity is expressed as:

$$S_m = \frac{\Delta V}{1 \text{ Pa}} \quad (13.3)$$

where  $\Delta V$  is the output voltage deflection

In most modern audio equipment, the amplifier's input impedances are substantially greater than the output impedance of the microphone. Thus the amplifier may be ignored and microphone output regarded as an open circuit. That makes the open circuit voltage measurement a useful tool in comparing microphone sensitivities.

The output voltage level is important to know for design of the interface amplifier. If at some high sound levels the microphone output voltage exceeds the amplifier linear range, the signal will go to saturation, resulting in distortions. In most practical cases, acoustic distortions result from the amplifier characteristics, rather than of a microphone.

### 13.1.4 Frequency Response

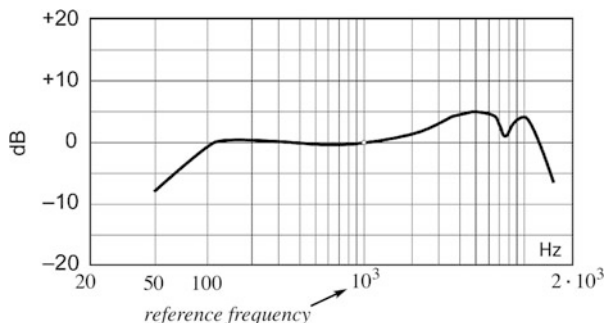
The ability of a microphone to respond to a specific frequency range is described by its frequency characteristic. The characteristic may indicate that some frequencies are exaggerated and others are attenuated (reduced). For example, a frequency response with the enhanced high frequencies means that the resulting audio output will sound more trebly than the original sound. An ideal "flat" frequency response means that the microphone is equally sensitive to all frequencies. In this case, no frequencies would be exaggerated or reduced resulting in a more accurate representation of the original sound. It could be said that a flat frequency response produces the purest audio experience. Yet, a perfectly flat response is not possible and even the best "flat response" microphones have some variations.

In many cases a flat frequency response is not always the most desirable option and a tailored frequency response is more useful. For example, a response pattern designed to emphasize the frequencies in a human voice would be well suited to picking up speech in an environment with lots of low-frequency background noise. To enhance recognition of speech, it may be desirable to enhance the higher frequency portion of the sound spectrum. This is especially desirable for the hearing aid microphones. Figure 13.2 illustrates a typical relative frequency response of a microphone intended for reproducing human voices. Naturally, for the ultrasonic or infrasonic microphones and hydrophones, the frequency responses are very different.

### 13.1.5 Intrinsic Noise

The self-noise or equivalent input noise level is the sound level that creates the same output voltage as the microphone does in the absence of sound. This represents the lowest point of the microphone's dynamic range. It is important to know the self-noise for recording low-level sounds. The noise is often stated

**Fig. 13.2** Relative frequency response of microphone for human hearing range. Reference frequency is selected at 1 kHz



**Fig. 13.3** 3-D directional sensitivity of a microphone

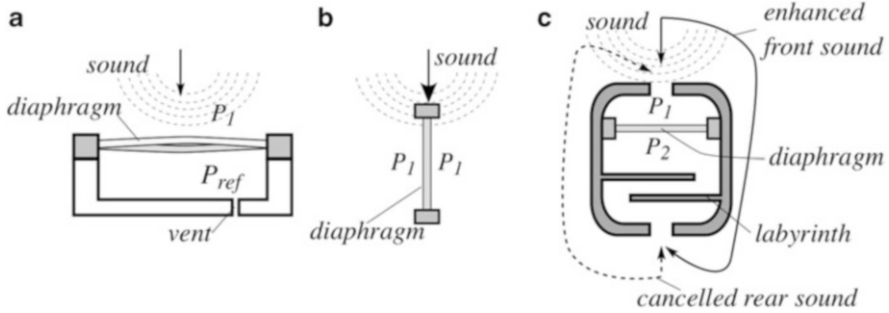


in dB(A), which is the equivalent loudness of the noise on a decibel scale frequency-weighted for how the ear hears, for example: “24 dBA SPL” (SPL means sound pressure level relative to 20  $\mu$ Pa). The lower the noise number the better. A quiet microphone typically measures 20 dBA SPL, however the super-quiet microphones exist with the noise level as low as 0 dBA SPL.

### 13.1.6 Directionality

A directional microphone has sensitivity that depends on the direction of the incident sound wave. A directional microphone is typically used to suppress unwanted sounds from directions other than that of the sound source of interest. Miniature directional microphone systems are often used in hearing aids to improve speech intelligibility in noisy environments. Directionality specifies spatial directions where a microphone is more or less sensitive, or not sensitive at all. Usually it is a graphical two- or three-dimensional representation of sensitivity variations in a polar system of coordinates. While a 3-D sensitivity diagram is more visually appealing (Fig. 13.3), in practice the 2-D polar diagrams are usually employed as being more descriptive.

Tailoring a microphone directionality is highly desirable for many applications when microphones should detect sounds from some predominant directions and



**Fig. 13.4** Shaping directional sensitivity of microphone. *Pressure* microphone senses signals arriving at the outer side of a diaphragm from all directions (a). *Pressure-gradient* diaphragm cancels equal-pressure sounds at its both sides (b), and nonuniform sensitivity formed by sound delay channel (c)

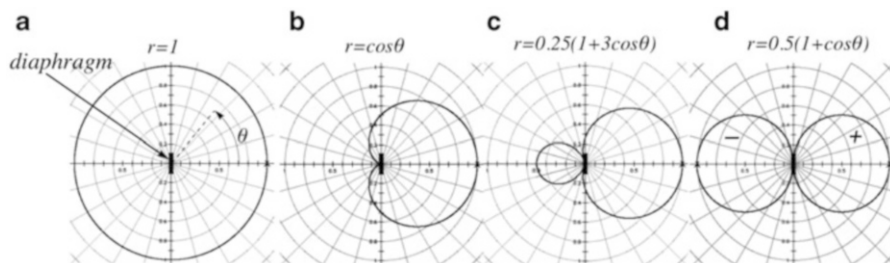
reject sounds from other directions. Figure 13.4a illustrates a concept of the so-called *pressure microphone* where the diaphragm is stretched over an enclosed chamber having a relatively constant internal atmospheric pressure. This means that the diaphragm is deflected by the sound waves arriving only at its outer surface. The degree of the diaphragm's deflection represents sound wave pressure  $P_1$  with respect to a relatively constant reference pressure  $P_{ref}$  inside the chamber. The diaphragm deflection is measured by transducers, some of which are described in this chapter.

To keep the reference pressure  $P_{ref}$  constant, slow changing atmospheric pressures shall be compensated for, otherwise the diaphragm may bulge out or cave out and will not respond to sounds. Thus, the chamber is not tightly sealed from the outside. It may contain a tiny vent hole for equalizing pressures inside and outside. Yet, the hole should not channel any significant level of the sound waves. This pressure microphone is *omnidirectional* because the diaphragm is deflected equally by the sound waves arriving from any direction. Since pressure is a scalar quantity that does not carry any information about the direction of the sound, the diaphragm responds only to the level of pressure. The omnidirectional polar diagram is illustrated as a circle with radius  $r = 1$  in Fig. 13.5a.

To make a microphone responsive to the direction of an incoming acoustic sound wave, the difference in acoustic pressure at minimum of two different points must be measured. The common method used in directional microphones is to measure the sound pressure with the help of two sound ports across a single diaphragm.

If the diaphragm is supported in such a manner that sound waves arrive at its both sides, such a microphone is called a *pressure-gradient* microphone and the diaphragm deflection is function of a differential pressure. If sound waves arrive in such a manner as pressures  $P_1$  are the same at both sides of the diaphragm and are in phase (Fig. 13.4b), the diaphragm will not move and the microphone is not sensitive at all. In other words, it is deaf to sounds on this particular axis. In contrast, sounds





**Fig. 13.5** Directionality polar diagrams: omnidirectional (a), cardioid (b), hyper-cardioid (c), and figure-8 (d). Equations on top describe curvatures in polar coordinates. Radius  $r$  is measure of microphone's sensitivity at angle  $\theta$  relative to front of microphone (the positive horizontal axis)

arriving perpendicular to the diaphragm will create a large pressure difference between the sides, and diaphragm will be moved a maximum amount.

A directional microphone contains at least two sound entry ports. The sound arriving at an angles between  $0^\circ$  and  $90^\circ$  reaches one port little sooner than the other port, causing a pressure difference on the diaphragm, resulting in a polar pattern that looks like a figure 8. It has the maximum sensitivity to sound on-axis normal to the diaphragm and the minimum sensitivity perpendicular to this. Figure 13.5d illustrates a figure-8 directionality diagram that indicates equal sensitivities at front and back of the diaphragm but a complete muting at the sides.

Note that positive pressure on the front produces the same output as a negative pressure on the back. In other words, a pressure-gradient microphone has polarity, since a positive pressure on the front of the microphone moves the diaphragm in the opposite direction to a positive pressure at the rear; the two lobes of the polar pattern are of the opposite polarity. This is the reason why the left lobe of figure-8 is marked with a minus sign, indicating the opposite phase to the right lobe. The phase becomes significant when we combine the microphone polar patterns to form more complex shapes, like a hypercardioid of Fig. 13.5c.

The above considerations suggest the ways of shaping directional diagrams by manipulating pressures at the front and backside of the diaphragm. Since the directional microphone subtracts the pressure on each side of the diaphragm, the sensitivity of these microphones is highly dependent on the separation distance between the sound ports. This separation distance needs to be significant as compared to the wavelength of the sound to get accurate results. When the distance between ports gets smaller in order to decrease the size of the microphone, the pressure difference,  $P_2 - P_1$ , between these two ports becomes too small to be detected accurately. As a result, it is challenging to design a directional microphone with small size and high sensitivity

Figure 13.5b shows a popular directionality shape called *cardioid* that is named so because it resembles shape of a heart (from the Greek καρδία—heart). However, originally the cardioid was not a primary microphone design, but was actually a combination of both pressure-operated and pressure-gradient components.

During the early development of microphones back in the 1930s, a cardioid response was achieved by mounting two separate microphone capsules—an omnidirectional and figure-8—within the same physical housing. Their outputs were combined electrically and the resulting polar pattern was a cardioid. The in-phase lobes were added, while the out-of-phase lobes were subtracted, resulting in a cardioid shape.

Most modern cardioid microphones employ a mechanical time-delay technique to maximize rejection of rearward sounds as illustrated in Fig. 13.4c. The microphone bottom chamber contains a labyrinth which is open to the rear. If sound arrives from the rear, its paths through the chamber to the bottom side of the diaphragm are sufficiently convoluted to take sound a finite time to travel, and that time is set equal to the time taken for sound to travel around the microphone from the bottom to the top (dotted line on the left). Thus, rearward sounds will arrive at both sides of the diaphragm near simultaneously and since  $P_1 \approx P_2$ , cancel out, while frontal sounds will be picked up with great sensitivity (because  $P_1 \gg P_2$ ) and the cardioid response results. By varying the rear chamber sizes and shapes, the sound ports number, and positions, it is possible to shape a variety of the directional sensitivities.

Shaping a more complex spatial coverage can be accomplished by arranging several omnidirectional or directional microphones and adding their output signals with different phase shifts. This can be accomplished, for example, by at least three discrete microphones which are individually directional with a cardioid pattern. The directional discrete microphones are positioned with respect to each other so that two microphones are always facing the sound source, while a third microphone is directed away from the sound source. The outputs of the three microphones are combined in a mixer by adding or subtracting their signals. The mixing can be optimized to negate signals from the unwanted sound sources. A  $180^\circ$  phase shifter is also used for offsetting the sound signals incident from the lateral directions, so that these signals are cancelled in the adder stage. This results in a directional pattern only toward the front of the arrangement, i.e., in the direction toward the desired sound source.

The polar patterns presented by manufacturers may be somewhat misleading. The real directional sensitivity patterns deviate from the ideal and often vary dramatically with frequency. Off-axis response can seriously alter the sound of a microphone in real-world use. In a room, there are reflections of the direct sound picked up off-axis and combined with the on-axis signal. The combination can alter the sound quality through frequency-dependent reinforcements and cancellations. One of the major differences between the high-quality microphones and others is the smoothness of the off-axis frequency response.

### 13.1.7 Proximity Effect

One of the most degrading effects to a cardioid microphone's frequency response is what is called *proximity effect*. It is a result of an artificial disbalance between the front and rear ports, where the rear port is forced to receive a much smaller sound

pressure, especially in a low-frequency range where the wavelengths are much longer. When a sound source gets closer to the front of the cardioid microphone the bass frequencies can be boosted up to as much as 18 dB in some cases. The closer the source the “boomier” the bass. Singers often use the proximity effect unconsciously, bringing the microphone closer to their lips for a warmer, more intimate tone.

---

## 13.2 Resistive Microphones

When the diaphragm vibrates, its motions are converted into variable electrical output. The methods of conversion of the diaphragm movement to electrical output are similar to the pressure sensors.

A piezoresistive effect has been popular for many years. In the past, resistive pressure transducer (pressure to electricity) was used quite extensively in microphones. The transducer consisted of a semiconductive powder (usually graphite) whose bulk resistivity was sensitive to pressure. Nowadays we would say that the powder possessed piezoresistive properties. However, these early devices had quite a limited dynamic range, poor frequency response, and a high-noise floor. A carbon microphone is a capsule containing carbon granules pressed between two metal plates. A voltage is applied across the metal plates, causing a small current to flow through the carbon. One of the plates, the diaphragm, vibrates under the incident sound waves, applying a varying pressure to the carbon. The changing pressure deforms the granules, causing the contact area between each pair of adjacent granules to change, and this modulates the electrical resistance of the mass of granules. The changes in resistance cause a corresponding change in the current flowing through the microphone, producing the output electrical signal. Carbon microphone was invented in the 1870s by the British inventor David E. Hughes.<sup>1</sup> These microphones were once commonly used in land-line telephones.

Presently, the same piezoresistive principle can be employed in the micromachined sensors, where stress sensitive resistors are the integral parts of a silicon diaphragm (see Sect. 11.5).

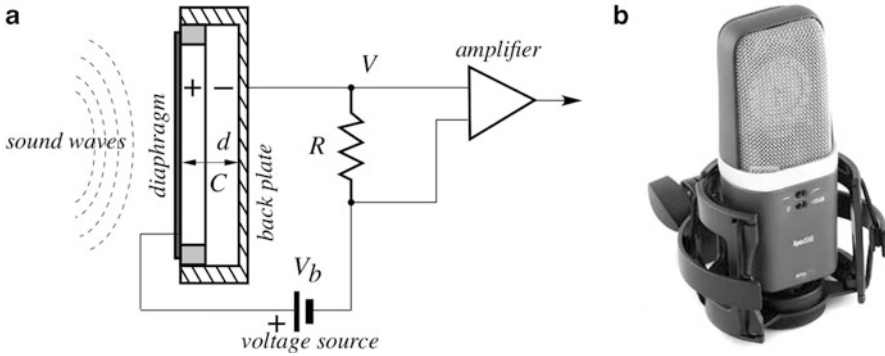
---

## 13.3 Condenser Microphones

If a parallel-plate capacitor is given an electric charge,  $q$ , voltage across its plates is governed by Eq. (4.19). On the other hand, according to Eq. (4.20) the capacitance depends on distance  $d$  between the plates. Thus, by solving these two equations for voltage we arrive at

---

<sup>1</sup> Even though D. E. Hughes invented the first microphone, Thomas Edison managed to secure a patent for himself.



**Fig. 13.6** Concept (a) and studio condenser microphone (b)

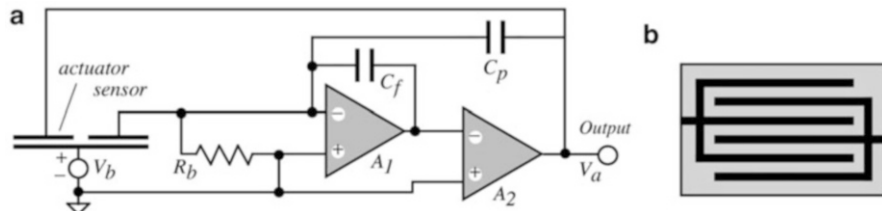
$$V = q \frac{d}{A\epsilon_0}, \quad (13.4)$$

where  $\epsilon_0 = 8.8542 \times 10^{-12} \text{ C}^2/\text{Nm}^2$  is the permittivity constant of free space (Sect. 4.1). The above equation is the theoretical basis for operation of the *condenser* microphones, which is the other way to say “capacitive” microphones. Thus, a capacitive microphone linearly converts a distance between the plates into electric voltage which can be further amplified and processed. The device essentially requires a source of an electric charge  $q$  whose magnitude directly determines the microphone sensitivity. The charge can be provided from a power supply having a voltage in the range from 10 to 200 V (Fig. 13.6).

Presently, many condenser microphones are fabricated with the silicon diaphragms that serve two purposes: to convert acoustic pressure into displacement, and to act as a moving plate of a capacitor. Some designs are described in [1–3]. To achieve high sensitivity, a bias voltage should be as large as possible, resulting in a large static deflection of the diaphragm, which may result in a reduced shock resistivity and lower dynamic range. Besides, if the air gap between the diaphragm and back plate is very small, the acoustic resistance of the air gap will reduce the mechanical sensitivity of the microphone at higher frequencies. For instance, at an air gap of 2  $\mu\text{m}$ , the upper cutoff frequency of only 2 kHz has been measured [1].

One way of improving the characteristics of a condenser microphone is to use a mechanical feedback from the output of the amplifier to the diaphragm [4]. Figure 13.7a shows a circuit diagram and Fig. 13.7b is a drawing of the interdigitized electrodes of the microphone. The electrodes serve different purposes—one is for conversion of a diaphragm displacement into voltage at the input of the amplifier  $A_1$ , while the other electrode is for converting feedback voltage  $V_a$  into a mechanical deflection by means of the electrostatic force. The mechanical feedback clearly improves linearity and the frequency range of the microphone, however, it significantly reduces the deflection which results in a lower sensitivity.

Another arrangement of a capacitive microphone is to use a radio frequency (RF) signal generated by a low-noise oscillator. The RF frequency is modulated by



**Fig. 13.7** Condenser microphone with mechanical feedback. Circuit diagram (a); interdigitized electrodes on diaphragm (b). (Adapted from [4])

the microphone capacitor. The oscillator may either be frequency modulated by the capacitance changes produced by the sound waves moving the capsule diaphragm, or the capsule may be part of a resonant circuit that modulates the amplitude of the fixed-frequency oscillator signal. Demodulation yields a low-noise audio frequency signal with a very low-source impedance. This technique permits use of a diaphragm with looser tension, which may be used to achieve wider frequency response due to higher acoustic compliance.

Condenser microphones are employed in a wide range of devices from telephone transmitters to inexpensive karaoke microphones to high-fidelity studio recording microphones. They generally produce a high-quality audio signal and are now the popular choice in laboratory and studio recording applications. For further reading on condenser microphones an excellent book may be recommended [5].

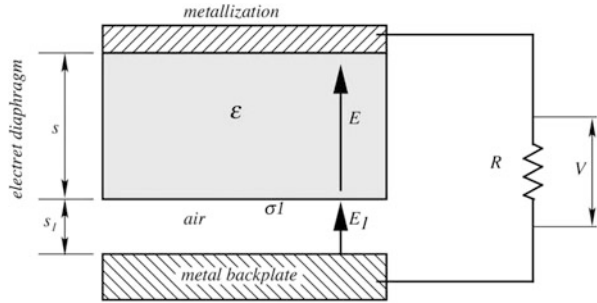
## 13.4 Electret Microphones

Electret microphone is a close relative to a condenser (capacitive) microphone. While a condenser microphone requires for operation a constant bias voltage, the electret generates its own electric field without the need for an external voltage source.

The first application of electret materials to microphones and earphones were described in 1928 [6]. Electret microphones are small, cheap, durable, and offer good performance at high frequencies. Most modern telephone handsets use electrets. This type of a microphone is a prime choice for use in smartphones, thus in 2015 over two Billion electret microphones were produced worldwide for various applications.

An electret material is a close relative to piezoelectric and pyroelectric materials. In effect, they are all electrets with the enhanced either piezoelectric or pyroelectric properties. An electret is a permanently electrically polarized dielectric material and can be considered an electrostatic equivalent of a permanent magnet. In microphones, electret is used in form of rather thin films made from Teflon, Mylar, and other polymers. The thickness ranges from 4 to 20  $\mu\text{m}$ . While all electret charges are subject to decay due to finite relaxation times, these changes

**Fig. 13.8** General structure of electret microphone. Thicknesses of layers are exaggerated for clarity (after [7])



are relatively slow—for high-quality electrets the relaxation times are many years—long enough for lifetimes of most practical microphones.

An electret microphone is an electrostatic transducer consisting of a metallized electret diaphragm and back plate separated from the diaphragm by an air gap (Fig. 13.8).

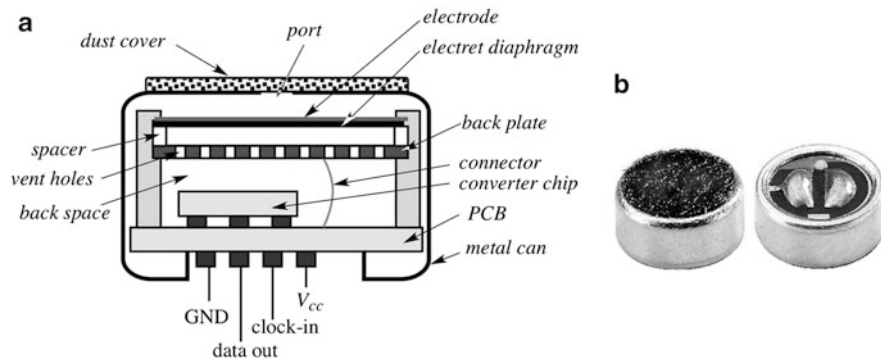
The upper metallization and metal back plate are connected through a resistor  $R$ . Voltage  $V$  across the resistor can be amplified and used as an output signal. It can be shown [8] that for a very large resistor  $R$  and sine-wave sound having circular frequency  $\omega$ , the microphone output voltage is:

$$V = \frac{4\pi\sigma_1 s}{s + s_1} \Delta \sin \omega t, \quad (13.5)$$

where  $\sigma_1$  is the electret surface charge,  $s$  is the electret thickness,  $s_1$  is the air gap, and  $\Delta$  is the diaphragm displacement. Thus, the deflected diaphragm generates voltage across the electrodes. That voltage is in phase with the diaphragm deflection.

The electret microphone differs from the condenser one in the sense that it does not require a d.c. bias voltage. For a comparable design dimensions and sensitivity, a condenser microphone would require well over 100 V bias. The mechanical tension of the membrane is generally kept at a relatively low value (about  $10 \text{ Nm}^{-1}$ ), so that the restoring force is determined by the air gap compressibility. To give the polymer permanent electret properties, the membrane may be fabricated either by a poling of the dielectric at high temperature while in a strong electric field or by electron beams. The temperature coefficient of sensitivity of the electret microphones is in the range of 0.03 dB/°C in the temperature range from  $-10$  to  $+50$  °C [9].

Foil-electret (diaphragm) microphones have more desirable features than any other capacitive microphone types. Among them is very wide frequency range from  $10^{-3}$  Hz and up to hundreds of MHz. They also feature a flat frequency response (within  $\pm 1$  dB), low harmonic distortion, low vibration sensitivity, good impulse response, and insensitivity to magnetic fields. Sensitivities of electret microphones are in the range of few mV/ $\mu\text{bar}$ .



**Fig. 13.9** Omnidirectional electret microphone with embedded processor having digital output (a) and module packaging (b)

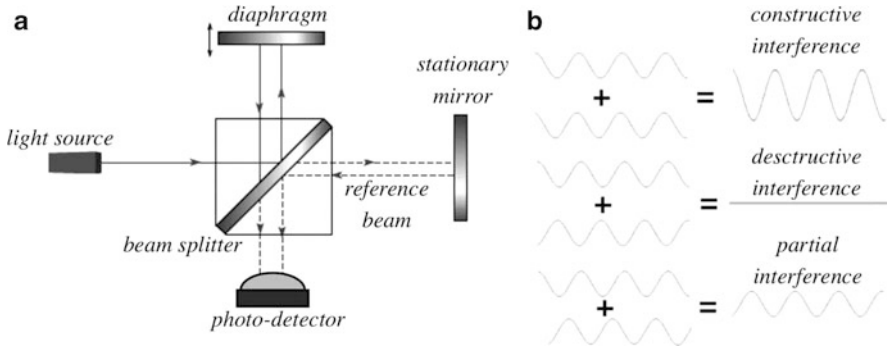
For operation in the infrasonic range, an electret microphone requires a miniature pressure equalization hole on the back plate. When used in the ultrasonic range, the electret is often given an additional bias (like a condenser microphone) on the top of its own polarization.

Electret microphones are the high-impedance sensors and thus require high-input impedance interface electronics. A JFET transistor has been the input of choice for many years. However, recently the monolithic amplifiers gain popularity. A more advanced electret microphone employs a built-in preamplifier, signal conditioner, and Sigma-Delta ADC (Fig. 13.9a). Thus, the output signal is in a digital format. The microphone back plate requires acoustic ports in the form of small holes between the electret gap and the backspace chamber. A commercial electret microphone is shown in Fig. 13.9b.

## 13.5 Optical Microphones

The limitations of piezoresistive and capacitive transducers for detection of very small diaphragm displacements, especially in the MEMS microphones, demand a need for alternative sensing techniques. Optical detection for displacement measurement through interferometry has been an alternative detection method for design of the microphones with improved performance for several demanding applications [10]. Although a variety of optical techniques have been investigated, most of them have not been successful in microscale implementations, due to integration difficulties. The optical detection scheme that is more feasible to integrate is the interferometric detection method shown in Fig. 13.10. In this method that is based on the Michelson interferometer,<sup>2</sup> the incoming beam of

<sup>2</sup> Albert A. Michelson, the American physicist, in 1907 was awarded a Nobel Prize for measurement the speed of light.



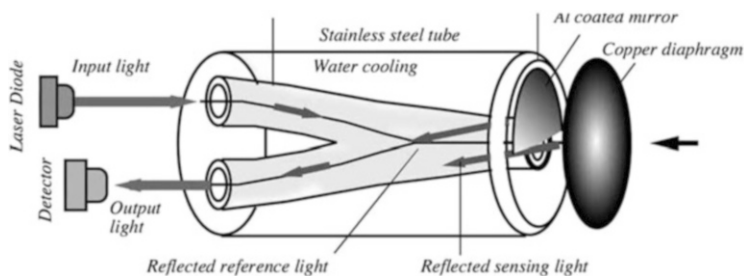
**Fig. 13.10** Concept of Michelson interferometric microphone (a) and interferences at different phases of the light beams (b) (adapted from [10])

light is split into two beams which are then passed along different paths. One beam serves as a reference, while the other beam bounces off the reflective vibrating diaphragm. When these two beams are combined, the interference takes place because of the path length difference due to the mechanical vibration of the diaphragm. This interference can be any combination of the constructive and destructive interferences depending on the displacement of the diaphragm. The detection of this interference with a photodetector makes it possible to obtain highly sensitive measurements of the diaphragm position.

Optical microphones are especially useful for the direct acoustic measurements in hostile environments, such as in turbojets or rocket engines, that require sensors which can withstand high heat and strong vibrations. The acoustic measurements under such hard conditions are required for computational fluid dynamics (CFD) code validation, structural acoustic tests, and jet noise abatement. These conditions demand use of robust diaphragms (plates), meaning that their displacements are very small. For such applications, a fiber-optic interferometric microphone can be quite suitable. One such design [11] is comprised of a single-mode temperature insensitive Michelson interferometer, and a reflective plate diaphragm. To provide an effect of interference between the incoming and outgoing light beams, two fibers are fused together and cleaved at the minimum tapered region (Fig. 13.11). The fibers are incorporated into a stainless steel tube which is water-cooled. The internal space in the tube is filled with epoxy, while the end of the tube is polished until the optical fibers are observed. Next, aluminum is selectively deposited to one of the fused fiber core ends to make its surface mirror reflective. This fiber serves as a reference arm of the microphone. The other fiber core is left open and serves as the sensing arm. Temperature insensitivity is obtained by the close proximity of the reference and sensing arms of the assembly.

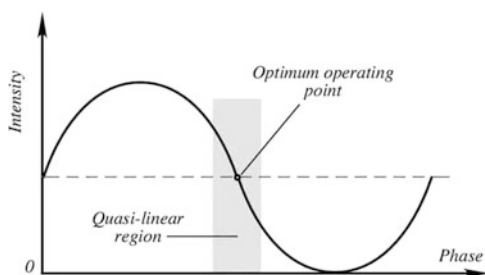
Light from a laser source (a laser diode operating near  $1.3 \mu\text{m}$  wavelength) enters one of the cores and propagates toward the fused end, where it is coupled to the other fiber core. When reaching the end of the core, light in the reference core is reflected from the aluminum mirror toward the input and output sides of the sensor. The portion





**Fig. 13.11** Fiber-optic interferometric microphone. Movement of the copper diaphragm is converted into light intensity in the detector

**Fig. 13.12** Intensity plot as function of reflected light phase



of light which goes toward the input is lost and makes no effect on the measurement, while the portion which goes to the output, strikes the detector's surface. That portion of light travels to the right in the sensing core, exits the fiber, and strikes the copper diaphragm. Part of the light is reflected from the diaphragm back toward the sensing fiber and propagates to the output end, along with the reference light. Depending on the position of the diaphragm, the phase of the reflected light will vary, thus becoming different from the phase of the reference light.

While traveling together to the output detector, the reference and sensing lights interfere with one another, resulting in the light intensity modulation. Therefore, the microphone converts the diaphragm displacement into a light intensity. Theoretically, the signal-to-noise ratio in such a sensor is obtainable in the order of 70–80 dB, thus resulting in an average minimum detectable diaphragm displacement as low as  $1 \text{ \AA}$  ( $10^{-10} \text{ m}$ ).

Figure 13.12 shows a typical plot of the optical intensity in the detector versus the phase for the interference patterns. To assure a better linearity of the transfer function, the operating point should be selected near the middle of the intensity, where the slope is the highest and the linearity is the best. The slope and the operating point may be changed by adjusting the wavelength of the laser diode. It is important for the deflection to stay within a quarter of the operating wavelength to maintain a proportional input.

The diaphragm is fabricated from a 0.05 mm foil with a 1.25 mm diameter. Copper is selected for the diaphragm due to its good thermal conductivity and

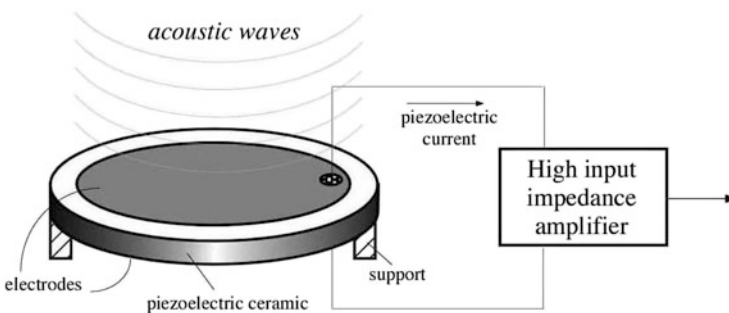
relatively low modulus of elasticity. The maximum acoustic frequency which can be transferred with the optical microphone is limited to about 100 kHz which is well above the desired working range needed for the structural acoustic testing.

## 13.6 Piezoelectric Microphones

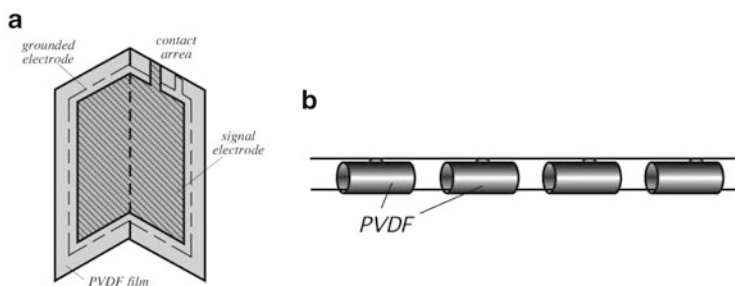
The piezoelectric effect can be used for the design of simple microphones because a piezoelectric crystal is a direct converter of a mechanical stress into an electric charge. The most frequently used material for the sensor is a piezoelectric ceramic, which can operate up to a very high-frequency limit. This is the reason, why piezoelectric sensors are used for transduction of ultrasonic waves. Still, even for the audible range, the piezoelectric microphones are employed quite extensively.

### 13.6.1 Low-Frequency Range

In a piezoelectric microphone, a diaphragm and displacement transducer are combined in one. Since the diaphragm is either made of or coated by a piezoelectric material, it flexing generates electric output. Typical applications are the voice activated devices and blood-pressure measurement apparatuses where the arterial Korotkoff sounds have to be detected. For such acoustically nondemanding applications, a piezoelectric microphone design is quite simple (Fig. 13.13). It consists of a piezoelectric ceramic disk with two electrodes deposited on the opposite sides for picking up the sound induced electric charge. The electrodes are connected to wires either by electrically conductive epoxy or by soldering. Since the output electrical impedance of such a microphone is very large, a high-input impedance amplifier is required. Such an amplifier, however, may have a degrading effect on the frequency response: the pick-up electrode capacitance together with a high output/input resistances form a first-order low-pass filter that cuts-off higher frequencies. This problem can be easily resolved by employing instead a charge-to-voltage converter as shown in Fig. 6.6c.



**Fig. 13.13** Piezoelectric microphone



**Fig. 13.14** Foldover piezoelectric acoustic pick-up (a) and arrangement of piezoelectric film hydrophone (b)

Piezoelectric films, PVDF, and copolymers, as described in Sect. 4.6.2, were used for many years as very efficient acoustic pick-ups in musical instruments [12]. One of the first applications for a piezoelectric film was an acoustic pick-up for a violin. Later, the film was introduced for a line of acoustic guitars as a saddle-mounted bridge pick-up, mounted in the guitar bridge. A very high fidelity of the pick-up led the way to a family of vibration sensing and accelerometer applications. Because of the low  $Q$ -factor<sup>3</sup> of the material, these transducers do not have the self-resonance of the hard ceramic pick-ups. Shielding can be achieved by a foldover design as shown in Fig. 13.14a. The sensing side is the slightly narrower electrode on the inside of the fold. The foldover technique provides a more sensitive pick-up than alternative shielding methods because the shield is formed by one of the film electrodes. For application in water, the film can be rolled in tubes, and many of such tubes can be connected in parallel (Fig. 13.14b).

### 13.6.2 Ultrasonic Range

Nowadays, use of the acoustic sensors is broader than detecting sound waves in air or water. They become increasingly popular for detecting mechanical vibrations in solid for operating such sensors as microbalances and *surface acoustic wave* devices (SAW). Applications range over measuring displacement, concentration of compounds, stress, force, temperature, etc. All such sensors are based on elastic motions in solid parts of the sensor and their major use is serving as parts in other, more complex sensors, for instance, in chemical detectors, accelerometers, pressure sensors, etc. In chemical and biological sensors, the acoustic path, where mechanical waves propagate, may be coated with chemically selective compound that interacts only with the material of interest (Sect. 18.6.1).

An excitation device (usually of a piezoelectric nature) forces atoms of the solid into vibratory motions about their equilibrium position. The neighboring atoms then

<sup>3</sup>  $Q$ -factor (quality factor) describes how the resonant bandwidth  $\Delta f$  relates to the center frequency  $f_r$ :  $Q = f_r/\Delta f$ .  $Q$  is an indicator of energy losses near the resonant frequency.

produce a restoring force, tending to bring the displaced atoms back to their original positions. In the acoustic sensors, vibratory characteristics, such as phase velocity and/or attenuation coefficient, are affected by the stimulus. In some sensors, the external stimuli, such as mechanical strain in the sensor's solid, increase the propagating speed of sound. In other sensors, which are called *gravimetric*, sorption of molecules or attachment of bacteria cause a reduction of acoustic wave velocity. And in other detectors, called the *acoustic viscosity sensors*, viscous liquid contacts the active region of an elastic wave sensor and the wave is attenuated.

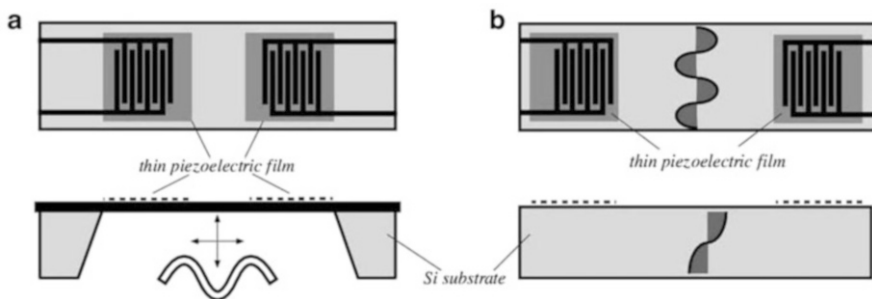
Acoustic waves propagating in solids have been used quite extensively in electronic devices such as electric filters, delay lines, microactuators, etc. The major advantage of the acoustic waves as compared with electromagnetic waves is their low velocity. Typical velocities in solids range from  $1.5 \times 10^3$  m/s to  $12 \times 10^3$  m/s, while the practical SAW utilize the range between  $3.8 \times 10^3$  m/s and  $4.2 \times 10^3$  m/s [13]. That is, acoustic velocities are five orders of magnitude smaller than those of electromagnetic waves. This allows for fabrication of miniature sensors operating with frequencies up to 5 GHz.

When the solid-state acoustic sensor is fabricated it is essential to couple the electronic circuit to its mechanical structure where the waves propagate. The most convenient effect to employ is the piezoelectric effect works in both ways: the mechanical stress induces electrical polarization charge so it acts as a microphone, and the applied electric field stresses the piezoelectric crystal making to act as a "speaker". Thus, the sensor generally has two piezoelectric transducers at both ends: one at the transmitting end for generation of acoustic waves and the other at the receiving end as a microphone for converting acoustic waves into electrical signal.

A design is a different in the MEMS structures. Since silicon does not possess piezoelectric effect, additional piezoelectric material must be deposited on the silicon waver in a form of a thin film [13]. Typical piezoelectric materials used for this purpose are zinc oxide (ZnO), aluminum nitride (AlN), and the so-called solid solution system of lead-zirconite-titanium oxides  $\text{Pb}(\text{Zr},\text{Ti})\text{O}_3$  known as PZT ceramic. When depositing thin films on a semiconductor material, several major properties must be taken into account. They are:

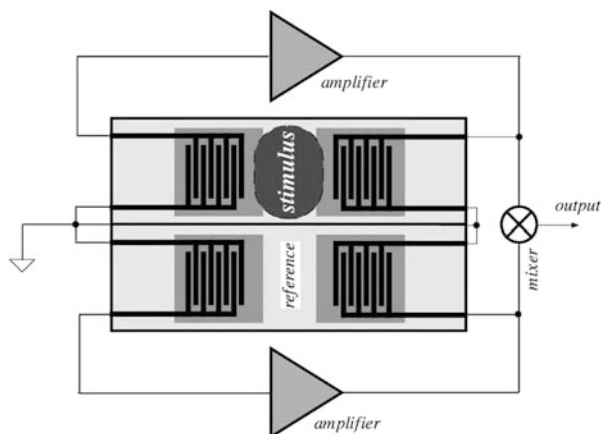
1. Quality of the adhesion to the substrate.
2. Resistance to the external factors (such as fluids which interact with the sensing surface during its operations).
3. Environmental stability (humidity, temperature, mechanical shock, and vibration).
4. Value of electromechanical coupling with the substrate.
5. Ease of processing by the available technologies.
6. Cost.

The strength of the piezoelectric effect in elastic-wave devices depends on configuration of the electrodes. Depending on the sensor design, for the bulk excitation (when the waves must propagate through the cross-sectional thickness of the sensor) the electrodes are positioned at the opposite sides and their area is quite large.



**Fig. 13.15** Ultrasonic sensors with flexural-plate mode (a) and surface acoustic-plate mode (b)

**Fig. 13.16** Differential SAW sensor



Several configurations for the solid-state acoustic sensors are known. They differ by the mode the waves propagate through the material. Figure 13.15 shows two most common versions: a sensor with flexural-plate mode (a) and with the acoustic-plate mode (b). In the former case, a very thin membrane is flexed by the left pair of the interdigitized electrodes and its vertical deflection induces response in the right pair of the electrodes that act as a microphone. As a rule, the membrane thickness is smaller than the wavelength of the oscillation. In the latter case, the waves are formed on the surface of a relatively thick plate. In either case, the space between the left and right pairs of the electrodes is used for interaction with the external stimuli, such as pressure, viscous fluid, gaseous molecules, or microscopic particles.

Many internal and external factors may contribute to propagation of acoustic wave and, subsequently, to change in frequency of oscillation, thus determination of a change in stimulus may be ambiguous and contain errors. An obvious solution to this problem is to use a differential technique, where two identical SAW devices are employed: one device is for sensing the stimulus and the other is used as a reference (Fig. 13.16). The reference device is shielded from stimulus, yet being

subjected to common factors, such as temperature, aging, vibrations, etc. The difference of the frequency changes of both oscillators is sensitive only to variations in the stimulus, thus canceling effects of spurious factors.

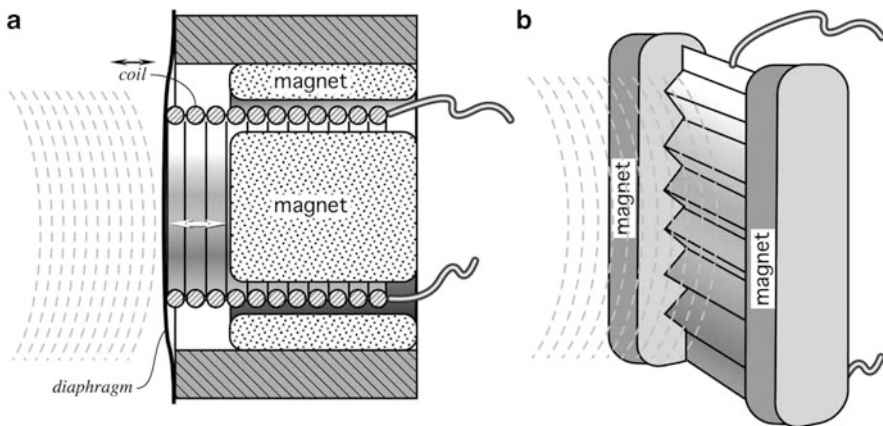
### 13.7 Dynamic Microphones

Dynamic microphones work via electromagnetic induction. They are robust, relatively inexpensive, and resistant to moisture. This, coupled with their potentially high gain (before feedback is applied) makes them ideal for on-stage uses.

*Moving-coil microphones* use the same dynamic principle as in a loudspeaker, only reversed, Fig. 13.17a. A small movable induction coil, positioned in the magnetic field of a permanent magnet, is attached to the diaphragm. When sound enters through the windscreen of the microphone (not shown in the figure), the sound waves move the diaphragm. When the diaphragm vibrates, the coil moves in the magnetic field, producing a varying voltage across the coil terminals. This is the result of electromagnetic induction. As it follows from Eq. (4.35), a variable magnetic field induces voltage in a coil. Thus, movement of the coil inside a permanent magnet generates the induced voltage in direct relationship with the rate of changing the magnetic field flux through the moving coil.

A single dynamic membrane will not respond linearly to all audio frequencies. Some microphones for this reason utilize multiple membranes for the different parts of the audio spectrum and then combine the resulting signals. Combining the multiple signals correctly is difficult and designs that do this are rare and tend to be expensive.

*Ribbon microphones* use a thin, usually corrugated metal ribbon suspended in a magnetic field (Fig. 13.17b). The ribbon is electrically connected to the microphone's output, and its vibration within the magnetic field generates the



**Fig. 13.17** Dynamic microphones: moving coil (a) and ribbon (b)

electrical signal. Ribbon microphones are similar to moving coil microphones in the sense that both produce sound by means of magnetic induction. Basic ribbon microphones detect sound in a bidirectional figure-8 pattern because the ribbon, which is open to sound both front and back, responds to the pressure gradient. Though the symmetrical front and rear pick-up can be a nuisance in normal stereo recording, the high-side rejection can be used to advantage in some applications, especially where a background noise rejection is required.

---

## References

1. Hohm, D., et al. (1989). A subminiature condenser microphone with silicon nitride membrane and silicon back plate. *The Journal of the Acoustical Society of America*, 85, 476–480.
2. Bergqvist, J., et al. (1990). A new condenser microphone in silicon. *Sensors and Actuators*, A21–A23, 123–125.
3. Sprengels, A. J., et al. (1989). Development of an electret microphone in silicon. *Sensors and Actuators*, 17(3&4), 509–512.
4. van der Donk, A. G. H., et al. (1991). Preliminary results of a silicon condenser microphone with internal feedback. In: *Transducers'91. International Conference on Solid-State Sensors and Actuators. Digest of technical papers* (pp. 262–265). IEEE.
5. Wong, S. K., et al. (Eds.). (1995). *AIP handbook of condenser microphones*. New York: AIP Press.
6. Nishikawa, S., et al. (1928). *Proc. Imp. Acad. Tokyo* (Vol. 4, p. 290).
7. Sessler, G. M. (Ed.). (1980). *Electrets*. Berlin: Springer.
8. Sessler, G. M. (1963). Electrostatic microphones with electret foil. *The Journal of the Acoustical Society of America*, 35(9), 1354–1357.
9. Griese, H. J. (1977). Paper Q29. *Proc. 9th Int. Conf. Acoust.*, Madrid.
10. Bicen, B. (2010). *Micromachined diffraction based optical microphones and intensity probes with electrostatic force feedback*. Ph.D. Dissertation, Georgia Institute of Technology. School of Mech. Eng.
11. Hellbaum, R. F., et al. (1991). An experimental fiber optic microphone for measurement of acoustic pressure levels in hostile environments. In *Sensors Expo Proceedings*. Peterborough: Helmers.
12. Piezo Film Sensors Technical Manual. (1999). Norristown, PA: Measurement Specialties. [www.msiusa.com](http://www.msiusa.com)
13. Motamedi, M. E., et al. (1994). Acoustic sensors. In S. M. Sze (Ed.), *Semiconductor sensors* (pp. 97–151). New York: John Wiley & Sons.

*“Water, taken in moderation, cannot hurt anybody”*

—Mark Twain

---

## 14.1 Concept of Humidity

The water content in surrounding air is an important factor for the well-being of humans and animals. The level of comfort is determined by a combination of two factors: relative humidity and ambient temperature. You may be quite comfortable at  $-30\text{ }^{\circ}\text{C}$  ( $-22\text{ }^{\circ}\text{F}$ ) in Siberia, where the air is usually very dry in winter, and feel quite miserable in Cleveland near lake Erie at  $0\text{ }^{\circ}\text{C}$  ( $+32\text{ }^{\circ}\text{F}$ ), where air may contain substantial amount of moisture.<sup>1</sup> Humidity is an important factor for operating certain equipment, for instance, high impedance electronic circuits, electrostatic sensitive components, high voltage devices, fine mechanisms, etc. A rule of thumb is to assure a relative humidity near 50 % at normal room temperature ( $20\text{--}25\text{ }^{\circ}\text{C}$ ). This may vary from as low as 38 % for the Class-10 clean rooms to 60 % in hospital operating rooms. Moisture is the ingredient common to most manufactured goods and processed materials. It can be said that a significant portion of the U.S. GNP (Gross National Product) is moisture [1].

Humidity can be measured by the instruments called *hygrometers* (from the Greek name *Hydra* of a mythological water monster-serpent). The first hygrometer was invented by Sir John Leslie (1766–1832) [2].

There are many ways to express moisture and humidity, often depending on industry or the particular application. Moisture of gases sometimes is expressed in pounds of water vapor per million cubic feet of gas. Moisture in liquids and solids is generally given as a percentage of water per total mass (wet weight basis), but may

---

<sup>1</sup> Naturally, here we disregard other comfort factors, such as economical, cultural, and political, otherwise I would not call Siberia a comfortable place. I spent some time there, so I know.



be given on a dry weight basis. Moisture in liquids with low water miscibility is usually expressed as parts per million by weight (PPM<sub>w</sub>).

The term *moisture* generally refers to the water content of any material, but for practical reasons, it is applied only to liquids and solids, while the term *humidity* is reserved for the water vapor content in gases. Here are some useful definitions.

*Moisture*—the amount of water contained in a liquid or solid by absorption or adsorption which can be removed without altering its chemical properties.

*Mixing ratio (humidity ratio), r*—the mass of water vapor per unit mass of dry gas.

*Absolute humidity (mass concentration or density of water vapor)*—the mass,  $m$ , of water vapor per unit volume  $v$  of wet gas:  $d_w = m/v$ . In other words, absolute humidity is the density of water vapor component. It can be measured, for example, by passing a measured quantity of air through a moisture-absorbing substance (such as silica-gel) which is weighed before and after the absorption. Absolute humidity is expressed in grams per cubic meter, or in grains per cubic foot. Since this measure is also a function of atmospheric pressure, it is not generally useful in engineering practice.

*Relative humidity (RH)* is the ratio of the actual vapor pressure of air at any temperature, to the maximum of saturation vapor pressure at the same temperature. Relative humidity in percents is defined as

$$H = 100 \frac{P_w}{P_s}, \quad (14.1)$$

where  $P_w$  is the partial pressure of water vapor and  $P_s$  is the pressure of saturated water vapor at a given temperature. The value of  $H$  expresses the vapor content as a percentage of the concentration required to cause the vapor saturation, that is, the formation of water droplets (dew) at that temperature. An alternative way to present RH is as a ratio of the mole fraction of water vapor in a space to the mole fraction of water vapor in the space at saturation.

The value of  $P_w$  together with partial pressure of dry air  $P_a$  is equal to pressure in the enclosure, or to the atmospheric pressure  $P_{\text{atm}}$  if the enclosure is open to the atmosphere:

$$P_w + P_a = P_{\text{atm}}. \quad (14.2)$$

At temperatures above the boiling point, water pressure could displace all other gases in the enclosure. The atmosphere volume would then consist entirely of superheated steam. In this case,  $P_w = P_{\text{atm}}$ . At temperatures above 100 °C, RH is a misleading indicator of moisture content because at these temperatures  $P_s$  is always more the  $P_{\text{atm}}$ , and maximum RH never can reach 100 %. Thus, at normal atmospheric pressure and temperature of 100 °C, the maximum RH is 100 %, while at 200 °C it is only 6 %. Above 374 °C, saturation pressures are not thermodynamically specified.

*Dewpoint temperature*—the temperature at which the partial pressure of the water vapor present would be at its maximum, or saturated vapor condition, with respect to equilibrium with a plain surface of ice. It also is defined as the temperature to which the gas-water vapor mixture must be cooled isobarically (at constant pressures) to induce frost or ice (assuming no prior condensation). The *dewpoint* is the temperature at which relative humidity is 100 %. In other words, the dewpoint is the temperature that the air must reach for the air to hold the maximum amount of moisture it can. When the temperature cools to the dewpoint, the air becomes saturated and fog, or dew, or frost can occur.

The following equations [3] calculate the dewpoint from relative humidity and temperature,  $t$ . All temperatures are in Celsius.

The saturation vapor pressure  $p_s$  over water surface is found from

$$p_s = 10^{0.66077 + 7.5 \frac{t}{237+t}} \quad (14.3)$$

and the dewpoint temperature is found from the approximation:

$$DP = \frac{237.3(0.66077 - \log_{10} p_w)}{\log_{10} p_w - 8.16077} t \quad (14.4)$$

where  $p_w = \frac{p_s \cdot RH}{100}$

Relative humidity displays an inverse relationship with the absolute temperature. This means that for the same absolute amount of moisture, the higher the temperature, the lower the RH.

Dewpoint temperature is usually measured with a chilled mirror. However, below 0 °C dewpoint, the measurement becomes uncertain as moisture eventually freezes and a crystal lattice growth will slowly occur, much like a snowflake. Nevertheless, moisture can exist for prolonged time below 0 °C in a liquid phase, depending on such variables as molecular agitation, rate of convection, sample gas temperature, contaminations, etc.

To calibrate humidity sensors, a reference source of humidity is required. There are several methods of producing a known humidity level. For example, one can generate a dry air (0 % humidity) and steaming moist air (100 % humidity) and then mix them in a known proportion. Yet, the most popular method is using saturated salt solutions in water. A dish with the saturated solution is placed in a closed box that is tightly sealed from the atmosphere. The solution generates relative humidity in the free space above the dish with good accuracy. The value of the relative humidity depends on the type of salt used (Table 14.1). Relative humidity above the saturated salt solution is very little dependent on temperature, but strongly dependent on temperature spatial uniformity. For an accuracy of  $\pm 2$  %RH a temperature uniformity inside the sealed box should be better than 0.5 °C.

To make a relative or absolute humidity sensor, any physical effect that relates to concentration of water molecules can be employed. One of the oldest sensors for measuring humidity was a hair tension transducer. The hair may be human or animal. Its tension is function of ambient humidity. If the hair is stretched between

**Table 14.1** Relative humidity of saturated salt solutions

Temperature (°C)	Lithium chloride solution LiCl, H <sub>2</sub> O	Magnesium chloride solution MgCl, 6H <sub>2</sub> O	Magnesium nitrate solution Mg(NO <sub>3</sub> ) <sub>2</sub> , 6H <sub>2</sub> O	Sodium chloride solution NaCl, 6H <sub>2</sub> O	Potassium chloride solution K <sub>2</sub> SO <sub>4</sub>
5	13	33.6 ± 0.3	58	75.7 ± 0.3	98.5 ± 0.9
10	13	33.5 ± 0.2	57	75.7 ± 0.2	98.2 ± 0.8
15	12	33.3 ± 0.2	56	75.6 ± 0.2	97.9 ± 0.6
20	12	33.1 ± 0.2	55	75.5 ± 0.1	97.6 ± 0.5
<b>25</b>	<b>11.3 ± 0.3</b>	<b>32.8 ± 0.3</b>	<b>53</b>	<b>75.3 ± 0.1</b>	<b>97.3 ± 0.5</b>
30	11.3 ± 0.2	32.4 ± 0.1	52	75.1 ± 0.1	97.0 ± 0.4
35	11.3 ± 0.2	32.1 ± 0.1	50	74.9 ± 0.1	96.7 ± 0.4
40	11.2 ± 0.2	31.6 ± 0.1	49	74.7 ± 0.1	96.4 ± 0.4
45	11.2 ± 0.2	31.1 ± 0.1	–	74.5 ± 0.2	96.1 ± 0.4
50	11.1 ± 0.2	30.5 ± 0.1	46	74.6 ± 0.9	95.8 ± 0.5
55	11.0 ± 0.2	29.9 ± 0.2	–	74.5 ± 0.9	–

From: Greenspan, L., Huang, P.H., Wahtstone, J.R., Aoro, R.M. 808 10 and OIML recommendations

two anchor points, the tension can be converted to electrical signal by any appropriate force sensor. Tension is stronger at dry air, while the hair relaxes at humid air. On this principle, the folk art “weather houses” were operating: human figure dolls changed positions under control of the hair tension and thus “predicting” weather.

Traditionally, RH was measured by the device called *aspirated psychrometer* (from the Latin *aspirātus*—*breathed upon* and the ancient Greek *ψυχρός*—*cold, frozen*) which is composed of two identical thermometers, where one has a dry mercury bulb, while the second bulb is wrapped around by a wet gauze with a wick immersed into a water to keep the gauze moist. Air is blown over both bulbs. When water or ice covers the wet bulb of the second thermometer, latent heat is removed from the surface of the bulb as the water evaporates, and the wet-bulb temperature becomes lower than the air (dry-bulb) temperature. At a lower humidity, water evaporates more actively, so that the wet-bulb temperature drops more. The aspirated psychrometer determines humidity by measuring the difference between the dry-bulb temperature and wet-bulb temperature:  $\Delta t = t_a - t_w$ . The RH is computed from the following formula:

$$RH(\%) = 100 \frac{p_w - A\Delta t}{p_s} \quad (14.5)$$

where  $A$  is a constant equal to 63 for a wet bulb and to 56 if the bulb is covered with ice,  $p_w$  is the water vapor pressure,  $p_s$  is the saturated water vapor pressure, and  $t_a$  and  $t_w$  are the Celsius temperatures of the dry and wet bulb, respectively.

The water vapor pressure is function of three factors: the atmospheric pressure  $P$ , the dry-wet bulb's thermal gradient  $\Delta t$ , and saturated water vapor pressure  $p_s$  at the air temperature:

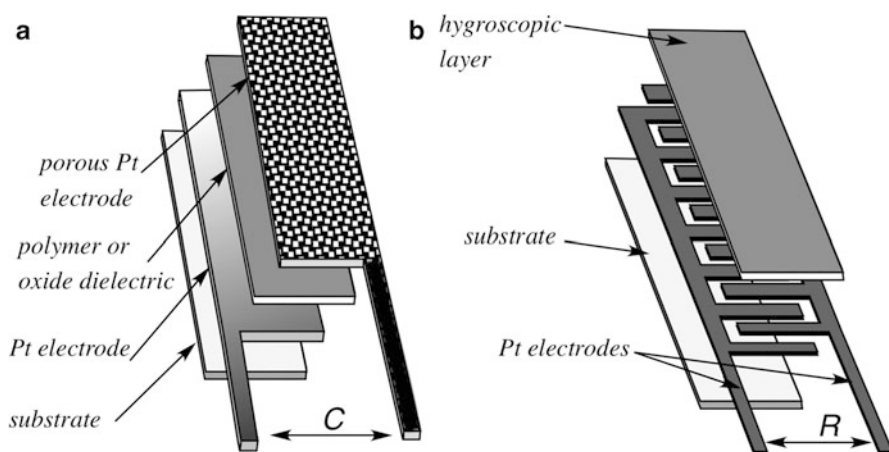
$$p_w = p_s - \frac{A}{755} P \Delta t \quad (14.6)$$

The aspirated psychrometer often is employed for calibrating the humidity sensors.

## 14.2 Sensor Concepts

To detect humidity level, a sensor in a hygrometer must be selective to water molecules and some of its internal properties should be modulated by the water molecule concentration. In other words, the sensor shall contain a converter of the  $H_2O$  vapor pressure into electrical signal. The most popular converters are based on capacitance and resistance that vary with humidity. We may say that these sensors are “bad” capacitors or resistors whose values are not stable—they change when these devices are subjected to moisture. Figure 14.1 illustrates general compositions of the capacitive (a) and resistive (b) humidity sensors.

In a capacitive sensor, a thin layer (polymer or oxide dielectric) whose dielectric properties depend on concentration of the absorbed moisture is sandwiched between two metal electrodes. The upper electrode is made porous to allow water molecules to reach the moisture sensitive dielectric layer and be absorbed. All layers are deposited on a substrate that may be ceramic. Capacitance  $C$  is measured between the electrodes by a conventional interface circuit.



**Fig. 14.1** Layers in capacitive (a) and resistive (b) humidity sensors

A resistive sensor contains a moisture-absorbing material whose electrical resistance is function of the absorbed water molecules. This sensing hygroscopic layer is positioned on the top of two interdigitized<sup>2</sup> metal electrodes and the entire assembly is built on a substrate. The resistance  $R$ , whose value depends on humidity, is measured between the electrodes.

For signal processing, either capacitance or resistance or both shall be converted into electrical signal by the appropriate circuit that depends on the conversion type: Z-to-V (voltage), or Z-to-F (frequency), or Z-to-D (digital) converter. When operating, the humidity-sensing element shall be measured only by an alternating current to remove the direct current component and avoid electrolysis (polarization) of the moisture sensitive material. The frequency of the a.c. is normally set within a range of 200 Hz–10 kHz.

---

### 14.3 Capacitive Humidity Sensors

An air-filled capacitor may serve as a relative humidity sensor because moisture in the atmosphere changes air electrical permittivity according to the following equation:

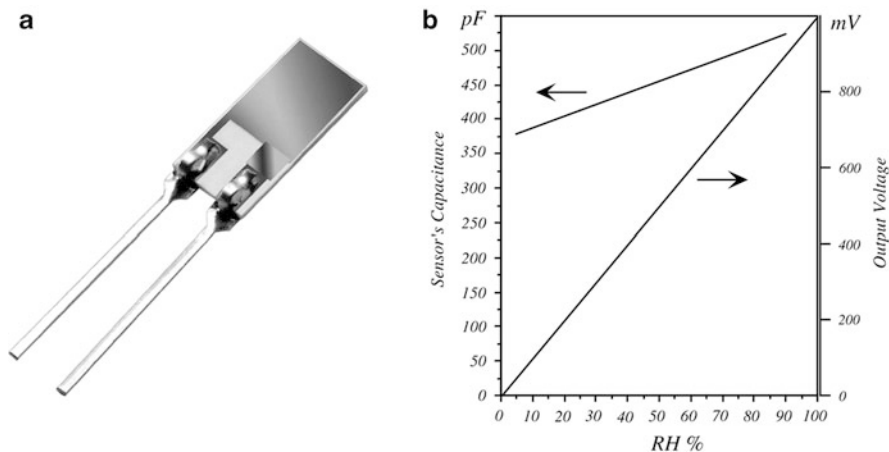
$$\kappa = 1 + \frac{211}{T} \left( p_w + \frac{48 p_s}{T} H \right) 10^{-6}, \quad (14.7)$$

where  $T$  is the absolute temperature in kelvin,  $p_w$  is the pressure of moist air in mmHg,  $p_s$  is the pressure in mmHg of saturated water-vapor at temperature  $T$ , and  $H$  is the relative humidity in %. Equation (14.7) shows that the dielectric constant of moist air, and, therefore, the capacitance, is proportional to the relative humidity. In spite of a good linearity, the air-filled capacitor as a humidity sensor has a low sensitivity and thus not practical.

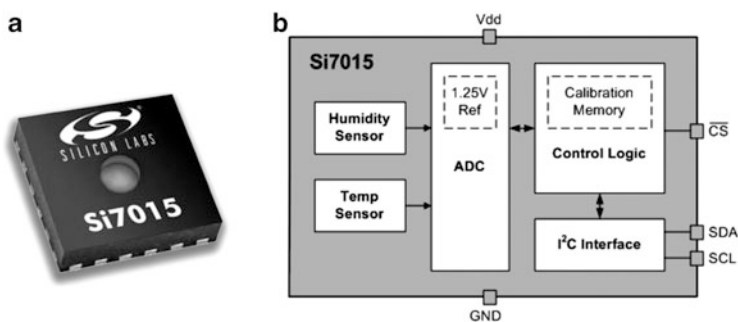
Instead of air, the space between the capacitor plates can be filled with an appropriate isolator whose dielectric constant changes significantly upon being subjected to humidity. A capacitive sensor may be formed of a hygroscopic polymer film with metallized electrodes deposited on the opposite sides. In one design [4] the dielectric was composed of a hydrophilic polymer thin film (8–12  $\mu\text{m}$  thick) made of cellulose acetate butyrate and the dimetylephtalate as plasticizer. The 8-mm-diameter gold porous disk electrodes (200  $\text{\AA}$  thick) were deposited on the polymer by the vacuum deposition. The film was suspended by a holder and the electrodes were connected to the terminals. The capacitance of such a sensor is approximately proportional to relative humidity  $H$

---

<sup>2</sup>Interdigitized term is an analogy of two joined hands whose fingers (digits) are positioned alternatively.



**Fig. 14.2** Capacitive relative humidity sensor (a) and its transfer function (b) for capacitance and output voltage from interface circuit

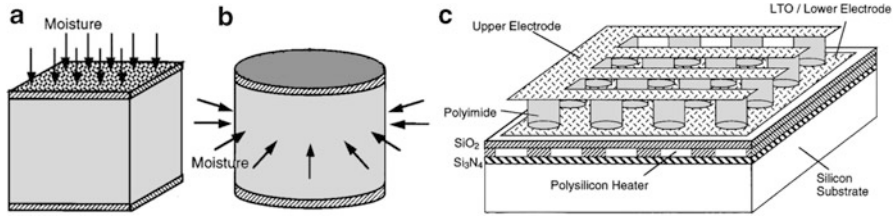


**Fig. 14.3** Integrated RH sensor packaging (a) and its functional diagram (b) (From Silicon Labs, Inc.)

$$C_h \approx C_o(1 + \alpha_h H), \tag{14.8}$$

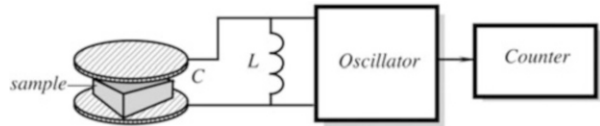
where  $C_o$  is the capacitance at  $H = 0$ .

A discrete capacitive RH sensor is shown in Fig. 14.2a and its transfer function (b) indicates that capacitance increase nearly linearly with the increase in humidity. This is due to a high dielectric constant of water. Note that the water dielectric constant also is function of temperature (see Fig. 4.7), thus the RH sensor requires a compensation by an auxiliary temperature sensor. This was implemented in commercially available integrated sensors, for example, in Si7015 produced by Silicon Labs (see Fig. 14.3). Note a circular opening in the packaging for receiving samples of air. Advantage of the integrated circuit is that in addition to the sensing elements (humidity and temperature) it incorporates the signal conditioners, ADC, calibration memory, compensation circuit, and a serial digital interface, such as  $I^2C$ .



**Fig. 14.4** Comparison of traditional (a) and cylindrical (b) moisture-sensing capacitors. Capacitive columns are connected in parallel (c) (Adapted from [5])

**Fig. 14.5** Capacitive moisture-sensing arrangement



Measurement humidity by a capacitive sensor may be a rather slow process because it takes time for the dielectric layer to absorb water molecules. Use of modern MEMS technology allows a dramatic speed enhancement by miniaturizing sizes of the sensing capacitors and increasing the exposed area of a dielectric material. One solution involves forming a multitude of cylindrical capacitive columns with the exposed side walls as shown in Fig. 14.4b and 14.4c [5].

While a traditional capacitive sensor has a porous upper electrode, the column capacitors form the exposed polyimide sides that absorb moisture much faster. The column diameter is only a few microns, allowing moisture to diffuse into them circumferentially. In addition, the sensor is augmented with a heating element. The heater is used to prevent condensation, after which a long recovery time is required, and during which the sensor remains inoperative. Multiple cylinders are connected in parallel as shown in Fig. 14.4c. This design speeds up the sensor response by about ten times.

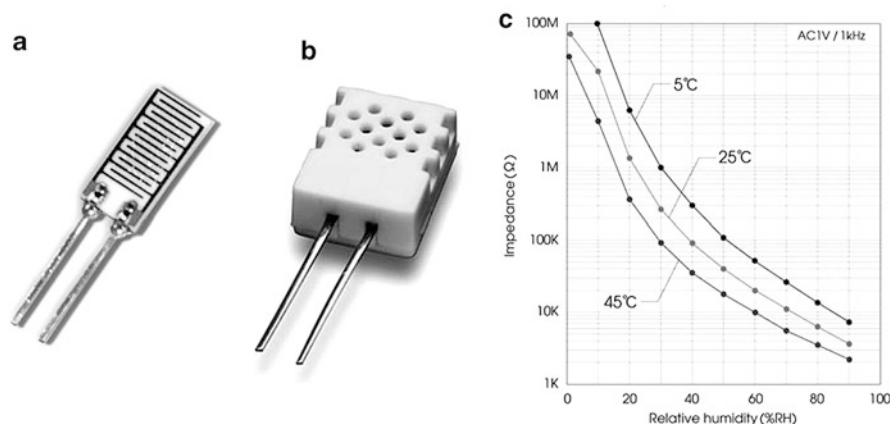
A capacitive technique can be used for measuring moisture in material samples [6]. Figure 14.5 shows a conceptual diagram of the capacitive measurement system where a dielectric constant of the sample changes the frequency of the LC-oscillator. This method of moisture measurement is quite useful in the process control of pharmaceutical products. Dielectric constants of most of the medical tablets are quite low (between 2.0 and 5.0) as compared with that of water (75–80 at room temperature). The sampled material is placed between two test plates which form a capacitor connected into an LC-oscillating circuit. The frequency is measured and related to moisture. The best way to reduce variations attributed to environmental conditions, such as temperature and room humidity, is a use of a differential technique. That is, the frequency shift  $\Delta f = f_o - f_1$  is calculated, where  $f_o$  and  $f_1$  are frequencies produced by the empty container and that filled with the sampled material, respectively. The method has some limitations, for instance, its accuracy is poor when measuring moistures below 0.5 %, the sample must be

clean of foreign particles having relatively high dielectric constants—examples are metal and plastic objects, a packing density, and a fixed sample geometry must be maintained.

## 14.4 Resistive Humidity Sensors

Resistances of many nonmetal conductors generally depend on their water content, as it was discussed in Sect. 4.5.4. This phenomenon is the basis of a resistive humidity sensor or *hygristor*. A basic design of a conductive hygrometric sensor is shown in Fig. 14.6a. The sensor is fabricated on a ceramic (alumina) substrate. The moisture-sensing material has a relatively low resistivity which changes significantly under varying humidity conditions. The material is deposited on the top of two interdigitized electrodes to provide a large contact area. When water molecules are absorbed by the upper layer, resistivity between the electrodes changes which can be measured by an electronic circuit. The first such sensor was developed by F. W. Dunmore in 1935 of a hygroscopic film consisting of 2–5 % aqueous solution of LiCl [7]. Another example of a conductive humidity sensor is the so-called Pope element which contains a polystyrene film treated with sulfuric acid to obtain the desired surface-resistivity characteristics.

Other promising materials for fabrication of a film for a conductivity sensor are solid polyelectrolytes. A long term stability and repeatability of these compounds, while generally not too great, can be significantly improved by using the interpenetrating polymer networks and carriers, and supporting media. When measured at 1 kHz, an experimental sample of such a film has demonstrated a change in impedance from 100 M $\Omega$  to 100  $\Omega$  while RH was changing from



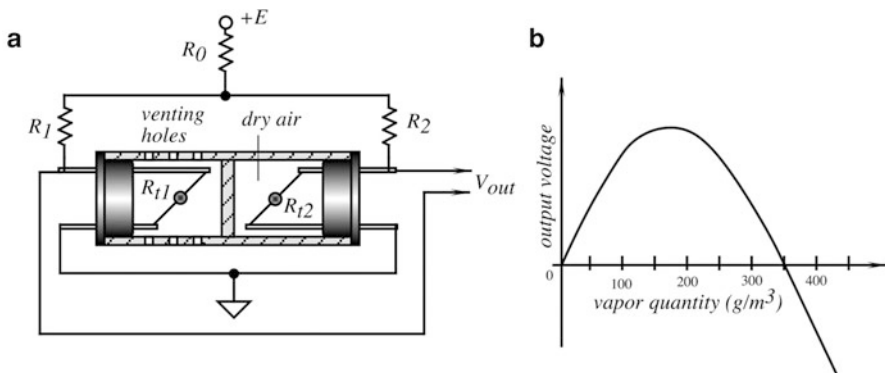
**Fig. 14.6** Substrate of hygristor carries interdigitized electrodes (a); commercial packaging of hygristor (b), and resistance-vs-RH characteristic at three different temperatures (courtesy of TDK)



0 to 90 % (Fig. 14.6c). For practical measurements conductometric humidity sensor can be mounted at the tip of a probe or mounted on a circuit board. Just as with the capacitive sensors, the output signal is strongly influenced by the air temperature. Thus, a signal conditioning circuit shall also receive a signal from an auxiliary temperature sensor. The hygristor's resistance is highly nonlinear, while its conductivity, being reciprocal to resistivity, demonstrates a reasonable linearity with respect to RH.

## 14.5 Thermal Conductivity Sensor

Using thermal conductivity of gas for measuring humidity can be accomplished by a differential thermistor-based sensor, Fig. 14.7a [8]. Two tiny thermistors ( $R_{t1}$  and  $R_{t2}$ ) are supported by thin wires to minimize thermal conductivity loss to the housing. The left thermistor is exposed to the outside gas through small venting holes, while the right thermistor is hermetically sealed in dry air. Both thermistors are connected into a bridge circuit ( $R_1$  and  $R_2$ ), which is powered by the reference voltage  $+E$ . The thermistors develop self-heating due to the passage of electric current resulting in release of Joule heat, thus their resistivities shall be fairly low—preferably from 10 to 50  $\Omega$ , otherwise the current would be too low for developing sufficient temperature rise up to 170  $^{\circ}\text{C}$  over the ambient temperature. Initially, the bridge is balanced in dry air to establish a zero reference point. The output of this sensor gradually increases as absolute humidity rises from zero. At about 150  $\text{g}/\text{m}^3$  it reaches the saturation and then decreases with a polarity change at about 345  $\text{g}/\text{m}^3$ , Fig. 14.7b. In this device, it is important to conduct measurement in a near-still air with very little air flow through the venting holes. Otherwise, air convection will cause additional cooling and thus cause errors in measurement.



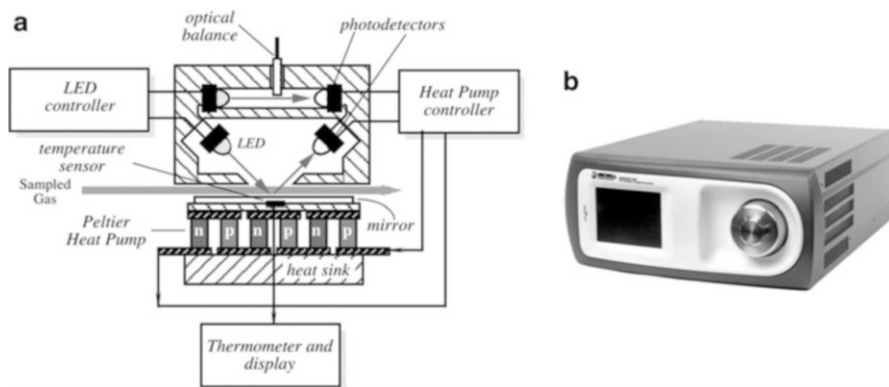
**Fig. 14.7** Absolute humidity sensor with self-heating thermistors. Design and electrical connection (a); output voltage (b)

## 14.6 Optical Hygrometers

### 14.6.1 Chilled Mirror

Most of the humidity sensors exhibit some repeatability problems, especially hysteresis with a typical value from 0.5 to 1 %RH. In precision process control, this may be a limiting factor, therefore indirect methods of humidity measurements should be considered. The most efficient method is a calculation of the absolute or relative humidity through dewpoint temperature by using Eq. (14.4). As was indicated above, the *dewpoint* is the temperature at which liquid and vapor phases of water (or any fluid for that matter) are in equilibrium. The temperature at which the vapor and solid phases are in equilibrium is called the *frostpoint*. At the dewpoint, only one value of saturation vapor pressure exist. Hence, absolute humidity can be measured from this temperature as long as the pressure is known. The optimum method of moisture measurement by which the minimum hysteresis effects are realized requires the use of optical hygrometry. The cost of an optical hygrometer is considerably greater, but if the benefit of tracking low-level moisture enhances product yield and quality, the cost is easily justified.

The basic idea behind the optical hygrometer is the use of a mirror whose surface temperature is precisely regulated by a thermoelectric heat pump. The mirror temperature is controlled at a threshold of formation of dew. Sampled air is pumped over the mirror surface and, if the mirror temperature crosses a dewpoint, releases moisture in the form of water droplets. The reflective properties of the mirror change at water condensation because water droplets scatter light rays. This can be detected by an appropriate photodetector. Figure 14.8 shows a simplified block diagram and a commercial instrument of a chilled mirror hygrometer. It is comprised of a heat pump operating on a Peltier effect. The pump removes heat from a thin mirrored surface which has an imbedded temperature sensor. That sensor is part of a digital thermometer which displays temperature of the mirror.



**Fig. 14.8** Chilled mirror dew point sensor with optical bridge (a) and commercial chilled mirror hygrometer (b) (Courtesy of Michell Instruments Ltd., Cambridgeshire, UK)

The hygrometer's circuit is of a differential type, where the top optocoupler, a light emitting diode (LED), and a photodetector, are used for the compensation of drifts, while the bottom optocoupler is for measuring the mirror reflectivity. The sensor's symmetry can be balanced by a wedged optical balance inserted into the light path of the upper optocoupler. The lower optocoupler is positioned at 45° angle with respect to the mirror. Above the dewpoint temperature, the mirror is dry and its reflectivity is the highest. The controller lowers temperature of the mirror through the heat pump. At the moment of the water condensation, the mirror reflectivity drops abruptly, which causes reduction in the photodetector photocurrent. The signals from the photodetector pass to the controller to regulate electric current through the heat pump to maintain its surface temperature at the level of a dewpoint, where no additional condensation or evaporation from the mirror surface occurs. Actually, water molecules are continuously being trapped and are escaping from the surface, but the average net level of the condensate density does not change once equilibrium is established.

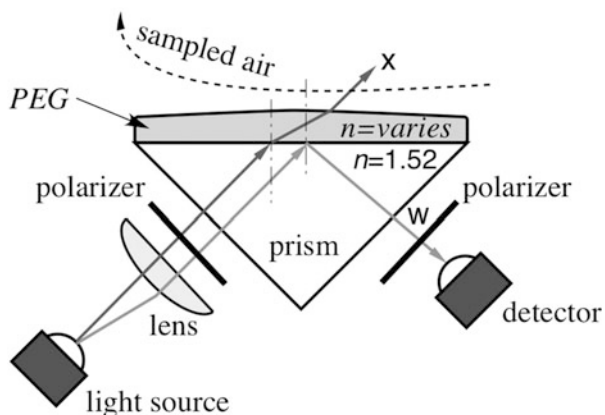
Since the sensed temperature of the mirrored surface precisely determines the actual prevailing dewpoint, this is considered the moisture's most fundamental and accurate method of measurement. Hysteresis is virtually eliminated and sensitivity is near 0.03 °C DP (dewpoint). From the dewpoint, all moisture parameters such as %RH, vapor pressure, etc. are obtainable once the prevailing temperature and pressure are known.

There are several problems associated with the method. One is a relatively high cost, the other is a potential mirror contamination, and the third is a relatively high-power consumption by the heat pump. Contamination problems can be virtually eliminated with use of particle filters and a special technique which deliberately cools the mirror well below the dewpoint to cause excessive condensation, with the following fast rewarming. This flashes out the contaminants keeping the mirror clean [9].

### 14.6.2 Light RH Sensors

Abilities of some materials to change their optical properties (polarization, refractive index, and light absorption) when subjected to water molecules are the basis for sensing by the light modulating RH sensors. An example of a humidity-sensing material is polyethylene glycol (PEG) that upon absorbing water molecules changes its refractive index and becomes swollen [10] that allows the RH measurement in a practical range from 10 to 95 %. PEG, which is a highly hydrophilic material, shows no monotonic linear response to humidity but gives different characteristics for various ranges of humidity levels both in index of refraction and in thickness. It undergoes a physical phase change from a semi-crystalline structure to a gel at around 80 % RH. At this phase-change point, a drastic decrease occurs in the index of refraction as well as a drastic increase in the swelling of the PEG film. If the PEG coating is hydrogenated in a vacuum chamber, hydrogen eliminates the effect on the humidity induced phase change.

**Fig. 14.9** Concept of light intensity modulation in the optical humidity sensor



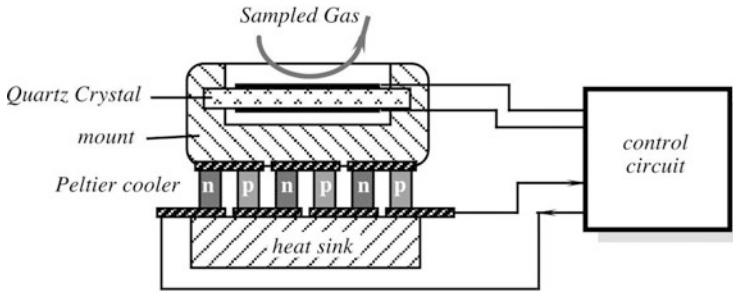
The PEG coating is used to make a light modulator as shown in Fig. 14.9. The sensor contains a prism whose upper plane is coated with a thin film of PEG. The effect of a total internal reflection (TIR) bouncing of the light generated by LED from the upper flat surface coated with the film and direct it to the photo detector as a beam  $w$ . The PEG film is being exposed to air that is drawn along the film surface.

To illustrate the concept, the drawing shows three optical effects working in concert under influence of the water molecules in the sampled air stream. The first effect is swelling of the PEG film that changes the amount of light reflected from the upper plane of the prism, the second is change in the PEG refractive index  $n$  that forces some light beams from being reflected toward the detector and diverted outwardly as a beam  $x$ , and the last effect is rotation of the light polarization by the PEG coating. A concept of the polarization rotation is shown in Fig. 8.36. Under the water molecules influence, light reflected from the PEG film changes its angle of polarization and thus after passing through a polarizing filter near the detector, its intensity is modulated in relation with the RH.

Another optical HR sensor responds to a variable color of the sensing material. A hygroscopic material can be impregnated with a dye that responds to the RH level. A polymer material with a dye is exposed to air for measuring RH. Change in the optical properties of a dye by humidity perhaps is due to association/dissociation complex the dye must be forming with the polymer carrier film or due to change in the pH level [11]. In the sensor, the polymer with a dye is placed in the path of an opto-coupler so that the light intensity can be converted into a variable electrical signal.

## 14.7 Oscillating Hygrometer

The idea behind the oscillating hygrometer is similar to that behind the optical chilled mirror sensor. The difference is that the measurement of the dewpoint is made not by the optical reflectivity of the surface, but rather by detecting a changing mass of the chilled plate. The chilled plate is fabricated of a thin quartz crystal, that is a part of an oscillating circuit. This implies the other name for the sensor: *the*



**Fig. 14.10** Oscillating hygrometer

*piezoelectric hygrometer*, because the quartz plate oscillation is based on the piezoelectric effect. A quartz crystal is thermally coupled to the Peltier cooler (see Sect. 4.9.2) which controls temperature of the crystal with a high degree of accuracy (Fig. 14.10). When the temperature drops to that of a dewpoint, a film of water vapor deposits on the exposed surface of the quartz crystal. Since the mass of the crystal changes, the resonant frequency of the oscillator shifts from  $f_o$  to  $f_1$ . The new frequency  $f_1$  corresponds to a given thickness of the water layer. The frequency shift controls current through the Peltier cooler, thus changing temperature of the quartz crystal to stabilize at the dewpoint temperature.

The major difficulty in designing the piezoelectric hygrometer is in providing an adequate thermal coupling between the cooler and the crystal, while maintaining small size of the crystal at a minimum mechanical loading [12]. This method may be employed by using the SAW sensors, similar to that of Fig. 13.15.

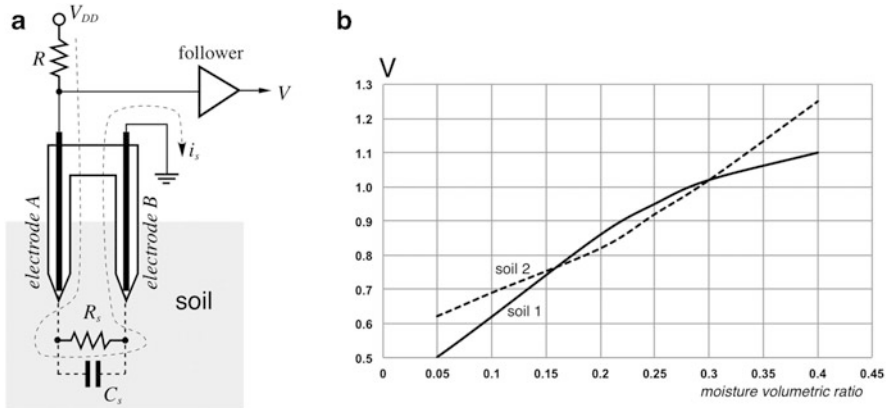
## 14.8 Soil Moisture

In agriculture and geology, investigation of soils is a serious business. Many soil moisture monitors operate on the principle of *conductivity* measurement. Pure water is not a good conductor of electricity. Since in a solution, the electrical current is transported by ions, the conductivity increases as the concentration of the ions increases. Thus, conductivity increases as water dissolves ionic species.

*Typical conductivity of waters*<sup>3</sup>:

Deionized water	$5.5 \times 10^{-6}$ S/m
Drinking water	0.005–0.05 S/m
Sea water	5 S/m

<sup>3</sup> Conductivity is measured in units of *siemens* (S) that is a reciprocal function of specific resistivity. See Sect. 4.5.1.



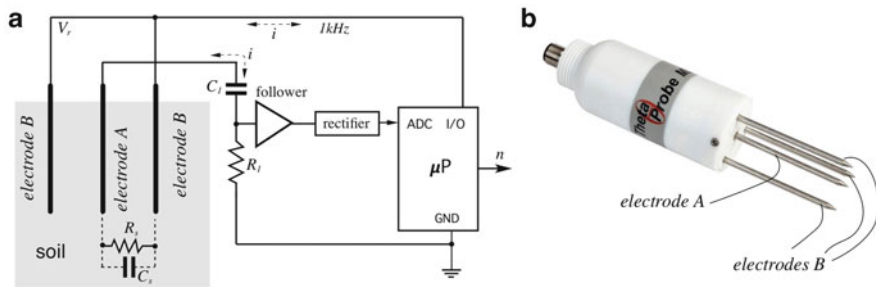
**Fig. 14.11** Soil conductivity meter with d.c. current (a) and transfer functions (b)

Soil is composed of a great variety of minerals and organic materials existing in solid, gaseous, and aqueous states. Water in soils, depending on the soil composition, ranges in conductivity from 0.01 to 8 S/m and is the main contributor to soil electrical conductivity.

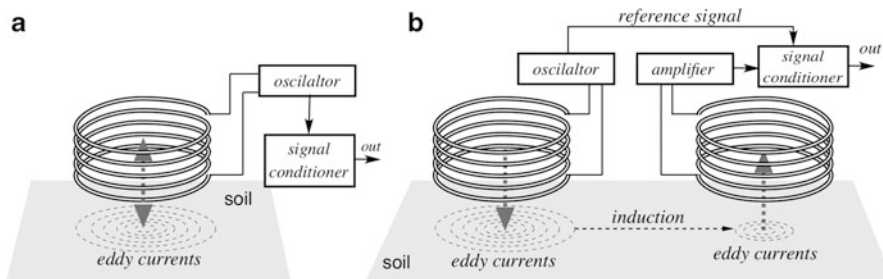
To monitor the soil water content, several methods are currently employed. One uses a simple two-electrode probe as shown in Fig. 14.11a where soil electrical resistivity  $R_s$  is measured by monitoring the voltage and current flow between the electrodes A and B that are inserted into the soil sample. Many hand-held moisture meters use a d.c. measurement circuit where current  $i_s$  passes through the soil. The circuit is a voltage divider consisting of a pull-up resistor  $R$  and soil resistance  $R_s$ . Note that a capacitance  $C_s$  between the electrodes makes no difference as long as direct current is used. As Fig. 14.11b illustrates, the output voltage clearly represents the soil water content [13]. Yet, this is not the most efficient way of measuring the soil resistivity as direct current causes the electrode polarization that changes the electrode-soil boundary resistance, resulting in errors after a prolonged use. In such sensors, to prevent accumulation of the electrolytic deposits, the electrodes shall be cleaned after each use.

To avoid the electrode polarization, measurement should be made with alternating current as illustrated in Fig. 14.12a. A typical probe has multiple electrodes, where a current injecting electrode A is placed in the center of the probe, Fig. 14.12b, while several (typically 3–5) return electrodes B are circumferentially positioned and connected in parallel. Thus, the soil impedance consisting of resistance  $R_s$  and capacitance  $C_s$  can be measured between the electrodes A and B by passing current  $i$  of frequency about 1 kHz. To remove a possible d.c. component from the current, the capacitor  $C_1$  is placed in series with resistor  $R_1$ . Voltage across the resistor is rectified and fed into the processor. Its magnitude relates to the soil impedance at the selected frequency.

Sometimes, soil impedance measurement should be made at the appreciable depth where using contact electrodes is impractical. In such cases, the



**Fig. 14.12** Multielectrode soil electrical impedance monitor (a) and commercial four-electrode probe (b) (Courtesy of Delta-T Devices Ltd, Cambridge, UK.)



**Fig. 14.13** Single (a) and dual (b) coil devices for noncontact measurement of electromagnetic conductivity of soil

electromagnetic conductivity measurement may be performed with use of eddy currents. Figure 14.13a shows soil with the eddy currents that are induced by a coil placed above the ground. The coil is driven by a high-frequency oscillator. The operating principle is similar to a metal detector, such as the one illustrated in Fig. 8.19. However, instead of metal, the coil would respond to circular induced currents in the electrically conductive soil. The higher the water content the stronger eddy currents. According to the Lenz law, these currents will oppose the coil a.c. current and thus can be measured.

Another arrangement for using eddy currents is shown in Fig. 14.13b that uses two coils—the transmitting and receiving. A transmitting coil is located at one end of the instrument. It induces circular eddy-current loops in the soil. The magnitude of these loops is directly proportional to the electrical conductivity of the soil where loops appear. Each current loop generates a secondary induced electromagnetic field that is proportional to the magnitude of the currents. A fraction of the secondary induced electromagnetic field is intercepted by the receiver coil of the instrument, and the sum of these induced signals is amplified and detected as the output voltage, which relates to a depth-weighted bulk soil electrical conductivity. The receiver coil measures amplitudes and phases of the secondary

magnetic field that will differ from those of the primary field as function of the soil properties (e.g., clay content, water content, and salinity), spacing of the coils and their distance from the soil surface [14].

---

## References

1. Quinn, F. C. (1985). The most common problem of moisture/humidity measurement and control. In: *Moisture and humidity. Proc. of the 1985 Int. Symp. on Moisture and Humidity* (pp. 1-5). ISA: Washington, DC.
2. Carter, E. F. (1966). Dictionary of inventions and discoveries. In F. Muller (Ed.), *Crane*. New York: Russak and Co.
3. Berry, F. A., Jr. (1945). *Handbook of meteorology* (p. 343). New York: McGraw-Hill Book Company.
4. Sashida, T., et al. (1985, April 15–18). An interchangeable humidity sensor for an industrial hygrometer. In: *Moisture and humidity. Proc. of the Intern. Symp. on Moisture and Humidity*, Washington, DC.
5. Kang, U., et al. (2000). A high-speed capacitive humidity sensor with on-chip thermal reset. *IEEE Transactions on Electron Devices*, 47(4), 702–710.
6. Carr-Brion, K. (1986). *Moisture sensors in process control*. New York: Elsevier Applied Science Publishers.
7. Norton, H. N. (1989). *Handbook of transducers*. Englewood Cliffs, NJ: Prentice Hall.
8. Hilhorst, M. A. (2000). A pore water conductivity sensor. *Soil Science Society of America Journal*, 64, 1922–1925.
9. Harding Jr., J. C. (1985, April 15–18). A chilled mirror dewpoint sensor/psychrometric transmitter for energy monitoring and control systems. In: *Moisture and humidity. Proc. of the Intern. Symp. on Moisture and Humidity*, Washington, DC.
10. Actkcoz, S., et al. (2008). Use of polyethylene glycol coatings for optical fibre humidity sensing. *Optical Review*, 15(2), 84–90.
11. Somani, P. R., et al. (2001). Charge transfer complex-forming dyes incorporated in solid polymer electrolyte for optical humidity sensing. *Sensors and Actuators B*, 80, 141–148.
12. Porlier, C. (1991). Chilled piezoelectric hygrometer: Sensor interface design. In: *Sensors Expo proceedings*, 107B-7. Dublin, NH: Helmers Publishing.
13. Moghaddam, M., et al. (2010). A wireless soil moisture smart sensor web using physics-based optimal control: Concept and initial demonstrations. *IEEE Journal of Selected Topics and Applied Earth Observations and Remote Sensing*, 3(4), 522–535.
14. Hendrickx, J. M. H., et al. (2002). Indirect measurement of solute concentration: Nonintrusive electromagnetic induction. In J. H. Dane & G. C. Topp (Eds.), *Methods of soil analysis. Part 4* (SSSA Book Ser. 5, pp. 1297–1306). Madison, WI: SSSA.



*“There is nothing more practical than a good theory”*

- Gustav Robert Kirchhoff

---

## 15.1 Introduction

Light is electromagnetic radiation (EMR) which consists of synchronized oscillations of electric and magnetic fields that propagate at the speed of light. The oscillations of the two fields are perpendicular to each other and perpendicular to the direction of energy and wave propagation, as shown in Fig. 5.1a. In the quantum theory of electromagnetism, EMR consists of photons—the elementary particles responsible for all electromagnetic interactions. A photon, while being a localized bundle of energy – a particle, is characterized by its wavelength and frequency. The entire wavelength (frequency) spectrum of the EMR is shown in Fig. 4.41. It spreads from very short wavelengths of  $\gamma$ -rays to the very long waves of the AM radio and even longer. Physicists often say “light” when they refer to ultraviolet (UV), visible, and infrared (IR) spectral ranges. The UV wavelengths range is approximately from 10 to 380 nm, visible range is approximately from 380 nm (violet) to 750 nm (red), while infrared is from 750 nm to about 1 mm. EMR in the spectral range from about 3 to 20  $\mu\text{m}$  is called *thermal radiation* since it covers natural radiation from objects being at temperatures that are not too hot to glow in the visible spectral range.

Detectors of EMR in the spectral range from UV to far-IR are called light detectors. A photodetector or light sensor absorbs quanta of light and produces, directly or indirectly, an electrical response. From the standpoint of a sensor designer, absorption of photons by a sensing element may result either in a quantum or thermal response. Therefore, all photodetectors are divided into two major groups that are called *quantum* and *thermal*.

The quantum detectors operate from the ultraviolet to mid-infrared spectral ranges, while thermal detectors are mostly useful in the mid- and far-infrared spectral ranges where their efficiency at room temperatures exceeds that of the quantum detectors. In this chapter, we cover both types. For description of highly sensitive photon sensors called *photomultipliers*, refer to Sect. 16.1.

### 15.1.1 Principle of Quantum Detectors

Solid-state quantum detectors (photovoltaic and photoconductive devices) rely on the interaction of individual photons with a crystalline lattice of semiconductor materials. When we say *photovoltaic* we mean the sensor that generates the output electric voltage in response to light. A *photoconductive* means a resistor whose electrical resistance is affected by the incident light. Their operations are based on the photoeffect that was discovered by A. Einstein, and brought him the Nobel Prize. In 1905, he made a remarkable assumption about the nature of light, that at least under certain circumstances the light energy was concentrated into localized bundles, later named photons. The energy of a single photon is given by

$$E = h\nu, \quad (15.1)$$

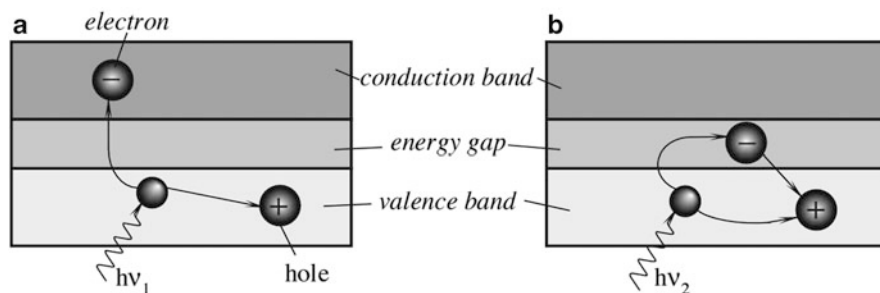
where  $\nu$  is the frequency of light and  $h = 6.626075 \times 10^{-34}$  J s (or  $4.13567 \times 10^{-15}$  eV s) is Planck's constant derived on the basis of the wave theory of light. When a photon strikes a surface of a conductor, it may result in the generation of a free electron. Part ( $\phi$ ) of the photon energy  $E$  is used to detach the electron from the surface, while the other part gives to the electron its kinetic energy. Thus, the photoelectric effect can be described as

$$h\nu = \phi + K_m, \quad (15.2)$$

where  $\phi$  is called the *work function* of the emitting surface and  $K_m$  is the maximum kinetic energy of the electron upon it exiting the surface. The similar processes occur when a semiconductor *pn*-junction is subjected to radiant energy: the photon transfers its energy to an electron and, if the energy is sufficiently high, the electron may become mobile which results in an electric current. If energy is not sufficient for liberating an electron, the photon energy is just converted to heat.

The periodic lattice of crystalline materials establishes the allowed energy bands for electrons that exist within that solid. The energy of any electron within the pure material must be confined to one of these energy bands that may be separated by gaps or ranges of forbidden energies. That is, the electron can have only "permitted" energies. Under certain conditions, electrons can jump over the forbidden barrier into the neighboring permitted energy band.

If light of a proper wavelength, that is having a sufficiently high energy of photons—see Eq. (15.1), strikes a semiconductor crystal, the concentration of



**Fig. 15.1** Photoeffect in a semiconductor for high (a) and low (b) energy photons

charge carriers (electrons and holes) in the crystal increases, which manifests in the increased conductivity of a crystal

$$\sigma = e(\mu_e n + \mu_h p), \quad (15.3)$$

where  $e$  is the electron charge,  $\mu_e$  is the electron mobility,  $\mu_h$  is the hole mobility, and  $n$  and  $p$  are the respective concentrations of electrons and holes<sup>1</sup> respectively.

Figure 15.1a shows energy bands of a semiconductor material, where  $E_g$  is the magnitude in eV of the forbidden band gap. The lower band is called the *valence band*, which corresponds to those electrons that are bound to specific lattice sites within the crystal. In the case of silicon or germanium, they are parts of the covalent bonding that constitute the interatomic forces within the crystal. The next higher-lying band is called the *conduction band* and represents electrons that are free to migrate through the crystal. Electrons in this band contribute to the electrical conductivity of the material. The two bands are separated by the band gap, the size of which determines the whether the material is classified as a semiconductor or an insulator. The number of electrons within the crystal is just adequate to completely fill all available sites within the valence band. In the absence of thermal excitation, both insulators and semiconductors would therefore have a configuration in which the valence band is completely full, and the conduction band completely empty. Under these imaginable circumstances, neither would theoretically show any electrical conductivity.

In a metal, the highest occupied energy band is not completely full. Therefore, electrons can easily migrate throughout the material. Metals are characterized by very high electrical conductivity. In insulators or semiconductors, on the other hand, the electron must first cross the energy band gap in order to reach the conduction band and the conductivity is therefore many orders of magnitude lower. For insulators, the forbidden energy band gap is usually 5 eV or more, whereas for semiconductors, the gap is considerably less (Table 15.1). Note that the longest the

<sup>1</sup> An electron hole is the lack of an electron at a position where one could exist in an atom or atomic lattice.

**Table 15.1** Band gaps and longest detectable wavelengths for various semiconductors (from various sources)

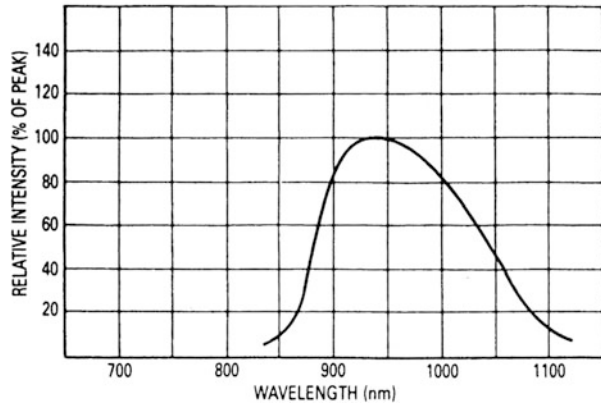
Material	Band gap (eV)	Longest detectable wavelength ( $\mu\text{m}$ )
SiC	2.0–7.0	0.18–0.62
C (diamond)	5.5	0.22
BN	5.0	0.25
NiO	4.0	0.31
ZnS	3.6	0.34
GaN	3.4	0.36
ZnO	3.3	0.37
CdS	2.41	0.52
CdSe	1.8	0.69
CdTe	1.5	0.83
GaAs	1.43	0.86
Si	1.12	1.10
Ge	0.67	1.85
PbS	0.37	3.35
InAs	0.35	3.54
Te	0.33	3.75
PbTe	0.3	4.13
PbSe	0.27	4.58
InSb	0.18	6.90

wavelength (lower frequency of a photon) the less energy is required to originate a photoeffect.

When the photon of frequency  $\nu_1$  strikes the crystal, its energy is high enough to separate the electron from its site in the valence band and push it through the forbidden energy gap into a conduction band at a higher energy level. In that band, the electron is free to serve as a current carrier. The deficiency of an electron in the valence band creates a hole that also serves as a current carrier that can move within the valence band. This is manifested in reduction of the specific resistivity of the material. On the other hand, Fig. 15.1b shows that a photon of lower frequency  $\nu_2$  does not have sufficient energy to push the electron through the forbidden energy gap. The photon energy is released as heat without creating current carriers.

The forbidden energy gap serves as a threshold below which the material is not light sensitive. However, the threshold is not abrupt. Throughout the photon-excitation process, the law of conservation of momentum applies. The momentum and density of hole-electron sites are higher at the center of both the valence and conduction bands, and fall to zero at the upper and lower ends of the bands. Therefore, the probability of an excited valence-band electron finding a site of like momentum in the conduction band is greater at the center of the bands, and the lowest at the ends of the bands. Therefore, the response of a material to photon energy increases from  $E_g$  gradually to its maximum and then falls back to zero at the energy corresponding to the difference between the bottom of the valence band and the top of the conduction band.

**Fig. 15.2** Spectral response of near-infrared photodiode



A typical spectral response of a semiconductive material is shown in Fig. 15.2. The light response of a bulk material can be altered by adding various impurities. They can be used to reshape and shift a spectral response of the material. All devices that directly convert photons of EMR into charge carriers are the *quantum detectors* that are generally produced in forms of *photodiodes*, *phototransistors*, and *photoresistors*.

When comparing the characteristics of different photodetectors, the following specifications usually should be considered:

*NEP* (noise equivalent power) is the amount of light equivalent to the intrinsic noise level of the detector. Stated differently, it is the light level required to obtain a signal-to-noise ratio equal to unity. Since the noise level is proportional to the square root of the bandwidth, the *NEP* is expressed in units of  $W/Hz^{-2}$ .

$$NEP = \frac{\text{noise current } (A/\sqrt{Hz})}{\text{radiant sensitivity at } \lambda_p (A/W)} \quad (15.4)$$

$D^*$  (*D-star*) refers to the *detectivity* of a detector's sensitive area of  $1 \text{ cm}^2$  and a noise bandwidth of 1 Hz

$$D^* = \frac{\sqrt{\text{area}(\text{cm}^2)}}{NEP} \quad (15.5)$$

Detectivity is another way to measure the sensor's signal-to-noise ratio. Detectivity is not uniform over the spectral range for the operating frequencies, therefore, the spectral content must be also specified. The detectivity is expressed in units of  $Hz^{-2}/W$ . It can be said, that the higher the value of  $D^*$ , the better the detector.

*IR cutoff wavelength* ( $\lambda_c$ ) represents the long wavelength limit of spectral response and often is listed as the wavelength at which the detectivity drops by 10 % of the peak value.

*Maximum current* is specified for photoconductive detectors (such as HgCdTe) which operate at constant currents. The operating current never should exceed the maximum limit.

*Maximum reverse voltage* is specified for Ge and Si photodiodes and photoconductive cells. Exceeding this voltage can cause the breakdown and severe deterioration of the sensor's performance.

*Radiant responsivity* is the ratio of the output photocurrent (or output voltage) divided by the incident radiant power at a given wavelength, expressed in A/W or V/W.

*Dark current*  $I_D$  for photodiodes is a leakage current at a reverse voltage when the diode is in complete darkness. This current generally is temperature-dependent and may vary from pA to  $\mu$ A. It approximately doubles for every 10 °C in temperature increase.

*Field of view* (FOV) is the angular measure of the volume of space where the sensor can respond to the source of radiation.

*Junction capacitance* ( $C_j$ ) is similar to the capacitance of a parallel plate capacitor. It should be considered whenever a high-speed response is required. The value of  $C_j$  drops with reverse bias and is higher for the larger diode areas.

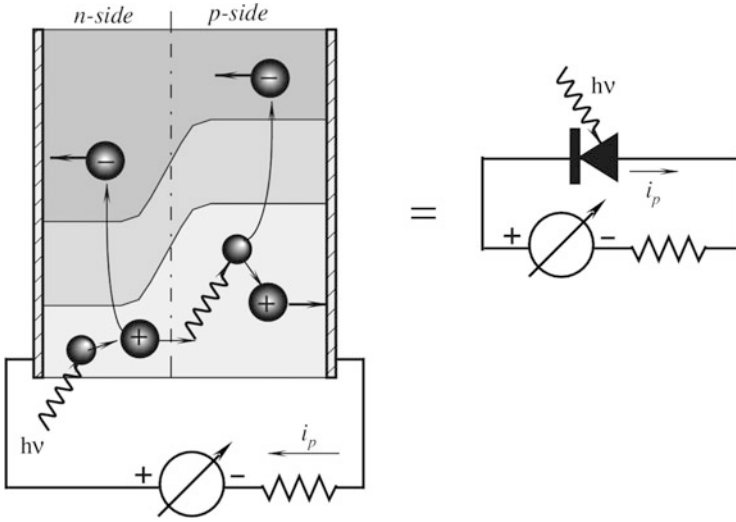
---

## 15.2 Photodiode

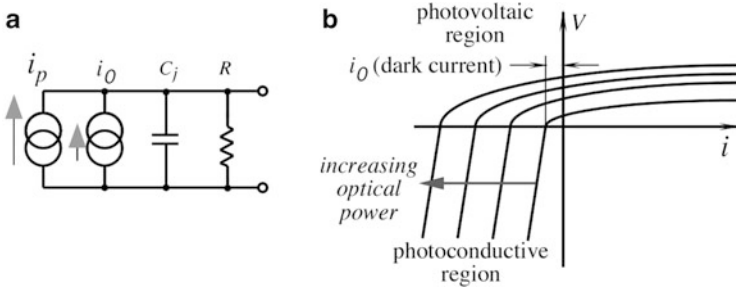
Photodiodes are semiconductive optical sensors, which if broadly defined, may even include solar batteries. However, here we consider only the information aspect of these devices rather than the power conversion. In a simple way, the operation of a photodiode can be described as follows.

If a *pn*-junction is *forward* biased (positive side of a battery is connected to the *p* side) and is exposed to light of proper frequency, the current increase will be very small with respect to a dark current. In other words, the bias current caused by the battery is much greater than the current generated by light and the diode is just a diode, not really useful for sensing light.

If the junction is *reverse biased* (Fig. 15.3), when light strikes the semiconductor the current will increase quite noticeably. The impinging photons create electron-hole pairs on both sides of the junction. When electrons enter the conduction band they start flowing toward the positive side of the battery. Correspondingly, the created holes flow to the negative terminal, meaning that photocurrent  $i_p$  flows in the network. Under dark conditions, dark current  $i_0$  is independent of the applied voltage and mainly is the result of thermal generation of charge carriers. It is a spurious current that should be as small as possible. Thus, a reverse-biased photodiode electrical equivalent circuit, Fig. 15.4a, contains two current sources and a *RC* network.



**Fig. 15.3** Structure of photodiode as energy bands. Plus terminal of battery is connected to cathode (n-side) of diode junction



**Fig. 15.4** Equivalent circuit of photodiode (a) and its volt-ampere characteristic (b)

The process of optical detection involves the direct conversion of optical energy (in form of photons) into an electrical signal (in form of electrons). If a probability that a photon of energy  $h\nu$  will produce an electron in a detection is  $\eta$ , then the average rate of production of electrons  $\langle r \rangle$  for an incident beam of optical power  $P$  is given by [1]:

$$\langle r \rangle = \frac{\eta P}{h\nu} \tag{15.6}$$

The production of electrons due to the incident photons at constant rate  $\langle r \rangle$  is randomly distributed in time and obeys Poisson statistics, so that the probability of the production of  $m$  electrons in some measurement time interval  $\tau$  is given by

$$p(m, \tau) = \langle r \rangle \tau \frac{1}{m!} e^{-\langle r \rangle \tau} \quad (15.7)$$

The statistics involved with optical detection are very important in the determination of minimum detectable signal levels and hence the ultimate sensitivity of the sensors. At this point, however, we just note that the *electrical current is proportional to the optical power* incident on the detector:

$$i = \langle r \rangle e = \frac{\eta e P}{h\nu}, \quad (15.8)$$

where  $e$  is the charge of an electron. A change in input power  $\Delta P$  (due to intensity modulation in a sensor, for instance) results in the output current  $\Delta i$ . Since power is proportional to squared current, the detector's electrical power output varies quadratically with input optical power, making it a "square-law" optical power detector.

The voltage-to-current response of a typical photodiode is shown in Fig. 15.4b. If we attach a high-input impedance voltmeter to the diode (corresponds to the case when  $i = 0$ , that is along the  $y$ -axis), we will observe that with increasing optical power, the voltage changes in a quite nonlinear fashion. In fact, variations are logarithmic. However, for the short circuit conditions ( $V = 0$ , that is along the  $x$ -axis), that is when the diode is connected to a current-to-voltage converter, such as in Fig. 15.6a, current varies linearly with the optical power. The current-to-voltage response of the photodiode is given by [2]:

$$i = i_0 \left( e^{eV/k_b T} - 1 \right) - i_s, \quad (15.9)$$

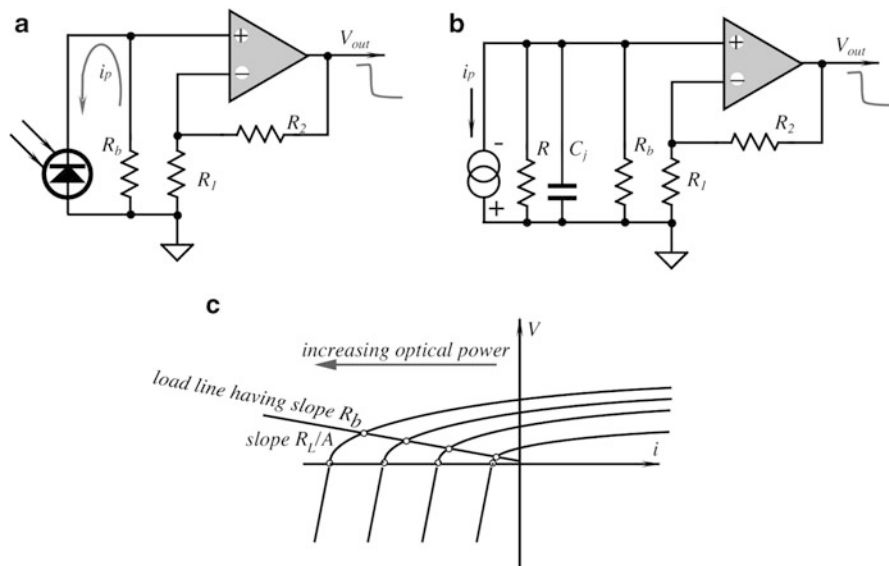
where  $i_0$  is a reverse "dark current" which is attributed to the thermal generation of electron-hole pairs,  $i_s$  is the current due to the detected optical signal,  $k_b$  is Boltzmann constant, and  $T$  is the absolute temperature. Combining Eqs. (15.8) and (15.9) yields:

$$i = i_0 \left( e^{eV/k_b T} - 1 \right) - \frac{\eta e P}{h\nu}, \quad (15.10)$$

which is the overall characteristic of a photodiode. Efficiency of the direct conversion of optical power into electric power is quite low. Typically, it is in the range of 5–10 %; however, it was reported that some experimental photocells were able to reach efficiency as high as 90 %. In the sensor technologies, however, photocells are generally not used.

There are two general operating modes for a photodiode: the *photoconductive* (PC) and the *photovoltaic* (PV). No bias voltage is applied for the PV mode. The result is that there is no dark current, so there is only thermal noise present. This allows much better sensitivities at low light levels. However, the speed response is worst due to an increase in  $C_j$  and responsivity to longer wavelengths is also reduced.



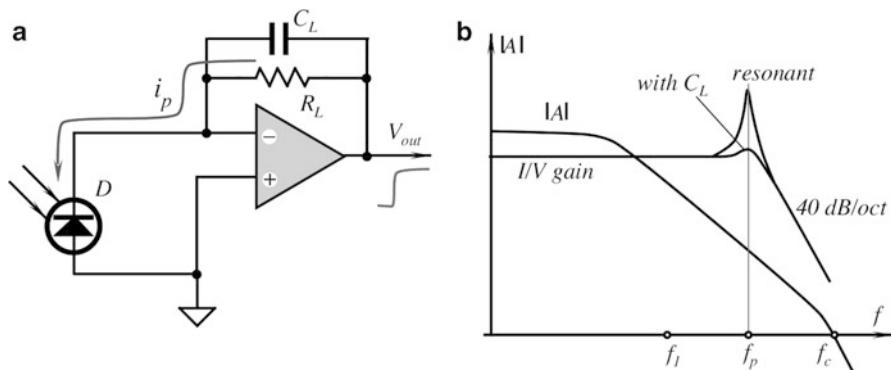


**Fig. 15.5** Connection of photodiode in a photovoltaic (PV) mode to noninverting amplifier (a); equivalent circuit (b); and loading characteristic (c)

Figure 15.5a shows a photodiode connected in a PV mode. In this connection, the diode operates as a current generating device which is represented in the equivalent circuit by a current source  $i_p$  in Fig. 15.5b. The load resistor  $R_b$  determines the voltage developed at the input of the amplifier and the slope of the load characteristic is proportional to that resistor as shown in Fig. 15.5c.

When using a photodiode in a photovoltaic mode, its large capacitance  $C_j$  may limit the speed response of the circuit. During operation with a direct resistive load, as in Fig. 15.5a, a photodiode exhibits a bandwidth limited mainly by its internal capacitance  $C_j$ . The equivalent circuit of Fig. 15.5b models such a bandwidth limit. The photodiode acts primarily as a current source. A large resistance  $R$  and the diode capacitance shunt the source. The capacitance ranges from 2 to 20,000 pF depending for the most part on the diode area. In parallel with the shunt, there is the amplifier's input capacitance (not shown) that results in a combined input capacitance  $C$ . The net input network determines the input circuit response rolloff of the virtual low-pass filter.

To avoid effect of the input capacitance, it is desirable to develop input voltage across the resistor and prevent it from charging the capacitance. This can be achieved by employing a current-to-voltage amplifier ( $I/V$ ) as shown in Fig. 15.6a. The amplifier and its feedback resistor  $R_L$  translate the diode current into a buffered output voltage with the excellent linearity. Added to the figure is a feedback capacitor  $C_L$  that provides a phase compensation. An ideal amplifier holds its two inputs at the same voltage (ground in the figure), thus the inverting input



**Fig. 15.6** Use of current-to-voltage converter (a) and frequency characteristics (b)

which is not directly connected to ground is called a *virtual ground*. The photodiode operates at zero voltage across its terminals which improves the response linearity and prevents charging the diode capacitance.

In practice, the amplifier's high but finite open-loop gain  $A$  limits the circuit performance by developing small, albeit nonzero voltage across the diode. Then, the break frequency is defined as

$$f_p = \frac{A}{2\pi R_L C} \approx A f_1 \quad (15.11)$$

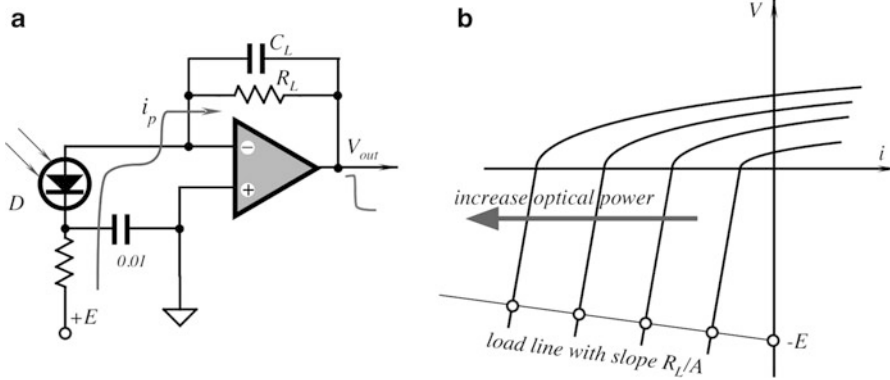
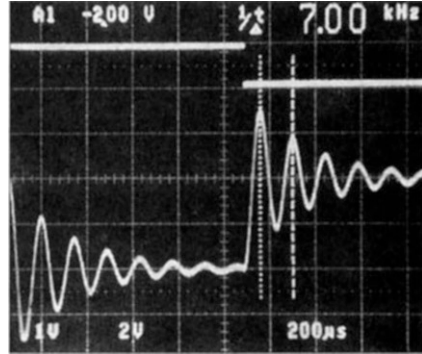
where  $A$  is the open-loop gain of the amplifier. Therefore, the break frequency is increased by a factor  $A$  as compared with  $f_1$ . It should be noted that when frequency increases, gain  $A$  declines, and the virtual load attached to the photodiode appears to be inductive. This results from the phase shift of gain  $A$ . Over most of the amplifier's useful frequency range,  $A$  has a phase lag of  $90^\circ$ . The  $180^\circ$  phase inversion by the amplifier converts this to a  $90^\circ$  phase lead which is specific for the inductive impedance. This inductive load resonates with the capacitance of the input circuit at a frequency equal to  $f_p$  (Fig. 15.6b) and may cause an oscillating response (Fig. 15.7) or the circuit instability. To restore stability, a compensating capacitor  $C_L$  is placed across the feedback resistor. Value of the capacitor can be found from:

$$C_L = \frac{1}{2\pi R_L f_p} = \sqrt{C C_c} \quad (15.12)$$

where  $C_c = 1/(2\pi R_L f_c)$ , and  $f_c$  is the unity-gain crossover frequency of the operational amplifier. The capacitor boosts the signal at the inverting input by shunting  $R_L$  at higher frequencies.

When using photodiodes for detection of low-level light, noise floor should be seriously considered. There are two main components of noise in a photodiode: shot

**Fig. 15.7** Response of photodiode with uncompensated circuit (Courtesy of Hamamatsu Photonics K.K.)



**Fig. 15.8** Photoconductive (PC) operating mode of photodiode. Circuit diagram (a); load characteristic (b)

noise and Johnson noise (see Sect. 6.7.1). Besides the sensor, noise from the interface amplifier and auxiliary components also should be accounted for.

For the photoconductive operating mode (PC), a reverse bias voltage is applied to the photodiode. The result is a wider depletion region, lower junction capacitance  $C_j$ , lower series resistance, shorter rise time, and linear response in photocurrent over a wider range of light intensities. However, as the reverse bias is increased, shot noise increases as well due to increase in a dark current. The PC mode circuit diagram is shown in Fig. 15.8a and the diode’s load characteristic in Fig. 15.8b. The reverse bias moves the load line into the third quadrant where the response linearity is better than that for the PV mode (the second quadrant). The load lines crosses the voltage axis at the point corresponding to the bias voltage  $E$ , while the slope is inversely proportional to the amplifier’s open-loop gain  $A$ . In this mode, the photodiode functions as a photosensitive resistor. The PC mode offers bandwidths to hundreds of MHz, providing an accompanying increase in the signal-to-noise ratio.

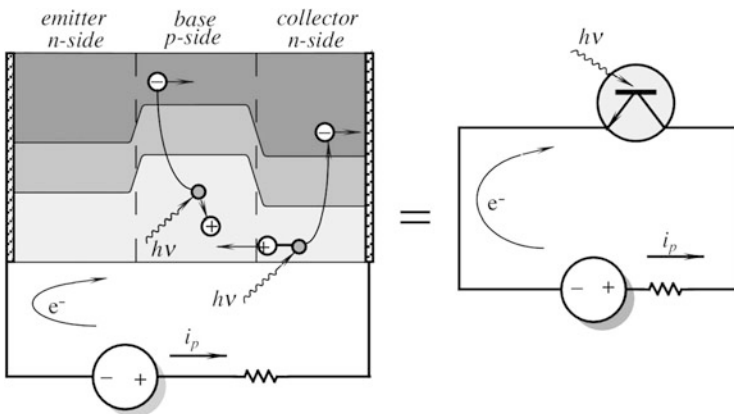
Presently, photodiodes together with interface electronic circuits are available in integral forms and known as *light-to-voltage converters*. Such an integrated circuit is comprised of a photodiode and current-to-voltage converter as shown in Fig. 15.6. An example is the device TSL257T from TAOS ([www.taosinc.com](http://www.taosinc.com)), which operates primarily in the visible spectral range from 400 to 800 nm.

### 15.3 Phototransistor

A photodiode directly converts photons into charge carriers, specifically one electron and one hole (hole-electron pair) per a photon. A phototransistor can do the same, and in addition it provides current gain, resulting in a much higher sensitivity. The collector–base junction is a reverse-biased diode that functions as described above. If the transistor is connected into a circuit containing a battery, a photoinduced current flows through the loop which includes the base-emitter region. This current is amplified by the phototransistor in the same manner as a conventional transistor amplifies the base current, resulting in a significant increase in the collector current.

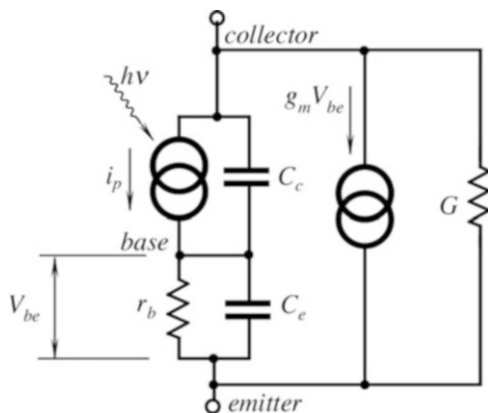
The energy bands for the phototransistor are shown in Fig. 15.9. The photoninduced base current is returned to the collector through the emitter and the external circuitry. In so doing, electrons are supplied to the base region by the emitter where they are pulled into the collector by the electric field. The sensitivity of a phototransistor is function of the collector–base diode quantum efficiency and also of the d.c. current gain of the transistor. Therefore, the overall sensitivity is a function of the collector current.

When subjected to varying ambient temperature, collector current changes linearly with a positive slope of about 0.00667 per °C. The magnitude of this temperature coefficient is primarily a result of the increase in current gain versus



**Fig. 15.9** Energy bands in phototransistor

**Fig. 15.10** Equivalent circuit of a phototransistor



temperature, since the collector–base photocurrent temperature coefficient is only about 0.001 per °C. The family of collector current versus collector voltage characteristics is very much similar to that of a conventional transistor. This implies that the circuits with phototransistors can be designed by using regular methods of transistor circuit techniques, except that its base should be used as an input of a photoinduced current. Since the actual photogeneration of the carriers occurs in the collector–base region, the larger the area of this region, the more carriers are generated, thus, the phototransistor is so designed to offer a large area to impinging light.

A phototransistor can be either a two-lead or a three-lead device. In the latter case, the base lead is available and the transistor may be used as a standard bipolar transistor with or without the additional capability of sensing light, thus giving a designer greater flexibility in circuit development. However, a two-lead device is the most popular as a dedicated photosensor.

When the base of the transistor is floating, it can be represented by an equivalent circuit shown in Fig. 15.10. Two capacitors  $C_c$  and  $C_e$  represent base–collector and base–emitter capacitances that are the speed limiting factors. Maximum frequency response of the phototransistor may be estimated from

$$f_1 \approx \frac{g_m}{2C_e}, \quad (15.13)$$

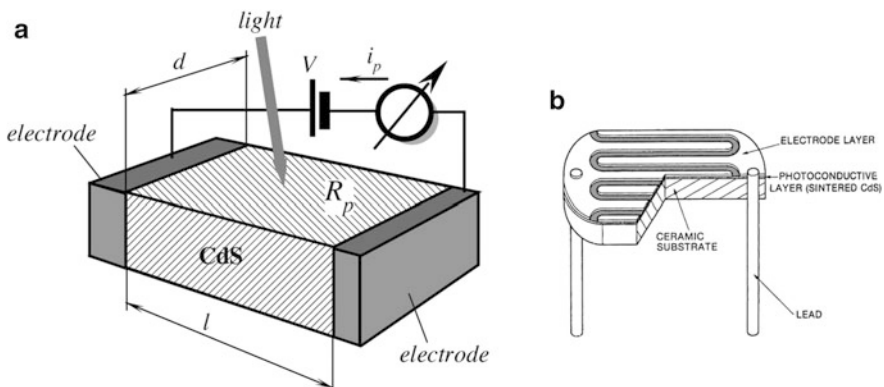
where  $f_1$  is the current-gain-bandwidth product and  $g_m$  is the transistor's forward transconductance.

Whenever a higher sensitivity of a photodetector is required, especially if high-response speed is not of concern, an integrated Darlington detector is recommended. It is comprised of a phototransistor whose emitter is coupled to the base of a regular bipolar transistor. Since a Darlington connection gives a current gain equal to the product of current gains of two transistors, the circuit proves to be an efficient way to make a sensitive light detector.

## 15.4 Photoresistor

A *photoresistor*, just as a photodiode, is a photoelectric device. It is a resistor whose resistance is called a *photoresistance*  $R_p$  that depends on incident light. The most common materials for its fabrication are cadmium sulfide (CdS) and cadmium selenide (CdSe) that are semiconductors whose resistances change upon light entering the surface. For its operation, a photoresistor requires a power source (excitation signal) because unlike a photodiode or phototransistor, it does not generate photocurrent—a photoeffect is manifested in change in the material's electrical resistance. Figure 15.11a shows a schematic diagram of a photoresistive cell. An electrode is set at each end of the photoconductor. In darkness, the resistance of the material is high. Hence, applied voltage  $V$  results in small dark current which is attributed to temperature effects. When light is incident on the surface, photocurrent  $i_p$  flows between its electrodes and through the battery.

The reason for the current increase is the following. Directly beneath the conduction band of the crystal is a donor level and there is an acceptor level above the valence band. In darkness, the electrons and holes in each level are almost crammed in place in the crystal, resulting in a high resistance of the semiconductor. When light illuminates the photoconductive crystal, photons are absorbed which result in the added-up energy in the valence-band electrons. This moves them into the conduction band, creating free holes in the valence band, increasing the conductivity of the material. Since near the valence band is a separate acceptor level that can capture free electrons not as easily as free holes, the recombination probability of the electrons and holes is reduced and the number of free electrons in the conduction band is high. Since CdS has a band gap of 2.41 eV, the absorption edge wavelength is  $\lambda = c/\nu \approx 515$  nm, which is in the visible spectral range. Hence, the CdS detects light shorter than 515 nm wavelengths (violet, blue, and green). Other photoconductors have different absorption edge



**Fig. 15.11** Structure of photoresistor (a) and plastic-coated photoresistor having serpentine shape (b)

wavelengths. For instance, while CdS is most sensitive at shorter wavelengths range, Si and Ge are most efficient in the near infrared.

The conductance of a semiconductor is given by:

$$\Delta\sigma = ef(\mu_n\tau_n + \mu_p\tau_p). \quad (15.14)$$

where  $\mu_n$  and  $\mu_p$  are the free electron and hole movements (cm/V s),  $\tau_n$  and  $\tau_p$  are the free electron and hole lives (sec),  $e$  is the charge of an electron, and  $f$  is the number of generated carriers per second per unit of volume. For a CdS sell  $\mu_n\tau_n \gg \mu_p\tau_p$ , hence, conductance by free holes can be ignored. Then the sensor becomes an  $n$ -type semiconductor. Thus:

$$\Delta\sigma = ef\mu_n\tau_n, \quad (15.15)$$

We can define sensitivity  $b$  of a photoresistor through a number of electrons generated by one photon (until the carrier lifespan ends):

$$b = \frac{\tau_n}{t_t}, \quad (15.16)$$

where  $t_t = l^2/V\mu_n$  is the transit time for the electron between the sensor's electrodes,  $l$  is distance between the electrodes, and  $V$  is applied voltage. Then, we arrive at:

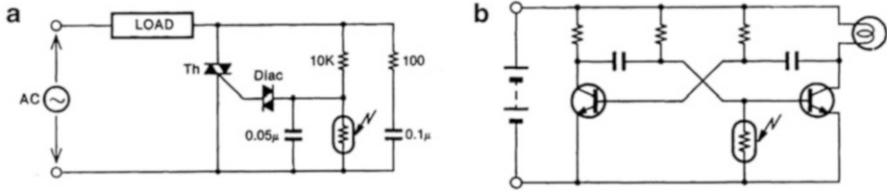
$$b = \frac{\mu_n\tau_n V}{l^2}. \quad (15.17)$$

For example, if  $\mu_n = 300 \text{ cm}^2/\text{V s}$ ,  $\tau_n = 10^{-3} \text{ s}$ ,  $l = 0.2 \text{ mm}$ , and  $V = 1.2 \text{ V}$ , then the sensitivity is 900, which means that a single photon releases for conduction 900 electrons, making a photoresistor to work as a photomultiplier. Indeed, a photoresistor is a very sensitive device!

It can be shown that for better sensitivity and lower cell resistance, a distance  $l$  between the electrodes should be reduced, while width of the sensor  $d$  should be increased. This suggests that the sensor should be very short and very wide. For practical purposes, this is accomplished by fabricating a sensor in a serpentine shape as shown in Fig. 15.11b).

Depending on the manufacturing process, the photoresistive cells can be divided into the sintered type, single-crystal type, and evaporated type. Of these, the sintered type offers high sensitivity and easier fabrication of large sensitive areas, which eventually translated into lower cost devices. The fabrication of CdS cells consists of the following steps.

1. Highly pure CdS powder is mixed with appropriate impurities and a fusing agent.
2. The mixture is dissolved in water.
3. The solution in form of paste is applied on the surface of a ceramic substrate and allowed to dry.



**Fig. 15.12** Examples of photoresistor applications: light switch (a) and beacon light (b) (Courtesy of Hamamatsu Photonics K.K.)

4. The ceramic subassemblies are sintered in a high-temperature oven to form a multicrystal structure. At this stage a photoconductive layer is formed.
5. Electrode layers and leads (terminals) are attached.
6. The sensor is packaged into a plastic or metal housing with or without a window.

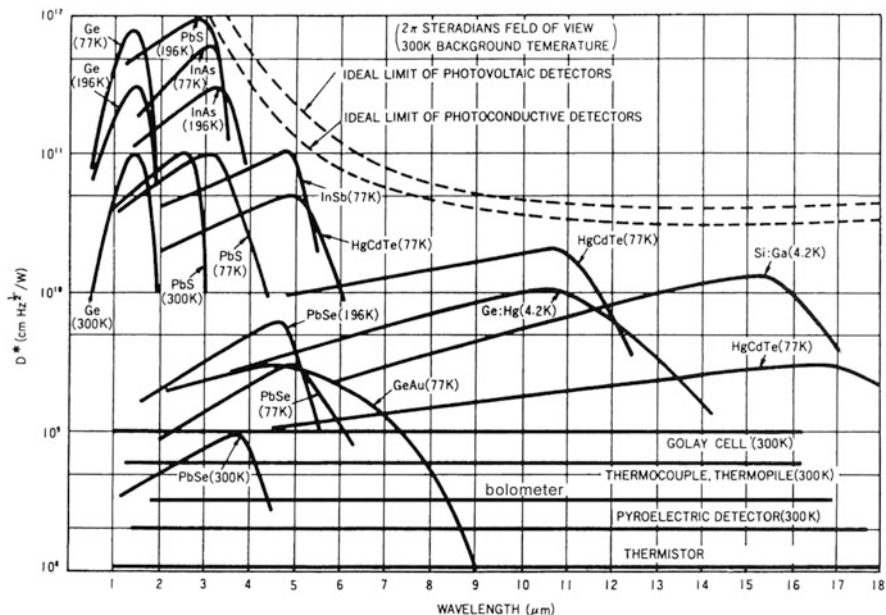
To tailor a spectral response of a photoresistor, the powder of step 1 can contain some variations, for instance, the addition of selenide or even the replacement of CdS for CdSe shifts the spectral response toward longer wavelengths (orange and red).

To illustrate, how photoresistors can be used, Fig. 15.12 shows two circuits. Circuit (a) shows an automatic light switch that turns lights on when illumination drops and voltage at the diac increases allowing a firing of a triac, Th. Circuit (b) shows a flashing beacon with a free running multivibrator, which is enabled at darkness, when resistance of a photoresistor becomes high and stops shunting the base of the right transistor. In these circuits, photoresistors work as a resistors whose resistances are modulated by light intensity. Note that in both circuits, the load lights should be shielded from the photoresistor, otherwise lights will provide a positive feedback to the photoresistor and the circuit start spuriously oscillate.

## 15.5 Cooled Detectors

For measurements of objects emanating photons on the range of 2 eV or higher, quantum detectors being at room temperatures are generally used. For the smaller energies (longer wavelengths) the narrower band gap semiconductors are required. However, even if a quantum detector has a sufficiently narrow energy band gap, at room temperatures its own intrinsic noise is much higher than a photoconductive signal. In other words, the detector will sense its own thermal radiation and the useful signal will be buried in noise. The noise level is temperature-dependent; therefore, when detecting the long-wavelength photons, a signal-to-noise ratio may become so small that an accurate measurement becomes impossible. This is the reason, why for operation in the mid and far infrared spectral ranges a photodetector not only should have a sufficiently narrow energy gap, but its temperature has to be





**Fig. 15.13** Operating ranges for some infrared detectors

lowered to the level where intrinsic noise is reduced to an acceptable level. Figure 15.13 shows typical spectral responses of many detectors with recommended operating temperatures.

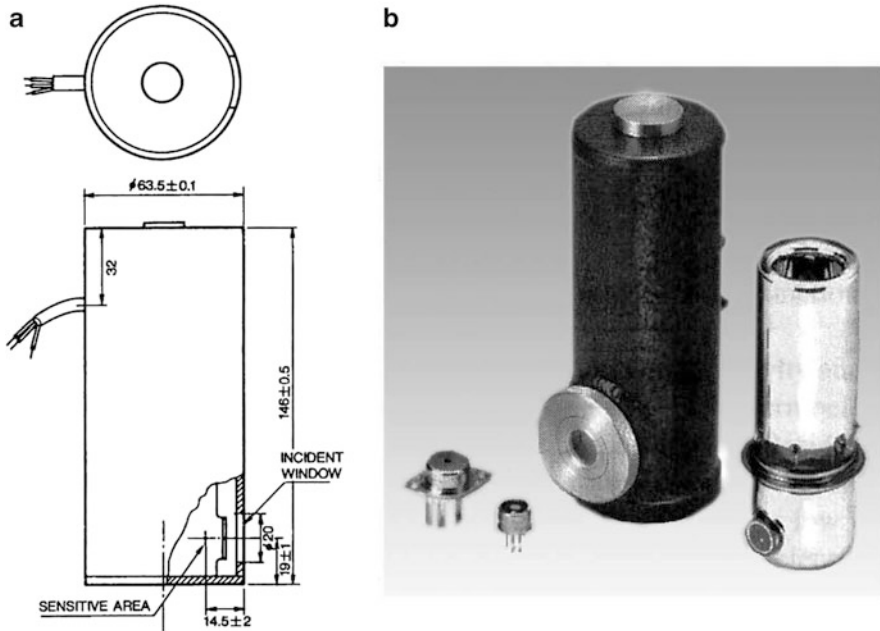
The operating principle of a cryogenically cooled detector is about the same as that of a photoresistor described in Sect. 15.4, except that it detects far-longer wavelengths at much lower temperatures. Thus, the sensor design becomes quite different. Depending on the required sensitivity and operating wavelength, the following crystals are typically used for this type of photoresistors: lead sulfide (PbS), indium arsenide (InAs), germanium (G), lead selenide (PbSe), and mercury-cadmium-telluride (HgCdTe).

Cooling shifts the spectral responses to longer wavelengths and increases sensitivity. However, the response speeds of PbS and PbSe become slower with cooling. Methods of cooling include Dewar cooling using dry ice, liquid nitrogen, liquid helium (Fig. 15.14), or thermoelectric coolers operating on the Peltier effect (see Sect. 4.9.2).

As an example, Table 15.2 lists typical specifications for an MCT photoconductive detector. MCT stands for the mercury-cadmium-telluride sensing element.

Applications of the cryogenically cooled quantum detectors include measurements of optical power over a broad spectral range, thermal temperature measurement and thermal imaging, detection of water content, and gas analysis.

Figure 15.15 depicts the gas absorption spectra for various molecules. Water strongly absorbs at 1.1, 1.4, 1.9, and 2.7  $\mu\text{m}$ . The gas analyzer makes use of



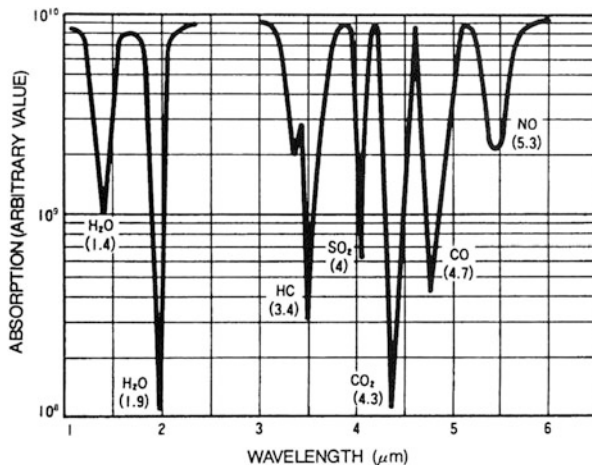
**Fig. 15.14** Cryogenically cooled MCT quantum infrared detectors. Dimensional drawing (in mm) of Dewar type (a); outside appearances of canned and Dewar detectors (b) (Courtesy of Hamamatsu Photonics K.K.)

**Table 15.2** Typical specifications for MCT far-infrared detectors

Sensitive area (mm)	Temperature (°C)	$I_p$ ( $\mu\text{m}$ )	$I_c$ ( $\mu\text{m}$ )	FOV (°)	Dark resist, $\text{k}\Omega$	Rise time, $\mu\text{s}$	Max current, mA	$D^*$ at $I_p$
1 × 1	-30	3.6	3.7	60	1	10	3	$10^9$
1 × 1	-196	15	16	60	20	1	40	$3 \times 10^9$

absorption in the infrared region of the spectrum. This allows fabrication of the spectrophotometers that measure the gas density. Also, similar sensors can be employed for measuring the automobile exhaust gases (CO, HC, CO<sub>2</sub>), for emission control (CO, SO, NO<sub>2</sub>), detecting fuel leakage (CH<sub>4</sub>, C<sub>3</sub>H<sub>2</sub>), etc. On the other hand, when measuring the IR radiation over appreciable distance, air humidity should be considered as water molecules will heavily absorb the IR light at specific wavelengths. Note that the spectral gas analysis not necessarily should be performed with the cooled quantum detectors. Modern *thermal* IR room temperature detectors have similar efficiencies and are much more convenient for use. These detectors (thermopiles and bolometers) are described below in Sects. 15.8.3 and 15.8.5.

**Fig. 15.15** Absorption spectra of gaseous molecules



## 15.6 Imaging Sensors for Visible Range

The CCD (Charge Coupled Device)<sup>2</sup> and CMOS (Complementary Metal Oxide Semiconductor) imaging sensors are two different technologies presently used for digitally capturing images in the visible spectral range. Each has unique strengths and weaknesses giving advantages in different applications.

Both types of the imagers convert light into electric charge and process it into electronic signals. In a CCD sensor, every pixel's charge is transferred through a very limited number of output nodes (often just one) to be converted to voltage, buffered, and sent off-chip as an analog signal. Then, the analog signal is digitized by an external ADC. All of the pixel can be devoted to light capture, and the output's uniformity (a key factor in image quality) is high. In a CMOS sensor, each pixel has its own charge-to-voltage conversion, and often the sensor also includes amplifiers, noise-correction, and digitization circuits, so that the chip outputs digital bits. These additional functions increase the design complexity and reduce the area available for light capture. With each pixel doing its own conversion, uniformity is lower. But the chip can be built to require less off-chip circuitry for basic operation.

CMOS imagers offer more integration (more functions on the chip), lower power dissipation (at the chip level), and the possibility of smaller system size, but they have often required tradeoffs between image quality and device cost. CMOS cameras may require fewer components and less power, but they still generally require companion chips to optimize image quality, increasing cost and reducing the advantage they gain from lower power consumption. CCD devices are less complex than CMOS, so they cost less to design. CCD fabrication processes also

<sup>2</sup> In 2009 Willard S. Boyle and George E. Smith received a Nobel Prize for their invention of CCD in 1969.

tend to be more mature and optimized; in general, it will cost less (in both design and fabrication) to yield a CCD than a CMOS imager for a specific high-performance application. The choice continues to depend on the application and the vendor more than the technology.

CCDs and CMOS imagers were both invented in the late 1960s and 1970. CCD became dominant, primarily because they gave far-superior images with the fabrication technology available. CMOS image sensors required more uniformity and smaller features than the silicon wafer foundries could not produce at the time. Nowadays, renewed interest in CMOS was based on expectations of lowered power consumption, camera-on-a-chip integration, and lowered fabrication costs. CCDs consume as much as 100 times more power than an equivalent CMOS sensor.

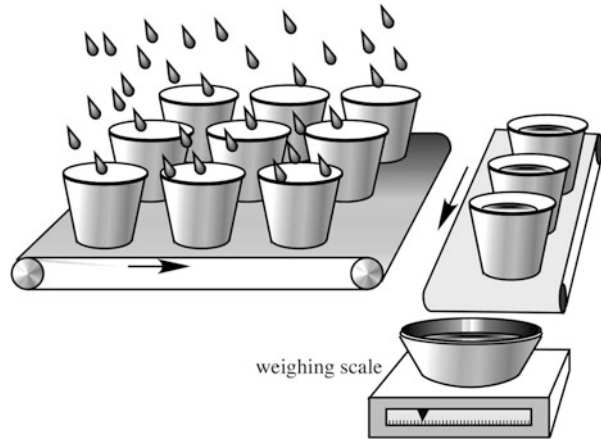
Both CCDs and CMOS imagers can offer excellent imaging performance when designed properly. CCDs have traditionally provided the performance benchmarks in the photographic, scientific, and industrial applications that demand the highest image quality (as measured in quantum efficiency and noise) at the expense of system size. Astronomers say that CCDs have a high quantum efficiency (QE), meaning that a large percentage of incoming photons are actually detected. While photographic plates might capture *one* photon out of every hundred, modern CCDs would capture *eighty* photons out of every hundred. This allows for a substantial decrease in exposure time. CCDs are also linear in nature, meaning that the signal they produce is directly proportional to the amount of light collected. This makes it easier to calculate the number of photons that hit the detector in the time of an exposure.

### 15.6.1 CCD Sensor

A CCD chip is divided into pixels. Each pixel has a potential well that collects the electrons produced by the photoelectric effect. At the end of an exposure (frame), each pixel has collected an amount of electrons (i.e., charge) proportional to the amount of light that fell onto it. The CCD is then read out by cycling the voltages applied to the chip in a process called “clocking.” Due to the structure of a CCD, clocking causes the charge in one pixel to be transferred to an adjacent pixel. To understand how the whole chip can operate, consider the following analogy suggested by Jerome Kristian and shown in Fig 15.16.

The incoming photons are represented by the raindrops, and the CCD chip is a 2D array of buckets. Each bucket represents a pixel, and the water it collects is the combined charge accumulation due to photoelectrons. Once the rain has stopped (the shutter is closed), conveyor belts move the columns of buckets down one row (the gates are clocked). The water in the buckets at the edge of the array pours into more buckets on a horizontal conveyor belt. This conveyor belt then pours these buckets one at a time into a container on a scale, that is a graduated cylinder (the readout electronics). The volume of water from each bucket is measured and rounded to the nearest milliliter (corresponding to the digital output of a CCD,

**Fig. 15.16** Analogy of the CCD operation

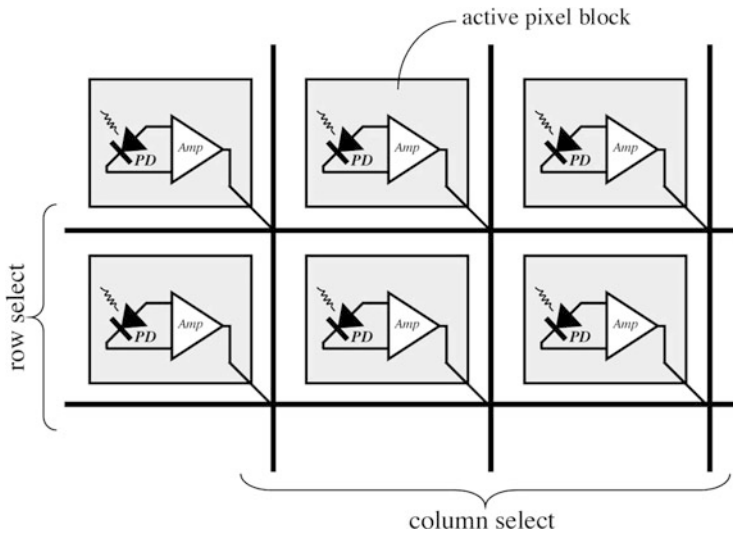


which reports the counts, or analog-to-digital units—ADUs, from each pixel). Then the image is formed by reconstructing the distribution of rainfall on the array.

Most CCDs have a setting called binning which causes them to read out in a slightly different manner. When binning is used, blocks of pixels are grouped together into “superpixels.” Each superpixel acts as one large pixel, with several results. Read times are faster, since fewer actual measurements of charge are performed. Each superpixel is also more sensitive, since it can collect more photons for a given exposure time, but this comes at the cost of resolution.

### 15.6.2 CMOS Imaging Sensors

Like CCDs, the CMOS imagers are made from silicon, but as the name implies, the process they are made in is called CMOS. This process is today the most common method of making processors and memories, meaning CMOS imagers take advantage of the process and cost advancements created by other high-volume devices. Because CMOS imagers are created in the same process as processors, memories, and other major components, CMOS imagers can integrate with these same components onto a single piece of silicon. Like CCDs, CMOS imagers include an array of photosensitive diodes (PD), one diode within each pixel. Unlike CCDs, however, each pixel in a CMOS imager has its own individual amplifier integrated inside (Fig. 15.17). Since each pixel has its own amplifier, the pixel is referred to as an “active pixel”. In addition, each pixel in a CMOS imager can be read directly on an  $x$ - $y$  coordinate system, rather than through the “bucket-brigade” process of a CCD. This means that while a CCD pixel always transfers a charge, a CMOS pixel always detects a photon directly, converts it to a voltage, and transfers the information directly to the output. Since CMOS pixel has an additional circuitry located next to it, the light sensitivity of a CMOS chip tends to be lower. Many of the photons arriving at the chip hit the circuitry instead of the photodiode.



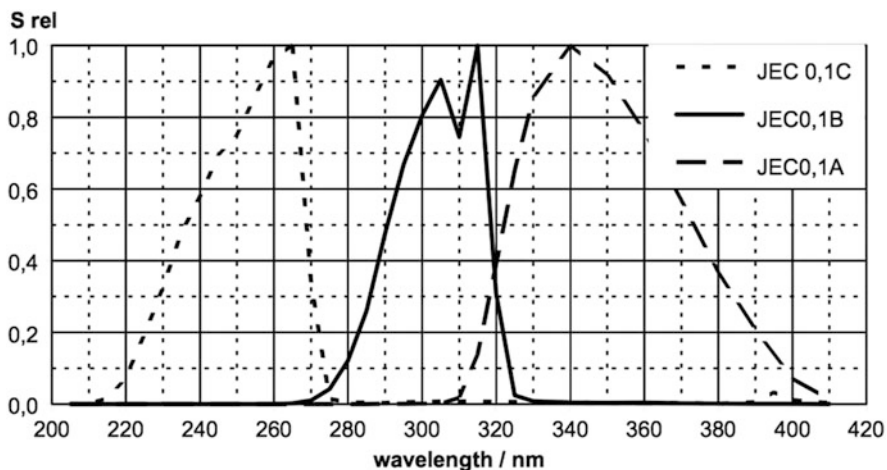
**Fig. 15.17** Organization of a CMOS imaging sensor

## 15.7 UV Detectors

### 15.7.1 Materials and Designs

As noted above, the UV spectral range of EMR is approximately from 10 to 380 nm. UV photons of very short wavelengths from 10 to 200 nm exist in Space and are strongly absorbed by the earth atmosphere, especially by oxygen molecules. The UV-C range from 100 to 280 nm is strongly absorbed by ozone in atmosphere and is damaging to microorganisms and other living cells. The UV-B (280–315 nm) is medium UV that is absorbed by ozone, while the UV-A is a weaker UV from 315 to 380 nm, also called a near-UV. This range is visible by insects and birds. Human eye cannot perceive UV since our lenses block most radiation in the wavelength range of 300–400 nm, while the shorter wavelengths are blocked by the cornea.

As compared to visible light, the UV photons are characterized by higher energy levels (Eq. 15.1) and thus can be sensed by quantum detectors. To tailor a spectrum response of a quantum detector, the gap of forbidden energies serves as a filter of the photons. Stronger photons (UV) jump the gap, while the weaker photons (visible and IR) are being stopped from entering the conduction band (see Fig. 15.1). This suggests the selection process of a semiconductive material for the UV sensing element—for UV photons the energy gap shall be wider to prevent detection of visible light.



**Fig. 15.18** Normalized (relative to maximum) spectral responses of various SiC UV photodiodes (from Laser Components GMBH)

Table 15.1 lists semiconductive materials such as NiO, ZnO, and ZnS that can be used for detection in the A, B, and C-UV ranges. Silicon carbide (SiC) is useful over a broad UV spectrum (Fig. 15.18). A design of a UV detector is similar to that of a visible light photodiode, however, its window or lens shall be fabricated of a material that is not opaque for the UV photons. Figure 5.5 shows that quartz is fairly transparent in the UV range (below 0.5  $\mu\text{m}$  of wavelength). However, manufacturers often apply filter coatings to limit transparency to desirable limits. Most of the UV-detectors are photodiodes with the enhanced responses in the selected UV-ranges.

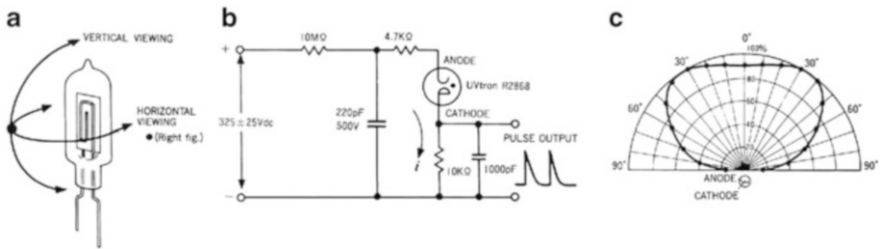
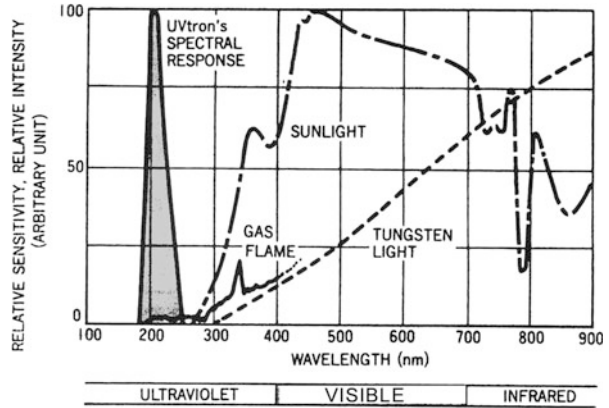
## 15.7.2 Avalanche UV Detectors

Detection of a gas flame is very important for security and fire prevention systems. In many respects it is a more sensitive way of detecting fire than a smoke detector, especially outdoors where smoke concentration may not reach a threshold level for the alarm triggering.

To detect burning gas, it is possible to use a unique feature of the flame—a noticeable portion of its optical spectrum is located in the ultraviolet (UV) spectral range (Fig. 15.19). Sunlight, after passing through the atmosphere loses a large portion of its UV spectrum located below 250 nm, while a gas flame contains UV components down to 180 nm. This makes it possible to design a narrow-bandwidth element for the UV spectral range which is selectively sensitive to flame and not sensitive to the sunlight or electric lights.

An example of such a device is shown in Fig. 15.20a. The element is a UV detector that makes use of a photoelectric effect in metals along with the gas

**Fig. 15.19** Electromagnetic spectra of various sources (Courtesy of Hamamatsu Photonics K.K.)



**Fig. 15.20** UV flame detector. Glass-filled tube (a); recommended operating circuit (b), angle of view in *horizontal plane* (c) (Courtesy of Hamamatsu Photonics K.K.)

multiplication effect (see Sect. 16.2). The detector is a rare-gas filled tube. The UV-transparent quartz housing assures wide angles of view in both horizontal and vertical planes (Fig. 15.20a, c). The device needs high voltage for operation and under normal conditions is not electrically conductive. Upon being optically exposed to a flame, the high-energy UV photons strike the cathode releasing free electrons to the gas-filled tube interior. Gas atoms receive an energy burst from the emitted electrons, which results in gas luminescence in the UV spectral range. This, in turn, causes more electrons to be emitted, which results in a higher UV luminescence. Thus, the element develops a fast avalanche-type electron multiplication making the anode-cathode region electrically conductive. Upon being exposed to a gas flame, the element works as a current switch producing a strong positive voltage spike at its output (Fig. 15.20b). It follows from the above description that the element generates UV radiation in response to the flame detection. Albeit being of a low intensity, the UV does not present harm to people, however it may lead to crosstalk between the similar neighboring sensors.



## 15.8 Thermal Radiation Detectors

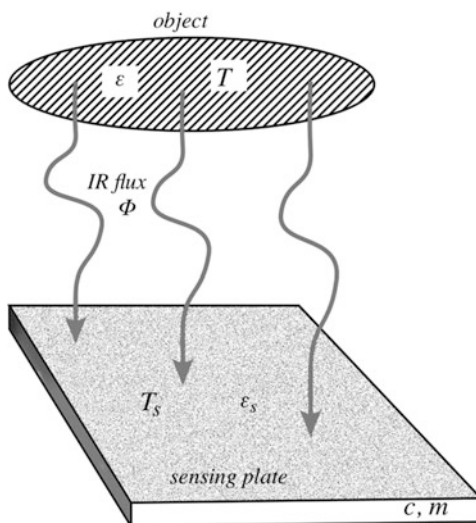
### 15.8.1 General Considerations

Thermal infrared (IR) detectors are primarily used for detecting EMR in the mid- and far-infrared (IR) spectral ranges. These are the prime sensors for noncontact thermometers which have been known in industry under the name of *pyrometers* from the Greek word  $\pi\upsilon\rho$  (fire). Today, noncontact methods of temperature measurement embrace a very broad range, including subzero temperatures, which are quite far away from that of flame. Therefore, *radiation* or *infrared* thermometry are more appropriate terms for this technology.

Photodiodes, phototransistors, and photoresistors that we described above belong to the class of quantum detectors, since their sensing mechanism is based on a direct conversion of quanta of light into electrical signal in the UV, visible, and near-infrared spectral ranges. However, in the mid- and far-infrared ranges ( $>3\ \mu\text{m}$  of a wavelength), quantum detectors have to be cryogenically cooled, otherwise their intrinsic noise will be unacceptably high. Thus, in those ranges, *thermal detectors* are employed instead. Their main advantage is that they work at room temperatures. The operating principle of thermal detectors is based on absorption or liberation of radiant energy and conversion of the captured energy into heat. Heat causes a temperature change of the sensing element. Then, change in temperature becomes the measure of the absorbed or liberated infrared (thermal) radiation. Below the mid-infrared range, thermal detectors are much less sensitive than quantum detectors.

Figure 15.21 illustrates a concept of a thermal IR detector whose key component is a *sensing plate* having high absorptivity (emissivity) in the thermal radiation spectral range. Any object naturally emanates infrared radiation flux in relation to

**Fig. 15.21** Concept of thermal radiation detector



its temperature  $T$  and surface emissivity  $\varepsilon$  (for description of emissivity refer to Sect. 4.12.3.1). A small portion of the flux is radiated toward the sensing plate. The plate has its own temperature  $T_s$  and emissivity  $\varepsilon_s$  and radiates its own IR flux. Thus, the net IR flux that exists between the object and sensing plate, according to Eq. (4.138) is

$$\Phi = A\varepsilon\varepsilon_s\sigma(T^4 - T_s^4), \quad (15.18)$$

where  $\sigma$  is the Stefan-Boltzmann constant and  $A$  is the geometry factor which depends on the optical coupling between the object and sensing plate. The optical coupling is shaped by the sensor components that channel the photon flux to the plate. The optical component may be a filter or lens having the specific transmission and a field of view (FOV). Also, the geometry factor depends on the sensing plate IR absorption area, and some other factors.

When the plate absorbs (or liberates) flux  $\Phi$ , the plate takes or releases heat  $Q = \Phi$ . Then according to Eq. (4.116) the plate's temperature changes by the value

$$\Delta T = \frac{Q}{cm} = \frac{\Phi}{cm}, \quad (15.19)$$

where  $c$  and  $m$  are the specific heat and mass of the sensing plate. By combining Eqs. (15.18) and (15.19) we arrive at the plate temperature change as function of the object's and plate's temperatures:

$$\Delta T = \frac{\Phi}{cm} = \frac{A\varepsilon_s\sigma}{cm}\varepsilon(T^4 - T_s^4) \quad (15.20)$$

A ratio in Eq. (15.20) represents then sensor's *thermal sensitivity* coefficient. The larger the temperature change  $\Delta T$  the higher the electrical output of the transducer, thus for a better signal-to-noise ratio, the design should maximize the sensitivity coefficient.

The sensing plate temperature change  $\Delta T$  is the measure of thermal radiation and thus shall be converted into the electrical output. The next step of a temperature-to-electricity conversion can be performed by several known transducers that are described in Chap. 17. The transducer defines the IR sensor type and functionality. Further in this chapter we discuss the most popular thermal IR sensors.

In summary, a typical thermal radiation sensor consists of:

1. A sensing plate—the component that absorbs EMR in the selected wavelength range and converts it to heat. The main requirements to the plate are a fast, predictable, and strong thermal response to absorbed EMR, and a good long-term stability.
2. Temperature-to-electricity transducer for the efficient conversion of the absorbed or liberated heat into electrical signal.

3. A housing, which shields its interior from environment. It should be hermetically sealed and filled either with dry air or inert gas, such as argon or nitrogen. The housing should have high thermal conductivity and thermal capacity for maintaining itself at a uniform and slow changing temperature. It is important to minimize all thermal couplings, including through radiation, between the sensing plate and housing, thus the inner surface of the housing that is exposed to the sensing plate should be coated with gold since gold has very low emissivity in the thermal spectral range.
4. A supporting structure to hold the sensing plate inside the housing and expose it only to thermal radiation arriving from the optical filter. The structure should have low thermal conductivity for minimizing a spurious conductive heat exchange between the housing and sensing plate.
5. A protective window or optical filter that is impermeable to environmental factors and substantially transparent in the wavelength of detection. The window may have a surface antireflective coating (ARC) to reduce reflective losses and filter out the undesirable portions of the light spectrum. Alternatively, a focusing lens or curved mirror may be used with or in place of the window. Preferably, the window should be well thermally coupled to the housing to closely follow its temperature.

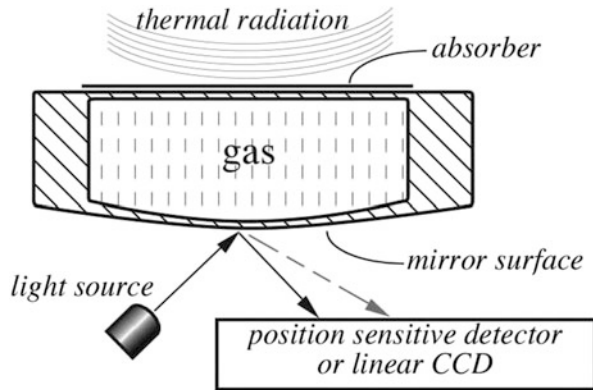
In a noncontact detection of thermal radiation, due to a small value of factor  $A$ , the sensing plate is rather poorly thermally coupled to the heat source. An IR sensor is usually positioned inside a radiation thermometer or thermal imaging camera that typically is near the ambient temperature, while the object may be either hot or cold. When the sensing plate is exposed to the object, after a short transitional time, the plate's temperature reaches a steady-state equilibrium with the object. However, an equilibrium does not mean being thermally equal, just steady. The sensing plate equilibrium temperature is always somewhere in-between the object's temperature and the initial temperature of the element, as illustrated in Fig. 17.5a. Typically, the plate temperature change is no greater than 1 °C, even for very large thermal gradients in Eq. (15.20). This is the reason why the thermal IR sensor shall be designed so that the sensing plate is well thermally decoupled from the housing, and thus a negligible heat from stray thermal sources that may exist in vicinity of the sensor would be minimized.

### 15.8.2 Golay Cells

The Golay cells [3] are the broadband thermal detectors of infrared radiation. They are extremely sensitive, but also extremely delicate. Just as any thermal radiation detector, the cell contains a heat absorbing plate that is a thin membrane.

The operating principle of the Golay cell is based on detection of a thermal expansion of gas trapped inside a sealed enclosure and conversion it into an electrical output. This is why these sensors sometimes are called *thermopneumatic* detectors. Figure 15.22 depicts an enclosed chamber having two membranes—the

**Fig. 15.22** Golay cell detector for thermal radiation



upper and lower. The upper membrane is for absorbing thermal radiation and thus it is coated with an IR thermal radiation absorber (e.g., goldblack<sup>3</sup>) [4], while the lower membrane has a mirror surface (e.g., coated with aluminum).

To monitor changes in the gas pressure, the mirror is illuminated by a light source. The incident light beam is reflected from the mirror and impinges on a position-sensitive detector (PSD), that is described in Sect. 7.5. The upper membrane is exposed to thermal radiation that is captured by the thermal radiation absorber. Temperature of the upper membrane increases and, in turn, warms up gas that is trapped inside the sensor's chamber. Gas expands and its pressure goes up. Increase in the gas pressure deflects the lower membrane that bulges out for the increase or caves in for the pressure decrease. A change in the mirror curvature deflects the reflected light beam. The reflected light impinges on the PSD at its various locations, depending on degree of the membrane bulging. The entire sensor may be micromachined using modern MEMS technology. The degree of the lower membrane deflection alternatively may be measured by different methods, for example by using a FP interferometer (see Sect. 8.5.4).

### 15.8.3 Thermopiles

A thermopile belongs to the class of passive infrared (PIR) detectors, meaning that it generates electric output in response to IR with no external power provided. The key element of the sensor is a thin membrane that can absorb thermal radiation. The membrane serves as an IR absorbing plate that was described above. The sensing process consists of several energy conversion steps: thermal radiation impinges on the surface of a membrane—the membrane temperature goes

<sup>3</sup> Goldblack is a thin coating of gold molecules deposited by evaporation on a surface in a N<sub>2</sub> atmosphere. It has high absorptivity of photons in a broad spectral range.

up—the temperature change is measured by a contact temperature sensor coupled to the membrane—the temperature sensor produces an electric output.

In a thermopile, a contact temperature sensor that is coupled to the membrane consists of a multitude of *thermocouples*<sup>4</sup> (see Sect. 17.8) embedded into the membrane. A single thermocouple is a low-sensitivity device generating tens of microvolts per one °C of a thermal gradient between its “hot” and “cold” junctions. Words “hot” and “cold” are the remnants of a traditional thermocouple jargon and used here conditionally since the junctions in reality are neither cold nor hot.

In any thermal radiation sensor, considering a rather poor thermal coupling with an object, temperature change of the membrane, when exposed to an object, may be very small, as low as 0.01 °C for small temperature gradients between the object and sensor. Thus, to improve a signal-to-noise ratio, a higher conversion factor from heat to voltage is required. This is achieved by increasing a number of thermocouples positioned on a surface or embedded into the membrane. Multiple thermocouples make a *thermopile*, like “piling up” thermocouples. A thermopile is a chain of serially connected thermocouples, typically ranging from 50 to 100 junctions that are positioned at a radiation absorbing area of the membrane. The chain will produce a 50–100 times stronger electrical signal. Originally, it was invented by Joule to increase the output signal of a thermoelectric sensor. He electrically connected several thermocouples in a series and *thermally* joined together their “hot” junctions and separately—“cold” junctions. Nowadays, the prime applications for thermopiles are for thermal detection of light in the mid- and far-infrared spectral ranges and measuring heat in chemical sensors.

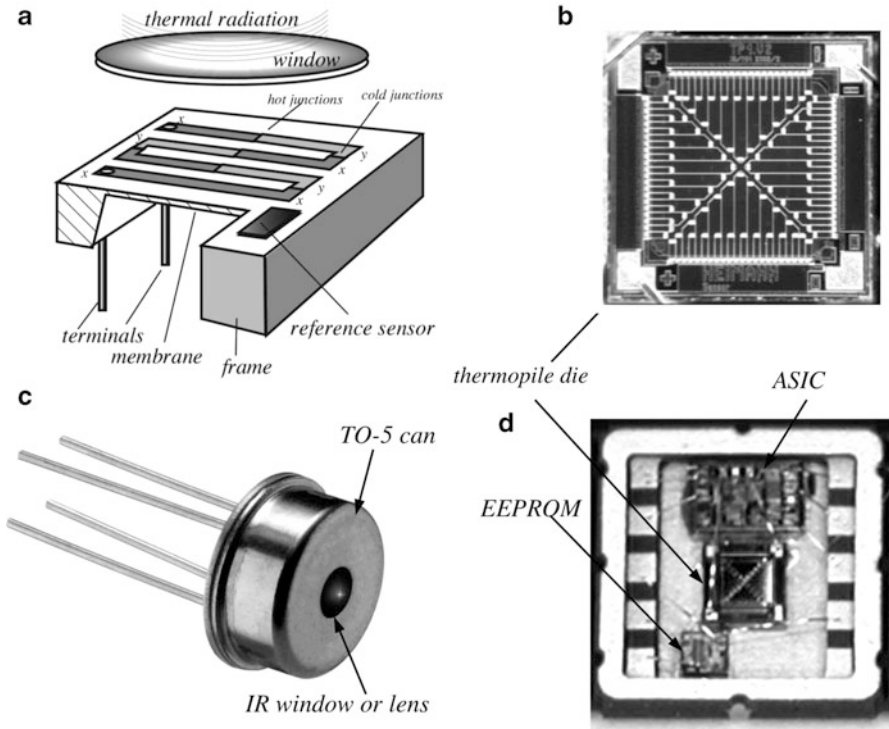
A conceptual drawing of a thermopile sensor is shown in Fig. 15.23a. The sensor consists of a silicon frame having a comparatively large thermal mass, so its temperature is relatively stable and not appreciably changing when the sensor receives thermal radiation. The frame is glued to the housing (not shown) for a better thermal stability. It supports a thin (<1 μm thick) membrane, just like a drum. The frame is the place where the “cold” junctions are deposited, while the membrane carries the “hot” junctions of the thermocouples.

The frame may be thermally coupled to a special reference temperature sensor or attached to a thermostat having a precisely known reference temperature. While a thermopile is a *relative* temperature sensor (measures only a temperature difference between the junctions), the reference sensor is of an *absolute* type (measures the frame temperature on the absolute scale: K or C or F). It may be a thermistor, semiconductor, etc. The purpose of that auxiliary sensor will be shown below.

When the IR sensor is not exposed to any object and completely shielded from any external thermal radiation, temperature gradient between the junctions is zero. At exposure to an external heat source, a temperature gradient between the hot and cold junctions arises and is converted into the output voltage by the thermopile

---

<sup>4</sup> A similar IR sensor called “microbolometer” instead of thermoelectric sensors uses another type of temperature sensors—the RTDs—*resistive temperature detectors*. It is described in Section 15.8.5.



**Fig. 15.23** Thermopiles for detecting thermal radiation. Conceptual drawing where  $x$  and  $y$  are different thermoelectric strips (a); micromachined thermopile sensor. Note the absorptive coating on the hot junctions in the center of the membrane (b); sensor in a TO-5 packaging (c); and thermopile SMD packaging includes ASIC and EEPROM (d) (Courtesy of Heimann Sensor GMBH)

junctions having an aggregated thermoelectric factor  $\alpha\Delta T$  for all junctions together):

$$V_{\text{out}} = \alpha\Delta T \quad (15.21)$$

The factor  $\alpha$  is not really a constant—it somewhat depends on the frame temperature  $T_s$ . For a better accuracy, its temperature coefficient  $g$  should be accounted for by a linear approximation<sup>5</sup>:

$$\alpha = \alpha_0[1 + g(T_s - T_{s0})], \quad (15.22)$$

<sup>5</sup> Strictly speaking the membrane and frame temperatures are slightly different, but for the most practical purposes a thermoelectric coefficient for the hot and cold junctions should be considered the same for all operating temperatures.

where  $\alpha_0$  is the thermoelectric coefficient at a calibrating temperature  $T_{s0}$ . Still, in a relatively narrow ambient operating range within  $\pm 5\text{--}7^\circ\text{C}$  from the calibrating temperature  $T_{s0}$ ,  $\alpha$  may be considered constant and equal to  $\alpha_0$  for most practical cases.

By combining Eqs. (15.20) and (15.21) we arrive at the thermopile output voltage as function of the object and the sensor (frame) temperatures:

$$V_{\text{out}} = \frac{A\varepsilon_s\sigma\alpha}{cm} \varepsilon(T^4 - T_s^4) \quad (15.23)$$

Evaluation of Eq. (15.23) shows that the sensor's sensitivity can be improved with increase in the optical coupling coefficient  $A$ , membrane's emissivity  $\varepsilon_s$ , and lowering the membrane mass  $m$ . It also improves with a correct selection of the type of thermocouple junctions ( $\alpha$ ) and membrane material ( $c$ ).

Note that the sensor's response is not a linear function of the thermal gradient—it is a differential 4th-order parabola of the absolute temperatures. However, since temperatures are in Kelvin, the nonlinearity is rather mild and for small temperature differences ( $T - T_s$ ) and not too stringent accuracy requirements, Eq. (15.23) may be approximated by a linear function.

A thermopile is a d.c. device whose output voltage follows its “hot-cold” junction temperature gradient according to Eq. (15.23). It can monitor a steady-state level of thermal radiation. Electrically, it can be modeled as a temperature controlled voltage source that is connected in series with a fixed resistor. The sensor is hermetically sealed in a metal can (Fig. 15.23c) with a hard infrared-transparent window that is transparent in a selected mid- and far-infrared spectral band. Sometimes, the window is called a *filter* since it allows only certain bandwidth to pass. Instead of a window, a focusing lens may be used to shape the sensor's field of view (FOV). A choice of materials for windows and lenses includes silicon, germanium, and zinc selenide. Alternatively to a metal can, a thermopile may be sealed inside a surface mountable SMD ceramic packaging as shown in Fig. 15.23d.

When a thermopile is used in the IR noncontact thermometers, the inverted Eq. (15.23) is used for computing the object's temperature in Kelvin:

$$T = \sqrt[4]{T_s^4 + V_{\text{out}} \frac{1}{\varepsilon} \frac{cm}{A\varepsilon_s\sigma\alpha}} = \sqrt[4]{T_s^4 + V_{\text{out}} \frac{S}{\varepsilon}}, \quad (15.24)$$

where  $S$  is the sensitivity factor that is determined during calibration of the IR thermometer. Note that the thermopile output voltage may be positive or negative, depending if the object is warmer or cooler than the sensor. The auxiliary reference sensor that is thermally coupled to the thermopile frame, measures  $T_s$ . Note that the object emissivity makes a strong contribution to accuracy and thus it shall be known. Since the emissivity is in a denominator, if it is too small, the uncertainty of measurement would grow dramatically. Thus surface temperatures of the low-emissivity objects (bare unoxidized metals) cannot be accurately measured by the IR sensors.

The best performance of a thermopile is characterized by high sensitivity, fast response, and low noise which may be achieved by using the junction materials having high thermoelectric coefficient  $\alpha$ , low thermal conductivity, and low-volume electric resistivity. The “hot” and “cold” junction pairs should have the thermoelectric coefficients of the opposite signs. This dictates selection of their materials. Unfortunately, most of metals having low electrical resistivity (gold, copper, silver) have only very poor thermoelectric coefficients. The higher electrical resistivity metals (especially bismuth and antimony) possess high thermoelectric coefficients and in the past they were selected for designing thermopiles. By doping these materials with Se and Te, the thermoelectric coefficient was improved up to  $230 \mu\text{V K}^{-1}$  [5]. Other thermocouple materials include the *p*-type silicon in junction with the aluminum strips deposited on a silicon membrane [6].

Table A.11 lists thermoelectric coefficients for selected elements. It is seen that coefficients for crystalline and polycrystalline silicon are very large and the volume resistivity is relatively low. The advantage of using silicon is in the possibility of employing a standard IC processes which results in a significant cost reduction. The resistivity and thermoelectric coefficients can be adjusted by the doping concentrations. However, the resistivity increases much faster than sensitivity, so the doping concentration has to be carefully optimized for the high sensitivity-low noise ratios.

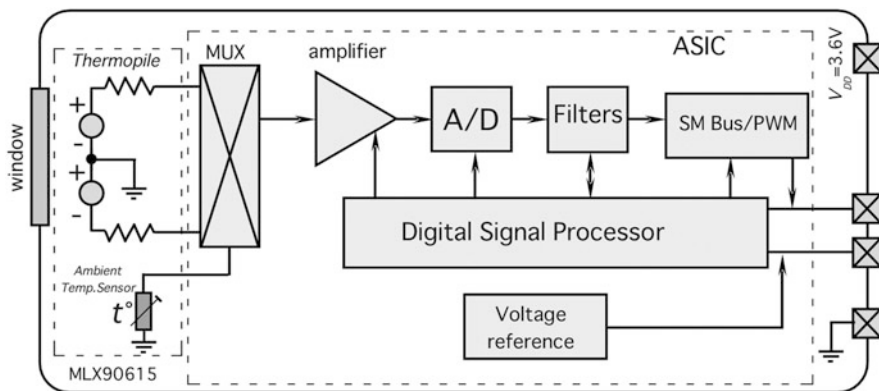
Methods of construction of the metal junction thermopiles may differ to some extent, but all incorporate vacuum deposition techniques and evaporation masks to apply the thermoelectric materials and IR absorbing coatings. To improve absorptivity (emissivity) of the infrared radiation, the “hot” junctions on the membrane are often coated with an absorber of thermal radiation. For example, they may be coated with Nichrome,<sup>6</sup> goldblack, organic paint, or carbon nanotubes. Figure 15.23b illustrates a silicon membrane with the deposited thermoelectric strips. When fabricating, the central part of the silicon substrate is removed by means of anisotropic etching from the back, leaving only about  $1 \mu\text{m}$  thin layer (membrane) of  $\text{SiO}_2\text{—Si}_3\text{N}_4$  on top, which has low thermal conductivity. Onto this membrane, thin conductors of two different thermoelectric materials (e.g., polysilicon and aluminum) are deposited. This allowed producing sensors with a negligible temperature coefficient of sensitivity ( $g$ ), which is an important factor for operation over broad ambient temperatures ranges. Note a position of the reference sensor that measures temperature of the frame that carries the “cold” junctions of the strips.

The modern trend in IR sensing technology is in integrating a thermopile sensor together with a signal conditioner that includes a low offset voltage amplifier, ADC, and other processing circuitry. A Belgium company Melexis ([www.melexis.com](http://www.melexis.com)) developed an entire noncontact IR thermometer MLX90615 in a miniature TO-46 can that contains a thermopile and data processing ASIC chip (Fig. 15.24). A small output signal from the thermopile is fed into a precision amplifier having an offset

---

<sup>6</sup> Alloy of 80 % nickel and 20 % chromium has emissivity (absorptivity) over 0.80.





**Fig. 15.24** Block-diagram of an integrated IR thermometer with a thermopile sensor

**Table 15.3** Typical specifications of a thermopile (HMS-M11 from Heimann Sensor GMBH)

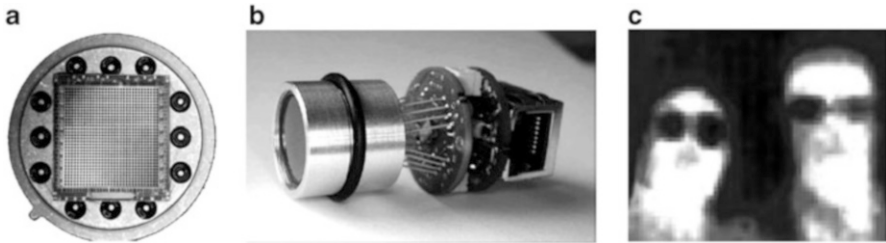
Parameter	Value	Unit	Conditions
Sensitive element size	$0.61 \times 0.61$	mm	
Output voltage	330	$\mu\text{V}$	for $\Delta T = 75 \text{ K}$
Noise	38	$\text{nV}/\sqrt{\text{Hz}}$	$25 \text{ }^\circ\text{C}$ , rms
Equivalent resistance	75	$\text{k}\Omega$	$25 \text{ }^\circ\text{C}$
Thermal time constant	<6	ms	
Angle of view (shaped by the IR lens)	20	Degree	10 % power level

voltage as small as  $0.5 \mu\text{V}$ . The digital signal processor (DSP) outputs the measured temperature or individual outputs from the IR and reference sensors with a 15-bit resolution. The packaging includes additional components, such as EEPROM memory<sup>7</sup> for storing the calibrating parameters. The device not only measures intensity of the IR radiation, but also computes temperature of the outside object whose IR signal is detected, and outputs the measured data over a serial link (SM Bus or PWM).

The thermopile operating frequency limit is mainly determined by a thermal capacity of the membrane, which is manifested through a thermal time constant. A thermopile sensor exhibits quite a low noise which primarily equals to a thermal noise of the sensor's equivalent resistance, that is of 20–100  $\text{k}\Omega$ . Typical properties of a thermopile sensor are given in Table 15.3.

It can be said that a thermopile as described above is a single-pixel thermal radiation sensor. Yet, an IR sensor with multiple thermopile pixels can be designed and used for a simultaneous detection of thermal radiation from multiple sources or

<sup>7</sup> ASIC means *Application Specific Integrated Circuit*. EEPROM means *Electrically Erasable Programmable Read-Only Memory*.



**Fig. 15.25** Thermopile thermal-imaging sensor. Sensing surface (a); imaging module (b); example of a thermal image (c) (Courtesy of Heimann Sensors GMBH)

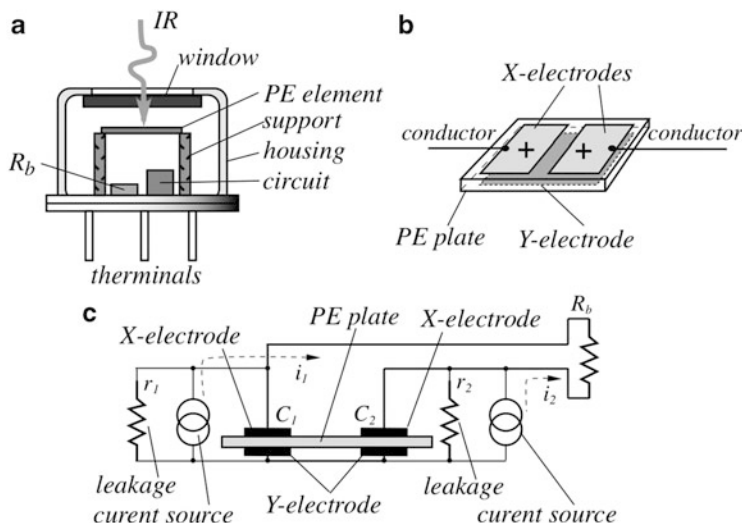
for thermal imaging. An example of such a sensor is shown in Fig. 15.25 where the thermopile pixels are arranged in a  $32 \times 31$  matrix. The number of junctions per pixel is 80 and the thermoelectric junctions materials are  $n$ -poly/ $p$ -poly Si. The pixels have size of  $150 \mu\text{m}$  and are positioned with a pitch of  $220 \mu\text{m}$ . The sensing module HTPA $32 \times 31$  from Heimann Sensors has the imbedded preamplifiers, multiplexer, and ADC. Advantage of the imaging module is that it does not require a cryogenic cooling and operates over a broad ambient temperature range.

#### 15.8.4 Pyroelectric Sensors

Just as a thermopile, a pyroelectric sensor belongs to the class of passive infrared (PIR) detectors, meaning that it generates electric output in response to IR radiation with no external power provided. Unlike a thermopile, this sensor can be called an a.c. sensor, as it is responsive only to a *variable part* of thermal radiation signal and very little responsive to a steady level of radiation. Refer to Sect. 4.7 for description of the pyroelectric effect.

The key element in a pyroelectric sensor is a thin plate fabricated of a pyroelectric ceramic that can develop surface electric charges when its temperature changes. The conversion steps in a pyroelectric sensor are as follows: infrared signal impinges on the pyroelectric plate—temperature of the plate goes up—electric charge is generated on the plate surface as long as temperature changes—electric charge is picked up and converted into electric voltage.

A pyroelectric sensing element consists of three essential components: the pyroelectric ceramic plate called “element” and two electrodes deposited on the opposite sides of the plate. In addition, several other components are required to make a practical device, such as the element supporting structure, a hermetically sealed housing, optical window or filter, electric terminals, etc. A typical construction of a pyroelectric sensor is shown in Fig. 15.26a. It is housed in a metal TO-5 or TO-39 can that provides electric shielding and protects its interior from environment. The can has an opening that is covered by a silicon window (IR filter) being



**Fig. 15.26** Dual pyroelectric (PE) sensor. PE element is supported at IR window (a); conductive electrodes are deposited on opposite sides of pyroelectric plate (b); equivalent circuit of dual PE-element (c)

substantially transparent in the mid- and far-infrared spectral ranges. The inner space of the can is filled with dry air or nitrogen.

The major problem in designing a pyroelectric detector is its sensitivity to mechanical stress and vibrations. Since a pyroelectric sensor possesses also the piezoelectric properties, the element is very much sensitive to minute mechanical vibrations. In other words, in addition to sensing heat flow, it behaves as a microphone or accelerometer. For a better mechanical noise rejection, the ceramic element shall be mechanically decoupled from the housing, especially from the electric terminals that are soldered to an external circuit board. Figure 15.26a shows the element being held by two ceramic supports that are designed to prevent stressing the element. In addition, to reduce the microphonic interferences, an electrical differential technique is typically employed, where two identical sensing elements are connected oppositely, serially, or in parallel. A differential connection not only cancels the electric charges resulted from mechanical vibrations, it also compensates for the rapid spurious thermal changes (thermal shocks).

In a differential design, two sensing elements are formed on a single-pyroelectric plate by depositing two pairs of electrodes for picking up the electric charge as shown in Fig. 15.25b. One upper X-electrode is either coated with the heat absorbing dielectric layer or fabricated of Nichrome, while the second upper X-electrode is either shielded from the IR radiation or gold-plated for a better reflectivity, resulting in almost no absorption of IR signal. Nichrome has high emissivity (absorptivity) and thus serves a dual purpose—for collecting electric charge from the pyroelectric plate (serves as an electrode) and absorbing thermal radiation. For applications in the PIR motion detectors (see Sect. 7.8.8), both

electrodes are exposed to the window (IR filter) and made to absorb the IR radiation. The bottom Y-electrode is common for both elements.

The metalized patterns on both sides of the plate form two serially connected capacitors  $C_1$  and  $C_2$  between the X and Y electrodes. Figure 15.26c shows the equivalent circuit of a dual pyroelectric (PE) element. Its ability to generate charges is represented by two current sources—one per element. The current sources generate currents  $i_1$  and  $i_2$  that are controlled by the heat flow and mechanical stress. Since electric currents from both elements flow through the load resistor  $R_b$  in the opposite directions, they will cancel each other, when equal—the case when the currents are produced by spurious in-phase interferences. If one of the PE elements does not receive IR signal but is subjected to the same interferences as the other element, voltage across the load resistor will represent the IR signal (no cancellation), while signals from interfering sources will be cancelled out.

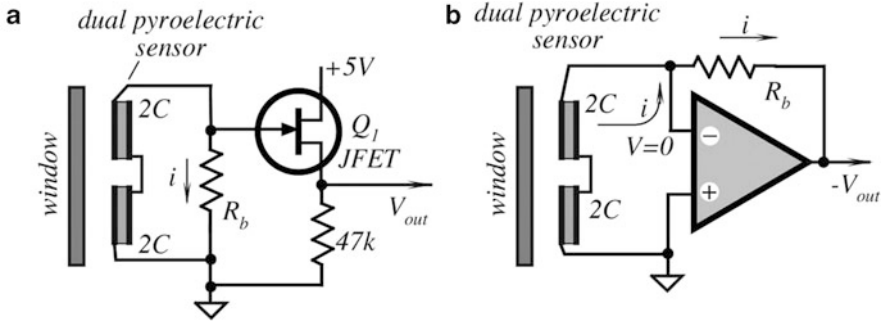
The sensor where the electrodes for both elements are deposited side-by-side on the same plate has the benefit of a good balance of the PE elements, resulting in a better rejection of common-mode interferences. Note that the sensing part of the ceramic plate exists only between the opposite electrodes. Portion of the pyroelectric plate that is not sandwiched between the electrodes does not participate in generation of a signal since electric charges from the electrode-free area are not picked up by the electrodes.

Pyroelectric elements have very high internal leakage resistances  $r_1$  and  $r_2$ . The leakage resistance  $r_1$  is connected in parallel with capacitance  $C_1$ , while  $r_2$  is in parallel with  $C_2$ . Values of  $r_1$  and  $r_2$  are very large—on the orders of  $10^{12}$ – $10^{14}$   $\Omega$ . To convert flowing pyroelectric charges (current) to voltage, it shall flow through a load resistor of a fixed value. In a practical sensor, the PE element is connected to an interface circuit that contains a load resistor  $R_b$  along with an impedance converter indicated as “circuit” in Fig. 15.26a. The converter may be either a voltage follower (for instance, a JFET) or a current-to-voltage converter with an operational amplifier.

The voltage follower (Fig. 15.27a) functions as an *impedance converter*—it converts sensor’s high-output impedance (a combination of capacitance  $C$  in parallel with the leakage and load resistances) into the lower output resistance of a follower. In this example, the output resistance is composed of the transistor’s transconductance in parallel with 47 k $\Omega$  in drain. A single-JFET follower is the most cost effective and simple circuit, however it suffers from two drawbacks. The first is dependence of its speed response on the so-called *electrical time constant*, that is a product of the sensor’s combined capacitance  $C$  and the load resistor  $R_b$ :

$$\tau_c = CR_b, \quad (15.25)$$

where  $C$  equals to serially connected  $C_1$  and  $C_2$ . For example, a typical dual sensor may have  $C = 40$  pF and  $R_b = 20$  G $\Omega$ , which yield  $\tau_c = 0.8$  s, corresponding to a first order low-pass filter with the upper cutoff frequency at 3 dB level equal to about 0.2 Hz—a very low frequency indeed! This makes the voltage follower suitable only for limited applications, where speed response is not important.



**Fig. 15.27** Impedance converters for pyroelectric sensors. Voltage follower with JFET (a); current-to-voltage converter with operational amplifier (b)

An example is a PIR motion detector (see Sect. 7.8.8). The second drawback of the circuit is a large offset voltage across the output resistor. This voltage depends on type of a JFET and is temperature dependent. Thus, the output  $V_{out}$  is the sum of two voltages: the offset voltage which can be as large as several volts, and a variable pyroelectric voltage which may be on the order of millivolts.

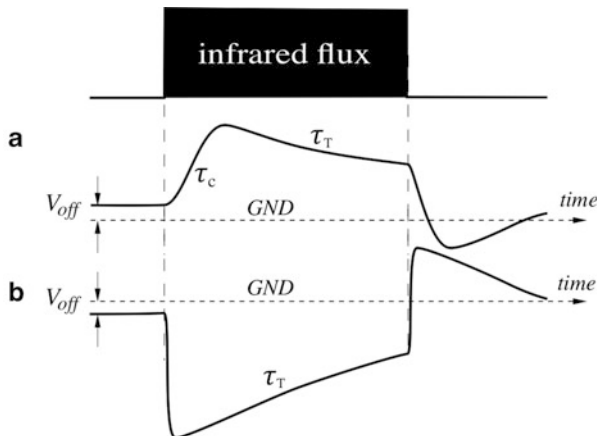
A more efficient, however, more expensive front stage circuit for a pyroelectric sensor is an  $I/V$  (current-to-voltage) converter, Fig. 15.27b. Its advantage is a faster response and insensitivity to capacitance of the sensing element. The element is connected to an inverting input of the operational amplifier which possesses properties of the so-called virtual ground (the similar circuits are shown in Figs. 15.6 and 15.8). That is, the voltage at the inverting input is constant and almost equal to that of a noninverting input, which in this circuit is grounded. Thus, the voltage across the sensor is forced by the feedback to stay near zero (ground) so the combined capacitance  $C$  has no chance to be charged. The output voltage follows the shape of the electric current (a flow of charges) generated by the sensor (see Fig. 4.28). For an optimal performance, the circuit should employ an operational amplifier with a low-bias current (1 pA or less). There are three major advantages in using this circuit: a fast response, insensitivity to capacitance of the pyroelectric element, and a low-output offset voltage. However, being a broadband circuit, a current-to-voltage converter may suffer from higher noise, thus resistor  $R_b$  should be shunted by a small capacitor to limit the bandwidth.

Both circuits, the JFET and  $I/V$  converter, transform pyroelectric current  $i_p$  into the output voltage  $V_{out}$ . According to the Ohm's law

$$V_{out} = i_p R_b. \tag{14.26}$$

For instance, if the pyroelectric current is 10 pA ( $10^{-11}$  A) and the load resistor is of  $2 \times 10^{10} \Omega$  (20 G $\Omega$ ), the output voltage swing is 200 mV. Note that in the absence of a pyroelectric current, the circuit bias current ( $I_B$ ) when passing through the input load resistor will produce the offset voltage  $V_{off}$ . Since the load resistor is of a very high resistance, the JFET transistor or operational amplifier must have low-input

**Fig. 15.28** Output signals of a voltage follower (a) and current-to-voltage converter (b) in response to a step function of thermal radiation



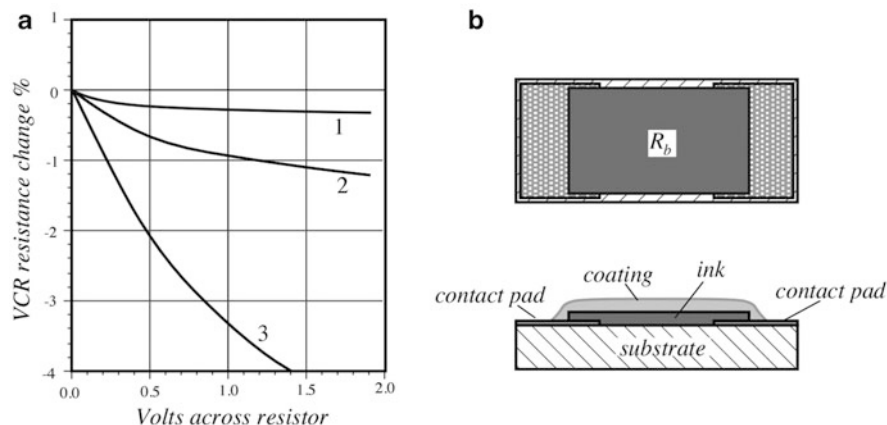
bias currents over the entire operating temperature range. CMOS OPAMs are generally preferable as their bias currents are less than 1 pA.

It should be noted that the circuits described above (Fig. 15.27) produce output signals of quite different shapes. The voltage follower's output voltage is a repetition of voltage across the element and  $R_b$ , Fig. 15.28a. It is characterized by two slopes: the leading slope having an electrical time constant  $\tau_c = CR_b$ , and the decaying slope having thermal time constant  $\tau_T$ . Voltage across the PE element in a current-to-voltage converter is essentially zero and, contrary to the follower, the input impedance of the converter is low. In other words, while the voltage follower acts as a voltmeter, the current-to-voltage converter acts as an ampermeter. The leading edge of its output voltage is fast (determined by a capacitance across  $R_b$ ) while the decaying slope is characterized by the same  $\tau_T$ . Thus, the converter's output voltage almost repeats shape of the sensor's pyroelectric current, Fig. 15.28b. Note that both circuits have some offset voltage  $V_{off}$ . However, in the current-to-voltage converter the offset voltage can be substantially compensated and an additional resistor equal to  $R_b$  is connected in series with a noninverting input of the OPAM.

Fabrication of the Gighm-range resistors that are essential for use with the pyroelectric sensors is not a trivial task. High-quality load resistors should have good environmental stability, low-temperature coefficient of resistance (TCR), and low voltage coefficient of resistance (VCR). The VCR is defined as

$$\xi = \frac{R_1 - R_{0.1}}{R_{0.1}} \cdot 100\%, \quad (15.27)$$

where  $R_1$  and  $R_{0.1}$  are the resistances measured, respectively, at 1 and 0.1 V across the resistor. Usually, VCR is negative, that is, the resistance value drops with increase in voltage across the resistor (Fig. 15.29a). Since the pyroelectric sensor's output is proportional to the product of the pyroelectric current and the bias resistor, VCR results in nonlinearity of the overall transfer function.



**Fig. 15.29** High-impedance resistor. VCRs for three different types of resistor (a); semi-conductive ink is deposited in alumina substrate (b)

A high-impedance resistor is fabricated by depositing a thin layer of a semiconductive ink on a ceramic (alumina) substrate, firing it in a furnace, and subsequent covering the surface with a protective coating. A high quality, relatively thick (at least  $50\ \mu\text{m}$  thick) hydrophobic coating is very important for protection against humidity, since even a small amount of water molecules may cause oxidation of the semiconductive layer. This will lead to a substantial increase in the resistance and a poor long-term stability. A typical design of a high-impedance resistor is shown in Fig. 15.29b.

In applications where high accuracy is not required, such as thermal radiation motion detection, the bias resistor can be replaced with one or two zero-biased parallel-opposite connected silicon diodes.

In practical applications, a distinction exists between two cases in which completely different demands have to be met with respect to the pyroelectric material and its radiative coupling with the environment [7]:

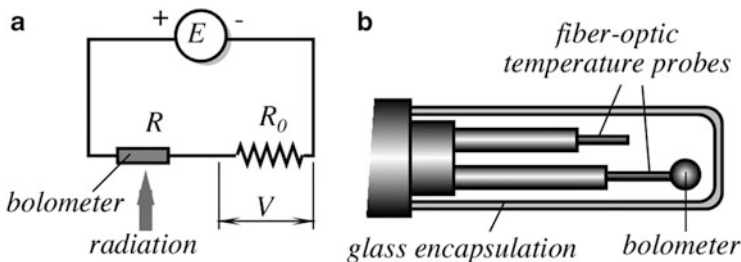
- (a) *Fast* sensors detect radiation of high intensity but very short duration (nanoseconds) of laser pulses, with a high repetition on the order of 1 MHz. The sensors are usually fabricated from single-crystal pyroelectrics, such as lithium tantalate ( $\text{LiTaO}_3$ ) or triglicinesulfate (TGS). This assures a high linearity of response. Usually, the pyroelectric material is bonded to a heat sink.
- (b) *Sensitive* sensors detect thermal radiation of low intensity, however, with a relatively low rate of change. Examples are the infrared thermometry and motion detection [8–10]. Detection of low level thermal radiation generally requires a good optical coupling with a heat source. Optical devices, such as focusing lenses and waveguides are generally employed. Contrary to a fast sensor, in these sensors, a thermal coupling between the PE element and environment (sensor's housing) shall be minimized. If well designed, such a

sensor can have the sensitivity approaching that of a cryogenically cooled quantum detector [6]. Commercial pyroelectric sensors are implemented on the basis of single crystals, such as TGS and  $\text{LiTaO}_3$ , or lead zirconate titanate (PZT) ceramics. PVDF film is also occasionally used, thanks to its high-speed response and good lateral resolution.

### 15.8.5 Microbolometers

Bolometers are miniature RTDs or thermistors (see Sects. 17.3 and 17.4) or other temperature-sensitive resistors which are mainly used for measuring r.m.s. of electromagnetic radiation over a broad spectral range from the mid-infrared to microwaves. The applications include IR temperature detection and imaging, measurements of local electromagnetic fields of high power, testing of microwave devices, RF antenna beam profiling, testing of high-power microwave weapons, monitoring of medical microwave heating, and others. The operating principle is based on a fundamental relationship between the absorbed electromagnetic signal and dissipated power [11]. The conversion steps in a bolometer are as follows: a resistor is exposed to electromagnetic radiation—radiation is absorbed by the resistor and converted into heat—the heat elevates resistor's temperature above the ambient—the temperature increase changes the bolometer's ohmic resistance—resistance is converted into electric output.

Below, we briefly outline the most common methods of the bolometer fabrication which evolved quite dramatically since Langley<sup>8</sup> invented a bolometer in 1881. A basic circuit for the voltage-biased bolometer application is shown in Fig. 15.30a. It consists of a bolometer (a temperature-sensitive resistor) having resistance  $R$ , a stable reference resistor  $R_0$ , and a bias voltage source  $E$ . The voltage  $V$  across  $R_0$  is the output signal of the circuit. It has the highest value when both



**Fig. 15.30** Equivalent circuit of electrically biased bolometer (a) and design of optical bolometer (b)

<sup>8</sup> Samuel Pierpont Langley (1834–1906) was an American astronomer and physicist.



resistors are equal. Sensitivity of the bolometer to the incoming electromagnetic (EM) radiation can be defined as [12]:

$$\beta_V = \frac{\alpha \varepsilon Z_T E}{4\sqrt{1 + (\omega \tau_T)^2}}, \quad (15.28)$$

where  $\alpha = (dR/dT)/R$  is the TCR (temperature coefficient of resistance) of the bolometer,  $\varepsilon$  is the surface emissivity,  $Z_T$  is the bolometer thermal resistance, which depends on its design and the supporting structure,  $\tau_T$  is the thermal time constant, which depends on  $Z_T$  and the bolometer's thermal capacity, and  $\omega$  is the frequency of the absorbed EMR.

Since the bolometer's temperature increase,  $\Delta T$  is

$$\Delta T = T - T_0 \approx P_E Z_T = \frac{E^2}{4R} Z_T, \quad (15.29)$$

and the resistance of RTD bolometer can be represented by a linear approximation

$$R = R_0(1 + \alpha_0 \Delta T), \quad (15.30)$$

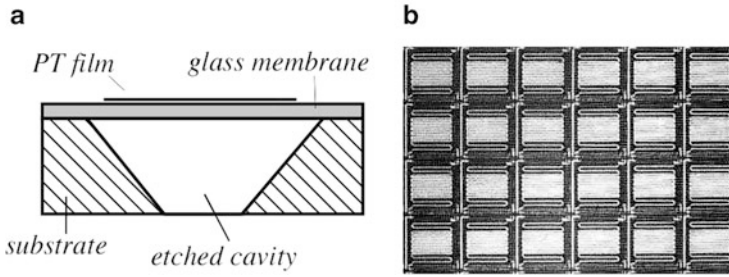
Equation (15.28) can be rewritten as:

$$\beta_V = \frac{1}{2} \varepsilon \alpha \sqrt{\frac{R_0 Z_T \Delta T}{(1 + \alpha_0 \Delta T) [1 + (\omega \tau_T)^2]}} \quad (15.31)$$

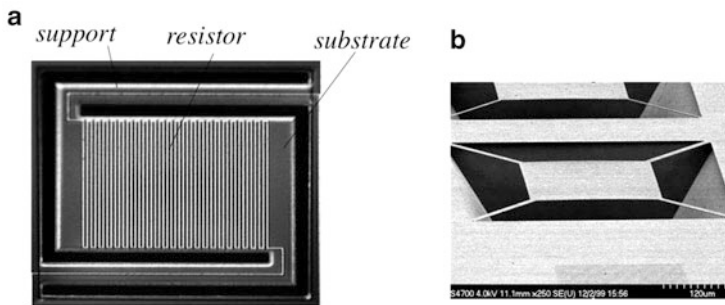
As follows from this equation, to improve the bolometer's responsivity, its electrical resistance and thermal impedance should be increased.

The bolometers were traditionally fabricated as miniature thermistors, suspended by tiny wires. Another popular method of bolometer fabrication is the use of metal film depositions [12, 13], usually of nichrome. As it follows from Eq. (15.29) one of the critical issues which always must be resolved when designing a bolometer (or any other accurate temperature sensor, for that matter) is to assure good thermal insulation of the sensing element from the supporting structure, connecting wires, and interface electronics. Otherwise, heat loss from the element may result in large errors and reduced sensitivity (see Fig. 17.1). One method to achieve this is to completely eliminate any metal conductors and to measure temperature of the bolometer by using a fiber optic technique, as it has been implemented in the E-field probe fabricated by Luxtron, Mountain View, CA [14]. In the design shown in Fig. 15.30b, a miniature heat absorbing ball is suspended at the end of an optical probe, and its temperature is measured by a fluoroptic<sup>®</sup> temperature sensor (see Sect. 17.9.1).

Modern bolometers for detecting IR radiation in the overall design are similar to thermopiles. Due to a miniature size, such sensors are called microbolometers. A microbolometer contains a frame with a stretched membrane across the frame



**Fig. 15.31** Platinum film bolometer. Glass membrane over etched cavity (a); array of bolometers (b)



**Fig. 15.32** Pattern of resistive film deposited on a substrate (a) and germanium film bolometer (b) floating over silicon cavity (courtesy of Prof. J. Shie)

opening. The membrane absorbs IR radiation and its temperature changes according to Eq. (15.20). A thermoresistive thin film material is deposited on surface of the micromachined silicon or glass membrane in a serpentine pattern as shown in Fig. 15.32a. In fact, the membrane is etched through to make suspending thermoresistors. The substrate sections where the resistor is deposited is held by an elongated support to reduce thermal conductive loss. This approach gains popularity with the increased demand for the focal-plane array sensors (FPA) that are required for thermal imaging. Figure 15.31b shows a microphotograph of an array with the microbolometers used for thermal imaging.

When an application does not need a high sensitivity and where cost of fabrication is a critical factor, a platinum film bolometer is an attractive choice. Platinum has a small, but predictive temperature coefficient of resistivity. A platinum film (having thickness of about  $500 \text{ \AA}$ ) may be deposited and photolithographically patterned over the thin glass membrane (Fig. 15.31a). The membrane is supported in the cavity etched in silicon by tiny extended leads. So the membrane plate is virtually floating over the V-grooved cavity in the Si substrate. This helps to dramatically minimize its thermal coupling with the substrate (increase the thermal resistance).

Besides platinum, many other materials may be used as temperature-sensitive resistors, for example, polysilicon, germanium (Fig. 15.32b), TaNO and others. The important issue when selecting a particular material is its compatibility with a standards CMOS process so that a full monolithic device can be fabricated on a single-silicon chip, including the interface electronic circuit. Thus, polysilicon is an attractive choice.

---

## References

1. Spillman, W. B., Jr. (1991). Optical detectors. In U. Eric (Ed.), *Fiber optic sensors* (pp. 69–97). New York, NY: John Wiley & Sons.
2. Verdeyen, J. T. (1981). *Laser electronics*. Englewood Cliffs, NJ: Prentice-Hall.
3. Golay, M. J. E. (1947). Theoretical consideration in heat and infra-red detection, with particular reference to the pneumatic detector. *Review of Scientific Instruments*, 18, 347.
4. Qian, D.-P., et al. (2013). Hardening and optimizing of the black gold thin film as the absorption layer for infrared detector. *Optics and Photonics Journal*, 3, 281–283.
5. Völklein, A., et al. (1991). High-sensitivity radiation thermopiles made of films. *Sensors and Actuators A*, 29, 87–91.
6. Schieferdecker, J., et al. (1995). Infrared thermopile sensors with high sensitivity and very low temperature coefficient. *Sensors and Actuators A*, 46–47, 422–427.
7. Meixner, H., et al. (1986). Infrared sensors based on the pyroelectric polymer polyvinylidene fluoride (PVDF). *Siemens Forsch-u Entwicl Ber Bd*, 15(3), 105–114.
8. Fraden, J. (1992). Active far infrared detectors. In J. F. Schooley (Ed.), *Temperature. Its measurement and control in science and industry* (Vol. 6, pp. 831–836). College Park, MD: American Institute of Physics.
9. Fraden, J. (1989). Radiation thermometer and method for measuring temperature. U.S. Patent No. 4,854,730, August 8, 1989.
10. Fraden, J. (1990). Active infrared motion detector and method for detecting movement, U.S. Patent No. 4,896,039, January 23, 1990.
11. Astheimer, R. W. (1984). Thermistor infrared detectors. *SPIE*, 443, 95–109.
12. Shie, J.-S., et al. (1991) Fabrication of micro-bolometer on silicon substrate by anisotropic etching technique (pp. 627–630). In *Transducers'91. International conference on solid-state sensors and actuators. Digest of technical papers*, ©IEEE, 1991.
13. Vogl, T. P., et al. (1962). Generalized theory of metal-film bolometers. *Journal of the Optical Society of America*, 52, 957–964.
14. Lentz, R. R., et al. (1989). Method and apparatus for measuring strong microwave electric field strengths. US Patent No. 4816634, 1989.

*“To understand something,  
means to derive it from quantum mechanics,  
which nobody understands.”*

-Joe Fineman

Fig. 4.41 shows a spectrum of the electromagnetic waves. On its left-hand side, there is a region of the  $\gamma$ -radiation. Then, there are the X-rays that, depending on the wavelengths, are divided into hard, soft, and ultrasoft rays. However, a spontaneous radiation from the matter not necessarily should be electromagnetic: there is the so-called *nuclear radiation*, which is emission of particles from the atomic nuclei. A spontaneous atomic decay can be of two types: the charged particles ( $\alpha$  and  $\beta$  particles, and protons), and uncharged particles, which are the neutrons. Some particles are complex like the  $\alpha$ -particles, which are the nuclei of helium atoms consisting of two neutrons, while other particles are generally simpler, like the  $\beta$ -particles which are either electrons or positrons. *Ionizing* radiations are given that name because as they pass through various media that absorbs their energy, additional ions, photons, or free radicals are created.

Certain naturally occurring elements are not stable but slowly decompose by throwing away a portion of their nucleus. This is called *radioactivity*. It was discovered in 1896 by Henry Becquerel while working on phosphorescent materials. These materials glow in the dark after exposure to light, and he thought that the glow produced in cathode ray tubes by X-rays might be connected with phosphorescence. He wrapped a photographic plate in black paper and placed various phosphorescent minerals on it. All results were negative until he used uranium ( $Z = 92$ )<sup>1</sup> salts. The result with these compounds was a deep blackening of the plate. These radiations were called Becquerel Rays.

---

<sup>1</sup> Z is the atomic number.

Besides the naturally occurring radioactivity, there are many manmade nuclei which are radioactive. These nuclei are produced in nuclear reactors, which may yield highly unstable elements. The other source of radiation is the Space from which the Earth is constantly bombarded by the particles.

Regardless of the sources or ages of radioactive substances, they decay in accordance with the same mathematical law. The law is stated in terms of number  $N$  of nuclei still undecayed, and  $dN$ , the number of nuclei which decay in a small interval  $dt$ . It was proven experimentally, that

$$dN = -\lambda N dt, \quad (16.1)$$

where  $\lambda$  is a decay constant specific for a given substance. From Eq. (16.1) it can be defined as a fraction of nuclei which decay in unit time

$$\lambda = -\frac{1}{N} \frac{dN}{dt}. \quad (16.2)$$

The SI unit of radioactivity is the *Becquerel* (Bq) which is equal to the activity of radionuclide decaying at the rate of one spontaneous transition per second. Thus, the becquerel is expressed in a unit of time:  $\text{Bq} = \text{s}^{-1}$ . To convert to the old historical unit which is the *curie*, the becquerel should be multiplied by  $3.7 \times 10^{10}$  (Table A.4).

The radiation absorbed dose is measured in *grays* (Gy). A gray is the absorbed dose when the energy per unit mass imparted to matter by ionizing radiation is 1 J/kg. That is,  $\text{Gy} = \text{J/kg}$ .

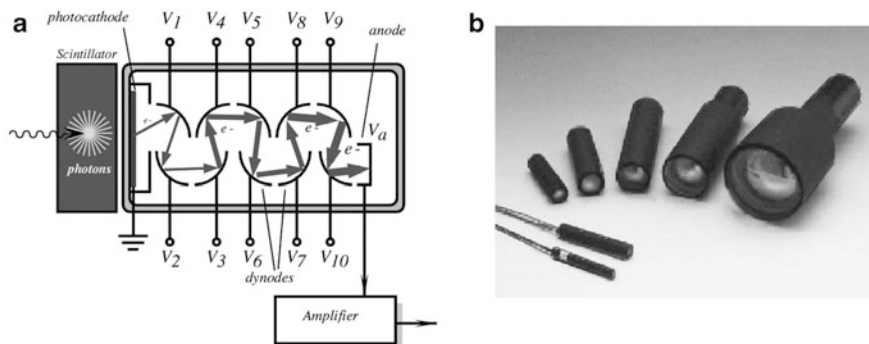
When it is required to measure exposure to X and  $\gamma$  rays, the dose of ionizing radiation is expressed in coulombs per kg, which is an exposure resulting in the production of 1 C of electric charge per 1 kg of dry air. In SI, a unit of C/kg replaces an older unit of *roentgen*.

The function of any radiation sensor depends on the manner in which the radiation interacts with the material of the detecting element. There are many excellent texts available on the subject of detecting radioactivity, for instance refs. [1, 2].

There are four general types of radiation detectors: the scintillation detectors, gaseous detectors, liquid detectors, and semiconductor detectors. Further, all detectors can be divided into two groups according to their functionality: the collision detectors and the energy detectors. The former merely detect the presence of a radioactive particle, while the latter can measure the radiative energy. That is, all detectors can be either quantitative or qualitative.

## 16.1 Scintillating Detectors

The operating principle of these detectors is based on the ability of certain materials to convert nuclear radiation into light. Thus, an optical photon detector in a combination with a scintillating material can form a radiation detector. It should



**Fig. 16.1** Scintillation detector with photomultiplier

be noted, however, that despite of a high efficiency of the conversion, the light intensity resulting from the radiation is extremely small. This demands photomultipliers to magnify signals to a detectable level.

The ideal scintillation material should possess the following properties:

1. It should convert the kinetic energy of charged particles into detectable light with a high efficiency.
2. The conversion should be linear. That is, the light produced should be proportional to the input energy over a wide dynamic range.
3. The post luminescence (the light decay time) should be short to allow fast detection.
4. The index of refraction of the material should be near that of glass to allow efficient optical coupling of the light to the photomultiplier tube.

The most widely used scintillators include the inorganic alkali halide crystals (of which sodium iodine is the favorite), and organic-based liquids and plastics. The inorganics are more sensitive, but generally slow, while organics are faster, but yield less light.

One of the major limitations of the scintillation counters is their relatively poor energy resolution. The sequence of events which leads to the detection involves many inefficient steps. Therefore, the energy required to produce one information carrier (a photoelectron) is in the order of 1000 eV or more, and the number of carriers created in a typical radiation interaction is usually no more than a few thousand. For example, the energy resolution for sodium iodine scintillators is limited to about 6 % when detecting 0.662 MeV  $\gamma$  rays, and is largely determined by the photoelectron statistical fluctuations. The only known way of reducing the statistical limit on energy resolution is to increase the number of information carriers per pulse. This can be accomplished by the use of the semiconductor detectors which are described below.

A general simplified arrangement of a scintillating sensor is shown in Fig. 16.1 in conjunction with a photomultiplier. The scintillator is attached to the front end of

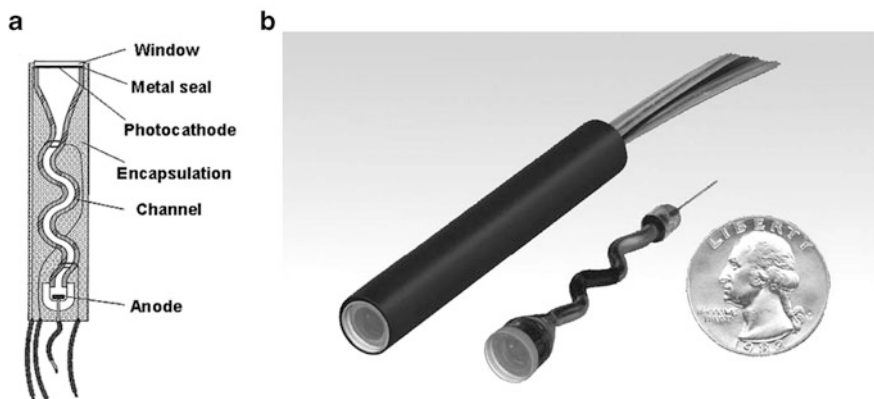
the photomultiplier (PM). The front end contains a photocathode which is maintained at a ground potential. There is a large number of special plates called *dynodes* positioned inside the PM tube in an alternating pattern, reminding shape of a “venetian blind.” Each dynode is attached to a positive voltage source in a manner that the farther the dynode from the photocathode, the higher is its positive potential. The last component in the tube is an anode, which has the highest positive potential, sometimes on the order of several thousand volts. All components of the PM are enveloped into a glass vacuum tube, which may contain some additional elements, like focusing electrodes, shields, etc.

Although the PM is called a photomultiplier, in reality it is an electron multiplier, as there are no photons, only electrons inside the PM tube during its operation. For illustration, let us assume that a  $\gamma$ -ray particle has a kinetic energy of 0.5 MeV (Mega-electron-Volt). It strikes the scintillating crystal resulting in a number of liberated photons. In a thallium-activated sodium iodine, the scintillating efficiency is about 13 %, and therefore total of  $0.5 \times 0.13 = 0.065$  MeV, or 65 keV of energy is converted into visible light with an average energy of 4 eV. Therefore, about 15,000 scintillating photons are produced per gamma pulse. This number is too small to be detected by an ordinary photodetector, and hence a multiplication effect is required before the actual detection takes place. Of 15,000 photons probably about 10,000 reach the photocathode, whose quantum efficiency is about 20 %. The photocathode serves to convert incident light photons into low-energy electrons. Therefore, the photocathode produces about 2000 electrons per pulse. Now, that number is to be multiplied in a PM. The PM tube is a linear device, that is, its gain is almost independent of the number of multiplied electrons.

Since all dynodes are at positive potentials ( $V_1 - V_{10}$ ), an electron released from the photocathode is attracted to the first dynode, liberating at impact with its surface several very low energy electrons. Thus, a multiplication effect takes place at the dynode. These electrons will be easily guided by the electrostatic field from the first to the second dynode. They strike the second dynode and produce more electrons which travel to the third dynode, and so on. The process results in an increasing number of available electrons (avalanche effect). An overall multiplication ability of a PM tube is in the order of  $10^6$ . As a result, about  $2 \times 10^9$  electrons will be available at a high voltage anode ( $V_a$ ) for production of electric current. This is a pretty strong electric current which can be easily processed by an electronic circuit. A gain of a PM tube is defined as

$$G = \alpha \delta^N, \quad (16.3)$$

where  $N$  is the number of dynodes,  $\alpha$  is the fraction of electrons collected by the PM tube,  $\delta$  is the efficiency of the dynode material, that is, the number of electrons liberated at impact. Its value ranges from 5 to 55 for a high yield dynode. The gain is sensitive to the applied high voltage, because  $\delta$  is almost a linear function of the inter-dynode voltage.



**Fig. 16.2** Channel photomultiplier: cross-sectional view (a) and external view with potted encapsulation at left and with no encapsulation at right (b). (Courtesy of PerkinElmer, Inc.)

A modern design of a photomultiplier is called the *Channel Photomultiplier* or CPM for short. It is the evolution of the classical photomultiplier tube PM. The modern CPM technology preserves the advantages of the classical PM while avoiding its disadvantages. Figure 16.2a shows a faceplate with a photocathode, the bent channel amplification structure and the anode. Like in the PM of Fig. 16.1, photons in the CPM are converted inside the photocathode into photoelectrons and accelerated in a vacuum towards the anode by an electrical field. Instead of the complicated dynode structure there is a bent thin semiconductive channel through which the electrons have to pass. Each time when electrons hit the wall of the channel, secondary electrons are emitted from the surface. At each collision, there is a multiplication of the secondary electrons resulting in an avalanche effect. Ultimately, an electron multiplication of  $10^9$  and more can be obtained. The resulting current can be read out at the anode. The CPM detector is potted with encapsulation material and is quite rugged as compared to the fragile PM. Magnetic field disturbance is negligibly small. Figure 16.2b shows images of the CPM. An important advantage of the CPM technology is its very low background noise. The term background noise refers to the measured output signal in the absence of any incident light. With classical PMs, the background noise originating from the dynode structure is generally a non-negligible part of the total background. As a result, the only effective source of background for the CPM is generated from thermal emission of the photocathode. Since the CPM is manufactured in a monolithic semiconductive channel structure, no charge-up effects might occur as known of classical PMs with isolating glass bulbs. Hence, extremely stable background conditions are observed. No sudden bursts occur. Also due to the absence of dynode noise, a very clean separation between an event created from a photo electron and electronic noise can be performed. This leads into a high stability of the signal over time.



## 16.2 Ionization Detectors

These detectors rely on the ability of some gaseous and solid materials to produce ion pairs in response to the ionization radiation. Then, positive and negative ions can be separated in an electrostatic field and measured.

Ionization happens because charged particles upon passing at a high velocity through an atom can produce sufficient electromagnetic forces, resulting in the separation of electrons, thus creating ions. Remarkably, the same particle can produce multiple ion pairs before its energy is expended. Uncharged particles (like neutrons) can produce ion pairs at collision with the nuclei.

### 16.2.1 Ionization Chambers

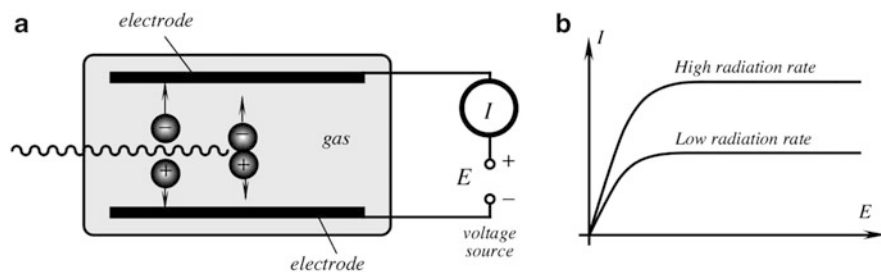
These radiation detectors are the oldest and most widely used. The ionizing particle causes ionization and excitation of gas molecules along its passing track. As a minimum, the particle must transfer an amount of energy equal to the ionization energy of the gas molecule to permit the ionization process to occur. In most gasses of interest for radiation detection, the ionization energy for the least tightly bound electron shells is between 10 and 20 eV [2]. However, there are other mechanisms by which the incident particle may lose energy within gas that do not create ions, for instance, moving gas electrons to a higher energy level without removing it. Therefore, the average energy lost by a particle per ion pair formed (called *W-value*) is always greater than the ionizing energy. The *W-value* depends on gas (Table 16.1), the type of radiation, and its energy.

In the presence of electric field, the drift of the positive and negative charges represented by the ions and electrons constitutes an electric current. In a given volume of gas, the rate of the formation of the ion pair is constant. For any small volume of gas, the rate of formation will be exactly balanced by the rate at which ion pairs are lost from the volume, either through recombination, or by diffusion or migration from the volume. If recombination is negligible and all charges are effectively collected, the steady state current is produced and it is an accurate measure of the rate of the ion pair formation. Figure 16.3a illustrates a basic structure of an ionizing chamber and the current/voltage characteristic.

A volume of gas is enclosed between the electrodes which produce an electric field. An electric current meter is attached in series with the voltage source  $E$  and

**Table 16.1** *W*-values for different gases [adapted from ref. [2]]

<i>W</i> -value (in eV/ion pair)		
Gas	Fast electrons	Alphas
A	27.0	25.9
He	32.5	31.7
N <sub>2</sub>	35.8	36.0
Air	35.0	35.2
CH <sub>4</sub>	30.2	29.0



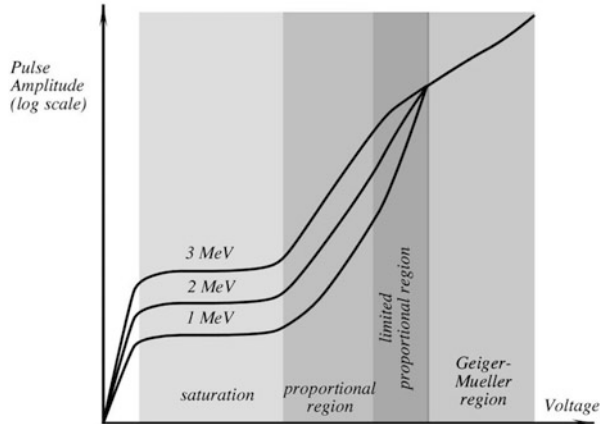
**Fig. 16.3** Simplified schematic of ionization chamber (a) and current vs. voltage characteristic (b)

the electrodes. There is no electrical conduction and no current under the no-ionization conditions. Incoming radiation produces, in the gas, positive and negative ions which are pulled by the electric field toward the corresponding electrodes forming an electric current. The current versus voltage characteristic of the chamber is shown in Fig. 16.3b. At relatively low voltages, the ion recombination rate is strong and the output current is proportional to the applied voltage, because higher voltage reduces the number of recombined ions. A sufficiently strong voltage completely suppresses all recombinations by pulling all available ions toward the electrodes, and the current becomes voltage independent. However, it still depends on the intensity of irradiation. This is the region which is called *saturation* and where the ionization chamber normally operates.

## 16.2.2 Proportional Chambers

The proportional chamber is a type of a gas-filled detector which almost always operates in a pulse mode and relies on the phenomenon of a gas multiplication. This is why these chambers are called the proportional counters. Due to gas multiplication, the output pulses are much stronger than in conventional ion chambers. These counters are generally employed in the detection and spectroscopy of low energy X-radiation and for the detection of neutrons. Contrary to the ionization chambers, the proportional counters operate at higher electric fields, which can greatly accelerate electrons that are liberated during the collision. If these electrons gain sufficient energy, they may ionize a neutral gas molecule, thus creating an additional ion pair. Hence, the process is of an avalanche type resulting in a substantial increase in the electrode current. The name for this process is *Townsend avalanche*. In the proportional counter, the avalanche process ends when the electron collides with the anode. Since in the proportional counter the electron must reach the gas ionization level, there is a threshold voltage after which the avalanche process occurs. In typical gases at atmospheric pressure, the threshold field level is on the order of  $10^6$  V/m.

**Fig. 16.4** Various operating voltages for gas-filled detectors (adapted from ref. [2])

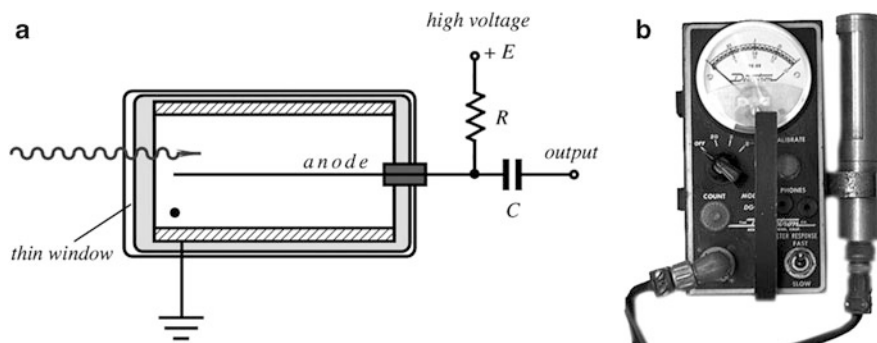


Differences between various gas counters are illustrated in Fig. 16.4. At very low voltages, the field is insufficient to prevent the recombination of ion pairs. In the saturation level, all ions are drifted to the electrodes. A further increase in voltage results in gas multiplication. Over some region of the electric field, the gas multiplication will be linear, and the collected charge will be proportional to the number of original ion pairs created during the ionization collision. An even further increase in the applied voltage can introduce nonlinear effects, which are related to the positive ions, due to their slow velocity.

### 16.2.3 Geiger–Müller (GM) Counters

The Geiger–Müller (GM) counter was invented<sup>2</sup> in 1928 and is still in use thanks to its simplicity, low cost, and ease of operation. The GM counter is different from other ion chambers by its much higher applied voltage (see Fig. 16.4). In the region of the GM operation, the output pulse amplitude does not depend on the energy of ionizing radiation and is strictly a function of the applied voltage. A GM counter is usually fabricated in form of a tube with an anode wire in the center, Fig. 16.5a. The tube is filled with a noble gas, such as helium or argon. A secondary component is usually added to the gas for the purpose of *quenching*, which is preventing of a retriggering of the counter after the detection. The retriggering may cause multiple pulses instead of the desired one. The quenching can be accomplished by several methods, among which are a short-time reduction of the high voltage applied to the tube, use of a high impedance resistor in series with the anode, and adding the

<sup>2</sup> Johannes (Hans) Wilhelm Geiger (1882–1945) was a German physicist. He is best known as the co-inventor of the GM counter and for the Geiger–Marsden experiment that discovered the atomic nucleus. He was a ‘loyal Nazi’ who unhesitatingly betrayed many of his former colleagues. Walther Müller (1905–1979) was a student of Geiger and a founder of a US company that produced tubes for the GM counters.



**Fig. 16.5** Conceptual circuit of Geiger–Müller (GM) counter. Symbol (*filled circle*) indicates gas (a) and vintage GM counter (b)

quench gas at concentrations of 5–10 %. Many organic molecules possess the proper characteristics to serve as a quench gas. Of these, ethyl alcohol and ethyl formate have proven to be the most popular.

In a typical avalanche created by a single original electron, the secondary ions are created. In addition to them, many excited gas molecules are formed. Within a few nanoseconds, these excited molecules return to their original state through the emission of energy in form of ultraviolet (UV) photons. These photons play an important role in the chain reaction occurring in the GM counter. When one of the UV-photons interacts by a photoelectric absorption in some other region of the gas, or at the cathode surface, a new electron is liberated which can subsequently migrate toward the anode, and will trigger another avalanche. In a Geiger discharge, the rapid propagation of the chain reaction leads to many avalanches which initiate at random radial and axial positions throughout the tube. Secondary ions are therefore formed throughout the cylindrical multiplying region which surrounds the anode wire. Hence, the discharge grows to envelope the entire anode wire, regardless of the position at which the primary initiating event occurred.

Once the Geiger discharge reaches a certain level, however, collective effects of all individual avalanches come into play and ultimately terminate the chain reaction. This point depends on the number of avalanches and not on the energy of the initiating particle. Thus, the GM current pulse is always of the same amplitude, which makes the GM counter just an indicator of irradiation, because all information on the ionizing energy is lost.

In the GM counter, a single particle of a sufficient energy can create about  $10^9$ – $10^{10}$  ion pairs. Because a single ion pair formed within the gas of the GM counter can trigger a full Geiger discharge, the counting efficiency for any charged particle that enters the tube is essentially 100 %. However, the GM counters are seldom used for counting neutrons because of a very low efficiency of counting. The efficiency of GM counters for  $\gamma$ -rays is higher for those tubes constructed with a cathode wall of high-Z material. For instance, bismuth ( $Z = 83$ ) cathodes have been widely used for the  $\gamma$ -detection in conjunction with gases of high atomic

numbers, such as xenon and krypton, which yield a counting efficiency up to 100 % for photon energies below about 10 keV.

A further improvement of GM counter is the so-called *wire chamber* that contains many parallel wires, arranged as a grid. A high voltage is applied to the wires with the metal casing being at a ground potential. As in the GM counter, a particle leaves a trace of ions and electrons, which drift toward the case or the nearest wire, respectively. By marking off the wires that had a pulse of current, one can see the particle's path.

### 16.2.4 Semiconductor Detectors

The best energy resolution in modern radiation detectors can be achieved in the semiconductor materials, where a comparatively large number of carriers for a given incident radiation event occurs. In these materials, the basic information carriers are *electron-hole pairs* created along the path taken by the charged particle through the detector. The charged particle can be either primary radiation, or a secondary particle. The electron-hole pairs in some respects are analogous to the ion pairs produced in the gas-filled detectors. When an external electric field is applied to the semiconductive material, the created carriers form a measurable electric current. The detectors operating on this principle are called solid-state or semiconductor diode detectors. The operating principle of these radiation detectors is the same as that of the semiconductor light detectors. It is based on the transition of electrons from one energy level to another when they gain or lose energy. For the introduction to the energy band structure in solids the reader should refer to Sect. 15.1.1.

When a charged particle passes through a semiconductor with the band structure shown in Fig. 15.1, the overall significant effect is the production of many electron-hole pairs along the track of the particle. The production process may be either direct or indirect, in that the particle produces high-energy electrons (or  $\Delta$  rays) which subsequently lose their energy in production more electron-hole pairs. Regardless of the actual mechanism involved, what is of interest to our subject is the average energy expended by the primary charged particle produces one electron-hole pair. This quantity is often called the "ionization energy." The major advantage of semiconductor detectors lies in the smallness of the ionization energy. The value of it for silicon or germanium is about 3 eV, compared with 30 eV required to create an ion pair in typical gas-filled detectors. Thus, the number of charge carriers is about ten times greater for the solid-state detectors for a given energy of a measured radiation.

To fabricate a solid-state detector, at least two contacts must be formed across a semiconductor material. For detection, the contacts are connected to the voltage source which enables carrier movement. The use of a homogeneous Ge or Si, however, would be totally impractical. The reason for that is in an excessively high leakage current caused by the material's relatively low resistivity (50 k $\Omega$  cm for silicon). The external voltage, when applied to the terminals of such a detector

may cause a current, which is 3–5 orders of magnitude greater than a minute radiation-induced electric current. Thus, the detectors are fabricated with the blocking junctions, which are reverse biased to dramatically reduce leakage current. In effect, the detector is a *semiconductor diode*, which readily conducts (has low resistivity) when its anode (*p* side of a junction) is connected to a positive terminal of a voltage source and the cathode (an *n* side of the junction) to the negative. The diode conducts very little (it has very high resistivity) when the connection is reversed, thus the name *reverse biasing* is implied. If the reverse bias voltage is made very large, in excess of the manufacturer specified limit, the reverse leakage current abruptly increases (the breakdown effect) which often may lead to a catastrophic deterioration of detecting properties or to the device destruction.

Several configurations of silicon diodes are currently produced. Among them diffused junction diodes, surface barrier diodes, ion implanted detectors, epitaxial layer detectors, and others. The diffused junction and surface barrier detectors find widespread applications for detection of  $\alpha$  particles and other short-range radiation. A good solid-state radiation detector should possess the following properties:

1. Excellent charge transport.
2. Linearity between the energy of the incident radiation and number of electron–hole pairs.
3. Absence of free charges (low leakage current).
4. Production of a maximum number of electron–hole pairs per unit of radiation.
5. High detection efficiency.
6. Fast response speed.
7. Large collection area.
8. Low cost.

When using semiconductor detectors, several factors should be seriously considered. Among them are the dead band layer of the detector and the possible radiation damage. If heavy charged particles or other weakly penetrating radiations enter the detector, there may be a significant energy loss before the particle reaches the active volume of the semiconductor. The energy can be lost in the metallic electrode and in a relatively thick silicon body immediately beneath the electrode. This thickness must be measured directly by the user if an accurate compensation is desirable. The simplest and most frequently used technique is to vary the angle of incidence of a monoenergetic charged particle radiation [2]. When the angle of incidence is zero (that is, perpendicular to the detector's surface) the energy loss in the dead layer is given by

$$\Delta E_o = \frac{dE_o}{dx} t, \quad (16.4)$$

where  $t$  is the thickness of the dead layer. The energy loss for an angle of incidence of  $\Theta$  is

$$\Delta E(\theta) = \frac{\Delta E_o}{\cos \Theta}. \quad (16.5)$$

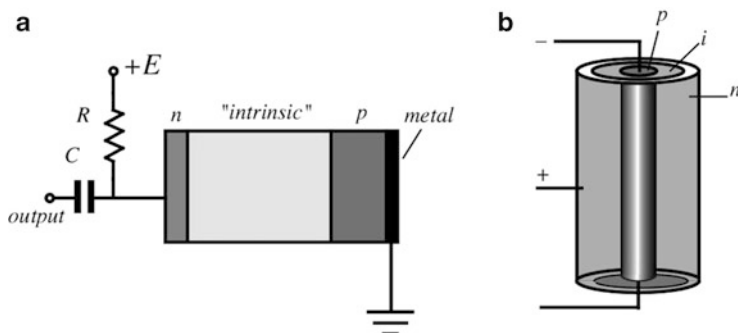
Therefore, the difference between the measured pulse height for angles of incidence of zero and  $\Theta$  is given by

$$E' = [E_o - \Delta E_o] - [E_o - \Delta E(\Theta)] = \Delta E_o \left( \frac{1}{\cos \Theta} - 1 \right). \quad (16.6)$$

If a series of measurements is made as the angle of incidence is varied, a plot of  $E'$  as a function of  $(1/\cos \Theta) - 1$  should be a straight line whose slope is equal to  $\Delta E_o$ . Using tabular data for  $dE_o/dx$  for the incident radiation, the dead layer thickness can be calculated from Eq. (16.4).

Any excessive use of the detectors may lead to some damage to the lattice of the crystalline structure, due to disruptive effects of the radiation being measured as it passes through the crystal. These effects tend to be relatively minor for lightly ionizing radiation ( $\beta$ -particles or  $\gamma$  rays), but can become quite significant under typical conditions of use for heavy particles. For example, prolonged exposure of silicon surface barrier detectors to fusion fragments will lead to a measurable increase in leakage current and a significant loss in energy resolution of the detector. With extreme radiation damage, multiple peaks may appear in the pulse height spectrum recorded for monoenergetic particles.

Mentioned above diffused junction diodes and surface barrier diodes are not quite suitable for detecting of penetrating radiation. The major limitation is in the shallow active volume of these sensors, which rarely can exceed 2–3 mm. This is not nearly enough, for instance, for a  $\gamma$ -ray spectroscopy. A practical method to make detectors for a more penetrating radiation is the so-called *ion-drifting* process. The approach consists of creating a thick region with a balanced number of donor impurities, which add either  $p$  or  $n$  properties to the material. Under ideal conditions, when the balance is perfect, the bulk material would resemble the pure (intrinsic) semiconductor without either  $p$  or  $n$  properties. However, in reality the perfect  $pn$  balance never can be achieved. In Si or Ge, the pure material with the highest possible purity tends to be of  $p$  type. To accomplish the desired compensation, the donor atoms must be added. The most practical compensation donor is lithium. The fabrication process involves a diffusing of lithium through the  $p$  crystal so that the lithium donors greatly outnumber the original acceptors, creating an  $n$  type region near the exposed surface. Then, temperature is elevated and the junction is reverse biased. This results in a slow drifting of lithium donors into the  $p$  type for the near perfect compensation of the original impurity. The process may take as long as several weeks. To preserve the achieved balance, the detector must be maintained at low temperature: 77 K for the germanium detectors. Silicon has very low ion mobility, thus the detector can be stored and operated at room temperature. However, the lower atomic number for silicon ( $Z = 14$ ) as compared with germanium ( $Z = 32$ ) means that the efficiency of silicon for detection of  $\gamma$  rays is very low and it is not widely used in the general  $\gamma$ -ray spectroscopy.



**Fig. 16.6** Lithium-drifted pin-junction detector. Structure of the detector (a); coaxial configuration of the detector (b)

**Table 16.2** Detecting properties of some semiconductive materials (adapted from ref. [2])

Material (operating temperature in K)	Z	Band gap, eV	Energy per electron-hole pair, eV
Si (300)	14	1.12	3.61
Ge (77)	32	0.74	2.98
CdTe (300)	48–52	1.47	4.43
HgI <sub>2</sub> (300)	80–53	2.13	6.5
GaAs (300)	31–33	1.43	4.2

A simplified schematic of a lithium-drifted detector is shown in Fig. 16.6a. It consists of three regions where the “intrinsic” crystal is in the middle. In order to create detectors of a larger active volume, the shape can be formed as a cylinder, Fig. 16.6b, where the active volumes of Ge up to 150 cm<sup>3</sup> can be realized. The germanium lithium-drifted detectors are designated as Ge(Li).

Regardless of the widespread popularity of the silicon and germanium detectors, they are not the ideal from certain standpoints. For instance, germanium must always be operated at cryogenic temperatures to reduce thermally generated leakage current, while silicon is not efficient for the detection of  $\gamma$  rays. There are some other semiconductors which are quite useful for detection of radiation at room temperatures. Among them are cadmium telluride (CdTe), mercuric iodine (HgI<sub>2</sub>), gallium arsenide (GaAs), bismuth trisulfide (Bi<sub>2</sub>S<sub>3</sub>), and gallium selenide (GaSe). Useful for radiation detectors properties of some semiconductive materials are given in Table 16.2.

Probably the most popular at the time of this writing is cadmium telluride which combines a relatively high Z-value (48 and 52) with a large enough band gap energy (1.47 eV) to permit room temperature operation. Crystals of high purity can be grown from CdTe to fabricate the intrinsic detector. Alternatively, chlorine doping is occasionally used to compensate for the excess of acceptors and to make the



material of a near-intrinsic type. Commercially available CdTe detectors range in size from 1 to 50 mm in diameter and can be routinely operated at temperatures up to 50 °C without an excessive increase in noise. Thus, there are two types of CdTe detectors available: the pure intrinsic type and the doped type. The former has high volume resistivity up to  $10^{10} \Omega \text{ cm}$ ; however, its energy resolution is not that great. The doped type has significantly better energy resolution; however, its lower resistivity ( $10^8 \Omega \text{ cm}$ ) leads to a higher leakage current. Besides, these detectors are prone to polarization which may significantly degrade their performance.

In the solid-state detectors, it is also possible to achieve a multiplication effect as in the gas-filled detectors. An analog of a proportional detector is called an *avalanche detector* which is useful for the monitoring of low-energy radiation. The gain of such a detector is usually in the range of several hundreds. It is achieved by creating within a semiconductor high-level electric fields.

---

### 16.3 Cloud and Bubble Chambers

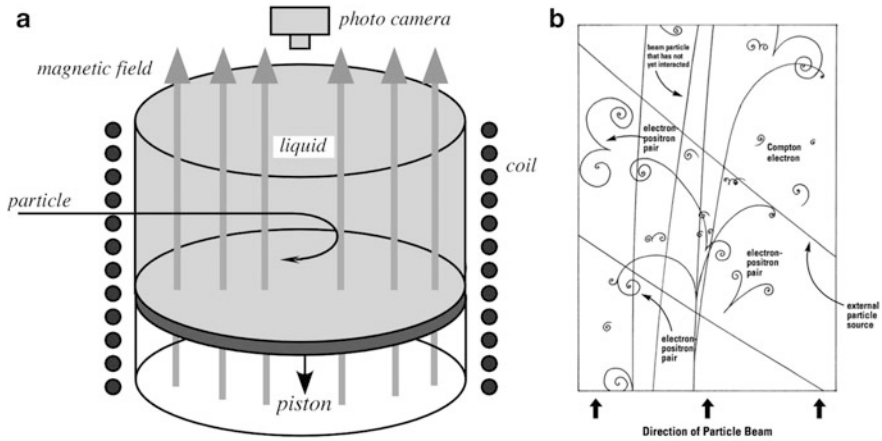
The cloud chamber, also known as the Wilson chamber,<sup>3</sup> is used for detecting particles of ionizing radiation. In its most basic form, a cloud chamber is a sealed environment containing a supercooled, supersaturated water or alcohol (e.g., methylated spirits) vapor, which is at the point of condensation. When an alpha particle or beta particle interacts with the mixture, it ionizes it. The resulting ions act as condensation nuclei, around which a mist will form. In other words, the vapor condenses into droplets when disturbed and ionized by the passage of a particle. A trail is left along the particle path because many ions are being produced along the path of the charged particle. These tracks have distinctive shapes (for example, an alpha particle's track is broad and straight, while an electron's is thinner and shows more evidence of deflection). The tracks are photographed and analyzed. When a vertical magnetic field is applied, positively and negatively charged particles will curve in opposite directions. There are different types of the cloud chambers. The expansion cloud chambers use a vacuum pump to briefly produce the right conditions for trails to form, while the diffusion type uses solid  $\text{CO}_2$  (dry ice) to cool the bottom of the chamber and produce a temperature gradient in which trails can be seen continuously.

A bubble chamber<sup>4</sup> is similar to the cloud chamber except that a liquid is used instead of vapor. Interestingly, a glass of champagne or beer is a kind of a bubble chamber where tiny bubble formations are triggered by the ionizing radiation coming from the environment and outer Space. For the physical experiments, a

---

<sup>3</sup>The cloud chamber was invented by a Scottish physicist Charles Thomas Rees Wilson (1869–1959).

<sup>4</sup>The bubble chamber was invented in 1952 by Donald A. Glaser, for which in 1960 he was awarded the Nobel Prize in Physics.



**Fig. 16.7** Bubble chamber (a) and ionizing tracks (b) (adapted from ref. [3])

bubble chamber is filled with a more prosaic and much colder liquid, such as liquid hydrogen. It is used for detecting electrically charged particles moving through it.

The bubble chamber is normally made by filling a large cylinder shown Fig. 16.7a with liquid hydrogen heated to just below its boiling point. As particles enter the chamber, a piston suddenly decreases its pressure, and the liquid enters into a superheated, metastable phase. Charged particles create an ionization track, around which the liquid vaporizes, forming microscopic bubbles. Bubble density around a track is proportional to a particle's energy loss.

Bubbles grow in size as the chamber expands, until they are large enough to be seen or photographed. Several cameras are mounted around it, allowing a three-dimensional image of an event to be captured. Bubble chambers with resolutions down to a few micrometers have been operated. A constant magnetic field is formed around the chamber by an electromagnet that causes charged particles to travel in helical paths whose radii are determined by their charge-to-mass ratios, Fig. 16.7b. Although bubble chambers were very successful in the past, they are of only limited use in current very-high-energy experiments for a variety of reasons, among which are the problem with the superheated phase that must be ready at the precise moment of collision, which complicates the detection of short-lived particles. Also, the bubble chambers are neither large nor massive enough to analyze high-energy collisions, where all products should be contained inside the detector.

## References

1. Evans, R. D. (1955). *The atomic nucleus*. New York, NY: McGraw-Hill.
2. Knoll, G. F. (1999). *Radiation detection and measurement* (3rd ed.). New York, NY: John Wiley and Sons.
3. The Elegant Universe. *Teacher's guide*. Nova ©pbs.org, 2012.

*When a scientist thinks of something, he asks, –‘Why?’  
When an engineer thinks of something, he asks, –‘Why not?’*

From prehistoric times people are aware of heat and trying to assess its intensity by measuring temperature. Perhaps the simplest, and certainly the most widely used, physical phenomenon for temperature sensing is thermal expansion. This forms the basis of the liquid-in-glass thermometers. For the electrical transduction, different methods of sensing are employed. Among them are: the resistive, thermoelectric, semiconductive, optical, acoustic, and piezoelectric detectors. For measuring temperature, the sensor shall be thermally coupled to the object. The coupling may be physical (contact) or remote (non-contact), but a thermal coupling always must be established for the sensor to produce a measurable electrical response.

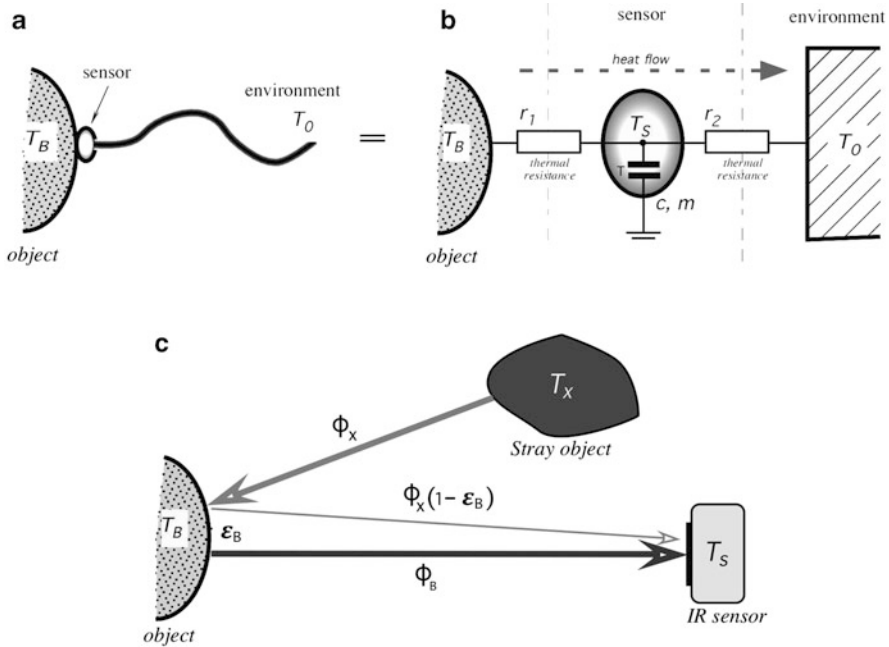
All temperature sensors can be divided into two classes: the *absolute* sensors and the *relative* sensors. An absolute temperature sensor measures temperature that is referenced to the absolute zero or any other fixed point on the absolute temperature scale, for example, 0 °C (273.15 K), 25 °C or any other arbitrarily selected reference temperature. Examples of the absolute sensors are thermistors and RTDs. A relative sensor measures a temperature difference between two objects, or thermal gradient. An example of a relative sensor is a thermocouple.

---

## 17.1 Coupling with Object

### 17.1.1 Static Heat Exchange

Taking a temperature essentially requires the transmission of a small portion of the object’s thermal energy to the sensor whose function is to convert that energy into an electrical signal. When a contact sensor (probe) is placed inside or on the object’s surface, heat conduction takes place through the boundary between the



**Fig. 17.1** Temperature sensor has thermal coupling with both object and connecting cable (a); equivalent thermal circuit for contact sensor (b); radiative coupling between object and IR noncontact sensor (c)

object and the probe. The sensing element in the probe warms up or cools down, i.e., it exchanges heat with the object. The same happens when heat is transferred by means of radiation—thermal energy in the form of infrared light is exchanged between surfaces of the sensor and the object. Any sensor, no matter how small, may disturb the measurement site and thus causes some error in temperature measurement. This applies to any methods of sensing: conductive, convective, and radiative. Thus, it's the engineering task to minimize the coupling error by an appropriate sensor design and correct measurement technique of which coupling between the sensor and object is the most critical part.

Let's discuss how coupling of a temperature sensor with an object affects accuracy? If a sensor is thermally coupled not only to the object whose temperature is measured, but also to some other items, an error is introduced. To be sure, a temperature sensor is *always* attached to something else besides the object of measurement. An example of "something else" for a contact sensor is a connecting cable shown in Fig. 17.1a that is physically attached to the object (by, e.g., clamping or adhesive). At the moment of attachment or when the object's temperature varies, the sensor's and object's temperatures are different. At any point of time, temperature of the sensor is  $T_S$ , while the object has true temperature  $T_B$  and then start coming closer to one another. The goal of a contact coupling is to bring  $T_S$  as close to  $T_B$  as possible, within the acceptable level of error.

In a practical system, one end of the cable is connected to a contact sensor, and thus is at temperature  $T_S$ . The other end is at some another temperature, for example, the ambient temperature  $T_0$  that may be quite different from  $T_S$ . The cable conducts both an electric signal and some heat from or to the sensor. Figure 17.1b shows a thermal circuit that includes the object, sensor, environment, and thermal resistances  $r_1$  and  $r_2$ . Thermal resistances should be clearly understood. A thermal resistance represents the ability of a matter to conduct thermal energy and is inversely related to thermal conductivity, that is  $r = l/\alpha$ . If an object is warmer than the environment, heat flows through the sensor in the direction indicated by an arrow.

The circuit of Fig. 17.1b resembles an electric circuit and indeed its properties can be evaluated by using the laws of electric circuits, such as Kirchhoff's<sup>1</sup> and Ohms laws. Note that a thermal capacitance of the sensor is represented by a capacitor. Assuming that we wait sufficiently long and all temperatures are settled on some steady-state levels, and also assuming that the object and environment temperatures are stable and not affected by their interconnection by the sensor, for such a steady state we may apply the law of conservation of energy. Consider that the thermal energy that flows from the object to the sensor is equal to the energy that outflows from the sensor to the environment. This allows us to write a static balance (equilibrium) equation:

$$\frac{T_B - T_S}{r_1} = \frac{T_B - T_0}{r_1 + r_2}, \quad (17.1)$$

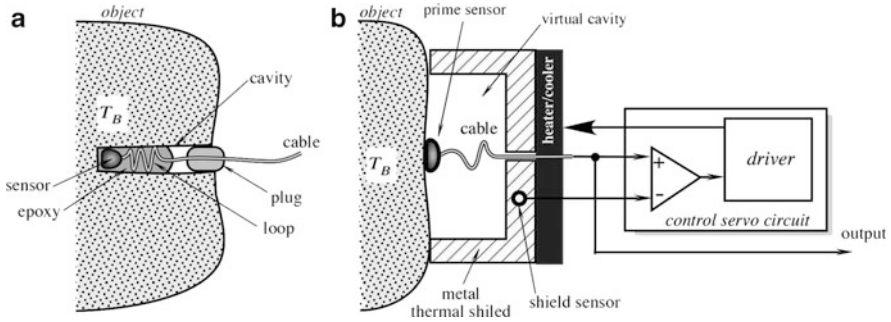
from which we derive the sensor's temperature as

$$T_S = T_B - (T_B - T_0) \frac{r_1}{r_2} = T_B - \Delta T \frac{r_1}{r_2}, \quad (17.2)$$

where  $\Delta T$  is a thermal gradient between the object and the surroundings. Let's take a closer look at Eq. (17.2). We can draw several conclusions from it. The first is that the sensor temperature  $T_S$  is different from that of the object  $T_B$ . The only exception is when the environment is at the same temperature as the object (a special case when  $\Delta T = T_B - T_0 = 0$ ). The second conclusion is that  $T_S$  will closely approach  $T_B$ , regardless of the gradient  $\Delta T$ , when the ratio  $r_1/r_2$  approaches zero. This means that for minimizing the measurement error we must improve a thermal coupling between the object and sensor ( $r_1 \rightarrow 0$ ) and thermally de-couple the sensor from surroundings as much as practical ( $r_2 \rightarrow \infty$ ). Often, it's not easy to do.

The best way of bringing  $\Delta T$  in Eq. (17.2) closer to zero is to embed the sensor into the object as shown in Fig. 17.2a. A cavity is formed inside the object where the sensor is placed, preferably with a thermal grease, epoxy or other method is used the thermally bond the sensor with the cavity walls. The cable near the sensor is shaped as a loop and also placed inside the cavity. This allows to equalize temperatures of

<sup>1</sup> Kirchhoff's law was originally conceived not for the electrical circuits but for plumbing.



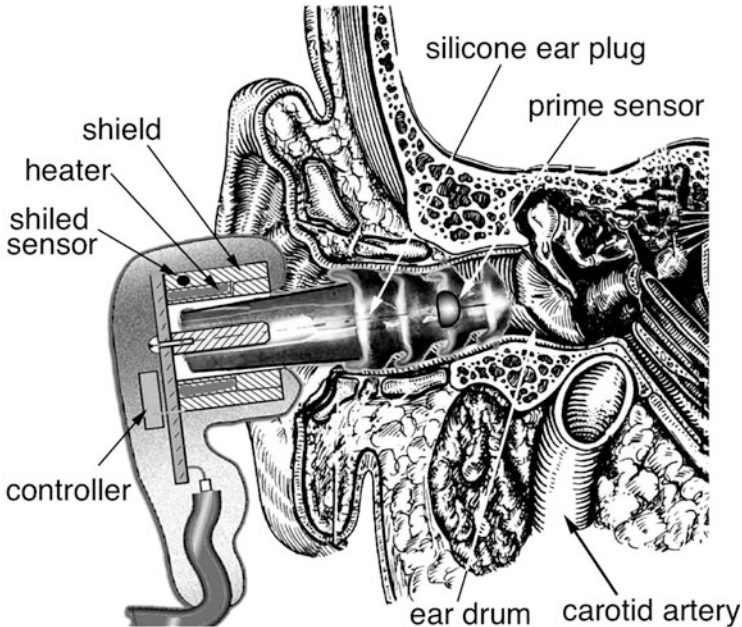
**Fig. 17.2** Embedded temperature sensor (a), surface temperature sensor with active driven thermal shield (b)

the sensor, cable, and cavity. Since the sensor and the proximal portion of the cable are not exposed to external temperatures, the measurement becomes significantly more accurate.

Forming a cavity inside an object is not always possible, thus a surface measurement becomes the only practical choice. As we just discussed, this is not a desirable arrangement for a contact measurement. Fortunately, there is a powerful technique to form a “virtual cavity” at the object’s surface [1], forcing  $\Delta T \rightarrow 0$ . To create a virtual cavity, the prime contact temperature sensor is provided with a surface thermal shield shown in Fig. 17.2b. Conceptually, this is a thermal equivalent to a driven capacitive shield (for example, see Figs. 6.4 and 7.20). The thermal driven shield is fabricated of a metal having a good thermal conductivity (e.g., aluminum) and contains two embedded components: a heater (and/or cooler) and another temperature sensor called the *shield temperature sensor*. Both sensors provide signals to the control servo-circuit that supplies power to the heater/cooler. The servo-circuit works to minimize the thermal gradient  $\Delta T$  between the prime and shield sensors. Preferably, the driven thermal shield touches the object’s surface all around the prime sensor, thus protects it from environment. The object surface and the shield form a virtual thermostatic cavity around the measurement spot. When a thermal gradient between both sensors approaches zero, the prime sensor becomes nearly totally thermally shielded from the environment. It’s very important to thermally decouple the prime sensor from the thermal shield, otherwise the circuit may become unstable.

This method was implemented in a medical body core thermometer [1] where the prime sensor was affixed to a pliant ear plug to touch the ear canal skin as shown in Fig. 17.3. The driven shield was positioned outside of the ear to cover the helix opening. Since interior of the ear canal was thermally shielded from the outside, this prime sensor provided accurate continuous non-invasive monitoring of patient’s temperature that is nearly the same as temperature of blood in the carotid artery.

A coupling problem may arise with a non-contact thermal (IR) radiation sensor (see Sect. 4.12.3). Heat exchange between the IR sensor and object is illustrated in



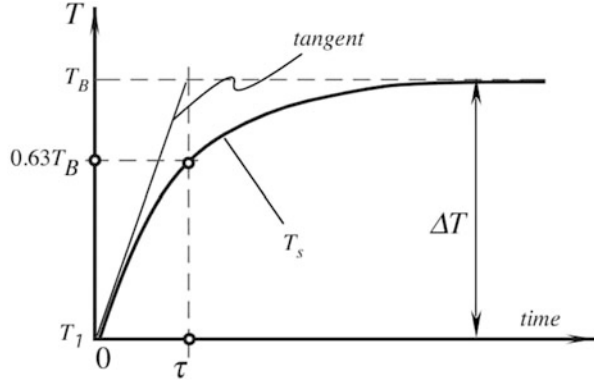
**Fig. 17.3** Sensor for noninvasive continuous monitoring of temperature through patient's ear canal. Driven shield temperature is forced to be nearly equal to temperature measured by the prime sensor that touches the ear canal skin

Fig. 17.1c. If the optical coupling between the object and sensor is not perfect, the sensor may receive undesirable thermal flux from a stray object having temperature  $T_x$ , even if that object is not within the field of view of the IR sensor. The object of measurement has temperature  $T_B$  and surface emissivity  $\epsilon_B$ , thus it emanates toward the IR sensor the useful flux  $\Phi_B$  in proportion to that emissivity. However, since  $\epsilon_B < 1$ , the object is somewhat reflective, hence a portion of the stray flux  $\Phi_x$  equal to  $\Phi_x(1 - \epsilon_B)$  will be reflected by the object toward the IR sensor. That spurious IR flux will cause error in measurement because it is added to the useful flux. Therefore, deficiency in the IR optical coupling between the object and noncontact sensor is a potential source of errors.

### 17.1.2 Dynamic Heat Exchange

Above, we evaluated the static, that is—time invariant, conditions of heat exchange between the sensor and object. Now let's consider a dynamic case when temperatures change with time. This occurs when either the object or the surrounding temperatures change or the sensor was just recently attached to the object and its temperature is not yet stabilized at the equilibrium. This equally

**Fig. 17.4** Temperature change of ideal sensor after being attached to object



relates to both the contact and noncontact IR sensors, thus below we discuss only the contact sensors.

Initially, let's consider an ideal case that requires making two assumptions: (1) a thermal resistance between the sensor and the environment is infinitely large ( $r_2 \rightarrow \infty$ ), meaning that the sensor will be perfectly thermally coupled to the object and to nothing else, and (2) the object's temperature doesn't change after the sensor is attached. In other words, the object is considered being much larger than the sensor and acts as an "infinite" heat source/sink. In other words, it has an infinitely large thermal capacity and infinitely high thermal conductivity. When the sensor is coupled to such an idealized object, the sensor's temperature profile will like the one shown in Fig. 17.4.

At a starting time  $t=0$  the temperature sensor having the initial temperature  $T_1$  comes in contact with the object having temperature  $T_B$ . After that, according to Newton's Law of Cooling the incremental amount of heat transferred from the object to the sensor is proportional to a temperature gradient between the instant sensor temperature  $T_s$  at a particular moment and a static temperature of the object  $T_B$ :

$$dQ = \alpha_1(T_B - T_s)dt, \quad (17.3)$$

where  $\alpha_1 = 1/r_1$  is the thermal conductivity of the sensor-object boundary. Note that  $T_s$  is changing while  $T_B$  is not. If the sensor has an average specific heat  $c$  and mass  $m$ , the heat absorbed by the sensor is

$$dQ = mc dT. \quad (17.4)$$

Since whatever heat is transferred the same heat is absorbed, Eqs. (17.3) and (17.4) are equal and yield the 1st-order differential equation

$$\alpha_1(T_B - T_s)dt = mc dT. \quad (17.5)$$



We denote the sensor's thermal time constant  $\tau_T$  as

$$\tau_T = \frac{mc}{\alpha_1} = mcr_1. \quad (17.6)$$

Then the differential equation takes form

$$\frac{dT}{T_B - T_s} = \frac{dt}{\tau_T} \quad (17.7)$$

This equation has a solution

$$T_s = T_B - \Delta T e^{-\frac{t}{\tau_T}} \quad (17.8)$$

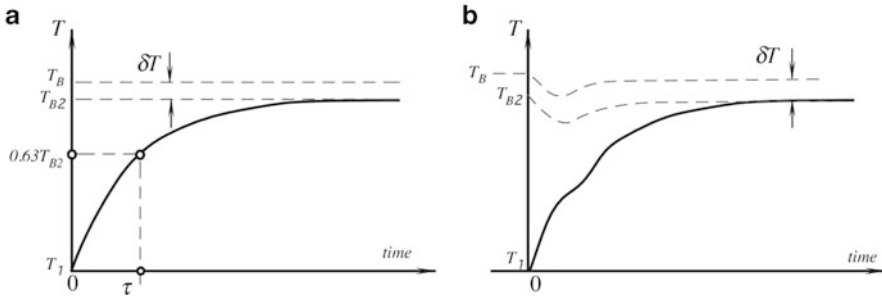
One time constant  $\tau_T$  is equal to the time required for temperature  $T$  to reach about 63.2 % of the initial gradient  $\Delta T = T_B - T_1$ . The smaller the time constant the faster the sensor responds to a change in temperature. The time constant can be minimized by reducing the size of the sensor (smaller  $m$ ) and by improving its coupling with the object (smaller  $r_1$ ).

If we wait for a long time ( $t \rightarrow \infty$ ) after attaching the sensor, Eq. (17.8) states, then the temperature of the sensor approaches temperature of the object:  $T_s = T_B$  which is the ideal equilibrium condition, so the sensor output can be used for computing the object's temperature. Theoretically, it takes infinite time to reach a perfect equilibrium between  $T_s$  and  $T_B$ —hardly anyone can wait that long! Fortunately, since only a finite accuracy is usually required, for most practical cases a quasi-equilibrium state may be considered after 5–10 time constants. For instance, after the waiting time  $t = 5\tau$  the sensor's temperature will differ from that of the object by 0.7 % of the initial gradient, while after ten time constants it will be within 0.005 %.

Now, we will study a more realistic case. Let us remove the first of the above assumptions and consider that a thermal coupling with the environment is not extremely large, that is  $r_2 \neq \infty$ . In other words, the sensor exchanges heat with other objects as well. Then the thermal time constant should be determined from

$$\tau_T = \frac{mc}{\alpha_1 + \alpha_2} = mc \frac{r_1}{1 + \frac{r_1}{r_2}} \quad (17.9)$$

and the sensor's response is shown in Fig. 17.5a. Note that now the sensor responds faster (a smaller time constant) but its temperature will never reach that of the object, no matter how long we wait. It may be higher or lower, but never equal, unless everything has the same temperature (e.g., the object, sensor and cable are inside a thermostat). Hence, due to a coupling to the environment, even at the equilibrium state, there will be a remaining thermal gradient  $\delta T$  which is the error.



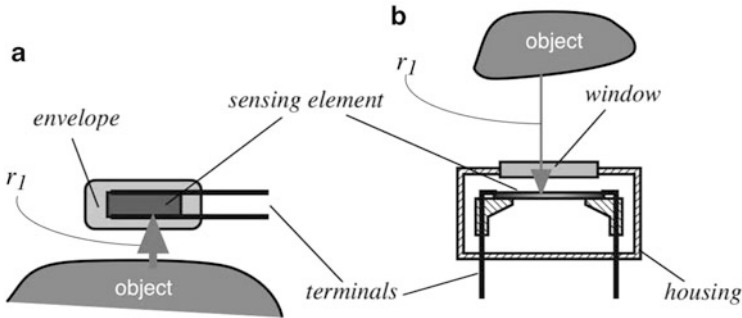
**Fig. 17.5** Temperature changes of sensor that is coupled to environment (a) and when the object has limited thermal conductivity (b)

Now let us remove the second assumption—we consider the object being not an ideal heat source or sink. This means that the object is not dramatically larger than the sensor or its thermal conductivity is relatively low. As a result of this “imperfection,” upon the attachment the sensor will disturb, at least temporarily, the measurement site. Figure 17.5b shows that upon the sensor attachment, the object’s temperature at the moment of contact deflects (cools down or warms up) and then will gradually return to some steady-state level. This causes a deviation of the sensor’s temperature profile from the ideal exponential function and a concept of a thermal time constant ( $\tau_T$ ) no longer will be applicable. The measurement site disturbance usually is difficult to evaluate or mitigate. In practice, this deviation becomes significant if one wishes to employ a predictive algorithm as described below, or a fast temperature tracking is required. The example is a medical axillary (under-the-armpit) thermometer that requires up to 3 min to equilibrate in spite of a relatively fast sensor. The problem is that the probe cools down the skin and it takes minutes for a capillary blood flow to reestablish the original temperature of the armpit.

### 17.1.3 Sensor Structure

A typical *contact* temperature sensor consists of the following components, Fig. 17.6a:

1. A sensing element—a device whose electrical properties vary in response to changes in temperature. Considering Eq. (17.9), a good sensing element should have low specific heat, small mass, strong and predictable sensitivity to temperature, and good long-term stability.
2. Terminals are the conductive pads or wires for interfacing between the sensing element and external electronic circuit. The terminals should have the lowest possible thermal conductivity and low electrical resistance (platinum is often the best compromise, yet expensive). Also, the terminals may be used for supporting



**Fig. 17.6** General structures of temperature sensors. Contact sensor (a) touches object for conductive heat transfer. IR sensor (b) exchanges heat with object through thermal radiation

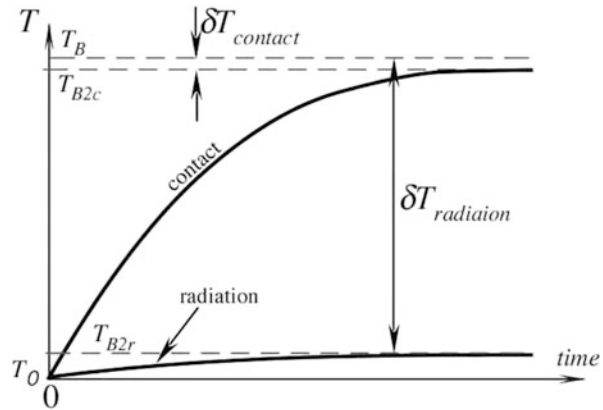
the sensing element so they should have a reasonable mechanical strength and stability.

3. A protective envelope is either a housing or coating which physically separates the sensing element from the environment, yet couples thermally. The envelope should have a low thermal resistance (high thermal conductivity), low thermal capacity, high electrical isolation properties, and be mechanically strong. It must be environmentally stable and impermeable to moisture and other compounds that may spuriously affect the sensing element.

A *noncontact* temperature sensor, Fig. 17.6b, is an optical thermal (IR) radiation sensor whose designs are covered in detail in Sect. 15.8. Like a contact sensor, it also contains a sensing element that is responsive to its own temperature. Temperature changes upon absorbing or liberating heat via radiation. The difference between the contact and noncontact is in the way of a heat transfer between the object and sensing element: in a contact sensor—it is through a thermal conduction by way of a physical contact, while in a noncontact sensor—it is through a thermal radiation (optically).

Either contact or noncontact sensors are thermally coupled to the objects through the respective thermal resistances  $r_1$ . However, that resistance for a contact sensor is much smaller than for an IR sensor. As a result, according to Eq. (17.2) the equilibrium temperatures for both sensors are quite different as shown in Fig. 17.7. While in a contact sensor the equilibrium temperature is closer to that of the object, the IR radiation sensor's temperature is much closer to temperature  $T_0$  of the instrument, resulting in a potentially very large thermal gradient  $\delta T_{\text{radiation}}$  between the sensor and object. For a contact sensor, the thermal gradient  $\delta T_{\text{contact}}$  is much smaller. In summary, for a contact sensor,  $r_1 \ll r_2$ , while for a noncontact IR sensor  $r_1 \gg r_2$ .

**Fig. 17.7** Difference in thermal responses between contact and noncontact (IR radiation) temperature sensors



### 17.1.4 Signal Processing of Sensor Response

When a temperature sensing element thermally couples to the object, its own temperature changes and the sensor generates an electric output signal. At some moment, the temperature change may come to a stop, meaning that the net heat flow through the sensor either ends or becomes steady. As long as the sensor's temperature keeps changing, the sensor either absorbs or liberates thermal energy. Thus, the sensor's response may be of two kinds: steady or changing. According to these conditions, to determine the object's temperature two basic methods of the signal processing can be employed: *equilibrium* and *predictive*. In the equilibrium method, a temperature measurement is complete when a thermal gradient between the object and sensing element inside the probe becomes steady. At that moment the sensor output represents the object temperature.

Reaching a thermal equilibrium between the object and sensor may be a slow process. For instance, a contact medical electronic thermometer measures temperature from a water bath in just 3 s (a good thermal coupling), yet it will take at least 3 min when temperature is measured axillary. In the equilibrium method, the end of measurement is determined when within a specified time interval the signal changes less than an acceptable error limit. For example, if within an interval of 1 s the temperature change is less than  $0.05\text{ }^{\circ}\text{C}$ , for a medical accuracy it may be considered steady enough.

#### 17.1.4.1 Predictive Algorithm

To shorten the measurement time, occasionally a predictive method is employed. It is based on inferring or anticipating the equilibrium temperature through computation of a variable rate of the sensor's temperature change. Thus, the end result is predicted well before a thermal equilibrium is established. A predictive method is often employed in clinical medical thermometers. It should be noted however, that the predictive method is inherently less accurate than the equilibrium method, due

to effects of noise, finite digital resolution, and assumptions about the sensor's response function.

As an illustration of a basic concept of the predictive technique, let us assume that upon contacting the object, temperature of the sensor follows an exponential function of Eq. (17.8). This is the only assumption we make. We have no prior knowledge of the starting temperature  $T_1$ , nor of the thermal time constant  $\tau_T$ . The goal of the algorithm is to compute the “would-be” equilibrium temperature  $T_B$  from several sequential measurements taken well before the actual equilibrium is achieved. According to the algorithm, we take just three sequential measurements with the equal time intervals  $t_0$  as shown in Fig. 17.8. The instantaneous sensor temperatures at these three points are  $T_x$ ,  $T_y$ , and  $T_z$ .

From Eq. (17.8), considering that each  $\Delta T$  is referred to the previously taken temperature point, values of  $T_y$  and  $T_z$  may be represented as:

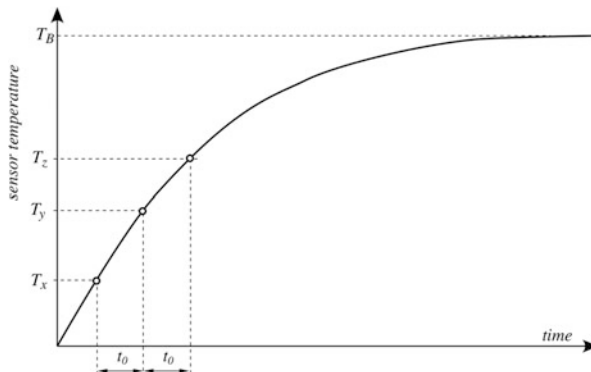
$$T_y = T_B - (T_B - T_x)e^{-\frac{t_0}{\tau_T}} \quad (17.10)$$

$$T_z = T_B - (T_B - T_y)e^{-\frac{t_0}{\tau_T}} \quad (17.11)$$

Remembering that  $\tau_T$  and  $t_0$  are constants, by manipulating Eqs. (17.10) and (17.11) we arrive at the predicted equilibrium temperature as function of three measured temperatures:

$$T_B = \frac{T_y^2 - T_x T_z}{2T_y - T_x - T_z} \quad (17.12)$$

This algorithm works and makes sense only during the temperature transient when values of the measured points ( $T_x$ ,  $T_y$  and  $T_z$ ) are not too close to one another. When the points are near the equilibrium level, the denominator in



**Fig. 17.8** Predicting equilibrium temperature from three data points taken at equal intervals

Eq. (17.12) approaches zero and the prediction error grows dramatically. The error greatly depends on noise, time delay  $t_0$ , and digital resolution of the ADC. The time delay preferably should be  $t_0 > 0.25\tau_T$ . Before applying the predictive algorithm, the sensor's signal shall be treated in a low-pass filter to limit its bandwidth to about  $0.2/\tau_T$  Hz and then converted in an ADC with at least 12-bit resolution.

This simple algorithm works well for many practical applications as long as the noise level is minimal, the object has a relatively high thermal conductivity and the sensor-object contact does not change until the last point  $T_z$  is taken.

When the sensor's response is not exponential, the equal-interval measurements (more than three points may be required) can be used for a curve fitting (see Sect. 2.1.2) to find a more realistic approximation of the temperature transient. Then, use the found approximation for predicting the equilibrium temperature.

---

## 17.2 Temperature References

When a temperature sensor is designed and fabricated, it is essential to assure its accuracy—a closeness of the response to the established standards of temperature. Thus, for calibration of any temperature sensor, a precision reference is required. Typically, a reference sensor is a very stable probe that, in turn, must be calibrated to even higher reference standard. The calibration scale depends on the selected standard. According to the *International Temperature Scale (ITS-90)*,<sup>2</sup> precision temperature instruments should be calibrated at reproducible equilibrium states of some materials. This scale designated kelvin temperatures by symbol  $T_{90}$  and the Celsius scale by  $t_{90}$ . In science and industry, the calibrating materials are certain chemical compounds (Table 17.1) whose temperature behavior at selected equilibrium states is governed by the fundamental laws of nature.

During calibration, the reference sensor is placed at a controlled pressure inside the material being at a specific physical state and the sensor response is measured. Then, it is moved to the next material and calibrated again. After being calibrated at several temperature points, the reference sensor may serve as a primary standard for calibrating other temperature sensors.

---

<sup>2</sup>The International Temperature Scale of 1990 was adopted by the *International Committee of Weights and Measures* at its meeting in 1989. This scale supersedes the International Practical Temperature Scale of 1968 (amended edition of 1975) and the 1976 Provisional Temperature Scale.

**Table 17.1** Temperature reference points

Temperature reference point description	°C
Triple point <sup>a</sup> of hydrogen	−259.34
Boiling point of normal hydrogen	−252.753
Triple point of oxygen	−218.789
Boiling point of nitrogen	−195.806
Triple point of argon	−189.352
Boiling point of oxygen	−182.962
Sublimation point of carbon dioxide	−78.476
Freezing point of mercury	−38.836
Triple point of water	0.01
Freezing point of water (water-ice mixture)	0.00
Boiling point of water	100.00
Triple point of benzoic acid	122.37
Freezing point of indium	156.634
Freezing point of tin	231.968
Freezing point of bismuth	271.442
Freezing point of cadmium	321.108
Freezing point of lead	327.502
Freezing point of zinc	419.58
Freezing point of antimony	630.755
Freezing point of aluminum	660.46
Freezing point of silver	961.93
Freezing point of gold	1064.43
Freezing point of copper	1084.88
Freezing point of nickel	1455
Freezing point of palladium	1554
Freezing point of platinum	1769

<sup>a</sup>Triple point is the equilibrium between the solid, liquid and vapor phases

## 17.3 Resistance Temperature Detectors (RTD)

Sir Humphry Davy had noted as early as 1821 that electrical resistances of various metals depend on temperature [2]. Sir William Siemens, in 1871, first outlined the use of a platinum resistance thermometer. In 1887 Hugh Callendar published a paper [3] where he described how to practically use platinum temperature sensors. The advantages of thermoresistive sensors are in simplicity of the interface circuits, sensitivity, and long-term stability. All such sensors can be divided into three groups: RTDs, semiconductors and thermistors. They belong to class of the absolute temperature sensors, that is, they can measure temperatures which are referenced to an absolute temperature scale.

The RTD term is usually pertinent to metal sensors, fabricated either in form of a wire or a thin film. Nowadays, this class also covers some semiconductor materials

with a pronounced sensitivity to temperature (e.g., germanium). Temperature dependence of resistivities of all metals and most alloys gives an opportunity to use them for temperature sensing (Table A.7). While virtually all metals can be employed for sensing, platinum is used almost exclusively because of its predictable response, long-term stability and durability. Tungsten RTDs are usually applicable for temperatures over 600 °C. All RTDs have positive temperature coefficients. Several types of them are available from various manufacturers:

1. Thin film RTDs are often fabricated of thin platinum or its alloys and deposited on a suitable substrate, such as a micromachined silicon membrane. The RTD is often made in a serpentine shape to ensure a sufficiently large length/width ratio.
2. Wire-wound RTDs, where the platinum winding is partially supported by a high temperature glass adhesive inside a ceramic tube. This construction provides a detector with the most stability for industrial and scientific applications.

Equation (4.58) gives a best fit 2nd-order approximation for platinum. In industry, it is customary to use separate approximations for the cold and hot temperatures. Callendar-van Dusen approximations represent approximations of the platinum transfer functions:

For the range from  $-200$  to  $0$  °C

$$R_t = R_0 [1 + At + Bt^2 + Ct^3(t - 100^\circ)]. \quad (17.13)$$

For the range from  $0$  to  $630$  °C it becomes identical to Eq. (4.58)

$$R_t = R_0 [1 + At + Bt^2]. \quad (17.14)$$

The constants  $A$ ,  $B$ , and  $C$  are determined by the properties of platinum used in the construction of the sensor. Alternatively, the Callendar-van Dusen approximation can be written as

$$R_t = R_0 \left\{ 1 + \alpha \left[ 1 - \delta \left( \frac{t}{100} \right) \left( \frac{t}{100} - 1 \right) - \beta \left( \frac{t}{100} \right)^3 \left( \frac{t}{100} - 1 \right) \right] \right\} \quad (17.15)$$

where  $t$  is the temperature in °C and the coefficients are related to  $A$ ,  $B$ , and  $C$  as

$$\begin{aligned} A &= \alpha \left( 1 + \frac{\delta}{100} \right) \\ B &= -\alpha\delta \times 10^{-4} \\ C &= -\alpha\beta \times 10^{-8}. \end{aligned} \quad (17.16)$$

The value of  $\delta$  is obtained by calibration at a high temperature, for example, at the freezing point of zinc (419.58 °C) and  $\beta$  is obtained while calibrating at a negative temperature.



To conform to the ITS-90, the Callendar-van Dusen approximation must be corrected. The correction is rather complex and the user should refer for details to the ITS-90. In different countries, some national specifications are applicable to RTDs. For instance, in Europe these are BS 1904: 1984; DIN 43760-1980; IEC 751:1983. In Japan it is JISC1604-1981. In the U.S.A. different companies have developed their own standards for the  $\alpha$ -values. For example, SAMA Standard RC21-4-1966 specifies  $\alpha = 0.003923 \text{ }^\circ\text{C}^{-1}$ , while in Europe DIN standard specifies  $\alpha = 0.003850 \text{ }^\circ\text{C}^{-1}$ , and the British Aircraft industry standard is  $\alpha = 0.003900 \text{ }^\circ\text{C}^{-1}$ .

Usually, RTDs are calibrated at standard points which can be reproduced in a laboratory with high accuracy (Table 17.1). Calibrating at these points allows for precise determination of approximation constants  $\alpha$  and  $\delta$ .

Typical tolerance for the wire-wound RTDs is  $\pm 10 \text{ m}\Omega$  which corresponds to about  $\pm 0.025 \text{ }^\circ\text{C}$ . Giving high requirements to accuracy, packaging isolation of the device should be seriously considered. This is especially true at higher temperatures where the resistance of isolators may drop significantly. For instance, a  $10 \text{ M}\Omega$  shunt resistor at  $550 \text{ }^\circ\text{C}$  results in the resistive error of about  $3 \text{ m}\Omega$  which corresponds to temperature error of  $-0.0075 \text{ }^\circ\text{C}$ .

---

## 17.4 Ceramic Thermistors

The term thermistor is a contraction of words *thermal* and *resistor*. The name is usually applied to metal-oxide sensors fabricated in forms of droplets, bars, cylinders, rectangular flakes, and thick films. Thermistors can be also fabricated of silicon and germanium (Sect. 17.5). A thermistor belongs to class of the absolute temperature sensors, that is, it can measure temperature that is referenced to an absolute temperature scale. All thermistors are divided into two groups: NTC (negative temperature coefficient) and PTC (positive temperature coefficient).

A conventional metal-oxide (ceramic) thermistor has a negative temperature coefficient, that is, its resistance decreases with increase in temperature. The NTC thermistor's resistance, as of any resistor, is determined by its physical dimensions and the material-specific resistivity. The relationship between the resistance and temperature is highly nonlinear (Fig. 4.18).

A ceramic thermistor (thermo-resistor) is fabricated of a crystalline material that essentially is a semiconductor. There is a similarity between a photo-resistor and a thermo-resistor in the way their resistances are modulated. A photoresistor, as described in Sect. 15.4, is characterized by the energy band gap (forbidden energies), while a thermo-resistor is characterized by the activation energy. Both the band gap and activation energy serve as the barriers for electrons, preventing them from moving, energy-wise, from the valence band to conduction band. For being able to jump through the band gap, the electron's energy shall be boosted up either by absorbing a photon or by gaining extra kinetic (thermal) energy. In more detail this process is described in Sect. 17.5.

Whenever a high accuracy is required, or the operating temperature range is wide, thermistor characteristics should not be taken directly from a manufacturer's data sheet. Typical tolerances of the nominal resistance (at 25 °C) for the mass produced thermistors may be rather wide:  $\pm 5\%$  is quite common, however for a higher price, a 1% or even better thermistors are readily available. Unless it was produced with tight tolerances, to reach a high accuracy, each low-tolerance thermistor needs to be individually calibrated over the entire operating temperature range.

Manufacturers can trim a ceramic thermistor by grinding its body to a required dimension that directly controls the nominal value of its resistance at a set temperature (typically 25 °C). This, however, increases cost. An alternative approach for an end-user is to individually calibrate thermistors. Calibration means that a thermistor has to be subjected to a precisely known temperature (a stirred water bath is often employed<sup>3</sup>) and its resistance is measured. This is repeated at several temperatures if a multi-point calibration is needed (Sect. 2.2). Naturally, a calibration is as good as the accuracy of a reference thermometer used during the calibration. To measure resistance of a thermistor, it is attached to a measurement circuit that passes through it an electric current. Depending on the required accuracy and production cost restrictions, a thermistor calibration can be based on use of one of several known approximations (models) of its temperature response.

When a thermistor is used as a temperature sensor, we assume that all its characteristics are based on the so-called zero-power resistance, meaning that electric current passing through a thermistor does not result in any noticeable temperature increase (Joule self-heating) which may affect accuracy of measurement. A static temperature increase of a thermistor due to a self-heating is governed by the following equation:

$$\Delta T_H = r \frac{N^2 V^2}{R_t} \quad (17.17)$$

where  $r$  is a thermal resistance from the thermistor to surroundings,  $V$  is the applied d.c. voltage during the resistance measurement,  $R_t$  is the resistance of a thermistor at a measured temperature, and  $N$  is a duty cycle of measurement (for example,  $N = 0.1$  means that constant voltage is applied to a thermistor only during 10% of the time.) For a continuous d.c. measurement,  $N = 1$ .

As follows from Eq. (17.17), a zero-power can be approached by selecting high resistance thermistors, increasing coupling to the object of measurement (reducing  $r$ ), and measuring its resistance at low voltages that are applied during short time intervals. Below in this chapter we will show effects of a self-heating on the thermistor response, but for now we assume that a self-heating results in a negligibly small error.

<sup>3</sup> Actually, water is not used with the unprotected thermistors. Mineral oil or Fluorinert<sup>®</sup> electronic fluid are more practical liquids.

To use a thermistor in the actual device, its transfer function (temperature dependence of a resistance) must be accurately established. Since that function is highly nonlinear (Fig. 4.18) and specific for each particular sensor, an analytical equation connecting the resistance and temperature is highly desirable. Several mathematical models of a thermistor transfer function have been proposed. It should be remembered, however, that any model is only an approximation and generally, the simpler the model the lesser accuracy should be expected. On the other hand, at a more complex model, calibration and practical use of a thermistor become more difficult. All present models are based on the experimentally established fact that logarithm of a thermistor's resistance  $R_t$  relates to its absolute temperature  $T$  by a polynomial equation:

$$\ln R_t = A_0 + \frac{A_1}{T} + \frac{A_2}{T^2} + \frac{A_3}{T^3}, \quad (17.18)$$

From this basic equation, three static transfer functions (models) have been proposed.

### 17.4.1 Simple Model

The Simple Model is the simplest approximation of the thermistor transfer function. Over a relatively narrow temperature range and accepting that some accuracy may be lost, we can eliminate two last terms in Eq. (17.18) and write it in form [4]:

$$\ln R_t \cong A + \frac{\beta}{T}, \quad (17.19)$$

where  $A$  is a dimensionless constant and  $\beta$  is another constant called the *material characteristic temperature* (in kelvin). If the thermistor's resistance  $R_0$  at the calibrating temperature  $T_0$  is known, then the resistance-temperature relationship (transfer function) is expressed as:

$$R_t = R_0 e^{\beta \left( \frac{1}{T} - \frac{1}{T_0} \right)} \quad (17.20)$$

Equation (17.20) is the most popular and widely used thermistor model. As shown in Sect. 17.5, it also can be derived from the Svante Arrhenius equation that describes the rate of chemical reactions as function of temperature. An obvious advantage of this model is a need to calibrate a thermistor at only one point ( $R_0$  at  $T_0$ ). This, however, assumes that value of  $\beta$  is already known, otherwise a two-point calibration is required to find the value of  $\beta$ :

$$\beta = \frac{\ln \frac{R_t}{R_0}}{\left( \frac{1}{T_t} - \frac{1}{T_0} \right)}, \quad (17.21)$$

where  $T_0$  and  $R_0$ ,  $T_1$  and  $R_1$  are two pairs of the corresponding temperatures and resistances at two calibrating points on the curve of Eq. (17.20). The value of  $\beta$  in this model is considered temperature independent, but may vary from part to part due to the manufacturing tolerances which typically are within  $\pm 1\%$ .

When the thermistor is used, its resistance  $R_t$  is measured. From that resistance, temperature in K can be computed from an *inverse transfer function* that is:

$$T = \left( \frac{1}{T_0} + \frac{\ln \frac{R_t}{R_0}}{\beta} \right)^{-1} \quad (17.22)$$

Error from the approximation of Eq. (17.20) is small near the calibrating temperature  $T_0$ , but increases noticeably while moving away from that point.

Beta ( $\beta$ ) specifies the thermistor curvature, but it does not directly describe its sensitivity, which is the negative temperature coefficient,  $\alpha$  that can be found by differentiating and normalizing Eq. (17.20)

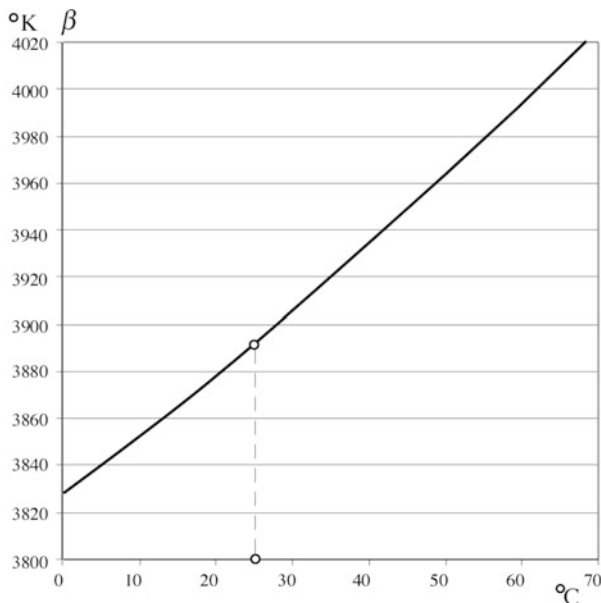
$$\alpha_r = \frac{1}{R_t} \frac{dR_t}{dT} = -\frac{\beta}{T^2} \quad (17.23)$$

It follows from Eq. (17.23) that the sensitivity depends on both: beta and temperature. Being a highly non-linear sensor, a thermistor is much more sensitive at lower temperatures while its sensitivity drops fast with a temperature increase. In the ceramic NTC thermistors, the sensitivity  $\alpha$  varies over the temperature range from  $-2\%$  (at the warmer side of the scale) to  $-8\%/^\circ\text{C}$  (at the cooler side of the scale), which implies that an NTC thermistor, albeit a nonlinear sensor, is a very sensitive device, roughly an order of magnitude more sensitive than any RTD. This is especially important for the applications where a high output signal over a relatively narrow temperature range is desirable. Examples are the medical electronic thermometers and home thermostats.

## 17.4.2 Fraden Model

In 1998, the author of this book proposed a further improvement of the Simple Model [5]. It is based on the experimental fact that in many thermistors, the characteristic temperature  $\beta$  is not a constant but rather a function of temperature (Fig. 17.9). Depending on the manufacturing process and type of a thermistor, the function may have either positive slope, as shown in the picture, or negative. Ideally,  $\beta$  should not change with temperature, but that is just a special case which can be seen only from the best manufacturers who tightly control composition of the ceramic material. In such cases, the Simple Model provides a quite accurate basis for temperature computation. But for a relatively inexpensive sensor, the Fraden model should be considered.

**Fig. 17.9** Value of  $\beta$  changes with temperature



It follows from Eqs. (17.18) and (17.19) that the thermistor material characteristic temperature  $\beta$  can be approximated as:

$$\beta = A_1 + BT + \frac{A_2}{T} + \frac{A_3}{T^2} \tag{17.24}$$

where  $A$  and  $B$  are constants. The evaluation of this equation shows that the third and fourth summands are very small as compared with the first two and for most practical cases can be removed. After elimination of two last terms, a model for  $\beta$  can be represented as a linear function of temperature:

$$\beta = A_1 + BT \tag{17.25}$$

Considering  $\beta$  a linear function of temperature, the Simple Model can be enhanced to improve its fidelity. Since  $\beta$  is no longer considered a constant, its linear approximation can be defined through at least one fixed point at some selected temperature  $T_b$  and a slope  $\gamma$ . Then, Eq. (17.25) can be written in form

$$\beta = \beta_b[1 + \gamma(T - T_b)], \tag{17.26}$$

where  $\beta_b$  is attributed to temperature  $T_b$ . A dimensionless coefficient  $\gamma$  has a meaning of a normalized change (a slope) in  $\beta$ :

$$\gamma = \left( \frac{\beta_x}{\beta_y} - 1 \right) \frac{1}{T_c - T_a}, \quad (17.27)$$

where  $\beta_x$  and  $\beta_y$  are two material characteristic temperatures at two  $T_a$  and  $T_c$  characterizing temperatures<sup>4</sup> that is equally spaced (up and down) from  $T_b$ . The value of  $\gamma$  depends on the thermistor material and the manufacturing process, so it may be considered more or less constant for a production lot of a particular type of a thermistor. Thus, it is usually sufficient to find  $\gamma$  for a lot or type of a thermistor rather than for each individual sensor.

By substituting Eq. (17.26) into Eq. (17.19) we arrive at the model of a thermistor:

$$\ln R_t \cong A + \frac{\beta_b [1 - \gamma(T_b - T)]}{T} \quad (17.28)$$

Solving Eq. (17.28) for resistance  $R_t$  yields the transfer function that represents the thermistor's resistance as function of its temperature:

$$R_t = R_0 e^{\beta_b [1 + \gamma(T - T_0)] \left( \frac{1}{T} - \frac{1}{T_0} \right)}, \quad (17.29)$$

where  $R_0$  is the resistance at calibrating temperature  $T_0$  and  $\beta_b$  is the characteristic temperature defined at two calibrating temperatures  $T_0$  and  $T_1$ . This is similar to a simple model of Eq. (17.20) with an introduction of an additional constant  $\gamma$ . Even though this model requires three points to define  $\gamma$  for a production lot, each individual thermistor still needs a two-point calibration. This makes the Fraden Model quite attractive for the low-cost high-volume applications that at the same time require higher accuracy. Note that the calibrating temperatures  $T_0$  and  $T_1$  preferably should be selected closer to the ends of the operating range, while temperature  $T_B$  should be selected near a middle of the operating range. See Table 17.2 for the practical equations. Errors in temperature computations are shown in Fig. 17.10.

### 17.4.3 Steinhart and Hart Model

Steinhart and Hart in 1968 proposed a model for the oceanographic range from  $-3$  to  $30$  °C [6] which in fact is useful for a much broader range. The model is based on Eq. (17.18) from which temperature can be calculated as:

<sup>4</sup>Note that  $\beta$  and  $T$  are in Kelvin. When temperature is indicated as  $t$ , the scale is in Celsius.

**Table 17.2** Practical use of three NTC thermistor models

	Simple model	Fraden model	Steinhart-Hart model
Maximum Error from 0 to 70 °C	±0.7 °C	±0.03 °C	±0.003 °C
Number of characterizing temperatures	2	3	0
Number of calibrating temperatures	2	2	3
Resistance-temperature dependence	$R_t = R_0 e^{\beta \left( \frac{1}{T} - \frac{1}{T_0} \right)}$	$R_t = R_0 e^{\beta_0 [1 + \gamma(T - T_0)] \left( \frac{1}{T} - \frac{1}{T_0} \right)}$	$R_t = e^{\left( A_0 + \frac{A_1}{T} + \frac{A_2}{T^2} + \frac{A_3}{T^3} \right)}$

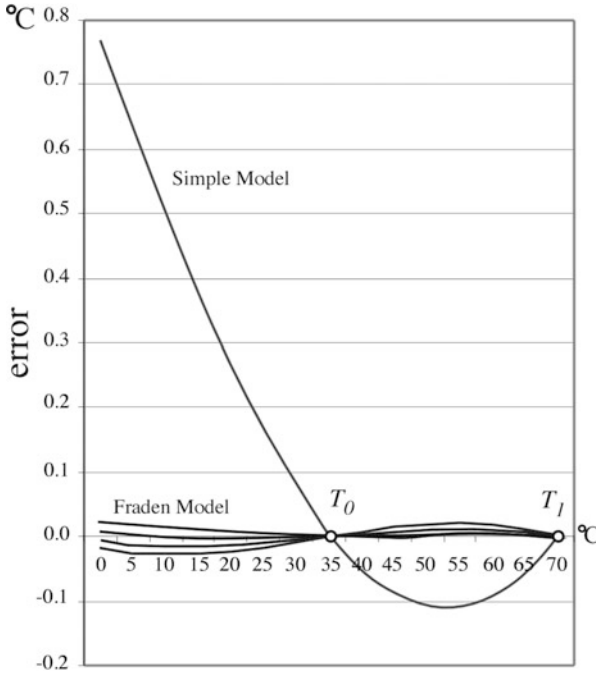
Characterizing a production lot or type of the thermistors

Characterizing points	No characterization required for a two-point calibration	$R_a, R_b, R_c$ at $T_a, T_b,$ and $T_c$ for a temperature range from $T_a$ to $T_c$ where $T_b$ is in the middle of the range	No characterization required
Characterizing factors	$\gamma = \left( \frac{\beta_x}{\beta_y} - 1 \right) \frac{1}{T_c - T_a}$ , where $\beta_x = \frac{\ln \frac{R_c}{R_0}}{\left( \frac{1}{T_c} - \frac{1}{T_0} \right)}$ , $\beta_y = \frac{\ln \frac{R_b}{R_0}}{\left( \frac{1}{T_b} - \frac{1}{T_0} \right)}$		

Calibrating an individual thermistor

Calibrating Points	$R_0$ at $T_0$ and $R_1$ at $T_1$	$R_0$ at $T_0$ and $R_1$ at $T_1$	$R_1$ at $T_1, R_2$ at $T_2,$ and $R_3$ at $T_3$
Analytic computation of temperature $T$ (in kelvin) from resistance $R$	$T = \left( \frac{1}{T_0} + \frac{\ln \frac{R}{R_0}}{\beta} \right)^{-1}$ where $\beta_m = \frac{\ln \frac{R_1}{R_0}}{\left( \frac{1}{T_1} - \frac{1}{T_0} \right)}$		
Insert resistance $R_t$ , the characterizing factors and the calibrating factors into the equation	$T = \left( \frac{1}{T_0} + \frac{\ln \frac{R_t}{R_0}}{\beta} \right)^{-1}$ where $\beta_m = \frac{\ln \frac{R_1}{R_0}}{\left( \frac{1}{T_1} - \frac{1}{T_0} \right)}$	$T = \left( \frac{1}{T_0} + \frac{\ln \frac{R_t}{R_0}}{\beta_0 [1 - \gamma(T - T_0)]} \right)^{-1}$ where $\beta_0 = \frac{\ln \frac{R_1}{R_0}}{\left( \frac{1}{T_1} - \frac{1}{T_0} \right)}$	$T = [A + B \ln R_t + C (\ln R_t)^3]^{-1}$ where $C = (G - \frac{ZH}{F}) \left[ \frac{-\frac{Z}{F} (\ln R_1^3 - \ln R_2^3)}{\ln R_1^3 - \ln R_2^3} \right]^{-1}$ $B = Z^{-1} [G - C (\ln R_1^3 - \ln R_2^3)]$ $A = T_1^{-1} - C \ln R_1^3 - B \ln R_1,$ $Z = \ln R_1 - \ln R_2, F = \ln R_1 - \ln R_3,$ $H = T_1^{-1} - T_3^{-1}, G = T_1^{-1} - T_2^{-1}$

Thermistor type or production lot should be characterized first to find *characterizing* factor (Fraden Model only). Individual thermistor is calibrated to determine *calibrating* factors. To compute temperature  $T$ , measure thermistor resistance  $R_t$  and calculate temperature with use of characterizing and calibrating factors. All temperatures are in K



**Fig. 17.10** Errors of Simple and Fraden models for a thermistor calibrated at two temperature points ( $T_0$  and  $T_1$ ) to determine  $\beta$ . Errors of Steinhart-Hart model are too small to be shown on this scale

$$T = \left[ \alpha_0 + \alpha_1 \ln R_t + \alpha_2 (\ln R_t)^2 + \alpha_3 (\ln R_t)^3 \right]^{-1} \tag{17.30}$$

Steinhart and Hart showed that the square term can be dropped without any noticeable loss in accuracy so the final equation becomes:

$$T = \left[ b_0 + b_1 \ln R_t + b_3 (\ln R_t)^3 \right]^{-1} \tag{17.31}$$

A correct use of the above equation assures accuracy in a millidegree range from 0 to 70 °C [7]. To find coefficients  $b$  for the above equation, a system of three equations should be solved after a thermistor is calibrated at three temperatures (Table 17.2). Thanks to a very close approximation, the Steinhart and Hart model became an industry standard for calibrating precision thermistors. Some manufacturers prefer to use the complete Eq. (17.30) while the others find the simplified version of Eq. (17.31) more practical. Extensive investigation of the Steinhart-Hart accuracy has demonstrated that even over a broader temperature range the approximation error does not exceed the measurement uncertainty of a couple of millidegrees [8]. Nevertheless, a practical implementation of the



approximation for the mass produced instruments is significantly limited by the need to calibrate each sensor at three or four temperature points.

A practical selection of the appropriate approximation depends on the required accuracy and cost constrains. Cost is affected by the number of temperature points at which the sensor is calibrated. Calibration of thermal sensors is time consuming and thus may be expensive. A complexity of mathematical computations is not a big deal, thanks to the computational power of modern processors. When the accuracy demand is not high, or cost is of a prime concern, or the application temperature range is narrow (typically  $\pm 5\text{--}10^\circ\text{C}$  from the calibrating temperature), the Simple Model is sufficient. The Fraden Model is preferred when a low cost and higher accuracy is a must. The Steinhart-Hart model should be used when the highest possible accuracy is required while the cost is not a major limiting factor.

To use a Simple Model, you need to know the values of  $\beta$  and the thermistor resistance  $R_0$  at a calibrating temperature  $T_0$ . To use Fraden Model, you need also know the value of  $\gamma$  which is not unique for each thermistor but is unique for a lot or a type. For the Steinhart-Hart Model you need to know three resistances at three calibrating temperatures. Table 17.2 provides equations for calibrating and computing temperatures from the thermistor resistances. Each model requires a series of computations if the equations to be resolved directly. However, in most practical cases these equations can be substituted by the look-up tables. To minimize size of a look-up table, a piece-wise linear approximation can be employed (see Sect. 2.1.6).

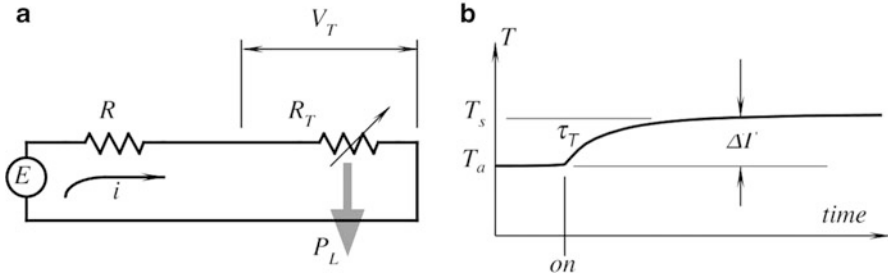
#### 17.4.4 Self-Heating Effect in NTC Thermistors

As it was mentioned above, when using an NTC thermistor, a self-heating effect should not be overlooked. A thermistor is an active type of a sensor, meaning it does require an excitation signal for its operation. The signal is usually either a d.c. or a.c. passing through the thermistor. The electric current causes a Joule heating and a subsequent increase in temperature. In some applications, this may be the source of errors since heat is coming not from the object but from inside of the sensor. However, in other applications, a self-heating is successfully employed for sensing fluid flow, thermal radiation and other stimuli.

Let us analyze the thermal effects in a thermistor, when electric power is applied. Figure 17.11a shows a voltage source  $E$  connected to a thermistor  $R_T$  through a current limiting resistor  $R$ .

When electric power  $P$  is applied to the circuit, the moment *on* in Fig. 17.11b, the rate at which energy is supplied to the thermistor must be equal the rate at which energy  $H_L$  is lost, plus the rate at which energy  $H_s$  is absorbed by the thermistor body. The absorbed energy is stored in the thermistor's thermal capacity  $C$ . The power balance equation is

$$\frac{dH}{dt} = \frac{dH_L}{dt} + \frac{dH_s}{dt}. \quad (17.32)$$



**Fig. 17.11** Current passing through thermistor causes self-heating (a); temperature of thermistor rises with thermal time constant  $\tau_T$ .  $P_L$  is thermal power lost to surroundings (b)

According to the law of conservation of energy, the rate at which thermal energy is supplied to the thermistor is equal to electric power delivered by voltage source  $E$

$$\frac{dH}{dt} = P = \frac{V_T^2}{R_T} = V_T i, \quad (17.33)$$

where  $V_T$  is the voltage drop across the thermistor. The rate at which thermal energy is lost from the thermistor to its surroundings is proportional to a temperature gradient  $\Delta T$  between the thermistor and surrounding temperature  $T_a$

$$P_L = \frac{dH_L}{dt} = \delta \Delta T = \delta(T_s - T_a), \quad (17.34)$$

where  $\delta$  is the so-called *dissipation factor* which is equivalent to the thermal conductivity from the thermistor to its surroundings. It is defined as a ratio of dissipated power and a temperature gradient (at a given surrounding temperature). The factor depends upon the sensor design, length and thickness of leadwires, thermistor material, supporting components, thermal radiation from the thermistor surface, and relative motion of medium in which the thermistor is located.

The rate of heat absorption is proportional to thermal capacity of the sensor assembly

$$\frac{dH_s}{dt} = C \frac{dT_s}{dt}. \quad (17.35)$$

This rate causes the thermistor's temperature  $T_s$  to rise above its surroundings.

Substituting Eqs. (17.34) and (17.35) into (17.33) we arrive at

$$\frac{dH}{dt} = P = Ei = \delta(T_s - T_a) + C \frac{dT_s}{dt}. \quad (17.36)$$

The above is a differential equation describing the thermal behavior of a thermistor when heat is generated by electric current. Let us solve it for a constant electric power supplied to the sensor:  $P = \text{const}$ . Then, solution of Eq. (17.36) is

$$\Delta T = (T_s - T_a) = \frac{P}{\delta} \left( 1 - e^{-\frac{\delta}{C}t} \right), \quad (17.37)$$

where  $e$  is the base of natural logarithms. The above solution indicates that upon applying electric power, the temperature of the sensor will exponentially rise above ambient. This specifies a transient condition which is characterized by a thermal time constant  $\tau_T = C\delta^{-1}$ . Here, the value of  $\delta^{-1} = r_T$  has a meaning of a thermal resistance between the sensor and its surroundings. The exponential transient is shown in Fig. 17.11b.

Upon waiting sufficiently long to reach a steady-state level  $T_s$ , the rate of change in Eq. (17.36) becomes equal to zero ( $dT_s/dt = 0$ ), then the rate of heat loss is equal to supplied power

$$\delta(T_s - T_a) = \delta\Delta T = V_T i. \quad (17.38)$$

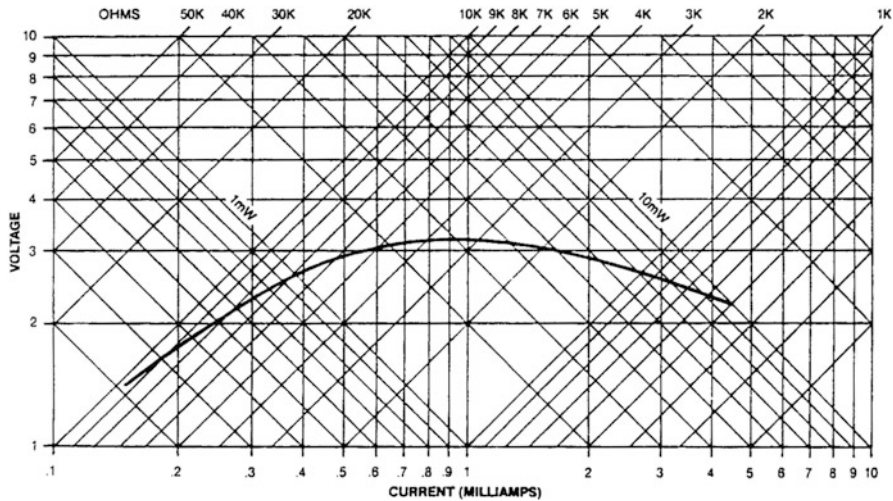
If by selecting a low-supply voltage and high resistances the current  $i$  is made very low, temperature rise,  $\Delta T$ , can be made negligibly small and the self-heating is virtually eliminated. Then, from Eq. (17.36) the temperature rate of change becomes

$$\frac{dT_s}{dt} = -\frac{\delta}{C}(T_s - T_a). \quad (17.39)$$

A solution of this differential equation is the same as of Eq. (17.8), which means that the sensor responds to heating either from the inside or outside with the same time constant  $\tau_T$ . Since the time constant depends on the thermistor coupling to the surroundings, it is usually specified for certain conditions, for instance,  $\tau_T = 1$  s at 25 °C, in still air, or 0.1 s at 25 °C, in stirred water. It should be kept in mind, that the above analysis represents a simplified model of heat flows. In reality, a thermistor response has a somewhat nonexponential shape due to a propagation of heat either from inside out or from outside through the entire thermistor body, including its protective coating.

All thermistor applications require the use of one of three basic characteristics:

1. The resistance vs. temperature characteristics of NTC thermistors are shown in Fig. 4.18. In most applications that are based on these characteristics, the self-heating effect is undesirable. Thus, the nominal resistance  $R_{T0}$  of the thermistor should be selected high and its coupling to the object should be maximized (increase in  $\delta$ ). The characteristic is primarily used for sensing and measuring temperature. Typical applications are contact electronic thermometers, thermostats and thermal breakers.



**Fig. 17.12** Voltage-current characteristic of NTC thermistor in still air at 25 °C (curvature of characteristic is due to self-heating effect)

2. The temperature versus time (or resistance versus time), are shown in Figs. 17.4 and 17.5.
3. The voltage versus current characteristic is important for applications where the self-heating effect is employed, or otherwise cannot be neglected. Power supply-loss balance is governed by Eq. (17.38). If variations in  $\delta$  are small (which is often the case) and the resistance versus temperature characteristic is known, then Eq. (17.39) can be solved for the static voltage versus current characteristic. That characteristic is usually plotted on log-log coordinates, where lines of constant resistance have a slope of +1 and lines of constant power have slope of  $-1$  (Fig. 17.12).

At very low currents (left side of Fig. 17.12), the power dissipated by the thermistor is negligibly small, and the characteristic is tangential to a line of constant resistance of the thermistor at a specified temperature. Thus, the thermistor behaves as a simple resistor, albeit temperature sensitive. That is, voltage drop  $V_T$  is proportional to current  $i$ .

As the current increases, the self-heating increases as well. This results in a decrease in the resistance of the thermistor. Since the resistance of the thermistor is no longer constant, the characteristics start to depart from the straight line. The slope of the characteristic ( $dV_T/di$ ) (the resistance at that temperature) drops with increase in current. The current increase leads to a further resistance drop that, in turn, increases the current. Eventually, current will reach its maximum value  $i_p$  at a voltage maximum value  $V_p$ . It should be noted that, at this point, a resistance of the thermistor is zero. Further increase in current  $i_p$  will result in continuing decrease in the slope, which means that the resistance has a negative value (right side of Fig. 17.12).

An even further increase in current will produce another reduction of resistance, where leadwire resistance becomes a contributing factor. A thermistor should never be operated under such conditions. A thermistor manufacturer usually specifies the maximum power rating for thermistors.

According to Eq. (17.38), self-heating thermistors can be used to measure variations in  $\delta$ ,  $\Delta T$ , or  $V_T$ . The applications where  $\delta$  vary, include vacuum manometers (Pirani gauges), anemometers, flow meters, fluid level sensors, etc. Applications where  $\Delta T$  is the stimulus include microwave power meters. The applications where  $V_T$  varies include some electronic circuits: automatic gain control, voltage regulation, volume limiting, etc.

### 17.4.5 Ceramic PTC Thermistors

All metals possess *positive temperature coefficients* (PTC). Their temperature coefficients of resistivity (TCR) are quite low (Table A.7) thus many of them are not very useful for temperature sensing that requires high sensitivity. The RTDs, as described above, have small positive temperature coefficients. In contrast, the ceramic PTC materials in certain and relatively narrow temperature ranges are characterized by very large temperature dependences.

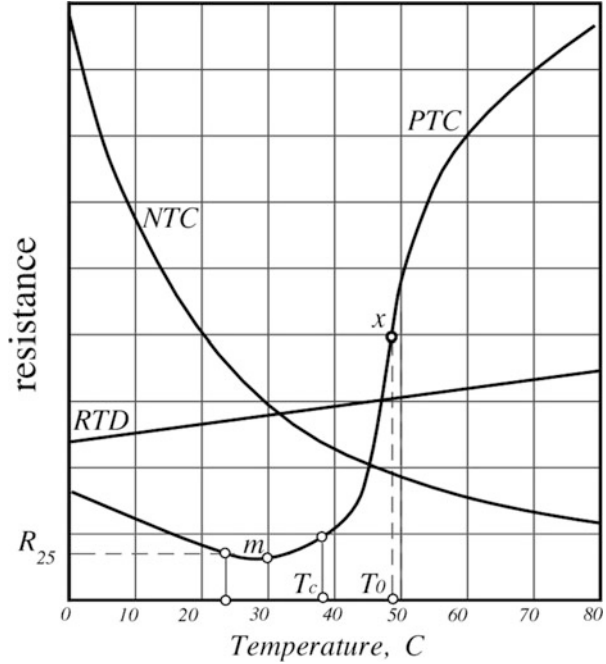
A PTC thermistors are fabricated of polycrystalline ceramic substances, where the base compounds, usually barium titanate or solid solutions of barium and strontium titanate (highly resistive materials), are made semiconductive by the addition of dopants [9]. Above the Curie temperature of a composite material, the ferroelectric properties change rapidly resulting in a rise in resistance, often several orders of magnitude. A typical transfer function curve for a ceramic PTC thermistor is shown in Fig. 17.13 in comparison with the NTC and platinum RTD responses. The shape of the curve does not lend itself to an easy mathematical approximation, therefore, manufacturers usually specify the PTC thermistors by a set of numbers:

1. Zero power resistance,  $R_{25}$ , at 25 °C, where self-heating is negligibly small.
2. Minimum resistance  $R_m$  is the value on the curve where thermistor changes its TCR from positive to negative value (point  $m$ ).
3. Transition temperature  $T_\tau$  is the temperature where resistance begins to change rapidly. It coincides approximately with the Curie point of the material. A typical range for the transition temperatures is from  $-30$  to  $+160$  °C.
4. TCR is defined in a standard form

$$\alpha = \frac{1}{R} \frac{\Delta R}{\Delta T}. \quad (17.40)$$

The coefficient changes very significantly with temperature and often is specified at point  $x$ , that is, at its highest value, which may be as large as  $2/^\circ\text{C}$ , meaning the change in resistance is 200 % per °C;

**Fig. 17.13** Transfer functions of PTC thermistor as compared with NTC thermistors and RTD



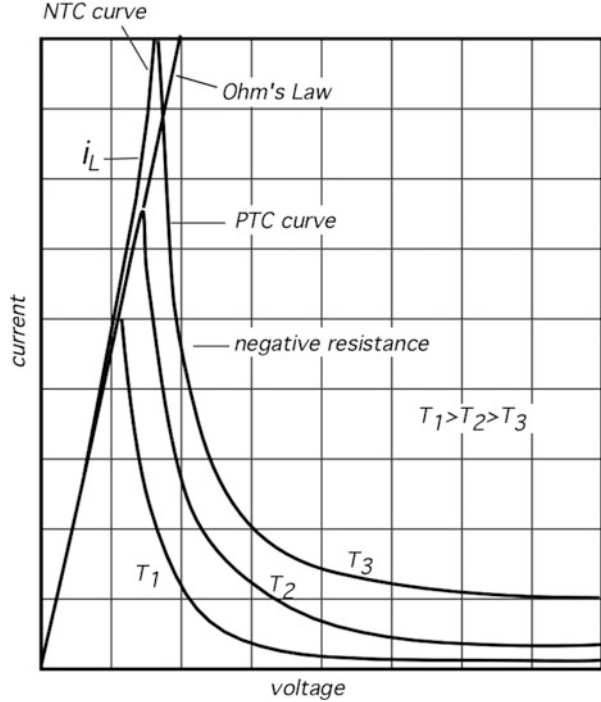
5. Maximum voltage  $E_{\max}$  is the highest value that the thermistor can withstand at any temperature.
6. Thermal characteristics are specified by a thermal capacity, a dissipation constant  $\delta$  (specified under given conditions of coupling to the environment) and a thermal time constant (defines speed response under specified conditions).

It is important to understand that for the PTC thermistors two factors play a key role: environmental temperature and a self-heating effect. Either one of these two factors shifts the thermistor's operating point.

The temperature sensitivity of a PTC thermistor is reflected in a volt-ampere characteristic of Fig. 17.14. A regular resistor with the near zero TCR, according to Ohm's law has a linear characteristic. An NTC thermistor has a positive curvature of the volt-ampere dependence. An implication of the negative TCR is that if such a thermistor is connected to a hard voltage source,<sup>5</sup> a self-heating due to Joule heat dissipation will result in resistance reduction. In turn, that will lead to further increase in current and more heating. If a heat outflow from the NTC thermistor is restricted, a self-heating may eventually cause overheating and a catastrophic destruction of the device.

<sup>5</sup> A hard voltage source means any voltage source having a near zero output resistance and capable of delivering unlimited current without change in voltage.

**Fig. 17.14** Volt-ampere characteristic of a PTC thermistor

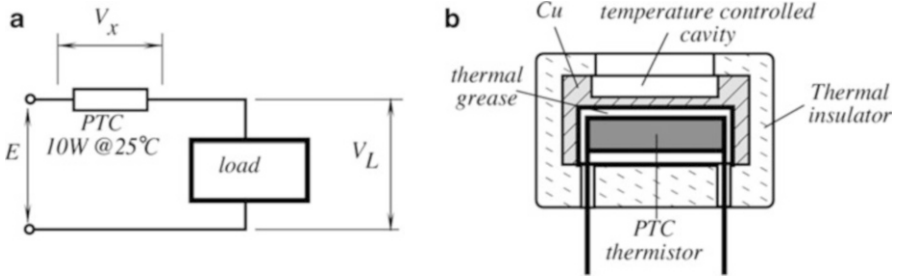


However, thanks to positive TCRs, metals do not overheat when connected to hard voltage sources and behave as self-limiting devices. For instance, a filament in an incandescent lamp does not burn out because the increase in its temperature results in increase in resistance which limits current. This self-limiting (self-regulating) effect is substantially enhanced in PTC thermistors. A shape of the volt-ampere characteristic indicates that in a relatively narrow temperature range the PTC thermistor possesses a negative resistance, that is:

$$R_x = - \frac{dV_x}{di} \tag{17.41}$$

This results in the creation of an internal negative feedback that makes this device a self-regulating thermostat. In the region of a negative resistance, any increase in voltage across the thermistor results in heat production which, in turn, increases the resistance and reduces heat production. As a result, the self-heating effect in a PTC thermistor produces enough heat to balance the heat loss on such a level that it maintains the device's temperature on a constant level  $T_0$  (Fig. 17.13). That temperature corresponds to point  $x$  where tangent to the curve has the highest value.

It should be noted that PTC thermistors are much more efficient when  $T_0$  is relatively high (over 100 °C) and their efficiency (the slope of the  $R-T$  curve near point  $x$ ) drops significantly at lower temperatures. By their very nature, PTC



**Fig. 17.15** Applications of PTC thermistors. Current limiting circuit (a); mini-thermostat (b)

thermistors are useful in the temperature range that is substantially higher than the operating ambient temperature.

There are numerous applications where the self-regulating effect of a PTC thermistor may be quite useful. We briefly mention four of them.

1. Circuit protection. A PTC thermistor may operate as a nondestructible (resettable) fuse in electric circuits, sensing excessive currents. Figure 17.15a shows a PTC thermistor connected in series with a power supply voltage  $E$  feeding the load with current  $i$ . A resistance of the PTC thermistor at room temperature is quite low (typically from 10 to 140  $\Omega$ ). Current  $i$  develops voltage  $V_L$  across the load and voltage  $V_x$  across the thermistor. It is assumed that  $V_L \gg V_x$ . Power dissipated by the thermistor  $P = V_x i$ , is lost to the surroundings and the thermistor's temperature is raised above ambient by a relatively small value. Whenever either ambient temperature becomes too hot, or load current increases dramatically (for instance, due to internal failure in the load), the heat dissipated by the thermistor elevates its temperature to a  $T_\tau$  region where its resistance starts increasing. This limits further current increase. Under the shorted-load conditions,  $V_x = E$ , current  $i$  drops to its minimal level. This will be maintained until normal resistance of the load is restored and, it is said, that the fuse resets itself. It is important to assure that  $E < 0.9E_{\max}$ , otherwise a catastrophic destruction of the thermistor may occur.
2. A miniature self-heating thermostat, Fig. 17.15b, for the microelectronic, biomedical, chemical, and other suitable applications can be designed with a single PTC thermistor. Its transition temperature must be appropriately selected. A thermostat consists of a dish, which is thermally insulated from the environment and thermally coupled to the thermistor. Thermal grease is recommended to eliminate a dry contact. The terminals of the thermistor are connected to a voltage source whose value may be estimated from the following formula:

$$E \geq 2\sqrt{\delta(T_\tau - T_a)R_{25}}, \quad (17.42)$$

where  $\delta$  is the heat dissipation constant which depends on thermal coupling to the environment and  $T_a$  is the ambient temperature. The thermostat's set point is



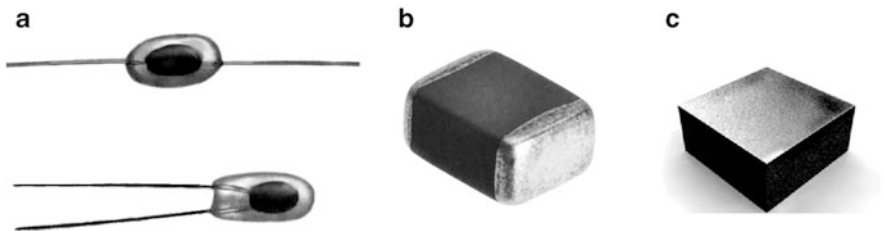
determined by the physical properties of the PTC ceramic material (Curie temperature) and due to internal thermal feedback, the device reliably operates within a relatively large range of the power supply voltages and ambient temperatures. Naturally, ambient temperature must be always less than  $T_{\tau}$ .

3. Time delay circuits can be created with the PTC thermistors thanks to a relatively long transition time between the application of electric power in its heating to a low resistance point.
4. Flowmeter and liquid level detectors that operate on principle of heat dissipation (thermo-anemometers as described in Sect. 12.3) can be made very simply with the PTC thermistors.

### 17.4.6 Fabrication

Generally, NTC ceramic thermistors can be classified into three major groups depending upon the method by which they are fabricated. The first group consists of bead-type thermistors. The beads may be bare, or coated with glass (Fig. 17.16), epoxy, or encapsulated into a metal jacket. Many of these beads have platinum alloy lead-wires, which are sintered into the ceramic body. The platinum is selected primarily because it combines a good electrical conductivity with a not-so-good thermal conductivity. When fabricated, a small portion of mixed metal oxide with a suitable binder is placed onto parallel lead-wires, which are under slight tension. After the mixture has been allowed to dry, or has been partly sintered, the strand of beads is removed from the supporting fixture and placed for the final sintering into a tubular furnace. The metal oxide shrinks onto the leadwires during this firing process and forms an intimate electrical bond. Then, the beads are individually cut from the strand, and given an appropriate coating.

Another type of a thermistor is a chip thermistor with surface contacts for the leadwires or direct soldering onto a circuit board. Usually, the chips are fabricated by a tape casting process, with subsequent screen-printing, spraying, painting or vacuum metallization of the surface electrodes. The chips are either bladed or cut into desired geometry. If desirable, the chips can be ground to meet the required



**Fig. 17.16** Glass coated axial and radial bead thermistors (a); surface mounted thermistor (b) and top-bottom uncoated chip thermistor (c)

tolerances. The chips are given two electrodes either axially or top-bottom. Presently, many thermistor chips are fabricated in standard forms (0201, 0402, 0603, and 0805 in the U.S. or 0603, 1005, 1608 and 2012—metric) for the surface-mounted assemblies on circuit boards.

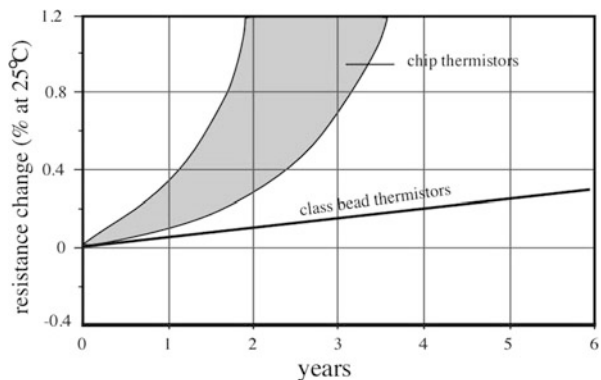
The third type of thermistors is fabricated by the depositing of semiconductive materials on a suitable substrate, such as glass, alumina, silicon, etc. These thermistors are preferable for integrated sensors and for a special class of thermal infrared detectors. A typical method of fabrication is silk-screening (see below).

Among the metallized surface contact thermistors, flakes and uncoated chips are the least stable. A moderate stability may be obtained by epoxy coating. The bead type with leadwires sintered into the ceramic body permit operation at higher temperatures, up to 550 °C. The metallized surface contact thermistors usually are rated up to 150 °C. Whenever a fast response time is required, bead thermistors are preferable: however, they are more expensive than the chip type. Besides, the bead thermistors are more difficult to trim to a desired nominal value. Trimming is usually performed by mechanical grinding of a thermistor at a selected temperature (usually 25 °C) to change its geometry and thus to bring its resistance to a specified value.

A thermistor can be produced in a process similar to making conventional thick-film resistors. The process involves screen-printing of conductive ink on a ceramic substrate. The ink for printing contains a powder with the thermistor characteristics, glass powder and organic binder. The thermistor powder is composed of oxides of Mn, Co, Ni, oxides of some noble metals such as Ru and other materials [10]. After printing, the thermistors fired in a furnace (sintered), then contact electrodes are printed at the edges of the thermistor pattern and fired again. Then, the substrates are cut into individual thermistors. Currently, high-quality thermistor inks (pastes) are commercially available from DuPont. Examples are pastes NTC40 and NTC50. The sensitivity  $\alpha$  for different pastes range from 0.2 to 3.7 % [11].

While using the NTC thermistors, one must not overlook possible sources of error. One of them is aging, which for the inexpensive sensors may be as large as +1 %/year. Figure 17.17 shows typical percentage changes in resistance values for

**Fig. 17.17** Long term stability of thermistors



the epoxy encapsulated chip thermistors as compared with the sintered glass encapsulated thermistors. A good environmental protection and pre-aging is a powerful method of sensor characteristic stabilizing. During pre-aging, the thermistor is maintained at +300 °C for at least 700 h. For a better protection, it may be further encapsulated into a stainless steel jacket and potted with epoxy. After pre-aging and encapsulation in glass and then into a stainless steel tube, a thermistor may have a drift as low as few millidegree per year.

## 17.5 Silicon and Germanium Thermistors

High-quality NTC thermistors can be successfully fabricated from monocrystalline or polycrystalline germanium or silicon [12, 13]. These thermistors have several advantages, among which their high sensitivity, tight manufacturing tolerances, small sizes, low cost, and ability to operate at cryogenic and high temperatures—from as low as 1 mK to as high as 500 °C. The discrete Si and Ge thermistors were developed by AdSem, Inc. ([www.adsem.com](http://www.adsem.com)) for a broad range of applications.

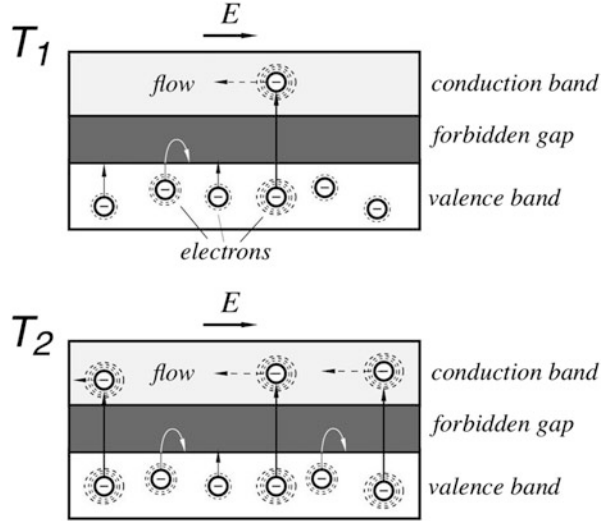
For operation at higher temperatures, thanks to use of the well developed standard semiconductor processes, the Si and Ge thermistors can be produced with tight tolerances and therefore do not require individual calibration in the temperature ranges from 0 to 500 °C (Si) and from –20 to 300 °C (Ge). Table 17.3 illustrates some characteristics of the discrete thermistors when operating at non-cryogenic temperatures. Since they are produced from a standard Si or Ge wafer, they can be combined in the same chip with other MEMS sensors, like pressure, humidity, acceleration, and many others.

Temperature dependence of resistance in semiconductors is function of the so-called *activation energy*. The term originally was proposed in 1889 by the Swedish scientist Svante Arrhenius to specify the minimum energy required to start a chemical reaction. The Arrhenius equation defines the rate of a chemical reaction as:

**Table 17.3** Typical characteristics of semiconductor higher temperature NTC thermistors (courtesy of AdSem, Inc.)

Parameter	Silicon	Germanium
Minimum dimensions (mm)	0.1 × 0.1 × 0.1	0.1 × 0.1 × 0.1
Operating temperatures (°C)	–10 to +500	–200 to +300
Beta at 25 °C (K)	6600	4700
Resistance range (Ohm) (for sizes 1 × 1 × 0.25 mm)	1 Ω to 5 MΩ	1 Ω to 500 kΩ
Tolerances	0 to +500 °C: ±0.1 °C 25 to +200 °C: ±0.05 °C	–40 to +25 °C: ±0.2 °C 25 to +300 °C: ±0.05 °C

**Fig. 17.18** At lower temperature  $T_1$  few electrons can jump the forbidden energy gap and resistance of material is high. At warmer temperature  $T_2$ , probability of jumping gap is higher and resistance is lower



$$k = Ae^{-\frac{E_a}{k_B T}} \quad (17.43)$$

where  $k_B$  is the Boltzmann constant,  $T$  is the absolute temperature,  $E_a$  is the activation energy of a reagent, and  $A$  is a constant. For the non-cryogenic temperatures, the same idea can be used for describing a minimum thermal energy that would be required to move an electron through the energy band gap of a semiconductor into the conduction band and, as a result, to change resistance of a semiconductor. Each semiconductor is characterized by its own activation energy  $E_a$ . The probability to excite a free carrier in a semiconductor due to a thermal agitation can be similarly expressed as:

$$P = P_0 e^{-\frac{E_a}{k_B T}} \quad (17.44)$$

This probability of a thermal excitation is translated into a thermally induced conductivity of a semiconductor. The higher probability of the electron excitation the smaller resistance. The sensing process is similar to a photoeffect that was described in Sect. 15.1.1 (see Fig. 15.1). Unlike a photo-resistor, an electron in a thermistor gets extra kinetic energy for jumping through the energy gap from a thermal agitation, rather than from absorption of a photon. Figure 17.18 illustrates a concept of a thermal effect in a semiconductor.

Any thermistor is a crystalline material, fabricated either of a special ceramic as described in Sect. 17.4 or from a Si or Ge wafer. The activation energy of a crystalline material in a simplified form can be considered as an equivalent to the gap of forbidden energies in the photoeffect. In a semiconductive crystalline material, most of the electrons have lower energies in the valence energy band, with a smaller number being in the conduction band. The valence band electrons are mostly bound in the crystal, while the conduction electrons are free to move through

the material, creating an electric current. Thus, resistivity of the material depends on number of electrons in the conduction band. When external electric field  $E$  is applied, electrons flow, making a current.

If temperature of the material is low ( $T_1$ ), the probability, Eq. (17.44), of an electron to have a sufficient energy for jumping the gap of forbidden energies is low.<sup>6</sup> Thermal agitations of the particles are statistically described by the Plank's Law, Eq. (4.129), where the most probable temperature is defined by the Wien's Law, Eq. (4.130). Slow vibrating ("colder") electrons either cannot dislodge from the crystal and enter the energy gap or, even if they can, they are turned back to the valence band. Few "hot" electrons jump the energy gap and participate in the electronic flow. The negatively charged electrons that are lost from the valence band, create holes—virtual positive charges that can contribute to electric current. A low number of the charge carriers (negative and positive) define a low conductivity (higher material resistance).

At a higher temperature  $T_2$ , more electrons are "hotter" and thus the probability of them to cross the energy gap is higher. As a result, a larger number of the electrons participate in the flow, resulting in a higher current and correspondingly—in lower resistance of the material.

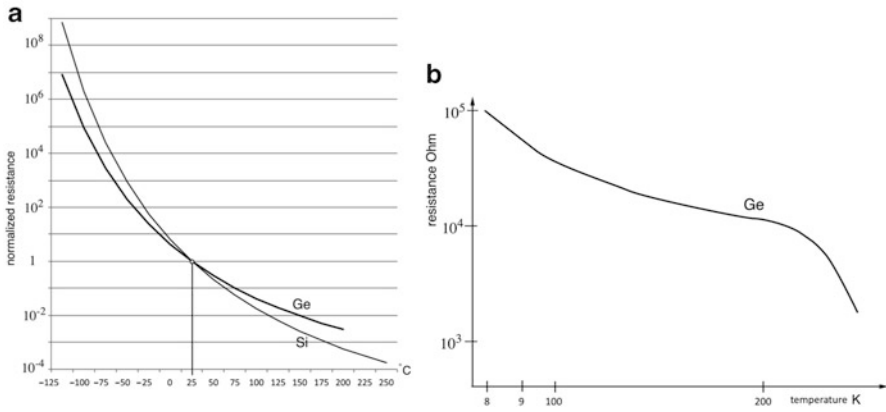
Remembering that the electrical resistance of a material is reciprocal of its conductance, the thermally related probability of crossing the energy gap defines the material resistance, and after simple mathematical manipulations of Eq. (17.44), the normalized resistance of a Ge or Si thermistor can be expressed as:

$$r = \frac{R(T)}{R_0} = e^{\frac{E_g}{k_B} \left( \frac{1}{T} - \frac{1}{T_0} \right)} = e^{\beta \left( \frac{1}{T} - \frac{1}{T_0} \right)}, \quad (17.45)$$

where  $\beta$  is a characteristic temperature of the semiconductor and  $R_0$  is the nominal resistance at a selected temperature  $T_0$ . The nominal resistance depends on the semiconductor type, its processing impurities and the sensor geometry. Note that Eq. (17.45) is the same as Eq. (17.20), meaning that the ceramic as well as Si and Ge thermistors are governed by the same law, where the activation energy defines the characteristic temperature and thus the sensitivity  $\alpha_r$ —see Eq. (17.23).

Figure 17.19a shows transfer functions of the Si and Ge thermistors for the non-cryogenic temperatures. A significant advantage of these thermistors is that they can be used also at the cryogenic range. During manufacturing, a dislocation doping [14] and doping by "hot" neutrons techniques [15] in combination with a regular impurity doping allows controlling the characteristics of Si and Ge to tailor them to specific temperature ranges. The cryogenic NTC thermistors with high interchangeability can be produced for the ranges 77–300, 20–300 and 1–300 K. There is a possibility of fabricating Si and Ge thermistors for the ultra-low range below 1 K (down to as low as 900  $\mu$ K).

<sup>6</sup>This mechanism is different for the cryogenic temperatures.



**Fig. 17.19** Static transfer functions of Si and Ge NTC thermistors at warmer temperatures (a) and of Ge at cryogenic temperatures (b)

To cover a super-wide operating temperature range (from a few mK up to 750 K) two Si thermistors can be joined in a single packaging: one thermistor for the cryogenic range, while the other—for higher temperatures. Besides, the Ge and Si thermistors are hardened for the operation at strong magnetic fields (up to 5 T) at liquid He temperatures, and have the increased radiation hardness for gamma-radiation and fast neutrons. As an example, Fig. 17.19b shows a temperature response of the Ge cryogenic thermistor having the chip size of  $0.25 \times 0.25 \times 0.7$  mm. Note that at this range the thermistor response is not governed by Eq. (17.45), since an electrical conduction of a semiconductor at such low temperatures primarily depends on impurities.

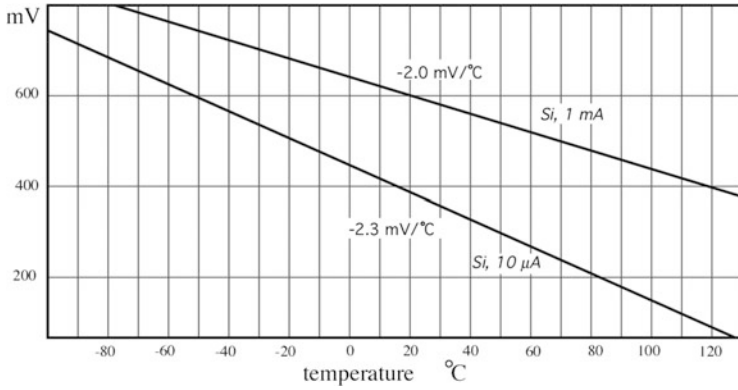
### 17.6 Semiconductor *pn*-Junction Sensors

A semiconductor *pn*-junction in a diode or bipolar transistor exhibits quite a strong thermal dependence [16]. If the forward biased junction is connected to a constant current generator, the voltage across the diode becomes a measure of the junction temperature, Fig. 17.21a. A very attractive feature of such a sensor is its high degree of linearity (Fig. 17.20) and possibility of integration with other components when the MEMS processing is used. Linearity allows a simple method of calibration using just two points to define a slope (sensitivity) and intercept.

The current-to-voltage equation of a *pn*-junction diode can be expressed as:

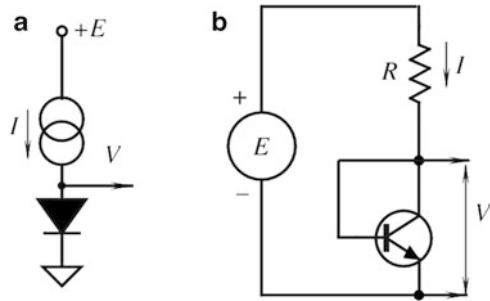
$$I = I_0 e^{\frac{qV}{2kT}}, \tag{17.46}$$

where  $I_0$  is the saturation current, which itself is a strong function of temperature. It can be shown that temperature-dependent voltage across the junction can be expressed as:



**Fig. 17.20** Voltage-temperature dependence of forward biased semiconductor junction under constant current conditions

**Fig. 17.21** Forward biased *pn*-junction temperature sensors. Diode (a); diode-connected transistor (b)



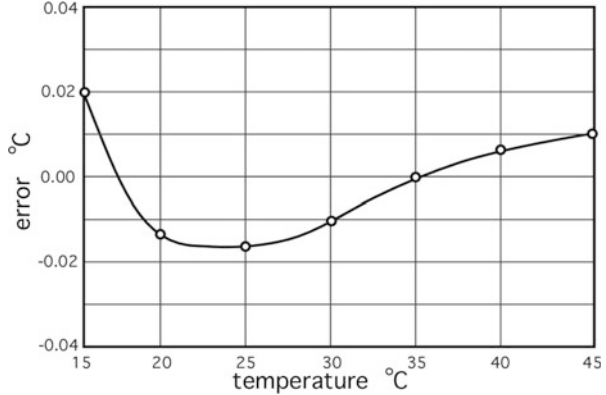
$$V = \frac{E_g}{q} - \frac{2kT}{q} (\ln K - \ln I), \tag{17.47}$$

where  $E_g$  is the energy band gap for silicon at 0 K (absolute zero),  $q$  is the charge of an electron and  $K$  is a temperature independent constant. It follows from the above equation that when the junction is operated under constant current conditions, the voltage linearly relates to temperature, and the slope (sensitivity) is given by:

$$b = \frac{dV}{dT} = -\frac{2k}{q} (\ln K - \ln I). \tag{17.48}$$

Typically, for a silicon junction operating at 10  $\mu\text{A}$ , the slope is approximately  $-2.3 \text{ mV}/^\circ\text{C}$  and it drops to about  $-2.0 \text{ mV}/^\circ\text{C}$  for a 1 mA current. Any diode or junction transistor can be used as a temperature sensor. A practical circuit for a transistor as a temperature sensor is shown in Fig. 17.21b. A voltage source  $E$  and a stable resistor  $R$  is used in place of a current source. Current through the transistor is determined as:

**Fig. 17.22** Error curve for silicon transistor (PN100) that is used as temperature sensor calibrated at 35 °C



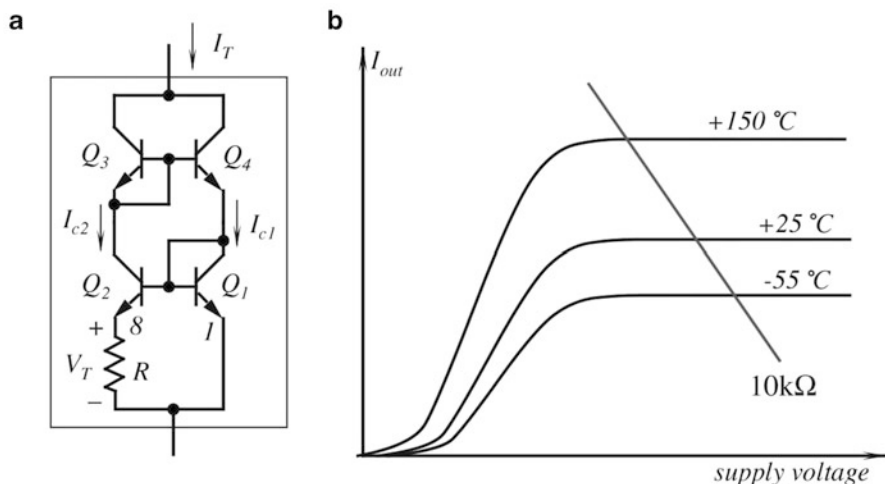
$$I = \frac{E - V}{R}. \quad (17.49)$$

It is recommended to use current on the order of  $I = 100 \mu\text{A}$ , therefore for  $E = 5 \text{ V}$  and  $V \approx 0.6 \text{ V}$ , the resistor  $R = (E - V)/I = 44 \text{ k}\Omega$ . When temperature of the diode increases, voltage  $V$  slightly drops which results in a minute increase in current  $I$ . According to Eq. (17.48), this causes some reduction in sensitivity which, in turn, is manifested as nonlinearity. However, the nonlinearity may be either small enough for a particular application, or it can be taken care of during the signal processing. This makes a transistor (diode) temperature sensor a very attractive device for many applications, due to its simplicity and very low cost. Figure 17.22 shows an error curve for the temperature sensors made with the PN100 transistor operating at  $100 \mu\text{A}$ . It is seen that the error is quite small and for many practical purposes no linearity correction is required.

A diode sensor can be formed in a silicon substrate in many monolithic MEMS sensors that may require temperature compensation. For instance, it can be diffused into a micromachined membrane of a silicon pressure sensor to compensate for temperature dependence of the piezoresistive elements.

Inexpensive, yet precise, semiconductor temperature sensors are fabricated by using the fundamental properties of transistors that allow to produce voltages that are proportional to absolute temperatures (in K). That voltage can be used directly or it can be converted into current [17]. The relationship between the base-emitter voltage ( $V_{be}$ ) and collector current of a bipolar transistor is the key property for producing a linear semiconductor temperature sensor. Figure 17.23a shows a simplified integrated circuit where transistors  $Q_3$  and  $Q_4$  form the so-called current mirror that forces two equal currents  $I_{C1} = I$  and  $I_{C2} = I$  into transistors  $Q_1$  and  $Q_2$ . The collector currents in these transistors are determined by a resistor  $R$ . In a monolithic circuit, transistor  $Q_2$  is actually made of several identical transistors connected in parallel, for example, 8. Therefore, the current density in  $Q_1$  is 8 times higher than that of each of transistors  $Q_2$ . The difference between base-emitter voltages of  $Q_1$  and  $Q_2$  is





**Fig. 17.23** Simplified circuit for semiconductor temperature sensor (a) and current-to-voltage curves (b)

$$\Delta V_{be} = V_{be1} - V_{be2} = \frac{kT}{q} \ln\left(\frac{rI}{I_{ceo}}\right) - \frac{kT}{q} \ln\left(\frac{I}{I_{ceo}}\right) = \frac{kT}{q} \ln r, \quad (17.50)$$

where  $r$  is a current ratio (equal to 8 in our example),  $k$  is the Boltzmann constant,  $q$  is the charge of an electron and  $T$  is temperature in K. Currents  $I_{ceo}$  are the same for both transistors. As a result, the current across resistor  $R$  produces voltage  $V_T = 179\text{ }\mu\text{V} \times T$  which is independent on the collector currents. Therefore, the total current through the sensor is

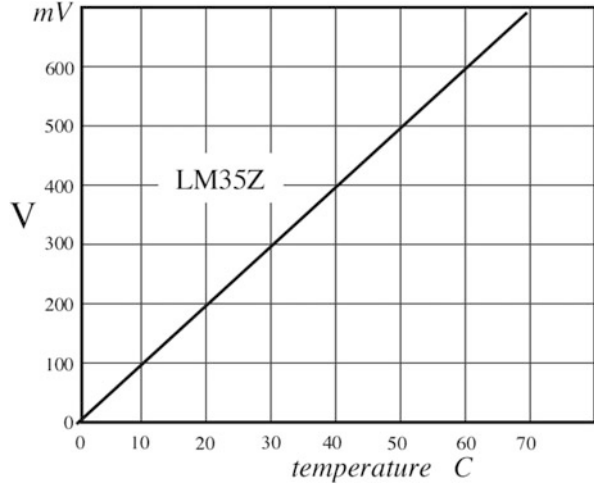
$$I_T = 2\frac{V_T}{R} = \left(2\frac{k}{qR} \ln r\right) T, \quad (17.51)$$

which for the currents ratio  $r = 8$  and resistor  $R = 358\text{ }\Omega$  produces a transfer function where current linearly depends on temperature with sensitivity  $I_T/T = 1\text{ }\mu\text{A/K}$ .

Figure 17.23b shows current-to-voltage curves for different temperatures. Note that the value in parenthesis of Eq. (17.51) is constant for a particular sensor design and may be precisely trimmed during the manufacturing process for a desired slope  $I_T/T$ . The current  $I_T$  may be easily converted into voltage. If, for example, a  $10\text{ k}\Omega$  resistor is connected in series with the sensor, the voltage across that resistor will be a linear function of the absolute temperature with a slope of  $10\text{ mV/K}$ .

The simplified circuit of Fig. 17.23a works according to the above equations only with the perfect transistors ( $\beta = \infty$ ). The practical monolithic sensors contain many additional components to overcome limitations of the real transistors. Several companies produce temperature sensors based on this principle. The examples are

**Fig. 17.24** Typical transfer function of LM35DZ semiconductor temperature sensor



LM35 from TI (voltage output circuit) and AD590 from Analog Devices (current output circuit).

Figure 17.24 shows a transfer function of a LM35Z temperature sensor which has a linear output internally trimmed for the Celsius scale with a sensitivity of 10 mV/°C. The function is quite linear where the nonlinearity error is confined within  $\pm 0.1^\circ$  and can be approximated by

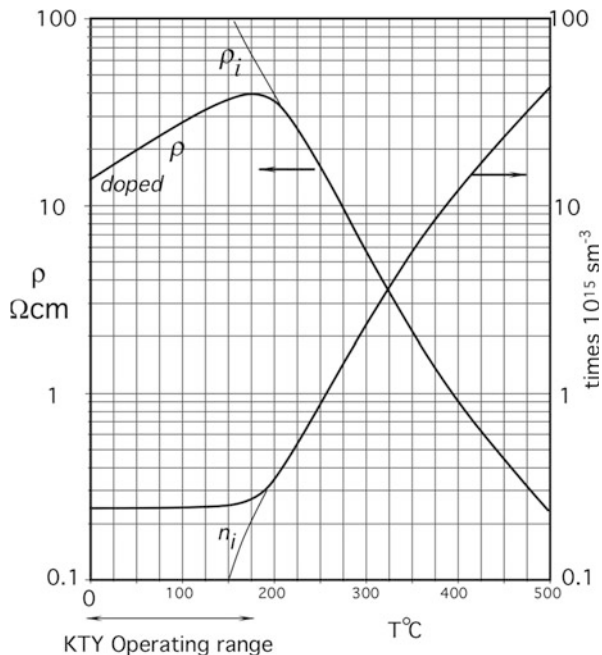
$$V_{\text{out}} = V_0 + at, \quad (17.52)$$

where  $t$  is the temperature in degrees C. Ideally,  $V_0$  should be equal to zero, however part-to-part variations of its value may be as large as  $\pm 10$  mV which correspond to an error of  $1^\circ\text{C}$ . The slope  $a$  may vary between 9.9 and 10.1 mV/°C, hence, for a high-accuracy application this sensor still may require a calibration to determine  $V_0$  and  $a$ .

## 17.7 Silicon PTC Temperature Sensors

Conductive properties of bulk silicon have been successfully implemented for fabrication of temperature sensors with the positive temperature coefficient (PTC). Nowadays, silicon resistive sensors are often incorporated into the micromachined structures for temperature compensation or direct temperature measurement. The discrete silicon sensors are also available, for example, the so-called KTY temperature detectors that originally were manufactured by Philips. Nowadays, such sensors are also produced by other manufacturers, such as Siemens. The Si PTC sensors have reasonably good linearity, and a high long-term stability (typically  $\pm 0.05$  K per year). The positive temperature coefficient makes them inherently safe for operation in the heating systems—a moderate overheating

**Fig. 17.25** Resistivity and number of free charge carriers for n-doped silicon



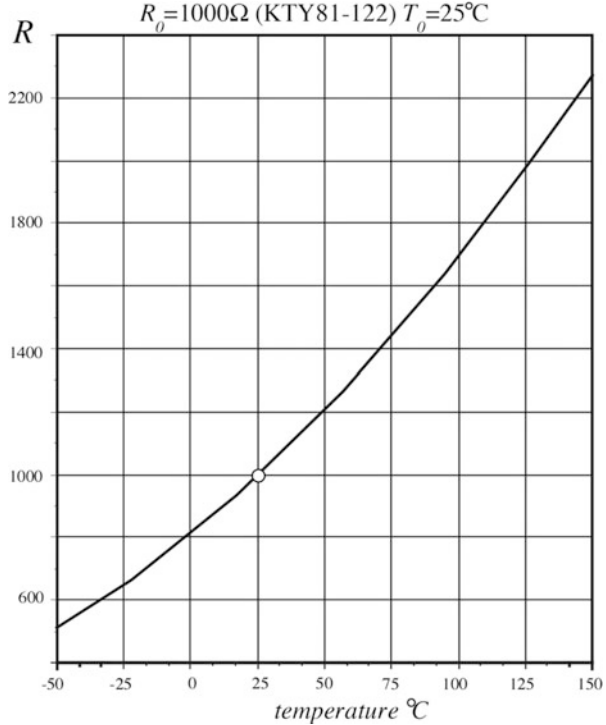
(below 200 °C) results in RTD's resistance increase and a self-protection. A silicon RTD belongs to the class of the absolute temperature sensors, that is, it can measure temperature that is referenced to the absolute temperature scales (K, C or F).

Pure silicon, either polysilicon or single crystal silicon, intrinsically has a negative temperature coefficient of resistance, Fig. 19.1b. However, when it's doped with an *n*-type impurity, in a certain temperature range, its temperature coefficient becomes positive (Fig. 17.25). This is the result of reducing a charge carrier mobility at lower temperatures. At higher temperatures, the number *n* of free charge carriers increases due to the number  $n_i$  of spontaneously generated charge carriers, and the intrinsic semiconductor properties of silicon predominate. Thus, at temperatures below 200 °C resistivity  $\rho$  has a positive temperature coefficient while over 200 °C it becomes negative. The basic KTY sensor consists of an *n*-type silicon cell having approximate dimensions of  $500 \times 500 \times 240 \mu\text{m}$ , metallized on one side and having contact areas on the other side.

A KTY sensor may be somewhat sensitive to a current direction, especially, at larger currents and higher temperatures. To alleviate this problem, a serially-opposite design is employed where two of the sensors are connected with the opposite polarities to form a dual sensor. These sensors are especially useful for the automotive applications.

A typical sensitivity of a PTC silicon sensor is on the order of 0.7 %/°C, that is, its resistance changes by 0.7 % per every °C. As for any other sensor with a mild nonlinearity, the KTY sensor transfer function may be approximated by a 2nd-order polynomial

**Fig. 17.26** Transfer function of KTY silicon temperature sensor



$$R_T = R_0 \left[ 1 + A(T - T_0) + B(T - T_0)^2 \right], \quad (17.53)$$

where  $R_0$  and  $T_0$  are the resistance ( $\Omega$ ) and temperature (K) at a reference point. For instance, for the KTY-81 sensors operating in the range from  $-55$  to  $+150$   $^{\circ}\text{C}$ , the coefficients are:  $A = 0.007874$   $\text{K}^{-1}$  and  $B = 1.874 \times 10^{-5}$   $\text{K}^{-2}$ . A typical transfer function of the sensor is shown in Fig. 17.26.

## 17.8 Thermoelectric Sensors

A thermoelectric contact sensor is called a *thermocouple* because at least two dissimilar conductors (a couple) are joined to form a junction. However, at least two of these junctions are needed to make a practical sensor. A thermocouple is a passive sensor, meaning it generates voltage in response to temperature and does not require any external excitation power. In other words, a thermocouple is a direct converter of thermal energy into electrical energy and because it's a voltage-generating sensor, sometimes thermocouple is called a "thermal battery."

The thermoelectric sensors belong to the class of *relative* sensors, because the voltage produced depends on a temperature *difference* between two thermocouple

junctions, in large part regardless of the absolute temperature of each junction. To measure temperature with a thermocouple, one junction will serve as a *reference* and its absolute temperature must be measured by a separate absolute sensor, such as a thermistor or RTD, or be thermally coupled to a material that is in a state of a known reference temperature (Table 17.1). Section 4.9 provides a physical background for a better understanding of the thermoelectric effect and Table A.10 lists some popular thermocouples that are designated by the letters originally assigned by the *Instrument Society of America* (ISA) and adopted by an American Standard ANSI MC 96.1. Detailed description of various thermocouples and their applications can be found in many excellent texts, for instance in [2, 18, 19].

The metals that are used to make thermocouples are:

Copper (Cu), Constantan (55 % Cu + 45%Ni), Iron (Fe), Chromel (90 % Ni + 10 % Cr), Alumel<sup>®</sup> (95 % Ni + 2 % Mn, 2 % Al), Nicrosil<sup>®</sup> (84.6 % Ni + 14.2 % Cr + 1.4 Si), Nisil<sup>®</sup> (95.5 % Ni + 4.4 % Si + 1 % Mg), Platinum (Pt), and Rhodium (Rh).

Below, we summarize the most important recommendations for the use of these standard thermocouples.

*Type T:* Copper (+) versus Constantan (–) is resistant to corrosion in moist atmosphere and suitable for subzero temperature measurements. Its use in air oxidizing environment is restricted to 370 °C (700 °F) due to the oxidation of the copper thermoelement. It may be used to higher temperatures in some other atmospheres.

*Type J:* Iron (+) versus Constantan (–) is suitable in vacuum and in oxidizing, reducing, or inert atmospheres, over the temperature range of 0–760 °C (32–1400 °F). The rate of oxidation in the iron thermoelement is rapid above 540 °C (1000 °F), and the use of heavy-gage wires is recommended when long life is required at the higher temperatures. This thermocouple is not recommended for use below the ice point because rusting and embrittlement of the iron thermoelement make its use less desirable than Type T.

*Type E:* Chromel<sup>®</sup> (+) versus Constantan (–) is recommended for use over the temperature range of –200 to 900 °C (–330 to 1600 °F) in oxidizing or inert atmospheres. In reducing atmospheres, alternately oxidizing or reducing atmospheres, marginally oxidizing atmospheres, and in vacuum, it is subject to the same limitations as type K. These thermocouples are suitable to subzero measurements since they are not subject to corrosion in atmospheres with high moisture content. Type E develops the highest e.m.f. per degree of all the commonly used types and is often used primarily because of this feature (see Fig. 4.36).

*Type K:* Chromel<sup>®</sup> (+) versus Alumel<sup>®</sup> (–) is recommended for use in an oxidizing or completely inert atmosphere over a temperature range of –200 to 1260 °C (–330 to 2300 °F). Due to the resistance to oxidation, type K is often used at temperatures above 540 °C. However, it should not be used in reducing atmospheres, in sulfurous atmospheres, and in a vacuum.

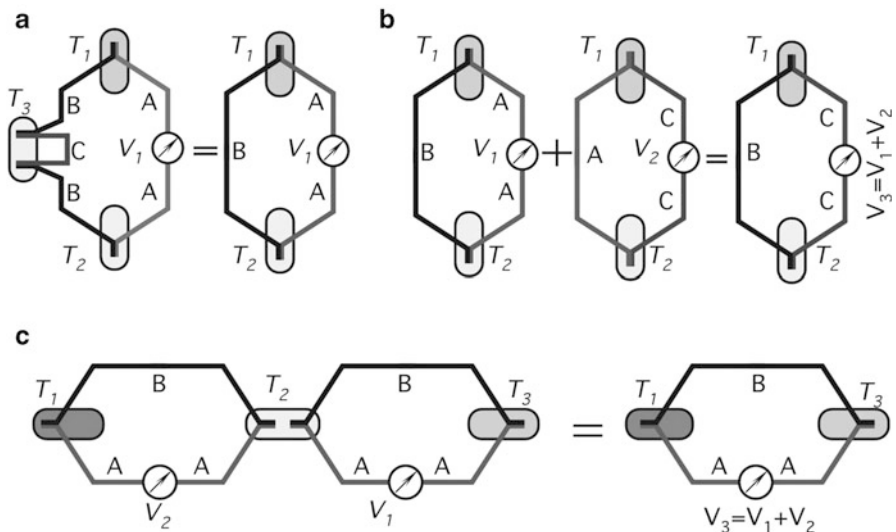
*Types R and S:* Pt/Rh (+) versus Pt (-) is recommended for continuous use in oxidizing or inert atmospheres over a temperature range of 0–1480 °C (32–2700 °F).

*Type B:* 30 % Pt/Rh (+) versus 6%Pt/Rh (-) is recommended for continuous use in oxidizing or inert atmospheres over the range of 870–1700 °C (1000–3100 °F). It is also suitable for short term use in a vacuum, but should not be used in reducing atmospheres, nor those containing metallic or nonmetallic vapors. It should never be directly inserted into a metallic primary protecting tube or well.

### 17.8.1 Thermoelectric Laws

For practical purposes, an application engineer shall be concerned with three basic laws which establish the fundamental rules for proper connection of thermocouples. Note that an interface electronic circuit must always be connected to two *identical* conductors, otherwise two parasitic thermocouples will be formed at the circuit and cause errors. These identical conductors may be formed from one of the thermocouple loop arms. That arm is broken for connecting the thermocouple to the voltage measuring circuit. The broken arm is indicated as material A in Fig. 17.27.

**Law No 1** A thermoelectric current can't be established in a homogeneous circuit by heat alone.



**Fig. 17.27** Illustrations for the thermoelectric laws

This law provides that a nonhomogeneous material is required for the generation of the Seebeck potential. If a conductor is homogeneous, regardless of the temperature distribution along its length, the resulting voltage is zero. The junction of two *dissimilar* conductors provides a condition for voltage generation.

**Law No. 2** The algebraic sum of the thermoelectric forces in a circuit composed of any number and combination of dissimilar materials is zero if all junctions are at a uniform temperature.

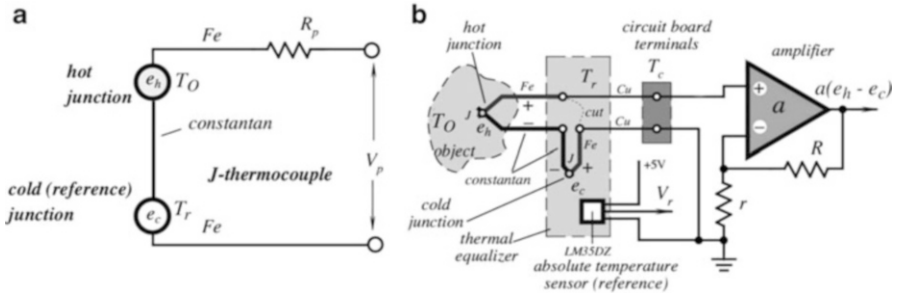
The law provides that an additional material  $C$  can be inserted into any arm of the thermoelectric loop without affecting the resulting voltage  $V_1$  as long as both additional joints are at the same temperature,  $T_3$  in Fig. 17.27a. There is no limitation on the number of inserted conductors, as long as both contacts for each insertion are at the same temperature. This implies that an interface circuit must be attached in such a manner as to assure a uniform temperature for both contacts. Another important consequence of the law is that thermoelectric joints may be formed by any technique, even if an additional intermediate material is involved (e.g., solder). The joints may be formed by welding, soldering, twisting, fusion, and so on without affecting accuracy of the Seebeck voltage. The law also provides a rule of *additive materials*, Fig. 17.27b: if thermoelectric voltages ( $V_1$  and  $V_2$ ) of two conductors ( $B$  and  $C$ ) with respect to a reference conductor ( $A$ ) are known, the voltage of a combination of these two conductors is the algebraic sum of their voltages against the reference conductor.

**Law No. 3** If two junctions at temperatures  $T_1$  and  $T_2$  produce Seebeck voltage  $V_2$ , and temperatures  $T_2$  and  $T_3$  produce voltage  $V_1$ , then temperatures  $T_1$  and  $T_3$  will produce  $V_3 = V_1 + V_2$ , Fig. 17.27c. This sometimes is called the law of intermediate temperatures. The law allows to calibrate a thermocouple at one temperature interval and then to use it at another interval. It also provides that extension wires of the same combination may be inserted into the loop without affecting accuracy.

The above laws provide for numerous practical circuits where thermocouples can be used in a great variety of combinations. They can be arranged for measuring the average temperature of an object, to measure the differential temperature between two objects, and to use other than thermocouple sensors for the reference junctions, etc.

It should be noted that thermoelectric voltage is quite small and the sensors, especially with long connecting wires are susceptible to various transmitted interferences. To increase the output signal, several thermocouples may be connected in series, while all reference junctions and all measuring junctions are maintained at the respective temperatures. Such an arrangement is called a *thermopile* (like piling up several thermocouples). Traditionally, the reference junctions are called *cold* and the measuring junctions are called *hot*.

Figure 17.28a shows an equivalent circuit for a thermocouple or thermopile. Each junction consists of a voltage source and a serial resistor. The voltage sources



**Fig. 17.28** Use of thermocouple. Equivalent circuit of thermocouple (a); front end of thermometer with semiconductor reference sensor and split thermoelectric wire (b)

represent the *hot* ( $e_h$ ) and *cold* ( $e_c$ ) junctions, while the resistances are combined in a resistor  $R_p$ . Seebeck potentials form the net voltage  $V_p = e_h - e_c$  that has a magnitude being function of the temperature differential between the object and reference junction ( $T_O - T_r$ ). The terminals of the circuit are assumed being fabricated of the same material, iron in this example of a *J*-thermocouple.

### 17.8.2 Thermocouple Circuits

In the past, thermocouples were often used with a reference cold junction immersed into a melting ice bath to maintain its temperature at 0 °C (thus, the name “cold” junction). This presents serious limitation for many practical uses. The second and third thermoelectric laws described above allow for simplified solutions. A “cold” junction can be maintained at any temperature, including ambient, as long as that temperature is precisely known. Therefore, a “cold” junction is thermally coupled to an additional reference temperature sensor. Usually, such a reference sensor is either a thermoresistive sensor (thermistor or RTD) or a semiconductor.

#### 17.8.2.1 Split Wire Circuit

Figure 17.28b shows connection of a thermocouple to an electronic circuit where one of the thermoelectric wires (iron) is cut (dotted line) and two copper wires are inserted into the split. The copper wires (the traces on a circuit board, for example) are connected to an amplifier. A “cold” (reference) junction is positioned on a “thermal equalizer” that is thermally joined to an absolute temperature reference sensor. The equalizer may be a copper or aluminum block. To avoid a dry contact, thermally conductive grease or epoxy should be applied for a better thermal tracking. A reference temperature detector in this example is a semiconductor sensor LM35DZ manufactured by Texas Instruments. The circuit has two outputs—one for the signal from the amplifier representing the Seebeck thermocouple voltage and the other for the reference signal  $V_r$ . The figure illustrates that connections to the input terminals of a circuit board and then to the amplifier’s



noninverting input and to the ground bus are made by the same type of wires (*Cu*). Both board terminals should be at the same temperature  $T_c$ , however, they not necessarily have to be at the “cold” junction temperature. This is especially important for the remote measurements, where circuit board temperature may be different from the reference “cold” junction temperature  $T_r$ .

For computing the absolute temperature of a hot junction ( $T_h$ ) from a thermocouple sensor, two signals are essentially required. The first is a thermocouple voltage from the amplifier having gain  $G$ , and the other is the reference sensor output voltage  $V_r$ . The amplifier output voltage is:

$$V = G(e_h - e_c) = G\alpha(T_O - T_r), \tag{17.54}$$

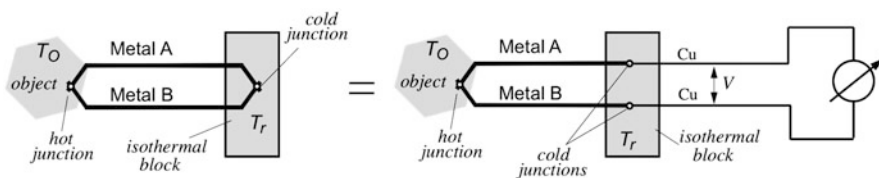
where  $\alpha_T$  [V/K] is the differential thermoelectric coefficient and  $T_r$  is the reference temperature as measured by the reference sensor. Thus, the object’s temperature is computed as:

$$T_O = \frac{V}{G\alpha} + T_r \tag{17.55}$$

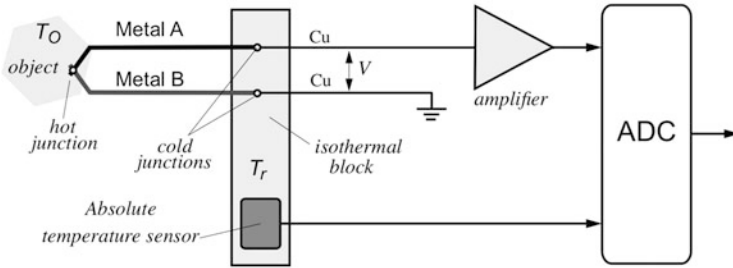
Signals from both the pre-amplifier and reference sensor may be digitized and used by a signal microprocessor for computing a sum with the appropriate scaling factors. Note that the thermoelectric coefficient  $\alpha_T$  is not necessarily a constant. It somewhat depends on temperature and thus shall be corrected for precision measurements.

### 17.8.2.2 Split Junction Circuit

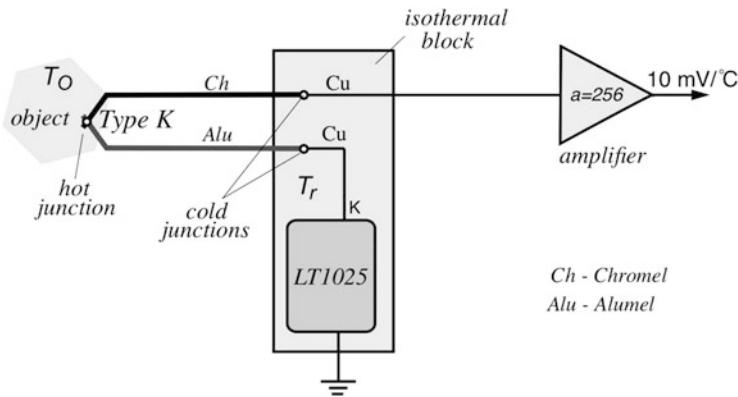
As follows for the second thermoelectric law, a wire may be inserted into a junction to form two more junctions without affecting accuracy, as long as the newly formed junctions are at the same temperature. The basic thermocouple circuit is illustrated in Fig. 17.29 (left side) where hot and cold junctions of two different metals A and B are respectively positioned on the object having temperature  $T_O$  and on the isothermal block (thermal equalizer) having reference temperature  $T_r$ . Yet, this arrangement is impractical as it is not connected to a meter. At the right side of Fig. 17.29, the cold (reference) junction is split and two copper wires are inserted to form two cold junctions. This will make no effect on the thermoelectric signals as



**Fig. 17.29** Cold junction is split to insert copper conductors for attaching to a voltmeter. The left and right circuits are thermoelectrically equivalent



**Fig. 17.30** Voltages from split-junction thermocouple and reference sensor are processed by ADC



**Fig. 17.31** Combining analog signals from thermocouple and reference integrated circuit

long as two cold junctions are at the same temperature. Two copper wires form a connection to the external voltmeter to monitor a differential thermocouple voltage. This split junction circuit is the most popular due to its simplicity and ease of practical use.

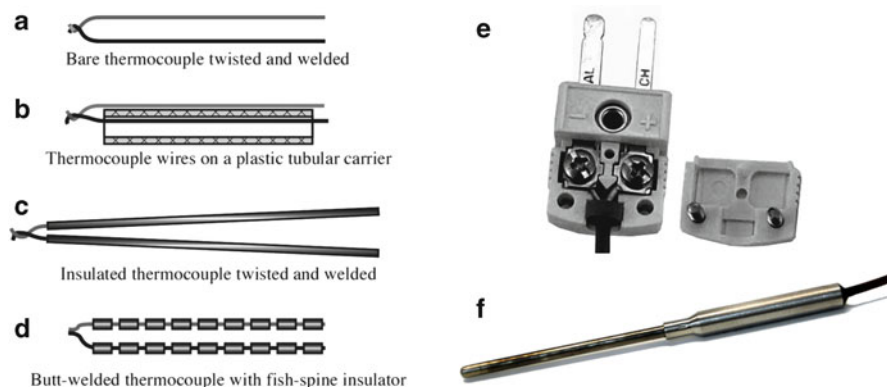
Figure 17.30 illustrates how two cold junctions are thermally coupled to a reference sensor that measures temperature  $T_r$  and both feed their signals to the analog-to-digital converter (ADC) for the further digital adding by a processor according to Eq. (17.55).

Adding the thermocouple and reference voltages not necessarily should be done by a computer. Figure 17.31 illustrates a concept of the analog adding of voltages from a thermocouple and reference temperature sensor to obtain a combined analog output signal. The thermocouple and reference voltages are connected in series. When adding up the voltages, the temperature sensitivities (volts per degree) of the thermocouple and reference sensor shall be closely matched. This was accomplished in the integrated thermocouple reference circuit LT1025 that has several scaling outputs for different types of thermocouples (type K is shown). Thus, the

combined output voltage represents the hot junction absolute temperature. It is fed to a common scaling amplifier whose gain is selected to provide a standardized output scale of  $10 \text{ mV}/^\circ\text{C}$ . Note that the integrated reference circuit shall be positioned on the same isothermal block (equalizer) that holds the cold junctions.

### 17.8.3 Thermocouple Assemblies

A complete thermocouple sensing assembly generally consists of one or more of the following: a sensing element assembly (the junction), a protective tube (ceramic or metal jackets), a thermowell (for some critical applications these are drilled solid bar stocks which are made to precise tolerances and are highly polished to inhibit corrosion), terminations (contacts which may be in the form of a screw type, open type, plug and jack-disconnect, military standard type connectors, etc.). Some typical thermocouple assemblies are shown in Fig. 17.32a–d. The wires may be left bare, or given electrical isolators. For high-temperature applications, the isolators may be of a fish-spine or ball ceramic type, which provide sufficient flexibility. If thermocouple wires are not electrically isolated, a measurement error may occur. Insulation is affected adversely by moisture, abrasion, flexing, temperature extremes, chemical attack, and nuclear radiation. A good knowledge of particular limitations of insulating materials is essential for accurate and reliable measurements. Some insulations have a natural moisture resistance. Teflon, polyvinyl chloride (PVC), and some forms of polyimides are examples of this group. With the fiber-type insulations, moisture protection results from impregnating with substances such as wax, resins, or silicone compounds. It should be noted that only one-time exposure to over-extreme temperatures cause evaporation of the impregnating materials and loss of protection. The moisture penetration is not confined to the sensing end of the assembly. For example, if a thermocouple passes



**Fig. 17.32** Some thermocouple assemblies (a–d). (e) Polarized jack for connecting thermopile wires to circuit (from Dataq Instruments) and (f) is thermocouple sealed in stainless steel tube (from RdF Corp.)

through hot or cold zones, condensation may produce errors in the measurement, unless adequate moisture protection is provided.

The basic types of flexible insulations for elevated temperature usage are fiberglass, fibrous silica, and asbestos (which should be used with proper precaution due to health hazard). In addition, thermocouples must be protected from atmospheres that are not compatible with the alloys. Protecting tubes serve the double purpose of guarding the thermocouple against mechanical damage and interposing a shield between the wires and the environment. The protecting tubes can be made of carbon steels (up to 540 °C in oxidizing atmospheres), stainless steel (up to 870 °C), ferric stainless steel (AISI 400 series), high-nickel alloys, Nichrome,<sup>7</sup> Inconel,<sup>8</sup> etc. (up to 1150 °C in oxidizing atmospheres). While the thermoelectric wires shall be well isolated and insulated from each other and from environment, the hot junction still must be in an intimate thermal coupling with the object of measurement.

Practically all base-metal thermocouple wires are annealed or given a “stabilizing heat treatment” by the manufacturer. Such treatment generally is considered sufficient, and seldom it is found advisable to further anneal the wire before testing or using. Although a new platinum and platinum-rhodium thermocouple wire as sold by some manufacturers already is annealed, it has become a regular practice in many laboratories to anneal all types R, S, and B thermocouples, whether new or previously used, before attempting an accurate calibration. This is accomplished usually by heating the thermocouple electrically in air. To anneal, the entire thermocouple is supported between two binding posts, which should be close together, so that the tension in the wires and stretching while hot are kept at a minimum. The temperature of the wire is conveniently determined with an optical pyrometer. Most of the mechanical strains are relieved during the first few minutes of heating at 1400–1500 °C.

Thin film thermocouples are formed by bonding junctions of foil metals. They are available in a free filament style with a removable carrier and in a matrix style with a sensor embedded in a thin laminated material. The foil having a thickness in the order of 5 μm (0.0002”) gives an extremely low mass and thermal capacity. Thin flat junctions may provide intimate thermal coupling with the measured surface. Foil thermocouples are very fast (a typical thermal time constant is 10 ms), and can be used with any standard interface electronic apparatuses. While measuring temperature with sensors having small mass, thermal conduction through the connecting wires always must be accounted for (see Fig. 17.1). Thanks to a very large length to thickness ratio of the film thermocouples (on the order of 1000) heat loss via wires usually is negligibly small.

To attach a film thermocouple to an object, several methods are generally used. Among them are various cements and flame or plasma sprayed ceramic coatings. For ease of handling, the sensors often are supplied on a temporary carrier of

---

<sup>7</sup> Trademark of the Driver-Harris Company.

<sup>8</sup> Trademark of the International Nickel Company.

polyimide film (Kapton, e.g.) which is tough, flexible, dimensionally stable, exceptionally heat resistant, and inert. While selecting cements, care must be taken to avoid corrosive compounds. For instance, cements containing phosphoric acid are not recommended for use with thermocouples having copper in one arm. Special isothermal connectors should be employed for electrical connections to the circuits, Fig. 17.32e.

---

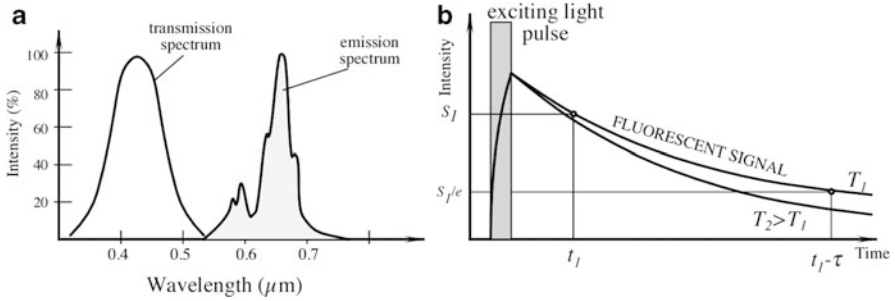
## 17.9 Optical Temperature Sensors

Temperature can be measured by the contact and noncontact methods. The noncontact instruments are generally associated with the infrared (IR) optical sensors that were covered in Sects. 4.12.3 and 15.8, however, there are other noncontact methods as described below. The need for noncontact temperature sensors exists when the surface measurement must be done fast. Also, they are needed for determining temperatures at hostile environments where very strong electrical, magnetic or electromagnetic fields, or very high voltages make measurements either too susceptible to interferences, or too dangerous for the operator. And also there are situations when it is just difficult to reach an object during a routine measurement. In medicine, noncontact IR measurements of body temperatures are preferable because they do not disturb the measurement sites (ear canal or skin surface), hygienic, and fast (typically from 1 to 2 s).

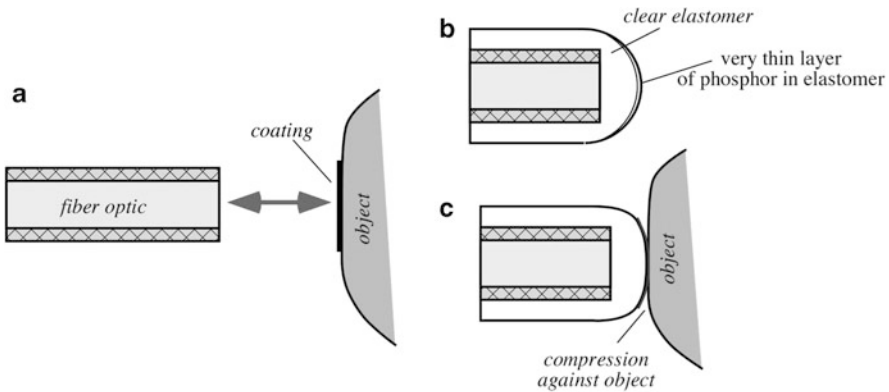
### 17.9.1 Fluoroptic Sensors

The fluoroptic sensors rely on the ability of a special phosphor compound to give away a fluorescent signal in response to light excitation. The compound can be directly painted over the measured surface and illuminated by an ultraviolet (UV) pulse, while observing the afterglow. The shape of the response afterglow pulse is function of temperature. The decay of the response afterglow is highly reproducible over a wide temperature range [20, 21]. As a sensing material, magnesium fluoromagnetite activated with tetravalent manganese is used. This is phosphor, long known in the lighting industry as a color corrector for mercury vapor street lamps, prepared as a powder by a solid-state reaction at approximately 1200 °C. It is thermally stable, relatively inert, benign from a biological standpoint, and insensitive to damage by most chemicals or by prolonged exposure to ultraviolet UV radiation. It can be excited to fluoresce by either UV or blue radiation. Its fluorescent emission is in the deep red region, and the fluorescent decay is essentially exponential.

To minimize crosstalk between the excitation and emission signals, they are passed through the bandpass filters, which reliably separate the related spectra, Fig. 17.33a. The pulsed excitation source, a Xenon flash lamp, can be shared among a number of optical channels in a multisensor system. The temperature measurement is made by measuring the rate of decay of the fluorescence, as shown in



**Fig. 17.33** Fluoroptic method of temperature measurement. Spectral responses of the excitation and emission signals (a); exponential decay of the emission signal for two temperatures ( $T_1$  and  $T_2$ ) (b); where  $e$  is the base of natural logarithms, and  $\tau$  is decay time constant (adapted from [20])

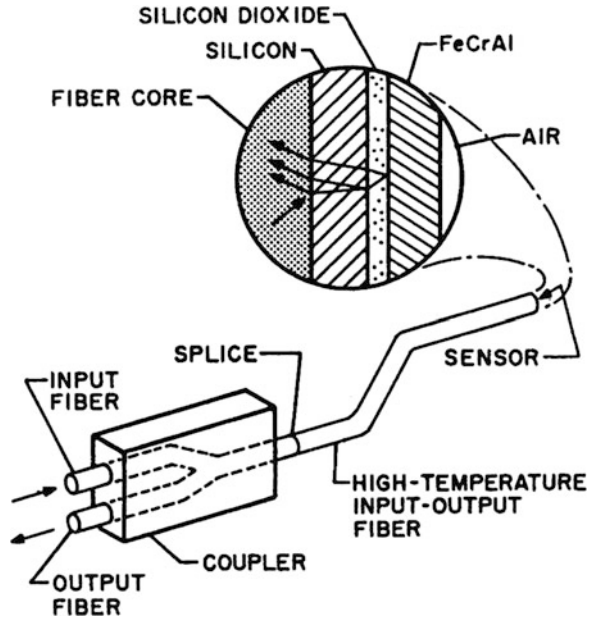


**Fig. 17.34** Placement of a phosphor compound in fluoroptic method. On surface of object (a); on tip of the probe (b and c) (adapted from [20])

Fig. 17.33b. In other words, a temperature is represented by the time constant  $\tau$  which drops fivefold over the temperature range from  $-200$  to  $+400$  °C. Since measurement of time is usually one of the simplest and most precise operations that can be performed by an electronic circuit, temperature can be measured with a good resolution and accuracy: about  $\pm 2$  °C over the above range without calibration.

Since the time constant is independent of the excitation intensity, a variety of designs is possible. For instance, the phosphor compound can be directly coated onto the surface of interest and the optic system can take measurement without a physical contact, Fig. 17.34a. This makes possible a continuous temperature monitoring without disturbing the measured site. In another design, a phosphor is coated on the tip of a pliable probe that can form a good contact area when touches the object, Fig. 17.34b, c.

**Fig. 17.35** Schematic of thin film optical temperature sensor



### 17.9.2 Interferometric Sensors

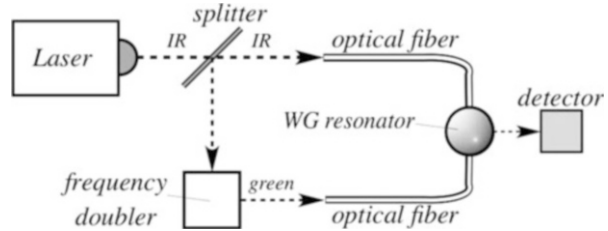
Another method of the optical temperature measurement is based on modulation of light intensity by interfering two light beams. One beam is a reference, while the other's travel through the temperature sensed medium is somewhat delayed, depending on temperature. This results in a phase shift and a subsequent extinction of the interference signal. For temperature measurement, a thin layer of silicon [22, 23] can be used because its refractive index changes with temperature (thermo-optic effect), thus modulating a light travel distance.

Figure 17.35 shows a concept of a thin film optical sensor. The sensor was fabricated by sputtering three layers onto the ends of the step-index multimode fibers with 100  $\mu\text{m}$  core diameters and 140  $\mu\text{m}$  cladding diameters [24]. The first layer is silicon coated with silicon dioxide. The FeCrAl layer on the end of the probe prevents oxidation of the underlying silicon. The fibers can be used up to 350  $^{\circ}\text{C}$ , however more expensive fibers with gold buffered coatings can be used up to 650  $^{\circ}\text{C}$ . The sensor is used with the LED light source operating in the range of 860 nm and a micro-optic spectrometer.

### 17.9.3 Super-High Resolution Sensing

Temperature measurements with super-high resolution are important for precision calorimetry, radio-astronomy and other fields of precision measurements. Yet, achieving extremely high resolution is limited by several interfering factors, such

**Fig. 17.36** Concept of whispering gallery mode (WGM) temperature sensor

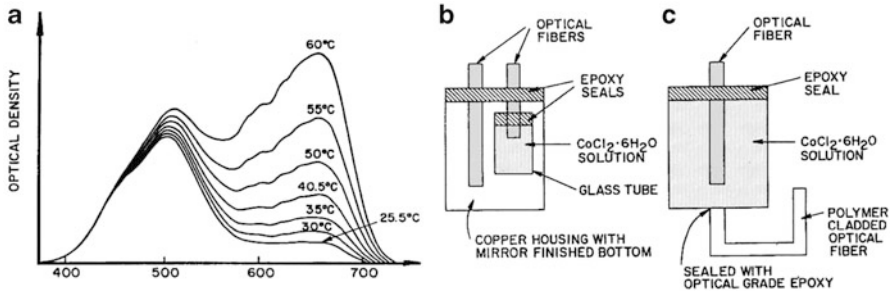


as thermal and electric noise, thermal expansion of materials, etc. In a laboratory setting, a super-high resolution as low as  $30 \text{ nK}/\sqrt{\text{Hz}}$  was achieved [25] by using an isotropic crystalline whispering-gallery mode (WGM) resonator. This resolution is so fine that it allows observing thermal jiggling of individual atoms. A concept of a WGM stems from the acoustic phenomenon observed in certain architectural structures having circular shapes. In such galleries, whispers could be heard across the circle but not at any intermediate position. Lord Rayleigh in 1914 developed a theory explaining that waves inside a circular cavity involve the resonance based on wave interference. The WGM waves are guided by a circular wall depending on its curvature, and the effect disappears for straight corridors. The same phenomenon was observed for the optical waves and can be used for various sensing, including a temperature sensing with the ultra-high resolution. The temperature sensor involves a round-shaped light resonator, like a disk or small sphere (radius about 5 mm) made of anisotropic material (e.g.,  $\text{MgF}_2$ ,  $\text{CaF}_2$ ). The circular device serves as a WGM resonator having an exceptionally high  $Q$  (resonance quality factor) on the order of  $10^8$ . The frequency of a WGM mode is affected by temperature dependence of the refractive index (thermo-optic effect) of the resonator and the thermal expansion of the resonator. The first dependence leads to temperature sensitivity solely within the optical mode, whereas in the latter, the mode frequency depends on temperature distribution throughout the entire resonator volume. The sensing device (Fig. 17.36) uses light of two frequencies (near IR and green). The near IR light is produced by a laser. Then, the laser beam is split into two, wherein one travels through the fiber optic guide to the WGM resonator, while the other first goes to the frequency doubler that outputs the green beam. When entering the WGM resonator, the waves of both frequencies interfere with each other and the resulting intensity is detected by an output photo-detector. The exit intensity greatly depends on the resonator temperature. The dependence results from change in the refractive index, while the thermal expansion effects are mostly cancelled due to a differential technique.

#### 17.9.4 Thermochromic Sensors

For biomedical applications, where electromagnetic interferences may present a problem, a temperature sensor can be fabricated with use of a thermochromic solution [26], such as cobalt chloride ( $\text{CoCl}_2 \cdot 6\text{H}_2\text{O}$ ).





**Fig. 17.37** Thermochromic solution sensor. Absorption spectra of cobalt chloride solution (a); reflective fiber coupling (b); transmissive coupling (c) (from [26])

The operation of this sensor is based on temperature dependence of a spectral absorption in the visible range of 400-800 nm by the thermochemical solution, Fig. 17.37a. This implies that the sensor should comprise a light source, photodetector and cobalt chloride solution that is thermally coupled with the object. Two possible designs are shown in Fig. 17.37b, c, where transmitting and receiving optical fibers are coupled through a cobalt chloride solution.

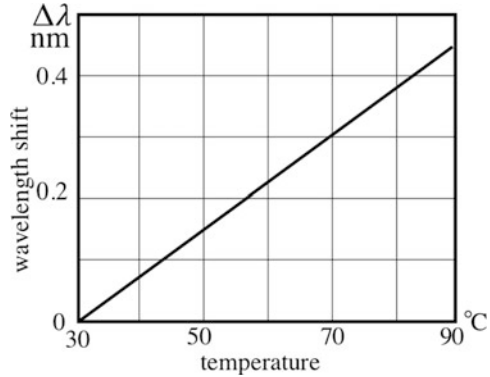
### 17.9.5 Fiber-Optic Temperature Sensors (FBG)

As it was described in Sect. 8.5.5 the Fiber Bragg Grating (FBG) sensor is sensitive to temperature. Advantages of these temperature sensors among others are immunity to EMI, absence of electrical conductors, stability, and ability to chain-connect multiple sensors in a single fiber. The operating principle of the FBG sensor is based on a thermal expansion of a fiber and a subsequent modulation of distance between the gratings having different refractive indices. The sensor has a temperature sensitivity described by Eq. (8.14) which we rewrite here as:

$$\frac{\Delta\lambda}{\lambda} = (\alpha_L + \alpha_n)T, \quad (17.56)$$

Practical values for the constants are  $\alpha_L = 0.55 \times 10^{-6} \text{ K}^{-1}$  and  $\alpha_n = 6.67 \times 10^{-6} \text{ K}^{-1}$  [27]. In one experiment [28], the reflected light from FBG was detected and measured by the optical spectrum analyzer. The wavelength shift exhibited quite a linear transfer function as shown in Fig. 17.38. The obvious practical limitation is a temperature range that shall not exceed physical and chemical stability of the fiber optic assembly. This sensor has a rather broad range of uses, including the aerospace applications, where some of the quantities that need to be measured are strain mapping, deformation, vibration detection, micrometeorite detection, distributed temperature measurements. They are also suitable for civil engineering, biomedical engineering, and embedding into smart structures for continuous monitoring of strain and temperature.

**Fig. 17.38** Transfer function of FBG temperature sensor



## 17.10 Acoustic Temperature Sensors

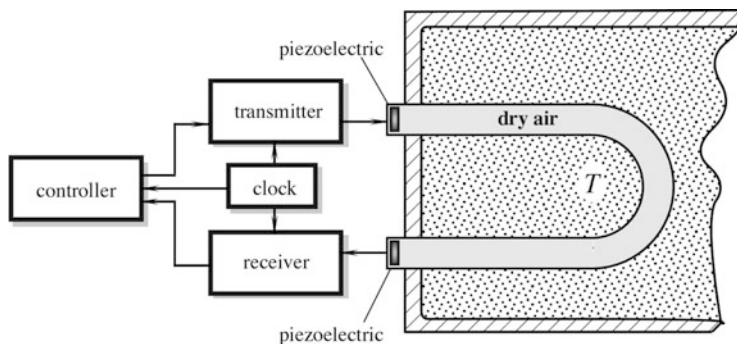
Under extreme conditions, temperature measurement may become a difficult task. These conditions include a cryogenic temperature range, high radiation levels inside nuclear reactors, etc. Another unusual condition is the temperature measurement inside a sealed enclosure with a known medium, in which no contact sensors can be inserted and the enclosure is not transmissive for infrared radiation. Under such restraining conditions, acoustic temperature sensors may come in quite handy. An operating principle of such a sensor is based on a relationship between temperature of the medium and speed of sound. For instance, in dry air at a normal atmospheric pressure the relationship is approximated by:

$$v \approx 331.5 \sqrt{\frac{T}{273.15 \text{ m/s}^2}} \quad (17.57)$$

where  $v$  is the speed of sound and  $T$  is the absolute temperature.

An acoustic temperature sensor (Fig. 17.39) is composed of three components: an ultrasonic transmitter, an ultrasonic receiver, and a gas filled hermetically sealed tube. The transmitter and receiver are ceramic piezoelectric plates that are acoustically decoupled from the tube to assure sound propagation primarily through the enclosed gas, which in most practical cases is dry air. Alternatively, the transmitting and receiving crystals may be incorporated into a sealed enclosure with a known content whose temperature has to be measured. That is, an intermediate tube is not necessarily required in cases where the internal medium, its volume and mass are held constant. When a tube is used, care should be taken to prevent its mechanical deformation and loss of hermeticity under the extreme temperature conditions. A suitable material for the tube is invar.

The clock of a low frequency (near 100 Hz) generates pulses that trigger the transmitter and disable the receiver, just like in a radar. The piezoelectric crystal



**Fig. 17.39** Acoustic thermometer with ultrasonic detection system

flexes and that causes a transmission of an ultrasonic wave along the tube. The receiving crystal is enabled before the wave arrives to its surface and converts it into an electrical transient, which is amplified and sent to the control circuit. The control circuit calculates the speed of sound by determining propagation time along the tube. Then, the corresponding temperature is determined from the calibration numbers stored in a look-up table. In another design, the thermometer may contain only one ultrasonic crystal which alternatively acts either as a transmitter, or as a receiver. In that case, the tube has a sealed empty end. The ultrasonic waves are reflected from the end surface and propagate back to the crystal, which before the moment of the wave arrival is turned into a reception mode. The electronic circuit [29] converts the received pulses into a signal that corresponds to the tube temperature.

A miniature temperature sensor can be fabricated with the surface acoustic waves (SAW) and plate waves (PW) techniques (see Sect. 13.6.2). The idea behind such a sensor is in temperature modulation of some mechanical parameters of a time-keeping element in the electronic oscillator [30, 31]. This leads to a change in the oscillating frequency. In effect, such an integral acoustic sensor becomes a direct converter of temperature into frequency. A typical sensitivity is in the range of several kilohertz per degree Kelvin.

## 17.11 Piezoelectric Temperature Sensors

Piezoelectric effect, in general, is a temperature dependent phenomenon. Thus, a temperature sensor based on variability of the oscillating frequency of a quartz crystal can be designed. Since quartz is an anisotropic medium, the resonant frequency of a plate is highly dependent on the crystallographic orientation of the plate—the so-called angle of cut. Thus, by selecting a cut, a negligibly small temperature sensitivity may be achieved (*AT*- and *BT*-cuts), or just the opposite—a cut with pronounced temperature dependence may be selected.

Temperature dependence of the resonant frequency may be approximated by a 3rd-order polynomial:

$$\frac{\Delta f}{f_0} = a_0 + a_1 \Delta T + a_2 \Delta T^2 + a_3 \Delta T^3 \quad (17.58)$$

where  $\Delta T$  and  $\Delta f$  are the temperature and frequency shifts respectively,  $f_0$  is the calibrating frequency and  $a$  are the coefficients. The first utilization of temperature dependence was made in 1962 by utilizing a non-rotated  $Y$ -cut crystal [32]. A very successful development of a linear temperature coefficient-cut (LC) was made by Hewlett-Packard [33]. The 2nd- and 3rd-order coefficients had been eliminated by selecting a doubly-rotated  $Y$ -cut. As a result, the sensor became highly linear with sensitivity ( $a_1$ ) 35 ppm/°C and the operating temperature range from  $-80$  to  $230$  °C with calibration uncertainty of 0.02 °C. With the advent of microprocessors, linearity became a less important factor and more sensitive, yet somewhat nonlinear quartz temperature sensors had been developed by using a slightly singly rotated  $Y$ -cut ( $Q = -4^\circ$ ) with sensitivity of 90 ppm/°C [34] and by utilizing a tuning-fork resonator in flexural and torsional modes [35, 36]. It should be noted however, that thermal coupling of the object of measurement with the oscillating plate is always difficult and, thus, all piezoelectric temperature sensors have relatively slow response as compared with thermistors and thermoelectrics.

---

## References

1. Fraden, J. et al. (2007). *Ear temperature monitor and method of temperature measurement*. U.S. Patent No. 7306565, 11 December 2007.
2. Benedict, R. P. (1984). *Fundamentals of temperature, pressure, and flow measurements* (3rd ed.). New York, NY: John Wiley & Sons.
3. Callendar, H. L. (1887). On the practical measurement of temperature. *Philosophical Transactions. Royal Society of London*, 178, 160.
4. Sapoff, M. (1999). Thermistor thermometers. In J. G. Webster (Ed.), *The measurement, instrumentation and sensors handbook* (pp. 3225–3241). Boca Raton, FL: CRC Press.
5. Fraden, J. (2000). A two-point calibration of negative temperature coefficient thermistors. *Review of Scientific Instruments*, 71(4), 1901–1905.
6. Steinhart, J. S., & Hart, S. R. (1968). Calibration curves for thermistors. *Deep Sea Research*, 15, 497.
7. Mangum, B. W. (1983). Triple point of succinonitrile and its use in the calibration of thermistor thermometers. *Review of Scientific Instruments*, 54(12), 1687.
8. Sapoff, M., et al. (1982). The exactness of  $\Delta t$  of resistance—temperature data. In J. E. Schooley (Ed.), *Temperature Its measurement and control in science and industry* (Vol. 5, p. 875). College Park, MD: American Institute of Physics.
9. Keystone Carbon Company. (1984). *Keystone NTC and PTC thermistors*. Catalogue © Keystone Carbon Company, St. Marys, PA.
10. Tosaki H et al. (1986) *Thick film thermistor composition*. U.S. Patent No. 4587040, 6 May 1986.
11. Zhiong J, et al. *Thick film thermistors printed on low temperature co-fired ceramic tapes*. University of Pensilvania. Retrieved from [http://repository.upenn.edu/meam\\_papers/117/](http://repository.upenn.edu/meam_papers/117/).
12. Villemant, C. M., et al. (1971). Thermistor. U.S. Patent No. 3,568,125, March 2, 1971.

13. Silver, E. H., et al. (2007). Method for making an epitaxial germanium temperature sensor. U.S. Patent No. 7232487, June 19, 2007.
14. Kozhukh, M. (1993). Low-temperature conduction in germanium with disorder caused by extended defects. *Nuclear Instruments & Methods, A329*, 453–466.
15. Kozhukh, M. (1993). Neutron doping of silicon in power reactors. *Journal of Physics: Condensed Matter*, 5, 2351–2376.
16. Sachse, H. B. (1975). *Semiconducting temperature sensors and their applications*. New York, NY: Wiley.
17. Timko, M. P. (1976). A two terminal IC temperature transducer. *IEEE Journal of Solid-State Circuits*, 11, 784–788.
18. Caldwell, F. R. (1962) Thermocouple materials. *NBS monograph 40. National Bureau of Standards*, 1 March 1962.
19. ASTM. (1993). *Manual on the use of thermocouples in temperature measurement. ASTM manual series: MNL: 12-93* (4th ed.). Philadelphia, PA: ASTM.
20. Wickersheim, K. A., et al. (1987). Fluoroptic thermometry. *Medical Electronics, February*, 84–91.
21. Fernicola, V. C., et al. (2000). Investigations on exponential lifetime measurements for fluorescence thermometry. *Review of Scientific Instruments*, 71(7), 2938–2943.
22. Schultheis, L., et al. (1988). Fiber-optic temperature sensing with ultrathin silicon etalons. *Optics Letters*, 13(9), 782–784.
23. Wolthuis, R., et al. (1991). Development of medical pressure and temperature sensors employing optical spectral modulation. *IEEE Transactions on Biomedical Engineering*, 38 (10), 974–981.
24. Beheim, G., et al. (1990). A sputtered thin film fiber optic temperature sensor. *Sensors, January*, 37–43.
25. Weng, W., et al. (2014). Nano-Kelvin thermometry and temperature control: Beyond the thermal noise limit. *PRL*, 112, 160801.
26. Hao, T., et al. (1990). An optical fiber temperature sensor using a thermochromic solution. *Sensors and Actuators A*, 24, 213–216.
27. Kersey, A. D., et al. (1997). Fiber grating sensors. *Journal of Lightwave Technology*, 15, 1442–1463.
28. Cazo, R. M., et al. Fiber Bragg Grating temperature sensor. Photonics Div., IEAv, São José dos Campos-SP-Brazil, e-mail: carmi@ieav.cta.br.
29. Williams, J. (1990). *Some techniques for direct digitization of transducer outputs, AN7, Linear Technology application handbook*. Milpitas, CA: Linear Technology.
30. Venema, A., et al. (1990). Acoustic-wave physical-electronic systems for sensors. *Fortschritte der Acustik der 16. Deutsche Arbeitsgemeinschaft für Akustik* (pp. 1155–1158).
31. Vellekoop, M. J., et al. (1990). *All-silicon plate wave oscillator system for sensor applications*. New York, NY: Proceedings of the IEEE Ultrasonic Symposium.
32. Smith, W. L., et al. (1963). Quartz crystal thermometer for measuring temperature deviation in the  $10^{-3}$  to  $10^{-6}$  °C range. *Review of Scientific Instruments*, 4, 268–270.
33. Hammond, D. L., et al. (1962). Linear quartz thermometer. *Instrumentation and Control Systems*, 38, 115.
34. Ziegler, H. (1984). A low-cost digital sensor system. *Sensors and Actuators*, 5, 169–178.
35. Ueda T, et al. (1986). *Temperature sensor utilizing quartz tuning fork resonator* (pp. 224–229). In Proceedings of the 40th annuals of frequency control symposium, Philadelphia, PA, 1986.
36. EerNisse E. P., et al. (1986). *A resonator temperature transducer with no activity dips*. (pp. 216–223). In Proceedings of the 40th annuals of frequency control symposium, Philadelphia, PA, 1986.

*Of all smells, bread;  
Of all tastes, salt.*

George Herbert, English poet

Sensors for measuring and detecting chemical and biological substances are pervasively employed yet are, for the most part, unobtrusive. They are used to help run our cars more efficiently, track down criminals, and monitor our environment and health. Examples of uses include monitoring of oxygen in automobile exhaust systems, glucose levels in samples from diabetics and carbon dioxide in the environment. In the laboratory, chemical detectors are the heart of key pieces of analytical equipment employed in the development of new chemicals and drugs and to monitor industrial processes. Progress has been impressive and the literature is full of interesting developments. Recent developments include a broad spectrum of technologies, such as improved screening systems for security applications [1] and miniaturization of systems once only used in laboratories [2]. Chemical sensors respond to stimuli produced by various chemicals or chemical reactions. These sensors are intended for *identification* and *quantification* of chemical species (including both liquid and gaseous phases). Chemical sensors can be stand-alone devices, or part of larger, more complex systems that include instrumentation for chemical reactions, separations, or other processes.

In industry, chemical sensors are used for process and quality control during plastics manufacturing and in the production of foundry metals where the amount of diffused gasses affects metal characteristics such as brittleness. They are used for environmental monitoring of workers to control their exposure to dangers and limit

---

This chapter is written in collaboration with Dr. Sanjay V. Patel (*Seacoast Science, Inc.*, sanjay@seacoastscience.com) and Prof. Todd E. Mlsna (*Mississippi State University*, tmlsna@chemistry.msstate.edu).

health risks. Chemical sensors find many new applications as *electronic noses*. An electronic nose generally uses many different types of sensor [3] in order to mimic the olfaction capabilities of mammals [4]. In medicine, chemical sensors are used to determine patient health by monitoring oxygen and trace gas content in the lungs and in blood samples. These sensors are often used for breathalyzers to test for blood alcohol levels, and as indicators of the digestion problems of patients. In the military, chemical sensors are used to detect fuel dumps and to warn soldiers of the presence of airborne chemical warfare agents. Chemical sensors are used to detect trace contaminants in liquids, and, for example, they are used to search for and monitor ground water contamination near military, civilian, and industrial sites, where significant amounts of chemicals are stored, used, or dumped [5]. Combinations of liquid and gas sensors are used in experimental military applications to monitor compounds produced from refineries and nuclear plants to verify compliance with weapons treaties.

---

## 18.1 Overview

### 18.1.1 Chemical Sensors

Traditionally, chemical sensing of unknown substances is done in an analytical laboratory with complex benchtop equipment including, for example, mass spectrometry, chromatography, nuclear magnetic resonance, X-ray and infrared technology. These methods are very accurate and it is possible to identify most classes of unknown chemicals with a high degree of confidence. However, the instruments are often expensive and require trained personnel to operate. Considerable efforts have been devoted to developing miniaturized, low cost sensing systems to address specific markets. Impressive advances have been made and many sensor systems are available at low cost but these miniaturized systems traditionally have problems with sensitivity, selectivity, baseline stability, and reproducibility. In this chapter we provide a brief overview of chemical sensors and sensing systems both for the analytical laboratory and miniaturized systems for mobile applications.

There is no universally accepted method to categorize the complete list of chemical detectors. For the purpose of this chapter we have grouped them into two main categories, one being transduction methods and the other being methods of implementation. We have further divided the methods of transduction into three classes including (1) sensors that measure electrical or electrochemical properties, (2) those that measure a change in a physical property, (3) and those that rely on absorption or release of optical or other wavelengths of electromagnetic radiation.

An impressive range of sensor technologies have been developed to respond to different chemical, physical, and optical properties to aid in the detection of chemical analytes. Some of these technologies, for example microcantilevers, can be used to measure chemical and/or physical properties, and thus are not easily classified.

### 18.1.2 Biochemical Sensors

*Biosensors* are a special class of chemical sensors. Evolution of species by means of natural selection led to extremely sensitive organs, which can respond to presence of just few molecules. Man-made sensors, while generally not as sensitive, employ biologically active materials in combination with several physical sensing elements, for example, amperometric or thermal. The bio-recognition element is actually a bioreactor on the top of the conventional sensor, so the response of the biosensor will be determined by the diffusion of the analyte, reaction products, co-reactants, or interfering species, and the kinetics of the recognition process. Examples of biological elements that may be detected qualitatively and quantitatively by the biosensors are: organisms, tissues, cells, organelles, membranes, enzymes, receptors, antibodies, and nucleic acids [6].

In fabrication of a biosensor, one of the key issues is *immobilization* of biochemical transducers on the physical or electrical transducer. The immobilizing layer or surface must confine the biologically active material on a sensing element and keep it from leaking out over the lifetime of the biosensor, allow contact to the analyte solution, allow any product to diffuse out of the immobilization layer, and not denature the biologically active material. Most of the biologically active materials used in biosensors are proteins or contain proteins in their chemical structures. To immobilize the proteins on the surface of the sensor, two basic techniques are employed: binding or physical retention. Adsorption and covalent binding are the two types of binding techniques. The retention involves separating the biologically active material from analyte solution with a layer on the surface of the sensor, which is permeable to the analyte and any products of the recognition reaction, but not to the biologically active material. Examples of biosensors are given in various sections in this chapter.

---

## 18.2 History

The history of man benefiting from sensing chemicals is rich and colorful. The first examples involved clever use of the animal kingdom including the miner's canary [7] employed to monitor air quality (Fig. 18.1). Early miners often worked in dangerous conditions without the benefit of modern ventilation systems. For hundreds of years miners would work side by side with caged canaries to warn of dangerous environmental conditions. Canaries are more sensitive than man to low levels of methane, carbon monoxide and diminished oxygen levels that can occur with a tunnel collapse or the release of pockets of trapped gases. As long as the canary lived the miner knew his air supply was safe. A dead canary alerted the miners of a potentially dangerous situation. In modern mines most canaries have been replaced with various types of personal, portable and fixed gas monitoring equipment [8].

Since prehistoric times canines were used for finding and tracking game. Today trained dogs are used for finding explosives and drugs in airports and other public places. A disproportionately large portion of the dog's brain is dedicated to smell



**Fig. 18.1** Canary in miner's cage



when compared to the human brain. As a result, dogs have demonstrated the ability to discriminate some odors at concentrations eight orders of magnitude lower than man. Ever since dogs have been domesticated 30,000 years ago [9] man has relied on the dog nose. From these modest beginnings chemical sensors have expanded beyond the animal kingdom, grown to become big business and are now pervasively employed. Reducing size and power and improving portability are the dominant industrial trends, with the goal of deploying chemical sensors in cell-phones and on unmanned vehicles. Recent advances in microfluidics have made miniaturized medical devices prevalent in the diagnostic analysis industry.

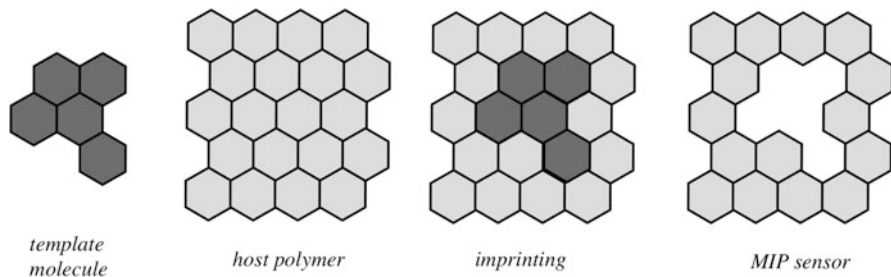
---

## 18.3 Chemical Sensor Characteristics

Most chemical sensors can be described using criteria and characteristics general to all sensors such as stability, repeatability, linearity, hysteresis, saturation, response time, and span (see Chap. 3) However, two special characteristics are unique and meaningful as applied to chemical detection. These are selectivity and sensitivity. Because chemical sensors are used both for identification and quantification, they need to be both selective and sensitive to a desired target species in a mixture of chemical species.

### 18.3.1 Selectivity

Selectivity describes the degree to which a sensor responds to only the desired target species, with little or no interference from non-target species. Therefore, one of the most important functions in the evaluation of a chemical sensor's performance is the qualification of its selectivity.



**Fig. 18.2** Creating lock-and-key MIP sensor (after [107])

Most sensors are not highly selective to one species, but respond to many different chemicals with varied sensitivity. Still, there are some types of sensors that can be very selective, by relying on selective materials or mechanisms. The signal processing mimicking that of live organisms often can dramatically enhance selectivity. Chemical sensors that rely on a physical or chemical interaction of analyte (the species that is subject of detection) can be generally divided into three groups [107]: lock-and-key, catalytic, and electrochemical.

### 18.3.1.1 Lock-and-Key

A chemical sensor having ideal selectivity should not respond to any analyte except just one specific chemical. Then, the question is—how to identify the correct chemical? In the lock-and-key approach, a specific molecule that is part of the sensing element binds only to the analyte of interest. Sometimes this approach is called the affinity sensing. Examples in biology are the antibodies, phages and nucleic acids. Biosensors including these types of interactions may require specialized fluidic systems to keep the biomaterials viable and allow for the optical or electrical transduction.

One affinity approach is to use the molecular imprintable polymers (MIP) that apply the lock-and-key principle: they recognize the molecular shape and size in a predictable way. The MIP is produced by creating an imprint of a template molecule, then removing the template and leaving a void in the polymer that becomes a negative image of the template (Fig. 18.2). The MIP imprint is a stable structure, both thermally and chemically, with a lifetime up to 8 years. MIP materials can be constructed and used with a variety of different transducers [73].

### 18.3.1.2 Catalytic Selectivity

A sensing element can be given a catalyst, such as an enzyme or metal, to help discriminate a specific analyte by activating or enhancing a chemical reaction. Detectors based on heated metal-oxides may contain catalysts and use the so-called “spillover” effect [60]. In this type of gas sensor, the catalyst helps to dissociate certain gas molecules, causing the dissociated atoms (or fragments) to spill over onto the surface of the sensing element. There they react with the

available oxygen on the metal-oxide surface, creating a measurable change. The rate of catalytic activity is highly dependent on temperature and many other factors.

One of the most efficient ways of achieving selectivity is by using sensors with the enzymatic reactions. Enzymes are a special kind of catalyst—proteins having molecular weight 6–4000 kDa, found in living organisms. They have two remarkable properties: (1) they are extremely selective to a given substance and (2) they are extraordinarily effective in increasing the rate of reactions. Therefore, they favorably contribute to both: the selectivity and the magnitude of the output signal. The maximum velocity of the reaction is proportional to the concentration of the enzyme.

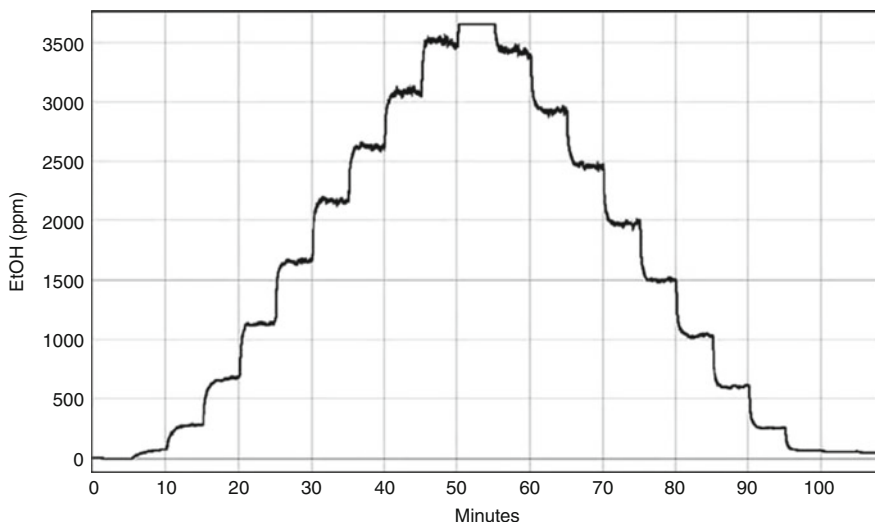
The enzyme-containing sensing element can be a heated probe, an electrochemical sensor, or an optical sensor. Enzymes operate only in an aqueous environment, so they are incorporated into immobilization matrices that are gels, specifically hydrogels. One common mode of operation is as follows: an enzyme is immobilized inside a layer into which the target chemical from the sample diffuses. When the enzyme reacts with the target chemical, it produces a chemical product or other effect, which can be detected.

### 18.3.1.3 Electrochemical Selectivity

Electrochemical sensors typically contain two or three electrodes having one as a “working” electrode, where the chemical interaction of interest takes place, while the others are the counter or auxiliary electrode and reference electrode. In some cases a reference electrode is used to force the system to help with measurement or controlling the electrochemical reactions. The sensor operation is similar to a battery, where a certain chemical reaction (oxidation or reduction) is induced to occur, with the application of a specific electrical potential or chemical species. The reaction usually produces a current or potential that can be detected. Examples are presented below.

## 18.3.2 Sensitivity

*Sensitivity* describes the minimal concentrations and concentration changes (then referred to as *resolution*) that can be successfully and repeatedly sensed by a device. Figures 18.3 and 18.4 display typical sets of data used to establish a sensors sensitivity and selectivity. For the chemical sensors, sensitivity is the synonym of resolution. Note that for the sensors described in the previous chapters of this book, the term sensitivity is often used as a synonym of “slope” when the transfer function of a sensor is linear, at least in a narrow range of the input stimuli. Calibration curves prepared using known standard chemicals at known concentrations in a similar way can be used to determine the slope of the plot of chemical concentration vs sensor response and thus establish the sensor sensitivity.



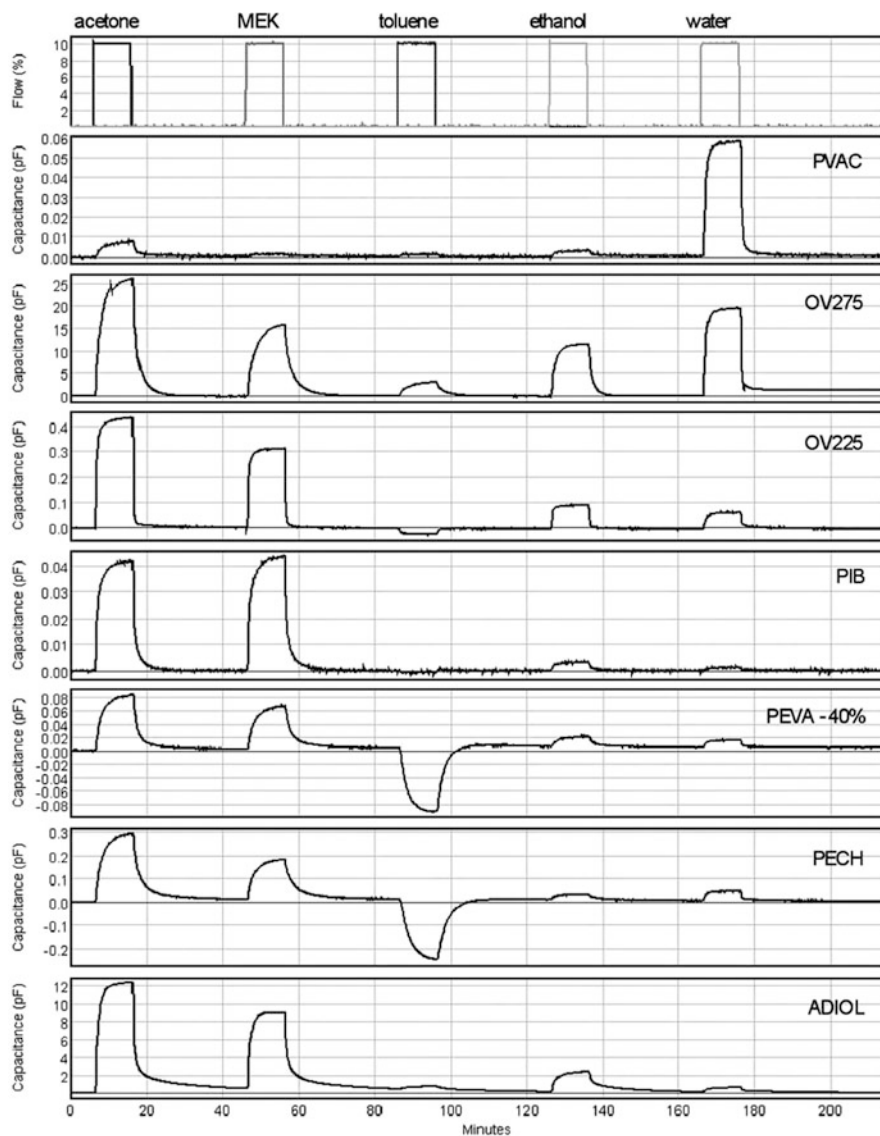
**Fig. 18.3** Metal-oxide semiconductor-based sensor response to increasing and decreasing concentrations of ethanol

## 18.4 Electrical and Electrochemical Sensors

Sensors that directly measure the electrical properties of a target analyte or the affect of the analyte on the electrical properties of another material are often the least expensive commercially available detectors. With these sensors, detection can be a reversible interaction or a destructive irreversible process resulting in analyte decomposition. These devices and supporting electronics are often simple in design and the resulting products can often be used in harsh applications. Sensors in this class include metal oxide semiconductors, electrochemical sensors, potentiometric sensors, conductometric sensors amperometric sensors, elastomeric chemiresistors, chemicapacitors, and ChemFET.

### 18.4.1 Electrode Systems

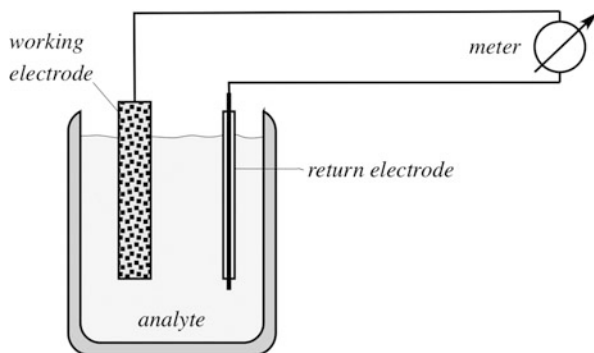
The electrochemical sensors are commercially available and very versatile. Depending on the operating mode, they can be divided into sensors that measure voltage (*potentiometric*), those that measure electric current (*amperometric*), and those which rely on the measurement of conductivity or resistivity (*conductometric*). In all these methods, special electrodes are used, where either a chemical reaction takes place, or the charge transport is modulated by the reaction. A fundamental rule of an electrochemical sensor is that it always requires a closed circuit, that is, an electric current (either DC or AC) must be able to flow in order to



**Fig. 18.4** Response of a capacitive VOC sensor array containing seven differently absorbing polymer coated chemicapacitors to pulses of acetone, methyl ethyl ketone, toluene, ethanol, and water at 25 °C

make a measurement. Since electric current flow essentially requires a closed loop, the sensor needs at least two electrodes, one of which often is called a *working electrode* (WE), while the other is called a *return electrode* or *counter electrode* or *auxiliary electrode* (Fig. 18.5). Both electrodes are immersed into the analyte or electrolyte. It should be noted however, that even though in a potentiometric sensor

**Fig. 18.5** Electrochemical cell with working and return electrodes



no flow of current is required for the voltage measurement, the loop still must be closed for measuring voltage. The sensor formed by these electrodes and electrolytes is called an *electrochemical cell*.

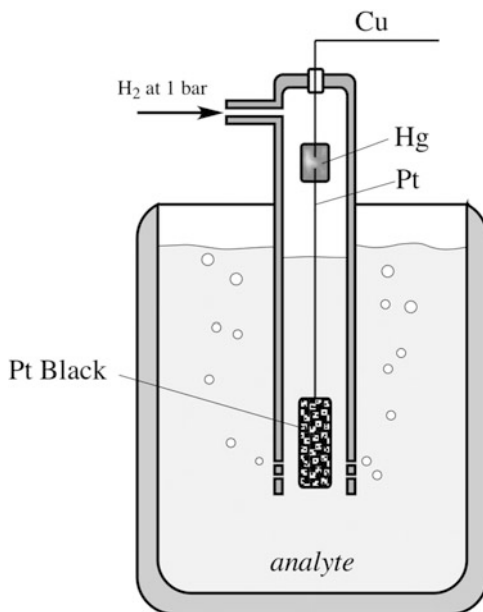
Analyte is a material that is analyzed. It may be dissolved in liquid to form electrolyte which is a medium that carries charges using ions instead of electrons. This directly limits the reactions that can take place and is the first stage of lending selectivity to the electrochemical sensor.

The electrodes in these sensing systems are often made of catalytic metals such as platinum or palladium, or they can be carbon-coated metals. Electrodes are designed to have high surface area to react with as much of the analyte as possible, producing the largest measurable signal. Electrodes can be treated (modified) to improve their reaction rates and extend their working life spans. The working electrode is where the targeted chemical reactions take place. The electrical signal is measured with respect to the reference electrode. Often, the return electrode serves as a reference electrode. Ideally, that electrode should not cause any chemical change to the analyte and the analyte should not modify the reference electrode. The reference electrode shall maintain a constant potential with respect to the analyte, regardless of its concentration or type.

Often, a reference electrode is surrounded by the “bridge solution,” so an electrical contact with the analyte is made through this buffer solution. A concentrated solution of potassium chloride is often selected for the bridge liquid. To prevent leaking the solution into the analyte, the reference electrode is made as an assembly of the metal electrode surrounded by a porous barrier (made of ceramic for example) that restricts the fluid flow. In the barrier, ions from both solutions diffuse to each other, but due to their different mobilities, they will diffuse at different rates. As a result, an electric charge will appear across the barrier in proportion to a difference in the ionic mobilities. Due to a bridge solution, the reference electrode potential is a sum of two potentials: one ( $e_r$ ) is from the electrode–bridge solution interface, while the other ( $e_j$ ) is from the bridge solution–analyte interface:

$$e_{\text{ref}} = e_r + e_j \quad (18.1)$$

**Fig. 18.6** Hydrogen reference electrode



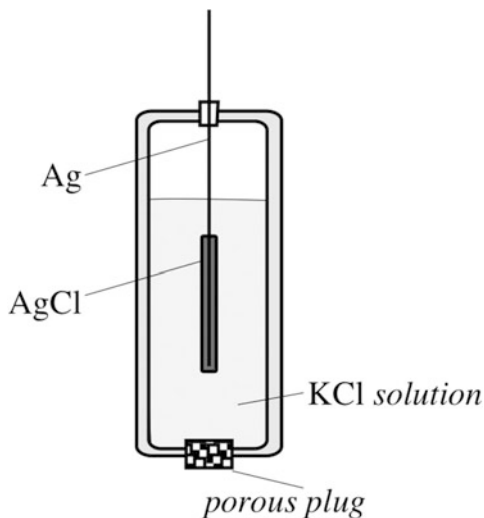
To account for this effect, before use, the sensor is calibrated with a standard analyte solution, so the reference potential becomes known.

There are two types of electrochemical interfaces from the viewpoint of the charge transfer: ideally polarized (purely capacitive) and nonpolarized. Some metals (e.g., Hg, Au, Pt) in contact with solutions containing only inert electrolyte (e.g.,  $\text{H}_2\text{SO}_4$ ) approach the behavior of the ideally polarized interface. Nevertheless, even in those cases a finite charge-transfer resistance exists at such an interface and excess charge leaks across with the time constant given by the product of the double-layer capacitance and the charge-transfer resistance ( $\tau = R_{ct}C_{dl}$ ).

Many analytes are aqueous solutions, thus it makes sense to use a reference electrode where hydrogen ions participate in the reaction. A standard hydrogen electrode (SHE) consists of a platinum foil surrounded by a platinum sponge called “platinum black” having very large surface area (Fig. 18.6). The platinum assembly is positioned inside a glass tube with a built-in small chamber where a drop of mercury is placed to make electrical contact between the platinum and copper wires for the external electrical connection. The Pt Black is dipped in the analyte solution for the electrochemical reaction. The glass tube has an inlet for pumping in  $\text{H}_2$  gas, while the base is perforated for escaping the excess of hydrogen.

When pure, dry hydrogen gas is passed through the inlet, it flows by the Pt Black sponge. Between the hydrogen gas that is adsorbed on the Pt surface and  $\text{H}^+$  of the solution, an equilibrium is established and an electrical double layer of the opposite charges is formed. The electric potential developed on the wire is called *hydrogen electrode potential*. It is defined as the potential that is developed between the hydrogen gas adsorbed on the Pt metal and  $\text{H}^+$  of the solution, when the hydrogen

**Fig. 18.7** Silver–silver chloride reference electrode



gas at a pressure of one atmosphere ( $\sim 1$  bar) is in equilibrium with  $H^+$  of unit concentration. The magnitude of SHE potential is considered to be zero. Since SHEs are difficult to prepare and maintain, they are rarely used in practice as reference electrodes. Their main purpose is for establishing the base potential for standardizing other reference electrodes. Thus, the potentials of the reference electrodes are measured on a *hydrogen scale*.

Other reference electrodes include the calomel electrode that consists of mercury with a layer of mercurous chloride ( $Hg_2Cl_2$ ) and silver–silver chloride ( $Ag/AgCl$ ) electrode. In many practical applications, the latter is preferable as it does not contain poisonous mercury and is much more temperature stable. This type of an electrode is widely used in electrophysiology to pick-up the EKG, EEG and other biological electrical potentials. In chemical sensors, silver electrodes suffer from a high solubility of  $AgCl$  in a concentrated potassium chloride solution, thus the electrode erodes, reducing its lifetime. Its construction is shown in Fig. 18.7. The standard potential of this electrode for a saturated solution is 0.1989 V.

### 18.4.2 Potentiometric Sensors

These sensors use the effect of the concentration on the equilibrium of the redox reactions occurring at the electrode–electrolyte interface in an electrochemical cell. An electrical potential may develop at this interface due to the redox reaction which takes place at the WE surface, where Ox denotes the oxidant,  $Z_e$  is the number of electrons involved in the redox reaction, and Red is the reduced product [10]:





This reaction occurs at one of the electrodes (cathodic reaction in this case) and is called a half-cell reaction. Under thermodynamical quasi-equilibrium conditions, the Nernst equation is applicable and can be expressed as

$$E = E_0 + \frac{RT}{nF} \ln \frac{C_0^*}{C_R^*}, \quad (18.3)$$

where  $C_0^*$  and  $C_R^*$  are the concentrations of Ox and Red, respectively,  $n$  is the number of electrons transferred,  $F$  is the Faraday constant,  $R$  is the gas constant,  $T$  is the absolute temperature, and  $E_0$  is the electrode potential at a standard state. In a potentiometric sensor, two half-cell reactions will take place simultaneously at each electrode. However, only one of the reactions should involve the sensing species of interest, while the other half-cell reaction is preferably reversible, noninterfering, and known.

The measurement of the cell potential of a potentiometric sensor should be made under zero-current or quasi-equilibrium conditions, thus a very high input impedance amplifier with a low bias current (which is called an *electrometer*<sup>1</sup>) is generally required. An ion-selective membrane is the key component of all potentiometric ion sensors. It establishes the reference with which the sensor responds to the ion of interest in the presence of various other ionic components in the sample. An ion-selective membrane forms a nonpolarized interface with the solution. A well-behaved membrane, i.e., one which is stable, reproducible, immune to adsorption and stirring effects, and also selective, has both high absolute and relative exchange-current density.

### 18.4.3 Conductometric Sensors

An electrochemical conductivity sensor measures the change in conductivity of the electrolyte in an electrochemical cell. An electrochemical sensor may involve a capacitive impedance resulting from the polarization of the electrodes and faradic or charge transfer process.

In a homogeneous electrolytic solution, the conductance of the electrolyte  $G$  ( $\Omega^{-1}$ ), is inversely proportional to  $L$ , which is the segment of the solution along the electrical field and directly proportional to  $A$ , which is the cross-sectional area perpendicular to the electric field [11]

$$G = \frac{\rho A}{L}, \quad (18.4)$$

where  $\rho$  ( $\Omega^{-1} \text{ cm}^{-1}$ ) is the specific conductivity of the electrolyte and is related quantitatively to the concentration and the magnitude of the charges of the ionic

---

<sup>1</sup> An electrometer is an instrument for measuring very small electric charges, currents or electrical potential differences. It is characterized by very low leakage currents, down to 1 fA.

species. According to Kohlrausch [12], the equivalent conductance of the solution at any concentration,  $C$  in mol/l or any convenient units, is given by

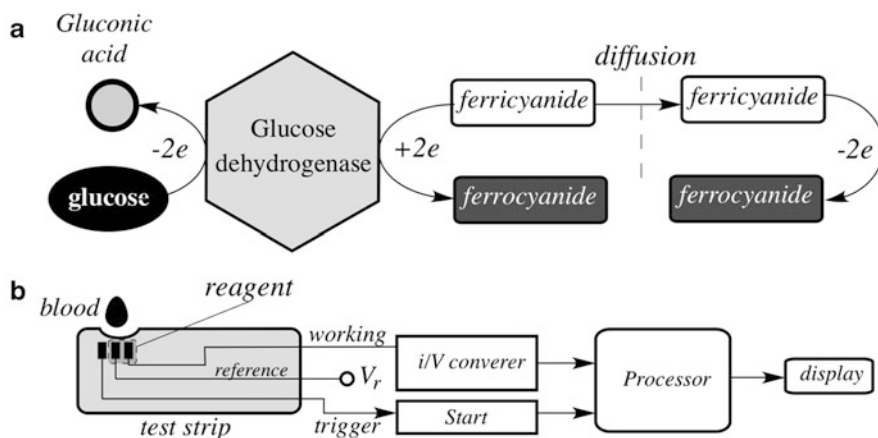
$$\Lambda = \Lambda_0 \beta \sqrt{C}, \quad (18.5)$$

where  $\beta$  is a characteristic of the electrolyte and  $\Lambda_0$  is the equivalent conductance of the electrolyte at an infinite dilution.

Measurement techniques of electrolytic conductance by an electrochemical conductivity sensor has remained basically the same over many years. Often, a Wheatstone bridge (similar to Fig. 18.11) is used with the electrochemical cell (the sensor) forming one of the resistance arms of the bridge. However, unlike the measurement of the conductivity of a solid, the conductivity measurement of an electrolyte is often complicated by the polarization of the electrodes at the operating voltage. A faradic or charge transfer process occurs at the electrode surfaces. Therefore, a conductivity sensor should be operated at a voltage where no faradic process could occur. Another important consideration is the formation of a double layer adjacent to each of the electrodes when a potential is imposed on the cell. This is described by the so-called Warburg impedance. Hence, even in the absence of the faradic process, it is essential to take into consideration the effect of the double layers during measurement of the conductance. The effect of the faradic process can be minimized by maintaining the high cell constant  $L/A$  of the sensor so that the cell resistance lies in the region between 1 and 50 k $\Omega$ . This implies using a small electrode surface area and large inter-electrode distance. This, however, reduces sensitivity of the Wheatstone bridge. Often the answer is in use of a multiple electrode configuration. Both effects of the double layers and the faradic process can be minimized by using a high frequency low amplitude alternating current. Another technique is to balance both the capacitance and the resistance of the cell by connecting a variable capacitor in parallel to the resistance of the bridge area adjacent to the cell.

An example of conductometric sensor is a blood glucose monitor. Conductivity of a blood sample cannot be directly tested to measure concentration of the glucose molecules, but using an electrochemical reaction, glucose can be used to generate a current. There are multiple chemical methods to achieve this. In one method, a drop of blood is applied to a test strip, where it is chemically preprocessed by a special reagent—enzyme (a protein catalyst) called glucose dehydrogenase. However, glucose and enzymes do not readily exchange electrons directly with the conductivity sensor electrode, so another chemical is required—a mediator to facilitate (or mediate) the electron transfer. The following steps take place in the glucose test strip, Fig. 18.8a:

- (a) Glucose in a blood sample first reacts with the enzyme glucose dehydrogenase. Glucose is oxidized by use of the atmospheric oxygen to gluconic acid and the enzyme is temporarily reduced by two electrons being transferred from the glucose molecule to the enzyme.



**Fig. 18.8** Concept of conductometric blood glucose sensor. Chemical reactions on a test strip (a); simplified block-diagram (b)

- (b) The reduced enzyme next reacts with the mediator ( $M_{ox}$ ), transferring a single electron to each of two mediator ions. The enzyme is returned to its original state, and the two  $M_{ox}$  ions are reduced to  $M_{red}$ .
- (c) At the sensor's electrode surface,  $M_{red}$  is oxidized back to  $M_{ox}$  (completing the circuit) and, after some incubation time that is required to complete the reactions and stabilize the process, the current passing through the modified sample is used to determine the concentration of glucose in the blood.

The enzyme glucose dehydrogenase is highly specific and accelerates the oxidation of glucose to gluconic acid. It is also less susceptible than glucose oxidase to common interferences. Its high specificity enables it to selectively react only with glucose in the presence of the thousands of compounds that could potentially interfere within the complex blood sample. This specificity is critical because glucose levels vary widely over time in a single healthy patient along with many other factors such as hematocrit, oxygen levels, metabolic by-products, and medications. The mediator in a test strip is potassium ferricyanide. The redox couple ferricyanide–ferrocyanide is capable of rapidly exchanging electrons with the working electrode. As a result, electrons are transferred between glucose and the electrode via enzyme and mediator and facilitate change in the reduction of electrical conductivity as function of glucose concentration.

Figure 18.8b illustrates a simplified block diagram of the blood glucose monitor that uses a conductometric method. The test strip has three electrodes that come in contact with the blood sample. The working electrode exchanges electrons with the mediator in the reagent. The reference electrode closes the current loop and provides a bias voltage that facilitates the chemical reaction and allows measurement of the sample conductivity, while the trigger electrode is for detecting the moment when the blood sample is applied to the strip. The Start circuit detects drop

in voltage that is caused by the blood conductivity. Electric current through the working electrode is a linear function of the number of released electrons. Thus, it is nearly proportional to concentration of glucose molecules in the blood sample.

Another example of a conductometric sensor is the *alcohol detector*. There are several methods of detecting blood alcohol wherein a direct blood test is the most accurate, albeit less convenient and slow. Screening for blood alcohol is used to determine whether an individual's blood alcohol content (BAC) is below or above a certain threshold value. In most practical cases, instead of sampling blood, screening is done by a *breathalyzer* to establish the breath alcohol content (BrAC). Conversion factors have been established to convert BrAC values into BAC values. The most commonly accepted conversion factor is 2100 [109]. To detect alcohol in breath, sample gas (breath) is injected into the sensing module of the breathalyzer. Of several possible ways of detecting breath alcohol, three possibilities are practical:

1. *Fuel cell* sensor devices are based on electrochemical reactions, in which alcohol in the gas phase is oxidized on a catalytic electrode surface to generate a quantitative electrical response.
2. *Infrared absorption* devices for breath sampling operate on the principle of infrared light being absorbed by alcohol molecules. The amount of light absorbed by the gas sample flowing through the sample cell can be taken as a measure of the alcohol content.
3. *Semiconductor* sensing element utilizes small, heated (300 °C) beads of a transition metal oxide, across which a voltage is applied to produce a small standing current. The current magnitude depends on the conductivity of the surface of the bead. Since the conductivity is affected by the amount of alcohol molecules adsorbed, it can be utilized as a measure for the alcohol concentration in the gas sample.

### 18.4.3.1 Amperometric Sensors

An example of an amperometric chemical sensor is a Clark oxygen sensor which was proposed in 1956 [13]. The operating principle of the electrode is based on the use of electrolyte solution contained within the electrode assembly to transport oxygen from an oxygen-permeable membrane to the metal cathode. The cathode current arises from a two-step oxygen-reduction process that may be represented as:

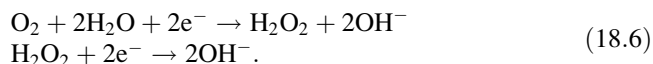
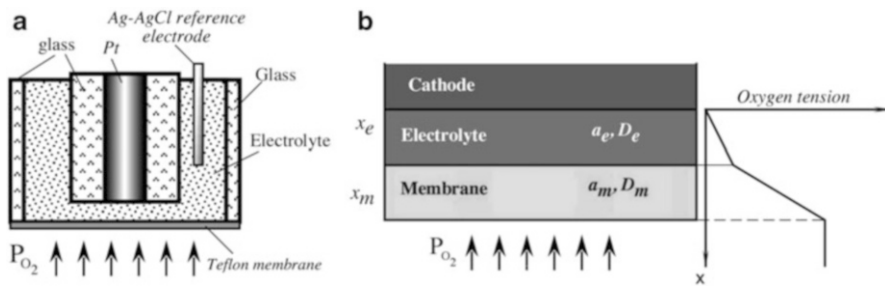


Figure 18.9a shows the membrane which is stretched across the electrode tip, allowing oxygen to diffuse through a thin electrolyte layer to the cathode. Both anode and cathode are contained within the sensor assembly, and no electrical contact is made with the outside sample. A first-order diffusion model of the Clark electrode is illustrated in Fig. 18.9b [14]. The membrane-electrolyte-electrode system is considered to act as a one-dimensional diffusion system with the partial pressure at the membrane surface equal to the equilibrium partial pressure  $p_o$  and



**Fig. 18.9** Clark electrode (a) and first-order one-dimensional model (b) of oxygen tension distribution throughout system (adapted from ref. [14])

that at the cathode equal to zero. It can be shown that the equilibrium steady-state electrode current is given by:

$$I \approx \frac{4Fa_m D_m p_{O_2}}{x_m}, \quad (18.7)$$

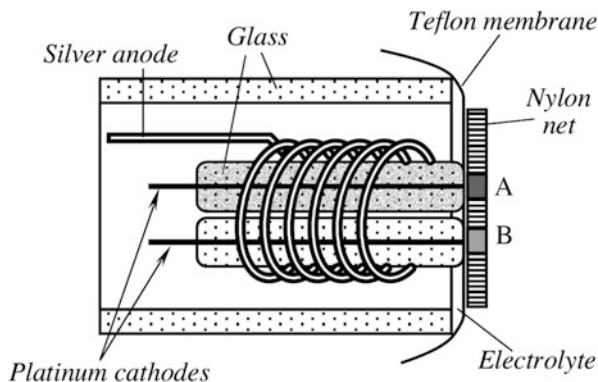
where  $A$  is the electrode area,  $\alpha_m$  is the solubility of oxygen in the membrane,  $F$  is the Faraday's constant,  $D_m$  is the diffusion constant, and  $x_m$  is the thickness of the membrane. It should be noted that the current is independent on the electrolyte thickness and diffusion properties. A Teflon<sup>®</sup> membrane can be used as an oxygen permeable film. We may define the sensor's sensitivity as a ratio of the current to the oxygen partial pressure

$$S = \frac{I}{p_{O_2}}. \quad (18.8)$$

For example, if the membrane is  $25 \mu\text{m}$  thick, and the cathode area is  $2 \times 10^{-6} \text{ cm}^2$ , then the sensitivity is approximately  $10^{-12} \text{ A/mmHg}$ .

An enzymatic type amperometric sensor can be built with a sensor capable of measuring the relative oxygen deficiency caused by the enzymatic reaction by using two Clark oxygen electrodes. The operating principle of the sensor is shown in Fig. 18.10. The sensor consists of two identical oxygen electrodes, where one (A) is coated with an active enzyme layer, while the other (B) with an inactive enzyme layer. An example of the application is a glucose sensor, where inactivation can be carried out either chemically, or by radiation, or thermally. The sensor is encapsulated into a plastic carrier with glass coaxial tubes supporting two Pt cathodes and one Ag anode. In the absence of the enzyme reaction, the flux of oxygen to these electrodes, and therefore the diffusion limiting currents, are approximately equal to one another. When glucose is present in the solution and the enzymatic reaction takes place, the amount of oxygen reaching the surface of the active electrode is reduced by the amount consumed by the enzymatic reaction, which results in a current imbalance.

**Fig. 18.10** Simplified schematic of an amperometric Clark oxygen sensor adapted for detecting glucose



#### 18.4.4 Metal Oxide Semiconductor (MOS) Chemical Sensors

The most common type of metal oxide based sensor (MOS) translates changes in concentration of a reactive species into changes in resistance. Development of these sensors began over 60 years ago when researchers discovered that the resistivity of a semiconductor changes with its chemical environment [15]. Germanium was used as an early model and clearly displayed measurable changes in resistance but suffered from problems with reproducibility for a range of reasons. Today metal-oxide sensors are commercially available, inexpensive, robust and serve in a number of different applications.

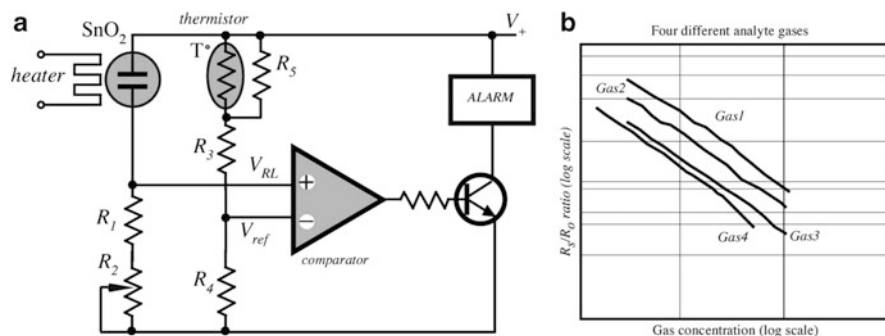
A metal-oxide-based sensor is generally comprised of a semiconducting sensitive layer, an electrical connection to measure the resistance of that layer, and a heater to control the temperature of the device [10]. After a reactive molecule chemisorbs on the metal-oxide surface a charge transfer takes place. When a metal oxide crystal such as  $\text{SnO}_2$  is heated at a certain high temperature in air, oxygen is adsorbed on the crystal surface and a surface potential is formed that inhibits electron flow. When the surface is exposed to oxidizable gases, such as hydrogen, methane, and carbon monoxide, the surface potential lowers and conductivity measurably increases [16]. As the concentration of the target chemical increases so does the magnitude of the change in resistance.

The relationship between the film's electrical resistance and a given oxidizable gas's concentration is described by the following empirical equation:

$$R_s = A[C]^{-\alpha}, \quad (18.9)$$

where  $R_s$  is the sensor electrical resistance,  $A$  is a constant specific for a given film composition,  $C$  is the gas concentration, and  $\alpha$  is the characteristic slope of  $R_s$  curve for that material and expected gas [17].

Metal oxide devices change resistivity in the presence of oxidizable gases and as such they require additional electronic circuitry to operate. A typical arrangement is to design the sensor as one leg in a Wheatstone bridge circuit (see Sect. 6.2.3) so



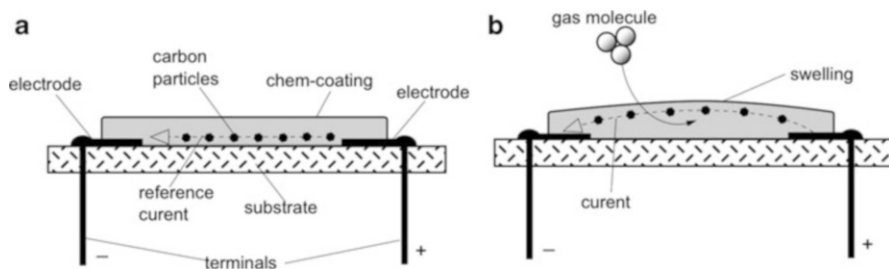
**Fig. 18.11** SnO<sub>2</sub> wheatstone bridge circuit (a) used for metal oxide sensors and responses to different gases (b)

that the changing resistance can be detected as an unbalancing of the potential drops observed across the bridge circuit, Fig. 18.11a. An NTC thermistor<sup>2</sup> with a linearizing parallel resistor is required to adjust the bridge balance point according to the sensor's temperature.

Since the sensor behaves as a variable resistor whose value is controlled by the gas species and gas concentration the voltage drop across it is proportional to its resistance and a plot of voltage drop vs. gas concentration is typically recorded. The response signal from the sensors is linear when plotted on logarithmic charts, Fig. 18.11b. The slopes and offsets of the curves produced by different oxidizable gases allow them to be distinguished from each other and quantified within certain concentration ranges where the curves do not overlap [18]. Optionally, the rate-of-change of the conductivity may be used to differentiate gases and concentrations [19]. The bulk conductivity can drift for these devices, but the rate-of-change of that conductivity when driven by a pulsed input is more stable and reproducible.

These solid-state sensors have the advantage of being small, having relatively low power consumption, low in cost, and can be easily batch-fabricated. The control and measurement circuitry can be fabricated on the silicon microchip as well, providing opportunities to design sensor packages containing monolithically integrated arrays of sensing elements along with the on-chip data acquisition and control systems. Several references to thin and thick film sensors on silicon devices have appeared based on a number of different materials for sensing a variety of gases [20, 21]. Tin oxide is the most prevalent pure film material studied [22–26]. In addition, Pt-doped [27, 28] and Pd-doped tin oxide films [29, 30] have been used to sense carbon monoxide, hydrogen, and hydrocarbons. Titania, in various forms and environments, has been used for sensing oxygen [31]. Rhodium-doped TiO<sub>2</sub> [32] has been used to sense hydrogen. Zinc oxide [33] has been used to sense hydrogen, carbon monoxide, and hydrocarbons. The electrical properties of these materials change with the adsorption, absorption, desorption, rearrangement, and reaction of

<sup>2</sup> Resistive temperature sensor having negative temperature coefficient (NTC)—see Chap. 17.



**Fig. 18.12** Swell-type chemo-resistor. Reference state (a) and detecting state (b)

gases on the surface or in the bulk. Many of these materials have catalytic properties, and the adsorption and/or surface reactions of gases contribute to changes in electrical conductivity.

### 18.4.5 Elastomer Chemiresistors

Elastomer chemiresistors or polymer conductive composites (also *polymer conductors* or simply “PCs”) are polymer films that adsorb chemical species and swell, increasing resistance as a *physical* response to the presence of a chemical species. These can be used as chemical detectors but do not truly employ a chemical reaction. The polymers are designed and/or treated to attract subsets of chemicals providing a degree of speciation or selectivity [34]. The PC sensors can respond to the presence of simple hydrocarbons such as isopropyl alcohol in only a couple of seconds, while less volatile chemicals, such as oils, may take 10–15 s. The PC element is not expected to be tolerant of corrosives, but barring such exposure should have a lifespan of months in normal operation. The typical PC sensing strategy uses several differently treated PC elements to produce an array, and then sample the array to produce a signature. Unlike metal oxide based sensors, the PCs do not require the high, controlled operating temperatures and therefore consume significantly less power. However, since the response is temperature dependent, a constant temperature of the PC should be maintained. This may be achieved by warming up the sensing element above ambient temperature (e.g., 40 °C), while during measurement maintaining that temperature on a stable level. In other words, the PC sensor should be augmented with a thermostat. In the manufacturing process, the PC film is impregnated with microscopic conductive particles [108], carbon black powder,<sup>3</sup> e.g., as shown in Fig. 18.12a. Initially, a reference current is established by the monitoring circuit in the absence of the odor of interest. When the specific odor is present in the air and absorbed by the coating, the bulk volume

<sup>3</sup>The mechanism of resistivity change is similar to that of a thick film force sensor shown in Fig. 10.4.



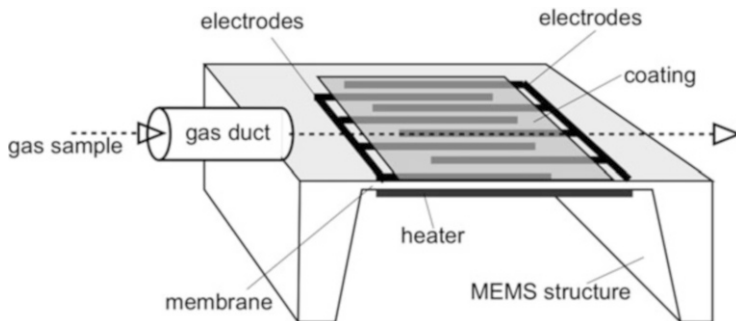
of the PC coating swells somewhat, causing increase in the average distance between the conductive particles, that in turn leads to increase in electrical resistance between the terminals. Subsequently, resistance is converted to electrical signal for processing, Fig. 18.12b.

Because swelling of the polymer begins immediately after exposure to the vapor, the resistance signals can be read in real-time or near-real-time. Currently, with sensing films having thickness on the order of 1  $\mu\text{m}$ , the swelling (and therefore resistance) response times to equilibrium film swelling values range from 0.1 to 100 s, depending on the vapor and the polymer through which the vapor must diffuse. More rapid responses to equilibrium could be simply obtained through reduction in the film thickness. Since the diffusion time is proportional to the square of the film thickness, decreasing the film thickness to the range of 0.1  $\mu\text{m}$  should provide a practically quick response. At small swellings, the film returns fully to its initial unswollen state after the vapor source is removed, and the film resistance on each array element returns back to its original value. The sensitivity of the conducting polymer composite based electronic nose compares highly favorably to other vapor detection systems.

To detect the presence of a liquid or vapor, a sensor usually must be specific to that particular agent at a certain concentration. That is, it should be selective to the liquid's physical and/or chemical properties. An example of such a sensor is a resistive detector of hydrocarbon fuel leaks. A detector is made of silicone (a nonpolar polymer) and carbon black composite. The polymer matrix serves as the sensing element and the conductive filler is used to achieve a relatively low volume resistivity, on the order of  $10\ \Omega\ \text{cm}$  in the initial stand-by state. The composition is selectively sensitive to the presence of a solvent with a large solvent-polymer interaction coefficient [35] and both the sensitivity and resistance can be modified by varying the conductive particle to polymer ratio. The sensor is fabricated in the form of a thin-film with a very large surface/thickness ratio. Whenever the solvent or vapor is exposed to the thin-film sensor, the polymer matrix swells resulting in the separation between conductive particles. This causes a conversion of the composite film from being more conductive to less conductive with a resistivity on the order  $10^9\ \Omega\ \text{cm}$ , or even higher. The response time for a thin-film sensor can be less than 1 s. The sensor returns to its normally conductive state when it is no longer in contact with the hydrocarbon fuel, making the device reusable.

An example of a swelling chemo-resistor for in an e-nose is a hydrogen sulfide ( $\text{H}_2\text{S}$ ) detector. Hydrogen sulfide is a toxic gas, which may be present in many environments and has a distinct smell of a rotten egg or decaying waste. In particular, it is responsible for a mouth malodor (halitosis). A level of  $\text{H}_2\text{S}$  gas at or above 100 parts per million (ppm) is immediately dangerous to life and health. The  $\text{H}_2\text{S}$  sensors require high sensitivity to fairly low levels of the gas and must also be able to discriminate  $\text{H}_2\text{S}$  from other gases that may be present and not give spurious readings affected by such other gases.

Just as in many breathalizers, to operate, the  $\text{H}_2\text{S}$  sensor's surface has to be heated well above ambient temperature to about 300  $^\circ\text{C}$ . This puts a significant



**Fig. 18.13** Concept of the H<sub>2</sub>S MEMS variable resistance sensor

strain on the sensing module power supply and also prolongs a response time of the sensor. To reduce both, a modern MEMS technology may be employed. Figure 18.13 illustrates a concept of the MEMS H<sub>2</sub>S sensor, where a silicon structure is formed with a substrate supporting a thin membrane having thickness on the order of 1  $\mu\text{m}$ . Such a membrane has low thermal capacity and thus can be warmed up to high temperature in a short time by a relatively low power.

Two inter-digitized (alternating) electrodes are formed on the membrane's upper surface. A selective coating is deposited by a sputtering and oxidizing technique on the top of the electrodes. The coating has a finite resistance that varies in relation with concentration of the H<sub>2</sub>S molecules in the gas sample. To form a sensing film, firstly a layer of a molybdenum sulfide, MoS<sub>2</sub>, having thickness no greater than 1000  $\text{\AA}$  is sputtered over the silicon membrane and the electrodes and subsequently a layer of tungsten oxide, WO<sub>x</sub>, of the same thickness are sputtered on. The resulting double-coating is then heated in air for several hours at a temperature of around 500  $^{\circ}\text{C}$ . This has both a sintering and oxidizing effect and generates a complex combination of metal oxides [110]. This coating combination does not consist merely of separate oxides of tungsten and molybdenum, but instead an ordered structure is formed which is an inseparable combination of the oxides and is in effect a type of crystal structure having both types of oxide contained within the same crystal lattice. The bottom of the silicon membrane is given a heater layer that during operation brings up the membrane temperature close to 300  $^{\circ}\text{C}$ . When in use, after the heater temperature is settled on a constant level, a sample of the outside gas is drawn over the membrane either by blowing into the gas duct, or sucking up by a miniature blower that augments the sensing module. The gas reacts with the coating whose electrical resistance changes accordingly to a concentration of the H<sub>2</sub>S molecules. The resistance can be easily measured by one of the conventional methods and related to the gas concentration. This sensor responds in few seconds and, what is also very important, has a fast clearing time, that is a quick readiness for the next measurement.

Recently nanomaterials have been used in place of carbon black to make fast-responding polymer composites for different applications [36]. These materials

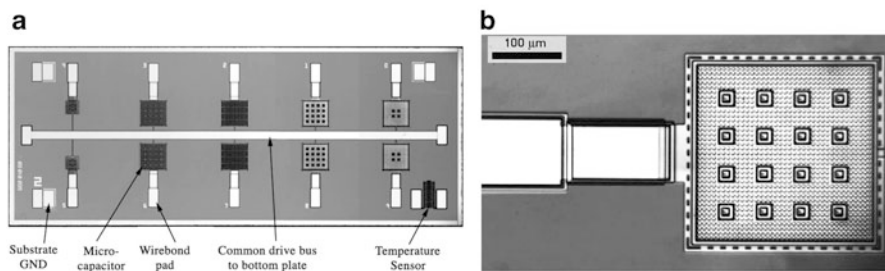
include carbon nanotubes [37], graphene [38], and metal nanoparticles [39]. In some cases, the polymers themselves have been spun into conductive fibers [40], or carbon nanotubes have been modified [41] to have some selective chemical functionality.

### 18.4.6 Chemicapacitive Sensors

A “chemicapacitive” sensor (or “chemicapacitor”) is a capacitor that has a selectively absorbing material, such as a polymer or other insulator, as a dielectric. When a chemical absorbs into the dielectric, its dielectric constant is altered, and correspondingly the capacitance of the sensor changes [42]. The most common type of commercially available chemicapacitor consists of water sensitive polymers and is used for humidity sensing (see Sect. 14.3). However, chemicapacitors are not limited to polymer dielectrics. Other materials have been used to broaden the range of detectable chemicals, sol–gel chemicapacitors, for example, can detect carbon dioxide [43]—although such materials often have to be heated to achieve optimal performance. More recently, polymers have been used to make low power sensors for volatile organic compounds (VOCs) [44].

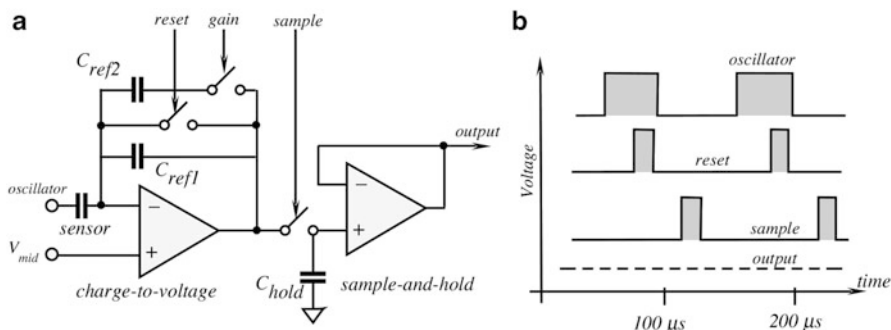
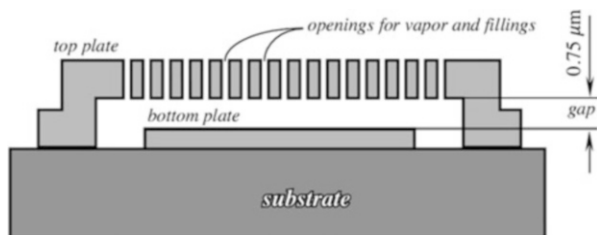
Chemicapacitors can be constructed using conventional thin film techniques, where conductive electrodes are arranged in either a parallel or interdigital layout, similar to Fig. 18.13. Typically, interdigitized electrodes consist of a single layer of metal deposited on a substrate to form two meshed combs. The polymer or other materials are deposited on top of the combs. Parallel-plate sensors [45] typically consist of a layer of metal deposited on a substrate, followed by a layer of insulator and finally a second, porous layer of metal on top of the insulator.

One example of a chemicapacitor is a MEMS-sensor based on micromachined capacitors [46] has been developed and commercialized. An example geometry is the square-shaped parallel-plate capacitor seen in Fig. 18.14. It has approximately 285  $\mu\text{m}$  on a side, with a 0.75  $\mu\text{m}$  vertical gap between the plates (Fig. 18.15). The top plate is perforated forming a waffle pattern, with silicon beams of 2.5  $\mu\text{m}$  and holes of 5  $\mu\text{m}$ . The 16 larger squares are the support posts, which together with the



**Fig 18.14** MEMS chip ( $2 \times 5$  mm) containing a variety of parallel-plate capacitor designs (a). Close-up top-view of a parallel-plate capacitor (b)

**Fig. 18.15** Cross-section diagram of the parallel-plate capacitor showing the 0.75  $\mu\text{m}$  gap



**Fig. 18.16** Capacitance measurement circuit (a) and timing diagrams (b)

outer edge of the square (also perforated) keep the top plate from flexing. The structures are made from conductive polycrystalline silicon, deposited on an insulating silicon nitride layer using commercially available semiconductor manufacturing methods [47].

These types of sensors can be made with varying geometries, and varying numbers of sensors and each sensor can receive a different analyte-sensitive coating. Each capacitor is filled with a polymer using an ink-jet [37]. The interaction between target analyte and polymer modifies the dielectric properties of the polymer resulting in a change in capacitance. Any capacitance measuring circuit can be used to measure these types of devices. These MEMS detector arrays operate well in ambient air at ambient pressures and temperatures, thus requiring no special compressed carrier gas and allowing for systems with decreased size and increased portability. They are now used commercially as the detectors for a gas chromatograph suitable for training students in academic laboratories.<sup>4</sup>

To measure the capacitance, a circuit applies a square wave voltage to the bottom plate. A charge/discharge readout circuit [48, 49] shown in Fig. 18.16 measures the capacitance of each sensor array using an oscillating charge/discharge drive voltage, and producing the corresponding output voltage,  $V_{\text{out}}$ :

<sup>4</sup> Vernier Mini Gas Chromatograph ([www.vernier.com/probes/gc-mini.html](http://www.vernier.com/probes/gc-mini.html)).

$$C_{\text{Sensor}} = \frac{(V_{\text{out}} - V_{\text{mid}})}{\Delta V_{\text{osc}}} \left( \sum C_{\text{ref}} \right), \quad (18.10)$$

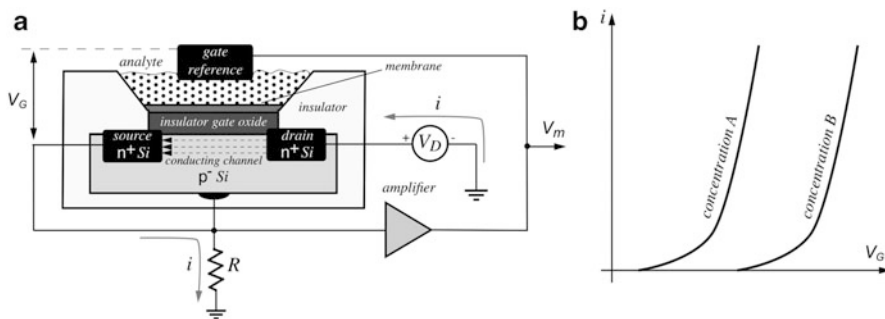
where  $V_{\text{mid}}$  is a virtual ground voltage or reference,  $\Delta V_{\text{osc}}$  the amplitude of the oscillator drive voltage,  $C_{\text{Sensor}}$  the capacitance of the capacitive sensor, and  $C_{\text{ref}}$  is the reference capacitance, which should be near or in the range of the capacitance of the sensor and is determined by the position of the gain switch. In the circuit, the reference capacitors are charged as the sensing capacitor discharges.

### 18.4.7 ChemFET

A conventional field effect transistor (FET) can be modeled as a voltage controlled resistor. The FET has *source*, *drain*, and *gate* terminals. When presenting FET as a variable resistor, the resistance is attributed to a narrow silicon channel between the source and drain, while the gate serves as a control terminal. The names of the terminals refer to their functions. Some FETs have a fourth terminal called the body, base, bulk, or substrate. This fourth terminal serves to bias the transistor into operation, but often it is not used in designs of electric circuits and typically is internally connected to the source terminal. Its presence is important when setting up the physical layout of an integrated circuit. The gate is insulated from the channel by a thin insulator—a layer of silicon dioxide ( $\text{SiO}_2$ ). Electrons in the FET “resistor” flow from the source terminal towards the drain terminal while the current magnitude is influenced by a control voltage applied between the source and gate.

The idea behind converting a FET into a chemical sensor is to augment the gate terminal with chemically sensitive components that would modify the source-gate voltage for controlling the source-drain resistance, and subsequently the source-drain current. The chemically selective gate material alters the gate potential at which the device begins to conduct and thus indicates the presence of specific chemical species. This modified FET was given the name ChemFET. Different materials applied to the gate react with different chemical species (gases or liquids) and provide differentiation of species. ChemFETs can be used for detecting  $\text{H}_2$  in air,  $\text{O}_2$  in blood, some military nerve gases,  $\text{NH}_3$ ,  $\text{CO}_2$ , and explosive gases [50]. Hydrogen gas-sensing ChemFETs use a palladium–nickel (Pd/Ni) film at their gate materials [51]. ChemFETs that are used for liquid sensing may employ a silver–silver chloride hydrogel (Ag/AgCl) bridge between the silicon dioxide ( $\text{SiO}_2$ ) gate isolator and a selective membrane that separates the gate from the analyte. The selective membrane is commonly polyvinyl chloride (PVC), polyurethane, silicone rubber, or polystyrene.

To detect a specific analyte, a ChemFET may use a small chamber that is positioned on the top of the gas- or ion-selective coating (or membrane) or series of coatings between its transistor gate and the analyte. A chemical sensitive element gives the device a control input that modifies the source-drain conduction in relationship with selected chemical species (analyte). Membrane-containing ChemFETs are commonly used to detect ions or biological molecules in liquids,



**Fig. 18.17** Liquid ChemFET construction and electrical connection for a feedback to the reference electrode (a) and volt-ampere characteristics (b)

Fig. 18.17a. When the membrane is placed into a contact with the test solution, for example, containing ions of the analyte, an additional potential  $\Delta V$  is generated at the membrane–electrolyte interface. This potential together with the bias voltage from the external source modifies the gate potential and thus modulates the current flow between the drain and source.

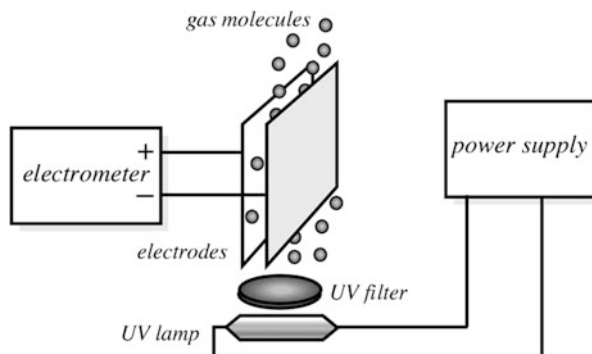
For an ion-selective ChemFET (ISFET) [52] the gate is replaced by or coated with a chemical selective electrolyte or other semiconductor material. If the ion-sensitive membrane is ion-penetrable, then the device is called a MEMFET (membrane-modified FET) and if the membrane is ion-impenetrable it is called a SURFET, since a surface potential is established by the ions. The gate coatings for the ChemFET can be enzyme membranes (ENFET) or ion-selective membranes. Ion-selective membranes produce a chemical sensor, while enzyme membranes can produce a biochemical-sensor. The enzyme membrane is made from polyaniline and is itself created using a voltammetric electrochemical process to produce this organic semiconductor [53]. The devices are inherently small and low in power consumption.

Just as in a conventional FET, the ChemFET is constructed using thin film techniques and commonly employs a *p*-type silicon body with two *n*-type silicon diffusion regions (source and drain). Operation of the ChemFET involves applying positive voltages to the gate and drain with respect to the source. The most popular circuit includes a feedback loop from the output to the reference gate electrode as shown in Fig. 18.17a. The feedback sets a constant current  $i$  through resistor  $R$ , depending on concentration of the analyte. When the concentration changes, the volt-ampere characteristic of the ChemFET shifts, Fig. 18.17b, and is measured as variation in the source-drain current.

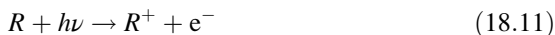
## 18.5 Photoionization Detectors

A photoionization detector (PID) typically uses high energy ultraviolet (UV) light to break molecules into positively charged ions. The molecules absorb the light energy resulting in temporary loss of electrons and the formation of positively

**Fig. 18.18** Concept of PID detector



charged ions. The molecules produce an electric current which is measured by an electrometer. Equation (18.11) shows a molecular species,  $R$ , being ionized by incident UV radiation, to an ion,  $R^+$  and electron.



The UV lamp is the heart of the detector and improvements in the UV lamp designs have led to significant reduction in cost and longer life expectancies. The wavelength of the UV light depends on the type of gas in the lamp employed. A popular choice is krypton which emits light with energies<sup>5</sup> of 10.0 and 10.6 eV. Xenon and argon lamps are also used occasionally.

When gas molecules pass by the UV lamp, they become ionized (Fig. 18.18). The free electrons are collected at a pair of closely placed electrode plates. These electrodes generate a signal in response to small changes in the electric field. The magnitude of the current flow is directly proportional to the gas concentration.

Each chemical has an ionization potential (IP), and gases with IP values below the rated eV output of the lamp will be ionized and thereby detected. For example, organic aromatic compounds and amines can be ionized by the 9.5 eV lamps, many aliphatic organic compounds require a 10.6 eV lamp and compounds such as acetylene, formaldehyde and methanol are more difficult to ionize and require an 11.7 eV lamp. Each lamp can ionize gases with ionization potentials below its eV rating but will not ionize gases with higher ionization potentials. Typically, portable PID systems are equipped with the 10.6 eV lamp because of its ability to ionize most volatile organic compounds. Isobutylene is often used to calibrate these devices. Each chemical will have a calibration factor, for a given lamp energy, which is related to the degree of ionization. The output of the PID sensor is typically linear below 200 ppm and will become saturated above 2000 ppm.

<sup>5</sup> The electron volt (eV) is a unit of energy. By definition, it is equal to the amount of kinetic energy gained by a single unbound electron when it accelerates through an electrostatic potential difference of 1 V. One eV is equal to  $1.60217653 \times 10^{-19}$  J.

## 18.6 Physical Transducers

Several types of chemical sensors rely on measurement of a physical property of an analyte or the affect of the analyte's interaction with another material for detection. Usually, no chemical reaction occurs at the sensing element. These sensor technologies can be reversible or destructive. Common, reversible technologies include those that require absorption of the analyte into a substrate sitting on a sensitive microbalance that can respond to changes in mass. These sensors include surface acoustic wave (SAW) devices, quartz crystal microbalances (QCMs) and microcantilevers. Destructive sensors may directly measure the molecular mass of an analyte, as in ion mobility spectrometry, or the quantity of heat released during complete oxidation, as in thermal or calorimetric sensors.

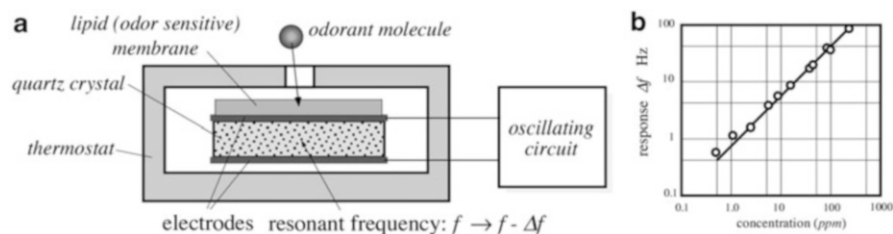
### 18.6.1 Acoustic Wave Devices

Acoustic wave devices can be used to make chemical sensors that detect very small mass change from adsorbed chemical molecules altering mechanical properties of a system, and are referred to as *mass*, *gravimetric*, or *microbalance sensors*. These devices are generally constructed from piezoelectric crystals or materials which can be oscillated at high frequencies (from kHz to GHz). In various types of these devices, acoustic waves are generated by an oscillator circuit, which allows the crystal to resonate. The resonant frequency of the sensor changes when the crystal is perturbed, typically the frequency decreases when the mass of the device increases during sorption [54]. The shift in the resonant frequency of a piezoelectric crystal is proportional to the additional mass that is deposited on the crystal surface. Depending upon how the circuit is constructed, a piezoelectric quartz oscillator resonates with a frequency that is called either a series ( $f_i$ ) or a parallel ( $f_{ar}$ ) resonant, see Fig. 7.1b. The frequency is function of the crystal mass and shape. For example, in one type of sensing structure, which in a simplified manner may be described as an oscillating plate whose natural frequency depends on its mass, the mass change and frequency are related by:

$$\frac{\Delta f}{f_o} = S_m \Delta m \quad (18.12)$$

where  $f_o$  is the unloaded natural oscillating frequency,  $\Delta f$  is the frequency shift:  $\Delta f = f_{\text{loaded}} - f_o$ ,  $\Delta m$  is the added mass per unit area, and  $S_m$  is called the sensitivity factor. The numerical value of  $S_m$  depends upon the design, material, and operating frequency (wavelength) of the acoustic sensor [47]. Since frequency and time are the easiest variables to measure by the electronic circuits the entire sensor's accuracy is determined virtually by the ability to assure that coefficient  $S_m$  is known and does not change during the measurement. Figure 18.19 shows an example of this type of a sensor.





**Fig. 18.19** Concept of microbalance vapor sensor (a) and its transfer function (b) for amylacetate gas

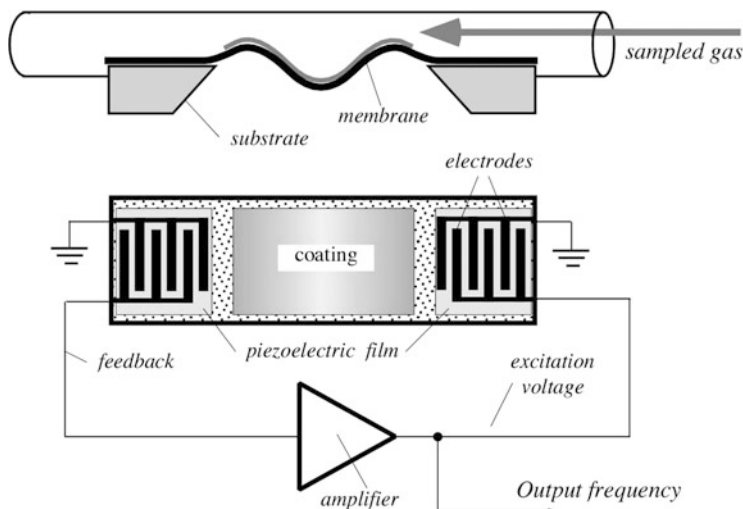
An electronic circuit measures the frequency shift, which can be related to a chemical concentration in the sampled gas. The absolute accuracy of the method depends on such factors as the mechanical clamping of the crystal, temperature, and therefore, calibration is usually required.

Generally speaking, there are four types of acoustic sensors widely used in chemical sensing research and products. These include quartz crystal microbalances (QCM), surface acoustic wave (SAW), acoustic plate mode (APM), and flexural-plate-wave (FPW) devices made from thin membranes. There are also several variations on these types of devices, which have been developed or adapted for specific uses. These variations include use of different modes of oscillation, resonance, and materials. Unlike a QCM, which operates at its resonant frequency, SAW, APM, and FPW devices are typically called “delay-line” devices. The delay refers to the time it takes for an applied electrical signal at one end (transmitter) of the device to propagate through the material (the acoustic wave) and to be measured at the opposing end (receiver).

Unlike the chemiresistors or chemicapacitors described in the earlier sections, the gravimetric transducers do not need to directly measure the properties of a sensitive layer; rather they indirectly measure the interaction of the layer with the environment. Generally speaking, all of the oscillating sensors are extremely sensitive. For instance, a typical sensitivity is on the range of  $5 \text{ MHz cm}^2/\text{kg}$ , which means that 1 Hz in frequency shift corresponds to about  $17 \text{ ng/cm}^2$  added mass. The dynamic range is quite broad: up to  $20 \text{ }\mu\text{g/cm}^2$ . To improve selectivity, devices may be coated with a chemical layer specific for the material of interest.

One type of a gravimetric detector is a surface acoustic wave sensor. SAW devices use propagating mechanical waves along a solid surface, which is in contact with a medium of lower density, such as air [55]. These waves are sometimes called Rayleigh waves after the man who predicted them in 1885. As with the other delay-line devices, the surface acoustic wave sensor is a transmission line with three essential components: the piezoelectric transmitter, the transmission line, typically with a chemically selective layer, and the piezoelectric receiver.<sup>6</sup> An electrical oscillator causes the electrodes of the transmitter to flex the substrate, thus

<sup>6</sup> See Sect. 13.6.2.



**Fig. 18.20** Flexural plate SAW gas sensor (deflection of membrane is exaggerated for clarity)

producing a mechanical, or acoustic, wave. The wave propagates along the transmission surface toward the receiver. The substrate may be fabricated of for example  $\text{LiNbO}_3$ , a material with a high piezoelectric coefficient [56]. However, the transmission line does not have to be piezoelectric, which opens several possibilities for designing the sensor of different materials, like silicon. The transmission surface interacts with the sample according to the selectivity of the coating, thus modulating the propagating waves. The waves are received at the other end and subsequently converted back to an electric form. Often, to reduce interferences and drifts, there is another reference sensor whose signal is subtracted from the test sensor's output.

Another type of a gravimetric sensor is shown in Fig. 18.20. The sensor is designed in form of a flexural thin silicon plate with two pairs of the interdigitized electrodes deposited by use of the sputtering technology. A thin piezoelectric  $\text{ZnO}$  thin film is deposited beneath the electrodes, so that the plate can be mechanically excited by the external electronic circuit. The piezoelectric film is needed to give silicon substrate piezoelectric properties. The top surface of the sensing plate can be coated with a thin layer of any number of different chemically selective materials. In this example, the entire sensor is positioned inside a tube where the sampled gas is blown through. The left and right pairs of the electrodes are connected to the oscillating circuit whose frequency  $f_0$  is determined by the natural mechanical frequency of the sensor's plate.

The circuit contains an amplifier whose output drives the excitation electrode. Thanks to a piezoelectric effect, this causes flexing the membrane and propagation of the deflection wave from right to left. The wave velocity is determined by the state of the membrane and its coating. Change in mechanical properties of the coating depends on its interaction with the sampled gas. Thus, the left electrodes

**Table 18.1** SAW chemical sensor coatings and materials (after [58])

Compound	Chemical coating	SAW substrate
Organic vapor	Polymer film	Quartz
SO <sub>2</sub>	TEA	Lithium niobate
H <sub>2</sub>	Pd	Lithium niobate, silicon
NH <sub>3</sub>	Pt	Quartz
H <sub>2</sub> S	WO <sub>3</sub>	Lithium niobate
Water vapor	Hygroscopic	Lithium niobate
NO <sub>2</sub>	PC	Lithium niobate, Quartz
NO <sub>2</sub> , NH <sub>3</sub> , NH <sub>3</sub> , SO <sub>2</sub> , CH <sub>4</sub>	PC	Lithium niobate
Vapor explosives, drugs	Polymer	Quartz
SO <sub>2</sub> , methane	C <sup>a</sup>	Lithium niobate

TEA triethanolamine, PC phthalocyanine

<sup>a</sup>No chemical coating used. Detection is based on changes in thermal conductivity produced by the gas

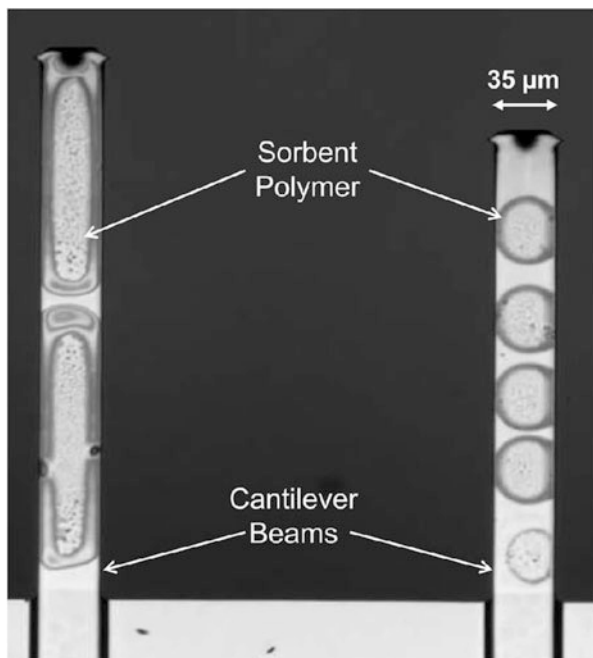
will detect piezoelectric response either sooner or later, depending how fast the wave goes through the membrane. The received signal is applied to the amplifier's input as a positive feedback voltage and causes the circuit to oscillate. The change in output frequency is a measure of the sampled gas concentration. The reference frequency is usually determined before sampling the gas.

A theoretical sensitivity of the flexural plate sensor is given by  $S_m = \frac{1}{2}\rho d$ , where  $\rho$  is the average density of the plate and  $d$  is its thickness [57]. At an operating frequency of 2.6 MHz the sensor has sensitivity on the order of  $-900 \text{ cm}^2/\text{g}$ . Thus, for example, if the sensor having the sensing area of  $0.2 \text{ cm}^2$  captures  $10 \text{ ng}$  ( $10^{-8} \text{ g}$ ) of material, the oscillating frequency is shifted by  $\Delta f = -900 \times 2.6 \times 10^6 \times 10^{-8} / 0.2 = -117 \text{ Hz}$ . Acoustic sensors are quite versatile and can be adapted for measuring variety of chemical compounds. The key to their efficiency is selection of the coating. Table 18.1 gives examples of various coatings for acoustic sensors.

## 18.6.2 Microcantilevers

Microcantilevers are devices shaped as miniature diving boards that are typically micromachined from silicon or other materials. Originally used in various types of surface probe microscopies (SPM) [58] they have since been adapted to detect chemicals [59, 60] and biological materials [61, 62]. As with chemiresistors and acoustic devices, a chemically sensitive sorbent coating can be added to the cantilever to enhance its sensitivity and selectivity to certain chemicals. Cantilevers have been shown to detect a wide range of chemical analytes from fixed gases such as hydrogen [42], to common volatile organic compounds [63], to explosives [64].

The length of these cantilevers is often in the range of 100–200  $\mu\text{m}$ , with a thickness range from 0.3 to 1  $\mu\text{m}$ . Since 1994, these devices have been developed for detecting a variety of chemicals by monitoring either the bending or frequency

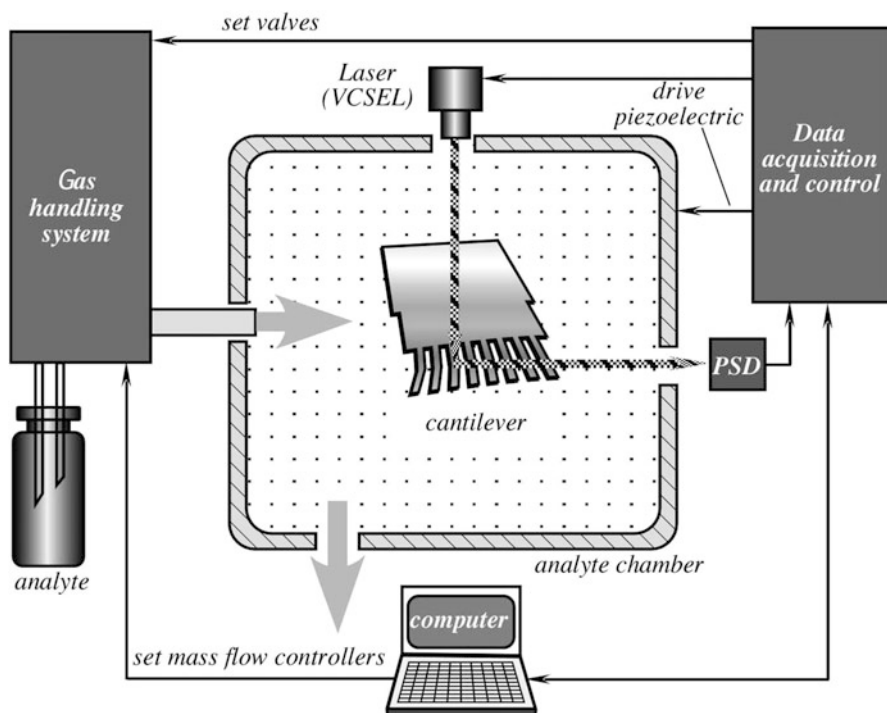


**Fig. 18.21** Standard optical microcantilevers used for surface probe microscopy that have been modified with an absorbent coating. The cantilever beam on the right has five drops of a sorbent polymer coating and the beam on the left has a continuous sorbent polymer coating covering the entire length

shift of an oscillating microcantilever [65–67]. The key to the sensitivity of these very thin devices is the high surface-to-volume ratio. This amplifies the effect of surface stresses due to interactions with chemicals.

When oscillated at its harmonic frequency, a cantilever can be used to detect sorbed mass, much like the acoustic devices described earlier. The resonance frequencies decrease due to the adsorbed mass and the more mass absorbed the greater the shift in frequency. Alternatively, the bending of a cantilever can be used to measure the change in surface stresses on the cantilever beam when a target chemical is preferentially absorbed to one of the surfaces of the cantilever by placing a selectively absorbent chemical coating on that surface (Fig. 18.21). Because surface stress is being monitored, diffusion into the coating is not necessary, and therefore, monolayer coatings are ideally suited for these devices.

The bending of the microcantilever is not caused by the weight of the absorbed chemical but by the absorption induced surface stresses due to changes in surface free energy. The cantilever will bend if the surface free-energy density change is comparable with the cantilevers spring constant. When chemicals come in contact with a coated cantilever, electrostatic repulsions, swelling, or other affects result in changes in surface stress, which ultimately result in measurable cantilever bending.



**Fig. 18.22** Concept of the measurement setup for optical cantilevers (adapted from ref. [53])

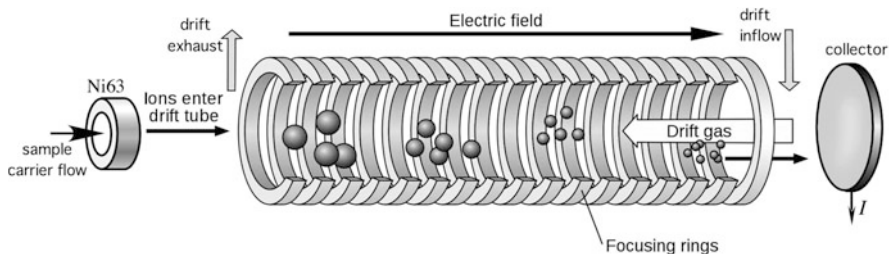
Cantilevers can be measured in many ways. Originally the sensing systems were based on optical (laser) detection (Fig. 18.22) being developed for SPM. Newer research has implemented thermal [65], capacitive [41], and piezoresistive [68] measurement techniques, thereby removing the need for lasers and associated optics, resulting in a simpler measurement circuit.

## 18.7 Spectrometers

Spectrometry (spectroscopy) is a class of powerful methods used to analyze chemical compositions based on energy or mass. There are several types of spectrometry, including:

*Mass Spectrometry (MS):* Sample molecules are ionized, and the mass to charge ratio of these ions is measured very accurately by electrostatic acceleration and magnetic field perturbation, providing a precise molecular weight.

*Ion mobility spectrometry (IMS):* a technique that detects and differentiates chemicals based on differential migration of ions under the influence of an electric field [69].



**Fig. 18.23** Principle of ion mobility spectrometry

*UV and visible spectroscopy:* Absorption of this (wavelengths of 200–800 nm) relatively high-energy light causes electronic excitation.

*Infrared spectroscopy:* Absorption of this lower energy radiation causes vibrational and rotational excitation of groups of atoms within the molecule.

*Nuclear magnetic resonance spectroscopy:* Absorption in the low-energy radiofrequency part of the spectrum causes excitation of nuclear spin states. NMR spectrometers are tuned to certain nuclei.

### 18.7.1 Ion Mobility Spectrometry

Ion mobility spectrometry has become the go-to technique for detection of contraband and explosives, due to its high sensitivity and selectivity. IMS both separates and detects chemicals, using differential migration of ions in an electric field. In IMS, gas phase species are required to be ionized, for example by high energy electrons from a radioactive  $^{63}\text{Ni}$  source. Ions travel in a gas stream through an electric deflection field that spatially separates the ions with respect to their ion mobility at atmospheric pressure. Ion species with different characteristics (mass, charge, and size) have different drift velocities, as in Eq. (18.13) where  $K$  is an ions mobility and  $v_d$  is its drift velocity (see Fig. 18.23). Ideally, individual ion beams develop that are spatially separated.

$$v_d = KE \quad (18.13)$$

By increasing the deflection voltage of the electric field all ion beams are successively directed onto the collector electrode, where the ion current  $I$  is measured. Differentiating the recorded  $I(V)$  curve results in the ion mobility spectrum. Under constant conditions the ion mobility  $K$  is a characteristic measure for a certain ion species. Typically an IMS will have a high resolution of  $R > 20$ :

$$R = t_d/W_{t,1/2} \quad (18.14)$$

where  $t_d$  is the drift time and  $W_{t,1/2}$  the temporal peak width measured at half of the maximum peak height.

Ion mobility spectrometers have become common in security and screening applications, such as in airports where they are used for drug [70], and explosives detection [71]. Such systems have been made into hand-held sniffers and bench-top instruments. Research and development of this detection technology remains very active with several groups around the world dedicated to advancing this analytical approach. Variations include different methods of ionization, the addition of chemicals to enhance ionization, and alternating electric fields to improve ion separation [72].

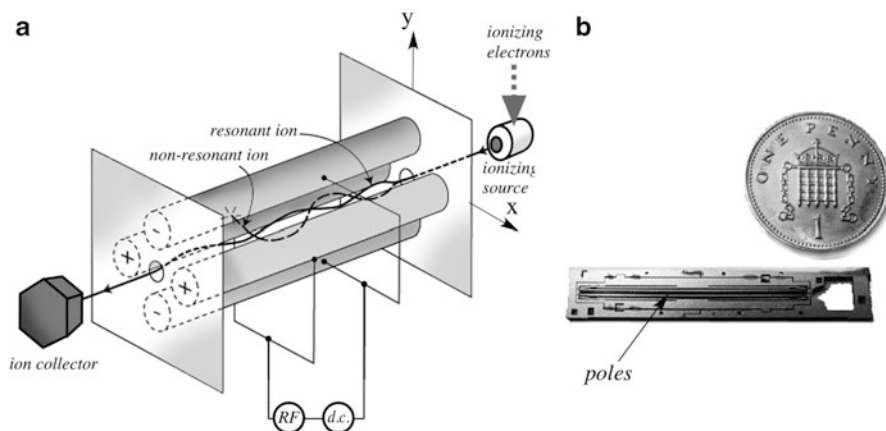
Recent advances in micro fabrication have allowed for miniaturization of the ion mobility drift tube and detectors to chip-sized devices, known as differential mobility spectrometry (DMS) or field asymmetric IMS (FAIMS) [6]. In this technique, as ions flow through the gas channel, an asymmetric AC voltage is applied (perpendicular to flow) with a DC bias. The result is that ions are filtered by field strength. Commercial FAIMS systems are available primarily for defense and screening applications.

## 18.7.2 Quadrupole Mass Spectrometer

Quadrupole mass filtering was invented in 1960 [74] and now is the most common mass analyzer. It is also known under other names such as a transmission quadrupole mass spectrometer (QMS) or quadrupole mass filter. Mass spectrometry is used to determine a specific molecular characteristic called mass-to-charge ( $m/z$ ) ratio. The spectrometer is fast, has a very wide dynamic range, and is quite efficient, albeit it is also quite expensive.

In a quadrupole mass spectrometer (QMS), the separation and determination of the molecule and fragment masses is controlled with high-frequency electric fields produced by the radiofrequency (RF) generator. The RF voltages are applied to four rod-shaped electrically conductive electrodes (quadrupole) placed in high vacuum, as shown in Fig. 18.24a. The filtering and determination of the ionized molecules is then implemented with a programmed modulation of the RF voltage amplitude with simultaneous superimposition of a DC voltage which can also be modulated.

The tested molecules are ionized by high-energy electrons, plasma, or with chemical reagents, and enter the space between four rods (poles). The alternating electric field produced by the rods accelerates ions out of the source region and into the quadrupole channel between the rods. As the ions travel through the channel, they are filtered according to their  $m/z$  ratio so that only a single  $m/z$  value ions can strike the detector inside the ion collector that is positioned at the opposite side from the source. The  $m/z$  ratio is determined by the RF and DC voltages applied to the electrodes. These voltages produce an oscillating electric field that functions as a bandpass filter to transmit only the selected  $m/z$  value. Thus, the molecules of the specific  $m/z$  are in resonance with the RF frequency and oscillate in the  $x$ - $y$  plane, while propagating toward the collector. On the other hand, the out of resonance



**Fig. 18.24** Concept of quadrupole mass spectrometer (a) and miniature QMS assembly made with MEMS technology (b) (from Imperial College London)

molecules go astray, hit the rods, and never reach the detector—in other words, they are rejected. The RF and DC fields are scanned (either by DC potential or frequency) to collect a complete mass spectrum. Recently attempts were made to develop QMS in a miniature form by using MEMS technologies, Fig. 18.24b.

## 18.8 Thermal Sensors

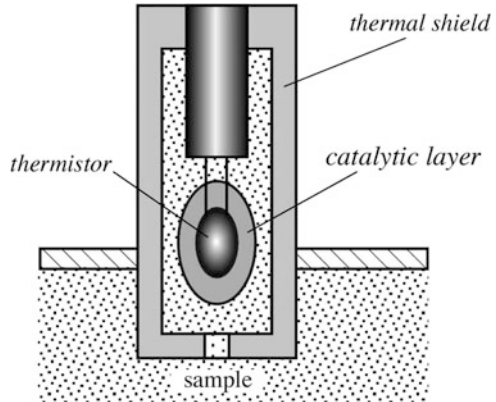
### 18.8.1 Concept

When the internal energy of a system changes, it is accompanied by an absorption or evolution of heat (as defined by the first law of thermodynamics). Therefore, a chemical reaction, which is associated with heat, can be detected by an appropriate thermal sensor, such as described in Chap. 17. These sensors operate on the basic principles that form the foundation of a *microcalorimetry*. The operating principle of a thermal sensor is rather simple: a temperature probe is coated with a chemically selective layer. Upon a chemical exposure, the probe measures transfer of heat during the reaction between the sample and the coating.

A simplified drawing of such a sensor is shown in Fig. 18.25. It contains a thermal shield to reduce heat loss to the environment and a thermistor coated by a catalytic layer. A biosensor based microcalorimeter may be made where the sensitive layer has an enzyme immobilized into a matrix. An example of such a sensor is the enzyme thermistor covered by an immobilized glucose oxidase (GOD). The enzymes are immobilized on the tip of the thermistor, which is then enclosed in a glass jacket in order to reduce heat loss to the surrounding solution. Another similar sensor with similarly immobilized bovine serum albumin is used as a reference. Both thermistors are connected as the arms of a Wheatstone bridge [73].



**Fig. 18.25** Schematic diagram of chemical thermal sensor

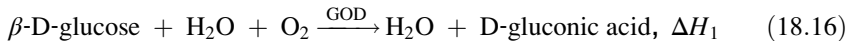


The temperature increase,  $dT$ , as a result of a chemical reaction is proportional to the incremental change in the enthalpy  $dH$

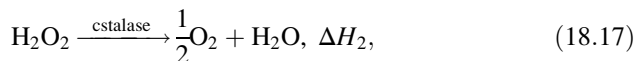
$$dT = \frac{1}{C_p} dH, \quad (18.15)$$

where  $C_p$  is the heat capacity of the sensing assembly.

The chemical reaction in the coating is



and

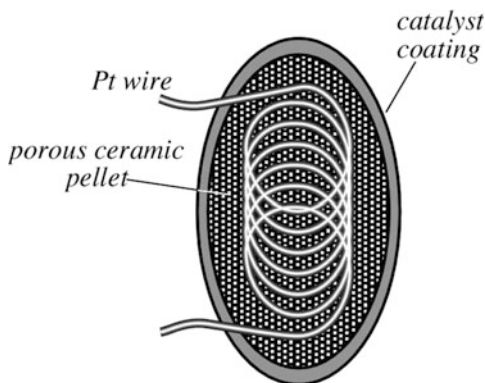


where  $\Delta H_1$  and  $\Delta H_2$  are partial enthalpies, the sum of which (for the above reaction) is approximately  $-80$  kJ/mol. The sensor responds linearly with the dynamic range depending on the concentration of hydrogen peroxide ( $\text{H}_2\text{O}_2$ ).

## 18.8.2 Pellister Catalytic Sensors

Pellisters and other catalytic sensors operate on the principle similar to thermal enzymatic sensors. Heat is liberated as a result of a catalytic reaction taking place at the surface of the sensor and the related temperature change inside the device is measured. Thus, the chemistry is similar to that of high temperature metal-oxide sensors, only the method of transduction is different. Catalytic gas sensors [10] have been designed specifically to detect low concentrations of flammable gases in ambient air inside mines. In a pellister, the platinum coil is imbedded in a pellet of  $\text{ThO}_2/\text{Al}_2\text{O}_3$  coated with a porous catalytic metal: palladium or platinum (Fig. 18.26).

**Fig. 18.26** Pellister or catalytic type thermal detector



The coil acts as both the heater and the resistive temperature detector (RTD). Naturally, any other type of heating element and temperature sensor can be successfully employed. When the combustible gas reacts at the catalytic surface, the heat evolved from the reaction increases the temperature of the pellet and of the platinum coil, thus increasing its resistance. There are two possible operating modes of the sensor. One is isothermal, where an electronic circuit controls the current through the coil to maintain a constant temperature. In the non-isothermal mode the sensor is connected as a part of a Wheatstone bridge whose output voltage is a measure of the gas concentration.

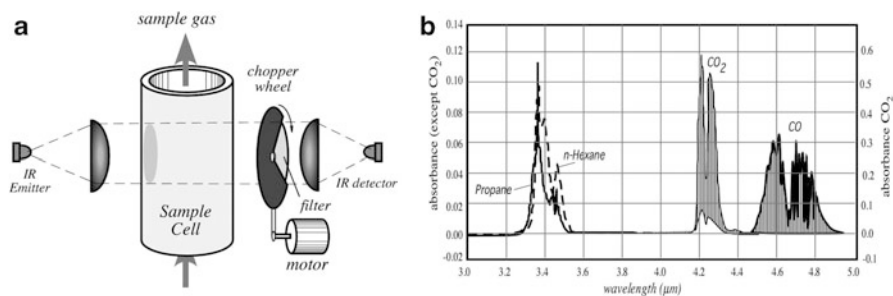
---

## 18.9 Optical Transducers

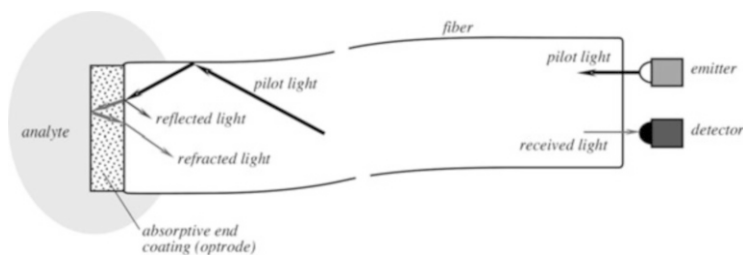
Optical transducers measure the interactions of various forms of light or electromagnetic radiation and a target chemical or a selective layer, by detecting the modulation of some properties of the radiation. Examples of such modulations are variations in intensity, polarization, and velocity of light in a medium. The presence of different chemicals in the analyte affects which wavelengths of light are modulated. Optical modulation is studied by spectroscopy, which provides information on various microscopic structures from atoms to polymer dynamics. In a general arrangement, the monochromatic radiation passes through a sample (which may be gas, liquid, or solid), and its properties are examined at the output. Alternatively, the sample may respond with a secondary radiation (e.g., induced luminescence), which is also measured.

### 18.9.1 Infrared Detection

Most chemicals can absorb infrared (IR) light at wavelengths representative of the types of bonds present. For these chemicals, the Lambert–Beer law can be used because the absorbance of the gas is proportional to the concentration. Most small portable systems employing this technology use non-dispersive IR (NDIR).



**Fig. 18.27** Non-dispersive IR (adapted from [74]) (a) and examples of absorption spectra (b)



**Fig. 18.28** Fiber optic gas sensor

In NDIR a polychromatic light source, typically a lamp or LED, is used to pass electromagnetic energy through a gas sample, Fig. 18.27a. Gases may be sampled using a fan or pump, or simply allowed to diffuse through a filter into an optically transparent cell, as is typically done in CO<sub>2</sub> sensors of this type. An optical filter is used in front of the light detector to limit the incoming light to only a particular wavelengths associated with a target analyte, Fig. 18.27b. The attenuated absorption of that wavelength by the chemical indicates its presence and concentration.

*Spectroscopic* systems for measuring optical absorption are useful for the UV and IR wavelengths and can be used to detect many chemicals, by producing a more complex absorbance signature in the form of a spectrum. Bench-top IR instruments typically use dispersive IR techniques. In these instruments a grate or prism is used to provide a broad wavelength range to select a specific wavelength of light to pass through the sample. In all strategies, the wavelength of the light source is routinely matched to the reactive energy of the optrode indicator to achieve a best possible electronic signal.

## 18.9.2 Fiber-Optic Transducers

*Fiber-optical* chemical sensors (Fig. 18.28) use a chemical reagent or sorbent phase to alter the amount or wavelength of light reflected by, absorbed by, or transmitted through a fiber wave-guide. A fiber optic sensor typically contains three parts, a

source of incident (pilot) light, an optrode, and a transducer (detector) to convert the changing photonic signal to an electrical signal. It is the optrode that contains the reagent phase membrane or indicator whose optical properties are affected by the analyte [75].

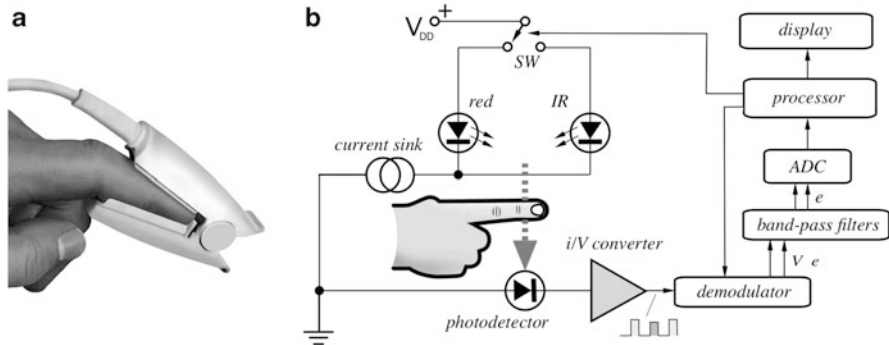
The location of the reagent, and the specific optical characteristic that is affected by it, vary from one type of the optical sensor to another. Simple polymer-coated fibers cover the polished lens end of a glass fiber with a reagent that absorbs incident light. Coating the cladding of a fiber instead of its polished end affects the reflection and refraction of the light. This is referred to as *evanescent wave sensing*. While the glass optical fiber is rugged and in many cases chemically resistant, the coating or indicator is not and becomes the weak component in the system [76].

Differential designs (to isolate all but reaction of interest) are often employed to split the original incoming light source and pass one through the reagent area while the other is unaltered. The two optical paths are either multiplexed to a single detector (transducer) or fed to different transducers to produce a difference signal used for sensing. One variation of the fiber optic sensors is the use of coated beads, which are attached or embedded into the end or a surface of an optical fiber [77]. These beads can be modified or coated to have chemical or biological sensitivity.

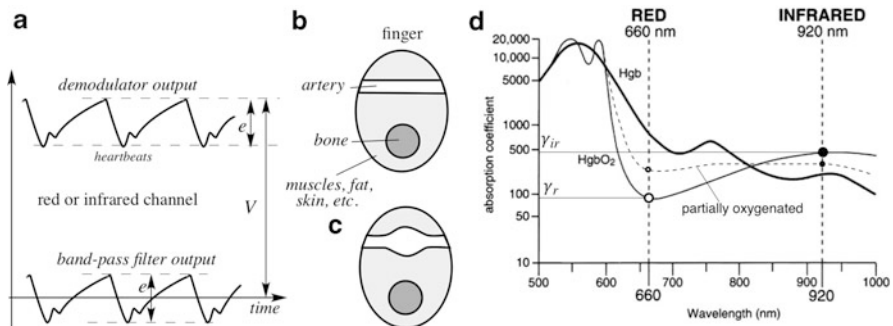
### 18.9.3 Ratiometric Selectivity (Pulse Oximeter)

A ratiometric technique (Sect. 6.2.1) is an efficient method for enhancing an optical selectivity when analyzing a specific property of a material. It requires taking a ratio of the light transmission intensity at two different wavelengths. The basic idea behind the technology is that certain chemicals transmit specific wavelengths of light more than similar chemicals. The ratiometric technique cancels signals from the interfering chemicals and nonspecific portions of the light spectra, thus allowing a higher degree of selectivity. To illustrate the concept, consider a *pulse oximeter*—a medical instrument for the in vivo noninvasive monitoring oxygenation of arterial blood hemoglobin. Word “noninvasive” means that no blood sample is drawn but rather the measurement is performed optically without penetrating the patient’s skin. The word “pulse” here means that only a variable pulsatile portion of the detected light is analyzed to eliminate the additive light components.

The blood oxygenation chemistry in a very simplified form is this. Oxygen is carried to all living cells in the body by the red blood cells where it is combined with molecules of hemoglobin (Hgb)—a protein having the oxygen-binding capacity. Hgb picks up oxygen in lungs, carries it to all organs and releases. It is vital that hemoglobin within the arterial blood carries the maximum possible amount of oxygen. Oxygen saturation, which is often referred to as  $\text{SaO}_2$  or  $\text{SpO}_2$ , is defined as the ratio of oxyhemoglobin ( $\text{HgbO}_2$ ) to the total concentration of Hgb within the blood ( $\text{HgbO}_2 + \text{Hgb}$ ). Usually, it is expressed as percent of the maximum possible oxygenation. In a healthy person under normal conditions arterial  $\text{SpO}_2$  is between



**Fig. 18.29** Pulse oximeter finger clip (a) and conceptual block-diagram (b)



**Fig. 18.30** Output voltages from demodulator and band-pass filter for either red or IR light (a); structure of finger including bone, various tissues and artery, before heartbeat (b); structure of finger with engorged artery following heartbeat (c), and absorption spectrum of oxygenated and deoxygenated hemoglobin (d)

96 and 98 %. If the level drops below 90 %, it is considered low, resulting in hypoxemia that can be sleep apnea, asthma crisis, pulmonary infection, etc.  $SpO_2$  levels below 80 % may compromise organ functions, such as the brain and heart, and should be promptly addressed. Venous blood is about 75 % saturated because oxygen was already released to the body organs.

The operating principle of a pulse oximeter is based on the red and infrared light absorption characteristics of oxygenated and deoxygenated hemoglobin. Body tissues allow transmission of more red and near infrared, while absorbing heavily blue, green, yellow, and mid-infrared lights. Oxygenated hemoglobin absorbs more infrared light while allowing more red light to pass through. Deoxygenated (or reduced) hemoglobin is the opposite—it absorbs more red light and allows more infrared light to pass through. Red light is in the 600–750 nm wavelength range, while infrared light is in the 850–1000 nm range. Figure 18.30d illustrates spectral absorption of two types of Hgb.

To take advantage of different light absorption by hemoglobin, a thin area of patient tissue (often—a tip of a finger or earlobe) is illuminated by two light sources (LEDs): one operates at the peak wavelength near 660 nm (red) and the second at 920 nm (near-infrared). Intensity of light that reaches the other side of the finger is detected by a photodetector and analyzed. The light sources are positioned inside the finger clip, Fig. 18.29a, at its upper portion, while the photodetector is at the opposite side of the finger. A conceptual block-diagram of a pulse oximeter is shown in Fig. 18.29b. The LEDs are turned on and off alternatively with a high rate (e.g., 1 kHz) by the switch SW, so only one at a time illuminates the finger. Their stability is assured by a constant current sink. The photodetector is common for both LEDs, hence its spectral response covers the visible and near IR regions of the optical spectrum. The detector's current passes to the current-to-voltage ( $i/V$ ) converter that produces the output pulses of variable amplitudes—alternatively for each LED. The pulses are demodulated to produce two analog voltages. Only one (red or IR) is shown in Fig. 18.30a as an example.

Figure 18.30b illustrates the structure of a finger that includes various tissues, such as muscles, nail, capillaries, fat, skin, and bone. There is also the artery full of blood—a pliant tube being in a relaxed state just before a heartbeat. Figure 18.30c shows that following a heartbeat, the artery engorges with blood and its volume expands.<sup>7</sup> This expansion leads to a larger absorption of light within the finger and the detected level of light drops as shown in Fig. 18.30a. The  $i/V$  converter generates the voltage pulses for each wavelength. These amplitude-modulated pulses are demodulated in a synchronous demodulator having two outputs: one for the red and the other for IR signal. The demodulated red and infrared voltages respectively are:

$$V_r \approx g_r k \left[ \frac{\Delta_0}{\Gamma_r} + \frac{\Delta_p f(t)}{\gamma_r} \right] = V_r + e_r \quad (18.18)$$

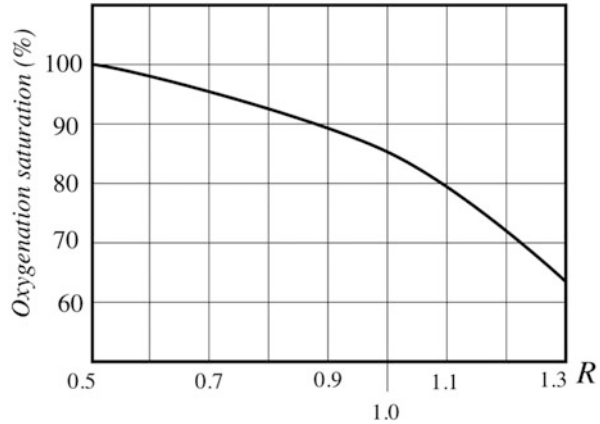
$$V_{ir} \approx g_{ir} k \left[ \frac{\Delta_0}{\Gamma_{ir}} + \frac{\Delta_p f(t)}{\gamma_{ir}} \right] = V_{ir} + e_{ir},$$

where  $g_r$  and  $g_{ir}$  are the red and IR respective LED brightness,  $k$  is the combined detector and  $i/V$  conversion scaling factor,  $\Delta_0$  is the finger equivalent thickness,  $\Delta_p$  is the arterial equivalent maximum volume engorgement,  $f(t)$  is a normalized variable heartbeat function of time,  $\gamma_r$  and  $\gamma_{ir}$  are the blood absorptions for each wavelength, and  $\Gamma_r$ ,  $\Gamma_{ir}$  are the maximum combined absorptions for the finger tissues at two wavelengths respectively. Note that the detected light intensity is inversely proportional to the absorption coefficients.

Each signal has two components: a constant (DC)  $V$  that reflects the total light absorption in a finger just before a heartbeat and a variable component,  $e$ , representing the light absorption being modulated by heartbeats. The magnitude

<sup>7</sup>This is a simplified model. In fact, the arterioles and capillaries also change their volumes with each heartbeat. However, the venous blood flow has almost no pulsatile component.

**Fig. 18.31** Experimentally determined relation between ratio  $R$  and hemoglobin oxygen saturation



of  $e$  is only about 1 % of  $V$ . The constant component depends on many factors (finger size, tissue composition, vasoconstriction, etc.), thus it carries a lot of unknown interfering variables, so it should be eliminated before further signal processing. It is removed by the band-pass filter (0.5–5 Hz) that allows only the variable components to pass for digitizing in the ADC:

$$\begin{aligned} e_r &= \frac{g_r k}{\gamma_r} \Delta_p f(t) \\ e_{ir} &= \frac{g_{ir} k}{\gamma_{ir}} \Delta_p f(t) \end{aligned} \quad (18.19)$$

To eliminate the constant or slow changing multiplicative factors in these equations, the processor computes the ratio  $R$ :

$$R = \frac{e_{ir}}{e_r} = \frac{g_{ir} \gamma_r}{g_r \gamma_{ir}} \approx \frac{\gamma_r}{\gamma_{ir}} \quad (18.20)$$

This final ratio assumes that the LED intensities  $g$  are adjusted to equal levels. Figure 18.30d shows that absorptions  $\gamma$  for a partially oxygenated hemoglobin, as indicated by the dotted line, varies for different ratios of  $\text{HgbO}_2$  and  $\text{Hgb}$ . The ratio of Eq. (18.20) is used as the measure of blood oxygenation. The relationship between  $R$  and  $\text{SpO}_2$  is established in clinical studies (Fig. 18.31) and used for calibrating the monitor.

### 18.9.4 Color Change Sensors

Sensing devices that change color upon exposure to certain chemical or biochemical species are a subset of optical sensors. Color change can be accomplished by many chemical pathways, such as acid–base reactions [78], hydration or solvation

[79], metal complex formation [80], shifts in surface plasmon resonance [81], or enzyme reactions [82] and have been used to detect gases [83, 84], liquids [85] and dissolved metals [86]. Acid–base indicating litmus paper is the most well-known optical indicating platform, where a pH sensitive chromophore is embedded into filter paper. Different chromophore containing molecules allow for detecting different pH transitions or ranges. Color change is also commonly used for indicating the presence of moisture, as in commercially available materials such as Drierite™ [87], a desiccant, calcium sulfate, which contains cobalt(II)chloride that turns from blue to pink as water is absorbed forming the hexahydrate.

Color change mechanisms have been implemented in a variety of sensing applications. The military has used chemical agent detecting paper (M8/M9 paper) to detect the presence of nerve and blister agents. These sheets can be wiped on a surface, or simply placed on personnel or equipment. A color change indicates possible exposure to certain chemical agents. For example, V-type nerve agents turn the M8 paper dark green, G-type nerve agents turn it yellow and blister agents (H) turn it red. M9 paper will turn pink, red, reddish-brown, or reddish-purple when exposed to liquid agent and can detect but not identify the specific agent.

Typically a human reader is required to detect the color change, but recent advances in optical detection technologies have allowed for miniaturization, quantitative analysis, and construction of arrays of detectors with varied selectivity [88]. Such devices compare the relative intensity of photodetector signals to reflected red, green and blue light and generate a quantitative measure of chemical exposure, often by using a ratiometric technique like in the pulse oximeter.

Similarly, Dräger tubes are commonly used for exposure monitoring applications [89]. These devices typically rely on one or more chemical reaction to change color of an indicating substance. Their color-change mechanism is easy to see, but may be difficult to quantify. They can also have many cross-sensitivities, to other chemicals [90]. Graduated tubes filled with these materials can be used to quantify the amount of chemical absorbed over a given period of time [91].

Enzyme Linked Immunosorbent Assay (ELISA) is a common type of colorimetric method, which uses antigen–antibody reactions [92] to react with target analytes in a multistep process, requiring either hands-on use or automation in a lab. Many types of biological and nonbiological chemicals can be detected using ELISA commercially available kits, including glucose, viruses [93], pesticides [94], or drugs. Color-changing immunoassay tests can be very specific and sensitive [95, 96], as is the case with commercially available pregnancy tests that detect human chorionic gonadotropin (hCG).

Color of a reflected or transmitted light can be accurately detected and measured by the RGB + IR color sensors that have 4 narrow-band color sensing channels: red for 615 nm of wavelength, green for 530 nm, blue for 460 nm, and near IR for 855 nm. The example of such a detector is S11059-02DT color sensor from Hamamatsu. It not only detects color at four different wavelength components but also presents the results of measurement as 16-bit numbers in a serial  $I^2C$  interface.



## 18.10 Multi-sensor Arrays

### 18.10.1 General Considerations

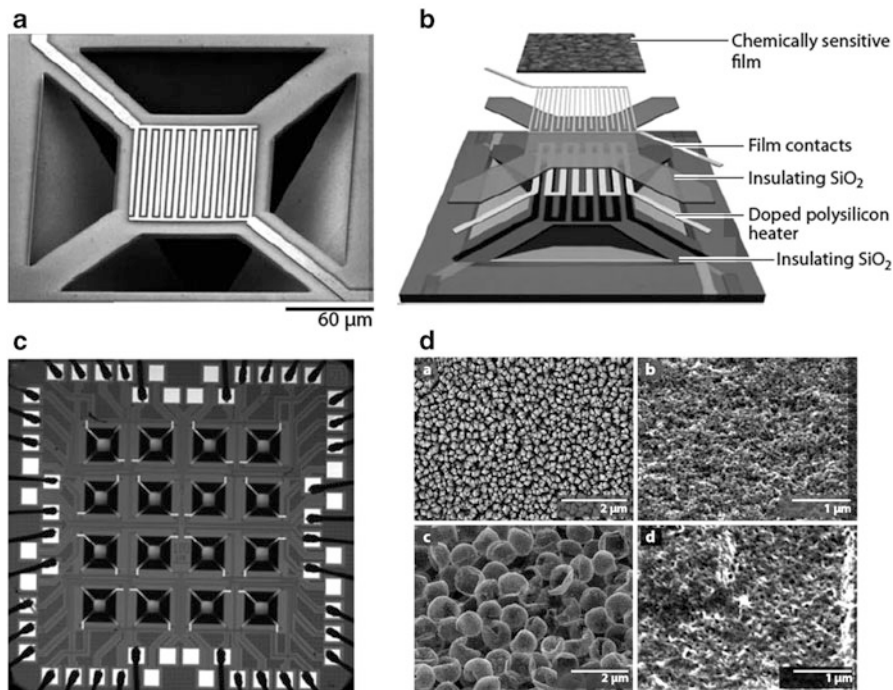
Processing multiple measurements from an individual chemical sensor, and from a number of different or independent sensors, can provide information needed to statistically reduce error and improve both selectivity and sensitivity of a chemical sensor [97] or chemical detection instrument. Since measurement error is a sum of systematic error and random error, the measurement error of an individual sensor can be statistically reduced via multiple samples by using statistics to reduce or eliminate the random error [98]. Multiple redundant sampling can provide enough data to reduce the measurement standard deviation by a factor of  $n^{0.5}$  where  $n$  is the number of redundant samples. The redundant samples may come from the same sensor, or multiple sensors of the same type, to further insure the best possible response [99]. This, however, is useful against random errors but is not efficient against systematic errors.

Responses from multiple independent sensors of *different* types can be combined (often referred to as sensor fusion) to provide overlapping reinforced responses that better span the sensors' response spaces leaving fewer gaps where analyte identification would be weak or unavailable.

### 18.10.2 Electronic Noses and Tongues

Two of the basic senses of humans, smell and taste, play a very important role in daily life for recognizing environmental conditions. Electronic smell and taste sensors (*e-noses* and *e-tongues*) have been intensely researched and developed due to their potentially broad commercial applications. They are very useful in the food industry, environmental protection, medicine, military, and other areas. The detection ability of these systems mainly depends on the ability of the sensitive materials to absorb or react with specific odors and ions. Although some achievements have been made, the e-noses and e-tongues still have significant limitations in sensitivity and specificity, compared with the biology binding of specific odorants and tastants to the olfactory and taste receptor cells.

The sensing parts of the e-noses and e-tongues are devices consisting of many similar, yet different sensing elements. An example of this multisensory approach is based on interactions between chemical species and semiconducting sensing materials placed on top of MEMS micro heater platforms developed at NIST [100–102]. The NIST electronic nose was comprised of eight types of sensors in the form of metal-oxide films deposited on the surfaces of 16 microheaters, with two copies of each material (Fig. 18.32). A polycrystalline silicon resistor was used for heating. A thermal time constant of the heater is a few milliseconds. In this example, different chemically sensitive films were deposited on the top of the different heaters: tin ( $\text{SnO}_2$ ), tin oxide coated with titanium oxide ( $\text{SnO}_2/\text{TiO}_2$ ), titanium oxide ( $\text{TiO}_2$ ), and titanium oxide coated with ruthenium oxide

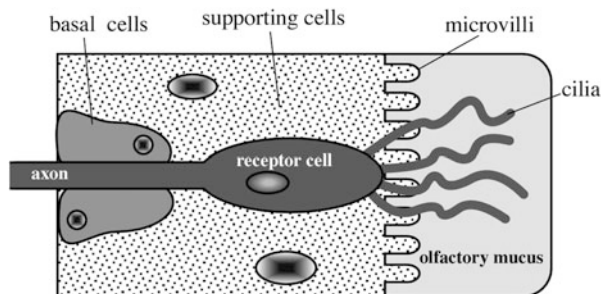


**Fig. 18.32** Top view of single chemical-sensor element (a); expanded schematic of critical components of microsensor device (b); 16-element microsensor array (c); scanning electron microscope images of variety of chemically sensitive films deposited on microhotplate-sensor platforms (d). Images are shown at different scales to highlight each film's nanostructure and morphology: (a) Polycrystalline metal oxide films deposited via chemical vapor deposition. Shown here is tin oxide (SnO<sub>2</sub>); titanium oxide (TiO<sub>2</sub>), TiO<sub>2</sub> layered on SnO<sub>2</sub>, and ruthenium (Ru) deposited on TiO<sub>2</sub> have also been used. (b) Mesoporous TiO<sub>2</sub> film applied by drop coating. (c) Drop-coated shells of Sb:SnO<sub>2</sub>. (d) Electrophoretically deposited nanostructured conductive polymer (here, colloidal polyaniline). Courtesy of Dr. Steven Semancik, NIST (stephen.semancik@nist.gov)

(TiO<sub>2</sub>/RuOx). These oxides are known to undergo chemical interactions with gas species ranging from surface-mediated oxidation of analyte gases to charge transfer upon analyte chemisorption. Since catalytic surface reaction rates vary with temperature, precise control of the individual heating elements allows for the ability to treat each of them as a collection of “virtual” sensors at 350 temperature increments between 150 and 500 °C, increasing the number of sensors to about 5600. The combination of the sensing films and the ability to vary the temperature gave the device the analytical equivalent of a snout full of sensory neurons.

A natural olfactory system is specialized to detect small airborne molecules at concentrations as low as a few parts per trillion and to discriminate among myriads of distinct compounds. In mammals, odorant molecules in the air enter the nostrils and bind with sensory neurons in the nose that convert the chemical interactions

**Fig. 18.33** Structure of olfactory neuron



into electrical signals that the brain interprets as a smell. The extraordinary performances of the olfactory and gustatory sensing are due to numerous receptors that are the sensory neurons and their subsequent neuronal processing. Each individual neuron can bind to multiple distinct molecules and ions with distinct affinities and specificities, though some receptors are relatively restricted to a set of few chemically related compounds. In humans, there are about 400 types of olfactory sensory receptors built into the many millions of cells in our nasal passages, allowing for detection of potentially billions of different scents [103]. Animals, such as dogs have hundreds more types of sensory neurons than humans. The process of olfactory perception begins when volatile compounds approach (via the respiratory air-stream) the nasal neuroepithelium where millions of distinct olfactory sensory cells reside.

Figure 18.33 shows a simplified diagram of the olfactory neuron. The perception occurs at tiny hair-like protrusions (cilia) from the receptor cells. The cilia are covered by mucus that captures the odorant molecules. The molecular properties of odorants that provide sensory properties are: low water solubility, high vapor pressure, low polarity, ability to dissolve in fat (lipophilicity), and surface activity. Electrical response of the receptor cell is transmitted via axon to the next level of signal processing. Nearly all chemical sensors suffer from a relatively short life due to drift and contamination of the sensing element. Nature solved this problem by frequent regeneration of all olfactory neurons that are replaced about every 40 days in humans—a very rare case of neural regeneration.

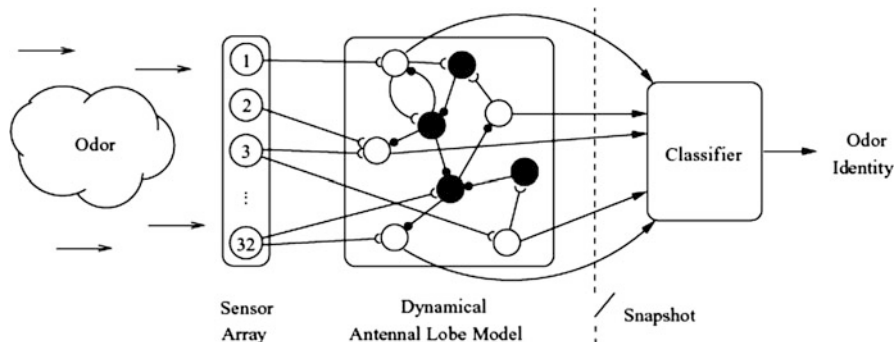
Receptors in the nasal cavities of mammals do not detect individual chemicals selectively, but use thousands of partially selective receptors that absorb inhaled chemicals. Each partially selective receptor may respond to a specific odorant strongly, weakly, or not at all, resulting in a distinct pattern that is sent to the brain for interpretation. The brain determines if this “smell” pattern has been detected before (learning and memory) and associates the chemical with a specific odor. Thus, different analytes give the brain different patterns, and these patterns determine the perception of the odor. It should be stressed that recognition of odorant species is not a job for any specific “olfactory sensor.” The odor or taste sensation and recognition are accomplished by a very complex system (brain) where the sensor is an integral part. A nose and tongue receptors are not just sensors but rather extensions of the brain.

Odor and taste recognition is a sequential process where the molecule identification is gradual by narrowing down a selection by means of a layered pattern recognition technique—from a coarse to fine signature of the odorant molecule. Generally, the recognition is faster and the sensitivity is better for more complex compounds. For example, there is a remarkable regularity in the sensitivity values for hydrocarbon alcohols such as methanol, ethanol, propanol, butanol, and pentanol. As the length of the chain increases, the sensitivity increases [104]. For a chain of eight carbon atoms (octanol) the human sensitivity is about 10 ppb (parts per billion), while for one carbon atom (methanol) it is 1 ppt (parts per thousand).

The sensation of taste is also initiated by the interaction of tastants with receptors and ion channels in the apical microvilli of taste receptor cells when some sapid molecules dissolve in saliva [3]. Subsequently, through a cellular signaling pathway gustatory signals are transduced gradually into the brain which integrates and analyzes these signals. Utilizing olfactory and gustatory cells as sensitive materials to develop a bioelectronic nose or tongue device is one of the emerging trends in the research and development of e-noses and e-tongues.

Much like people detect and remember many different smells and tastes and then use that knowledge to generalize about the perceptions they have not encountered before, the e-nose and e-tongue also need to be trained to recognize the chemical signatures of different smells before it can deal with unknowns. The current trend is a bionic approach based on combination of the multiple sensors and a signal processing by neural networks or their computer-based equivalents. The main idea is to use many sensors of different types and process data in a way that resembles data processing by living brains [105]. Electronic noses and tongues are less of a sensor or instrument and more of a measurement strategy.

Since the e-nose and e-tongue sensing cells in an array are relatively slow to respond, produce intrinsic noise and have relatively low selectivity, the bionic methods of signal processing become more popular. They employ the adaptive and learning (trainable) neural-network software in the DSP and can yield quite impressive results by responding to dynamics of the changing outputs of the sensing array [111]. This neural processing has three advantages: faster speed response, improved signal-to-noise ratio, and better selectivity. Figure 18.6 illustrates an array of multiple CP sensors that are exposed to an odorant [112]. The dynamical approach utilizes time transients of the sensor responses without waiting for their settling on constant levels. Each sensor in the array is predominantly sensitive to a specific odorant and coupled to one or more inputs of the neural network that responds to the rates of the signal changes and their magnitudes (Fig. 18.34). Noisy and slow sensor responses are refined by the neural system formed as a multiple coupling of the excitatory (white circles) and inhibitory (black circles) dynamical units. Such processing improves accuracy of detection and speeds up the analyte recognition.



**Fig. 18.34** Dynamical processing of the e-nose signals by a neural network (from ref. [112])

## 18.11 Specific Difficulties

The difficulty of developing chemical sensors (and systems) vs. other sensors (such as temperature, pressure, and humidity) is that interactions with chemicals during the sensing process can result in permanent changes in the sensor. This typically results in drift in the sensor baseline which can adversely affect sensor calibration. For example, electrochemical cells, which employ liquid electrolytes (material that conducts electrical current via charged ions, not electrons), consume a small amount of electrolyte with each measurement requiring that the electrolyte be replenished eventually. Chemical FET sensors operating in aqueous solutions may build up carbonic acid at the gate–membrane interface, which etches its components, and absorbent polymer coatings can become oxidized in harsh environments.

Also, unlike pressure or temperature sensors which have comparatively few conditions under which they need to be modeled to operate, chemical sensors are often exposed to nearly unlimited numbers of chemical combinations. This introduces interference responses, for example many chemical sensors have some degree of sensitivity to water. Therefore, when developing a sensor system to operate in the environment, the operator must account for changes in humidity when calibrating the system.

Ceramic bead-type and other catalytic hydrocarbon sensors begin to sinter ( $\sim 400^\circ\text{C}$ ), and bulk platinum electrodes and heating elements begin to evaporate at elevated ( $1000^\circ\text{C}$ ) temperatures, limiting their life spans and their usefulness for long-term continuous monitoring [106]. This evaporation rate is even higher in the presence of combustible gases. The loss of the platinum metal results in a change in the resistance of the wire that introduces offset error into the sensor reading, and leads to early burn-out of the heating platinum coil.

Chemical poisoning can affect many sensors such as the catalytic bead devices where, chlorinated, sulfur and lead containing compounds can irreversibly bind to the sensing element, inhibiting the oxidation of the hydrocarbon species, and

producing an inaccurate false-low reading. Filters are commonly used with any chemical sensor if it is to be subjected to an environment containing a characteristic poison. Judicious selection of the filter material is required to eliminate only the poisoning agent without an associated reduction in the target analyte (the chemical species being exposed to the sensor).

Surface Acoustical Wave devices that use species-selective adsorptive films can be poisoned *mechanically* by species that adsorb, but which do not desorb returning the mass of the device back to its original (calibrated) state. Similarly, gas-selective coatings on fiber-optic devices also may be poisoned by non-removable species, permanently reducing the optical reflectance and indicating a false positive.

Another problem unique to chemical sensors is the significant chemical reaction changes that occur at different concentration levels. For example, certain reactive hydrocarbon devices (metal oxide devices, voltammetric devices, etc.) require mixtures near stoichiometric (balanced chemical reactions) so that required minimal levels of both target analyte hydrocarbons and needed oxygen are available to feed the measurement reaction. If the hydrocarbon levels are too high (or better stated as the accompanying oxygen levels are too low) then only a fraction of the hydrocarbons will react producing a false negative reading.

---

## References

1. Jacoby, M. (2009). Keepers of the gate. *Chemical and Engineering News*, 87(22), 10–13.
2. Zheng, O., et al. (2009). Handheld miniature ion trap mass spectrometers. *Analytical Chemistry*, 81(7), 2421–2425.
3. Nagle, H. T., et al. (1998). The how and why of electronic noses. *IEEE Spectrum*, 35, 22–34.
4. Amoore, J. E., et al. (1964). The stereochemical theory of odor. *Scientific American*, 210, 42–99.
5. Ho, C. K., et al. (2002). In-situ chemiresistor sensor package for real-time detection of volatile organic compounds in soil and groundwater. *Sensors*, 2, 23–34.
6. Dewa, A. S., et al. (1994). Biosensors. In S. M. Sze (Ed.), *Semiconductor sensors* (pp. 415–472). New York, NY: John Wiley & Sons.
7. Kim, T. (2009, February 16). Canary in the old growth. *High Country News*.
8. For a wealth of information on Mine Safety Gas Monitoring Equipment is the United States Department of Labor. *Mine Safety & Health Administration (MSHA) website*. Retrieved from <http://www.msha.gov>.
9. Clutton-Brock, J. (1995). Origins of the dog: domestication and early history. In J. Serpell (Ed.), *The domestic dog, its evolution, behaviour and interactions with people* (pp. 7–20). Cambridge: Cambridge University Press.
10. Gentry, S. J. (1988). Catalytic devices. In T. E. Edmonds (Ed.), *Chemical sensors*. New York, NY: Chapman and Hall.
11. Cobbold, R. S. C. (1974). *Transducers for biomedical measurements*. New York, NY: John Wiley & Sons.
12. [www.askiitians.com/jit-jee-chemistry/physical-chemistry/Kohlrausch-law.aspx](http://www.askiitians.com/jit-jee-chemistry/physical-chemistry/Kohlrausch-law.aspx)
13. Tan, T. C., & Liu, C. C. (1991). Principles and fabrication materials of electrochemical sensors. In Kodansha Ltd (Ed.), *Chemical sensor technology* (Vol. 3). Tokyo: Kodansha Ltd.
14. Clark, L. C. (1956). Monitor and control of blood and tissue oxygen tension. *Transactions – American Society for Artificial Internal Organs*, 2(p), 41–46.

15. Madou, M. J., et al. (1989). *Chemical sensing with solid state devices*. Waltham, MA: Academic.
16. Wolfrum, E. J., et al. (2006). Metal oxide sensor arrays for the detection, differentiation, and quantification of volatile organic compounds at sub-parts-per-million concentration levels. *Sensors and Actuators B*, *115*, 322–329.
17. Persaud, K., et al. (1982). Analysis of discrimination mechanisms in the mammalian olfactory system using a model nose. *Nature*, *299*, 352–355.
18. Sberveglieri, G. (1992). *Gas sensors: principles, operations, and developments* (p. 8, 148, 282, 346–408). Boston, MA: Kluwer.
19. Blum, L. J. (1997). *Bio- and chemi-luminescent sensors* (pp. 6–32). River Edge, NJ: World Scientific Publishing Co. Pte. Ltd.
20. Sberveglieri, G. (1995). Recent developments in semiconducting thin-film gas sensors. *Sensors and Actuators B*, *23*, 103–109.
21. Demarne, V., et al. (1992). Thin film semiconducting metal oxide gas sensors. In G. Sberveglieri (Ed.), *Gas sensors* (pp. 89–116). Dordrecht: Kluwer.
22. Malyshe, V., et al. (1992). Gas sensitivity of SnO<sub>2</sub> and ZnO thin-film resistive sensors to hydrocarbons, carbon monoxide, and hydrogen. *Sensors and Actuators B*, *10*, 11–14.
23. Hoefer, U., et al. (1994). CO and CO<sub>2</sub> thin-film SnO<sub>2</sub> gas sensors on Si substrates. *Sensors and Actuators B*, *22*, 115–119.
24. Demarne, V., et al. (1988). An integrated low-power thin-film CO gas sensors on silicon. *Sensors and Actuators B*, *13*, 301–313.
25. Barsan, N., et al. (1995). The temperature dependence of the response of SnO<sub>2</sub>-based gas sensing layers to O<sub>2</sub>, CH<sub>4</sub>, and CO. *Sensors and Actuators B*, *26–27*, 45–48.
26. Van Geloven, P., et al. (1989). Tin(IV) oxide gas sensors: thick-film versus metallo-organic based sensors. *Sensors and Actuators B*, *17*, 361–368.
27. Schierbaum, K. D., et al. (1993). Specific palladium and platinum doping for SnO<sub>2</sub>-based thin film sensor arrays. *Sensors and Actuators B*, *13–14*, 143–147.
28. Sulz, G., et al. (1993). Ni, In, and Sb implanted Pt and V catalyzed thin-film SnO<sub>2</sub> gas sensors. *Sensors and Actuators B*, *16*, 390–395.
29. Tournier, G., et al. (1995). Selective detection of CO and CH<sub>4</sub> with gas sensors using SnO<sub>2</sub> doped with palladium. *Sensors and Actuators B*, *26–27*, 24–28.
30. Huck, R., et al. (1993). Spillover effects in the detection of H<sub>2</sub> and CH<sub>4</sub> by sputtered SnO<sub>2</sub> films with Pd and PdO deposits. *Sensors and Actuators B*, *17*, 355–359.
31. Saji, K., et al. (1983). Characteristics of TiO<sub>2</sub> oxygen sensor in nonequilibrium gas mixtures. In T. Seiyama, K. Fueki, J. Shiokawa, & S. Suzuki (Eds.), *Chemical sensors, proceedings of the international meeting on chemical sensors, Fukuoka Japan* (pp. 171–176). Tokyo: Elsevier.
32. Mumuera, G., et al. (1989). Mechanism of hydrogen gas-sensing at low temperatures using Rh/TiO<sub>2</sub> systems. *Sensors and Actuators B*, *18*, 337–348.
33. Egashira, M., et al. (1989). Gas-sensing characteristics of Li<sup>+</sup>-doped and undoped ZnO whiskers. *Sensors and Actuators B*, *18*, 349–360.
34. Grate, J. W., et al. (1990). Role of selective sorption in chemiresistor sensors for organophosphorus detection. *Analytical Chemistry*, *62*(18), 1927–1934.
35. Eastman, M. P., et al. (1999). Application of the solubility parameter concept to the design of chemiresistor arrays. *Journal of the Electrochemical Society*, *146*, 3907–3913. doi:10.1149/1.1392571.
36. Liu, Q., et al. (2014). Nanomaterials for analysis and monitoring of emerging chemical pollutants. *Trends in Analytical Chemistry*, *58*, 10–22.
37. Sharma, S., et al. (2014). MWCNT-conducting polymer composite based ammonia gas sensors: A new approach for complete recovery process. *Sensors and Actuators B: Chemical*, *194*, 213–219.
38. Benz, M., et al. (2012). Freestanding chemiresistive polymer composite ribbons as high-flux sensors. *Journal of Applied Polymer Science*, *125*(5), 3986–3995.

39. Garg, N., et al. (2010). Robust gold nanoparticles stabilized by trithiol for application in chemiresistive sensors. *Nanotechnology*, 21, 405501.
40. Kwon, O., & Seok, O. (2012). Seok multidimensional conducting polymer nanotubes for ultrasensitive chemical nerve agent sensing. *Nano Letters*, 12(6), 2797–2802.
41. Penza, M., et al. (2010). Metalloporphyrins-modified carbon nanotubes networked films-based chemical sensors for enhanced gas sensitivity. *Sensors and Actuators B: Chemical*, 144(2:17), 387–394.
42. Hierlemann, A., et al. (2000). Application-specific sensor systems based on cmos chemical microensors. *Sensors and Actuators B: Chemical*, 70, 2–11.
43. Endres, H.-E., et al. (1999). A capacitive CO<sub>2</sub> sensor system with suppression of the humidity interference. *Sensors and Actuators B: Chemical*, 57, 83–87.
44. Patel, S. V., et al. (2003). Chemicapacitive microsensors for volatile organic compound detection. *Sensors and Actuators B*, 96(3), 541–553.
45. Fotis, E. (2002). A new ammonia detector based on thin film polymer technology. *Sensors*, 19(5), 73–75.
46. Mlsna, T. E., et al. (2006). Chemicapacitive microsensors for chemical warfare agent and toxic industrial chemical detection. *Sensors and Actuators B: Chemical*, 116(1-2), 192–201.
47. The Multi-User MEMS Process (MUMPs) from MEMSCAP, Inc. (Durham, NC) is used to manufacture the these chemicapacitive sensor chips.
48. Britton, C. L., et al. (2000). Multiple-input microcantilever sensors. *Ultramicroscopy*, 82, 17–21.
49. Baselt, D. R., et al. (2003). Design and performance of a microcantilever-based hydrogen sensor. *Sensors and Actuators B: Chemical*, 88(2), 120–131.
50. Polk, B. J. (2002). ChemFET arrays for chemical sensing microsystems. *IEEE*, 2002, 732–735.
51. Wilson, D. M., et al. (2001). Chemical sensors for portable, handheld field instruments. *IEEE Sensor Journal*, 1(4), 256–274.
52. Janata, J. (1989). *Principles of chemical sensors, Chapter 4*. New York, NY: Plenum.
53. Kharitonov, A. B., et al. (2000). Enzyme monolayer-functionalized field-effect transistors for biosensor applications. *Sensors and Actuators, B*, 70(1–3), 222–231.
54. Ballantine, D. S., et al. (1997). *Acoustic wave sensors: Theory, design and physicochemical applications*. Boston, MA: Academic.
55. Ristic, V. M. (1983). *Principles of acoustic devices*. New York: Wiley and Sons.
56. Nieuwenhuizen, M. S., et al. (1986). Transduction mechanism in SAW gas sensors. *Electronics Letters*, 22, 184–185.
57. Wenzel, S. W., et al. (1989). Analytic comparison of the sensitivities of bulk-surface-, and flexlural plate-mode ultrasonic gravimetric sensors. *Applied Physics Letters*, 54, 1976–1978.
58. Binnig, G., et al. (1986). Atomic force microscope. *Physical Review Letters*, 56, 930–933.
59. Battiston, F. M., et al. (2001). A chemical sensor based on a microfabricated cantilever array with simultaneous resonance-frequency and bending readout. *Sensors and Actuators B: Chemical*, 77, 122–131.
60. Sharma, S., et al. (2012). Review article: a new approach to gas sensing with nanotechnology. *Philosophical Transactions of the Royal Society A, Mathematical, Physical and Engineering Sciences*, 370(1967), 2448-24-73.
61. Hansen, K. M., et al. (2001). Cantilever-based optical deflection assay for discrimination of DNA single-nucleotide mismatches. *Analytical Chemistry*, 73, 1567–1571.
62. Baselt, D. R., et al. (2001). A biosensor based on magnetoresistance technology. *Biosensors & Bioelectronics*, 13, 731–739.
63. Betts, T. A., et al. (2000). Selectivity of chemical sensors based on micro-cantilevers coated with thin polymer films. *Analytica Chimica Acta*, 422, 89–99.
64. Senesac, L. R., et al. (2009). Micro-differential thermal analysis detection of adsorbed explosive molecules using microfabricated bridges. *Review of Scientific Instruments*, 80, 035102.



65. Thundat, T., et al. (1995). Detection of mercury-vapor using resonating microcantilevers. *Applied Physics Letters*, 66(13), 1695–1697.
66. Thundat, T., et al. (1995). Vapor detection using resonating microcantilevers. *Analytical Chemistry*, 67(3), 519–521.
67. Pinnaduwaige, L. A., et al. (2004). Detection of trinitrotoluene via deflagration on a microcantilever. *Journal of Applied Physics*, 95, 5871–5875.
68. Datskos, P. G., et al. (1996). Remote infrared radiation detection using piezoresistive microcantilevers. *Applied Physics Letters*, 69(20), 2986–2988.
69. Creaser, C., et al. (2004). Ion mobility spectrometry: a review. Part 1. Structural analysis by mobility measurement. *The Analyst*, 129, 984–994.
70. Wu, C., et al. (2000). Secondary electrospray ionization ion mobility spectrometry/mass spectrometry of illicit drugs. *Analytical Chemistry*, 72(2), 396–403.
71. Tam, M., et al. (2004). Secondary electrospray ionization-ion mobility spectrometry for explosive vapor detection. *Analytical Chemistry*, 76(10), 2741–2747.
72. Rhykerd, C. L., et al. (1999). Guide for the selection of commercial explosives detection systems for law enforcement applications. *NIJ Guide* 100-99, NCJ 178913. Retrieved September, 1999, from [www.ojp.usdoj.gov/nij/pubs-sum/178913.htm](http://www.ojp.usdoj.gov/nij/pubs-sum/178913.htm).
73. Kriz, D., et al. (1997). Molecular imprinting: New possibilities for sensor technology. *Analytical Chemistry*, 69(11), 345A–349A. doi:10.1021/ac971657e.
74. Dybko, A., et al. (2000). Fiber optic chemical sensors. Retrieved from [www.ch.pw.edu.pl/~dybko/csrg/fiber/operating.html](http://www.ch.pw.edu.pl/~dybko/csrg/fiber/operating.html).
75. Seiler, K., et al. (1992). Principles and mechanisms of ion-selective optodes. *Sensors and Actuators B*, 6, 295–298.
76. Walt, D. R. (2000). Molecular biology: Bead based fiber-optic arrays. *Science*, 287(5452), 451.
77. Chen, H. X., et al. (2010). Colorimetric optical pH sensor production using a dual-color system. *Sensors and Actuators B: Chemical*, 146(1), 278–282.
78. Kreno, L. E., et al. (2011). Metal–organic framework materials as chemical sensors. *Chemical Reviews*, 112(2), 1105–1125.
79. Xu, Z., et al. (2010). Sensors for the optical detection of cyanide ion. *Chemical Society Reviews*, 39(1), 127–137.
80. Vilela, D., et al. (2012). Sensing colorimetric approaches based on gold and silver nanoparticles aggregation: Chemical creativity behind the assay. A review. *Analytica Chimica Acta*, 751, 24–43.
81. Miranda, O. R., et al. (2011). Colorimetric bacteria sensing using a supramolecular enzyme–nanoparticle biosensor. *Journal of the American Chemical Society*, 133(25), 9650–9653.
82. Mader, H. S., et al. (2010). Optical ammonia sensor based on upconverting luminescent nanoparticles. *Analytical Chemistry*, 82(12), 5002–5004.
83. Feng, L., et al. (2010). A simple and highly sensitive colorimetric detection method for gaseous formaldehyde. *Journal of the American Chemical Society*, 132(12), 4046–4047.
84. Burgess, I. B., et al. (2011). Wetting in color: Colorimetric differentiation of organic liquids with high selectivity. *ACS Nano*, 6(2), 1427–1437.
85. Quang, D. T., et al. (2010). Fluoro- and chromogenic chemodosimeters for heavy metal ion detection in solution and biospecimens. *Chemical Reviews*, 110(10), 6280–6301.
86. <http://www.drierite.com/>
87. Janzen, M. C., et al. (2006). Colorimetric sensor arrays for volatile organic compounds. *Analytical Chemistry*, 78, 3591–3600.
88. Doran, J. W., et al. (1996). Field and laboratory tests of soil respiration. *Methods for Assessing Soil Quality*, 1996, 231–245.
89. Dräger Safety AG & Co. KGaA. (2008). *Dräger-Tubes & CMS-handbook* (15th ed., p. 114). Lübeck: Dräger Safety AG & Co. KGaA.
90. Costello, B. P., et al. (2008). A sensor system for monitoring the simple gases hydrogen, carbon monoxide, hydrogen sulfide, ammonia and ethanol in exhaled breath. *Journal of Breath Research*, 2(3), 037011.

91. R&D Systems, Inc. *ELISA development guide*. Retrieved January 12, 2015, from <http://www.rndsistemas.com/pdf/edbapril02.pdf>.
92. Jiao, Y., et al. (2012). Preparation and evaluation of recombinant severe fever with thrombocytopenia syndrome virus nucleocapsid protein for detection of total antibodies in human and animal sera by double-antigen sandwich enzyme-linked immunosorbent assay. *Journal of Clinical Microbiology*, 50(2), 372–377.
93. Pesticides and companies providing ELISA systems are listed at: <http://www.aoac.org/testkits/TKDATA7.HTM>.
94. Rissin, D. M., et al. (2010). Single-molecule enzyme-linked immunosorbent assay detects serum proteins at subfemtomolar concentrations. *Nature Biotechnology*, 28(6), 595–599.
95. Immunoassay methods of acetochlor: Detection Review of existing immunoassay kits for screening of acetochlor and other acetanilides in water. Acetochlor Registration Partnership. Retrieved March, 1995, from <http://www.epa.gov/oppefed1/aceto/elisa.htm>.
96. Gottuk, D. T., et al. (1999). *Identification of fire signatures for shipboard multi-criteria fire detection systems* (pp. 48–87). Washington, DC: NRL/MR/6180-99-8386, Naval Research Laboratory.
97. Einax, J. W., et al. (1997). *Chemometrics in environmental analysis* (pp. 2–75). VCH: Weinheim.
98. Prasad, L., et al. (1994). Fault-tolerant sensor integration using multiresolution decomposition. *Physical Review E*, 49(4), 3452–3461.
99. Raman, B., et al. (2009). Designing and optimizing microsensor arrays for recognizing chemical hazards in complex environments. *Sensors and Actuators B*, 137, 617–629.
100. Raman, B., et al. (2008). Bioinspired methodology for artificial olfaction. *Analytical Chemistry*, 80, 8364.
101. Meier, D. C., et al. (2009). Detecting chemical hazards with temperature-programmed microsensors: Overcoming complex analytical problems with multidimensional databases. *Annual Review of Analytical Chemistry*, 2, 463–484.
102. Bushdid, C., et al. (2014). Humans can discriminate more than 1 trillion olfactory stimuli. *Science*, 343, 1370–1372.
103. Cometto-Muñiz, J. E., et al. (1990). Thresholds for odor and nasal pungency. *Physiology and Behaviour*, 48, 719–725.
104. Wang, P., et al. (2007). Olfactory and taste cell sensor and its applications in biomedicine. *Sensors and Actuators A*, 139, 131–138.
105. Edmonds, T. E. (Ed.). (1988). *Chemical sensors*. New York, NY: Blackie and Son Ltd.
106. Wilson, D. (2014). Interference and selectivity in portable chemical sensors (Chapter 54). In J. G. Webster & H. Eren (Eds.), *Measurement, instrumentation and sensors handbook*. Boca Raton, FL: CRC Press.
107. Burl, M. C., et al. (2001). Assessing the ability to predict human percepts of odor quality from the detector responses of a conducting polymer composite-based electronic nose. *Sensors and Actuators B*, 72, 149–159.
108. Jones, A. W. (1976). Precision, accuracy and relevance of breath alcohol measurements. *Modern Problems of Pharmacopsychiatry*, 11, 65–78.
109. Jones, E., et al. (1989). *Hydrogen sulfide sensor*. U.S. Patent No. 4822465.
110. Rabinovich, M., et al. (2008). Transient dynamics for neural processing. *Science*, 321, 48–50.
111. Muezzinoglu, M. K., et al. (2009). Chemosensor-driven artificial antennal lobe transient dynamics enable fast recognition and working memory. *Neural Computation*, 21, 1018–1103.
112. RAE Systems Inc., Theory and operation of NDIR Sensors, *Technical Note TN-169*. rev 1 wh.04-02.

*“Any sufficiently advanced technology is indistinguishable from magic.”*

-Arthur C. Clarke

Methods of sensor fabrication are numerous and specific for each particular design. They comprise processing of semiconductors, optical components, metals, ceramics, and plastics. Here, we briefly overview some materials and the most popular processing techniques.

---

## 19.1 Materials

### 19.1.1 Silicon as Sensing Material

Silicon is present in the sun and stars and is a principle component of a class of meteorites known as *aerolites*. Silicon is the second most abundant material on Earth, being exceeded only by oxygen—it makes up to 25.7 % of the earth’s crust, by weight. Silicon is not found free in nature, but occurs chiefly as the oxide, and as silicates. Some oxides are sand, quartz, rock crystal, amethyst, clay, mica, etc. Silicon is prepared by heating silica and carbon in an electric furnace, using carbon electrodes. There are also several other methods for preparing the element. Crystalline silicon has a metallic luster and grayish color.<sup>1</sup> The Czochralski process is commonly used to produce single crystals of silicon used for the solid-state semiconductors and micro-machined sensors. Silicon is a relatively inert element,

---

<sup>1</sup> *Silicon* should not be confused with *silicone* which is made by hydrolyzing silicon organic chloride, such as dimethyl silicon chloride. Silicones are used as insulators, lubricants, and for production of silicone rubber.

**Table 19.1** Effects in the silicon-based sensors [1]

Stimuli	Effects
Radiant	Photovoltaic effect, photoelectric effect, photoconductivity, photomagneto-electric effect
Mechanical	Piezoresistivity, lateral photoelectric effect, lateral photovoltaic effect
Thermal	Seebeck effect, temperature dependence of conductivity and junction, Nernst effect
Magnetic	Hall effect, magneto-resistance, Suhi effect
Chemical	Ion-sensitivity

but it is attacked by halogens and dilute alkali. Most acids, except hydrofluoric, do not affect it. Elemental silicon transmits infrared radiation and is commonly used as windows and lenses in the mid- and far-infrared sensors.

Silicon atomic weight is  $28.0855 \pm 0.0003$ , and its atomic number is 14. Its melting point is  $1410^\circ\text{C}$  and boiling point is  $2355^\circ\text{C}$ . Specific gravity at  $25^\circ\text{C}$  is 2.33 and valence is 4.

Properties of silicon are well studied and its applications to sensor designs have been extensively researched around the world. The material is inexpensive and can now be produced and processed controllably to unparalleled standards of purity and perfection. Silicon exhibits a number of physical effects which are quite useful for the sensor applications (Table 19.1).

Unfortunately, silicon does not possess the piezoelectric effect (or perhaps—fortunately because in many sensors piezoelectricity would generate interferences). Most effects of silicon such as the Hall effect, the Seebeck effect, and the piezo-resistance are quite large; however, a major problem with silicon is that its responses to many stimuli show a substantial temperature sensitivity. For instance: strain, light, and magnetic field responses are temperature dependent. When silicon does not display the proper effect, it is possible to deposit layers of materials with the desired sensitivity on top of the silicon substrate. For instance, sputtering of the ZnO thin films is used to form piezoelectric transducers which are useful for fabrication of SAW (surface acoustic waves) devices and accelerometers. In the later case, the strain at the support end of an etched micromechanical cantilever is detected by a ZnO overlay.

Silicon itself exhibits very useful mechanical properties which nowadays are widely used to fabricate such devices as pressure transducers, temperature sensors, force and tactile detectors by employing the MEMS technologies. Thin film and photolithographic fabrication procedures make it possible to realize a great variety of extremely small, high precision mechanical structures using the same processes that have been developed for electronic circuits. High-volume batch-fabrication techniques can be utilized in the manufacture of complex, miniaturized mechanical components which may not be possible with other methods. Table A.14 presents a comparative list of mechanical characteristics of silicon and other popular crystalline materials.

Although single-crystal silicon (SCS) is a brittle material, yielding catastrophically (not unlike most oxide-based glasses) rather than deforming plastically

**Table 19.2** Standard silicon wafers

Diameter (inch)	Diameter (mm)	Thickness (micron)
1	25.4	250
2	51	275
3	76	375
4	100	525
5	130	625
6 (5.9)	150	675
8 (7.9)	200	725
12 (11.8)	300	775

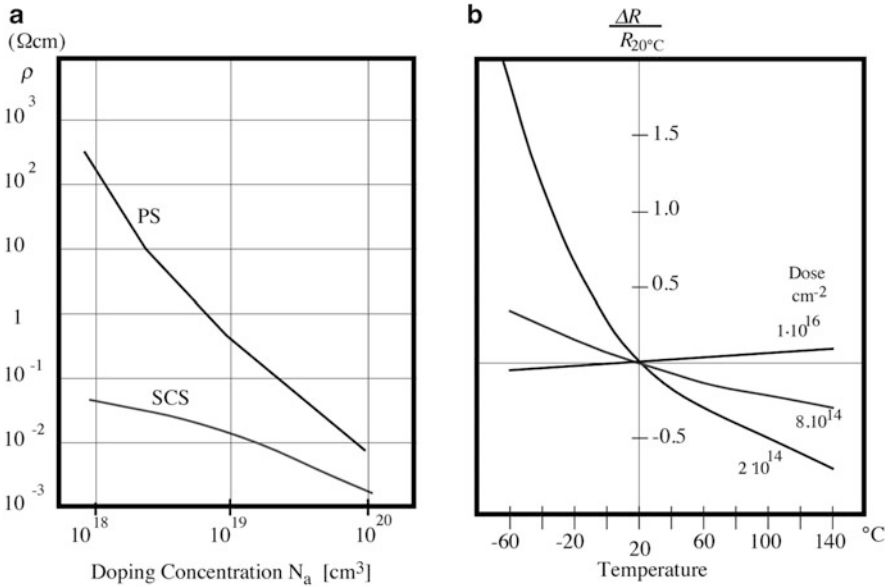
(like most metals), it certainly is not as fragile as is often believed. The Young's modulus of silicon ( $1.9 \times 10^{12}$  dyn/cm or  $27 \times 10^6$  psi) has a value of that approaching stainless steel and is well above that of quartz and most of glasses. The misconception that silicon is extremely fragile is based on the fact that it is often obtained in thin slices (Table 19.2) which are only 250–775  $\mu\text{m}$  thick. Even stainless steel at these dimensions is very easy to deform inelastically.

As mentioned above, many of the structural and mechanical disadvantages of SCS can be alleviated by deposition of thin films. Sputtered quartz, for example, is utilized routinely by industry to passivate integrated circuit chips against airborne impurities and mild atmospheric corrosion effects. Another example is a deposition of silicon nitrate (Table A.14) which has a hardness second only to diamond. Anisotropic etching is the key technology for micromachining of miniature three dimensional structures in silicon. Two etching systems are of practical interest. One based on ethylenediamine and water with some additives. The other consists of purely inorganic alkaline solutions like KOH, NaOH, or LiOH.

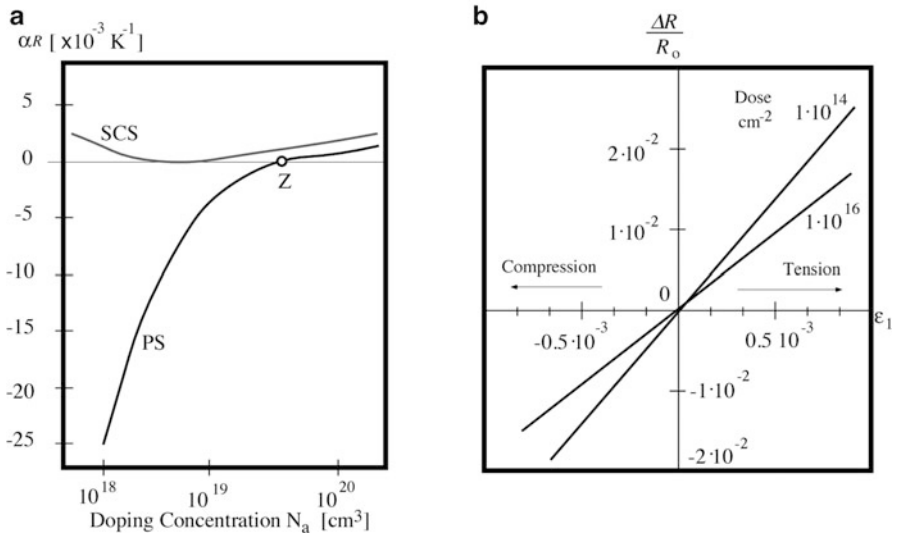
Forming the so-called *polysilicon* (PS) materials allows developing sensors with unique characteristics. Polysilicon layers (on the order of 0.5  $\mu\text{m}$ ) may be formed by vacuum deposition onto oxidized silicon wafer with an oxide thickness of about 0.1  $\mu\text{m}$  [2]. Polysilicon structures are doped with boron by a technique known in the semiconductor industry as LPCVD (low-pressure chemical vapor deposition).

Figure 19.1a shows resistivity of boron doped LPCVD polysilicon in a comparison with SCS. Resistivity of PS layers is always higher than that of a single crystal material, even when the boron concentration is very high. At low doping concentrations the resistivity climbs rapidly, so that only the impurity concentration range is of interest to a sensor fabrication. The resistance change of PS with temperature is not linear. Through selected doping, Fig. 19.1b, the temperature coefficient of resistance may be selected over a wide range, both positive and negative (see Sects. 17.8 and 17.9). Generally, at non-cryogenic temperatures the temperature coefficient of resistance (TCR) increases with decreased doping concentration.

Figure 19.2a shows that the temperature sensitivity of PS is substantially higher than that of SCS and can be controlled by doping. It is interesting to note that at a specific doping concentration, the resistance becomes insensitive to temperature variations (point Z).



**Fig. 19.1** Specific resistivity of boron doped silicon (a); temperature coefficient of resistivity of silicon for different doping concentrations (b)



**Fig. 19.2** Temperature coefficient as function of doping (a) and piezoresistive sensitivity of silicon (b)

For the development of sensors for pressure, force, or acceleration, it is critical to know the strain sensitivity of PS resistors expressed through the gauge factor. Figure 19.2b shows curves of the relative resistance change of boron doped PS resistors, referenced to the resistance value  $R_0$  under no-stress conditions, as a function of longitudinal strain  $\epsilon_1$ . The parameter varies with the implantation dose. It can be seen that the resistance decreases with compression and increases under tension. It should be noted that the gauge factor, the slope of the line in Fig. 19.2b, is temperature dependent. PS resistors are capable of realizing at least as high a level of long-term stability as any can be expected from resistors in SCS, since surface effects play only a secondary role in device characteristics.

### 19.1.2 Plastics

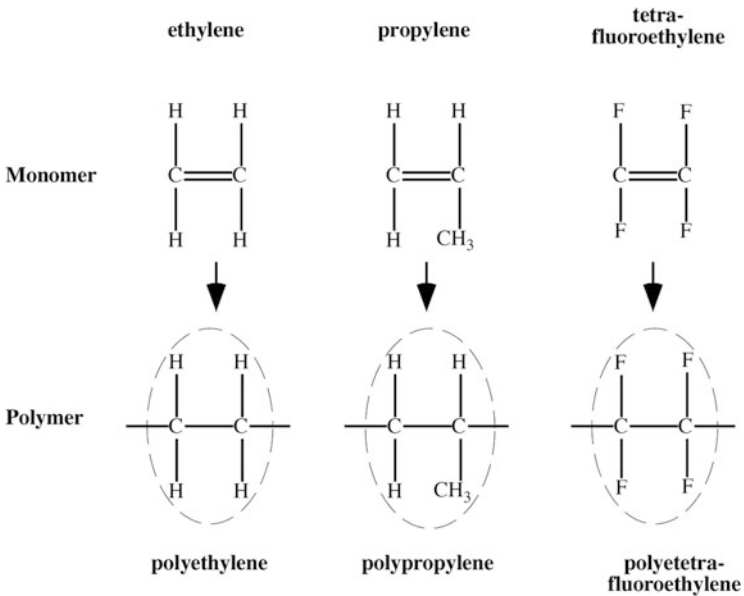
Plastics are synthetic materials made from chemical raw materials called *monomers*. A monomer (one chemical unit) such as ethylene is reacted with other monomer molecules to form long chains of repeating ethylene units, forming the polymer polyethylene. In a similar manner, polystyrene is formed from styrene monomers. The polymers consist of carbon atoms in combination with other elements. Polymer chemists use only eight elements to create thousands of different plastics. These elements are: carbon (C), hydrogen (H), nitrogen (N), oxygen (O), fluorine (F), silicon (Si), sulfur (S), and chlorine (Cl). Combining these elements in various ways produce extremely large and complex molecules.

Each atom has a limited capacity (energy bonds) for joining with other atoms, and every atom within a molecule must have all its energy bonds satisfied if the compound is to be stable. For example, hydrogen can bond only to one other atom, while carbon or silicon must attach to four other atoms to satisfy its energy bonds. Thus, H–H and H–F are stable molecules, while C–H and Si–Cl are not. Figure 19.3 shows all eight atoms and the corresponding energy bonds.

Adding more carbon atoms in a chain and more hydrogen atoms to each carbon atom creates heavier molecules. For example, ethane gas ( $C_2H_6$ ) is heavier than methane gas because it contains additional carbon and two hydrogen atoms. Its molecular weight is 30. Then, the molecular weight can be increased in the increments of 14 (one carbon+two hydrogen), until the compound pentane ( $C_5H_{12}$ ) is reached. It is too heavy to be gas and indeed it is liquid at room temperature. Further additions of  $CH_2$  groups makes progressively heavier liquid until  $C_{18}H_{38}$  is reached. It is solid—paraffin wax. If we continue and grow larger molecules, the wax becomes harder and harder. At about  $C_{100}H_{202}$  the material with a molecular weight 1402 is tough enough and is called a low-molecular weight *polyethylene*, the simplest of all thermoplastics. Continuing the addition of more  $CH_2$  groups further increases the toughness of the material until medium molecular weight (between 1000 and 5000 carbons) and high-molecular weight polyethylene. Polyethylene, being the simplest polymer (Fig. 19.4), has many useful properties in the sensor technologies. For example, the polyethylene is reasonably transparent in

**Fig. 19.3** Atomic building blocks for polymers

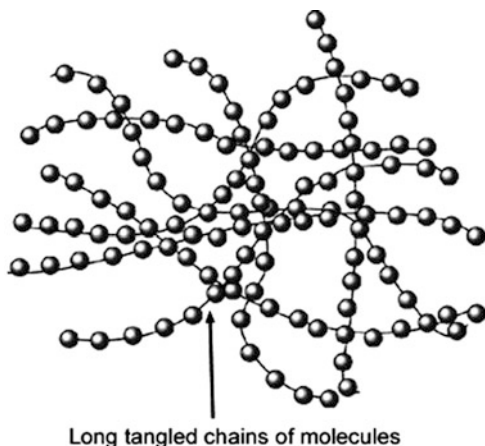
Element	Atomic weight	Energy Bonds
Hydrogen	1	-H 1
Carbon	12	$\begin{array}{c}   \\ -C- \\   \end{array}$ 4
Nitrogen	14	$\begin{array}{c}   \\ -N- \\   \end{array}$ 3
Oxygen	16	-O- 2
Fluorine	19	-F 1
Silicon	28	$\begin{array}{c}   \\ -Si- \\   \end{array}$ 4
Sulfur	32	-S- 2
Chlorine	35	-Cl 1



**Fig. 19.4** Monomers and their respective polymer units



**Fig. 19.5** Molecular chains of thermoplastic polymer



the mid- and far-infrared spectral ranges and thus is used for fabrication of infrared Fresnel lenses.

By applying heat, pressure and catalysts, monomers are grown into long chains. The process is called polymerization. Chain length (molecular weight) is important because it determines many properties of a plastic. The major effects of the increased length are increased toughness, creep resistance, stress-crack resistance, melt temperature, melt viscosity, and difficulty of processing. After polymerization is completed, the finished polymer chains resemble long intertwined bundles of spaghetti with no physical connections between chains. Such a polymer is called *thermoplastic* (heat-moldable) polymer (Fig. 19.5).

If chains are packed closer to one another, a denser polyethylene is formed which in effect results in formation of crystals. Crystallized areas are stiffer and stronger. Such polymers are more difficult to process since they have higher and sharp melt temperatures. That is, instead of softening, they quickly transform into low-viscosity liquids. On the other hand, amorphous thermoplastics soften gradually, but they do not flow as easily as crystalline plastics. The examples of amorphous polymers are ABS, polystyrene, polycarbonate, polysulfone, and polyetherimide. Crystalline plastics include polyethylene, polypropylene, nylon, PVDF, acetal, and others.

Below is a non-exhaustive list of thermoplastics.

*ABS* (acrylonitrile-butadiene-styrene) is very tough, yet hard and rigid. Fair chemical resistance and low water absorption. Good dimensional stability. Some grades may be electroplated.

*Acrylic* has high optical clarity and excellent resistance to outdoor weathering. This is hard, glossy material with good electrical properties. It is available in a variety of colors.

*Fluoroplastics* comprise a large family of materials (PTFE, FEP, PFA, CTFE, ECTFE, ETFE, and PFDf) with excellent electrical properties and chemical

resistance, low friction and outstanding stability at high temperatures. However, their strength is moderate and cost is high. One example is polytetrafluoroethylene (PTFE) which is known as DuPont brand Teflon.

*Nylon* (polyimide) has outstanding toughness and wear resistance with low coefficient of friction. Good electrical and chemical properties. However, it is hygroscopic and dimensional stability is worst than in most other plastics.

*Polycarbonate* has highest impact resistance. It is transparent with excellent outdoor stability and resistance to creep under load. It may have some problems with chemicals.

*Polyester* has excellent dimensional stability but is not suitable for outdoor use or for service in hot water.

*Polyethylene* is lightweight, inexpensive with excellent chemical stability and good electrical properties. Moderate transparency in broad spectral range from visible to far infrared. Has poor dimensional and thermal stability.

*Polypropylene* has outstanding resistance to flex and stress cracking with excellent chemical and electrical properties with good thermal stability. It is lightweight and cheap. Optical transparency is good down to far-infrared spectral range. However, absorption and scattering of photons in mid-infrared range is higher than in polyethylene.

*Polyurethane* is tough and extremely abrasion and impact-resistant. Can be made into films and foams. Has good chemical and electrical properties; however, UV exposure degrades its quality.

*Polybutadiene* is a synthetic rubber has a high resistance to wear. It has been used to coat or encapsulate electronic assemblies, offering extremely high electrical resistivity. It exhibits a recovery of 80 % after stress is applied.

*Polyvinyl chloride* (PVC), is the third most widely used thermoplastic polymer after polyethylene and polypropylene. PVC is cheap, durable, and easy to assemble. It can be made softer and more flexible by the addition of plasticizers, the most common being phthalates. In electronics, it is used in to make flexible tubing and electrical cable insulation.

Other type of plastics is called *thermoset* in which polymerization (curing) is done in two stages: one—by the material manufacturer and the other—by the molder. An example is phenolic which during the molding process is liquefied under pressure, producing a cross-linking reaction between molecular chains. After it has been molded, a thermoset plastic has virtually all its molecules interconnected with strong physical bonds, which are not heat reversible. In effect, curing a thermoset is like cooking an egg. Once it is cooked, it will remain hard. In general, thermoset plastics resist higher temperatures and provide greater dimensional stability. This is the reason why such thermoset plastics as polyester (reinforced) used to make boat hulls and circuit-breaker components, epoxy is used to make printed circuit boards, and melamine is used to make dinnerware.

On the other hand, thermoplastics offer higher impact strength, easier processing, and better adaptability to complex designs than do thermosets.

The thermoplastics that are most useful in sensor-related applications are the following.

*Alkyd* has excellent electrical properties and very low moisture absorption.

*Allyl* (diallyl phthalate) has outstanding dimensional stability and high heat and chemical resistance.

*Epoxy* has exceptional mechanical strength, electrical properties and adhesion to most of materials.

*Phenolic* is a low-cost material. Color is limited to black and brown.

*Polyester* (thermoplastic version) has a great variety of colors, may be transparent or opaque. Shrinkage is high.

If two different monomers (*A* and *B*) are combined in a polymerization reaction, such a polymer is called *copolymer*. Final properties of copolymer depend on ratio of components *A* and *B*.

Polymer mechanical properties can be modified by providing additives, such as fibers to increase strength and stiffness, plastisizers for flexibility, lubricants for easier molding, or UV stabilizers for better performance in sun light.

Another good way to control properties of plastics, is to make polymer alloys or blends. Primarily this is done to retain properties of each component.

*Conductive plastics*. Being wonderful electrical isolators, plastic materials often require lamination with metal foil, painting with conductive paint, or metallization to give them electrical conductive properties, required for shielding. Another way of providing electrical conductivity is mixing plastics with conductive additives (for instance, graphite or metal fibers) or building composite plastic parts incorporating metal mesh.

*Piezoelectric plastics* are made from PVF<sub>2</sub>, PVDF and copolymers which are crystalline materials. Initially, they do not possess piezoelectric properties and must be poled either in high voltage or by corona discharge (Sect. 4.6.2). Metal electrodes are deposited on both sides of the film either by silk-screening or vacuum metallization. These films, in some applications are used instead of ceramics, thanks to their flexibility and stability against mechanical stress. Another advantage of the piezoelectric plastics is they ability to be formed into any desirable shape.

A polymer that is very useful for the sensing technologies is *Kapton* which is a *polyimide* (PI) film developed by DuPont. It is a thermoset material with density of 1.42 g/cm<sup>3</sup> and low thermal conductivity of 0.12 W/(m K). PI remains stable in a wide range of temperatures, from near the absolute zero of -273 °C to +400 °C. Among other things, PI is used in flexible printed circuits that can be employed to connect sensors to rigid printed circuit boards (PCB). A flexible PI printed circuit board can be made as thin as 50 μm and even thinner. These boards are flexible and can withstand close to a million bends. PI is also commonly used as a material for windows of all kinds at X-ray sources (synchrotron beam-lines and X-ray tubes)

and X-ray detectors. Its high mechanical and thermal stability as well as high transmittance to X-rays make it the preferred material. It also does not suffer from radiation damage. However, PI has relatively poor resistance to mechanical abrasion.

### 19.1.3 Metals

From the sensor designer standpoint, there are two classes of metals: nonferrous and ferrous. Ferrous metals, like steel, are often used in combination with magnetic sensors to measure motion, distance, magnetic field strength, etc. Also, they are quite useful as magnetic shields. Nonferrous metals, on the other hand, are permeable to magnetic fields and used whenever these fields are of no concern.

Nonferrous metals offer a wide variety of mechanical and electrical properties. When selecting a metal, one must consider not only its physical properties but also ease of mechanical processing. For example, copper has excellent thermal and electrical properties, yet it is difficult to machine, so in many instances aluminum should be considered as a compromise alternative, especially where soldering is not required.

*Aluminum* has a high strength-to-weight ratio and possesses its own anticorrosion mechanism. When exposed to air, aluminum does not oxide progressively, like iron would do. The protection is provided by a microscopic oxide coating which forms on the surface and seals the bare metal from environment.

There are hundreds of aluminum alloys. They can be processed by many ways, like drawing, casting, stamping. Some alloys can be soldered and welded. Besides excellent electrical properties, aluminum is a superb reflector of light over nearly entire spectrum from UV to radio waves. Aluminum coatings are widely used for mirrors and waveguides. In the mid- and far-infrared ranges, the only superior to aluminum reflector is gold.

On a negative side, aluminum is difficult to solder. In “normal” soldering of copper, removal of the copper oxide is relatively easy with mild organic and inorganic fluxes. However, because the rapid formation of an aluminum oxide layer and the difficulty in removing that oxide layer, the solder cannot wet the aluminum surface. This is the reason for using a special flux such as an organic amine-based flux (up to 285 °C), inorganic fluxes (chloride or fluoride up to 400 °C), and complex fluoroaluminate salts (above 550 °C).

*Beryllium* has several remarkable properties. Its low density (two thirds that of aluminum) is combined with high modulus per weight (five times that of steel), high specific heat, excellent dimensional stability and transparency to X-rays. However, it is expensive metal. Like aluminum, beryllium forms a protective coating on its surface, thus resisting to corrosion. It may be processed by many conventional methods, including powder cold pressing. The metal is used as X-ray windows, optical platforms, mirror substrates, satellite structures.

*Magnesium* is a very light metal with high strength-to-weight ratio. Due to its low modulus of elasticity, it can absorb energy elastically which gives its good damping characteristics. The material is very easy to process by most of metal working techniques.

*Nickel* allows designing very tough structures which are also resistant to corrosion. When compared with steel, the nickel alloys have ultrahigh strength and high modulus of elasticity. Its alloys include binary systems with copper, silicon, and molybdenum. Nickel and its alloys preserve their mechanical properties down to cryogenic temperatures and at high temperatures up to 1200 °C. Nickel is used in high-performance superalloys such as Inconel, Monel (Ni–Cu), Nichrome (Ni–Cr), and Ni–Cr–Fe alloys.

*Copper* combines very good thermal and electrical conductivity properties (second only to pure silver) with corrosion resistance and relative ease of processing. However, its strength-to-weight ratio is relatively poor. Copper is also difficult to machine since it is too soft. Copper and its alloys—the brasses and bronzes come in variety of forms, including films. Brasses are alloys which contain zinc and other designated elements. Bronzes comprise main groups: copper–tin–phosphorus (phosphor bronze), copper–tin–lead–phosphorus (lead phosphor bronzes), and copper–silicon (silicon bronzes) alloys. Under the outdoor condition, copper develops a blue-green patina. This can be prevented by applying acrylic coating. Copper alloy with beryllium has excellent mechanical properties and used to make springs.

*Lead* is the most impervious of all common metals to X-rays and  $\gamma$ -radiation. It resists attack by many corrosive chemicals, most types of soil, marine, and industrial environment. It has low melting temperature, ease of casting and forming, good sound and vibration absorption. It possesses natural lubricity and wear resistance. Lead is rarely used in pure form. Its most common alloys are “hard lead” (1–13 % of antimony), calcium and tin alloys which have better strength and hardness.

*Platinum* is a silver-white precious metal that is extremely malleable, ductile and corrosion resistant. Its positive temperature coefficient of resistance is very stable and reproducible which allows its use in temperature sensing.

*Gold* is extremely soft and chemically inert metal. It can only be attacked by *aqua regia* and by sodium and potassium in presence of oxygen. One gram of pure gold can be worked into a leaf covering 5000 cm<sup>2</sup> and only less than 0.1  $\mu\text{m}$  thick. Mainly, it is used for plating and alloyed with other metals like copper, nickel, and silver. In sensor applications, gold is used for fabricating electrical contacts and plating mirrors and waveguides that operate in the mid- and far-infrared spectral ranges.

*Silver* is least costly of all precious metals. It is very malleable and corrosion resistant. It has the highest electrical and thermal conductivity of all metals.

*Palladium, iridium, and rhodium* resemble and behave like platinum. They are used as electrical coatings to produce hybrid and printed circuit boards and various ceramic substrates with electrical conductors. Another application is in fabrication of high quality reflectors operating in broad spectral range, especially at elevated temperatures or highly corrosive environments. Iridium has the best corrosion resistance of all metals and thus used in the most critical applications.

*Molybdenum* maintains its strength and rigidity up to 1600 °C. The metal and its alloys are readily machinable by conventional tools. In nonoxidizing environments, it resists attacks by most of acids. Its prime application is for high-temperature devices, such as heating elements and reflectors of intense infrared radiation for high-temperature furnaces. Molybdenum has low coefficient of thermal expansion and resists erosion by molten metals.

*Tungsten* in many respects is similar to molybdenum, but can operate even at higher temperatures. A thermocouple sensor fabricated of tungsten is alloyed with 25 % of rhenium and used with another wire—with 5 % of rhenium.

*Zinc* is seldom used alone, except for coating, and mainly used as an additive in many alloys.

#### 19.1.4 Ceramics

In sensor technologies, ceramics are very useful *crystalline* materials thanks to their structural strength, thermal stability, light weight, resistance to many chemicals, ability to bond with other materials, and excellent electrical properties. Although most metals form at least one chemical compound with oxygen, only a handful of oxides are useful as the principal constituent of ceramics. Examples are *alumina* and *beryllia*. The natural alloying element in the alumina is silica; however, alumina can be alloyed also with chromium, magnesium, calcium, and other elements.

Several metal carbides and nitrides qualify as ceramics. Most commonly used are boron carbide and nitride and aluminum nitride (Table A.24). Whenever fast heat transfer is of importance, aluminum nitride shall be considered, while silicon carbide has high dielectric constant, which makes it attractive for designing capacitive sensors. Due to their hardness, most ceramics require special processing. A precise and cost-effective method of cutting various shapes of ceramic substrates is scribing, machining, and drilling by use of computer-controlled CO<sub>2</sub> laser. Ceramics for the sensor substrates are available from many manufacturers in thickness ranging from 0.1 to 10 mm.

#### 19.1.5 Structural Glasses

Glass is *amorphous* solid material made by fusing silica with a basic oxide. Although its atoms never arrange themselves into crystalline structure, atomic spacing in glass is quite tight. Glass is characterized by optical transparency,

availability in many colors, hardness, and resistance to most chemicals except hydrofluoric acid (Table A.25). Most glasses are based on the silicate system and made from three major components: silica ( $\text{SiO}_2$ ), lime ( $\text{CaCO}_3$ ), and sodium carbonate ( $\text{Na}_2\text{CO}_3$ ). Nonsilicate glasses include phosphate glass (which resists hydrofluoric acid), heat absorbing glasses (made with  $\text{FeO}$ ), and systems based on oxides of aluminum, vanadium, germanium, and other metals. An example of such specialty glass is arsenic trisulfate ( $\text{As}_2\text{S}_3$ ) known as AMTIR which is substantially transparent in mid- and far-infrared spectral range and is used for fabricating infrared optical devices (see below).

*Borosilicate* glass is the oldest type of glass that is substantially resistant to thermal shock. In the trademark Pyrex<sup>®</sup>, some of the  $\text{SiO}_2$  molecules are replaced by boric oxide. This glass has a low coefficient of thermal expansion and thus is used for fabricating optical mirrors (like in telescopes).

*Lead-alkali* glass (lead glass) contains lead monoxide ( $\text{PbO}$ ) which increases its index of refraction. Also, it is a better electrical insulator. In the sensor technologies, it is used for fabricating optical windows, prisms and as a shield against nuclear radiation. Other glasses include aluminosilicate glass (in which  $\text{Al}_2\text{O}_3$  replaces some silica), 96 % silica, and fused silica.

Another class of glass is *light-sensitive* glasses that are available in three grades. Photochromatic glass darkens when exposed to ultraviolet radiation and clears when UV is removed or glass is heated. Some photochromatic compositions remain darkened for a week or longer. Others fade within few minutes when UV is removed. The photosensitive glass reacts to UV in a different manner: if it is heated after exposure, it turns from clear to opal. This allows to create some patterns within the glass structure. In a similar manner, the germanium-doped silica glass can change its refractive index when exposed to strong UV light (see Sect. 8.5.5). Moreover, the exposed opalized glass is much more soluble in hydrofluoric acid which allows for efficient etching technique.

## 19.1.6 Optical Glasses

### 19.1.6.1 Visible and Near Infrared Ranges

Most optical glasses are mixtures of silica obtained from beds of fine sand or from pulverized sandstone; an alkali to lower the melting point, usually a form of soda or, for finer glass, potash; lime as a stabilizer; and cullet (waste glass) to assist in melting the mixture. The properties of glass are varied by adding other substances, commonly in the form of oxides, e.g., lead, for brilliance and weight; boron, for thermal and electrical resistance; barium, to increase the refractive index; cerium, to absorb infrared rays; metallic oxides, to impart color; and manganese, for decolorizing.

Optical glasses are classified by their main chemical components and are identified by refractive index. Since refractive index is function of a wavelength,

**Table 19.3** Wavelengths of Spectral Lines and Refractive Indices for some Glasses and Plastics (glasses are from *Pilkington Special Glass Ltd*)

Wavelength (nm)	Spectral line	Element	Refractive index			
			Glass BSC517642	Glass LAF744447	Plastic acrylic	Plastic polycarbonate
1013.98	t	Hg	1.507	1.726		
852.11	S	Cs	1.510	1.730		
768.19	A'	K				
706.52	r	He				
656.27	C	H	1.514	1.739	1.489	1.578
643.85	C'	Cd				
632.8	632.8	He-Ne Laser				
589.29	D	Na			1.492	1.584
587.56	d	He	1.516	1.744		
546.07	e	Hg	1.518	1.748		
486.13	F	H			1.498	1.598
479.99	F'	Cd	1.522	1.756		
435.83	g	Hg	1.526	1.765		
404.66	h	Hg	1.530	1.773		
365.01	i	Hg	1.536	1.787		

it is measured at specific spectral lines of spectrum produced by various elements. Examples of the spectral lines and the corresponding refractive indices of some glasses and clear plastics are given in Table 19.3.

Quality and durability of glasses depend on the environment to which they are subjected. In various processes of fabricating optical components such as lenses and prisms, surface deterioration is often encountered and recognized as dimming, staining, and latent scratching. These surface defects are caused by chemical reactions of the glass constituents with water in the surrounding environment or with detergents in the cleaning fluids. A high refractive index leads to weaker surfaces.

Polished glass exposed to high humidity and rapid temperature variations may “sweat.” Water vapor may condense to form droplets on the glass surface. Some of the glass components that dissolve in the droplets may in turn attack the glass surface and react with gaseous elements in the air (e.g., CO<sub>2</sub>). The reaction products form as white spots or a cloudy film as the glass surface dries. It is called “dimming.” Water contact causes chemical reactions (ion exchange between cations in the glass and hydronium ions H<sub>3</sub>O<sup>+</sup> in water) which result in a silica-rich surface layer that causes an interference color on that layer. It is called “staining.” Fine scratches created on the glass surfaces during polishing will sometimes grow to a large visible size when the surfaces are exposed to corrosive ions out of inorganic builders in a detergent used for cleaning.



**Table 19.4** Properties of chalcogenide glasses (courtesy of *Amorphous Materials, Inc.* Garland, Texas, USA)

	AMTIR-1	AMTIR-2	AMTIR-3	AMTIR-4	AMTIR-5	AMTIR-6	C1
Composition	Ge-As-Se	As-Se	Ge-Sb-Se	As-Se	As-Se	As-S	As-Se-Te
Transmission range, $\mu\text{m}$	0.7–12	1.0–14	1.0–12	1.0–12	1.0–12	0.6–8	1.2–14
Refr. index at 10 $\mu\text{m}$	2.4981	2.7613	2.6027	2.6431	2.7398	2.3807	2.8051
Upper use temp, $^{\circ}\text{C}$	300	150	250	90	130	150	120

**Table 19.5** Crystalline Infrared Materials

Material	Useful spectral range ( $\mu\text{m}$ )	Appx. refractive index
Magnesium fluoride	0.5–9.0	1.36
Zinc sulfide	0.4–14.5	2.25
Calcium fluoride	<0.4–11.5	1.42
Zinc selenide	0.5–22.0	2.44
Magnesium oxide	<0.4–9.5	1.69
Calcium telluride	0.9–31.0	2.70
Silicon	1.2–8.0	3.45
Germanium	1.3–22.0	4.00

### 19.1.6.2 Mid- and Far-Infrared Ranges

For operation in the range of thermal radiation (mid- and far-infrared), the silicon based amorphous glasses have very high coefficient of absorption and thus cannot be used. The alternatives are the crystalline materials (e.g., germanium and silicon), some polymers (polyethylene and polypropylene) and special chalcogenide glasses containing selenium. These glasses can be drawn into fibers to form fiber optic sensors and thermal radiation transmission lines. To produce lenses and prisms they can be molded, just like the silicon based glasses or plastics. This can dramatically simplify production and lower cost as compared with the crystalline materials that as a rule require grinding and polishing. Examples of the most popular chalcogenide glasses are given in Table 19.4. Note the relatively low, as compared with Si and Ge, refractive indices, meaning that the AMTIR glasses have lower IR reflectance.

An alternative to the AMTIR glasses is the use of crystalline materials having substantial transmission in the mid- and far-infrared ranges. The most popular IR materials and their properties are given in Table 19.5. Note that a high refractive index results in a high coefficient of reflection. This may cause an undesirable loss in the signal intensity. To reduce reflection, anti-reflection (AR) coating is recommended.

## 19.2 Nano-materials

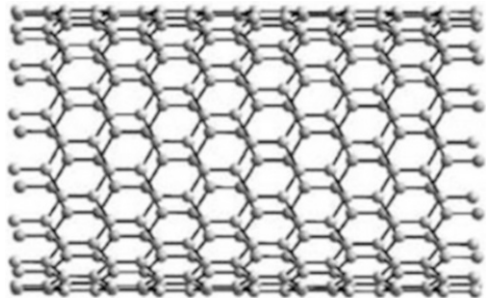
The idea to fabricate functional devices on atomic scales first was expressed in 1959 by the great physicist Richard Feynman. He described a possibility for scientists to manipulate and control individual atoms and molecules. Later, Professor Norio Taniguchi suggested the term *nano-technology*. For nearly 40 years nanotechnology was a somewhat emotional term, more of a wishful thinking than a real thing. While it referred to dimensions of a device on a nanometer ( $10^{-9}$  m) scale, most of the sub-miniature elements had sizes about a thousand times larger—in a micrometer ( $10^{-6}$  m) range. Nowadays, this technology progresses very rapidly. Presently, we can produce nano-materials and devices in sizes from 1 to 100 nm, approaching those of atoms. An atom has a diameter of about 0.1 nm, yet an atomic nucleus is much smaller—about 0.00001 nm.

Nano-scale materials are proving attractive for a new generation of sensors due to their unique electrical and mechanical properties [3]. For example, they are used to create fast-responding sensors with good sensitivity and selectivity for the detection of chemical species and biological agents [4].

One of the nano-materials being of a great interest for sensing is the CNT—carbon nanotubes [5]. In a nanotube, molecules of carbon are arranged in a tubular shape with a remarkable length-to-diameter ratio of 28 million which is significantly larger than any other known material [6]. The tubes are rolled of a large graphite sheet called graphene (Fig. 19.6). The diameter of a nanotube is just few nanometers while the length is several millimeters. The tubes are characterized by extremely large surface area for a given volume. The tensile strength is over 100 times larger than that of stainless steel. CNTs are the strongest and stiffest materials yet discovered in terms of tensile strength and elastic modulus. They have a very large Young's modulus in their axial direction (see Table 19.6). The Young modulus value of a single-walled nano-tube (SWNT) is estimated as high as 1–1.8 Tpa [7].

All CNT exhibit strong anisotropic thermal conductivity. They are very good thermal conductors along the tube, exhibiting a property known as “ballistic conduction,” but good thermal insulators laterally to the tube axis. Thermal conductivity of CNT is on the order of 6000 W/(m K) at room temperature, comparing to the best metal heat conductor—silver, that has thermal conductivity 419 W/

**Fig. 19.6** Graphite nanotube of “armchair” type



**Table 19.6** Mechanical properties of single-walled nanotube (SWNT) and multi-walled nanotube (MWNT) in comparison with other materials

Material	Young modulus (GPa)	Tensile strength (GPa)	Density (g/cm <sup>3</sup> )
Single wall nanotube	1054	150	n/a
Multi wall nanotube	1200	150	2.6
Steel	208	0.4	7.8
Epoxy	3.5	0.005	1.25
Wood	16	0.008	0.6

(m K). The temperature stability of CNT is estimated to be about 750 °C in air. It is expected that low-defect CNTs will have very low coefficients of thermal expansion. This makes the nanotube materials attractive for fabricating temperature and infrared sensors. At least in theory, the tubes can carry electric currents thousand times stronger than copper. Their final usage, however, may be limited by their potential toxicity.

## 19.3 Surface Processing

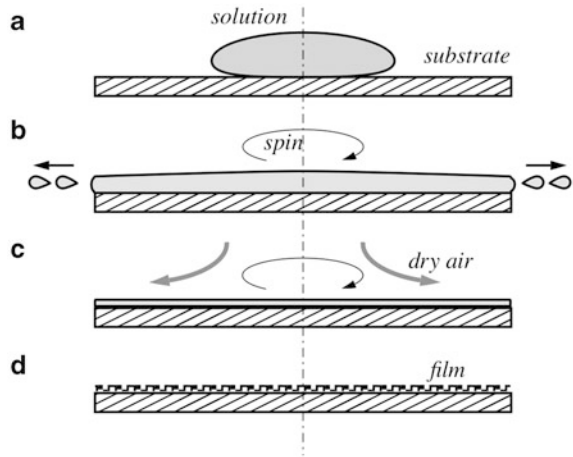
Surface processing is required to give a sensing element certain properties which it otherwise does not possess. For example, to enhance absorption of thermal radiation by a mid- and far-infrared sensor, the surface of a sensing element may be coated with a material having high IR photon absorptivity, for instance nichrome. A piezoelectric film may be applied to a silicon wafer to give it piezoelectric properties. The thick films are often used for fabrication of pressure sensors or microphones where flexible membranes are the key components. Several methods may be used to deposit thin and relatively thin (often referred to as “thick”) layers of films on a substrate or semiconductor wafer. Among them are the spin-casting, vacuum deposition, sputtering, electroplating, and screen printing [8].

### 19.3.1 Spin Casting

The spin casting (coating) process involves use of a thin-film material dissolved in a volatile liquid solvent (Fig. 19.7). The solution is poured on the substrate (a) and the sample is rotated in a high speed – typically over 10 rotations per second. The centrifugal forces spread the material (b) and the excess is flung off the sides. Airflow dries the majority of the solvent off (c) and after the solvent evaporates, a thin layer of film remains on the sample (d). This technique is often used for deposition of organic materials, especially for fabricating humidity and chemical sensors. The thickness depends on solubility of the deposited material and typically is in the range from 0.1 to 50 µm.

The advantages of spin coating are the simplicity and relative ease with which a process can be set up coupled with the thin and fairly uniform coating that can be

**Fig. 19.7** Concept of spin casting



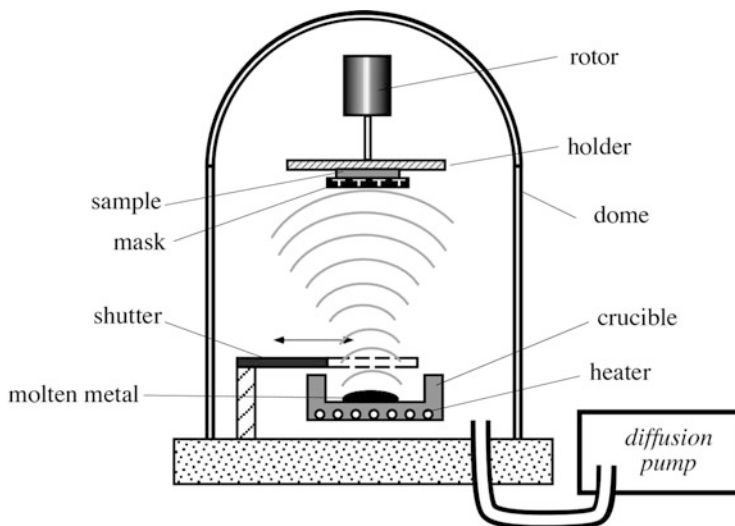
achieved. Due to the ability to have high spin speeds the high airflow leads to fast drying times which in turn results in high consistency at both macroscopic and nano length scales. Yet, since the process relies on the flow of the solution, it may not yield a uniform film or can form island (film-free areas) when the sample has a nonflat surface. Besides, the material may have tendency to shrinkage. Finally, the material usage is typically very low, at around 10 % or less, with the rest being flung off the side and wasted. Whilst this is not usually an issue for research environments, it is clearly wasteful for manufacturing. Nevertheless, in many cases the process is useful and often the only acceptable method of deposition.

### 19.3.2 Vacuum Deposition

A metal can be converted into gaseous form and then deposited on the surface of the sample. The evaporation system consists of a vacuum chamber (Fig. 19.8) where diffuse pump evacuates air down to  $10^{-6}$ – $10^{-7}$  Torr of pressure. A deposited material is placed into a ceramic crucible which is heated by tungsten filament above the metal melting point. An alternative method of heating is use of an electron beam.

On a command from the control device, the shutter opens and allows the metal atoms emanated from the molten metal to deposit on the sample. Parts of the sample which shall remain free of the deposited material are protected by the mask. The deposited film thickness is determined by the evaporation time and the vapor pressure of the metal. Hence, materials with low melting point are easy to deposit, for instance aluminum. In general, vacuum deposited films have large residual stress and thus this technique is used mainly for depositing only thin layers.

Since the molten material is virtually a point source of atoms, it may cause both nonuniform distribution of the deposited film and the so-called shadowing effect where the edges of the masked pattern appear blurry. Two methods may help to



**Fig. 19.8** Deposition of thin metal film in vacuum chamber

alleviate this problem. One is use of multiple sources where more than one crucible (often three or four) is used. Another method is rotation of the target.

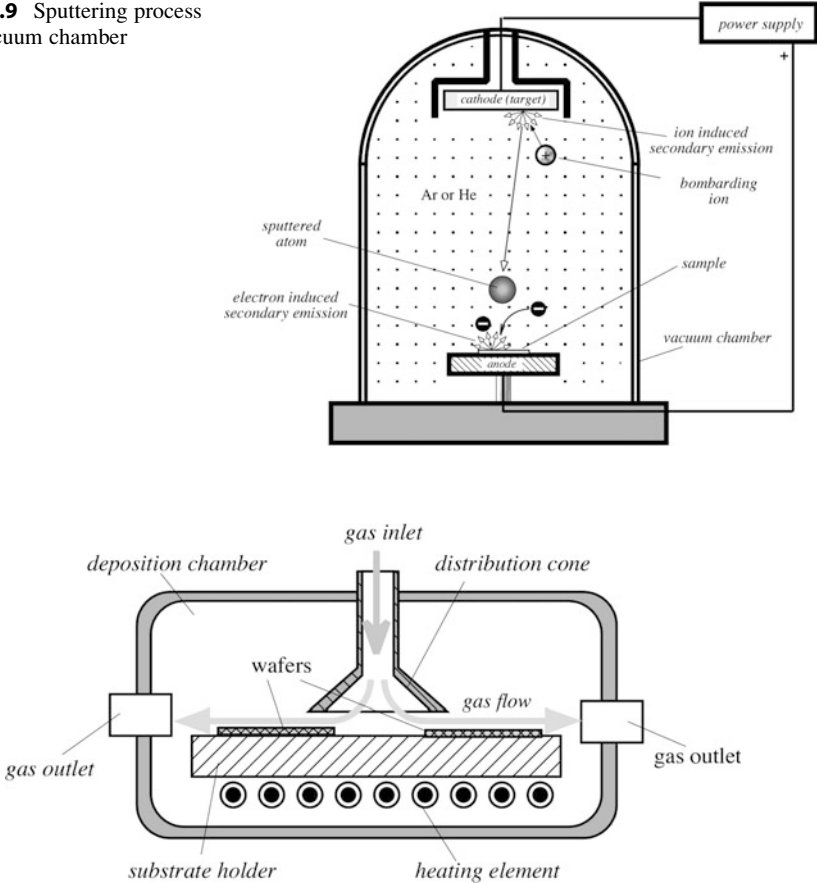
When using the vacuum deposition, one shall pay attention to introduction of spurious materials into the chamber. For instance, even minuscule amount of oil leaking from the diffuse pump will result in burning of organic materials and co-deposition on the sample of such undesirable compounds as carbohydrates.

### 19.3.3 Sputtering

As in the vacuum deposition method, sputtering is performed in a vacuum chamber (Fig. 19.9); however, after evacuation of air, an inert gas, such as argon or helium, is introduced into the chamber at about  $2 \times 10^{-6}$ – $5 \times 10^{-6}$  Torr. An external high voltage DC or AC power supply is attached to the cathode (target) which is fabricated of the material which has to be deposited on the sample. The sample is attached to the anode at some distance from the cathode. High voltage ignite plasma of the inert gas and the gas ions bombard the target. The kinetic energy of the bombarding ions is sufficiently high to free some atoms from the target surface. Hence, the escaped sputtered atoms deposit on the surface of the sample.

The sputtered techniques yields better uniformity, especially if magnetic field is introduced into the chamber allowing for better directing atoms toward the anode. Since this method does not require high temperature of the target, virtually any material, including organic, can be sputtered. Moreover, materials from more than one target can be deposited at the same time (co-sputtering) permitting controlled

**Fig. 19.9** Sputtering process in a vacuum chamber



**Fig. 19.10** Simplified structure of a CVD reactor chamber

ratio of materials. For example, this can be useful for sputtering nichrome (Ni and Cr) electrodes on the surface of pyroelectric sensors.

### 19.3.4 Chemical Vapor Deposition (CVD)

A chemical vapor phase deposition (CVD) process is an important technique for production of optical, optoelectronic and electronic devices. For the sensor technologies, it is useful for forming optical windows and fabrication of semiconductor sensors where thin and thick crystalline layers have to be deposited on the surface.

The CVD process takes place in a deposition (reaction) chamber, one of the versions of which in a simplified form is shown in Fig. 19.10.

The substrates or wafers are positioned on a stationary or rotating table (the substrate holder) whose temperature is elevated up to the required level by the heating elements. The top cover of the chamber has an inlet for the carrier  $H_2$  gas, which can be added by various precursors and dopants. These additives, while being carried over the heated surface of the substrate, form a film layer. The gas mixture flows from the distribution cone over the top surface of the wafers and exits through the exhaust gas outlets. This is accompanied by the production of chemical by-products that are exhausted out of the chamber along with unreacted precursor gases.

The average gas pressure in the chamber may be near 1 atm, or somewhat lower. For example, a layer 6000 Å of  $Ga_{0.47}In_{0.53}As$  can be grown on the InP substrate at 1 atm and 630 °C with a rate of 1.4 Å/s [4].

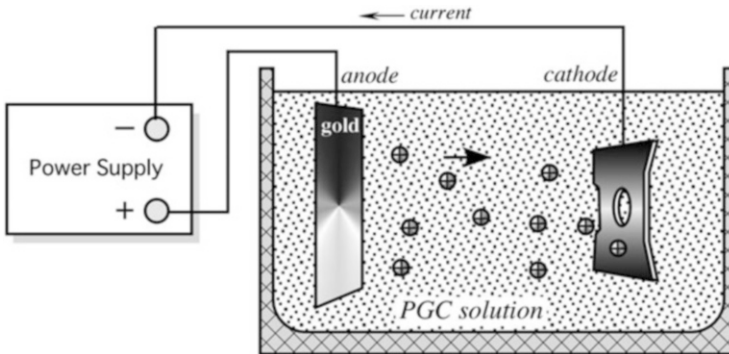
In the sensor technologies, especially in MEMS structures, CVD has a number of advantages as a method for depositing thin films. One of the primary advantages is that CVD films are generally quite conformal, i.e., that the film thickness on the sidewalls of features is comparable to the thickness on the top. This means that films can be applied to elaborately shaped MEMS structures, including the insides and undersides of features, and that high-aspect ratio holes and other features can be completely filled.

CVD also has a number of disadvantages. One of the primary disadvantages lies in the properties of the precursors. Ideally, the precursors need to be volatile at near-room temperatures. This is nontrivial for a number of elements in the periodic table, although the use of metal-organic precursors has eased this situation. CVD precursors can also be toxic ( $Ni(CO)_4$ ), explosive ( $B_2H_6$ ), or corrosive ( $SiCl_4$ ). The by-products of CVD reactions can also be hazardous ( $CO$ ,  $H_2$ , or  $HF$ ). Some of these precursors, especially the metal-organic precursors, can also be quite costly. The other major disadvantage is the fact that the films are usually deposited at elevated temperatures. This puts some restrictions on the kind of substrates that can be coated. More importantly, it leads to stresses in films deposited on materials with different thermal expansion coefficients, which can cause mechanical instabilities in the films deposited of the miniature structures.

### 19.3.5 Electroplating

Electroplating is a deposition of a metal coating on an electrically conductive object by using electric current. The result is a thin, smooth, even coat of metal on the object. Modern electrochemistry was invented by the Italian chemist Luigi V. Brugnatelli in 1805. Brugnatelli used Alessandro Volta's invention of 5 years earlier—the voltaic pile, to facilitate the first electroplating.

The process used in electroplating is called *electrodeposition* and is analogous to a galvanic cell acting in reverse. The part to be coated is placed into a bath or tank containing a solution of one or more metal salts. The part that requires plating is connected to an electrical circuit, forming the cathode (negative) of the circuit while an electrode (typically of the same metal to be plated) forms the anode—a



**Fig. 19.11** Gold plating in a bath (PGC means *potassium gold cyanide* salt used for gold plating)

positive electrode. When an electrical current is passed through the circuit, metal ions in the solution take up excess electrons at the part.

The anode and cathode in the electroplating cell are connected to a DC power supply (Fig. 19.11). The metal of the anode is oxidized to form cations with a positive charge. These cations associate with the anions in the solution. The cations are reduced at the cathode to deposit in the metallic state.

A popular practical process that is different from the bath plating called *brush electroplating*. The selected areas or entire part are plated using a brush saturated with the plating solution. The brush, typically a stainless-steel body wrapped with a cloth material that both holds the plating solution and prevents direct contact with the item being plated, is connected to the positive side of a low voltage DC power supply. The part to be plated is connected to the negative terminal. The brush acts as the anode, but typically does not contribute any plating material, although sometimes the brush is made from or contains the plating material in order to extend the life of the plating solution.

The plating most commonly is done by a single metallic element, not an alloy. However, some alloys can be electrodeposited, notably brass and tin/lead alloy.

Often, direct deposition of a metal on a part (substrate) is not the most efficient way of plating, mainly for the reliability reasons. Let us for example consider electroplating with a metal that has inherently poor adhesion to the substrate. In such a case, a “strike” (the under-plating) can be first deposited. A typical strike is a very thin (less than  $0.1\ \mu\text{m}$  thick) plating of an aid metal having high quality and good adherence to the plated material. The strike is “friendly” or compatible with both—the metal and the substrate. The strike serves as a foundation for the subsequent plating processes. One example of this situation is a notably poor adhesion of electrolytic nickel on zinc alloys. The solution is to use the copper strike first, since copper has good adherence to most materials.

In the sensing technologies, one of the most frequently used metals for plating is gold. It serves to provide corrosion-resistant electrically conductive layers on copper conductors, printed circuit boards and also as an excellent reflector for use



in the mid- and far-infrared spectral ranges. However, plating gold directly on copper, if not done correctly, may pose serious problems because the copper atoms tend to diffuse through the gold layer, causing tarnishing of its surface and formation of an oxide and/or sulfide layer. In an IR reflector, this will result in degradation of performance due to a dramatic reduction in reflectivity. A layer of a suitable barrier metal, usually nickel, is deposited on the copper substrate before the gold plating. The layer of under-plating nickel provides mechanical backing for the gold layer, improving its wear resistance. It also reduces the impact of micro-pores that may be present in the gold layer.

---

## 19.4 MEMS Technologies

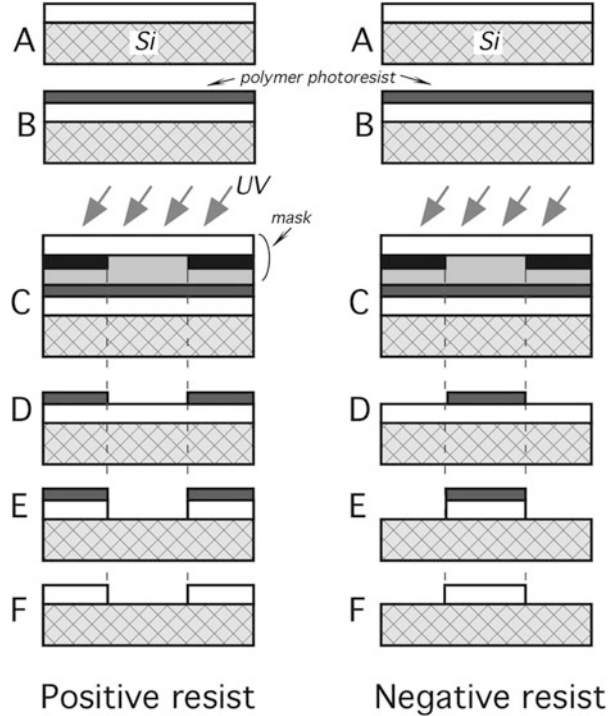
Present trend in the sensor technologies is undoubtedly shifted toward the micro-miniaturization or *microsystem technologies*, known as MST. A subset of these is known as *micro-electro-mechanical systems* or MEMS for short [9]. A MEMS device has electrical and mechanical components, which means there must be at least one moving or deformable part and that electricity must be part of its operation. Another subset is called MEOMS which stands for micro-electro-optical systems. As the name implies, at least one optical component is part of the device. Most of the sensors that are fabricated with use of MEMS or MEOMS are three-dimensional devices with dimensions in the order of micrometers. In fact, MEMS and *nano-technology* are different labels of micro-engineering, since both are concerned with fabrication of micro-miniature structures. One main criterion of MEMS is that there are at least some elements having some sort of mechanical functionality whether or not these elements can move.

The two constructional technologies of microengineering are *microelectronics* and *micromachining*. Microelectronics, producing electronic circuitry on silicon chips, is a very well developed technology. Micromachining is the name for the techniques used to produce the structures and moving parts of microengineered devices. One of the main goals of microengineering is to be able to integrate microelectronic circuitry into micromachined structures, to produce completely integrated systems (microsystems). Such systems typically have the same advantages of low cost, reliability and small size as silicon chips produced in the microelectronics industry.

Presently, there are three micromachining techniques that are in use or are extensively used by the industry. *Silicon micromachining* is given most prominence, since this is one of the better developed micromachining techniques. Silicon is the primary substrate material used in the production microelectronic circuitry and so is the most suitable candidate for the eventual production of microsystems.

The *Excimer Laser* is an ultraviolet laser which can be used to micromachine a number of materials without heating them, unlike many other lasers which remove material by burning or vaporizing it. The Excimer laser lends itself particularly to the machining of organic materials (polymers etc.).

**Fig. 19.12** Positive and negative photolithography



*LIGA*. The acronym comes from the German name for the process (*Lithographie, Galvanoformung, Abformung*). LIGA uses lithography, electroplating, and molding processes to produce microstructures.

### 19.4.1 Photolithography

Photolithography is the basic technique used to define the shape of micromachined structures in the three techniques outlined below. The technique is essentially the same as that used in the microelectronics industry

Figure 19.12a shows a thin film of some material (e.g., silicon dioxide) on a substrate of some other material (e.g., a silicon wafer). The goal of the process is to selectively remove some silicon dioxide (oxide) so that it only remains in particular areas on the silicon wafer, Fig. 19.12f. The process begins with producing a mask. This will typically be a chromium pattern on a glass plate. The wafer is then coated with a polymer which is sensitive to ultraviolet light, Fig. 19.12b, called a photoresist. Ultraviolet light is then shone through the mask onto the photoresist, Fig. 19.12c. The photoresist is then developed which transfers the pattern on the mask to the photoresist layer, Fig. 19.12d.

There are two types of photoresist, termed positive (lefts side of Fig. 19.12) and negative (right side of Fig. 19.12). Where the ultraviolet light strikes the positive resist it weakens the polymer, so that when the image is developed the resist is washed away where the light struck it—transferring a positive image of the mask to the resist layer. It is similar to glass-plate photography. The opposite occurs with the negative resist. Where the ultraviolet light strikes negative resist it strengthens the polymer, so when developed the resist that was not exposed to ultraviolet light is washed away—a negative image of the mask is transferred to the resist.

A chemical (or some other method) is then used to remove the oxide where it is exposed through the openings in the resist, Fig. 19.12e. Finally the resist is removed leaving the patterned oxide, Fig. 19.12f.

## 19.4.2 Silicon Micromachining

There is a number of basic techniques that can be used to pattern thin films that have been deposited on a silicon wafer, and to shape the wafer itself, to form a set of basic microstructures (bulk silicon micromachining). The techniques for depositing and patterning thin films can be used to produce quite complex microstructures on the surface of silicon wafer (surface silicon micromachining). Electrochemical *etching* is the basic silicon micromachining technique. Silicon *bonding* techniques can also be utilized to extend the structures produced by silicon micromachining techniques into multilayer structures.

### 19.4.2.1 Basic Techniques

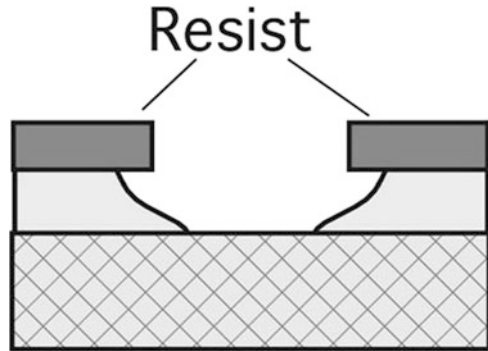
There are three basic techniques associated with silicon micromachining. These are the deposition of thin films of materials, the removal of material (patterning) by wet chemical etchants, and the removal of material by dry etching techniques. Another technique that is utilized is the introduction of impurities into the silicon to change its properties (i.e., doping).

### 19.4.2.2 Thin Films

There are a number of different techniques that facilitate the deposition or formation of very thin films (on the order of micrometers, or even much less) of different materials on a silicon wafer (or other suitable substrate). These films can then be patterned using photolithographic techniques and suitable etching techniques. Common materials include silicon dioxide (oxide), silicon nitride, polycrystalline silicon (polysilicon or poly), and aluminum. A number of other materials can be deposited as thin films, including noble metals such as gold. However, noble metals will contaminate microelectronic circuitry causing it to fail, so any silicon wafers with noble metals on them have to be processed using equipment specially set aside for the purpose. Noble metal films are often patterned by a method known as “lift off,” rather than wet or dry etching.

Often, photoresist is not tough enough to withstand the etching required. In such cases a thin film of a tougher material (e.g., oxide or nitride) is deposited and

**Fig. 19.13** Isotropic etching under the mask



patterned using photolithography. The oxide/nitride then acts as an etch mask during the etching of the underlying material. When the underlying material has been fully etched the masking layer is stripped away.

### 19.4.2.3 Wet Etching

Wet etching is a blanket name that covers the removal of material by immersing the wafer in a liquid bath of the chemical etchant. Wet etchants fall into two broad categories; isotropic etchants and anisotropic etchants. Isotropic etchants attack the material being etched at the same rate in all directions. Anisotropic etchants attack the silicon wafer at different rates in different directions, and so there is more control of the shapes produced. Some etchants attack silicon at different rates depending on the concentration of the impurities in the silicon (concentration dependent etching).

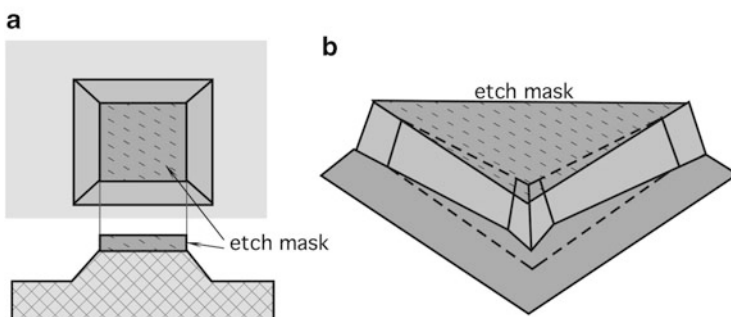
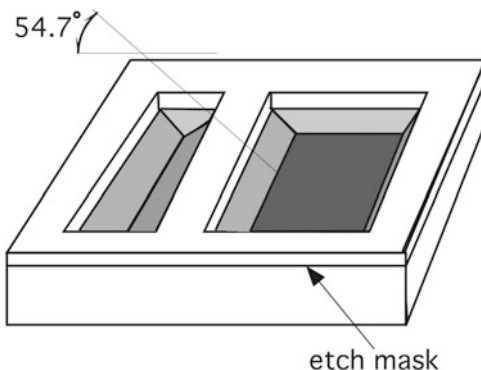
Isotropic etchants are available for oxide, nitride, aluminum, polysilicon, gold, and silicon. Since isotropic etchants attack the material at the same rate in all directions, they remove material horizontally under the etch mask (undercutting) at the same rate as they etch through the material. This is illustrated for a thin film of oxide on a silicon wafer in Fig. 19.13 using an etchant that etches the oxide faster than the underlying silicon (e.g., hydrofluoric acid).

Anisotropic etchants are available to etch different crystal planes in silicon at different rates. The most popular anisotropic etchant is potassium hydroxide (KOH), since it is the safest to use.

Etching is done on a silicon wafer. Silicon wafers are slices that have been cut from a large ingot of silicon that was grown from a single seed crystal. The silicon atoms are all arranged in a crystalline structure, so the wafer is monocrystalline silicon (as opposed to polycrystalline silicon mentioned above). When purchasing silicon wafers, it is possible to specify that they have been sliced with the surface parallel to a particular crystal plane.

The simplest structures that can be formed using KOH to etch a silicon wafer with the most common crystal orientation (100) are shown in Fig. 19.14. These are the V-shaped grooves, or pits with right angled corners and sloping side walls. Using

**Fig. 19.14** Simple structures etched by KOH



**Fig. 19.15** Mesa structures

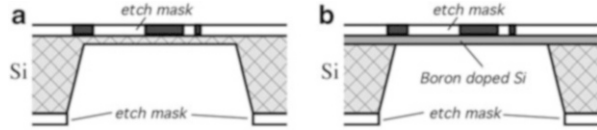
wafers with different crystal orientations can produce grooves or pits with vertical walls.

Both oxide and nitride etch slowly in KOH. Oxide can be used as an etch mask for short periods in the KOH etch bath (i.e., for shallow grooves and pits). For long periods, nitride is a better etch mask as it etches more slowly in the KOH.

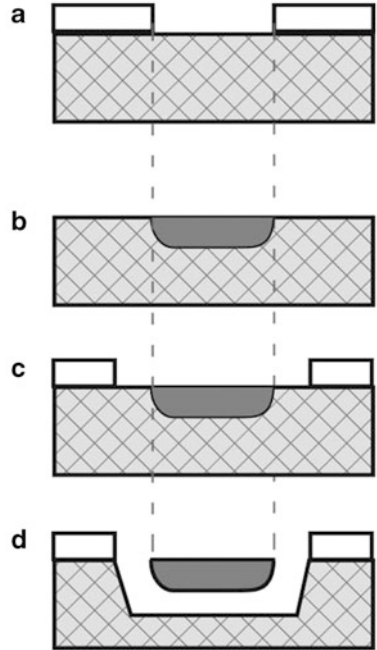
KOH can also be used to produce mesa structures, Fig. 19.15a. When etching mesa structures the corners can become beveled, Fig. 19.15b, rather than right angle corners. This has to be compensated for in some way. Typically the etch mask is designed to include additional structures on the corners. These compensation structures are designed so that they are etched away entirely when the mesa is formed to leave  $90^\circ$  corners. One problem with using compensation structures to form the right-angled mesa corners is that they put a limit on the minimum spacing between the mesas.

Fabrication of a diaphragm is one of the most popular sensor processes. It is used to produce accelerometers, pressures sensor, infrared temperature sensors (thermopiles and micro-bolometers) and many others. Silicon diaphragms from about  $50\ \mu\text{m}$  thick upwards can be made by etching through an entire wafer with KOH, Fig. 19.16a. The thickness is controlled by timing the etch, and so is subject to errors.

**Fig. 19.16** Micromachining of a diaphragm or membrane



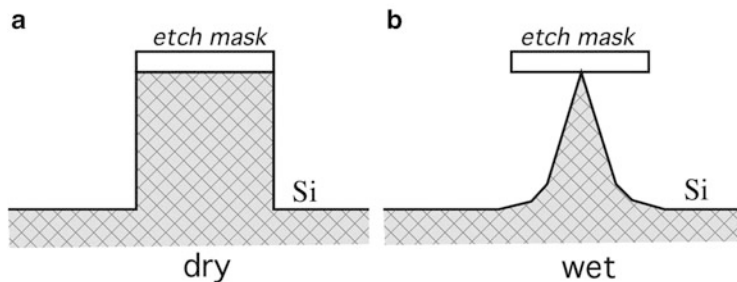
**Fig. 19.17** Etching around the boron doped silicon



#### 19.4.2.4 Concentration-dependent Etching

Thinner diaphragms, of up to about  $20\ \mu\text{m}$  thick, can be produced using boron to stop the KOH etch, Fig. 19.16b. This is called the concentration-dependent etching. The thickness of the diaphragm is dependent on the depth to which the boron is diffused into the silicon, which can be controlled more accurately than the simple timed KOH etch. High levels of boron in silicon will reduce the rate at which it is etched in KOH by several orders of magnitude, effectively stopping the etching of the boron rich silicon. The boron impurities are usually introduced into the silicon by a process known as *diffusion*.

Besides the diaphragms, many other structures can be built by the concentration dependent etching. A thick oxide mask is formed over the silicon wafer and patterned to expose the surface of the silicon wafer where the boron is to be introduced, Fig. 19.17a. The wafer is then placed in a furnace in contact with a boron diffusion source. Over a period of time boron atoms migrate into the silicon wafer. Once the boron diffusion is completed, the oxide mask is stripped off,



**Fig. 19.18** Dry etching of pointed structure

Fig. 19.17b. A second mask may then be deposited and patterned, Fig. 19.17c, before the wafer is immersed in the KOH etch bath. The KOH etches the silicon that is not protected by the mask, and etches around the boron-doped silicon, Fig. 19.17d. Boron can be driven into the silicon as far as 20  $\mu\text{m}$  over periods of 15–20 h; however, it is desirable to keep the time in the furnace as short as possible.

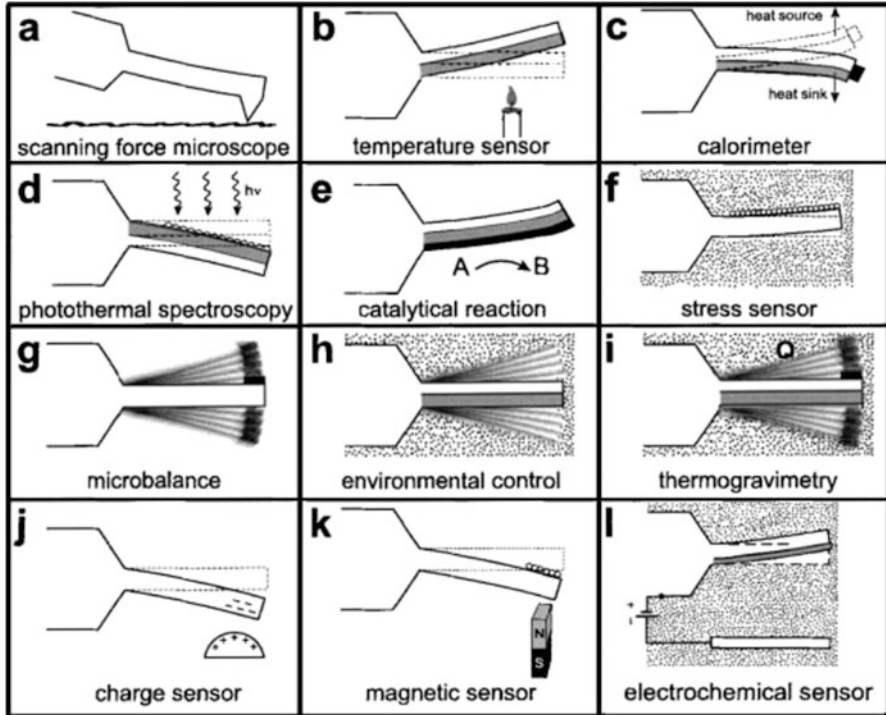
#### 19.4.2.5 Dry Etching

The most common form of dry etching for micromachining applications is *reactive ion etching* (RIE). Ions are accelerated towards the material to be etched, and the etching reaction is enhanced in the direction of travel of the ion, thus RIE is an anisotropic etching technique. Deep trenches and pits (up to ten or a few tens of microns) of arbitrary shape and with vertical walls can be etched in a variety of materials including silicon, oxide and nitride. Unlike anisotropic wet etching, RIE is not limited by the crystal planes in the silicon. A combination of dry etching and isotropic wet etching can be used to form very sharp points. First, a column with vertical sides is etched away using an RIE, Fig. 19.18a. A wet etch is then used, which undercuts the etch mask leaving a very fine point, Fig. 19.18b, the etch mask is then removed. Very fine points like this can be fabricated on the end of cantilever beams as probes for use, for example, in tactile sensors.

### 19.4.3 Micromachining of Bridges and Cantilevers

Cantilevers and narrow bridges are frequently employed on the MEMS sensors thanks to a very large spectrum of applications (e.g., Fig. 15.32b). One of the applications for these beams and bridges is the resonant sensors. The structure can be set vibrating at its fundamental frequency. Anything causing a change in the mass, length, etc. of the structure will register as a change frequency. Care has to be taken to ensure that only the quantity to be measured causes a significant change in frequency.

Figure 19.19 illustrates some popular uses of the micro-cantilevers. In many sensors, the cantilever ability to flex under various stimuli can be detected by embedded piezo-resistive sensors. Examples include strains developed under



**Fig. 19.19** Uses of a micromachined cantilever sensors (adapted from ref. [10])

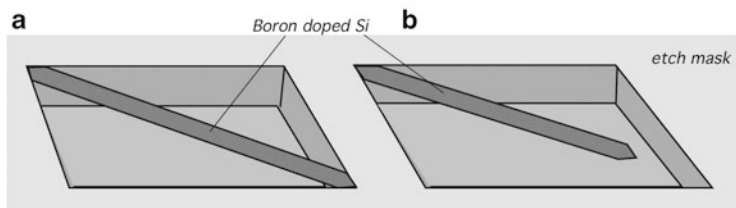
various chemical reactions (e), nonuniform absorption (b) of heat and electrostatic forces (j).

Concentration dependent etching can be used to produce narrow bridges or cantilever beams. Figure 19.20a shows a bridge, defined by a boron diffusion, spanning a pit that was etched from the front of the wafer in KOH. A cantilever beam (a bridge with one end free) produced by the same method is shown in Fig. 19.20b. The bridge and beam project across the diagonal of the pit to ensure that they will be etched free by the KOH. More complex structures are possible using this technique, but care must be taken to ensure that they will be etched free by the KOH.

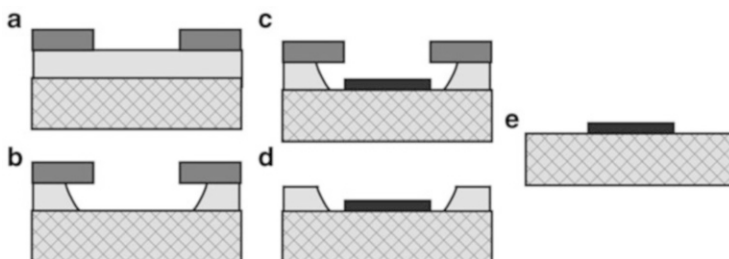
#### 19.4.4 Lift-Off

Lift-off is a stenciling technique often used to pattern noble metal films. There are a number of different techniques, but here we will outline just one that is an assisted lift-off method. A thin film of the assisting material (e.g., oxide) is deposited. A layer of resist is put over this and patterned, as for photolithography, to expose the oxide in the pattern desired for the metal, Fig. 19.21a. The oxide is then wet etched





**Fig. 19.20** Etching of bridge and cantilever



**Fig. 19.21** Lift-off technique

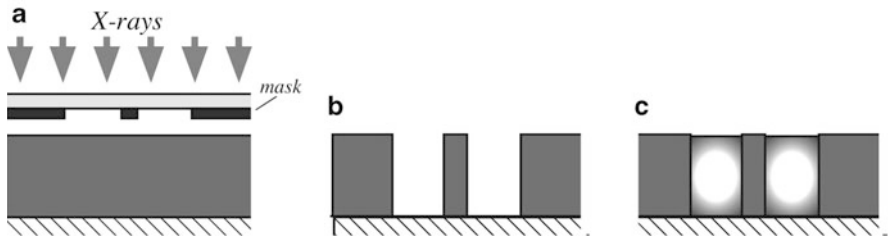
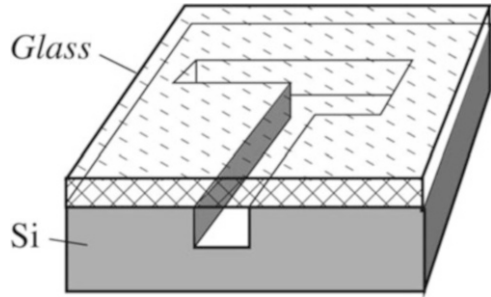
so as to undercut the resist, Fig. 18.17b. The metal is then deposited on the wafer, typically by a process known as evaporation, Fig. 19.21c. The metal pattern is effectively stenciled through the gaps in the resist, which is then removed lifting off the unwanted metal with it, Fig. 19.21d. The assisting layer is then stripped off too, leaving the metal pattern alone, Fig. 19.21e.

### 19.4.5 Wafer Bonding

There are a number of different methods available for bonding micromachined silicon wafers together, or to other substrates, to form more complex devices. A method of bonding silicon to glass that appears to be gaining in popularity is anodic bonding (electrostatic bonding). The silicon wafer and glass substrate are brought together and heated to a high temperature. A large electric field is applied across the join, which causes an extremely strong bond to form between the two materials. Figure 19.22 shows a glass plate bonded over a channel etched into a silicon wafer (RIE).

It is also possible to bond silicon wafers directly together using gentle pressure, under water (direct silicon bonding). Other bonding methods include using an adhesive layer, such as a glass, or photoresist. Whilst anodic bonding and direct silicon bonding form very strong joins, they suffer from some disadvantages, including the requirement that the surfaces to be joined are very flat and clean.

**Fig. 19.22** Bonding of glass to silicon



**Fig. 19.23** LIGA technique to produce metal structure

Wafer bonding techniques can potentially be combined with some of the basic micromachined structures to form the membranes, cantilevers, valves, pumps, etc. of a microfluid handling system that may be parts of chemical sensors.

### 19.4.6 LIGA

LIGA is capable of creating very finely defined microstructures of up to 1000  $\mu\text{m}$  high. In the process as originally developed, a special kind of photolithography using X-rays (X-ray lithography) is used to produce patterns in very thick layers of photoresist. The X-rays from a synchrotron source are shone through a special mask onto a thick photoresist layer (sensitive to X-rays) which covers a conductive substrate, Fig. 19.23a. This resist is then developed (Fig. 19.23b). The pattern formed is then electroplated with metal, Fig. 19.23c. The metal structures produced can be the final product; however, the metal structure can be used as a micro-mold that can be filled with various materials, such as a plastic to produce the finished structures in that material. As the synchrotron source makes LIGA expensive, alternatives are being developed. These include high voltage electron beam lithography which can be used to produce structures of the order of 100  $\mu\text{m}$  high, and excimer lasers capable of producing structures of up to several hundred microns high.

Naturally, electroplating is not limited to use with the LIGA process, but may be combined with other processes and more conventional photolithography to produce microstructures.

---

## References

1. Middelhoek, S., et al. (1985). Smart sensors: when and where? *Sensors and actuators*, 8(1), 39–48. Elsevier Sequoya.
2. Obermier, E., et al. (1986). Characteristics of polysilicon layers and their application in sensors. In: *IEEE solid-state sensors workshop*.
3. Honeychurch, K. C. (Ed.). (2014). *Nanosensors for chemical and biological applications*. Sawston: Woodhead Publishing.
4. Frijlink, P. M., et al. (1991). Layer uniformity in a multiwafer MOVPRE reactor for III-V compounds. *Journal of Crystal Growth*, 107, 167–174.
5. Ratner, M., et al. (2003). *Nanotechnology. A gentle introduction to the next big idea*. New York City, NY: Pearson Education, Inc.
6. Popov, V. N. (2004). Carbon nanotubes: properties and application. *Materials Science and Engineering*, R43, 61–102.
7. Varshney, K. (2014). Carbon nanotubes: a review on synthesis, properties and applications. *International Journal of Engineering Research and General Science*, 2(4), 660–667.
8. Rancourt, J. D. (1996). *Optical thin films – User's handbook*. New York, NY: McGraw-Hill.
9. Gad-El-Hak, M. (Ed.). (2006). *MEMS – Introduction and fundamentals* (2nd ed.). Boca Raton, FL: CRC Press.
10. Lang, H. P., et al. (1999). An artificial nose based on a micromechanical cantilever array. *Analytica Chimica Acta (Elsevier)*, 393, 59–65.

---

# Appendix

**Table A.1** Chemical symbols for the elements

Ac	Actinium	Co	Cobalt	In	Indium	Os	Osmium	Sm	Samarium
Ag	Silver	Cr	Chromium	Ir	Iridium	P	Phosphorous	Sn	Tin
Al	Aluminum	Cs	Cesium	K	Potassium	Pa	Protactinium	Sr	Strontium
Am	Americium	Cu	Copper	Kr	Krypton	Pb	Lead	Ta	Tantalum
Ar	Argon	Dy	Dysprosium	La	Lanthanum	Pd	Palladium	Tb	Terbium
As	Arsenic	Er	Erbium	Li	Lithium	Pm	Promethium	Tc	Technetium
At	Astatine	Es	Einsteinium	Lr	Lawrencium	Po	Polonium	Te	Tellurium
Au	Gold	Eu	Europium	Lu	Lutetium	Pr	Praseodymium	Th	Thorium
B	Boron	F	Fluorine	Md	Mendelevium	Pt	Platinum	Ti	Titanium
Ba	Barium	Fe	Iron	Mg	Magnesium	Pu	Plutonium	Tl	Thallium
Be	Beryllium	Fm	Fermium	Mn	Manganese	Ra	Radium	Tm	Thulium
Bi	Bismuth	Fr	Francium	Mo	Molybdenum	Rb	Rubidium	U	Uranium
Bk	Berkelium	Ga	Gallium	N	Nitrogen	Re	Rhenium	V	Vanadium
Br	Bromine	Gd	Gadolinium	Na	Sodium	Rh	Rhodium	W	Tungsten
C	Carbon	Ge	Germanium	Nb	Niobium	Rn	Radon	Xe	Xenon
Ca	Calcium	H	Hydrogen	Nd	Neodymium	Ru	Ruthenium	Y	Yttrium
Cd	Cadmium	He	Helium	Ne	Neon	S	Sulfur	Yb	Ytterbium
Ce	Cerium	Hf	Hafnium	Ni	Nickel	Sb	Antimony	Zn	Zinc
Cf	Californium	Hg	Mercury	No	Nobelium	Sc	Scandium	Zr	Zirconium
Cl	Chlorine	Ho	Holmium	Np	Neptunium	Se	Selenium		
Cm	Curium	I	Iodine	O	Oxygen	Si	Silicon		

**Table A.2** SI multiples

Factor	Prefix	Symbol	Factor	Prefix	Symbol
$10^{18}$	exa	E	$10^{-1}$	deci	d
$10^{15}$	peta	P	$10^{-2}$	centi	c
$10^{12}$	tera	T	$10^{-3}$	milli	m
$10^9$	giga	G	$10^{-6}$	micro	$\mu$
$10^6$	mega	M	$10^{-9}$	nano	n
$10^3$	kilo	k	$10^{-12}$	pico	p
$10^2$	hecto	h	$10^{-15}$	femto	f
$10^1$	deca	da	$10^{-18}$	atto	a

**Table A.3** Derivative SI units

Quantity	Name of unit	Expression in terms of basic units
Area	square meter	$m^2$
Volume	cubic meter	$m^3$
Frequency	hertz (Hz)	$s^{-1}$
Density (concentration)	kilogram per cubic meter	$kg/m^3$
Velocity	meter per second	m/s
Angular velocity	radian per second	rad/s
Acceleration	meter per second squared	$m/s^2$
Angular acceleration	radian per second squared	$rad/s^2$
Volumetric flow rate	cubic meter per second	$m^3/s$
Force	newton (N)	$kg\ m/s^2$
Pressure	newton per square meter ( $N/m^2$ ) or pascal (Pa)	$kg/m\ s^2$
Work energy heat torque	joule (J), newton-meter (N m) or watt-second (W s)	$kg\ m^2/s^2$
Power heat flux	watt (W) Joule per second (J/s)	$kg\ m^2/s^3$
Heat flux density	watt per square meter ( $W/m^2$ )	$kg/s^3$
Specific heat	joule per kilogram degree (J/kg deg)	$m^2/s^2\ deg$
Thermal conductivity	watt per meter degree ( $W/m\ deg$ ) or ( $J\ m/s\ m^2\ deg$ )	$kg\ m/s^3\ deg$
Mass flow rate (mass flux)	kilogram per second	kg/s
Mass flux density	kilogram per square meter-second	$kg/m^2\ s$
Electric charge	coulomb (C)	A s
Electromotive force	volt (V) or (W/A)	$kg\ m^2/A\ s^3$
Electric resistance	ohm ( $\Omega$ ) or (V/A)	$kg\ m^2/A^2\ s^3$
Electric conductivity	ampere per volt-meter (A/V m)	$A^2\ s^3/kg\ m^3$
Electric capacitance	farad (F) or (A s/V)	$A^3\ s^4/kg\ m^2$
Magnetic flux	weber (Wb) or (V s)	$kg\ m^2/A\ s^2$
Inductance	henry (H) or (V s/A)	$kg\ m^2/A^2\ s^2$
Magnetic permeability	henry per meter (H/m)	$kg\ m/A^2\ s^2$
Magnetic flux density	tesla (T) or weber per square meter ( $Wb/m^2$ )	$kg/A\ s^2$
Magnetic field strength	ampere per meter	A/m
Magnetomotive force	ampere	A
Luminous flux	lumen (lm)	cd sr
Luminance	candela per square meter	$cd/m^2$
Illumination	lux (lx) or lumen per square meter ( $lm/m^2$ )	$cd\ sr/m^2$

**Table A.4** SI conversion multiples (to make a conversion to SI, a non-SI value should be multiplied by a number given in the table)

<b>Acceleration: (m/s<sup>2</sup>)</b>			
ft/s <sup>2</sup>	0.3048	gal	0.01
free fall (g)	9.80665	in/s <sup>2</sup>	0.0254
<b>Angle: radian (rad)</b>			
degree	0.01745329	second	$4.848137 \times 10^{-6}$
minute	$2.908882 \times 10^{-4}$	grade	$1.570796 \times 10^{-2}$
<b>Area: (m<sup>2</sup>)</b>			
acre	4046.873	hectare	$1 \times 10^4$
are	100.00	mi <sup>2</sup> (US statute)	$2.589998 \times 10^6$
ft <sup>2</sup>	$9.290304 \times 10^{-2}$	yd <sup>2</sup>	0.8361274
<b>Bending Moment or torque: (N m)</b>			
dyne cm	$1 \times 10^{-7}$	lbf in	0.1129848
kgf m	9.806650	lbf ft	1.355818
ozf in	$7.061552 \times 10^{-3}$		
<b>Electricity and magnetism<sup>a</sup></b>			
ampere hour	3600 coulomb (C)	EMU of inductance	$8.987 \times 10^{11}$ henry (H)
EMU of capacitance	$10^9$ farad (F)	EMU of resistance	$8.987 \times 10^{11}$ ( $\Omega$ )
EMU of current	10 ampere (A)	faraday	$9.65 \times 10^{19}$ coulomb (C)
EMU of elec. potential	$10^{-8}$ volt (V)	gamma	$10^{-9}$ tesla (T)
EMU of inductance	$10^{-9}$ henry (H)	gauss	$10^{-4}$ tesla (T)
EMU of resistance	$10^{-9}$ ohm ( $\Omega$ )	gilbert	0.7957 ampere (A)
ESU of capacitance	$1.112 \times 10^{-12}$ farad (F)	maxwell	$10^{-8}$ weber (Wb)
ESU of current	$3.336 \times 10^{-10}$ ampere (A)	mho	1.0 siemens (S)
EMU of elec. potential	299.79 volt (V)	ohm centimeter	0.01 ohm meter ( $\Omega$ m)
<b>Energy (work): joule (J)</b>			
British thermal unit (Btu)	1055	kilocalorie	4187
calorie	4.18	kW h	$3.6 \times 10^6$
calorie (kilogram)	4184	ton (nuclear equiv. TNT)	$4.184 \times 10^9$
electronvolt	$1.60219 \times 10^{-19}$	therm	$1.055 \times 10^8$
erg	$10^{-7}$	W h	3600
ft lbf	1.355818	W s	1.0
ft-poundal	0.04214		
<b>Force: newton (N)</b>			
dyne	$10^{-5}$	ounce-force	0.278
kilogram-force	9.806	pound-force (lbf)	4.448
kilopond (kp)	9.806	poundal	0.1382
kip (1000 lbf)	4448	ton-force (2000 lbf)	8896

(continued)

**Table A.4** (continued)

<b>Heat</b>			
Btu ft/(h ft <sup>2</sup> °F) (thermal conductivity)	1.7307 W/(m K)	cal/cm <sup>2</sup>	4.18 × 10 <sup>4</sup> J/m <sup>2</sup>
Btu/lb	2324 J/kg	cal/(cm <sup>2</sup> min)	697.3 W/m <sup>2</sup>
Btu/(lb °F) = cal/(g °C) (heat capacity)	4186 J/(kg K)	cal/s	4.184 W
Btu/ft <sup>3</sup>	3.725 × 10 <sup>4</sup> J/m <sup>3</sup>	°F h ft <sup>2</sup> /Btu (thermal resistance)	0.176 K m <sup>2</sup> /W
cal/(cm s °C)	418.4 W/(m K)	ft <sup>2</sup> /h (thermal diffusivity)	2.58 × 10 <sup>-5</sup> m <sup>2</sup> /s
<b>Length: meter (m)</b>			
angstrom	10 <sup>-10</sup>	microinch	2.54 × 10 <sup>-8</sup>
astronomical unit	1.495979 × 10 <sup>11</sup>	micrometer (micron)	10 <sup>-6</sup>
chain	20.11	mil	2.54 × 10 <sup>-5</sup>
fermi (femtometer)	10 <sup>-15</sup>	mile (nautical)	1852.000
foot	0.3048	mile (international)	1609.344
inch	0.0254	pica (printer's)	4.217 × 10 <sup>-3</sup>
light year	9.46055 × 10 <sup>15</sup>	yard	0.9144
<b>Light</b>			
cd/in. <sup>2</sup>	1550 cd/m <sup>2</sup>	lambert	3.183 × 10 <sup>3</sup> cd/m <sup>2</sup>
footcandle	10.76 lx (lux)	lm/ft <sup>2</sup>	10.76 lm/m <sup>2</sup>
footlambert	3.426 cd/m <sup>2</sup>		
<b>Mass: kilogram (kg)</b>			
carat (metric)	2 × 10 <sup>-4</sup>	ounce (troy or apothecary)	3.110348 × 10 <sup>-2</sup>
grain	6.479891 × 10 <sup>-5</sup>	pennyweight	1.555 × 10 <sup>-3</sup>
gram	0.001	pound (lb avoirdupois)	0.4535924
hundredweight (long)	50.802	pound (troy or apothecary)	0.3732
hundredweight (short)	45.359	slug	14.5939
kgf × s <sup>2</sup> /m	9.806650	ton (long, 2240 lb)	907.184
ounce (avoirdupois)	2.834952 × 10 <sup>-2</sup>	ton (metric)	1000
<b>Mass: per unit time (includes Flow)</b>			
perm (0 °C)	5.721 × 10 <sup>-11</sup> kg/(Pa s m <sup>2</sup> )	lb/(hp h) SPC—specific fuel consumption	1.689659 × 10 <sup>-7</sup> kg/J
lb/h	1.2599 × 10 <sup>-4</sup> kg/s	ton (short)/h	0.25199 kg/s
lb/s	0.4535924 kg/s		
<b>Mass per unit volume (includes Density and Capacity): (kg/m<sup>3</sup>)</b>			
oz (avoirdupois)/gal (UK liquid)	6.236	oz (avoirdupois)/gal (US liquid)	7.489
oz (avoirdupois)/in. <sup>3</sup>	1729.99	slug/ft <sup>3</sup>	515.3788
lb/gal (US liquid)	11.9826 kg/m <sup>3</sup>	ton (long)/yd <sup>3</sup>	1328.939

(continued)



**Table A.4** (continued)

<b>Power: watt (W)</b>			
Btu (International)/s	1055.056	horsepower (electric)	746
cal/s	4.184	horsepower (metric)	735.499
erg/s	$10^{-7}$	horsepower (UK)	745.7
horsepower (550 ft lbf/s)	745.6999	ton of refrigeration (12,000 Btu/h)	3517
<b>Pressure or stress: pascal (Pa)</b>			
atmosphere, standard	$1.01325 \times 10^5$	dyne/cm <sup>2</sup>	0.1
atmosphere, technical	$9.80665 \times 10^4$	foot of water (39.2 °F)	2988.98
bar	$10^5$	poundal/ft <sup>2</sup>	1.488164
centimeter of mercury (0 °C)	1333.22	psi (lbf/in. <sup>2</sup> )	6894.757
centimeter of water (4 °C)	98.0638	torr (mmHg, 0 °C)	133.322
<b>Radiation units</b>			
curie	$3.7 \times 10^{10}$ becquerel (Bq)	rem	0.01 sievert (Sv)
rad	0.01 gray (Gy)	roentgen	$2.58 \times 10^{-4}$ C/kg
<b>Temperature</b>			
° Celsius	TK = t°C + 273.15 K	° Fahrenheit	T°C = (t°F - 32)/1.8 °C
° Fahrenheit	TK = (t°F + 459.67)/1.8 K	° Rankine	TK = T°R/1.8
<b>Velocity (includes Speed): (m/s)</b>			
ft/s	0.3048	mi/h (International)	0.44704
in./s	$2.54 \times 10^{-2}$	rpm (r/min)	0.1047 rad/s
knot (International)	0.51444		
<b>Viscosity: (Pa s)</b>			
centipose (dynamic viscosity)	$10^{-3}$	lbf × s/in <sup>2</sup>	6894.757
centistokes (kinematic viscosity)	$10^{-6}$	rhe	$10 \times 1/(\text{Pa s})$
poise	0.1	slug/(ft s)	47.88026
poundal s/ft <sup>2</sup>	1.488164	stokes	$10^{-4}$ m <sup>2</sup> /s
lb/(ft s)	1.488164		
<b>Volume (includes capacity): (m<sup>3</sup>)</b>			
acre-foot	1233.489	gill (US)	$1.182941 \times 10^{-4}$
barrel (oil, 42 gal)	0.1589873	in. <sup>3</sup>	$1.638706 \times 10^{-5}$
bushel (U.S.)	$3.5239 \times 10^{-2}$	litre	$10^{-3}$
cup	$2.36588 \times 10^{-4}$	ounce (US fluid)	$2.957353 \times 10^{-5}$
ounce (U.S. fluid)	$2.95735 \times 10^{-5}$	pint (US dry)	$5.506105 \times 10^{-4}$

(continued)

**Table A.4** (continued)

ft <sup>3</sup>	$2.83168 \times 10^{-2}$	pint (US liquid)	$4.731765 \times 10^{-4}$
gallon (Canadian, U.K. liquid)	$4.54609 \times 10^{-3}$	tablespoon	$1.478 \times 10^{-5}$
gallon (U.S. liquid)	$3.7854 \times 10^{-3}$	ton (register)	2.831658
gallon (U.S. dry)	$4.40488 \times 10^{-3}$	yd <sup>3</sup>	0.76455

<sup>a</sup>ESU means electrostatic *cgs* unit; EMU means electromagnetic *cgs* unit

**Table A.5** Dielectric constants of some materials at room temperature (25 °C)

Material	$\kappa$	Frequency (Hz)	Material	$\kappa$	Frequency (Hz)
Air	1.00054	0	Paraffin	2.0–2.5	10 <sup>6</sup>
Alumina ceramic	8–10	10 <sup>4</sup>	Plexiglas	3.12	10 <sup>3</sup>
Acrylics	2.5–2.9	10 <sup>4</sup>	Polyether sulfone	3.5	10 <sup>4</sup>
ABS/Polysulfone	3.1	10 <sup>4</sup>	Polyesters	3.22–4.3	10 <sup>3</sup>
Asphalt	2.68	10 <sup>6</sup>	Polyethylene	2.26	10 <sup>3</sup> –10 <sup>8</sup>
Beeswax	2.9	10 <sup>6</sup>	Polypropylenes	2–3.2	10 <sup>4</sup>
Benzene	2.28	0	Polyvinyl chloride	4.55	10 <sup>3</sup>
Carbon tetrachloride	2.23	0	Porcelain	6.5	0
Cellulose nitrate	8.4	10 <sup>3</sup>	Pyrex glass (7070)	4.0	10 <sup>6</sup>
Ceramic (titanium dioxide)	14–110	10 <sup>6</sup>	Pyrex glass (7760)	4.5	0
Cordierite	4–6.23	10 <sup>4</sup>	Rubber (neoprene)	6.6	10 <sup>3</sup>
Compound for thick film capacitors	300–5000	0	Rubber (silicone)	3.2	10 <sup>3</sup>
Diamond	5.5	10 <sup>8</sup>	Rutile ⊥ optic axis	86	10 <sup>8</sup>
Epoxy resins	2.8–5.2	10 <sup>4</sup>	Rutile    optic axis	170	10 <sup>8</sup>
Ferrous oxide	14.2	10 <sup>8</sup>	Silicone resins	3.4–4.3	10 <sup>4</sup>
Flesh (skin, blood, muscles)	97	40 × 10 <sup>6</sup>	Tallium chloride	46.9	10 <sup>8</sup>
Flesh (fat, bones)	15	40 × 10 <sup>6</sup>	Teflon	2.04	10 <sup>3</sup> –10 <sup>8</sup>
Lead nitrate	37.7	6 × 10 <sup>7</sup>	Transformer oil	4.5	0
Methanol	32.63	0	Vacuum	1	—
Nylon	3.5–5.4	10 <sup>3</sup>	Water	78.5	0
Paper	3.5	0			

**Table A.6** Properties of magnetic materials (adapted from *Sprague*, CN-207 Hall effect IC applications, 1986)

Material	MEP (G Oe) $\times 10^6$	Residual induction (G) $\times 10^3$	Coercive force (Oe) $\times 10^3$	Temperature coefficient %/ $^{\circ}\text{C}$	Cost
R. E.-Cobalt	16	8.1	7.9	-0.05	highest
Alnico 1,2,3,4	1.3-1.7	5.5-7.5	0.42-0.72	-0.02 to -0.03	medium
Alnico 5,6, 7	4.0-7.5	10.5-13.5	0.64-0.78	-0.02 to -0.03	medium/high
Alnico 8	5.0-6.0	7-9.2	1.5-1.9	-0.01 to 0.01	medium/high
Alnico 9	10	10.5	1.6	-0.02	high
Ceramic 1	1.0	2.2	1.8	-0.2	low
Ceramic 2,3,4,6	1.8-2.6	2.9-3.3	2.3-2.8	-0.2	low/medium
Ceramic 5,7,8	2.8-3.5	3.5-3.8	2.5-3.3	-0.2	medium
Cunife	1.4	5.5	0.53	-	medium
Fe-Cr	5.25	13.5	0.6	-	medium/high
Plastic	0.2-1.2	1.4	0.45-1.4	-0.2	lowest
Rubber	0.35-1.1	1.3-2.3	1-1.8	-0.2	lowest

**Table A.7** Resistivities ( $\rho$ )  $10^{-8}\Omega$  m (at room temperature) and temperature coefficients of resistivity (TCR)  $10^{-3}/^{\circ}\text{K}$  of some materials at room temperature

Material	$\rho$	TCR ( $\alpha$ )	Material	$\rho$	TCR ( $\alpha$ )
Alumina <sup>a</sup>	$>10^{20}$		Palladium	10.54	3.7
Aluminum (99.99 %)	2.65	3.9	Platinum	10.42	3.7
Beryllium	4.0	0.025	Platinum + 10 % Rhodium	18.2	
Bismuth	$10^6$		Polycrystalline glass <sup>a</sup>	$6.3 \times 10^{14}$	
Brass (70Cu, 30Zn)	7.2	2.0	Rare earth metals	28-300	
Carbon	3500	-0.5	Silicon (very sensitive to purity)	$(3.4-15) \times 10^6$	
Chromium plating	14-66		Silicon bronze (96Cu, 3Si, 1Zn)	21.0	
Constantan (60Cu, 40Ni)	52.5	0.01	Silicon nitride	$10^{19}$	
Copper	1.678	3.9	Silver	1.6	6.1
Evanohm (75Ni, 20Cr, 2.5Al, 2.5Cu)	134		Sodium	4.75	
Germanium (polycrystalline)	$46.10^6$		Stainless steel (cast)	70-122	

(continued)

**Table A.7** (continued)

Material	$\rho$	TCR ( $\alpha$ )	Material	$\rho$	TCR ( $\alpha$ )
Gold	2.24	3.4	Tantalum	12.45	3.8
Iridium	5.3		Tantalum carbide	20	
Iron (99.99 %)	9.71	6.5	Tin	11.0	4.7
Lead	22	3.36	Titanium	42	
Manganese	185		Titanium and its alloys	48–199	
Manganin	44	0.01	Titanium carbides	105	
Manganin (84Cu, 12Mn, 4Ni)	48		Tungsten	5.6	4.5
Mercury	96	0.89	Zinc	5.9	4.2
Mullite <sup>a</sup>	10 <sup>21</sup>		Zircon <sup>a</sup>	>10 <sup>20</sup>	
Nichrome	100	0.4	Zirconium and its alloys	40–74	
Nickel	6.8	6.9			

<sup>a</sup>Volume resistivity**Table A.8** Properties of piezoelectric materials at 20 °C

	PVDF	BaTiO <sub>3</sub>	PZT	Quartz	TGS
Density ( $\times 10^3$ kg/m <sup>3</sup> )	1.78	5.7	7.5	2.65	1.69
Dielectric constant, $\epsilon_r$	12	1700	1200	4.5	45
Elastic modulus (10 <sup>10</sup> N/m)	0.3	11	8.3	7.7	3
Piezoelectric constant (pC/N)	$d_{31} = 20$ $d_{32} = 2$ $d_{33} = -30$	78	110	2.3	25
Pyroelectric constant (10 <sup>-4</sup> C/m <sup>2</sup> K)	4	20	27	–	30
Electromechanical coupling constant (%)	11	21	30	10	–
Acoustic impedance (10 <sup>6</sup> kg/m <sup>2</sup> s)	2.3	25	25	14.3	–

**Table A.9** Physical properties of pyroelectric materials (from Meixner, H., Mader, G. and Kleinschmidt, P. Infrared sensors based on the pyroelectric polymer polyvinylidene fluoride (PVDF). *Siemens Forsch.-u. Entwickl. Ber. Bd.*, vol. 15, No. 3, pp: 105–114, 1986)

Material	Curie Temperature, °C	Thermal Conductivity, W/(mK)	Relative Permittivity, $\epsilon_r$	Pyroelectric Charge Coef., C/(m <sup>2</sup> K)	Pyroelectric Voltage Coef., V/(mK)	Coupling, $k_p^2$ (%)
<i>Single crystals</i>						
TGS	49	0.4	30	$3.5 \times 10^{-4}$	$1.3 \times 10^6$	7.5
LiTaO <sub>3</sub>	618	4.2	45	$2.0 \times 10^{-4}$	$0.5 \times 10^6$	1.0
<i>Ceramics</i>						
BaTiO <sub>3</sub>	120	3.0	1000	$4.0 \times 10^{-4}$	$0.05 \times 10^6$	0.2
PZT	340	1.2	1600	$4.2 \times 10^{-4}$	$0.03 \times 10^6$	0.14
<i>Polymers</i>						
PVDF	205	0.13	12	$0.4 \times 10^{-4}$	$0.40 \times 10^6$	0.2
<i>Polycrystalline layers</i>						
PbTiO <sub>3</sub>	470	2 (monocrystal)	200	$2.3 \times 10^{-4}$	$0.13 \times 10^6$	0.39

Note: The above figures may vary depending on manufacturing technologies

**Table A.10** Characteristics of thermocouple types

Junction materials	Sensitivity $\mu\text{V}/^\circ\text{C}$ (at 25 $^\circ\text{C}$ )	Temperature range ( $^\circ\text{C}$ )	Applications	Designation
Copper/constantan	40.9	-270 to +600	Oxidation, reducing, inert, vacuum. Preferred below 0 $^\circ\text{C}$ . Moisture resistant	T
Iron/constantan	51.7	-270 to +1000	Reducing and inert atmosphere. Avoid oxidation and moisture	J
Chromel/alumel	40.6	-270 to 1300	Oxidation and inert atmospheres	K
Chromel/constantan	60.9	-200 to 1000		E
Pt (10 %)/Rh-Pt	6.0	0-1550	Oxidation and inert atmospheres, avoid reducing atmosphere and metallic vapors	S
Pt (13 %)/Rh-Pt	6.0	0-1600	Oxidation and inert atmospheres, avoid reducing atmosphere and metallic vapors	R
Silver-Paladium	10.0	200-600		
Constantan-Tungsten	42.1	0-800		
Silicon-Aluminum	446	-40 to 150	Used in thermopiles and micromachined sensors	

**Table A.11** Thermoelectric coefficients and volume resistivities of selected elements (Adapted from J. Schieferdecker et al. Infrared thermopile sensors with high sensitivity and very low temperature coefficient. *Sensors and Actuators A* 46-47, pp: 422-427, 1995)

Element	$\alpha$ ( $\mu\text{V K}^{-1}$ )	$\rho$ ( $\mu\Omega \text{ m}$ )
<i>p</i> -Si	100-1000	10-500
<i>p</i> -Poly-Si	100-500	10-1000
Antimony (Sb)	32	18.5
Iron (Fe)	13.4	0.086
Gold (Au)	0.1	0.023
Copper (Cu)	0	0.0172
Silver (Ag)	-0.2	0.016
Aluminum (Al)	-3.2	0.028
Platinum (Pt)	-5.9	0.0981
Cobalt (Co)	-20.1	0.0557
Nickel (Ni)	-20.4	0.0614
Bismuth (Bi)	-72.8	1.1
<i>n</i> -Si	-100 to -1000	10-500
<i>n</i> -Poly-Si	-100 to -500	10-1000

**Table A.12** Thermocouples for very low and very high temperatures

Materials	Useful range, °C	Approx sensitivity, $\mu\text{V}/^\circ\text{C}$
Iron-constantan	down to $-272$	$-32$
Copper-constantan	down to $-273$	$-22.9$
Cromel-alumel	down to $-272$	$-23.8$
Tantalum-tungsten	up to 3000	6.1
Tungsten—tungsten(50)/molybdenum	up to 2900	2.8
Tungsten -tungsten(20)/rhenium	up to 2900	12.7

**Table A.13** Densities ( $\text{kg}/\text{m}^3$ ) of some materials, at 1 atm pressure and  $0^\circ\text{C}$ 

Best laboratory vacuum	$10^{-17}$	Silica	1938–2657
Hydrogen	0.0899	Graphite recrystallized	1938
Helium	0.1785	Borosilicate glass (TEMPAX <sup>®</sup> ) <sup>a</sup>	2200
Methane	0.7168	Asbestos fibers	2400–3300
Carbon monoxide	1.250	Silicon	2333
Air	1.2928	Polycrystalline glass	2518–2600
Oxygen	1.4290	Aluminum	2700
Carbon dioxide	1.9768	Mullite	2989–3293
Plastic foams	10–600	Silicon nitride	3183
Benzene	680–740	Alumina ceramic	3322–3875
Alcohol	789.5	Zinc alloys	5200–7170
Turpentine	860	Vanadium	6117
Mineral oil	900–930	Chromium	7169
Natural rubber	913	Tin and its alloys	7252–8000
Polyethylene, low density	913	Stainless steel	8138
Ice	920	Bronzes	8885
Polyethylene, high density	950	Copper	8941
Carbon and graphite fibers	996–2000	Cobalt and its alloys	9217
Water	1000	Nickel and its alloys	9245
Nylon 6	1100	Bismuth	9799
Hydrochloric acid (20 %)	1100	Silver	10,491
Acrylics	1163–1190	Lead and its alloys	11,349
Epoxies	1135–2187	Palladium	12,013
Coal tar	1200	Mercury	13,596
Phenolic	1246–2989	Molybdenum	13,729
Glycerin	1260	Tantalum and its alloys	16,968
PVC	1350	Gold	19,320
Saran fibers	1700	Tungsten and its alloys	19,653
Sulfuric acid (20 %)	1700	Platinum	21,452
Polyester	1800	Iridium	22,504
Beryllium and its alloys	1855–2076	Osmium	22,697

<sup>a</sup>TEMPAX<sup>®</sup> is a registered trademark of Schott Glaswerke, Mainz, Germany

**Table A.14** Mechanical properties of some solid materials

Material	Modulus of elasticity (GPa)	Poisson's ratio ( $\nu$ )	Density ( $\text{kg/m}^3$ )
Aluminum	71	0.334	2700
Beryllium copper	124	0.285	8220
Brass	106	0.324	8530
Copper	119	0.326	8900
Glass	46.2	0.245	2590
Lead	36.5	0.425	11,380
Molybdenum	331	0.307	10,200
Phosphor bronze	11	0.349	8180
Steel (carbon)	207	0.292	7800
Steel (stainless)	190	0.305	7750

**Table A.15** Mechanical properties of some crystalline materials (from Petersen, K. E. Silicon as a mechanical material. *Proc. IEEE*, vol. 70, No. 5, pp: 420–457, May 1, 1982)

Material	Yield strength, $10^{10}$ dyne/cm <sup>2</sup>	Knoop hardness, kg/mm <sup>2</sup>	Young's modulus, $10^{12}$ dyne/cm <sup>2</sup>	Density, g/cm <sup>3</sup>	Thermal conductivity, W/cm°C	Thermal expansion, $10^{-6}/^\circ\text{C}$
Diamond <sup>a</sup>	53	7000	10.35	3.5	20.0	1.0
SiC <sup>a</sup>	21	2480	7.0	3.2	3.5	3.3
TiC <sup>a</sup>	20	2470	4.97	4.9	3.3	6.4
Al <sub>2</sub> O <sub>3</sub> <sup>a</sup>	15.4	2100	5.3	4.0	0.5	5.4
Si <sub>3</sub> N <sub>4</sub> <sup>a</sup>	14	3486	3.85	3.1	0.19	0.8
Iron <sup>a</sup>	12.6	400	1.96	7.8	0.803	12.0
SiO <sub>2</sub> (fibers)	8.4	820	0.73	2.5	0.014	0.55
Si <sup>a</sup>	7.0	850	1.9	2.3	1.57	2.33
Steel (max. strength)	4.2	1500	2.1	7.9	0.97	12.0
W	4.0	485	4.1	19.3	1.78	4.5
Stainless steel	2.1	660	2.0	7.9	0.329	17.3
Mo	2.1	275	3.43	10.3	1.38	5.0
Al	0.17	130	0.70	2.7	2.36	25.0

<sup>a</sup>Single crystal

**Table A.16** Speed of sound waves (gases at 1 atm pressure, solids in long thin rods)

Medium	speed (m/s)
Rubber	40–150
Air (dry at 20 °C)	344
Steam (134 °C)	494
Hydrogen (20 °C)	1330
Water (fresh)	1433
Water (sea)	1519
Lead	1190
Concrete	3200–3600
Brass	3475
Copper	3810
Aluminum	3100–6320
Gold	3240
Class	3962
Hardwood	3962
Brick	4176
Pyrex <sup>®</sup> glass	5640
Steel	6100
Diamond	12,000
Beryllium	12,890

**Table A.17** Coefficient ( $\alpha$ ) of linear thermal expansion of some materials (per °C  $\times 10^{-6}$ )

Material	$\alpha$	Material	$\alpha$
Alnico I (permanent magnet)	12.6	Nylon	90
Alumina (polycrystalline)	8.0	Phosphor-bronze	9.3
Aluminum	25.0	Platinum	9.0
Brass	20.0	Plexiglas (lucite)	72
Cadmium	30.0	Polycarbonate (ABS)	70
Chromium	6.0	Polyethylene (high density)	216
Comol (permanent magnet)	9.3	Silicon	2.6
Copper	16.6	Silver	19.0
Fused quartz	0.27	Solder 50–50	23.6
Glass (Pyrex <sup>®</sup> )	3.2	Steel (SAE 1020)	12.0
Glass (regular)	9.0	Steel (stainless: type 304)	17.2
Gold	14.2	Teflon	99
Indium	18.0	Tin	13.0
Invar	0.7	Titanium	6.5
Iron	12.0	Tungsten	4.5
Lead	29.0	Zinc	35.0
Nickel	11.8		



**Table A.18** Specific heat and thermal conductivity of some materials (at 25 °C)

Material	Specific heat, J/kg °C	Thermal conductivity, W/m °C	Density, kg/m <sup>3</sup>
Air (1 atm)	995.8	0.024	1.2
Alumina	795	6	4000
Aluminum	481	88–160	2700
Bakelite	1598	0.23	1300
Brass	381	26–234	8500
Chromium	460	91	
Constantan	397	22	8800
Copper	385	401	8900
Diamond		99–232	
Fiberglass	795	0.002–0.4	60
Germanium		60	
Glass (Pyrex)	780	0.1	2200
Glass (regular)		1.9–3.4	
Gold	130	296	19,300
Graphite		112–160	
Iron	452	79	7800
Lead	130	35	11,400
Manganin	410	21	8500
Mercury	138	8.4	13,500
Nickel and its alloys	443	6–50	8900
Nylon	1700	0.24	1100
Platinum	134	73	21,400
Polyester	1172	0.57–0.73	1300
Polyurethane foam		0.024	40
Silicon	668	83.7	2333
Silicone oil	1674	0.1	900
Silver	238	419	10,500
Stainless steel	460	14–36	8020
Styrofoam	1300	0.003–0.03	50
Teflon TFE	998	0.4	2100
Tin	226	64	7300
Tungsten	139	96.6	19,000
Water	4184	0.6	1000
Zinc	389	115–125	7100

**Table A.19** Typical emissivities of different materials (from 0 to 100 °C)

Material	Emissivity	Material	Emissivity
Blackbody (ideal)	1.00	Green leaves	0.88
Cavity radiator	0.99–1.00	Ice	0.96
Aluminum (anodized)	0.70	Iron or steel (rusted)	0.70
Aluminum (oxidized)	0.11	Nickel (oxidized)	0.40
Aluminum (polished)	0.05	Nickel (unoxidized)	0.04
Aluminum (rough surface)	0.06–0.07	Nichrome (80Ni-20Cr) (oxidized)	0.97
Asbestos	0.96	Nichrome (80Ni-20Cr) (polished)	0.87
Brass (dull tarnished)	0.61	Oil	0.80
Brass (polished)	0.05	Silicon	0.64
Brick	0.90	Silicone Rubber	0.94
Bronze (polished)	0.10	Silver (polished)	0.02
Carbon filled latex paint	0.96	Skin (human)	0.93–0.96
Carbon lamp black	0.96	Snow	0.85
Chromium (polished)	0.10	Soil	0.90
Copper (oxidized)	0.6–0.7	Stainless steel (buffed)	0.20
Copper (polished)	0.02	Steel (flat rough surface)	0.95–0.98
Cotton cloth	0.80	Steel (ground)	0.56
Epoxy resin	0.95	Tin plate	0.10
Glass	0.95	Water	0.96
Gold	0.02	White paper	0.92
Gold-black	0.98–0.99	Wood	0.93
Graphite	0.7–0.8	Zinc (polished)	0.04

**Table A.20** Refractive indices (*n*) of some materials

Material	<i>n</i>	wavelength (μm)	Note
Vacuum	1		
Air	1.00029		
Acrylic	1.5	0.41	
AMTIR-1 (Ge <sub>33</sub> As <sub>12</sub> Se <sub>55</sub> )	2.6 2.5	1 10	Amorphous glass <sup>a</sup>
AMTIR-3 (Ge <sub>28</sub> Sb <sub>12</sub> Se <sub>60</sub> )	2.6	10	Amorphous glass <sup>a</sup>
As <sub>2</sub> S <sub>3</sub>	2.4	8.0	Amorphous glass <sup>a</sup>
CdTe	2.67	10.6	
Crown glass	1.52		
Diamond	2.42	0.54	Excellent thermal conductivity
Fused silica (SiO <sub>2</sub> )	1.46	3.5	
Borosilicate glass	1.47	0.7	TEMPAX <sup>®b</sup> Transparent: 0.3–2.7μm
GaAs	3.13	10.6	Laser windows

(continued)

**Table A.20** (continued)

Material	$n$	wavelength ( $\mu\text{m}$ )	Note
Germanium	4.00	12.0	
Heaviest flint glass	1.89		
Heavy flint glass	1.65		
Irtran 2 (ZnS)	2.25	4.3	Windows in IR sensors
KBr	1.46	25.1	Hygroscopic
KCl	1.36	23.0	Hygroscopic
KRS-5	2.21	40.0	Toxic
KRS-6	2.1	24	Toxic
NaCl	1.89	0.185	Hygroscopic, corrosive
Polyethylene	1.54	8.0	Low cost IR windows/lenses
Polystyrene	1.55		
Pyrex 7740	1.47	0.589	Good thermal and optical properties
Quartz	1.458	0.589	
Sapphire ( $\text{Al}_2\text{O}_3$ )	1.59	5.58	Chemically resistant
Silicon	3.42	5.0	Windows in IR sensors
Silver bromide (AgBr)	2.0	10.6	Corrosive
Silver chloride (AgCl)	1.9	20.5	Corrosive
Skin (human)	1.38		
Water [20 °C]	1.33		
Ytterbium fluoride ( $\text{YbF}_3$ )	1.52	0.22–12	Used for ARC on windows/lenses
ZnSe	2.4	10.6	IR windows, brittle

<sup>a</sup>Available from Amorphous Materials, Inc. Garland, TX, USA: [amorphousmaterials.com](http://amorphousmaterials.com)

<sup>b</sup>TEMPAX<sup>®</sup> is a registered trademark of Schott Glasswerke, Mainz, Germany

**Table A.21** Characteristics of C–Zn and Alkaline cells (from Powers R.A. Batteries for low power electronics. In: *Proceedings of the IEEE*, Vol. 83, No. 4, pp: 687–693, April 1995)

Battery	Wh/L	Wh/kg	Drain rate	Shelf life
Carbon–Zinc	150	85	Low–medium	2 years
Alkaline	250	105	Medium–high	5 years

**Table A.22** Lithium–manganese dioxide primary cells (from Powers R.A. Batteries for low power electronics. In: *Proceedings of the IEEE*, Vol. 83, No. 4, pp: 687–693, April 1995)

Construction	Voltage	Capacity (mA h)	Rated d.c. current (mA)	Pulse current (mA)	Energy sensity (W h/L)
Coin	3	30–1000	0.5–7	5–20	500
Cyl. wound	3	160–1300	20–1200	80–5000	500
Cyl. bobbin	3	650–500	4–10	60–200	620
Cyl. “D” cell	3	10,000	2500		575
Prismatic	3	1150	18		490
Flat	3 /6	150–1400	20–125		290

**Table A.23** Typical characteristics of “AA”-size secondary cells

System	Volts	Capacity (mA h)	Rate (C) <sup>a</sup>	W h/L	W h/kg	Cycles	Loss/Mo (%)
NiCad	1.2	1000	10	150	60	1000	15
Ni-MH	1.2	1200	2	175	65	500	20
Pb Acid	2	400	1	80	40	200	2
Li Ion (CoO <sub>2</sub> )	3.6	500	1	225	90	1200	8
Li/MnO <sub>2</sub>	3	800	0.5	280	130	200	1

<sup>a</sup>Note: Discharge rate unit, C, (in mA) is equal numerically to the nominal capacity (in mA h).

**Table A.24** Miniature secondary cells and batteries

Manufacturer	Part	Type	Size	Capacity (mAh)	Voltage	Price \$ (approx.)
Avex Corp. Bensalem, PA, 800-345-1295		RAM	AA	1.4	1.5	1
GN National Electric Inc. Pomona, CA 909-598-1919	GN-360	NiCd	15.5 × 19 mm	60	3.6	1.10
GP Batteries USA, San Diego, CA 619-674-5620	Green-Charge	NiMH	2/3AA, AA, 2/3AF, 4/5AF	600–2500	1.2	2–7
Gould, Eastlake, OH 216-953-5084	3C120M	LiMnO <sup>2</sup>	3 × 4 × 0.12 cm	120	3	2.71
House of Batteries Inc., Huntington Beach, CA, 800-432-3385	Green Cell	NiMH	AA, 4/5A, 7/5A	1200–2500	1–2	3.50–12
Maxell Corp., Fairlawn, NJ 201-794-5938	MHR-AAA	NiMH	AAA	410	1.2	4
Moli Energy Ltd., Maple Ridge, BC, Canada, 604-465-7911	MOLICEL	Li-ion	18(dia) × 65 mm	1200	3.0–4.1	25
Plainview Batteries, Inc., Plainview, NY 516-249-2873	PH600	NiMH	48 × 17 × 7.7 mm	600	1.2	4
Power Conversion, Inc., Elmwood Park, NJ 201-796-4800	MO4/11	LiMnO <sub>2</sub>	1/2AA	1000	3.3	5–8
Power Sonic Corp., Redwood City, CA, 415-364-5001	PS-850AA	NiCd	AA	850	1.2	1.75
Rayovac Corp., Madison, WI 608-275-4690	Renewal	RAM	AA, AAA	1200, 600	1.5	from 0.50
Renata US, Richardson, TX 214-234-8091	CR1025	Li	10 mm	25	3.0	0.50
Sanyo Energy (USA), San Diego, CA, 691-661-7992	Twicell	NiMH	10.4 × 44.5 × 67 mm	450	1.2	3.85
Saft America, Inc., San Diego, CA, 619-661-7992	VHAA	NiMH	AA	1100	1.2	2.95
Tadiran Electronics, Port Washington, NY, 516-621-4980		Li	1/AA-DD packs	370 mAh to 30 Ah	3–36	1+
Toshiba America, Deerfield, IL, 800-879-4963	LSQ8	Li-ion	8.6 × 3.4 × 48 mm	900	3.7	12–15
Ultralife Batteries, Inc., Newark, NJ, 315-332-7100	U3VL	Li	25.8 × 44.8 × 16.8	3600	3.0	4.60
Varta Batteries, Inc., Elmsford, NY 914-592-2500		NiMH	AAA-F	300–8000	1.2	0.80+

*Li-ion* lithium-ion, *LiMnO<sup>2</sup>* lithium manganese dioxide, *NiCd* nickel-cadmium, *NiMH* nickel-metal hydride, *RAM* rechargeable alkaline manganese

**Table A.25** Electronic ceramics (between 25 and 100 °C)

	96 % Alumina (Al <sub>2</sub> O <sub>3</sub> )	Beryllia (BeO)	Boron nitride (BN)	Aluminum nitride (AlN)	Silicon carbide (SiC)	Silicon (Si)
Hardness, Knopp (kg/mm <sup>2</sup> )	2000	1000	280	1200	2800	–
Flexural Strength (10 <sup>5</sup> N/m <sup>2</sup> )	3.0	1.7–2.4	0.8	4.9	4.4	–
Thermal conductivity (W/(m K))	21	250	60	170–200	70	150
Thermal expansion (10 <sup>-6</sup> /K)	7.1	8.8	0.0	4.1	3.8	3.8
Dielectric strength (kV/mm)	8.3	19.7	37.4	14.0	15.4	–
Dielectric loss (10 <sup>-4</sup> tan delta at 1 MHz)	3–5	4–7	4	5–10	500	–
Dielectric constant, $\kappa$ (at 10 MHz)	10	7.0	4.0	8.8	40	–

**Table A.26** Properties of glasses

	Soda-lime	Borosilicate	Lead glass	Aluminosilicate	Fused silica	96 % silica
Modulus of elasticity ( $10^6$ psi)	10.2	9.0	8.5–9.0	12.5–12.7	10.5	9.8
Softening temperature ( $^{\circ}$ F)	1285	1510	932–1160	1666–1679	2876	2786
Coefficient of thermal expansion ( $10^{-6}$ ; in./in. $^{\circ}$ C)	8.5–9.4	3.2–3.4	9–12.6	4.1–4.7	0.56	0.76
Thermal conductivity (BTU—in./h ft $^2$ $^{\circ}$ F)	7.0	7.8	5.2	9.0	9.3	10.0
Density (lb/in. $^3$ )	0.089	0.081	0.103–0.126	0.091–0.095	0.079	0.079
Electrical resistivity (Log $10\Omega$ cm)	12.4	14	17	17	17	17
Refractive index	1.525	1.473	1.540–1.560	1.530–1.547	1.459	1.458

---

# Index

## A

A/D converters, 5  
    successive approximation, 234  
    voltage-to-frequency, 228  
Absolute zero, 134  
Absorption, 9, 164  
Absorptivity, 146, 186  
Accelerated life test, 64  
Acceleration, 733  
Accelerometer  
    characteristics, 396  
    piezoelectric, 405  
    piezoresistive, 404  
    thermal, 406  
Accuracy, 8, 39  
Active sensor, 5  
Aging, 59  
Alternating magnetic field, 142  
Ampere, 10  
Amplifiers, 198–199  
    bridge, 216  
    charge, 201  
    current, 203  
    differential, 304  
    noninverting, 201  
Angular acceleration, 733  
Angular velocity, 733  
Antenna, 564  
Area, 733  
Atmosphere, 431, 736  
Attenuation, 166  
Avalanche detector, 582

## B

Band gap. *See* Energy gap  
Barometer, 429, 434  
Barrel tubes, 433  
Beamsplitter, 391

Bellows, 415, 433  
Below mid infrared, thermal detectors, 549  
Bernoulli, 429, 456  
Bias current, 196, 199  
Bimetal coil, 399  
Bolometer, 564  
Boltzmann constant, 245, 532  
Bootstrapping, 198  
Bourdon tubes, 433  
Boyle, 429  
Bridge, 213, 214  
    amplifiers, 216  
    disbalanced, 214  
    null-balanced, 215  
Btu, 133

## C

Cadmium sulfide (CdS), 538  
Cadmium telluride (CdTe), 581  
Calibration, 42  
Calorie, 133, 734  
Candela, 10  
Capacitance, 77, 733  
Capacitive gauge, 342  
Capacitive sensor, 342–345  
Capacitor, 77, 402, 534  
    bypass, 255  
Car, 5, 290  
Cavity, 151  
The Celsius, 134  
Charge, 9, 290, 302, 475, 657  
Coatings, 169, 186  
Coil, 93, 346, 442  
Collectors, 185  
Common-mode rejection, 248  
Comparator, 290, 296  
Complementary metal oxide semiconductor  
    (CMOS), 196, 245



- Concentrators, 185–186  
 Conductive rubber, 323  
 Conductivity, 9, 99, 527  
 Conductor, 99  
 Constantan, 417  
 Convection, 141, 463  
 Conversion multiples, 734  
 Core, 347  
 Coulomb, 733  
 Coulomb law, 73  
 Cryogenic light detectors, 540  
 Curie, 105, 114, 736  
 Curie temperature, 62, 350, 425, 611, 615  
 Current generators, 220  
   mirrors, 222  
 Current limiting, 614  
 Current pumps. *See* Current generators
- D**
- Damping factor, 54  
 Data acquisition, 4, 5  
 Dead band, 8  
 Decibel, 39  
 Density, 430, 733, 746  
 Diaphragm, 437, 441  
 Dielectric constant, 79, 81, 301  
 Digital representation, 226  
 Diode, 80, 445, 533, 578  
 Dipole moment, 115  
 Displacement, 320, 402, 455  
 Displacement measurements, 287  
 Displacement sensor, 364, 370  
 Dissipation factor, 608  
 Divider, 209  
 Doping, 701  
 Doppler effect, 273  
 Dynode, 572
- E**
- Eddy currents, 349  
 Einstein, 526  
 Electric charge, 70–76  
 Electric current, 10, 96, 97  
 Electric dipole, 74  
 Electric field, 9, 72, 96, 143, 293  
 Electric force, 71  
 Electric lights control, 271  
 Electric potential, 76  
 Electrical conductivity, 71  
 Electricity, 70  
 Electrode, 292, 422, 473, 659
- Electrolyte, 399, 659  
 Electromagnetic radiation, 525  
 Electromotive force (*e.m.f.*), 90, 262  
 Electron-volt, 156  
 Emissivity, 9, 146, 147, 186, 301, 306  
   spatial diagrams, 149  
 Encoding disks, 371  
 Energy bands, 526, 536, 578  
 Energy gap, 528  
 Energy management, 271  
 Excitation, 7, 49, 50, 218–225, 346
- F**
- Fahrenheit, 134  
 False positive detection, 272  
 Farad, 77, 733  
 Faraday, 79, 90, 472  
 Faraday cage, 74  
 The Faraday's constant, 660  
 Faraday's law, 90  
 Ferromagnetics, 346  
 Fiber optics, 179–183, 366, 392  
 Fiber-optic sensors, 364–365  
 Fiber-optics, 444  
 Field lines, 72  
 Field of view, 296  
 Film, 186  
 Flow dynamics, 453–455  
 Flowmeter, 615  
 Fluoroptics, 565  
 Flux, 9, 72, 144, 166, 733  
 Flux density, 306  
 Focus, 175  
 Force, 403, 430, 733  
 Force-sensitive resistor (FSR), 325  
 Franklin, 70  
 Frequency, 733  
   corner, 196  
   natural, 52, 54  
   resonant, 52, 397  
 Frequency response, 195  
 Full-scale output (FSO), 39
- G**
- Gain-bandwidth product, 200  
 Galileo, 413  
 Gallon, 737  
 Gas multiplication, 547  
 Gauge, 103, 435  
 Gauge factor, 103  
 Gauging, 348

Gauss' law, 72  
Geiger-Mueller counters, 576–578  
Germanium, 580  
Gold, 172, 739, 745, 747  
Gold-black, 186, 747  
Grating sensors, 370–371  
Gravitational sensors, 399  
Ground loops, 259–261  
Ground planes, 258  
Guarding, 197

## H

Hall coefficient, 121  
Hall effect, 119–123, 700  
Hall sensor, 119  
Heat flow, 116  
Heat flux, 733  
Heat transfer, 133  
Heater, 406, 463  
Henry, 90, 91, 472, 733  
Hermistor, 564  
Hydrophone, 370  
Hygrometer, 507  
Hysteresis, 8, 43–44, 353

## I

Image, 297, 305  
Impedance  
  output, 48, 195  
Impedance conversion, 201  
Inaccuracy, 39  
Inductance, 733  
Induction, 90–95  
Inductor, 91  
Infrared, 144, 541  
Infrasound, 129  
Interference, 243  
Ionization detectors, 574–582  
Isolator, 71

## J

JFET, 196, 303, 475, 560  
Johann Seebeck (1770–1831), 123  
Joule, 76, 137, 733

## K

Kelvin, 10, 134  
Keyboards, 318  
Kilogram, 10, 414

King's law, 463  
Kirchhoff law, 58

## L

Langevin, P., 105  
Leakage current, 197  
The Leakage resistance, 116  
Length, 10  
Lens, 174, 286, 296, 299  
  facet, 298  
  Fresnel, 304  
  pinhole, 300  
Level detector, 365, 615  
Light, 155  
Light detectors, 155  
Light-emitting diodes (LEDs), 285, 444  
Linear expansion, 135  
Linearity, 8, 45  
  independent, 45  
Linear variable differential transformer  
  (LVDT), 346, 415  
Lithium, 580  
Load resistance, 200  
Lumen, 167, 734  
Luminance, 734  
Luminescence, 548

## M

Magnet, 361  
Magnetic field, 90, 119, 349, 358, 474  
Magnetic flux, 9, 346, 353, 442, 473  
Magnetic resistance, 346, 442  
Magnetoresistance, 358  
Magnetostrictive detector, 361–362  
Mask, 297  
Mass, 10, 55, 56, 405, 453  
Mean-time-between-failures (MTBF), 61  
Measurand, 2  
Mechanical load, 339  
Membrane, 326, 434  
  ion-selective, 656  
Mercury cadmium-telluride (HgCdTe), 541  
Mercury switch, 399  
Metal oxide, 187  
Metal oxide semiconductor (MOS), 206  
Meter, 10  
Microcalorimetry, 679  
Micromachining, 700  
Microphone  
  electret, 495  
Microwaves, 274, 564

- Mirrors, 170, 444  
Mole, 10  
Motion detectors, 271  
Movements, 292, 295  
Multiplexer, 5, 347  
Mutual inductance, 93
- N**  
Navigation systems, 397  
Newton, 55, 59, 162, 413, 414, 733  
Nichrome, 186, 417, 634, 747  
Noise  
    additive, 248  
    current, 244  
    inherent, 244  
    Johnson, 245  
    mechanical, 258  
    multiplicative, 250  
    peak-to-peak, 247  
    pink, 246  
    popcorn, 245  
    Schottky, 245  
    Seebeck, 261  
    sources, 243  
    thermal, 245  
    transmitted, 247, 257  
    white, 245  
Noise equivalent power (NEP), 529  
Nonlinearity, 44–45
- O**  
Offset voltage, 196, 199  
Ohm, 733  
Ohm's law, 93, 98  
Operational amplifier, 199, 534, 561  
Optical distortions, 169  
Optical materials, 164  
Optical sensors, 362–371  
Optics, 143  
Oscillators, 224  
    LC, 224, 225  
    RC, 224, 225  
Output format, 8  
Output resistance, 201
- P**  
Pascal, 429  
Passive-infrared (PIR), 302  
Peltier, 123–129  
Permittivity, 9  
Permittivity constant, 72  
Phase shift, 52  
Photoconductivity, 700  
Photodiode, 530  
Photoeffect, 286, 526  
Photometry, 166–168  
Photomultiplier, 571  
Photon, 525, 572  
Photon detector, 570  
Photoresistor, 301, 538  
Phototransistor, 536  
Photovoltaic effect, 700  
Piezoelectric effect, 104–113, 195,  
    197, 274, 422, 474, 585,  
    673, 700, 736  
Piezoelectric films, 320  
Piezoresistive effect, 416  
Piezoresistivity, 700  
Planck, 526  
Planck's constant, 156  
Plate, 435  
Platinum, 100, 416, 634, 738, 745  
Polarization, 80, 116  
Polarized light, 363  
Poling, 75  
Polymer, 325, 425  
Polymer piezo/pyroelectric film, 109  
Polynomial, 100  
Polysilicon, 701  
Polyvinylidene fluoride (PVDF), 304, 320,  
    322, 424  
Position sensitive detector (PSD), 285  
Potential, 9  
Potentiometer, 336  
Pound, 414  
Precession, 386  
Pressure, 733  
    absolute, 439  
    differential, 439  
Pressure sensor  
    mercury, 432  
    piezoresistive, 435  
Pressure transducers, 318  
Price, 65  
Primary pyroelectricity, 115  
Prism, 365  
Proportional chamber, 575  
Proximity detector, 363–364  
Proximity sensor, 350  
Pyroelectric effect, 113–119, 474, 558  
Pyroelectric coefficient, 307  
Pyroelectric detector, 75  
Pyroelectric sensor, 305  
Pyroelectricity, 114  
Pyroelectrics, 302

**Q**

Quantum detectors, 526  
 Quartz, 71, 105, 745, 748  
 Quenching, 576

**R**

Radian, 10  
 Radiation, 133  
 Radiation detectors, 569  
 Radioactivity, 569  
 Range meters, 273  
 Ratiometric technique, 209  
 Reflection, 9, 146, 161  
 Reflective coefficient, 164, 174  
 Reflector, 364  
 Refraction, 161  
 Refractive index, 9, 162, 169  
 Reliability, 61  
 Repeatability, 46  
 Resistance, 96–104, 703  
 Resistance temperature detector (RTD),  
     100, 564  
 Resistivity, 98, 701  
 Resistor, 98  
 Resolution, 8, 47  
 Robots, 291, 295  
 Rotary variable differential transformer  
     (RVDT), 346  
 Rotation, 386

**S**

Sagnac effect, 390  
 Scintillating detectors, 570–573  
 Second, 10  
 Secondary pyroelectricity, 115  
 Security, 271, 295  
 Security system, 7  
 Seebeck, 629, 700  
 Selectivity, 8  
 Self-induction, 91  
 Sensor, 424, 599, 610, 611  
     acoustic, 640  
     amperometric, 659  
     angular, 359  
     array, 297  
     breeze, 474  
     capacitive, 440  
     catalytic, 680  
     classification, 7  
     conductometric, 656  
     definition, 2  
     differential, 248

displacement, 365  
 eddy currents, 350  
 electrochemical, 651  
 electromagnetic, 472  
 enzyme, 650  
 far infrared, 301  
 flow, 453  
 fuel detection, 664  
 gas, 680  
 gas flame, 547  
 grating, 370  
 Hall effect, 353  
 ionizing radiation, 569  
 magnetic, 347  
 magnetoresistive, 359  
 magnetostrictive, 361  
 navigation, 386  
 noncontact, 4  
 occupancy, 271  
 optical, 362  
 optoelectronic, 295, 443, 550  
 oscillating, 671  
 output format, 4  
 piezoelectric, 320, 362, 405, 474  
     cable, 424  
 piezoresistive, 404  
 platinum, 597, 598  
 pn-junction, 620  
 position, 285  
 potentiometric, 655  
 pressure gradient, 456  
 proximity, 348, 350, 364  
 reliability, 63  
 RTD, 597  
 self-heating, 610  
 tactile, 318  
 temperature, 551, 564, 593  
 the pressure concept was primarily based on  
     the pioneering work of Evangelista.i.  
     Torricelli, 429  
 thermal, 406, 458  
 thermistor, 599  
     characteristics, 610  
     NTC, 599  
     PTC, 611  
 thermoelectric, 626  
 transverse, 348  
 triboelectric, 292  
 ultrasonic, 273, 470  
 VRP, 442  
 Shielding  
     electric, 252  
     magnetic, 256  
 SI multiples, 733

Signal conditioner, 4  
 Signal conditioning, 60, 198  
 Signal format, 3, 4  
 Silicon, 122, 286, 326, 354, 406, 435,  
     444, 580, 621, 624–626,  
     699, 747, 748  
 Silicon nitrate, 701  
 Silicone rubber, 747  
 Skin (human), 156, 747  
 Slug, 414  
 Snell's law, 161  
 Solenoid, 5, 92  
 Solid angle, 10  
 Sound, 129  
 Specific heat, 9, 137, 733  
 Speed of light, 143  
 Speed of response, 8  
 Spring, 415  
 Stability, 8  
 Stefan-Boltzmann law, 145, 301, 305  
 Steradian, 10, 167  
 Stimulus, 1  
     definition, 2  
 Storage conditions, 59  
 Strain gauge, 414  
 Stress, 104, 416, 436  
 Surface acoustic wave (SAW), 672  
 Switched capacitor, 205  
 Synchronous detector, 347  
 Systems of units, 10

**T**

Temperature coefficient of resistivity  
     (TCR), 99  
 Temperature, 9, 97, 99, 114, 301, 417, 457,  
     550, 585  
     reference points, 597  
 Temperature detector, 211  
 Tesla, 733  
 Thermal conductivity, 9, 139, 590, 733  
 Thermal expansion, 585  
 Thermal radiation, 118  
 Thermal resistance, 57  
 Thermal shock, 62  
 Thermal time constant, 118  
 Thermal transport (flow sensors), 458  
 Thermistors, 7, 100, 214, 302, 599, 679  
 Thermoanemometer, 463  
 Thermocouple, 627, 741  
     assemblies, 633  
     film, 634  
     laws, 628

Thermoelectrics, 114  
 Thermometer, 585  
 Thermopiles, 302, 552, 629  
 Thermostat, 399, 553  
 Time, 10  
 Time constant, 51, 57, 560, 591  
 Toothed wheel, 359  
 Torque, 734  
 Toys, 271, 295  
 Transformer, 346, 442  
 Transmission  
     four-wire, 243  
     two-wire, 242  
 Transmittance, 164  
 Transparency, 162  
 Triangular measurement, 286  
 Triboelectric effect, 60, 70  
 Tungsten, 100, 739

**U**

Ultrasound, 129  
 Ultraviolet (UV), 155, 547  
 Units of measurements, 10–11  
 US Customary systems, 414

**V**

Velocity, 464, 733  
 Velocity detectors, 273  
 Velocity of light, 162  
 Viscosity, 9, 736  
 Volt, 733  
 Voltage follower, 201, 560  
 Voltage gain, 198  
 Voltage reference, 223  
 Volume, 733

**W**

Water, 81, 134, 169, 737, 746–748  
 Waveguide, 361  
 Weber, 733  
 Wheatstone bridge, 212, 359,  
     417, 432, 437  
 Window, 169  
 Wiper, 337  
 W-value, 574

**Y**

Young's modulus, 701